plants

Special Issue Reprint

10th Anniversary of *Plants*

Recent Advances and Perspectives
Volume II

Edited by
Milan Stankovic, Paula Baptista and Petronia Carillo

mdpi.com/journal/plants

MDPI

10th Anniversary of *Plants*—Recent Advances and Perspectives—Volume II

10th Anniversary of *Plants*—Recent Advances and Perspectives—Volume II

Editors

Milan Stankovic
Paula Baptista
Petronia Carillo

MDPI

Basel • Beijing • Wuhan • Barcelona • Belgrade • Novi Sad • Cluj • Manchester

Editors

Milan Stankovic
University of Kragujevac
Kragujevac
Serbia

Paula Baptista
Polytechnic Institute
of Bragança
Bragança
Portugal

Petronia Carillo
University of Campania
"Luigi Vanvitelli"
Caserta
Italy

Editorial Office
MDPI
St. Alban-Anlage 66
4052 Basel, Switzerland

This is a reprint of articles from the Special Issue published online in the open access journal *Plants* (ISSN 2223-7747) (available at: https://www.mdpi.com/journal/plants/special_issues/10th_anniversary_plants).

For citation purposes, cite each article independently as indicated on the article page online and as indicated below:

Lastname, A.A.; Lastname, B.B. Article Title. *Journal Name* **Year**, *Volume Number*, Page Range.

Volume II
ISBN 978-3-0365-8420-1 (Hbk)
ISBN 978-3-0365-8421-8 (PDF)
doi.org/10.3390/books978-3-0365-8421-8

Set
ISBN 978-3-0365-8372-3 (Hbk)
ISBN 978-3-0365-8373-0 (PDF)

Contents

About the Editors

Milan Stankovic

Milan Stanković is an associate professor at the Department of Biology and Ecology, Faculty of Science, University of Kragujevac, Republic of Serbia and Head of Department of Biology and Ecology (2016-). His scientific and teaching careeer started at the Department of Biology and Ecology, Faculty of Science, University of Kragujevac (2008). He acquired his PhD degree in Plant Science (2012) at the same university and completed his postdoctoral research at the Université François-Rabelais de Tours, France. At the Faculty of Science, he was appointed as an assistant professor (2013), as well as an associate professor (2019), and he teaches several BSc, MSc, and PhD courses on plant science. His current research is focused on plant biology, ecology, and phytochemistry. Dr. Stanković is the (co-)author of over 300 references including articles in peer-reviewed journals, edited books, book chapters, conference papers, meeteng abstracts, etc. He is currently working as an associate editor of *Plants* (2012-).

Paula Baptista

Paula Baptista is currently an associate professor at the Polytechnic Institute of Bragança (Portugal), the coordinator of the topic "Sustainable Agriculture and Innovative Agro-food Chains" of the Mountain Research Center (CIMO, http://cimo.ipb.pt/web/), and the general secretary of the International Organisation for Biological Control (IOBC-WPRS). More recently, she has become a member of the Plant Health (PLH) Panel of EFSA. She holds a bachelor's degree in agricultural engineering (1996, University of Trás-os-Montes), a master's degree in quality control (2000, University of Porto), and a PhD in science (2007, University of Minho). Her main interests are focused on agricultural microbiology and biotechnology, and in particular on the exploitation of beneficial microorganisms to improve plant health and yield. Her specific lines of research include the identification and characterization of microbial biological control agents, and the study of the molecular bases of plant(s)–pathogen(s)–biocontrol agent(s) interactions using '-omics' approaches. Her research has led to the publication of more than 150 ISI papers.

Petronia Carillo

Petronia Carillo has been a full professor of agronomy at the University of Campania "Luigi Vanvitelli" in Caserta, Italy, since 2020, where she teaches agronomy, plant physiology, and post-harvest physiology. She was an associate professor of plant physiology (2010–2020) and permanent researcher of plant physiology (1999–2010) at the Second University of Naples, Italy. She studied at University Federico II of Naples, Italy, where she received her Ph.D. in plant physiology (1996) and MS (1992). She was a guest scientist at the Botanical Institute, Ruprecht-Karls-University of Heidelberg, Germany (4 months, 2000), and Max Planck Institute of Molecular Plant Physiology of Golm-Potsdam Germany (2–3 months a year from 2001 to 2010 and shorter visits from 2011 to 2020). She currently studies the metabolic and physiological responses of species of agronomic interest to nutrient deficiency, salt stress, and the type of cultivation (conventional, biological, hydroponic, eustress, microgravity, and the use of biostimulants).

plants

MDPI

Review

Engineering Considerations to Produce Bioactive Compounds from Plant Cell Suspension Culture in Bioreactors

Elizabeth Alejandra Motolinía-Alcántara [1], Carlos Omar Castillo-Araiza [2], Mario Rodríguez-Monroy [3], Angélica Román-Guerrero [1,*] and Francisco Cruz-Sosa [1,*]

[1] Departamento de Biotecnología, Universidad Autónoma Metropolitana-Iztapalapa, Av. Ferrocarril de San Rafael Atlixco 186, Ciudad de México 09310, Mexico; eama@xanum.uam.mx
[2] Departamento de Ingeniería de Procesos e Hidráulica, Universidad Autónoma Metropolitana-Iztapalapa, Av. Ferrocarril de San Rafael Atlixco 186, Ciudad de México 09310, Mexico; coca@xanum.uam.mx
[3] Centro de Desarrollo de Productos Bióticos (CEPROBI), Departamento de Biotecnología, Instituto Politécnico Nacional (IPN), Yautepec 62731, Mexico; mrmonroy@ipn.mx
* Correspondence: arogue@xanum.uam.mx (A.R.-G.); cuhp@xanum.uam.mx (F.C.-S.); Tel.: +52-55-5804-4600 (ext. 2847) (A.R.-G.)

Abstract: The large-scale production of plant-derived secondary metabolites (PDSM) in bioreactors to meet the increasing demand for bioactive compounds for the treatment and prevention of degenerative diseases is nowadays considered an engineering challenge due to the large number of operational factors that need to be considered during their design and scale-up. The plant cell suspension culture (CSC) has presented numerous benefits over other technologies, such as the conventional whole-plant extraction, not only for avoiding the overexploitation of plant species, but also for achieving better yields and having excellent scaling-up attributes. The selection of the bioreactor configuration depends on intrinsic cell culture properties and engineering considerations related to the effect of operating conditions on thermodynamics, kinetics, and transport phenomena, which together are essential for accomplishing the large-scale production of PDSM. To this end, this review, firstly, provides a comprehensive appraisement of PDSM, essentially those with demonstrated importance and utilization in pharmaceutical industries. Then, special attention is given to PDSM obtained out of CSC. Finally, engineering aspects related to the bioreactor configuration for CSC stating the effect of the operating conditions on kinetics and transport phenomena and, hence, on the cell viability and production of PDSM are presented accordingly. The engineering analysis of the reviewed bioreactor configurations for CSC will pave the way for future research focused on their scaling up, to produce high value-added PDSM.

Keywords: medicinal plant; bioactive compounds; plant-derived secondary metabolites (PDSM); cell suspension culture (CSC); bioreactor engineering

Citation: Motolinía-Alcántara, E.A.; Castillo-Araiza, C.O.; Rodríguez-Monroy, M.; Román-Guerrero, A.; Cruz-Sosa, F. Engineering Considerations to Produce Bioactive Compounds from Plant Cell Suspension Culture in Bioreactors. *Plants* **2021**, *10*, 2762. https://doi.org/10.3390/plants10122762

Academic Editors: Milan S. Stankovic, Paula Baptista and Petronia Carillo

Received: 9 November 2021
Accepted: 6 December 2021
Published: 14 December 2021

1. Introduction

The plant world has been exploited for thousands of years by human cultures for preventing pain, producing pleasure, usage in religious ceremonies, and treating different diseases and illnesses. Recently, the World Health Organization (WHO) estimated that 80 percent of people worldwide rely on herbal medicines for some aspect of their primary healthcare importance. Medicinal plants have great significance in the health industry. Today, almost 25% of modern medicines are obtained or derived from natural sources [1–3]. To this end, according to a recent report by the British Broadcasting Corporation (BBC), plant-derived drugs will grow from USD 29.3 billion in 2017 to around USD 39.2 billion by 2022, with a compound annual growth rate (CAGR) of 6.1% per year for the same period.

The chemical entities responsible for the biological activity in medicinal plants are organic molecules classified as secondary metabolites. Although there are more than 50,000 plant species used for medicinal purposes, bioactive compounds in plant tissues

generally account for less than 1% (wt.), leading to the overexploitation, threatening, or extinction of vegetal species [4–6]. In agreement with Süntar et al. [7], half of the drugs used for clinical treatments are obtained out of natural sources, accounting for 185 chemical compounds approved by the FDA [8]. Due to the growing interest in obtaining phytochemicals from plant-derived secondary metabolites (PDSM), the use of biotechnologies based on the plant cell culture (PCC) results in a promising, sustainable, and environmentally friendly way of overcoming the problems related to either the traditional cultivation of medicinal plants (including variations in crop quality associated with drought or flood crops, diseases or pest attacks on plants, or the chemical synthesis of bioactive compounds, allowing a better control in the quality and higher yields of the desired products to be achieved.

Academia and industry, nowadays, aim their research on PCC for large-scale production of bioactive compounds by using callus cells, immobilized cells, embryos, roots, shoots, and suspended cells [9,10]. Among PCC, the plant cell suspension culture (CSC) is one of the processes that presents excellent scaling-up attributes for producing plant-derived secondary metabolites (PDSM). Nevertheless, although the use of CSC seems an attractive bioreaction concept for large-scale production of bioactive compounds [11–13], there is a lack of information related to the engineering of the bioreactor technology because of the complex interaction between the operational variables and its performance regarding microbiology, thermodynamics, kinetics, and transport phenomena, which, in turn, impact on the production and quality of PDSM.

This review, in its first part, states the main bioactive compounds found in plants with great commercial relevance, giving an overview of the types of compounds and their different biological activities, and stressing the relevance of PCC for satisfying the today's demand for bioactive compounds. The second part is focused on the production of bioactive compounds by CSC, summarizing the engineering strategies followed in the literature for achieving large-scale production and indicating the characteristics required from plant tissues to obtain CSC with adequate properties. Bioreactor configurations implemented for CSC are also described in this section. Because of its impact on the design and scale-up of CSC, the third part elucidates the impact of the bioreactor configuration and operational conditions on the performance of plant cell cultures during the production of PDSM.

2. Bioactive Compounds in Plants

Medicinal plants are considered as a resource for bioactive compounds that can be used for obtaining pharmacopeial or non-pharmacopeial drugs, contributing to the rising interest and demand for plant-derived phytochemicals [14–16]. Their main activities include antioxidant, anti-inflammatory, antiproliferative, anticancer, anti-neurodegenerative disorders, and chronic diseases, among other health properties [17]. These bioactive compounds are considered as plant-derived secondary metabolites (PDSM) since, in contrast to the primary metabolites, they do not play an active role in the direct metabolic process or growth of the plant, but their importance relies on their interactions with biotic and abiotic stresses in defense of the plant viability [7,18,19].

PDSM are classified in three main groups: (i) terpenes and terpenoid compounds formed by 5-C isopentanoid units, (ii) phenolic compounds derived from the shikimic acid pathway, and (iii) nitrogen and sulfur comprising compounds (Figure 1) synthesized from common amino acids [18]. Their classification is based on their composition, structure, the pathway used for their biosynthesis, and their chemical nature (solubility, polarity, reactivity) [17,20–22]. PSDM are normally produced out of specific plant species or taxonomy [18]. Table 1 describes the main characteristics and biological activities reported for the three groups of PDSM.

PDSM are, in general, extracted from roots and aerial parts of the plant, with typical yields below 1% wt. Their production usually takes very long cultivation times for reaching the plant maturity and ensuring the highest PDSM production, thus requiring large amounts of plant material for satisfying the demand of bioactive compounds in the food

and pharmaceutical industries, and leading to the overexploitation and extinction of the vegetal species, despite the risk of unpredictable differences in the homogeneity and quality of the extracted vegetal due to environmental factors during cultivation [16,18,23,24]. Therefore, it is important to implement novel technologies that allow the production of bioactive compounds in more sustainable and better controlled processes. Among the biotechnological strategies proposed in the literature to produce PDSM out of PCC, the root culture, shoot culture, hairy root culture, and cell suspension culture are some of the most studied in the laboratory scale.

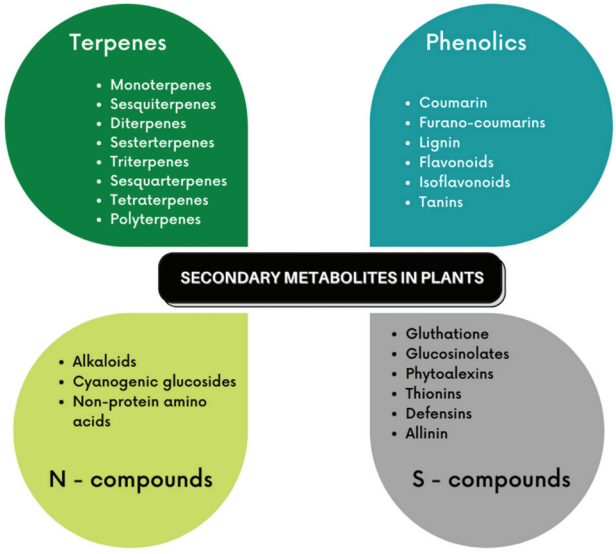

Figure 1. Classification and types of PDSM.

Table 1. Characteristics and biological activities reported for PDSM in medicinal plants.

Compound	Characteristics	Representative Compounds	Biological/ Pharmacological Properties	References
Alkaloids	Complex organic molecules with a heterocyclic nitrogen ring. ↑ 10,000 compounds isolated ↑ 300 families of plants	Piperine; nicotine, vasicine; theobromine; caffeine; aconitine; atropine; quinine; capsaicin, ephedrine; paclitaxel; morphine; berberine; vincristine;	Chemotherapeutic agents; antiproliferative; antimicrobial and antiparasitic activities; analgesic, anti-hyperglycemic, Alzheimer's and Parkinson's diseases, stroke, epilepsy, fungicide.	[25–29]
Phenolic compounds	They are diverse in structure, and present in common the hydroxylated aromatic rings. ↑ 8000 different compounds identified ↑ 300 families of plants	*Simple phenolics*: hydroquinone, pyrogallol acid. *Single phenolic ring*: gallic acid, salicylic acid, caffeic acid, hydroxycinnamic acids. *Two phenolic rings:* Xanthones, stilbenes, flavonoids. *Quinines:* Benzoquinones, naphtaquinones anthraquinones, tannins and lignans.	Antioxidant, anti-inflammatory, anticarcinogenic, cardiovascular protective effect, antidiabetic, anti-obesity, antihemolytic, antibacterial, liver protection, antiatherogenic, antiviral, neuroprotective functions.	[30–35]
Terpenes	Synthesized from acetate via the mevalonic acid pathway. They comprise natural hydrocarbons with isoprene blocks. ↑ 23,000 compounds identified.	*Monoterpenes:* menthol. *Sesquiterpenes:* zingiberene. *Diterpenes:* retinol. *Triterpenes*: squalene. *Tetraterpene*: β-carotene.	Anti-hypertensive activity, antimicrobial, insecticide, fungicide, antioxidant, anticonvulsant, anti-tumor and neurotrophic effects, immune function, skin protection, UV protection, anticancer, antiparasitic, antihyperglycemic.	[28–30,36,37]
Sulfur-rich compounds (SRGs)	The structure is composed of a β-D-glucosyl residue linked by a sulfur atom. About 137 SRGs identified in plants	Glutathione, glucosinolates, phytoalexines, thionines,	Enzyme regulator, intercellular signaling molecule, antitumor effect, Burkitt lymphoma treatment, anticancer.	[38–41]

3. Plant Cell Culture

Plant cell culture (PCC) is nowadays recognized as a promising, renewable, sustainable, and environmentally friendly alternative to obtain PDSM out of wild plants. PCC accounts for the virtues of whole-plant cultivation systems and offers significant advantages, such as controlled manufacture due to standardized environmental conditions, i.e., it is not seasonal dependent, makes use of low amounts of water, and pesticides and herbicides are not required, achieving better quality in the desired product [42,43]. The establishment of different types of plant cell cultures are aimed for regenerating organs or somatic embryos for plant propagation, virus elimination, genetic manipulation, germplasm storage, and for in vitro production of PDSM [44,45]. The main differences found in the literature about in vitro plant cell cultures with whole wild plants comprise a higher cell growth intensity, the mechanisms of synthesis and reserve organelles for PDSM, and the concentration of PDSM. Despite most of the PDSM contents recovered in plant cell cultures usually being lower than those obtained in wild plants, there are some successful cases where super-producer strains have been achieved [46,47]. According to the literature [48], PCC is defined as the process where plant cells or plant tissues are isolated from plant organs and cultivated under artificial environmental conditions, taking advantage of plants' regeneration ability by means of cuttings or explants. Thus, the resultant proliferated plant cells maintain the genetic information from the donor plant. In the literature [49], it has been elucidated how PCC works as a technological platform where chromosome doubling and artificial polyploidy induction are favored by getting the overexpression of key genes involved in the synthesis of PDSM and, hence, favoring the production of both high-value bioactive compounds and plants with more agronomical potency. Plant cell cultures include the production of callus and immobilized cells, embryos, roots, shoots, and cell suspensions, extending the advantages of manipulation with a better understanding about the intricate mechanisms of synthesis of PDSM [44].

3.1. Types of Cell Cultures

Calluses relate to the massive growth of cells and the buildup of agglomerated dedifferentiated cells, that may be able to revamp the complete plant, acquiring features like meristematic cells and developing new stem cells, which are able to form new individual plants [50]. Somatic embryos are obtained by the tissue formation from somatic cells or callus, having as the main objective the micropropagation of species seeds. Hairy roots culture is usually obtained by the infection of plant cells with *Agrobacterium rhizogenes*, resulting in the transformation of callus into differentiated tissues [48].

Even though there are several studies where the production of PDSM from callus cultures and differentiated cells/tissues are used, the cell suspension culture from dedifferentiated cells is mostly preferred [51,52]. Cell suspension cell culture (CSC) is considered as a simple and cost-effective method, allowing suitable conditions for cells to produce compounds identical to those from parental cells to be achieved, offering advantages such as setting stable systems for continuous PDSM production with homogeneity in yields and quality, as well as offering the possibility of synthesizing new compounds and greater potential for PDSM commercial application [51,53]. Therefore, CSC has been demonstrated to be the selected biotechnological tool for obtaining high-value PDSM, such as taxol [53,54], resveratrol [55,56], and ginsenosides [57], among others. To this end, further discussions will be centered on CSC for producing PDSM at laboratory and larger scales using different bioreactor configurations. Table 2 shows recent successful examples where plant cell culture is used for producing PDSM with pharmacological relevance.

Table 2. PDSM from medicinal plants successfully produced in the in vitro plant cell culture, bioactivities, and yield comparison.

Compound	Plant Species	Biological Activity/ Pharmaceutical Use	Extraction Yield		Type of Culture	Ref.
			Mother Plant	In Vitro Cell Culture		
Shikonin	*Lithospermum erythrorhizon* *Alkanna tinctoria* Tausch *Echium plantagineum* L.	Anticancer, antibacterial, anti-inflammatory, hepatic steatosis attenuator, antitumor, and antioxidants	10−20 mg/g	150−200 mg/g 36.25 mg/L	CSC HRC	[58–62] [63]
Anthraquinones	*Morinda citrifolia* *Rubia cordifolia* *Senna obtusifolia*	Antimicrobial, antifungal, hypotensive, analgesic, antimalarial, gastroprotective, antioxidant, hepatoprotective and antileukemic, and mutagenic functions	3 mg/g	100–200 mg/g	HRC CCC CSC	[64–67]
Rosmarinic acid	*Ocimum basilicum* *Origanum vulgare* *Satureja khuzistanica* *Coleus blumei* *Salvia officinalis*	Antioxidant, anti-inflammatory, antiviral activities	8.78–9.4 mg/g 23.53 mg/g 12 mg/g 30 mg/g 30 mg/g	12.32–21.28 mg/g 31.25 mg/g 38 mg/g 270 mg/g 360 mg/g	CSC CSC CSC CSC CSC	[68,69] [70,71] [72,73] [32]
Berberine	*Thalictrum minus* *Coptis japonica* *Coscinium fenestratum*	Effects antitumor, anticancer, lower blood lipid, lower blood glucose, anti-osteoporosis, anti-osteoarthritis, antibiotic, and anti-inflammatory	0.1 mg/g 20–40 mg/g 1 mg/g	0.8 mg/mL 132 mg/g 178 mg/g	CSC CSC CCC	[74–79]
Ginsenosides	*Panax ginseng* *Panax japonicus* *Panax notoginseng*	Antitumor, immunological, anti-inflammation, anticancer, antidiabetic, and cardiovascular-protective	0.015–8 mg/g	36.4–80 mg/g 3.4–28.9 mg/g 15.1–105.6 mg/g 20–50 mg/g 60 mg/g 71.94 mg/g 40 mg/g	HRC CSC ARC CSC CCC ARC CSC	[57,80,81]
Diosgenin	*Dioscorea deltoidea* *Dioscorea bulbifera* *Helicteres isora* L.	Anticancer, antidiabetic, anticoagulant, antithrombosis, anti-inflammatory, antiviral, anti-ageing	0.4−3 mg/g 1–5 mg/g	72 mg/g 3.5–16 mg/g 12 mg/g 8.64 mg/L 23 mg/g	CSC CCC CCC CSC CCC	[82] [83] [84]
Ajmalicine	*Catharanthus roseus*	Antihypertensive, obstructive circulatory diseases treatment	3 mg/g	63 mg/L 10 mg/g 34 mg/L	CCC CSC HRC	[85] [86,87]
Paclitaxel	*Taxus chinensis*	Anticancer	0.02 mg/g	1.5 mg/g	CSC	[88]
Podophyllotoxin	*Linum narbonense* *Juniperus chinensi* *Linum flavum*	Vigorous antimitotic and antiviral activities and anticancer	0.5 mg/g 0.025 mg/g 1.6 mg/g	1.57 mg/g 189.91 mg/g 2 mg/g	CCC CSC CSC	[89]
Artemisinin	*Artemisia annua* L.	Treat multi-drug-resistant strains of falciparum malaria	1–15 mg/g	9.33–110.2 mg/L	CSC	[90,91]
Phenolic Acids (rosmarinic, chlorogenic, and ferulic acid)	*Verbena officinalis*	Antimicrobial, secretolytic, expectorant, and diuretic agent	136.59 mg/g	126.55 mg/g 189.91 mg/g	CCC CSC	[92]
Resveratrol	*Vitis vinifera* L.	Reduced coronary heart disease mortality rates and atherosclerosis, inhibiting low-density lipoprotein oxidation, and carcinogenesis	NR	277.89 µg/g	CSC	[7]

CSC means cell suspension culture; HRC means hairy root culture; CCC means callus cell culture, ARC adventitious root culture; NR means not reported.

3.2. Plant Cell Suspension Culture

Plant cell suspension culture (CSC) represents a cost-effective and simple biological process for the synthesis of PDSM at large scales [51]. This production concept takes advantage of plant cells as biosynthetically totipotent structures, being capable of obtaining bioactive compounds with identical properties to those contained in plant stem cells, offering potential advantages regarding quality and yield of PDSM [51,93]. To this end, although there are engineering challenges, CSC offers greater potential for industrial applications in large-scale bioreactors than plant tissue and organ cultures. Although the latter ones offer better genetic stability in propagated cells, the design of the bioreactors for their maintenance usually requires greater investments and careful experimentation in the preliminary scale-up stage [42,94].

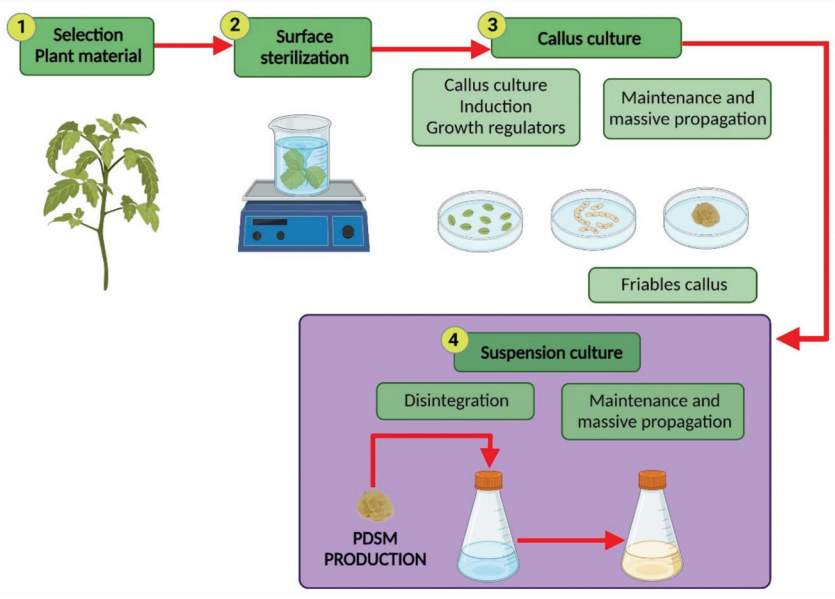

Figure 2. General steps for obtaining cell suspension culture. PDSM means plant-derived secondary metabolites. * Schemes were created with BioRender.com.

Success in the operation of suspension cultures depends on the induction and obtention of friable callus (stage 3) through the exposure to growth regulators, such as auxins and cytokinin. The final step (stage 4) comprises the transfer and maintenance of this cell culture in a liquid. CSC may become unstable when subjected to prolonged culture times, causing differences in the quality and quantity of PDSM; this behavior is due to the consumption and reduced availability of nutrients in the culture media, in addition to genetic variations that can restrict the conservation of the high-yield cell line [9]. Among the strategies used for improving the production of PDSM in CSC is the modification in the culture media composition (different carbon, nitrogen, and phosphorous sources) for optimizing the nutrient availability during the culture time [6,9], and the use of biotic or abiotic elicitors that trigger the defense response from plant cells promoting the secondary metabolism through the introduction of chemical or physical stresses [7,51,95]. Biotic elicitors are complex compounds derived from biological sources, including plant-derived polysaccharides, such as pectin and cellulose, and microbial-derived polysaccharides, such as chitin and glucan [6,44], and plant immune-signaling molecules, such as jasmonic acid [96], salicylic acid [97,98], and methyl jasmonate [96]. Abiotic elicitors include inorganic salts, heavy metals, UV irradiation, high salinity, and pressure [99].

3.3. Commercial Production of PDSM from CSC

The current production of various drugs, cosmetics, and food ingredients is obtained using plant cell cultures, especially in the form of CSC, as these offer several advantages over other technologies, such as better control during the production of PDSM, a larger feasibility for the scaling up of the process, and shorter production cycles, being environmentally responsible and sustainable processes. The application of CSC to obtain commercial products dates back to the 1960s [7,9,24,100]. Table 3 shows a selection of plant cell extracts that have been successfully manufactured at a commercial scale for pharmaceutical purposes. So, by way of history, the first report about industrial manufacturing of bioactive compounds derived from CSC was found for Shikonin from *L. erythrorhizon* by Mitsui Petrochemical Ind., now Mitsui Chemicals, Inc. (Tokyo, Japan). To date, Taxol®, manufactured by Phyton Biotech, Inc. (Delta, BC, Canada), and Genexol, the commercial name for paclitaxel compound by Samyang Genex, represent the cancer drugs with greater demand in the market, with annual sales reaching up to 200–300 kg per year [101]. In agreement with the information available at the website for manufacturers, the production volume for PDSM increases from a few cubic meters to 75 m^3 equivalent, to reach 880 m^3 per year [102].

Table 3. Plant-derived products manufactured from plant CSC which have entered into the pharmaceutical industry. The list of products makes no claim to be complete.

Product	Species	Pharmaceutical Use	Manufacturer, Tradename, and Scale of Production	Type of Culture	Reference
Rosmarinic acid	*Coleus blumei*	Anti-inflammatory	ANattermann & Cie. Gmbh, www.sanofi.de (accessed on 30 October 2021)	CSC	[103]
Echinacea polysaccharides	*Echinacea purpurea*	Immunostimulant, anti-inflammatory	Diversa, 75,000 L bioreactor	CSC	[100,104]
Berberines	*Thalictrum minun*	Anticancer; antibiotic; anti-inflammatory	Mitsui Chemicals, Inc., (75,000 Lbr)	CSC	[105]
	Coptis japonica		https://www.mitsuichemicals.com/ (accessed on 30 October 2021)	CSC	
Podophyllotoxin	*Podophyllum* spp.	Anticancer	Nippon Oil Company, Ltd. https://www.freepatentsonline.com/5336605.html (accessed on 30 October 2021)	CSC OC	[106] [107]
Docetaxel	*Taxus baccata*	Ovarian cancer treatment	Phyton Biotech, Inc., Taxotere (150 kg/year) https://phytonbiotech.com/ (accessed on 30 October 2021)	CSC	[108,109]
Paclitaxel	*Taxus* spp.	Anticancer: FDA approved for the treatment of ovarian, breast, and lung cancers	Phyton Biotech, Inc., Taxol ® (1000 kg/year) https://phytonbiotech.com/ (accessed on 30 October 2021)	CSC	[110]
			Samyang Genex Corporation., Genexol (32,000 Lbr) https://samyangbiopharm.com/eng/ProductIntroduce/injection01 (accessed on 30 October 2021)	CSC	[111] [112]
Scopolamine	*Duboisia* spp.	Anticholinergic; antimuscarinic; motion sickness, nausea, and intestinal cramping	Sumitomo Chemical Co., Ltd., Tokyo, Japan (50–20,000 Lbr) https://www.sumitomo-chem.co.jp/pharma-chem/ (accessed on 30 October 2021)	HRC	[113,114]
Shikonin	*Lithospermum erythrorhizon*	Anti-HIV, antitumor, anti-inflammatory	Xi'an NEO Biotech, Shikonin 95% http://www.extractneo.com/about (accessed on 30 October 2021)	CSC	[100]

CSC: cell suspension culture; HRC: hairy root culture; OC: organ culture.

3.4. Typical Bioreactor Configurations

Bioreactors are defined as containers used to provide a controlled environment to transfer nutrients and oxygen to cell cultures in adequate concentrations that allow the cell to maintain its primary and secondary metabolic activity. Because plant cells, as well as other micro-organisms, are more sensitive and less stable than chemical compounds, biore-

actor designs must be robust enough to provide a greater degree of control over process disturbances and contamination and achieve high productivities, high quality products, and cost effectiveness. The bioreactor design and its optimal operation depend on the determination of the operating conditions giving rise to the required product formation, minimizing the cost of the process [115]. The most common bioreactor configurations utilized for commercial and large-scale production consist in stirred tank bioreactor (STB), wave stirred bioreactor (WSB), air-lift bioreactor (ALB), and bubble column (BC). The selection of the bioreactor configuration is frequently established by its optimal performance in terms of metabolic activity and kinetics of cell cultures, economic costs, and its flexible operation regarding maintenance of cultures by controlling operational conditions, such as temperature, pH, aseptic, mixing, aeration, and scalability. Table 4 shows some characteristics, advantages, and disadvantages of these types of bioreactors.

Table 4. Comparison of bioreactor configurations commonly used for plant cell culture.

Bioreactor Configuration	Schematic Diagram *	Description	Advantages	Disadvantages	Ref.
Bubble column (BC)	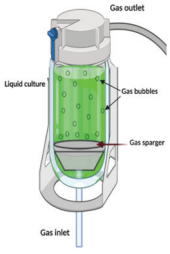	It is classified in the pneumatic-type bioreactor. They are constructed in cylindric columns where gas injection represents the only energy entrance to the system. BC bioreactors operate under constant bubbling where gas flows from the bottom to the top through nozzles, perforated plates, or spray rings, allowing not only the aeration process, but also helping the mixing and circulation of the fluid, without the need to install mechanical accessories.	Simple structure as no mechanical force is required to shake. Easier maintenance and reduces the risk of contamination due to the lack of mobile parts. Reduced effect of the shear stress.	High foam formation under high gas flow rates. Poor oxygen transfer capabilities. Poor fluid mixing in highly viscous fluids. High levels of foaming under high-aeration conditions	[24,94,116]
Airlift (ALB)	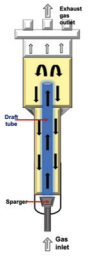	It is classified in the pneumatic-type bioreactor. This configuration is considered reasonably like STR, excepting for the impeller. They are tower reactors where fluid broth is mixed with a gas stream, which is compressed and injected at the bottom of the discharge pipe. The gas–fluid mix allows the creation ofdifferences in density and upward displacement. It is more suitable for hairy root and somatic embryo cultures.	Easy maintenance and reduces the risk of contamination due to the absence of mobile parts. Reduced effect of the shear stress. Higher oxygen transfer than that in BC. The energy required is provided by the compressed gas.	High levels of foam formation under high gas flow rates. Poor fluid mixing in highly viscous fluids. Relatively poor oxygen transfer capabilities.	[24,117–119]

Table 4. *Cont.*

Bioreactor Configuration	Schematic Diagram *	Description	Advantages	Disadvantages	Ref.
Stirred tank bioreactor (STB)	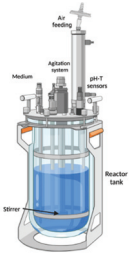	It is grouped in the mechanically agitated bioreactor. This bioreactor consists in a mixer (turbine or propeller) installed within the tank reactor and may be equipped with gassing inlet stream. It can operate in batch, semi-continuous, or continuous mode [117,120].	Efficient fluid mixing systems. High oxygen mass transfer capability. Convenient for high-viscous fluids. Comply with Good Manufacturing Practices. Easy scale-up. Highly adaptable to production scale and products. Impeller alternative.	High energy cost owing to mechanical agitation. Contamination risk with mechanical seal. Some cells and metabolites are susceptible to shearing generated by the impeller and bursting gas bubbles. Depending on the operation mode, this configuration can represent high costs of maintenance, cleaning, and startup.	[94,117,120,121]

* Schemes were created with BioRender.com.

Engineering Aspects in the Plant Cell Suspension Culture

Engineers designing or optimizing bioreactor technologies must both consider the effect of operating conditions on the complex interaction between transport phenomena, thermodynamics, growth kinetics, metabolic activity, and maintenance of plant cell cultures and, based on it, propose methodologies to transfer information observed in flask cultures to larger bioreactor scales. Some operational conditions are critical because they can cause a decrease in biomass, a low PDSM production, or a loss of cell viability. Table 5 shows some CSC that have been successfully scaled from flask cultures to large-scale bioreactors.

Table 5. Comparison of operating conditions used for SCC in flask and bioreactor to produce PDSM. The list of examples makes no claim to be complete.

Species	Compounds	Operation Variables Evaluated		Biomass Production		PDSM Production	Ref.
		In Shake Flask	In Bioreactor	In Shake Flask	In Bioreactor		
Scrophularia striata	Phenylethanoid glycosides	50 mL SCC in 100 mL flask 110 rpm 25 °C	5.0 L SCC in STR 10 L Fg: 0.5–1.0 L/min 110–170 rpm 25 ± 1 °C Darkness	14.16 g/L	15.64 g/L	The acteoside content in CSC in the bioreactor was about threefold higher than that in the shake flask	[122]
Buddleja cordata	Verbascoside, linarin and hydroxycinnamic acids	50 mL SCC in 250 mL flasks 110 rpm 26 ± 2 °C	STR 2 L Fg: 1 vvm (ring diffuser Rushton impeller 400 rpm 26 ± 2 °C 16/8 h light to dark photoperiod	11.8 g/L	13.62 g/L	The content of phenolics was twofold higher in STR.	[123,124]
Rubia tinctorum	Anthraquinone	25 mL SCC in 250 mL flasks 100 rpm 25 ± 2 °C 16/8 h photoperiod (140 µmol m^{-2} s^{-1})	1.0 L SCC in STR 2 L Fg: 1 vvm Turbine impeller 450 rpm 25 ± 2 °C 16/8 h photoperiod (140 µmol m^{-2} s^{-1})	330 g/L	220 g/L	Anthroquinone production was 2.5 times higher in STR	[125]

Table 5. *Cont.*

Species	Compounds	Operation Variables Evaluated		Biomass Production		PDSM Production	Ref.
		In Shake Flask	In Bioreactor	In Shake Flask	In Bioreactor		
Arnebia sp.	Shikonin	25 mL CSC in 250 mL flasks 100 rpm 25 ± 2 °C Continuous light (70 μmol/m^2 s ^{1})	Air-lift bioreactor 2 L working volume 25 ± 2 °C Fg: 2 L/min (sparger ring)	1249.2 g/L	480 g/L	The shikonin content was 2.6 times higher in the bioreactor than in the flask. Production remained without significant differences in both bioreactors	[126]
			STR 2 L Six-blade turbine impeller 100 rpm Fg: 2 L/min 25 ± 2 °C	1249.2 g/L	450 g/L		
Ocinum basilicum	Rosmarinic acid	100 rpm 25 ± 2 °C	7 L CSC in STR 10 L Marine impeller 100 rpm Fg: 25 L/min	Biomass was 8.4 times higher in bioreactor than in flask		Production increased 1.66 times in bioreactor	[69]
Satureja khuzistanica	Rosmarinic acid	200 mL CSC in 1 L flask 110 rpm 25 °C	1 L CSC in culture bags 2 L Batch mode 20–30 rpm 25 °C Fg: 0.1 vvm Darkness	13.6 g/L	18.7 g/L	Production increased 2.5 times in bioreactor	[127]
Vitis labrusca L.	Resveratrol	100 mL CSC in 300 mL flasks 110 rpm 23 °C Darkness	STR 5 L Marine impeller 110 rpm Fg: 0.15 vvm	NR	≈35 g DW	Production increased 1.15 times in bioreactor	[128]
Santalum album L.	Squalene	100 mL CSC in 250 L flask 90 rpm 28 °C	Airlift bioreactor 7 L Batch mode 70–80 rpm Fg: 4 L/min 28 ± 2 ° C	1.05 mg/g	1.25 mg/g	Production increased 1.71 times in bioreactor in four weeks of culture	[129]

NR means Not reported.

The scaling up of CSC carried out in a flask culture demands the use of bioreactor engineering to characterize the impact of operating conditions on growth kinetics, cell deactivation, and transport phenomena and, hence, on the metabolic activity and production rates of PDSM. To this end, in what follows, main aspects to be considered during the scaling up of CSC, from the screening of plant cells to the industrial-scale bioreactor design, are mentioned and analyzed.

The screening of a set of plant cells is considered as the first stage during the scaling up of CSC [42,94]. Screening takes place in shake flasks. In these laboratory bioreactors, hydrodynamic and transport phenomena negatively impact on the growth kinetics, cell viability, metabolic activity, and production rates of PDSM. For instance, in these bioreactors, the production of PDSM involves two-phase systems (liquid culture phase and cell culture phase) neglecting the effect of operating conditions, including the impact of the oxygen concentration, on the microscopic and macroscopic performance of the shake flask. In this context, apparent results regarding cell growth kinetics, cell viability rates, and production rates of PDSM are observed. In these conditions, promising plant cells are identified and selected to be evaluated in larger bioreactor configurations, such as those presented in Table 4.

The second step accounts for characterization of cell growth kinetics, cell viability rates, metabolic activity, and production rates of PDSM under controlled operating conditions in

bench-scale bioreactors with similar configurations to those systems to be implemented at the commercial scale, i.e., bench-scale bioreactors accounting for three phases (liquid–gas–cells) (see Table 4). Thus, during the analysis of bench-scale systems, the coupling of experimentation with mathematical modeling is essential for stating the basis for the scaling up of CSC [130–132]. Herein, cell growth kinetics and production rates of PDSM are the main response variables to maximize during CSC. It is worth mentioning that their experimental and theoretical characterization makes possible the connection between the microscopic world of the metabolic cell activity and the macroscopic world of the bioreactor performance and, hence, the downstream processing. Besides, the experimental characterization of these cell mechanisms and their analysis using mathematical models lead to the construction of the engineering tool for the scaling up and optimization of the bioreactor configuration, allowing a better understanding of CSC during the production of PDSM. In particular, the use of bench-scale bioreactors allows for identifying and controlling those operating conditions where transport phenomena favor the kinetics of the CSC.

Based on the kinetics, since in CSC it is not possible to develop intrinsic kinetic models, there are two types of models that can be developed in bench-scale bioreactors: extrinsic ones, where transport phenomena are explicitly included during the modeling of the bioreactor; and apparent ones, where transport phenomena resistances impact during the experimentation but they are not considered during the modeling of the bench-scale bioreactors [131,133–137]. Thus, to determine extrinsic kinetic models, it is recommended to carry out a regime analysis to identify and model those transport phenomena limiting the production of PDSM. Experiments make possible the development of the corresponding model, relating kinetics with macroscopic variables, namely the concentration of substrates and PDSM, cell growth, and cell viability involved during the operation of the bench-scale bioreactor. The kinetic model depends on the quality of the experimental data and it is only reliable for the range of operational conditions utilized during its development. When the kinetic model is based on metabolic steps of the reaction, the mathematical complexity increases but leads to a better physical representation of the CSC during the production of PDSM. Besides, the loss of cell viability caused by operational aspects, i.e., a toxic compound, cell shear stress, or cell sintering, is modeled by empirical expressions whose parameters involve physical meaning [138], such as the generalized power law equation (GPLE) [139–141]. Finally, the Monod model offers an adequate explanation for the reaction rates of growing cells, but it has no mechanistic basis [142,143]. Moreover, the Monod model is only applicable when cells are in a metabolic equilibrium, namely when the composition of the macromolecules in the cell remains in a pseudo-steady state during the CSC. Table 6 presents some kinetic models to describe cell growth rate. It is worth mentioning that, in transient experiments, when the concentration of a substrate or PDSM is brusquely modified, Monod kinetics are not suitable and the kinetic model must account for the cell metabolism [138,144]. There are, in the literature, several models that have no mechanistic grounds but account for some biological features of the cell growth [138,145]. These models offer an acceptable description of the cell growth and metabolic activity due to fluctuation in the concentration of substrates and products. In these models, cell mass is divided into compartments, and the rate of formation of each compartment has different stoichiometry and kinetics.

Table 6. Models used to describe kinetics and deactivation in whole cells [137,140–142].

Mathematical Equation	Conventional Name
$r_x = \mu = \frac{\mu_{max}[S_i]}{[S_i]+K_m}$ $r_s = Y_{xs}\mu$	Monod kinetics
$r_x = \mu = \frac{\mu_{max}[S_i]}{([S_i]^2/K_i)+[S_i]+K_m}$ $r_s = Y_{xs}\mu$	Expanded Monod kinetics
$r_x = \mu = \frac{\mu_{max}[S_i]}{[S_i]+K_m}\left(1-\frac{[P]}{[P]_{max}}\right)$ $r_s = Y_{xs}\mu$	Expanded Monod kinetics
$r_x = \mu = \mu_{max}(1-\exp(-[S_i]/K_m))$ $r_s = Y_{xs}\mu$	Monod's teacher Tessier kinetics.
$r_x = \mu = \frac{\mu_{max}[S_i]}{[S_i]+K_sX}$ $r_s = Y_{xs}\mu$	Contois kinetics.
$r_x = \mu = \mu_{max}\left(1-\frac{X}{K_s}\right)$ $r_s = Y_{xs}\mu$	Logistic kinetics.
$\frac{d\theta_x}{dt} = -k_{in}(\theta_x-\theta_{ss})^m$ $r = r_s = \theta_x\frac{k[S_i]}{[S_i]+K_m}$	Cell deactivation kinetics

In bench-scale bioreactors, it is experimentally complicated to minimize transport resistances [139–141,146]. In the fluid bulk, concentration, temperature, or radiative gradients can be present. Hydrodynamics impact on mass and heat transfer mechanisms from the gas phase to the liquid phase and from the liquid phase to the cell phase. Moreover, cell growth can impact on mass and heat transfer mechanisms. Although complicated, a proper kinetic analysis must account for the effect of fluid dynamics on transport phenomena and, hence, on cell growth, cell viability, and metabolic activity.

During the screening at the laboratory bioreactors or during the operation of the bench-scale bioreactor, the response surface methodology (RSM) is a potential tool to guide experimental designs. RSM leads to the following advantages [147–151]:

(1) It defines an establishment of the relationship between responses (yield, cell viability, oxygen concentration, etc.) and control operating conditions (temperature, pressure, initial concentration, power input, agitation rate, etc.).
(2) It predicts the effect of control operating condition on responses.
(3) It gives inferences on the significance of the operating conditions on the performance of the reactor.
(4) It allows the determination of the operating window where the bioreactor meets its best performance.

On the above end, RSM couples experimental designs, and mathematical and statistical methods [152,153]. Firstly, an experimental design is proposed; the evaluation of this experimental design constitutes the so-called response surface design (RSD). The suitability of the RSD depends on its orthogonally, ratability, and uniform precision [153]. Secondly, the empirical model is then developed; it is approximated by a polynomial equation that accounts for elements that consist of powers and cross-product powers, constant coefficients referred to as parameters, and a random experimental error. Albeit empirical, first-degree and second-degree polynomial equations are usually used to fit observations and carry out the optimization. To this end, every model and its reliability depends on the RSD, i.e., first-order designs are used to fit observations with the first-degree models, and observations out of second-order designs are fitted with second-degree models [152–154]. The most common first-order designs are 2k factorial, Plackett–Burman, and simplex designs, while the most common second-order designs are 3k factorial, central composite, and the Box–Behnken designs. Note that the choice of a proper RSD is essential since the quality of prediction, as measured by the size of the prediction variance, depends on it; thus, the

lower the variance, the better the fit of the responses. On this basis, a single RSD is not able to satisfy all criteria, but it is considered as robust if it meets the assumptions related to the model and the error distribution [152,153]. Finally, the assessing of the results uses both statistical tests, i.e., F-value, t-value, and confidence interval, and graphical tests, i.e., variance dispersion graphs, fraction of design space plots, and quantile plots. Graphical methods [149,150] based on quantile dispersions have also been used to compare experimental designs for estimating variance components in an analysis of variance (ANOVA) situation. RSM can lead to the identification of the operational window where CSC presents its higher yields to PDSM, which, in turn, will be essential in the conceptual design and scaling up of the bioreactor configuration.

Because of the advent of computation in the last years, the bioreactor design not only depends on empirical, but also deterministic approaches, which allows the proper determination of hydraulics, fluid dynamics, mass transport, heat transfer, radiative transfer, and kinetics from different bioreactor configurations at various scales. This information is transferred to design and scale up the industrial bioreactor. The design of this reactor strongly depends on the development of a model coupling kinetics and transport phenomena at both the cell and bioreactor level, including the fluid and the gas phase. This is, however, a complex task, since it needs experiments and mathematical solutions that are not trivial. It is worth stressing that, during the construction of this model, fluid dynamics are yet the bottleneck during the scaling up of a bioreactor configuration because of their impact on transport phenomena, kinetics, and, hence, on the global production of PDSM.

Based on the above, a model accounting for kinetic, deactivation, and all transport mechanisms should be developed from the laboratory to the bench scale. This model should be constructed following a framework based on computational fluid dynamics (CFD). The model needs to be validated at the bench scale before using it to design the industrial bioreactor. The preliminary dimensions of the reactor need to be obtained from the utilization of the practical know-how reported in the literature or experimental and modeling results obtained at the bench scale. It will make the scaling up process more efficient and reliable. Developing a model for the use of CFD allows the consideration of fluid dynamics along with its effect on transport phenomena, which leads to obtaining operating conditions where mixing, hydrodynamics, and transport phenomena are improved without affecting the operating cost of the process. A criterion when designing the industrial-scale bioreactor is to achieve a compromise between operating expenses and yield of the PDSM. At the end of the scaling-up process, the experimentation and investment cost as that compared using an empirical or heuristic approach will be significantly minimized.

In addition to the aforementioned, the scaling up of CSC becomes more challenging when observing how operating conditions impact on the production of PDSM. Operating conditions influence in different scenarios and magnitudes the performance of cell cultures during the production of PDSM, from the supply of nutrients (oxygen, light, ionic strength, pH) to the implementation of mechanical and pneumatic work to keep the process operating in optimal conditions. In further sections, a discussion about the main operating variables in bioreactors and their effect on the performance of cell culture will be provided.

3.5. Effect of Operating Variables on the Bioreactor Performance

3.5.1. Temperature

It is a key variable that must be kept under control because its increment impacts on kinetics, inducing the premature senescence of the culture, and produces the loss of viability, such that it reduces the yield of PDSM. On the other hand, temperature may also act as an abiotic elicitor. Temperature in bioreactors has varied between 23 and 30 °C [155,156], although most of the works have fixed it at 25 °C [122,123]. Most temperature control systems consist of the use of temperature probes and jackets or coils used as a heat transfer system to activate metabolic reactions or cool the bioreactor because of the heat generated by exothermic metabolic reactions. Heating or cooling systems also used in bioreactors are electric heaters or steam streams for the former, and cooling water or refrigerants in

cooling towers for the latter [115]. Species such as *Catharanthus roseus* and *Lavanda vera* exhibited the best kinetic cell performance at 30 °C, leading to a constant production rate of PDSM when CSC was carried out in stirred tank bioreactors [157,158].

3.5.2. Light

Cell irradiation by use of visible light is one of the most important elements when designing CSC bioreactors, since photons affect the growth and morphogenesis of cell cultures both in in vivo and in vitro conditions. Plant cell cultures vary their physiological response to the light exposure because of photolytic reactions, significantly influencing the synthesis and production of secondary metabolites, such that yields are a function of the type of species, growth stage, type of light, and time of exposure to light. In plant cell cultures, the use of 12/16 h light/dark photoperiod is the most frequent condition, although total darkness and continuous light exposure have also been reported [52,159,160]. Some examples recently reported in the literature about the effect of light exposure in CSC are for *Vitis vinifera* [159], *Theobroma cacao* [161], *Clinacanthus nutans* (Burm. f.) Lindau [162], *Catharanthus roseus* (L.) G Don. [163], and *Artemisia absinthium* [164], where higher production of PDSM were obtained under light exposure. On the other hand, species such as *Plumbago europaea* L. [160] showed 1.7 times the production of plumbagina, the main bioactive compound, when CSC were cultured in darkness; besides, *Ajuga bracteosa* exhibited a higher concentration of PDSM and antioxidant activity when its CSC was subjected to darkness and methyl jasmonate as elicitor [165], and *Ruta graveolens* with a 3.14-fold increase in total flavonoid content [166].

3.5.3. pH

pH is one of the factors influencing the growth and production rates of PDSM; therefore, it is a critical operating condition in small- and large-scale plant cell culture. It provides the proper balance of acidity/alkalinity to the culture to avoid cell breakage. The initial pH in plant cell cultures usually ranges between 5.5 and 6.0; abrupt changes during the culture can cause variations or loss of the nutrient uptake. One of the most relevant challenges during the operation of the bioreactor is the successful implementation of an efficient pH control system. The bioreactor behavior depends on the change in pH, modifying the cell growth and the production of PDSM and being widely dependent of the species related to the plant [13,156,167,168].

3.5.4. Mixing

In cell cultures, the production of biomass and PDSM is highly dependent on the conversion of substrates into products, this conversion and reaction rates are mediated and controlled by transport mechanisms toward and from the place where the conversion occurs. In every bioreactor, fluid dynamics impact how substrate and inoculum are transported to the liquid bulk and how PDSM are removed. In batch operations, fluid dynamics occasioned by mixing prevents local exhaustion of substrates such as oxygen [169]. Mixing and fluid dynamics are a function of the bioreactor configuration and impact the performance of CSC, such that, when properly controlled, they minimize interfacial mass and heat transport resistances, decreasing temperature and concentration gradients in the bioreactor bulk and, hence, having homogeneous distribution of the components or conditions in the culture medium [170].

The characteristic time related to mixing in bioreactors influences heat production, oxygen mass transfer, and C-substrate consumption in the cultures [24,169]. For instance, the characteristic time related to heat production (mainly due to metabolic heat) is defined as the time necessary to heat up the content in the vessel by 1 °C, while the mixing characteristic time is usually considered as the one for smoothing out temperature gradients occasioned by the metabolic reactions. In most bioreactor configurations, mixing times range from 10 to 100 s, such that heat will not be accumulated.

The characteristic time for mass transport is defined as the characteristic time required for the decrease in oxygen concentration once the gas flow rate is discontinued, this time is not related to a critical time for the micro-organism. Depending on the bioreactor configuration, the capacity of oxygen transfer rate (OTR) will vary [170]. Despite STR exhibiting better OTR, it has some restrictions related to the dispersion of gas through the vessel, because the higher transfer occurred near the sparger, reducing the concentration of dissolved oxygen in the aqueous medium. In this sense, the respective characteristic time for oxygen depletion in STR is considered as the critical time when it is assumed that all the oxygen is transferred close to the impeller. On the other hand, bubble column bioreactors are not excluded for exhibiting oxygen depletion; in this configuration, the oxygen is transferred at all the positions in the column, and even though the oxygen transfer is mainly observed near the sparger, it is greater than that for STR. Thus, the characteristic time for depletion is based on the concentration of oxygen dissolved outside the region of the sparger [170–172].

The last characteristic time associated to the mixing process in bioreactors is related to the relationship between cell growth rate and bulk substrate concentration. Since the Monod model describes adequately this phenomenon, this equation is used to determine the characteristic time for substrate consumption. This characteristic time will be larger than the one for mixing time and fluid dynamics calculated for the bioreactor. Thus, cell growth rate and consumption substrate rate strongly depend on the transport phenomena resistances and, hence, characteristic times involved in every bioreactor configuration.

Considerations of Cell Culture Properties on the Mixing Process

Plant CSC is effectively set up in small-scale bioreactors, exhibiting excellent production of secondary metabolites, but, when it comes to working with larger scales, the situation is not that simple. Cell cultures tend to form flocs and agglomerates when the daughter cells are not completely separated from the stem ones after cell division; these agglomerate systems are constituted from several hundreds of cells, ranging in particle sizes around 0.5 cm diameter, depending on the cell line, culture conditions, and growth stage [16,111,173]. These agglomerated structures lead to the formation of heterogeneous populations creating microenvironments (larger intra-agglomerate transport resistances) that limit the substrate and oxygen transfer rates, causing low rates of growth and PDSM production. Some studies have demonstrated that the production of specialized high value-added PDSM depends on the formation of aggregates and their size [174–177]. For example, growth characteristics and qualitative composition of PDSM in *Phlojodicarpus sibiricus* cell cultures were directly correlated with the level of cell aggregation, being more favorable in aggregates of 10–30 cells than in aggregates of >50 cells [174]. Small aggregates (~400 μm) within *Taxus* suspension cultures produced four times more paclitaxel than larger aggregates (~1100 μm) [178].

However, despite intra-aggregate diffusion limitations, it has been reported that the formation of large aggregates may favor the production of PDSM, as is the case with cell suspension cultures of *Psoralea corylifolia*, where an aggregate size of 1200–2000 μm favored the production of phytoestrogens compared to sizes of 800–1200 μm [179]. Moreover, the formation of cell aggregates can also be favored by the secretion of extracellular polysaccharides (ECP), contributing to greater cell adhesion. Therefore, aggregation patterns coupled with high biomass concentrations and ECP secretions result in culture mediums with non-Newtonian characteristics [180].

One of the most logical and simplest ways to overcome these concerns could be related to the increase in the stirring speed, because it will break the flocs and cell agglomerates, facilitating the substrate and oxygen uptake and, therefore, increasing the growth rate and conversion to desired products [174,181]. Nevertheless, plant cells, as with other micro-organisms, are sensitive to shearing, and surpassing their resistance umbral to hydrodynamic stress may induce their cell wall breakage, causing the loss of valuable products [124,180,182]. Besides, plant cell cultures are characterized by being viscous and

highly dense suspensions that behave as non-Newtonian fluids, which also contributes to restricting the flow regime and the heat and mass transfer mechanisms, leading to zones with gradients of concentration and temperature, and, therefore, to dead zones of mixing in the bioreactor [42,173]. For this reason, in CSC the mixing is often evaluated in terms of its impact on the biological performance (growth rate and productivity) of the bioreactor technology.

A clear example that the aggregate size is an important parameter for the production of high added-value PDSM is the production of Paclitaxel by *Taxus chinensis* cultures. The authors of [176,181] showed that mechanical shear helps disintegration, favoring production by having small aggregates (194 μm) compared to the control, in which large aggregates (600 μm) were obtained that directly affected production.

3.5.5. Aeration

Aeration, as well as mixing, is one of the most important operating variables, both acting synergistically in bioreactors by maintaining aerobic conditions [183], helping to desorb volatile products, eliminating the metabolic heat, contributing to the synthesis of PDSM, and having a beneficial effect on power consumption [10]. In most of bioreactor configurations, gas stream is split by highly porous spargers in the form of bulb diffusers, sintered filters, or perforated plates, where gas bubbles are generated on the bottom of the vessel and rise through the culture medium, producing pneumatic mixing. The mass transfer will depend on the type of sparger and gas flow rate. Despite physiological differences between microbial and plant cell cultures, the use of excessive aeration conditions might cause foam generation due to the presence of extracellular proteins [184].

CSC in plants generally exhibits a doubling time of about 2–5 days, longer than that required by bacteria cells (0.5–1 h) [42,185]. For this reason, slower growth rates in plant cells lead to low oxygen demand, with a direct relationship to the cell concentration. High cell densities in the bioreactors may not be as desirable because it can cause limitations and inadequate concentrations of dissolved oxygen. The oxygen uptake rate (OUR) in CSC is commonly used for monitoring the physiology and oxygen demand by plant cells; this parameter is dependent on the cell culture line, culture conditions, and the growth rate [170]. Typical OUR values for plant CSC range from 5 to 10 mmol O_2/L h), a lower requirement when compared to that for microbial cells (10–90 mmol O_2/L h). Another important parameter considered for the establishment of aeration conditions is the oxygen transfer rate (OTR); it must be high enough to provide the required oxygen concentration to meet the respiratory demands of the cells (OUR), favoring the growth and production of the desired compounds, but not too high that it can hinder them. To overcome these difficulties, the concentration of dissolved oxygen must be kept above the critical level of cell oxygen consumption, which has been reported to be 15–20% oxygen saturation content in pure water (1.3 to 1.6 g/m^3) [11,77]. Dissolved oxygen concentration is not a variable that can be used for scaling criteria, and instead the volumetric mass transfer coefficient (kLa) and the air flow rate are used (vvm). kLa is a function of both agitation and aeration and is affected by various factors, such as geometric and operational characteristics of the reactor (stirring speed, aeration rate, fluid hydrodynamics, media composition, cell type, morphology, and concentration), which must, therefore, be analyzed when designing the bioreactor [186]. In agreement to the literature [24], to achieve an OUR around 5 to 10 mmol O_2/L h) in plant CSC, a typical kLa value between 10 and 50 h^{-1} is required. In Table 7, some of the operating conditions used in bioreactors and their effect on the CSC are described.

Other variables related to the aeration process in bioreactors are the superficial velocity of the gas, which permits the calculation and inference of the air bubbles' behavior in the bioreactor, and the observation of their coalescence in the medium. The superficial velocity is controlled by the aeration rate [119,187] showed that plant cell cultures, when subjected to hydrodynamic stresses, can change their color and increase the PDSM production as a defense mode. Nevertheless, as mentioned above, aeration also has an effect on the mixing

and mass transfer, so low aeration conditions will lead to poorly homogeneous conditions and limitations on cell growth due to the presence of sedimentation, or the development of microenvironments due to concentrations gradients. On the other hand, the increase in aeration could overcome these disadvantages, but also, the increase in shearing occurrs, making it necessary to establish the fragility of the cells to define the intensities of aeration that maintain an adequate level of homogeneity, without affecting the cell growth nor the production of PDSM.

Table 7. Conditions used in bioreactors and their effect on the SCC.

Species	Compounds	Bioreactor	Operating Conditions	Operation Variables	Effect of the Operating Variable	Ref.
B. cordata	Phenolics (phenylethanoid glycoside and flavonoid contents)	STR of 2 L (ring diffuser) and 3 L (sintered diffuser), Rushton impeller	26 ± 2 °C, photoperiod of 16 h light (50 µmol/m^2 s)/8 h darkness Fg: 0.1 vvm	Stirring speeds (120 and 400 rpm)	In both bioreactors, a higher shear stress was observed at rates of 400 rpm, affecting the growth phases and parameters, resulting in the decrease in PDSM.	[124]
R. cordifolia	Anthraquinones	STR of 8 L	25 ± 0.1 °C, gamma-irradiated cell cultures, the agitation speed of the impeller was 60 rpm, working volume 5 L	Impeller type (helical ribbon, Rushton turbine)	Helical ribbon provided a homogeneous mix and lower shear stress compared to Rushton turbine.	[66]
R. tinctorum	Antraquinones	Baffled flask	25 ± 2 °C, the cultures were grown in presence or in absence of light with a 16 h photoperiod using cool white fluorescent tubes at a light intensity of approximately 90 mol/m^2 s	Stirring speeds (100, 360 rpm)	The speed at 360 rpm had a negative effect on cell growth; however, it favored the production of PDSM	[188]
R. tinctorum	Antraquinones	STR of 1.5 L, turbine impeller	25 ± 2 °C, working volume of 1.0 L Fg: 1 vvm	Shear stress (450 rpm)	The speed of agitation affected cell viability; however, it favored the production of PDSM.	[125]
Arnebia sp.	Shikonin	Air-lif of 2 L	25 ± 2 °C, the dissolved oxygen (2 L/min)	Bioreactor-type	No significant differences were obtained in the growth and production of PDSM in both bioreactors.	[126]
		STR of 2 L, six-blade turbine impellers	25 ± 2 °C, 100 rpm, dissolved oxygen (2 L/min)			
V. officinalis	Phenylpropanoid glycosides (Verbascoside) (Isoverbascoside)	STR	23 ± 1 °C, photoperiod, 33 rpm and continuous Fg: 0.5 vvm	Bioreactor-type	The production of PDSM was significantly higher in the STR bioreactor	[92]
	Phenolic acids (Ferulic and Rosmarinic acid)	Balloon bioreactor (BB)				
T. minus	Berberine	STR of 2 L, Rushton turbine	25 °C in the dark, working volume (1.75 L) Fg: 0.1 vvm	Stirrer speeds of 100–900 rpm	The 250-rpm speed favored cell growth and PDSM production	[77]
			25 °C in the dark, working volume (1.75 L) and 250 rpm Fg: 0.1 vvm,	Dissolved oxygen fluctuations (25, 35 and 50%)	Fluctuations in dissolved oxygen tension affected berberine accumulation in the *T. minus* cultures depending on the average oxygen level achieved. Reductions in berberine production were observed not only as the average dissolved oxygen tension declined below 35% air saturation	

Table 7. *Cont.*

Species	Compounds	Bioreactor	Operating Conditions	Operation Variables	Effect of the Operating Variable	Ref.
D. deltoidea	Steroid glycosides	BC of 20 and 630 L	26 ± 0.5 °C in darkness, working volume of 15 L and 550 L, semi-continuous regime. Fg: 0.1 to 1.0 vvm depending on the growth phase of cell culture, OD was maintained at 10–40% of saturation volume	Bioreactor volume	No significant effect of bioreactor volume was obtained on cell growth and PDSM production.	[182]

PDSM: plant-derived secondary metabolites; STR: stirred tank reactor; Fg: aeration flow rate; vvm: gas volumetric flow rate per unit volume of culture medium.

4. Conclusions

To conclude, plants are a rich source of bioactive compounds of pharmacological interest, known as PDSM; due to their low production in nature, obtaining them leads to overexploitation and extinction of the species of interest. As an alternative ecological solution, plant cell culture, particularly CSC, stands out as one of the most efficient and promising technologies for producing PDSM in bioreactors. The selection and design of the bioreactor for the production of PDSM out of CSC is a complex task, which depends on two factors: on the one hand, the properties of the cells that vary according to the species under study (shear stress, aggregate formation, and rheology) and, on the other hand, transport phenomena related to the bioreactor configuration. The operating conditions in the bioreactor impact cell performance, such that the mixing and aeration are factors influencing fluid dynamics and, hence, mass transfer and heat transfer at both inter- and intracell levels. Thus, the optimization of bioreactors by elucidating the effect of the operating condition on the cell properties is essential for obtaining larger yields of PDSM. Despite the arduous research in this field, few PDSMs are commercialized at an industrial level. To this end, more studies focused on correlating the operating variables with kinetics and transport phenomena are needed to understand the behavior of plant cells, providing more bases for optimal growth and maximum production of PDSM in bioreactors.

This review provided updated information that helps the reader to understand the behavior of plant cells growing in suspension, identifying the key parameters to relate PDSM productivity with the optimization of operating variables in bioreactors, which will help future research in the scaling of PDSM with high added value, resulting in the development of new successful biotechnological processes.

Author Contributions: Conceptualization, E.A.M.-A., A.R.-G. and F.C.-S.; investigation, E.A.M.-A.; resources, F.C.-S., M.R.-M.; writing—original draft preparation, E.A.M.-A.; writing—review and editing, A.R.-G., C.O.C.-A. and F.C.-S.; project administration, F.C.-S. All authors have read and agreed to the published version of the manuscript.

Funding: This research was partially funded by the Consejo Nacional de Ciencia y Tecnología (CONACyT), scholarship grant of E.A.M.-A. (616138).

Acknowledgments: The authors give thanks to the Consejo Nacional de Ciencia y Tecnología (CONACyT) for the scholarship grant of E.A.M.-A. (616138).

Conflicts of Interest: The authors declare no conflict of interest.

Abbreviations

k_{in}	deactivation constant.
K_m	affinity constant.
K_s	substrate inhibition constant.
m	deactivation order.
n	reaction order value affecting the concentration of substrate and affinity constant.
r and r_s	the specific consumption rate of substrate i.
r_x	the specific rate of biomass formation.
r_{max}	the maximum specific consumption rate of substrate i.
$[S_i]$	the concentration of substrate i.
X	the concentration of biomass.
$Y_{x/s}$	biomass yield from substrate.
μ	the specific rate of biomass formation.
μ_{max}	the maximum specific rate of biomass formation
θ_X	dimensionless cell deactivation.
θ_{ss}	residual dimensionless activity.

References

1. Zafar, T.; Shrivastava, V.K.; Shaik, B. *Pharmaceutical Biotechnology in Herbal Neuroprotection*; Springer: Singapore, 2018; pp. 221–228.
2. Süntar, I. Traditional Medicine for Wound Management. *Evid.-Based Complement. Altern. Med.* **2017**, *2017*, 4214382.
3. Elkordy, A.A.; Haj-Ahmad, R.R.; Awaad, A.S.; Zaki, R.M. An overview on natural product drug formulations from conventional medicines to nanomedicines: Past, present and future. *J. Drug Deliv. Sci. Technol.* **2021**, *63*, 102459. [CrossRef]
4. Georgiev, M.I.; Eibl, R.; Zhong, J.-J. Hosting the plant cells in vitro: Recent trends in bioreactors. *Appl. Microbiol. Biotechnol.* **2013**, *97*, 3787–3800. [CrossRef]
5. Steingroewer, J.; Bley, T.; Georgiev, V.; Ivanov, I.; Lenk, F.; Marchev, A.; Pavlov, A. Bioprocessing of differentiated plant in vitro systems. *Eng. Life Sci.* **2013**, *13*, 26–38. [CrossRef]
6. Bhaskar, R.; Xavier, L.S.E.; Udayakumaran, G.; Kumar, D.S.; Venkatesh, R.; Nagella, P. Biotic elicitors: A boon for the in-vitro production of plant secondary metabolites. *Plant Cell Tissue Organ Cult.* **2021**, *147*, 1–18. [CrossRef]
7. Süntar, I.; Çetinkaya, S.; Haydaroğlu, Ü.S.; Habtemariam, S. Bioproduction process of natural products and biopharmaceuticals: Biotechnological aspects. *Biotechnol. Adv.* **2021**, *50*, 107768. [CrossRef]
8. Newman, D.J.; Cragg, G.M. Natural products as sources of new drugs over the nearly four decades from 01/1981 to 09/2019. *J. Nat. Prod.* **2020**, *83*, 770–803. [CrossRef]
9. Ochoa-Villarreal, M.; Howat, S.; Hong, S.; Jang, M.O.; Jin, Y.-W.; Lee, E.-K.; Loake, G.J. Plant cell culture strategies for the production of natural products. *BMB Rep.* **2016**, *49*, 149–158. [CrossRef]
10. Süntar, I. Importance of Ethnopharmacological Studies in Drug Discovery: Role of Medicinal Plants. *Phytochem. Rev.* **2019**, *5*, 1199–1209. [CrossRef]
11. Georgiev, M.I.; Weber, J.; Maciuk, A. Bioprocessing of plant cell cultures for mass production of targeted compounds. *Appl. Microbiol. Biotechnol.* **2009**, *83*, 809–823. [CrossRef]
12. Doran, P.M. Bioreactors, stirred tank for culture of plant cells. *Encycl. Ind. Biotechnol.* **2010**, *1*, 1–35. [CrossRef]
13. Ruffoni, B.; Pistelli, L.; Bertoli, A.; Pistelli, L. Plant Cell Cultures: Bioreactors for Industrial Production. *Adv. Exp. Med. Biol.* **2010**, *698*, 203–221. [CrossRef] [PubMed]
14. Namdeo, A.G.; Ingawale, D.K. Ashwagandha: Advances in plant biotechnological approaches for propagation and production of bioactive compounds. *J. Ethnopharmacol.* **2021**, *271*, 113709. [CrossRef]
15. Kolewe, M.E.; Gaurav, V.; Roberts, S.C. Pharmaceutically active natural product synthesis and supply via plant cell culture technology. *Mol. Pharm.* **2008**, *5*, 243–256. [CrossRef]
16. Georgiev, M.I.; Weber, J. Bioreactors for plant cells: Hardware configuration and internal environment optimization as tools for wider commercialization. *Biotechnol. Lett.* **2014**, *36*, 1359–1367. [CrossRef]
17. Taroncher, M.; Vila-Donat, P.; Tolosa, J.; Ruiz, M.J.; Rodríguez-Carrasco, Y. Biological activity and toxicity of plant nutraceuticals: An overview. *Curr. Opin. Food Sci.* **2021**, *42*, 113–118. [CrossRef]
18. Jamwal, K.; Bhattacharya, S.; Puri, S. Plant growth regulator mediated consequences of secondary metabolites in medicinal plants. *J. Appl. Res. Med. Aromat. Plants* **2018**, *9*, 26–38. [CrossRef]
19. Wang, S.; Alseekh, S.; Fernie, A.R.; Luo, J. The structure and function of major plant metabolite modifications. *Mol. Plant* **2019**, *12*, 899–919. [CrossRef] [PubMed]
20. Nielsen, E.; Temporiti, M.E.E.; Cella, R. Improvement of phytochemical production by plant cells and organ culture and by genetic engineering. *Plant Cell Rep.* **2019**, *38*, 1199–1215. [CrossRef]
21. Verma, N.; Shukla, S. Impact of various factors responsible for fluctuation in plant secondary metabolites. *J. Appl. Res. Med. Aromat. Plants* **2015**, *2*, 105–113. [CrossRef]
22. Zhong, J.-J. Plant secondary metabolites. *Compr. Biotechnol.* **2011**, 324–333. [CrossRef]

23. Sajc, L.; Grubisic, D.; Vunjak-Novakovic, G. Bioreactors for plant engineering: An outlook for further research. *Biochem. Eng. J.* **2000**, *4*, 89–99. [CrossRef]
24. Werner, S.; Maschke, R.W.; Eibl, D.; Eibl, R. Bioreactor technology for sustainable production of plant cell-derived products. In *Bioprocessing of Plant In Vitro Systems*; Springer: Cham, Switzerland, 2018; pp. 413–432. [CrossRef]
25. Casciaro, B.; Mangiardi, L.; Cappiello, F.; Romeo, I.; Loffredo, M.R.; Iazzetti, A.; Calcaterra, A.; Goggiamani, A.; Ghirga, F.; Mangoni, M.L.; et al. Naturally-occurring Alkaloids of plant origin as potential antimicrobials against antibiotic-resistant infections. *Molecules* **2020**, *25*, 3619. [CrossRef]
26. Islam, M.T.; Mubarak, M.S. Pyrrolidine alkaloids and their promises in pharmacotherapy. *Adv. Tradit. Med.* **2020**, *20*, 13–22. [CrossRef]
27. Tran, N.; Pham, B.; Le, L. Bioactive compounds in anti-diabetic plants: From herbal medicine to modern drug discovery. *Biology* **2020**, *9*, 252. [CrossRef]
28. Rodriguez-Garcia, A.; Hosseini, S.; Martinez-Chapa, S.O.; Cordell, G.A. Multi-target activities of selected Alkaloids and Terpenoids. *Mini-Rev. Org. Chem.* **2017**, *14*, 272–279. [CrossRef]
29. Shehadeh, M.; Suaifan, G.; Abu-Odeh, A. Plants secondary metabolites as blood glucose-lowering molecules. *Molecules* **2021**, *26*, 4333. [CrossRef]
30. Sharifi-Rad, J.; Rajabi, S.; Martorell, M.; López, M.D.; Toro, M.T.; Barollo, S.; Armanini, D.; Fokou, P.V.T.; Zagotto, G.; Ribaudo, G.; et al. Plant natural products with anti-thyroid cancer activity. *Fitoterapia* **2020**, *146*, 104640. [CrossRef]
31. Shah, S.M.A.; Akram, M.; Riaz, M.; Munir, N.; Rasool, G. Cardioprotective potential of plant-derived molecules: A scientific and medicinal approach. *Dose-Response* **2019**, *17*, 1559325819852243. [CrossRef]
32. Smetanska, I. *Sustainable Production of Polyphenols and Antioxidants by Plant In Vitro Cultures*; Springer: Berlin/Heidelberg, Germany, 2018; ISBN 9783319545998.
33. Suresh, Y.; Rajasekar, G.; Lavanya, T.; Lakshminarsimhulu, B.; Reddy, K.S.; Reddy, S.R. Antioxidant and antidiabetic properties of isolated fractions from methanolic extract derived from the whole plant of *Cleome viscosa* L. *Future J. Pharm. Sci.* **2020**, *6*, 1–18. [CrossRef]
34. Croft, K.D.; Yamashita, Y.; O'Donoghue, H.; Shirasaya, D.; Ward, N.C.; Ashida, H. Screening plant derived dietary phenolic compounds for bioactivity related to cardiovascular disease. *Fitoterapia* **2018**, *126*, 22–28. [CrossRef] [PubMed]
35. Olivares-Vicente, M.; Barrajon-Catalan, E.; Herranz-Lopez, M.; Segura-Carretero, A.; Joven, J.; Encinar, J.A.; Micol, V. Plant-derived polyphenols in human health: Biological activity, metabolites and putative molecular targets. *Curr. Drug Metab.* **2018**, *19*, 351–369. [CrossRef] [PubMed]
36. Eljounaidi, K.; Lichman, B.R. Nature's chemists: The discovery and engineering of phytochemical biosynthesis. *Front. Chem.* **2020**, *8*, 1041. [CrossRef] [PubMed]
37. Jahangeer, M.; Fatima, R.; Ashiq, M.; Basharat, A.; Qamar, S.A.; Bilal, M.; Iqbal, H.M. Therapeutic and biomedical potentialities of terpenoids—A review. *J. Pure Appl. Microbiol.* **2021**, *15*, 471–483. [CrossRef]
38. Zaynab, M.; Fatima, M.; Abbas, S.; Sharif, Y.; Umair, M.; Zafar, M.H.; Bahadar, K. Role of secondary metabolites in plant defense against pathogens. *Microb. Pathog.* **2018**, *124*, 198–202. [CrossRef]
39. Sonigra, P.; Meena, M. Metabolic profile, bioactivities, and variations in the chemical constituents of essential oils of the ferula genus (*Apiaceae*). *Front. Pharmacol.* **2021**, *11*, 2328. [CrossRef] [PubMed]
40. Blažević, I.; Montaut, S.; Burčul, F.; Olsen, C.E.; Burow, M.; Rollin, P.; Agerbirk, N. Glucosinolate structural diversity, identification, chemical synthesis and metabolism in plants. *Phytochemistry* **2020**, *169*, 112100. [CrossRef]
41. Maina, S.; Misinzo, G.; Bakari, G.; Kim, H.-Y. Human, animal and plant health benefits of glucosinolates and strategies for enhanced bioactivity: A systematic review. *Molecules* **2020**, *25*, 3682. [CrossRef]
42. Eibl, R.; Meier, P.; Stutz, I.; Schildberger, D.; Hühn, T.; Eibl, D. Plant cell culture technology in the cosmetics and food industries: Current state and future trends. *Appl. Microbiol. Biotechnol.* **2018**, *102*, 8661–8675. [CrossRef]
43. Karki, U.; Fang, H.; Guo, W.; Unnold-Cofre, C.; Xu, J. Cellular engineering of plant cells for improved therapeutic protein production. *Plant Cell Rep.* **2021**, *40*, 1087–1099. [CrossRef] [PubMed]
44. Narayani, M.; Srivastava, S. Elicitation: A stimulation of stress in in vitro plant cell/tissue cultures for enhancement of secondary metabolite production. *Phytochem. Rev.* **2017**, *16*, 1227–1252. [CrossRef]
45. Woo, H.-A.; Ku, S.S.; Jie, E.Y.; Kim, H.; Kim, H.-S.; Cho, H.S.; Jeong, W.-J.; Park, S.U.; Min, S.R.; Kim, S.W. Efficient plant regeneration from embryogenic cell suspension cultures of Euonymus alatus. *Sci. Rep.* **2021**, *11*, 15120. [CrossRef]
46. Ali, A.M.A.; El-Nour, M.E.M.; Yagi, S.M. Total phenolic and flavonoid contents and antioxidant activity of ginger (*Zingiber officinale* Rosc.) rhizome, callus and callus treated with some elicitors. *J. Genet. Eng. Biotechnol.* **2018**, *16*, 677–682. [CrossRef] [PubMed]
47. Babich, O.; Sukhikh, S.; Pungin, A.; Ivanova, S.; Asyakina, L.; Prosekov, A. Modern trends in the in vitro production and use of callus, suspension cells and root cultures of medicinal plants. *Molecules* **2020**, *25*, 5805. [CrossRef]
48. Furusaki, S.; Takeda, T. Bioreactors for plant cell culture. *Compr. Biotechnol.* **2017**, 519–530. [CrossRef]
49. Niazian, M. Application of genetics and biotechnology for improving medicinal plants. *Planta* **2019**, *249*, 953–973. [CrossRef] [PubMed]

50. Kwon, Y.-W.; Lee, S.-H.; Kim, A.-R.; Kim, B.J.; Park, W.-S.; Hur, J.; Jang, H.; Yang, H.-M.; Cho, H.-J.; Kim, H.-S. Plant callus-derived shikimic acid regenerates human skin through converting human dermal fibroblasts into multipotent skin-derived precursor cells. *Stem Cell Res. Ther.* **2021**, *12*, 346. [CrossRef]
51. Gonçalves, S.; Romano, A. Production of plant secondary metabolites by using biotechnological tools. In *Secondary Metabolites, Sources and Applications*; IntechOpen: London, UK, 2018. [CrossRef]
52. Isah, T.; Umar, S.; Mujib, A.; Sharma, M.P.; Rajasekharan, P.E.; Zafar, N.; Frukh, A. Secondary metabolism of pharmaceuticals in the plant in vitro cultures: Strategies, approaches, and limitations to achieving higher yield. *Plant Cell Tissue Organ Cult.* **2018**, *132*, 239–265. [CrossRef]
53. Prasad, G.D.; Sudina, B.; Janardan, L.; Rajani, S.; Rosario, G.-G.M. Establishment of regenerative callus, cell suspension system, and molecular characterization of *Taxus wallichiana* Zucc. for the in vitro production of Taxol. *J. Appl. Pharm. Sci.* **2020**, *11*, 22–34. [CrossRef]
54. Sharma, K.; Zafar, R. Optimization of methyl jasmonate and β-cyclodextrin for enhanced production of taraxerol and taraxasterol in (*Taraxacum officinale* Weber) cultures. *Plant Physiol. Biochem.* **2016**, *103*, 24–30. [CrossRef] [PubMed]
55. Chastang, T.; Pozzobon, V.; Taidi, B.; Courot, E.; Clément, C.; Pareau, D. Resveratrol production by grapevine cells in fed-batch bioreactor: Experiments and modelling. *Biochem. Eng. J.* **2018**, *131*, 9–16. [CrossRef]
56. Jeong, Y.J.; Park, S.H.; Park, S.-C.; Kim, S.; Kim, T.H.; Lee, J.; Kim, S.W.; Ryu, Y.B.; Jeong, J.C.; Kim, C.Y. Induced extracellular production of stilbenes in grapevine cell culture medium by elicitation with methyl jasmonate and stevioside. *Bioresour. Bioprocess.* **2020**, *7*, 40643. [CrossRef]
57. Le, K.-C.; Jeong, C.-S.; Lee, H.; Paek, K.-Y.; Park, S.-Y. Ginsenoside accumulation profiles in long- and short-term cell suspension and adventitious root cultures in Panax ginseng. *Hortic. Environ. Biotechnol.* **2018**, *60*, 125–134. [CrossRef]
58. Malik, S.; Cusido, R.M.; Mirjalili, M.H.; Moyano, E.; Palazon, J.; Bonfill, M. Production of the anticancer drug taxol in *Taxus baccata* suspension cultures: A review. *Process. Biochem.* **2011**, *46*, 23–34. [CrossRef]
59. Sahakyan, N.; Petrosyan, M.; Trchounian, A. The activity of Alkanna species in vitro culture and intact plant extracts against antibiotic resistant bacteria. *Curr. Pharm. Des.* **2019**, *25*, 1861–1865. [CrossRef]
60. Gwon, S.Y.; Ahn, J.; Jung, C.H.; Moon, B.; Ha, T.-Y. Shikonin attenuates hepatic steatosis by enhancing beta oxidation and energy expenditure via AMPK activation. *Nutrients* **2020**, *12*, 1133. [CrossRef]
61. Jeziorek, M.; Damianakos, H.; Kawiak, A.; Laudy, A.E.; Zakrzewska, K.; Sykłowska-Baranek, K.; Chinou, I.; Pietrosiuk, A. Bioactive rinderol and cynoglosol isolated from *Cynoglossum columnae* Ten. in vitro root culture. *Ind. Crop. Prod.* **2019**, *137*, 446–452. [CrossRef]
62. Rat, A.; Naranjo, H.D.; Krigas, N.; Grigoriadou, K.; Maloupa, E.; Alonso, A.V.; Schneider, C.; Papageorgiou, V.P.; Assimopoulou, A.N.; Tsafantakis, N.; et al. Endophytic bacteria from the roots of the medicinal plant *Alkanna tinctoria* Tausch (Boraginaceae): Exploration of plant growth promoting properties and potential role in the production of plant secondary metabolites. *Front. Microbiol.* **2021**, *12*, 113. [CrossRef] [PubMed]
63. Fu, J.-Y.; Zhao, H.; Bao, J.-X.; Wen, Z.-L.; Fang, R.-J.; Fazal, A.; Yang, M.-K.; Liu, B.; Yin, T.-M.; Pang, Y.-J.; et al. Establishment of the hairy root culture of *Echium plantagineum* L. and its shikonin production. *3 Biotech* **2020**, *10*, 429. [CrossRef]
64. Baque, A.; Shiragi, H.K.; Moh, S.-H.; Lee, E.-J.; Paek, K.-Y. Production of biomass and bioactive compounds by adventitious root suspension cultures of *Morinda citrifolia* (L.) in a liquid-phase airlift balloon-type bioreactor. *Vitr. Cell. Dev. Biol. Anim.* **2013**, *49*, 737–749. [CrossRef]
65. Veremeichik, G.; Bulgakov, V.; Shkryl, Y.; Silantieva, S.; Makhazen, D.; Tchernoded, G.; Mischenko, N.; Fedoreyev, S.; Vasileva, E. Activation of anthraquinone biosynthesis in long-cultured callus culture of *Rubia cordifolia* transformed with the rolA plant oncogene. *J. Biotechnol.* **2019**, *306*, 38–46. [CrossRef] [PubMed]
66. Mariadoss, A.; Satdive, R.; Fulzele, D.P.; Ramamoorthy, S.; Zayed, H.; Younes, S.; Rajasekaran, C. Enhanced production of anthraquinones by gamma-irradiated cell cultures of *Rubia cordifolia* in a bioreactor. *Ind. Crop. Prod.* **2020**, *145*, 111987. [CrossRef]
67. Kowalczyk, T.; Sitarek, P.; Toma, M.; Rijo, P.; Domínguez-Martíne, E.; Falcó, I.; Sánchez, G.; Śliwiński, T. Enhanced accumulation of betulinic acid in transgenic hairy roots of *Senna obtusifolia* growing in the Sprinkle Bioreactor and evaluation of their biological properties in various biological models. *Chem. Biodivers.* **2021**, *18*, e2100455. [CrossRef] [PubMed]
68. Açıkgöz, M.A. Effects of sorbitol on the production of phenolic compounds and terpenoids in the cell suspension cultures of *Ocimum basilicum* L. *Biologia* **2021**, *76*, 395–409. [CrossRef]
69. Pandey, P.; Singh, S.; Banerjee, S. *Ocimum basilicum* suspension culture as resource for bioactive triterpenoids: Yield enrichment by elicitation and bioreactor cultivation. *Plant Cell Tissue Organ Cult.* **2019**, *137*, 65–75. [CrossRef]
70. Li, Y.-P.; Tang, D.-B.; Wang, X.-Q.; Wang, M.; Zhang, Q.-F.; Liu, Y.; Shen, B.-Y.; Chen, J.-G.; Yin, Z.-P. Development of *Origanum vulgare* cell suspension culture to produce polyphenols and the stimulation effect of salicylic acid elicitation and phenylalanine feeding. *Biotechnol. Bioprocess Eng.* **2021**, *26*, 456–467. [CrossRef]
71. Gonçalves, S.; Moreira, E.; Grosso, C.; Andrade, P.B.; Valentão, P.; Romano, A. Phenolic profile, antioxidant activity and enzyme inhibitory activities of extracts from aromatic plants used in Mediterranean diet. *J. Food Sci. Technol.* **2017**, *54*, 219–227. [CrossRef]
72. Sahraroo, A.; Mirjalili, M.H.; Corchete, P.; Babalar, M.; Moghadam, M.R.F. Establishment and characterization of a *Satureja khuzistanica* Jamzad (*Lamiaceae*) cell suspension culture: A new in vitro source of rosmarinic acid. *Cytotechnology* **2016**, *68*, 1415–1424. [CrossRef]

73. Sahraroo, A.; Mirjalili, M.H.; Babalar, M.; Zarei, A. Enhancement of rosmarinic acid production by *Satureja khuzistanica* cell suspensions: Effects of phenylalanine and sucrose. *SABRAO J. Breed. Genet.* **2018**, *50*, 25–35.
74. Och, A.; Podgórski, R.; Nowak, R. Biological activity of berberine—A summary update. *Toxins* **2020**, *12*, 713. [CrossRef]
75. Khan, T.; Krupadanam, D.; Anwar, S.Y. The role of phytohormone on the production of berberine in the calli cultures of an endangered medicinal plant, turmeric (*Coscinium fenestratum* L.). *Afr. J. Biotechnol.* **2008**, *7*, 3244–3246. [CrossRef]
76. Yamada, Y.; Yoshimoto, T.; Yoshida, S.T.; Sato, F. Characterization of the promoter region of biosynthetic enzyme genes involved in Berberine Biosynthesis in *Coptis japonica*. *Front. Plant Sci.* **2016**, *7*, 1352. [CrossRef]
77. Cheung, C.K.-L.; Leksawasdi, N.; Doran, P.M. Bioreactor scale-down studies of suspended plant cell cultures. *AIChE J.* **2018**, *64*, 4281–4288. [CrossRef]
78. Tabata, M. Transport and secretion of natural products in plant cell cultures. *Planta Med.* **1991**, *57*, S21–S26. [CrossRef]
79. Sato, F.; Yamada, Y. High berberine-producing cultures of coptis japonica cells. *Phytochemistry* **1984**, *23*, 281–285. [CrossRef]
80. Hou, M.; Wang, R.; Zhao, S.; Wang, Z. Ginsenosides in *Panax* genus and their biosynthesis. *Acta Pharm. Sin. B* **2021**, *11*, 1813–1834. [CrossRef] [PubMed]
81. Adil, M.; Jeong, B.R. In vitro cultivation of *Panax ginseng* C.A. Meyer. *Ind. Crop. Prod.* **2018**, *122*, 239–251. [CrossRef]
82. Nazir, R.; Kumar, V.; Gupta, S.; Dwivedi, P.; Pandey, D.K.; Dey, A. Biotechnological strategies for the sustainable production of diosgenin from *Dioscorea* spp. *Appl. Microbiol. Biotechnol.* **2021**, *105*, 569–585. [CrossRef] [PubMed]
83. Shaikh, S.; Shriram, V.; Khare, T.; Kumar, V. Biotic elicitors enhance diosgenin production in *Helicteres isora* L. suspension cultures via up-regulation of CAS and HMGR genes. *Physiol. Mol. Biol. Plants* **2020**, *26*, 593–604. [CrossRef]
84. Deshpande, H.A.; Bhalsing, S.R. Isolation and characterization of diosgenin from in vitro cultured tissues of *Helicteres isora* L. *Physiol. Mol. Biol. Plants* **2013**, *20*, 89–94. [CrossRef]
85. Das, A.; Sarkar, S.; Bhattacharyya, S.; Gantait, S. Biotechnological advancements in *Catharanthus roseus* (L.) G. Don. *Appl. Microbiol. Biotechnol.* **2020**, *104*, 4811–4835. [CrossRef]
86. Thakore, D.; Srivastava, A.; Sinha, A.K. Mass production of Ajmalicine by bioreactor cultivation of hairy roots of *Catharanthus roseus*. *Biochem. Eng. J.* **2017**, *119*, 84–91. [CrossRef]
87. Alamgir, A.N.M. Cultivation of herbal drugs, biotechnology, and in vitro production of secondary metabolites, high-value medicinal plants, herbal wealth, and herbal trade. In *Therapeutic Use of Medicinal Plants and Their Extracts: Volume 1*; Springer: Berlin/Heidelberg, Germany, 2017; pp. 379–452, ISBN 9783319638621.
88. Changxing, L.; Galani, S.; Hassan, F.-U.; Rashid, Z.; Naveed, M.; Fang, D.; Ashraf, A.; Qi, W.; Arif, A.; Saeed, M.; et al. Biotechnological approaches to the production of plant-derived promising anticancer agents: An update and overview. *Biomed. Pharmacother.* **2020**, *132*, 110918. [CrossRef] [PubMed]
89. Kumar, P.; Sharma, P.; Kumar, V.; Kumar, A. Plant resources: In vitro production, challenges and prospects of secondary Metabolites from medicinal plants. *Ind. Biotechnol.* **2019**, *2019*, 89–104. [CrossRef]
90. Salehi, M.; Karimzadeh, G.; Naghavi, M.R. Synergistic effect of coronatine and sorbitol on artemisinin production in cell suspension culture of *Artemisia annua* L. cv. Anamed. *Plant Cell Tissue Organ Cult.* **2019**, *137*, 587–597. [CrossRef]
91. Kayani, W.K.; Kiani, B.H.; Dilshad, E.; Mirza, B. Biotechnological approaches for artemisinin production in Artemisia. *World J. Microbiol. Biotechnol.* **2018**, *34*, 54. [CrossRef] [PubMed]
92. Kubica, P.; Szopa, A.; Kokotkiewicz, A.; Miceli, N.; Taviano, M.; Maugeri, A.; Cirmi, S.; Synowiec, A.; Gniewosz, M.; Elansary, H.; et al. Production of Verbascoside, Isoverbascoside and Phenolic acids in callus, suspension, and bioreactor cultures of *Verbena officinalis* and biological properties of biomass extracts. *Molecules* **2020**, *25*, 5609. [CrossRef]
93. Yue, W.; Ming, Q.-L.; Lin, B.; Rahman, K.; Zheng, C.-J.; Han, T.; Qin, L.-P. Medicinal plant cell suspension cultures: Pharmaceutical applications and high-yielding strategies for the desired secondary metabolites. *Crit. Rev. Biotechnol.* **2016**, *36*, 215–232. [CrossRef]
94. Valdiani, A.; Hansen, O.K.; Nielsen, U.B.; Johannsen, V.K.; Shariat, M.; Georgiev, M.I.; Omidvar, V.; Ebrahimi, M.; Dinanai, E.T.; Abiri, R. Bioreactor-based advances in plant tissue and cell culture: Challenges and prospects. *Crit. Rev. Biotechnol.* **2018**, *39*, 20–34. [CrossRef]
95. Thakur, M.; Bhattacharya, S.; Khosla, P.K.; Puri, S. Improving production of plant secondary metabolites through biotic and abiotic elicitation. *J. Appl. Res. Med. Aromat. Plants* **2019**, *12*, 1–12. [CrossRef]
96. Nabi, N.; Singh, S.; Saffeullah, P. Responses of in vitro cell cultures to elicitation: Regulatory role of jasmonic acid and methyl jasmonate: A review. *Vitr. Cell. Dev. Biol. Anim.* **2021**, *57*, 341–355. [CrossRef]
97. Khan, T.; Khan, T.; Hano, C.; Abbasi, B.H. Effects of chitosan and salicylic acid on the production of pharmacologically attractive secondary metabolites in callus cultures of *Fagonia indica*. *Ind. Crop. Prod.* **2019**, *129*, 525–535. [CrossRef]
98. Kehie, M.; Kumaria, S.; Tandon, P. Biotechnological enhancement of capsaicin biosynthesis in cell suspension cultures of Naga King Chili (*Capsicum chinense* Jacq.). *Bioprocess Biosyst. Eng.* **2016**, *39*, 205–210. [CrossRef]
99. Schenke, D.; Utami, H.P.; Zhou, Z.; Gallegos, M.-T.; Cai, D. Suppression of UV-B stress induced flavonoids by biotic stress: Is there reciprocal crosstalk? *Plant Physiol. Biochem.* **2019**, *134*, 53–63. [CrossRef]
100. Lange, B.M. Commercial-scale tissue culture for the production of plant natural products: Successes, failures and outlook. In *Biotechnology of Natural Products*; Springer: Cham, Switzerland, 2018; pp. 189–218. [CrossRef]
101. Marketwatch. Available online: https://www.marketwatch.com/press-release/paclitaxel-market-size-in-2021-87-cagr-with-top-countries-data-competition-strategies-share-industry-analysis-by-top-manufactures-growth-insights-and-forecasts-to-2026-2021-08-06 (accessed on 8 December 2021).

102. Frense, D. Taxanes: Perspectives for biotechnological production. *Appl. Microbiol. Biotechnol.* **2007**, *73*, 1233–1240. [CrossRef]
103. Espinosa-Leal, C.A.; Puente-Garza, C.A.; García-Lara, S. In vitro plant tissue culture: Means for production of biological active compounds. *Planta* **2018**, *248*, 1–18. [CrossRef] [PubMed]
104. Wagner, H.; Stuppner, H.; Schäfer, W.; Zenk, M. Immunologically active polysaccharides of *Echinacea purpurea* cell cultures. *Phytochemistry* **1988**, *27*, 119–126. [CrossRef]
105. DiCosmo, F.; Misawa, M. Plant cell and tissue culture: Alternatives for metabolite production. *Biotechnol. Adv.* **1995**, *13*, 425–453. [CrossRef]
106. Giri, A.; Narasu, M.L. Production of podophyllotoxin from *Podophyllum hexandrum*: A potential natural product for clinically useful anticancer drugs. *Cytotechnology* **2000**, *34*, 17–26. [CrossRef]
107. Sasheva, P.; Ionkova, I. Small Cells for Big Ideas: The Cytotoxic Podophyllotoxin and the Long Journey in Discovering Its Biosynthetic Pathway. In *Biotechnology and Production of Anti-Cancer Compounds*; Federal University of Maranhao: Sao Luis, Brazil, 2017. [CrossRef]
108. Rao, K.; Chodisetti, B.; Gandi, S.; Giri, A.; Kishor, P.B.K. Cadmium chloride elicitation of *Abutilon indicum* cell suspension cultures for enhanced stigmasterol production. *Plant Biosyst. Int. J. Deal. All Asp. Plant Biol.* **2021**, *155*, 1–6. [CrossRef]
109. Ojha, T.; Hu, Q.; Colombo, C.; Wit, J.; van Geijn, M.; van Steenbergen, M.J.; Bagheri, M.; Königs-Werner, H.; Buhl, E.M.; Bansal, R.; et al. Lyophilization stabilizes clinical-stage core-crosslinked polymeric micelles to overcome cold chain supply challenges. *Biotechnol. J.* **2021**, *16*, 2000212. [CrossRef] [PubMed]
110. McElroy, C.; Jennewein, S. Taxol® biosynthesis and production: From forests to fermenters. In *Biotechnology of Natural Products*; Springer: Berlin/Heidelberg, Germany, 2017; pp. 145–185.
111. Chattopadhyay, S.; Farkya, S.; Srivastava, A.; Bisaria, V.S. Bioprocess considerations for production of secondary metabolites by plant cell suspension cultures. *Biotechnol. Bioprocess Eng.* **2002**, *7*, 138–149. [CrossRef]
112. Lee, S.-W.; Kim, Y.-M.; Cho, C.H.; Kim, Y.T.; Kim, S.M.; Hur, S.Y.; Kim, J.-H.; Kim, B.-G.; Kim, S.-C.; Ryu, H.-S.; et al. An open-label, randomized, parallel, phase ii trial to evaluate the efficacy and safety of a cremophor-free polymeric micelle formulation of paclitaxel as first-line treatment for ovarian cancer: A Korean gynecologic oncology group study (KGOG-3021). *Cancer Res. Treat.* **2018**, *50*, 195–203. [CrossRef] [PubMed]
113. Muranaka, T.; Ohkawa, H.; Yamada, Y. Continuous production of scopolamine by a culture of *Duboisia leichhardtii* hairy root clone in a bioreactor system. *Appl. Microbiol. Biotechnol.* **1993**, *40*, 219–223. [CrossRef]
114. D'Amelia, V.; Docimo, T.; Crocoll, C.; Rigano, M. Specialized metabolites and valuable molecules in crop and medicinal plants: The evolution of their use and strategies for their production. *Genes* **2021**, *12*, 936. [CrossRef]
115. Singh, J.; Kaushik, N.; Biswas, S. Bioreactors—Technology & design analysis. *Scitech J.* **2014**, *1*, 28–36.
116. Esperança, M.N.; Mendes, C.E.; Rodriguez, G.Y.; Cerri, M.O.; Béttega, R.; Badino, A.C. Sparger design as key parameter to define shear conditions in pneumatic bioreactors. *Biochem. Eng. J.* **2020**, *157*, 107529. [CrossRef]
117. Barragán, L.P.; Figueroa, J.; Durán, L.R.; González, C.A.; Hennigs, C. *Fermentative Production Methods*; Elsevier: Amsterdam, The Netherlands, 2016; pp. 189–217.
118. Zhang, T.; We, C.; Ren, Y.; Feng, C.; Wu, H. Advances in airlift reactors: Modified design and optimization of operation conditions. *Rev. Chem. Eng.* **2017**, *33*, 163–182. [CrossRef]
119. Kumar, N.; Gupta, R.; Bansal, A. Effect of surface tension on hydrodynamics and mass transfer coefficient in airlift reactors. *Chem. Eng. Technol.* **2020**, *43*, 995–1004. [CrossRef]
120. Tervasmäki, P.; Latva-Kokko, M.; Taskila, S.; Tanskanen, J. Effect of oxygen transfer on yeast growth—Growth kinetic and reactor model to estimate scale-up effects in bioreactors. *Food Bioprod. Process.* **2018**, *111*, 129–140. [CrossRef]
121. Fitzpatrick, J.J. Insights from mathematical modelling into energy requirement and process design of continuous and batch stirred tank aerobic bioreactors. *ChemEngineering* **2019**, *3*, 65. [CrossRef]
122. Ahmadi-Sakha, S.; Sharifi, M.; Niknam, V. Bioproduction of phenylethanoid glycosides by plant cell culture of *Scrophularia striata* Boiss.: From shake-flasks to bioreactor. *Plant Cell Tissue Organ Cult.* **2016**, *124*, 275–281. [CrossRef]
123. Estrada-Zúñiga, M.E.; Cruz-Sosa, F.; Rodriguez-Monroy, M.; Verde-Calvo, J.R.; Vernon-Carter, E.J. Phenylpropanoid production in callus and cell suspension cultures of *Buddleja cordata* Kunth. *Plant Cell Tissue Organ Cult.* **2009**, *97*, 39–47. [CrossRef]
124. Vazquez-Marquez, A.M.; Zepeda-Gómez, C.; Burrola-Aguilar, C.; Bernabé-Antonio, A.; Nieto-Trujillo, A.; Cruz-Sosa, F.; Rodríguez-Monroy, M.; Estrada-Zúñiga, M.E. Effect of stirring speed on the production of phenolic secondary metabolites and growth of *Buddleja cordata* cells cultured in mechanically agitated bioreactor. *Plant Cell Tissue Organ Cult.* **2019**, *139*, 155–166. [CrossRef]
125. Busto, V.; Rodriguez-Talou, J.; Giulietti, A.; Merchuk, J. Effect of shear stress on Anthraquinones production by *Rubia tinctorum* suspension cultures. *Biotechnol. Prog.* **2008**, *24*, 175–181. [CrossRef]
126. Gupta, K.; Garg, S.; Singh, J.; Kumar, M. Enhanced production of napthoquinone metabolite (shikonin) from cell suspension culture of *Arnebia* sp. and its up-scaling through bioreactor. *3 Biotech* **2014**, *4*, 263–273. [CrossRef]
127. Khojasteh, A.; Mirjalili, M.H.; Palazon, J.; Eibl, R.; Cusido, R.M. Methyl jasmonate enhanced production of rosmarinic acid in cell cultures of *Satureja khuzistanicain* a bioreactor. *Eng. Life Sci.* **2016**, *16*, 740–749. [CrossRef]
128. Lambert, C.; Lemaire, J.; Auger, H.; Guilleret, A.; Reynaud, R.; Clément, C.; Courot, E.; Taidi, B. Optimize, modulate, and scale-up resveratrol and resveratrol dimers bioproduction in *Vitis labrusca* L. Cell suspension from Flasks to 20 L Bioreactor. *Plants* **2019**, *8*, 567. [CrossRef]

129. Rani, A.; Meghana, R.; Kush, A. Squalene production in the cell suspension cultures of Indian sandalwood (*Santalum album* L.) in shake flasks and air lift bioreactor. *Plant Cell Tissue Organ Cult.* **2018**, *135*, 155–167. [CrossRef]
130. Salehi, M.; Farhadi, S.; Moieni, A.; Safaie, N.; Ahmadi, H. Mathematical modeling of growth and paclitaxel biosynthesis in *Corylus avellana* cell culture responding to fungal elicitors using multilayer perceptron-genetic algorithm. *Front. Plant Sci.* **2020**, *11*, 1148. [CrossRef]
131. Maschke, R.; Geipel, K.; Bley, T. Modeling of plant in vitro cultures: Overview and estimation of biotechnological processes. *Biotechnol. Bioeng.* **2014**, *112*, 1–12. [CrossRef] [PubMed]
132. Villegas, A.; Arias, J.P.; Aragón, D.; Ochoa, S.; Arias, M. Structured model and parameter estimation in plant cell cultures of *Thevetia peruviana*. *Bioprocess Biosyst. Eng.* **2016**, *40*, 573–587. [CrossRef]
133. Chattopadhyay, S.; Bisaria, V.S.; Srivastava, A.K. Enhanced production of Podophyllotoxin by *Podophyllum hexandrum* using in situ cell retention bioreactor. *Biotechnol. Prog.* **2003**, *19*, 1026–1028. [CrossRef] [PubMed]
134. Prakash, G.; Srivastava, A.K. Modeling of azadirachtin production by *Azadirachta indica* and its use for feed forward optimization studies. *Biochem. Eng. J.* **2006**, *29*, 62–68. [CrossRef]
135. Amdoun, R.; Khelifi, L.; Khelifi-Slaoui, M.; Amroune, S.; Benyoussef, E.-H.; Thi, D.V.; Assaf-Ducrocq, C.; Gontier, E. Influence of minerals and elicitation on *Datura stramonium* L. tropane alkaloid production: Modelization of the in vitro biochemical response. *Plant Sci.* **2009**, *177*, 81–87. [CrossRef]
136. Thakore, D.; Srivastava, A.K.; Sinha, A.K. Model based fed batch cultivation and elicitation for the overproduction of ajmalicine from hairy roots of *Catharanthus roseus*. *Biochem. Eng. J.* **2015**, *97*, 73–80. [CrossRef]
137. Salehi, M.; Farhadi, S.; Moieni, A.; Safaie, N.; Hesami, M. A hybrid model based on general regression neural network and fruit fly optimization algorithm for forecasting and optimizing paclitaxel biosynthesis in *Corylus avellana* cell culture. *Plant Methods* **2021**, *17*, 13. [CrossRef]
138. Villadsen, J.; Nielsen, J.; Lidén, G. Chemicals from metabolic pathways. In *Bioreaction Engineering Principles*; Springer: Boston, MA, USA, 2011; pp. 7–62. ISBN 97814419968792.
139. Melgarejo-Torres, R.; Castillo-Araiza, C.O.; López-Ordaz, P.; Torres-Martínez, D.; Gutiérrez-Rojas, M.; Lye, G.; Huerta-Ochoa, S. Kinetic mathematical model for ketone bioconversion using *Escherichia coli* TOP10 pQR239. *Chem. Eng. J.* **2014**, *240*, 1–9. [CrossRef]
140. Palmerín-Carreño, D.; Castillo-Araiza, C.; Rutiaga-Quiñones, O.; Verde-Calvo, J.; Huerta-Ochoa, S. Kinetic, oxygen mass transfer and hydrodynamic studies in a three-phase stirred tank bioreactor for the bioconversion of (+)-valencene on *Yarrowia lipolytica* 2.2ab. *Biochem. Eng. J.* **2016**, *113*, 37–46. [CrossRef]
141. Castillo-Araiza, C.; Palmerín-Carreño, D.; Prado-Barragán, A.; Huerta-Ochoa, S. On the conceptual design of a partitioning technology for the bioconversion of (+)-valencene to (+)-nootkatone on whole cells: Experimentation and modelling. *Chem. Eng. Process. Process. Intensif.* **2017**, *122*, 493–507. [CrossRef]
142. Liu, Y. A simple thermodynamic approach for derivation of a general Monod equation for microbial growth. *Biochem. Eng. J.* **2006**, *31*, 102–105. [CrossRef]
143. Liu, Y. Overview of some theoretical approaches for derivation of the Monod equation. *Appl. Microbiol. Biotechnol.* **2007**, *73*, 1241–1250. [CrossRef]
144. Wang, J.D.; Levin, P.A. Metabolism, cell growth and the bacterial cell cycle. *Nat. Rev. Genet.* **2009**, *7*, 822–827. [CrossRef]
145. Henson, A.M. Dynamic modeling of microbial cell populations. *Curr. Opin. Biotechnol.* **2003**, *14*, 460–467. [CrossRef]
146. Daugulis, A.J. Partitioning bioreactors. *Curr. Opin. Biotechnol.* **1997**, *8*, 169–174. [CrossRef]
147. Kalil, S.; Maugeri, F.; Rodrigues, M. Response surface analysis and simulation as a tool for bioprocess design and optimization. *Process. Biochem.* **2000**, *35*, 539–550. [CrossRef]
148. Ríos-Morales, D.; Castillo-Araiza, C.O.; Vizcarra-Mendoza, M.G. Study of the agglomeration mechanism of a natural organic solid in a bench-scale wet fluidized bed using statistical analysis and discretized population balance. *Chem. Eng. Commun.* **2014**, *201*, 23–40. [CrossRef]
149. Khuri, A.I.; Mukhopadhyay, S. Response surface methodology. *Wiley Interdiscip. Rev. Comput. Stat.* **2010**, *2*, 128–149. [CrossRef]
150. Dellino, G.; Kleijnen, J.P.; Meloni, C. Robust optimization in simulation: Taguchi and response surface methodology. *Int. J. Prod. Econ.* **2010**, *125*, 52–59. [CrossRef]
151. Anderson-Cook, C.M.; Borror, C.M.; Montgomery, D.C. Response surface design evaluation and comparison. *J. Stat. Plan. Inference* **2009**, *139*, 629–641. [CrossRef]
152. Montgomery, D.C. *Design and Analysis of Experiments*; John Wiley: Hoboken, NJ, USA, 2013; ISBN 9781118146927.
153. Box, G. JS hunter, WG hunter. *Stat. Exp. Des. Innov. Discov.* **2005**, *21*, 303–304. [CrossRef]
154. Hanrahan, G.; Lu, K. Application of factorial and response surface methodology in modern experimental design and optimization. *Crit. Rev. Anal. Chem.* **2006**, *36*, 141–151. [CrossRef]
155. Malik, S.; Bhushan, S.; Sharma, M.; Ahuja, P.S. Physico-chemical factors influencing the shikonin derivatives production in cell suspension cultures of *Arnebia euchroma* (Royle) Johnston, a medicinally important plant species. *Cell Biol. Int.* **2011**, *35*, 153–158. [CrossRef] [PubMed]
156. Nartop, P. Engineering of biomass accumulation and secondary metabolite production in plant cell and tissue cultures. In *Plant Metabolites and Regulation under Environmental Stress*; Academic Press: Cambridge, MA, USA, 2018; pp. 169–194. [CrossRef]

157. Ten Hoopen, H.J.G.; Vinke, J.L.; Moreno, P.; Verpoorte, R.; Heijnen, J.J. Influence of temperature on growth and ajmalicine production by *Catharantus roseus* suspension cultures. *Enzym. Microb. Technol.* **2002**, *30*, 56–65. [CrossRef]
158. Georgiev, M.; Pavlov, A.; Ilieva, M. Rosmarinic acid production by *Lavandula vera* MM cell suspension: The effect of temperature. *Biotechnol. Lett.* **2004**, *26*, 855–856. [CrossRef] [PubMed]
159. Ali, M.; Abbasi, B.H. Light-induced fluctuations in biomass accumulation, secondary metabolites production and antioxidant activity in cell suspension cultures of *Artemisia absinthium* L. *J. Photochem. Photobiol. B Biol.* **2014**, *140*, 223–227. [CrossRef]
160. Beigmohamadi, M.; Movafeghi, A.; Sharafi, A.; Jafari, S.; Danafar, H.; Beigmohammadi, M. Cell suspension culture of *Plumbago europaea* L. Towards production of Plumbagin. *Iran. J. Biotechnol.* **2019**, *17*, 46–54. [CrossRef] [PubMed]
161. Gallego, A.M.; Rojas, L.F.; Valencia, W.G.; Atehortúa, L.; Urrea, A.I.; Fister, A.S.; Guiltinan, M.J.; Maximova, S.N.; Pabón-Mora, N. Transcriptomic analyses of cacao flavonoids produced in photobioreactors. *BMC Genom.* **2021**, *22*, 551. [CrossRef]
162. Bong, F.J.; Subramaniam, S.; Chew, B.L. Effects of light illumination and subculture frequency on biomass production in cell suspension cultures of *Clinacanthus nutans*. *Malays. Appl. Biol.* **2021**, *50*, 197–204.
163. Zavala-Ortiz, D.; Veracruz, T.N.; Martínez-Montero, M.; Guedon, E.; Marc, A.; Ebel, B.; Barradas-Dermitz, D.; Hayward-Jones, P.; Mata-Rosas, M.; Aguilar-Uscanga, M. Interest of cellular differentiation in the production of vincristine and vinblastine in suspension cultures of *Catharanthus roseus* (L.) G Don. *Rev. Mex. Ing. Química* **2021**, *20*, 807–821. [CrossRef]
164. Andi, S.A.; Gholami, M.; Ford, C.M.; Maskani, F. Impact of light irradiance on the biosynthesis of ABA-elicited phenolic compounds in suspension-cultured *Vitis vinifera* L. cells. *Plant Cell Tissue Organ Cult.* **2021**, *146*, 387–400. [CrossRef]
165. Ali, H.; Khan, M.A.; Ullah, N.; Khan, R.S. Impacts of hormonal elicitors and photoperiod regimes on elicitation of bioactive secondary volatiles in cell cultures of *Ajuga bracteosa*. *J. Photochem. Photobiol. B Biol.* **2018**, *183*, 242–250. [CrossRef]
166. Sharifi, Y.; Omran, V.G.; Ghavami, T.S.T.; Gharakhili, A.N.; Ebrahimzadeh, M.A. Effect of Salicylic acid on Phenols and flavonoids content and DPPH scavenging activity in cell suspension culture of Iranian sodab (*Ruta graveolens*). *Tabari Biomed. Stud. Res. J.* **2020**, *1*, 18–21. [CrossRef]
167. Khoo, H.E.; Azlan, A.; Tang, S.T.; Lim, S.M. Anthocyanidins and anthocyanins: Colored pigments as food, pharmaceutical ingredients, and the potential health benefits. *Food Nutr. Res.* **2017**, *61*, 1361779. [CrossRef]
168. Zhou, H.; Purdie, J.; Wang, T.; Ouyang, A. pH measurement and a rational and practical pH control strategy for high throughput cell culture system. *Biotechnol. Prog.* **2009**, *26*, 872–880. [CrossRef]
169. Riet, K.; van der Lans, R. *Mixing in Bioreactor Vessels*; Elsevier: Amsterdam, The Netherlands, 2011; pp. 63–80.
170. Garcia-Ochoa, F.; Gomez, E.; Santos, V.E. Fluid dynamic conditions and oxygen availability effects on microbial cultures in STBR: An overview. *Biochem. Eng. J.* **2020**, *164*, 107803. [CrossRef]
171. Garcia-Ochoa, F.; Gomez, E. Bioreactor scale-up and oxygen transfer rate in microbial processes: An overview. *Biotechnol. Adv.* **2009**, *27*, 153–176. [CrossRef] [PubMed]
172. Thomas, J.A.; Liu, X.; DeVincentis, B.; Hua, H.; Yao, G.; Borys, M.C.; Aron, K.; Pendse, G. A mechanistic approach for predicting mass transfer in bioreactors. *Chem. Eng. Sci.* **2021**, *237*, 116538. [CrossRef]
173. Yela, A.C.A.; Chiquiza-Montaño, L.N.; Hoyos, R.; Orozco-Sánchez, F. Rheology and mixing analysis of plant cell cultures (*Azadirachta indica*, *Borojoa patinoi* and *Thevetia peruviana*) in shake flasks. *Biochem. Eng. J.* **2016**, *114*, 18–25. [CrossRef]
174. Khandy, M.T.; Kochkin, D.V.; Tomilova, S.V.; Klyushin, A.G.; Galishev, B.A.; Nosov, A.M. Growth and biosynthetic characteristics of *Phlojodicarpus sibiricus* cell suspension cultures. *Russ. J. Plant Physiol.* **2021**, *68*, 569–578. [CrossRef]
175. Tomilova, S.V.; Khandy, M.T.; Kochkin, D.V.; Galishev, B.A.; Klyushin, A.G.; Nosov, A.M. Effect of Synthetic Auxin analogs (2.4-D and α-NAA) on growth and biosynthetic characteristics of suspension cell culture of *Tribulus terrestris* L. *Russ. J. Plant Physiol.* **2020**, *67*, 636–645. [CrossRef]
176. Gaid, M.; Wucherpfennig, T.; Scholl, S.; Krull, R. Challenges for the Cultivation of Plant Cells on the Example of Hypericum Perforatum and Taxus Chinensis. *Ref. Ser. Phytochem.* **2016**. [CrossRef]
177. Wilson, A.S.; Cummings, E.M.; Roberts, S.C. Multi-scale engineering of plant cell cultures for promotion of specialized metabolism. *Curr. Opin. Biotechnol.* **2014**, *29*, 163–170. [CrossRef]
178. Kolewe, M.E.; Henson, M.A.; Roberts, S.C. Analysis of aggregate size as a process variable affecting paclitaxel accumulation in Taxus suspension cultures. *Biotechnol. Prog.* **2011**, *27*, 1365–1372. [CrossRef] [PubMed]
179. Satdive, R.K.; Shinde, A.N.; Singh, S.K.; Kamble, S.; Singh, S.; Malpathak, N.; Fulzele, D.P. Aggregate cell suspension cultures of *Psoralea corylifolia* improved phytoestrogens production. *Biotechnol. Bioprocess Eng.* **2015**, *20*, 373–379. [CrossRef]
180. Kieran, P.M.; Malone, D.M.; MacLoughlin, P.F. Effects of hydrodynamic and interfacial forces on plant cell suspension systems. *Mol. Biominer.* **2000**, *67*, 139–177. [CrossRef]
181. Wilson, S.A.; Maindarkar, S.N.; McKee, M.C.; Vilkhovoy, M.; Henson, M.A.; Roberts, S.C. A population balance model to modulate shear for the control of aggregation in Taxus suspension cultures. *Biotechnol. Prog.* **2020**, *36*, e2932. [CrossRef] [PubMed]
182. Titova, M.; Popova, E.; Konstantinova, S.; Kochkin, D.; Ivanov, I.; Klyushin, A.; Titova, E.; Nebera, E.; Vasilevskaya, E.; Tolmacheva, G.; et al. Suspension cell culture of *Dioscorea deltoidea*—A renewable source of biomass and Furostanol Glycosides for food and pharmaceutical industry. *Agronomy* **2021**, *11*, 394. [CrossRef]
183. Maischberger, T. Optimized process and bioreactor characterization. *Chem. Ing. Tech.* **2019**, *91*, 1719–1723. [CrossRef]
184. Yasin, M.; Jang, N.; Lee, M.; Kang, H.; Aslam, M.; Bazmi, A.A.; Chang, I.S. Bioreactors, gas delivery systems and supporting technologies for microbial synthesis gas conversion process. *Bioresour. Technol. Rep.* **2019**, *7*, 100207. [CrossRef]

185. Huang, T.-K.; McDonald, K.A. Bioreactor engineering for recombinant protein production in plant cell suspension cultures. *Biochem. Eng. J.* **2009**, *45*, 168–184. [CrossRef]
186. Martínez-Corona, J.I.; Cisneros-Garza, R.R.; Robledo-Padilla, F.; Parra, R.; Treviño-Martínez, A.S.; Alvarez, A.J. Optical approach for measuring oxygen mass transfer in stirred Tank Bioreactors. *Int. J. Chem. React. Eng.* **2017**, *15*, 15. [CrossRef]
187. Salazar-Magallón, J.A.; De La Peña, A.H. Production of antifungal saponins in an airlift bioreactor with a cell line transformed from *Solanum chrysotrichum* and its activity against strawberry phytopathogens. *Prep. Biochem. Biotechnol.* **2020**, *50*, 204–214. [CrossRef] [PubMed]
188. Busto, V.D.; Calabró-López, A.; Rodríguez-Talou, J.; Giulietti, A.M.; Merchuk, J.C. Anthraquinones production in *Rubia tinctorum* cell suspension cultures: Down scale of shear effects. *Biochem. Eng. J.* **2013**, *77*, 119–128. [CrossRef]

plants

MDPI

Article

Metamitron, a Photosynthetic Electron Transport Chain Inhibitor, Modulates the Photoprotective Mechanism of Apple Trees

Yuval Tadmor [1], Amir Raz [2,3], Shira Reikin-Barak [4], Vivek Ambastha [5], Eli Shemesh [6], Yehoram Leshem [3,5], Omer Crane [4], Raphael A. Stern [3,4], Martin Goldway [2,3], Dan Tchernov [6] and Oded Liran [1,6,*]

1 Group of Agrophysics Studies, MIGAL—Galilee Research Institute, Kiryat Shemona, Upper Galilee 11016, Israel; yuvalt@migal.org.il
2 Group of Molecular Genetics in Agriculture, MIGAL—Galilee Research Institute, Kiryat Shemona, Upper Galilee 11016, Israel; amirr@migal.org.il (A.R.); Goldway@migal.org.il (M.G.)
3 Faculty of Sciences and Technology, Tel-Hai Academic College, Kiryat-Shemona, Upper Galilee 12208, Israel; yoril@migal.org.il (Y.L.); raffi@migal.org.il (R.A.S.)
4 Northern R&D, Kiryat Shemona, Upper Galilee 11016, Israel; shirrb@gmail.com (S.R.-B.); omerc@migal.org.il (O.C.)
5 Group of Plant Development and Adaptation, MIGAL—Galilee Research Institute, Kiryat Shemona, Upper Galilee 11016, Israel; viveka@migal.org.il
6 Morris Kahn Marine Research Station, Department of Marine Biology, Leon H. Charney School of Marine Sciences, University of Haifa, Mt. Carmel, Haifa 3498838, Israel; eshemesh@univ.haifa.ac.il (E.S.); dtchernov@univ.haifa.ac.il (D.T.)
* Correspondence: odedl@migal.org.il

Citation: Tadmor, Y.; Raz, A.; Reikin-Barak, S.; Ambastha, V.; Shemesh, E.; Leshem, Y.; Crane, O.; Stern, R.A.; Goldway, M.; Tchernov, D.; et al. Metamitron, a Photosynthetic Electron Transport Chain Inhibitor, Modulates the Photoprotective Mechanism of Apple Trees. *Plants* **2021**, *10*, 2803. https://doi.org/10.3390/plants10122803

Academic Editor: Michael Moustakas

Received: 18 November 2021
Accepted: 15 December 2021
Published: 17 December 2021

Abstract: Chemical thinning of apple fruitlets is an important practice as it reduces the natural fruit load and, therefore, increases the size of the final fruit for commercial markets. In apples, one chemical thinner used is Metamitron, which is sold as the commercial product Brevis® (Adama, Ashdod, Israel). This thinner inhibits the electron transfer between Photosystem II and Quinone-b within light reactions of photosynthesis. In this study, we investigated the responses of two apple cultivars—Golden Delicious and Top Red—and photosynthetic light reactions after administration of Brevis®. The analysis revealed that the presence of the inhibitor affects both cultivars' energetic status. The kinetics of the photoprotective mechanism's sub-processes are attenuated in both cultivars, but this seems more severe in the Top Red cultivar. State transitions of the antenna and Photosystem II repair cycle are decreased substantially when the Metamitron concentration is above 0.6% in the Top Red cultivar but not in the Golden Delicious cultivar. These attenuations result from a biased absorbed energy distribution between photochemistry and photoprotection pathways in the two cultivars. We suggest that Metamitron inadvertently interacts with photoprotective mechanism-related enzymes in chloroplasts of apple tree leaves. Specifically, we hypothesize that it may interact with the kinases responsible for the induction of state transitions and the Photosystem II repair cycle.

Keywords: apple; Golden Delicious; Top Red; fruitlet thinners; photosynthesis; light reactions; electron transport rate; photoprotective mechanism; state transitions; PSII repair cycle

1. Introduction

The chemical thinning of pip fruit trees is an essential practice in agriculture as it reduces the natural fruit load, which results in larger fruits and enhanced economic value [1]. The chemical thinner's main purpose is to decrease sugar supply to the fruitlet and thus encourage it to drop [2,3]. One way to reduce carbohydrate synthesis is to use photosynthesis-related herbicides that inhibit the photosynthetic electron transport chain [2]. The most common photosynthetic herbicides include 3-(3,4-DiChlorophenyl)-1,1-diMethylUrea (DCMU, commercial name—Diuron) and 4-Amino-4,5-dihydro-3-methyl-6-phenyl-1,2,4-triazin-5-one (metamitron, commercial name—Brevis®). While DCMU has

been substantially researched over the years [4], Metamitron's mechanism of action and its correct application dosage for apple trees is still a subject of debate [5].

Most of the sunlight energy absorbed in the photosynthetic apparatus is directed towards photochemistry and Electron Transport Rate (ETR) [6]. However, not all the absorbed energy can be used. In fact, the physical properties of the chlorophyll a molecule present an inherent difficulty in the photosynthetic apparatus. When the chlorophyll holds energy for prolonged time without the ability to transfer it forward, the chlorophyll changes its chemical energetic state and may interact with molecular oxygen, a reaction that results in Reactive Oxygen Species (ROS) [7]. ROS will damage the photosynthetic apparatus, reducing its capability to synthesize sugars. Then, the photosynthetic apparatus will commence several energy dissipation processes in order to mitigate the probability to induce ROS [8].

These processes are termed Non Photochemical Quenching (NPQ) [9], and are activated in response to the duration of the stress. Essentially, there are three major processes within NPQ that are activated at different time scales:

a. Energy related (qE, several seconds) [10], responsible for the epoxidation of special carotenoids (Xanthophylls) located on the Light Harvesting Complexes (LHC, photosynthetic antenna). Upon epoxidation, these Xanthophylls change their chemical activity from light harvesting to energy dissipation and thus prevent light energy from reaching the reaction centers of PhotoSystem II (PSII).
b. State transition related (qT, minutes) [11], responsible for transition of the LHCII between the two central photosynthetic complexes—PSII and Photosystem I (PSI). This results in a different allocation of absorbed energy between the two photosystems and reduces the damage to PSII.
c. Photoinhibition dependent (qI, hours) [12], with prolonged stress, ROS will eventually accumulate in the vicinity of PSII and destroy the D1 subunit an important component of the reaction center [13]. The destruction of D1 results in a non-active PSII. The damaged D1 are marked for replacement via a regulated process that replaces the damaged unit with a de novo synthesized copy [14].

At the molecular level, two out of the three NPQ processes involve phosphorylation kinases of the State TraNsition (STN) family [15,16]. The first process is LHCII transfer between the reaction centers. Upon excess illumination, the trans-thylakoid membrane potential increases, and this induces STN7 activity [17]. Then, this kinase phosphorylates LHCII which results in the disconnection from PSII supercomplexes [15]. In the second process, the PSII repair cycle is comprised of a distinct set of steps which enables a rapid replacement of damaged D1 subunit [18]. PSII supercomplexes with damaged D1 are designated for a repair through phosphorylation via the STN8 pathway [16]. Then, a set of serine proteases cleave the transmembrane Psb-a protein (D1) at specific locations, thus exposing it to the repair complex [13].

When an ETR herbicide is applied, the absorbed light energy cannot be utilized in the light reactions. This event increases the probability of ROS accumulation, and damage to PSII. In fact, using such specific PSII inhibitors signals to the photosynthetic apparatus that the electron transport chain is reduced downstream PSII. This state mimics photosynthetic stress which, in turn, induces the photoprotective mechanisms [19,20]. Characterizing the response of the photosynthesis physiology in the presence of the inhibitor can then be performed with chlorophyll fluorescence methods [21,22]. These incorporate the fact that the photochemistry is linked to fluorescence emission via the interplay between the three fates of energy utilization within the apparatus—photochemistry, heat dissipation and fluorescence emission [6]. The most common examination includes a light response curve that examines the magnitude of the electron transport rate against a gradient of light intensities [23]. This curve includes several key parameters that explain the response of the apparatus to light: a. Light Use Efficiency (LUE)—the initial linear slope receives units of electrons excited in photochemistry to the amount of photons absorbed in the process [24,25]; b. The concave part of the curve marks the transition between photo-

chemical to non-photochemical energy quenching, where absorbed energy is also being dissipated by other photoprotective mechanisms [26] to photochemistry [27]. Additional examinations using chlorophyll fluorescence include, but are not limited to, electron transitions within the PSII complex itself (OJIP test—[28]), and determining energy distribution between photochemistry and non-photochemical processes [29].

In this study, we report that Metamitron, an electron transport chain inhibitor, obtains an additional activity on top of its primary role. It interacts with the photoprotective mechanism of apple trees. We present evidence of two additional activities: it promotes a forced state transition of LHCII to PSI site in Top Red (TR) but not Golden Delicious (GD) cultivars; and interferes with the PSII repair cycle in both cultivars. These actions force the apparatus off balance which results in an unexpected photosynthetic physiology after Metamitron application.

2. Results

2.1. Parameterization of Light Response Curves of Two Cultivars of Apple Trees Leaves

Light response curves of PSII activity were performed with a background of Brevis® in order to characterize the photosynthetic response to a block at the PSII site. Light response curves of GD (Figure 1A) exhibited a logarithmic response for the control group with the ETR reaching up to 60 μmol e^- m^{-2} s^{-1}. The initial linear slope stretches until 100 μmol photons m^{-2} s^{-1}, at which point the concave part of the curve starts to level out at 300 μmol photons m^{-2} s^{-1} towards its maximum activity. An increase in the inhibitor concentration results in a gradual decrease of the curve's plateau. At 0.64% inhibitor concentration, the curve reaches a local maximum at 300 μmol photons m^{-2} s^{-1} and rapidly declines to zero, and at a concentration of 1.28% of inhibitor, there is no viable ETR at any light intensity. Light Use Efficiency (LUE), the initial linear slope of the light response curve (Figure 1B) of GD, shows a logarithmic decay towards the minimum LUE and then levels out at and above 0.32% inhibitor concentration. The LUE does not reach a zero rate, even at a concentration of 0.64–1.28% inhibitor. This means that at very low light intensities, there is still a minimum photosynthetic rate in the presence of the inhibitor. Effective antenna size (Figure 1C) presented a sigmoid behavior. The inflection point is found within the range of 0.08% to 0.16% inhibitor concentration, concomitant with a statistically significant decrease in the LUE data for this cultivar. Maximum photosynthetic activity (Figure 1D) presented a rate of logarithmic decay with a complete arrest in activity at the two highest inhibitor concentrations, as expected.

The TR (Figure 2A) ETR response to the Brevis® inhibitor gradient was much more disorganized than that recorded for the GD cultivar. In the light response curve graph, there seems to be two groups of responses: below and above 0.16% inhibitor concentration. The light response curves for the control and the first group, presented a steeper increase in electron transport rate when compared with the same increase in the GD cultivar. Then, the activity reaches a maximum on the concave part of the curve at 500 μmol photons m^{-2} s^{-1} and not on the plateau. Finally, the curve starts to decline with greater light intensity, implying for development of photoinhibition of the TR cultivar at light intensities above 1000 μmol photons m^{-2} s^{-1}. Additionally, the maximum activity reached was ~44 μmol e^- m^{-2} s^{-1} which is 75% of the maximum activity of the GD. With increase in inhibitor concentration, the curve magnitude decreases. The ETR curve does not reach zero in presence of even the highest inhibitor concentration. In fact, at 1.28% inhibitor concentration, the maximum rate reaches a higher activity than the 0.64% inhibitor concentration-related curve. When inspecting the LUE data (Figure 2B), the two groups are visible as expected, with the 0.16% inhibitor concentration corresponding statistically to the second group, that of the 0.32% inhibition concentration. There was no statistically significant difference between the LUE in the first group, as expected. Moreover, there was no gradual decrease in the efficiency. It seems as if above 0.16% inhibitor concentration, there is a "breaking point" and a forced decrease in the performance of PSII activity. When analyzing the effective antenna size (Figure 2C), there seems to be no organized decline

with increasing concentration of the inhibitor, and on top of that, there is no statistical significance between the responses. This implies that the inhibitor interferes with some regulation pathway in control of the reactivity of PSII antenna to attenuation in light intensities. Finally, the maximum activity of TR (Figure 2D) is also divided into two activity groups, where each group has a similar appearance within themselves with no statistically significant difference. The only difference found between the two groups was the "breaking point" above 0.16% inhibitor concentration. Here, activity decreased to ~25% of the control sample activity. However, as seen for the ETR, this does not completely inhibit the activity of PSII.

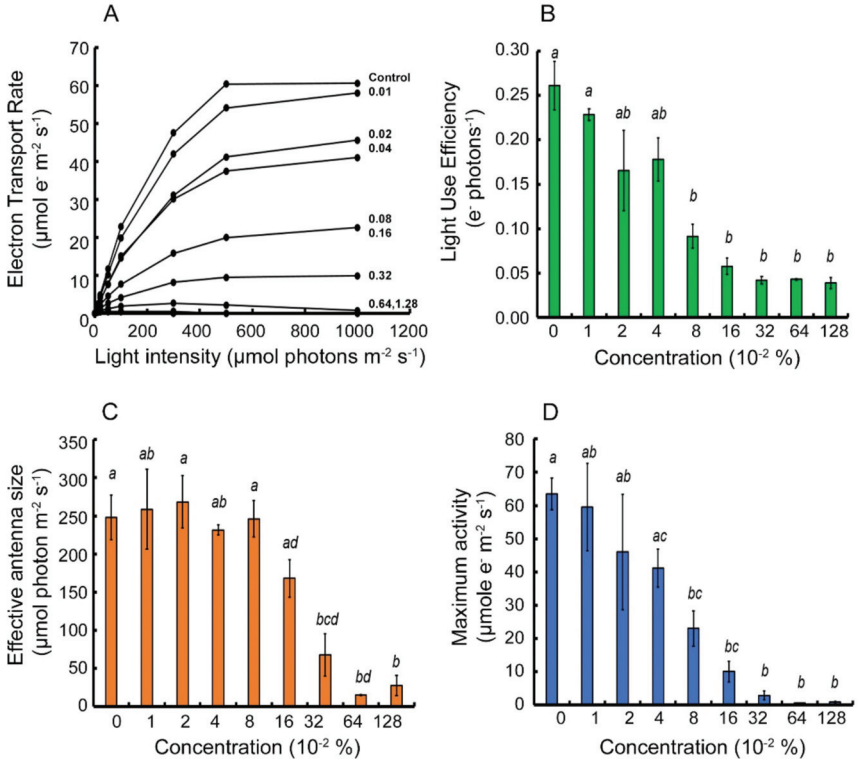

Figure 1. Parameterization of light response curves of Apple (*Malus domestica*) cultivar "Golden Delicious" that experienced a Brevis® inhibitor gradient for 2 days under laboratory conditions. Panel (**A**) represents light response curves data. Panels (**B**–**D**) represent the parametrization variables-Light Use Efficiency (LUE) (green), Effective antenna size (orange), and maximum Electron Transport Rate (ETR) (blue), respectively. Each column is an average of three biological repeats. Error bars represent standard error of the mean. Amount of inhibitor is given in percentage. Letter notations describe statistically significant difference at $p < 0.05$.

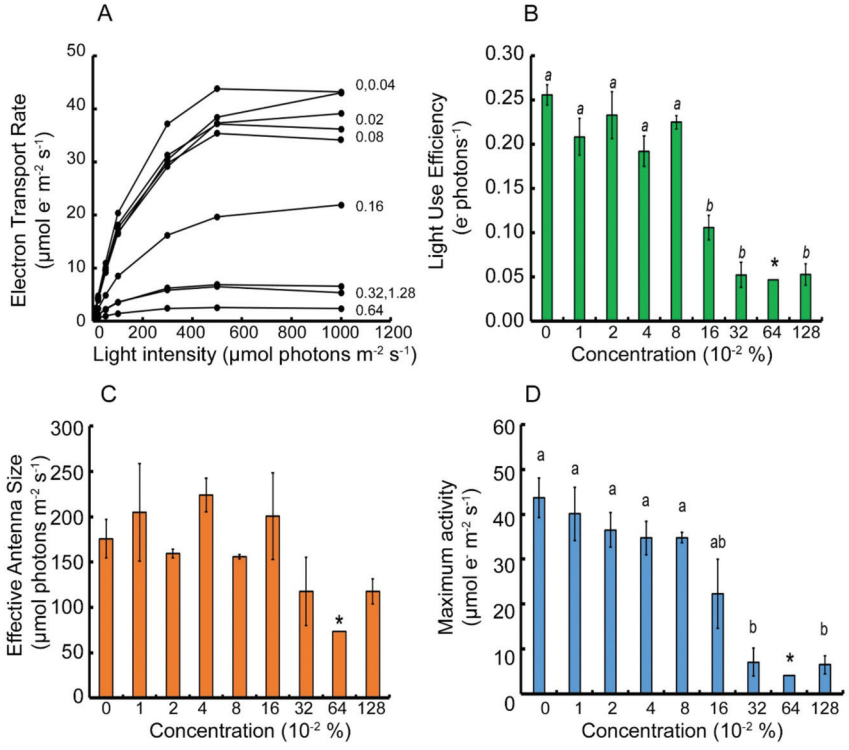

Figure 2. Parameterization of light response curves of Apple (*Malus domestica*) cultivar "Top Red" that experienced a Brevis® inhibitor gradient for 2 days under laboratory conditions. Panel (**A**) represents light response curves data. Panels (**B**–**D**) represent the parametrization variables-Light Use Efficiency (LUE) (green), Effective antenna size (orange), and maximum Electron Transport Rate (ETR) (blue), respectively. The asterisk in the panels represent two biological repeats only, therefore no error bars are present. Each column is an average of three biological repeats. Error bars represent standard error of the mean. Inhibitor is given in percentage. Letter notations describe statistically significant difference at $p < 0.05$.

2.2. Analysis of the Photoprotective Mechanism's Response to the Metamitron Inhibitor

The yield of each of the three outcomes of light energy utilization by the photosynthetic apparatus was suggested by formulations in Kramer et al. (2004) (Figure 3). The yield of energy distribution was performed for the two apple cultivars, GD and TR, for the data recorded on the light response curve at three light intensities (Figure 3): a. 50 µmol photons m^{-2} s^{-1} (Figure 3A,B) which is found at the range of the initial linear slope of both of the cultivars and therefore relates to the LUE; b. 300 µmol photons m^{-2} s^{-1} (Figure 3C,D) which is found at the concave part of the curve and therefore relates to the antenna size attenuations of each cultivar; c. 1000 µmol photons m^{-2} s^{-1} (Figure 3E,F) which relates to the maximum ETR for each cultivar measured in this study.

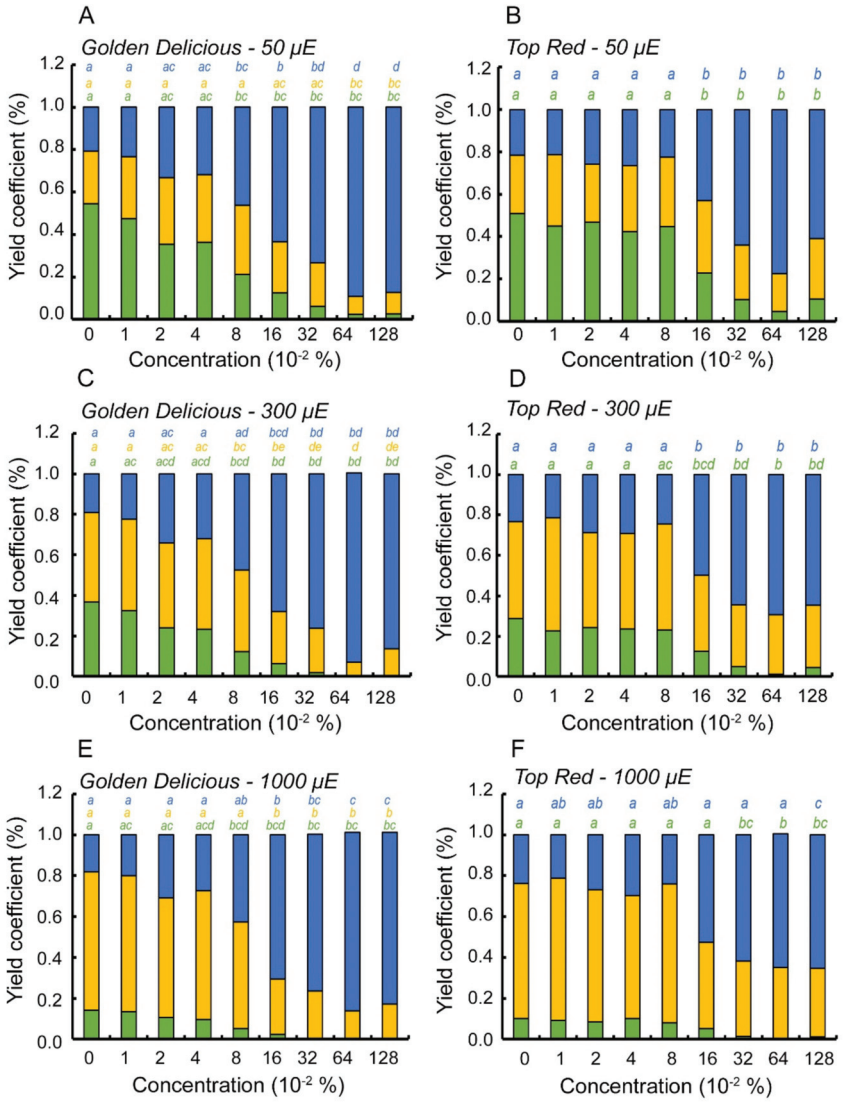

Figure 3. Quantum yields of absorbed energy distribution between the three outcomes of light energy utilization in two apple cultivars with Brevis® inhibitor. Panels (**A**,**C**,**E**) and (**B**,**D**,**F**) represent results of light energy utilization distribution analysis across three light intensities extracted from the light response curve, for Golden Delicious and Top Red cultivars, respectively. Each column comprises three stacked bars which are summed to 1. The colors green, yellow and blue represent effective quantum yield of PSII photochemistry (Φ_{PSII}), quantum yield of regulated non-photochemical energy loss in PSII (Φ_{NPQ}) and quantum yield of non-regulated energy loss in PSII (Φ_{NO}), respectively. Each bar represents three biological repeats. Letter notations describe statistically significant differences ($p < 0.05$). µE is µmol photon m^{-2} s^{-1}.

The control group for GD at each of the three light intensities (Figure 3A,C,F, leftmost bar) presented a classic energy yield distribution, where at 50 µmol photons m^{-2} s^{-1}, 60% of the energy was diverted to photochemistry (green fraction of the bar, Φ_{II}). This fraction of quantum yield decreases with an increase in light intensity until 1000 µmol photons m^{-2} s^{-1},

where the photochemistry yield reached below 20% (green fraction of the leftmost bar at Figure 3F). The quantum yield of regulated non-photochemical energy loss in PSII (Φ_{NPQ}) increases with light intensity in the control up to 60% of the total absorbed energy at maximum light intensity (yellow fraction of the leftmost bar at Figure 3E). The fraction of energy lost by non-regulated processes in PSII (Φ_{NO}) (blue fraction of the leftmost bar in the three panels, Figure 3A,C,E), remains constant at the 20% mark for each light intensity; this implies that under natural conditions, the ROS scavenging mechanism is efficient for this cultivar. With increasing concentration of the inhibitor there is a gradual decline in the photochemistry quantum yield for each of the three light intensities. The energy is diverted to the non-regulated loss of energy in PSII (Φ_{NO}) and implies that the accumulation of triplet chlorophylls is expected (see the blue fraction of bars in each of the panels Figure 3A,C,E). The regulated non-photochemical energy loss in PSII (Φ_{NPQ}) shows a statistically significant attenuation when passing the 0.08–0.16% of inhibitor concentration (note the yellow lettering in Figure 3A,C,E), as expected.

The energetic distribution between the three outcomes of light energy utilization in the case of the TR cultivar presented similar apparatus behavior from the control to that of the GD cultivar (Figure 3B,D,F). The energy lost by the non-regulated processes was slightly increased at 300 μmol photons m^{-2} s^{-1} when compared with that of the GD. The same phenomenon of energy lost by non-regulated NPQ, with increase in the concentration of the inhibitor, is seen for the TR when compared to the GD. However, one striking difference between the two cultivars is that there was no statistically significant difference between the yield of energy diverted to the regulated NPQ in any of the inhibitor concentration (note that there is almost no difference in magnitude of the yellow fraction of the bars in any of the three light intensities-Figure 3B,D,F). In addition, in TR and as seen before, there was no gradual decline in either of the three yields after an increase in inhibitor concentration. Instead, there is a "breaking point" between 0.08% to 0.16% inhibitor concentrations. The two groups below and above this threshold are significantly different from each other.

In order to explain the differences of allocated absorbed energy to the regulated non-photochemical energy loss in PSII (Φ_{NPQ}) process between the two cultivars (yellow fraction of bars in Figure 3), we analyzed the relaxation kinetics of each of the photoprotective mechanisms of NPQ. That is, energy dependent quenching (qE), state transition dependent quenching (qT) and photoinhibition dependent quenching (qI) were examined against the background of the inhibitor gradient (Tables 1 and 2 for GD and TR, respectively). The quenching values of each process were assessed over 10 days after application of the inhibitor, so as to track the response of the photoprotective mechanism along the natural decomposition rate of the inhibitor. The data presented on day 2 relates to the analysis performed in the previous steps shown. In the case of GD (Table 1), there was no difference between the dates for the level of energy dependent quenching (qE). This was expected, since there was no trans-thylakoid membrane potential created due to the presence of the inhibitor. There was a slight increasing trend each day, which may imply a generation of a proton potential gradient due to cyclic electron transport. The only statistically significant difference was found on the second day after application, where the energetic state was different between the 0.01% and 0.05% inhibitor concentrations. The state transition dependent quenching mechanism (Table 1, qT column) increased with inhibitor concentration, as expected due to the inhibition of electron transport downstream PSII. There was a statistically significant difference between the control and maximum inhibitor concentration, which implies that antennas are transferred from the PSII to the PSI site in order to reduce absorbed light energy reaching the PSII reaction center. Here, again the significant difference was present only two days after spraying, where the rest of the time there was no statistically significant difference. This implies a desensitizing effect of the inhibitor on the process. Eventually, the photoinhibition dependent quenching (Table 1, qI column) showed a decline in values with increasing concentration of the inhibitor. This increase was not statistically different on any of the dates except the second day after application. This is a surprising result, as the repair cycle does not increase its activity

in the presence of the PSII inhibitor, which exposes the complex to an elevated level of absorbed energy. This increases the probability of ROS accumulation in the reaction center vicinity and therefore requires a replacement of damaged subunits. This also implies a desensitization of this mechanism by the inhibitor.

Table 1: Quantum yield of the photoprotective pathways of apple cultivar "Golden Delicious" on the background of Brevis® inhibitor gradient and over time. Each value is an average of three biological repeats performed in duplicates, and the error values are standard error of the mean. Letter notations describe statistically significant difference ($p < 0.05$).

Days	Concentration (%)	Quantum Yield of Process ‡		
		qE	qT	qI
2	0	0.156 ± 0.090 ^{ab}	0.096 ± 0.012 ^{a}	0.536 ± 0.120 ^{ab}
	0.01	0.143 ± 0.032 ^{a}	0.136 ± 0.011 ^{ab}	0.473 ± 0.049 ^{a}
	0.05	0.336 ± 0.016 ^{b}	0.166 ± 0.005 ^{b}	0.257 ± 0.023 ^{b}
	0.5	0.227 ± 0.027 ^{ab}	0.154 ± 0.011 ^{b}	0.411± 0.039 ^{ab}
5	0	0.278 ± 0.081	0.149 ± 0.045	0.520 ± 0.186
	0.01	0.134 ± 0.076	0.105 ± 0.023	0.527 ± 0.132
	0.05	0.223 ± 0.022	0.171 ± 0.024	0.439 ± 0.076
	0.5	0.255 ± 0.045	0.189 ± 0.010	0.389 ± 0.068
7	0	0.114 ± 0.026	0.132 ± 0.027	0.710 ± 0.245
	0.01	0.063 ± 0.033	0.094 ± 0.034	0.521 ± 0.080
	0.05	0.168 ± 0.046	0.176 ± 0.033	0.524 ± 0.093
	0.5	0.152 ± 0.028	0.176 ± 0.014	0.498 ± 0.008
10	0	0.087 ± 0.012	0.129 ± 0.017	0.471 ± 0.030
	0.01	0.121 ± 0.020	0.127 ± 0.024	0.484 ± 0.038
	0.05	0.161 ± 0.020	0.173 ± 0.007	0.439 ± 0.022
	0.5	0.166 ± 0.033	0.170 ± 0.08	0.466 ± 0.042

‡ qE-Energy dependent quenching, qT-State transition dependent quenching, qI-photoinhibition dependent quenching.

The TR cultivar presents a different, and to some extent opposite, behavior to the GD cultivar performance with respect to its photoprotective mechanisms (Table 2). The energetic dependent quenching of the TR (Table 2, qE column) increases with increasing concentration of the inhibitor. Although there is no statistical significance between the inhibitor concentration responses, it seems that the trans-thylakoid membrane potential increases, which implies for increased cyclic electron transport. This is because the inhibitor blocks electron transport downstream PSII, so the only source of electrons during the light period may be that of the PSI. The state transition dependent quenching magnitude (Table 2, qT column) decreases substantially with increasing concentration of the inhibitor for each time instance, implying a desensitization of the process with the application of the inhibitor. This, in fact, is surprising and requires an explanation for which of the two photosystems the antenna is found in this case. The only significant difference is found on the 5th day, but this trend repeats itself along the whole 10-day range. These results corroborate the decrease in magnitude of energy allocated to the regulated non-photochemical energy loss in PSII (Φ_{NPQ}) process as analyzed in the previous step (Figure 3B). Finally, the photoinhibition dependent quenching of TR (Table 2, qI column) seems to relax with increasing concentration of the inhibitor up until the 5th day after application. Starting at the 7th day, there is a flip in the reactivity of this process, whereby the qI portion increases with increase in inhibitor concentration, probably due to the natural degradation of the inhibitor. The fact that there is a decrease in qI fraction during the first days after application, implies a desensitization of this process, because if the inhibitor concentration is higher, then more PSII complexes are blocked, and more energy is lost to the non-regulated dissipation mechanism (Figure 3, blue portion of graph in panels 3A, C, E). This behavior is not seen in the case of the GD as mentioned, and it also implies that a

modulated repair mechanism of PSII in this cultivar may affect both the characteristics of electron transport rate and, by that, the quantum yield distribution profile as seen in the previous steps.

Table 2: Quantum yield of the photoprotective pathways of apple trees "Top Red" on the background of Brevis® inhibitor gradient with time. Each value is an average of three biological repeats performed in duplicates, and the error values are standard error of the mean. Letter notation describe statistically significant difference at $p < 0.05$.

Days	Concentration (%)	Quantum Yield of Process ‡		
		qE	qT	qI
2	0	0.165 ± 0.003	0.140 ± 0.009	0.465 ± 0.028 [a]
	0.01	0.194 ± 0.030	0.135 ± 0.014	0.430 ± 0.048 [a]
	0.05	0.198 ± 0.022	0.138 ± 0.004	0.437 ± 0.028 [a]
	0.5	0.241 ± 0.061	0.099 ± 0.048	0.285 ± 0.069 [b]
5	0	0.149 ± 0.006	0.148 ± 0.017 [a]	0.471 ± 0.044 [a]
	0.01	0.123 ± 0.006	0.133 ± 0.004 [a]	0.500 ± 0.002 [a]
	0.05	0.143 ± 0.015	0.130 ± 0.012 [a]	0.535 ± 0.036 [a]
	0.5	0.199 ± 0.060	0.067 ± 0.020 [b]	0.243 ± 0.015 [b]
7	0	0.145 ± 0.018	0.154 ± 0.014	0.455 ± 0.032
	0.01	0.116 ± 0.040	0.122 ± 0.017	0.528 ± 0.073
	0.05	0.151 ± 0.025	0.160 ± 0.022	0.439 ± 0.060
	0.5	0.263 ± 0.087	0.133 ± 0.042	0.509 ± 0.133
10	0	0.040 ± 0.018	0.059 ± 0.019	0.534 ± 0.029 [a]
	0.01	0.062 ± 0.018	0.089 ± 0.008	0.581 ± 0.005 [a]
	0.05	0.045 ± 0.041	0.078 ± 0.033	0.626 ± 0.038 [a]
	0.5	0.039 ± 0.022	0.033 ± 0.011	1.046 ± 0.121 [b]

‡ qE-Energy dependent quenching, qT-State transition dependent quenching, qI-Photoinhibition dependent quenching.

2.3. Metamitron Interferes with the Photoprotective Mechanism in Apple Trees

In view of the attenuated performance of both the state transitions and photoinhibition dependent quenching, a 77K fluorescence was analyzed. The 77K fluorescence spectrum presented a difference in fluorescent peak magnitudes of PSII (685 nm) and PSI (720–740 nm) in relation to the location of the antenna complex LHCII (Figure 4). GD that was exposed to a 0.6% inhibitor concentration presented a slight increase in the PSI peak over that of PSII (Figure 4A, green curve). This implies that there was an event of state transition after application of the inhibitor. Addition of DCMU, an inhibitor with similar mechanism of activity, did not show this phenomenon (Figure 4A, red curve). This implies that this phenotype is related only to Metamitron presence. There was almost no difference between these spectra and the control which was sprayed only with water (Figure 4A, blue curve). Contrary to this, the TR cultivar presented a very different fluorescence spectrum when Metamitron was applied (Figure 4B, green curve). Here, there was a very high magnitude in the fluorescence emitted from PSI—an increase in 15% fluorescence than PSII, which was not visible for GD and also not seen for TR when applied with DCMU (Figure 4B, compare green and red curves). There was a slight expansion of the PSI peak in the case of TR applied with DCMU, but this was not significant when compared to the control (Figure 4B, blue curve). These results imply that Metamitron encourages the transition state between the two photosystems when the apparatus was trying to avoid ROS accumulation in the vicinity of PSII, and the transfer of the antenna to PSI. These results corroborate the characteristics of the light response curve seen in Figure 2, where there was no statistical significance between the 0.64% and the control treatment. This suggests that the apparatus of at least the TR cultivar cannot regulate this process within the photoprotective mechanism when the Metamitron inhibitor is applied.

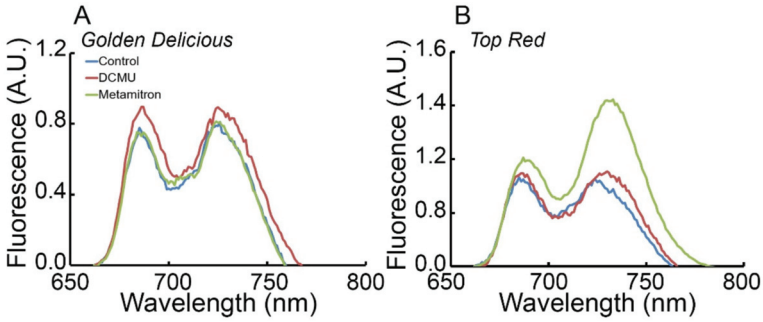

Figure 4. The 77K fluorescence spectra of apple tree leaves of two cultivars experiencing photosynthetic inhibition by Metamitron. Panels (**A**,**B**) represent Golden Delicious and Top Red cultivars, respectively. There are three treatments in each panel-control (only buffer), 3-(3,4-dichlorophenyl)-1,1-dimethylurea (DCMU), 4-Amino-4,5-dihydro-3-methyl-6-phenyl-1,2,4-triazin-5-one (Metamitron) in colors of Blue, Magenta and Green, respectively. Each curve is an average of three biological repeats.

In view of the desensitization of the repair cycle of PSII in the TR cultivar, a Western blot analysis was performed on the D1 subunits with and without phosphorylation, to understand the dynamics between damaged D1 sent for degradation and the de novo synthesis of the new copy. In addition to these, OEC-33 scaffold subunit (Psb-O) was also checked, as it is very sensitive to the presence of ROS. In the case of GD (Figure 5A), non-phosphorylated Psb-a subunit (D1) shows a uniform appearance throughout all the concentrations of the inhibitor, and the same as the control (Figure 5A, upper panel). Phosphorylated Psb-a* showed strong bands in the control for both non-cleaved Psb-a* (35 kda) and cleaved product Psb-a* (25 kda). However, with increase in inhibitor concentration, GD's cleaved Psb-a* decreased almost completely at 0.01% of the inhibitor (Figure 5A, middle panel), while the non-cleaved product was present at the same strength of the control only at the lower inhibitor concentrations. In the rest of the lanes, this subunit and cleavage product were very faint. The cleaved product of GD's Psb-a* disappears completely above the concentration of 0.16%. The Psb-O subunit was also presented uniformly in the case of GD (Figure 5A, lower panel), despite very faint lines of cleaved product below the 35 kda band and between 0.01% and 0.08% inhibitor concentration.

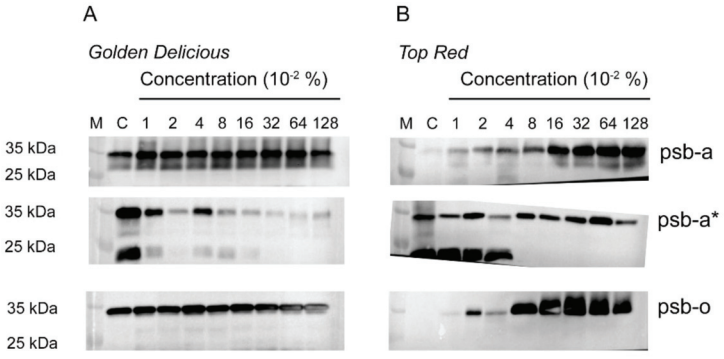

Figure 5. Western blot of three subunits of PSII for two apple cultivars exposed to a concentration gradient of the Brevis® inhibitor. Panels (**A**,**B**) represent information for Golden Delicious and Top Red cultivars, respectively. Each sample includes three different leaf extracts. Psb-a, psb-a* and psb-o stand for D1, D1-phosphorylated and OEC-33 (Oxygen Evolving Center) subunits of PSII. M, C are Marker and Control (without Brevis), respectively.

The TR cultivar presented an arrested repair cycle of Psb-a (Figure 5B, upper panel). The control showed only a faint accumulation of Psb-a in contrast to the accumulation of this subunit which started at 0.01% inhibitor concentration; this increased substantially starting from the 0.16% inhibitor concentration. This implies that de novo copies of Psb-a are accumulated but may not be inserted into the thylakoid membrane. Phosphorylated Psb-a* presented a similar behavior between the control (where strong bands occur both for the intact and cleaved fragment). Starting from 0.08%, there was a complete disappearance of the cleaved product of Psb-a*. Instead, there was a mirror representation of the phosphorylated, non-cleaved Psb-a*. This implies that the non-cleaved phosphorylated subunit was not removed from the damaged PSII. This also explains the accumulation of the de novo synthesized copies recorded (compare Figure 5B upper and middle panels). Finally, the Psb-O subunit deteriorates starting at 0.08%, where a smear of the protein is visible (Figure 5B lower panel). This goes in line with the fact that damaged Psb-a* are not cleaved and thus are not being sent out of the PSII complex; this results in accumulation of ROS. Altogether, these results point to the fact that Metamitron interacts with at least two photoprotection mechanisms pathways and modulates their activity.

3. Discussion

This study provides evidence that Brevis® (Adama, Israel), a Metamitron-based commercial chemical thinner, which is used as an inhibitor of the photosynthetic electron transport chain, interacts with the photoprotective mechanism of the photosynthetic apparatus of both apple cultivars Golden Delicious (GD) and Top Red (TR). Several photosynthetic physiological protocols were performed and provide proof that Metamitron suppresses the PSII repair cycle and forces a state transition of LHCII from PSII to PSI. These secondary activities related to the inhibitor, affect each of the photoprotective and light harvesting processes within the chloroplasts of TR. GD apparatus is also affected by the inhibitor, however to a lesser extent. The damaged D1 subunits of TR are accumulating within the thylakoid membranes in application of at least 0.08% inhibitor, and this results in accumulated ROS that disintegrates the Psb-O subunit (Figure 5B, lower panel). The Psb-O band profile in the gel is a sensitive marker for ROS accumulation within the chloroplasts, as was first suggested by Henmi et al. (2004) [30]. In their work, the researchers noted a degradation of Psb-O in response to very high light stress on the apparatus; they suggested that this degradation was caused by ROS. In the current study, there is a smear behavior seen in the gel of Psb-O when the inhibitor reaches above 0.04%, corroborating the damage by ROS in this cultivar. The accumulation of ROS at the vicinity of PSII encourages the LHCII to transfer to PSI in order to minimize energy flowing towards PSII (Figure 4B); this should decrease the accumulation of ROS [9]. In turn, the accumulation of ROS in the vicinity of PSII in the TR affects the response of this cultivar to increased light intensities on the background of the inhibitor. First, the relaxation of the repair cycle of TR is silenced as the inhibitor concentration increases (Table 2, photoinhibition dependent quenching (qI column)), and the qT state transition dependent quenching decreases as well, implying that after the forced transfer, the apparatus is stuck in this position (Table 2, qT column). This results in a non-statistically significant difference in antenna size in the case of the TR cultivar (Figure 2C). It also explains why there is no complete arrest of photosynthetic activity regardless of the very high concentration of the inhibitor (Figure 2A,D). This is probably since damaged PSII continues to work partially and are not being repaired. Rosa et al. (2021) show that at 0.2% administration of Metamitron in apple trees the ROS scavenging pathway is activated [4] This corroborates our findings that depend on a much higher concentration of Metamitron, and imply that ROS may indeed increase, which is verified on PSII complex molecular level. The modulation of photoprotective mechanisms was less indicative in the case of GD, although the fragmented D1 disappeared at the lowest concentration of the inhibitor (Figure 5A). In the GD case, the photoprotective mechanisms kept operating despite the attenuated performance of the repair cycle of damaged PSII. The gradual diversion of energy from regulated non-photochemical energy loss in PSII (Φ_{NPQ})

to non-regulated loss of energy in PSII (Φ_{NO}) is already documented and corroborated by the study of Klughammer and Schreiber (2008). In their paper, the researchers explain that with the closure of PSII and the decrease of the maximum fluorescence signal, most of the absorbed energy is diverted to non-regulated processes such as thermal decay, triplet chlorophyll, etc. Moreover, Wen et al. (2021) present evidence that in the model organism *Arabidopsis thaliana*, Deg-1 serine protease which is responsible for the cleavage of the phosphorylated Psb-a* is silenced, there is a marked decline in the electron transport rate [31]. Therefore, with an increase in inhibitor concentration there is a higher probability of the increase in ROS which interacts with the excited triplet chlorophyll within PSII. Finally, the light response curve of the GD is not harmed as expected in view of the intact Psb-a units (Figure 5A). GD presented a concave profile of carbon assimilation towards 1000 μmol photons m^{-2} s^{-1} [32], while other cultivars were shown to reach maximum photosynthetic activity already at 300 μmol photons m^{-2} s^{-1} [33]; both corroborate our results.

We therefore suggest that the commercial product Brevis® interacts with at least two different photoprotective mechanisms of apple trees—the state transition and repair cycle of PSII. We suspect that this interaction may involve the STN kinases as both photoprotective mechanisms involved with these enzymes were affected by the presence of the inhibitor (Figure 6). Therefore, applying Metamitron affects not only electron transport rate out of PSII, but also modulates the photoprotection mechanism. In turn, this attenuates the capability of the apple trees to defend themselves from photosynthetic stress when applied with the Metamitron-based inhibitors.

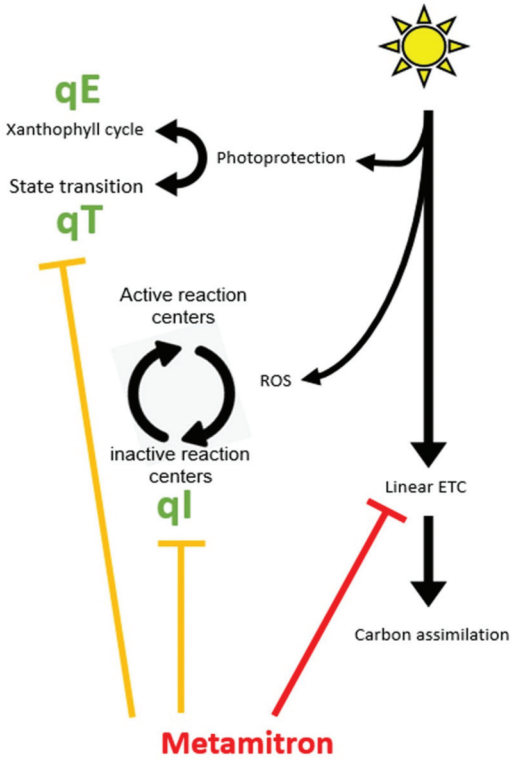

Figure 6. Metamitron activity model in view of this study. ETC refers to Electron Transport Chain. The bold red line represents the Metamitron primary mode of action blocking electron transport rate, and the bold orange lines represent its secondary activity, as revealed in this study.

The main limitation of this study is the fact that, except for the DCMU-positive control during the 77K fluorescence assay, we did not compare the commercial inhibitor activity to that of the pure substances Metamitron (4-Amino-4,5-dihydro-3-methyl-6-phenyl-1,2,4-triazin-5-one) and to DCMU (3-(3,4-dichlorophenyl)-1,1-dimethylurea). However, the analysis of an OJIP test (Supplementary Figure S1) that examines the extent of inhibition within PSII on a gradient of inhibitor concentrations, was similar to the evidence presented by Abbaspoor et al. (2006). Moreover, there is a large body of evidence for this commercial inhibitor in relation to PSII inhibition [5,34], specifically in apple trees. In the case of DCMU, the non-regulated loss of energy in PSII (Φ_{NO}) increases with inhibitor concentration and decreases the photochemical activity as shown in other studies [35,36]. An additional limitation is the fact that we did not corroborate the results of this study in outdoor conditions. The fact that the commercial inhibitor is metabolized with time in the plant tissues, together with the different activity profile between TR and GD, requires future study. Specifically, studying the attenuation over time of the inhibition under field conditions with the natural degradation of the inhibitor. Secondly, there was a discrepancy between the increase in inhibitor concentration and the decline in the regulated NPQ process, but there was a statistically significant increase in the qT portion in GD (Figure 3E compared to Table 1). We explain this discrepancy as such: while the photosynthetic apparatus cannot use the regulated NPQ processes, the antennas are still stuck in state-2 transition (on PSI, Figure 4B), so the relaxation for this process is prolonged. In addition, the other two quenching processes (Table 1, qE and qI) are not statistically significant. This corroborates the decline in the overall NPQ activity and was translated as a decrease in its quantum yield portion, as seen in Figure 3E for GD.

Lastly, it is noted that the greatest activity of this inhibitor under outdoor conditions occurred when the apple trees were shaded [37]. The evidence brought forth in this study provides an explanation why this is the case. This is because when the trees are shaded, there is less chance that the photosynthetic apparatus will push for induction of photoprotective pathways. Therefore, there would be less interaction between Brevis® and the induced photoprotective enzymatic cascades. This lets the inhibitor perform its primary task, which is to inhibit the ETR within the photosynthetic apparatus and to reduce sugar synthesis.

Practical implication of the secondary activity of Metamitron will be to incorporate it into carbon balance models that predict the efficacy of fruitlet thinning depending on light and temperature [38]. The data gathered in this study should be considered to determine the optimal concentration of the inhibitor and its application timing. Under high irradiance, there is a higher chance that the Metamitron would interact with other components within the photosynthetic apparatus and attenuate the tree's response to photosynthetic stress. At the crop level, it would be beneficial to research the response of other apple cultivars to Metamitron with respect to the photoprotective mechanisms within photosynthesis. This will expand our understanding of the different phenotypes of photoprotection within apple cultivars and contribute to our overall understanding of photosynthetic activity and photoprotection in this species. As Metamitron is being gradually introduced into other fruit species—e.g., citrus [39], peach [40], pears [41]—it will be beneficial to examine Metamitron reactivity with the photoprotective mechanisms of other fruit species as well. Finally, the reactivity of the photoprotective mechanisms to the inhibition of the ETR, as suggested in this study may be merely an extreme reaction of the NPQ pathways to the presence of the inhibitor, yet, both effects seen in the photoprotection are governed by the same family of kinases—STN8, which induces the serine protease responsible for cleavage of D1 and STN7 for phosphorylation of the LHC. It was implied that it interacts specifically with enzymes of this family. We, therefore, suggest to conduct a molecular investigation in order to establish a mechanistic model for Metamitron modulation of the respected cascades and to expand our understanding of its mode of action within the photosynthetic apparatus.

4. Materials and Methods

4.1. Plant Material & Chemicals Application

The experiment was conducted on two apple cultivars 'Golden Delicious' (GD) and 'Top Red' (TR), from the Fichman experimental farm in Israel (33.13199, 35.8059; *Malus domestica Bork.*). Branches were cut when fruitlet diameter was between 6–8 mm, corresponding to nine days after full bloom. The branches were acclimated for 24 h prior to experimentation in a growing room kept at 24.5 °C with 50 µmol photon m^{-2} s^{-1} cool white fluorescence light (OSRAM L36, W/840) and a 16:8 light:dark cycle. Each vase included three branches from three different trees of one cultivar in the experimental farms, for a total of 18 vases and 54 branches total for the two cultivars. Brevis® (ADAMA, Ashdod, Israel) consists of a 15% active ingredient Metamitron (4-Amino-3-methyl-6-phenyl-1,2,4-triazin-5-one) that was dissolved in Double Distilled Water (DDW) according to the manufacturer instructions. A set of nine different concentrations were prepared in 1 L volumes: control (only DDW), 0.01%, 0.02%, 0.04%, 0.08%, 0.16%, 0.32%, 0.64% and 1.28%; these were sprayed in the morning after the 24 h acclimation in the growth chamber.

4.2. Chlorophyll a Fluorescence Measurements

A Pulse Amplitude Modulation (PAM)-based portable fluorometer (FlouroPen FP-100Max, Photon Systems Instruments, Brno, Czech Republic) with various pre-configured protocols was used. Experiments were carried out in green light by adhering green filter papers to headlight torches. The temperature was kept constant at 24.5 °C. The following protocols were used:

a. OJIP [28] (Supplementary Figure S1): The OJIP transient is a fast recording of the initial increase in fluorescence upon illumination of dark-adapted leaves. Leaves were adapted to the dark for 20 min. The OJIP initials stand for: O (F_0) measured 50 µs after illumination starts, J—first intermediate step measured after 2 ms, I—second intermediate step measured after 30 ms, and P—Fm (maximum fluorescence) [42];

b. Light response curve [23,43]: This protocol records maximum quantum yield in the dark and then effective quantum yield in series, each after an illumination period. In such a way, by gradually increasing the light, information regarding light use efficiency, characteristic light intensity and maximum activity of PSII can be extracted from the data. Maximum quantum yield is calculated as:

$$Fv/Fm = \frac{F_m - F_0}{F_m} \quad (1)$$

where F_m and F_0 are maximum and minimum fluorescence measured after dark adaptation time, respectively. Effective quantum yield is calculated in the same manner as equation (1), where it is considered effective because it is recorded during or at the end of a light period just before closing or changing the light intensity. LC3 pre-configured measurement was used with 7 steps increase in actinic light intensity within the PAM-fluorometer: 10, 20, 50, 100, 300, 500, 1000 µmol photons m^{-2} s^{-1}. Parameterization of the light response curve followed Eilers and Peeters (1988) formulation [43]: A linear regression curve was fitted to the logarithmic data with the following fit equation:

$$p = \frac{I}{aI^2 + bI + c} \quad (2)$$

where p and I are the photosynthetic activity and light intensity, respectively. The coefficients a, b and c are used to minimize the fit over the logarithmic data in order to extract the required information. Their initial values at the start of the fitting procedure are calculated directly from the acquired data:

$$a = \frac{1}{sI_m^2} \quad (3)$$

$$b = \frac{1}{P_m} - \frac{2}{sI_m} \tag{4}$$

$$c = \frac{1}{s} \tag{5}$$

where s, I_m and P_m are the initial linear slope, the light intensity at maximum photosynthetic activity, and the maximum photosynthetic activity reached. Then, after the fitting procedure is finished, reverse equations are used to extract the information needed:

$$LUE = \frac{1}{s} \tag{6}$$

$$\text{Effective Antenna Size}(I_k) = \frac{c}{b + 2\sqrt{ac}} \tag{7}$$

$$\text{Maximum activity} = \frac{1}{b + 2\sqrt{ac}} \tag{8}$$

c. Light energy utilization distribution was calculated as suggested by Kramer et al. (2004) [29] where the puddle model [44] was taken into account during calculation:

$$\Phi_{II} = \frac{F'_m - F'_s}{F'_m} \tag{9}$$

$$NPQ = \frac{F_m - F'_m}{F'_m} \tag{10}$$

$$\Phi_{NO} = \frac{1}{NPQ + 1 + \Phi_{II}(F_m/F_0 - 1)} \tag{11}$$

$$\Phi_{NPQ} = 1 - \Phi_{II} - \Phi_{NO} \tag{12}$$

where Φ_{II} is the effective quantum yield of PSII, F'_m and F'_s are the maximum and steady state fluorescence measured during light, respectively; NPQ initials stand for Non-Photochemical Quenching, Φ_{NO} represents the quantum yield of non-regulated loss in PSII, and Φ_{NPQ} is the quantum yield of regulated non-photochemical energy loss in PSII.

d. Relaxation kinetics [45] were calculated during an induction-relaxation pre-configured measurement (NPQ1) in the portable fluorometer. The induction period was given at 60 s at an intensity of 50 µmol photons m^{-2} s^{-1} (comparable to the ambient light intensity the leaves experienced during acclimation in the growth chamber). Then, the relaxation period after illumination in the dark was given at 88 s, during which three saturating pulses are fired at a pre-set intervals of 26 s each in the dark. The calculations for each of the coefficients are:

$$qE = \frac{F'^2_m - F'^1_m}{F_m - F_0} \tag{13}$$

$$qT = \frac{F'^3_m - F'^2_m}{F_m - F_0} \tag{14}$$

$$qI = \frac{F_m - F'^3_m}{F_m - F_0} \tag{15}$$

where $F'^{\#}m$ is the number of the saturating pulse during the relaxation part of the induction- relaxation protocol.

4.3. The 77K Fluorescence Assay

Samples of apple tree leaves sprayed with 0.6% pure Metamitron (Sigma-aldrich, Rehovot, Israel), 0.096% DCMU (Sigma-aldrich, Israel), and DDW, were cut two days

after administration and kept in liquid nitrogen until measurement. Then, each leaf was crushed with a mortar and pestle with liquid nitrogen and thawed in 1 mL PBS (1:10 with DDW, Sigma-aldrich, Israel). Immediately after thawing, a sample was loaded into a Pasteur pipette and was mounted into a Dewar cuvette filled with liquid nitrogen in spectrofluorometer (Cary-Varian, Agilent, Santa Clara, CA, USA). Preliminary tests were performed on the leaves in order to determine the volume of buffer and, therefore, the correct concentration used, which eliminates self-re-absorption of the fluorescence signal by the sample. Finally, each spectrum was pre-processed before comparison, and the data was normalized to the 685 nm peak and shifted on the *Y*-axis to zero by the first point in the curve (662 nm).

4.4. SDS-PAGE and Western Analysis

Apple tree leaves were homogenized with a mortar and pestle in the dark at 4 °C within liquid nitrogen, and then proteins were extracted with a lysis buffer (20% SDS, 1.5 M Tris pH 8.8), 1 mM PMSF and 1% phosphatase inhibitor (p0044, Sigma-aldrich). Samples were centrifuged at 4 °C, 14,000 RPM for 10 min and total protein was assessed with Bradford assay [46]. A total of 25 µgr total proteins were loaded in each well onto an SDS-PAGE [47] and transferred to a PVDF membrane (Amersham Biosciences, Amersham, UK), blocked for two hours in 5% (*v/v*) skim milk, and incubated with primary antibodies: De-phosphorylated Psb-a (1:10,000) (AS05-084, Sigma-aldrich), phosphorylated Psb-a (1:10,000) (AS13-2669, Agrisera) or Psb-o (AS05-092, Agrisera) (1:5,000) diluted according to the manufacturer's recommendations. The membrane was then incubated with a goat α-rabbit –HRP conjugated secondary antibody (1:20,000) (AS09-602, Agrisera) and developed with an ECL-bright (AS16-ECL-N-10, Agrisera).

4.5. Statistical Analysis

Each group of control or treatments within this study included 3 samples from each of the three branches taken from different trees in the orchard. Statistical procedures were performed as described in Liran et al. (2020) [48]. Groups were checked for normal distribution with Shapiro–Wilk's test and homogeneity of variances with Levene's test. If both tests were satisfied, analysis of variance (ANOVA) was selected. Pairwise comparisons were checked with Tukey's HSD test. If the homogeneity of variance test was violated, Welch's ANOVA was used instead and Games–Howell (for epsilon < 0.75) or Greenhouse–Geisser (for epsilon > 0.75) post hoc comparison tests were used. If the normality criteria were violated, a Kruskal–Wallis's a-parametric ANOVA was used with Dunn's procedure and a Bonferroni adjustment were made for the pairwise comparisons.

For inspection of differences between groups in time, a repeated measures ANOVA was used if Mauchly's sphericity test was satisfied. If homoscedasticity was not violated, pair-wise comparisons were checked with Pearson's correlation tests and Bonferroni adjustments. If homoscedasticity test failed, a Spearman's rank non-parametric correlation test was used instead. If Mauchly's sphericity test was violated, a Friedman's a-parametric ANOVA was applied with pair-wise comparisons with Bonferroni's adjustments. Statistical significance was set to $p < 0.05$. Statistical analyses were carried out in Statistical Product and Service Solution (SPSS) (IBM, Chicago, IL, USA).

Supplementary Materials: The following are available online at https://www.mdpi.com/article/10.3390/plants10122803/s1, Figure S1: Brevis® active ingredient Metamitron obtains a PSII acceptor side inhibition profile in OJIP measurement in "Top-Red" cultivar.

Author Contributions: Conceptualization, Y.L., O.C., R.A.S., D.T. and O.L.; Data curation, Y.T., A.R., S.R.-B., V.A. and E.S.; Formal analysis, Y.T., A.R., S.R.-B., V.A., E.S., O.C., R.A.S., M.G. and O.L.; Funding acquisition, O.L.; Investigation, Y.T., A.R., S.R.-B., V.A., E.S., Y.L., O.C., R.A.S., M.G. and O.L.; Methodology, Y.L., O.C., R.A.S., M.G., D.T. and O.L.; Project administration, O.L.; Resources, A.R., Y.L., O.C., M.G., D.T. and O.L.; Supervision, Y.L., O.C., R.A.S., M.G., D.T. and O.L.; Validation, Y.T., A.R., S.R.-B., V.A., E.S., O.C., R.A.S. and O.L.; Visualization, Y.T., A.R. and O.L.; Writing—original draft, Y.T., V.A., Y.L., O.C., R.A.S., M.G., D.T. and O.L.; Writing—review and editing, Y.T., V.A., Y.L.,

O.C., R.A.S., M.G., D.T. and O.L. All authors have read and agreed to the published version of the manuscript.

Funding: This work was supported by "ICA in Israel" (Grant number PR20000032) and the Chief Scientist of the Israeli Ministry of Agriculture and Rural Development (Grant number 21-37-0011).

Data Availability Statement: Data is available upon request from the corresponding author.

Acknowledgments: The authors would like to extend their gratitude to Amos Naor for his persistence, good advice, friendship and fruitful discussions regarding this work.

Conflicts of Interest: The authors declare no conflict of interest.

References

1. Dennis, F.G., Jr. The History of Fruit Thinning. *Plant Growth Regul.* **2000**, *31*, 1–16. [CrossRef]
2. Greene, D.; Costa, G. Fruit Thinning in Pome- and Stone-Fruit: State of the Art. *Acta Hortic.* **2013**, *998*, 93–102. [CrossRef]
3. Lakso, A.N.; Johnson, R.S. A Simplified Dry Matter Production Model for Apple Using Automatic Programming Simulation Software. *Acta Hortic.* **1990**, *276*, 141–148. [CrossRef]
4. Rosa, N.; Lidon, F.C.; Rodrigues, A.P.; Pais, I.P.; Scotti-Campos, P.; Asín, L.; Oliveira, C.M.; Ramalho, J.C. Implications of Nighttime Temperature on Metamitron Impacts on the Photosynthetic Machinery Functioning of Malus x Domestica Borkh. *J. Plant Physiol.* **2021**, *261*, 153427. [CrossRef]
5. Stern, R.A. The Photosynthesis Inhibitor Metamitron Is a Highly Effective Thinner for 'Golden Delicious' Apple in a Warm Climate. *Fruits* **2015**, *70*, 127–134. [CrossRef]
6. Baker, N.R. Chlorophyll Fluorescence: A Probe of Photosynthesis In Vivo. *Annu. Rev. Plant Biol.* **2008**, *59*, 89–113. [CrossRef]
7. Müller, P.; Li, X.-P.; Niyogi, K.K. Non-Photochemical Quenching. A Response to Excess Light Energy. *Plant Physiol.* **2001**, *125*, 1558–1566. [CrossRef]
8. Pinnola, A.; Bassi, R. Molecular Mechanisms Involved in Plant Photoprotection. *Biochem. Soc. Trans.* **2018**, *46*, 467–482. [CrossRef]
9. Messant, M.; Krieger-Liszkay, A.; Shimakawa, G. Dynamic Changes in Protein-Membrane Association for Regulating Photosynthetic Electron Transport. *Cells* **2021**, *10*, 1216. [CrossRef] [PubMed]
10. Ruban, A.V. Nonphotochemical Chlorophyll Fluorescence Quenching: Mechanism and Effectiveness in Protecting Plants from Photodamage. *Plant Physiol.* **2016**, *170*, 1903–1916. [CrossRef] [PubMed]
11. Schansker, G.; Tóth, S.Z.; Strasser, R.J. Dark Recovery of the Chl a Fluorescence Transient (OJIP) after Light Adaptation: The QT-Component of Non-Photochemical Quenching Is Related to an Activated Photosystem I Acceptor Side. *Biochim. Biophys. Acta (BBA)-Bioenerget.* **2006**, *1757*, 787–797. [CrossRef]
12. Foyer, C.H. Reactive Oxygen Species, Oxidative Signaling and the Regulation of Photosynthesis. *Environ. Exp. Bot.* **2018**, *154*, 134–142. [CrossRef]
13. Aro, E.-M.; McCaffery, S.; Anderson, J.M. Photoinhibition and D1 Protein Degradation in Peas Acclimated to Different Growth Irradiances. *Plant Physiol.* **1993**, *103*, 835–843. [CrossRef]
14. Melis, A. Photosystem-II Damage and Repair Cycle in Chloroplasts: What Modulates the Rate of Photodamage in Vivo? *Trends Plant Sci.* **1999**, *4*, 130–135. [CrossRef]
15. Rochaix, J.-D.; Lemeille, S.; Shapiguzov, A.; Samol, I.; Fucile, G.; Willig, A.; Goldschmidt-Clermont, M. Protein Kinases and Phosphatases Involved in the Acclimation of the Photosynthetic Apparatus to a Changing Light Environment. *Philos. Trans. R. Soc. B Biol. Sci.* **2012**, *367*, 3466–3474. [CrossRef] [PubMed]
16. Bonardi, V.; Pesaresi, P.; Becker, T.; Schleiff, E.; Wagner, R.; Pfannschmidt, T.; Jahns, P.; Leister, D. Photosystem II Core Phosphorylation and Photosynthetic Acclimation Require Two Different Protein Kinases. *Nature* **2005**, *437*, 1179–1182. [CrossRef]
17. Bellafiore, S.; Barneche, F.; Peltier, G.; Rochaix, J.-D. State Transitions and Light Adaptation Require Chloroplast Thylakoid Protein Kinase STN7. *Nature* **2005**, *433*, 892–895. [CrossRef]
18. Theis, J.; Schroda, M. Revisiting the Photosystem II Repair Cycle. *Plant Signal Behav.* **2016**, *11*, e1218587. [CrossRef]
19. Mattoo, A.K.; Pick, U.; Hoffman-Falk, H.; Edelman, M. The Rapidly Metabolized 32,000-Dalton Polypeptide of the Chloroplast Is the "Proteinaceous Shield" Regulating Photosystem II Electron Transport and Mediating Diuron Herbicide Sensitivity. *Proc. Natl. Acad. Sci. USA* **1981**, *78*, 1572–1576. [CrossRef]
20. Allakhverdiev, S.I.; Nishiyama, Y.; Takahashi, S.; Miyairi, S.; Suzuki, I.; Murata, N. Systematic Analysis of the Relation of Electron Transport and ATP Synthesis to the Photodamage and Repair of Photosystem II in Synechocystis. *Plant Physiol.* **2005**, *137*, 263–273. [CrossRef]
21. Schreiber, U.; Schliwa, U.; Bilger, W. Continuous Recording of Photochemical and Non-Photochemical Chlorophyll Fluorescence Quenching with a New Type of Modulation Fluorometer. *Photosynth. Res.* **1986**, *10*, 51–62. [CrossRef]
22. Genty, B.; Briantais, J.-M.; Baker, N.R. The Relationship between the Quantum Yield of Photosynthetic Electron Transport and Quenching of Chlorophyll Fluorescence. *Biochim. Biophys. Acta (BBA)-Gen. Subj.* **1989**, *990*, 87–92. [CrossRef]
23. Maxwell, K.; Johnson, G.N. Chlorophyll Fluorescence—A Practical Guide. *J. Exp. Bot.* **2000**, *51*, 659–668. [CrossRef]
24. Henley, W.J. Measurement and Interpretation of Photosynthetic Light-Response Curves in Algae in the Context of Photoinhibition and Diel Changes. *J. Phycol.* **1993**, *29*, 729–739. [CrossRef]

25. Long, S.P.; Humphries, S.; Falkowski, P.G. Photoinhibition of Photosynthesis in Nature. *Annu. Rev. Plant Biol.* **1994**, *45*, 633–662. [CrossRef]
26. Kroon, B.; Prézelin, B.B.; Schofield, O. Chormatic Regulation of Quantum Yields for Photosystem II Charge Separation, Oxygen Evolution, and Carbon Fixation in Heterocapsa Pygmaea (Pyrrophyta). *J. Phycol.* **1993**, *29*, 453–462. [CrossRef]
27. Jassby, A.D.; Platt, T. Mathematical Formulation of the Relationship between Photosynthesis and Light for Phytoplankton. *Limnol. Oceanogr.* **1976**, *21*, 540–547. [CrossRef]
28. Strasser, R.J.; Tsimilli-Michael, M.; Srivastava, A. Analysis of the Chlorophyll a Fluorescence Transient. In *Chlorophyll a Fluorescence*; Springer: Berlin, Germany, 2004; pp. 321–362.
29. Kramer, D.M.; Johnson, G.; Kiirats, O.; Edwards, G.E. New Fluorescence Parameters for the Determination of QA Redox State and Excitation Energy Fluxes. *Photosynth. Res.* **2004**, *79*, 209. [CrossRef]
30. Henmi, T.; Miyao, M.; Yamamoto, Y. Release and Reactive-Oxygen-Mediated Damage of the Oxygen-Evolving Complex Subunits of PSII during Photoinhibition. *Plant Cell Physiol.* **2004**, *45*, 243–250. [CrossRef]
31. Klughammer, C.; Schreiber, U. Complementary PS II Quantum Yields Calculated from Simple Fluorescence Parameters Measured by PAM Fluorometry and the Saturation Pulse Method. *PAM Appl. Notes* **2008**, *1*, 201–247.
32. Wen, X.; Yang, Z.; Ding, S.; Yang, H.; Zhang, L.; Lu, C.; Lu, Q. Analysis of the Changes of Electron Transfer and Heterogeneity of Photosystem II in Deg1-Reduced Arabidopsis Plants. *Photosynth. Res.* **2021**, *150*, 159–177. [CrossRef] [PubMed]
33. Greer, D.H. Photon Flux Density and Temperature-Dependent Responses of Photosynthesis and Photosystem II Performance of Apple Leaves Grown in Field Conditions. *Funct. Plant Biol.* **2015**, *42*, 782–791. [CrossRef]
34. Campbell, R.J.; Marini, R.P.; Birch, J.B. Canopy Position Affects Light Response Curves for Gas Exchange Characteristics of Apple Spur Leaves. *J. Am. Soc. Hortic. Sci.* **1992**, *117*, 467–472. [CrossRef]
35. McArtney, S.J.; Obermiller, J.D.; Arellano, C. Comparison of the Effects of Metamitron on Chlorophyll Fluorescence and Fruit Set in Apple and Peach. *HortScience* **2012**, *47*, 6. [CrossRef]
36. Pfündel, E.; Klughammer, C.; Schreiber, U. Monitoring the Effects of Reduced PS II Antenna Size on Quantum Yields of Photosystems I and II Using the Dual-PAM-100 Measuring System. *PAM Appl. Notes* **2008**, *1*, 21–24.
37. Robinson, T.L.; Lakso, A.N. Advances in Predicting Chemical Thinner Response of Apple Using a Carbon Balance Model. *N. Y. Fruit Q.* **2011**, *19*, 15–20. [CrossRef]
38. Lakso, A.N.; Robinson, T.L. Decision Support for Apple Thinning Based on Carbon Balance Modeling. In Proceedings of the IX International Symposium on Modelling in Fruit Research and Orchard Management 1068, Saint-Jean-sur-Richelieu, QC, Canada, 19–23 June 2011; pp. 235–242.
39. Stander, O.P.J.; Botes, J.; Krogscheepers, C. The Potential Use of Metamitron as a Chemical Fruit-Thinning Agent in Mandarin. *HortTechnology* **2018**, *28*, 28–34. [CrossRef]
40. De Mello Farias, R.; Barreto, C.F.; Schiavon, A.V.; Hellwig, C.G.; Martins, C.R.; Malgarim, M.B.; Mello-Farias, P.C. Effect of Chemical Thinning Season Using Metamitron on Peaches 'Sensação'Quality. *J. Exp. Agric. Int.* **2017**, *19*, 1–7.
41. Elsysy, M.A.; Hubbard, A.; Einhorn, T.C. Postbloom Thinning of 'Bartlett'Pear with Metamitron. *HortScience* **2020**, *55*, 174–180. [CrossRef]
42. Ariyarathna, R.A.I.S.; Weerasena, S.L.; Beneragama, C. Application of Polyphasic OJIP Chlorophyll Fluorescent Transient Analysis as an Indicator for Testing of Seedling Vigour of Common Bean (*Phaseolus Vulgaris* L.). *Trop. Agric. Res.* **2020**, *31*, 106. [CrossRef]
43. Eilers, P.H.C.; Peeters, J.C.H. A Model for the Relationship between Light Intensity and the Rate of Photosynthesis in Phytoplankton. *Ecol. Model.* **1988**, *42*, 199–215. [CrossRef]
44. Lavergne, J.; Trissl, H.-W. Theory of Fluorescence Induction in Photosystem II: Derivation of Analytical Expressions in a Model Including Exciton-Radical-Pair Equilibrium and Restricted Energy Transfer between Photosynthetic Units. *Biophys. J.* **1995**, *68*, 2474–2492. [CrossRef]
45. Lichtenthaler, H.K.; Buschmann, C.; Knapp, M. How to Correctly Determine the Different Chlorophyll Fluorescence Parameters and the Chlorophyll Fluorescence Decrease Ratio R Fd of Leaves with the PAM Fluorometer. *Photosynthetica* **2005**, *43*, 379–393. [CrossRef]
46. Bradford, M.M. A Rapid and Sensitive Method for the Quantitation of Microgram Quantities of Protein Utilizing the Principle of Protein-Dye Binding. *Anal. Biochem.* **1976**, *72*, 248–254. [CrossRef]
47. Laemmli, U.K. Cleavage of Structural Proteins during the Assembly of the Head of Bacteriophage T4. *Nature* **1970**, *227*, 680–685. [CrossRef]
48. Liran, O.; Shir, O.M.; Levy, S.; Grunfeld, A.; Shelly, Y. Novel Remote Sensing Index of Electron Transport Rate Predicts Primary Production and Crop Health in L. Sativa and Z. Mays. *Remote Sens.* **2020**, *12*, 1718. [CrossRef]

plants

MDPI

Article

Classification and Characterization of the Manoor Valley's (Lesser Himalaya) Vegetation from the Subtropical-Temperate Ecotonal Forests to the Alpine Pastures along Ecological Variables

Inayat Ur Rahman [1,2,*], Aftab Afzal [1,*], Zafar Iqbal [1], Mashail Nasser Alzain [3], Al-Bandari Fahad Al-Arjani [4], Abdulaziz A. Alqarawi [5], Elsayed Fathi Abd_Allah [5], Niaz Ali [1], Shazia Sakhi [6], Muhammad Azhar Khan [1], Uzma Khan [1], Farhana Ijaz [1,*], Samina Mumtaz [7] and Eduardo Soares Calixto [8,9]

1 Department of Botany, Hazara University, Mansehra 21300, Pakistan; zafar.iqbal@hu.edu.pk (Z.I.); niazalitk25@gmail.com (N.A.); azharfinal@gmail.com (M.A.K.); uzmaqau2003@yahoo.com (U.K.)
2 William L. Brown Center, Missouri Botanical Garden, 4344 Shaw Blvd, St. Louis, MO 63110, USA
3 Department of Biology, College of Sciences, Princess Nourah Bint Abdulrahman University, Riyadh 11451, Saudi Arabia; mnAlZain@pnu.edu.sa
4 Botany and Microbiology Department, College of Science, King Saud University, Riyadh 11451, Saudi Arabia; aalarjani@ksu.edu.sa
5 Department of Plant Production, College of Food and Agriculture Science, King Saud University, Riyadh 11451, Saudi Arabia; alqarawi@ksu.edu.sa (A.A.A.); eabdallah@ksu.edu.sa (E.F.A.)
6 Center of Plant Sciences and Biodiversity, University of Swat, Swat 19200, Pakistan; shaziasakhi@gmail.com
7 Department of Animal Sciences, Karakoram International University, Gilgit-Baltistan 15100, Pakistan; samina@kiu.edu.pk
8 Department of Biology, University of Missouri, St. Louis, MO 63166, USA; calixtos.edu@gmail.com
9 Entomology and Nematology Department, University of Florida, Gainesville, FL 32611, USA
* Correspondence: hajibotanist@outlook.com (I.U.R.); draftab@hu.edu.pk (A.A.); fbotany@yahoo.com (F.I.)

Citation: Rahman, I.U.; Afzal, A.; Iqbal, Z.; Alzain, M.N.; Al-Arjani, A.-B.F.; Alqarawi, A.A.; Abd_Allah, E.F.; Ali, N.; Sakhi, S.; Khan, M.A.; et al. Classification and Characterization of the Manoor Valley's (Lesser Himalaya) Vegetation from the Subtropical-Temperate Ecotonal Forests to the Alpine Pastures along Ecological Variables. *Plants* **2022**, *11*, 87. https://doi.org/10.3390/plants11010087

Academic Editor: Daniel Sánchez-Mata

Received: 8 October 2021
Accepted: 29 November 2021
Published: 28 December 2021

Abstract: Plant species are distributed in different types of habitats, forming different communities driven by different sets of environmental variables. Here, we assessed potential plant communities along an altitudinal gradient and their associations with different environmental drivers in the unexplored Manoor Valley (Lesser Himalaya), Pakistan. We have implemented various ecological techniques and evaluated phytosociological attributes in three randomly selected 50 m-transects within each stand (a total of 133) during different seasons for four years (2015–2018). This phytosociological exploration reported 354 plant species representing 93 different families. The results revealed that the Therophytic life form class dominated the flora, whereas Nanophyll dominated the leaf size spectra. There were a total of twelve plant communities identified, ranging from the lowest elevations to the alpine meadows and cold deserts. The maximum number of species were found in *Cedrus–Pinus–Parrotiopsis* community (197 species), in the middle altitudinal ranges (2292–3168 m). Our results showed that at high altitudes, species richness was reduced, whereas an increase in soil nutrients was linked to progression in vegetation indicators. We also found different clusters of species with similar habitats. Our study clearly shows how altitudinal variables can cluster different plant communities according to different microclimates. Studies such as ours are paramount to better understanding how environmental factors influence ecological and evolutionary aspects.

Keywords: vegetation structure; environmental variables; PC-ORD; plant community assembly; Himalaya

1. Introduction

The study of vegetation classification based on species co-occurrence [1,2] and its relationship to ecological variables [3] is known as phytosociology. This field has specified major

strategies and methodologies that may be linked to vegetation mapping [4,5], and biodiversity conservation [6]. Plant biodiversity research generally focuses on species diversity [7–9] and species-level measurement [10]. It is greatly influenced by a variety of environmental variables [11–13], such as climatic, edaphic, and geographic variables [13–18]. Plant associations/communities with a well-defined structure in respect to ecological variables can be described physiognomically as well as floristically [19–21]. Floristic diversity and biological spectra rely on topography as well as other environmental variables. For instance, biological spectrum mirrors the existing ecological and natural surroundings [22,23]. They are the plant characteristics that have been widely applied in vegetation research [24]. High mountains are major hotspots for endemics across the world [25–28].

It is well understood that altitude is a complex factor along which many environmental gradients [29] and species diversity [15,30] change accordingly. Biological as well as the environmental gradients interact to govern the distribution of species richness all around the altitudinal gradient [31–33]. The species richness of higher plant species has been reported to have increased in temperate latitudes [34]. The relationship between vegetation and ecological diversity is reflected as a percentage of the ecosystem's overall quality [35]. The altitudinal gradient has a greater influence on temperature in mountainous regions than latitude, and the rate of decrease is considerably faster in summer than in winter, resulting in altitudinal vegetation zonation [29].

Plant species are found in a diverse range of environments, forming different communities driven by different sets of environmental variables [6,36,37]. Many ecological experts have recognized distinct types of forests in Pakistan [38–41], but it is not clear how and which environmental variables drive plant diversity and community structure in most alpine ecosystems. In this context, we used different multivariate approaches to assess potential plant communities along an altitudinal gradient and their associations with different environmental drivers, namely climatic, edaphic, and physiographic variables. In sum, we assessed (i) which potential plant communities are present in the subtropical-temperate ecotonal forests to the alpine pastures; (ii) which plant species are most representative each plant community; (iii) which environmental variables most determine plant community structure in this region; and (iv) which species are distribution in each community based on their biological spectrum (life form and leaf size). Since there is a significant variability in environmental gradients with respect to the altitude and different plant species are adapted to a set of micro-climatic conditions [42–44], we hypothesized that there would be different plant communities along the elevational gradient, with specific plants related to particular sets of environmental variables. Importantly, statistical methodologies in vegetation ecology, such as multivariate analysis [45], have evolved in recent decades, allowing researchers to evaluate the impact of ecological variables on large groups of plants [6,43,46–48]. Therefore, we took advantage of these advanced statistical approaches to assess viable low-dimensional summaries of field information by advantageous and objective means [49].

2. Materials and Methods

2.1. Study Area

Geographically, the Manoor Valley [4,50,51] is situated in the north-western part of Pakistan (34.68165 N to 34.83869 N latitude and 73.57520 E to 73.73182 E longitude; 1580 to 4677 m elevation above sea level) and is part of the Himalayan mountain range. The multiple elevational layers of the research area are depicted on a georeferenced map (Figure 1). The wide gap in in elevation demonstrates that the climate differs from lower altitudinal ranges [4] to the alpine meadows [42]. The study area is located on the Indian Plate's north-western boundary [52], which has immense phytogeographic and floristic significance.

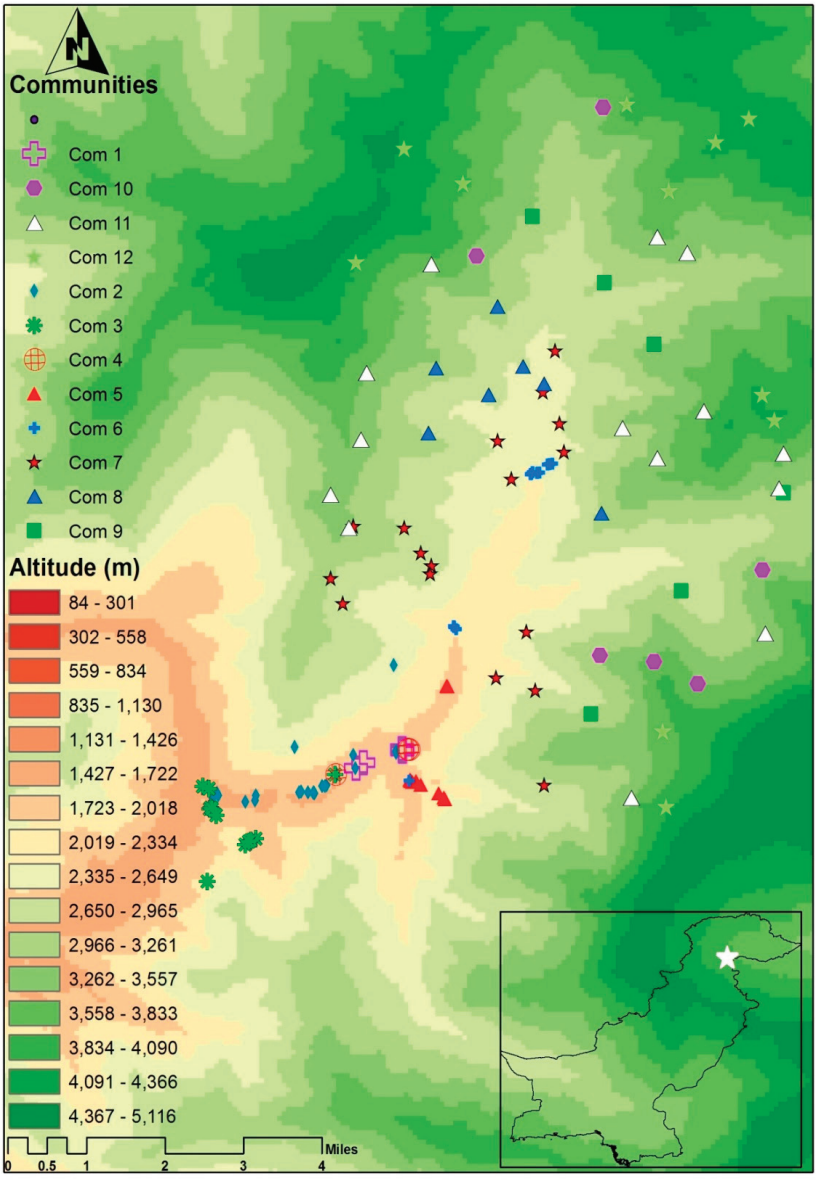

Figure 1. GIS map (generated using ArcGIS version 10.1) depicting the altitudinal layers and distribution pattern of communities of the studied area (Manoor Valley). Com 1: *Salix–Sorbaria–Impatiens*, Com 2: *Indigofera–Juglans–Isodon*, Com 3: *Cedrus–Cynodon–Isodon*, Com 4: *Indigofera–Parrotiopsis–Bistorta*, Com 5: *Sambucus–Cedrus–Desmodium*, Com 6: *Indigofera–Cedrus–Pinus*, Com 7: *Cedrus–Pinus–Parrotiopsis*, Com 8: *Pinus–Viburnum–Cedrus*, Com 9: *Abies–Picea–Juniperus*, Com 10: *Juniperus–Sibbaldia–Juniperus*, Com 11: *Sibbaldia–Bergenia–Rheum*, Com 12: *Poa–Bistorta–Primula*.

2.2. Vegetation Sampling and Herbarium work

The vegetation of the study area (Manoor Valley) was surveyed and quantified [53] during four consecutive years, from 2015 to 2018, along the environmental variables [43]. The line transect method was adopted for vegetation sampling [54–58]. The study area was

subdivided into 133 stands (sampling plots). Each stand was replicated thrice (three transects of 50 m in each stand) [53,59]. The interval between each transect was 100 m and the interval between the stands was 200 m. The phytosociological attributes (i.e., density, frequency and their relative values, and importance value (IV)) were employed on the recorded data of each stand [4,60,61]. The species were further ranked with the highest IV and considered the representative species [19,62]. Similarly, plant communities were designated based on three dominant species [63–66]. Moreover, both attributes of the biological spectrum (life form and leaf size spectra) were recognized by the following [67]. Methods for collecting specimens, their labelling, pressing, drying, poisoning, and mounting were adopted by the following [68,69]. Their identification was achieved with the aid of Flora of Pakistan [70–72] and submitted to the Herbarium of Hazara University, Mansehra (Pakistan).

2.3. Ecological Variables

The slope angle, aspect and exposure were recorded at each stand using a clinometer, while the altitude, longitude, and latitude were recorded by the Global Positioning System (GPS). Two hundred grams of soil samples from three randomly selected transects within each sampling stand (0–30 cm depth) were collected [73] and mixed thoroughly to make a composite sample [74], stored in a sterile polythene bag and labeled. All the samples were submitted to the Soil and Water Testing Laboratory at the Model Farm Service Center in Mansehra, Pakistan, for analysis of various physicochemical parameters such as soil pH [75], and texture (loam, clay, silt and sand) [76], organic matter (OM%) [77], nitrogen (N) [78], potassium (K), phosphorous (P) [79], calcium carbonate ($CaCO_3$) [80–82], and electric conductivity (EC) [76]. Moreover, other climatic variables were measured by a small remote weather station (Kestrel 4000 weather and environmental tracker) like temperature, humidity, wind speed (WS), barometric pressure (BP), wet bulb (WB), heat index (HI), and dew point (DP) to record the data at each transect and then average values were calculated at stand level [43].

2.4. Statistical Analyses

Multivariate analysis was carried out to analyze the recorded data of species and ecological variables resulting from the field observations [49,83] to find out the relationship among them [84,85]. The recorded species and sampled stands were constrained in association to the ecological variables [86,87], which were divided into geographic, slope aspect, edaphic, and climatic variables. For the identification and classification of plant communities [53], the two-way indicator species analysis (TWINSPAN) was processed using PC-ORD version 5.0 [87–89]. A georeferenced map was generated with ArcGIS version 10.1 to depict the distribution pattern of plant communities.

Canonical correspondence analysis (CCA) was used to ordinate species and samples along the ecological variables [90,91] using CANOCO version 5 [92,93], and we performed a variation partitioning test (partial CCA) to evaluate how explanatory attributes (climatic, edaphic, geographic, and slope) drive the plant species distribution. First, we built the best model with the lowest number of variables (those that most explain variance), through the *step* function in R. Next, we also evaluated multicollinearity between variables of the final model using Variance Inflation Factor (VIF), and we removed any variable with VIF >10, one at a time. Non-multidimensional scaling ordination (NMDS) [89,94] was performed using the software R 4.0.1 [95–97]. NMDS was conducted to evaluate the correlation of recognized plant communities with their associated species.

3. Results

A total of 12 plant communities were recognized, each representing for different indicator species. Each community was associated to a set of variables, but altitude, Slope (ES), Slope (SE), Slope (SW), Slope (WN), electric conductivity (EC) and heat index were the most significant variables driving species distribution in the present study. Therophytes and

Hemicryptophytes, and Nanophyll, were the most frequent type of life form and leaf size, respectively, present in the communities found. Below we discuss these results in detail.

3.1. TWINSPAN Classification

TWINSPAN, which is based partitioning reciprocal averaging ordination space, was used to classify 354 species and 133 stands. Two large different clusters, which show a high cluster heterogeneity value (Lambda = 0.814). One of these clusters had eight different communities and was formed by 93 sampling sites, while the other cluster presented four communities structured into 40 sites. Furthermore, different subdivisions observed were within these two large groups with cluster heterogeneity values of less than 0.4: a total of 12 major plant communities were recognized, from subtropical-temperate ecotonal forests (1580 m) to the alpine meadows and cold deserts (4278 m) of the Manoor Valley, Lesser Himalayas. Each community was composed of different groups of indicator species recorded at different altitudes (Figure 1).

3.2. Vegetation Characterization of Plant Communities

In total, 12 major plant communities were established by TWINSPAN. All the twelve recognized plant communities were indicated with distinct symbols and colours. The GIS map shows the elevational layer and communities of the study area—illustrating the recognition and distribution of plant communities (Figure 1) along the ecological variables (Figures 2 and 3 and Supplementary data Figures S1–S4).

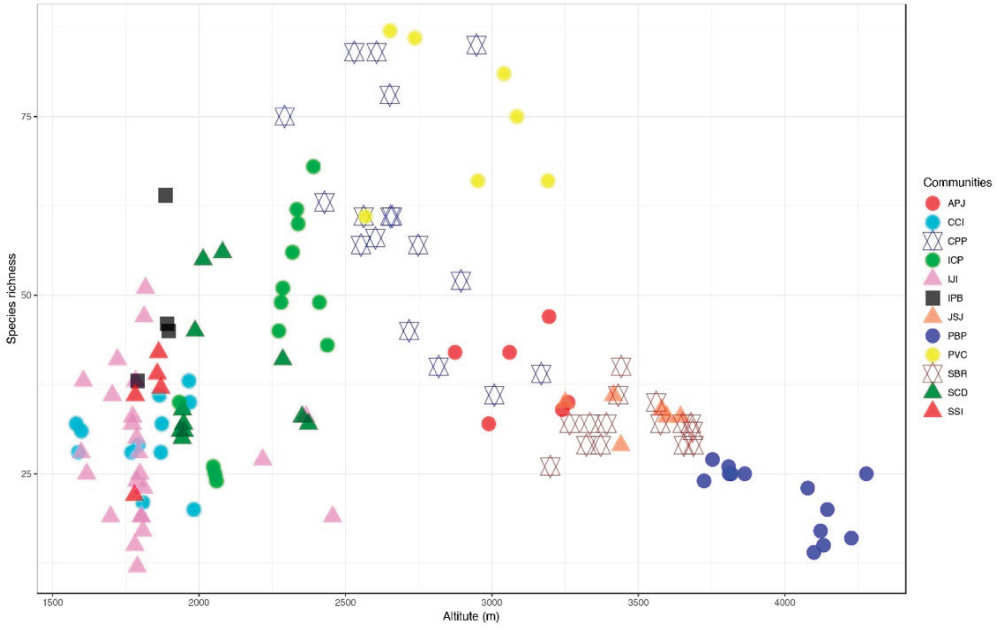

Figure 2. The relationship between the altitude and the species richness of 12 plant communities.

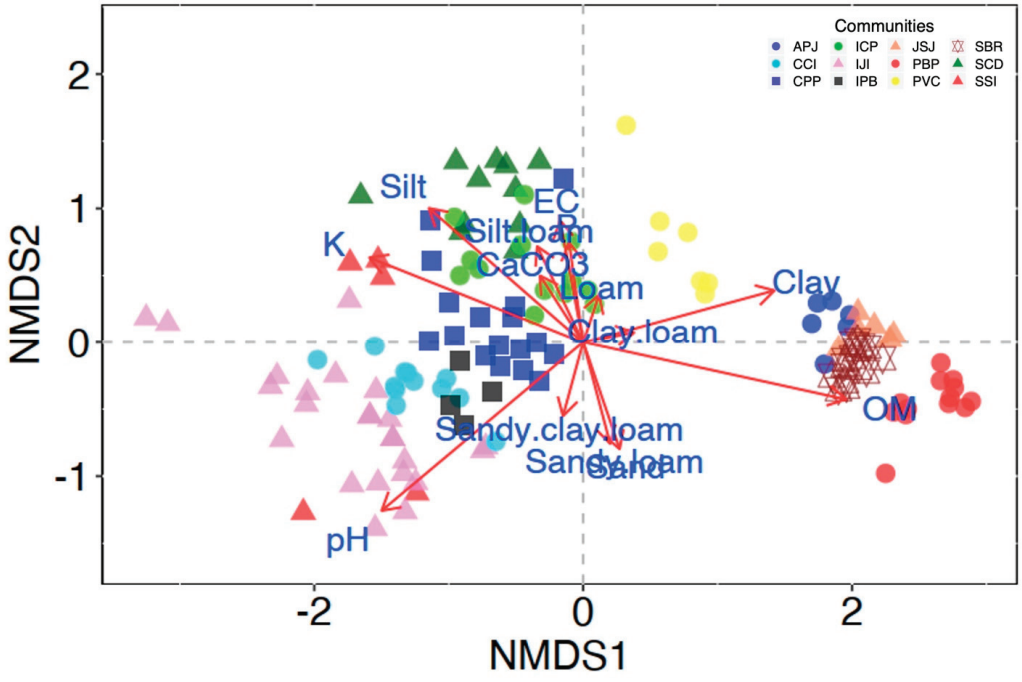

Figure 3. The NMDS ordination reveals the relationship between communities and edaphic variables. The length of the arrows illustrates the influence range, while the direction shows the correlation of the variables with plant communities. Plant communities that are close together or on the same axis have a positive correlation. The codes represent community types.

3.2.1. *Salix–Sorbaria–Impatiens* Community

This community (SSI) was recorded between altitudinal ranges of 1782.3–1869.5 m (5 stands) with 65 associated species. The indicator plant species of the SSI community were *Salix alba*, *Sorbaria tometosa and Impatiens bicolor* with highest IV values of 9.12, 5.51, and 5.29, respectively. Other frequent species were *Clematis grata*, *Bromus secalinus*, *Fragaria nubicola*, *Rumex nepalensis*, *Ficus carica*, *Salvia moorcroftiana*, *Indigofera heterantha*, *Bistorta amplexicaulis*, *Crotalaria* sp., *Filipendula vestita* and *Desmodium elegans*. Rare species with lower IV values included *Withania somnifera, Trachyspermum amii*, *Clinopodium vulgare*, *Paspalum dilatatun*, *Piptatherum aequiglume*, *Bauhinia variegata* and *Salix tetrasperma*. The life form spectra was dominated by Therophytes (36.92% of species), followed by Hemicryptophytes with 15.38% of species (Table 1). Nanophyll dominated the leaf size spectra with 30.77% of the species, followed by Mesophyll and Microphyll with 27.69% species each (Table 1). The ecological variables that strong and positively influenced the SSI community were pH (6.5–7), temperature (26.1–27.2 °C), HI (26.8–29.1), and BP (808.1–816.1) (Supplementary data Figure S1). Other important variables such as altitude and windspeed (0–1.5 m/s) were found in negative association with SSI community. Nevertheless, the SSI community's species diversity was restricted by low OM (0.65–1.15%) and P (9.6 mg/kg) (Figure 3 and Supplementary data Figure S2).

Table 1. Percentage of plant species recorded in each plant community according to the biological spectrum (life form) and leaf size.

	Plant Communities											
	SSI	**IJI**	**CCI**	**IPB**	**SCD**	**ICP**	**CPP**	**PVC**	**APJ**	**JSJ**	**SBR**	**PBP**
Life form												
Chamaephytes	9.23	10.71	12.68	10.23	10.68	7.09	8.79	5.94	9.84	0.00	12.00	12.82
Geophytes	4.62	5.36	9.86	6.82	7.77	9.22	0.00	11.39	9.84	11.36	8.00	10.26
Hemicryptophytes	15.38	22.32	25.35	25.00	0.00	25.53	27.47	30.69	40.98	56.82	48.00	53.85
Liana	3.08	0.89	2.82	1.14	1.94	0.00	1.65	0.99	0.00	0.00	0.00	0.00
Megaphanerophytes	0.00	3.57	2.82	1.14	5.83	2.13	1.65	2.97	6.56	0.00	0.00	0.00
Mesophanerophytes	13.85	7.14	0.00	3.41	9.71	4.96	2.75	1.98	3.28	0.00	0.00	0.00
Microphanerophytes	4.62	5.36	1.41	3.41	0.97	2.13	0.55	0.50	0.00	2.27	0.00	0.00
Nanophanerophytes	12.31	10.71	9.86	11.36	19.42	11.35	14.84	11.88	0.00	11.36	8.00	0.00
Parasitic	0.00	0.89	1.41	1.14	0.00	0.00	0.00	0.00	0.00	0.00	0.00	0.00
Therophytes	36.92	33.04	33.80	36.36	43.69	37.59	42.31	33.66	29.51	18.18	24.00	23.08
Leaf size												
Aphyllous	1.54	0.89	1.33	1.14	0.76	1.42	0.00	0.00	1.52	2.04	2.00	2.63
Leptophyll	10.77	10.71	10.67	15.91	19.08	17.02	17.77	16.84	24.24	26.53	28.00	21.05
Macrophyllous	1.54	5.36	6.67	1.14	6.11	7.09	5.58	5.61	3.03	2.04	2.00	2.63
Mesophyll	27.69	20.54	10.67	13.64	14.50	16.31	14.72	15.31	10.61	14.29	10.00	15.79
Microphyll	27.69	26.79	30.67	22.73	28.24	26.95	30.96	28.06	27.27	20.41	20.00	28.95
Nanophyll	30.77	35.71	40.00	45.45	31.30	31.21	30.96	34.18	33.33	34.69	38.00	28.95

Plant communities: *Salix–Sorbaria–Impatiens* (SSI), *Indigofera–Juglans–Isodon* (IJI), *Cedrus–Cynodon–Isodon* (CCI), *Indigofera–Parrotiopsis–Bistorta* (IPB), *Sambucus–Cedrus–Desmodium* (SCD), *Indigofera–Cedrus–Pinus* (ICP), *Cedrus–Pinus–Parrotiopsis* (CPP), *Pinus–Viburnum–Cedrus* (PVC), *Abies–Picea–Juniperus* (APJ), *Juniperus–Sibbaldia–Juniperus* (JSJ), *Sibbaldia–Bergenia–Rheum* (SBR), *Poa–Bistorta–Primula* (PBP).

3.2.2. *Indigofera–Juglans–Isodon* Community

This plant community (IJI) was recognized in 24 stands at an altitude ranging from 1597 to 2456 m with 113 associated species (Table 1). *Indigofera heterantha*, *Juglans regia*, and *Isodon rugosus* were recognized as the indicator species that dominated the community with IV values of 6.94, 5.00, and 4.37, respectively. Other co-dominant species were *Cynodon dactylon*, *Ziziphus* sp., *Micromeria biflora*, *Leptopus chinensis*, *Rumex hastatus*, *Ailanthus altissima* and *Impatiens bicolor*. Moreover, species that were rarely recorded in this community were *Dactylis glomerata*, *Achyranthes aspera*, *Lamium album*, *Bupleurum longicaule*, *Ricinus communis*, *Malus domestica*, *Pyrus pashia*, *Dodonaea viscosa*, *Filipendula vestita*, *Lactuca tatarica*, *Pinus roxburghii* and *Xanthium strumarium*. Therophytes dominated the biological spectrum with 33.04% of plant species, followed by Hemicryptophytes (22.32%), Chamaephytes and Nanophanerophytes (10.71%) each (Table 1). Nanophyllous class dominated the leaf size spectra, accounting for 35.71% of plant species, followed by microphyll (26.79%), and mesophyll (20.54%). The IJI community was supported by abundant limestone, granite, and sandstone. High temperatures (32.5 °C), pH (5.7–7.1), K (200–235 mg/kg), and HI (26.8–29.1) all had an impact on the indicators of the IJI community and their associated species, which were distributed on a slope angle of 28–75° (Figure 3 and Supplementary data Figures S1–S4).

3.2.3. *Cedrus–Cynodon–Isodon* Community

This community (CCI) was recognized in 12 stands between altitudes of 1580.8–1982 m. *Cedrus deodara* (11.77 IV), *Cynodon dactylon* (10.42 IV) and *Isodon rugosus* (6.02 IV) were recorded as the leading indicators of this plant community. Other co-dominant species were *Dryopteris wallichiana*, *Oxalis corniculate*, *Medicago sativa*, *Cyperus rotundus*, *Fragaria nubicola*, *Adiantum capillus-veneris*, *Impatiens bicolor*, *Trifolium repens*, *Clematis grata*, *Artemisia absinthium*, *Leptodermis virgata*, *Convolvulus arvensis*, *Tagetes minuta*, *Cirsium arvense*, *Persicaria capitata* and *Hedera nepalensis*. Nonetheless, *Silybum marianum*, *Dicliptera bupleuroides*, *Cichorium intybus*, *Pteridium aquilinum*, *Geranium nepalense*, *Conyza japonica*, *Malvastrum coromandelianum*, *Saussurea* sp., *Pinus roxburghii*, *Achyranthes bidentata* and *Pyrus pashia* were found

as the rare species with lower IV values. Therophytes dominated the life form spectra with 33.80% of species, followed by Hemicryptophytes with 25.35% of species, Chamaephytes with 12.68% of species, Nanophanerophytes and Geophytes each with 9.86% of species (Table 1). Nanophyll dominated the leaf size spectra with 40% of the species, followed by Microphyll with 30.67% of the species, and Leptophyll and Mesophyll with 10.67% of the species. Atmospheric humidity (53.6–74.9%), DP (15.5–19.1%), temperature (20.9–28.4 °C), EC (0.56–2.24 dsm^{-1}), OM (0.6–1.25%) and pH (5.9–7.3), were the most influential ecological variables that influenced the composition as well as distribution of plant species of CCI community. Aspect (N-E), slope angle (24–50°), and silty loam soil texture were also important significant variables of the CCI community (Supplementary data Figures S1–S4).

3.2.4. *Indigofera–Parrotiopsis–Bistorta* Community

The IPB community was recognized on the aspect (W-N) with a slope angle (45–80°) in four stands at an altitudinal range of 1789.6–1896.3 m, which has a total of 87 species associated species (Table 1). *Indigofera heterantha*, *Parrotiopsis jacquemontii*, *Bistorta amplexicaule* were recorded as the dominant species in this community with highest IV values of 12.34, 9.05 and 6.18, respectively. Other characteristic species based IV were *Indigofera hebepetala*, *Clematis grata*, *Bromus secalinus*, *Cynodon dactylon*, *Clinopodium vulgare*, *Cynoglossum glochidiatum*, *Urochloa panicoides*, *Isodon rugosus*, *Pimpinella stewartia*, *Berberis lycium*, *Dysphania ambrosioides*, *Pyrus pashia* and *Poa infirma*. Rare species of this community with minimum IV values were *Leptodermis virgata*, *Cynoglossum apenninum*, *Commelina benghalensis*, *Cannabis sativa*, *Bergenia ciliata*, *Crotalaria* sp., *Malva neglecta*, *Ficus carica*, *Salix alba*, *Achyranthes bidentata*, *Malvastrum coromandelianum*, *Cyperus odoratus*, *Fraxinus hookeri* and *Malva parviflora*. Therophytes dominated the life form spectra with 36.36% of plant species, followed by Hemicryptophytes with 25% of species. Nanophyll led the leaf size spectra with 45.45% of species, followed by Microphyll with 22.73% of the species (Table 1). The strongest environmental variables of this IPB community were pH (6.4–6.6), DP (18.6–21.4), and WB (20.8–23.8) and (Supplementary data Figures S1 and S4).

3.2.5. *Sambucus–Cedrus–Desmodium* Community

This plant community (SCD) was recorded with a total of 129 associates in 11 stands between the altitudinal ranges of 1936 to 2373.8 m. *Sambucus weightiana* (5.25 IV), *Cedrus deodara* (5.05 IV), Desmodium elegans (4.1 IV) were recognized as the topmost dominant species. *Sorbaria tomentosa*, *Dactylis glomerata*, *Heracleum candicans*, *Dryopteris wallichiana*, *Pennisetum orientale*, *Onopordum acanthium*, *Fragaria nubicola*, *Foeniculum vulgare*, *Parrotiopsis jacquemontiana* and *Phragmites latissimus* were other co-dominant species with lower IV values as compared to the community indicators. Nonetheless, *Phytolacca latbenia*, *Pleurospermum stellatum*, *P. stylosum*, *Seseli libanotis*, *Torilis japonica*, *Vicia sativa*, *Vincetoxicum petrense*, *Corydalis carinata*, *Polygonatum verticillatum*, *Salix tetrasperma*, *Sida cordata*, *Thalictrum pedunculatum*, *Lindelofia* sp., *Spiraea vaccinifolia* and *Trachyspermum amii* were found as the rare species with less IV values. Therophytic class dominated the life form spectrum, accounting for 43.69% of plant species, followed by nanophanerophytes (19.42%). Nanophyllous leaf size class dominated the SCD community with 31.30% of species, followed by Microphyll (28.24%) and Leptophyll (19.08%). Moreover, one aphyllous plant species was also found in SCD community (Table 1). The most influential ecological variables that influenced the composition of SCD community were K (210–228 mg/kg), P (12.8 mg/kg), pH (5.2–6.9), and EC (3.3 dsm^{-1}), and loamy soil texture (Figure 3), which were distributed on a slope angle of 25–85° (Supplementary data Figures S1–S4).

3.2.6. *Indigofera–Cedrus–Pinus* Community

This plant community was recognized in 12 stands on the N-W aspect between altitudinal ranges of 1932.3–2437.8 m, which has 141 associated species (Table 1). *Indigofera heterantha* (10.16 IV), *Cedrus deodara* (5.75 IV) and *Pinus wallichiana* (5.66 IV) were recorded as the leading indicators of this plant community with the highest IV values. Other co-

dominant species were *Viburnum grandiflorum*, *Cynodon dactylon*, *Heracleum candicans*, *Bistorta amplexicaulis*, *Poa infirma*, *Isodon rugosus*, *Lathyrus aphaca*, *Prunella vulgaris*, *Plantago major*, *Juglans regia*, *Impatiens brachycentra*, *Pennisetum orientale*, *Euphrasia himalayica* and *Pimpinella stewartii*. Nonetheless, rare species with lower IV values included *Epilobium hirsutum*, *Helianthus annuus*, *Salvia nubicola*, *Epimedium elatum*, *Sonchus asper*, *Avena sativa*, *Conyza japonica*, *Portulaca oleracea*, *Prunus armeniaca*, *Alcea rosea*, *Bauhinia variegata*, *Cotoneaster acuminatus*, *Lotus corniculatus*, *Lindelofia* sp., *Cornus macrophylla* and *Lavatera cachemiriana*. Therophytes dominated the life form spectra accounting 37.59% of all the species in the ICP community, followed by Hemicryptophytes (25.53%), Nanophanerophytes (11.35%), and geophytes (9.22%). The nanophyllous class dominated the leaf size spectra with 31.21% of species, followed by Microphyll (26.95%), and Leptophyll (17.02%). Nonetheless, aphyllous species accounted for the least number of species in the ICP community (1.42% of species, Table 1). The strongest ecological variables that significantly influenced the composition of plant species of ICP community associates were $CaCO_3$ (7.5 mg/kg), humidity (49.2–68.5%), and soil texture (silty loam) (Figure 3 and Supplementary data Figures S1–S4).

3.2.7. *Cedrus–Pinus–Parrotiopsis* Community

CPP community was recorded in 17 stands between the altitudinal ranges of 2292–3168 m. The highest number of species (197 species) were recorded in this plant community (Table 1 and Figure 2). *Cedrus deodara* (19.88 IV), *Pinus wallichiana* (17.26 IV) and *Parrotiopsis jacquemontii* (8.5 IV) were recognized as the topmost dominant species. Other co-dominant species with lower IV values than the community indicators included *Cynodon dactylon*, *Oxalis corniculata*, *Clinopodium vulgare*, *Isodon rugosus*, *Indigofera heterantha*, *Impatiens bicolor*, *Fragaria nubicola*, *Geranium wallichianum* and *Clematis grata* were. Moreover, species that were rarely recorded in this community were *Rhynchosia pseudo-cajan*, *Sorbus tomentosa*, *Euphorbia helioscopia*, *Galium asparagifolium*, *Hyoscyamus niger*, *Silene conoidea*, *Poa infirma*, *Rosa webbiana*, *Galium aparine*, *Rumex nepalensis*, *Smilax glaucophylla*, *Spiranthes sinensis* and *Vicia sativa*. Therophytes dominated the life form spectra with 42.31% of species, followed by Hemicryptophytes with 27.47% of species. The microphyllous and Nanophyllous classes dominated the leaf size spectra, accounting for 30.96% of species, followed by Leptophyll (17.77%) and mesophyll (14.72%) (Table 1). Loamy and silty loamy texture, P (11.12 mg/kg), and K (214.6 mg/kg) were all influencing variables for the CPP community (Figure 3 and Supplementary data Figures S1–S4). As a result, the highest species diversity was observed in this CPP community.

3.2.8. *Pinus-Viburnum-Cedrus* Community

The PVC community was recognized on the northern aspect between altitudinal ranges of 2568–3191 m in 7 stands with a total of 195 associated plant species. *Pinus wallichiana-Viburnum grandiflorum-Cedrus deodara* were recorded as the dominant species in this community with highest IV values of 17.98, 16.43, and 9.92, respectively. Other co-dominant and characteristic plant species were *Abies pindrow*, *Arisaema jacquemontii*, *Juniperus squamata*, *Juniperus communis*, *Picea smithiana*, *Fragaria nubicola*, *Cynodon dactylon*, *Quercus incana*, *Urochloa panicoides* and *Bergenia stracheyi*. Moreover, rare species of this PVC community with lower IV values included *Impatiens bicolor*, *Lotus corniculatus*, *Rumex nepalensis*, *Epilobium latifolium*, *Helianthus annuus*, *Inula cuspidata*, *Platanus orientalis*, *Pleurospermum stylosum*, *Pteracanthus urticifolius* and *Swertia paniculata*. Therophytes dominated the life form with 33.66% of species, followed by Hemicryptophytes with 30.69% of species, and Nanophanerophytes with 11.88% of species (Table 1). Nanophyllous dominated the leaf size spectra, accounting for 34.18% of plant species, followed by Microphyll (18.06%) and Leptophyll (16.84%) (Table 1). OM (2.12%), K (215.7 mg/kg), P (11.9 mg/kg), and EC (2.12 dsm^{-1}) were the most effective ecological variables that had a positive influence on the species diversity of the PVC community (Supplementary data Figures S1–S4).

3.2.9. *Abies–Picea–Juniperus* Community

This community (APJ) was recorded at the middle altitudinal range (2874–3260 m) of the north-western aspect of the study area with 66 associated plant species (Table 1). The indicators of the APJ community are *Abies pindrow* (26.17 IV), *Picea smithiana* (23.77 IV), and *Juniperus squamata* (21.77 IV). *Thymus linearis*, *Bistorta affinis*, *Bergenia stracheyi*, *Rheum australe*, and *Poa infirma* are some of the herb layer's co-dominant species, while *Juniperus communis* and *Cotoneaster microphyllus* are the distinguishing species of the shrubby layer. Furthermore, *Quercus incana* and *Pinus wallichiana* are the major tree layer associates with the APJ community. The APJ community is characterised by a preference for the shade. In comparison to sub-alpine (JSJ) and alpine (SBR) communities, hill slopes get less direct sunlight. The shade effect was significantly influenced by the tree layer's larger canopy cover. Hemicryptophytes dominated the life form classes with 40.98% of species, followed by Therophytes (29.51%), Chamaephytes, and Geophytes (9.84%) each. The nanophyllous class dominated the leaf size spectra, accounting for 33.33% of plant species, followed by Microphyll (27.27%) and Leptophyll (24.24%) (Table 1). Low K (205.4 mg/kg) and low EC (1.4 dsm^{-1}) were the most significant ecological variables that played a vital role in the formation of the APJ community. Moreover, the APJ community was hosted by a clay-loamy soil texture (Supplementary data Figures S1–S4) with a low pH (Figure 3).

3.2.10. *Juniperus–Sibbaldia–Juniperus* Community

With a total of 40 associated species, this community (JSJ) was observed in six stands varying in altitude from 3250 to 3644 m (Table 1). The indicators of the JSJ community are shrubs, i.e., *Juniperus squamata*, *Sibbaldia procumbens*, *Juniperus squamata*. The tree layer was represented by the only species (*Rhododendron arboreum*). Other shrubby layer associates of the JSJ community includes *Cotoneaster microphyllus*, and *Juniperus excelsa*, while the herb layer associates were *Bergenia stracheyi*, *Bistorta affinis*, *Caltha palustris*, *Dracocephalum nutans*, *Primula hazarica*, *Poa infirma* and *Rheum australe*. Hemicryptophytes dominated the life form spectra, accounting for 56.82% of plant species, followed by Therophytes (18.18%), Geophytes and Nanophanerophytes (11.36%) each (Table 1). The leaf size spectrum was dominated by Nanophyllous class (34.69% of plant species), followed by Leptophyll (26.53% of plant species), Microphyll (20.41% of plant species) and Mesophyll (14.29% of plant species). Low EC (0.85 dsm^{-1}), temperature (7.4–13.8 °C), WS (2–3 m/s) and DP (12.8–15.5) all had a significant impact on the JSJ community. As a result, these ecological variables constrain the species diversity of JSJ community (Supplementary data Figures S1–S4).

3.2.11. *Sibbaldia–Bergenia–Rheum* Community

This community (SBR) was identified at the higher altitudinal ranges (3199–3688 m) above the timber line at latitude (N = 34.69472–34.79333) and longitude (E = 73.60278–73.68639). The SBR community represents subalpine vegetation, having *Sibbaldia procumbens* (10.78 IV), *Bergenia stracheyi* (8.37 IV), and *Rheum australe* (7.75 IV) as the indicator species, for a total of 53 associated species. The herbaceous species dominated the vegetation, although some nanophanerophytes occur at comparatively lower altitudes, i.e., *Juniperus squamata*, *J. communis*, *J. excelsa* and *Cotoneaster microphyllus*. Nevertheless, other herbaceous co-dominants were *Poa alpina*, *P. infirma*, *Bistorta affinis*, and *Primula hazarica*. This subalpine community develops in between the timberline and alpine meadows, regardless of slope aspect, and overlaps with the alpine community (*Poa-Bistorta-Primula*) at most of the elevations. Hemicryptophytes dominated the life form spectra with 48% of species, followed by Therophytes (24% of species) and chamaephytes (12% of species). The Nanophyllous class dominated the leaf size spectra, accounting for 38% of all species, followed by Leptophyll (18%) and microphyll (20%) (Table 1). The altitude and WS (2.5–5 m/s) had a significant impact on this plant community. The indicators, as well as other associated species were also found to be temperature sensitive. The soil texture hosting the SBR community was mainly clay, with the lowest K (197–216.6 mg/kg) and pH (4.8–5.8) values and maximum OM (0.98–2.28%) concentration (Figure 3). Moreover, the SBR community was found to be

negatively associated with ecological variables such as humidity, $CaCO_3$, HI, WB, BP, and slope angle (Supplementary data Figures S1, S3 and S4).

3.2.12. *Poa-Bistorta-Primula* Community

The *Poa-Bistorta-Primula* Community (PBP) was recognized as the highest altitudinal (3724–4278 m) alpine and cold desert plant community recorded at a latitude (N = 34.69306–34.83861) and a longitude (E = 73.60750–73.69444). *Poa alpina* (17.32 IVI), *Bistorta affinis* (15.03 IV), and *Primula rosea* (9.07 IV) are the indicator species of PBP community. Other co-dominant species are *Rheum australe*, *Bergenia stracheyi* and *Androsace hazarica*. This plant community included a total of 39 species. However, tree and shrub layers (Phanerophytes and Nanophanerophytes) were entirely absent from these alpine meadows. Moreover, this alpine community (PBP) has a low species richness as compared to other plant communities (Figure 2 and Table 1). Extremely low temperatures are a hallmark of the growth period due to high elevation. Xeric conditions compounded such harsh environments, and a relatively short growth season was recorded from July to September. Hemicryptophytes contributed 53.85% of the species, followed by Therophytes (23.08%), Chamaephytes (12.82%), and Geophytes (10.26%). Microphyll and Nanophyll classes dominated the leaf size spectra with 28.95% of species each, followed by Leptophyll (21.05%) (Table 1). Higher altitude and WS (3.5–8 m/s), as well as low temperature had a strong impact on the indicators and other associates of PBP community. The soil texture hosting this community was sandy in nature (Figure 3), with the lowest K (196–206.9 mg/kg) and pH (4.9–5.6) and maximum OM (1.15–2.64%) concentration. Furthermore, the PBP community was found to be negatively associated with ecological variables such as humidity, $CaCO_3$, HI, WB, BP, and slope angle (Supplementary data Figures S1–S4).

3.3. Non-Metric Multidimensional Scaling (NMDS)

All the data based on 354 plant species in 133 sampled stands were categorized into 12 plant communities using NMDS. Plant communities that are close together or on the same axis have a positive correlation, whereas communities that are far apart or on different axes have a negative correlation. The *Poa–Bistorta–Primula*, *Sibbaldia–Bergenia–Rheum*, and *Juniperus–Sibbaldia–Juniperus* communities, for example, had a positive association with one another but negatively correlated with the *Indigofera–Juglans–Isodon*, and *Indigofera-Cedrus–Pinus* communities (Figure 4). All these relationships could be attributed to patterns in the variables of their host environment. For example, the former plant communities were found at elevations of 3724–4278 m, 3199–3688 m, and 3250–3644 m, respectively, while the latter plant communities were found at lower elevations (1597–2456 m and 1932.3–2437.8 m), respectively. Moreover, four stands (S38, S39, S40, S41 and S42) are correlated with each other and shaped the SSI community. The PBP community identified in 13 stands can be seen far apart from the other plant communities. Only the three most representative plant species for each community are plotted.

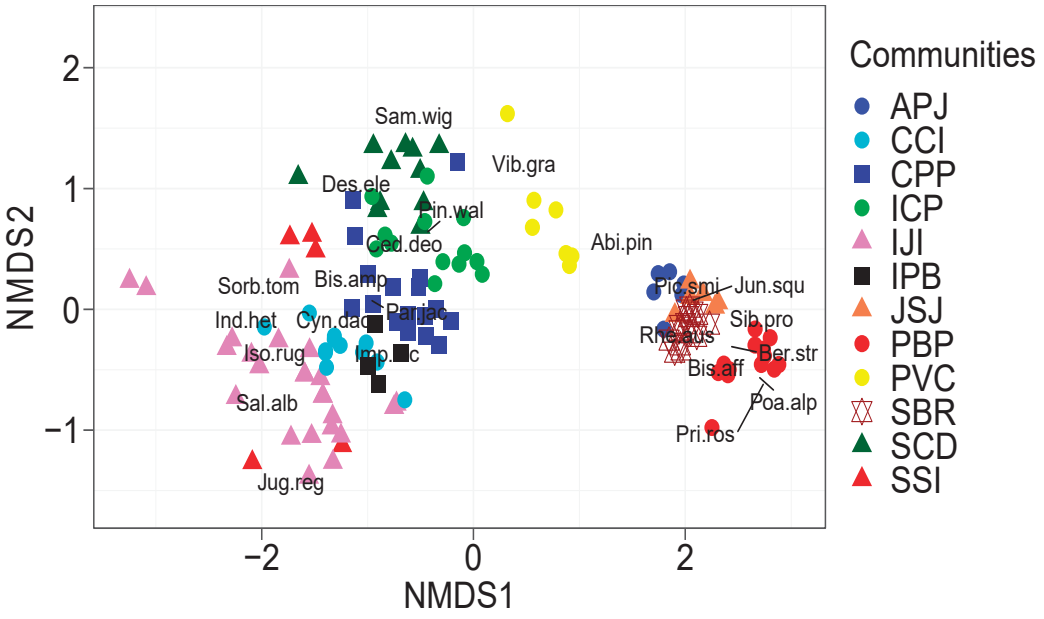

Figure 4. NMDS ordination is based on plant species that are in association with sampled stands and grouped into communities Plant communities that are close together or on the same axis and have a positive correlation. Only the three most representative plant species for each community are plotted. Some species are present in different communities and due to that, the total number of species are not 36.

3.4. Canonical Correspondence Analysis (CCA)

The CCA and variation partitioning tests showed that the total inertia results of CCA was 8.626, where our final variables (Altitude, Slope ES, Slope SE, Slope SW, Slope WN, EC, heat index) together explained 22.6% of variation. CCA model was significant (χ^2 = 1.951; pseudo-F value = 4.529; $p < 0.001$). For the 8 explanatory variables, we tested simple term effects. Simple term effects showed that all variables were significant (χ^2_{range} = 0.104–0.785; pseudo-F value$_{[range]}$ = 1.93–14.59; $p < 0.006$; Table 1). Finally, the two first axis were also highly significant ($p < 0.001$). Table 2 displays the significance level of the testing results regarding the influence of environmental variables on the vegetation of the Manoor Valley. The PBP, SBR and JSJ plant communities revealed positive association with altitude (Supplementary data Figures S1–S4). All these plant communities were found at the higher altitudes (3724–4278 m, 3199–3688 m, and 3250–3644 m), respectively. The slope angle, on the other hand, has a negative relationship with altitude. The IJI and ICP plant communities are in positive association with slope angle. This strong influential association might be due to the occurrence of these plant communities in the lower (1597–2456 m) and middle (1932.3–2437.8 m) altitudinal ranges.

Table 2. Detailed numerical results of variations partitioning (partial CCA) for groups of variables.

Gradient Class	Variation (adj)	% of Explained	Eigen Values				F	*p*
			Axis 1	Axis 2	Axis 3	Axis 4		
Edaphic	9.8	18.7	0.6211	0.1887	0.1135	0.0904	2.1	0.002
Climatic	9.8	13.9	0.7210	0.1138	0.0841	0.0546	3.4	0.002
Physio-graphic	18.1	25.5	0.7641	0.2903	0.2176	0.1624	3.4	0.002
Aspect	9.1	15.3	0.4280	0.1675	0.1417	0.1206	2.5	0.002

4. Discussion

Plant species are distributed in diverse types of habitats, forming different communities driven by different sets of environmental variables [6]. The aspect stimulates habitat diversification and promotes micro-environmental variation in the vegetation structure [36,37]. As a result, the composition of different units is observed as a reflection of changing habitat settings along environmental variables [38]. Here, we used different multivariate approaches to assess potential plant communities along an altitudinal gradient and their association with different environmental drivers. Our study documented 354 plant species belonging to 93 families. The current research area is located at the elevations ranging from 1580 m to 4278 m, with varying environmental conditions that are reflected in a rich and diverse flora. Our results showed that at high altitudes, species richness was reduced, whereas an increase in soil nutrients was linked to progression in vegetation indicators. We also found different clusters of species with similar habitats. Our study clearly shows how altitudinal variables can cluster different plant communities according to different microclimates.

In the current vegetational sampling of a remote valley (Manoor Valley, Himalaya), 12 major plant communities were established by TWINSPAN from the lower ranges to the alpine meadows. The CPP communities (197 species) in the middle altitudinal habitats (2292–3168 m) have the most plant species. Ordination methods have commonly been used to show species distribution and community structure along ecological variables [98,99]. Similarly, a researcher investigated the vegetation of the western Himalayas and identified five distinct communities, the most abundant of which were found on north-facing slopes at middle altitudes, where the moisture levels were highest [6]. Thirteen major groups were identified in the vegetation of Kammanassie areas using the TWINSPAN classification [100]. These results, along with ours, show evidence that elevational variables are suitable places to evaluate how changes in environmental variables drive plant community structure and diversity. In addition, these results also show that multivariate approaches are powerful tools for community analysis [43] and can be considered in new ecological studies as statistical methods.

As the study area is in the Himalayan belt, the vegetation was primarily of a Sino-Japanese nature. The plant communities were classified based upon climatic (i.e., temperature, HI, DP, WB, BP, and WS), edaphic (i.e., soil pH, EC, OM, P, K, $CaCO_3$, soil texture), and topographic variables (i.e., altitude, altitudinal density, latitude, longitude, slope angle, different exposures, and aspects). The vegetation was classified into different communities/associations [101,102] represented by dominant species based on their importance values [20,103]. At lower elevational ranges (1580.8–2456 m), the plant communities with dominant species were *Salix alba*, *Sorbaria tometosa*, and *Impatiens bicolor* (SSI), *Indigofera heterantha, Juglans regia*, and *Isodon rugosus* (IJI), *Cedrus deodara, Cynodon dactylon*, and *Isodon rugosus* (CCI), *Indigofera heterantha, Parrotiopsis jacquemontii*, and *Bistorta amplexicaule* (IPB), and *Sambucus weightiana, Cedrus deodara*, and *Desmodium elegans* (SCD) respectively. Similar indicators were recorded by other researchers during a field survey in the Himalayas of Pakistan [104].

The vegetation in the upper altitudinal ranges includes *Pinus wallichiana, Abies pindrow, Indigofera heterantha* and *Viburnum grandiflorum*, which are the representatives of moist temperate forests. These plant species are the temperate zone representatives [30,39,41,105,106]. These plant associations were shaped by the impact of various environmental gradients. Ecosystems respond to numerous simultaneous changes in the environment as these variations differ the diversity and distribution of communities [107,108]. Vegetation in distributions more closely resembles the changes in soil characteristics [109–111]. Our results revealed that soil characteristics such as EC, pH, soil texture, OM, K and P had a great impact on plant community distribution and association. Soil variables, altitude, latitude, slope aspect and angle also had a strong influence on species richness, as previously reported by [112].

Dissimilar plant communities were described as those with less than 65% similarity [113,114]. The communities' similarities were due to shrubs, trees, and perennial plants,

while the communities' dissimilarities were due to Therophytes. The maximum similarity index was noted between SBR and JSJ communities (55.53%), followed by JSJ and APJ communities with 39.71% of similarity. The highest similarity between communities may be due to similar environmental conditions [30], which leads to changes in the species' habitat. The highest dissimilarity was observed between PBP and IPB communities, JSJ and SSI communities (99.94% each), followed by IJI and PBP communities (99.92%), SSI and PBP communities (99.91%). These results follow the findings of [6,53]. Maximum dissimilarity between communities might be due to wide altitudinal variation among communities [30,115], which represents the presence of different set of species adapted to different set of climatic variables [112,116–118].

5. Conclusions

To the best of our knowledge, this is the only valley within the Himalayas of Pakistan that has never been explored before, due to its harsh terrain and geographical location. The current study revealed that the sampled area has rich species diversity. The study provides the first ever detailed insights into the spatial distribution and vegetation mapping in response to environmental variables in the study area. The flora of the Manoor Valley consists of 354 plant species belonging to 93 families, distributed into a total of 12 major plant communities, from the lowest altitude to the alpine zones. The *Cedrus–Pinus–Parrotiopsis* community resided at the middle altitudinal ranges (2292–3168 m) was recorded with highest number of associates (197 species). Our study clearly shows how altitudinal variables can cluster different plant communities according to different microclimates, which can be a proxy for future studies evaluating the impacts of climate change on plant communities. Studies such as ours are paramount to better understand how environmental factors influence ecological and evolutionary aspects.

Supplementary Materials: The following supporting information can be downloaded at: https://www.mdpi.com/article/10.3390/plants11010087/s1. Figure S1: Canonical correspondence analysis: (a) & (c) the contour plot shows the count of species at each axis, (b) Distribution of plant species along the edaphic variables, (d). Distribution of plant species along the climatic variables. Figure S2: Canonical correspondence analysis: (a). the contour plot shows the count of species at each axis, (b). Distribution of plant species along the slope aspects. Figure S3: Canonical correspondence analysis: (a) Distribution of stands along the edaphic variables, (b) and (c) Van Dobben circles show the correlation of species in association to edaphic variables and among them, i.e., red circle shows the positive and blue indicates the negative correlation. Figure S4: Canonical correspondence analysis: (a) Association of sampling sites along the climatic variables, (b). Association of sampling sites along the slope aspects.

Author Contributions: I.U.R.: Conceptualization, Methodology, Software, Data curation, Writing—Original draft preparation. A.A.: Supervision, Visualization. Z.I.: Supervision, Methodology, Validation. M.N.A., A.-B.F.A.-A., A.A.A. and E.F.A.: Resources, helped in revision, Validation. N.A., S.S., M.A.K., U.K., F.I. and S.M.: helped in revision, Reviewing and Editing. E.S.C.: Reviewing and Editing, Validation. All authors have read and agreed to the published version of the manuscript.

Funding: The authors would like to extend their sincere appreciation to the Researchers Supporting Project Number (RSP-2021/134), King Saud University, Riyadh, Saudi Arabia.

Acknowledgments: The first author is thankful to Bougand Bassuner (Lehmann Building, Missouri Botanical Garden, St. Louis, MO, USA) for providing support and guidance using ArcGIS software. The authors would like to extend their sincere appreciation to the Researchers Supporting Project Number (RSP-2021/134), King Saud University, Riyadh, Saudi Arabia.

Conflicts of Interest: The authors declare no conflict of interest.

References

1. Capelo, J. Using species abundance and phylogeny conjointly to approach vegetation classification: A case study on Macaronesia's woody vegetation. *J. Veg. Sci.* **2020**, *31*, 616–633. [CrossRef]
2. Czortek, P.; Orczewska, A.; Dyderski, M.K. Niche differentiation, competition or habitat filtering? Mechanisms explaining co-occurrence of plant species on wet meadows of high conservation value. *J. Veg. Sci.* **2021**, *32*, e12983. [CrossRef]

3. Černý, T.; Kopecký, M.; Petřík, P.; Song, J.; Šrůtek, M.; Valachovič, M.; Altman, J.; Doležal, J. Classification of K orean forests: Patterns along geographic and environmental gradients. *Appl. Veg. Sci.* **2015**, *18*, 5–22. [CrossRef]
4. Rahman, I.U. Ecophysiological Plasticity and Ethnobotanical Studies in Manoor Area, Kaghan Valley, Pakistan. Ph.D. Thesis, Hazara University, Mansehra, Pakistan, 2020.
5. Haq, F. Phytosociological Attributes of Different Vegetational Zones of Nandiar Khuwar Catchment Area. Ph.D. Thesis, Hazara University, Mansehra, Pakistan, 2015.
6. Khan, S.M. Plant Communities and Vegetation Ecosystem Services in the Naran Valley, Western Himalaya. Ph.D. Thesis, University of Leicester, Leicester, UK, 2012.
7. Loreau, M.; Naeem, S.; Inchausti, P.; Bengtsson, J.; Grime, J.P.; Hector, A.; Hooper, D.U.; Huston, M.A.; Raffaelli, D.; Schmid, B. Biodiversity and ecosystem functioning: Current knowledge and future challenges. *Science* **2001**, *294*, 804–808. [CrossRef] [PubMed]
8. Hamilton, A.J. Species diversity or biodiversity? *J. Environ. Manage.* **2005**, *75*, 89–92. [CrossRef] [PubMed]
9. Chiarucci, A.; Bacaro, G.; Scheiner, S.M. Old and new challenges in using species diversity for assessing biodiversity. *Philos. Trans. R. Soc. B Biol. Sci.* **2011**, *366*, 2426–2437. [CrossRef]
10. Field, R.; Hawkins, B.A.; Cornell, H.V.; Currie, D.J.; Diniz-Filho, J.A.F.; Guégan, J.-F.; Kaufman, D.M.; Kerr, J.T.; Mittelbach, G.G.; Oberdorff, T.; et al. Spatial species-richness gradients across scales: A meta-analysis. *J. Biogeogr.* **2009**, *36*, 132–147. [CrossRef]
11. Kullman, L. Alpine flora dynamics—A critical review of responses to climate change in the Swedish Scandes since the early 1950s. *Nord. J. Bot.* **2010**, *28*, 398–408. [CrossRef]
12. Jabis, M.D. Climate Change Impacts in Alpine Plant Communities. Ph.D. Thesis, UC Berkeley, Berkeley, CA, USA, 2018.
13. Malanson, G.P.; Nelson, E.L.; Zimmerman, D.L.; Fagre, D.B. Alpine plant community diversity in species–area relations at fine scale. *Arctic, Antarct. Alp. Res.* **2020**, *52*, 41–46. [CrossRef]
14. Dvorský, M.; Doležal, J.; De Bello, F.; Klimešová, J.; Klimeš, L. Vegetation types of East Ladakh: Species and growth form composition along main environmental gradients. *Appl. Veg. Sci.* **2011**, *14*, 132–147. [CrossRef]
15. Pauli, H.; Gottfried, M.; Dullinger, S.; Abdaladze, O.; Akhalkatsi, M.; Alonso, J.L.B.; Coldea, G.; Dick, J.; Erschbamer, B.; Calzado, R.F.; et al. Recent Plant Diversity Changes on Europe's Mountain Summits. *Science* **2012**, *336*, 353–355. [CrossRef]
16. Steinbauer, M.J.; Grytnes, J.-A.; Jurasinski, G.; Kulonen, A.; Lenoir, J.; Pauli, H.; Rixen, C.; Winkler, M.; Bardy-Durchhalter, M.; Barni, E.; et al. Accelerated increase in plant species richness on mountain summits is linked to warming. *Nature* **2018**, *556*, 231–234. [CrossRef] [PubMed]
17. Adair, K.L.; Lindgreen, S.; Poole, A.M.; Young, L.M.; Bernard-Verdier, M.; Wardle, D.A.; Tylianakis, J.M. Above and belowground community strategies respond to different global change drivers. *Sci. Rep.* **2019**, *9*, 1–11. [CrossRef] [PubMed]
18. Brun, P.; Zimmermann, N.E.; Graham, C.H.; Lavergne, S.; Pellissier, L.; Münkemüller, T.; Thuiller, W. The productivity-biodiversity relationship varies across diversity dimensions. *Nat. Commun.* **2019**, *10*, 1–11. [CrossRef]
19. Curtis, J.T.; McIntosh, R. The interrelations of certain analytic and synthetic phytosociological characters. *Ecology* **1950**, *31*, 434–455. [CrossRef]
20. Dufrêne, M.; Legendre, P. Species assemblages and indicator species: The need for a flexible asymmetrical approach. *Ecol. Monogr.* **1997**, *67*, 345–366. [CrossRef]
21. Paudel, P.K.; Sipos, J.; Brodie, J.F. Threatened species richness along a Himalayan elevational gradient: Quantifying the influences of human population density, range size, and geometric constraints. *BMC Ecol.* **2018**, *18*, 1–8. [CrossRef]
22. Hussain, F.; Shah, S.M.; Badshah, L.; Durrani, M.J. Diversity and ecological characteristics of flora of Mastuj valley, district Chitral, Hindukush range, Pakistan. *Pak. J. Bot* **2015**, *47*, 495–510.
23. Rahman, I.U.; Afzal, A.; Iqbal, Z.; Ijaz, F.; Ali, N.; Asif, M.; Alam, J.; Majid, A.; Hart, R.; Bussmann, R.W. First insights into the floristic diversity, biological spectra and phenology of Manoor valley, Pakistan. *Pakistan J. Bot.* **2018**, *50*, 1113–1124.
24. Rahman, I.U.; Hart, R.; Afzal, A.; Iqbal, Z.; Abdallah, E.F.; Alqarawi, A.A.; Ijaz, F.; Ali, N.; Kausar, R.; Muzammil, S.; et al. Phenological plasticity in Berberis lycium Royle along temporal and altitudinal gradients. *Appl. Ecol. Environ. Res.* **2019**, *17*, 331–341. [CrossRef]
25. Cañadas, E.M.; Fenu, G.; Peñas, J.; Lorite, J.; Mattana, E.; Bacchetta, G. Hotspots within hotspots: Endemic plant richness, environmental drivers, and implications for conservation. *Biol. Conserv.* **2014**, *170*, 282–291. [CrossRef]
26. Noroozi, J.; Talebi, A.; Doostmohammadi, M.; Rumpf, S.B.; Linder, H.P.; Schneeweiss, G.M. Hotspots within a global biodiversity hotspot—Areas of endemism are associated with high mountain ranges. *Sci. Rep.* **2018**, *8*, 10345. [CrossRef] [PubMed]
27. Kidane, Y.O.; Steinbauer, M.J.; Beierkuhnlein, C. Dead end for endemic plant species? A biodiversity hotspot under pressure. *Glob. Ecol. Conserv.* **2019**, *19*, e00670. [CrossRef]
28. Noroozi, J.; Naqinezhad, A.; Talebi, A.; Doostmohammadi, M.; Plutzar, C.; Rumpf, S.B.; Asgarpour, Z.; Schneeweiss, G.M. Hotspots of vascular plant endemism in a global biodiversity hotspot in Southwest Asia suffer from significant conservation gaps. *Biol. Conserv.* **2019**, *237*, 299–307. [CrossRef]
29. Givnish, T.J. On the causes of gradients in tropical tree diversity. *J. Ecol.* **1999**, *87*, 193–210. [CrossRef]
30. Iqbal, Z.; Zeb, A.; Abd_Allah, E.F.; Rahman, I.U.; Khan, S.M.; Ali, N.; Ijaz, F.; Anwar, Y.; Muzammil, S.; Alqarawi, A.A.; et al. Ecological assessment of plant communities along the edaphic and topographic gradients of biha valley, District Swat, Pakistan. *Appl. Ecol. Environ. Res.* **2018**, *16*. [CrossRef]
31. Klanderud, K.; Birks, H.J.B. Recent increases in species richness and shifts in altitudinal distributions of Norwegian mountain plants. *The Holocene* **2003**, *13*, 1–6. [CrossRef]

32. Odland, A.; Birks, H.J.B. The altitudinal gradient of vascular plant richness in Aurland, western Norway. *Ecography (Cop.).* **1999**, *22*, 548–566. [CrossRef]
33. Weckström, J.; Korhola, A. Patterns in the distribution, composition and diversity of diatom assemblages in relation to ecoclimatic factors in Arctic Lapland. *J. Biogeogr.* **2001**, *28*, 31–45. [CrossRef]
34. Heywood, V.H.; Watson, R.T. *Global Biodiversity Assessment*; Cambridge University Press: Cambridge, UK, 1995; Volume 1140.
35. McGrady-Steed, J.; Morin, P.J. Biodiversity, density compensation, and the dynamics of populations and functional groups. *Ecology* **2000**, *81*, 361–373. [CrossRef]
36. Luo, Z.; Tang, S.; Li, C.; Fang, H.; Hu, H.; Yang, J.; Ding, J.; Jiang, Z. Environmental effects on vertebrate species richness: Testing the energy, environmental stability and habitat heterogeneity hypotheses. *PLoS ONE* **2012**, *7*, e35514. [CrossRef] [PubMed]
37. Yang, Z.; Liu, X.; Zhou, M.; Ai, D.; Wang, G.; Wang, Y.; Chu, C.; Lundholm, J.T. The effect of environmental heterogeneity on species richness depends on community position along the environmental gradient. *Sci. Rep.* **2015**, *5*, 15723. [CrossRef] [PubMed]
38. Smith, M.; Facelli, J.; Cavagnaro, T. Interactions between soil properties, soil microbes and plants in remnant-grassland and old-field areas: A reciprocal transplant approach. *Plant Soil* **2018**, *433*, 127–145. [CrossRef]
39. Champion, S.H.; Seth, S.K.; Khattak, G.M. *Forest Types of Pakistan*; Pakistan Forest Institute: Peshawar, Pakistan, 1965.
40. Beg, A.R. *Wildlife Habitats of Pakistan*; Pakistan Forest Institute: Peshawar, Pakistan, 1975.
41. Ahmed, M.; Husain, T.; Sheikh, A.H.; Hussain, S.S.; Siddiqui, M.F. Phytosociology and structure of Himalayan forests from different climatic zones of Pakistan. *Pakistan J. Bot.* **2006**, *38*, 361.
42. Rahman, I.-U.; Afzal, A.; Abd_Allah, E.F.; Iqbal, Z.; Alqarawi, A.A.; Hashem, A.; Calixto, E.S.; Ali, N.; Asmarayani, R. Composition of plant communities driven by environmental gradients in alpine pastures and cold desert of northwestern Himalaya, Pakistan. *Pakistan J. Bot.* **2021**, *53*, 655–664. [CrossRef]
43. Rahman, I.U.; Afzal, A.; Iqbal, Z.; Bussmann, R.W.; Alsamadany, H.; Calixto, E.S.; Shah, G.M.; Kausar, R.; Shah, M.; Ali, N.; et al. Ecological gradients hosting plant communities in Himalayan subalpine pastures: Application of multivariate approaches to identify indicator species. *Ecol. Inform.* **2020**, *60*, 101162. [CrossRef]
44. Rahman, I.U.; Afzal, A.; Iqbal, Z.; Hart, R.; Abd_Allah, E.F.; Alqarawi, A.A.; Alsubeie, M.S.; Calixto, E.S.; Ijaz, F.; Ali, N.; et al. Response of plant physiological attributes to altitudinal gradient: Plant adaptation to temperature variation in the Himalayan region. *Sci. Total Environ.* **2020**, *706*, 135714. [CrossRef]
45. Rahman, I.U.; Calixto, E.S.; Afzal, A.; Iqbal, Z.; Ali, N.; Ijaz, F.; Shah, M.; Hakeem, K.R. Advanced multivariate and computational approaches in agricultural studies. In *Essentials of Bioinformatics, Volume II: In Silico Life Sciences: Medicine*; Shaik, N.A., Hakeem, K.R., Banaganapall, B., Elango, R., Eds.; Springer International Publishing: Cham, Switzerland, 2019; pp. 93–102. ISBN 9783030193171.
46. Gehlhausen, S.M.; Schwartz, M.W.; Augspurger, C.K. Vegetation and microclimatic edge effects in two mixed-mesophytic forest fragments. *Plant Ecol.* **2000**, *147*, 21–35. [CrossRef]
47. Sánchez-Rojas, G.; Gallina, S. Factors affecting habitat use by mule deer (*Odocoileus hemionus*) in the central part of the Chihuahuan Desert, Mexico: An assessment with univariate and multivariate methods. *Ethol. Ecol. Evol.* **2000**, *12*, 405–417. [CrossRef]
48. Kleyer, M.; Dray, S.; Bello, F.; Lepš, J.; Pakeman, R.J.; Strauss, B.; Thuiller, W.; Lavorel, S. Assessing species and community functional responses to environmental gradients: Which multivariate methods? *J. Veg. Sci.* **2012**, *23*, 805–821. [CrossRef]
49. Gauch, H.G.; Gauch, H.G., Jr. *Multivariate Analysis in Community Ecology*; Cambridge University Press: Cambridge, UK, 1982; ISBN 0521282403.
50. Rahman, I.U.; Afzal, A.; Iqbal, Z.; Abd-Allah, E.F.; Alqarawi, A.A.; Calixto, E.S.; Ali, N.; Ijaz, F.; Kausar, R.; Alsubeie, M.S.; et al. Role of multivariate approaches in floristic diversity of Manoor valley (*Himalayan region*) Pakistan. *Appl. Ecol. Environ. Res.* **2019**, *17*, 1475–1498. [CrossRef]
51. Rahman, I.U.; Ijaz, F.; Afzal, A.; Iqbal, Z.; Ali, N.; Khan, S.M. Contributions to the phytotherapies of digestive disorders: Traditional knowledge and cultural drivers of Manoor Valley, Northern Pakistan. *J. Ethnopharmacol.* **2016**, *192*, 30–52. [CrossRef] [PubMed]
52. Clift, P.D.; Giosan, L.; Blusztajn, J.; Campbell, I.H.; Allen, C.; Pringle, M.; Tabrez, A.R.; Danish, M.; Rabbani, M.M.; Alizai, A. Holocene erosion of the Lesser Himalaya triggered by intensified summer monsoon. *Geology* **2008**, *36*, 79–82. [CrossRef]
53. Haq, F.; Ahmad, H.; Iqbal, Z.; Alam, M.; Aksoy, A. Multivariate approach to the classification and ordination of the forest ecosystem of Nandiar valley western Himalayas. *Ecol. Indic.* **2017**, *80*, 232–241. [CrossRef]
54. Buckland, S.T.; Anderson, D.R.; Burnham, K.P.; Laake, J.L.; Borchers, D.L.; Thomas, L. *Introduction to Distance Sampling: Estimating Abundance of Biological Populations*; Oxford Univ. Press: Oxford, UK, 2001.
55. Buckland, S.T.; Anderson, D.R.; Burnham, K.P.; Laake, J.L.; Borchers, D.L.; Thomas, L. *Advanced Distance Sampling*; Oxford University Press: Oxford, UK, 2004; Volume 2.
56. Buckland, S.T.; Newman, K.B.; Fernández, C.; Thomas, L.; Harwood, J. Embedding population dynamics models in inference. *Stat. Sci.* **2007**, *22*, 44–58. [CrossRef]
57. Anderson, D.R.; Burnham, K.P.; Laake, J.L. *Distance Sampling: Estimating Abundance of Biological Populations*; Chapman &Hall: London, UK, 1993.
58. Le Moullec, M.; Pedersen, Å.Ø.; Yoccoz, N.G.; Aanes, R.; Tufto, J.; Hansen, B.B. Ungulate population monitoring in an open tundra landscape: Distance sampling versus total counts. *Wildl. Biol.* **2017**, *2017*, 4. [CrossRef]
59. Kent, M. *Vegetation Description and Data Analysis: A Practical Approach*, 2nd ed.; John Wiley & Sons: Hoboken, NJ, USA, 2012; ISBN 1119962390.

60. Qadir, S.A.; Qureshi, S.Z.; Ahmed, M.A. A phytosociological survey of the Karachi University Campus. *Vegetatio* **1966**, *13*, 339–362. [CrossRef]
61. Rahman, M.M.; Mahmud, M.A.A.; Shahidullah, M.; Nath, T.K.; Jashimuddin, M. The competitiveness of the phytosociological attributes of the protected areas in Bangladesh with that in the other tropical countries. *J. Sustain. For.* **2016**, *35*, 431–450. [CrossRef]
62. Curtis, J.T. *The Vegetation of Wisconsin: An Ordination of Plant Communities*; University of Wisconsin Press: Madison, WI, USA, 1959; ISBN 0299019438.
63. Son, H.-J.; Park, S.-H.; Lee, D.-H.; Song, J.-H.; Park, H.-W.; Park, W.-G. Growing environment characteristics and vegetation structure of Vaccinium Oldhamii Miq. native habitats in Korea. *For. Sci. Technol.* **2019**, *15*, 33–43. [CrossRef]
64. Tian, Z.; Li, H.; Li, W.; Gan, X.; Zhang, X.; Fan, Z. Structural characteristics and niches of dominant tree populations in Tetracentron sinense communities: Implications for conservation. *Bot. Sci.* **2018**, *96*, 157–167. [CrossRef]
65. Lou, Y.; Pan, Y.; Gao, C.; Jiang, M.; Lu, X.; Xu, Y.J. Response of plant height, species richness and aboveground biomass to flooding gradient along vegetation zones in floodplain wetlands, Northeast China. *PLoS ONE* **2016**, *11*, e0153972. [CrossRef]
66. Song, J.H.; Cheong, E.J.; Kim, H.; Kim, M.S.; Kim, S.H. Variation of morphological characteristics and anthocyanin contents from fruit of Vaccinium oldhamii in Korea. *J. Korean Soc. For. Sci.* **2015**, *104*, 193–197. [CrossRef]
67. Raunkiaer, C. *The Life Forms of Plants and Statistical Plant Geography; Being the Collected Papers of C. Raunkiaer*; Clarendon Press: Oxford, UK, 1934.
68. Ijaz, F. Biodiversity and Traditional uses of Plants of Sarban Hills, Abbottabad. Ph.D. Thesis, Hazara University, Manehra, Pakistan, 2014.
69. Ijaz, F.; Rahman, I.; Iqbal, Z.; Alam, J.; Ali, N.; Khan, S. Ethno-ecology of the healing forests of Sarban Hills, Abbottabad, Pakistan: An economic and medicinal appraisal. In *Plant and Human Health*; Ozturk, K.R.H., Ed.; Springer International Publishing AG: Berlin/Heidelberg, Germany, 2018; pp. 675–706.
70. Nasir, E.; Ali, S.I. *Flora West of Pakistan*.; National Herbarium: Karachi, Pakistan, 1971.
71. Ali, S.I.; Nasir, Y.J. *Flora of Pakistan*; Department of Botany, University of Karachi, Karachi and National Herbarium: Islamabad, Pakistan, 1989.
72. Ali, S.I.; Qaiser, M. *Flora of Pakistan*; Department of Botany, University of Karachi: Karachi, Pakistan, 1995.
73. Haq, F.; Ahmad, H.; Iqbal, Z. Vegetation description and phytoclimatic gradients of subtropical forests of Nandiar Khuwar catchment District Battagram. *Pakistan J. Bot.* **2015**, *47*, 1399–1405.
74. Ravindranath, N.H.; Ostwald, M. *Carbon Inventory Methods: Handbook for Greenhouse Gas Inventory, Carbon Mitigation and Roundwood Production Projects*; Springer International Publishing AG: Berlin/Heidelberg, Germany, 2007.
75. Mc Lean, E.O. *Soil pH and Lime requirement. n Methods of Soil Analysis Part 2 Chemical and Microbiological Properties*; Page, A.L., Miller, R.H., Keeney, D.R., Eds.; American Society of Agronomy, Inc. Soil Science Society of America, Inc.: Madison, WI, USA, 1982; pp. 199–223.
76. Wilson, M.J.; Bayley, S.E. Use of single versus multiple biotic communities as indicators of biological integrity in northern prairie wetlands. *Ecol. Indic.* **2012**, *20*, 187–195. [CrossRef]
77. Nelson, D.W.; Sommers, L.E. Total carbon, organic carbon, and organic matter. In *Methods ofSoil Analysis. Part 3. Chemical Method*; Sparks, D.L., Page, A.L., Helmke, P.A., Loeppert, R.H., Soltanpour, P.N., Tabatabai, M.A., Johnston, C.T., Summer, M.E., Eds.; Soil Science Society of America and American Society of Agronomy: Madison, WI, USA, 1996; pp. 961–1010.
78. Paul, A.E.; Berry, E.H. The Kjeldahl nitrogen method and its modifications. *J. Assoc. Off. Agric. Chem.* **1921**, *5*, 108–132. [CrossRef]
79. Soltanpour, P.N.; Workman, S. Modification of the NH4 HCO3-DTPA soil test to omit carbon black. *Commun. Soil Sci. Plant Anal.* **1979**, *10*, 1411–1420. [CrossRef]
80. Soltanpour, P.N. Determination of nutrient availability and elemental toxicity by AB-DTPA soil test and ICPS. In *Advances in Soil Science*; Springer: New York, NY, USA, 1991; pp. 165–190.
81. Rahman, I.U.; Afzal, A.; Iqbal, Z.; Ijaz, F.; Khan, S.M.; Khan, S.A.; Shah, A.H.; Khan, K.; Ali, N. Influence of different nutrients application in nutrient deficient soil on growth and yield of onion. *Bangladesh J. Bot.* **2015**, *44*, 613–619. [CrossRef]
82. Rahman, I.U.; Ijaz, F.; Afzal, A.; Iqbal, Z. Effect of foliar application of plant mineral nutrients on the growth and yield attributes of chickpea (Cicer arietinum L.) Under nutrient deficient soil conditions. *Bangladesh J. Bot.* **2017**, *46*, 111–118.
83. Gilliam, F.S.; Saunders, N.E. Making more sense of the order: A review of Canoco for Windows 4.5, PC-ORD version 4 and SYN-TAX 2000. *J. Veg. Sci.* **2003**, *14*, 297–304. [CrossRef]
84. Šmilauer, P.; Lepš, J. *Multivariate Analysis of Ecological Data Using CANOCO*, 2nd ed.; Cambridge University Press: Cambridge, UK, 2014.
85. Mayor, J.R.; Sanders, N.J.; Classen, A.T.; Bardgett, R.D.; Clément, J.C.; Fajardo, A.; Lavorel, S.; Sundqvist, M.K.; Bahn, M.; Chisholm, C.; et al. Elevation alters ecosystem properties across temperate treelines globally. *Nature* **2017**, *542*, 91–95. [CrossRef]
86. Knapp, A.K.; Fay, P.A.; Blair, J.M.; Collins, S.L.; Smith, M.D.; Carlisle, J.D.; Harper, C.W.; Danner, B.T.; Lett, M.S.; McCarron, J.K. Rainfall variability, carbon cycling, and plant species diversity in a mesic grassland. *Science* **2002**, *298*, 2202–2205. [CrossRef] [PubMed]
87. McCune, B. PC-ORD: An integrated system for multivariate analysis of ecological data. *Abstr. Bot.* **1986**, *10*, 221–225.
88. Rahman, I.U.; Afzal, A.; Iqbal, Z.; Hashem, A.; Al-Arjani, A.-B.F.; Alqarawi, A.A.; Abd_Allah, E.F.; Abdalla, M.; Calixto, E.S.; Sakhi, S. Species Distribution Pattern and Their Contribution in Plant Community Assembly in Response to Ecological Gradients of the Ecotonal Zone in the Himalayan Region. *Plants* **2021**, *10*, 2372. [CrossRef]

89. Terzi, M.; Bogdanović, S.; D'Amico, F.S.; Jasprica, N. Rare plant communities of the Vis Archipelago (Croatia). *Bot. Lett.* **2019**, *167*, 1–14. [CrossRef]
90. Jackson, D.A.; Somers, K.M. Putting things in order: The ups and downs of detrended correspondence analysis. *Am. Nat.* **1991**, *137*, 704–712. [CrossRef]
91. Hill, M.O.; Gauch, H.G. Detrended Correspondence Analysis: An Improved Ordination Technique. *Vegetatio* **1980**, *42*, 47–58. [CrossRef]
92. ter Braak, C.J.F.; Smilauer, P. *CANOCO Reference Manual and CanoDraw for Windows User's Guide: Software for Canonical Community Ordination (Version 4.5)*; Canoco: Ithaca NY, USA, 2002.
93. Šmilauer, P.; Lepš, J. *Multivariate Analysis of Ecological Data Using CANOCO 5*; Cambridge University Press: Cambridge, UK, 2014; ISBN 110769440X.
94. Oksanen, J.; Kindt, R.; Legendre, P.; O'Hara, B.; Stevens, M.H.H.; Oksanen, M.J.; Suggests, M. The vegan package. *Community Ecol. Packag.* **2007**, *10*, 719.
95. Ricklefs, R.E. Evolutionary diversification and the origin of the diversity–environment relationship. *Ecology* **2006**, *87*, S3–S13. [CrossRef]
96. Becker, A.; Körner, C.; Brun, J.-J.; Guisan, A.; Tappeiner, U. Ecological and Land Use Studies Along Elevational Gradients. *Mt. Res. Dev.* **2007**, *27*, 58–65. [CrossRef]
97. R Core Team. *R: A Language and Environment for Statistical Computing*; R Foundation for Statistical Computing: Vienna, Austria, 2020.
98. Kent, M.; Ballard, J. Trends and problems in the application of classification and ordination methods in plant ecology. *Vegetatio* **1988**, *78*, 109–124. [CrossRef]
99. Digby, P.G.N.; Kempton, R.A. *Multivariate Analysis of Ecological Communities*; Springer Science & Business Media: Berlin/Heidelberg, Germany, 2012; Volume 5, ISBN 9400931352.
100. Cleaver, G.; Brown, L.R.; Bredenkamp, G.J. The phytosociology of the vermaaks, marnewicks and buffelsklip valleys of the kammanassie nature reserve, western cape. *Koedoe* **2005**, *48*, 1–16. [CrossRef]
101. Cáceres, M.; Legendre, P. Associations between species and groups of sites: Indices and statistical inference. *Ecology* **2009**, *90*, 3566–3574. [CrossRef]
102. Reed, M.; Dougill, A.; Baker, T. Participatory indicator development: What can ecologists and local communities learn from each other. *Ecol. Appl.* **2008**, *18*, 1253–1269. [CrossRef]
103. Magiera, A.; Feilhauer, H.; Waldhardt, R.; Wiesmair, M.; Otte, A. Mapping Plant Functional Groups in Subalpine Grassland of the Greater Caucasus. *Mt. Res. Dev.* **2018**, *38*, 63–72. [CrossRef]
104. Haq, F.; Ahmad, H.; Iqbal, Z. Vegetation composition and ecological gradients of subtropical-moist temperate ecotonal forests of Nandiar Khuwar catchment, Pakistan. *Bangladesh J. Bot.* **2015**, *44*, 267–276. [CrossRef]
105. Sher, H.; Al_yemeni, M. Economically and ecologically important plant communities in high altitude coniferous forest of Malam Jabba, Swat, Pakistan. *Saudi J. Biol. Sci.* **2011**, *18*, 53–61. [CrossRef]
106. Rahman, I.U.; Khan, N.; Ali, K. Classification and ordination of understory vegetation using multivariate techniques in the Pinus wallichiana forests of Swat Valley, northern Pakistan. *Sci. Nat.* **2017**, *104*, 24. [CrossRef] [PubMed]
107. Dukes, J.; Mooney, H. Does global change increase the success of biological invaders? *Trends Ecol. Evol.* **1999**, *1*, 135–139. [CrossRef]
108. Reich, P.B. Elevated CO_2 reduces losses of plant diversity caused by nitrogen deposition. *Science* **2009**, *326*, 1399–1402. [CrossRef]
109. Jafari, M.; Jafarian Jeloudar, Z. Vegetation community in relation to the soil characteristics of Rineh rangeland, Iran. *Casp. J. Environ. Sci.* **2010**, *8*, 141–150.
110. Kabir, M.; Iqbal, M.Z.; Farooqi, Z.R.; Shafiq, M. Vegetation pattern and soil characteristics of the polluted industrial area of Karachi. *Pak. J. Bot* **2010**, *42*, 661–678.
111. Shaheen, H.; Riffat, A.; Salika, M.; Firdous, S.S. Impacts of roads and trails on floral diversity and structure of Ganga-Choti forest in Kashmir Himalayas. *Bosque* **2018**, *39*, 71–79. [CrossRef]
112. Khan, S.M.; Harper, D.M.; Page, S.; Ahmad, H. Species and community diversity of vascular flora along environmental gradient in Naran Valley: A multivariate approach through indicator species analysis. *Pak. J. Bot* **2011**, *43*, 2337–2346.
113. Ellenberg, D.; Mueller-Dombois, D. *Aims and Methods of Vegetation Ecology*; Wiley: New York, NY, USA, 1974.
114. Srivastava, S.; Shukla, R.P. Similarity and difference of species among various plant communities across grassland vegetation of north-eastern Uttar Pradesh. *Trop. Plants Res.* **2016**, *3*, 364–369.
115. Shaheen, H.; Ullah, Z.; Khan, S.M.; Harper, D.M. Species composition and community structure of western Himalayan moist temperate forests in Kashmir. *For. Ecol. Manage.* **2012**, *278*, 138–145. [CrossRef]
116. Bano, S.; Khan, S.M.; Alam, J.; Alqarawi, A.A.; Abd_Allah, E.F.; Ahmad, Z.; Rahman, I.U.; Ahmad, H.; Aldubise, A.; Hashem, A. Eco-Floristic studies of native plants of the Beer Hills along the Indus River in the districts Haripur and Abbottabad, Pakistan. *Saudi J. Biol. Sci.* **2018**, *25*, 801–810. [CrossRef]
117. Amagai, Y.; Kudo, G.; Sato, K. Changes in alpine plant communities under climate change: Dynamics of snow-meadow vegetation in northern Japan over the last 40 years. *Appl. Veg. Sci.* **2018**, *21*, 561–571. [CrossRef]
118. Jiménez-Alfaro, B.; Girardello, M.; Chytrý, M.; Svenning, J.-C.; Willner, W.; Gégout, J.-C.; Agrillo, E.; Campos, J.A.; Jandt, U.; Kącki, Z.; et al. History and environment shape species pools and community diversity in European beech forests. *Nat. Ecol. Evol.* **2018**, *2*, 483–490. [CrossRef]

plants

MDPI

Review

Genomic and Meiotic Changes Accompanying Polyploidization

Francesco Blasio [1], Pilar Prieto [2], Mónica Pradillo [1] and Tomás Naranjo [1,*]

[1] Departamento de Genética, Fisiología y Microbiología, Facultad de Biología, Universidad Complutense de Madrid, 28040 Madrid, Spain; franblas@ucm.es (F.B.); pradillo@bio.ucm.es (M.P.)
[2] Plant Breeding Department, Institute for Sustainable Agriculture, Agencia Estatal Consejo Superior de Investigaciones Científicas (CSIC), Alameda del Obispo s/n, Apartado 4048, 14080 Cordova, Spain; pilar.prieto@ias.csic.es
* Correspondence: toranjo@bio.ucm.es

Abstract: Hybridization and polyploidy have been considered as significant evolutionary forces in adaptation and speciation, especially among plants. Interspecific gene flow generates novel genetic variants adaptable to different environments, but it is also a gene introgression mechanism in crops to increase their agronomical yield. An estimate of 9% of interspecific hybridization has been reported although the frequency varies among taxa. Homoploid hybrid speciation is rare compared to allopolyploidy. Chromosome doubling after hybridization is the result of cellular defects produced mainly during meiosis. Unreduced gametes, which are formed at an average frequency of 2.52% across species, are the result of altered spindle organization or orientation, disturbed kinetochore functioning, abnormal cytokinesis, or loss of any meiotic division. Meiotic changes and their genetic basis, leading to the cytological diploidization of allopolyploids, are just beginning to be understood especially in wheat. However, the nature and mode of action of homoeologous recombination suppressor genes are poorly understood in other allopolyploids. The merger of two independent genomes causes a deep modification of their architecture, gene expression, and molecular interactions leading to the phenotype. We provide an overview of genomic changes and transcriptomic modifications that particularly occur at the early stages of allopolyploid formation.

Keywords: allopolyploidy; interspecific hybridization; unreduced gametes; cytological diploidization; genomic changes

Citation: Blasio, F.; Prieto, P.; Pradillo, M.; Naranjo, T. Genomic and Meiotic Changes Accompanying Polyploidization. *Plants* **2022**, *11*, 125. https://doi.org/10.3390/plants11010125

Academic Editors: Milan S. Stankovic, Paula Baptista and Petronia Carillo

Received: 3 December 2021
Accepted: 29 December 2021
Published: 3 January 2022

Publisher's Note: MDPI stays neutral with regard to jurisdictional claims in published maps and institutional affiliations.

1. Introduction

Polyploidy, defined as the presence of three or more complete sets of chromosomes in a cell or organism, is an important feature of genome evolution in many eukaryote taxa. Polyploids have been documented in yeasts, insects, and vertebrates [1] but polyploidy is pervasive and especially prominent in the evolutionary history of plants, with both recent and ancient events occurring particularly in lineages such as the Angiosperms [2]. Polyploids are usually classified according to their mode of origin as autopolyploids, those having three of more genomes of a given species, and allopolyploids, which originated after interspecific hybridization followed by chromosome doubling [3].

Early cytogeneticists assumed the pattern of chromosome pairing at the first meiotic division as a reliable criterion to identify homologous and homoeologous relationships between the chromosome sets of a polyploid organism. The frequency of multivalents was used as a cytological parameter to distinguish between auto- and allopolyploids [4]. A high level of multivalent pairing at metaphase I suggests homology between chromosome sets and hence autopolyploidy. In contrast, a preferential formation of bivalents likely results from the presence of non-homologous (homoeologous) parental chromosome sets, hence indicating allopolyploidy. Consistent with this notion, a survey consisting of 171 reports on neopolyploids yielded a higher frequency of multivalents at diakinesis and

metaphase I in autopolyploids (28.8%) than in allopolyploids (8.3%) [5]. Such multivalent frequencies suggested partial cytological diploidization of many autopolyploids and complete cytological diploidization of most allopolyploids. However, differentiation between auto- and allopolyploids is not absolute, since almost exclusive bivalent formation was observed in some autopolyploids while some allopolyploids show multivalent formation. This variable pairing pattern is more consistent with a gradient of divergence between the genomes concurring in polyploids than with a strict differential behavior between auto- and allopolyploids.

Since the Modern Synthesis, allopolyploidy has been considered for decades to be more prevalent than autopolyploidy in the evolution of Angiosperms [6]. This trend continues today, but it is now recognized that both are extremely important in nature [2,3]. Soltis and coworkers [7] propose two main reasons for the widespread omission of autopolyploidy as a significant speciation mechanism: (i) autopolyploidy was traditionally considered extremely rare in nature, (ii) many of plant systematists adhered to a species concept based on morphological features, in which diploids and polyploids were considered as different cytotypes of a single species. In contrast, Lewis [1] proposed a significant contribution of autopolyploidy to plant speciation, especially among herbaceous perennial taxa. Further studies support that autopolyploids are frequently, though they may be lost or remain undetected [2]. Ramsey and Schemske [3] estimated a rate of autotetraploid formation of 10^{-5} similar to the genic mutation rate, which implies that allotetraploid formation can only reach such a incidence after a high frequency of interspecific hybridization (0.2% for selfing taxa, 2.7% for outcrossing taxa). They concluded that autopolyploids may often be formed at a higher frequency than allopolyploids.

Polyploid organisms may undergo major changes in genomic structure and phenotypic development, relative to their diploid counterparts, which provide them a broader basis for evolution. The presence of four alleles per locus in autotetraploids, or more in higher levels of ploidy, confers an increased heterozygosity to autopolyploids in comparison with that of their diploid progenitors. This fact allows the beneficial masking of deleterious genes. A high level of heterozygosity derived from the presence of homoeoalleles is also present in allopolyploids, which is accompanied of additivity of the merged parental genomes as well as the occurrence of instantaneous reproductive isolation, and a tendency to suffer less inbreeding depression than diploids [8]. Phenotypic and morphological changes known to be induced by polyploidy are those associated with variation in flower number and flowering time [9], root architecture and plant structure, or alterations in plant physiology such as abiotic stress tolerance [10].

The advent of the new genomic tools has led to the development of a number of molecular and genomic studies focused on the rapid changes induced by allopolyploidy, which have been revealed to occur at the genetic and epigenetic level, together with major alterations in the transcriptional landscape [11,12]. Allopolyploid formation requires the adaptation of two nuclear genomes within a single cytoplasm, which may involve programmed genetic and epigenetic changes during the initial generations following genome fusion. Early generations of synthetic allopolyploids show rapid and extensive restructuring of the merged genomes, including chromosome rearrangements and changes in the chromosome number [13–18] as well as epigenetic modifications, such as, transposon activation, chromatin modifications and altered methylation patterning [19–24]. In this first phase of allopolyploid evolution, the conflict between the merged genomes modifies the gene expression profile, which is often associated with phenotypic modifications of the new polyploid plants [25–28]. However, allopolyploids of recent origin commonly display phenotypic instability, low fertility and low embryonic viability [22], but their persistence accompanied of successful genetic readjustments may lead to stable genomic variants that express fertile and well adapted phenotypes on an evolutionary time scale of hundreds or thousands of generations [29]. This second phase of genome evolution includes either sub- or neofunctionalization of duplicated genes to form novel genetic functions and gene complex [30–36] or the loss of redundant copies [37]. Reduction of genomic

redundancy converts the polyploid organism into a diploid one, which is often referred to as genetic diploidization. Thus, genetic diploidization is considered an evolutionary process of a wider time scale than that of the cytological diploidization which happens at the primitive allopolyploid stage and concerns genetic systems involved in control of meiotic pairing [38,39].

The evolutionary history of seed plants and Angiosperms is full of Whole Genome Doubling (WGD) events [40,41] with each subsequent polyploidy superimposed on the genomic remnants surviving from earlier rounds of polyploidy. Genomic complexity of modern Angiosperm genomes ranges from those that underwent few polyploidization events (e.g., *Amborella*, *Allium*, *Olea*, *Theobroma*) to others that reflect as many as 128 (*Saccharum*), 144 (*Gossypium*), and even 288 (*Brassica*) genomic multiplication processes [42]. Recurrent polyploidization is usually accompanied of chromosome rearrangements and reduction of chromosome number as well as a large-scale loss of duplicated genes and repetitive sequences. Such genome reorganizations, while harboring the vestigial marks of ancient polyploidy events, lead to chromosome constitutions that facilitate a cytological diploid-like behavior of the extant species [42].

Advances in understanding the extent of polyploidy in plant speciation, driven largely by the explosive development of genomic tools, have occurred in parallel with a number of reports showing evidence of mitotic and meiotic cell division alterations involved in the formation of polyploids [43]. On the other hand, recent identification of genes controlling the diploid-like meiotic behavior of allopolyploids such as wheat or *Brassica* will contribute to understand their origin and their mode of action [38,39]. In this review, we will discuss the cytological and molecular mechanisms that underlay the pathways leading to polyploids formation, including interspecific hybridization, chromosome doubling, cytological diploidization and genetic and epigenetic changes produced at the onset of allopolyploidy.

2. Interspecific Hybridization

Plant hybridization has been important to humans since the commencement of domestication of plants and animals during the Neolithic era. In the mid of the eighteenth century, hybridization was considered as a reproduction mode that could yield sterile plants with intermediate phenotype [44–46]. In the beginning of the nineteenth century, hybridization was largely used as a source of variation for plants of agronomical or ornamental importance. Its main biological relevance relied on its use as a tool to prove if two different plants deserve the species status [44]. When the hybrid obtained in a cross between two different plants was sterile such plants were considered to belong to different species while, if the offspring was fertile, they were considered as varieties of the same species. However, different naturalists challenged this idea in the second half of the nineteenth century [44]. The Mendel's work on plant hybridization [47] and its rediscovery by de Vries, Correns and Tschermak in 1900 [48–50] established the path to reveal the hereditarily determined plant diversity, which, in fact, led to the emergence of genetics. The invariable offspring of homozygotes formulated in the Mendelian principles led Lotsy [51] to propose that hybridization has played a determinant evolutionary role assuming that a new combination of traits arises only by crossing. Wingë [52] proposed that new and stable species emerge by the duplication of the chromosome number of an interspecific hybrid (i.e., allopolyploidy). Evidence supporting this hypothesis was quickly reported in different plant species [53,54]. Müntzing [55] proposed a second mechanism in which hybridization may produce new and stable species. He postulated that later generation hybrids could, by chance, lead to new combinations of parental chromosomes and alleles that were homozygous for a unique combination of chromosomal sterility factors. The new hybrid population would be fertile, stable, and at the same ploidy level as its parents but partially isolated from its progenitors due to chromosome differentiation [55,56].

The formation of interspecific hybrids may be conditioned by an important aspect of the biology of the organisms, the breeding system. In plant species the mode of reproduction is sexual or asexual. Sexual reproduction takes place by self-cross, outcross or mixed. The

type of sex system (hermaphroditism, monoecy or dioecy) contributes to reinforce the mode of sexual reproduction. While dioecy, and to a large extent monoecy, determine outcross reproduction, hermaphroditism ensures exclusive or dominant self-crossing. Breeding system changes along evolution even between closely related species. All changes do not occur with the same frequency, that is, the outcrossing system, which appears mainly in the ancestral lineages, is often lost and evolves to inbreeding while the transition of highly inbreeding species to outcrossing is rare [57].

Interspecific hybridization requires some rate of outcrossing of the concerned species. Outcrossing rates vary among different taxa. Most Angiosperms (87.5% [58]) are pollinated by insects and other animals and show intermediate outcrossing rates while wind-pollination species, which are mainly found among Gymnosperms and few Angiosperms families such as Poaceae, show a bimodal outcrossing-inbreeding species distribution [57–59].

Given the abundance of animal-pollinated species, pollinators often alternate visits to flowers of plant species flowering at the same time and within the flight pattern, which causes interspecific pollen transference. Hybridization between a given pair of species is usually asymmetric in that one species may act preferentially as male or female [60]. Effective hybridization requires a transition through several steps, foreign pollen arrival on a stigma, which generates competitive interactions with conspecific grains for adhesion and germination. Pollen must germinate and form the pollen tube, which is more likely between close relatives, as they may have similar pollen-pistil compatibility. Finally, sperm should be released to fertilize the egg.

Competitive interactions between conspecific and heterospecific pollen grains have a negative impact on fertility whereby Angiosperms evolved multiple prezygotic and postzygotic barriers to minimize the effect of fitness reduction. Prezygotic barriers impede hybridization and include prepollination isolation and gametic selection [61]. Hybrid sterility, caused either by gene incompatibilities or chromosome rearrangements, is a common form of postzygotic reproductive isolation in plants [62]. Prepollination isolation prevents the anticipated arrival of competitive foreign pollen grains on a stigma. These barriers include adaptations such as flowering asynchrony either during the day or along the year, or divergence in floral traits conditioning the pollinator preference or the mechanical interaction between flower and pollinator during visits. Various forms of gametic isolation, including stigma incompatibility and suppression of pollen tube growth, counteract foreign pollen germination deposited on a stigma. Modifications of the structure or chemical composition of stigma as well as factors controlling pollen recognition and self-incompatibility may contribute to increase incompatibility with foreign pollen. Self-incompatibility and interspecific incompatibility show similarities in the molecular mechanisms controlling the pollen-pistil interactions, since pollen of self-compatible species deposited on stigma of self-incompatible relatives is rejected but not in the reciprocal hybridization [63]. Pollen deposited on the stigma of a distantly related species usually fails to germinate, but this is not the case between closely related species. In such cases, divergence between species in pollen tube performance in the style may cause either a more disruptive development of the foreign pollen tube or mismatches in the size of both structures, which contribute to avoid interspecific hybridization [61]. An additional evolutionary strategy to avoid interspecific hybridization involves a shift in the mating system toward earlier self-pollination, which reduces the opportunity of fertilization after the arrival of foreign pollen to stigma [61].

Despite genetic isolation barriers arisen in the evolution, interspecific hybridization is a relatively frequent biological phenomenon. Whitney and coworkers studied the pattern of hybridization in a sample of approximately 10% of 352,000 Angiosperm species [64]. They investigated 37,000 species included in 3212 genera of 282 families from eight regional floras covering parts of North America and Australia, continental Europe and two island groups (British Isles and Hawaii). Interspecific hybrids occurred with a frequency of 0.09 hybrids per non hybrid species. Both families and genera had different hybridization propensity, but a given group usually showed the same hybridization pattern across

regions, which suggests that genetic constitution of each group is more relevant than environmental conditions. This hybridization frequency based on floristic surveys was probably underestimated, and more accurate estimates are expected to be obtained through implementation of genomic tools. Natural hybridization has been reported in 22 of the 25 most important crops of the world and is also common among invasive species [65].

Interspecific hybridization may represent a source of phenotypic innovation [62]. Although interspecific hybrids usually show a low fertility, the offspring obtained allows to extend hybridization to further generations, which may display transgressive trait variation, that is, a gain or a loss of valuable traits with respect to the parental species. On the other hand, recurrent backcrosses of the hybrids with one of the parental species give rise to introgression of alien genes in any of the parental species and represent a common way of gene flow between species in hybrid zones [62].

While interspecific hybridization and subsequent WGD (allopolyploidy) represents a common mode of speciation in plants, homoploid hybrid speciation is rare. Some hybrid lineages found in *Helianthus*, and probably in other genera, have achieved reproductive isolation without variation of the ploidy level [62]. Darlington [66] proposed an inverse relationship between the fertility of an interspecific hybrid and the fertility of the allopolyploid generated from the homoploid hybrid by doubling its chromosome number. He argued that homoploid hybrids between closely related species will show a high level of meiotic pairing and fertility, while the fertility of the corresponding allopolyploids will be reduced because of uneven segregation of chromosomes from multivalents involving both homologues (equivalent chromosomes from the same genome) and homoeologues (equivalent chromosomes from related genomes). In contrast, homoploid hybrids between distant species will be sterile due to chromosome pairing failure, but allopolyploids will be fertile due to preferential formation of homologous bivalents at meiosis. Comparison of the mean genetic distance between the parental species of homohybrids and allopolyploids in different taxa led to the conclusion that polyploid formation occurs at random regardless the level of phylogenetic divergence between the parental species while homoploid hybrids tend to be formed among progenitors closely related [67].

3. Mechanisms and Frequency of WGD in Plants

3.1. Pathways for WGD in Plants

The occurrence of WGD in interspecific hybrids contributes to stabilize their meiotic behavior strongly disrupted when homoeologous chromosomes fail to pair. Meiotic pairing regularization ensures a high degree of fertility of new allopolyploids, whose genomic integrity may persist through generations. Thus, upon hybridization, WGD drives allopolyploid induction and speciation. However, our understanding of the processes affecting the initial formation of polyploids within diploid populations is one of unexplored issues of polyploidy evolution [68]. Cytological alterations reported in the last two decades, such as meiotic non-reduction giving rise to 2n gametes and somatic doubling, have been implicated in the formation of individuals with changed ploidy level [43]. Union of unreduced gametes, rather than somatic doubling, has been considered as the most likely method of polyploid formation in plants [69,70].

Meiotic non-reduction or meiotic restitution is the outcome of cellular alterations in any of the two meiotic divisions that switch meiosis into a mitotic-like division, generating two diploid spores out of a diploid mother cell instead four haploid spores. An autotetraploid individual can be originated either in one-step process consisting in the fusion of unreduced egg and unreduced sperm or in a two-steps process that involves formation of a triploid intermediate after fusion of an unreduced gamete with a normal haploid gamete, followed of self-fertilization of the triploid or crossing with a diploid [3]. Most gametes produced by triploids are not functional because of their aneuploid constitution, but triploids generate a low number of euploid gametes ($\times$, $2\times$ and even $3\times$) which are involved in the formation of the autotetraploid. Allotetraploids can be formed in one-step process from interspecific

hybrids, but the triploid bridge is also possible as triploid interspecific hybrids have been observed in different taxa [3].

3.2. Cellular Mechanisms, and Their Genetic Control, Causing Plants Meiotic Restitution

Cellular defects giving rise to meiotic restitution have been classified in two main groups, namely First Division Restitution (FDR) and Second Division Restitution (SDR), which yield 2n gametes genetically equivalent to those produced by a loss of the first meiotic division or the second meiotic division, respectively [43,71–73]. In the absence of recombination, the FDR-type is comparable to a mitotic division and 2n gametes retain the parental genome constitution, but when one crossover is formed between two homologues the parental constitution is retained in only two of the four chromatids. Unreduced gametes produced in the SDR-type contain the two sister chromatids of the same parental or recombinant chromosome. Cellular defects causing meiotic restitution have been classified in three main types: alterations of meiotic spindle dynamics, disturbed formation of meiotic cell plate, and omission of any of the two meiotic divisions [43,71–73].

Spindle dynamics in any of the two meiotic divisions may be altered by structural defects in microtubules nucleation, spindle organization and orientation, and kinetochore functioning, which usually generate unbalanced chromosome segregation and aneuploidy, but occasionally induce a meiotic restitution event. Formation of curved spindle and disturbed attachment of microtubules to kinetochores impede chromosome segregation and block cell plate formation in the first meiotic division of interspecific wheat-rye hybrids, yielding a restituted nucleus, which undergoes the second meiotic division to form unreduced gametes [74]. Other alterations in the spindle organization disturb its bipolar orientation causing monopolar, multipolar or apolar arrangements of microtubules. Meiocytes with monopolar spindle, in interspecific hybrids of Triticeae, or apolar spindle, in maize meiotic mutants, omit chromosome segregation at anaphase I yielding unreduced gametes [75,76]. Abnormal spindle geometry in the second meiotic division has been documented as a source of unreduced gametes formation in dicotyledons microsporogenesis [71]. Proper chromosome number reduction is produced when the two spindles adopt a perpendicular orientation in the second meiotic division, followed by cytokinesis to yield the four microspores. Disturbed arrangements such as fused spindles and parallel spindles generate a dyad with 2n nuclei while a tripolar spindle produce a triad containing two n and one 2n nuclei [77–80]. However, fused, parallel and tripolar spindles may appear in the same flower and probably represent different phenotypic expressions of the same cellular defect [79–82].

Alterations of spindle dynamics are under strong genetic control. Up to date, a list of 23 genes of *Arabidopsis*, whose mutations cause meiotic restitution, have been reported [83]. Instances of *Arabidopsis* genes with mutations that induce the formation of unreduced 2n microspores through alteration of the second meiotic division spindles arrangement are *AtPS1*, *JASON* and *AFH14* [79,80,84]. Protein AFH14 is involved in the control of cell division trough interactions with microtubules and microfilaments. The mode of action of *AtPS1* on spindle organization is unknown. The AtPS1 protein has been suggested to play its regulatory function via RNA decay [80]. The JASON protein positively regulates the *AtPS1* expression, which suggests that JASON controls the organization of the second meiotic division spindles through AtPS1 [80]. On the other hand, the origin of tetraploid potato cultivars and related wild species has been attributed to a high frequency of the *ps* (parallel spindles) allele, which induces the formation of 2n gametes [85,86]. In carnation, *Dianthus caryophyllus*, the *DcPS1* (*Dianthus caryophyllus Parallel Spindle 1*) gene, which encodes a protein with domains suggesting a regulatory function, induces the formation of unreduced gametes through alteration of spindle orientation in the male second meiotic division [87].

Abnormal cytokinesis, either in the first or in the second meiotic division, represents another major mode of unreduced gametes production both in microsporogenesis and macrosporogenesis. In monocotyledons, cytokinesis occurs at the end of the two divi-

sions of both male and female meiosis, but, in the spermatocytes of most dicotyledons, cytokinesis takes place at the end of the second division. Premature cytokinesis in the first meiotic division of microsporocytes although reported in some dicotyledons species is not a relevant mechanism of meiotic restitution [71,78]. Incomplete or no cell plate formation at any meiotic division has been observed in different species and represents an important mechanism of FDR- or SDR-type unreduced gametes [88–93]. Cellular defects such as disturbed microtubule array biogenesis or reduction of microtubules stability [94–97] anomalous transport of cell wall material, disturbed fusion of membrane vesicles [98] and reduced deposition of callose [99] may prevent cell plate formation in meiotic cells. The chromatin regulator Male Meiocyte Death 1 (MMD1/DUET), a PHD-finger protein that binds with H3K4methylation sites, is involved in the control of multiple processes in *Arabidopsis* male meiosis. A hypomorphic *mmd1/duet* mutant allele causes defects in microtubule organization and cytokinesis, which leads to meiotic restitution [83]. Disturbed spindle elongation or orientation may also induce cytokinesis alterations. This is the case of potato and *Populus* meiocytes, where disturbed spindle orientation causes defects in interzonal radial microtubules array formation followed of cell plate formation failure and unreduced gametes [78,100].

Loss of any of the two meiotic cell divisions is another source of meiotic restitution. The absence of the first meiotic division abolishes both homologous recombination and chromosome number reduction. Chromosomes divide at anaphase II separating sister chromatids in two FDR-type nuclei with the parental genetic constitution [101–104]. This phenomenon is observed in apomictically reproducing species and is termed diplosporous apomeiosis [105–108]. In fact, the three components of apomixis, apomeiosis, parthenogenesis and functional endosperm development, are uncoupled in many crops leading to their partitioning [109]. Mutation of the *Arabidopsis* gene *DYAD/SWITCH1* (*SWI1*), a regulator of meiotic chromosome organization, causes apomeiosis [102]. The transformation of meiosis into a mitotic division was also shown in the triple *osd1/Atrec8/Atspo11-1* mutant of *Arabidopsis*, called *MiMe*, where the *Atspo11-1* and *Atrec8* mutations produce sister chromatids separation at anaphase I, and the *osd1* mutation prevents the second division [103]. Sister chromatids separate in the first meiotic division while the second meiotic division is omitted. The *Dominant nonreduction4* (*Dnr4*) of maize is defective in chromatin condensation during meiosis and shows a diplosporous phenotype with frequent unreduced gametes formation [104]. *Dnr4* codes for AGO104, a member of the ARGONAUTE family proteins, which is needed for non-CG methylation of centromeric and knob-repeat DNA. Mutation in protein-coding genes, such as *Arabidopsis* protein DYAD/SWITCH1 [110], maize DMT102 and DMT103 DNA-methyltransferases [111], and APOLLO (APOmixis-Linked Locus) histidine exonuclease of *Boechera* [112], induce a complete omission of the first meiotic division and yield meiocytes that undergo equational cell division to produce 2n megaspores.

Failure of separation of sister chromatids in the second meiotic division because of delayed dissolution of centromeric cohesion yields dyads with SDR-type 2n nuclei [103,113]. Mutations in the *Arabidopsis* genes *GIGC1/OSD1* (*GIGAS CELL1/OMISSION OF SECOND DIVISION1*) and *CYCA1;2* (*A1-TYPE CYCLIN*), also called *TAM* (*TARDY ASYNCRONOUS MEIOSIS*), cause the second division blocking after normal chromosome segregation in the first division, generating dyads containing SDR-type 2n nuclei [103,113]. OSD1 is involved in the maintenance of the activity of cyclin-dependent kinases and promotes meiotic division through inhibition of the APC/C (Anaphase Promoting Control/Cyclosome) [114]. The A-type cyclin CYCA1;2 encoded by TAM is involved in regulation of cell cycle progression through the formation of a complex with CDKA;1 [115].

3.3. Meiotic Restitution in Interspecific Hybrids

The absence of homologous chromosomes in interspecific hybrids restrict meiotic pairing to homoeologous chromosomes, which show a variable synaptic pattern conditioned by the degree of affinity between the parental genomes. Such a meiotic irregularity

affects chromosome segregation at anaphase I and causes a high frequency of non-viable gametes. However, some interspecific hybrids between Triticeae species are capable of producing small or sometimes large numbers of seeds, which usually have a duplicated chromosome number [116–122]. Hybrids between phylogenetically distant species, such as wheat x rye, lack meiotic recombination and form, almost exclusively, univalents at metaphase I. These univalents either show a monopolar orientation and segregate to one pole at anaphase I [75,118] or once positioned at the cell equator do not move to the poles [118], or after segregation at anaphase I undergo a centripetal migration from the poles toward the cell center at telophase I [74], yielding in all instances one restituted cell, which undergoes a normal second division. Sister kinetochores of chromosomes forming bivalents orient syntelically at the first meiotic division, but those of univalents may show either syntelic or amphitelic orientation [123]. Sister kinetochores of univalents undergoing monopolar segregation, as well as those moving from the poles towards the cell center and rejoined on the equator at telophase I, should adopt a synthelic orientation. In contrast, univalents staying at the cell equator are oriented amphitelically. This was demonstrated in a study [124] on the orientation of sister kinetochores in meiocytes of durum wheat cultivar Langdon, which orient syntelically in the bivalents formed in tetraploid plants but amphitelically in the univalents produced in polyhaploids and interspecific hybrids with *Ae. tauschii.* Persistence of sister centromere cohesion until anaphase II counteracted the tension created by amphitelic orientation and maintained univalents at the cell equator contributing to generate the restituted nucleus. Univalents formed in interspecific hybrids may also divide equationally at anaphase I. When all univalents behave in this way, the second meiotic division is lost and meiosis is converted in a single mitotic division, which is called single-division meiosis (SDM). SDM has been observed in interspecific hybrids of durum wheat and *Ae. longissima* [120,125] and in hybrids of durum and bread wheat with other *Aegilops* species or rye [126,127]. Both FDR and SDM meiotic restitution types coexist in the same hybrid [125–127]. Failure of synapsis in polyhaploids and interspecific hybrids was considered essential in determining the type of centromere orientation of chromosomes at metaphase I and anaphase I. Cytomixis, a migration of cytoplasmatic or nuclear materials between adjacent cells, has also been reported as source of meiotic restitution in hybrids between the parental species of peanut (*Arachis hypogea*, L) [128].

Jauhar and coworkers [118] suggested that in interspecific hybrids, meiotic restitution and its frequency largely depend on the presence of univalents caused by the lack of homologous partner rather than genetic defects. Consistent with this assumption is the behavior of ABDD hybrids obtained in the cross of *T. turgidum* (AABB) × tetraploid *Ae. tauschii* (DDDD), which do not undergo meiotic restitution while the ABD *T. turgidum* × *Ae. tauschii* hybrids do [129]. A similar conclusion was inferred from the occurrence of meiotic restitution induced by the formation of univalents in durum wheat haploids, which is absent in haploids of the 5D-5B substitution line where homoeologous bivalents are formed [118]. Similarly, asynapsis induced by low temperature in nulli 5D-tetra 5B plants of hexaploid wheat Chinese Spring generates meiotic restitution [130]. Thus, failure of synapsis more than absence of a homologous partner is responsible of meiotic restitution induced by univalents formation in hybrids. However, genetic factors were also suggested to be involved in the induction of unreduced gametes in genomic combinations involving durum wheat and *Ae. longissima* chromosomes [125]. Accordingly, genetic differences between *T. turgidum* genotypes are responsible of differences in the frequency of chromosome doubling observed in hybrids with rye or *Ae. tauschii* [131–134]. An allele causing meiotic restitution in such hybrids has been located on chromosome 4A in cultivar Langdon [135,136] and one quantitative trait locus (QTL) on chromosome 3B [137]. Genetic variation in the promotion of unreduced gametes formation through meiotic restitution in ABD hybrids was also observed in *Ae. tauschii*, which seems to be under the control of six QTLs [138]. *Ae. triuncialis* shows also genetic variation in its ability to promote chromosome doubling in hybrids with wheat [139]. Studies in haploids of wheat-rye substitution lines revealed that univalents divided equationally at anaphase I in the presence of chromosome 6R but reductionally

when 2R was present [140]. Thus, these two rye chromosomes cause antagonist effects on meiotic restitution, 6R is a promoter chromosome and 2R a suppressor one of meiotic restitution. A further study confirmed these results and that chromosome 1R and 5R carry also genetic information that promotes equational division of univalents and SDM [127].

Cytological mechanisms leading to meiotic restitution in interspecific hybrids between species sharing a relatively high level of genetic affinity are similar to those reported in hybrids between more distant species, but genotypes of unreduced 2n gametes formed show usually a higher frequency of homoeologous recombination than those produced in a strict FDR-type mechanism. Bivalents and multivalents formed by homoeologous chromosomes in metaphase I, combined with separation of sister chromatids of univalents, generate dyads with unusual chromosome constitution consisting in nulli-disomies and associated translocations of homoeologues [141]. This process of unreduced gametes formation was first detected in hybrids of *Lilium* and termed indeterminate (IMR)-type of meiotic restitution [142]. Polyploids formed from such unreduced gametes show a mixture of two copies- and four copies-chromosomal regions, are called segmental allopolyploids [143], and have been detected in different taxa through cytological approaches or genome sequencing [144–148].

3.4. Stress-Induced Meiotic Restitution

Plant meiosis is extremely sensitive to environmental conditions. Abiotic stresses, such as low and high temperatures, salt stress, osmotic shock and water deficit, have a negative impact on male gamete development and cause a considerable reduction of male fertility [149,150]. Adverse conditions are also a source of meiotic restitution in species or hybrids of genera *Rosa*, *Solanum*, *Populus*, *Impatiens*, *Agave*, *Lotus*, *Ipomnoeoa*, *Capsicum*, *Triticum*, *Arabidopsis* or *Medicago* [43]. Heat stress or short period of cold induce meiotic restitution through irregularities on spindle organization or orientation, alteration of cell cycle regulation, defects on cell wall formation, or failure on synapsis and chiasma formation [43]. A more frequent formation on unreduced gametes in extreme environments has been suggested based on the observation that polyploids are more prevalent in such conditions [151]. This assumption in association with the coincidence of a burst of ancient polyploidization events with the Cretaceous-Paleogene extinction, occurred 66 million years ago, suggesting that polyploid establishment is promoted during times of environmental stress [152,153].

3.5. Premeiotic and Postmeiotic WGD in Plants

Apart from meiotic non-reduction, diploid gametes can also be generated by premeiotic or postmeiotic WGD [154]. Premeiotic WGD may be the result of two different cytological abnormalities, syncyte formation and cytomixis. The syncytium is formed because of defects in cell wall construction and, when it is followed of nuclear fusion, polyploid cells arise, which generate diploid gametes. This was observed in the tomato mutant *pmcd1* (*pre-meiotic cytokinesis defect 1*), tetraploid meiocytes originate from nuclear fusion events in syncytial premeiotic germ line cells, ectopically generated by alterations in cell wall formation [155]. Cytomixis leading to WGD was reported in *Dactylis glomerata* [156]. Migration of chromosomes through cytomictic channels was observed during the entire first meiotic division from pachytene to telophase I. The number of bivalents in some meiocytes at diakinesis indicated the formation of some polyploid cells, which generate unreduced gametes. Postmeiotic chromosome doubling occurs by defects in cytokinesis after the second meiotic division. Cold treatment disturbs the phragmoplast construction by destabilization of radial microtubule arrays at the tetrad stage in *Arabidopsis* [91]. Defects in microtubule organization cause also errors in cell wall formation in the *tetraspore* (*tes*)/*stud* mutant of *A. thaliana*, the absence of cytokinesis generates a monad with four nuclei, some of which may be fused [157]. Postmeiotic cytokinesis is regulated by the mitogen-activated protein kinase (MAPK) signaling pathway. *TES/STUD/AtNACK2*, *MKK6/ANQ1*, and *MPK4* are the three main components of this MAPK signaling cascade and mutations of these

genes cause failure of microspore mother cell cytokinesis, which results in over-size mature multinucleate pollen grains [95].

3.6. Frequency of Unreduced Gametes Formation in Natural Plant Populations

The importance of 2n gametes for polyploid evolution raises the question of how frequent and variable 2n gametes are in natural populations. The estimation of the frequency and variation of unreduced gametes in natural populations has been rather limited. Most reports were based in a few number of populations in a small number of species and suggested a low frequency of 2n gametes [158–163]. The most relevant study to compare the frequency and variation of 2n gametes formation within and among taxa was carried out by Kreiner and coworkers in 60 populations from 24 species of Brassicaceae [164]. The presence of unreduced male gametes was detected by flow cytometry, which establishes the level of ploidy by quantification of the DNA content of pollen nuclei. Variation of 2n gametes production was assessed among species, among populations within species, and among individuals within populations. Most of the variation in 2n gametes production was among individuals within populations. The proportion of 2n gametes per plant ranged from 0 to 85.6%, with an average frequency of 1.93% among all plants and 2.52% across species. Variation in 2n gamete production was related to reproductive system; asexual species produced significantly more 2n gametes than mixed-mating and outcrossing species. The conclusion was drawn that in situations of low selective pressure, 2n gametes can be maintained and individuals with high frequency of unreduced gametes are important to generate polyploid offspring.

4. Cytological Diploidization of Allopolyploids

After WGD, multivalents at metaphase I lead to missegregation, gametic aneuploidy and low fertility [165,166]. In this landscape, natural selection should favor a diploid-like meiosis (cytological diploidization) with bivalent chromosome configurations, even though there are four or more sets of homologous/homoeologous chromosomes, to overcome the reduction in fertility derived from meiotic irregularities. As explained above, autopolyploids and allopolyploids face different meiotic challenges for balanced segregation of homologous chromosomes during diploidization [5,167]. We will address below specific examples of these situations concerning mainly allopolyploid species among monocots and dicots.

4.1. Monocots

4.1.1. Wheat

Bread wheat is one of the most important crops in the world. It is the only allopolyploid species in which an extensive amount of work has been carried out to study cytological diploidization and identify genes involved in the genetic control of recombination [168–170], particularly among homoeologous chromosomes [171,172]. This allopolyploid species, and tetraploid (pasta) wheat, arose by combining related genomes. Bread wheat (*Triticum aestivum* L., 2n = 6x = 42) comprises three subgenomes (A, B, and D) derived from three different but related diploid species. Each subgenome contains seven pairs of homologous (equivalent) chromosomes. Similarly, allotetraploid wheat (*T. turgidum* L., 2n = 4x = 28), commonly known as durum (or pasta) wheat, has also two subgenomes (A and B) with seven pairs of homologues each. Chromosomes from different subgenomes are named homoeologues since they evolved from a common ancestor and preserve a considerable degree of genetic affinity [173]. The presence of homoeologous chromosomes, which share a high degree of gene synteny and DNA sequence homology, makes the process of recognition and pairing during meiosis more complicated because each wheat chromosome needs to distinguish between its equivalent (homologue) and the similar/related (homoeologue) from the other subgenomes. Hence, despite its genome complexity, wheat behaves as diploid during meiosis (Figure 1). This means that chromosomes associate regularly in pairs of homologues to successfully recombine and segregate correctly in

anaphase I. This high efficiency of chromosome associations in pairs during meiosis has a great effect on wheat fertility but, on the other hand, has a negative effect preventing pairing and recombination between wheat chromosomes and those from related species in the framework of breeding.

Numerous challenges at the cytological, genetic, and epigenetic levels were overcome to preserve fertility in the newly formed allopolyploids, particularly in annual and predominantly self-pollinated species such as wheat and wheat related species [174]. At the cytological level, the diploid-like meiotic behavior in wheat has been traditionally explained through the action of several *Ph* (*Pairing homoeologous*) genes, which restricted chromosome associations to homologous chromosomes [175–177]. Among these *Ph* genes, the *Ph1* locus, located on the long arm of chromosome 5B, was described as the major chromosome pairing locus in wheat [178]. Other loci such as *Ph2* located on the short arm of chromosomes 3D, or another suppressor located on the short arm of chromosome 3A, have also an effect on meiosis, although their impact is much weaker than the one of the *Ph1* locus [176,179,180].

The *Ph1* locus has been intensively studied during some decades due to its key implications in meiosis and therefore in breeding. Several hypotheses have tried to explain how *Ph1* restricts recombination to homologous chromosomes (reviewed in [38]). The *Ph1* locus was described controlling homologous chromosome pairing in bread wheat [175,181–183]. The presence of the *Ph1* locus affects also the dynamics of telomere bouquet formation by delaying it, what suggests that chromosomes might have more time to check potential pairing and consequently, correct homologous chromosome pairing could be facilitated [184]. Suppression of homoeologous crossovers (COs) instead of preventing chromosome associations between homoeologues has been also assessed to the *Ph1* locus [185–189].

Recently, the *ZIP4* gene has been associated to the *Ph1* phenotype. *ZIP4* was included during polyploidization in the same region of chromosome 5B and consists in one extra copy of the major new meiotic gene *ZIP4*, named *TaZIP4-B2*, that duplicated and diverged from chromosome 3B [172,186]. Hence, hexaploid wheat has four copies of *ZIP4*, one copy on chromosomes 3A, 3B and 3D, and a fourth copy inserted on chromosome 5B, which corresponds to the duplicated and diverged *TaZIP4-B2* [190].

The new finding of the *TaZIP4-B2* gene as the candidate to explain the effect of the *Ph1* locus on recombination suggests that *TaZIP4-B2* has a stronger effect in meiosis than previously explained for *ZIP4* in other model species studies [190,191]. In *Arabidopsis* and rice, *ZIP4* is only necessary for homologous CO and not for pairing and synapsis, although in yeast, *ZIP4* is needed for both CO and synapsis [191–194]. In addition, *ZIP4* can also participate as a scaffold protein that facilitates the assembly of protein complexes and promoting homologous COs [190,191,195]. Studies in wheat comparing two *TaZIP4-B2* TILLING mutants, one *TaZIP4-B2* CRISPR mutant and the Sears *ph1b* deletion mutant have revealed that all four mutants display an equivalent level of COs between homoeologous chromosomes in hybrids with the same wild relative [196]. Due to the fact that *TaZIP4-B2* TILLING and CRISPR mutants are of recent origin, the possibility that chromosome rearrangements accumulated over generations in the *ph1b* mutant could also modify the meiotic phenotype derived from the absence of the wild *Ph1* allele, seems unlikely. In addition, large-scale genome sequencing and RNA analysis have recently shown that homoeologous wheat chromosomes did not display wide gene loss or expression changes after polyploidization [197,198], suggesting that a key factor quickly evolved upon wheat polyploidization to regulate the behavior of its several genomes at the onset of meiosis, and consequently fertility is also preserved. Altogether, after several decades of studying the diploid-like behavior of polyploid wheat, the duplicated and diverged *TaZIP4-B2* copy inserted on wheat chromosome 5B seems to be the key regulator, responsible for both the suppression of homoeologous COs and the promotion of homologous pairing-synapsis phenotypes, which has been historically defined on wheat chromosome 5B. Nevertheless, the molecular mechanisms behind its phenotype remains to be elucidated.

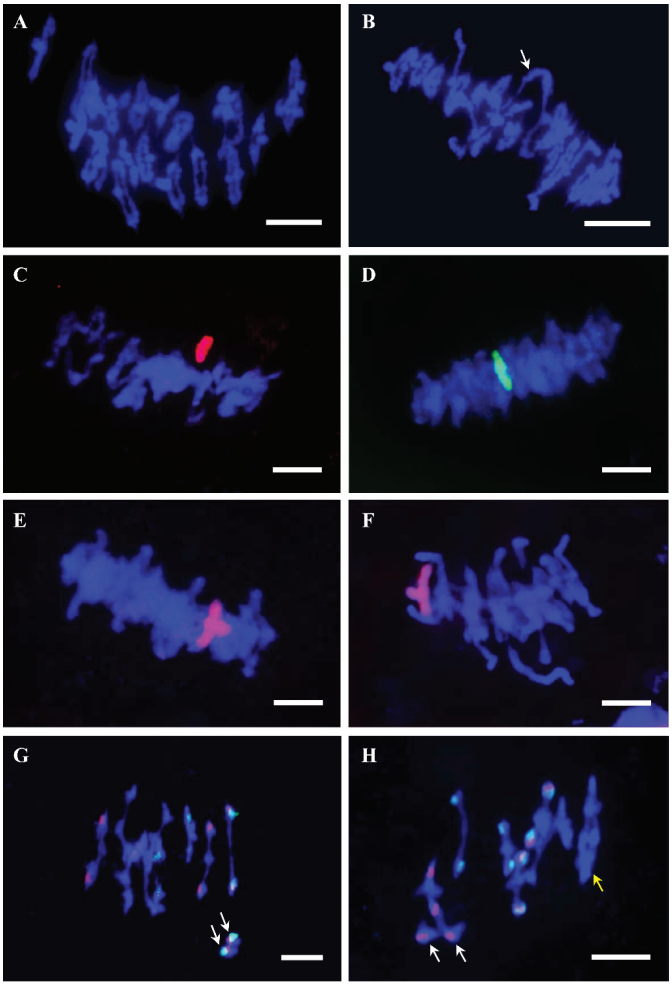

Figure 1. Diploid behavior during meiosis in allopolyploids and autopolyploids. (**A**,**B**) Chromosome associations at metaphase I in the presence and in the absence of the *Ph1* locus in wheat (*T. aestivum*; AABBDD). (**A**) Representative image showing regular bivalent formation in the presence of *Ph1*. (**B**) Formation of multivalents (arrow) in the absence of *Ph1*. (**C**–**F**) Fluorescence in situ hybridization showing chromosome associations at metaphase I in wheat lines carrying chromosomes from wheat related species, both in the presence and in the absence of the *Ph1* locus. Introgressed homologous chromosomes are visualized associated in disomic lines independently of the presence of the *Ph1* locus, although aberrant chromosome associations can be observed in the absence of the *Ph1* locus (**F**). (**C**) Wheat + pair $6H^{v}$ from *Hordeum vulgare* (red), *Ph1Ph1*. (**D**) Wheat + pair $6H^{ch}$ from *Hordeum chilense* (green), *Ph1Ph1*. (**E**) Wheat + pair 6P from *Agropyron cristatum* (in red), *Ph1Ph1*. (**F**) Wheat + pair 6P from *Agropyron cristatum* (in red), *ph1ph1*. (**G**,**H**) Chromosome associations at metaphase I in a natural autotetraploid line from *A. thaliana*. 45S rDNA and 5S rDNA regions are detected in green and red, respectively, to identify the chromosomes. (**G**) Metaphase I showing a pair of univalents (arrows). (**H**) Metaphase I exhibiting univalents (white arrows) and a quadrivalent (yellow arrow). Bars for (**A**–**F**): 10 μm. Bars for (**G**,**H**): 5 μm.

4.1.2. Wheat-Related Polyploid Species

Among allopolyploid *Aegilops* species, regardless the degree of divergence between homoeologous genomes, the control of the diploid-like meiosis operates by means of restriction of synapsis to homologous chromosomes and suppression of chiasma formation in the infrequent homoeologous associations [199]. A similar system controlling restriction of chromosome synapsis initiation to homologous chromosomes has also been reported in allopolyploid species of *Avena* [200], *Festuca* [201], and wild forms of *T. turgidum* and *T. timopheevii* [202]. Surprisingly, the strictly disomic inheritance displayed by the cultivated wheat *T. timopheevii* is achieved though synaptonemal complex (SC) multivalents are relatively frequent during prophase I [203]. The high efficiency of the diploidizing mechanism of *Aegilops* is noticeable, at least in *Ae. ventricosa*, since it also operates in the synthetic amphiploid *Ae. ventricosa-S. cereale* despite its recent origin and the presence of rye genomes [199].

4.1.3. Other Polyploid Species Included in the Poaceae Family

In the *Zea* genus, which includes allotetraploid species with 2n = 20 chromosomes, such as maize, *Zea mays* L., and teosintes, and the alloautooctoploid species *Z. perennis* (2n = 40), a paring regulator locus (*PrZ*), whose expression is suppressed by colchicine, has been recently reported [204]. Poggio and González postulated that, in *Z. perennis*, *PrZ* would affect independently the A and B maize genomes, being relevant the threshold of homology, the fidelity of pairing in each genomes and the ploidy level [204]. To the best of our knowledge, no other genes related to maize cytological diploidization have been described so far.

Little efforts have been carried out to shed some light on the diploid-like behavior of rice polyploids. The genus *Oryza* has 24 species, two of them (*O. sativa* and *O. glaberrima*) are cultivated and 22 are wild species. Among the 22 wild species, six are in the primary gene pool of *O. sativa* complex and share the A genome. Another group of 10 wild species, under the *O. officinalis* complex, includes tetraploid species with genome constitution, BBCC (*O. punctata* and *O. minuta*) or CCDD (*O. latifolia*, *O. alta* and *O. grandiglumis*). All species of this complex belong to the secondary gene pool and are cross incompatible with *O. sativa*. The other six wild species are most distantly related and highly cross incompatible to *O. sativa* and include tetraploids with genome formula HHJJ and HHKK [205]. Particularly in the *O. officinalis* complex, the largest of the *Oryza* genus, genomic relationships were found extremely complicated. For example, the BBCC tetraploid species formed independently with different parenthood in three polyploidization events [206–209]. Furthermore, three tetraploid species with CCDD genomes were assumed to be formed by one polyploidization event, where the CC genome progenitor was the maternal parent [206,209–212]. All these works revealed that the C genome seems to be the pivotal genome in all the tetraploids rice species.

Nevertheless, a *Ph1*-like system has not been identified so far in the genus *Oryza*. Recent studies have been focused on the temporal evolutionary dynamics of four polyploid genomes at both genetic and expression levels. Orthologous genomic sequences adjacent to the *DEP1* locus, a major grain yield QTL in cultivated rice, from four *Oryza* polyploids and their likely diploid genome donors or close relatives have been studied [213]. Genome dominance of this locus was not detected in the lately formed BBCC polyploid, *O. minuta*, and its short-term reactions to allopolyploidy is mainly displayed as a high fraction of homoeologous gene pairs showing imbalanced expression. In addition, an ongoing diploidization progression has been detected in this genus, suggesting that the expression divergence conducted by changes of selective restriction might plays an important function in the long-term diploidization [213].

4.2. Dicots

4.2.1. *Brassica napus*

As it happens in allopolyploid wheats, in allohaploids (AC, 2n = 1x = 19) from oilseed rape (*Brassica napus*, AACC; 2n = 4x = 38) homoeologous chromosome pairing during meiosis is genetically controlled by a major QTL named *PrBn* for *PAIRING REGULATOR IN B. NAPUS* [17,214–216]. *PrBn* has an effect on the frequency but not on the distribution of chiasmata between homoeologous chromosomes [217]. In addition to this locus, in this species, other six minor QTLs have slight additive and *PrBn*-independent effects on non-homologous chromosome recombination frequency [218]. *PrBn* was identified by exploiting natural variation for high and low homoeologous recombination in *B. napus* haploids. However, all *B. napus* allotetraploid accessions display a diploid-like meiotic behavior regardless the genotype at the *PrBn* locus [214,217]. Therefore, the mode of action of *PrBn* seems to be different from that of *Ph1* in wheat. Unlike *PrBn*, no natural polymorphism has been described for *Ph1* in hexaploid wheat and, in contrast to *Ph1*, *PrBn* is not required for regular bivalent formation during meiosis in the allopolyploid *B. napus*. Since the suppression of homoeologous pairing by *PrBn* is not essential, the mechanism of meiotic stability in *Brassica* remains unclear.

Attempts have been made to identify the candidate gene, but this has not been possible, even though it has been mapped to chromosome C9 [214]. Annotated genes within the QTL region includes *RPA1C* (*REPLICATION PROTEIN A 1C*) and *MUS81* (*MMS and UV SENSITIVE 81*). RPA1C functions in double-stranded break (DSB) repair during meiosis in *Arabidopsis thaliana* [219] and MUS81 is an endonuclease involved in the formation of crossovers (COs) [220]. However, expression analyses on meiocytes isolated from the two lines used to map the *PrBn* locus, *Darmor-bzh* and *Yudal*, revealed no differences [221].

Cifuentes and coworkers [215] found that two meiotic phenotypes of *B. napus*, differing in the chiasma frequency at metaphase I, could be explained by the segregation of two alleles at *PrBn*. These alleles came from different parental *B. oleracea* (CC, 2n = 2x = 18) genotypes. In a similar study, Sheidai [222] found variability in pairing and chiasma frequency associated to different *B. napus* accessions. Mason and Batley [223] suggest that genetic control of chromosome pairing in *B. napus* could arise either by mutation in the newly formed allotetraploid or through the accumulation of minor alleles inherited from the diploid parents. Interestingly, in contrast to the regular bivalent formation in *B. napus* lines, resynthesized allotetraploids (obtained by hybridization of the parental species *B. oleracea* and *B. rapa*) display a high frequency of homoeologous bivalents and even multivalents [224]. Exploiting these differences, Higgins and coworkers [225] identified recently three QTLs that contributed to the control of homoeologous recombination. One of these QTLs, *BnaPh1* (*B. NAPUS PAIRING HOMOEOLOGOUS 1*), is the major contributor to variation of the recombination pattern. This QTL locates in a homoeologous region of that carrying *PrBn*, which includes also RPA1C and MUS81. It is possible that one of these genes or another not yet characterized could be responsible of the meiotic phenotypes of established and resynthesized lines [225]. In addition, the regions around the minor QTLs include *MSH3*, a gene involved in DNA repair [226], but it is not clear whether this gene may be considered a candidate [225].

4.2.2. Arabidopsis

In the last decade, the *Arabidopsis* genus has risen as an excellent model for analyzing the consequences of WGD on meiosis [227]. This genus includes several polyploids of different ages and origins. In addition, the diploid progenitors of the polyploids are still found in nature. *Arabidopsis suecica* (2n = 4x = 26) and *A. kamchatica* (2n = 4x = 32) are allotetraploids, whereas *A. arenosa* and *A. lyrata* can be found in diploid (2n = 2x = 16) or tetraploid (2n = 4x = 32) populations.

Arabidopsis suecica and *A. kamchatica* present a diploid-like meiotic behavior and disomic inheritance [228]. However, *A. suecica* neotetraploids (obtained by the hybridization of autotetraploid *A. thaliana* and *A. arenosa*) display multivalents and reduced pollen viabil-

ity [229]. A QTL named *BOY NAMED SUE* (*BYS*), together with other multiple genomic loci, seems to be involved in controlling homoeologous recombination in this allotetraploid species [229]. Furthermore, different chromosomal rearrangements might have contributed to the cytological diploidization [230]. A recent study has reported that *A. suecica* genome is colinear with the ancestral genomes of *A. thaliana* and *A. arenosa*, showing no subgenome dominance in expression and stable transposon dynamics, but with an upregulation of meiotic genes in the *A. thaliana* subgenome [231]. All these data suggest that even though the diploid progenitors of the *A. suecica* are quite divergent, a genetic control system should evolve to achieve meiotic diploidization.

Arabidopsis arenosa is an outcrossing species highly diverse that can be found in both diploid and tetraploid populations. Cytogenetic studies in tetraploids have revealed that most of homologous chromosomes associate randomly as bivalents during meiosis [232,233]. It has been hypothesized that a slower progression through prophase I could contribute to this diploidization [233]. In contrast, extensive multivalent formation and reduced fertility is observed in synthetic neotetraploids obtained from colchicine treated diploids [232]. On the other hand, *A. arenosa* diploid lines display a higher frequency of chiasmata per bivalent compared to the established autotetraploid [232]. These data support the idea that either the reduction of CO frequency or the increase of CO interference promote the formation of bivalents over multivalents, to achieve balanced chromosome segregation during meiosis in polyploids [234]. Indeed, CO interference, measured by localizing E3 ligase HEI10 foci, is strong in established autotetraploid plants of *A. arenosa*, but weak in synthetic neotetraploids of this species [235]. In this context, it is important to highlight that the reduction in chiasma frequency has also been observed in other established autotetraploid species [236]. However, there are species in which chiasma frequency increases by 75% over that in diploids [237]. To add more complexity, it is remarkable to note that some natural autotetraploids form multivalents with no substantial reduction in fertility compared to diploids [238].

Interestingly, signatures of selection found in meiotic genes of *A. arenosa* might be the consequence of genomic changes leading to genomic stability. These genes include elements related to the cohesin complex (*SMC3*, *REC8/SYN1*, and *PDS5*), components of the meiotic axes and synaptonemal complex (SC) (*ASY1*, *ASY3*, *ZYP1a*, and *ZYP1b*), and homologous recombination factors (*PRD3*) [232,239,240]. For this reason, it has been suggested that the diploid-like pairing of *A. arenosa* is the consequence of modifications in the structural components of the meiotic chromosomes. Specifically, for ASY1, a single amino-acid change within the HORMA protein domain was found at a very high frequency in tetraploid populations, whereas it was detected at a very low frequency in diploids [239]. The presence of this *ASY1* mutant allele in tetraploids is associated with a reduced formation of multivalents [241]. Likewise, in established autotetraploid plants of *A. lyrata*, the frequency of multivalents and chiasma distribution is associated with the segregation of an *ASY3* allele [242].

In the model species most commonly used for meiosis studies, *A. thaliana* (2n = 2x = 10), some natural tetraploid accessions have been found, but the cytogenetic studies performed have been scarce [243,244]. However, studies that focus on the analysis of colchicine-induced polyploids are more abundant [245–247] (Figure 1). Santos and coworkers [246] demonstrated that the high multivalents frequency observed in the first generation of *A. thaliana* autotetraploids decreases in successive generations of self-crossing, suggesting rapid adaptation to WGD. Remarkably, this cytological diploidization does not affect all chromosomes equally, since the small chromosomes suffer a more rapid decline of the frequency of multivalents. In a subsequent study, Parra-Nunez [248] reported that genetic differences between accessions have also an influence on chromosome associations during meiosis.

4.2.3. *Solanum tuberosum*

Most cultivated potatoes, which represent the third most important food crop in the world, are autotetraploid (2n = 4x = 48) with an intriguing origin and evolution [249]. Despite the presence of four sets of homologous chromosomes, bivalents are commonly observed at metaphase I, although multivalent formation occurs sometimes [250]. The absence of preferences for pairing/synapsis and recombination between homologous chromosomes, together with outcrossing and a high level of heterozygosity, result in a large number of allelic combinations due to a polysomic pattern of inheritance [250].

It is important to establish the mechanism leading to bivalent formation in this autotetraploid to compare it with that responsible of the diploid-like meiotic behavior of allopolyploids. Cytogenetic studies have been difficult in potato due to the small size of chromosomes, but the use of bacterial artificial chromosomes (BACs) as probes in FISH experiments allowed the identification of individual chromosomes [251,252]. In an elegant study, He and coworkers [253] applied oligonucleotide-based painting probes to identify four different potato chromosomes. They demonstrated that the four homologous chromosomes form a SC quadrivalent configuration in 66–78% of pachytene meiocytes. However, cells with one chiasmate quadrivalent at metaphase I were reduced to 21–42%. The reduction in the frequency of quadrivalents as meiosis progresses has also been observed in wheat, and this mechanism (transformation of SC zygotene-pachytene quadrivalents into pairs of bivalents at metaphase I) has been proposed as a possible mechanism of diploidization of polyploid species [236,254].

Other studies have been focused on the comparison between diploid and tetraploid potato varieties. Remarkably, the CO frequency per bivalent (at least for some individual chromosomes) in certain tetraploid varieties was lower than in a diploid variety [255]. This observation concurs with the idea of reduction in the mean chiasma frequency per cell in the evolution of autotetraploid species [234]. Taking into account that in potato open chromatin regions, marked by H3K4me3, present a higher CO frequency [256], several epigenetic mechanisms, in addition to genetic factors, might be involved in the variation of this recombination landscape.

5. Readjustments of the Merged Genomes

5.1. Genomic Changes

Genomes from two diverged species that merge are usually unstable at early stages of allopolyploid formation and experience massive genetic changes including structural variation caused by deletions, inversions, translocations or homoeologous exchanges, together with epigenetic changes, such as transposable element (TE) activation and transcriptional gene silencing mediated by small RNAs, resulting in heritable loss of gene expression from previously active genes [8,257–260].

Genome sizes of polyploids are typically smaller than expected, suggesting that genome downsizing is a common readjustment in the diploidization process [261]. The loss of genetic material is a non-random process. It particularly affects to house-keeping genes or nuclear-encoded organellar genes [35,262], whereas genes involved in signal transduction and transcription are preferentially retained [263].

In wheat, allopolyploidization causes an immediate and non-random loss of both, coding and non-coding DNA sequences. Specifically, tetraploid wheat (*T. durum*) shows a reduction of 2–10% in the DNA content relative to the summed amounts of its diploid progenitors [264]. A similar situation occurs in the hexaploid wheat (*T. aestivum*) [265]. In this species, the rDNA loci of the A and D subgenomes have been lost in the evolution [265]. The DNA loss has contributed to increase the divergence between the homoeologous chromosomes, favoring its diploid-like meiotic behavior [174,264,266]. However, although many duplicated genes were lost, several copies of some of them are retained. Gene retention could serve as source of variation for natural selection to enhance possible adaptation to environmental changes [263]. In this context, the three homoeologous copies of most wheat meiotic genes are retained and show balanced expression to ensure proper

meiotic progression [198]. There are, however, exceptions: the copy of the meiotic gene *SPO11-2* in subgenome A is not expressed, while its homoeologues in the other two subgenomes are functional [267]. Gene retention could also involve the acquisition of a novel expression domain or a new and beneficial role (neofunctionalization). This process has been reported for specific transcription factors, allowing the acquisition of different roles in regulatory development and plant morphology [268,269].

On the other hand, gene subfunctionalization involves the expression of duplicated genes in a tissue-specific way or in different developmental stages. It also ensures balanced expression among the different subgenomes [260,270]. The analysis of 727 RNAseq data sets in *T. aestivum* indicates that around 15–20% of genes present a tissue-specific differentiated homoeologous expression [271]. In the *Brassica* genus, the two paralogous genes *SHORT SUSPENSOR* (*SSP*) and *BRASSINOSTEROID KINASE 1* (*BSK1*) acquired different roles in the evolution. While *BSK1* retains its original role in hormonal transduction, *SSP* diverged to acquire a new function in zygote elongation by losing the kinase domain [272].

In addition to rearrangements affecting the copy number of genes, exons or small repeats, larger structural mutations resulting from reciprocal and non-reciprocal homoeologous exchanges abound in polyploids [273]. These rearrangements, involving small telomeric regions, intercalary segments of variable size, and even entire chromosome arms, alter the copy number of large genomic portions containing genic and non-genic DNA sequences, which is a representative feature of segmental allopolyploids. Extensive and repeated pattern of chromosomal variation has been reported in different populations of the natural allopolyploid *Tragopogon miscellus*, formed multiple times in the past 90 years [148]. Other segmental allopolyploids are quinoa, *Chenopodium quinoa* [274], tobacco, *Nicotiana tabacum* [275], *Brassica* [276,277], peanuts, *Arachis hypogaea* [278,279], and the synthetic allotetraploid rice obtained from the cross *O. sativa* subsp *indica* × *O. sativa* subsp *japonica* [280,281]. The complexity of chromosomal rearrangements can increase over generations, providing a very wide genomic diversity, on which natural selection can act promoting adaptation of neopolyploids. In fact, in *Brassica*, segmental allopolyploidy promoted phenotypic diversification of traits such as glucosinolate metabolism, flowering time or disease resistance [276].

Investigation of the constitution and evolution of subgenomes present in different allotetraploid plant species has shown that one subgenome, called dominant subgenome, tends to preserve more genes than the other subgenome. In addition, genes of the dominant subgenome tend to be more expressed than their homoeologous counterparts retained in the recessive subgenome [282]. Genome dominance involves events such as chromosome rearrangements of the types indicated above, which increase the dominant genome size instead of the submissive one, a preference in gene silencing of the submissive genome through epigenetic changes, or preference in activation of TEs from the dominant genome [270]. The occurrence of genome dominance normally appears following the hybridization process, throughout the first generations [283,284], or through multiple rounds of polyploidy [282]. In most cases, genome dominance manifests by upregulation or downregulation of the dominant or submissive genome, respectively [270,284,285]. The main elements responsible for this dominance would probably be trans–acting factors, that is, regulatory proteins such as transcription factors that operate through sequence-specific DNA-binding motifs. Dominance seems to arise in the genome with the most efficient factors [286]. For example, in the new synthetic allopolyploid *Cucumis sativus* × *C. hystryx* drastic changes at genomic level emerge rapidly after hybridization, while others occur in later generations at a slower rate. The study has revealed that the *C. sativum* subgenome is dominant, preserving more sequences and showing a higher expression level than the *C. hystryx* genome [287]. However, in tetraploid cotton, downregulation of the homoeologous gene copies of the submissive genome is mediated by both, cis- and trans-regulatory elements from the dominant genome [288]. Nevertheless, genome dominance is not present in all plant species. In *Oryza*, the short-term responses to genome merger are manifested in a high proportion of homoeologous gene pairs showing unequal expression [213].

5.2. Changes in the Activity of Transposable Elements (TEs)

Hybridization and polyploidization frequently trigger TE activation [269]. This has important consequences since TEs are the most abundant element in the genome of many plants. For example, in wheat, these elements represent about 85% of the genome [289].

TEs play a key role in plant evolution, since they are source of genetic diversity, allowing adaptation to new environments [290–293]. The repetitive nature of TEs offers numerous sequences scattered through the whole genome, which are potential sites for recombination and, therefore, represent a major source of chromosome rearrangements. TEs may represent a substrate for new genes and gene functions [294] and can provide promoters or transcriptional regulatory elements that change gene expression levels [295]. In addition, TEs transposition can create insertions and/or other mutations along the genome sequence, which might confer an adaptive advantage to new species [296]. Specifically, TEs seems to be involved in the adaptation to different stresses by modification of the expression of stress-related genes [297]. This phenomenon has been reported in the case of aluminum resistance genes [298] or in genes involved in the response to different diseases in pepper [299]. In wheat, Poretti and coworkers [300] showed how a specific class of TEs, Miniature Inverted-repeat Transposable Elements (MITEs), contribute to the regulation of neighboring genes via micro RNAs (miRNAs), increasing the immune response to the powdery mildew pathogen. In a meiotic context, TEs, providing sequence homology, are also involved in the modification of the recombination pattern along the chromosomes [301,302].

Hybridization and polyploidization not only allow the combination of two different TE populations, and siRNAs controlling them, but also affect the expression of flanking genes [295]. In addition to offer new regulatory sequences, TEs can also be the source of small RNAs that affect gene expression [260]. The reactivation of LTRs (Long Terminal Repeats) in resynthesized hexaploid wheat produces alterations in the expression of neighboring genes [303,304]. Similar results were observed in different species such as synthetic *Arabiposis* polyploids [22], synthetic *Cucumis* polyploids [287], or *Gossypium* [305], among others. TEs can also experience an increase in copy number following the hybridization, as it has been reported in tobacco [306] or *Brassica* [307]. Exceptions have been found, for example in *A. arenosa*, where polyploidization caused no change in the copy number [308].

5.3. Changes at the Gene Expression and Regulatory Level

The expression level of duplicated genes in allopolyploids, instead of being exclusively additive relative to that of progenitors, suffers a deep modification called "transcriptome shock" [309]. Gene expression changes, including genome dominance and non-additive expression patterns, have been reported in synthetic and natural polyploid species of various taxa, such as, *Arabidopsis* [310], *Tragopogon* [311], *Coffea* [312], *Gossypium* [288], *Oryza* [313], *Mimulus* [314] and *Triticum* [315,316]. The transcriptomic adjustment to the polyploid condition might take place either during the first generations, after the hybridization and/or WGD, or after a long term period [317]. For example, Zhao and coworkers [262], reported that among the homoeologous gene pairs of the A and B subgenomes, either from natural tetraploid wheat or extracted from hexaploid wheat, with differential expression relative to a synthetic tetraploid, most of them had only one differentially expressed copy, which was more often that of the B subgenome. In addition, differentially expressed genes were more abundant in the A and B extracted subgenomes than in those of the natural tetraploid wheat. This suggests that chromatin remodeling produced to adjust gene expression levels is an irreversible process that initiates at early generations and increases with the course of evolution. The non-additive expression pattern means that the expression level of a particular gene in a polyploid plant is not equal to the average of the gene expression levels in the two parents [318]. This has been observed in synthetic *Arabidopsis* allotetraploids (*A. thaliana* × *A. arenosa*) where around 6% of the genes differ in their expression level relative to the mid-parental value. Most of these genes were also differentially expressed among progenitors and non-additive gene regulation was derived from repression in 65% of genes [310].

As stated above, factors, such as TEs, genome dominance and cis- and trans-regulatory elements, contribute to gene expression regulation. In fact, the merge of two genomes could generate new forms of interactions between parental regulatory factors [286]. It has been demonstrated that the level of interactions between trans-factors of polyploids is about 54–64% higher than those found in diploids [319]. In wheat, polyploidization caused mainly elimination of redundant genes as well as appearance of inter-subgenome trans-regulation [262]. In addition, the merge of two different small RNA populations (such as miRNAs and siRNAs) can trigger the emergence of new regulatory mechanisms in allopolyploids [320,321]. Expression of these small RNAs can also be non-additively regulated [322]. In this context, a high siRNA density at genes associated with TEs has been reported to have a negative effect on gene expression of the D genome in nascent allohexaploid wheat [323].

However, modification of gene expression can be also influenced by epigenetic changes such as alterations in the pattern of methylation of histones and DNA [318]. Indeed, a study carried out on hexaploid wheat and its progenitor *Ae. tauschii* showed that modification of the methylation pattern is responsible of altered expression in 11% of genes [324]. Accordingly, changes of histone and DNA methylation are responsible of the Nucleolar Organizing Region (NOR) silencing in the subgenome A of a synthetic allotetraploid wheat, causing its further elimination [325]. Nucleolar dominance controlled by changes on methylation of DNA and histones has been also observed in the allopolyploid *A. suecica* (*A. thaliana* × *A. arenosa*), where the rRNA genes from *A. thaliana* are silenced while those from *A. arenosa*, are transcribed [259,326]. Likewise, DNA methylation changes observed in synthetic allopolyploid *B. napus* (AACC), affect mainly to silencing of genes of the C genome [327].

Epigenetic changes may also modulate the polyploid phenotype. For instance, *A. suecica* shows late flowering compared to its progenitors. In these species, the flowering time is controlled by two genes, the *FLOWERING LOCUS C* (*FLC*), that repress flowering, and *FRIGIDA* (*FRI*) that upregulates *FLC*. In *A. suecica* both *FLC* copies, from *A. thaliana* and *A. arenosa*, are upregulated by H3K4 trimethylation (H3K4me3) and H3K9 acetylation causing flowering delay [328]. The photoperiod in domesticated allotetraploid cotton (*G. barbadense* × *G. hirsutum*, AADD genomes) is also modified relative to the parental species. The *CONSTANT-LIKE 2* (*COL2*) gene is hypermethylated in both wild species, which is responsible of plant photoperiod sensitivity. During the domestication process, hypermethylation disappeared in *COL2* of the D genome, contributing to photoperiod insensitivity of the allotetraploid. This epigenetic change has allowed to produce cotton in different environments (such as subtropical) [329].

The merger and doubling of independent genomes profoundly impact their genetic architecture, the expression mode of merged genes, and the physiological machinery responsible of the allopolyploid phenotype. However, changes in genome organization, gene expression and molecular interactions do not occur only suddenly after hybridization but are cumulative throughout the polyploid evolution. Feldman and Levy [174] distinguished between revolutionary changes, that is, those arising in the early stages of allopolyploid formation and evolutionary changes, namely, changes produced more gradually over time. Understanding the impact that revolutionary and evolutionary changes have had on allopolyploid evolution is essential for a comprehensive knowledge of the dimension of the temporal progression needed to become a stable and well adapted allopolyploid species. As suggested by Nieto-Ferliner and coworkers [260] revolutionary changes most likely represent the tip of the iceberg as compared to later evolutionary innovations. Despite the advances produced in the last decades with the use of genomic tools for probing genomes and transcriptomes, the way by which polyploidization leads to phenotypic diversity and evolutionary diversification is poorly understood [260]. Consequently, it is also unknown how the different are the evolutionary patterns of allopolyploids relative to diploids.

6. Conclusions

Speciation by allopolyploidy is a complex evolutionary process that initiates with interspecific hybridization and is followed of the hybrid chromosome number duplication, cytological diploidization of the primitive allopolyploid and genetical diploidization derived from cumulative genomic changes over evolutionary timescale. Interspecific hybridization seems to be a relatively frequent phenomenon among plants conditioned by the reproductive system. Interpecific hybridization has been exploited in several research experiments for interspecific gene transfer. In addition, very valuable information on the genetic and epigenetic changes triggered by the genome merger has been obtained from synthetic hybrids and allopolyploids. WGD is also starting to be quantified and different cellular defects have been identified as responsible of the production of unreduced gametes. While the chromosome constitution of the hybrids may be responsible, at least in part, or the production of 2n gametes, there is evidence that the parental genotypes are also important to achieve WGD. On the other hand, there is accumulated evidence that meiotic and mitotic cell divisions are indeed highly vulnerable to environmental stress. Interspecific hybridization and WGD may facilitate genetic diversification and even provide an emergent saltational speciation as response to environment changes. The cytological diploidization depends on genetic systems evolved at the early allopolyploid stage that suppress recombination between homoeologous chromosomes. The locus *Ph1* in wheat is the best studied example, but the genetic basis of the diploid-like behavior is unknown in most allopolyploids. Understanding the mode of action of homoeologous recombination suppressors has also implication in their application for useful gene introgression into crops through meiotic recombination. To establish how the different are the mechanisms responsible of the cytological diploidization of autopolyploids and allopolyploids is also of great importance, since many autopolyploids show also preferential bivalent formation at meiosis. Genomic changes and transcriptomic modifications generated in the primitive allopolyploid can increase in complexity in the course of evolution giving rise to phenotypic innovations, which can be exposed to natural selection or drift. The advent of high-throughput molecular genetics and advances in DNA sequencing technologies provide experimental tools to investigate changes produced during the evolutionary trajectory of extant allopolyploid species and identify relevant genomics signatures of their cryptic long-term modifications capable of generating adaptation and speciation.

Author Contributions: Conceptualization and design, T.N. Writing, the four authors, F.B., M.P., P.P. and T.N., have made a substantial, direct and intellectual contribution to write the manuscript. All authors have read and agreed to the published version of the manuscript.

Funding: P.P. research lab is supported by P20_00971 grant from the Consejería de Transformación Económica, Industria, Conocimiento y Universidades/Cofinanciación FEDER 80%—Programa Operativo FEDER de Andalucía 2014-2020 and the PID2019-103996RB-I00 grant from the MCIN/AEI/10.13039/501100011033. T.N. and M.P. acknowledge the support of the Ministry of Science and Innovation of Spain (PID2020-118038GB-I00) and of the European Union (Marie Curie ITN, MEICOM 765212). M.P. is part of the International Plant Nucleus Consortium (IPNC) and COST Action n° CA 16212 'In Depth'. F.B. is a PhD fellow funded by the European Union (Marie Curie ITN, MEICOM 765212).

Institutional Review Board Statement: Not applicable.

Informed Consent Statement: Not applicable.

Acknowledgments: Authors deeply thanks Zuny Cifuentes and María del Carmen Calderón from P.P. lab for providing microscopy images.

Conflicts of Interest: The authors declare no conflict of interest.

References

1. Lewis, W.H. *Polyploidy: Biological Relevance*; Plenum Press: New York, NY, USA, 1980; pp. 1–583. [CrossRef]
2. Soltis, D.E.; Visger, C.J.; Soltis, P.S. The Polyploidy Revolution Then...and Now: Stebbins Revisited. *Am. J. Bot.* **2014**, *101*, 1–22. [CrossRef]
3. Ramsey, J.; Schemske, D.W. Pathways, Mechanisms, and Rates of Polyploid Formation in Flowering Plants. *Annu. Rev. Ecol. Syst.* **1998**, *29*, 467–501. [CrossRef]
4. Jackson, R.C. Polyploidy and Diploidy: New Perspectives on Chromosome Pairing and Its Evolutionary Implications. *Am. J. Bot.* **1982**, *69*, 1512–1523. [CrossRef]
5. Ramsey, J.; Schemske, D.W. Neopolyploidy in Flowering Plants. *Annu. Rev. Ecol. Syst.* **2002**, *33*, 589–639. [CrossRef]
6. Soltis, P.S.; Soltis, D.E. The Role of Genetic and Genomic Attributes in the Success of Polyploids. *Proc. Natl. Acad. Sci. USA* **2000**, *97*, 7051–7057. [CrossRef] [PubMed]
7. Soltis, D.E.; Soltis, P.S.; Schemske, D.W.; Hancock, J.F.; Thompson, J.N.; Husband, B.C.; Judd, W.S. Autopolyploidy in Angiosperms: Have We Grossly Underestimated the Number of Species? *Taxon* **2007**, *56*, 13–30. [CrossRef]
8. Qiu, T.; Liu, Z.; Liu, B. The Effects of Hybridization and Genome Doubling in Plant Evolution via Allopolyploidy. *Mol. Biol. Rep.* **2020**, *47*, 5549–5558. [CrossRef]
9. Schranz, M.E.; Osborn, T.C. Novel Flowering Time Variation in the Resynthesised Polyploid *Brassica Napus*. *J. Hered.* **2000**, *91*, 242–246. [CrossRef]
10. Cohen, H.; Fait, A.; Tel-Zur, N. Morphological, Cytological and Metabolic Consequences of Autopolyploidization in *Hylocereus* (Cactaceae) Species. *BMC Plant Biol.* **2013**, *13*, 173. [CrossRef]
11. Feldman, M.; Levy, A.A. Allopolyploidy—A Shaping Force in the Evolution of Wheat Genomes. *Cytogenet. Genome Res.* **2005**, *109*, 250–258. [CrossRef] [PubMed]
12. Adams, K.L.; Wendel, J.F. Polyploidy and Genome Evolution in Plants. *Curr. Opin. Plant Biol.* **2005**, *8*, 135–141. [CrossRef]
13. Chen, Z.J.; Ni, Z. Mechanisms of Genomic Rearrangements and Gene Expression Changes in Plant Polyploids. *BioEssays* **2006**, *28*, 240–252. [CrossRef]
14. Song, K.; Lu, P.; Tang, K.; Osborn, T.C. Rapid Genome Change in Synthetic Polyploids of Brassica and Its Implications for Polyploid Evolution. *Proc. Natl. Acad. Sci. USA* **1995**, *92*, 7719–7723. [CrossRef]
15. Nicolas, S.D.; Le Mignon, G.; Eber, F.; Coriton, O.; Monod, H.; Clouet, V.; Huteau, V.; Lostanlen, A.; Delourme, R.; Chalhoub, B.; et al. Homeologous Recombination Plays a Major Role in Chromosome Rearrangements That Occur During Meiosis of *Brassica Napus* Haploids. *Genetics* **2007**, *175*, 487–503. [CrossRef]
16. Gaeta, R.T.; Chris Pires, J. Homoeologous Recombination in Allopolyploids: The Polyploid Ratchet. *New Phytol.* **2010**, *186*, 18–28. [CrossRef]
17. Grandont, L.; Jenczewski, E.; Lloyd, A. Meiosis and Its Deviations in Polyploid Plants. *Cytogenet. Genome Res.* **2013**, *140*, 171–184. [CrossRef]
18. Lipman, M.J.; Chester, M.; Soltis, P.S.; Soltis, D.E. Natural Hybrids between *Tragopogon mirus* and *T. miscellus* (Asteraceae): A New Perspective on Karyotypic Changes Following Hybridization at the Polyploid Level. *Am. J. Bot.* **2013**, *100*, 2016–2022. [CrossRef]
19. Shaked, H.; Kashkush, K.; Ozkan, H.; Feldman, M.; Levy, A.A. Sequence Elimination and Cytosine Methylation Are Rapid and Reproducible Responses of the Genome to Wide Hybridization and Allopolyploidy in Wheat. *Plant Cell* **2001**, *13*, 1749–1759. [CrossRef] [PubMed]
20. Kashkush, K.; Feldman, M.; Levy, A.A. Gene Loss, Silencing and Activation in a Newly Synthesized Wheat Allotetraploid. *Genetics* **2002**, *160*, 1651–1659. [CrossRef] [PubMed]
21. Madlung, A.; Masuelli, R.W.; Watson, B.; Reynolds, S.H.; Davison, J.; Comai, L. Remodeling of DNA Methylation and Phenotypic and Transcriptional Changes in Synthetic *Arabidopsis* Allotetraploids. *Plant Physiol.* **2002**, *129*, 733–746. [CrossRef] [PubMed]
22. Madlung, A.; Tyagi, A.P.; Watson, B.; Jiang, H.; Kagochi, T.; Doerge, R.W.; Martienssen, R.; Comai, L. Genomic Changes in Synthetic *Arabidopsis* Polyploids. *Plant J.* **2005**, *41*, 221–230. [CrossRef] [PubMed]
23. Chen, Z.J. Genetic and Epigenetic Mechanisms for Gene Expression and Phenotypic Variation in Plant Polyploids. *Annu. Rev. Plant Biol.* **2007**, *58*, 377–406. [CrossRef] [PubMed]
24. Gaeta, R.T.; Pires, J.C.; Iniguez-Luy, F.; Leon, E.; Osborn, T.C. Genomic Changes in Resynthesized *Brassica Napus* and Their Effect on Gene Expression and Phenotype. *Plant Cell* **2007**, *19*, 3403–3417. [CrossRef]
25. Adams, K.L.; Wendel, J.F. Novel Patterns of Gene Expression in Polyploid Plants. *Trends Genet.* **2005**, *21*, 539–543. [CrossRef] [PubMed]
26. Comai, L.; Tyagi, A.P.; Winter, K.; Holmes-Davis, R.; Reynolds, S.H.; Stevens, Y.; Byers, B. Phenotypic Instability and Rapid Gene Silencing in Newly Formed *Arabidopsis* Allotetraploids. *Plant Cell* **2000**, *12*, 1551–1567. [CrossRef] [PubMed]
27. Wang, J.; Tian, L.; Madlung, A.; Lee, H.S.; Chen, M.; Lee, J.J.; Watson, B.; Kagochi, T.; Comai, L.; Chen, Z.J. Stochastic and Epigenetic Changes of Gene Expression in *Arabidopsis* Polyploids. *Genetics* **2004**, *167*, 1961–1973. [CrossRef]
28. Stupar, R.M.; Bhaskar, P.B.; Yandell, B.S.; Rensink, W.A.; Hart, A.L.; Ouyang, S.; Veilleux, R.E.; Busse, J.S.; Erhardt, R.J.; Buell, C.R.; et al. Phenotypic and Transcriptomic Changes Associated With Potato Autopolyploidization. *Genetics* **2007**, *176*, 2055–2067. [CrossRef]
29. Mayrose, I.; Zhan, S.H.; Rothfels, C.J.; Magnusn-Ford, K.; Barker, M.S.; Rieseberg, L.H.; Otto, S.P. Recently Formed Polyploid Plants Diversify at Lower Rates. *Science* **2011**, *333*, 1257. [CrossRef]

30. Sémon, M.; Wolfe, K.H. Consequences of Genome Duplication. *Curr. Opin. Genet. Dev.* **2007**, *17*, 505–512. [CrossRef]
31. Tate, J.A.; Joshi, P.; Soltis, K.A.; Soltis, P.S.; Soltis, D.E. On the Road to Diploidization? Homoeolog Loss in Independently Formed Populations of the Allopolyploid *Tragopogon miscellus* (Asteraceae). *BMC Plant Biol.* **2009**, *9*, 80. [CrossRef]
32. Zhang, P.G.; Huang, S.Z.; Pin, A.L.; Adams, K.L. Extensive Divergence in Alternative Splicing Patterns after Gene and Genome Duplication during the Evolutionary History of *Arabidopsis*. *Mol. Biol. Evol.* **2010**, *27*, 1686–1697. [CrossRef]
33. Hu, C.; Lin, S.Y.; Chi, W.T.; Charng, Y.Y. Recent Gene Duplication and Subfunctionalization Produced a Mitochondrial GrpE, the Nucleotide Exchange Factor of the Hsp70 Complex, Specialized in Thermotolerance to Chronic Heat Stress in *Arabidopsis*. *Plant Physiol.* **2012**, *158*, 747–758. [CrossRef] [PubMed]
34. Xu, G.; Guo, C.; Shan, H.; Kong, H. Divergence of Duplicate Genes in Exon-Intron Structure. *Proc. Natl. Acad. Sci. USA* **2012**, *109*, 1187–1192. [CrossRef] [PubMed]
35. De Smet, R.; Adams, K.L.; Vandepoele, K.; Van Montagu, M.C.E.; Maere, S.; Van De Peer, Y. Convergent Gene Loss Following Gene and Genome Duplications Creates Single-Copy Families in Flowering Plants. *Proc. Natl. Acad. Sci. USA* **2013**, *110*, 2898–2903. [CrossRef] [PubMed]
36. Roulin, A.; Auer, P.L.; Libault, M.; Schlueter, J.; Farmer, A.; May, G.; Stacey, G.; Doerge, R.W.; Jackson, S.A. The Fate of Duplicated Genes in a Polyploid Plant Genome. *Plant J.* **2013**, *73*, 143–153. [CrossRef] [PubMed]
37. Koh, J.; Soltis, P.S.; Soltis, D.E. Homeolog Loss and Expression Changes in Natural Populations of the Recently and Repeatedly Formed Allotetraploid *Tragopogon mirus* (Asteraceae). *BMC Genome* **2010**, *11*, 97. [CrossRef]
38. Naranjo, T.; Benavente, E. The Mode and Regulation of Chromosome Pairing in Wheat-Alien Hybrids (Ph Genes, an Updated View). In *Alien Introgression in Wheat: Cytogenetics, Molecular Biology, and Genomics*, 1st ed.; Molnár-Láng, M., Ceoloni, C., Doležel, J., Eds.; Springer: Cham, Switzerland, 2015; pp. 133–162. [CrossRef]
39. Svačina, R.; Sourdille, P.; Kopecký, D.; Bartoš, J. Chromosome Pairing in Polyploid Grasses. *Front. Plant Sci.* **2020**, *11*, 1056. [CrossRef]
40. Jiao, Y.; Wickett, N.J.; Ayyampalayam, S.; Chanderbali, A.S.; Landherr, L.; Ralph, P.E.; Tomsho, L.P.; Hu, Y.; Liang, H.; Soltis, P.S.; et al. Ancestral Polyploidy in Seed Plants and Angiosperms. *Nature* **2011**, *473*, 97–100. [CrossRef]
41. Paterson, A.H.; Wang, X.; Li, J.; Tang, H. Ancient and Recent Polyploidy in Monocots. In *Polyploidy Genome Evolution*; Soltis, P.S., Soltis, D.E., Eds.; Springer: Berlin/Heidelberg, Germany, 2012; pp. 93–108. [CrossRef]
42. Wendel, J.F. The Wondrous Cycles of Polyploidy in Plants. *Am. J. Bot.* **2015**, *102*, 1753–1756. [CrossRef]
43. De Storme, N.; Mason, A. Plant Speciation through Chromosome Instability and Ploidy Change: Cellular Mechanisms, Molecular Factors and Evolutionary Relevance. *Curr. Plant Biol.* **2014**, *1*, 10–33. [CrossRef]
44. Robert, H. *Plant Hybridization before Mendel*; Princeton University Press: Princeton, NJ, USA; Elsevier: Princeton, NJ, USA, 1929.
45. Zirkle, C. *The Beginnings of Plant Hybridization. Morris Arboretum Monographs. I*; University of Pennsylvania Press, Philadelphia (Humphrey Milford, Oxford University Press): London, UK, 1935; pp. 1–248.
46. López-Caamal, A.; Tovar-Sánchez, E. Genetic, Morphologica, and Chemical Patterns of Plant Hybridization. *Rev. Chil. Hist. Nat.* **2014**, *87*, 16. [CrossRef]
47. Mendel, G. Versuche Über Pflanzen-Hybriden. In *Verhandlungen des Naturforschenden Vereines in Brünn*; Verlage des Vereines: Brünn, Czechoslovakia, 1866; pp. 3–47.
48. De Vries, H. Das Spaltungsgesetz Der Bastarde. *Ber. Der Dtsch. Bot. Ges.* **1900**, *18*, 83–90. [CrossRef]
49. Correns, C. Mendel's Regel Über Das Verhalten Der Nachkommenschaft Der Rassenbastarde. *Ber. Der Dtsch. Bot. Ges.* **1900**, *18*, 158–168.
50. Tschermak, E. Ueber Künstliche Kreuzung Bei Pisum Sativum. *Ber. Der Dtsch. Bot. Ges.* **1900**, *18*, 232–239. [CrossRef]
51. Lotsy, J.P. *Evolution by Means of Hybridization*; Martinus Nijhoff: The Hague, The Netherlands, 1916; p. 166.
52. Winge, Ø. The Chromosomes, Their Numbers and General Importance. *C.R. Trav. Lab. Carlsb.* **1917**, *13*, 131–275.
53. Stebbins, G.L. *Variation and Evolution in Plants*; Columbia University Press: New York, NY, USA, 1950; pp. 1–643. [CrossRef]
54. Soltis, D.E.; Soltis, P.S. Molecular Data and the Dynamic Nature of Polyploidy. *CRC Crit. Rev. Plant Sci.* **1993**, *12*, 243–273. [CrossRef]
55. Müntzing, A. Outlines to a Genetic Monograph of the Genus *Galeopsis*. *Hereditas* **1930**, *13*, 185–341. [CrossRef]
56. Rieseberg, L.H. Hybrid Origins of Plant Species. *Annu. Rev. Ecol. Syst.* **2003**, *28*, 359–389. [CrossRef]
57. Charlesworth, D. Evolution of Plant Breeding Systems. *Curr. Biol.* **2006**, *16*, R726–R735. [CrossRef]
58. Ollerton, J.; Winfree, R.; Tarrant, S. How Many Flowering Plants Are Pollinated by Animals? *Oikos* **2011**, *120*, 321–326. [CrossRef]
59. Aide, T.M. The Influence of Wind and Animal Pollination on Variation in Outcrossing Rates. *Evolution* **1986**, *40*, 434–435. [CrossRef]
60. Tiffin, P.; Olson, M.S.; Moyle, L.C. Asymmetrical Crossing Barriers in Angiosperms. *Proc. Biol. Sci.* **2001**, *268*, 861–867. [CrossRef]
61. Moreira-Hernández, J.I.; Muchhala, N. Importance of Pollinator-Mediated Interspecific Pollen Transfer for Angiosperm Evolution. *Annu. Rev. Ecol. Evol. Syst.* **2019**, *50*, 191–217. [CrossRef]
62. Yakimowski, S.B.; Rieseberg, L.H. The Role of Homoploid Hybridization in Evolution: A Century of Studies Synthesizing Genetics and Ecology. *Am. J. Bot.* **2014**, *101*, 1247–1258. [CrossRef]
63. Bedinger, P.A.; Broz, A.K.; Tovar-Mendez, A.; McClure, B. Pollen-Pistil Interactions and Their Role in Mate Selection. *Plant Physiol.* **2017**, *173*, 79–90. [CrossRef]

64. Whitney, K.D.; Ahern, J.R.; Campbell, L.G.; Albert, L.P.; Kin, M.S. Patterns of Hybridization in Plants. *Perspect. Plant Ecol. Evol. Syst.* **2010**, *12*, 175–182. [CrossRef]
65. Ellstrand, N. *Dangerous Liaisons? When Cultivated Plants Mate with Their Wild Relatives*; Johns Hopkins University Press: Baltimore, MD, USA, 2003; p. 244.
66. Darlington, C.D. *Recent Advances in Cytology*, 2nd ed.; P. Blakiston's Son & Co.: Philadelphia, PA, USA, 1937; pp. 1–671.
67. Buggs, R.J.A.; Soltis, P.S.; Soltis, D.E. Does Hybridization between Divergent Progenitors Drive Whole-Genome Duplication? *Mol. Ecol.* **2009**, *18*, 3334–3339. [CrossRef]
68. Soltis, D.E.; Buggs, R.J.A.; Doyle, J.J.; Soltis, P.S. What We Still Don't Know about Polyploidy. *Taxon* **2010**, *59*, 1387–1403. [CrossRef]
69. de Wet, J.M. Origins of Polyploids. *Polyploidy Biol. Revel.* **1979**, *13*, 3–15. [CrossRef]
70. Harlan, J.R.; de Wet, J.M.J. On Ö. Winge and a Prayer: The Origins of Polyploidy. *Bot. Rev.* **1975**, *41*, 361–390. [CrossRef]
71. Bretagnolle, F.; Thompson, J.D. Gametes with the Somatic Chromosome Number: Mechanisms of Their Formation and Role in the Evolution of Autopolyploid Plants. *New Phytol.* **1995**, *129*, 1–22. [CrossRef]
72. Brownfield, L.; Köhler, C. Unreduced Gamete Formation in Plants: Mechanisms and Prospects. *J. Exp. Bot.* **2011**, *62*, 1659–1668. [CrossRef]
73. de Storme, N.; Geelen, D. Sexual Polyploidization in Plants—Cytological Mechanisms and Molecular Regulation. *New Phytol.* **2013**, *198*, 670–684. [CrossRef]
74. Shamina, N.; Dorogova, N.; Goncharov, N.; Orlova, A.; Trunova, S. Abnormalities of Spindle and Cytokine Behavior Leading to the Formation of Meiotic Restitution Nuclei in Intergeneric Cereal Hybrids. *Cell Biol. Int.* **1999**, *23*, 863–870. [CrossRef]
75. Shamina, N.V.; Silkova, O.G.; Seriukova, E.G. Monopolar Spindles in Meiosis of Intergeneric Cereal Hybrids. *Cell Biol. Int.* **2003**, *27*, 657–664. [CrossRef]
76. Shamina, N.; Dorogova, N.; Trunova, S. Radial Spindle and the Phenotype of the Maize Meiotic Mutant, Dv. *Cell Biol. Int.* **2000**, *24*, 729–736. [CrossRef] [PubMed]
77. Conicella, C.; Genualdo, G.; Errico, A.; Frusciante, L.; Monti, L.M. Meiotic Restitution Mechanisms and 2n Pollen Formation in a *Solanum tuberosum* Dihaploid and in Dihaploid x Wild Species Hybrids. *Plant Breed.* **1996**, *115*, 157–161. [CrossRef]
78. Conicella, C.; Capo, A.; Cammareri, M.; Errico, A.; Shamina, N.; Monti, L.M. Elucidation of Meiotic Nuclear Restitution Mechanisms in Potato through Analysis of Microtubular Cytoskeleton. *Euphytica* **2003**, *133*, 107–115. [CrossRef]
79. D'Erfurth, I.; Jolivet, S.; Froger, N.; Catrice, O.; Novatchkova, M.; Simon, M.; Jenczewski, E.; Mercier, R. Mutations in AtPS1 (*Arabidopsis thaliana* Parallel Spindle 1) Lead to the Production of Diploid Pollen Grains. *PLoS Genet.* **2008**, *4*, e1000274. [CrossRef] [PubMed]
80. De Storme, N.; Geelen, D. The *Arabidopsis* Mutant *jason* Produces Unreduced First Division Restitution Male Gametes through a Parallel/Fused Spindle Mechanism in Meiosis II. *Plant Physiol.* **2011**, *155*, 1403–1415. [CrossRef] [PubMed]
81. Becerra Lopez-Lavalle, L.A.; Orjeda, G. Occurrence and Cytological Mechanism of 2n Pollen Formation in a Tetraploid Accession of *Ipomoea batatas* (Sweet Potato). *J. Hered.* **2002**, *93*, 185–192. [CrossRef] [PubMed]
82. Zhang, J.F.; Wei, Z.Z.; Li, D.; Li, B. Using SSR Markers to Study the Mechanism of 2n Pollen Formation in *Populus* × *Euramericana* (Dode) Guinier and *P. popularis*. *Ann. For. Sci.* **2009**, *66*, 506. [CrossRef]
83. Liu, B.; Jin, C.; De Storme, N.; Schotte, S.; Schindfessel, C.; De Meyer, T.; Geelen, D. A Hypomorphic Mutant of PHD Domain Protein Male Meiocytes Death 1. *Genes* **2021**, *12*, 516. [CrossRef]
84. Li, Y.; Shen, Y.; Cai, C.; Zhong, C.; Zhu, L.; Yuan, M.; Ren, H. The Type II *Arabidopsis* Formin14 Interacts with Microtubules and Microfilaments to Regulate Cell Division. *Plant Cell* **2010**, *22*, 2710–2726. [CrossRef]
85. Iwanaga, M.; Peloquin, S.J. Origin and Evolution of Cultivated Tetraploid Potatoes via 2n Gametes. *Theor. Appl. Genet.* **1982**, *61*, 161–169. [CrossRef]
86. Watanabe, K.; Peloquin, S.J. Occurrence of 2n Pollen and Ps Gene Frequencies in Cultivated Groups and Their Related Wild Species in Tuber-Bearing *Solanums*. *Theor. Appl. Genet.* **1989**, *78*, 329–336. [CrossRef] [PubMed]
87. Zhou, X.; Mo, X.; Gui, M.; Wu, X.; Jiang, Y.; Ma, L.; Shi, Z.; Luo, Y.; Tang, W. Cytological, Molecular Mechanisms and Temperature Stress Regulating Production of Diploid Male Gametes in *Dianthus caryophyllus* L. *Plant Physiol. Biochem.* **2015**, *97*, 255–263. [CrossRef] [PubMed]
88. Pfeiffer, T.W.; Bingham, E.T. Abnormal Meiosis in Alfalfa, *Medicago sativa*: Cytology of 2N Egg and 4N Pollen Formation. *Can. J. Genet. Cytol.* **1983**, *25*, 107–112. [CrossRef]
89. Pagliarini, M.S.; Takayama, S.Y.; De Freitas, P.M.; Carraro, L.R.; Adamowski, E.V.; Silva, N.; Batista, L.A.R. Failure of Cytokinesis and 2n Gamete Formation in Brazilian Accessions of *Paspalum*. *Euphytica* **1999**, *108*, 129–135. [CrossRef]
90. Boldrini, K.R.; Pagliarini, M.S.; Do Valle, C.B. Abnormal Timing of Cytokinesis in Microsporogenesis in *Brachiaria humidicola* (Poaceae: Paniceae). *J. Genet.* **2006**, *85*, 225–228. [CrossRef] [PubMed]
91. De Storme, N.; Copenhaver, G.P.; Geelen, D. Production of Diploid Male Gametes in *Arabidopsis* by Cold-Induced Destabilization of Postmeiotic Radial Microtubule Arrays. *Plant Physiol.* **2012**, *160*, 1808–1826. [CrossRef]
92. Premachandran, M.N.; Lalitha, R. Microsporogenesis in a Fertile *Saccharum Officinarum* × *Erianthus Arundinaceus* Hybrid with Floral Abnormalities. *J. Sugarcane Res.* **2012**, *2*, 11–17.
93. Gómez-Rodríguez, V.M.; Rodríguez-Garay, B.; Barba-Gonzalez, R. Meiotic Restitution Mechanisms Involved in the Formation of 2n Pollen in *Agave tequilana* Weber and *Agave angustifolia* Haw. *Springerplus* **2012**, *1*, 1–7. [CrossRef] [PubMed]

94. Yang, C.Y.; Spielman, M.; Coles, J.P.; Li, Y.; Ghelani, S.; Bourdon, V.; Brown, R.C.; Lemmon, B.E.; Scott, R.J.; Dickinson, H.G. TETRASPORE Encodes a Kinesin Required for Male Meiotic Cytokinesis in *Arabidopsis*. *Plant J.* **2003**, *34*, 229–240. [CrossRef] [PubMed]
95. Zeng, Q.; Chen, J.G.; Ellis, B.E. AtMPK4 Is Required for Male-Specific Meiotic Cytokinesis in *Arabidopsis*. *Plant J.* **2011**, *67*, 895–906. [CrossRef] [PubMed]
96. Krupnova, T.; Stierhof, Y.D.; Hiller, U.; Strompen, G.; Müller, S. The Microtubule-Associated Kinase-like Protein RUNKEL Functions in Somatic and Syncytial Cytokinesis. *Plant J.* **2013**, *74*, 781–791. [CrossRef]
97. Oh, S.A.; Bourdon, V.; Dickinson, H.G.; Twell, D.; Park, S.K. *Arabidopsis* Fused Kinase TWO-IN-ONE Dominantly Inhibits Male Meiotic Cytokinesis. *Plant Reprod.* **2014**, *27*, 7–17. [CrossRef]
98. Shamina, N.V.; Shatskaya, O.A. Two Novel Meiotic Restitution Mechanisms in Haploid Maize (*Zea Mays* L.). *Russ. J. Genet.* **2011**, *47*, 438–445. [CrossRef]
99. Enns, L.C.; Kanaoka, M.M.; Torii, K.U.; Comai, L.; Okada, K.; Cleland, R.E. Two Callose Synthases, GSL1 and GSL5, Play an Essential and Redundant Role in Plant and Pollen Development and in Fertility. *Plant Mol. Biol.* **2005**, *58*, 333–349. [CrossRef]
100. Zhang, Z.; Kang, X. Cytological Characteristics of Numerically Unreduced Pollen Production in *Populus tomentosa* Carr. *Euphytica* **2010**, *173*, 151–159. [CrossRef]
101. Tavoletti, S. Cytological Mechanisms of 2n Egg Formation in a Diploid Genotype of *Medicago sativa* Subsp. Falcata. *Euphytica* **1994**, *75*, 1–8. [CrossRef]
102. Ravi, M.; Marimuthu, M.P.A.; Siddiqi, I. Gamete Formation without Meiosis in *Arabidopsis*. *Nature* **2008**, *451*, 1121–1124. [CrossRef]
103. D'Erfurth, I.; Jolivet, S.; Froger, N.; Catrice, O.; Novatchkova, M.; Mercier, R. Turning Meiosis into Mitosis. *PLoS Biol.* **2009**, *7*, e1000124. [CrossRef]
104. Singh, M.; Goel, S.; Meeley, R.B.; Dantec, C.; Parrinello, H.; Michaud, C.; Leblanc, O.; Grimanelli, D. Production of Viable Gametes without Meiosis in Maize Deficient for an ARGONAUTE Protein. *Plant Cell* **2011**, *23*, 443–458. [CrossRef]
105. Grimanelli, D.; Leblanc, O.; Espinosa, E.; Perotti, E.; González De León, D.; Savidan, Y. Mapping Diplosporous Apomixis in Tetraploid *Tripsacum*: One Gene or Several Genes? *Heredity* **1998**, *80*, 33–39. [CrossRef]
106. Van Dijk, P.J.; Bakx-Schotman, J.M.T. Formation of Unreduced Megaspores (Diplospory) in Apomictic Dandelions (*Taraxacum officinale*, s.l.) is Controlled by a Sex-Specific Dominant Locus. *Genetics* **2004**, *166*, 483–492. [CrossRef]
107. Noyes, R.D. Inheritance of Apomeiosis (Diplospory) in *Fleabanes* (Erigeron, Asteraceae). *Heredity* **2004**, *94*, 193–198. [CrossRef] [PubMed]
108. Ozias-Akins, P. Apomixis: Developmental Characteristics and Genetics. *CRC Crit. Rev. Plant Sci.* **2007**, *25*, 199–214. [CrossRef]
109. Kaushal, P.; Dwivedi, K.K.; Radhakrishna, A.; Srivastava, M.K.; Kumar, V.; Roy, A.K.; Malaviya, D.R. Partitioning Apomixis Components to Understand and Utilize Gametophytic Apomixis. *Front. Plant Sci.* **2019**, *10*, 256. [CrossRef] [PubMed]
110. Agashe, B.; Prasad, C.K.; Siddiqi, I. Identification and Analysis of DYAD: A Gene Required for Meiotic Chromosome Organisation and Female Meiotic Progression in *Arabidopsis*. *Development* **2002**, *129*, 3935–3943. [CrossRef] [PubMed]
111. Garcia-Aguilar, M.; Michaud, C.; Leblanc, O.; Grimanelli, D. Inactivation of a DNA Methylation Pathway in Maize Reproductive Organs Results in Apomixis-like Phenotypes. *Plant Cell* **2010**, *22*, 3249–3267. [CrossRef] [PubMed]
112. Corral, J.M.; Vogel, H.; Aliyu, O.M.; Hensel, G.; Thiel, T.; Kumlehn, J.; Sharbel, T.F. A Conserved Apomixis-Specific Polymorphism Is Correlated with Exclusive Exonuclease Expression in Premeiotic Ovules of Apomictic *Boechera* Species. *Plant Physiol.* **2013**, *163*, 1660–1672. [CrossRef] [PubMed]
113. d'Erfurth, I.; Cromer, L.; Jolivet, S.; Girard, C.; Horlow, C.; Sun, Y.; To, J.P.C.; Berchowitz, L.E.; Copenhaver, G.P.; Mercier, R. The CYCLIN-A CYCA1;2/TAM Is Required for the Meiosis I to Meiosis II Transition and Cooperates with OSD1 for the Prophase to First Meiotic Division Transition. *PLoS Genet.* **2010**, *6*, e1000989. [CrossRef] [PubMed]
114. Cromer, L.; Heyman, J.; Touati, S.; Harashima, H.; Araou, E.; Girard, C.; Horlow, C.; Wassmann, K.; Schnittger, A.; de Veylder, L.; et al. OSD1 Promotes Meiotic Progression via APC/C Inhibition and Forms a Regulatory Network with TDM and CYCA1;2/TAM. *PLoS Genet.* **2012**, *8*, e1002865. [CrossRef] [PubMed]
115. Bulankova, P.; Riehs-Kearnan, N.; Nowack, M.K.; Schnittger, A.; Riha, K. Meiotic Progression in *Arabidopsis* Is Governed by Complex Regulatory Interactions between SMG7, TDM1, and the Meiosis I–Specific Cyclin TAM. *Plant Cell* **2010**, *22*, 3791–3803. [CrossRef]
116. Kihara, H.; Lilienfeld, F. A New Synthesized 6x-wheat. *Hereditas* **1949**, *35*, 307–319. [CrossRef]
117. Wagenaar, E.B. Meiotic Restitution and the Origin of Polyploidy. i. Influence of Genotype on Polyploid Seedset in a *Triticum crassum* × *T. turgidum* Hybrid. *Can. J. Genet. Cytol.* **1968**, *10*, 836–843. [CrossRef]
118. Jauhar, P.P.; Dogramaci-Altuntepe, M.; Peterson, T.S.; Almouslem, A.B. Seedset on Synthetic Haploids of Durum Wheat: Cytological and Molecular Investigations. *Crop Sci.* **2000**, *40*, 1742–1749. [CrossRef]
119. Matsuoka, Y.; Nasuda, S. Durum Wheat as a Candidate for the Unknown Female Progenitor of Bread Wheat: An Empirical Study with a Highly Fertile F1 Hybrid with *Aegilops tauschii* Coss. *Theor. Appl. Genet.* **2004**, *109*, 1710–1717. [CrossRef]
120. Tiwari, V.K.; Rawat, N.; Neelam, K.; Randhawa, G.S.; Singh, K.; Chhuneja, P.; Dhaliwal, H.S. Development of *Triticum turgidum* Subsp. Durum—*Aegilops longissima* Amphiploids with High Iron and Zinc Content through Unreduced Gamete Formation in F1 Hybrids. *Genome* **2008**, *51*, 757–766. [CrossRef]
121. You-wei, Y.; Zhang, L.; Yen, Y.; Zheng, Y.; Liu, D. Cytological Evidence on Meiotic Restitution in Pentaploid F1 Hybrids between Synthetic Hexaploid Wheat and *Aegilops variabilis*. *Caryologia* **2010**, *63*, 354–358. [CrossRef]

122. Matsuoka, Y. Evolution of Polyploid *Triticum* Wheats under Cultivation: The Role of Domestication, Natural Hybridization and Allopolyploid Speciation in Their Diversification. *Plant Cell Physiol.* **2011**, *52*, 750–764. [CrossRef]
123. Naranjo, T.; Lacadena, J.R. Wheat Univalent Orientation at Anaphase I in Wheat-Rye Derivatives. *Chromosoma* **1982**, *84*, 653–661. [CrossRef]
124. Cai, X.; Xu, S.S.; Zhu, X. Mechanism of Haploidy-Dependent Unreductional Meiotic Cell Division in Polyploid Wheat. *Chromosoma* **2010**, *119*, 275–285. [CrossRef]
125. Pignone, D. Non-Reductional Meiosis in a *Triticum turgidum* ×*Aegilops longissima* Hybrid and in Backcrosses of Its Amphidiploid with *T. turgidum* (Poaceae). *Plant Syst. Evol.* **1993**, *187*, 127–134. [CrossRef]
126. Silkova, O.G.; Shchapova, A.I.; Shumny, V.K. Meiotic Restitution in Amphihaploids in the Tribe *Triticeae*. *Russ. J. Genet.* **2011**, *47*, 383–393. [CrossRef]
127. Silkova, O.G.; Loginova, D.B. Sister Chromatid Separation and Monopolar Spindle Organization in the First Meiosis as Two Mechanisms of Unreduced Gametes Formation in Wheat-Rye Hybrids. *Plant Reprod.* **2016**, *29*, 199–213. [CrossRef] [PubMed]
128. García, A.V.; Ortiz, A.M.; Silvestri, M.C.; Custodio, A.R.; Moretzsohn, M.C.; Lavia, G.I. Occurrence of 2n Microspore Production in Diploid Interspecific Hybrids between the Wild Parental Species of Peanut (*Arachis hypogaea* L., Leguminosae) and Its Relevance in the Genetic Origin of the Cultigen. *Crop Sci.* **2020**, *60*, 2420–2436. [CrossRef]
129. Wang, C.J.; Zhang, L.Q.; Dai, S.F.; Zheng, Y.L.; Zhang, H.G.; Liu, D.C. Formation of Unreduced Gametes Is Impeded by Homologous Chromosome Pairing in Tetraploid *Triticum turgidum* × *Aegilops tauschii* Hybrids. *Euphytica* **2010**, *175*, 323–329. [CrossRef]
130. Ressurreição, F.; Barão, A.; Viegas, W.; Delgado, M. Haploid Independent Unreductional Meiosis in Hexaploid Wheat. In *Meiosis Molecular Mechanism Cytogenetics Diversity*; Swan, A., Ed.; InTechOpen: London, UK, 2012; pp. 321–330. [CrossRef]
131. Xu, S.; Dong, Y. Fertility and Meiotic Mechanisms of Hybrids between Chromosome Autoduplication Tetraploid Wheats and *Aegilops* Species. *Genome* **1992**, *35*, 379–384. [CrossRef]
132. Zhang, L.Q.; Yen, Y.; Zheng, Y.L.; Liu, D.C. Meiotic Restriction in Emmer Wheat Is Controlled by One or More Nuclear Genes That Continue to Function in Derived Lines. *Sex. Plant Reprod.* **2007**, *20*, 159–166. [CrossRef]
133. Zhang, L.Q.; Liu, D.C.; Zheng, Y.L.; Yan, Z.H.; Dai, S.F.; Li, Y.F.; Jiang, Q.; Ye, Y.Q.; Yen, Y. Frequent Occurrence of Unreduced Gametes in *Triticum turgidum-Aegilops tauschii* Hybrids. *Euphytica* **2010**, *172*, 285–294. [CrossRef]
134. Tanaka, M. Newly Synthesized Amphidiploids from the Hybrids Emmer Wheats x *Aegilops squarrosa* Varieties. *Wheat Inf. Serv.* **1961**, *8*, 8.
135. Xu, S.J.; Joppa, L.R. Mechanisms and Inheritance of First Division Restitution in Hybrids of Wheat, Rye, and *Aegilops squarrosa*. *Genome* **1995**, *38*, 607–615. [CrossRef]
136. Xu, S.J.; Joppa, L.R. First-Division Restitution in Hybrids of Langdon Durum Disomic Substitution Lines with Rye and *Aegilops squarrosa*. *Plant Breed.* **2000**, *119*, 233–241. [CrossRef]
137. Hao, M.; Luo, J.; Zeng, D.; Zhang, L.; Ning, S.; Yuan, Z.; Yan, Z.; Zhang, H.; Zheng, Y.; Feuillet, C.; et al. QTug.Sau-3B Is a Major Quantitative Trait Locus for Wheat Hexaploidization. *Genes Genome Genet.* **2014**, *4*, 1943–1953. [CrossRef] [PubMed]
138. Matsuoka, Y.; Nasuda, S.; Ashida, Y.; Nitta, M.; Tsujimoto, H.; Takumi, S.; Kawahara, T. Genetic Basis for Spontaneous Hybrid Genome Doubling during Allopolyploid Speciation of Common Wheat Shown by Natural Variation Analyses of the Paternal Species. *PLoS ONE* **2013**, *8*, e68310. [CrossRef]
139. Mirzaghaderi, G.; Fathi, N. Unreduced Gamete Formation in Wheat: *Aegilops triuncialis* Interspecific Hybrids Leads to Spontaneous Complete and Partial Amphiploids. *Euphytica* **2015**, *206*, 67–75. [CrossRef]
140. Silkova, O.G.; Dobrovolskaya, O.B.; Shchapova, A.I.; Shumny, V.K. Features of the Regulation of Meiotic Restitution in Androgenic Haploids of Wheat-Rye Substitution Lines 2R(2D)1, 2R(2D)3, and 6R(6A) (*Triticum aestivum* L., Cultivar Saratovskaya 29/*Secale cereale* L., Cultivar Onokhoiskaya). *Russ. J. Genet.* **2009**, *45*, 1062–1066. [CrossRef]
141. Oleszczuk, S.; Lukaszewski, A.J. The Origin of Unusual Chromosome Constitutions among Newly Formed Allopolyploids. *Am. J. Bot.* **2014**, *101*, 318–326. [CrossRef]
142. Lim, K.B.; Ramanna, M.S.; De Jong, J.H.; Jacobsen, E.; Van Tuyl, J.M. Indeterminate Meiotic Restitution (IMR): A Novel Type of Meiotic Nuclear Restitution Mechanism Detected in Interspecific Lily Hybrids by GISH. *Theor. Appl. Genet.* **2001**, *103*, 219–230. [CrossRef]
143. Stebbins, G.L. Types of Polyploids: Their Classification and Significance. *Adv. Genet.* **1947**, *1*, 403–429. [CrossRef] [PubMed]
144. Gaut, B.S.; Doebley, J.F. DNA Sequence Evidence for the Segmental Allotetraploid Origin of Maize. *Proc. Natl. Acad. Sci. USA* **1997**, *94*, 6809–6814. [CrossRef] [PubMed]
145. Boff, T.; Schifino-Wittmann, M.T. Segmental Allopolyploidy and Paleopolyploidy in Species of *Leucaena Benth*: Evidence from Meiotic Behaviour Analysis. *Hereditas* **2003**, *138*, 27–35. [CrossRef] [PubMed]
146. Shinohara, W.; Ushio, Y.; Seo, A.; Nakato, N.; Kono, M.; Kudoh, H.; Tobe, H.; Murakami, N. Evidence for Hybrid Origin and Segmental Allopolyploidy in Eutetraploid and Aneutetraploid *Lepisorus thunbergianus* (Polypodiaceae). *Syst. Bot.* **2010**, *35*, 20–29. [CrossRef]
147. Xiong, Z.; Gaeta, R.T.; Pires, J.C. Homoeologous Shuffling and Chromosome Compensation Maintain Genome Balance in Resynthesized Allopolyploid *Brassica napus*. *Proc. Natl. Acad. Sci. USA* **2011**, *108*, 7908–7913. [CrossRef]

148. Chester, M.; Gallagher, J.P.; Symonds, V.V.; Da Silva, A.V.C.; Mavrodiev, E.V.; Leitch, A.R.; Soltis, P.S.; Soltis, D.E. Extensive Chromosomal Variation in a Recently Formed Natural Allopolyploid Species, *Tragopogon miscellus* (Asteraceae). *Proc. Natl. Acad. Sci. USA* **2012**, *109*, 1176–1181. [CrossRef]
149. De Storme, N.; Geelen, D. The Impact of Environmental Stress on Male Reproductive Development in Plants: Biological Processes and Molecular Mechanisms. *Plant. Cell Environ.* **2014**, *37*, 1–18. [CrossRef]
150. Fuchs, L.K.; Jenkins, G.; Phillips, D.W. Anthropogenic Impacts on Meiosis in Plants. *Front. Plant Sci.* **2018**, *9*, 1429. [CrossRef]
151. Mable, B.K. 'Why Polyploidy Is Rarer in Animals than in Plants': Myths and Mechanisms. *Biol. J. Linn. Soc.* **2004**, *82*, 453–466. [CrossRef]
152. Vanneste, K.; Baele, G.; Maere, S.; Van De Peer, Y. Analysis of 41 Plant Genomes Supports a Wave of Successful Genome Duplications in Association with the Cretaceous-Paleogene Boundary. *Genome Res.* **2014**, *24*, 1334–1347. [CrossRef] [PubMed]
153. Mason, A.S.; Pires, J.C. Unreduced Gametes: Meiotic Mishap or Evolutionary Mechanism? *Trends Genet.* **2015**, *31*, 5–10. [CrossRef] [PubMed]
154. Loginova, D.B.; Silkova, O.G. Mechanisms of Unreduced Gamete Formation in Flowering Plants. *Russ. J. Genet.* **2017**, *53*, 741–756. [CrossRef]
155. De Storme, N.; Geelen, D. Pre-Meiotic Endomitosis in the Cytokinesis-Defective Tomato Mutant *pmcd1* Generates Tetraploid Meiocytes and Diploid Gametes. *J. Exp. Bot.* **2013**, *64*, 2345–2358. [CrossRef] [PubMed]
156. Falistocco, E.; Tosti, N.; Falcinelli, M. Cytomixis in Pollen Mother Cells of Diploid *Dactylis*, One of the Origins of 2n Gametes. *J. Hered.* **1995**, *86*, 448–453. [CrossRef]
157. Spielman, M.; Preuss, D.; Li, F.L.; Browne, W.E.; Scott, R.J.; Dickinson, H.G. Tetraspore is Required for Male Meiotic Cytokinesis in *Arabidopsis thaliana*. *Development* **1997**, *124*, 2645–2657. [CrossRef] [PubMed]
158. De Haan, A.; Maceira, N.O.; Lumaret, R.; Delay, J. Production of 2n Gametes in Diploid Subspecies of *Dactylis glomerata* L. 2. Occurrence and Frequency of 2n Eggs. *Ann. Bot.* **1992**, *69*, 345–350. [CrossRef]
159. Maceira, N.O.; De Haan, A.A.; Aret, R.L.; Billon, M.; Delay, J. Production of 2n Gametes in Diploid Subspecies of *Dactylis glomerata* L. 1. Occurrence and Frequency of 2n Pollen. *Ann. Bot.* **1992**, *69*, 335–343. [CrossRef]
160. Bretagnolle, F. Pollen Production and Spontaneous Polyploidization in Diploid Populations of *Anthoxanthum alpinum*. *Biol. J. Linn. Soc.* **2001**, *72*, 241–247. [CrossRef]
161. Ramsey, J. Unreduced Gametes and Neopolyploids in Natural Populations of *Achillea borealis* (Asteraceae). *Heredity* **2006**, *98*, 143–150. [CrossRef]
162. Sheidai, M.; Jafari, S.; Taleban, P.; Keshavarzi, M. Cytomixis and Unreduced Pollen Grain Formation in *Alopecurus* L. and *Catbrosa Beauv*. (Poaceae). *Cytologia* **2009**, *74*, 31–41. [CrossRef]
163. Kovalsky, I.E.; Solís Neffa, V.G. Evidence of 2n Microspore Production in a Natural Diploid Population of *Turnera sidoides* Subsp. Carnea and Its Relevance in the Evolution of the *T. sidoides* (Turneraceae) Autopolyploid Complex. *J. Plant Res.* **2012**, *125*, 725–734. [CrossRef] [PubMed]
164. Kreiner, J.M.; Kron, P.; Husband, B.C. Frequency and Maintenance of Unreduced Gametes in Natural Plant Populations: Associations with Reproductive Mode, Life History and Genome Size. *New Phytol.* **2017**, *214*, 879–889. [CrossRef]
165. Comai, L. The Advantages and Disadvantages of Being Polyploid. *Nat. Rev. Genet.* **2005**, *6*, 836–846. [CrossRef] [PubMed]
166. Zielinski, M.L.; Mittelsten Scheid, O. Meiosis in Polyploid Plants. *Polyploidy Genome Evol.* **2012**, 33–55. [CrossRef]
167. Doyle, J.J.; Egan, A.N. Dating the Origins of Polyploidy Events. *New Phytol.* **2010**, *186*, 73–85. [CrossRef] [PubMed]
168. Boden, S.A.; Shadiac, N.; Tucker, E.J.; Langridge, P.; Able, J.A. Expression and Functional Analysis of TaASY1 during Meiosis of Bread Wheat (*Triticum aestivum*). *BMC Mol. Biol.* **2007**, *8*, 65. [CrossRef]
169. Boden, S.A.; Langridge, P.; Spangenberg, G.; Able, J.A. TaASY1 Promotes Homologous Chromosome Interactions and Is Affected by Deletion of Ph1. *Plant J.* **2009**, *57*, 487–497. [CrossRef] [PubMed]
170. De Bustos, A.; Pérez, R.; Jouve, N. Characterization of the Gene Mre11 and Evidence of Silencing after Polyploidization in *Triticum*. *Theor. Appl. Genet.* **2007**, *114*, 985–999. [CrossRef]
171. Sutton, T.; Whitford, R.; Baumann, U.; Dong, C.; Able, J.A.; Langridge, P. The Ph2 Pairing Homoeologous Locus of Wheat (*Triticum aestivum*): Identification of Candidate Meiotic Genes Using a Comparative Genetics Approach. *Plant J.* **2003**, *36*, 443–456. [CrossRef]
172. Griffiths, S.; Sharp, R.; Foote, T.N.; Bertin, I.; Wanous, M.; Reader, S.; Colas, I.; Moore, G. Molecular Characterization of Ph1 as a Major Chromosome Pairing Locus in Polyploid Wheat. *Nature* **2006**, *439*, 749–752. [CrossRef] [PubMed]
173. Sears, E.R. Nullisomic-Tetrasomic Combinations in Hexaploid Wheat. *Chromosom. Manip. Plant Genet.* **1966**, 29–45. [CrossRef]
174. Feldman, M.; Levy, A.A. Genome Evolution Due to Allopolyploidization in Wheat. *Genetics* **2012**, *192*, 763–774. [CrossRef] [PubMed]
175. Riley, R.; Chapman, V. Genetic Control of the Cytologically Diploid Behaviour of Hexaploid Wheat. *Nature* **1958**, *182*, 713–715. [CrossRef]
176. Driscoll, C.J. Genetic suppression of homoeologous chromosome pairing in hexaploid wheat. *Can. J. Genet. Cytol.* **1972**, *14*, 39–42. [CrossRef]
177. Martinez-Perez, E.; Shaw, P.; Moore, G. The Ph1 Locus Is Needed to Ensure Specific Somatic and Meiotic Centromere Association. *Nature* **2001**, *411*, 204–207. [CrossRef]
178. Sears, E.R. Genetic Control of Chromosome Pairing in Wheat. *Annu. Rev. Genet.* **1976**, *10*, 31–51. [CrossRef]

179. Mello-Sampayo, T. Genetic Regulation of Meiotic Chromosome Pairing by Chromosome 3D of *Triticum aestivum*. *Nat. New Biol.* **1971**, *230*, 22–23. [CrossRef]
180. Prieto, P.; Moore, G.; Reader, S. Control of Conformation Changes Associated with Homologue Recognition during Meiosis. *Theor. Appl. Genet.* **2005**, *111*, 505–510. [CrossRef] [PubMed]
181. Sears, E.R. Induced Mutant with Homoeologous Pairing in Common Wheat. *Can. J. Genet. Cytol.* **1977**, *19*, 585–593. [CrossRef]
182. Okamoto, M. Asynaptic Effect of Chromosome V. *Wheat Inf. Serv.* **1957**, *5*, 6.
183. Sears, R.E. Intergenomic Chromosome Relationships in Hexaploid Wheat. *Proc. Int. Congr. Genet.* **1958**, *2*, 258–259.
184. Richards, D.M.; Greer, E.; Martin, A.C.; Moore, G.; Shaw, P.J.; Howard, M. Quantitative Dynamics of Telomere Bouquet Formation. *PLoS Comput. Biol.* **2012**, *8*, e1002812. [CrossRef]
185. Moore, G. The Control of Recombination in Wheat by *Ph1* and Its Use in Breeding. *Methods Mol. Biol.* **2014**, *1145*, 143–153. [CrossRef]
186. Rey, M.D.; Martín, A.C.; Higgins, J.; Swarbreck, D.; Uauy, C.; Shaw, P.; Moore, G. Exploiting the *ZIP4* Homologue within the Wheat *Ph1* Locus Has Identified Two Lines Exhibiting Homoeologous Crossover in Wheat-Wild Relative Hybrids. *Mol. Breed.* **2017**, *37*, 1–11. [CrossRef]
187. Calderón, M.C.; Rey, M.D.; Martín, A.; Prieto, P. Homoeologous Chromosomes From Two *Hordeum* Species Can Recognize and Associate During Meiosis in Wheat in the Presence of the *Ph1* Locus. *Front. Plant Sci.* **2018**, *9*, 585. [CrossRef]
188. Calderón, M.C.; Prieto, P. Wild and Cultivated Homoeologous Barley Chromosomes Can Associate and Recombine in Wheat in the Absence of the *Ph1* Locus. *Agron* **2021**, *11*, 147. [CrossRef]
189. Martín, A.C.; Rey, M.D.; Shaw, P.; Moore, G. Dual Effect of the Wheat *Ph1* Locus on Chromosome Synapsis and Crossover. *Chromosoma* **2017**, *126*, 669–680. [CrossRef] [PubMed]
190. Martín, A.C.; Alabdullah, A.K.; Moore, G. A Separation-of-Function *ZIP4* Wheat Mutant Allows Crossover between Related Chromosomes and Is Meiotically Stable. *Sci. Rep.* **2021**, *11*, 21811. [CrossRef]
191. Chelysheva, L.; Gendrot, G.; Vezon, D.; Doutriaux, M.P.; Mercier, R.; Grelon, M. Zip4/Spo22 Is Required for Class I CO Formation but Not for Synapsis Completion in *Arabidopsis thaliana*. *PLoS Genet.* **2007**, *3*, e83. [CrossRef] [PubMed]
192. Shen, Y.; Tang, D.; Wang, K.; Wang, M.; Huang, J.; Luo, W.; Luo, Q.; Hong, L.; Li, M.; Cheng, Z. ZIP4 in Homologous Chromosome Synapsis and Crossover Formation in Rice Meiosis. *J. Cell Sci.* **2012**, *125*, 2581–2591. [CrossRef]
193. Tsubouchi, T.; Zhao, H.; Roeder, G.S. The Meiosis-Specific zip4 Protein Regulates Crossover Distribution by Promoting Synaptonemal Complex Formation Together with zip2. *Dev. Cell* **2006**, *10*, 809–819. [CrossRef]
194. Dubois, E.; De Muyt, A.; Soyer, J.L.; Budin, K.; Legras, M.; Piolot, T.; Debuchy, R.; Kleckner, N.; Zickler, D.; Espagne, E. Building Bridges to Move Recombination Complexes. *Proc. Natl. Acad. Sci. USA* **2019**, *116*, 12400–12409. [CrossRef]
195. Perry, J.; Kleckner, N.; Börner, G.V. Bioinformatic analyses implicate the collaborating meiotic crossover/chiasma proteins Zip2, Zip3, and Spo22/Zip4 in ubiquitin labeling. *Proc. Natl. Acad. Sci. USA* **2005**, *102*, 17594–17599. [CrossRef]
196. Rey, M.D.; Martín, A.C.; Smedley, M.; Hayta, S.; Harwood, W.; Shaw, P.; Moore, G. Magnesium Increases Homoeologous Crossover Frequency During Meiosis in *ZIP4* (*Ph1* Gene) Mutant Wheat-Wild Relative Hybrids. *Front. Plant Sci.* **2018**, *9*, 509. [CrossRef]
197. Ramírez-González, R.H.; Borrill, P.; Lang, D.; Harrington, S.A.; Brinton, J.; Venturini, L.; Davey, M.; Jacobs, J.; Van Ex, F.; Pasha, A.; et al. The Transcriptional Landscape of Polyploid Wheat. *Science* **2018**, *361*, eaar6089. [CrossRef]
198. Alabdullah, A.K.; Borrill, P.; Martin, A.C.; Ramirez-Gonzalez, R.H.; Hassani-Pak, K.; Uauy, C.; Shaw, P.; Moore, G. A Co-Expression Network in Hexaploid Wheat Reveals Mostly Balanced Expression and Lack of Significant Gene Loss of Homeologous Meiotic Genes Upon Polyploidization. *Front. Plant Sci.* **2019**, *10*, 1–24. [CrossRef] [PubMed]
199. Cuñado, N.; Blazquez, S.; Melchor, L.; Pradillo, M.; Santos, J.L. Understanding the Cytological Diploidization Mechanism of Polyploid Wild Wheats. *Cytogenet. Genome Res.* **2005**, *109*, 205–209. [CrossRef] [PubMed]
200. Jones, M.; Rees, H.; Jenkins, G. Synaptonemal Complex Formation in *Avena* Polyploids. *Heredity* **1989**, *63*, 209–219. [CrossRef]
201. Thomas, H.M.; Thomas, B.J. Synaptonemal Complex Formation in Two Allohexaploid *Festuca* Species and a Pentaploid Hybrid. *Heredity* **1993**, *71*, 305–311. [CrossRef]
202. Martinez, M.; Naranjo, T.; Cuadrado, C.; Romero, C. The Synaptic Behaviour of the Wild Forms of *Triticum turgidum* and *T. timopheevii*. *Genome* **2001**, *44*, 517–522. [CrossRef]
203. Martinez, M.; Naranjo, T.; Cuadrado, C.; Romero, C. Synaptic Behaviour of the Tetraploid Wheat *Triticum timopheevii*. *Theor. Appl. Genet.* **1996**, *93*, 1139–1144. [CrossRef]
204. Poggio, L.; González, G.E. Cytological Diploidization of Paleopolyploid Genus *Zea*: Divergence between Homoeologous Chromosomes or Activity of Pairing Regulator Genes? *PLoS ONE* **2018**, *13*, e0189644. [CrossRef]
205. Jena, K.K. The Species of the Genus *Oryza* and Transfer of Useful Genes from Wild Species into Cultivated Rice, *O. Sativa*. *Breed. Sci.* **2010**, *60*, 518–523. [CrossRef]
206. Ge, S.; Sang, T.; Lu, B.R.; Hong, D.Y. Phylogeny of Rice Genomes with Emphasis on Origins of Allotetraploid Species. *Proc. Natl. Acad. Sci. USA* **1999**, *96*, 14400–14405. [CrossRef] [PubMed]
207. Dally, A.M.; Second, G. Chloroplast DNA Diversity in Wild and Cultivated Species of Rice (Genus *Oryza*, Section *Oryza*). Cladistic-Mutation and Genetic-Distance Analysis. *Theor. Appl. Genet.* **1990**, *80*, 209–222. [CrossRef]
208. Kanno, A.; Hirai, A. Comparative Studies of the Structure of Chloroplast DNA from Four Species of *Oryza*: Cloning and Physical Maps. *Theor. Appl. Genet.* **1992**, *83*, 791–798. [CrossRef]

209. Wang, Z.Y.; Second, G.; Tanksley, S.D. Polymorphism and Phylogenetic Relationships among Species in the Genus *Oryza* as Determined by Analysis of Nuclear RFLPs. *Theor. Appl. Genet.* **1992**, *83*, 565–581. [CrossRef] [PubMed]
210. Aggarwal, R.K.; Brar, D.S.; Nandi, S.; Huang, N.; Khush, G.S. Phylogenetic Relationships among *Oryza* Species Revealed by AFLP Markers. *Theor. Appl. Genet.* **1999**, *98*, 1320–1328. [CrossRef]
211. Bao, Y.; Ge, S. Origin and Phylogeny of *Oryza* Species with the CD Genome Based on Multiple-Gene Sequence Data. *Plant Syst. Evol.* **2004**, *249*, 55–66. [CrossRef]
212. Jena, K.K.; Kochert, G. Restriction Fragment Length Polymorphism Analysis of CCDD Genome Species of the Genus *Oryza* L. *Plant Mol. Biol.* **1991**, *16*, 831–839. [CrossRef] [PubMed]
213. Zou, X.; Du, Y.; Wang, X.; Wang, Q.; Zhang, B.; Chen, J.; Chen, M.; Doyle, J.J.; Ge, S. Genome Evolution in *Oryza* Allopolyploids of Various Ages: Insights into the Process of Diploidization. *Plant J.* **2021**, *105*, 721–735. [CrossRef] [PubMed]
214. Jenczewski, E.; Eber, F.; Grimaud, A.; Huet, S.; Lucas, M.O.; Monod, H.; Chèvre, A.M. PrBn, a Major Gene Controlling Homeologous Pairing in Oilseed Rape (*Brassica Napus*) Haploids. *Genetics* **2003**, *164*, 645–653. [CrossRef] [PubMed]
215. Cifuentes, M.; Grandont, L.; Moore, G.; Chèvre, A.M.; Jenczewski, E. Genetic Regulation of Meiosis in Polyploid Species: New Insights into an Old Question. *New Phytol.* **2010**, *186*, 29–36. [CrossRef]
216. Jenczewski, E.; Alix, K. From Diploids to Allopolyploids: The Emergence of Efficient Pairing Control Genes in Plants. *CRC Crit. Rev. Plant Sci.* **2004**, *23*, 21–45. [CrossRef]
217. Nicolas, S.D.; Leflon, M.; Monod, H.; Eber, F.; Coriton, O.; Huteau, V.; Chèvre, A.M.; Jenczewski, E. Genetic Regulation of Meiotic Cross-Overs between Related Genomes in *Brassica napus* Haploids and Hybrids. *Plant Cell* **2009**, *21*, 373–385. [CrossRef]
218. Liu, Z.; Adamczyk, K.; Manzanares-Dauleux, M.; Eber, F.; Lucas, M.O.; Delourme, R.; Chèvre, A.M.; Jenczewski, E. Mapping *PrBn* and Other Quantitative Trait Loci Responsible for the Control of Homeologous Chromosome Pairing in Oilseed Rape (*Brassica napus* L.) Haploids. *Genetics* **2006**, *174*, 1583–1596. [CrossRef]
219. Aklilu, B.B.; Soderquist, R.S.; Culligan, K.M. Genetic Analysis of the Replication Protein A Large Subunit Family in *Arabidopsis* Reveals Unique and Overlapping Roles in DNA Repair, Meiosis and DNA Replication. *Nucleic Acids Res.* **2014**, *42*, 3104–3118. [CrossRef]
220. Berchowitz, L.E.; Francis, K.E.; Bey, A.L.; Copenhaver, G.P. The Role of *AtMUS81* in Interference-Insensitive Crossovers in *A. thaliana*. *PLoS Genet.* **2007**, *3*, 1355–1364. [CrossRef] [PubMed]
221. Blary, A. Towards a Functional Characterization of Meiotic Recombination in Rapeseed: Analysis of the Meiotic Transcriptome and Hyper-Recombinant Mutants. Ph.D. Thesis, Université Paris-Saclay, Saint-Aubin, France, 2016.
222. Sheidai, M.; Noormohamadi, Z.; Sotodeh, M. Cytogenetic Variability In Several Canola (*Brassica napus*) Cultivare. *Caryologia* **2014**, *59*, 267–276. [CrossRef]
223. Mason, A.S.; Batley, J. Creating New Interspecific Hybrid and Polyploid Crops. *Trends Biotechnol.* **2015**, *33*, 436–441. [CrossRef]
224. Szadkowski, E.; Eber, F.; Huteau, V.; Lodé, M.; Huneau, C.; Belcram, H.; Coriton, O.; Manzanares-Dauleux, M.J.; Delourme, R.; King, G.J.; et al. The First Meiosis of Resynthesized *Brassica napus*, a Genome Blender. *New Phytol.* **2010**, *186*, 102–112. [CrossRef]
225. Higgins, E.E.; Howell, E.C.; Armstrong, S.J.; Parkin, I.A.P. A Major Quantitative Trait Locus on Chromosome A9, *BnaPh1*, Controls Homoeologous Recombination in *Brassica napus*. *New Phytol.* **2021**, *229*, 3281–3293. [CrossRef]
226. Culligan, K.M.; Hays, J.B. *Arabidopsis* MutS Homologs-AtMSH2, AtMSH3, AtMSH6, and a Novel AtMSH7-Form Three Distinct Protein Heterodimers with Different Specificities for Mismatched DNA. *Plant Cell* **2000**, *12*, 991–1002. [CrossRef]
227. Lloyd, A.; Bomblies, K. Meiosis in Autopolyploid and Allopolyploid *Arabidopsis*. *Curr. Opin. Plant Biol.* **2016**, *30*, 116–122. [CrossRef] [PubMed]
228. Comai, L.; Tyagi, A.P.; Lysak, M.A. FISH Analysis of Meiosis in *Arabidopsis* Allopolyploids. *Chromosom. Res.* **2003**, *11*, 217–226. [CrossRef]
229. Henry, I.M.; Dilkes, B.P.; Tyagi, A.; Gao, J.; Christensen, B.; Comaia, L. The Boy Named sue Quantitative Trait Locus Confers Increased Meiotic Stability to an Adapted Natural Allopolyploid of *Arabidopsis*. *Plant Cell* **2014**, *26*, 181–194. [CrossRef] [PubMed]
230. Pontes, O.; Neves, N.; Silva, M.; Lewis, M.S.; Madlung, A.; Comai, L.; Viegas, W.; Pikaard, C.S. Chromosomal Locus Rearrangements Are a Rapid Response to Formation of the Allotetraploid *Arabidopsis suecica* Genome. *Proc. Natl. Acad. Sci. USA* **2004**, *101*, 18240–18245. [CrossRef] [PubMed]
231. Burns, R.; Mandáková, T.; Gunis, J.; Soto-Jiménez, L.M.; Liu, C.; Lysak, M.A.; Novikova, P.Y.; Nordborg, M. Gradual Evolution of Allopolyploidy in *Arabidopsis suecica*. *Nat. Ecol. Evol.* **2021**, *5*, 1367–1381. [CrossRef] [PubMed]
232. Yant, L.; Hollister, J.D.; Wright, K.M.; Arnold, B.J.; Higgins, J.D.; Franklin, F.C.H.; Bomblies, K. Meiotic Adaptation to Genome Duplication in *Arabidopsis arenosa*. *Curr. Biol.* **2013**, *23*, 2151–2156. [CrossRef] [PubMed]
233. Higgins, J.D.; Wright, K.M.; Bomblies, K.; Franklin, F.C.H. Cytological Techniques to Analyze Meiosis in *Arabidopsis arenosa* for Investigating Adaptation to Polyploidy. *Front. Plant Sci.* **2014**, *4*, 546. [CrossRef]
234. Bomblies, K.; Jones, G.; Franklin, C.; Zickler, D.; Kleckner, N. The Challenge of Evolving Stable Polyploidy: Could an Increase in "Crossover Interference Distance" Play a Central Role? *Chromosoma* **2016**, *125*, 287–300. [CrossRef]
235. Morgan, C.; White, M.A.; Franklin, F.C.H.; Zickler, D.; Kleckner, N.; Bomblies, K. Evolution of Crossover Interference Enables Stable Autopolyploidy by Ensuring Pairwise Partner Connections in *Arabidopsis arenosa*. *Curr. Biol.* **2021**, *31*, 4713–4726.e4. [CrossRef]
236. Davies, A.; Jenkins, G.; Rees, H. Diploidisation of *Lotus corniculatus* L. (Fabaceae) by Elimination of Multivalents. *Chromosoma* **1990**, *99*, 289–295. [CrossRef]

237. Wallace, A.J.; Callow, R.S. Meiotic Variation in an Intergenomic Autopolyploid Series. I. Chiasma Frequency. *Genome* **1995**, *38*, 122–132. [CrossRef]
238. Wentworth, J.E.; Gornall, R.J. Cytogenetic Evidence for Autopolyploidy in *Parnassia palustris*. *New Phytol.* **1996**, *134*, 641–648. [CrossRef]
239. Hollister, J.D.; Arnold, B.J.; Svedin, E.; Xue, K.S.; Dilkes, B.P.; Bomblies, K. Genetic Adaptation Associated with Genome-Doubling in Autotetraploid *Arabidopsis arenosa*. *PLoS Genet.* **2012**, *8*, e1003093. [CrossRef] [PubMed]
240. Wright, K.M.; Arnold, B.; Xue, K.; Surinova, M.; O'Connell, J.; Bomblies, K. Selection on Meiosis Genes in Diploid and Tetraploid *Arabidopsis arenosa*. *Mol. Biol. Evol.* **2015**, *32*, 944–955. [CrossRef] [PubMed]
241. Morgan, C.; Zhang, H.; Henry, C.E.; Franklin, C.F.H.; Bomblies, K. Derived Alleles of Two Axis Proteins Affect Meiotic Traits in Autotetraploid *Arabidopsis arenosa*. *Proc. Natl. Acad. Sci. USA* **2020**, *117*, 8980–8988. [CrossRef] [PubMed]
242. Seear, P.J.; France, M.G.; Gregory, C.L.; Heavens, D.; Schmickl, R.; Yant, L.; Higgins, J.D. A Novel Allele of ASY3 Is Associated with Greater Meiotic Stability in Autotetraploid *Arabidopsis lyrata*. *PLoS Genet.* **2020**, *16*, e1008900. [CrossRef] [PubMed]
243. Henry, I.M.; Dilkes, B.P.; Young, K.; Watson, B.; Wu, H.; Comai, L. Aneuploidy and Genetic Variation in the *Arabidopsis thaliana* Triploid Response. *Genetics* **2005**, *170*, 1979–1988. [CrossRef]
244. Chao, D.Y.; Dilkes, B.; Luo, H.; Douglas, A.; Yakubova, E.; Lahner, B.; Salt, D.E. Polyploids Exhibit Higher Potassium Uptake and Salinity Tolerance in *Arabidopsis*. *Science* **2013**, *341*, 658–659. [CrossRef]
245. Weiss, H.; Maluszynska, J. Chromosomal Rearrangement in Autotetraploid Plants of *Arabidopsis thaliana*. *Hereditas* **2000**, *133*, 255–261. [CrossRef]
246. Santos, J.L.; Alfaro, D.; Sanchez-Moran, E.; Armstrong, S.J.; Franklin, F.C.H.; Jones, G.H. Partial Diploidization of Meiosis in Autotetraploid *Arabidopsis thaliana*. *Genetics* **2003**, *165*, 1533–1540. [CrossRef]
247. Yu, Z.; Haage, K.; Streit, V.E.; Gierl, A.; Torres Ruiz, R.A. A Large Number of Tetraploid *Arabidopsis thaliana* Lines, Generated by a Rapid Strategy, Reveal High Stability of Neo-Tetraploids during Consecutive Generations. *Theor. Appl. Genet.* **2009**, *118*, 1107–1119. [CrossRef] [PubMed]
248. Parra-Nunez, P.; Pradillo, M.; Santos, J.L. Competition for Chiasma Formation between Identical and Homologous (But Not Identical) Chromosomes in Synthetic Autotetraploids of *Arabidopsis thaliana*. *Front. Plant Sci.* **2019**, *9*, 1924. [CrossRef] [PubMed]
249. Felcher, K.J.; Coombs, J.J.; Massa, A.N.; Hansey, C.N.; Hamilton, J.P.; Veilleux, R.E.; Buell, C.R.; Douches, D.S. Integration of Two Diploid Potato Linkage Maps with the Potato Genome Sequence. *PLoS ONE* **2012**, *7*, e36347. [CrossRef]
250. Bourke, P.M.; Voorrips, R.E.; Visser, R.G.F.; Maliepaard, C. The Double-Reduction Landscape in Tetraploid Potato as Revealed by a High-Density Linkage Map. *Genetics* **2015**, *201*, 853–863. [CrossRef] [PubMed]
251. Dong, F.; Song, J.; Naess, S.K.; Helgeson, J.P.; Gebhardt, C.; Jiang, J. Development and Applications of a Set of Chromosome-Specific Cytogenetic DNA Markers in Potato. *Theor. Appl. Genet.* **2000**, *101*, 1001–1007. [CrossRef]
252. Tang, X.; De Boer, J.M.; Van Eck, H.J.; Bachem, C.; Visser, R.G.F.; De Jong, H. Assignment of Genetic Linkage Maps to Diploid *Solanum tuberosum* Pachytene Chromosomes by BAC-FISH Technology. *Chromosom. Res.* **2009**, *17*, 899–915. [CrossRef]
253. He, L.; Braz, G.T.; Torres, G.A.; Jiang, J. Chromosome Painting in Meiosis Reveals Pairing of Specific Chromosomes in Polyploid *Solanum* Species. *Chromosoma* **2018**, *127*, 505–513. [CrossRef] [PubMed]
254. Naranjo, T.; Corredor, E. Clustering of Centromeres Precedes Bivalent Chromosome Pairing of Polyploid Wheats. *Trends Plant Sci.* **2004**, *9*, 214–217. [CrossRef] [PubMed]
255. Choudhary, A.; Wright, L.; Ponce, O.; Chen, J.; Prashar, A.; Sanchez-Moran, E.; Luo, Z.; Compton, L. Varietal Variation and Chromosome Behaviour during Meiosis in *Solanum tuberosum*. *Heredity* **2020**, *125*, 212–226. [CrossRef] [PubMed]
256. Marand, A.P.; Jansky, S.H.; Zhao, H.; Leisner, C.P.; Zhu, X.; Zeng, Z.; Crisovan, E.; Newton, L.; Hamernik, A.J.; Veilleux, R.E.; et al. Meiotic Crossovers Are Associated with Open Chromatin and Enriched with Stowaway Transposons in Potato. *Genome Biol.* **2017**, *18*, 203. [CrossRef] [PubMed]
257. Kenan-Eichler, M.; Leshkowitz, D.; Tal, L.; Noor, E.; Melamed-Bessudo, C.; Feldman, M.; Levy, A.A. Wheat Hybridization and Polyploidization Results in Deregulation of Small RNAs. *Genetics* **2011**, *188*, 263–272. [CrossRef] [PubMed]
258. Li, Q.; Rana, K.; Xiong, Z.; Ge, X.; Li, Z.; Song, H.; Qian, W. Genetic and Epigenetic Alterations in Hybrid and Derived Hexaploids between *Brassica napus* and *B. oleracea* Revealed by SSR and MSAP Analysis. *Acta Physiol. Plant.* **2019**, *41*, 1–9. [CrossRef]
259. Song, Q.; Chen, J.Z. Epigenetic and Developmental Regulation in Plant Polyploids. *Curr. Opin. Plant Biol.* **2015**, *24*, 101–109. [CrossRef]
260. Nieto Feliner, G.; Casacuberta, J.; Wendel, J.F. Genomics of Evolutionary Novelty in Hybrids and Polyploids. *Front. Genet.* **2020**, *11*, 1–21. [CrossRef]
261. Wang, X.; Morton, J.A.; Pellicer, J.; Leitch, I.J.; Leitch, A.R. Genome Downsizing after Polyploidy: Mechanisms, Rates and Selection Pressures. *Plant J.* **2021**, *107*, 1003–1015. [CrossRef]
262. Zhao, N.; Dong, Q.; Nadon, B.D.; Ding, X.; Wang, X.; Dong, Y.; Liu, B.; Jackson, S.A.; Xu, C. Evolution of Homeologous Gene Expression in Polyploid Wheat. *Genes* **2020**, *11*, 1401. [CrossRef]
263. Xu, C.; Nadon, B.D.; Do Kim, K.; Jackson, S.A. Genetic and Epigenetic Divergence of Duplicate Genes in Two Legume Species. *Plant Cell Environ.* **2018**, *41*, 2033–2044. [CrossRef]
264. Eilam, T.; Anikster, Y.; Millet, E.; Manisterski, J.; Feldman, M. Genome Size in Diploids, Allopolyploids, and Autopolyploids of Mediterranean *Triticeae*. *J. Bot.* **2010**, *2010*, 1–12. [CrossRef]

265. Brenchley, R.; Spannagl, M.; Pfeifer, M.; Barker, G.L.A.; D'Amore, R.; Allen, A.M.; McKenzie, N.; Kramer, M.; Kerhornou, A.; Bolser, D.; et al. Analysis of the Bread Wheat Genome Using Whole-Genome Shotgun Sequencing. *Nature* **2012**, *491*, 705–710. [CrossRef] [PubMed]
266. Liu, B.; Vega, J.M.; Feldman, M. Rapid Genomic Changes in Newly Synthesized Amphiploids of *Triticum* and *Aegilops*. II. Changes in Low-Copy Coding DNA Sequences. *Genome* **1998**, *41*, 535–542. [CrossRef]
267. Benyahya, F.; Nadaud, I.; Da Ines, O.; Rimbert, H.; White, C.; Sourdille, P. SPO11.2 Is Essential for Programmed Double-Strand Break Formation during Meiosis in Bread Wheat (*Triticum aestivum* L.). *Plant J.* **2020**, *104*, 30–43. [CrossRef] [PubMed]
268. Rensing, S.A. Gene Duplication as a Driver of Plant Morphogenetic Evolution. *Curr. Opin. Plant Biol.* **2014**, *17*, 43–48. [CrossRef] [PubMed]
269. Vicient, C.M.; Casacuberta, J.M. Impact of Transposable Elements on Polyploid Plant Genomes. *Ann. Bot.* **2017**, *120*, 195–207. [CrossRef]
270. Glombik, M.; Bačovský, V.; Hobza, R.; Kopecký, D. Competition of Parental Genomes in Plant Hybrids. *Front. Plant Sci.* **2020**, *11*. [CrossRef]
271. Takahagi, K.; Inoue, K.; Mochida, K. Gene Co-Expression Network Analysis Suggests the Existence of Transcriptional Modules Containing a High Proportion of Transcriptionally Differentiated Homoeologs in Hexaploid Wheat. *Front. Plant Sci.* **2018**, *9*, 1–10. [CrossRef]
272. Liu, S.L.; Adams, K.L. Dramatic Change in Function and Expression Pattern of a Gene Duplicated by Polyploidy Created a Paternal Effect Gene in the *Brassicaceae*. *Mol. Biol. Evol.* **2010**, *27*, 2817–2828. [CrossRef]
273. Mason, A.S.; Wendel, J.F. Homoeologous Exchanges, Segmental Allopolyploidy, and Polyploid Genome Evolution. *Front. Genet.* **2020**, *11*, 1014. [CrossRef] [PubMed]
274. Jarvis, D.E.; Ho, Y.S.; Lightfoot, D.J.; Schmöckel, S.M.; Li, B.; Borm, T.J.A.; Ohyanagi, H.; Mineta, K.; Michell, C.T.; Saber, N.; et al. The Genome of *Chenopodium quinoa*. *Nature* **2017**, *542*, 307–312. [CrossRef] [PubMed]
275. Chen, S.; Ren, F.; Zhang, L.; Liu, Y.; Chen, X.; Li, Y.; Zhang, L.; Zhu, B.; Zeng, P.; Li, Z.; et al. Unstable Allotetraploid Tobacco Genome Due to Frequent Homeologous Recombination, Segmental Deletion, and Chromosome Loss. *Mol. Plant* **2018**, *11*, 914–927. [CrossRef] [PubMed]
276. Hurgobin, B.; Golicz, A.A.; Bayer, P.E.; Chan, C.K.K.; Tirnaz, S.; Dolatabadian, A.; Schiessl, S.V.; Samans, B.; Montenegro, J.D.; Parkin, I.A.P.; et al. Homoeologous Exchange Is a Major Cause of Gene Presence/Absence Variation in the Amphidiploid *Brassica napus*. *Plant Biotechnol. J.* **2018**, *16*, 1265–1274. [CrossRef]
277. Samans, B.; Snowdon, R.; Mason, A.S. Homoeologous Exchanges and Gene Losses Generate Diversity and Differentiate the *B. napus* Genome from That of Its Ancestors. In *Brassica Napus Genome*; Liu, S., Snowdon, R., Chalhoub, B., Eds.; Springer: Cham, Switzerland, 2018; pp. 131–148. [CrossRef]
278. Bertioli, D.J.; Jenkins, J.; Clevenger, J.; Dudchenko, O.; Gao, D.; Seijo, G.; Leal-Bertioli, S.C.M.; Ren, L.; Farmer, A.D.; Pandey, M.K.; et al. The Genome Sequence of Segmental Allotetraploid Peanut *Arachis hypogaea*. *Nat. Genet.* **2019**, *51*, 877–884. [CrossRef]
279. Zhuang, W.; Chen, H.; Yang, M.; Wang, J.; Pandey, M.K.; Zhang, C.; Chang, W.C.; Zhang, L.; Zhang, X.; Tang, R.; et al. The Genome of Cultivated Peanut Provides Insight into Legume Karyotypes, Polyploid Evolution and Crop Domestication. *Nat. Genet.* **2019**, *51*, 865–876. [CrossRef]
280. Sun, Y.; Wu, Y.; Yang, C.; Sun, S.; Lin, X.; Liu, L.; Xu, C.; Wendel, J.F.; Gong, L.; Liu, B. Segmental Allotetraploidy Generates Extensive Homoeologous Expression Rewiring and Phenotypic Diversity at the Population Level in Rice. *Mol. Ecol.* **2017**, *26*, 5451–5466. [CrossRef]
281. Li, N.; Xu, C.; Zhang, A.; Lv, R.; Meng, X.; Lin, X.; Gong, L.; Wendel, J.F.; Liu, B. DNA Methylation Repatterning Accompanying Hybridization, Whole Genome Doubling and Homoeolog Exchange in Nascent Segmental Rice Allotetraploids. *New Phytol.* **2019**, *223*, 979–992. [CrossRef]
282. Woodhouse, M.R.; Cheng, F.; Pires, J.C.; Lisch, D.; Freeling, M.; Wang, X. Erratum: Origin, Inheritance, and Gene Regulatory Consequences of Genome Dominance in Polyploids. *Proc. Natl. Acad. Sci. USA* **2014**, *111*, 6527. [CrossRef] [PubMed]
283. He, L.Q.; Tang, R.H.; Jiang, J.; Xiong, F.Q.; Huang, Z.P.; Wu, H.N.; Gao, Z.K.; Zhong, R.C.; He, X.H.; Han, Z.Q. Rapid Gene Expression Change in a Novel Synthesized Allopolyploid Population of Cultivated Peanut×*Arachis doigoi* Cross by CDNA-SCoT and HFO-TAG Technique. *J. Integr. Agric.* **2017**, *16*, 1093–1102. [CrossRef]
284. Zhu, W.; Hu, B.; Becker, C.; Doğan, E.S.; Berendzen, K.W.; Weigel, D.; Liu, C. Altered Chromatin Compaction and Histone Methylation Drive Non-Additive Gene Expression in an Interspecific *Arabidopsis* Hybrid. *Genome Biol.* **2017**, *18*, 1–16. [CrossRef]
285. Combes, M.C.; Hueber, Y.; Dereeper, A.; Rialle, S.; Herrera, J.C.; Lashermes, P. Regulatory Divergence between Parental Alleles Determines Gene Expression Patterns in Hybrids. *Genome Biol. Evol.* **2015**, *7*, 1110–1121. [CrossRef] [PubMed]
286. Hu, G.; Wendel, J.F. Cis–Trans Controls and Regulatory Novelty Accompanying Allopolyploidization. *New Phytol.* **2019**, *221*, 1691–1700. [CrossRef] [PubMed]
287. Yu, X.; Wang, P.; Li, J.; Zhao, Q.; Ji, C.; Zhu, Z.; Zhai, Y.; Qin, X.; Zhou, J.; Yu, H.; et al. Whole-Genome Sequence of Synthesized Allopolyploids in *Cucumis* Reveals Insights into the Genome Evolution of Allopolyploidization. *Adv. Sci.* **2021**, *8*, 1–15. [CrossRef]
288. Yoo, M.J.; Szadkowski, E.; Wendel, J.F. Homoeolog Expression Bias and Expression Level Dominance in Allopolyploid Cotton. *Heredity* **2013**, *110*, 171–180. [CrossRef] [PubMed]

289. Wicker, T.; Gundlach, H.; Spannagl, M.; Uauy, C.; Borrill, P.; Ramírez-González, R.H.; De Oliveira, R.; Mayer, K.F.X.; Paux, E.; Choulet, F. Impact of Transposable Elements on Genome Structure and Evolution in Bread Wheat. *Genome Biol.* **2018**, *19*, 1–18. [CrossRef]
290. Yu, X.; Zhai, Y.; Wang, P.; Cheng, C.; Li, J.; Lou, Q.; Chen, J. Morphological, Anatomical and Photosynthetic Consequences of Artificial Allopolyploidization in *Cucumis*. *Euphytica* **2021**, *217*, 5. [CrossRef]
291. Bourque, G.; Burns, K.H.; Gehring, M.; Gorbunova, V.; Seluanov, A.; Hammell, M.; Imbeault, M.; Izsvák, Z.; Levin, H.L.; Macfarlan, T.S.; et al. Ten Things You Should Know about Transposable Elements. *Genome Biol.* **2018**, *19*, 1–12. [CrossRef]
292. Bariah, I.; Keidar-Friedman, D.; Kashkush, K. Where the Wild Things Are: Transposable Elements as Drivers of Structural and Functional Variations in the Wheat Genome. *Front. Plant Sci.* **2020**, *11*, 1–9. [CrossRef]
293. Venkatesh; Nandini, B. Miniature Inverted-Repeat Transposable Elements (MITEs), Derived Insertional Polymorphism as a Tool of Marker Systems for Molecular Plant Breeding. *Mol. Biol. Rep.* **2020**, *47*, 3155–3167. [CrossRef]
294. Lisch, D. How Important Are Transposons for Plant Evolution? *Nat. Rev. Genet.* **2013**, *14*, 49–61. [CrossRef]
295. Quesneville, H. Twenty years of transposable element analysis in the Arabidopsis thaliana genome. *Mob. DNA* **2020**, *11*, 11–13.
296. Arkhipova, I.R. Neutral Theory, Transposable Elements, and Eukaryotic Genome Evolution. *Mol. Biol. Evol.* **2018**, *35*, 1332–1337. [CrossRef] [PubMed]
297. Quadrana, L.; Etcheverry, M.; Gilly, A.; Caillieux, E.; Madoui, M.A.; Guy, J.; Bortolini Silveira, A.; Engelen, S.; Baillet, V.; Wincker, P.; et al. Transposition Favors the Generation of Large Effect Mutations That May Facilitate Rapid Adaption. *Nat. Commun.* **2019**, *10*, 1–10. [CrossRef] [PubMed]
298. Pereira, J.F.; Ryan, P.R. The Role of Transposable Elements in the Evolution of Aluminium Resistance in Plants. *J. Exp. Bot.* **2019**, *70*, 41–54. [CrossRef] [PubMed]
299. Kim, S.; Park, J.; Yeom, S.I.; Kim, Y.M.; Seo, E.; Kim, K.T.; Kim, M.S.; Lee, J.M.; Cheong, K.; Shin, H.S.; et al. New Reference Genome Sequences of Hot Pepper Reveal the Massive Evolution of Plant Disease-Resistance Genes by Retroduplication. *Genome Biol.* **2017**, *18*, 1–11. [CrossRef] [PubMed]
300. Poretti, M.; Praz, C.R.; Meile, L.; Kälin, C.; Schaefer, L.K.; Schläfli, M.; Widrig, V.; Sanchez-Vallet, A.; Wicker, T.; Bourras, S. Domestication of High-Copy Transposons Underlays the Wheat Small RNA Response to an Obligate Pathogen. *Mol. Biol. Evol.* **2020**, *37*, 839–848. [CrossRef]
301. Kent, T.V.; Uzunović, J.; Wright, S.I. Coevolution between Transposable Elements and Recombination. *Philos. Trans. R. Soc. B Biol. Sci.* **2017**, *372*, 20160458. [CrossRef]
302. Choudhury, R.R.; Rogivue, A.; Gugerli, F.; Parisod, C. Impact of Polymorphic Transposable Elements on Linkage Disequilibrium along Chromosomes. *Mol. Ecol.* **2019**, *28*, 1550–1562. [CrossRef]
303. Kashkush, K.; Yaakov, B. Methylation, Transcription, and Rearrangements of Transposable Elements in Synthetic Allopolyploids. *Int. J. Plant Genom.* **2011**, *2011*, 569826. [CrossRef]
304. Kashkush, K.; Feldman, M.; Levy, A.A. Transcriptional Activation of Retrotransposons Alters the Expression of Adjacent Genes in Wheat. *Nat. Genet.* **2003**, *33*, 102–106. [CrossRef]
305. Cheng, H.; Sun, G.; He, S.; Gong, W.; Peng, Z.; Wang, R.; Lin, Z.; Du, X. Comparative Effect of Allopolyploidy on Transposable Element Composition and Gene Expression between *Gossypium hirsutum* and Its Two Diploid Progenitors. *J. Integr. Plant Biol.* **2019**, *61*, 45–59. [CrossRef]
306. Petit, M.; Guidat, C.; Daniel, J.; Denis, E.; Montoriol, E.; Bui, Q.T.; Lim, K.Y.; Kovarik, A.; Leitch, A.R.; Grandbastien, M.A.; et al. Mobilization of Retrotransposons in Synthetic Allotetraploid Tobacco. *New Phytol.* **2010**, *186*, 135–147. [CrossRef]
307. Sarilar, V.; Palacios, P.M.; Rousselet, A.; Ridel, C.; Falque, M.; Eber, F.; Chèvre, A.M.; Joets, J.; Brabant, P.; Alix, K. Allopolyploidy Has a Moderate Impact on Restructuring at Three Contrasting Transposable Element Insertion Sites in Resynthesized *Brassica napus* Allotetraploids. *New Phytol.* **2013**, *198*, 593–604. [CrossRef]
308. Baduel, P.; Quadrana, L.; Hunter, B.; Bomblies, K.; Colot, V. Relaxed Purifying Selection in Autopolyploids Drives Transposable Element Over-Accumulation Which Provides Variants for ocal Adaptation. *Nat. Commun.* **2019**, *10*. [CrossRef] [PubMed]
309. Das Gupta, M.; Tsiantis, M. Gene Networks and the Evolution of Plant Morphology. *Curr. Opin. Plant Biol.* **2018**, *45*, 82–87. [CrossRef]
310. Wang, J.; Tian, L.; Lee, H.S.; Wei, N.E.; Jiang, H.; Watson, B.; Madlung, A.; Osborn, T.C.; Doerge, R.W.; Comai, L.; et al. Genomewide Nonadditive Gene Regulation in *Arabidopsis* Allotetraploids. *Genetics* **2006**, *172*, 507–517. [CrossRef] [PubMed]
311. Tate, J.A.; Ni, Z.; Scheen, A.C.; Koh, J.; Gilbert, C.A.; Lefkowitz, D.; Chen, Z.J.; Soltis, P.S.; Soltis, D.E. Evolution and Expression of Homeologous Loci in *Tragopogon miscellus* (Asteraceae), a Recent and Reciprocally Formed Allopolyploid. *Genetics* **2006**, *173*, 1611. [CrossRef] [PubMed]
312. Combes, M.C.; Cenci, A.; Baraille, H.; Bertrand, B.; Lashermes, P. Homeologous Gene Expression in Response to Growing Temperature in a Recent Allopolyploid (*Coffea arabica* L.). *J. Hered.* **2012**, *103*, 36–46. [CrossRef] [PubMed]
313. Xu, C.; Bai, Y.; Lin, X.; Zhao, N.; Hu, L.; Gong, Z.; Wendel, J.F.; Liu, B. Genome-Wide Disruption of Gene Expression in Allopolyploids but Not Hybrids of Rice Subspecies. *Mol. Biol. Evol.* **2014**, *31*, 1066–1076. [CrossRef] [PubMed]
314. Edger, P.P.; Smith, R.; McKain, M.R.; Cooley, A.M.; Vallejo-Marin, M.; Yuan, Y.; Bewick, A.J.; Ji, L.; Platts, A.E.; Bowman, M.J.; et al. Subgenome Dominance in an Interspecific Hybrid, Synthetic Allopolyploid, and a 140-Year-Old Naturally Established Neo-Allopolyploid Monkeyflower. *Plant Cell* **2017**, *29*, 2150–2167. [CrossRef] [PubMed]

315. Chagué, V.; Just, J.; Mestiri, I.; Balzergue, S.; Tanguy, A.M.; Huneau, C.; Huteau, V.; Belcram, H.; Coriton, O.; Jahier, J.; et al. Genome-Wide Gene Expression Changes in Genetically Stable Synthetic and Natural Wheat Allohexaploids. *New Phytol.* **2010**, *187*, 1181–1194. [CrossRef]
316. Wang, X.; Zhang, H.; Li, Y.; Zhang, Z.; Li, L.; Liu, B. Transcriptome Asymmetry in Synthetic and Natural Allotetraploid Wheats, Revealed by RNA-Sequencing. *New Phytol.* **2016**, *209*, 1264–1277. [CrossRef]
317. Flagel, L.; Udall, J.; Nettleton, D.; Wendel, J. Duplicate Gene Expression in Allopolyploid Gossypium Reveals Two Temporally Distinct Phases of Expression Evolution. *BMC Biol.* **2008**, *6*, 1–9. [CrossRef]
318. Ding, M.; Chen, Z.J. Epigenetic Perspectives on the Evolution and Domestication of Polyploid Plant and Crops. *Curr. Opin. Plant Biol.* **2018**, *42*, 37–48. [CrossRef]
319. Bao, Y.; Hu, G.; Grover, C.E.; Conover, J.; Yuan, D.; Wendel, J.F. Unraveling Cis and Trans Regulatory Evolution during Cotton Domestication. *Nat. Commun.* **2019**, *10*, 1–12. [CrossRef]
320. Wendel, J.F.; Jackson, S.A.; Meyers, B.C.; Wing, R.A. Evolution of Plant Genome Architecture. *Genome Biol.* **2016**, *17*, 1–14. [CrossRef]
321. D'Ario, M.; Griffiths-Jones, S.; Kim, M. Small RNAs: Big Impact on Plant Development. *Trends Plant Sci.* **2017**, *22*, 1056–1068. [CrossRef] [PubMed]
322. Crisp, P.A.; Hammond, R.; Zhou, P.; Vaillancourt, B.; Lipzen, A.; Daum, C.; Barry, K.; De Leon, N.; Buell, C.R.; Kaeppler, S.M.; et al. Variation and Inheritance of Small RNAs in Maize Inbreds and F1 Hybrids. *Plant Physiol.* **2020**, *182*, 318–331. [CrossRef]
323. Li, A.; Liu, D.; Wu, J.; Zhao, X.; Hao, M.; Geng, S.; Yan, J.; Jiang, X.; Zhang, L.; Wu, J.; et al. MRNA and Small RNA Transcriptomes Reveal Insights into Dynamic Homoeolog Regulation of Allopolyploid Heterosis in Nascent Hexaploid Wheat. *Plant Cell* **2014**, *26*, 1878–1900. [CrossRef] [PubMed]
324. Lu, F.H.; McKenzie, N.; Gardiner, L.J.; Luo, M.C.; Hall, A.; Bevan, M.W. Reduced Chromatin Accessibility Underlies Gene Expression Differences in Homologous Chromosome Arms of Diploid *Aegilops tauschii* and Hexaploid Wheat. *Gigascience* **2021**, *9*, 1–11. [CrossRef]
325. Guo, X.; Han, F. Asymmetric Epigenetic Modification and Elimination of RDNA Sequences by Polyploidization in Wheat. *Plant Cell* **2014**, *26*, 4311–4327. [CrossRef]
326. Lawrence, R.J.; Earley, K.; Pontes, O.; Silva, M.; Chen, Z.J.; Neves, N.; Viegas, W.; Pikaard, C.S. A Concerted DNA Methylation/Histone Methylation Switch Regulates rRNA Gene Dosage Control and Nucleolar Dominance. *Mol. Cell* **2004**, *13*, 599–609. [CrossRef]
327. Xu, Y.; Zhong, L.; Wu, X.; Fang, X.; Wang, J. Rapid Alterations of Gene Expression and Cytosine Methylation in Newly Synthesized *Brassica napus* Allopolyploids. *Planta* **2009**, *229*, 471–483. [CrossRef] [PubMed]
328. Wang, J.; Tian, L.; Lee, H.S.; Chen, Z.J. Nonadditive Regulation of FRI and FLC Loci Mediates Flowering-Time Variation in *Arabidopsis* Allopolyploids. *Genetics* **2006**, *173*, 965–974. [CrossRef] [PubMed]
329. Song, Q.; Zhang, T.; Stelly, D.M.; Chen, Z.J. Epigenomic and Functional Analyses Reveal Roles of Epialleles in the Loss of Photoperiod Sensitivity during Domestication of Allotetraploid Cottons. *Genome Biol.* **2017**, *18*, 1–14. [CrossRef] [PubMed]

plants

MDPI

Article

Root Morphology, Allometric Relations and Rhizosheath of Ancient and Modern Tetraploid Wheats (*Triticum durum* Desf.) in Response to Inoculation with *Trichoderma harzianum* T-22

Rocco Bochicchio [1,*], Rosanna Labella [1], Antonella Vitti [1,2], Maria Nuzzaci [1], Giuseppina Logozzo [1] and Mariana Amato [1,*]

[1] School of Agriculture, Forestry, Food and Environmental Sciences, University of Basilicata, 85100 Potenza, Italy; rosannalabella@yahoo.it (R.L.); avitti@unisa.it (A.V.); maria.nuzzaci@unibas.it (M.N.); giuseppina.logozzo@unibas.it (G.L.)

[2] Department of Pharmacy, University of Salerno, 84100 Salerno, Italy

* Correspondence: bochicchiorocco@gmail.com (R.B.); mariana.amato@unibas.it (M.A.)

Abstract: Early root traits and allometrics of wheat are important for competition and use of resources. They are under-utilized in research and un-explored in many ancient wheats. This is especially true for the rhizosheath emerging from root-soil interactions. We investigated root morphology, root/shoot relations and the amount of rhizosheath of four tetrapoid wheat seedlings (30 days after emergence): the italian landrace Saragolle Lucana and modern varieties Creso, Simeto and Ciclope, and tested the hypothesis that inoculation with *Trichoderma harzianum* T-22 (T-22) enhances rhizosheath formation and affects wheat varieties differently. Overall growth of non-inoculated plants showed different patterns in wheat varieties, with Saragolle and Ciclope at the two extremes: Saragolle invests in shoot rather than root mass, and in the occupation of space with highest ($p < 0.05$) shoot height to the uppermost internode (5.02 cm) and length-to-mass shoot (97.8 cm g^{-1}) and root (more than 140 m g^{-1}) ratios. This may be interpreted as maximizing competition for light but also as a compensation for low shoot efficiency due to the lowest ($p < 0.05$) recorded values of optically-measured chlorophyll content index (22.8). Ciclope invests in biomass with highest shoot (0.06 g) and root (0.04 g) mass and a thicker root system (average diameter 0.34 mm vs. 0.29 in Saragolle) as well as a highest root/shoot ratio (0.95 g g^{-1} vs. 0.54 in Saragolle). Rhizosheath mass ranged between 22.14 times that of shoot mass in Ciclope and 43.40 in Saragolle (different for $p < 0.05$). Inoculation with *Trichoderma* increased the amount of rhizosheath from 9.4% in Ciclope to 36.1% in Simeto and modified root architecture in this variety more than in others. Ours are the first data on roots and seedling shoot traits of Saragolle Lucana and of *Trichoderma* inoculation effects on rhizosheath. This opens to new unreported interpretations of effects of *Trichoderma* inoculation on improving plant growth.

Keywords: root length; root/shoot ratio; specific root length; Saragolle Lucana; seed coating

Citation: Bochicchio, R.; Labella, R.; Vitti, A.; Nuzzaci, M.; Logozzo, G.; Amato, M. Root Morphology, Allometric Relations and Rhizosheath of Ancient and Modern Tetraploid Wheats (*Triticum durum* Desf.) in Response to Inoculation with *Trichoderma harzianum* T-22. *Plants* **2022**, *11*, 159. https://doi.org/10.3390/plants11020159

Academic Editors: Milan S. Stankovic, Paula Baptista and Petronia Carillo

Received: 14 December 2021
Accepted: 5 January 2022
Published: 7 January 2022

1. Introduction

Root morphological traits explain a large part of the physiology of roots [1] and the plant's ability to respond to inputs and environmental constraints [2]. Belowground indicators and allometric relations between and within shoot and root are therefore commented in terms of strategy of plants in dealing with anthropic and natural factors and their ability to provide products and ecosystem services [3,4].

Root traits and allometric relations have therefore been strongly suggested for inclusion in selection criteria for plants (e.g., [5,6] and for the evaluation of agronomic practices [2]). Translating seedling traits into mature plants morphology and behavior, though, is the object of controversy. For wheat many studies report that seedling traits are not related to root architecture at anthesis due to interactions with the environment

(e.g., [7,8]). Nevertheless early traits correlate well with vegetative growth, field establishment, exploration of the environment and competition [9] and may relate to later root traits if referred to specific functions such as penetration of hard layers or specific environmental conditions [5,10].

In wheat, root traits have been shown to differ between varieties (e.g., [7,11,12]) and desirable traits are different based on environmental constraints [5]. Plant phenotyping on 36 genotypes chosen along the key steps of evolution in tetraploid wheat from wild emmer to emmer to durum wheat indicates that domestication has changed shoot and root mass and biometric traits [13], although [14] showed that experimental growth conditions such as soil type may affect the extent and direction of the observed changes therefore conclusions are not easy to generalize. It is still considered essential to explore both genetic variation within modern genotypes, and traits of landraces and ancient wheats [3]. Based on root biometrics and allometric relations ancient or underutilized wheat germplasm has been classified in the water-spending plant type [15] since their extended root systems with high length density allows them cope with drought avoidance via rapid uptake of water. This allows to face dry spells without reducing yield, but at the cost of high water consumption, and is considered an efficient strategy in environments where wheat can rely on in-season rainfall with occasional water shortages, as opposed to water-saving wheat varieties which are more successful in environments where wheat grows on stored water [4]. Nevertheless, in spite of the low harvest index of tall ancient phenotypes in high input conditions, some ancient wheats may provide valuable traits in erratic environment and input due to high plasticity in carbon allocation which results in favorable allometry or root traits under drought [3,12]. Research on root and allocation traits of ancient wheats though is still scarce.

Differences in soil-plant interactions between and within plant species are also related to root exudation and relations with rhizosphere organisms. In tetraploid wheat [14] showed that in addition to a strong effect of soil type, genotypic differences were found in the composition of rhizosphere metabolites between domestication groups, as some of the metabolites have high heritability and [16] found that wheat cultivar variability was linked to root traits such as mass, surface area and volume, but also to carbohydrate exudation and diversity of groups of associated rhizospheric organisms.

The rhizosheath is defined as the portion of soil that adheres to the root system of certain plant species [17]. It is a trait emerging from root-soil interactions via the exudation of mucilages which are responsible for key properties of the rhizosheath by binding soil, affecting root hydration, plant water relations and resilience in dry environments [18–20], soil stability [20] and relations with soil chemicals [21]. The extent of rhizosheath depends on soil conditions, especially water content [22]. Since it is related to exudates produced by roots and associated microflora, and given its key role in root physiology, the rhizosheath may be considered as a plant-related trait [20]. It is affected by plant species [23,24] and variety [19,25]. In wheat varietal differences have been shown [19] but the production of rhizosheath in ancient wheats has not been investigated yet.

The filamentous ascomycetous *Trichoderma* spp. (family *Hypocreaceae*) are avirulent opportunistic plant symbiont fungi able to colonize soil, plant roots and plant debris. These fungi exhibit different activities for agriculture applications related to their biological functions, such as plant growth promotion, biocontrol of plant disease, organic matter decomposition, bioremediation of pesticides [26].

In particular, *Trichoderma* spp. are known to ameliorate plant performance thanks to their double ability to improve plant growth and development, and to induce plant defense responses against several pathogens, insects and abiotic stress [19,27–30]. For this reason *Trichoderma*-based products are a major source of registered biofertilizers and biofungicides that can be used in crop sustainable management as biostimulants and for plant disease control [31–33]. Seed coating with a commercial product containing *Trichoderma harzianum* T-22 has been shown to improve seedling vigor and also to enhance the protection against the fungal pathogen *Fusarium culmorum* in the susceptible durum wheat (*Triticum durum* L.)

cv. Karim [34]. When applied to seeds, the spores of some strains of *Trichoderma* can germinate rapidly, and within few days hyphae and branching filaments grow from the seed onto the emerging radicle [30]. On the other hand, *Trichoderma atroviride* applied as growth medium or seed treatment induced a diverse and distinctively modulated wheat (*Triticum aestivum* L.) root exudate metabolic profile during root colonization [35].

The effects of *Trichoderma*-based biostimulants and/or biopesticides on nutrient uptake, crop growth and systemic resistance have been indicated as species- and genotype-dependent [36,37]. Changes in phytohormone levels, in particular auxins and cytokinins have been established to be one of the direct mechanism by which *T. harzianum* is able to promote tree plant growth and cell wall suberification in the exoderm and endoderm [38,39]. Furthermore, different degrees of *Trichoderma* strain-dependent in root colonization of wheat have been demonstrated due to a diverse production of eight different phytohormones, including gibberellins, abscisic acid (ABA), salicylic acid (SA), auxin IAA (indole-3-acetic acid), and cytokinins [40]. *Trichoderma* spp. has also been shown to increase plant lateral root growth and root hair via IAA (promoting elongation) [41,42] and other mechanisms like plasma membrane H+ATP-ase activation which promotes cell growth [43].

Trichoderma spp. are frequently found in agricultural soils as common inhabitants of the rhizosphere because they grow along the entire length of plant root system, colonizing the first or second layer of root epidermis cells [44]. They have also been isolated in the rhizosheath of plants [22], but the ability of *Trichoderma* spp. to affect the amount of rhizosheath soil binding to plants upon inoculation has not been investigated so far.

Among ancient tetraploid wheats Saragolle Lucana was the first italian landrace enrolled in the Italian Wheat Landrace Conservation Registry in 2014 (https://www.gazzettaufficiale.it/eli/gu/2014/01/28/22/sg/pdf, accessed date 1 December 2021). Its early biometrics, root morphology and interactions with plant growth promoting organisms have not been investigated.

We conducted a research on Saragolle Lucana compared with three italian tetraploid wheats corresponding to different times of release and breeding history, inoculated with *Trichoderma harzianum* T-22 (T-22) with the aim of testing the following hypotheses:

(1) that allocation, root traits and rhizosheath soil adhering to roots of Saragolle Lucana are different from those of modern wheats

(2) That T-22 inoculation enhances rhizosheath formation

(3) That effects of T-22 inoculation on plant growth, allocation and early root traits differ between an ancient wheat and modern varieties.

2. Results

2.1. Overall Growth

The height of plants at the uppermost node (Figure 1a) showed significantly highest values for Saragolle and was not significantly different among the other wheat varieties within the control treatment. Values were not significantly affected by *Trichoderma* inoculation except for the Ciclope variety which showed a significant increase, but remained lower than in Saragolle. The same trend was found for height at the tip of the last fully expanded leaf (data not shown). Shoot dry biomass was not significantly different between varieties in the control treatment, but *Trichoderma* caused a significant increase in shoot dry biomass for Saragolle (Figure 1b), whereas it decreased biomass accumulation in Creso. *Trichoderma* inoculation also resulted in a significant increase of the Chlorophyll content index CCI by 45% for Saragolle (Figure 1c) whereas for all varieties non-significant variations were found. The lowest CCI values were recorded for Saragolle control plants (Figure 1c).

Root biomass (Figure 1d) in control plants was significantly lowest for Saragolle and highest for Ciclope, and for the latter variety it was significantly higher in the control than in the *Trichoderma* treatment. Upon inoculation the root mass of Simeto was not significantly different from that of Ciclope. In the control treatment total plant biomass was highest for Ciclope (0.114 g) and lowest for Saragolle (0.084 g), but for the latter variety it increased to 0.092 g upon inoculation with T-22.

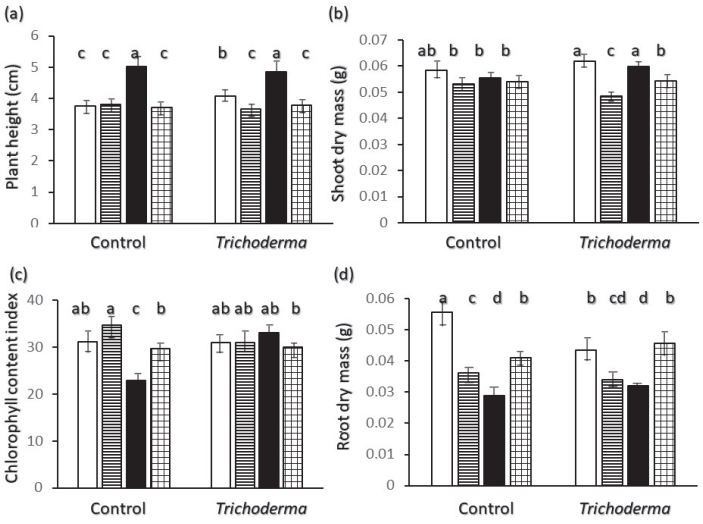

Figure 1. Interaction of wheat variety x *Trichoderma harzianum* T-22 inoculation on overall growth data: (**a**) height to the uppermost node; (**b**) shoot dry mass; (**c**) Chlorophyll Content Index; (**d**) root dry mass. Color code of bars: white = Ciclope; horizontal stripes = Creso; black = Saragolle; grid = Simeto. Vertical segments on each bar indicate standard deviation $n = 6$. Different letters on each bar designate significantly different values for $p < 0.05$ at the Tukey's post hoc mean separation test.

2.2. Root Biometrics

Non-inoculated plants showed a significantly higher total length of root structures (Figure 2a) in Ciclope and Saragolle compared to other varieties, whereas root surface (Figure 2b) and volume (Figure 2d) were highest in Ciclope, and this corresponds to a thicker root system characterized by a higher average diameter in the latter variety (Figure 2c). *Trichoderma* made roots of Ciclope finer on average as shown by a root diameter decrease by 9.0 % (Figure 2c) and thicker in Simeto with an increase in diameter by 8.7%.

The effect of T-22 was also to increase root length, surface and volume in Simeto (Figure 2a,b,d), whereas for the other varieties such root trait values were reduced or did not show significant differences.

Most of the root system length was due to very fine roots (<0.5 mm diameter) (Figure 3a), and in control plants a significantly lower percentage of finest root length was found in Ciclope with around 86% roots in this class than in the other varieties were finest roots represented more than 90% of the total root length. Conversely a higher percentage of roots were found for Ciclope in the diameter classes of 0.5 mm up to 1.5 mm (Figure 3b,c).

At diameters higher than 1.5 mm no significant differences were found due to high variability. *Trichoderma* inoculation significantly increased the proportion of very fine roots for Ciclope (Figure 3a) but values stayed significantly lower than those of Saragolle and Creso. A corresponding reduction in the proportion of roots in the 0.50–1 mm and 1–1.5 mm classes was shown for Ciclope upon inoculation (Figure 3b,c). The only variety showing a decrease in very fine roots (<0.5 mm) and an increase in the 0.50–1 mm class in the *Trichoderma* treatment was Simeto, and this corresponds to an increase in average root diameter upon inoculation for this variety as shown in Figure 2c.

Length data in absolute values (Figure 4) show that Saragolle had more than 390 cm of total length of very fine roots per plant (Figure 4a), which is the highest value between varieties but not significantly higher than Ciclope in the control and Simeto in the T-22 treatment. Absolute total length corresponding to higher diameter classes up to 1.5 mm (Figure 4b,c), instead, was significantly higher in Ciclope. Simeto is the only variety where

the absolute value of root length increased upon inoculation in the <0.5 and 0.5–1 mm diameter classes.

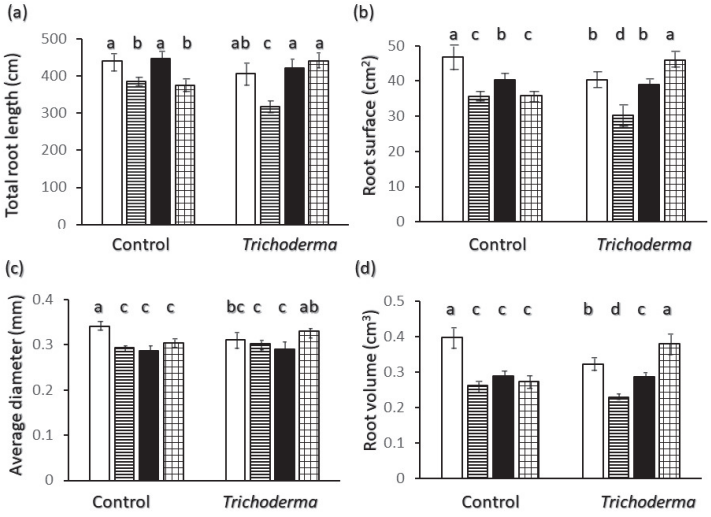

Figure 2. Interaction of wheat variety x *Trichoderma harzianum* T-22 inoculation on root biometrics: (**a**) total length of root structures; (**b**) root surface; (**c**) average diameter; (**d**) root volume. Color code of bars: white = Ciclope; horizontal stripes = Creso; black = Saragolle; grid = Simeto. Vertical segments on each bar indicate standard deviation $n = 3$. Different letters on each bar designate significantly different values for $p < 0.05$ at the Tukey's post hoc mean separation test.

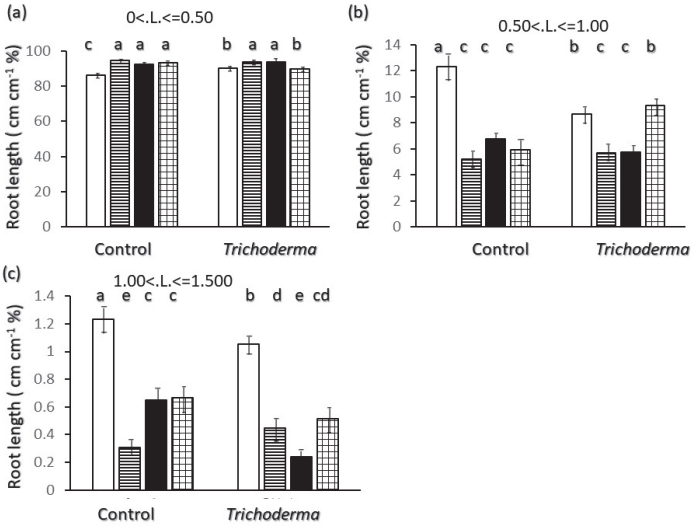

Figure 3. Interaction of wheat variety x *Trichoderma harzianum* T-22 inoculation on root length percent distribution by diameter class: (**a**) diameter class < 0.5 mm; (**b**) diameter class 0.5 < d < 1 mm; (**c**) diameter class 1 < d < 1.55 mm. Color code of bars: white = Ciclope; horizontal stripes = Creso; black = Saragolle; grid = Simeto. Vertical segments on each bar indicate standard deviation $n = 3$. Different letters on each bar designate significantly different values for $p < 0.05$ at the Tukey's post hoc mean separation test.

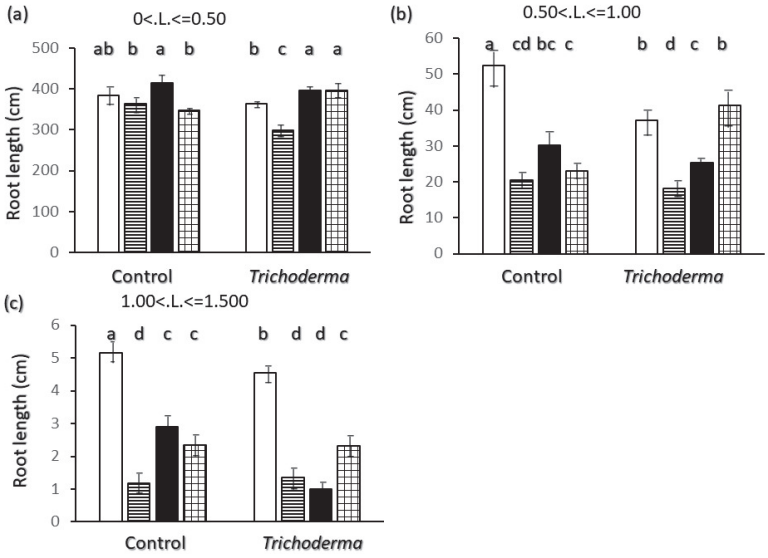

Figure 4. Interaction of wheat variety x *Trichoderma harzianum* T-22 inoculation on root length values by diameter class: (**a**) diameter class < 0.5 mm; (**b**) diameter class 0.5 < d < 1 mm; (**c**) diameter class 1 < d < 1.55 mm. Color code of bars: white = Ciclope; horizontal stripes = Creso; black = Saragolle; grid = Simeto. Vertical segments on each bar indicate standard deviation $n = 3$. Different letters on each bar designate significantly different values for $p < 0.05$ at the Tukey's post hoc mean separation test.

Figure 5 reports root surface in the finest root class. Control plants showed that absolute values (Figure 5a) of Ciclope were higher than those of Simeto but in percentage of the whole root system (Figure 5b) the former variety showed significantly lower values than the other varieties in this diameter class. Patterns of absolute (Figure 5a) and percent (Figure 5b) values of very fine root surface of plants treated with T-22 are parallel to the corresponding values of root length (Figures 3a and 4a).

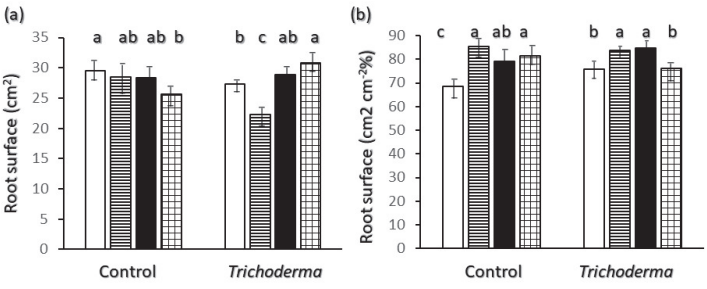

Figure 5. Interaction of wheat variety x *Trichoderma harzianum* T-22 inoculation on root surface in the diameter class < 0.5 mm: (**a**) total length of root structures; (**b**) percent length of root structures. Color code of bars: white = Ciclope; horizontal stripes = Creso; black = Saragolle; grid = Simeto. Vertical segments on each bar indicate standard deviation $n = 3$. Different letters on each bar designate significantly different values for $p < 0.05$ at the Tukey's post hoc mean separation test.

2.3. Allometric Relations

Figure 6 reports mass and length relations between different plant traits. The two extremes for root to shoot mass and length ratios (Figure 6a,b) in control plants are Saragolle and Ciclope. Plant root mass (Figure 6a) corresponds to little over 55% of the shoot mass

for Saragolle, and almost 95% in Ciclope, and root length (Figure 6b) is almost 8 times the shoot length for Saragolle and almost 13 times for Ciclope. Upon inoculation with *Trichoderma* Ciclope is shown to invest proportionally significantly less in roots in terms of mass (Figure 6b) and length (Figure 6b) whereas Simeto invests proportionally more, but these two varieties still show significantly higher values than Saragolle for the mass ratio (Figure 6a) and than Saragolle and Creso for the length ratio (Figure 6b). The root system's ratio of length to weight (Figure 6c) shows higher values for Saragolle and Creso, and lowest for Ciclope, corresponding to a thicker root system. The effect of *Trichoderma* was to significantly increase specific root length only in the two varieties characterized by lower values: Ciclope and Simeto, but even so they were still significantly lower than values of Saragolle and Creso. The ratio of shoot height to biomass (Figure 6d) show that values were significantly and considerably higher in Saragolle than in the modern wheats showing a higher proportional investment in height than in biomass for this ancient wheat. Values decreased significantly upon T-22 inoculation for Saragolle only (Figure 6d).

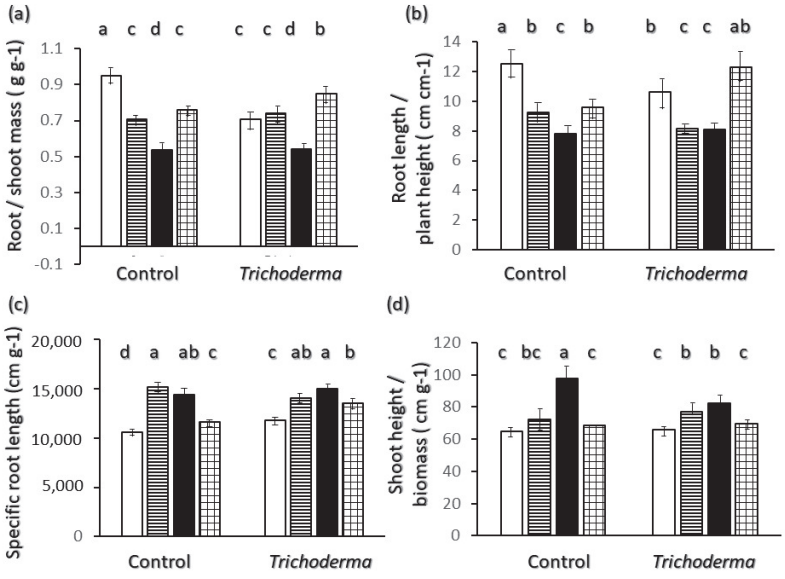

Figure 6. Interaction of wheat variety x *Trichoderma harzianum* T-22 inoculation on Allometric relations of plant parts: (**a**) root to shoot mass ratio $n = 6$; (**b**) root length to plant height ratio Vertical segments on each bar indicate standard deviation n=3; (**c**) specific root length $n = 3$; (**d**) shoot height to biomass ratio $n = 6$. Color code of bars: white = Ciclope; horizontal stripes = Creso; black = Saragolle; grid = Simeto. Different letters on each bar designate significantly different values for $p < 0.05$ at the Tukey's post hoc mean separation test.

2.4. Rhizosheath

Figure 7 reports data on rhizosheat amount and relations with root traits. The dry weight of rhizosheath was lowest for Saragolle and highest for Simeto (Figure 7a).

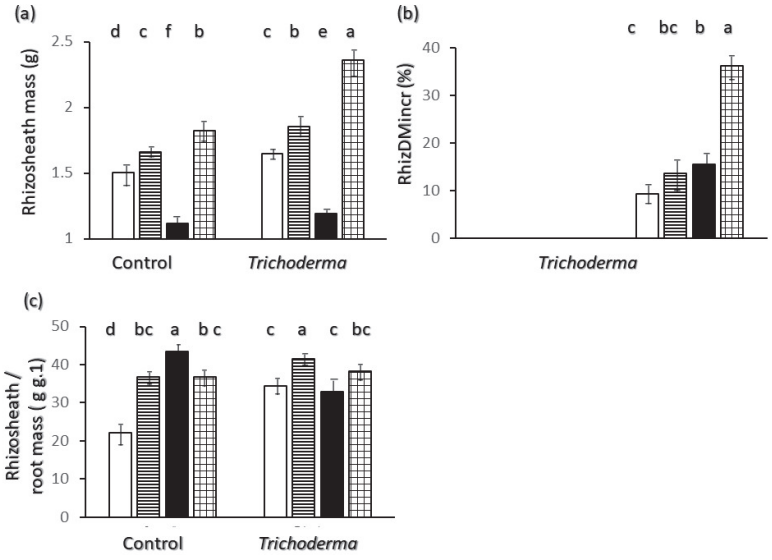

Figure 7. Rhizosheath mass data and indices. Interaction of wheat variety x *Trichoderma harzianum* T-22 inoculation on (**a**) rhizosheath mass; (**c**) rhizosheath/root mass ratio. Main effect of wheat variety on rizosheath percent weight gain upon inoculation RhizDMIncr (**b**). Color code of bars: white = Ciclope; horizontal stripes = Creso; black = Saragolle; grid = Simeto. Vertical segments on each bar indicate standard deviation $n = 3$. Different letters on each bar designate significantly different values for $p < 0.05$ at the Tukey's post hoc mean separation test.

Upon inoculation with T-22 the amount of rhizosheath was higher than in the control for all varieties (Figure 7a). The percent increase (Figure 7b) was lower than 10% in Ciclope and higher than 35% for Simeto. Figure 7c shows that the proportion of rhizosheath to root weight was quite high: the rhizosheath amounted to more than 20 times the weight of roots in Ciclope (the significantly lowest value) and more than 43 times in Saragolle (the significantly highest value) for control plants. Upon inoculation with *Trichoderma* values for Saragolle were significantly lower than in the control while for Ciclope and Creso they were higher or not different, and in general the range of values between varieties was narrower (Figure 7c); in inoculated plants Creso showed a significantly higher value than other varieties. (Figure 7c).

3. Discussion

Shoot and Root Growth and Relations

Data in our experiment show different patterns of biomass allocation and root morphology in the early growth of wheat varieties. The two opposite extremes of overall behavior for non-inoculated plants are the ancient wheat Saragolle and the modern variety Ciclope. Saragolle shows the tallest seedling (Figure 1a) and a shoot growth characterized by a very high proportional investment in height per unit biomass (Figure 6d), as well as the lowest root mass (Figure 1d) and proportional investment in root mass (Figure 6a) and length (Figure 6b). Ciclope shows the highest shoot (Figure 1b) and root (Figure 1d) dry mass and the highest proportional mass and length investment in roots (Figure 6a,b); shoots show the lowest investment in height per unit biomass(Figure 6c).

Patterns of growth and morphology of wheat varieties have been commented in terms of strategy [4]. Also, allocation of assimilates between above- and below-ground plant parts is classically analyzed within the framework of hypotheses derived from the functional balance theory [45], whereby the relative sizes of roots and shoots are an inverse function of their activity. Typical activities for shoot and root within this framework are

respectively capture and conversion of light into assimilated carbon, and uptake and transport of nutrients [46] and water. According to this theory a plant exhibiting efficient photosynthesis will have a relatively small shoot compared to a plant with inefficient light capture, which will need a larger shoot mass to provide a unit mass of roots with the assimilates it needs. Along this line the early patterns of mass accumulation and partitioning shown by Saragolle with tall plants and a low root/shoot ratio indicate a competition-oriented strategy, especially for light, and possibly the need to compensate for lower efficiency in resource acquisition. This corresponds to a lower chlorophyll content index of Saragolle (Figure 1c) compared to modern wheats, and points to a less efficient capture and conversion of light. A functional-balance type interpretation is also corroborated by a higher root/shoot ratio exhibited by Saragolle upon T-22 inoculation in coincidence with a significantly higher CCI, therefore a more efficient shoot. Low chlorophyll content values for ancient wheats compared to modern varieties were reported by [3], as in our experiment, and commented in terms of lower yield potential. Conversely a high CCI and investment in belowground biomass allocation for Ciclope suggests a higher shoot efficiency and a strategy oriented towards root growth and soil resource acquisition. This resulted in the highest total biomass produced in our experiment.

Regarding belowground morphology and allometry only, two different root physiognomies emerge: Saragolle and Creso are characterized by a finer root system (lower biomass-Figure 1d, diameter-Figure 2c and higher specific root length-Figure 6c) whereas the more recent Ciclope and Simeto exhibit a thick system with high biomass and diameter and lower specific root length, and show a high presence of roots larger than 0.5 mm diameter in control plants for Ciclope and inoculated plants for Simeto. The high mass investment and thickness-though-allows a high surface and volume. In spite of the lowest mass investment in roots, thanks to a finer root system Saragolle has absolute values of total (Figure 2a) and fine (Figure 4a) root length as high as Ciclope and a higher percentage of fine roots like Creso and Simeto (Figure 3a). This allows a comparable absolute surface but a higher percent surface than Ciclope (Figure 5). This adds to aboveground patterns in drawing the strategy of Saragolle as strongly oriented towards the occupation of space by maximizing the length of shoots and root per unit biomass. No data on the root system of Saragolle are available in the literature for comparison but the root profile of Saragolle emerging from our results corresponds to the profile set by [3,11] for ancient wheats including underutilized species: a high root length and specific root length with investment in lengths and surfaces rather than mass. Authors emphasize how this type of plants achieve a more extensive root system, resulting in higher soil volume exploration and acquisition capacities for below-ground resources compared to modern wheats, and this is achieved by using fewer assimilates to build up root length, surface and volume.

Differences between ancient wheats and modern dwarf lines were investigated by [47] who found a higher root length in modern lines from gel chamber experiments but a lower length from field experiments. They also report that in spite of differences in length, root diameter was not altered by dwarfing genes and hypothesized a direct effect of dwarfing alleles on root growth during seedling establishment, rather than a secondary partitioning effect. Root systems of high length or length density have been identified as successful in limiting drought damage to yield, but there is no consensus as to whether root length in surface [7] or deep [5] layers is more desirable, and this is also linked to weather and water supply patterns [11,48]. Root mass seems more correlated with nutrient uptake than with water relations [49]. A large percentage of fine roots in ancient wheats is discussed in terms of advantage in fast water uptake during drought (water spenders) but not water use efficiency [11].

The variation in rhizosheath mass between varieties found in our experiment is comparable or lower than that reported in the literature. For wheat a three-fold variation of rhizosheath to root mass between varieties has been reported [19] whereas in our case the minimum value found in control Ciclope was about half that of control Saragolle which showed the maximum value of relative rhizosheath mass (Figure 7c). This is due to the

much lower root mass of Saragolle compared to Ciclope which more than compensates the lowest absolute value of rhizosheath mass (Figure 7a). Finding Ciclope and Saragolle at the opposite extremes for relative rhizosheath mass data confirms what discussed for the opposite profiles of such two varieties regarding shoot and root growth. Simeto was the variety with highest absolute values of rhizosheath and percent increase of rhizosheath mass upon inoculation with T-22. Rhizosheath results add to growth and morphology in showing that Simeto had a distinctive profile where a rather large and thick root system is accompanied by a higher response to inoculation and a large amount of rhizosheath. This is somewhat contrary to literature reports where a larger rhizosheath is found in finer root systems (e.g., [23]). Also a comparison of ancient and modern wheats inoculated with Plant Growth Promoting Rhizobacteria (PGPR) suggests a reduced ability of modern cultivars to interact with PGPR [50]. The higher absolute and percent response of Simeto to inoculation with a fungal product based on *Trichoderma harzianum* T-22 in our data does not confirm a lower ability of modern wheats to entertain relations and respond to rhizosphere interactions.

Rhizosheaths have been mainly reported in terms of adaptation to arid environments [20] by enhancing water retention and preventing root dehydration whereas the role in water uptake is controversial [18]. Wheat varieties with larger rhizosheath have been shown to sustain higher transpiration in dry condition and stay alive beyond the permanent wilting point of varieties with smaller rhizosheath [19]. Alterations in soil porosity due to mucilages involved in rhizosheath formation [20] may play a role in continuity of water movement in conditions of alternating water supply. Rhizosheats also play a role in plant nutrition and soil penetration (e.g., [51]) therefore species and varietal differences in rhizosheath may be viewed as a generally advantageous trait, especially in conditions of low input and alternating conditions.

All wheat varieties showed a significantly higher rhizosheat mass in response to *Trichoderma* inoculation and this allows us to reject the null hypothesys with respect to the effect of T-22 on rhizosheath enhancement. To the best of our knowledge this is the first report of such an effect and it opens the way to new interpretations of effects of *Trichoderma* inoculation on improving plant growth: besides documented mechanisms based on growth hormones and resistance to pathogens (e.g., [30,39]), *Trichoderma* treatments may promote a better performance of plants through rhizosheath-mediated improvements of water relations [18], nutrition [51] and soil structure [20,21].

4. Materials and Methods

The experimental design was a factorial combination of (A) four tetraploid wheats (*Triticum durum* Desf., 2n = 4x = 28; AABB genome) and (B) two inoculation treatments with six replications.

4.1. Tetraploid Wheats

Italian tetraploid wheats consisted of three modern hard wheat varieties released in different years and an ancient wheat landrace:

Creso (1974, Yaktana-54/Norin 10-B//2*Cappelli-63/3/3*Tehuacan-60/4/Capelli-B144);

Simeto (1988, Capeiti-8/Valnova)

Creso and Simeto varieties were obtained by mutagenesis and crosses involving old wheat materials;

Ciclope (Trinakria/Berillo//Valnova/Trinakria) variety released in 2006, selected from crosses between breeding lines [52,53];

Saragolle Lucana: the first Italian landrace enrolled in the Italian Wheat Landrace Conservation Registry in 2014 (https://www.gazzettaufficiale.it/eli/gu/2014/01/28/22/sg/pdf, accessed date: 1 December 2021). It is an ancient durum wheat population safeguarded from the risk of genetic erosion through in situ/on farm conservation and

cultivation in the northern Basilicata (Sud Italy) area by the "Associazione Lucana Cerealisti di Antiche Varietà, ALCAV".

All four tetraploid wheats are referred to as varieties in the text.

4.2. Inoculation Treatments

Inoculation treatments were:

(i) Seed coating with a spores suspension of the commercial formulation Trianum P (Koppert, Berkel en Rodenrijs, The Netherlands) containing *Trichoderma harzianum* Rifai KRL-AG2 (T-22);

(ii) Seed coating with water (control without T-22).

4.3. Seedling Growth Conditions

Seeds were selected for weight uniformity within variety (Saragolle Lucana 68.5 ± 0.46 mg; Creso 48.6 ± 0.32 mg; Simeto 50.6 ± 0.33 mg; Ciclope 64.6 ± 0.41 mg). They were surface-sterilized with 0.6% Na-hypochlorite solution for 2 min, then with 70% ethanol for 2 min and then rinsed three times with sterile dH_2O.

Seeds for the *Trichoderma* treatment were coated with a mixture of a T-22 suspension at concentration of 10^6 spores mL^{-1}, or water as control, in 4 μL $seed^{-1}$ of Tween-20, applied to seeds guaranteeing a homogeneous distribution by continuous rotation, until complete adhesion and absorption, according to [34,54].

Two seeds were sown per pot, irrigated and thinned to 1 seedling per pot after 9 days. Pots were cylinders of 25 cm length and 2.8 cm diameter and were filled with 172.0 g +/− of a field collected silty loam soil with the following characteristics: sand (50–2000 μm) 43.6%, silt (2–50 μm) 34.2%, clay < 2 μm) 22.1%., pH 6.8; N 1.9 g kg^{-1}; phosphates (P_2O_5) 50.3 g kg^{-1}; potassium oxide (K_2O) 1430 g kg^{-1}.

Pots were arranged randomly in a custom-built growth cabinet and grown for 20 days after emergence (average T = 21.5 °C; average relative humidity 33.6%). After filling pots were brought to field capacity and thereafter irrigated every 3 days to replace 100% of gravimetrically-determined evapotranspiration.

4.4. Measurements

At the end of the experiment the following measurements were made:

Chlorophyll content index (CCI) on three leaves per plant with a leaf transmittance leaf clip chlorophyll concentration meter (MC-100 Apogee instruments U.S.A.):

$$CCI = T_{931}/T_{653}$$

where T_{931} = Leaf transmittance at 931 nm; T_{653} = Leaf transmittance at 653 nm

Biometric measurements: plant height to the uppermost internode and to the tip of the last fully expanded leaf, above-ground plant fresh and dry (after oven drying at 70 °C until constant weight) biomass after clipping at the soil level. The bottom of pots was removed and the soil was gently pushed from the bottom. On three replications the root system was extracted by washing over a mesh of 0.5 mm and placed in a transparent tray (200 × 250 mm) with a 4-mm to 5-mm deep layer of water and scanned by STD 4800 Image Acquisition System at 1200 DPI. After scanning roots were blotted and weighed to obtain the fresh root mass, then oven dried at 70 °C until constant weight to obtain the root dry mass. Root morphology was determined on scanned images using WinRhizo.

ArabidopsisV2009c image analysis software (Regent Instruments Inc., QC, Canada). The following traits were measured: total length (cm), surface area (cm^2), mean diameter (mm), volume (cm^3). All parameters were assessed on a plant basis, and the distribution of length, surface and volume were then classified into seven diameter classes from 0.0 to 3.5 mm in 0.5 mm increments. No roots with diameter larger than 3.5 mm were found.

We then calculated root to shoot biomass ratio (g g^{-1}), root length to plant height ratio (cm cm^{-1}), specific root length (root length per unit of root biomass (cm g^{-1}) and shoot height to mass ratio (cm g^{-1}).

On three replications the mass of rhizosheat soil was determined as follows: the root system was held by the plant basis and gently shaken free of bulk soil. The root was then transferred to a clean sheet of paper and the soil which was not firmly attached to roots was gently brushed off with a soft brush. The soil which remained attached to roots after this treatment was considered rhizosheath soil. The rhizosheath-root complex was then weighed to determine the fresh mass (RRhizFM g plant^{-1}), oven-dried at 105 °C and weighed again to obtain the dry mass (RRhizDM g plant^{-1}). Roots were thereafter washed over a 0.5 mm mesh, blotted and weighed to obtain the fresh root mass (RFM g plant^{-1}), then oven dried at 70 °C until constant weight to obtain the root dry mass (RDM g plant^{-1}). The rhizosheath soil fresh (RhizFM) and dry (RhizDM) mass were then calculated as:

$$\text{RhizFM} = \text{RRhizFM-RFM g plant}^{-1}$$

and

$$\text{RhizDM} = \text{RRhizDM-RDM g plant}^{-1}$$

We then calculated the percent increase of RhizDM following inoculation (RhizDMincr) as:

$$\text{RhizDMincr} = 100 * (\text{RhizDM of inoculated plants-RhizDM of control plants})/\text{RhizDm of control plants.}$$

As a consequence of the described procedures we had 6 replicated for the following variables: plant height, shoot dry mass, chlorophyll content index, root dry mass, and derived indices; the number of replicates was 3 for root length, surface area, diameter, volume, RhizFM, RhizDM, RhizDMincr and derived indices.

One-Way ANOVA was performed to test the significance of the main factor (A) wheat variety on RhizDMinc. Two-way ANOVA was performed to test the significance of the factorial combination of the two main factors (A) wheat variety and (B) inoculation treatments and their interaction for all other traits. Mean separation was performed using the post-hoc test of Tukey at p 0.05.

Author Contributions: Conceptualization, R.B., M.N., G.L. and M.A.; methodology, R.B. and M.N.; investigation, R.B. and R.L.; data curation, R.B, R.L and A.V.; writing-original draft preparation, R.B. and M.A.; writing-review and editing, A.V., M.N. and G.L.; funding acquisition, M.A. All authors have read and agreed to the published version of the manuscript.

Funding: This research was partly funded by the project "Ottimizzazione degli input per la sostenibilità della cerealicoltura lucana-CERESO" PSR Basilicata 2014-2020-Misura 16 "Cooperazione"-Sottomisura 16.2 grant number CUP B41F19000030002.

Data Availability Statement: Data presented in this study are available on request from the corresponding author.

Conflicts of Interest: The authors declare no conflict of interest. The funders had no role in the design of the study; in the collection, analyses, or interpretation of data; in the writing of the manuscript, or in the decision to publish the results.

References

1. Hanslin, H.M.; Bischoff, A.; Hovstad, K.A. Root growth plasticity to drought in seedlings of perennial grasses. *Plant Soil* **2019**, *440*, 551–568. [CrossRef]
2. Agren, G.I.; Franklin, O. Root: Shoot ratios, optimization and nitrogen productivity. *Ann. Bot.* **2003**, *92*, 795–800. [CrossRef] [PubMed]
3. Nakhforoosh, A.; Grausgruber, H.; Kauland, H.P.; Bodner, G. Dissection of drought response of modern and underutilized wheat varieties according to Passioura's yield-water framework. *Front. Plant Sci.* **2015**, *6*, 570. [CrossRef] [PubMed]
4. Nakhforoosh, A.; Bodewein, T.; Fiorani, F.; Bodner, G. Identification of water use strategies at early growth stages in durum wheat from shoot phenotyping and physiological measurements. *Front. Plant Sci.* **2016**, *7*, 1155. [CrossRef] [PubMed]
5. Richards, R.A. Genetic Opportunities to Improve Cereal Root Systems for Dryland Agriculture. *Plant Prod. Sci.* **2008**, *11*, 12–16. [CrossRef]

6. Wasson, A.P.; Richards, R.A.; Chatrath, R.; Misra, S.C.; Prasad, S.V.S.; Rebetzke, G.J.; Kirkegaard, J.A.; Christopher, J.; Watt, M. Traits and selection strategies to improve root systems and water uptake in water-limited wheat crops. *J. Exp. Bot.* **2012**, *63*, 3485–3498. [CrossRef]
7. Motzo, R.; Atene, G.; Deidda, M. Genotypic variation in durum wheat root systems at different stages of development in a Mediterranean environment. *Euphytica* **1992**, *66*, 197–206. [CrossRef]
8. Rich, S.M.; Christopher, J.; Richards, R.; Watt, M. Root phenotypes of young wheat plants grown in controlled environments show inconsistent correlation with mature root traits in the field. *J. Exp. Bot.* **2020**, *71*, 4751–4762. [CrossRef]
9. Watt, M.; Moosavi, S.; Cunningham, S.C.; Kirkegaard, J.A.; Rebetzke, G.J.; Richards, R.A. A rapid, controlled-environment seedling root screen for wheat correlates well with rooting depths at vegetative, but not reproductive, stages at two field sites. *Ann. Bot.* **2020**, *112*, 447–455. [CrossRef]
10. Figueroa-Bustos, V.; Palta, J.A.; Chen, Y.; Siddique, K.H.M. Characterization of Root and Shoot Traits in Wheat Cultivars with Putative Differences in Root System Size. *Agronomy* **2018**, *8*, 109. [CrossRef]
11. Nakhforoosh, A.; Grausgruber, H.; Kaul, H.P.; Bodner, G. Wheat root diversity and root functional characterization. *Plant Soil* **2014**, *380*, 211–229. [CrossRef]
12. Akman, H.; Akgun, N.; Tamkoc, A. Screening for root and shoot traits in different wheat species and wild wheat relatives. *Bot. Sci.* **2017**, *95*, 147–154. [CrossRef]
13. Gioia, T.; Nagel, K.A.; Beleggia, R.; Fragasso, M.; Ficco, D.B.; Pieruschka, R.; Vita, P.D.; Fiorani, F.; Papa, R. Impact of domestication on the phenotypic architecture of durum wheat under contrasting nitrogen fertilization. *J. Exp. Bot.* **2015**, *66*, 5519–5530. [CrossRef]
14. Iannucci, A.; Fragasso, M.; Beleggia, R.; Nigro, F.; Papa, R. Evolution of the Crop Rhizosphere: Impact of Domestication on Root Exudates in Tetraploid Wheat (*Triticum turgidum* L.). *Front. Plant Sci.* **2017**, *8*, 2124. [CrossRef] [PubMed]
15. Levitt, J. *Responses of Plants to Environmental Stresses*; Academic Press: New York, NY, USA, 1980.
16. Iannucci, A.; Canfora, L.; Nigro, F.; De Vita, P.; Beleggia, R. Relationships between root morphology, root exudate compounds and rhizosphere microbial community in durum wheat. *Appl. Soil Ecol.* **2021**, *158*, 103781. [CrossRef]
17. Pang, J.; Ryan, M.H.; Siddique, K.H.M.; Simpson, R.J. Unwrapping the rhizosheath. *Plant Soil.* **2017**, *418*, 129–139. [CrossRef]
18. Ahmadi, K.; Zarebanadkouki, M.; Ahmed, M.A.; Ferrarini, A.; Kuzyakov, Y.; Kostka, S.I.; Carminati, A. Rhizosphere engineering: Innovative improvement of root environment. *Rhizosphere* **2017**, *3*, 176–184. [CrossRef]
19. Basirat, M.; Mousavi, S.M.; Abbaszadeh, S.A.; Ebrahimi, M.; Zarebanadkouki, M. The rhizosheath: A potential root trait helping plants to tolerate drought stress. *Plant Soil* **2019**, *445*, 565–575. [CrossRef]
20. Amato, M.; Bochicchio, R.; Mele, G.; Labella, R.; Rossi, R. Soil structure and stability in the spermosphere of myxosdiaspore chia (*Salvia hispanica* L.). *Soil Res.* **2018**, *57*, 546–558. [CrossRef]
21. Di Marsico, A.; Scrano, L.; Amato, M.; Gàmiz, B.; Real, M.; Cox, L. Influence of mucilage from seeds of chia (*Salvia hispanica* L.) as an amendment, on the sorption-desorption of herbicides in agricultural soils. *Sci. Tot. Env.* **2018**, *625*, 531–538. [CrossRef]
22. Watt, M.; Mc Cully, M.E.; Canny, M.J. Formation and stabilization of rhizosheaths of *Zea mays* L. *Plant Physiol.* **1994**, *106*, 179–186. [CrossRef] [PubMed]
23. Hartnett, D.C.; Wilson, G.W.; Ott, J.; Setshogo, M. Variation in root system traits among african semi-arid savanna grasses: Implications for drought tolerance. *Austral. Ecol.* **2013**, *38*, 383–392. [CrossRef]
24. Brown, L.K.; George, T.S.; Neugebauer, K.; White, P.J. The rhizosheath—A potential trait for future agricultural sustainability occurs in orders throughout the angiosperms. *Plant Soil* **2017**, *418*, 115–128. [CrossRef]
25. Ndour, P.M.S.; Barry, C.M.; Tine, D.; de la Fuente Cantó, C.; Gueye, M.; Barakat, M.; Ortet, P.; Achouak, W.; Ndoye, I.; Sine, B.; et al. Pearl millet genotype impacts micro-bial diversity and enzymatic activities in relation to root-adhering soil aggregation. *Plant Soil* **2021**, *464*, 109–129. [CrossRef]
26. Zin, N.A.; Badaluddin, N.A. Biological functions of *Trichoderma* spp. for agriculture applications. *Ann. Agric. Sci.* **2020**, *65*, 168–178.
27. Woo, S.L.; Lorito, M. Exploiting the interactions between fungal antagonists, pathogens and the plant for biocontrol. In *Novel Biotechnologies for Biocontrol Agent Enhancement and Management*; Vurro, M., Gressel, J., Eds.; NATO Security through Science Series; Springer: Dordrecht, The Netherlands, 2006; pp. 107–130.
28. Vitti, A.; La Monaca, E.; Sofo, A.; Scopa, A.; Cuypers, A.; Nuzzaci, M. Beneficial effects of *Trichoderma harzianum* T-22 in tomato seedlings infected by *Cucumber mosaic virus* (CMV). *Biocontrol* **2015**, *60*, 135–147. [CrossRef]
29. Vitti, A.; Pellegrini, E.; Nali, C.; Lovelli, S.; Sofo, A.; Valerio, M.; Scopa, A.; Nuzzaci, M. *Trichoderma harzianum* T-22 induces systemic resistance in tomato infected by *Cucumber Mosaic Virus*. *Front. Plant Sci.* **2016**, *7*, 1520. [CrossRef] [PubMed]
30. Harman, G.; Khadka, R.; Doni, F.; Uphoff, N. Benefits to plant health and productivity from enhancing plant microbial symbionts. *Front. Plant Sci.* **2021**, *11*, 610065. [CrossRef] [PubMed]
31. Woo, S.; Ruocco, M.; Vinale, F.; Nigro, M.; Marra, R.; Lombardi, N.; Pascale, A.; Lanzuise, S.; Manganiello, G.; Lorito, M. *Trichoderma*-based products and their widespread use in agriculture. *Open Mycol. J.* **2014**, *8*, 71–126. [CrossRef]
32. Vitti, A.; Sofo, A.; Scopa, A.; Nuzzaci, M. Sustainable agricultural practices in disease defence of traditional crops in Southern Italy: The case study of tomato cherry protected by *Trichoderma harzianum* T-22 Against *Cucumber Mosaic Virus* (CMV). In *The Sustainability of Agro-Food and Natural Resource Systems in the Mediterranean Basin*; Vastola, A., Ed.; Springer: Heidelberg, Germany, 2015; pp. 133–143.

33. Sarrocco, S.; Vannacci, G. Preharvest application of beneficial fungi as a strategy to prevent postharvest mycotoxin contamination: A review. *Crop. Prot.* **2018**, *110*, 160–170. [CrossRef]
34. Kthiri, Z.; Jabeur, M.B.; Machraoui, M.; Gargouri, S.; Hiba, K.; Hamada, W. Coating seeds with Trichoderma strains promotes plant growth and enhance the systemic resistance against Fusarium crown rot in durum wheat. *Egypt J. Biol. Pest. Control* **2020**, *30*, 1–10. [CrossRef]
35. Lucini, L.; Colla, G.; Miras Moreno, M.B.; Bernardo, L.; Cardarelli, M.; Terzi, V.; Bonini, P.; Rouphaelf, Y. Inoculation of *Rhizoglomus irregulare* or *Trichoderma atroviride* differentially modulates metabolite profiling of wheat root exudates. *Phytochemistry* **2019**, *157*, 158–167. [CrossRef] [PubMed]
36. Fiorentino, N.; Ventorino, V.; Woo, S.L.; Pepe, O.; De Rosa, A.; Gioia, L.; Romano, I.; Lombardi, N.; Napolitano, M.; Colla, G.; et al. *Trichoderma*-based biostimulants modulate rhizosphere microbial populations and improve N uptake efficiency, yield and nutritional quality of leafy vegetables. *Fron. Plant Sci.* **2018**, *9*, 743. [CrossRef] [PubMed]
37. Tucci, M.; Ruocco, M.; De Masi, L.; De Palma, M.; Lorito, M. The beneficial effect of *Trichoderma* spp. on tomato is modulated by the plant genotype. *Mol. Plant Pathol.* **2011**, *12*, 341–354. [PubMed]
38. Sofo, A.; Scopa, A.; Manfra, M.; De Nisco, M.; Tenore, G.; Troisi, J.; Di Fiori, R.; Novellino, E. *Trichoderma harzianum* strain T-22 induces changes in phytohormone levels in cherry rootstocks (*Prunus cerasus* × *P. canescens*). *Plant Growth Regul.* **2011**, *65*, 421–425. [CrossRef]
39. Sofo, A.; Tataranni, G.; Xiloyannis, C.; Dichio, B.; Scopa, A. Direct effects of Trichoderma harzianum strain T-22 on micropropagated GiSeLa6® (*Prunus cerasus* × *Prunus canescens*) rootstocks. *Environ. Exp. Bot.* **2012**, *76*, 33–38. [CrossRef]
40. Illescas, M.; Pedrero-Méndez, A.; Pitorini-Bovolini, M.; Hermosa, R.; Monte, E. Phytohormone Production Profiles in *Trichoderma* Species and Their Relationship to Wheat Plant Responses to Water Stress. *Pathogens* **2021**, *10*, 991. [CrossRef]
41. Contreras-Cornejo, H.A.; Macias-Rodriguez, L.; Cortes-Penagos, C.; Lopez-Bucio, J. *Trichoderma virens*, a plant beneficial fungus, enhances biomass production and promotes lateral root growth through an auxin-dependent mechanism in Arabidopsis. *Plant Physiol.* **2009**, *149*, 1579–1592. [CrossRef] [PubMed]
42. Contreras-Cornejo, H.A.; Macias-Rodriguez, L.; Alfaro-Cuevas, R.; Lopez-Bucio, J. Trichoderma spp. improve growth of Arabidopsis seedlings under salt stress through enhanced root development, osmolyte production, and Na+ elimination through root exudates. *Mol. Plant-Microbe Interact.* **2014**, *27*, 503–514. [CrossRef]
43. López-Coria, M.; Hernández-Mendoza, J.L.; Sánchez-Nieto, S. *Trichoderma asperellum* Induces Maize Seedling Growth by Activating the Plasma Membrane H+-ATPase. *Mol. Plant Microbe Interact.* **2016**, *29*, 797–806. [CrossRef]
44. Harman, G.E.; Howell, C.R.; Viterbo, A.; Chet, I.; Lorito, M. Trichoderma species—Opportunistic, avirulent plant symbionts. *Nat. Rev. Microbiol.* **2004**, *2*, 43–56. [CrossRef]
45. Brouwer, R. Nutritive influences on the distribution of dry matter in the plant. *Neth. J. Agric. Sci.* **1962**, *10*, 399–408. [CrossRef]
46. Davidson, R.L. Effect of root/leaf temperature differentials on root/shoot ratios in some pasture grasses and clover. *Ann. Bot.* **1969**, *33*, 561–569. [CrossRef]
47. Wojciechowski, T.; Gooding, M.J.; Ramsay, L.; Gregory, P.J. The effects of dwarfing genes on seedling root growth of Wheat. *J. Exp. Bot.* **2009**, *60*, 2565–2573. [CrossRef] [PubMed]
48. Nakhforoosh, A.; Nagel, K.A.; Fiorani, F.; Bodner, G. Deep soil exploration vs. topsoil exploitation: Distinctive rooting strategies between wheat landraces and wild relatives. *Plant Soil* **2021**, *459*, 397–421. [CrossRef] [PubMed]
49. Bakhshandeh, S.; Kertesz, M.A.; Corneo, P.E.; Dijkstra, F.A. Dual-labeling with 15N and H218O to investigate water and N uptake of wheat under different water regimes. *Plant Soil* **2016**, *408*, 429–441. [CrossRef]
50. Valente, F.G.; Le Gouis, J.; Moënne-Loccoz, Y.; Prigent–Combaret, C. Ancient wheat varieties have a higher ability to interact with plant growth-promoting rhizobacteria. *Plant Cell Environ.* **2019**, *43*, 246–260. [CrossRef] [PubMed]
51. Haling, R.E.; Brown, L.K.; Bengough, A.G.; Young, I.M.; Hallett, P.D.; White, P.J.; George, T.S. Root hairs improve root penetration, root–soil contact, and phosphorus acquisition in soils of different strength. *J. Exp. Bot* **2013**, *64*, 3711–3721. [CrossRef]
52. Marzario, S.; Logozzo, G.; David, J.L.; Zeuli, P.S.; Gioia, T. Molecular Genotyping (SSR) and Agronomic Phenotyping for Utilization of Durum Wheat (Triticum durum Desf.) Ex Situ Collection from Southern Italy: A Combined Approach Including Pedigreed Varieties. *Genes* **2018**, *9*, 465. [CrossRef] [PubMed]
53. Mangini, G.; Gadaleta, A.; Colasuonno, P.; Marcotuli, I.; Signorile, A.M.; Simeone, R.; Vita, P.D.; Mastrangelo, A.M.; Laidò, G.; Pecchioni, N.; et al. Genetic dissection of the relationships between grain yield components by genome-wide association mapping in a collection of tetraploid wheats. *PLoS ONE* **2018**, *13*, e0190162.
54. Kthiri, Z.; Jabeur, M.B.; Chairi, F.; López-Cristoffanini, C.; López-Carbonell, M.; Serret, M.D.; Araus, J.L.; Karmous, C.; Hamada, W. Exploring the Potential of Meyerozyma guilliermondii on Physiological Performances and Defense Response against Fusarium Crown Rot on Durum Wheat. *Pathogens* **2021**, *10*, 52. [CrossRef] [PubMed]

plants

MDPI

Review

Metal Detoxification in Land Plants: From Bryophytes to Vascular Plants. STATE of the Art and Opportunities

Elisa Fasani [1,†], Mingai Li [2,†], Claudio Varotto [2], Antonella Furini [1,*] and Giovanni DalCorso [1,*]

[1] Department Biotechnology, University of Verona, Str. Le Grazie 15, 37131 Verona, Italy; elisa.fasani@univr.it
[2] Department of Biodiversity and Molecular Ecology, Research and Innovation Centre, Fondazione Edmund Mach, Via E. Mach 1, 38010 San Michele all' Adige, Italy; mingai.li@fmach.it (M.L.); claudio.varotto@fmach.it (C.V.)
* Correspondence: antonella.furini@univr.it (A.F.), giovanni.dalcorso@univr.it (G.D.)
† These authors contributed equally to this work.

Abstract: Potentially toxic elements are a widespread concern due to their increasing diffusion into the environment. To counteract this problem, the relationship between plants and metal(loid)s has been investigated in the last 30 years. In this field, research has mainly dealt with angiosperms, whereas plant clades that are lower in the evolutive scale have been somewhat overlooked. However, recent studies have revealed the potential of bryophytes, pteridophytes and gymnosperms in environmental sciences, either as suitable indicators of habitat health and elemental pollution or as efficient tools for the reclamation of degraded soils and waters. In this review, we summarize recent research on the interaction between plants and potentially toxic elements, considering all land plant clades. The focus is on plant applicability in the identification and restoration of polluted environments, as well as on the characterization of molecular mechanisms with a potential outlet in the engineering of element tolerance and accumulation.

Keywords: heavy metals; evolution; hyperaccumulation

Citation: Fasani, E.; Li, M.; Varotto, C.; Furini, A.; DalCorso, G. Metal Detoxification in Land Plants: From Bryophytes to Vascular Plants. STATE of the Art and Opportunities. *Plants* **2022**, *11*, 237. https://doi.org/10.3390/plants11030237

Academic Editors: Milan S. Stankovic, Paula Baptista and Petronia Carillo

Received: 30 December 2021
Accepted: 15 January 2022
Published: 18 January 2022

Publisher's Note: MDPI stays neutral with regard to jurisdictional claims in published maps and institutional affiliations.

1. Introduction

Elements that have a density of more than 5 g/cm^3 are defined as heavy metals (HMs) [1]. They are present mainly in rock formations, from where they can be released either by natural erosive processes or anthropical intervention; only a limited number of heavy metals are soluble under physiological conditions and thus, bioavailable to living organisms. A certain number of HM is essential for the normal metabolic functioning of organisms (i.e., iron [Fe], molybdenum [Mo], manganese [Mn], zinc [Zn], nickel [Ni], copper [Cu] and cobalt [Co]); both their deficiency and excess can lead to physiological stress due to nutritional imbalance and toxicity. Others (such as arsenic [As], silver [Ag], mercury [Hg], antimony [Sb], cadmium [Cd] and lead [Pb]) have no known biological function and are toxic even when present at low concentration. More recently, the nomenclature *heavy metals* have encountered opposition between researchers, also because some toxic elements, such as As or selenium (Se), are not actual metals, but metalloids or non-metal elements; to overcome this issue, a great variety of definitions have been proposed (for an overview about this topic, refer to an opinion by Duffus [2])). In 2019, Pourret and Hursthouse [3] proposed the term *potentially toxic elements* (PTE) instead of heavy metals in studies concerning environmental science. We will adopt this term throughout the manuscript, therefore, including heavy metals under the chemical point of view, together with metalloids and other elements important for their toxicity towards living organisms; in cases where just genuine heavy metals are considered, we will refer to these with the abbreviation HMs.

Environmental pollution caused by a variety of anthropic activities has substantially increased the presence of PTEs in the biosphere, posing serious threats to all forms of

life [4]. PTE contamination can easily reach aquatic systems and soils and subsequently the food chain [5]. Pollution by metals or metalloids not only impacts crop production and quality but also affects atmosphere and water quality and endangers the health and life of plants, animals and human beings. Indeed, when essential PTEs are present in excess or unessential ones are introduced in the body even in small doses, they can cause adverse health effects in both acute and chronic dosing [6]. Symptoms of PTE toxicity in humans include neurological defects, cardiovascular, liver and kidney failure, and, if not promptly recognized as due to PTE exposure, can lead to severe clinical conditions [7,8]. Similarly, when the elevated concentrations of PTE are present in the soil they interfere with plant nutrient uptake, leading to toxicity symptoms and growth inhibition on most plant species [9].

At the cellular level, toxic or excess PTEs can displace and substitute metallic cofactors from enzymes and other proteins, such as transcription factors, altering enzyme activity and the expression patterns of numerous genes; in addition, the imbalance of metal homeostasis leads to damages to lipids, proteins and nucleic acids. The major toxicity route is the production of free radicals and *reactive oxygen species* (ROS), causing oxidative damage [10], followed by the activation of the activity of enzymes that contribute to ROS detoxification [11]. Thus, to minimize the induced damages, plants, as well as other organisms, have developed tightly regulated mechanisms to selectively take up essential elements and use them in metabolic functions, and to avoid or metabolically inactivate toxic/excessive ions. Enzymatic and non-enzymatic defense mechanisms are in charge of ROS control. Enzymatic scavenging of ROS is operated by antioxidants, such as superoxide dismutases (SOD), catalases (CAT), peroxidases (POD) and glutathione reductases as well as non-enzymatic antioxidant molecules including organic acids, glutathione, ascorbic acids, alpha-tocopherols and others [12]. In addition, intracellular and extracellular chelation mechanisms are crucial for PTE detoxification. The binding of PTEs to amino acids, metallothioneins and phytochelatins guarantees that excess or toxic elements are metabolically unavailable and eventually sequestered outside the cytoplasm (e.g., in vacuoles or cell wall) preventing their entrance into energy organelles [13]. Among land plants, different species have evolved various degrees of tolerance to PTEs, with consequent implications in their ability to survive and grow in contaminated areas. A variety of morphological and physiological properties are responsible for the capacity of different species to bind metals on their surfaces or to take them up intracellularly [14]. In this review we summarize actual knowledge on the plant—PTE relationship, taking into consideration the main land plant taxa, i.e., bryophytes and pteridophytes for spore-bearing plants, and gymnosperms and angiosperms as seed-bearing plants.

2. Spore-Bearing Plants

2.1. Bryophytes

Bryophyte is a class of non-vascular green land plants constituted by around 15,000 species [15]. As revealed by recent phylogenomic reconstructions [16,17], the three lineages of bryophytes (hornworts, mosses and liverworts) likely form a monophyletic clade which is the sister group to tracheophytes. Bryophytes are small, possess both simple morphology and anatomy with a dominant haploid life cycle, and are able to disperse either by spores or by vegetative propagules, such as fragments of leaf and thallus or specialized structures with a high regeneration capacity [15,18,19]. Bryophytes grow in diverse habitats, such as soil, tree trunks, barks and branches, as well as rock surfaces, and take the mineral nutrients required for their growth directly from the substances dissolved in the moist substrates they live on [20]. Due to the absence of epidermal cuticles and the high surface-to-volume ratio, bryophytes are highly susceptible to environmental impacts. In addition, their high ion-exchange capacity, ion chelation and wide geographical distribution make bryophytes excellent biological organisms for monitoring PTE pollution.

Because of anthropogenic activities associated with urbanization and industrial development, more and more non-degradable hazardous PTEs have been released into

the environment and entered natural habitats. Among the three lineages of bryophytes, mosses [21–24] and liverworts [25,26] have been widely explored as biological tools to assess PTE pollution in both terrestrial and aquatic environments. Bryophytes are, in fact, able to accumulate large quantities of HMs over their entire surface, either from the atmosphere or from the substrate, without visible negative impacts on their growth and development [27]. Positive correlations between PTE cellular accumulation and environmental levels have been identified in a range of bryophytes [28], confirming the relevance of these simple plants as biomonitors. Interestingly, there is a great variation in the accumulation of specific PTEs among different species and habitats [29]. For instance, the mosses *Funaria hygrometrica* and *Warnstorfia fluitans* accumulate large quantities of Pb and As, respectively [30,31]. The liverwort *Marchantia polymorpha* accumulates high levels of Cu, Zn and Cd [32,33]. Bryophytes have also the capacity to concentrate rare earth elements [34]. Thus, the evergreen bryophytes allow following the presence of specific elements and their deposition patterns in the respective environment over defined time spans.

Despite their apparent structural simplicity, bryophytes have developed a set of different strategies to tolerate elemental stress. As a general mechanism, they can produce cell wall barriers to prevent PTEs from entering their protoplasts [35]. For example, the moss *Scorpiurum circinatum* was shown to immobilize toxic metal ions in its cell walls [36]; similarly, excessive Zn intake was blocked by the cell wall and plasma membrane in the moss *Pohilia drummondii* [37]. However, the molecular regulation of cell wall biosynthesis and composition still needs further elucidation to understand their role in PTE tolerance in bryophytes. In addition to cell walls, differences in cation exchange capacities and transporter activity in the plasma membrane could generate different elemental tolerance among different species of this clade [38]. Inside the cell, chelation of ions by cysteine-rich oligopeptides glutathione (GSH) and phytochelatins (PCs) is a fundamental approach employed for PTE detoxification; ligand synthesis, accumulation in the cytoplasm and sequestration into vacuoles by ATP-binding cassette (ABC) transporters have been demonstrated to confer tolerance to different extents [39,40]. Although both GSH and PCs have been identified in all three lineages of bryophytes [41], the main contributor to metal chelation is apparently different among the species. At least with regards to Cd, its detoxification is mainly driven by GSH in the case of the moss *Leptodictyum riparium* [42], whereas PCs play essential roles in the liverwort *M. polymorpha* [43]. In addition to ion chelation, the antioxidant defense system, comprising a diverse array of enzymatic and non-enzymatic components, is also an efficient and sophisticated regulator to cope with oxidative stress induced by PTEs [44]. For instance, modulation of the activity of antioxidant enzymes (CATs and PODs) was observed in the *moss Hypnum plumaeforme* [45], as well as in the aquatic bryophyte *Fontinalis antipyretica* subjected to metal exposure [46]. Thus, despite the application of these mechanisms being species-specific, the measurement of intracellular ROS content and/or of antioxidant activity provides an effective overview for the overall intracellular redox state in response to PTE stress.

2.2. Pteridophytes

Pteridophytes are a paraphyletic group of plants encompassing ferns and other related clades (lycophytes and monilophytes; [47]), that constitute the second largest group among land plants [48]. Despite the crown age of pteridophytes dating back to about 400 million years before the present [49], the majority of extant pteridophyte species result from a secondary diversification that took place concomitantly to angiosperm diversification [50]. The patterns of adaptive evolution and diversification in extant pteridophytes, therefore, largely parallel those observed in flowering plants [51]. Ferns represent the large majority among the ca. 13,000 species of pteridophytes currently recognized [47], thus constituting a group of primary interest to study the evolution of metal(loid) tolerance and hyperaccumulation in vascular plants and their potential use in phytoremediation [52–55]. In particular, some aquatic ferns from genera *Salvinia* and *Azolla* (family Salviniaceae) can accumulate with good efficiency a wide range of PTE like Au, Cd, Cr, Cs, Cu, Mn, Ni, Pb, Sr and Zn [56–58];

in view of this, they could be useful for the phytoremediation of contaminated wastewaters like industrial effluents and sewage water [53,58–64].

In the genus *Salvinia*, several species (*S. auriculata*, *S. biloba*, *S. herzogii*, *S. minima*, *S. molesta*, *S. natans* and *S. rotundifolia*) have the capacity to accumulate PTEs in sufficiently high amounts to be used for efficient wastewater depuration (e.g., [65–75]), reaching accumulation ranges of 6000–18,000 mg Kg^{-1} dry weight for Cd, Cr, Cu, Fe, Ni and Pb [57,64,76,77]. Natural variation in the capacity to accumulate PTEs exists among species, as in the case of *Azolla*, another aquatic fern genus with good potential for wastewater phytoremediation. *Azolla caroliniana*, for instance, can accumulate As, Cd, Cr, Hg and Pb in the range between 284–963 mg Kg^{-1}, while *A. filiculoides* has been reported to accumulate about 10 times as much Cd, Cr, Cu and Pb (6500–9300 mg Kg^{-1}). By contrast, *A. pinnata* is a Pb accumulator (ca. 2700 mg Kg^{-1}) but can accumulate amounts of Cr, Cu, Hg and Cd (ca. 210–740 mg Kg^{-1}) comparable to those of *A. caroliniana* [64].

Additionally, several species of land ferns have been reported to grow in soils contaminated by a variety of different PTEs and are thus, considered valuable ecological indicators of metal pollution [78]. Recent surveys of fern species that are abundant in mining areas reveal a good potential for the exploitation of some of them (especially from the *Pityrogramma* and *Pteris* genera) for mine rehabilitation and/or metal recovery [79–81]. Among the seven orders currently recognized of leptosporangiate ferns (subclass Polypodiidae, the most represented among ferns), [82], metal tolerance and accumulation has been studied most intensively in the Polypodiales order, where representative species from more than 13 genera have been characterized so far [53,64]. The most promising Polypodiales genera for phytoremediation are *Adiantum*, *Asplenium*, *Athyrium*, *Azolla*, *Blechnum*, *Nephrolepis*, *Pellaea* and *Pteris*, which display a high degree of natural variation in their ability to accumulate or hyperaccumulate different metals and the metalloid As. For instance, accumulation of Cd varies from only 4.1 mg Kg^{-1} in *Nephrolepis cordifolia* to 1095 mg Kg^{-1} in *Athyrium yokoscense*; Pb varies between 62 mg Kg^{-1} in *Pteris falcata* to 2040–3464 in *Athyrium yokoscense*; Zn from 216 mg Kg^{-1} in *Blechnum nudum* to 2422 mg Kg^{-1} in *Athyrium yokoscense*; As from 814 mg Kg^{-1} in *Athyrium yokoscense* to 14,500 mg Kg^{-1} in *Pteris vittata* [64].

Among the species investigated, three gained recent and widespread attention for their outstanding accumulation capacity of PTEs, namely *Athyrium yokoscense*, *Pityrogramma calomelanos* and *Pteris vittata*. Among them, *A. yokoscense* is the one with the broadest specificity and overall highest accumulation levels. Indeed, *A. yokoscense* can not only accumulate Cd and Pb to about 1000 mg Kg^{-1} and 10,000 mg Kg^{-1}, respectively [83,84], but is also highly tolerant and accumulates Zn and Cu up to more than 9000 mg Kg^{-1} and 3300 mg Kg^{-1} in the roots, respectively [85]. *A. yokoscense* is also an efficient As accumulator, with concentrations of this metalloid reaching up to 922 mg Kg^{-1} and 2192 mg Kg^{-1} in above-ground and below-ground organs, respectively [86]. By comparison, *P. calomelanos* and *P. vittata* display a lower capacity to accumulate metals, but they accumulate As to higher levels than *A. yokoscense* [79,86]. *P. calomelanos* can accumulate large amounts of As (>8000 mg Kg^{-1} dry mass) mostly in its fronds, while in the rhizoids As concentration does not exceed 310 mg Kg^{-1} dry mass [87,88]. Similarly, *P. vittata* commonly accumulates As mainly in above-ground organs in concentrations up to 7500 mg Kg^{-1} without any detectable toxic effects, but even higher concentrations of As in fronds (>22,000 mg Kg^{-1}) have also been reported [89,90]. Both bioconcentration factor (BCF; the ratio between As concentration in plant tissues and As concentration in soil) and translocation factor (TF; the ratio between As concentration in fronds and As concentration in roots) of *P. vittata* can reach impressively high values, respectively up to 63 and 25 [91,92]. For these reasons, in recent years *P. vittata* has become a valuable model to elucidate the molecular mechanisms for As hyperaccumulation [93]. Both the diploid sporophyte and the haploid gametophyte of *Pteris vittata* can withstand the major forms of environmental arsenic, arsenate (As(V)) and arsenite (As(III)) [90]. According to a recent model of As hyperaccumulation in *P. vittata* gametophyte cells [94], arsenate is taken up into the cytoplasm by the phosphate transporter PvPht1;3 [95], while arsenite uptake is mediated by Tonoplast Intrinsic Protein

4 (PvTIP4) [96]. Once inside the cell, arsenite is directly transported across the tonoplast membrane by the PvACR3 transporter [97] for long-term storage in the vacuole as free arsenite [98]. On the other hand, cytoplasmic arsenate can undergo two different fates: (i) it can be reduced to arsenite by the arsenate reductase PvACR2 [99], or (ii) converted to 1-arseno-3-phosphoglyerate (1-As-3-PG) by PvGAPC1, an unusual glyceraldehyde 3-phosphate dehydrogenase with a very high affinity for arsenate [94]. The Organic Cation Transporter protein (PvOCT4) transports 1-As-3-PG into cytoplasmic vesicles, where it is reduced to arsenite by PvGSTF1, a glutathione S-transferase with arsenate reductase activity, and/or by PvACR2. Fusion of the vesicles to the tonoplast releases the arsenite into the vacuole [94].

3. Seed-Bearing Plants: Gymnosperms and Angiosperms

Progressing with evolution, Spermatophyta, i.e., seed-bearing vascular plants, comprise two sister groups, gymnosperms and flowering plants, angiosperms. If the first represent roughly 1% of total plant diversity and are confined mostly to boreal environments and high-elevation lands, angiosperms account for almost 90% of all plant species and are widespread in all Earth's ecosystems (the rest are non-seed bearing plants, [100]). On the other hand, the former group can be roughly approximated with conifers, which are the most diverse group worldwide, clustering more than 600 species [100,101].

3.1. Gymnosperms

Published literature regarding PTE accumulation in gymnosperms is scarce if compared to angiosperms. The majority of published papers deal with the exploitation of gymnosperms as biological monitors [102]. In this context, as previously mentioned for bryophytes, plants are helpful (*i*) to estimate the actual environmental contamination in a particular site, due to the HMs or radionuclides deposition on leaves, and (*ii*) to record contamination across time, e.g., the temporal evolution of PTE availability in the environment, analyzing metal content in bark sheets [103]. Interestingly, while for some authors utilization of biological material for environmental quality monitoring is rather accepted as reliable and affordable [101], recent works pointed out that the usefulness of coniferous trees as bioindicators of pollution may be debatable, especially for those elements that can act as micronutrients. More robust data can be obtained on non-essential elements, such as Cd, Pb, or Hg, whose absorption and mobility across the plant tissues are limited [103]. The effect of PTEs on gymnosperms has been studied, revealing that also members of this clade are characterized by great variability in terms of sensitivity to metal(loid) ions, depending on the element utilized, the plant species considered and the cultural conditions. Indeed, most experiments have been carried out on a laboratory scale, such as in vitro or hydroponic cultures, analyzing germination and behavior of seedlings or young trees [102]. A range of publications deals with the accumulation of trace elements in needles of plants growing in contaminated areas, highlighting that plant behavior in metal uptake largely depends on the species, the metal considered and the environmental context. As for the latter, the presence of airborne pollution and soil elemental levels influence direct uptake via needles, root absorption and translocation processes [104]. For instance, four-year-old *Pinus sylvestris* plants resulted to be more sensitive to Ni and less to Cu, even though both metals determine injuries on fine roots and needles [105]. In *Picea abies* treated with Cd, Pb, Cu, and Zn, the harshest effects were produced by Cd on germination and by Cu and Pb on growth [106].

Common mechanisms, shared with angiosperm relatives, have been pointed out, such as the activity of antioxidant enzymes; for example, superoxide dismutase induction by excess Zn in *P. sylvestris* [107], or increase in peroxidase activity in *P. abies* grown in soil contaminated with Cd [108] counteract the negative effects due to metal-induced ROS production. The response to PTEs in the growth substrate is highly dependent on the plant species and the metal concentrations applied. For example, treating a *P. abies* cell culture with Cd and As induced the synthesis of GSH-S transferases, enzymes known to be

involved in contrasting oxidative damages and membrane lipid peroxidation. Interestingly, Pb treatment does not induce the same effect [109].

Additionally, PCs already mentioned non-protein thiols, are involved in metal ion chelation and detoxification by transport and compartmentalization to specific cell districts, such as the vacuole [110]. The production of PCs in response to treatment with metal ions, such as Cd has been confirmed for a long time in coniferous plants (i.e., *Pinus*, *Abies* and *Picea*), *Gingko biloba* and *Cycas revoluta* [111]. Additionally, Fe, Mn and Pb enhanced PC accumulation in needles of *P. sylvestris* grown in contaminated sites, consistently with the increased amount of metals accumulated in the same tissues [101]. A similar effect in stimulating PC accumulation was reported in *Picea rubens* cell suspensions treated with excess Zn and Cd [112].

Considering degraded soils and the possibility of reclamation by means of reforestation, the understanding of plant tolerance to PTE abundance helps in choosing the right species for reforestation of a particular site. According to this, recent literature has emerged dealing with pollution tolerance and maintenance of fitness upon growth on polluted sites. For instance, Curguz et al., [106] found that seedlings of *P. abies* are particularly tolerant to high soil concentrations of Zn, Cd, Cu and Pb, and the spruce could be selected for reforestation in Serbia, whose subsoil was reported to be contaminated with these metals. Another example considered reclamation of polluted soils due to mining activities in Northern Africa by phytostabilization of metals with ecto-mycorrhized *Pinus halepensis*. Indeed, the presence of ectomycorrhizae significantly reduced root-to-shoot translocation of Zn and Cd, enhancing *P. halpensis* tolerance toward these metals [113]. Coniferous plants are particularly adapted to cold-climate regions. *P. sylvestris*, thanks to its high adaptability, is frequently proposed for remediation of soil polluted by industrial activities, and can, therefore, be suitable for reforestation of degraded boreal lands, even though its ability to tolerate and accumulate PTEs is much lower compared to herbaceous species (see later in the text) [114,115]. Indeed, recent experiments showed that *P. sylvestris* behaves as more sensitive in comparison with angiosperm: root and shoot growth of *P. sylvestris* is inhibited by Pb, Zn, and Cd treatment, which also perturbed plant mineral nutrition [113]. Moreover, germination and seedling growth were also inhibited in *P. sylvestris* challenged with moderate (50 μM) Zn excess, and metal accumulation increased in seedling roots rather than in stems, pointing to a retention of the contaminant in the root [107]. Similarly, in four-week-old hybrid *Larix* (*L. x eurolepis*), double Cd accumulation has been detected in roots compared to shoots [116]. Such accumulation in roots rather than in shoots of gymnosperms has been described frequently [102], pointing to a retention of the excess PTE in the roots to preserve photosynthetic tissues from potentially toxic ion concentrations. The accumulation and compartmentation of toxic ions have evolved as a tolerance strategy and allowed plant growth and reproduction in metalliferous soils (either naturally contaminated or degraded by anthropogenic activities).

3.2. Angiosperms and the Evolution of the Hyperaccumulation and Hypertolerance Traits

Adopted by both pteridophytes and angiosperms, worth of note is the evolution of the hypertolerance and hyperaccumulation traits (Figure 1), which are not represented in woody plant species belonging to the gymnosperms [102,117,118]. In angiosperms, due to the relative easiness of intra- and inter-specific crosses, both traits have been extensively studied in experiments with segregating populations derived by crosses between phylogenetically closed species characterized by opposite behavior in terms of metal accumulation and tolerance. Genetic determinants of the two traits, organized in quantitative trait loci, are different; indeed, PTE tolerance can be achieved through two opposite mechanisms. Some plants tend to exclude toxic ions from absorption, thereby limiting the root-to-shoot translocation of the metals to physiological concentrations and are, therefore, tolerant but not accumulators of the PTE. Conversely, other species evolved the ability to accumulate great amounts of PTE in their aerial parts, where the ions are sequestered in apposite cell tissues and/or compartments, removing them from the cytosolic environment [119]. These

species are both tolerant and, due to their accumulation ability, defined hyperaccumulators (for a review, see [120]).

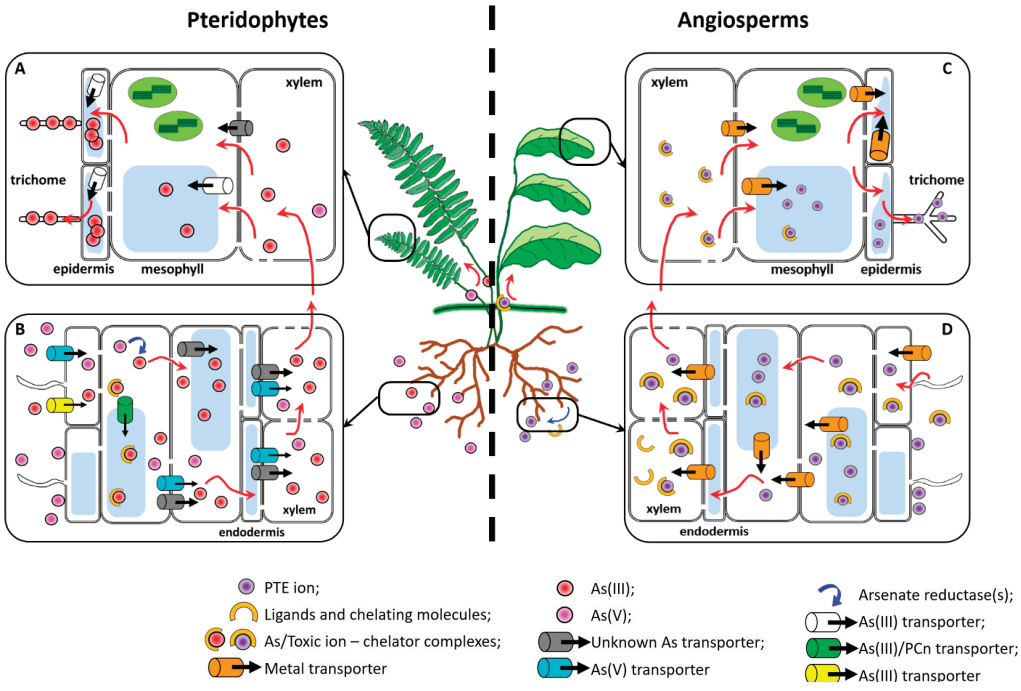

Figure 1. Similarities and differences between hyperaccumulation in ferns and in angiosperm hyperaccumulator plants. In Pteridophytes, As hyperaccumulation is a complex process involving both As(III) and As(V). While As(V) is the major form taken up from the soil, As(III) is the prevalent form transported and stored in the plant. A key process in determining the relative balance of As(III) and As(V) is the reduction of arsenate to arsenite by arsenate reductases in the roots (**B**). As is partly sequestered in the vacuoles both as free As(III) and As(III)/phytochelatin complexes (depicted for simplicity in different cells), but the majority is loaded into the xylem with the contribution of unidentified transporters. (**A**). After unloading from the xylem in the fronds, As(III) is stored in the vacuoles of mesophyll and especially epidermal cells and trichomes, where As concentrations reach the highest values [94,98]. In Angiosperms, the main genetic determinants of heavy metal hyperaccumulation are constitutively overexpressed in hyperaccumulators species. Coded proteins are involved in metal transport and homeostasis. For instance, as highlighted in (**D**), in the root of hyperaccumulator plants a variety of membrane transporters are involved in the transport of metal ions towards the shoot, decreasing root vacular accumulation in favor of an enhanced root-to-shoot transport. Additionally, overproduction of ligands, both intracellularly and secreted into the rhizosphere, (such as Histidine, required for Ni hypertolerance and hyperaccumulation [110]) plays a role as hyperaccumulation determinant, binding to HM ions and adjuvating their transport through the xylem sap. (**C**). Once translocated towards the shoot, by the action of overexpressed vacuolar and plasma membrane transporters, HM ions are sequestered in vacuoles of mesophyll and epidermis cells and in leaf cell walls respectively, and, in some species, such as *Arabidopsis halleri*, in cell trichomes [120]. As mentioned in the text, such sequestration is important to exclude the toxic ions from energy handling organelles, such as chloroplasts and mitochondria.

Among angiosperms, species able to hyperaccumulate PTE are distributed in many families and genera, showing that the trait has evolved independently many times. Up to now, more than 700 species have been demonstrated to hyperaccumulate one or more

PTEs and are listed in the Global Hyperaccumulator Database (http://hyperaccumulators.smi.uq.edu.au/collection/ accessed on 30 December 2021) which is constantly updated. Interestingly, two families are more represented in this database, i.e., Brassicaceae and Phyllanthaceae, and members of these families are currently considered as models for studying metal hyperaccumulation in angiosperms, such as *Arabidopsis halleri*, *Noccaea* spp., *Alyssum* spp.

Interestingly, several genes that take part in metal transport and homeostasis, and those that encode metal chelators and are involved in the stress response, have been correlated with the hyperaccumulation trait; however, these determinants are not specific of hyperaccumulators but are rather constitutively overexpressed in these species, conferring them the ability to tolerate and accumulate in specific plant organs and/or tissues, huge amounts of metal ions [121]. Mechanisms induced in angiosperms to tolerate excess PTE, as well as those enacted by hyperaccumulators, have been extensively studied and reported in the literature [120]. The first examples are the enhanced accumulation of ion chelating compounds, such as histidine or nicotianamine, involved in hyperaccumulation of Ni in *Alyssum* and Zn in *A. halleri* respectively [122,123]. The overexpression of transporter proteins involved in root-to-shoot metal translocation was also correlated to hyperaccumulation. Such overexpression has been reported, in some cases, as the result of genomic DNA expansion and/or promoter modification, driving enhanced mRNA transcription, as in the case of the Zn transporter HMA4 of *A. halleri* [124]. However, plant capacity for PTE tolerance and accumulation cannot be ascribed to a limited number of genetic determinants, but rather to a whole reorganization of developmental, nutritional and metabolic processes [119,125], whose extent is still under study.

4. Conclusions and Future Perspectives

Deep knowledge of the interaction between plants and metal ions/metalloids in soil, both toxic or nutrient elements, is an essential base for a successful application of non-vascular and vascular plants for the identification and reclamation of PTE-polluted environments. In addition to the more straightforward approaches, such knowledge allows for manipulation of PTE tolerance and accumulation in target plant species. From a biotechnological point of view, there are two main fields of application of genetic engineering of the plant actors, leading to either improved metal accumulation or exclusion from the cellular environment. Firstly, biotechnology may aim to tailor PTE content in edible plant parts, by enhancing the transport and accumulation of essential metal(oid)s for human nutrition (i.e., biofortification), or reducing the accumulation of toxic elements in crops cultivated on risky lands. Secondly, an increase in the accumulation of toxic elements in above-ground plant tissues is significant for phytoremediation purposes, in view of adopting engineered plants to remove HMs from contaminated soils or waters.

The in-depth insight that is being currently gained regarding the genetics of metal(loid) tolerance and accumulation is a valuable source of genetic information (considering both coding and non-coding sequences) that could be employed to control ion accumulation in particular plant tissues or districts. Recent reviews detail the high number of experiments aimed at modulating metal(oid) accumulation in plants, adopting as a system a variety of model plants, trees and edible crops [126,127]. Moreover, even if most literature concerns flowering plants as "gene donors" (generally overlooking the prokaryotic kingdom as well as spore-bearing plants), attention has recently moved toward pteridophytes. For instance, the *P. vittata* As transporter PvACR3, localized in the tonoplast of the gametophyte, is able to enhance resistance to As-contaminated growth substrates in transgenic *A. thaliana* plants, even though it localizes to the plasma membrane in *A. thaliana* cells [128]. Interestingly, during evolution, the ACR3 gene was lost from the angiosperm genomes [128].

The new breeding techniques, such as CRISPR/Cas-mediated genome editing, enable the targeting of specific sites on the DNA, allowing to precisely modify up to a single nucleotide in the sequence, obtaining highly predictable modifications and transgene-free organisms that could be of particular interest for a concrete application.

Author Contributions: Conceptualization, A.F. and G.D.; Writing—review and editing, E.F., M.L., C.V., A.F. and G.D. All authors have read and agreed to the published version of the manuscript.

Funding: This research received no external funding.

Institutional Review Board Statement: Not applicable.

Informed Consent Statement: Not applicable.

Data Availability Statement: The study did not report any data.

Conflicts of Interest: The authors declare no conflict of interest.

References

1. Holleman, A.F.; Wiberg, E. *Lehrbuch der Anorganischen Chemie*; Walter de Gruyter: Berlin, Germany, 1985; p. 868.
2. Duffus, J.H. "Heavy Metals"-a meaningless term? *Pure Appl. Chem.* **2002**, *74*, 793–807. [CrossRef]
3. Pourret, O.; Hursthouse, A. It's Time to Replace the Term "Heavy Metals" with "Potentially Toxic Elements" When Reporting Environmental Research. *Int. J. Environ. Res. Public Health* **2019**, *16*, 4446. [CrossRef] [PubMed]
4. Rai, P.K. Heavy metal phytoremediation from aquatic ecosystems with special reference to macrophytes. *Crit. Rev. Environ. Sci.* **2009**, *39*, 697–753. [CrossRef]
5. Fytianos, K.; Katsianis, G.; Triantafyllou, P.; Zachariadis, G. Accumulation of heavy metals in vegetables grown in an industrial area in relation to soil. *Bull. Environ. Contam. Toxicol.* **2001**, *67*, 423–430. [CrossRef]
6. Wieczorek-Dąbrowska, M.; Tomza-Marciniak, A.; Pilarczyk, B.; Balicka-Ramisz, A. Roe and red deer as bioindicators of heavy metals contamination in north-western Poland. *Chem. Ecol.* **2013**, *29*, 100–110. [CrossRef]
7. Jarup, L. Hazards of heavy metal contamination. *Br. Med. Bull.* **2003**, *68*, 167–182. [CrossRef] [PubMed]
8. Wirth, J.J.; Mijal, R.S. Adverse effects of low level heavy metal exposure on male reproductive function. *Syst. Biol. Reprod. Med.* **2010**, *56*, 147–167. [CrossRef]
9. Hall, J.L. Cellular mechanisms for heavy metals detoxification and tolerance. *J. Exp. Bot.* **2002**, *53*, 1–11. [CrossRef]
10. Kakkar, P.; Jaffery, F.N. Biological markers for metal toxicity. *Environ. Toxicol. Pharmacol.* **2005**, *19*, 335–349. [CrossRef] [PubMed]
11. Jan, A.T.; Azam, M.; Siddiqui, K.; Ali, A.; Choi, I.; Haq, Q.M.R. Heavy Metals and Human Health: Mechanistic Insight into Toxicity and Counter Defense System of Antioxidants. *Int. J. Mol. Sci.* **2015**, *16*, 29592–29630. [CrossRef]
12. Sytar, O.; Kumar, A.; Latowski, D.; Kuczynska, P.; Strzałka, K.; Prasad, M.N.V. Heavy metal-induced oxidative damage, defense reactions, and detoxification mechanisms in plants. *Acta Physiol. Plant* **2013**, *35*, 985–999. [CrossRef]
13. Tennstedt, P.; Peisker, D.; Böttcher, C.; Trampczynska, A.; Clemens, S. Phytochelatin Synthesis Is Essential for the Detoxification of Excess Zinc and Contributes Significantly to the Accumulation of Zinc. *Plant Physiol.* **2009**, *149*, 938–948. [CrossRef] [PubMed]
14. Salemaa, M.; Derome, J.; Helmisaari, H.S.; Nieminen, T.; Vanha-Majamaa, I. Element accumulation in boreal bryophytes, lichens and vascular plants exposed to heavy metal and sulfur deposition in Finland. *Sci. Total Environ.* **2004**, *324*, 141–160. [CrossRef] [PubMed]
15. Frahm, J.P. Diversity, dispersal and biogeography of bryophytes (mosses). *Biodivers. Conserv.* **2008**, *17*, 277–284. [CrossRef]
16. Puttick, M.N.; Morris, J.L.; Williams, T.A.; Cox, C.J.; Edwards, D.; Kenrick, P.; Pressel, S.; Wellman, C.H.; Schneider, H.; Pisani, D.; et al. The Interrelationships of Land Plants and the Nature of the Ancestral Embryophyte. *Curr. Biol.* **2018**, *28*, 733–745.e2. [CrossRef]
17. Harris, B.J.; Harrison, C.J.; Hetherington, A.M.; Williams, T.A. Phylogenomic Evidence for the Monophyly of Bryophytes and the Reductive Evolution of Stomata. *Curr. Biol.* **2020**, *30*, 2001–2012.e2. [CrossRef] [PubMed]
18. Hutsemekers, V.; Dopagne, C.; Vanderpoorten, A. How far and how fast do bryophytes travel at the landscape scale? *Divers. Distrib.* **2008**, *14*, 483–492. [CrossRef]
19. Shimamura, M. Marchantia polymorpha: Taxonomy, phylogeny and morphology of a model system. *Plant Cell Physiol.* **2016**, *57*, 230–256. [CrossRef]
20. Coelho, M.C.M.; Gabriel, R.; Hespanhol, H.; Borges, P.A.V.; Ah-Peng, C. Bryophyte diversity along an elevational gradient on pico island (Azores, portugal). *Diversity* **2021**, *13*, 162. [CrossRef]
21. Zechmeister, H.G.; Dirnböck, T.; Hülber, K.; Mirtl, M. Assessing airborne pollution effects on bryophytes-lessons learned through long-term integrated monitoring in Austria. *Environ. Pollut.* **2007**, *147*, 696–705. [CrossRef]
22. Zvereva, E.L.; Kozlov, M.V. Impacts of industrial polluters on bryophytes: A meta-analysis of observational studies. *Water Air Soil Pollut.* **2011**, *218*, 573–586. [CrossRef]
23. Chen, Y.E.; Cui, J.M.; Yang, J.C.; Zhang, Z.W.; Yuan, M.; Song, C.; Yang, H.; Liu, H.M.; Wang, C.Q.; Zhang, H.Y.; et al. Biomonitoring heavy metal contaminations by moss visible parameters. *J. Hazard. Mater.* **2015**, *296*, 201–209. [CrossRef]
24. Di Palma, A.; González, A.G.; Adamo, P.; Giordano, S.; Reski, R.; Pokrovsky, O.S. Biosurface properties and lead adsorption in a clone of *Sphagnum palustre* (Mosses): Towards a unified protocol of biomonitoring of airborne heavy metal pollution. *Chemosphere* **2019**, *236*, 124375. [CrossRef]
25. Samecka-Cymerman, A.; Marczonek, A.; Kempers, A.J. Bioindication of heavy metals in soil by liverworts. *Arch. Environ. Contam. Toxicol.* **1997**, *33*, 162–171. [CrossRef]

26. Vásquez, C.; Calva, J.; Morocho, R.; Donoso, D.A.; Benítez, Á. Bryophyte communities along a tropical urban river respond to heavy metal and arsenic pollution. *Water* **2019**, *11*, 813. [CrossRef]
27. Sassmann, S.; Wernitznig, S.; Lichtscheidl, I.K.; Lang, I. Comparing copper resistance in two bryophytes: *Mielichhoferia elongata* Hornsch. versus *Physcomitrella patens* Hedw. *Protoplasma* **2010**, *246*, 119–123. [CrossRef] [PubMed]
28. Papadia, P.; Barozzi, F.; Migoni, D.; Rojas, M.; Fanizzi, F.P.; Di Sansebastiano, G.P. Aquatic mosses as adaptable bio-filters for heavy metal removal from contaminated water. *Int. J. Mol. Sci.* **2020**, *21*, 4769. [CrossRef] [PubMed]
29. Shaw, J.; Antonovics, J.; Anderson, L.E. Inter- and intraspecific variation of mosses in tolerance to copper and zinc. *Evolution* **1987**, *41*, 1312–1325.
30. Itouga, M.; Hayatsu, M.; Sato, M.; Tsuboi, Y.; Kato, Y.; Toyooka, K.; Suzuki, S.; Nakatsuka, S.; Kawakami, S.; Kikuchi, J.; et al. Protonema of the moss *Funaria hygrometrica* can function as a lead (Pb) adsorbent. *PLoS ONE* **2017**, *12*, e0189726. [CrossRef]
31. Sandhi, A.; Landberg, T.; Greger, M. Phytofiltration of arsenic by aquatic moss (*Warnstorfia fluitans*). *Environ. Pollut.* **2018**, *237*, 1098–1105. [CrossRef]
32. Sharma, S. Marchantia polymorpha L.: A Bioaccumulator. *Aerobiologia* **2007**, *23*, 181–187. [CrossRef]
33. Ares, Á.; Itouga, M.; Kato, Y.; Sakakibara, H. Differential Metal Tolerance and Accumulation Patterns of Cd, Cu, Pb and Zn in the Liverwort *Marchantia polymorpha* L. *Bull. Environ. Contam. Toxicol.* **2018**, *100*, 444–450. [CrossRef]
34. Pratas, J.; Favas, P.J.C.; Varun, M.; D'Souza, R.; Paul, M.S. Distribution of rare earth elements, thorium and uranium in streams and aquatic mosses of Central Portugal. *Environ. Earth Sci.* **2017**, *76*, 156. [CrossRef]
35. Krzesłowska, M.; Rabęda, I.; Lewandowski, M.; Samardakiewicz, S.; Basińska, A.; Napieralska, A.; Mellerowicz, E.J.; Wozny, A. Pb induces plant cell wall modifications-In particular-The increase of pectins able to bind metal ions level. In Proceedings of the E3S Web of Conferences, 16th International Conference on Heavy Metals in the Environment, Rome, Italy, 23–27 September 2012; EDP Sciences: Les Ulis, France, 2013; Volume 1.
36. Basile, A.; Sorbo, S.; Pisani, T.; Paoli, L.; Munzi, S.; Loppi, S. Bioacumulation and ultrastructural effects of Cd, Cu, Pb and Zn in the moss *Scorpiurum circinatum* (Brid.) Fleisch. & Loeske. *Environ. Pollut.* **2012**, *166*, 208–211. [PubMed]
37. Lang, I.; Wernitznig, S. Sequestration at the cell wall and plasma membrane facilitates zinc tolerance in the moss *Pohlia drummondii*. *Environ. Exp. Bot.* **2011**, *74*, 186–193. [CrossRef]
38. Shakya, K.; Chettri, M.K.; Sawidis, T. Impact of heavy metals (copper, zinc, and lead) on the chlorophyll content of some mosses. *Arch. Environ. Contam. Toxicol.* **2008**, *54*, 412–421. [CrossRef] [PubMed]
39. Degola, F.; De Benedictis, M.; Petraglia, A.; Massimi, A.; Fattorini, L.; Sorbo, S.; Basile, A.; Di Toppi, L.S. A Cd/Fe/Zn-responsive phytochelatin synthase is constitutively present in the ancient liverwort *Lunularia cruciata* (L.) dumort. *Plant Cell Physiol.* **2014**, *55*, 1884–1891. [CrossRef]
40. Lane, T.S.; Rempe, C.S.; Davitt, J.; Staton, M.E.; Peng, Y.; Soltis, D.E.; Melkonian, M.; Deyholos, M.; Leebens-Mack, J.H.; Chase, M.; et al. Diversity of ABC transporter genes across the plant kingdom and their potential utility in biotechnology. *BMC Biotechnol.* **2016**, *16*, 47. [CrossRef]
41. Petraglia, A.; De Benedictis, M.; Degola, F.; Pastore, G.; Calcagno, M.; Ruotolo, R.; Mengoni, A.; Di Toppi, L.S. The capability to synthesize phytochelatins and the presence of constitutive and functional phytochelatin synthases are ancestral (plesiomorphic) characters for basal land plants. *J. Exp. Bot.* **2014**, *65*, 1153–1163. [CrossRef]
42. Bellini, E.; Maresca, V.; Betti, C.; Castiglione, M.R.; Fontanini, D.; Capocchi, A.; Sorce, C.; Borsò, M.; Bruno, L.; Sorbo, S.; et al. The moss *Leptodictyum riparium* counteracts severe cadmium stress by activation of glutathione transferase and phytochelatin synthase, but slightly by phytochelatins. *Int. J. Mol. Sci.* **2020**, *21*, 1583. [CrossRef]
43. Li, M.; Barbaro, E.; Bellini, E.; Saba, A.; di Toppi, L.S.; Varotto, C. Ancestral function of the phytochelatin synthase C-terminal domain in inhibition of heavy metal-mediated enzyme overactivation. *J. Exp. Bot.* **2020**, *71*, 6655–6669. [CrossRef] [PubMed]
44. Inupakutika, M.A.; Sengupta, S.; Devireddy, A.R.; Azad, R.K.; Mittler, R. The evolution of reactive oxygen species metabolism. *J. Exp. Bot.* **2016**, *67*, 5933–5943. [CrossRef] [PubMed]
45. Sun, S.Q.; He, M.; Cao, T.; Zhang, Y.C.; Han, W. Response mechanisms of antioxidants in bryophyte (*Hypnum plumaeforme*) under the stress of single or combined Pb and/or Ni. *Environ. Monit. Assess.* **2009**, *149*, 291–302. [CrossRef]
46. Dazy, M.; Masfaraud, J.F.; Férard, J.F. Induction of oxidative stress biomarkers associated with heavy metal stress in *Fontinalis antipyretica* Hedw. *Chemosphere* **2009**, *75*, 297–302. [CrossRef]
47. Smith, A.R.; Pryer, K.M.; Schuettpelz, E.; Korall, P.; Schneider, H.; Wolf, P.G. A classification for extant ferns. *Names* **2006**, *55*, 705–731. [CrossRef]
48. Prance, G.T. Discovering the plant world. *Taxon* **2001**, *50*, 345–359. [CrossRef]
49. Niklas, K.J.; Tiffney, B.H.; Knoll, A.H. Patterns in vascular land plant diversification. *Nature* **1983**, *303*, 614–616. [CrossRef]
50. Schneider, H.; Schuettpelz, E.; Pryer, K.M.; Cranfill, R.; Magallón, S.; Lupia, R. Ferns diversified in the shadow of angiosperms. *Nature* **2004**, *428*, 553–557. [CrossRef]
51. Kreft, H.; Jetz, W.; Mutke, J.; Barthlott, W. Contrasting environmental and regional effects on global pteridophyte and seed plant diversity. *Ecography* **2010**, *33*, 408–419. [CrossRef]
52. Drăghiceanu, O.A.; Dobrescu, C.M.; Soare, L.C. Applications of pteridophytes in phytoremediation. *Curr. Trends Nat. Sci.* **2014**, *3*, 68–73.
53. Praveen, A.; Pandey, V.C. Pteridophytes in phytoremediation. *Environ. Geochem. Health* **2020**, *42*, 2399–2411. [CrossRef]

54. Prabhu, S.G.; Srinikethan, G.; Hegde, S. Potential of Pteridophytes in Heavy Metal Phytoremediation. *Int. J. Res. Eng. Technol.* **2016**, *5*, 1–9.
55. Tiwari, S.; Sarangi, B.K.; Anusha, P.; Pandey, R.A. Metal Hyperaccumulating Ferns: Progress and Future Prospects. In *Recent Advances towards Improved Phytoremediation of Heavy Metal Pollution*; Leung, D.W.M., Ed.; Bentham Science Publishers: Sharjah, United Arab Emirates, 2013; ISBN 978-1-60805-787-0.
56. Sukumaran, D. Phytoremediation of heavy metals from industrial effluent using constructed wetland technology. *Appl. Ecol. Environ. Sci.* **2013**, *1*, 92–97. [CrossRef]
57. Dhir, B.; Sharmila, P.; Saradhi, P.P.; Sharma, S.; Kumar, R.; Mehta, D. Heavy metal induced physiological alterations in *Salvinia natans*. *Ecotoxicol. Environ. Saf.* **2011**, *74*, 1678–1684. [CrossRef] [PubMed]
58. Bennicelli, R.; St\kepniewska, Z.; Banach, A.; Szajnocha, K.; Ostrowski, J. The ability of *Azolla caroliniana* to remove heavy metals (Hg (II), Cr (III), Cr (VI)) from municipal waste water. *Chemosphere* **2004**, *55*, 141–146. [CrossRef] [PubMed]
59. Cohen-Shoel, N.; Barkay, Z.; Ilzycer, D.; Gilath, I.; Tel-Or, E. Biofiltration of toxic elements by Azolla biomass. *Water Air Soil Pollut.* **2002**, *135*, 93–104. [CrossRef]
60. Stepniewska, Z.; Bennicelli, R.P.; Balakhina, T.I.; Szajnocha, K.; Banach, A.M.; Wolinska, A. Potential of *Azolla caroliniana* for the removal of Pb and Cd from wastewaters. *Int. Agrophys.* **2005**, *19*, 251–255.
61. Rakhshaee, R.; Khosravi, M.; Ganji, M.T. Kinetic modeling and thermodynamic study to remove Pb (II), Cd (II), Ni (II) and Zn (II) from aqueous solution using dead and living *Azolla filiculoides*. *J. Hazard. Mater.* **2006**, *134*, 120–129. [CrossRef]
62. Rai, P.K. Phytoremediation of Hg and Cd from industrial effluents using an aquatic free floating macrophyte *Azolla pinnata*. *Int. J. Phytoremediat.* **2008**, *10*, 430–439. [CrossRef]
63. Mashkani, S.G.; Ghazvini, P.T.M. Biotechnological potential of *Azolla filiculoides* for biosorption of Cs and Sr: Application of micro-PIXE for measurement of biosorption. *Bioresour. Technol.* **2009**, *100*, 1915–1921. [CrossRef]
64. Dhir, B. Role of Ferns in Environmental Cleanup. In *Current Advances in Fern Research*; Fernández, H., Ed.; Springer International Publishing: Cham, Switzerland, 2018; pp. 517–531; ISBN 978-3-319-75103-0.
65. Nichols, P.B.; Couch, J.D.; Al-Hamdani, S.H. Selected physiological responses of *Salvinia minima* to different chromium concentrations. *Aquat. Bot.* **2000**, *68*, 313–319. [CrossRef]
66. Hoffmann, T.; Kutter, C.; Santamaria, J. Capacity of *Salvinia minima* Baker to tolerate and accumulate As and Pb. *Eng. Life Sci.* **2004**, *4*, 61–65. [CrossRef]
67. Olguin, E.J.; Hernández, E.; Ramos, I. The effect of both different light conditions and the pH value on the capacity of *Salvinia minima* Baker for removing cadmium, lead and chromium. *Acta Biotechnol.* **2002**, *22*, 121–131. [CrossRef]
68. Olguin, E.J.; Sánchez-Galván, G.; Pérez-Pérez, T.; Pérez-Orozco, A. Surface adsorption, intracellular accumulation and compartmentalization of Pb (II) in batch-operated lagoons with *Salvinia minima* as affected by environmental conditions, EDTA and nutrients. *J. Ind. Microbiol. Biotechnol.* **2005**, *32*, 577–586. [CrossRef]
69. Espinoza-Quinones, F.R.; Zacarkim, C.E.; Palacio, S.M.; Obregon, C.L.; Zenatti, D.C.; Galante, R.M.; Rossi, N.; Rossi, F.L.; Pereira, I.R.A.; Welter, R.A.; et al. Removal of heavy metal from polluted river water using aquatic macrophytes *Salvinia* sp. *Braz. J. Phys.* **2005**, *35*, 744–746. [CrossRef]
70. Molisani, M.M.; Rocha, R.; Machado, W.; Barreto, R.C.; Lacerda, L.D. Mercury contents in aquatic macrophytes from two reservoirs in the Paraba do Sul: Guandú river system, SE Brazil. *Braz. J. Biol.* **2006**, *66*, 101–107. [CrossRef] [PubMed]
71. Suñe, N.; Sánchez, G.; Caffaratti, S.; Maine, M.A. Cadmium and chromium removal kinetics from solution by two aquatic macrophytes. *Environ. Pollut.* **2007**, *145*, 467–473. [CrossRef]
72. Sánchez-Galván, G.; Monroy, O.; Gómez, J.; Olguin, E.J. Assessment of the hyperaccumulating lead capacity of Salvinia minima using bioadsorption and intracellular accumulation factors. *Water Air Soil Pollut.* **2008**, *194*, 77–90. [CrossRef]
73. Fuentes, I.I.; Espadas-Gil, F.; Talavera-May, C.; Fuentes, G.; Santamaria, J.M. Capacity of the aquatic fern (*Salvinia minima* Baker) to accumulate high concentrations of nickel in its tissues, and its effect on plant physiological processes. *Aquat. Toxicol.* **2014**, *155*, 142–150. [CrossRef] [PubMed]
74. Kumari, S.; Kumar, B.; Sheel, R. Bioremediation of Heavy Metals by Serious Aquatic Weed, *Salvinia*. *Int. J. Curr. Microbiol. Appl. Sci.* **2016**, *5*, 355–368. [CrossRef]
75. Emiliani, J.; Oyarce, W.G.L.; Salvatierra, L.M.; Novo, L.A.B.; Pérez, L.M. Evaluation of Cadmium Bioaccumulation-Related Physiological Effects in *Salvinia biloba*: An Insight towards Its Use as Pollutant Bioindicator in Water Reservoirs. *Plants* **2021**, *10*, 2679. [CrossRef] [PubMed]
76. Banerjee, G.; Sarker, S. The role of *Salvinia rotundifolia* in scavenging aquatic Pb (II) pollution: A case study. *Bioprocess Eng.* **1997**, *17*, 295–300. [CrossRef]
77. Dhir, B.; Sharmila, P.; Saradhi, P.P. Potential of aquatic macrophytes for removing contaminants from the environment. *Crit. Rev. Environ. Sci. Technol.* **2009**, *39*, 754–781. [CrossRef]
78. Chang, J.S.; Yoon, I.H.; Kim, K.W. Heavy metal and arsenic accumulating fern species as potential ecological indicators in As-contaminated abandoned mines. *Ecol. Indic.* **2009**, *9*, 1275–1279. [CrossRef]
79. Claveria, R.J.R.; Perez, T.R.; Perez, R.E.C.; Algo, J.L.C.; Robles, P.Q. The identification of indigenous Cu and As metallophytes in the Lepanto Cu-Au Mine, Luzon, Philippines. *Environ. Monit. Assess.* **2019**, *191*, 185. [CrossRef] [PubMed]
80. Ha, N.T.H.; Nga, T.T.H.; Minh, N.N.; Anh, B.T.K.; Hang, N.T.A.; Duc, N.A.; Nhuan, M.T.; Kim, K.W. Uptake of arsenic and heavy metals by native plants growing near Nui Phao multi-metal mine, northern Vietnam. *Appl. Geochem.* **2019**, *108*, 104368. [CrossRef]

81. Prasetia, H.; Sakakibara, M.; Takehara, A.; Sueoka, Y. Heavy metals accumulation by *Athyrium yokoscence* in a mine area, Southwestern Japan. *IOP Conf. Ser. Earth Environ. Sci.* **2017**, *71*, 12025. [CrossRef]
82. Christenhusz, M.J.M.; Chase, M.W. Trends and concepts in fern classification. *Ann. Bot.* **2014**, *113*, 571–594. [CrossRef]
83. Morishita, T.; Boratynski, J.K. Accumulation of cadmium and other metals in organs of plants growing around metal smelters in Japan. *Soil Sci. Plant Nutr.* **1992**, *38*, 781–785. [CrossRef]
84. Kamachi, H.; Komori, I.; Tamura, H.; Sawa, Y.; Karahara, I.; Honma, Y.; Wada, N.; Kawabata, T.; Matsuda, K.; Ikeno, S.; et al. Lead tolerance and accumulation in the gametophytes of the fern *Athyrium yokoscense*. *J. Plant Res.* **2005**, *118*, 137–145. [CrossRef]
85. Nishizono, H.; Suzuki, S.; Ishii, F. Accumulation of heavy metals in the metal-tolerant fern, *Athyrium yokoscense*, growing on various environments. *Plant Soil* **1987**, *102*, 65–70. [CrossRef]
86. Van, T.K.; Kang, Y.; Fukui, T.; Sakurai, K.; Iwasaki, K.; Aikawa, Y.; Phuong, N.M. Arsenic and heavy metal accumulation by *Athyrium yokoscense* from contaminated soils. *Soil Sci. Plant Nutr.* **2006**, *52*, 701–710. [CrossRef]
87. Francesconi, K.; Visoottiviseth, P.; Sridokchan, W.; Goessler, W. Arsenic species in an arsenic hyperaccumulating fern, *Pityrogramma calomelanos*: A potential phytoremediator of arsenic-contaminated soils. *Sci. Total Environ.* **2002**, *284*, 27–35. [CrossRef]
88. Corzo Remigio, A.; Edraki, M.; Baker, A.J.M.; van der Ent, A. Root responses to localised soil arsenic enrichment in the fern *Pityrogramma calomelanos* var. *austroamericana grown in rhizoboxes*. *Plant Physiol. Biochem.* **2021**, *164*, 147–159. [CrossRef]
89. Ma, L.Q.; Komar, K.M.; Tu, C.; Zhang, W.; Cai, Y.; Kennelley, E.D. A fern that hyperaccumulates arsenic. *Nature* **2001**, *409*, 579. [CrossRef] [PubMed]
90. Danh, L.T.; Truong, P.; Mammucari, R.; Foster, N. A Critical Review of the Arsenic Uptake Mechanisms and Phytoremediation Potential of Pteris Vittata. *Int. J. Phytoremediation* **2014**, *16*, 429–453. [CrossRef]
91. Tu, C.; Ma, L.Q. Effects of Arsenic Concentrations and Forms on Arsenic Uptake by the Hyperaccumulator Ladder Brake. *J. Environ. Qual.* **2002**, *31*, 641–647. [CrossRef]
92. Zheng, J.; Niu, T.; Wu, G.; Chen, W. One magic pteridophyte (*Pteris vittata* L.): Application in remediating arsenic contaminated soils and mechanism of arsenic hyperaccumulation. *Front. Agric. China* **2010**, *4*, 293–298. [CrossRef]
93. Vandana, U.K.; Gulzar, A.B.M.; Singha, L.P.; Bhattacharjee, A.; Mazumder, P.B.; Pandey, P. Hyperaccumulation of arsenic by *Pteris vittata*, a potential strategy for phytoremediation of arsenic-contaminated soil. *Environ. Sustain.* **2020**, *3*, 169–178. [CrossRef]
94. Cai, C.; Lanman, N.A.; Withers, K.A.; DeLeon, A.M.; Wu, Q.; Gribskov, M.; Salt, D.E.; Banks, J.A. Three Genes Define a Bacterial-Like Arsenic Tolerance Mechanism in the Arsenic Hyperaccumulating Fern *Pteris vittata*. *Curr. Biol.* **2019**, *29*, 1625–1633.e3. [CrossRef]
95. Ditusa, S.F.; Fontenot, E.B.; Wallace, R.W.; Silvers, M.A.; Steele, T.N.; Elnagar, A.H.; Dearman, K.M.; Smith, A.P. A member of the Phosphate transporter 1 (Pht1) family from the arsenic-hyperaccumulating fern *Pteris vittata* is a high-affinity arsenate transporter. *New Phytol.* **2016**, *209*, 762–772. [CrossRef]
96. He, Z.; Yan, H.; Chen, Y.; Shen, H.; Xu, W.; Zhang, H.; Shi, L.; Zhu, Y.G.; Ma, M. An aquaporin PvTIP4;1 from *Pteris vittata* may mediate arsenite uptake. *New Phytol.* **2016**, *209*, 746–761. [CrossRef] [PubMed]
97. Indriolo, E.; Na, G.N.; Ellis, D.; Salt, D.E.; Banks, J.A. A vacuolar arsenite transporter necessary for arsenic tolerance in the arsenic hyperaccumulating fern *Pteris vittata* is missing in flowering plants. *Plant Cell* **2010**, *22*, 2045–2057. [CrossRef] [PubMed]
98. Lombi, E.; Zhao, F.J.; Fuhrmann, M.; Ma, L.Q.; McGrath, S.P. Arsenic distribution and speciation in the fronds of the hyperaccumulator *Pteris vittata*. *New Phytol.* **2002**, *156*, 195–203. [CrossRef]
99. Ellis, D.R.; Gumaelius, L.; Indriolo, E.; Pickering, I.J.; Banks, J.A.; Salt, D.E. A novel arsenate reductase from the arsenic hyperaccumulating fern *Pteris vittata*. *Plant Physiol.* **2006**, *141*, 1544–1554. [CrossRef]
100. Condamine, F.L.; Silvestro, D.; Koppelhus, E.B.; Antonelli, A. The rise of angiosperms pushed conifers to decline during global cooling. *Proc. Natl. Acad. Sci. USA* **2020**, *117*, 28867–28875. [CrossRef]
101. Kandziora-Ciupa, M.; Ciepał, R.; Nadgórska-Socha, A.; Barczyk, G. Accumulation of heavy metals and antioxidant responses in *Pinus sylvestris* L. needles in polluted and non-polluted sites. *Ecotoxicology* **2016**, *25*, 970–981. [CrossRef]
102. Saladin, G. Phytoextraction of Heavy Metals: The Potential Efficiency of Conifers. In *Heavy Metal Contamination of Soils*; Springer International Publishing: Cham, Switzerland, 2015; pp. 333–353.
103. Rodríguez Martin, J.A.C.; Gutiérrez, M.; Torrijos, N. Nanos Wood and bark of *Pinus halepensis* as archives of heavy metal pollution in the Mediterranean Region. *Environ. Pollut.* **2018**, *239*, 438–447. [CrossRef]
104. Zeiner, M.; Juranović Cindrić, I. Accumulation of Major, Minor and Trace Elements in Pine Needles (*Pinus nigra*) in Vienna (Austria). *Molecules* **2021**, *26*, 3318. [CrossRef] [PubMed]
105. Kukkola, E.; Rautio, P.; Huttunen, S. Stress indications in copper- and nickel-exposed Scots pine seedlings. *Environ. Exp. Bot.* **2000**, *43*, 197–210. [CrossRef]
106. Curguz, V.G.; Raicevic, V.; Veselinovic, M.; Tabakovic-Tosic, M.; Vilotic, D. Influence of heavy metals on seed germination and growth of *Picea abies* L. Karst. *Polish J. Environ. Stud.* **2012**, *21*, 355–361.
107. Ivanov, Y.V.; Savochkin, Y.V.; Kuznetsov, V.V. Scots pine as a model plant for studying the mechanisms of conifers adaptation to heavy metal action: 2. Functioning of antioxidant enzymes in pine seedlings under chronic zinc action. *Russ. J. Plant Physiol.* **2012**, *59*, 50–58. [CrossRef]
108. Radotic, K.; Ducic, T.; Mutavdic, D. Changes in peroxidase activity and isoenzymes in spruce needles after exposure to different concentrations of cadmium. *Environ. Exp. Bot.* **2000**, *44*, 105–113. [CrossRef]

109. Schröder, P.; Fisher, C.; Debus, R.; Wenzel, A. Reaction of detoxification mechanisms in suspension cultured spruce cells (*Picea abies* L. Karst.) to heavy metals in pure mixture and in soil eluates. *Environ. Sci. Pollut. Res.* **2003**, *10*, 225–234. [CrossRef]
110. DalCorso, G.; Manara, A.; Furini, A. An overview of heavy metal challenge in plants: From roots to shoots. *Metallomics* **2013**, *5*, 1117–1132. [CrossRef]
111. Gekeler, W.; Grill, E.; Winnacker, E.L.; Zenk, M.H. Survey of the Plant Kingdom for the Ability to Bind Heavy Metals through Phytochelatins. *Z. Für Nat. C* **1989**, *44*, 361–369. [CrossRef]
112. Thangavel, P.; Long, S.; Minocha, R. Changes in phytochelatins and their biosynthetic intermediates in red spruce (*Picea rubens* Sarg.) cell suspension cultures under cadmium and zinc stress. *Plant Cell Tissue Organ Cult.* **2007**, *88*, 201–216. [CrossRef]
113. Hachani, C.; Lamhamedi, M.S.; Cameselle, C.; Gouveia, S.; Zine El Abidine, A.; Khasa, D.P.; Béjaoui, Z. Effects of Ectomycorrhizal Fungi and Heavy Metals (Pb, Zn, and Cd) on Growth and Mineral Nutrition of *Pinus halepensis* Seedlings in North Africa. *Microorganisms* **2020**, *8*, 2033. [CrossRef] [PubMed]
114. Chudzińska, E.; Diatta, J.B.; Wojnicka-Półtorak, A. Adaptation strategies and referencing trial of Scots and black pine populations subjected to heavy metal pollution. *Environ. Sci. Pollut. Res. Int.* **2014**, *21*, 2165–2177. [CrossRef]
115. Wegiel, A.; Bielinis, E.; Polowy, K. Heavy metals accumulation in Scots pine stands of different densities growing on not contaminated forest area (northwestern Poland). *Austrian J. For. Sci.* **2018**, *35*, 259–281.
116. Moussavou Moudouma, C.F.; Riou, C.; Gloaguen, V.; Saladin, G. Hybrid larch (*Larix x eurolepis* Henry): A good candidate for cadmium phytoremediation? *Environ. Sci. Pollut. Res.* **2013**, *20*, 1889–1894. [CrossRef] [PubMed]
117. Ivanov, Y.V.; Kartashov, A.V.; Ivanova, A.I.; Savochkin, Y.V.; Kuznetsov, V.V. Effects of zinc on Scots pine (*Pinus sylvestris* L.) seedlings grown in hydroculture. *Plant Physiol. Biochem.* **2016**, *102*, 1–9. [CrossRef] [PubMed]
118. Pulford, I.D.; Watson, C. Phytoremediation of heavy metal-contaminated land by trees-A review. *Environ. Int.* **2003**, *29*, 529–540. [CrossRef]
119. Schvartzman, M.S.; Corso, M.; Fataftah, N.; Scheepers, M.; Nouet, C.; Bosman, B.; Carnol, M.; Motte, P.; Verbruggen, N.; Hanikenne, M. Adaptation to high zinc depends on distinct mechanisms in metallicolous populations of *Arabidopsis halleri*. *New Phytol.* **2018**, *218*, 269–282. [CrossRef]
120. Manara, A.; Fasani, E.; Furini, A.; DalCorso, G. Evolution of the metal hyperaccumulation and hypertolerance traits. *Plant Cell Environ.* **2020**, *43*, 2969–2986. [CrossRef]
121. Verbruggen, N.; Hanikenne, M.; Clemens, S. A more complete picture of metal hyperaccumulation through next-generation sequencing technologies. *Front. Plant Sci.* **2013**, *4*, 388. [CrossRef]
122. Ingle, R.A.; Mugford, S.T.; Rees, J.D.; Campbell, M.M.; and Smith, J.A.C. Constitutively high expression of the histidine biosynthetic pathway contributes to nickel tolerance in hyperaccumulator plants. *Plant Cell* **2005**, *17*, 2089–2106. [CrossRef]
123. Deinlein, U.; Weber, M.; Schmidt, H.; Rensch, S.; Trampczynska, A.; Hansen, T.H.; Husted, S.; Schjoerring, J.K.; Talke, I.N.; Krämer, U.; et al. Elevated nicotianamine levels in *Arabidopsis halleri* roots play a key role in zinc hyperaccumulation. *Plant Cell* **2012**, *24*, 708–723. [CrossRef] [PubMed]
124. Corso, M.; An, X.; Jones, C.Y.; Gonzalez-Doblas, V.; Schvartzman, M.S.; Malkowski, E.; Willats, W.G.T.; Hanikenne, M.; Verbruggen, N. Adaptation of *Arabidopsis halleri* to extreme metal pollution through limited metal accumulation involves changes in cell wall composition and metal homeostasis. *New Phytol.* **2021**, *230*, 669–682. [CrossRef] [PubMed]
125. Hanikenne, M.; Talke, I.N.; Haydon, M.J.; Lanz, C.; Nolte, A.; Motte, P.; Kroymann, J.; Weigel, D.; Kraemer, U. Evolution of metal hyperaccumulation required cisregulatory changes and triplication of HMA4. *Nature* **2008**, *453*, 391–396. [CrossRef] [PubMed]
126. Rai, K.K.; Pandey, N.; Meena, R.P.; Rai, S.P. Biotechnological strategies for enhancing heavy metal tolerance in neglected and underutilized legume crops: A comprehensive review. *Ecotoxicol. Environ. Saf.* **2021**, *208*, 111750. [CrossRef] [PubMed]
127. Koźmińska, A.; Wiszniewska, A.; Hanus-Fajerska, E.; Muszyńska, E. Recent strategies of increasing metal tolerance and phytoremediation potential using genetic transformation of plants. *Plant Biotechnol. Rep.* **2018**, *12*, 1–14. [CrossRef] [PubMed]
128. Chen, Y.; Xu, W.; Shen, H.; Yan, H.; Xu, W.; He, Z.; Ma, M. Engineering arsenic tolerance and hyperaccumulation in plants for phytoremediation by a PvACR3 transgenic approach. *Environ. Sci. Technol.* **2013**, *47*, 9355–9362. [CrossRef] [PubMed]

plants

MDPI

Article

Addition of Medicinal Plants Increases Antioxidant Activity, Color, and Anthocyanin Stability of Black Chokeberry (*Aronia melanocarpa*) Functional Beverages

Desislava Teneva, Daniela Pencheva, Ani Petrova, Manol Ognyanov, Yordan Georgiev and Petko Denev *

Laboratory of Biologically Active Substances, Institute of Organic Chemistry with Centre of Phytochemistry, Bulgarian Academy of Science, 139 Ruski Blvd., 4000 Plovdiv, Bulgaria; Desislava.Teneva@orgchm.bas.bg (D.T.); Daniela.Klisurova@orgchm.bas.bg (D.P.); Ani.Petrova@orgchm.bas.bg (A.P.); Manol.Ognyanov@orgchm.bas.bg (M.O.); Yordan.Georgiev@orgchm.bas.bg (Y.G.)
* Correspondence: petko.denev@orgchm.bas.bg; Tel.: +359-3264-2759

Abstract: The present study investigates the effect of the addition of medicinal plants, such as lady's mantle, lavender, rosehip, and meadowsweet, on the chemical composition, antioxidant activity, and color intensity of ready-to-drink aronia nectar during pasteurization and long-term storage. Pasteurization caused a significant decrease in anthocyanin content of aronia nectar, which reduced to 20% of the initial value after four months of storage. Herbs provided different protection to aronia anthocyanins that degraded more slowly during the four-month storage compared to pasteurized control without herbs. The addition of medicinal plants enriched aronia nectar with phenolic compounds and increased its antioxidant activity by up to 52% in meadowsweet-aronia nectar. Moreover, it was accompanied by a color intensity magnification due to co-pigmentation of aronia anthocyanins and herbal phenolics. In contrast to anthocyanins, which constantly degraded during the whole period, color intensity began to stabilize after 30 days, demonstrating that co-pigmentation was progressively established during the time and rosehip provided the best stabilization of aronia nectar color. Current research demonstrates for the first time that medicinal plants such as lady's mantle, rosehip, and especially meadowsweet can be used to increase antioxidant activity, color, and anthocyanin stability of black chokeberry functional beverages.

Keywords: black chokeberry (*Aronia melanocarpa*); anthocyanin stability; antioxidant activity; herbs; co-pigmentation; color stability; functional foods/beverages

Citation: Teneva, D.; Pencheva, D.; Petrova, A.; Ognyanov, M.; Georgiev, Y.; Denev, P. Addition of Medicinal Plants Increases Antioxidant Activity, Color, and Anthocyanin Stability of Black Chokeberry (*Aronia melanocarpa*) Functional Beverages. *Plants* **2022**, *11*, 243. https://doi.org/10.3390/plants11030243

Academic Editors: Milan S. Stankovic, Paula Baptista and Petronia Carillo

Received: 22 December 2021
Accepted: 15 January 2022
Published: 18 January 2022

Publisher's Note: MDPI stays neutral with regard to jurisdictional claims in published maps and institutional affiliations.

1. Introduction

Aronia melanocarpa, also known as black chokeberry, is a deciduous shrub that belongs to the *Rosaceae* family. Nowadays, chokeberries are cultivated as an important industrial crop and are processed into juices, nectars, wines, jams, and food-grade colorants. *Aronia melanocarpa* fruits are a good source of dietary fiber, vitamin B complex, carotenoids, tocopherols, vitamin C, and vitamin K, macroelements (K, Ca, P, Mg, Na), and microelements (Zn, Fe, Se, Cu, Mo, Cr, Mn, Si, Ni, B, V) [1]. Black chokeberry fruits reveal numerous health benefits and are among the richest sources of polyphenols and particularly anthocyanins in the plant kingdom [2,3]. Besides strong antioxidant and immunomodulatory activities, the beneficial health effects of chokeberry include gastroprotective, hypotensive, lipid-lowering, anticarcinogenic, neuroprotective, and cardioprotective effects [4–8]. Therefore, *Aronia melanocarpa* is recognized as a valuable medicinal plant [9]. The four major anthocyanins in *Aronia melanocarpa* are cyanidin-3-*O*-galactoside, cyanidin-3-*O*-arabinoside, cyanidin-3-*O*-glucoside, and cyanidin-3-*O*-xyloside [10]. In the past 20 years, the health benefits of anthocyanins have become a subject of numerous studies [11–13]. Anthocyanins act as antioxidants and show numerous health benefits, including anticancer, antiatherogenic, and anti-inflammatory effects [14]. Besides their health benefits, anthocyanins in foods are an

important quality parameter that affects customers' preferences. Anthocyanin stability in foods is affected by numerous factors, such as pH, solvents, temperature, and the presence of oxygen, enzymes, and other concomitant substances. The duration of heating during food processing has a strong influence on anthocyanin stability. Sadilova, Stintzing, and Carle have observed that elderberry anthocyanin content was very sensitive to thermal treatment and several studies reported anthocyanin reduction with an increase in temperature [15–17]. The heat-labile factors can force anthocyanin destruction, which could be accelerated by endogenous enzymes in fruits that cause pigment destruction during juice processing [17]. García-Viguera and Zafrilla have reported that temperature plays a critical role in anthocyanin loss during storage [18], whereas Kasparaviciene and Briedis revealed that eight-hour storage of black currant and black chokeberry juice concentrates at 60 °C resulted in a reduction in anthocyanins by 31% and 35%, and antioxidant activity decreased by 26% and 56%, respectively [19].

The combination of the attractive color of anthocyanins and their biological activities make the preservation of these pigments in foodstuffs and beverages an important technological problem. Co-pigmentation is one of the main mechanisms for the natural stabilization of anthocyanins. The co-pigmentation phenomenon occurs when a pigment (anthocyanin) and a co-pigment (colorless substance) form non-covalent complexes. It is observed as a bathochromic shift and hyperchromic effect, which stabilizes and modulates anthocyanin color, contributing to more intense color. However, it should be noted that most of the studies investigating co-pigmentation are performed in model systems, either with isolated and purified anthocyanins, or with model foods/beverages involving pure phenolic compounds [20,21].

As one of the richest sources of anthocyanins in the plant kingdom, black chokeberries and their products are thoroughly studied in regard to chemical composition and health benefits. However, studies regarding the stabilization of aronia anthocyanins through co-pigmentation are scarce. In our recent study, we investigated in model systems the co-pigmentation of anthocyanins isolated from black chokeberry with polyphenolic co-pigments and herbal extracts [22]. The investigated compounds provoked different co-pigmentation effects, accompanied by a color intensity (CI) magnification. The effect was profound at high co-pigment/pigment ratios, not characteristic for plant matter, and unachievable from a practical point of view. The addition of herbal extracts to purified anthocyanins led to a significant hyperchromic effect at much lower pigment/co-pigment ratios compared to pure compounds. Another study, using model beverages, revealed that chlorogenic acid enhanced the CI of aronia juice and that purified pigment from aronia had smaller co-pigmentation effects in comparison to fruit juice, indicating the participation of natural co-pigments present in fruits [23]. Furthermore, two studies investigated the effect of the addition of herbal extracts on the polyphenol content and composition of aronia juices without evaluating the effect on CI [24,25].

As a result of our previous study and literature review, we hypothesized that, except in model systems with purified anthocyanins, herbal extracts could exert their protective effect on black chokeberry anthocyanins and color stability in real food matrices. Moreover, this could be achieved in low concentrations, which are achievable in food processing, thus opening perspectives for potential practical application in the production of aronia-based functional foods. Therefore, the current study aimed to investigate the effect of the addition of herbs (lady's mantle, lavender, rosehip, and meadowsweet) on the chemical composition, color stability, and antioxidant activity of ready-to-drink nectar from black chokeberry fruits after pasteurization and four-month storage. Namely, meadowsweet, lavender, and lady's mantle extracts showed co-pigmentation with chokeberry anthocyanins in the above-mentioned study, whereas rosehip was chosen because of its high antioxidant potential and the observed synergistic effect in in vitro antioxidant activity, when mixed with aronia extracts [26]. Furthermore, it is known that co-pigmentation is progressively established during food storage and studies evaluating the co-pigmentation of aronia anthocyanins

with herbal extracts during processing and storage of real food matrices such as aronia drinks are required [27].

2. Results and Discussion

2.1. Effect of Herb Addition on Chemical Composition, Color Intensity, and Antioxidant Activity of Black Chokeberry Nectar

In the European Union, there are strict regulations towards the requirements for fruit-based drinks, including fruit juices and fruit nectars [28]. According to them, fruit nectar is "The fermentable but unfermented product which is obtained by adding water with or without the addition of sugars and/or honey to fruit juice, to fruit purée and/or to concentrated fruit purée, and/or to a mixture of those products". In our study, we chose four popular herbs to enrich aronia nectar with polyphenolic compounds and to investigate their effect on anthocyanin degradation and color stability after thermal pasteurization and four-month storage. The content of anthocyanins, polyphenols, as well as antioxidant activity and CI of black chokeberry nectar with 40% fruit content and aronia-herbal nectars are presented in Table 1. As it is evident from the results, black chokeberry nectar is a very rich source of polyphenols—3020.0 mg/L and particularly anthocyanins—700.4 mg/L, rendering very high oxygen radical absorbance capacity (ORAC) antioxidant activity of 63,878 µmol trolox equivalents (TE)/l. The addition of all herbs in a concentration of 2% significantly increased ($p < 0.05$) the polyphenol content of chokeberry nectar reaching 40%, when rosehip or meadowsweet extracts were added to the nectar. The increase in peroxyl radical scavenging activity (ORAC value) was even more significant ($p < 0.05$), exceeding 50% in the case of meadowsweet extract. Hydroxyl radical averting capacity (HORAC value) of chokeberry with meadowsweet was 29.6% higher than the pure chokeberry nectar ($p < 0.05$). Herb addition led to a decrease in anthocyanin content due to the soaking effect of aronia extract on dry herbs. As a result, CI of mixed aronia-herbal products decreased in all cases ($p < 0.05$), from 42.8 for pure aronia nectar to 36.8 for chokeberry with lavender nectar. The addition of herbs to aronia nectar was related to an increase in colored hue, which was significant ($p < 0.05$) for rosehip and lady's mantle and could be attributed to carotenoid content of rosehip and brownish pigments in dry lady's mantle aerial parts.

Table 1. Anthocyanin and polyphenol content, antioxidant activity, color intensity, and color hue of black chokeberry nectar with or without herb addition.

	Chokeberry	Chokeberry with Lavender	Chokeberry with Meadowsweet	Chokeberry with Rosehip	Chokeberry with Lady's Mantle
Anthocyanin content, mg/L	700.4 ^{c} ± 16.0	587.0 ^{a} ± 12.5	642.9 ^{b} ± 13.5	571.9 ^{a} ± 19.7	565.2 ^{a} ± 21.1
Total polyphenol content, mg/L	3020.0 ^{a} ± 65.4	3395.7 ^{b} ± 59.4	4177.2 ^{d} ± 120.3	4281.4 ^{d} ± 88.7	3851.5 ^{c} ± 53.3
ORAC [1], µmol TE/L	63,878 ^{a} ± 190	73,198 ^{b} ± 1750	96,973 ^{d} ± 1488	91,713 ^{d} ± 3322	78,227 ^{c} ± 2319
HORAC [2], µmol GAE [3]/L	14,556 ^{a} ± 32	16,336 ^{c} ± 54	18,860 ^{d} ± 745	15,158 ^{b} ± 873	15,612 ^{b} ± 203
CI [4]	42.8 ^{b} ± 1.0	36.8 ^{a} ± 2.3	39.6 ^{a} ± 2.4	40.0 ^{a} ± 1.6	39.3 ^{a} ± 1.6
Color hue	9.0 ^{ab} ± 0.8	9.8 ^{abc} ± 0.6	8.7 ^{a} ± 0.4	11.7 ^{d} ± 1.0	10.7 ^{cd} ± 0.6

[1] Oxygen radical absorbance capacity; [2] Hydroxyl radical averting capacity; [3] Gallic acid equivalents; [4] Color intensity. Results are presented as mean values ± standard deviation (SD). There are no significant differences among values marked with the same superscript letters in individual lines.

The addition of herbs to increase polyphenol content and antioxidant activity of aronia-based products have been investigated by other authors, as well. For example, Skapska et al. used *Cistus*, green tea, and nettle to fortify 80% aronia extracts with additional antioxidants [24]. Similar to our findings, the authors found that the addition of herbal extracts to aronia extract increases its antioxidant activity, measured by several in vitro assays, such as ORAC, ABTS, and DPPH. Moreover, a synergistic effect of selected herbal extracts was noted in total antioxidant capacity. In our study, the ORAC value of 40% aronia nectar was similar to their results for 80% aronia extract. This could be due to either difference in the raw material or the technological processing since our recent study demonstrated that black chokeberry fruits and functional drinks differ significantly in

their chemical composition and antioxidant activity [29]. In another study, Sidor et al. investigated the effect of adding aqueous cinnamon and clove extracts on polyphenol loss in cloudy and clarified chokeberry juices [25]. The authors demonstrated that the addition of plant extracts prior to the pasteurization process influenced the content of phenolic compounds in the chokeberry juice and also observed a slight decrease in the anthocyanin content after the addition of herbal extracts.

In general, medicinal plants lack or are poor in anthocyanins, but are rich in other classes of phenolic compounds that could act as co-pigments to anthocyanins. The content of the major phenolic compounds of black chokeberry nectar, without and with herb addition, are presented in Table 2. Besides being a rich source of anthocyanins (cumulative content—700.4 mg/L), pure chokeberry nectar is a very rich source of several other classes of phenolic compounds (hydroxycinnamic acids, flavonols, and flavan-3-ols). Similarly to anthocyanin content, the content of other phenolic components such as neochlorogenic acid and quercetin decreased after the addition of herbs, again related to the soaking effect of aronia extract on dried herbs. On the other hand, the addition of herbs during extraction enriched chokeberry nectar with additional phenolics, such as *p*-coumaric and ellagic acids, and rosmarinic acid in the case of lavender (corresponding chromatograms are shown in Supplementary Figure S1). The addition of meadowsweet to aronia nectar increased significantly both the content of epicatechin from 42.4 mg/L to 115.3 mg/L ($p < 0.05$) and quercetin-3-glucoside from 116 mg/L to 145.5 mg/L, ($p < 0.05$), whereas the addition of 2% lady's mantle during black chokeberry extraction increased the content of rutin in the product with 225% ($p < 0.05$). It is known that these flavonoids and particularly quercetin derivatives are strong chain-breaking antioxidants. Moreover, a recent study revealed that quercetin and epicatechin are the strongest antioxidants in black chokeberry fruits. However, due to the relatively low content, their contribution to the antioxidant activity of the fruits is not so significant compared to proanthocyanidins [3]. As it is demonstrated here, the addition of meadowsweet and lady's mantle to aronia nectar enriched it in these flavonoids, which could explain the significantly higher ORAC activity of these two products when compared to pure aronia nectar ($p < 0.05$) (Table 1).

Table 2. Major phenolic constituents (mg/L) of black chokeberry nectar with or without herb addition.

	Chokeberry	Chokeberry with Lavender	Chokeberry with Meadowsweet	Chokeberry with Rosehip	Chokeberry with Lady's Mantle
Gallic acid	-	-	$34.9^{a} \pm 3.4$	$57.2^{b} \pm 4.8$	$32.4^{a} \pm 4.1$
Neochlorogenic acid	$322.1^{b} \pm 18.5$	$242.1^{a} \pm 12.4$	$273.3^{a} \pm 16.5$	$254.3^{a} \pm 21.0$	$240.2^{a} \pm 20.3$
Chlorogenic acid	$269.1^{b} \pm 11.2$	$181.6^{a} \pm 10.8$	$280.6^{b} \pm 19.6$	$273.8^{b} \pm 28.1$	$283.1^{b} \pm 21.2$
Caffeic acid	-	$19.9^{a} \pm 2.6$	-	-	-
Epicatechin	$42.4^{a} \pm 3.1$	$50.7^{ab} \pm 4.8$	$115.3^{c} \pm 9.6$	$53.9^{b} \pm 4.1$	$53.7^{b} \pm 2.3$
p-Coumaric acid	-	$17.4^{b} \pm 1.2$	$16.9^{b} \pm 2.1$	$11.7^{a} \pm 0.9$	$20.5^{b} \pm 0.8$
Ferulic acid	-	$22.1^{a} \pm 0.8$	$58.3^{c} \pm 3.1$	$45.2^{b} \pm 2.1$	$47.2^{b} \pm 4.0$
Rutin	$178.0^{a} \pm 8.1$	$124.7^{a} \pm 9.6$	$188.4^{b} \pm 9.2$	$172.8^{b} \pm 5.1$	$579.8^{c} \pm 14.6$
Ellagic acid	-	-	$34.2^{a} \pm 1.2$	$49.5^{b} \pm 2.9$	$65.9^{c} \pm 4.1$
Quercetin-3-glucoside	$116.0^{a} \pm 7.2$	$132.7^{ab} \pm 5.6$	$176.2^{c} \pm 9.9$	$145.5^{b} \pm 13.1$	$118.8^{a} \pm 10.5$
Rosmarinic acid	-	$29.2^{a} \pm 0.2$	-	-	-
Quercetin	$14.5^{b} \pm 0.8$	$6.2^{a} \pm 0.2$	$12.3^{b} \pm 0.6$	$8.7^{a} \pm 0.9$	$8.4^{a} \pm 1.0$

Results are presented as mean values ± SD. There are no significant differences among values marked with the same superscript letters in individual lines ($p < 0.05$).

2.2. Changes in Chemical Composition, Color Intensity, and Antioxidant Activity of Black Chokeberry Nectar, without and with Herbs, during Pasteurization and Storage

2.2.1. Changes in Anthocyanin Content and Polyphenol Constituents of Black Chokeberry Nectar, without and with Herbs, during Pasteurization and Storage

Anthocyanins are particularly desired components in foods because on the one hand, they render the food an attractive red color, but on the other, due to their numerous health benefits, they increase functional and health-promoting properties of foods [22]. Because of their unstable nature, anthocyanins are readily destroyed during processing and storage, and the natural stabilization of anthocyanins with co-pigments is an important problem of practical significance. The rate of degradation of anthocyanins increases during processing

and storage as temperature increases and follows first-order kinetics [30]. The increase in temperature causes hydrolysis of the glycosidic bonds, which leads to a loss in anthocyanin color and formation of brown chalcones [31]. Several studies have shown that aronia anthocyanins are prone to degradation during technological processing and especially heating. For example, Hwan and Ki investigated the effects of different factors (pH, temperature, light, sugars, organic acids, etc.) on the stability of anthocyanins extracted from *Aronia melanocarpa* and revealed that high temperatures and prolonged heating substantially reduced anthocyanin content [32]. Another study demonstrated that a decrease of anthocyanins in aronia drinks as a result of thermal pasteurization treatment could be diminished by high-pressure carbon dioxide preservation, which can be explained by a much lower heat dose during the latter process during storage [24]. Similar results were observed by Wilkes et al. after pasteurization of chokeberry juice. Moreover, anthocyanin losses were paralleled by increased polymeric color values, indicating that the small amounts of anthocyanins remaining were present in large part in polymeric forms [33]. Therefore, adding herbal extracts to anthocyanin-rich foods is an interesting approach to delay their degradation [34,35]. Figure 1 depicts the changes in anthocyanin content of the studied beverages after pasteurization (90°C, 10 min). Since co-extraction of chokeberry mesh and herbs led to a decrease of chokeberry nectar anthocyanin content, results are presented as percent of the initial anthocyanin content of the corresponding sample before pasteurization (Panel A) and compared to the content of anthocyanins in the control nectar without herb addition (Panel B). Our results showed that indeed anthocyanins in aronia nectar were degraded rapidly after thermal treatment at 90 °C and their degradation was constant during the whole monitoring period of 120 days, reaching about 20% of the initial value.

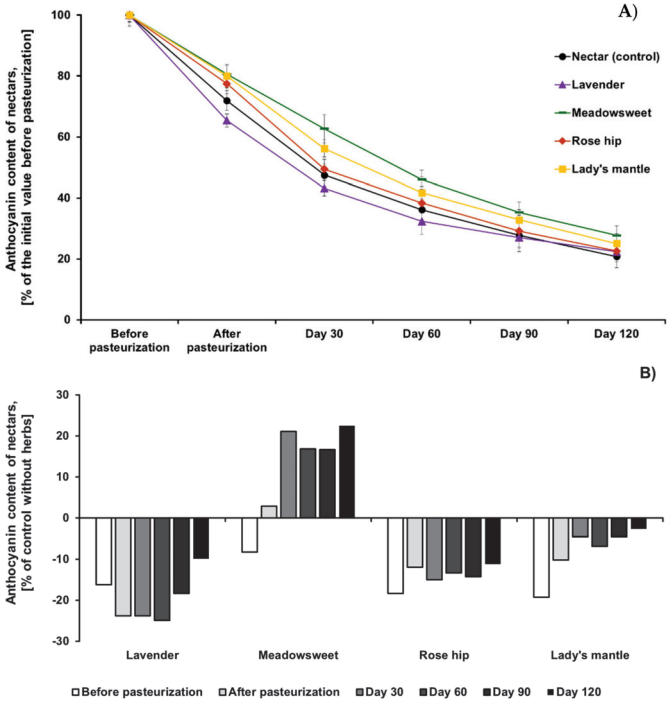

Figure 1. Changes of anthocyanin content of black chokeberry nectar, with or without the addition of herbs, after pasteurization and during storage: (**A**) expressed as a percent of the sample before pasteurization; (**B**) expressed as percent from the control (nectar without herb) at the corresponding time point.

The addition of meadowsweet, rosehip, and lady's mantle reduced anthocyanin degradation in all time points. Interestingly, the protective effect of the herbal extracts was most pronounced at shorter storage periods (30 days and 60 days), whereas after 120 days of storage differences in anthocyanin degradation were smaller. For example, anthocyanins from chokeberry nectar degraded with 32% and 19.8% less when meadowsweet was added in the extraction, respectively, after 30 and 60 days of storage. As it could be seen from Figure 1, Panel B, all herbs tended to protect black chokeberry anthocyanins during pasteurization and storage. However, the effect was most pronounced with meadowsweet. Although the initial content of anthocyanins in chokeberry-meadowsweet beverage was lower than that in pure aronia nectar, the content of anthocyanins immediately after pasteurization was higher than the control and increased significantly during storage. This is evidence that meadowsweet extract protected aronia anthocyanins from degradation during pasteurization and storage.

2.2.2. Changes in Color Intensity of Black Chokeberry Nectar, without and with Herbs, during Pasteurization and Storage

Quite often, food color is only related to anthocyanin content, and CI or color expression is not taken into consideration. As already discussed, the co-pigmentation phenomenon could significantly increase CI at the same levels of anthocyanins in the sample [3]. However, it should be noted that most of the studies investigating co-pigmentation are in model systems with isolated and purified anthocyanins since real food matrices are more difficult to investigate, especially when herbs are added to the system. Usually, co-pigmentation is observed as a bathochromic shift and/or hyperchromic effect, which stabilizes and modulates anthocyanin color, contributing to a more intense color [20,21]. However, the addition of colored herbs during extraction could mask both hyperchromic and bathochromic effects. Therefore, we used CI as a marker for color expression. This method was proposed by Glories for the evaluation of wine color and later adopted in many studies [36–39].

The changes of CI of the studied beverages after thermal treatment and during storage are shown in Figure 2. Although anthocyanins are the main color pigments in the studied beverages, the trend of CI change was completely different from that of anthocyanin degradation. Thermal treatment led to a significant drop in CI (Figure 2, Panel A), probably due to anthocyanin degradation that occurred during pasteurization. In all cases, CI decreased within the first 30 days of storage. However, this process occurred at a slower rate in comparison to anthocyanin degradation (Figure 1). In the case of lavender, meadowsweet, and lady's mantle, this decrease continued to the 60th day of storage, and after that, CI showed a trend towards stabilization. In the case of rosehip, stabilization of CI began after 30 days of storage. Due to the decreased anthocyanin content of mixed aronia-herbal beverages, their CI before pasteurization was lower than that of the nectar without herbs (Figure 2, Panel B). In all studied beverages, there was a trend for increased CI in comparison to control nectar. Although aronia-lavender nectar showed a trend for CI stabilization during storage, the absolute value of CI did not pass the value of the nectar at the corresponding time point. However, in all other cases (meadowsweet, rosehip, and lady's mantle), after approximately 30 days of storage, the absolute values of CI exceeded that of the control nectar. For example, after 120 days of storage, aronia nectar with added rosehip had a CI that was 31.2% higher than that of the pure chokeberry nectar. Interestingly, the color of pure aronia nectar, which had the highest rate of anthocyanin degradation, also showed a trend for stabilization after approximately 60 days of storage. This is probably due to the high native content of hydroxycinnamic acids, epicatechin, and proanthocyanidins in aronia berries, which are strong co-pigments for aronia anthocyanins and could explain the elevated anthocyanin and color stability of aronia in comparison to other berries with non-acylated anthocyanins [22].

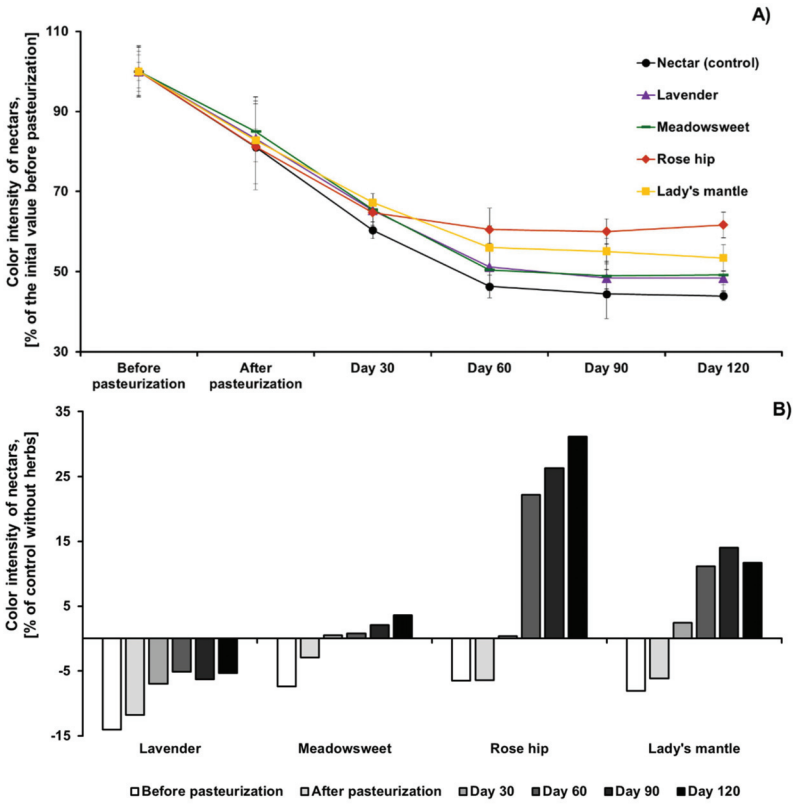

Figure 2. Changes in color intensity of black chokeberry nectar, with or without the addition of herbs, after pasteurization and during storage: (**A**) Expressed as percent before pasteurization; (**B**) Expressed as percent from the control (nectar without herb) at the corresponding time point.

2.2.3. Changes in Antioxidant Activity of Black Chokeberry Nectar, without and with Herbs, during Pasteurization and Storage

Measuring the antioxidant activity of foodstuffs is important from two aspects. Firstly, antioxidant components could protect food primary and secondary metabolites from oxidation, rancidity, and resulting degradation, and, therefore, preserve food quality. Secondly, food antioxidants taken with the diet could exert their antioxidant-related effects in the body, thus promoting human health [40]. Interestingly, we demonstrated that functional beverages obtained from the same batch of aronia fruits, which differed in their polyphenol content and antioxidant activity due to different technological processing, revealed different biological activity as well. This was demonstrated in a rat model of indomethacin-induced gastric ulcers, and the gastroprotective effect of aronia juices was related to their polyphenol content and antioxidant activity [5]. Furthermore, the effect was increased by enriching aronia juice with polyphenols from lady's mantle.

In order to monitor the antioxidant activity changes after thermal treatment and during storage, we employed three different assays. ORAC is an indicator for the peroxyl radical scavenging capacity of antioxidants via hydrogen atom transfer, whereas analysis for total polyphenols relies on a single electron transfer. HORAC is an indicator of the ability of an antioxidant to prevent the formation of hydroxyl radicals during Fenton-like reactions [41]. Figure 3 presents data on the changes in antioxidant activity after thermal treatment and during 120 days of storage. As already stated, the addition of herbs significantly increased the polyphenol content of chokeberry nectar, and antioxidant

activity measured by all three assays stayed comparatively stable during the whole period of storage and monitoring. These results correlate well with the total polyphenol content, which is kept more stable than anthocyanins during storage. From these results, it could be concluded that anthocyanin degradation did not significantly affect the antioxidant activity of aronia beverages. Anthocyanin degradation, caused by high temperature, results in the formation of benzoic acid derivatives and coumarins, with preserved hydroxyl groups and antioxidant activity [42,43]. In a previous study, we demonstrated that chokeberry proanthocyanidins were the major contributor to aronia antioxidant activity and, therefore, anthocyanin degradation did not significantly affect fruit antioxidant properties [3].

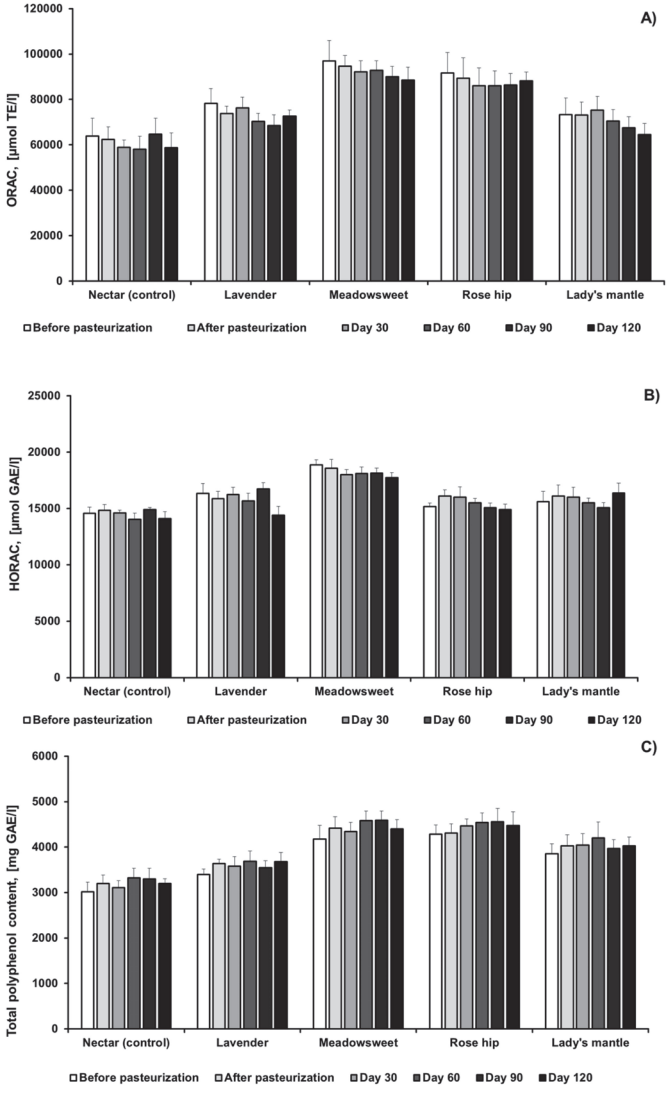

Figure 3. Changes in (**A**) ORAC (Oxygen radical absorbance capacity); (**B**) HORAC (Hydroxyl radical averting capacity) antioxidant activities and (**C**) total polyphenol content during thermal processing and storage of black chokeberry nectar with or without the addition of herbs. TE (trolox equivalents); GAE (Gallic acid equivalents). Results are presented as mean values ± SD.

It is very difficult to relate the observed herb-induced magnification of anthocyanin or color stability with the observed antioxidant properties of aronia-herbal beverages. The extract of meadowsweet protected to the highest extent aronia anthocyanins from degradation during storage, but rosehip extract provided the best stabilization of aronia nectar color. Usually, there is a good correlation between polyphenol content and antioxidant activity, and it is known that certain phenolics could prevent or delay anthocyanin degradation [44]. Furthermore, the effectiveness of phenolic compounds as co-pigments is not related to the polyphenol content and resulting antioxidant properties, indicating that the qualitative phenolic composition of the extracts is more important than the total polyphenol content [22].

3. Materials and Methods

3.1. Chemicals

Cyanidin-3-*O*-galactoside chloride (≥97%), cyanidin-3-*O*-arabinoside chloride (≥97%), and cyanidin-3-*O*-glucoside chloride (≥97%) were purchased from Extrasynthese S.A. (Genay Cedex, France). Chlorogenic acid (≥95%), caffeic acid (≥98%), ferulic acid (≥99%), *p*-coumaric acid (≥98%), rutin (≥94%), epicatechin (≥90%), quercetin-3-*O*-glucoside (≥90%), quercetin (≥98%), rosmarinic acid (≥98%), ellagic acid (≥95%), neochlorogenic acid (≥98%), gallic acid (100%), Trolox (≥98%), fluorescein (FL) disodium salt (100%), and 2,2′-Azobis(2-amidinopropane) dihydrochloride (AAPH) (≥98%) were purchased from Sigma-Aldrich (Steinheim, Germany) and Folin–Ciocalteu's phenol reagent was purchased from Merck (Darmstadt, Germany). All other solvents used were of analytical grade and purchased from local distributors.

3.2. Plant Materials

Black chokeberry fruits were cultivated from Dimitar Sokolov (Gotse Delchev, Latitude: 41.5667, Longitude: 23.7333, Bulgaria) and harvested in the stage of full maturity in August 2020. Fresh fruits were frozen and stored at −18 °C by Vitanea Ltd. (Plovdiv, Bulgaria) and delivered frozen prior to extraction and analysis.

Cut herbs (size 1–4 mm): common lavender (*Lavandula angustifolia* Mill.) aerial parts, lady's mantle (*Alchemilla glabra* Neygenf.) aerial parts, and meadowsweet (*Filipendula ulmaria* L.) aerial parts, produced by Herbal pharmacy No. 1, Plovdiv were purchased from "Pharmacy 36.6", Plovdiv, Bulgaria. Dried deseeded rosehips (*Rosa canina* L.) fruits (Size 2–8 mm, batch number RSPLH01032021L) were purchased from Balevski and Kirov Ltd. (Tryavna, Gabrovo region, Bulgaria).

3.3. Preparation of Beverages

Black chokeberry nectar with 40% fruit content was prepared according to a previously reported procedure [29]. Briefly, frozen aronia fruits were defrosted at room temperature and homogenized in a laboratory blender. After that, 400 g of fruit homogenate were mixed with 600 mL ultrapure water, transferred to a brown-glass bottle, and incubated in a thermostatic water bath shaker (NUVE, Asagi Ovecler Ankara, Turkey) for 1 h, at 60 °C. After that, solid fruit residue was separated from the clear aronia nectar by pressing through a cheesecloth.

For the preparation of mixed aronia-herbal beverages, 400 g of fruit homogenate were mixed with 600 mL ultrapure water and 20 g (2% *w*/*v*) of the respective herb (lavender, lady's mantle, meadowsweet, or rosehip). Mixtures were transferred in brown-glass bottles and incubated in a thermostatic water bath shaker (NUVE, Asagi Ovecler Ankara, Turkey) for 1 h, at 60 °C. After that, solid fruit-herbal residues were separated from the clear nectars by pressing through a cheesecloth.

All extraction procedures were repeated 5 times in order to collect approximately 3.5 L of all nectars necessary for the whole experiment. 50 mL from all samples were separated for analysis before thermal treatment, whereas the remaining amounts were subjected to pasteurization.

3.4. Pasteurization and Storage of Black Chokeberry Nectars with or without Herb Addition

Pasteurization of fruit nectars was performed according to Rabie et al., with slight modifications [45]. Briefly, filtrated nectars were poured in 250 mL glass bottles, capped with twist-off metal caps, transferred into a 90 °C water bath, and pasteurized for 10 min minutes. Pasteurized nectars were cooled to room temperature in a cold water bath for 30 min. In total, 10 bottles were kept from each nectar—2 parallel samples for each time point (after pasteurization; and 30, 60, 90, and 120 days of storage).

Pasteurized bottles were kept in a dark place at 20.0 ± 1.0 °C for the whole storage period. Two bottles from each sample/nectar were randomly chosen, either after pasteurization or at the corresponding time points of storage, and opened immediately before analysis.

3.5. Color Evaluation

CI and color hue were calculated according to Bimpilas et al. via the following formulas [37]:

$$CI = A_{420} + A_{520} + A_{620}$$

$$\text{Color hue} = A_{420}/A_{520}$$

where: A_{420}, $A_{520,}$ and A_{620} are the absorbance values measured at 420 nm, 520 nm, and 620 nm, respectively.

Using this method, the absorbance of samples was measured at 420 nm (yellow), 520 nm (red), and 620 nm (blue), thus reflecting the% contribution of different pigment categories to the expressed color. All spectrophotometric measurements were performed at a Biowave DNA spectrophotometer using a 0.05 mm optical path glass cell (Biochrom WPA, Cambridge, United Kingdom). Results for color intensity and color hue were recalculated for 1 mm optical path.

3.6. Total Polyphenol Content Analysis

Total polyphenols were determined according to the method of Singleton and Rossi, with the Folin–Ciocalteu's reagent [46]. Gallic acid was employed as a calibration standard, and results were expressed in mg gallic acid equivalents (GAE) per liter of extract ± SD, (n = 6).

3.7. HPLC Determination of Anthocyanins

The quantitation of anthocyanins was conducted on a Nexera-i LC2040C Plus UHPLC system (Shimadzu Corporation, Kyoto, Japan) with a UV detector and a binary pump. The system was controlled by LabSolutions (ver. 5.98) software (Shimadzu Corp.). A wavelength of 520 nm was used. Anthocyanins were separated using an Agilent TC-C18 column (5 μm, 4.6 × 250 mm) at 25 °C. The following mobile phases were used: 5% formic acid (A) and 100% methanol (B) at a flow rate of 1.0 mL/min. The gradient condition started with 15% B and linearly increased to 30% B at 20 min. The sample injection volume was 20 μL. The results were calculated from the relationship between the peak area response and concentration, using linear regression for each analyte. The R-squared values (R^2) were >0.99 for all calibration curves. Anthocyanins were identified by comparing the retention times of unknown analytes with analytical grade standards (cyanidin-3-*O*-galactoside, cyanidin-3-*O*-arabinoside, and cyanidin-3-*O*-glucoside). The total anthocyanin content was expressed as the sum of the content of the three anthocyanins and expressed as mg per liter of extract ± SD (n = 4).

3.8. HPLC Analysis of Phenolic Compounds

The main polyphenol compounds of aronia and herbal extracts were quantified on a Nexera-i LC2040C Plus UHPLC system (Shimadzu Corporation, Kyoto, Japan) with a UV detector and a binary pump. A wavelength of 280 nm was used. The separation of phenolics was performed on an Agilent TC-C18 column (5 μm, 4.6 mm × 250 mm) at

25 °C. The mobile phases constituted 0.5% acetic acid (A) and 100% acetonitrile (B) at a flow rate of 0.8 mL/min. The gradient condition started with 14% B, between 6 min and 30 min linearly increased to 25% B, then to 50% B at 40 min. The sample injection volume was 20 µL. The results were calculated from the relationship between the peak area response and concentration, using linear regression for each analyte. The R-squared values (R^2) were >0.99 for all calibration curves. All phenolic compounds were identified by comparing the retention times of unknown analytes with analytical grade standards (chlorogenic acid, caffeic acid, ferulic acid, *p*-coumaric acid, rutin, epicatechin, quercetin-3-*O*-glucoside, quercetin, rosmarinic acid, ellagic acid, neochlorogenic acid) and expressed as mg per liter of extract ± SD (n = 4).

3.9. Oxygen Radical Absorbance Capacity (ORAC) Assay

Oxygen Radical Absorbance Capacity was measured according to the method of Ou, Hampsch-Woodill, and Prior [47] with some modifications [48]. Solutions of AAPH, FL, and trolox were prepared in a phosphate buffer (75 mmol/L, pH 7.4). Samples were diluted in the phosphate buffer as well. The reaction mixture (total volume 200 µL) contained FL—(170 µL, final concentration 5.36×10^{-8} mol/L), AAPH—(20 µL, final concentration 51.51 mmol/L), and sample—10 µL. The FL solution and sample were incubated at 37 °C for 20 min directly in a microplate reader, and AAPH (dissolved in buffer at 37 °C) was added. The mixture was incubated for 30 s before the initial fluorescence was measured. After that, the fluorescence readings were taken at the end of every cycle (1 min) after shaking. For the blank, 10 µL of phosphate buffer was used instead of the extract. Trolox solutions (6.25; 12.5; 25 and 50 µmol/L) were used for defining the standard curve. ORAC was measured using a FLUOstar OPTIMA plate reader (BMG Labtech, Germany), excitation wavelength of 485 nm and emission wavelength of 520 nm were used. ORAC values were expressed in µmol TE per liter of extract ± SD (n = 8).

3.10. Hydroxyl Radical Averting Capacity (HORAC) Assay

HORAC was performed as described by Ou et al. [49]. Briefly, hydrogen peroxide solution of 0.55 M was prepared in distilled water. 4.6 mM Co(II) was prepared as follows: 15.7 mg of $CoF_2 \cdot 4H_2O$ and 20 mg of picolinic acid were dissolved in 20 mL of distilled water. FL—170 µL (60 nM, final concentration) and 10 µL of the sample were incubated at 37 °C for 10 min directly in the FLUOstar plate reader. After incubation 10 µL H_2O_2 (27.5 mM, final concentration) and 10 µL of Co(II) (230 µM final concentration) solutions were subsequently added. The initial fluorescence was measured, after which the readings were taken every minute after shaking. For the blank sample, a phosphate buffer solution was used. 100, 200, 600, 800, and 1000 µM gallic acid solutions (in phosphate buffer 75 mM, pH = 7.4) were used for building the standard curve. Measurements were performed on a FLUOstar OPTIMA fluorometer (BMG LABTECH, Offenburg, Germany). The excitation wavelength of 485 nm and emission wavelength of 520 nm was used. The results were expressed in micromole gallic acid equivalents (µmol GAE) per liter of extract ± SD (n = 8).

3.11. Statistical Analysis

All samples were prepared and analyzed in duplicates. The HPLC analyses were performed twice for every single sample (n = 4), whereas other analyses were run at least in triplicates for each sample (n = 6). Results were expressed as mean values ± standard deviations. One-way analysis of variance (ANOVA) and Student's t-test were used to evaluate the differences of the mean between groups. *p* values less than 0.05 were considered to be significant. Microsoft Excel, 2013 (Microsoft Corporation, Redmond, WA, USA) was used in the analyses.

4. Conclusions

The current work provides evidence for the first time that the addition of herbs during the processing of black chokeberry fruits can successfully increase polyphenol content,

antioxidant activity, color, and anthocyanin stability of resulting functional beverages, thus increasing their functionality and consumers' acceptance. However, different herbs provided different protective effects. Meadowsweet extracts protected to the highest extent aronia anthocyanins from degradation, but rosehip provided the best stabilization of aronia nectar color during storage. Therefore, each herbal material should be investigated for its ability to increase anthocyanin and/or color stability of foods. Interestingly, CI decreased with a different pattern from anthocyanin degradation, thus revealing that the co-pigmentation effect in chokeberry nectar with herbal phenolics was established after the first month of beverage storage. Our research findings could find practical application in the industrial production of aronia-based functional drinks with enhanced antioxidant activity and stabilized anthocyanins, and color for the prevention and supplementation of oxidative stress-related diseases.

Supplementary Materials: The following supporting information can be downloaded at: https://www.mdpi.com/article/10.3390/plants11030243/s1, Figure S1. UHPLC elution pattern of phenolic constituents: (A) chokeberry with meadowsweet; (B) chokeberry with lavender; (C) chokeberry with rose hip; (D) chokeberry with lady's mantle; (E) chokeberry (control).

Author Contributions: Conceptualization, P.D.; methodology, P.D.; investigation, D.T., D.P., A.P., M.O., Y.G.; resources, P.D.; writing—original draft preparation, P.D., D.T.; writing—review and editing, M.O., Y.G.; supervision, P.D.; project administration, P.D.; funding acquisition, P.D. All authors have read and agreed to the published version of the manuscript.

Funding: This research was supported by the Bulgarian National Science Fund, grant No. DN 09/20. Part of the laboratory equipment used in the study was purchased with the financial support of Operational Program "Science and Education for Smart Growth" 2014–2020, co-financed by European Union through the European Structural and Investment Funds, Grant BG05M2OP001-1.002-0012.

Institutional Review Board Statement: Not applicable.

Informed Consent Statement: Not applicable.

Data Availability Statement: Data is contained within the article.

Acknowledgments: We greatly acknowledge Vasil Georgiev from Laboratory of Cell Biosystems, The Stephan Angeloff Institute of Microbiology, Bulgarian Academy of Sciences for providing a Biowave DNA spectrophotometer for color evaluation measurements.

Conflicts of Interest: The authors declare no conflict of interest.

References

1. Sidor, A.; Gramza-Michałowska, A. Black chokeberry *Aronia melanocarpa* L. a qualitative composition, phenolic profile and antioxidant potential. *Molecules* **2019**, *24*, 3710. [CrossRef] [PubMed]
2. Denev, P.; Kratchanov, C.; Ciz, M.; Lojek, A.; Kratchanova, M. Bioavailability and antioxidant activity of black chokeberry (*Aronia melanocarpa*) polyphenols: In vitro and in vivo evidences and possible mechanisms of action. A Review. *Compr. Rev. Food Sci. Food Saf.* **2012**, *11*, 471–489. [CrossRef]
3. Denev, P.; Číž, M.; Kratchanova, M.; Blazheva, D. Black chokeberry (*Aronia melanocarpa*) polyphenols reveal different antioxidant, antimicrobial and neutrophil-modulating activities. *Food Chem.* **2019**, *284*, 108–117. [CrossRef]
4. Bushmeleva, K.; Vyshtakalyuk, A.; Terenzhev, D.; Belov, T.; Parfenov, A.; Sharonova, N.; Nikitin, E.; Zobov, V. Radical scavenging actions and immunomodulatory activity of *Aronia melanocarpa* propylene glycol extracts. *Plants* **2021**, *10*, 2458. [CrossRef] [PubMed]
5. Banach, M.; Wiloch, M.; Zawada, K.; Cyplik, W.; Kujawski, W. Evaluation of antioxidant and anti-inflammatory activity of anthocyanin-rich water-soluble aronia dry extracts. *Molecules* **2020**, *25*, 4055. [CrossRef]
6. Daskalova, E.; Delchev, S.; Topolov, M.; Dimitrova, S.; Uzunova, Y.; Valcheva-Kuzmanova, S.; Kratchanova, M.; Vladimirova-Kitova, L.; Denev, P. *Aronia melanocarpa* (Michx.) Elliot fruit juice reveals neuroprotective effect and improves cognitive and locomotor functions of aged rats. *Food Chem. Toxicol.* **2019**, *132*, 110674. [CrossRef] [PubMed]
7. Daskalova, E.; Delchev, S.; Vladimirova-Kitova, L.; Kitov, S.; Denev, P. Black chokeberry (*Aronia melanocarpa*) functional beverages increase HDL-cholesterol levels in aging rats. *Foods* **2021**, *10*, 1641. [CrossRef]
8. Gajic, D.; Saksida, T.; Koprivica, I.; Vujicic, M.; Despotovic, S.; Savikin, K.; Jankovi, T.; Stojanovic, I. Chokeberry (*Aronia melanocarpa*) fruit extract modulates immune response in vivo and in vitro. *J. Funct. Foods* **2020**, *66*, 2–9. [CrossRef]
9. Valcheva-Kuzmanova, S.; Belcheva, A. Current knowledge of *Aronia melanocarpa* as a medicinal plant. *Folia Med.* **2006**, *48*, 11–17.

10. Dorneanu, R.; Cioanca, O.; Chifiriuc, O.; Albu, E.; Tuchiluș, C.; Mircea, C.; Salamon, I.; Hăncianu, M. Synergic benefits of *Aronia melanocarpa* anthocyanin-rich extracts and antibiotics used for urinary tract infections. *Farmacia* **2017**, *65*, 778–783.
11. Spinardi, A.; Cola, G.; Gardana, C.; Mignani, I. Variation of anthocyanin content and profile throughout fruit development and ripening of highbush blueberry cultivars grown at two different altitudes. *Front. Plant Sci.* **2019**, *19*, 3–5. [CrossRef]
12. Fan, R.; Sun, Q.; Zeng, J.; Zhang, X. Contribution of anthocyanin pathways to fruit flesh coloration in pitayas. *Plant Biol.* **2020**, *20*, 361. [CrossRef]
13. Ponder, A.; Hallmann, E.; Kwolek, M.; Srednicka-Tober, D.; Kazimierczak, R. Genetic differentiation in anthocyanin content among berry fruits. *Mol. Biol.* **2021**, *43*, 4. [CrossRef] [PubMed]
14. Brand, M.H.; Connolly, B.A.; Levine, L.H.; Richards, J.T.; Shine, S.M.; Spencer, L.E. Anthocyanins, total phenolics, ORAC and moisture content of wild and cultivated dark-fruited *Aronia* species. *Sci. Hortic.* **2017**, *224*, 332–342. [CrossRef]
15. Sadilova, E.; Stintzing, F.C.; Carle, R. Thermal degradation of acylated and nonacylated anthocyanins. *J. Food Sci.* **2006**, *71*, 504–512. [CrossRef]
16. Rhim, J.W. Kinetics of thermal degradation of anthocyanin pigment solutions driven from red flower cabbage. *Food Sci. Biotechnol.* **2002**, *11*, 361–364.
17. Brownmiller, C.; Howard, L.R.; Prior, R.L. Processing and storage effects on monomeric anthocyanins, percent polymeric color, and antioxidant capacity of processed blueberry. *J. Food Sci.* **2008**, *73*, 72–79. [CrossRef]
18. García-Viguera, C.; Zafrilla, P. Changes in anthocyanins during food processing: Influence on color. In *Chemistry and Physiology of Selected Food Colorants*; Ames, J.M., Hofmann, T., Eds.; American Chemical Society: Washington, DC, USA, 2001; Volume 4, pp. 56–65.
19. Kasparaviciene, G.; Briedis, V. Stability and antioxidant activity of black currant and black aronia berry juices. *Medicina* **2003**, *39* (Suppl. 2), 65–69. (In Lithuanian)
20. Asen, S.; Stewart, R.N.; Norris, K.H. Co-pigmentation of anthocyanins in plant tissues and its effect on color. *Phytochemistry* **1972**, *11*, 1139–1144. [CrossRef]
21. Trouillas, P.; Sancho-Garcia, J.C.; De Freitas, V.; Gierschner, J.; Otyepka, M.; Dangles, O. Stabilizing and modulating color by copigmentation: Insights from theory and experiment. *Chem. Rev.* **2016**, *116*, 4937–4982. [CrossRef] [PubMed]
22. Klisurova, D.; Petrova, I.; Ognyanov, M.; Georgiev, Y.; Kratchanova, M.; Denev, P. Co-pigmentation of black chokeberry (*Aronia melanocarpa*) anthocyanins with phenolic co-pigments and herbal extracts. *Food Chem.* **2019**, *279*, 162–170. [CrossRef]
23. Wilska-Jeszka, J.; Korzuchowska, A. Anthocyanins and chlorogenic acid copigmentation—Influence on the colour of strawberry and chokeberry juices. *Z. Lebensm. Unters. Forsch.* **1996**, *203*, 38–42. [CrossRef]
24. Skąpska, S.; Marszałek, K.; Woźniak, L.; Zawada, K.; Wawer, I. Aronia dietary drinks fortified with selected herbal extracts preserved by thermal pasteurization and high pressure carbon dioxide. *LWT-Food Sci. Technol.* **2017**, *85*, 423–426. [CrossRef]
25. Sidor, A.; Drożdżyńska, A.; Brzozowska, A.; Szwengiel, A.; Gramza-Michałowska, A. The effect of plant additives on the stability of polyphenols in cloudy and clarified juices from black chokeberry (*Aronia melanocarpa*). *Antioxidants* **2020**, *9*, 801. [CrossRef] [PubMed]
26. Kratchanova, M.; Denev, P.; Kratchanov, C. Rosehip extract synergistically increase antioxidant activity of fruit and herb extracts. *Bulg. Chem. Commun.* **2014**, *46A*, 59–64.
27. Gonzalez-Manzano, S.; Dueñas, M.; Rivas-Gonzalo, J.C.; Escribano-Bailón, M.T.; Santos-Buelga, C. Studies on the copigmentation between anthocyanins and flavan-3-ols and their influence in the colour expression of red wine. *Food Chem.* **2009**, *114*, 649–656. [CrossRef]
28. Directive 2012/12/EU of the European parliament and of the Council amending Council Directive 2001/112/EC relating to fruit juices and certain similar products intended for human consumption. *Off. J. Eur. Union* **2012**, L115/1–L115/11.
29. Denev, P.; Kratchanova, M.; Petrova, I.; Klisurova, D.; Georgiev, Y.; Ognyanov, M.; Yanakieva, I. Black chokeberry (*Aronia melanocarpa* (Michx.) Elliot) fruits and functional drinks differ significantly in their chemical composition and antioxidant activity. *J. Chem.* **2018**, *2018*, 9574587. [CrossRef]
30. Ahmed, J.; Shivhare, U.S.; Raghavan, G.S.V. Thermal degradation kinetics of anthocyanin and visual colour of plum puree. *Eur. Food Res. Technol.* **2004**, *218*, 525–528. [CrossRef]
31. Adams, J.B. Thermal degradation of anthocyanins with particular reference to the 3-glycosides of cyanidin. I. In acidified aqueous solution at 100 °C. *J. Sci. Food Agric.* **1973**, *24*, 747–762. [CrossRef]
32. Hwang, E.-S.; Ki, K.-N. Stability of the anthocyanin pigment extracted from aronia (*Aronia melancocarpa*). *Korean J. Food Sci. Technol.* **2013**, *45*, 416–421. [CrossRef]
33. Wilkes, K.; Howard, L.R.; Brownmiller, C.; Prior, R.L. Changes in chokeberry (*Aronia melanocarpa* L.) polyphenols during juice processing and storage. *J. Agric. Food Chem.* **2014**, *62*, 4018–4025. [CrossRef] [PubMed]
34. Chung, I.-M.; Park, I.; Seung-Hyun, K.; Thiruvengadam, M.; Rajakumar, G. Plant-mediated synthesis of silver nanoparticles: Their characteristic properties and therapeutic applications. *Nanoscale Res. Lett.* **2016**, *11*, 40. [CrossRef]
35. Jensen, M.B.; López-de-Dicastillo Bergamo, C.A.; Payet, R.M.; Liu, X.; Konczak, I. Influence of copigment derived from Tasmannia pepper leaf on Davidson's plum anthocyanins. *J. Food Sci.* **2011**, *76*, C447–C453. [CrossRef]
36. Glories, Y. La couleur des vins rouges. 2e partie: Mesure, origine et interprétation. *J. Int. Sci. Vigne du Vin.* **1984**, *18*, 253–271. [CrossRef]

37. Pérez-Magariño, S.; González-San José, M.L. Polyphenols and colour variability of red wines made from grapes harvested at different ripeness grade. *Food Chem.* **2006**, *96*, 197–208. [CrossRef]
38. Bimpilas, A.; Panagopoulou, M.; Tsimogiannis, D.; Oreopoulou, V. Anthocyanin copigmentation and color of wine: The effect of naturally obtained hydroxycinnamic acids as cofactors. *Food Chem.* **2016**, *197*, 39–46. [CrossRef] [PubMed]
39. Remini, H.; Mertz, C.; Belbahi, A.; Achir, N.; Dornier, M.; Madani, K. Degradation kinetic modelling of ascorbic acid and colour intensity in pasteurized blood orange juice during storage. *Food Chem.* **2015**, *173*, 665–673. [CrossRef] [PubMed]
40. National Academy of Sciences, Institute of Medicine. Panel on dietary antioxidants and related compounds: Vitamin C, vitamin E, selenium, and α-carotene and other carotenoids: Overview, antioxidant definition, and relationship to chronic disease. In *Dietary Reference Intakes for Vitamin C, Vitamin E, Selenium, and Carotenoids*; National Academies Press: Washington, DC, USA, 2000; pp. 35–57.
41. Číž, M.; Čížová, H.; Denev, P.; Kratchanova, M.; Slavov, A.; Lojek, A. Different methods for control and comparison of the antioxidant properties of vegetables. *Food Control* **2010**, *21*, 518–523. [CrossRef]
42. Furtado, P.; Figueiredo, P.; Chaves das Neves, H.; Pina, F. Photochemical and thermal degradation of anthocyanidins. *J. Photochem. Photobiol. A Chem.* **1993**, *75*, 113–118. [CrossRef]
43. Seeram, N.P.; Bourquin, L.D.; Nair, M.G. Degradation products of cyanidin glycosides from tart cherries and their bioactivities. *J. Agric. Food Chem.* **2001**, *49*, 4924–4929. [CrossRef] [PubMed]
44. Roidoung, S.; Dolan, K.; Siddiq, M. Gallic acid as a protective antioxidant against anthocyanin degradation and color loss in vitamin-C fortified cranberry juice. *Food Chem.* **2016**, *210*, 422–427. [CrossRef]
45. Rabie, M.A.; Soliman, A.Z.; Diaconeasa, Z.S.; Constantin, B. Effect of pasteurization and shelf life on the physicochemical properties of physalis (*Physalis peruviana* L.) Juice. *J. Food Process. Preserv.* **2015**, *39*, 1051–1060. [CrossRef]
46. Singleton, V.L.; Rossi, J.A.J. Colorimetry of total phenolics with phosphomolybdic-phosphotungstic acid reagents. *Am. J. Enol. Vitic.* **1965**, *16*, 144–158.
47. Ou, B.; Hampsch-Woodill, M.; Prior, R.L. Development and validation of an improved oxygen radical absorbance capacity assay using fluorescein as the fluorescence probe. *J. Agric. Food Chem.* **2001**, *49*, 4619–4626. [CrossRef] [PubMed]
48. Denev, P.; Ciz, M.; Ambrozova, G.; Lojek, A.; Yanakieva, I.; Kratchanova, M. Solid-phase extraction of berris' anthocyanins and evaluation of their antioxidative properties. *Food Chem.* **2010**, *123*, 1055–1061. [CrossRef]
49. Ou, B.; Hampsch-Woodill, M.; Flanagan, J.; Deemer, E.K.; Prior, R.L.; Huang, D.J. Novel fluorometric assay for hydroxyl radical prevention capacity using fluorescein as the probe. *J. Agric. Food Chem.* **2002**, *50*, 2772–2777. [CrossRef] [PubMed]

plants

MDPI

Review

Biotechnological Advances in Pharmacognosy and In Vitro Manipulation of *Pterocarpus marsupium* Roxb.

Anees Ahmad [1,2], Naseem Ahmad [1], Mohammad Anis [1], Mohammad Faisal [3], Abdulrahman A. Alatar [3], Eslam M. Abdel-Salam [3], Ram Pratap Meena [4] and Iyyakkannu Sivanesan [5,*]

1 Plant Biotechnology Laboratory, Department of Botany, Aligarh Muslim University, Aligarh 202002, India; aneesqadriamu@gmail.com (A.A.); naseembot@gmail.com (N.A.); anism1@rediffmail.com (M.A.)
2 Pharmacognosy Laboratory, Drug Standardization Research Institute, Central Council for Research in Unani Medicine, Ministry of AYUSH, Government of India, New Delhi 110058, India
3 Department of Botany & Microbiology, College of Science, King Saud University, P.O. Box 2455, Riyadh 11451, Saudi Arabia; faisalm15@yahoo.com (M.F.); aalatar@ksu.edu.sa (A.A.A.); eabdelsalam@ksu.edu.sa (E.M.A.-S.)
4 Chemistry Laboratory, Central Council for Research in Unani Medicine (CCRUM), Ministry of AYUSH, New Delhi 110058, India; ccrumdsr2017@gmail.com
5 Department of Bioresources and Food Science, Institute of Natural Science and Agriculture, Konkuk University, 1 Hwayang-dong, Gwangjin-gu, Seoul 05029, Korea
* Correspondence: siva74@konkuk.ac.kr

Abstract: Trees are vital resources for economic, environmental, and industrial growth, supporting human life directly or indirectly through a wide variety of therapeutic compounds, commodities, and ecological services. *Pterocarpus marsupium* Roxb. (Fabaceae) is one of the most valuable multipurpose forest trees in India and Sri Lanka, as it is cultivated for quality wood as well as pharmaceutically bioactive compounds, especially from the stem bark and heartwood. However, propagation of the tree in natural conditions is difficult due to the low percentage of seed germination coupled with overexploitation of this species for its excellent multipurpose properties. This overexploitation has ultimately led to the inclusion of *P. marsupium* on the list of endangered plant species. However, recent developments in plant biotechnology may offer a solution to the overuse of such valuable species if such advances are accompanied by technology transfer in the developing world. Specifically, techniques in micropropagation, genetic manipulation, DNA barcoding, drug extraction, delivery, and targeting as well as standardization, are of substantial concern. To date, there are no comprehensive and detailed reviews of *P. marsupium* in terms of biotechnological research developments, specifically pharmacognosy, pharmacology, tissue culture, authentication of genuine species, and basic gene transfer studies. Thus, the present review attempts to present a comprehensive overview of the biotechnological studies centered on this species and some of the recent novel approaches for its genetic improvement.

Keywords: biotechnological tools; DNA barcoding; ethnomedicine; in vitro culture; genetic improvement

Citation: Ahmad, A.; Ahmad, N.; Anis, M.; Faisal, M.; Alatar, A.A.; Abdel-Salam, E.M.; Meena, R.P.; Sivanesan, I. Biotechnological Advances in Pharmacognosy and In Vitro Manipulation of *Pterocarpus marsupium* Roxb.. *Plants* **2022**, *11*, 247. https://doi.org/10.3390/plants11030247

Academic Editor: Milan S. Stankovic

Received: 27 December 2021
Accepted: 17 January 2022
Published: 18 January 2022

1. Introduction

Forest trees provide valuable resources for economic, environmental, and industrial development. Indeed, these plants sustain human life directly or indirectly, which supply a wide range of goods and ecological services essential for survival and prosperity. The medicinal plants used in traditional medicine all over the world are a potentially rich source of therapeutic compounds. Population increase along with rapid technological advances are putting tremendous pressure on natural genetic resources, especially in developing countries, where such resources are rapidly declining, and more species face extinction [1]. The more than 70 species in the pantropical genus *Pterocarpus* (Fabaceae) are also faced with development pressure [2]. The use of different plant parts in *Pterocarpus* spp. to treat

illnesses since ancient times has been well documented [3–8]. The species has received much attention in experimental studies because of the growing evidence of potential bioactivities. The increasing demand for wood has led to unsustainable harvesting from wild sources of three species of *Pterocarpus*, namely *Pterocarpus marsupium*, *P. santalinus*, and *P. indicus*, which are now recognized as threatened species [9]. Besides the pharmaceutical value of *Pterocarpus* species, the wood is also valuable for bridge and boat building, as well as small-scale construction materials, plywood, veneer, and specialty wood for musical instruments [10].

The increase in public awareness of phytochemical-based drugs and the rapid growth of plant-based pharmacological industries have led to a greater demand for, and overexploitation of, natural flora. An increase in subsistence or non-commercial harvesting, as well as recent climatic changes have harmed many plant species, including *Pterocarpus* spp. One possible biotechnical response to the decline of some species is micropropagation, which capitalizes on the totipotent nature of plant cells [11]. In vitro propagation through tissue culture plays an important role in mass multiplication, plant improvement, plant breeding, regeneration of elite or superior clones, exchange of planting materials, secondary metabolites production, and germplasm conservation [12,13]. However, conventional propagation practice is time-consuming and labor-intensive and requires the availability of many plants for plantation or afforestation. Notwithstanding these challenges, plant cell, tissue, and organ culture techniques will become increasingly important in the cultivation of medicinal, as well as aromatic, plants by providing healthy and disease-free planting stock that can be widely utilized in commercial propagation and reforestation programs [14,15]. The information on actual genetic structure and the cryptic number of the differentiated genetic resources are valuable aids not only for developing in vitro regeneration protocols but also for the conservation of these medicinal plants. Many adulterants of *Pterocarpus* plant materials are available in the market, and they affect the efficacy of the drug; in some cases, these adulterants might be toxic and can prove to be lethal. A DNA barcoding technique can be effectively utilized to characterize and authenticate *Pterocarpus* and the detection of adulterants [16]. This technique is an alternative for rapid and robust species identification of genuine plant materials for the herbal drug industry [17].

P. marsupium propagates only by seed; the germination rate has been reported to be less than 30%, apparently because of the hard fruit coat coupled with poor viability and pod setting [18]. The mature fruits are harvested from the trees in April and May or before they drop to the ground. Pathogenic infections of fallen fruit also affect the germination rate under natural conditions [19]. Ahmad [20] recommended freshly collected seeds as a good planting source for obtaining healthy plantlets. The oleo-resin exudates of this species contain several unique active constituents, including vijyayosin, pterosupin, marsupsin, and pterostilbene, all of which show a wide range of pharmacological activity [21]. In addition, the National Medicinal Plant Board (NMPB) of India has estimated that the annual trade value of *P. marsupium* is approximately 300–500 metric tons per year and that each mature tree (10–15 years) produces approximately 0.5–0.6 tons of dry heartwood, valued at US $ 1200–1500 for each mature tree in the international market. Due to the aforementioned increased interest in recent years in the pharmaceutical, as well as the economic value of *P. marsupium*, the government of India has begun to encourage programs for large-scale cultivation and conservation of this species. The high demand for oleo-resin and wood, unsustainable harvesting practices, anthropogenic threats, and lack of regeneration, have together resulted in the rapid decline of natural populations. Furthermore, illegal harvesting of oleo-resin by damaging or wounding the wood can cause the trees to be susceptible to pests or diseases. Thus, uncontrolled extraction of oleo-resin could lead to adult mortality in combination with fragmentation and a low regeneration rate, threatening the persistence of the species.

Despite the enormous ethnobotanical value of *P. marsupium*, there is limited information on its genetic structure. Data on intraspecific relatedness is vital for selecting the best genotypes for plant breeding, effective population management, and conservation of

germplasm. Given that genetic diversity allows populations to adapt to changing environments, the investigation of the genetic diversity of *P. marsupium* is not only important for species conservation, but also for the development and utilization of germplasm for improvement of this valuable but threatened medicinal plant. *P. marsupium* is a highly valuable medicinal plant but is a threatened species in India. Efforts for the conservation and propagation of this tree species will ultimately lead to the development of policies to make the species available for general use at a low cost. In view of these facts, it is of paramount importance to develop biotechnological techniques that ensure rapid propagation, multiplication, and authentication of the species for optimal germplasm conservation. With this goal in mind, we review the biotechnological advances made to date in *P. marsupium* concerning pharmacognosy, in vitro culture, multiplication, and genetic improvement.

2. Botanical Description of *P. marsupium*

Pterocarpus marsupium Roxb., a legume, commonly known as "Bijasal" or "Indian Kino Tree," (Figure 1) is a valuable multipurpose, as well as industrially important, forest tree. Ahmad and Anis [22] suggested that it is a potential herbal drug yielding tree in India. Generally, the tree is found in dry mixed deciduous tropical forests and flourishes in the open sun under "80" to "200" cm moderate rainfall. It is commonly found in central and peninsular India, mainly in the forested regions of Madhya Pradesh, Chhattisgarh, Maharashtra, Andhra Pradesh, some areas of Uttar Pradesh, and sub-Himalayan tracts, up to 1000 m altitude [20].

Figure 1. *Pterocarpus marsupium* Roxb. (22°23′25″ N and 84°21′44″ E, Chhattisgarh state of India).

The species performs best in fertile, deep, clayey loam soil with good drainage and can tolerate extreme temperatures during the summer season. Wild populations have rapidly disappeared, and even single young saplings are rarely found in the forest. The International Union for the Conservation of Nature (IUCN) evaluated *P. marsupium* as a vulnerable species based on autogenic reproductive deficiency [10]. In addition, this species has been categorized by several researchers or conservation agencies as vulnerable [23], depleted [24], fast disappearing [25], endangered [26], critically endangered in Nepal [27], and vulnerable in Sri Lanka [28]. *P. marsupium* can be identified in the wild by its upright bole, longitudinally fissured bark, imparipinnate leaf arrangement (5–7 leaflets, 8–13 cm long), coriaceous, dark green and shiny leaves, scented yellow flowers in large panicles (1–5 cm long), and orbicular and winged fruits with flat pods. Each pod contains one to three seeds, bony and convex in shape. Flowering begins in November and continues up to March. The mature tree attains a height of up to 30 m and a girth up to 2.5 m, with clear and straight bole [29].

3. Phytochemistry and Therapeutic Values of *P. marsupium*

3.1. Active Constituents

A large number of important phytochemicals, such as glucosides, sesquiterpene and vijayoside (Table 1) have been isolated from aqueous extract of heartwood of *P. marsupium* [30]. The extract of heartwood contains pterostilbene (Figure 2A, pterosupin) (Figure 2O, marsupsin (Figure 2M), and liquiritigenin (Figure 2N), (−)-epicatechin) (Figure 2H) [31,32]. Bark extract contains several reputed phytochemicals such as 3-*o*-methyl-D-glucose (Figure 3C), n-hexadecanoic acid (Figure 3D), 1,2-benzenedicarboxylic acid (Figure 3E), tetradecanoic acid, (Figure 3F), 9,12-octadecadienoic acid (Z,Z) (Figure 3G), D-friedoolean-14-en-3-one (Figure 3H), and lupeol (Figure 2J) [33]. At least eleven bioactive compounds, namely pterocarposide (Figure 2P), 2,6-dihydroxyphenyl glucopyranoside (Figure 2Q), pteroside (Figure 3I), vijayoside (Figure 3J), pterosupol, marsuposide, epicatechin, quercetin (Figure 3M), vanillic acid (Figure 3N), formononetin (Figure 3O), and naringenin have been extracted from the heartwood of *P. marsupium* [21]. The most important bioactive compounds extracted from *P. marsupium* are presented in Table 1. Structures of bioactive compounds of *P. marsupium* are shown in Figures 2 and 3.

Table 1. Important bioactive compounds extracted from *Pterocarpus marsupium* (in chronological order).

Plant Parts	Extract Preparation	Technique *	Bioactive Compound	References
Heartwood	Ethyl acetate	C-SG	Pterostilbene (Figure 2A) (2S)-7-Hydroxyflavanone (Figure 2B) Isoliquiritigenin (Figure 2C) 7,4′-Dihydroxyflavone 7-rutinoside (Figure 2D) 5-Deoxykaempferol (Figure 2E) *p*-Hydroxybenzaldehyde (Figure 2F) 3-(4-Hydroxyphenyl) lactic acid (Figure 2G)	[34]
Bark	Ethanolic extract	C-SG	(−)-Epicatechin (Figure 2H)	[35]
P. marsupium extract	Ethyl acetate	C-SG	Naringenin (Figure 2I) Lupeol (Figure 2J)	[36]
Roots	Ethanolic extract	C-SG	7-Hydroxy-6, 8-dimethyl flavanone-7-*O*-α-L-arabinopyranoside (Figure 2K) 7,8,4′-Trihydroxy-3′, 5′-dimethoxy flavanone-4′-*O*-β-D-glucopyranoside (Figure 2L)	[37]

Table 1. *Cont.*

Plant Parts	Extract Preparation	Technique *	Bioactive Compound	References
Heartwood	Ethyl acetate	Thin Layer Chromatography	Marsupsin (Figure 2M) Liquiritigenin (Figure 2N)	[31]
Heartwood	Ethyl acetate	C-SG	Pterosupin (Figure 2O)	[32]
Heartwood	Aqueous extract	C-SG	Pterocarposide (Figure 2P)	[38]
Heartwood	Aqueous extract	Coulman chromatography over Sephadex LH-20	1-(2′,6′-Dihydroxyphenyl)-β-D-glucopyranoside (Figure 2Q) Pteroisoauroside (Figure 2R)	[39]
Heartwood	Aqueous extract	C-SG	Marsuposide (Figure 3A) Sesquiterpene (Figure 3B)	[30]
Leaves	Methanolic extract	UV-spectrophotometer	Phenolics	[40]
Wood and bark	Ethanolic extract	GC-MS	3-*O*-Methyl-d-glucose (Figure 3C) n-Hexadecanoic acid (Figure 3D) 1,2-Benzenedicarboxylic acid (Figure 3E) Tetradecanoic acid (Figure 3F) 9,12-Octadecadienoic acid (Z,Z) (Figure 3G) D-Friedoolean-14-en-3-one (Figure 3H)	[33]
Apical stem bark	Methanolic extract	Followed standard protocols	Alkaloids Glycosides Flavonoids Terpenoids	[41]
Heartwood	Ethanolic extract	C-SG	Pteroside (Figure 3I) Vijayoside (Figure 3J) *C*-β-D-Glucopyranosyl-2,6-dihydroxyl benzene (Figure 3K)	[42]
Heartwood	Ethanolic extract	C-SG and HPLC	(+)-Dihydrorobinetin (Figure 3L) Pterosupol	[43]
Heartwood	Methanolic extract	LC-MS-MS	Quercetin (Figure 3M) Vanillic acid (Figure 3N) Formononetin (Figure 3O)	[21]
Heartwood	Methanolic extract	HPLC and FTIR	Liquiritigenin	[44]

* Technique—Phytochemical compound identification techniques used, C-SG—Chromatography over Silica Gel, GC-MS—Gas Chromatography-Mass Spectrometry, LC-MS-MS—Liquid Chromatography with Tandem Mass Spectrometry, HPLC—High-Performance Liquid Chromatography, FTIR—Fourier Transform Infrared Spectroscopy.

3.2. Medicinal Properties

Ethno-medicine: Given the substantial evidence of its pharmacological properties, *P. marsupium* has potential as an herbal drug yielding tree; indeed, it has been used to cure several diseases in the Indian traditional medicine system for many centuries [30,45]. The flowers of the tree are used in the treatment of fever, and the heartwood powder is useful in treating chest pain, body pain, and indigestion [46]. Trivedi [47] reported that a paste made from wood and seeds is useful in treating diabetic anemia. In addition, Yesodharan and Sujana [48] have suggested that heartwood is useful in the treatment of body pain and diabetes. Interestingly, a cup made of the wood of *P. marsupium* heartwood is used for drinking water to control blood sugar levels in "Ayurvedic" medicine [49]. Aqueous infusions of the bark have also been used to treat diabetic patients since ancient times [50]. The stem bark is used to treat urinary discharge and piles, and the resin-gum is applied externally in the treatment of leucorrhoea [51]. The medicinal values of the active constituents or aqueous extracts of *P. marsupium* are shown in Table 2.

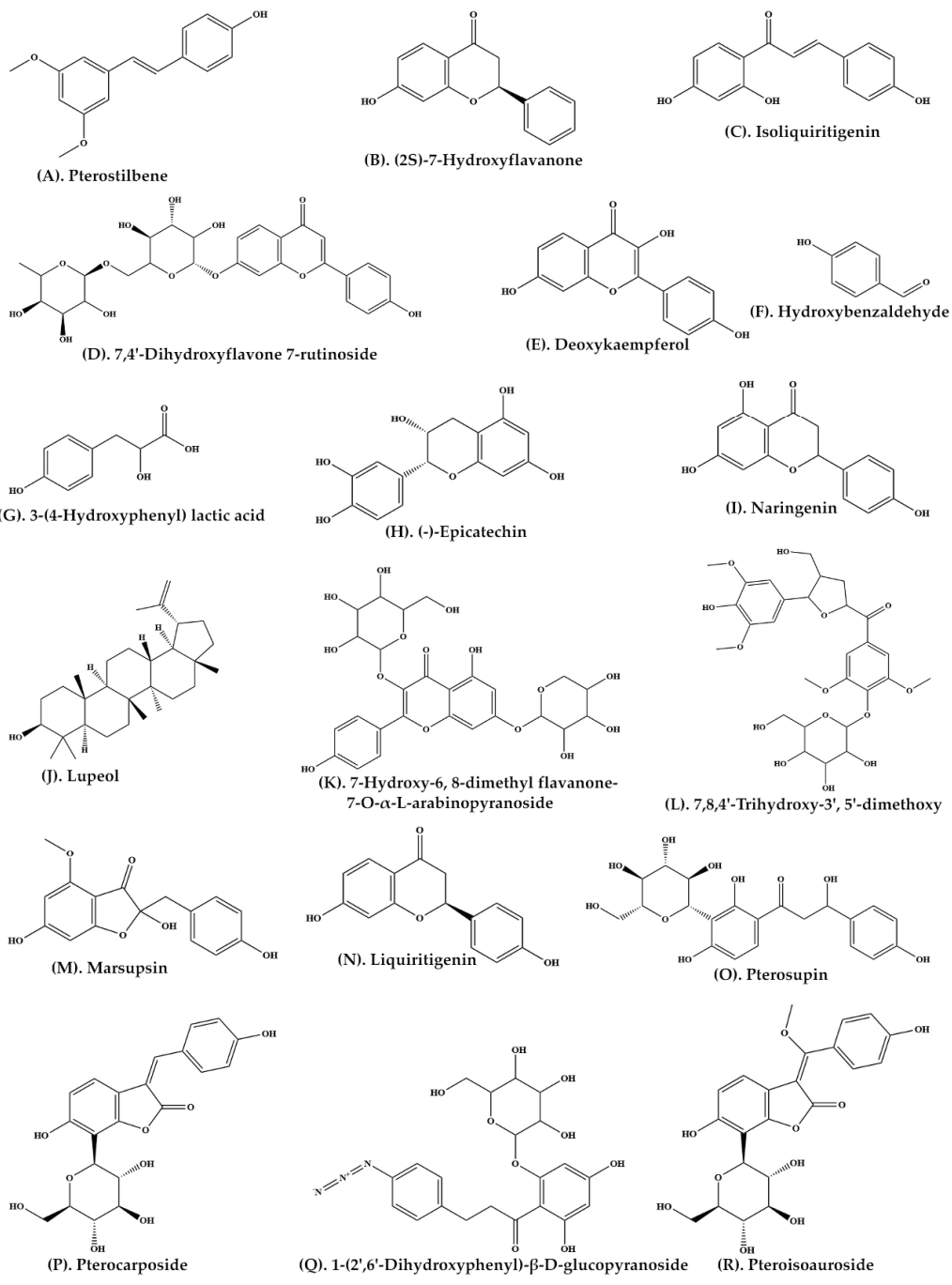

Figure 2. Molecular structure of bioactive compounds extracted from *Pterocarpus marsupium* Roxb.

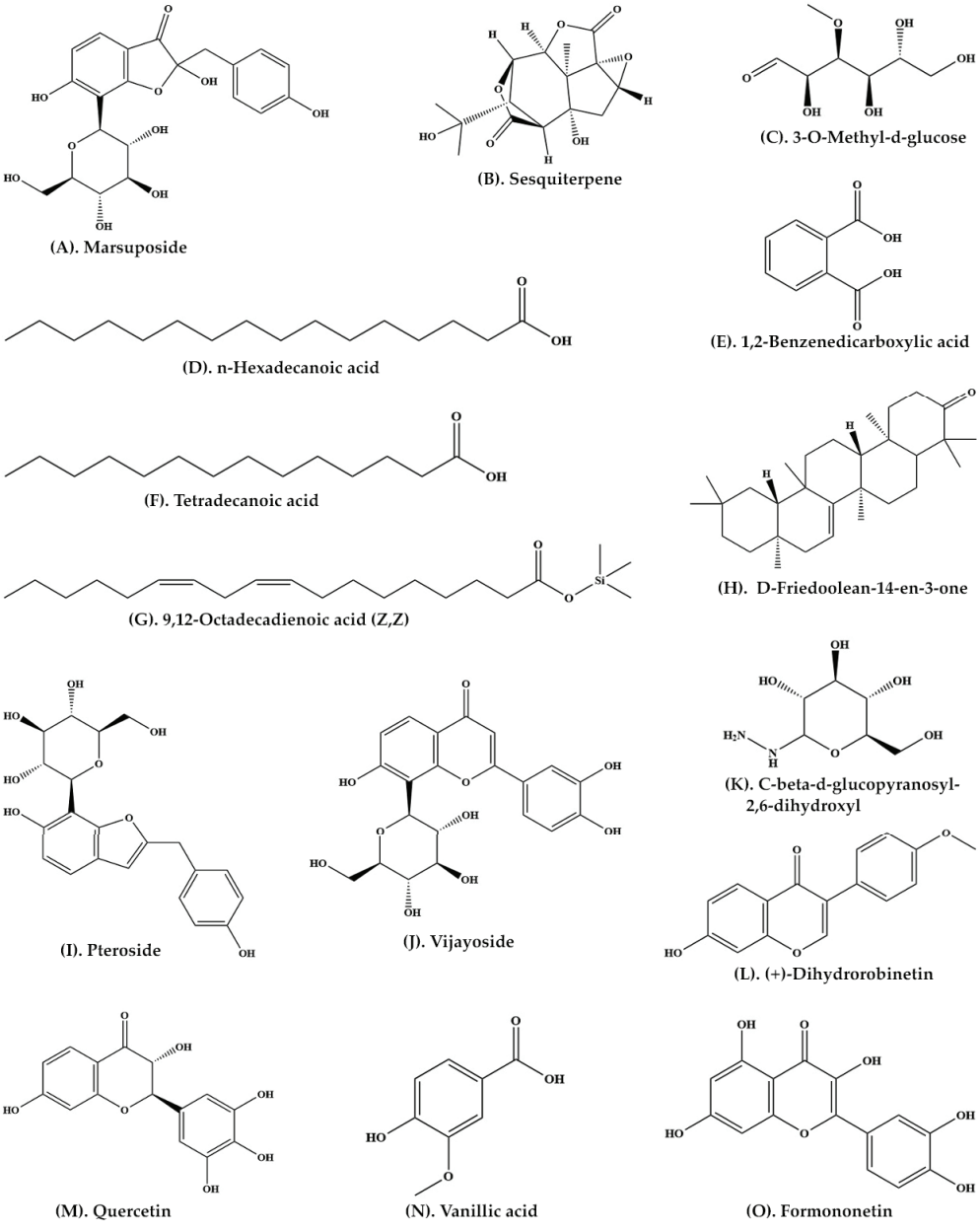

Figure 3. Molecular structure of bioactive compounds extracted from *Pterocarpus marsupium* Roxb.

Table 2. Potential activities of some important bioactive compounds or aqueous extracts of *Pterocarpus marsupium* (in chronological order).

S.N.	Extracts/Bioactive Compound	Potential Activities	References
1	(−)-Epicatechin (Figure 2H)	No effect on central nervous system Cardiac stimulant activity Anti-diabetic	[35]
2	Flavonoids	Anti-hyperlipidemic	[31]
3	Phenolics	Anti-hyperglycemic	[32]
4	Pterostilbene (Figure 2A)	Cyclooxygenase-2 (COX-2) inhibition	[52]
5	Pterostilbene and 3,5-hydroxypterostilbene	Induce apoptosis in tumor cells	[53]
6	5,7,2-4 tetrahydroxy isoflavone 6-6 glucoside	Cardiotonic	[45]
7	Pterostilbene	Anti-cancerous Anti-inflammatory Analgesic	[54]
8	Phenolics	Anti-oxidant	[40]
9	Pterostilbene	Anti-cancerous Anti-proliferative	[55]
10	Bark extract	Anti-oxidant Analgesic	[56]
11	Extract of bark and wood	Anti-diabetic Anti-hyperlipidemic	[57]
12	Extract of apical stem bark	Anti-microbicidal	[41]
13	Phenolic-*C*-glycosides	Anti-diabetic	[42]
14	Pterostilbene	Novel telomerase inhibitor	[58]
15	Heartwood extract	Dipeptidyl peptidase-4 (DPP-4) inhibition activity	[59]
16	Heartwood extract	Anti-glycation Sorbitol accumulation	[60]
17	Pterostilbene	Inhibition of aldose reductase Inhibition of platelet aggregation	[61]
18	Heartwood extract	Reduction in body weight Anti-diabetic Anti-hyperlipidemic	[62]
19	(+)-Dihydrorobinetin (Figure 3L)	Radical scavenging activity	[43]
20	Heartwood extract	In vitro lipid lowering activity	[21]
21	Liquiritigenin (Figure 2N)	Hypoglycemic activity	[44]
22	Pterostilbene	Sun (UV rays) protective capacity	[63]

Anti-diabetic properties: Heartwood extract of *P. marsupium* was primarily used in the Ayurvedic system of medicine for treating diabetic patients and has been compared to proprietary drugs often prescribed to treat diabetes, such as metformin, which is mainly an anti-hyperglycemic medicine [64,65]. In earlier studies, an extract of *P. marsupium* bark was found to contain (−)-epicatechin, an anti-diabetic compound that promotes regeneration of pancreatic β-cells [66]. Subsequently, Manickam, Ramanathan, Farboodniay Jahromi, Chansouria, and Ray [32] reported two of the most important phenolic constituents of the heartwood, namely marsupsin and pterostilbene, which significantly reduced the blood glucose level in hyperglycemic rats. In yet another study [67], both of these compounds (marsupsin and pterostilbene) were shown to have insulin-like activities similar to those of metformin (1,1-dimethylbiguanide), an important hypoglycemic compound that stimulates glycolysis and inhibits glucose absorption in the intestine. These results indicate that both pterostilbene and marsupsin are powerful anti-diabetic agents that might be useful in the treatment of non-insulin-dependent diabetes mellitus patients.

Suppression of platelet aggregation: The oral administration of an extract from the leaves or stem bark of *P. marsupium* has been shown to inhibit the reduction of platelets, which suggests action against platelet aggregation. The heartwood extract, containing pterostilbene, also exhibited suppressive effects on platelet aggregation [52]. Another

study [68] suggested that pterostilbene is a derivative of resveratrol—commonly known as one of the potent inhibitors of platelet aggregation. In a comparative study of pterostilbene and resveratrol [61] it was found that 50 μM pterostilbene resulted in 91% inhibition of platelet aggregation in rats, compared with 84% reduction after an equimolar dose of resveratrol. These results clearly indicate that pterostilbene is a potential substitute of resveratrol for platelet aggregation inhibition.

Dipeptidyl peptidase-4 (DPP-4) inhibition activity: Dipeptidyl peptidase-4 (DPP-4) is an intrinsic membrane protein dispersed in several tissues, including intestinal epithelial cells, renal proximal tubules, and the cells of the lungs, liver, kidney, and placenta [69]. Presently, there are three important DPP-4 inhibitors, namely Sitagliptin, Vidagliptin, and Saxagliptin, that are commercially available in the international market and used for the treatment of type-2 diabetes and Alzheimer's disease (Type-2 diabetes is one of the major risk factors associated with Alzheimer's disease). In several scientific studies, we note that it has been suggested that heartwood extract of *P. marsupium* has dipeptidyl pepdase-4 (DPP-4) inhibition properties in the treatment of type-2 diabetes and Alzheimer's disease [59,70].

Cardiotonic activity: The aqueous extract of *P. marsupium* heartwood contains 5,7,2-4 tetrahydroxy isoflavone 6-6 glycoside, which is a potent antioxidant believed to prevent cardiovascular disease [45]. Digoxin, isolated from *Digitalis lanata*, is a most effective cardiotonic medicine but shows some acute side effects, such as gynaecomastia, irregular heartbeat, and poor kidney function [71]. Mohire, Salunkhe, Bhise, and Yadav [45] reported interesting results from a comparative study of the aqueous extract of *P. marsupium* heartwood and digoxin on the positive intropic and negative chronotropic effects on the heart (frog). They found that the heartwood extract showed a decrease in a heartbeat (negative chronotropic) and an increase in the height of force of concentration (positive intropic) effect. In comparison, a low concentration of digoxin increases the height of force of concentration (20%), which is four times less than the height of force of concentration produced by an aqueous extract of *P. marsupium* heartwood (80%). These results clearly suggest that the therapeutic efficacy of *P. marsupium* heartwood extract is much higher than that of digoxin. Thus, the limitations of digoxin can be overcome by using an aqueous extract of *P. marsupium* heartwood, which has been found to have excellent cardiotonic activity as well as a wide margin of safety compared with digoxin.

Lipid-lowering capacity: The condition of obesity is characterized by the deposition of extra fat along with high levels of fatty acids, glycerol, and pro-inflammatory markers, which can indicate a diabetic phenotype [72]. A continuous increase in body mass and weight gain increases the likelihood of type-1 and -2 diabetes [73]. In a recent experiment, Singh, Bajpai, Gupta, Gaikwad, Maurya, and Kumar [21] demonstrated that heartwood extract of *P. marsupium* potentially reduced the extra fat accumulation in adipocytes cells and was also conducive to the successful treatment of diabetic patients.

Cyclooxygenase (COX-2) inhibition and anti-inflammatory activities: Cyclooxygenase (COX) plays an important role in body tissue inflammation and inflammatory pain. It is the rate-limiting enzyme in the conversion of arachidonic acid to prostaglandin. A survey of the literature shows that there are principally three isoforms of COX that have been identified: COX-1 [74], COX-2 [75], and COX-3 [76]. Among these, COX-2 plays an important role during inflammation since it is the main agent to induce prostaglandin production during inflammation. In a study by Hougee, Faber, Sanders, de Jong, van den Berg, Garssen, Hoijer, and Smit [52], it was reported that pterostilbene—the active compound found in heartwood extract of *P marsupium*—shows selective COX-2 inhibitory activity in humans. In addition, pterostilbene is a stimulating compound used in the treatment of several inflammatory diseases [77].

Anticancer, anti-proliferative, analgesic, and antioxidant activities: Pterostilbene is a naturally occurring stilbenoid phytochemical synthesized in plants via the phenylpropanoid pathway [78]. Research has shown that it is a structural analog of various highly bioactive compounds such as stilbene and resveratrol [60,79]. Because pterostilbene (*trans*-3,5-dimethoxy-4′-hydroxystilbene) has a close structural similarity with resveratrol (3,5,4′-

trihydroxy-trans-stilbene), it yields a large number of health benefits (Table 2). A number of researchers believe that pterostilbene has more potential bioactivities (i.e., anticancer, antioxidant, anti-inflammatory) than resveratrol [54,80,81]. In addition, Ferrer, et al. [82], Tolomeo, Grimaudo, Cristina, Roberti, Pizzirani, Meli, Dusonchet, Gebbia, Abbadessa, Crosta, Barucchello, Grisolia, Invidiata and Simoni [53], and Chakraborty, Gupta, Ghosh and Roy [55] reported that pterostilbene did not show any cytotoxic effect against normal human cells and inhibited certain types of cancerous cells.

4. Propagation of *Pterocarpus marsupium*

The plant consists of various organs and tissues, which in turn are made up of different individual cells. Plants are propagated through various methods: direct seed culture, explant cultures (from plant cells, tissues, organs, mature or immature zygotic embryo) on artificial media under aseptic conditions. Micropropagation is one of the best methods for obtaining genetically identical clones of donor plants [13]. This method has been extensively utilized for regeneration and conservation of various tree species, including *Melia azedarach* [83], *Acacia ehrenbergiana* [84], *Albizia lebbeck* [85], *Lagerstroemia speciosa* [86], *Cassia alata* [87], and *Erythriana variegata* [88]. Such propagation methods make possible the mass multiplication of new cultivars of valuable medicinal woody trees that would otherwise take several years to develop via conventional methods. In the following sections, the important methods adopted for the propagation of *P. marsupium* are discussed concerning the existing literature.

4.1. Mechanism of Seed Germination

Seed germination, the most common method for multiplication in flowering plants, is a process in which physio-morphological changes result in the activation of the embryo. As the seed absorbs water before germination, the seed embryo elongates. Shu, et al. [89] have proposed that once the radicle has grown out from the seed layers, the process of seed germination is complete. The processes involved in seed germination and how they are affected by different physio-morphological barriers have been well documented in a wide range of plant families, including Fabaceae [90,91]. The moisture content of seeds and the ambient storage temperature are key factors in promoting seed viability. Generally, seeds of many plants fail to germinate (due to a number of factors) and subsequently pass through a phase of dormancy that delays the whole life cycle of the plant. Different treatments have been found to improve germination and seedling growth. Furthermore, the promotive role of plant growth regulators on the breaking of seed dormancy and germination has been studied from time to time in many plant species. The general mechanism of seed germination and different factors affecting the germination rate are discussed below.

Seed germination and formation of the seedling: The process of seed germination—the resumption of growth of the embryo, leading to the formation of a seedling—is supported by environmental conditions that favor vegetative development, such as suitable temperature, required level of humidity, and the availability of oxygen and inhibitory substance, if any.

Seed development: Embryogenesis can be divided into three phases of approximately equal duration. The first phase begins with the zygote undergoing embryogenesis concomitant with endosperm proliferation. This is basically a phase of cell division and cell differentiation. The second phase, the accumulation of storage compounds to support the process, marks the end of cell division. In the third or final phase, the embryo becomes tolerant to desiccation. In this process, a seed dehydrates, losing up to 90% of its water. As a consequence of dehydration, metabolism comes to a stop and the seed enters a quiescent stage as a mature seed.

Hormonal balance of seed development: Abscisic acid (ABA) is the principal hormone involved in maturation and dormancy of an embryo. The content of ABA is very low during early embryogenesis, peaks (reaches maturation) during mid-embryogenesis, and declines when the seed attains maturity. However, some other hormones are also induced in the overall response of seed development. An example is the peak of ABA production in seeds, which coincides with a decline in the level of IAA and gibberellins [89,92]. Thus, an interaction between two or more hormones is a recurring theme in seed development in general. One difficulty in interpreting hormonal balance in seeds is that not all tissues in the seed are of the same genotype [93]. In a seed, the embryo and endosperm are the products of the female and male genotype products, whereas the seed coat is the exclusive product of the genome.

Seed dormancy: Dormancy of the seed, an adaptive feature, is a temporal delay in the process of germination and thus allows for (a) time for seed dispersal, (b) delay of germination until the onset of favorable conditions, and (c) maximization of seedling survival. If the environmental conditions are not suitable for germination, the seeds released in a dormant state remain in a dormant state. Embryo-imposed dormancy is intrinsic to the embryo. It is not affected by the seed coat or other surrounding tissues. The embryo dormancy is primarily due to the presence of an inhibitor such as ABA and the absence of a promoter such as gibberellin [89]. Finkelstein, et al. [94] reported that dormant seeds can be made to germinate subject to certain environmental conditions. Many species, such as tropical tree legumes, produce seeds with a tough seed coat, which protects against germination by restricting uptake of water and exchange of O_2. These limitations can be removed by scarification. (In nature, abrasion by sand, microbial action, or passage through an animal's gut have the same effect.) In some cases, the seeds are treated with mineral acid. Many seeds lose their dormancy while lying exposed on the ground during storage. During seed germination, an activated embryo requires the food reserves of cotyledons in dicot seeds and the endosperm in monocot seeds [95]. Food reserves, such as starch and proteins, are broken down by a variety of hydrolytic enzymes into sugars and amino acids.

4.2. Propagation from Seed

The fruits of *P. marsupium* are orbicular winged pods (samara) and are the only planting material used (Figure 4A). The germination rate is very low (less than 30%) in natural conditions [96], probably due to the seeds being enclosed within a hard fruit coat and stony pericarp, resulting in what can be called mechanical dormancy [97]. The mechanical excision of the hard fruit coat is a tedious and labor-intensive task. Sometimes, pathogenic infection also restricts the natural propagation rate of *P. marsupium* [19]. Therefore, to overcome these constraints and improve the seed germination rate, several methods have been suggested, including seed viability test, wet-heat treatment, physical and acid scarification of seeds, excision of fruit coat by sharp scissors, and using different culture media compositions and seed orientations [19,20,98].

In the process of seed embryo growth, combinations of several cellular and metabolic pathways are coordinated by a complex regulatory network that regulates seed dormancy [89]. This period of growth is crucial to plant survival, given that the seed must germinate only when conditions—temperature, light, gases, water, seed coats, mechanical restrictions, hormonal structure, and level—are favorable. However, several plants show adaptive traits that promote survival under stressful conditions [94]. Many wild species that have been domesticated show a low level of seed dormancy compared to wild relatives, which ensures higher emergence rates after sowing [99,100]. However, the loss of seed dormancy is undesirable when it results in rapid germination of newly matured seeds and consequently extensive losses in quality and quantity of the crop, which presents problems for pre-harvest management, as well as industrial consumption [101].

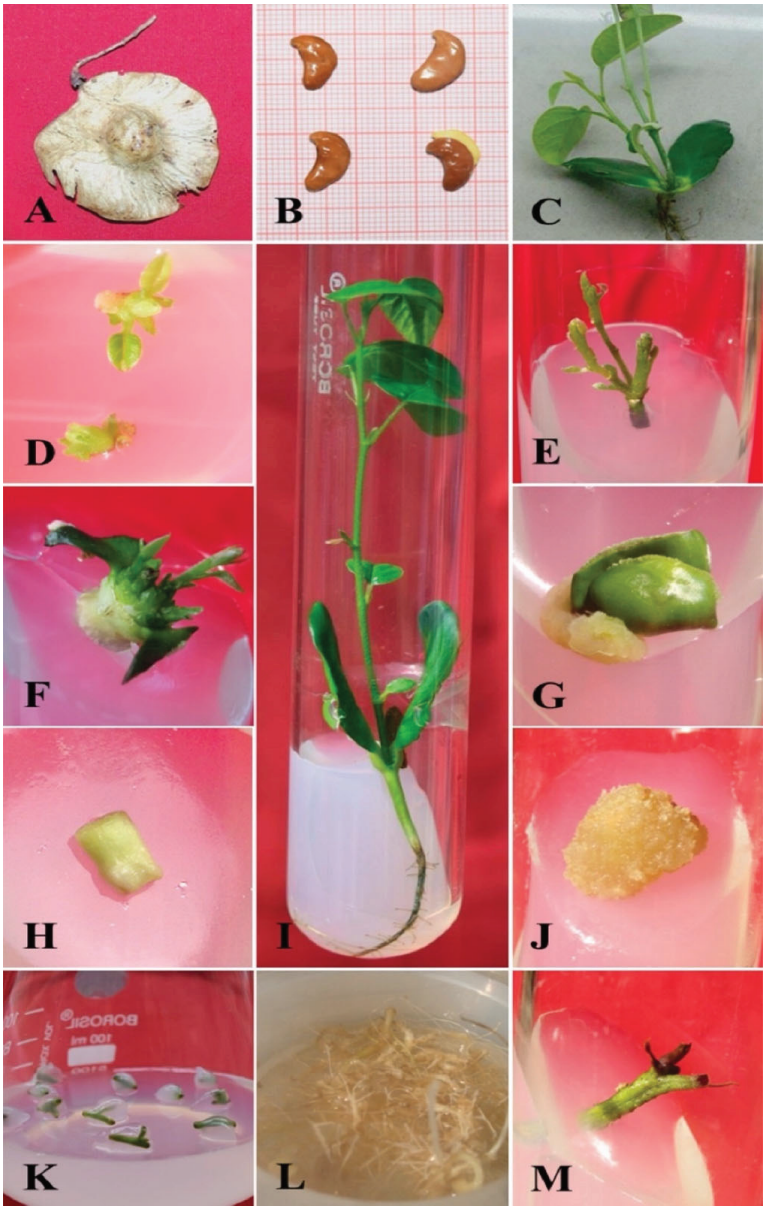

Figure 4. Different sources of explants (or planting materials) used for in vitro propagation of *Pterocarpus marsupium* Roxb. (**A**) Winged fruit, (**B**) 24 h presoaked seeds, (**C**) Intact seedling, (**D**) Shoot tip culture, (**E**) Juvenile nodal segment culture, (**F**) Cotyledonary node culture, (**G**) Cotyledonary leaf culture, (**H**) Hypocotyl segment culture, (**I**) Axenic seedling culture, (**J**) Callus culture via hypocotyl segment, (**K**) Synthetic seed culture, (**L**) Root culture, (**M**) Mature nodal segment culture.

In the case of ex vitro germination, any mechanism that will improve the absorbency of fruit coat could result in an improved percentage of seed germination. Wet heat therapy and physical fruit scarifications weaken the enclosure structure, which improves imbibition and thus enhances the germination rate of the seed. Generally, all these approaches are used more commonly in many plants' fruit and seed dormancy pretreatments. They help to remove the many inhibitors partially and also to decrease the enclosure structure of fruits [102]. Sometimes, seeds' long exposure to hot water may affect the embryo and reduce germination. The contrasting effects of hot wet therapy on the germination of *P. marsupium* and *P. santalinus* were stated by Kalimuthu and Lakshmanan [97]. It was observed that 24 h presoaked seeds (Figure 4B) showed decreased seed germination. Physically scarified seeds have been shown to be more successful in many cases relative to non-scarified and wet heat-treated seeds. Many physical limitations, such as gasses and the diffusion of moisture, are regulated by the thick seed coat of several plants, particularly the Fabaceae family. The high degree of impermeability is largely due to the presence of palisade coating in the seed coat of some legumes [103,104]. The dormancy seed, therefore, induces significant uncertainty in the germination of seed. Physical scarification of seeds has demonstrated that the increased germination rate is possibly attributed to the diffusion of water and gases, mainly by fissures, which causes various biochemical reactions after the rejuvenation of the embryo into a seedling [105,106]. In addition, improved germination patterns in chemically scarified seeds have also been documented relative to other treatments. Barmukh and Nikam [107] suggested that untreated seeds had a 28.2% germination rate within 15 days, whereas physically scarified seeds had a 55.3% germination rate. The treatment of H_2SO_4 for 30 min resulted in a maximum of 78–85% germination in ex vitro conditions. Treatment of scarification 30 min with concentrated H_2SO_4 can be enhanced, consistent and fast germination of seed for the development of *P. marsupium* seedlings. At this stage, the seedlings attained the height of 0.4 m after 8 months, and they were successfully acclimatized under field conditions. The removal of a chemical inhibitor and a scarification of H_2SO_4 seed coat is well explored in a variety of experimental studies on the seed germination of plants [108]. The practice of seed germination includes many important elements for the production of a mature plant under sufficient acid treatment and environmental conditions. The seed coat has an embryonic axis consisting of a radicle, plumule and cotyledons. Long exposure of fruit/seed to acid scarification was morphologically compromised embryonic axis, radicle, plumule, slow development of seedlings, cotyledonary leaf chlorosis, and leaf burnt on the margins [109,110]. All these characteristics are detrimental and decrease the food storage potential that sustains the embryo and its development until it has the ability to absorb sunlight and become autotrophic. In an earlier study, Kalimuthu and Lakshmanan [97] suggested that various combinations of sulphuric acid pretreatment had not changed in the germination of *P. santalinus* and *P. marsupium*, whereas in another study, *P. santalinus* fruit pods were pretreated with 1% H_2SO_4 for 4 days or concentrated H_2SO_4 for 5 min, the most effective treatment for seed germination was found [111]. In addition, Barmukh and Nikam [107] reported that the chemical scarification of seeds with concentrated H_2SO_4 for 30 min is the most effective treatment for homogenous and rapid germination of *P. marsupium*.

Several scientific studies have shown that early seed germination and seedling growth are tightly controlled by numerous hormonal signal molecules [90,112]. Different combinations of media, such as MS [113], B_5 [114], and WH [115], were utilized for the assessment of in vitro seed germination in *P. marsupium* [116]; the highest seed germination rate (96%) was reported on half-strength-MS medium after 20 days. The orientation of the seed can sometimes be a significant factor in improving in vitro seed germination in many plant species [117]. In another study, Mishra, Rawat, Nema, and Shirin [19] reported that *P. marsupium* seeds cultured on a half-strength MS medium in a horizontal position showed maximum germination (78.23%). The results clearly showed that the seed orientation and strength of the medium both have a strong effect on in vitro seed germination (a significantly higher germination rate was obtained with horizontally cultured seeds com-

pared with vertically cultured seeds). Similarly, the horizontal orientation of *Hardwickia binata* seeds significantly enhanced the germination rate compared with vertical orientation [118]. One more important aspect observed during in vitro germination practice is the optimization of an appropriate culture medium and the combination with plant hormones. Husain, Anis, and Shahzad [98] reported a maximum of 80% in vitro seed germination on half-strength MS medium enriched with 0.25 mg/L gibberellic acid, after six days of seed culture. This study clearly demonstrated that the combination of the appropriate media at the right strength along with the incorporation of plant growth regulator (GA_3) enhanced the germination rate. Ahmad et al. [119] reported various allied parameters on in vitro seed germination, i.e., highest percent germination (91.3%), speed germination (29.0 seeds/day), coefficient germination (8.23%), mean germination time (12.15 days), and mean seedling height (10.31 cm) within 21 days of *P. marsupium* seed culture on 0.50 µM GA_3 augmented MS medium. The enhanced concentration of GA_3 promotes the rupture of seed testa and endosperm [120]. The use of culture media augmented with GA_3 has been reported in many studies aimed at improving germination along with better elongation of the plantlets of different species [121–123]. It is also reported that GA3 regulated the synthesis of α-amylase in the aleuronic layer of seeds by upregulating the α-amylase gene, SLN1, and GAMYB transcription factors, thereby promoting germination [124]. Furthermore, DELLA mediated inhibition of BZR1 transcription factor has been shown to promote plantlet elongation [125]. GA_3 stimulates the synthesis of mRNA, which is specific for α-amylase release and is assumed to be one of the factors for improving the rate of seed germination [126].

4.3. Micropropagation through Various Methods

In vitro propagation basically depends on the choice of appropriate explants (pieces of tissue used to initiate cultures) to serve as the preliminary experimental planting material. For multiple shoot bud induction (or bud breaking), the most frequently used explants are those that contain meristematic cells, such as cotyledonary nodes (CN), nodal segments (NS), immature zygotic embryo (IZE), hypocotyl segment (HS), shoot tips and root tip explants. The different types of explants obtained from 7-day-old axenic seedlings of *P. marsupium* are shown in Figure 4C–M. The cell division potential is highest in these tissues, which apparently yield the much-needed growth-regulating substances, such as cytokinins and auxins [127]. In vitro propagation highlights the potential of morphogenic responses on various explants of *P. marsupium* under the regime of different plant hormone combinations. However, the morphogenic potential of explants of various organs varies and some do not grow at all. Explants derived from juvenile seedlings are frequently used for organogenesis under the regime of different plant growth regulators, as they are easily established in axenic culture and have a greater morphogenic potential than do mature explants obtained from donor mother plants [128–131]. The axenic seedlings of *P. marsupium* are a suitable source for obtaining axenic planting material (or explants) as they are aseptically grown from sterilized seeds. Multiple shoot bud induction during plant cell, tissue, and organ culture greatly depend on the type of plant growth regulators (PGR) applied, and their concentration, uptake, transport, and metabolism, and the endogenous hormone levels of explants [132,133]. Endogenous levels of cytokinins in explants are available in various forms, such as free bases, nucleotides, ribosides, *O*-glucosides, and *N*-glucosides [134]. Exogenously supplemented PGRs can modulate the action of enzymes that control the level of endogenous hormones and enzymes [135]. In the next section, we will cover the progress made to date in in vitro propagation of *P. marsupium* through various explants under PGR regimes.

4.3.1. Cotyledonary Node Culture

Cotyledonary node (CN) explants obtained from axenic seedlings of *P. marsupium* have been shown to have the highest regeneration frequency among explants [22,25,136,137]. Similarly, CN explants have been reported to show significantly greater morphogenic potential than do other explants in many tree species, including *Dalbergia sissoo* [138], *Acacia ehrenbergiana* [84], *Eucalyptus saligna* [139], *Lawsonia inermis* [140], *Prosopis cineraria* [141], and *Aegle marmelos* [142]. A variety of cytokinins, i.e., *meta*-topolin (*m*T), 6-benzyl adenine (BA), Kinetin (Kn), 2-isopentenyladenine (2iP), and thidiazuron (TDZ) has been used for *P. marsupium* micropropagation. In Table 3, we have summarized the in vitro propagation successes in this species.

Table 3. In vitro propagation protocols for *Pterocarpus marsupium* (in chronological order).

Explants	Source	Media Compositions (Multiplication) *	Culture Response	Media Compositions (Rhizogenesis)	Rooting Response	Plantlets Survival Rate	References
Shoot tip	AS/MT	MS + 0.2 mg·L^{-1} BAP	Ca-Dm	-	-	-	[96]
Aseptic seeds	-	MS basal medium	ISG (95–100%)	-	-	>68%	[26]
Nodal segment	35-d-old-AS	MS + 0.2 mg·L^{-1} IBA	IO	MS + 0.2 mg·L^{-1} IBA	RF		
Cotyledonary node	20-d-old-AS	MS + 4.44 µM BA+ 0.26 µM NAA	SM (85%)	½ MS + 9.84 µM IBA	RF (IVR)	52%	[136]
Cotyledonary node	18-d-old-AS	MS + 5.0 µM BA + 0.25 µM IAA	SM (75%)	2-step-method: PT on ½ MS (liquid) + 200 µM IBA	MRI (40–50%)	-	[25]
				FT on ½ MS (semi-solid) + 0.5 µM IBA	ER (IVR)		
Aseptic seeds	-	½ MS 0.25 mg·L^{-1} GA_3	ISG (80%)	-	-	-	[98]
Cotyledonary node	18-d-old-AS	2-step-method: SIM: MS + 0.4 µM TDZ	MSI (90%)	2-step-method: PT on ½ MS (liquid) + 200 µM IBA	MRI (65%)	70%	[137]
		FT on SEM: MS + 5.0 µM BA	ES (90%)	FT on ½ MS + 0.5 µM IBA + 3.96 µM PG	ER (IVR)		
Nodal segment	18-d-old-AS	MS + 4.0 µM BA + 0.5 µM IAA + 20 µM AdS	SM (85%)	2-step-method: PT on ½ MS (liquid) + 100 µM IBA + 15.84 µM PG	MRI (70%)	75%	[143]
				FT on ½ MS (semi-solid) + 0.5 µM IBA	ER (IVR)		
Hypocotyl	12-d-old-AS	MS + 5.0 µM 2,4-D + 1.0 µM BA	Ca-Fm (90%)	½ MS + 1.0 µM BA	SEG (56%)	60%	[144]
		MS + 0.5 µM BA + 0.1 µM NAA + 10 µM ABA	SEs (51%)				
Aseptic seed	-	½ MS basal medium	ISG (96%)	-	-	-	[116]
Cotyledonary node	18-d-old-AS	MS + 1.0 mg·L^{-1} BAP + 0.5 mg·L^{-1} NAA	SM (70%)	-	-	-	
Aseptic seed	-	½ MS basal medium	ISG (78.23%)	-	-	-	[19]
Immature zygotic embryo	Green fruits	MS + 3.0 mg·L^{-1} BA + 0.5 mg·L^{-1} IAA	SM (93.8%)	2-step-method: PT on ½ MS (liquid) + 3.0 mg·L^{-1} IBA	MRI (70.8%)	74%	[56]
				FT on ½ MS basal medium	ER (IVR)		
Immature cotyledon	9-d-old-AS	3-step-method: MS + 1.07 µM NAA	Ca-Fm (60.41%)	2-step-method:		95%	[145]
		FT on MS + 8.9 µM BAP + 1.07 µM NAA	MSI (60.41%)	PT on ½ MS (liquid) + 19.6 µM IBA	MRI (75%)		
		FT on MS + 4.4 µM BAP	ES	FT on ½ MS + 2.85 µM IBA	ER (IVR)		
Nodal segment	10-y-old-MT	2-step-method: MS + 13.95 µM Kn + 568 µM AA + 260 µM CA + 605 µM AmS + 217 µM AdS	MSBB (64.44%)	½ MS + 4.92 µM IBA	RF (42%) (IVR)	-	[146]
		FT on MS + 9.3 µM Kn + 0.54 µM NAA + 568 µM AA + 260 µM CA + 605 µM AmS + 217 µM AdS	ES				
Nodal segment	4-w-old-AS	2-step-method: PT on ½ MS (liquid) + 10.0 µM TDZ	MSBB (96%)	2-step-method: PT on ½ MS (liquid) + 150 µM IBA	MRI (80%)	75%	[147]
		FT on MS (semisolid) + 5.0 µM *m*T + 1.0 µM NAA	ES (70%)	FT on ½ MS + 1.5 µM IBA	ER (IVR)		
Cotyledonary node	20-d-old-AS	MS + 7.5 µM *m*T + 1.0 µM NAA	SM (85%)	2-step-method: PT on ½ MS (liquid) + 100 µM IBA	MRI (75%)	80%	[20]
				FT on ½ MS + 1.0 µM IBA	ER (IVR)		

Table 3. *Cont.*

Explants	Source	Media Compositions (Multiplication) *	Culture Response	Media Compositions (Rhizogenesis)	Rooting Response	Plantlets Survival Rate	References
Immature zygotic embryo	Green fruits	MS + 5.37 µM NAA MS + 2.69 µM NAA + 4.4 µM BA + 3% Sucrose	SEs (67.3%)	½ MS + 5.8 µM GA_3	SEG (70%)	78%	[148]
Shoot tip	7-d-old-AS	MS + 7.0 µM *m*T + 1.0 µM NAA	SM (80%)	2-step-method: PT on ½ MS (liquid) + 250 µM IBA FT on Soilrite	MRI (67.7%) ER (EVR)	96.7%	[149]
In vitro seedling	Seed	MS + 0.5 µM GA_3 + 0.5 µM TDZ	SM (85%)	2-step-method: PT on ½ MS (liquid) + 100 µM IBA FT on ½ MS + 0.5 µM GA_3	MRI (80%) ER (IVR)	86.7%	[150]
Aseptic seeds	-	½ MS 0.5 µM GA_3	ISG (91.3%)	-	-	-	[119]

* AA—Ascorbic acid, ABA—Abscisic acid, AdS—Adenine sulphate, AmS—Ammonium sulphate, AS—Axenic seedling, BA—6-benzyladenine, CA—Citric acid, Ca-Dm—Callus-dead mass, Ca-Fm—Callus-fresh mass, d—days, ER—Elongation of roots, ES—Elongation of shoots, EVR—Ex vitro rooting, FT—Followed to transfer, GA_3—Gibberellic acid, h—hours, IBA—Indole-3-butyric acid, IO—Indirect organogenesis, IVR—In vitro rooting, ISG—In vitro seed germination, Kn—Kinetin, MRI—Multiple root induction, MSBB—Multiple shoot bud break, MSI—Multiple shoot induction, MT—Mature tree, *m*T—*Meta*-topolin, NAA—α-naphthalene acetic acid, PG—Phloroglucinol, PT—Pretreatment, RF—Root formation, SEG—Somatic embryos germination, SEM—Shoot elongation medium, SEs—Somatic embryos, SIM—Shoot induction medium, SM—Shoot multiplication, TB—1,2,3-trihydroxy benzene, TDZ—Thidiazuron, w—week, y—year, 2,4-D—2,4-dichlorophenoxyacetic acid.

Ahmad and Anis [22] reported that the highest number of shoots was obtained in CN explants when cultured on 7.5 µM *m*T containing MS medium, which is better than BA for shoot multiplication in *P. marsupium*. The superiority of *m*T over other cytokinins for in vitro propagation has been well documented in many species [151–155]. *Meta*-topolin, a benzyladenine analog [*N* 6-(3-hydroxybenzylamino) purine] is a highly active aromatic cytokinin [156] and differs from BA by having a hydroxyl group in the aromatic side chain (Figure 5), which facilitates the formation of a *O*-glycoside [155] capable of rapid conversion to the active form of nucleosides, nucleotides, or free bases when required [152]. Furthermore, these bases can be converted by N^6- and N^9-glycosylation or alanine conjugates of the purine ring into biologically inactive forms, i.e., stable derivatives [157–159]. Although BA is a widely used cytokinin in micropropagation systems, it has sometimes inhibited rooting efficiency, toxicity, and abnormal growths such as basal callus formation in many species [154,156,160,161]. The undesirable properties of BA may be due to its N^7- and N^9-glycosylation or conjugation with alanine that results in biological inactivation by the formation of chemically stable derivatives [156,162]. Therefore, utilization of *m*T in plant tissue culture has gained increasing interest due to reports of various important parameters, such as improved rate (%) of seed germination [163,164], enhanced multiple shoot induction [165,166], increased shoot length and quality [167–169], successful rooting [170,171], better quality of regenerated plantlets [164,172], easy acclimatization [171,173], alleviation of hyper-hydricity [171,174], delayed senescence [175–177], improved histogenic stability [178,179], alleviated shoot tip necrosis [179], improved physiological and biochemical activities [156,158,176], increased yield [180], and improved biomass content [22,156,173].

Interestingly, while Husain, Anis, and Shahzad [137] observed several shoots from CN explants when cultured on MS medium containing only 0.4 µM TDZ (Thidiazuron), yet the proliferation and shoot elongation remained undifferentiated for one months before these TDZ-exposed cultures were moved to the 5.0 µM BA fortified medium, which in turn induced the proliferation and subsequent shoot elongation. Studies specifically suggested that constant TDZ exposure inhibited shoot elongation [181]. In order to counteract such an antagonistic influence of TDZ, TDZ-exposed cultures have been moved to a secondary medium either free of hormones or supplemented by another PGR such as BA for development and elongation. Thidiazuron (N-phenyl N′-1,2,3-thiazol-5-yl urea) is a synthetic phenylurea having a potent cytokinin-like activity [182]. TDZ is widely used as an alternative to cytokinin in the plant tissue culture system (Figure 6A–C). It is a more powerful plant growth regulator (PGR) relative to other cytokinins for the induction of multiple de novo shoots in many plant species [88,183–185]. Murthy et al. [186] reported

that exogenous usage of TDZ in culture media increased the endogenous amount of plant hormones, especially auxins and cytokinins, in micropropagation practices. TDZ also influences the cytokinins biosynthetic or metabolic processes of cytokinins responsible for controlling the concentration of endogenous levels of purine metabolites [187]. Several researchers concluded that augmentation of TDZ in culture media showed a favorable response on axillary shoot bud induction or bud breaks. However, in many plant species such as *Rhododendron* [188], *Adhathoda beddomei* [189], *Dalbergia sissoo* [138], and *Rauvolfia tetraphylla* [190,191], these shoot buds have not been elongated and proliferated. Many research studies have strongly indicated that such a detrimental impact of TDZ-exposed crops could be due to the existence of phenyl groups and have demonstrated many drawbacks, including bunching of microshoot, fasciation, hyperhydricity, low microshoot efficiency, and inhibition of rooting ability [192–195]. Another study by Huetteman and Preece [196] addressed the issue of shoot elongation by following a two-step culture strategy consisting of a primary medium fortified with TDZ for the induction of multiple shoot buds, followed by their transfer to a secondary medium fortified with another plant hormone (i.e., BA) that promotes shoot elongation. Such a type of culture strategy of using primary medium (shoot bud breaking/induction medium) and secondary medium (shoot elongation medium) has been successfully applied to a several tree species [137,147,197–199].

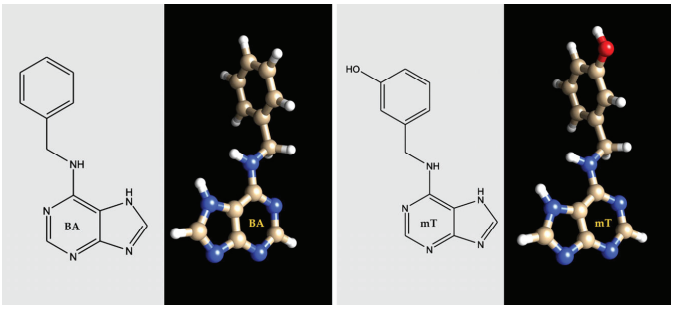

Figure 5. Comparative molecular structure of 6-benzyladenine (BA) and *meta*-topolin (*m*T).

Figure 6. In vitro shoot morphogenesis in *Pterocarpus marsupium* Roxb. (**A**) Multiple shoots on MS + 0.5 µM TDZ, after 3 weeks. (**B**) Multiplication on MS + 5.0 µM *m*T, after 6 weeks. (**C**) Multiple shoots proliferation on MS + 0.5 µM GA_3 + 0.5 µM TDZ + 1.0 µM NAA, after 9 weeks.

Anis, Husain, and Shahzad [25] examined the responses of CN explants of *P. marsupium* to optimize the maximum shoot multiplication under BA and Kn regimen alone or in combination with auxins and obtained good response when cultured on MS medium fortified with 5 μM BA which produced 7.83 shoots per CN explant within 6 weeks of culture. Whereas Kn induced a single shoot, and no significant response was detected. Meanwhile, the explants cultured on the BA fortified medium showed significant shoot growth, and were considered to be more responsive than Kn. The superiority of BA over Kn for multiple shoot induction from CN explant has been reported earlier in *Pterocarpus* species [136,200,201]. BA and Kn cytokinins are commonly used in plant tissue culture systems. However, the efficacy of BA over Kn in in vitro morphogenesis has been well documented in several plant species, such as *Curcuma zedoaria* [202], *Aegle marmelos* [203], *Andrographis paniculata* [204], *Albizia lebbeck* [205], *Terminalia bellirica* [206], *Acacia ehrenbergiana* [84], and *Acacia gerrardii* [207]. In addition, Kn has also been shown to be efficient in successfully developing in vitro propagation protocols for several species [208–211].

Chand and Singh [136] have developed a protocol for in vitro plant regeneration through CN of *P. marsupium*. An average of 9.5 shoots per CN explant were induced on MS medium containing 4.44 μM BA and 0.26 μM NAA in 85% cultures after 15 weeks. According to Chand and Singh, BA was more effective than Kn for multiple shoot formation from the CN explant of *P. marsupium*. It has been found that auxins could not induce shoot multiplication when used alone and that the cytokinin unaided produced very few shoots, whereas the combination of cytokinin and auxin underwent profusion of regeneration. Many studies have shown that a lower dose of auxins is needed in combination with cytokinin to boost the multiplication rate in many plant species [83,84,212–214]. α-naphthalene acetic acid (NAA), indole-3-acetic acid (IAA), and indole-3-butyric acid (IBA) are widely used in shoot multiplication, proliferation, and rooting cultures. Recently, the MS medium fortified with 7.5 μM *m*T and 1.0 μM NAA exhibited the highest frequency of shoot regeneration in *P. marsupium* [22]. Thus, the use of cytokinin to auxin in a ratio proven to be successful in high in vitro shoot regeneration instead of using cytokinin alone. The need for a low auxin concentration in combination with cytokinin can also regulate the endogenous cytokinin level by inhibiting the cytokinin biosynthesis gene, such as isopentenyl transferase (*PsIPT1* and *PsIPT2*) in micropropagated cultures [215,216]. Such type of synergistic effect of cytokinins (BA, Kn, or *m*T) with auxins (IAA, IBA, or NAA) on shoot multiplication and proliferation has been reported by several researchers in many plants' species [217–219]. Cytokinin-auxin has also been associated with many physiological and developmental mechanisms, such as in vitro somatic embryo induction, apical dominance, cell cycle modulation, lateral root induction, control of senescence, and vascular tissues formation [135,220]. Tippani, Nanna, Mamidala, and Thammidala [148] also reported that the addition of auxin (NAA) with cytokinin (BA) to the medium increased the frequency of somatic embryo differentiation rather than BA individually in the medium. In that study, it was concluded that the MS medium containing 4.40 μM BA in combination with 2.69 μM NAA was the most suitable phytohormone combination for indirect organogenesis practice in *P. marsupium*. Several scientific studies have indicated that auxin controls the biosynthesis pathway of cytokinin through the unique activation of *IPT5* and *IPT7* genes [221,222]. In addition to these, several other studies have indicated that cytokinin and auxin jointly regulate their metabolism and signaling pathways [126,223]. As a result, both hormones were considered to be a key signaling molecules regulating the morphogenic response of plants.

4.3.2. Nodal Segment Culture

A successful and efficient regeneration protocol from the nodal segment of *P. marsupium* was established by Ahmad, Ahmad, and Anis [147]. The NS is a good source of axillary shoot multiplication in the tissue culture system, and even a single explant can give rise to multiple copies of true-to-type plantlets within a few months. A two-fold culture strategy was applied to address the problem of shoot elongation. Primarily, the authors

evaluated the effect of TDZ on nodal explant for axillary buds breaking on half-strength MS (liquid) medium containing 10 μM TDZ for 8 days. Thereafter, pretreated NS were transferred to a secondary medium containing different concentrations of *meta*-topolin. TDZ-pretreated NS—when transferred to MS medium supplemented with 5.0 μM *m*T in combination with 1.0 μM NAA—gave the best results, producing the highest number of shoots within eight weeks of culture. A similar culture strategy using shoot bud breaking (primary medium) and subsequent shoot elongation (secondary medium) has been effectively applied in many tree species, for example, *Acacia catechu* [224], *Eucalyptus grandis* [225], *Acacia sinuate* [198], *Lagerstroemia parviflora* [226], *Malus alba* [199], *Melia azedarach* [83], *Balanites aegyptiaca* [227], and *Acacia ehrenbergiana* [84].

Generally, in woody species, NS inoculated on hormone-free MS medium do not show any response, but shoot induction has been observed in cytokinin-augmented MS medium. Husain, Anis, and Shahzad [143] reported that the addition of 20 μM adenine sulfate (AdS) in MS medium containing 4.0 μM BA and 0.5 μM IAA improved the establishment of nodal explant cultures. A nucleotide base of adenine in the form of AdS can induce cell growth and significantly promote multiple shoot growth. AdS provide an additional nitrogen source to the cell, and this form of nitrogen can generally be taken up more rapidly than inorganic nitrogen. In a number of studies, the application of AdS in culture medium is recommended because it promotes the regeneration capacity of explants, especially in woody species such as *Tectona grandis* [228], *Bauhinia vahlii* [229], and *Melia azedarach* [230]. However, in the place of AdS, some other adjuvants, such as silver nitrate ($AgNO_3$), casein hydrolysate (CH), polyvinylpyrrolidone (PVP), activated charcoals, coconut water, amino acids, and vitamins have been used in the culture medium for inducing shoot/root organogenesis and somatic embryogenesis [231]. Fuentes et al. [232] found that the addition of $AgNO_3$ and fructose promoted somatic embryogenesis in *Coffea canephora*, whereas CH in combination with ammonium chloride has been shown to be the best combination in culture media to promote embryo germination as well as plant regeneration in *Sapindus mukorossi* [233].

4.3.3. Shoot Tip Culture

Now-a-days, shoot tip culture techniques have been attracting interest by plant tissue culturists mainly due to their possible usage in large areas such as clonal multiplication of vegetatively propagated crop plants, virus elimination, genetic modification, germplasm conservation, etc. The most desirable aspect of shoot tip culture is that it has an advantage over other in vitro processes, the ability to preserve a high degree of genetic integrity among regenerants. Nehra and Kartha [234] have thoroughly reviewed the different facets of shoot tip culture and its commercial applications in many fields. Many researchers have used shoot tip explants to establish an effective in vitro regeneration protocol in several woody species. Sharma et al. [235] induced multiple shoots of *Bougainvillea glabra* from shoot tip explants culture on medium supplemented with of 0.5 mg/L BAP and 1.5 mg/L IAA. Multiple shoots were successfully achieved in shoot tip explant of *Catha edulis* (mature tree) when cultured on MS medium supplemented with 0.3 mg/L BA and 3.0 mg/L IAA by Hamid [236]. Kaur and Kant [237] reported a successful micropropagation protocol for *Acacia catechu* through shoot tip explants. It produced the highest number of shoots when cultured on MS medium containing 1.5 mg/L BAP plus 1.5 mg/L Kn. Shoot tip explants obtained from 20-day-old in vivo germinated seedling of *Pterocarpus santalinus* proliferated into multiple shoots on 1.0 mg/L BAP in combination with 0.1 mg/L fortified MS medium [238]. Similarly, Al-Sulaiman and Barakat [239] successfully induced multiple shoots of *Ziziphus spina-christi* from shoot tip on MS medium supplemented with 1.0 mg/L BA and 0.1 mg/L NAA. Recently, Hussain et al. [240] reported the highest differentiation of shoots *Tecoma stans* by culturing shoot tip on 7.5 μM BA and 0.5 μM NAA enriched MS medium. Their studies indicate that the formulation of PGRs in culture media for shoot tip culture depends mainly on plant species. Shoot tip culture is the most appropriate method for obtaining both virus-free and true-to-type clones. Up to now, only a single

report has been published on successful in vitro regeneration of *P. marsupium* through shoot tip explants [149]. The highest shoot bud differentiation was achieved in this investigation at 7.0 μM *m*T plus 1.0 μM NAA, whereas Das and Chatterjee [96] attempted to regenerate multiple shoots from the shoot tip of *P. marsupium*. Initially, it was observed that shoot tip explants grew at 0.2 mg/L of BAP enriched MS medium, but after some time, it did not grow and eventually became necrotic on the same medium. As a result, these studies demonstrate that the formulation of culture media, PGRs and culture conditions plays an important role in effective shoot tip culture.

4.3.4. Immature Zygotic Embryos Culture

In plant tissue culture systems, the combination of PGRs plays an important role in determining the morphogenic response of explants. Mature tissues, which lack undifferentiated totipotent cells, respond poorly to regeneration treatments. Tippani, Vemunoori, Yarra, Nanna, Abbagani, and Thammidala [56] used immature zygotic embryos (IZEs) of a *P. marsupium* as the explant source, which, unlike other types of explants, is rich in meristematic cells. The researchers induced the highest frequency of shoot regeneration (93.8%) on MS medium fortified with 3.0 mg/L BA in combination with 0.5 mg/L IAA, which resulted in a maximum of 17.3 shoots per IZE explant. Subsequently, when these cultures were sub-cultured on MS medium containing a reduced concentration of 1.0 mg L^{-1} BA, an improvement in the average number of shoot (27.2) per IZE explant as well as increase in the average shoot length (4.5 cm) were documented. The potential use of IZEs to establish a plant regeneration system through shoot organogenesis and somatic embryogenesis has been verified in many tree species; for example, *Bixa orellana* [241], *Chamaecyparis obtusa* [242], *Pinus oocarpa* [243], and *Sapium sebiferum* [244]. IZEs are considered a reliable source of explants, and the combination of 2,4-D and Kn is generally recommended for somatic embryogenesis in several woody species angiosperms and gymnosperms [245].

In addition, the rate of multiplication of in vitro shoots depends greatly on the subculture of proliferating explants on a fresh medium. It is also imperative that as the number of cells, tissues, or organs becomes excessively high, there is a need to increase the amount of a culture or to increase the organ numbers for in vitro propagation. During extended cultures, the level of nutrients in the medium is significantly depleted, and as result of the development of certain harmful metabolites, a decline in relative humidity in culture vessels has resulted in the drying of developing cultures. Apóstolo et al. [246] advocated that the high humidity in culture flask or culture tubes helps to boost rapid growth. Thus, a repetitive sub-culture strategy can help in inducing multiple shoots, followed by improved rooting [217,247]. Several researchers have introduced a repeated sub-culture approach to improve multiplication rates in several plant species such as *Feronia limonia* [248], *Pterocarpus santalinus* [249], *Balanites aegyptiaca* [217], *Spondias mangifera* [250], *Arnebia hispidissima* [251], and *Tetrastigma hemsleyanum* [252].

4.3.5. Intact Seedling Culture

Multiple shoot induction directly from the seed explant (also called intact seedling culture) is another method for rapid in vitro propagation (Figure 4C). The significant aspect of this regeneration protocol is that shoot differentiation occurs directly from the CN of the seedling, eliminating the need for an explant preparation step. Our literature review found that the intact seedling method greatly reduces many difficulties such as the cost of culture, time of regeneration protocol, and other considerations such as the age and size of the explant and its orientation in the culture vessel. However, it should be noted that these very same factors are thought to have an important role in successful regeneration, especially in leguminous tees. Malik and Saxena [253] reported that the rate of shoot multiplication via the intact seedling method in *Phaseolus vulgaris* was higher than that obtained from the explant method. Bhuyan et al. [254] developed a high throughput shoot multiplication protocol through intact seedling propagation of *Murraya koenigii* cultured on 5.0 mg/L BA and 0.4 mg/L GA_3 in MS medium. The authors found that the application of GA_3 to the

medium had no stimulatory effect on shoot multiplication per intact seedling, whereas it did exhibit a remarkable effect on shoot elongation. Hussain, et al. [255] reported that the shoot multiplication rate from intact seedlings of *Sterculia urens* was highest when cultured on MS medium containing 5.0 μM BA, 0.4 μM GA_3, and 0.1% ascorbic acid. Perveen, Anis, and Aref [85] successfully developed an in vitro regeneration protocol for *Albizia lebbeck* through the intact seedling method. In this trial, the highest shoot multiplication response was obtained from the highest dose of 5.0 μM TDZ (primary medium) followed by transfer to a lower dose (0.5 μM) of TDZ (secondary medium). Cumulatively, the results of these studies are clear evidence that intact seedling cultures are greatly influenced by the formulation of the growth regulator and that excision of the explant is not necessary for in vitro shoot multiplication. In case of *P. marsupium*, Ahmad, Anis, Khanam and Alatar [149] reported only direct shoot multiplication from the intact seedling method. The optimum culture, containing 0.50 μM GA_3, induced the maximum seed germination response along with better shoot growth when compared to cultures with TDZ. Similarly, cultures treated with TDZ exhibited a higher shoot multiplication rate than did those treated with GA_3. However, it was found that the two hormones combined together at an optimal level (TDZ at 0.50 μM and GA_3 at 0.50 μM) resulted in the most effective treatment for germination response, shoot multiplication, and subsequent shoot elongation per explant. The authors [149] hypothesized that the improvement in protocol performance was due to the interaction of the two hormones, with successful regulation both in terms of biosynthesis and signal transduction.

4.3.6. Somatic Embryogenesis

In somatic embryogenesis (SE), a single cell or group of somatic cells initiate the developmental pathway that leads to the formation of NZEs. This means that the embryos have no connection with pre-existing vascular tissue within the maternal callus. Williams and Maheswaran [256] suggested that somatic embryos can differentiate from pre-embryogenic determined cells, leading to direct embryogenesis. There are two well-defined methods for SE: the direct method (without callus) and the indirect method (with a callus-intervening phase). SE has been widely exploited in many plant breeding activities, such as mass-scale propagation, shortening of the breeding cycle, development of synthetic seeds, and genetic transformation of industrially important crops [127,231]. Currently, there are only a few published reports of SE in *P. marsupium* (Table 1). Differentiation of the somatic embryo can occur directly on the callus induction medium, whereas in many cases a combination of different media and hormones is required for callus induction, somatic embryo formation, and morphogenesis of shoot and plantlet conversion [144]. Recently, Tippani, Nanna, Mamidala, and Thammidala [148] developed an improved protocol for in vitro plantlet regeneration via SE from IZE explants of *P. marsupium*. Dedifferentiated tissues were induced profusely in 96.6% callus from IZE explants when cultured on a callus induction medium, i.e., MS plus 5.37 μM NAA. The callus was successfully induced to produce somatic embryos when cultured onto differentiation medium, i.e., MS consisting of 2.69 μM NAA and 4.40 μM BA. Lastly, maturation of somatic embryos into plantlets has been accomplished with the use of half-strength MS fortified with GA_3 (5.80 μM). Chaturani et al. [257] reported that IZEs are an ideal explant to obtain the highest culture initiation and multiplication under in vitro conditions. There are many reports available on the utilization of IZE explants for inducing SE in tree species such as *Pinus oocarpa* [243] and *Fraxinus mandshurica* [258].

In addition, there have been many reports of the efficacy of HSs, obtained from aseptic seedlings, to achieve indirect SE in many plant species [259,260]. Husain, Anis, and Shahzad [144] achieved SE from the callus, derived from hypocotyl segment (excised from12-day-old axenic seedlings) of *P. marsupium*. Primarily, callus formation occurred on callus induction medium, i.e., MS containing 2,4-D (5.0 μM) and BA (1.0 μM). Secondarily, the calluses were successfully converted into somatic embryos when they were sub-cultured onto differentiation medium; i.e., MS containing 0.5 μM BA and 0.1 μM NAA in combination with 10 μM ABA. Husain, Anis, and Shahzad [144] also suggested that

maturation of somatic embryos takes place by the addition of ABA, a growth inhibitor, which creates stress conditions that are conducive to the development and maturation of somatic embryos of *P. marsupium*. It may be possible that ABA interacts synergistically with both hormones (auxin-cytokinin) and stimulates maximum somatic embryo maturation. SE formation has occurred in many leguminous tree species via various explant sources such as immature cotyledon in *Acacia catechu* [261], immature cotyledon in *Hardwickia binata* [262], endosperms in *A. nilotica* [263], embryonic axes with cotyledons in *Albizzia julibrissin* [264], IZEs in *Acacia mangium* [265], and immature cotyledon in *Pterocarpus marsupium* [145].

4.4. Rooting and Acclimatization

Rhizogenesis of in vitro raised microshoots is often problematic in woody species and leads to significant economic consequences because of losses at this stage [266,267]. The development of a well-rooted system is vital for the successful establishment of in vitro raised microshoots in field conditions. Therefore, adventitious root formation is an important step for in vitro regeneration of various woody plants [268]. The use of auxins affects the in vitro root formation of microshoots raised in tissue culture [269]. Some important factors (type and concentration of auxin and treatment duration) play crucial roles in root induction [270,271]. IBA is an important exogenous auxin utilized for in vitro root induction in several plant species because it has shown more resistance to photodegradation, adherence to microshoots, and inactivation by biological action [272]. The stimulatory effect of IBA on induction of rooting may be due to successive rooting gene activation and better uptake, transportation, and stability compared with other auxins [159,273]. This type of two-step rooting strategy has been applied in many tree species [147,274]. In the first step, the distal ends of microshoots are dipped in a half-strength MS (liquid) medium containing a high dose of auxin (IBA) over a filter paper bridge for several days. In the second step, these pretreated microshoots are transferred onto half-strength MS (semisolid) medium, fortified with a lower dose of IBA, and cultured for one month (Figure 7A–F). Regenerated microshoots of *P. marsupium* have been affected by high dose IBA pretreatments, which improves the rate of rooting response, the number of roots per microshoot, and their subsequent length [25,56,143].

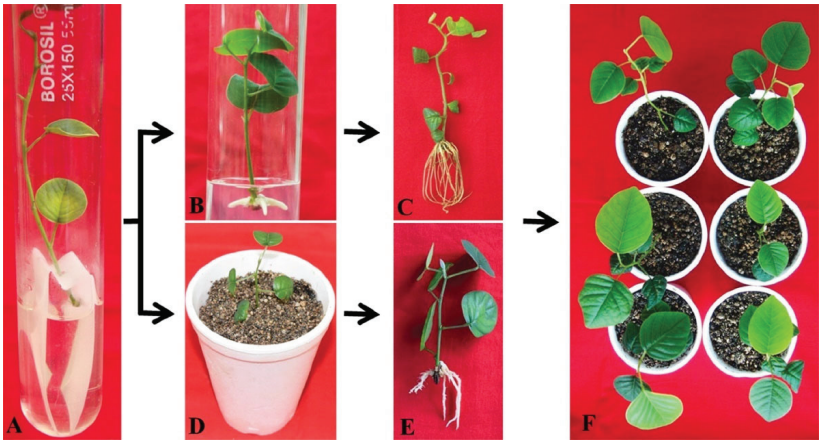

Figure 7. Two step rooting strategy for root formation in microshoots of *Pterocarpus marsupium* Roxb. (**A**) Pretreatment of microshoot in liquid medium employing filter paper bridge; (**B**) Pretreated microshoot transferred onto semi-solid medium containing phytagel for in vitro root formation; (**C**) 4-week-old in vitro rooted microshoot; (**D**) Pretreated microshoot transferred onto Soilrite (a synthetic soil) for ex vitro root formation; (**E**) 4-week-old ex vitro rooted microshoot; (**F**) Acclimatized plantlet in Soilrite.

Ahmad and Anis [22] have reported that root forming efficiency in *m*T-derived microshoots is higher compared to BA-derived microshoots. Rhizogenesis in microshoots was carried out via a two-step rooting procedure. For the purpose, distal ends of microshoots were pre-treated with a high dose of IBA (100 μM) augmented $\frac{1}{2}$ MS (liquid) medium for 5 days, followed by their transfer onto the half-strength of MS (semisolid) medium containing a low dose of IBA (1.0 μM) resulting in a successful root induction response. Ludwig-Müller [273] proposed that several factors, such as better absorption of auxin, transport, and stabilization over other auxins, and the subsequent genes, are responsible for the in vitro root formation. However, an inhibitory effect of BA on in vitro root development and low acclimation rates has also been recorded in many plant species [172,275]. On the other hand, a profound impact of *meta*-topolin on in vitro rooting and acclimatization of regenerated plantlets has also been identified in several species [161,173,276]. Exogenous doses of auxin in the culture medium are commonly used in different plants to induce in vitro rhizogenesis in regenerated microshoots [84,277,278]. Auxins serve as a central regulator of adventitious root formation. Specifically, it stimulates the preparation of pericycle cells that induce lateral roots [279,280]. De Smet [281] has reported several research studies on the use of auxin for the initiation and growth of lateral roots in isolated microshoots. The addition of exogenous auxin to the culture medium induces new primordial lateral root unrelated to acropetal branching in many plant species, including *Arabidopsis* [282]. In an experiment performed by Ilina, Kiryushkin, Semenova, Demchenko, Pawlowski and Demchenko [280], the main lateral root of the pericycle cells undergoes asymmetric anticline arises three adjacent pericycle cells. After some time, all active pericycle cells are arrested in the basal portion of the elongation region [283]. Since some of the pericycle cells that left the basal portion of the root apical meristem in the G1 phase of the cell cycle may begin the cell division of the cells involved in the induction of primordia's lateral roots [284].

Jaiswal, Choudhary, Arya, and Kant [146] reported that being a woody perennial *P. marsupium* is difficult for in vitro rhizogenesis. In vitro root induction in microshoots found that IBA was more effective than the other auxin and $\frac{1}{2}$ MS medium containing 4.92 μM IBA induced 2.14 roots per microshoots with an average root length of 1.24 cm in 42.2% cultures. On the other hand, in an experiment performed by Tippani, Vemunoori, Yarra, Nanna, Abbagani and Thammidala [56], the best response was recorded on MS medium containing 3.0 mg L-1 IBA pretreatment for 24 h, followed by transfer onto hormone-free MS medium, produced a maximum number of 3.2 roots per microshoot with mean root length of 2.9 cm in 70.8% cultures after 15 days of transfer. According to De Klerk et al. [285], high doses of auxin pretreatment are needed during the initial root induction process, but in many cases during root elongation, a high dose of any growth regulator becomes inhibitory. A large number of researchers have proposed IBA as the best rooting hormone in many plant species like *Kigelia pinnata* [286], *Terminalia arjuna* [287], *Albizia lebbeck* [85], and *Syzygium cumini* [214]. On the other hand, in *P. marsupium* microshoots, Husain, Anis, and Shahzad [137] applied a two-step rooting protocol for in vitro root induction. In the first step, the distal end of microshoots was pulse-treated with 200 μM IBA for 4 days and on filter paper bridge on $\frac{1}{2}$ MS (liquid) medium, followed by step-two with subsequent transfer of these pulse-treated shoots to 0.6% agar-gelled $\frac{1}{2}$ MS containing 0.2 μM IBA in combination with 3.96 μM phenolic acids (phloroglucinol). At this stage, the maximum number of 4.4 roots per microshoot with a mean root length of 4.0 cm was obtained in 65% of cultures after 4 weeks. In several tree species, the stimulatory effect of phloroglucinol has been documented [288–290]. Interestingly, De Klerk et al. [291] suggested that phloroglucinol in combination with auxin had a synergistic effect in inhibiting peroxidase activity in the culture, thereby protecting the endogenous auxin from peroxidase-catalyzed oxidation. Subsequently, an in vitro rooting response in microshoots of *P. marsupium* was also observed when it was grown on the primary liquid MS medium followed by switch to the secondary hormone-free semisolid half-strength MS medium. The highest root formatting frequency (70%) was achieved with a maximum

3.8 roots per microshoot on an average root length of 3.9 cm on the MS medium containing 100 μM IBA and 15.84 μM phloroglucinol after 4 weeks of culture [143]. Ahmad, Ahmad, Anis, Alatar, Abdel-Salam, Qahtan, and Faisal [150] recently reported an improvement in the in vitro rooting response in *P. marsupium* by pre-treating microshoot with 100 μM IBA for 5 days and then transferring to medium of containing 0.50 μM GA_3. This combination has been shown to be the highest in vitro rooting in microshoots. Improvement in rooting response was hypothesized that IBA would be stored in basal ends of microshoots during pretreatment and would be actively used when interacted with GA_3.

Recently, many tissue culturists have focused on ex vitro rhizogenesis in microshoots because ex vitro rooted plantlets produce a better developed root system compared with those of in vitro raised plantlets [129,292,293]. The ex-vitro rooting strategy is practical and cost-effective, requiring less time, less labor, fewer chemicals, and only minimal equipment compared with the requirements of in vitro rooting practice. Many researchers have reported that ex vitro rooted plantlets have good quality roots with minimum damage, are easy to acclimatize, and have a high survival rate because they do not require any additional acclimatization before being transplanted in natural conditions [85,129,294–296]. A major breakthrough in ex vitro rooting was achieved by Ahmad, Anis, Khanam, and Alatar [149] via a two-step rooting procedure. In this process, microshoots were isolated from in vitro grown cultures and subjected to the pretreatment of basal ends in optimized doses of IBA, followed by transfer onto various potting substrates. The best rooting response was obtained when the basal ends of microshoots were treated with 250 μM IBA for 5 days, followed by transfer to Soilrite, where a maximum of 3.63 roots per microshoot and mean root length of 3.59 cm, as well as the highest rooting frequency 67.7%, were recorded 4 weeks after transplantation. The authors reported that the ex-vitro rooted plantlets of *P. marsupium* were successfully acclimatized, with 96.7% survival rate [149]. Similarly, ex vitro rooting in regenerated microshoots has been achieved in a large number of woody species, including *Tectona grandis* [297], *Nyctanthes arbor-tristris* [298], *Vitex negundo* [183], *Malus zumi* [299], *Melia azedarach* [83], and *Tecomella undulata* [300]. In the study by Ahmad and Anis [22], the hardening of regenerated plantlets of *P. marsupium* was achieved by the well-rooted shootlets being gently removed from the culture vessel and washed with running tap water to remove any adherent; after which the plantlets were transplanted to Thermocol cups (10-cm diameter) containing sterile Soilrite. Other researchers have covered the culture cups with transparent polyethylene bags as a safeguard to ensure high humidity and placed the cups under 16/8 h (day/night) in culture room conditions [147,301]. These polybags were gradually opened in order to acclimatize the plantlets to natural conditions. Finally, the acclimatized plantlets were successfully shifted to normal garden soil under natural daylight conditions. Generally, tissue culture-raised plantlets have low photosynthetic rate because regenerated plantlets have underdeveloped photosynthetic apparatuses [302]. The improvement in photosynthetic pigment contents in regenerated plantlets is possible during acclimatization, as noted by several researchers [303,304]. The substantial increment in photosynthetic pigment content with high light intensity promotes the pigment biosynthesis enzyme, which is vital to synthesis of photosynthetic pigment content [305]. There have been several investigations of the abrupt decrease in photosynthetic pigment contents during the initial days followed by a continuous increase during the acclimatization processes in many plants [131,306,307].

5. Molecular Studies of *P. marsupium*

5.1. Genetic Fidelity Assay

Plant tissue culture techniques are an important tool in the clonal propagation of genetically uniform plants that possess desirable traits. Many researchers have suggested that the existence of somaclonal variations among sub-clones of an elite parental line is a potential drawback during micropropagation practice [240,308]. Javed, Alatar, Anis, and El-Sheikh [88] advocated that genetic uniformity of regenerated plantlets is a prerequisite to sustain the desired genotypes. The application of phytohormones at elevated concentra-

tions and continuous sub-culturing of cultures for long periods hinders the maintenance of genetic stability [22]. The consequences of unintended mutations and the mixing of regenerated plantlets could mean that much time and money is wasted before the mistakes are discovered. Therefore, it is necessary to validate the uniformity of the regenerated plants at the genetic level through molecular markers, given that variability induced by continuous practice of in vitro propagation cannot be detected phenotypically because the structural differences in the gene products are not sufficient enough to alter the phenotypes [309]. Although many approaches have been attempted to detect genetic homogeneity (i.e., true-to-type clones) among regenerants, the most suitable technique appears to be DNA-based molecular markers. Such markers are not affected by environmental factors and can be analyzed using genomic DNA from any growth stage; therefore, these markers are very useful in analyzing genetic fidelity in a large number of plant species. RAPD and ISSR have become more popular among the different molecular marker techniques, as they do not require any prior DNA sequence information [87,191,310].

There have been scores of studies on genetic fidelity analysis by using RAPD and ISSR techniques in regenerated plants of different species such as *Moringa peregrina* [311], *Alhagi maurorum* [312], *Terminalia bellerica* [313], *Morus alba* [314], *Lawsonia inermis* [140], *Platanus orientalis* [315], *Erythrina variegata* [88], *Tecoma stans* [240]. Their simplicity, cost-effectiveness, and requirement of low quantity DNA are some reasons for the selection of these markers for genetic fidelity analysis [311,314,316–318].

Although DNA-based markers have been shown to be an effective technique to assess genetic fidelity in a number of plant species, there are few documented techniques particular to *P. marsupium*. In one recent study [149], assessment of genetic fidelity in *P. marsupium* regenerants was achieved using DNA-based ISSR primers. The authors of this study obtained a total of 35 bands, with an average of 4.38 bands per primer, in a monomorphic banding pattern. In an earlier study, Ahmad and Anis [22] had used a total of 29 RAPD primers to detect genetic fidelity among regenerated plantlets of *P. marsupium*; the results were monomorphic DNA bands exhibiting complete genetic uniformity. In still earlier work, Tippani, Vemunoori, Yarra, Nanna, Abbagani, and Thammidala [56] reported that four ISSR primers produced a monomorphic banding pattern regenerated when compared with mother plant. In a later experiment [148], eight ISSR primers were used for DNA amplification, producing a clear, reproducible, and monomorphic DNA banding pattern demonstrating genetic fidelity among regenerants of *P. marsupium* derived through the SE method. Taken together, this research confirms the efficacy of regeneration protocols for true-to-type plant breeding in general and *P. marsupium* in particular.

5.2. DNA Barcoding

Presently, several adulterants of *Pterocarpus* species are available in the international trade market [16]. Scientific authentication of genuine species is vital for the herbal drug industry; however, the conventional approach for the identification of authentic species is not sufficient. The difficulty lies in the fact that most of the physical and anatomical characteristics (i.e., wood density, grain, and color) of *Pterocarpus* species are very similar to its adulterants. DNA barcoding offers an alternative and feasible taxonomic tool for rapid and robust species identification in general [17,319–321] and could be an effective technique to distinguish *Pterocarpus* and its adulterants. Jiao, Yu, Wiedenhoeft, He, Li, Liu, Jiang, and Yin [16] developed a DNA barcode to distinguish adulterants of six commercially important species of *Pterocarpus* (*P. marsupium*, *P. santalinus*, *P. indicus*, *P. erinaceus*, *P. zenkeri*, *P. angolensis*). An array of genes, including *ITS2*, *matK*, *ndhF-rpl32*, and *rbcL*, have been utilized to discriminate *Pterocarpus* species through TaxonDNA and tree-based analytical methods. Jiao, Yu, Wiedenhoeft, He, Li, Liu, Jiang, and Yin [16] suggested that two of these genes, namely *matK* and *rbcL*, are the core DNA barcodes for authentication of many plant species. The *ITS2* regions are standard DNA barcodes, especially used in identifying adulterants of industrially important medicinal plants [9,322]. Similarly, *ndhF-rpl32*, an intergenic spacer gene of cpDNA, has the potential to be used for DNA barcoding of

a large number of species [323–325]. Consequently, many researchers in this field have recommended DNA barcodes as well-known tools for authenticating genuine herbal raw materials in quality control programs and forensic studies [326–328].

5.3. Genetic Transformation

Establishment of in vitro propagation protocols is a prerequisite for genetic manipulation studies because in traditional breeding techniques—such as backcrossing and selfing—it is difficult to fix desirable alleles in a particular genetic background [13]. Successful transfer of genes of interest through genetic transformation technique has been well documented in many tree species [329–331]. Gorpenchenko et al. [332] established a successful genetic transformation process in *Panax ginseng* through callus-based shoot organogenesis. Similarly, Tippani, Yarra, Bulle, Porika, Abbagani, and Thammidala [145] demonstrated genetic transformation in *P. marsupium* through callus-based organogenesis using immature cotyledon explants obtained from 9-day-old axenic seedlings. Callus formation occurred on callus induction medium containing MS fortified with 1.07 µM NAA for 2 weeks. Subsequently, the callus was co-cultivated with *A. tumefaciens* (harboring the binary plasmid with *uidA* and *hpt* genes) and cultured on MS augmented with BAP (8.9 µM), NAA (1.07 µM), and acetosyringone (200 µM) for 2 days. These cultures were then transferred onto MS containing BAP (8.9 µM), NAA (1.07 µM), hygromycin (20 mg/L), and cefotaxime (250 mg/L) for multiple shoot induction, followed by transfer to shoot elongation MS medium containing BAP (4.40 µM), hygromycin (15 mg/L), and cefotaxime (200 mg/L). Putatively transformed microshoots were rooted on MS medium containing BA (2.85 µM) in combination with hygromycin (20 mg/L), after dip treatment of the distal ends of *P. marsupium* for 24 h in MS medium fortified with IBA (19.60 µM). Tippani, Yarra, Bulle, Porika, Abbagani, and Thammidala [145] validated the gene transfer into putatively regenerated plants through RT-PCR and GUS assay. Interestingly, Jube and Borthakur [333] proposed that the rate of transformation in woody species is meager because excised explants produce several harmful phenolic compounds. On a contrary note, there are many reports published on *A. tumefaciens*-mediated transformation in leguminous woody trees [330,331].

6. Conclusions and Future Prospects

The commercial productivity of tree plantations could be increased by reducing the genetic diversity of forest species and achieving greater homogeneity of tree phenotypes. Currently, many factors, such as increasing demand from pharmaceutical companies and timber-based industries and the overall decline of the global forest cover, as well as the impacts of climate change, have all motivated forestry decision-makers to raise the productivity of natural forests. There is also an increasing demand for aromatic and herbal drug yielding plants because natural products are seen to be non-toxic and have fewer side effects. Our comprehensive survey of the literature revealed that knowledge of the pharmacognosy, ethnobotany, and micropropagation of *P. marsupium*—a species of high value globally and in India—is rather limited and has only appeared in the past three decades. Plant biotechnology has opened new avenues for the generation of novel genetic variability, and techniques in this field now offer greater selection and are increasingly more precise and reproducible. Such techniques have broad applications in a number of important areas, for example, genetically modified food, feed, and fiber.

Micropropagation of *P. marsupium* can offer great advantages over traditional methods. Such advances can help researchers meet their goals in numerous specialties: plant breeding, plant biotechnology, germplasm conservation, rapid propagation of genetically modified plants, secondary metabolites biosynthesis, germplasm exchange, extensive collection within minimum space, supply of important planting material for wild population recovery, and molecular and ecological studies. Moreover, before developing any regeneration protocol, information on actual genetic variability and the cryptic number of the differentiated genetic resources are essential for both the genetic improvement of the species

and its conservation. Before developing an effective method to maintain the genetic diversity of any targeted species, it must first be quantified. A promising method in regeneration programs is the use of DNA-based molecular markers.

Advances in DNA barcoding will help in the authentication of key forest species such as *P. marsupium* and may eventually lead to the formulation of legislation ensuring the public's access to this plant at a reasonable cost. There are several substituted for *P. marsupium* wood on the market, and they can be less effective as medicines and, in some circumstances, fatal due to the toxicity of the substituted plant material as an open access, worldwide library of reference barcode sequences continues to be collected, DNA barcoding may be a viable answer to species authentication, allowing non-taxonomists to identify specimens. In vitro propagation and genetic diversity analysis of *P. marsupium* can be used effectively to select superior populations of the species for breeding programs aimed at improving productivity, wood quality, and chemical constituents, thereby helping to inform plans for conservation and sustainable use of this valuable plant species. More importantly, critical elements of an effective conservation strategies need to be discussed.

Author Contributions: Conceptualization, A.A., N.A. and M.A.; methodology, A.A., N.A. and M.F. software, A.A., N.A., M.F. and E.M.A.-S.; validation, A.A., N.A. and M.A.; formal analysis, A.A., N.A., M.F., A.A.A., E.M.A.-S., R.P.M. and I.S.; investigation, A.A., N.A. and M.A.; data curation, A.A., N.A. and M.A.; writing—original draft preparation, A.A., N.A. and M.F.; writing—review and editing, M.A., A.A.A., E.M.A.-S., M.F., R.P.M. and I.S.; supervision, M.A. and N.A. All authors have read and agreed to the published version of the manuscript.

Funding: Deanship of Scientific Research, King Saud University: RGP175.

Institutional Review Board Statement: Not applicable.

Informed Consent Statement: Not applicable.

Data Availability Statement: Not applicable.

Acknowledgments: This article was supported by the KU Research Professor Program of Konkuk University.

Conflicts of Interest: The authors declare no conflict of interest.

References

1. Keenan, R.J.; Reams, G.A.; Achard, F.; de Freitas, J.V.; Grainger, A.; Lindquist, E. Dynamics of global forest area: Results from the FAO Global Forest Resources Assessment 2015. *For. Ecol. Manag.* **2015**, *352*, 9–20. [CrossRef]
2. Klitgaard, B.; Lavin, M.D. Dalbergieae: Legumes of the world. In *Legumes of the World*; Lewis, G.P., Schrire, B., MacKinder, B., Lock, M., Eds.; Royal Botanic Gardens Kew: Richmond, UK, 2005; pp. 307–335.
3. Baker, E.G. *The Leguminosae of Tropical Africa*; Erasmus Press: Ghent, Belgium, 1929.
4. Bentham, G. A Synopsis of Dalbergieae: A Tribe of the Leguminosae. *J. Proc. Linn. Soc.* **1860**, *4*, 65–80. [CrossRef]
5. De Candolle, A.P. *Memoires sur la Famille des Legumineuses*; Auguste Belin: Paris, France, 1825.
6. Lewis, G.P. *Legumes of Bahia*; Royal Botanic Gardens Kew: Richmond, UK, 1987.
7. Rojo, J.P. *Pterocarpus (Leguminosae-Papilionaceae) Revised for the World*; Verlag Von J. Cramer: Lehre, Germany, 1972.
8. Taubert, P. Leguminosae. In *Die Natürlichen Pflanzenfamilien*; Engler, A., Prantl, K., Eds.; Engelmann: Lemgo, Germany, 1894.
9. Saslis-Lagoudakis, C.H.; Klitgaard, B.B.; Forest, F.; Francis, L.; Savolainen, V.; Williamson, E.M.; Hawkins, J.A. The use of phylogeny to interpret cross-cultural patterns in plant use and guide medicinal plant discovery: An example from *Pterocarpus* (Leguminosae). *PLoS ONE* **2011**, *6*, e22275. [CrossRef] [PubMed]
10. Barstow, M. *Pterocarpus marsupium. The IUCN Red List of Threatened Species 2017: E. T34620A67802995*; IUCN: Colombo, Sri Lanka, 2017.
11. Anis, M.; Ahmad, N. *Plant Tissue Culture: Propagation, Conservation and Crop Improvement*; Springer: Singapore, 2016.
12. Phillips, G.C.; Garda, M. Plant tissue culture media and practices: An overview. *In Vitr. Cell. Dev. Biol.-Plant* **2019**, *55*, 242–257. [CrossRef]
13. Dobránszki, J.; da Silva, J.A.T. Micropropagation of apple—A review. *Biotechnol. Adv.* **2010**, *28*, 462–488. [CrossRef]
14. Teixeira da Silva, J.A.; Kher, M.M.; Soner, D.; Nataraj, M. Red sandalwood (*Pterocarpus santalinus* L. f.): Biology, importance, propagation and micropropagation. *J. For. Res.* **2019**, *30*, 745–754. [CrossRef]
15. Teixeira da Silva, J.A.; Zeng, S.; Godoy-Hernández, G.; Rivera-Madrid, R.; Dobránszki, J. *Bixa orellana* L. (achiote) tissue culture: A review. *In Vitr. Cell. Dev. Biol.-Plant* **2019**, *55*, 231–241. [CrossRef]
16. Jiao, L.; Yu, M.; Wiedenhoeft, A.C.; He, T.; Li, J.; Liu, B.; Jiang, X.; Yin, Y. DNA Barcode Authentication and Library Development for the Wood of Six Commercial *Pterocarpus* Species: The Critical Role of Xylarium Specimens. *Sci. Rep.* **2018**, *8*, 1945. [CrossRef]

17. Kress, W.J. Plant DNA barcodes: Applications today and in the future. *J. Syst. Evol.* **2017**, *55*, 291–307. [CrossRef]
18. Kalimuthu, K.; Lakshmanan, K. Preliminary investigation on micropropagation of *Pterocarpus marsupium* Roxb. *Indian J. For.* **1994**, *17*, 192–195.
19. Mishra, Y.; Rawat, R.; Nema, B.; Shirin, F. Effect of Seed Orientation and Medium Strength on in vitro Germination of *Pterocarpus marsupium* Roxb. *Not. Sci. Biol.* **2013**, *5*, 476–479. [CrossRef]
20. Ahmad, A. *In Vitro Morphogenesis and Assessment of Genetic Diversity in Pterocarpus marsupium Roxb. Using Molecular Markers*; Aligarh Muslim University: Aligarh, India, 2019.
21. Singh, P.; Bajpai, V.; Gupta, A.; Gaikwad, A.N.; Maurya, R.; Kumar, B. Identification and quantification of secondary metabolites of *Pterocarpus marsupium* by LC–MS techniques and its in-vitro lipid lowering activity. *Ind. Crops Prod.* **2019**, *127*, 26–35. [CrossRef]
22. Ahmad, A.; Anis, M. *Meta*-topolin Improves *In Vitro* Morphogenesis, Rhizogenesis and Biochemical Analysis in *Pterocarpus marsupium* Roxb.: A Potential Drug-Yielding Tree. *J. Plant Growth Regul.* **2019**, *38*, 1007–1016. [CrossRef]
23. World Conservation Monitoring Centre (WCMC). *Pterocarpus Marsupium. The IUCN Red List of Threatened Species*; WCMC: Cambridge, UK, 1998.
24. Chaudhuri, A.B.; Sarkar, D.D. *Biodiversity Endangered: India's Threatened Wildlife and Medicinal Plants*; Scientific: Jodhpur, India, 2002.
25. Anis, M.; Husain, M.K.; Shahzad, A. In vitro plantlet regeneration of *Pterocarpus marsupium* Roxb., an endangered leguminous tree. *Curr. Sci.* **2005**, *88*, 861–863.
26. Tiwari, S.; Shah, P.; Singh, K. In vitro propagation of *Pterocarpus marsupium* Roxb.: An endangered medicinal tree. *Indian J. Biotechnol.* **2004**, *3*, 422–425.
27. Garzuglia, M. *Threatened, Endangered and Vulnerable Tree Species: A Comparison between FRA 2005 and the IUCN Red List*; Forest Resources Assessment (FRA) Working Paper 108/E; FAO, Forestry Department: Rome, Italy, 2005.
28. MOE. *Ministry of Environment, The National Red List 2012 of Sri Lanka: Conservation Status of the Fauna and Flora*; Ministry of Environment: Colombo, Sri Lanka, 2012.
29. NMPB. *National Medicinal Plant Board, Department of AYUSH, Ministry of Health and Family Welfare, Government of India, Agro Techniques of Selected Medicinal Plants*; TERI Press: New Delhi, India, 2008.
30. Maurya, R.; Singh, R.; Deepak, M.; Handa, S.S.; Yadav, P.P.; Mishra, P.K. Constituents of *Pterocarpus marsupium*: An ayurvedic crude drug. *Phytochemistry* **2004**, *65*, 915–920. [CrossRef] [PubMed]
31. Jahromi, M.A.F.; Ray, A.B.; Chansouria, J.P.N. Antihyperlipidemic Effect of Flavonoids from *Pterocarpus marsupium*. *J. Nat. Prod.* **1993**, *56*, 989–994. [CrossRef]
32. Manickam, M.; Ramanathan, M.; Farboodniay Jahromi, M.A.; Chansouria, J.P.N.; Ray, A.B. Antihyperglycemic Activity of Phenolics from *Pterocarpus marsupium*. *J. Nat. Prod.* **1997**, *60*, 609–610. [CrossRef]
33. Maruthupandian, A.; Mohan, V. GC-MS analysis of some bioactive constituents of *Pterocarpus marsupium* Roxb. *Int. J. Chem. Tech. Res.* **2011**, *3*, 1652–1657.
34. Maurya, R.; Ray, A.; Duah, F.; Slatkin, D.; Schiff, P., Jr. Constituents of *Pterocarpus marsupium*. *J. Nat. Prod.* **1984**, *47*, 179–181. [CrossRef]
35. Chakravarthy, B.; Gode, K. Isolation of (-)-epicatechin from *Pterocarpus marsupium* and its pharmacological actions. *Planta Med.* **1985**, *51*, 56–59. [CrossRef] [PubMed]
36. Tripathi, J.; Joshi, T. Flavonoids from *Pterocarpus marsupium*. *Planta Med.* **1988**, *54*, 371–372. [CrossRef]
37. Tripathi, J.; Joshi, T. Phytochemical Investigation of Roots of *Pterocarpus marsupium*. Isolation and Structural Studies of Two New Flavanone Glycosides. *Z. Nat. C* **1988**, *43*, 184–186. [CrossRef] [PubMed]
38. Handa, S.; Singh, R.; Maurya, R.; Satti, N.; Suri, K.; Suri, O. Pterocarposide, an isoaurone C-glucoside from *Pterocarpus marsupium*. *Tetrahedron Lett.* **2000**, *41*, 1579–1581. [CrossRef]
39. Suri, K.; Satti, N.; Gupta, B.; Suri, O. 1-(2′, 6′-Dihydroxyphenyl)-β-glucopyranoside, a novel C-glycoside from *Pterocarpus marsupium*. *Indian J. Chem.* **2003**, *42*, 432–433. [CrossRef]
40. Mutharaian, N.; Sasikumar, J.M.; Pavai, P.; Bai, V.N. In vitro antioxidant activity of *Pterocarpus marsupium* Roxb. Leaves. *Int. J. Biomed. Pharm. Sci.* **2009**, *3*, 29–33.
41. Patil, U.H.; Gaikwad, D.K. Phytochemical screening and microbicidal activity of stem bark of *Pterocarpus marsupium*. *Int. J. Pharm. Sci. Res.* **2011**, *2*, 36–40.
42. Mishra, A.; Srivastava, R.; Srivastava, S.P.; Gautam, S.; Tamrakar, A.K.; Maurya, R.; Srivastava, A.K. Antidiabetic activity of heart wood of *Pterocarpus marsupium* Roxb. and analysis of phytoconstituents. *Indian J. Exp. Biol.* **2013**, *51*, 363–374. [PubMed]
43. Deguchi, T.; Miyamoto, A.; Miyamoto, K.; Kawata-Tominaga, T.; Yoshioka, Y.; Iwaki, M.; Murata, K. Determination of (+)-Dihydrorobinetin as An Active Constituent of the Radical-Scavenging Activity of Asana (*Pterocarpus marsupium*) Heartwood. *Nat. Prod. Commun.* **2019**, *14*, 1–5. [CrossRef]
44. Yadav, V.K.; Mishra, A. In vitro & in silico study of hypoglycemic potential of *Pterocarpus marsupium* heartwood extract. *Nat. Prod. Res.* **2019**, *33*, 3298–3302. [CrossRef] [PubMed]
45. Mohire, N.C.; Salunkhe, V.R.; Bhise, S.B.; Yadav, A.V. Cardiotonic activity of aqueous extract of heartwood of *Pterocarpus marsupium*. *Indian J. Exp. Biol.* **2007**, *45*, 532–537. [PubMed]
46. Bressers, J. *Botany of Ranchi District, Bihar, India*; Catholic Press: Ranchi, India, 1951; p. 96.
47. Trivedi, P.C. *Medicinal Plants Traditional Knowledge*; I.K. International Publishing House: New Delhi, India, 2006.

48. Yesodharan, K.; Sujana, K. Ethnomedicinal knowledge among *Malamalasar* tribe of Parambikulam wildlife sanctuary, Kerala. *Indian J. Tradit. Knowl.* **2007**, *6*, 481–485.
49. Chopra, R.N.; Nayar, R.L.; Chopra, I.C. *Glossary of Indian Medicinal Plants*; Council of Scientific and Industrial Research: New Dehli, India, 1956; p. 78.
50. Anonymous. *The Wealth of India*; CSIR: New Delhi, India, 1969; Volume III.
51. Pullaiah, T. *Medicinal Plants of Andhra Pradesh (India)*; Regency Publication: New Delhi, India, 1999; p. 165.
52. Hougee, S.; Faber, J.; Sanders, A.; de Jong, R.B.; van den Berg, W.B.; Garssen, J.; Hoijer, M.A.; Smit, H.F. Selective COX-2 Inhibition by a *Pterocarpus marsupium* Extract Characterized by Pterostilbene, and its Activity in Healthy Human Volunteers. *Planta Med.* **2005**, *71*, 387–392. [CrossRef]
53. Tolomeo, M.; Grimaudo, S.; Cristina, A.D.; Roberti, M.; Pizzirani, D.; Meli, M.; Dusonchet, L.; Gebbia, N.; Abbadessa, V.; Crosta, L.; et al. Pterostilbene and 3′-hydroxypterostilbene are effective apoptosis-inducing agents in MDR and BCR-ABL-expressing leukemia cells. *Int. J. Biochem. Cell Biol.* **2005**, *37*, 1709–1726. [CrossRef]
54. Remsberg, C.M.; Yáñez, J.A.; Ohgami, Y.; Vega-Villa, K.R.; Rimando, A.M.; Davies, N.M. Pharmacometrics of pterostilbene: Preclinical pharmacokinetics and metabolism, anticancer, antiinflammatory, antioxidant and analgesic activity. *Phytother. Res.* **2008**, *22*, 169–179. [CrossRef]
55. Chakraborty, A.; Gupta, N.; Ghosh, K.; Roy, P. In vitro evaluation of the cytotoxic, anti-proliferative and anti-oxidant properties of pterostilbene isolated from *Pterocarpus marsupium*. *Toxicol. In Vitr.* **2010**, *24*, 1215–1228. [CrossRef]
56. Tippani, R.; Vemunoori, A.K.; Yarra, R.; Nanna, R.S.; Abbagani, S.; Thammidala, C. Adventitious shoot regeneration from immature zygotic embryos of Indian Kino tree (*Pterocarpus marsupium* Roxb.) and genetic integrity analysis of in vitro derived plants using ISSR markers. *Hortic. Environ. Biotechnol.* **2013**, *54*, 531–537. [CrossRef]
57. Maruthupandian, A.; Mohan, V. Antidiabetic, antihyperlipidaemic and antioxidant activity of *Pterocarpus marsupium* Roxb. in alloxan induced diabetic rats. *Int. J. Pharm. Tech. Res.* **2011**, *3*, 1681–1687.
58. Tippani, R.; Jaya Shankar Prakhya, L.; Porika, M.; Sirisha, K.; Abbagani, S.; Thammidala, C. Pterostilbene as a potential novel telomerase inhibitor: Molecular docking studies and its in vitro evaluation. *Curr. Pharm. Biotechnol.* **2013**, *14*, 1027–1035. [CrossRef]
59. Kosaraju, J.; Madhunapantula, S.V.; Chinni, S.; Khatwal, R.B.; Dubala, A.; Muthureddy Nataraj, S.K.; Basavan, D. Dipeptidyl peptidase-4 inhibition by *Pterocarpus marsupium* and *Eugenia jambolana* ameliorates streptozotocin induced Alzheimer's disease. *Behav. Brain Res.* **2014**, *267*, 55–65. [CrossRef]
60. Gupta, P.; Jain, V.; Pareek, A.; Kumari, P.; Singh, R.; Agarwal, P.; Sharma, V. Evaluation of effect of alcoholic extract of heartwood of *Pterocarpus marsupium* on in vitro antioxidant, anti-glycation, sorbitol accumulation and inhibition of aldose reductase activity. *J. Tradit. Complementary Med.* **2017**, *7*, 307–314. [CrossRef] [PubMed]
61. Murata, K.; Deguchi, T.; Yasuda, M.; Endo, R.; Fujita, T.; Matsumura, S.; Yoshioka, Y.; Matsuda, H. Improvement of Blood Rheology by Extract of Asana, *Pterocarpus marsupium*-Suppression of Platelet Aggregation Activity and Pterostilbene, as a Main Stilbene in the Extract. *Nat. Prod. Commun.* **2017**, *12*, 1089–1093. [CrossRef]
62. Qadeer, F.; Abidi, A.; Fatima, F.; Rizvi, D.A. Effect of *Pterocarpus marsupium* in animal model of high carbohydrate diet-induced metabolic syndrome. *Natl. J. Physiol. Pharm. Pharmacol.* **2018**, *8*, 1509–1514. [CrossRef]
63. Majeed, M.; Majeed, S.; Jain, R.; Mundkur, L.; Rajalakshmi, H.R.; Lad, P.; Neupane, P. A Randomized Study to Determine the Sun Protection Factor of Natural Pterostilbene from *Pterocarpus marsupium*. *Cosmetics* **2020**, *7*, 16. [CrossRef]
64. Satyavati, G.V.; Gupta, A.K.; Tandon, N. *Medicinal Plants of India*; ICMR Publications: New Delhi, India, 1987; Volume 2, p. 533.
65. Grover, J.K.; Yadav, S.; Vats, V. Medicinal plants of India with anti-diabetic potential. *J. Ethnopharmacol.* **2002**, *81*, 81–100. [CrossRef]
66. Chatterjee, A.; Pakrashi, S.C. *The Treatise on Indian Medicinal Plants*; Publications and Information Directorate: New Delhi, India, 1992; Volume 2.
67. Grover, J.K.; Vats, V.; Yadav, S.S. *Pterocarpus marsupium* extract (Vijayasar) prevented the alteration in metabolic patterns induced in the normal rat by feeding an adequate diet containing fructose as sole carbohydrate. *Diabetes Obes. Metab.* **2005**, *7*, 414–420. [CrossRef] [PubMed]
68. Messina, F.; Guglielmini, G.; Curini, M.; Orsini, S.; Gresele, P.; Marcotullio, M.C. Effect of substituted stilbenes on platelet function. *Fitoterapia* **2015**, *105*, 228–233. [CrossRef] [PubMed]
69. Green, B.D.; Flatt, P.R.; Bailey, C.J. Dipeptidyl peptidase IV (DPP IV) inhibitors: A newly emerging drug class for the treatment of type 2 diabetes. *Diabetes Vasc. Dis. Res.* **2006**, *3*, 159–165. [CrossRef]
70. Kosaraju, J.; Gali, C.C.; Khatwal, R.B.; Dubala, A.; Chinni, S.; Holsinger, R.M.D.; Madhunapantula, V.S.R.; Muthureddy Nataraj, S.K.; Basavan, D. Saxagliptin: A dipeptidyl peptidase-4 inhibitor ameliorates streptozotocin induced Alzheimer's disease. *Neuropharmacology* **2013**, *72*, 291–300. [CrossRef]
71. Beard, E.L., Jr. The American Society of Health System Pharmacists. *JONA's Healthc. Law Ethics Regul.* **2001**, *3*, 78–79. [CrossRef] [PubMed]
72. Smith, U. Abdominal obesity: A marker of ectopic fat accumulation. *J. Clin. Investig.* **2015**, *125*, 1790–1792. [CrossRef]
73. Al-Goblan, A.S.; Al-Alfi, M.A.; Khan, M.Z. Mechanism linking diabetes mellitus and obesity. *Diabetes Metab. Syndr. Obes.* **2014**, *7*, 587–591. [CrossRef]
74. Holtzman, M.J.; Turk, J.; Shornick, L.P. Identification of a pharmacologically distinct prostaglandin H synthase in cultured epithelial cells. *J. Biol. Chem.* **1992**, *267*, 21438–21445. [CrossRef]

75. Hla, T.; Neilson, K. Human cyclooxygenase-2 cDNA. *Proc. Natl. Acad. Sci. USA* **1992**, *89*, 7384–7388. [CrossRef] [PubMed]
76. Chandrasekharan, N.V.; Dai, H.; Roos, K.L.T.; Evanson, N.K.; Tomsik, J.; Elton, T.S.; Simmons, D.L. COX-3, a cyclooxygenase-1 variant inhibited by acetaminophen and other analgesic/antipyretic drugs: Cloning, structure, and expression. *Proc. Natl. Acad. Sci. USA* **2002**, *99*, 13926–13931. [CrossRef] [PubMed]
77. Sander, S.; Smit, H.; Garssen, J.; Faber, J.; Hoijer, M. *Pterocarpus marsupium* extract exhibits antiinflammatory activity in human subjects. *Planta Med.* **2005**, *71*, 387–392.
78. Kodan, A.; Kuroda, H.; Sakai, F. A stilbene synthase from Japanese red pine (*Pinus densiflora*): Implications for phytoalexin accumulation and down-regulation of flavonoid biosynthesis. *Proc. Natl. Acad. Sci. USA* **2002**, *99*, 3335–3339. [CrossRef]
79. Frémont, L. Biological effects of resveratrol. *Life Sci.* **2000**, *66*, 663–673. [CrossRef]
80. Stivala, L.A.; Savio, M.; Carafoli, F.; Perucca, P.; Bianchi, L.; Maga, G.; Forti, L.; Pagnoni, U.M.; Albini, A.; Prosperi, E.; et al. Specific Structural Determinants Are Responsible for the Antioxidant Activity and the Cell Cycle Effects of Resveratrol. *J. Biol. Chem.* **2001**, *276*, 22586–22594. [CrossRef]
81. Rimando, A.M.; Cuendet, M.; Desmarchelier, C.; Mehta, R.G.; Pezzuto, J.M.; Duke, S.O. Cancer Chemopreventive and Antioxidant Activities of Pterostilbene, a Naturally Occurring Analogue of Resveratrol. *J. Agric. Food Chem.* **2002**, *50*, 3453–3457. [CrossRef] [PubMed]
82. Ferrer, P.; Asensi, M.; Segarra, R.; Ortega, A.; Benlloch, M.; Obrador, E.; Varea, M.T.; Asensio, G.; Jordá, L.; Estrela, J.M. Association between pterostilbene and quercetin inhibits metastatic activity of B16 melanoma. *Neoplasia* **2005**, *7*, 37–47. [CrossRef] [PubMed]
83. Husain, M.K.; Anis, M. Rapid in vitro multiplication of *Melia azedarach* L. (a multipurpose woody tree). *Acta Physiol. Plant.* **2009**, *31*, 765–772. [CrossRef]
84. Javed, S.B.; Anis, M.; Khan, P.R.; Aref, I.M. In vitro regeneration and multiplication for mass propagation of *Acacia ehrenbergiana* Hayne: A potential reclaiment of denude arid lands. *Agrofor. Syst.* **2013**, *87*, 621–629. [CrossRef]
85. Perveen, S.; Anis, M.; Aref, I.M. In vitro plant regeneration of *Albizia lebbeck* (L.) from seed explants. *For. Syst.* **2013**, *22*, 241–248. [CrossRef]
86. Vijayan, A.; Padmesh Pillai, P.; Hemanthakumar, A.S.; Krishnan, P.N. Improved in vitro propagation, genetic stability and analysis of corosolic acid synthesis in regenerants of *Lagerstroemia speciosa* (L.) Pers. by HPLC and gene expression profiles. *Plant Cell Tissue Organ Cult.* **2015**, *120*, 1209–1214. [CrossRef]
87. Ahmed, M.R.; Anis, M.; Alatar, A.A.; Faisal, M. In vitro clonal propagation and evaluation of genetic fidelity using RAPD and ISSR marker in micropropagated plants of *Cassia alata* L.: A potential medicinal plant. *Agrofor. Syst.* **2017**, *91*, 637–647. [CrossRef]
88. Javed, S.B.; Alatar, A.A.; Anis, M.; El-Sheikh, M.A. *In Vitro* Regeneration of Coral Tree from Three Different Explants Using Thidiazuron. *HortTechnology* **2019**, *29*, 946–951. [CrossRef]
89. Shu, K.; Liu, X.-d.; Xie, Q.; He, Z.-h. Two Faces of One Seed: Hormonal Regulation of Dormancy and Germination. *Mol. Plant* **2016**, *9*, 34–45. [CrossRef]
90. Miransari, M.; Smith, D.L. Plant hormones and seed germination. *Environ. Exp. Bot.* **2014**, *99*, 110–121. [CrossRef]
91. Ludewig, K.; Zelle, B.; Eckstein, R.L.; Mosner, E.; Otte, A.; Donath, T.W. Differential effects of reduced water potential on the germination of floodplain grassland species indicative of wet and dry habitats. *Seed Sci. Res.* **2014**, *24*, 49–61. [CrossRef]
92. White, C.N.; Rivin, C.J. Gibberellins and seed development in maize. II. Gibberellin synthesis inhibition enhances abscisic acid signaling in cultured embryos. *Plant Physiol.* **2000**, *122*, 1089–1097. [CrossRef] [PubMed]
93. Tuan, P.A.; Kumar, R.; Rehal, P.K.; Toora, P.K.; Ayele, B.T. Molecular Mechanisms Underlying Abscisic Acid/Gibberellin Balance in the Control of Seed Dormancy and Germination in Cereals. *Front. Plant Sci.* **2018**, *9*, 668. [CrossRef] [PubMed]
94. Finkelstein, R.; Reeves, W.; Ariizumi, T.; Steber, C. Molecular Aspects of Seed Dormancy. *Annu. Rev. Plant Biol.* **2008**, *59*, 387–415. [CrossRef]
95. Lee, K.P.; Lopez-Molina, L. A seed coat bedding assay to genetically explore in vitro how the endosperm controls seed germination in *Arabidopsis thaliana*. *J. Vis. Exp.* **2013**, *2013*, e50732. [CrossRef]
96. Das, T.; Chatterjee, A. in vitro studies of *Pterocarpus marsupium*—An endangered tree. *Indian J. Plant Physiol.* **1993**, *36*, 269–272.
97. Kalimuthu, K.; Lakshmanan, K. Effect of different treatments on pod germination of *Pterocarpus species*. *Indian J. For.* **1995**, *18*, 104–106.
98. Husain, M.K.; Anis, M.; Shahzad, A. Seed germination studies in *Pterocarpus marsupium* Roxb., an important multipurpose tree. *Hamdard Med.* **2007**, *50*, 112–115.
99. Lenser, T.; Theißen, G. Molecular mechanisms involved in convergent crop domestication. *Trends Plant Sci.* **2013**, *18*, 704–714. [CrossRef]
100. Meyer, R.S.; Purugganan, M.D. Evolution of crop species: Genetics of domestication and diversification. *Nat. Rev. Genet.* **2013**, *14*, 840–852. [CrossRef]
101. Simsek, S.; Ohm, J.-B.; Lu, H.; Rugg, M.; Berzonsky, W.; Alamri, M.S.; Mergoum, M. Effect of pre-harvest sprouting on physicochemical changes of proteins in wheat. *J. Sci. Food Agric.* **2014**, *94*, 205–212. [CrossRef]
102. Baskin, C.C.; Baskin, J.M. *Seeds: Ecology, Biogeography and Evolution of Dormancy and Germination*, 2nd ed.; Academic Press: San Diego, CA, USA, 1998.
103. Rolston, M.P. Water impermeable seed dormancy. *Bot. Rev.* **1978**, *44*, 365–396. [CrossRef]
104. Khan, A.A. Hormonal regulation of primary and secondary seed dormancy. *Isr. J. Bot.* **1980**, *29*, 207–224. [CrossRef]

105. Bewley, J.D.; Bradford, K.J.; Hilhorst, H.W.M.; Nonogaki, H. *Seeds: Physiology of Development, Germination and Dormancy*, 3rd ed.; Springer: New York, NY, USA, 2013.
106. Tigabu, M.; Oden, P. Effect of scarification, gibberellic acid and temperature on seed germination of two multipurpose *Albizia* species from Ethiopia. *Seed Sci. Technol.* **2001**, *29*, 11–20.
107. Barmukh, R.; Nikam, T. Promotion of seed germination in *Pterocarpus marsupium* Roxb. *Indian J. Plant Physiol.* **2008**, *13*, 143–150.
108. Baskin, J.M.; Baskin, C.C.; Spooner, D.M. Role of temperature, light and date: Seeds were exhumed from soil on germination of four wetland perennials. *Aquat. Bot.* **1989**, *35*, 387–394. [CrossRef]
109. Azad, S.; Manik, M.R.; Hasan, S.; Matin, A. Effect of different pre-sowing treatments on seed germination percentage and growth performance of *Acacia auriculiformis*. *J. For. Res.* **2011**, *22*, 183. [CrossRef]
110. Tadros, M.J.; Samarah, N.H.; Alqudah, A.M. Effect of different pre-sowing seed treatments on the germination of *Leucaena leucocephala* (Lam.) and *Acacia farnesiana* (L.). *New For.* **2011**, *42*, 397–407. [CrossRef]
111. Dayanand, T.; Lohidas, T. Effect of different treatments on pod germination of red sanders (*Pterocarpus santalinus* Linn.). *Indian J. For.* **1988**, *11*, 87–88.
112. Park, J.; Kim, Y.-S.; Kim, S.-G.; Jung, J.-H.; Woo, J.-C.; Park, C.-M. Integration of auxin and salt signals by the NAC transcription factor NTM2 during seed germination in *Arabidopsis*. *Plant Physiol.* **2011**, *156*, 537–549. [CrossRef] [PubMed]
113. Murashige, T.; Skoog, F. A Revised Medium for Rapid Growth and Bio Assays with Tobacco Tissue Cultures. *Physiol. Plant.* **1962**, *15*, 473–497. [CrossRef]
114. Gamborg, O.L.; Miller, R.A.; Ojima, K. Nutrient requirements of suspension cultures of soybean root cells. *Exp. Cell Res.* **1968**, *50*, 151–158. [CrossRef]
115. White, P.R. *The Cultivation of Animal and Plant Cells*, 2nd ed.; Ronald Press: New York, NY, USA, 1963.
116. Ahmad, N.; Alia, A.; Khan, F.; Kour, A.; Khan, S. In vitro seed germination and shoot multiplication of *Pterocarpus marsupium* Roxb.—An endangered medicinal tree. *Researcher* **2012**, *4*, 20–24.
117. Lee, J.-H.; Kim, Y.-K.; Oh, E.-Y.; Jung, K.-Y.; Ko, K.-S. Optimization of in vitro seed germination of *Taraxacum platycarpum*. *Korean J. Environ. Agric.* **2009**, *28*, 403–408. [CrossRef]
118. Masilamani, P.; Singh, B.G.; Chinnusamy, C.; Annadurai, K. Short communication: Influence af seed orientation and depth of sowing on germination and vigour of Anjan (*Hardwickia binata* Roxb). *Trop. Agric. Res. Ext.* **1999**, *2*, 76–78.
119. Ahmad, A.; Siddique, I.; Varshney, A. Selection of Elite Genotype of a Multipurpose Forest Tree (*Pterocarpus marsupium* Roxb.) from Naturally Grown Populations in Central India. In *Propagation and Genetic Manipulation of Plants*; Siddique, I., Ed.; Springer: Singapore, 2021; pp. 101–119.
120. Lee, S.; Cheng, H.; King, K.E.; Wang, W.; He, Y.; Hussain, A.; Lo, J.; Harberd, N.P.; Peng, J. Gibberellin regulates *Arabidopsis* seed germination via RGL2, a GAI/RGA-like gene whose expression is up-regulated following imbibition. *Genes Dev.* **2002**, *16*, 646–658. [CrossRef] [PubMed]
121. Varshney, A.; Anis, M.; Aref, I. Control of bioregulants on plant resurgence in vitro from mature seeds of Egyptian myrobalan tree (*Balanites aegyptiaca* del.)—A plant affluent in saponins. *Int. J. Pharm. Sci. Rev. Res.* **2013**, *22*, 23–28.
122. Justamante, M.S.; Ibáñez, S.; Villanova, J.; Pérez-Pérez, J.M. Vegetative propagation of argan tree (*Argania spinosa* (L.) Skeels) using in vitro germinated seeds and stem cuttings. *Sci. Hortic.* **2017**, *225*, 81–87. [CrossRef]
123. Khazaei Kojori, Z.; Rezaei, M.; Sarkhosh, A.; Gharangik, S. The effects of bud-scale removing and gibberellin (GA3) on dormancy break of apricot (*P. armeniaca* L.) vegetative buds. *J. Appl. Hortic.* **2018**, *20*, 50–54. [CrossRef]
124. Gubler, F.; Chandler, P.M.; White, R.G.; Llewellyn, D.J.; Jacobsen, J.V. Gibberellin signaling in barley aleurone cells. Control of SLN1 and GAMYB expression. *Plant Physiol.* **2002**, *129*, 191–200. [CrossRef] [PubMed]
125. Li, Q.-F.; He, J.-X. Mechanisms of signaling crosstalk between brassinosteroids and gibberellins. *Plant. Signal. Behav.* **2013**, *8*, e24686. [CrossRef]
126. Weiss, D.; Ori, N. Mechanisms of cross talk between gibberellin and other hormones. *Plant Physiol.* **2007**, *144*, 1240–1246. [CrossRef]
127. Gantait, S.; Kundu, S.; Das, P.K. *Acacia*: An exclusive survey on in vitro propagation. *J. Saudi Soc. Agric. Sci.* **2018**, *17*, 163–177. [CrossRef]
128. Fatima, N.; Anis, M. Role of growth regulators on in vitro regeneration and histological analysis in Indian ginseng (*Withania somnifera* L.) Dunal. *Physiol. Mol. Biol. Plants* **2012**, *18*, 59–67. [CrossRef] [PubMed]
129. Ahmad, N.; Javed, S.B.; Khan, M.I.; Anis, M. Rapid plant regeneration and analysis of genetic fidelity in micropropagated plants of *Vitex trifolia*: An important medicinal plant. *Acta Physiol. Plant.* **2013**, *35*, 2493–2500. [CrossRef]
130. Nagar, D.S.; Jha, S.K.; Jani, J. Direct adventitious shoot bud formation on hypocotyls explants in *Millettia pinnata* (L.) Panigrahi-a biodiesel producing medicinal tree species. *Physiol. Mol. Biol. Plants* **2015**, *21*, 287–292. [CrossRef] [PubMed]
131. Perveen, S.; Khanam, M.N.; Anis, M.; Atta, H.A.E. in vitro mass propagation of *Murraya koenigii* L. *J. Appl. Res. Med. Aromat. Plants* **2015**, *2*, 60–68. [CrossRef]
132. Howell, S.H.; Lall, S.; Che, P. Cytokinins and shoot development. *Trends Plant Sci.* **2003**, *8*, 453–459. [CrossRef]
133. Santner, A.; Estelle, M. Recent advances and emerging trends in plant hormone signalling. *Nature* **2009**, *459*, 1071–1078. [CrossRef] [PubMed]
134. Moubayidin, L.; Di Mambro, R.; Sabatini, S. Cytokinin–auxin crosstalk. *Trends Plant Sci.* **2009**, *14*, 557–562. [CrossRef] [PubMed]
135. Chandler, J.W.; Werr, W. Cytokinin–auxin crosstalk in cell type specification. *Trends Plant Sci.* **2015**, *20*, 291–300. [CrossRef]

136. Chand, S.; Singh, A.K. in vitro shoot regeneration from cotyledonary node explants of a multipurpose leguminous tree *Pterocarpus marsupium* Roxb. *In Vitr. Cell. Dev. Biol.-Plant* **2004**, *40*, 464–466. [CrossRef]
137. Husain, M.K.; Anis, M.; Shahzad, A. In vitro propagation of Indian Kino (*Pterocarpus marsupium* Roxb.) using Thidiazuron. *In Vitr. Cell. Dev. Biol.-Plant* **2007**, *43*, 59–64. [CrossRef]
138. Pradhan, C.; Kar, S.; Pattnaik, S.; Chand, P.K. Propagation of *Dalbergia sissoo* Roxb. through in vitro shoot proliferation from cotyledonary nodes. *Plant Cell Rep.* **1998**, *18*, 122–126. [CrossRef]
139. Da Silva, A.L.L.; Gollo, A.L.; Brondani, G.E.; Horbach, M.A.; Oliveira, L.; Machado, M.P.; Lima, K.; Costa, J. Micropropagation of *Eucalyptus saligna* Sm. from cotyledonary nodes. *Pak. J. Bot.* **2015**, *47*, 311–318.
140. Moharana, A.; Das, A.; Subudhi, E.; Naik, S.K.; Barik, D.P. High frequency shoot proliferation from cotyledonary node of *Lawsonia inermis* L. and validation of their molecular finger printing. *J. Crop Sci. Biotechnol.* **2018**, *20*, 405–416. [CrossRef]
141. Venkatachalam, P.; Jinu, U.; Gomathi, M.; Mahendran, D.; Ahmad, N.; Geetha, N.; Sahi, S.V. Role of silver nitrate in plant regeneration from cotyledonary nodal segment explants of *Prosopis cineraria* (L.) Druce.: A recalcitrant medicinal leguminous tree. *Biocatal. Agric. Biotechnol.* **2017**, *12*, 286–291. [CrossRef]
142. Gupta, A.; Thomas, T.; Khan, S. Regeneration of *Aegle marmelos* (l.) Through Enhanced Axillary Branching from Cotyledenory Node. *UK J. Pharm. Biosci.* **2018**, *6*, 24. [CrossRef]
143. Husain, M.K.; Anis, M.; Shahzad, A. In vitro propagation of a multipurpose leguminous tree (*Pterocarpus marsupium* Roxb.) using nodal explants. *Acta Physiol. Plant.* **2008**, *30*, 353–359. [CrossRef]
144. Husain, M.K.; Anis, M.; Shahzad, A. Somatic embryogenesis and plant regeneration in *Pterocarpus marsupium* Roxb. *Trees* **2010**, *24*, 781–787. [CrossRef]
145. Tippani, R.; Yarra, R.; Bulle, M.; Porika, M.; Abbagani, S.; Thammidala, C. in vitro plantlet regeneration and *Agrobacterium tumefaciens*-mediated genetic transformation of Indian Kino tree (*Pterocarpus marsupium* Roxb.). *Acta Physiol. Plant.* **2013**, *35*, 3437–3446. [CrossRef]
146. Jaiswal, S.; Choudhary, M.; Arya, S.; Kant, T. Micropropagation of adult tree of *Pterocarpus marsupium* Roxb. using nodal explants. *J. Plant Dev.* **2015**, *22*, 21–30.
147. Ahmad, A.; Ahmad, N.; Anis, M. Preconditioning of Nodal Explants in Thidiazuron-Supplemented Liquid Media Improves Shoot Multiplication in *Pterocarpus marsupium* (Roxb.). In *Thidiazuron: From Urea Derivative to Plant Growth Regulator*; Ahmad, N., Faisal, M., Eds.; Springer: Singapore, 2018; pp. 175–187.
148. Tippani, R.; Nanna, R.S.; Mamidala, P.; Thammidala, C. Assessment of genetic stability in somatic embryo derived plantlets of *Pterocarpus marsupium* Roxb. using inter-simple sequence repeat analysis. *Physiol. Mol. Biol. Plants* **2019**, *25*, 569–579. [CrossRef] [PubMed]
149. Ahmad, A.; Anis, M.; Khanam, M.N.; Alatar, A.A. Direct shoot organogenesis from shoot tip explants of a highly medicinal valued tree *Pterocarpus marsupium* Roxb. *In Vitr. Cell. Dev. Biol.-Plant* **2020**, *56*, 670–681. [CrossRef]
150. Ahmad, A.; Ahmad, N.; Anis, M.; Alatar, A.A.; Abdel-Salam, E.M.; Qahtan, A.A.; Faisal, M. Gibberellic acid and thidiazuron promote micropropagation of an endangered woody tree (*Pterocarpus marsupium* Roxb.) using in vitro seedlings. *Plant Cell Tissue Organ Cult. (PCTOC)* **2021**, *144*, 449–462. [CrossRef]
151. Kubalakova, M.; Strnad, M. The effects of aromatic cytokinins (populins) on micropropagation and regeneration of sugar beet in vitro. *Biol. Plant* **1992**, *34*, 578–579.
152. Strnad, M.; Hanuš, J.; Vaněk, T.; Kamínek, M.; Ballantine, J.A.; Fussell, B.; Hanke, D.E. *Meta*-topolin, a highly active aromatic cytokinin from poplar leaves (*Populus* × *canadensis* Moench., cv. Robusta). *Phytochemistry* **1997**, *45*, 213–218. [CrossRef]
153. Amoo, S.O.; Finnie, J.F.; Van Staden, J. The role of *meta*-topolins in alleviating micropropagation problems. *Plant Growth Regul.* **2011**, *63*, 197–206. [CrossRef]
154. Aremu, A.O.; Bairu, M.W.; Szüčová, L.; Dolezal, K.; Finnie, J.; Van Staden, J. Assessment of the role of meta-topolins on in vitro produced phenolics and acclimatization competence of micropropagated 'Williams' banana. *Acta Physiol. Plant.* **2012**, *34*, 2265–2273. [CrossRef]
155. Werbrouck, S.P.O.; Strnad, M.; Van Onckelen, H.A.; Debergh, P.C. *Meta*-topolin, an alternative to benzyladenine in tissue culture? *Physiol. Plant.* **1996**, *98*, 291–297. [CrossRef]
156. Gentile, A.; Jàquez Gutiérrez, M.; Martinez, J.; Frattarelli, A.; Nota, P.; Caboni, E. Effect of *meta*-Topolin on micropropagation and adventitious shoot regeneration in *Prunus* rootstocks. *Plant Cell Tissue Organ Cult.* **2014**, *118*, 373–381. [CrossRef]
157. Drewes, F.E.; Van Staden, J. The effect of 6-benzyladenine derivatives on the rooting of *Phaseolus vulgaris* L. primary leaf cuttings. *Plant Growth Regul.* **1989**, *8*, 289–296. [CrossRef]
158. Mala, J.; Machova, P.; Cvrckova, H.; Karady, M.; Novak, O.; Mikulik, J.; Dostal, J.; Strnad, M.; Dolezal, K. The role of cytokinins during micropropagation of wych elm. *Biol. Plant.* **2013**, *57*, 174–178. [CrossRef]
159. Liu, J.; Moore, S.; Chen, C.; Lindsey, K. Crosstalk Complexities between Auxin, Cytokinin, and Ethylene in *Arabidopsis* Root Development: From Experiments to Systems Modeling, and Back Again. *Mol. Plant* **2017**, *10*, 1480–1496. [CrossRef] [PubMed]
160. Magyar-Tábori, K.; Dobránszki, J.; Teixeira da Silva, J.A.; Bulley, S.M.; Hudák, I. The role of cytokinins in shoot organogenesis in apple. *Plant Cell Tissue Organ Cult.* **2010**, *101*, 251–267. [CrossRef]
161. Naaz, A.; Hussain, S.A.; Anis, M.; Alatar, A.A. *Meta*-topolin improved micropropagation in *Syzygium cumini* and acclimatization to *ex vitro* conditions. *Biol. Plant.* **2019**, *63*, 174–182. [CrossRef]

162. Webster, C.A.; Jones, O.P. Micropropagation of some cold-hardy dwarfing rootstocks for apple. *J. Hortic. Sci.* **1991**, *66*, 1–6. [CrossRef]
163. Huyluoğlu, Z.; Ünal, M.; Palavan-Ünsal, N. Cytological evidences of the role of *meta*-topolin and Benzyladenin in barley root tips. *Adv. Mol. Biol.* **2008**, *2*, 31–37.
164. Bairu, M.W.; Kulkarni, M.G.; Street, R.A.; Mulaudzi, R.B.; Van Staden, J. Studies on seed germination, seedling growth, and in vitro shoot induction of *Aloe ferox* Mill., a commercially important species. *HortScience* **2009**, *44*, 751–756. [CrossRef]
165. De Diego, N.; Montalbán, I.; Moncaleán, P. in vitro regeneration of *Pinus* spp. adult trees: New method for obtaining clonal plants. *Acta Hortic.* **2008**, *865*, 361–365. [CrossRef]
166. Nas, M.N.; Bolek, Y.; Sevgin, N. The effects of explant and cytokinin type on regeneration of *Prunus microcarpa*. *Sci. Hortic.* **2010**, *126*, 88–94. [CrossRef]
167. Meyer, E.M.; Touchell, D.H.; Ranney, T.G. *In Vitro* Shoot Regeneration and Polyploid Induction from Leaves of *Hypericum* Species. *HortScience* **2009**, *44*, 1957–1961. [CrossRef]
168. Niedz, R.P.; Evens, T.J. The effects of benzyladenine and *meta*-topolin on in vitro shoot regeneration of a *Citrus citrandarin* rootstock. *Res. J. Agric. Biol. Sci.* **2010**, *6*, 45–53.
169. Vasudevan, R.; Van Staden, J. Cytokinin and explant types influence in vitro plant regeneration of Leopard Orchid (*Ansellia africana* Lindl.). *Plant Cell Tissue Organ Cult.* **2011**, *107*, 123–129. [CrossRef]
170. Magyar-Tábori, K.; Dobránszky, J.; Jámbor-Benczúr, É.; Bubán, T.; Lazányi, J.; Szalai, J.; Ferenczy, A. Post-effects of cytokinins and auxin levels of proliferation media on rooting ability of in vitro apple shoots (Malus domestica Borkh.) 'Red Fuji'. *Int. J. Hortic. Sci.* **2001**, *7*, 26–29. [CrossRef]
171. Bairu, M.W.; Stirk, W.A.; Dolezal, K.; Van Staden, J. Optimizing the micropropagation protocol for the endangered *Aloe polyphylla*: Can *meta*-topolin and its derivatives serve as replacement for benzyladenine and zeatin? *Plant Cell Tissue Organ Cult.* **2007**, *90*, 15–23. [CrossRef]
172. Bairu, M.W.; Stirk, W.A.; Doležal, K.; van Staden, J. The role of topolins in micropropagation and somaclonal variation of banana cultivars 'Williams' and 'Grand Naine' (*Musa* spp. AAA). *Plant Cell Tissue Organ Cult.* **2008**, *95*, 373–379. [CrossRef]
173. Valero-Aracama, C.; Kane, M.E.; Wilson, S.B.; Philman, N.L. Substitution of benzyladenine with *meta*-topolin during shoot multiplication increases acclimatization of difficult- and easy-to-acclimatize sea oats (*Uniola paniculata* L.) genotypes. *Plant Growth Regul.* **2010**, *60*, 43. [CrossRef]
174. Dobránszky, J.; Jámbor-Benczúr, E.; Reményi, M.L.; Magyar-Tábori, K.; Hudák, I.; Kiss, E.; Galli, Z. Effects of aromatic cytokinins on structural characteristics of leaves and their post-effects on subsequent shoot regeneration from in vitro apple leaves of 'Royal Gala'. *Int. J. Hortic. Sci.* **2005**, *11*, 41–46. [CrossRef]
175. Čatský, J.; Pospíšilová, J.; Kamínek, M.; Gaudinová, A.; Pulkrábek, J.; Zahradníček, J. Seasonal changes in sugar beet photosynthesis as affected by exogenous cytokininN6-(m-hydroxybenzyl)adenosine. *Biol. Plant.* **1996**, *38*, 511–518. [CrossRef]
176. Palavan-Ünsal, N.; Çağ, S.; Çetin, E.; Büyüktunçer, D. Retardation of senescence by *meta*-topolin in wheat leaves. *J. Cell Mol. Biol.* **2002**, *1*, 101–108.
177. Wojtania, A. Effect of Meta-topolin on in vitro propagation of Pelargonium × hortorum and Pelargonium × hederaefolium cultivars. *Acta Soc. Bot. Pol.* **2011**, *79*, 101–106. [CrossRef]
178. Bogaert, I.; Van Cauter, S.; Werbrouck, S.; Dolezal, K. New aromatic cytokinins can make the difference. *Acta Hortic.* **2004**, *725*, 265–270. [CrossRef]
179. Bairu, M.; Jain, N.; Stirk, W.; Doležal, K.; Van Staden, J. Solving the problem of shoot-tip necrosis in Harpagophytum procumbens by changing the cytokinin types, calcium and boron concentrations in the medium. *S. Afr. J. Bot.* **2009**, *75*, 122–127. [CrossRef]
180. Zhang, C.; Whiting, M.D. Improving 'Bing' sweet cherry fruit quality with plant growth regulators. *Sci. Hortic.* **2011**, *127*, 341–346. [CrossRef]
181. Murch, S.J.; Saxena, P.K. Molecular fate of thidiazuron and its effects on auxin transport in hypocotyls tissues of *Pelargonium* × *hortorum* Bailey. *Plant Growth Regul.* **2001**, *35*, 269–275. [CrossRef]
182. Guo, B.; Abbasi, B.H.; Zeb, A.; Xu, L.L.; Wei, Y.H. Thidiazuron: A multi-dimensional plant growth regulator. *Afr. J. Biotechnol.* **2011**, *10*, 8984–9000. [CrossRef]
183. Ahmad, N.; Anis, M. Rapid clonal multiplication of a woody tree, *Vitex negundo* L. through axillary shoots proliferation. *Agrofor. Syst.* **2007**, *71*, 195–200. [CrossRef]
184. Dhavala, A.; Rathore, T.S. Micropropagation of *Embelia ribes* Burm f. through proliferation of adult plant axillary shoots. *In Vitr. Cell. Dev. Biol.-Plant* **2010**, *46*, 180–191. [CrossRef]
185. Singh, M.; Jaiswal, V.; Jaiswal, U. Thidiazuron-induced anatomical changes and direct shoot morphogenesis in *Dendrocalamus strictus* Nees. *Can. J. Pure Appl. Sci.* **2014**, *8*, 2901–2904.
186. Murthy, B.N.S.; Murch, S.J.; Saxena, P.K. Thidiazuron-induced somatic embryogenesis in intact seedlings of peanut (Arachis hypogaea): Endogenous growth regulator levels and significance of cotyledons. *Physiol. Plant.* **1995**, *94*, 268–276. [CrossRef]
187. Zhang, C.G.; Li, W.; Mao, Y.F.; Zhao, D.L.; Dong, W.; Guo, G.Q. Endogenous Hormonal Levels in Scutellaria baicalensis Calli Induced by Thidiazuron. *Russ. J. Plant Physiol.* **2005**, *52*, 345–351. [CrossRef]
188. Preece, J.E.; Imel, M.R. Plant regeneration from leaf explants of *Rhododendron* 'P.J.M. Hybrids'. *Sci. Hortic.* **1991**, *48*, 159–170. [CrossRef]

189. Sudha, C.; Seeni, S. in vitro multiplication and field establishment of *Adhatoda beddomei* C. B. Clarke, a rare medicinal plant. *Plant Cell Rep.* **1994**, *13*, 203–207. [CrossRef] [PubMed]
190. Faisal, M.; Ahmad, N.; Anis, M. Shoot multiplication in *Rauvolfia tetraphylla* L. using thidiazuron. *Plant Cell Tissue Organ Cult.* **2005**, *80*, 187–190. [CrossRef]
191. Hussain, S.A.; Ahmad, N.; Anis, M. Synergetic effect of TDZ and BA on minimizing the post-exposure effects on axillary shoot proliferation and assessment of genetic fidelity in Rauvolfia tetraphylla (L.). *Rend. Lincei Sci. Fis. Nat.* **2018**, *29*, 109–115. [CrossRef]
192. Lu, C.-Y. The use of thidiazuron in tissue culture. *In Vitr. Cell. Dev. Biol.-Plant* **1993**, *29*, 92–96. [CrossRef]
193. Singh, S.K.; Syamal, M.M. A short pre-culture soak in thidiazuron or forchlorfenuron improves axillary shoot proliferation in rose micropropagation. *Sci. Hortic.* **2001**, *91*, 169–177. [CrossRef]
194. Ahmad, N.; Siddique, I.; Anis, M. Improved plant regeneration in *Capsicum annuum* L. from nodal segments. *Biol. Plant.* **2006**, *50*, 701–704. [CrossRef]
195. Faisal, M.; Anis, M. Thidiazuron induced high frequency axillary shoot multiplication in *Psoralea corylifolia*. *Biol. Plant.* **2006**, *50*, 437–440. [CrossRef]
196. Huetteman, C.A.; Preece, J.E. Thidiazuron: A potent cytokinin for woody plant tissue culture. *Plant Cell Tissue Organ Cult.* **1993**, *33*, 105–119. [CrossRef]
197. Fasolo, F.; Zimmerman, R.H.; Fordham, I. Adventitions shoot formation on excised leaves of in vitro grown shoots of apple cultivars. *Plant Cell Tissue Organ Cult.* **1989**, *16*, 75–87. [CrossRef]
198. Vengadesan, G.; Ganapathi, A.; Prem Anand, R.; Ramesh Anbazhagan, V. in vitro propagation of *Acacia sinuata* (Lour.) Merr. via cotyledonary nodes. *Agrofor. Syst.* **2002**, *55*, 9–15. [CrossRef]
199. Thomas, T. Thidiazuron Induced Multiple Shoot Induction and Plant Regeneration from Cotyledonary Explants of Mulberry. *Biol. Plant.* **2003**, *46*, 529–533. [CrossRef]
200. Patri, S.; Bhatnagar, S.; Bhojwani, S.S. Preliminary investigations on micropropagation of a leguminous timber tree: *Pterocarpus santalinus*. *Phytomorphology* **1988**, *38*, 41–45.
201. Anuradha, M.; Pullaiah, T. in vitro seed culture and induction of enhanced axillary branching in Pterocarpus santalinus and *Pterocarpus marsupium*: A method for rapid multiplication. *Phytomorphology* **1999**, *49*, 157–163.
202. Loc, N.H.; Duc, D.T.; Kwon, T.H.; Yang, M.S. Micropropagation of zedoary (*Curcuma zedoaria* Roscoe): A valuable medicinal plant. *Plant Cell Tissue Organ Cult.* **2005**, *81*, 119–122. [CrossRef]
203. Nayak, P.; Behera, P.R.; Manikkannan, T. High frequency plantlet regeneration from cotyledonary node cultures of *Aegle marmelos* (L.) Corr. *In Vitr. Cell. Dev. Biol.-Plant* **2007**, *43*, 231–236. [CrossRef]
204. Purkayastha, J.; Sugla, T.; Paul, A.; Solleti, S.; Sahoo, L. Rapid in vitro multiplication and plant regeneration from nodal explants of *Andrographis paniculata*: A valuable medicinal plant. *In Vitr. Cell. Dev. Biol.-Plant* **2008**, *44*, 442–447. [CrossRef]
205. Perveen, S.; Varshney, A.; Anis, M.; Aref, I.M. Influence of cytokinins, basal media and pH on adventitious shoot regeneration from excised root cultures of *Albizia lebbeck*. *J. For. Res.* **2011**, *22*, 47–52. [CrossRef]
206. Phulwaria, M.; Rai, M.K.; Harish; Gupta, A.K.; Ram, K.; Shekhawat, N.S. An improved micropropagation of *Terminalia bellirica* from nodal explants of mature tree. *Acta Physiol. Plant.* **2011**, *34*, 299–305. [CrossRef]
207. Varshney, A.; Anis, M.; Rasheed, M.; Khan, P.; Aref, I. Assessment of changes in physiological and biochemical behaviors in Grey-haired Acacia tree (*Acacia gerrardii*)—An important plant of arid region. *Int. J. Sci. Res. Eng. Res.* **2013**, *4*, 1134–1156.
208. Gururaj, H.B.; Giridhar, P.; Ravishankar, G.A. Micropropagation of *Tinospora cordifolia* (Willd.) Miers ex Hook. F & Thoms—A multipurpose medicinal plant. *Curr. Sci.* **2007**, *92*, 23–26.
209. Chaudhary, H.; Sood, N. Purification and partial characterization of lectins from in vitro cultures of *Ricinus communis*. *Plant Tissue Cult. Biotechnol.* **2008**, *18*, 89–102. [CrossRef]
210. Harisharanraj, R.; Suresh, K.; Saravanababu, S. Rapid clonal propagation of *Rauvolfia tetraphylla* L. *Acad. J. Plant Sci.* **2009**, *2*, 195–198.
211. Ozudogru, E.A.; Kaya, E.; Kirdok, E.; Issever-Ozturk, S. in vitro propagation from young and mature explants of thyme (*Thymus vulgaris* and *T. longicaulis*) resulting in genetically stable shoots. *In Vitr. Cell. Dev. Biol.-Plant* **2011**, *47*, 309–320. [CrossRef]
212. Siddique, I.; Anis, M.; Aref, I.M. *In Vitro* Adventitious Shoot Regeneration via Indirect Organogenesis from Petiole Explants of *Cassia angustifolia* Vahl.—A Potential Medicinal Plant. *Appl. Biochem. Biotechnol.* **2010**, *162*, 2067–2074. [CrossRef]
213. Parveen, S.; Shahzad, A. Factors affecting in vitro plant regeneration from cotyledonary node explant of *Senna sophera* (L.) Roxb. a highly medicinal legume. *Afr. J. Biotechnol.* **2014**, *13*, 413–422. [CrossRef]
214. Naaz, A.; Hussain, S.A.; Naz, R.; Anis, M.; Alatar, A.A. Successful plant regeneration system via *de novo* organogenesis in *Syzygium cumini* (L.) Skeels: An important medicinal tree. *Agrofor. Syst.* **2019**, *93*, 1285–1295. [CrossRef]
215. Ferguson, B.J.; Beveridge, C.A. Roles for Auxin, Cytokinin, and Strigolactone in Regulating Shoot Branching. *Plant Physiol.* **2009**, *149*, 1929–1944. [CrossRef]
216. Müller, D.; Leyser, O. Auxin, cytokinin and the control of shoot branching. *Ann. Bot.* **2011**, *107*, 1203–1212. [CrossRef]
217. Anis, M.; Varshney, A.; Siddique, I. in vitro clonal propagation of *Balanites aegyptiaca* (L.) Del. *Agrofor. Syst.* **2010**, *78*, 151–158. [CrossRef]
218. Faisal, M.; Alatar, A.A.; Ahmad, N.; Anis, M.; Hegazy, A.K. An Efficient and Reproducible Method for in vitro Clonal Multiplication of *Rauvolfia tetraphylla* L. and Evaluation of Genetic Stability using DNA-Based Markers. *Appl. Biochem. Biotechnol.* **2012**, *168*, 1739–1752. [CrossRef] [PubMed]

219. Siddique, I.; Javed, S.B.; Al-Othman, M.R.; Anis, M. Stimulation of in vitro organogenesis from epicotyl explants and successive micropropagation round in *Cassia angustifolia* Vahl.: An important source of sennosides. *Agrofor. Syst.* **2013**, *87*, 583–590. [CrossRef]
220. Danova, K.; Motyka, V.; Todorova, M.; Trendafilova, A.; Krumova, S.; Dobrev, P.; Andreeva, T.; Oreshkova, T.; Taneva, S.; Evstatieva, L. Effect of Cytokinin and Auxin Treatments on Morphogenesis, Terpenoid Biosynthesis, Photosystem Structural Organization, and Endogenous Isoprenoid Cytokinin Profile in *Artemisia alba* Turra *In Vitro*. *J. Plant Growth Regul.* **2018**, *37*, 403–418. [CrossRef]
221. Nordström, A.; Tarkowski, P.; Tarkowska, D.; Norbaek, R.; Astot, C.; Dolezal, K.; Sandberg, G. Auxin regulation of cytokinin biosynthesis in *Arabidopsis thaliana*: A factor of potential importance for auxin-cytokinin-regulated development. *Proc. Natl. Acad. Sci. USA* **2004**, *101*, 8039–8044. [CrossRef]
222. Ioio, R.D.; Nakamura, K.; Moubayidin, L.; Perilli, S.; Taniguchi, M.; Morita, M.T.; Aoyama, T.; Costantino, P.; Sabatini, S. A Genetic Framework for the Control of Cell Division and Differentiation in the Root Meristem. *Science* **2008**, *322*, 1380–1384. [CrossRef]
223. Rashotte, A.M.; Carson, S.D.B.; To, J.P.C.; Kieber, J.J. Expression profiling of cytokinin action in *Arabidopsis*. *Plant Physiol.* **2003**, *132*, 1998–2011. [CrossRef]
224. Kaur, K.; Verma, B.; Kant, U. Plants obtained from the Khair tree (*Acacia catechu* Willd.) using mature nodal segments. *Plant Cell Rep.* **1998**, *17*, 427–429. [CrossRef]
225. Barrueto Cid, L.P.; Machado, A.C.M.G.; Carvalheira, S.B.R.C.; Brasileiro, A.C.M. Plant regeneration from seedling explants of *Eucalyptus grandis* × *E. urophylla*. *Plant Cell Tissue Organ Cult.* **1999**, *56*, 17–23. [CrossRef]
226. Tiwari, S.K.; Kashyap, M.K.; Ujjaini, M.M.; Agrawal, A.P. in vitro propagation of *Lagerstromia parviflora* Roxb. from adult tree. *Indian J. Exp. Biol.* **2002**, *40*, 212–215.
227. Siddique, I.; Anis, M. Direct plant regeneration from nodal explants of *Balanites aegyptiaca* L. (Del.): A valuable medicinal tree. *New For.* **2009**, *37*, 53–62. [CrossRef]
228. Devi, Y. Rapid cloning of elite teak (*Tectona grandis* Linn.) by in vitro multiple shoot production. *Indian J. Exp. Biol.* **1994**, *32*, 668–671.
229. Dhar, U.; Upreti, J. In vitro regeneration of a mature leguminous liana (*Bauhinia vahlii* Wight & Arnott). *Plant Cell Rep.* **1999**, *18*, 664–669. [CrossRef]
230. Husain, M.K.; Anis, M. In vitro proliferation of shoots of *Melia azedarach* L. from mature trees. In *Biotechnology for a Better Future*; D'Souza, L., Anuradha, M., Nivas, S., Hegde, S., Rajendra, K., Eds.; SAC: Mangalore, India, 2004; pp. 294–301.
231. Giri, C.C.; Shyamkumar, B.; Anjaneyulu, C. Progress in tissue culture, genetic transformation and applications of biotechnology to trees: An overview. *Trees* **2004**, *18*, 115–135. [CrossRef]
232. Fuentes, S.R.L.; Calheiros, M.B.P.; Manetti-Filho, J.; Vieira, L.G.E. The effects of silver nitrate and different carbohydrate sources on somatic embryogenesis in *Coffea canephora*. *Plant Cell Tissue Organ Cult.* **2000**, *60*, 5–13. [CrossRef]
233. Sinha, R.K.; Majumdar, K.; Sinha, S. Somatic embryogenesis and plantlet regeneration from leaf explants of *Sapindus mukorossi* Gaertn.: A soapnut tree. *Curr. Sci.* **2000**, *78*, 620–623.
234. Nehra, N.S.; Kartha, K.K. Meristem and Shoot Tip Culture: Requirements and Applications. In *Plant Cell and Tissue Culture*; Vasil, I.K., Thorpe, T.A., Eds.; Springer: Dordrecht, The Netherlands, 1994; pp. 37–70.
235. Sharma, A.K.; Prasad, R.N.; Chaturvedi, H.C. Clonal propagation of *Bougainvillea glabra* 'Magnifica' through shoot apex culture. *Plant Cell Tissue Organ Cult.* **1981**, *1*, 33–38. [CrossRef]
236. Hamid, M.E. *In Vitro* Propagation of *Catha edulis*. *HortScience* **1991**, *26*, 212. [CrossRef]
237. Kaur, K.; Kant, U. Clonal propagation of *Acacia catechu* Willd. by shoot tip culture. *Plant Growth Regul.* **2000**, *31*, 143–145. [CrossRef]
238. Balaraju, K.; Agastian, P.; Ignacimuthu, S.; Park, K. A rapid in vitro propagation of red sanders (*Pterocarpus santalinus* L.) using shoot tip explants. *Acta Physiol. Plant.* **2011**, *33*, 2501. [CrossRef]
239. Al-Sulaiman, M.A.; Barakat, M.N. in vitro shoot multiplication of *Ziziphus spina-christi* by shoot tip culture. *Afr. J. Biotechnol.* **2010**, *9*, 850–857.
240. Hussain, S.A.; Anis, M.; Alatar, A.A. Efficient In Vitro Regeneration System for *Tecoma stans* L., Using Shoot Tip and Assessment of Genetic Fidelity Among Regenerants. *Proc. Natl. Acad. Sci. India Sect. B Biol. Sci.* **2020**, *90*, 171–178. [CrossRef]
241. Borges de Paiva Neto, V.; Ribeiro da Mota, T.; Campos Otoni, W. Direct organogenesis from hypocotyl-derived explants of annatto (*Bixa orellana*). *Plant Cell Tissue Organ Cult.* **2003**, *75*, 159–167. [CrossRef]
242. Taniguchi, T.; Kurita, M.; Itahana, N.; Kondo, T. Somatic embryogenesis and plant regeneration from immature zygotic embryos of Hinoki cypress (*Chamaecyparis obtusa* Sieb. et Zucc.). *Plant Cell Rep.* **2004**, *23*, 26–31. [CrossRef] [PubMed]
243. Lara-Chavez, A.; Flinn, B.S.; Egertsdotter, U. Initiation of somatic embryogenesis from immature zygotic embryos of Oocarpa pine (*Pinus oocarpa* Schiede ex Schlectendal). *Tree Physiol.* **2011**, *31*, 539–554. [CrossRef] [PubMed]
244. Hou, J.; Wu, Y.; Shen, Y.; Mao, Y.; Liu, W.; Zhao, W.; Mu, Y.; Li, M.; Yang, M.; Wu, L. Plant regeneration through somatic embryogenesis and shoot organogenesis from immature zygotic embryos of *Sapium sebiferum* Roxb. *Sci. Hortic.* **2015**, *197*, 218–225. [CrossRef]
245. Dunstan, D.I.; Tautorus, T.E.; Thorpe, T.A. Somatic embryogenesis in woody plants. In *In Vitro Embryogenesis in Plants*; Thorpe, T.A., Ed.; Kluwer Academic Publishers: Dordrecht, The Netherlands, 1995.
246. Apóstolo, N.M.; Brutti, C.B.; Llorente, B.E. Leaf anatomy of *Cynara scolymus* L. in successive micropropagation stages. *In Vitr. Cell. Dev. Biol.-Plant* **2005**, *41*, 307–313. [CrossRef]

247. Fatima, N.; Ahmad, N.; Ahmad, I.; Anis, M. Interactive Effects of Growth Regulators, Carbon Sources, pH on Plant Regeneration and Assessment of Genetic Fidelity Using Single Primer Amplification Reaction (SPARS) Techniques in *Withania somnifera* L. *Appl. Biochem. Biotechnol.* **2015**, *177*, 118–136. [CrossRef] [PubMed]
248. Hiregoudar, L.V.; Kumar, H.G.; Murthy, H.N. in vitro culture of *Feronia limonia* (L.) Swingle from hypocotyl and internodal explants. *Biol. Plant.* **2005**, *49*, 41–45. [CrossRef]
249. Prakash, E.; Khan, P.S.S.V.; Rao, T.J.V.S.; Meru, E.S. Micropropagation of red sanders (*Pterocarpus santalinus* L.) using mature nodal explants. *J. For. Res.* **2006**, *11*, 329–335. [CrossRef]
250. Tripathi, M.; Kumari, N. Micropropagation of a tropical fruit tree *Spondias mangifera* Willd. through direct organogenesis. *Acta Physiol. Plant.* **2010**, *32*, 1011–1015. [CrossRef]
251. Shekhawat, M.S.; Shekhawat, N.S. Micropropagation of *Arnebia hispidissima* (Lehm). DC. and production of alkannin from callus and cell suspension culture. *Acta Physiol. Plant.* **2010**, *33*, 1445–1450. [CrossRef]
252. Peng, X.; Zhang, T.-t.; Zhang, J. Effect of subculture times on genetic fidelity, endogenous hormone level and pharmaceutical potential of *Tetrastigma hemsleyanum* callus. *Plant Cell Tissue Organ Cult.* **2015**, *122*, 67–77. [CrossRef]
253. Malik, K.; Saxena, P. Regeneration in *Phaseolus vulgaris* L.: High-frequency induction of direct shoot formation in intact seedlings by N6-benzylaminopurine and thidiazuron. *Planta* **1992**, *186*, 384–389. [CrossRef] [PubMed]
254. Bhuyan, A.K.; Pattnaik, S.; Chand, P.K. Micropropagation of Curry Leaf Tree [*Murraya koenigii* (L.) Spreng.] by axillary proliferation using intact seedlings. *Plant Cell Rep.* **1997**, *16*, 779–782. [CrossRef] [PubMed]
255. Hussain, T.M.; Chandrasekhar, T.; Gopal, G.R. Micropropagation of *Sterculia urens* Roxb., an endangered tree species from intact seedlings. *Afr. J. Biotechnol.* **2008**, *7*, 95–101.
256. Williams, E.G.; Maheswaran, G. Somatic Embryogenesis: Factors Influencing Coordinated Behaviour of Cells as an Embryogenic Group. *Ann. Bot.* **1986**, *57*, 443–462. [CrossRef]
257. Chaturani, G.; Subasinghe, S.; Jayatilleke, M.; Mapalana, K.; Lanka, S. In vitro establishment, germination and growth performance of Red sandal wood (*Pterocarpus santalinus* L.). *Trop. Agric. Res. Ext.* **2006**, *9*, 116–130.
258. Yang, L.; Li, Y.; Shen, H. Somatic embryogenesis and plant regeneration from immature zygotic embryo cultures of mountain ash (*Sorbus pohuashanensis*). *Plant Cell Tissue Organ Cult.* **2012**, *109*, 547–556. [CrossRef]
259. Ashok Kumar, H.G.; Murthy, H.N.; Paek, K.Y. Somatic embryogenesis and plant regeneration in *Gymnema sylvestre*. *Plant Cell Tissue Organ Cult.* **2002**, *71*, 85–88. [CrossRef]
260. Junaid, A.; Mujib, A.; Bhat, M.A.; Sharma, M.P. Somatic embryo proliferation, maturation and germination in *Catharanthus roseus*. *Plant Cell Tissue Organ Cult.* **2006**, *84*, 325–332. [CrossRef]
261. Rout, G.R.; Samantaray, S.; Das, P. Somatic embryogenesis and plant regeneration from callus culture of *Acacia catechu*—A multipurpose leguminous tree. *Plant Cell Tissue Organ Cult.* **1995**, *42*, 283–285. [CrossRef]
262. Das, A.B.; Rout, G.R.; Das, P. In vitro somatic embryogenesis from callus culture of the timber yielding tree *Hardwickia binata* Roxb. *Plant Cell Rep.* **1995**, *15*, 147–149. [CrossRef]
263. Garg, L.; Bhandari, N.N.; Rani, V.; Bhojwani, S.S. Somatic embryogenesis and regeneration of triploid plants in endosperm cultures of *Acacia nilotica*. *Plant Cell Rep.* **1996**, *15*, 855–858. [CrossRef]
264. Austin Burns, J.; Wetzstein, H.Y. Embryogenic cultures of the leguminous tree *Albizia julibrissin* and recovery of plants. *Plant Cell Tissue Organ Cult.* **1998**, *54*, 55–59. [CrossRef]
265. Xie, D.Y.; Hong, Y. Regeneration of *Acacia mangium* through somatic embryogenesis. *Plant Cell Rep.* **2001**, *20*, 34–40. [CrossRef]
266. De Klerk, G.-J. Rooting of microcuttings: Theory and practice. *In Vitr. Cell. Dev. Biol.-Plant* **2002**, *38*, 415–422. [CrossRef]
267. Wiszniewska, A.; Nowak, B.; Kołton, A.; Sitek, E.; Grabski, K.; Dziurka, M.; Długosz-Grochowska, O.; Dziurka, K.; Tukaj, Z. Rooting response of *Prunus domestica* L. microshoots in the presence of phytoactive medium supplements. *Plant Cell Tissue Organ Cult.* **2016**, *125*, 163–176. [CrossRef]
268. Ilczuk, A.; Jacygrad, E. The effect of IBA on anatomical changes and antioxidant enzyme activity during the in vitro rooting of smoke tree (*Cotinus coggygria* Scop.). *Sci. Hortic.* **2016**, *210*, 268–276. [CrossRef]
269. Yan, Y.-H.; Li, J.-L.; Zhang, X.-Q.; Yang, W.-Y.; Wan, Y.; Ma, Y.-M.; Zhu, Y.-Q.; Peng, Y.; Huang, L.-K. Effect of naphthalene acetic acid on adventitious root development and associated physiological changes in stem cutting of *Hemarthria compressa*. *PLoS ONE* **2014**, *9*, e90700. [CrossRef] [PubMed]
270. Naija, S.; Elloumi, N.; Jbir, N.; Ammar, S.; Kevers, C. Anatomical and biochemical changes during adventitious rooting of apple rootstocks MM 106 cultured in vitro. *Comptes Rendus Biol.* **2008**, *331*, 518–525. [CrossRef] [PubMed]
271. Zhang, J.-Y.; Guo, Z.-R.; Zhang, R.; Li, Y.-R.; Cao, L.; Liang, Y.-W.; Huang, L.-B. Auxin Type, Auxin Concentration, and Air and Substrate Temperature Difference Play Key Roles in the Rooting of Juvenile Hardwood Pecan Cuttings. *HortTechnology* **2015**, *25*, 209–213. [CrossRef]
272. Elmongy, M.S.; Cao, Y.; Zhou, H.; Xia, Y. Root Development Enhanced by Using Indole-3-butyric Acid and Naphthalene Acetic Acid and Associated Biochemical Changes of In Vitro Azalea Microshoots. *J. Plant Growth Regul.* **2018**, *37*, 813–825. [CrossRef]
273. Ludwig-Müller, J. Indole-3-butyric acid in plant growth and development. *Plant Growth Regul.* **2000**, *32*, 219–230. [CrossRef]
274. Rajeswari, V.; Paliwal, K. In vitro propagation of *Albizia odoratissima* L.F. (Benth.) from cotyledonary node and leaf nodal explants. *In Vitr. Cell. Dev. Biol.-Plant* **2006**, *42*, 399–404. [CrossRef]
275. Werbrouck, S.P.O.; van der Jeugt, B.; Dewitte, W.; Prinsen, E.; Van Onckelen, H.A.; Debergh, P.C. The metabolism of benzyladenine in *Spathiphyllum floribundum* 'Schott Petite' in relation to acclimatisation problems. *Plant Cell Rep.* **1995**, *14*, 662–665. [CrossRef]

276. Khanam, M.N.; Javed, S.B.; Anis, M.; Alatar, A.A. *meta*-Topolin induced in vitro regeneration and metabolic profiling in *Allamanda cathartica* L. *Ind. Crops Prod.* **2020**, *145*, 111944. [CrossRef]
277. Khanam, M.N.; Anis, M. Organogenesis and efficient in vitro plantlet regeneration from nodal segments of *Allamanda cathartica* L. using TDZ and ultrasound assisted extraction of quercetin. *Plant Cell Tissue Organ Cult.* **2018**, *134*, 241–250. [CrossRef]
278. Hussain, S.A.; Ahmad, N.; Anis, M.; Hakeem, K.R. Development of an efficient micropropagation system for *Tecoma stans* (L.) Juss. ex Kunth using thidiazuron and effects on phytochemical constitution. *In Vitr. Cell. Dev. Biol.-Plant* **2019**, *55*, 442–453. [CrossRef]
279. Du, Y.; Scheres, B. Lateral root formation and the multiple roles of auxin. *J. Exp. Bot.* **2018**, *69*, 155–167. [CrossRef] [PubMed]
280. Ilina, E.L.; Kiryushkin, A.S.; Semenova, V.A.; Demchenko, N.P.; Pawlowski, K.; Demchenko, K.N. Lateral root initiation and formation within the parental root meristem of *Cucurbita pepo*: Is auxin a key player? *Ann. Bot.* **2018**, *122*, 873–888. [CrossRef] [PubMed]
281. De Smet, I. Lateral root initiation: One step at a time. *New Phytol.* **2012**, *193*, 867–873. [CrossRef] [PubMed]
282. Lloret, P.G.; Casero, P.J. Lateral root initiation. In *Plant Roots—The Hidden Half*, 3rd ed.; Waisel, Y., Eshel, A., Kafkafi, U., Eds.; Marcel Dekker Inc.: New York, NY, USA, 2002; pp. 127–156.
283. Demchenko, N.P.; Demchenko, K.N. Resumption of DNA Synthesis and Cell Division in Wheat Roots as Related to Lateral Root Initiation. *Russ. J. Plant Physiol.* **2001**, *48*, 755–764. [CrossRef]
284. Vieten, A.; Vanneste, S.; Wisniewska, J.; Benkova, E.; Benjamins, R.; Beeckman, T.; Luschnig, C.; Friml, J. Functional redundancy of PIN proteins is accompanied by auxin-dependentcross-regulation of PIN expression. *Development* **2005**, *132*, 4521–4531. [CrossRef]
285. De Klerk, G.-J.; Brugge, J.T.; Marinova, S. Effectiveness of indoleacetic acid, indolebutyric acid and naphthaleneacetic acid during adventitious root formation in vitro in *Malus* 'Jork 9'. *Plant Cell Tissue Organ Cult.* **1997**, *49*, 39–44. [CrossRef]
286. Thomas, T.D.; Puthur, J.T. Thidiazuron induced high frequency shoot organogenesis in callus from *Kigelia pinnata* L. *Bot. Bull. Acad. Sin* **2004**, *45*, 307–313.
287. Pandey, S.; Singh, M.; Jaiswal, U.; Jaiswal, V.S. Shoot initiation and multiplication from a mature tree of *Terminalia arjuna* Roxb. *In Vitr. Cell. Dev. Biol.-Plant* **2006**, *42*, 389–393. [CrossRef]
288. James, D.J. Adventitious root formation 'in vitro' in apple rootstocks (*Malus pumila*) I. Factors affecting the length of the auxin-sensitive phase in M.9. *Physiol. Plant.* **1983**, *57*, 149–153. [CrossRef]
289. Zanol, G.; Fortes, G.d.L.; Campos, A.; Da Silva, J.; Centellas, A. in vitro rooting and peroxidase activity of apple rootstocks cv." Marubakaido" treated with indolebutyric acid and floroglucinol. *Rev. Bras. De Fisiol. Veg.* **1998**, *10*, 65–68.
290. Hammatt, N.; Grant, N.J. Micropropagation of mature British wild cherry. *Plant Cell Tissue Organ Cult.* **1997**, *47*, 103–110. [CrossRef]
291. De Klerk, G.-J.; van der Krieken, W.; De Jong, J.C. Review the formation of adventitious roots: New concepts, new possibilities. *In Vitr. Cell. Dev. Biol.-Plant* **1999**, *35*, 189–199. [CrossRef]
292. Borkowska, B. Morphological and physiological characteristics of micropropagated strawberry plants rooted in vitro or ex vitro. *Sci. Hortic.* **2001**, *89*, 195–206. [CrossRef]
293. Sharma, S.; Gambhir, G.; Srivastava, D.K. In vitro differentiation and plant regeneration from root and other explants of juvenile origin in pea (*Pisum sativum* L.). *Legume Res.* **2017**, *40*, 1020–1027. [CrossRef]
294. Bellamine, J.; Penel, C.; Greppin, H.; Gaspar, T. Confirmation of the role of auxin and calcium in the late phases of adventitious root formation. *Plant Growth Regul.* **1998**, *26*, 191–194. [CrossRef]
295. Liu, Z.; Li, Z. Micropropagation of *Camptotheca acuminata* decaisne from axillary buds, shoot tips, and seed embryos in a tissue culture system. *In Vitr. Cell. Dev. Biol.-Plant* **2001**, *37*, 84–88. [CrossRef]
296. Yan, H.; Liang, C.; Yang, L.; Li, Y. In vitro and ex vitro rooting of *Siratia grosvenorii*, a traditional medicinal plant. *Acta Physiol. Plant.* **2010**, *32*, 115–120. [CrossRef]
297. Tiwari, S.K.; Tiwari, K.P.; Siril, E.A. An improved micropropagation protocol for teak. *Plant Cell Tissue Organ Cult.* **2002**, *71*, 1–6. [CrossRef]
298. Siddique, I.; Anis, M.; Jahan, A. Rapid multiplication of *Nyctanthes arbor-tristis* L. through in vitro axillary shoot proliferation. *World J. Agri. Sci* **2006**, *2*, 188–192.
299. Xu, J.; Wang, Y.; Zhang, Y.; Chai, T. Rapid in vitro multiplication and *ex vitro* rooting of *Malus zumi* (Matsumura) Rehd. *Acta Physiol. Plant.* **2007**, *30*, 129–132. [CrossRef]
300. Varshney, A.; Anis, M. Improvement of shoot morphogenesis in vitro and assessment of changes of the activity of antioxidant enzymes during acclimation of micropropagated plants of Desert Teak. *Acta Physiol. Plant.* **2012**, *34*, 859–867. [CrossRef]
301. Alam, N.; Anis, M.; Javed, S.B.; Alatar, A.A. Stimulatory effect of copper and zinc sulphate on plant regeneration, glutathione-*S*-transferase analysis and assessment of antioxidant activities in *Mucuna pruriens* L. (DC). *Plant Cell Tissue Organ Cult.* **2020**, *141*, 155–166. [CrossRef]
302. Amâncio, S.; Rebordão, J.P.; Chaves, M.M. Improvement of acclimatization of micropropagated grapevine: Photosynthetic competence and carbon allocation. *Plant Cell Tissue Organ Cult.* **1999**, *58*, 31–37. [CrossRef]
303. Kadleček, P.; Tichá, I.; Čapková, V.; Schäfer, C. Acclimatization of Micropropagated Tobacco Plantlets. In *Photosynthesis: Mechanisms and Effects: Volume I–V, Proceedings of the XIth International Congress on Photosynthesis, Budapest, Hungary, 17–22 August 1998*; Garab, G., Ed.; Springer: Dordrecht, The Netherlands, 1998; pp. 3853–3856.
304. Pospisilova, J.; Ticha, I.; Kadlecek, P.; Haisel, D.; Plzakova, S. Acclimatization of Micropropagated Plants to *Ex Vitro* Conditions. *Biol. Plant.* **1999**, *42*, 481–497. [CrossRef]

305. Yang, Y.-J.; Tong, Y.-G.; Yu, G.-Y.; Zhang, S.-B.; Huang, W. Photosynthetic characteristics explain the high growth rate for *Eucalyptus camaldulensis*: Implications for breeding strategy. *Ind. Crops Prod.* **2018**, *124*, 186–191. [CrossRef]
306. Lavanya, M.; Venkateshwarlu, B.; Devi, B.P. Acclimatization of neem microshoots adaptable to semi-sterile conditions. *Indian J. Biotechnol.* **2009**, *8*, 218–222.
307. Faisal, M.; Anis, M. Effect of light irradiations on photosynthetic machinery and antioxidative enzymes during ex vitro acclimatization of *Tylophora indica* plantlets. *J. Plant Interact.* **2010**, *5*, 21–27. [CrossRef]
308. Nayak, S.A.; Kumar, S.; Satapathy, K.; Moharana, A.; Behera, B.; Barik, D.P.; Acharya, L.; Mohapatra, P.K.; Jena, P.K.; Naik, S.K. In vitro plant regeneration from cotyledonary nodes of *Withania somnifera* (L.) Dunal and assessment of clonal fidelity using RAPD and ISSR markers. *Acta Physiol. Plant.* **2013**, *35*, 195–203. [CrossRef]
309. Javed, S.B.; Alatar, A.A.; Anis, M.; Faisal, M. Synthetic seeds production and germination studies, for short term storage and long distance transport of *Erythrina variegata* L.: A multipurpose tree legume. *Ind. Crops Prod.* **2017**, *105*, 41–46. [CrossRef]
310. Goyal, A.K.; Pradhan, S.; Basistha, B.C.; Sen, A. Micropropagation and assessment of genetic fidelity of *Dendrocalamus strictus* (Roxb.) nees using RAPD and ISSR markers. *3 Biotech* **2015**, *5*, 473–482. [CrossRef] [PubMed]
311. Al Khateeb, W.; Bahar, E.; Lahham, J.; Schroeder, D.; Hussein, E. Regeneration and assessment of genetic fidelity of the endangered tree *Moringa peregrina* (Forsk.) Fiori using Inter Simple Sequence Repeat (ISSR). *Physiol. Mol. Biol. Plants* **2013**, *19*, 157–164. [CrossRef]
312. Agarwal, T.; Gupta, A.K.; Patel, A.K.; Shekhawat, N.S. Micropropagation and validation of genetic homogeneity of *Alhagi maurorum* using SCoT, ISSR and RAPD markers. *Plant Cell Tissue Organ Cult.* **2015**, *120*, 313–323. [CrossRef]
313. Dangi, B.; Khurana-Kaul, V.; Kothari, S.L.; Kachhwaha, S. Micropropagtion of *Terminalia bellerica* from nodal explants of mature tree and assessment of genetic fidelity using ISSR and RAPD markers. *Physiol. Mol. Biol. Plants* **2014**, *20*, 509–516. [CrossRef]
314. Saha, S.; Adhikari, S.; Dey, T.; Ghosh, P. RAPD and ISSR based evaluation of genetic stability of micropropagated plantlets of *Morus alba* L. variety S-1. *Meta Gene* **2016**, *7*, 7–15. [CrossRef] [PubMed]
315. Kuzminsky, E.; Alicandri, E.; Agrimi, M.; Vettraino, A.M.; Ciaffi, M. Data set useful for the micropropagation and the assessment of post-vitro genetic fidelity of veteran trees of *P. orientalis* L. *Data Brief* **2018**, *20*, 1532–1536. [CrossRef] [PubMed]
316. Antony Ceasar, S.; Lenin Maxwell, S.; Bhargav Prasad, K.; Karthigan, M.; Ignacimuthu, S. Highly efficient shoot regeneration of *Bacopa monnieri* (L.) using a two-stage culture procedure and assessment of genetic integrity of micropropagated plants by RAPD. *Acta Physiol. Plant.* **2010**, *32*, 443–452. [CrossRef]
317. Gupta, A.K.; Harish; Rai, M.K.; Phulwaria, M.; Agarwal, T.; Shekhawat, N.S. *In Vitro* Propagation, Encapsulation, and Genetic Fidelity Analysis of *Terminalia arjuna*: A Cardioprotective Medicinal Tree. *Appl. Biochem. Biotechnol.* **2014**, *173*, 1481–1494. [CrossRef]
318. Saeed, T.; Shahzad, A.; Ahmad, N.; Parveen, S. High frequency conversion of non-embryogenic synseeds and assessment of genetic stability through ISSR markers in *Gymnema sylvestre*. *Plant Cell Tissue Organ Cult.* **2018**, *134*, 163–168. [CrossRef]
319. Jiao, L.; Yin, Y.; Cheng, Y.; Jiang, X. DNA barcoding for identification of the endangered species Aquilaria sinensis: Comparison of data from heated or aged wood samples. *Holzforschung* **2014**, *68*, 487–494. [CrossRef]
320. Hajibabaei, M.; Singer, G.A.C.; Hebert, P.D.N.; Hickey, D.A. DNA barcoding: How it complements taxonomy, molecular phylogenetics and population genetics. *Trends Genet.* **2007**, *23*, 167–172. [CrossRef]
321. Lee, S.Y.; Ng, W.L.; Mahat, M.N.; Nazre, M.; Mohamed, R. DNA Barcoding of the Endangered Aquilaria (Thymelaeaceae) and Its Application in Species Authentication of Agarwood Products Traded in the Market. *PLoS ONE* **2016**, *11*, e0154631. [CrossRef]
322. Chen, S.; Yao, H.; Han, J.; Liu, C.; Song, J.; Shi, L.; Zhu, Y.; Ma, X.; Gao, T.; Pang, X.; et al. Validation of the ITS2 Region as a Novel DNA Barcode for Identifying Medicinal Plant Species. *PLoS ONE* **2010**, *5*, e8613. [CrossRef] [PubMed]
323. Timme, R.E.; Kuehl, J.V.; Boore, J.L.; Jansen, R.K. A comparative analysis of the *Lactuca* and *Helianthus* (Asteraceae) plastid genomes: Identification of divergent regions and categorization of shared repeats. *Am. J. Bot.* **2007**, *94*, 302–312. [CrossRef]
324. Shaw, J.; Lickey, E.B.; Schilling, E.E.; Small, R.L. Comparison of whole chloroplast genome sequences to choose noncoding regions for phylogenetic studies in angiosperms: The tortoise and the hare III. *Am. J. Bot.* **2007**, *94*, 275–288. [CrossRef]
325. Song, Y.; Dong, W.; Liu, B.; Xu, C.; Yao, X.; Gao, J.; Corlett, R.T. Comparative analysis of complete chloroplast genome sequences of two tropical trees *Machilus yunnanensis* and *Machilus balansae* in the family Lauraceae. *Front. Plant Sci.* **2015**, *6*, 662. [CrossRef] [PubMed]
326. Lv, T.; Teng, R.; Shao, Q.; Wang, H.; Zhang, W.; Li, M.; Zhang, L. DNA barcodes for the identification of Anoectochilus roxburghii and its adulterants. *Planta* **2015**, *242*, 1167–1174. [CrossRef] [PubMed]
327. Pei, N.; Chen, B.; Kress, W.J. Advances of Community-Level Plant DNA Barcoding in China. *Front. Plant Sci.* **2017**, *8*, 225. [CrossRef]
328. Li, D.-Z.; Gao, L.-M.; Li, H.-T.; Wang, H.; Ge, X.-J.; Liu, J.-Q.; Chen, Z.-D.; Zhou, S.-L.; Chen, S.-L.; Yang, J.-B.; et al. Comparative analysis of a large dataset indicates that internal transcribed spacer (ITS) should be incorporated into the core barcode for seed plants. *Proc. Natl. Acad. Sci. USA* **2011**, *108*, 19641–19646. [CrossRef]
329. Campbell, M.M.; Brunner, A.M.; Jones, H.M.; Strauss, S.H. Forestry's fertile crescent: The application of biotechnology to forest trees. *Plant Biotechnol. J.* **2003**, *1*, 141–154. [CrossRef]
330. Yang, M.; Xie, X.; Zheng, C.; Zhang, F.; He, X.; Li, Z. *Agrobacterium tumefaciens*-mediated genetic transformation of *Acacia crassicarpa* via organogenesis. *Plant Cell Tissue Organ Cult.* **2008**, *95*, 141–147. [CrossRef]

331. Thangjam, R.; Sahoo, L. in vitro regeneration and *Agrobacterium tumefaciens*-mediated genetic transformation of *Parkia timoriana* (DC.) Merr.: A multipurpose tree legume. *Acta Physiol. Plant.* **2012**, *34*, 1207–1215. [CrossRef]
332. Gorpenchenko, T.Y.; Kiselev, K.V.; Bulgakov, V.P.; Tchernoded, G.K.; Bragina, E.A.; Khodakovskaya, M.V.; Koren, O.G.; Batygina, T.B.; Zhuravlev, Y.N. The *Agrobacterium rhizogenes rolC*-gene-induced somatic embryogenesis and shoot organogenesis in *Panax ginseng* transformed calluses. *Planta* **2006**, *223*, 457–467. [CrossRef] [PubMed]
333. Jube, S.; Borthakur, D. Development of an *Agrobacterium*-mediated transformation protocol for the tree-legume *Leucaena leucocephala* using immature zygotic embryos. *Plant Cell Tissue Organ Cult.* **2009**, *96*, 325–333. [CrossRef] [PubMed]

plants

MDPI

Article

Calmodulin Domain Protein Kinase PiCDPK1 Regulates Pollen Tube Growth Polarity through Interaction with RhoGDI

Nolan Scheible †, Gyeong Mee Yoon †,‡ and Andrew G. McCubbin *

School of Biological Sciences and Center for Reproductive Biology, Washington State University, Pullman, WA 99164, USA; nolan.scheible@wsu.edu (N.S.); yoong@purdue.edu (G.M.Y.)

* Correspondence: amccubbin@wsu.edu

† These authors contributed equally to this work.

‡ Current address: Department of Botany and Plant Pathology, Purdue University, West Lafayette, IN 47907, USA.

Abstract: The pollen-specific calcium-dependent protein kinase PiCDPK1 of *Petunia inflata* has previously been shown to regulate polarity in tip growth in pollen tubes. Here we report the identification of a Rho Guanine Dissociation Inhibitor (PiRhoGDI1) as a PiCDPK1 interacting protein. We demonstrate that PiRhoGDI1 and PiCDPK1 interact in a yeast 2-hybrid assay, as well as in an in vitro pull-down assay, and that PiRhoGDI1 is phosphorylated by PiCDPK1 in vitro. We further demonstrate the PiRhoGDI1 is capable of rescuing the loss of growth polarity phenotype caused by over-expressing PiCDPK1 in vivo using stable transgenic plants. We confirmed that PiRhoGDI1 interacts with a pollen-expressed ROP GTPase isoform consistent with the established role of RhoGDIs in negatively regulating GTPases through their membrane removal and locking them in an inactive cytosolic complex. ROP is a central regulator of polarity in tip growth, upstream of Ca^{2+}, and PiCDPK1 over-expression has been previously reported to lead to dramatic elevation of cytosolic Ca^{2+} through a positive feedback loop. The discovery that PiCDPK1 impacts ROP regulation via PiRhoGDI1 suggests that PiCDPK1 acts as RhoGDI displacement factor and leads us to propose a model which we hypothesize regulates the rapid recycling of ROP GTPase at the pollen tube tip.

Keywords: pollen; tip growth; calcium; calcium dependent protein kinase; Rho Guanine Dissociation Inhibitor; ROP GTPase; RhoGDI displacement factor; polarity

Citation: Scheible, N.; Yoon, G.M.; McCubbin, A.G. Calmodulin Domain Protein Kinase PiCDPK1 Regulates Pollen Tube Growth Polarity through Interaction with RhoGDI. *Plants* **2022**, *11*, 254. https://doi.org/10.3390/plants11030254

Academic Editors: Milan S. Stankovic, Paula Baptista and Petronia Carillo

Received: 30 December 2021
Accepted: 17 January 2022
Published: 19 January 2022

1. Introduction

Highly polarized growth is a characteristic of a number of specialized eukaryotic cell types including animal neurons, fungal hyphae, and higher plant pollen tubes and root hairs. These cells grow by a process known as "tip growth" in which expansion/extension is continuously restricted to an apical domain [1]. Pollen tubes extend to form a conduit through which sperm cells are transported through female floral tissues to the ovules, and thus are critical to sexual reproduction in higher plants. In addition to their biological significance, they provide a tractable model with which to study tip growth. Though pollen is multicellular, it consists of relatively inactive sperm cells located within a highly active vegetative cell that grows to form a pollen tube, providing an opportunity to investigate polar growth at the cellular level with relative ease.

Ca^{2+} has long been known to play a pivotal role in regulating pollen tube growth [2–6]. Growing tubes exhibit a steep-tip-focused free Ca^{2+} gradient, the perturbance of which results in reversible cessation of tip growth [3,7,8]. Calcium dependent protein kinases, particularly Calmodulin-domain-like protein kinases (CDPKs) have been implicated as being one of the immediate sensors and response elements to this Ca^{2+} signal, their kinase activity being activated by elevated Ca^{2+} levels leading to phosphorylation of downstream components of these signaling pathways [9]. Expression profiling data indicate that 16 CDPK isoforms are expressed in pollen in *Arabidopsis thaliana* and knock-out mutants of 6 of the 13 tested exhibit mutant phenotypes in pollen germination and or tube growth [9].

Over-expression of *Petunia inflata CDPK1* (PiCDPK1) in pollen causes depolarized growth, whereas expression of a constitutively active mutant version of this isoform severely inhibits growth [10]. An analysis of a double-knock out of the functionally redundant isoforms of *A. thaliana CPKs-17* and *-34* (the At*CPK* isoforms most closely related to PiCDPK1) provided genetic corroboration of the biological and broader phylogenetic relevance of these results. Double T-DNA insertion mutants of *AtCPK-17* and *-34* exhibited a ~3 fold reduction in pollen tube growth rate and 350 fold reduction in transmission efficiency [11]. Identification of the downstream targets of protein kinases is key to understanding their biological function. AtCPK34 was recently implicated in modulating the activity of two pollen-specific aquaporins, NIP4-1 and NIP4-2, through phosphorylation of the Serine-267 residue [12]. Of the other *A. thaliana* CPK isoforms that are expressed in pollen, reports suggest that *AtCPK2* and *20* participate in regulating anion concentrations in pollen tubes by phosphorylating and thereby mediating the activity of the anionic membrane channel SLAH [13]. AtCPK11 and 24, with the former capable of phosphorylating the latter, participate in regulating the inward movement of potassium through the channel SPIK1 [9]. AtCPK32 interacts with and phosphorylates a cyclic nucleotide-gated calcium channel and is key for maintenance of the tip-focused calcium gradient [14]. Though the immediate downstream targets of PiCDPK1 in tip growth have not been identified, over-expression of PiCDPK1 causes a dramatic elevation of Ca^{2+} at the pollen tube tip, which as it is Ca^{2+}-activated, suggests the possibility that it may be involved in a positive feedback loop [10]. Combined these studies suggest that CPK gene family members and their interactions with downstream effectors are critical components of Ca^{2+} signaling pathways in pollen tube growth.

Signaling upstream of Ca^{2+} involves the action of a class of plant-specific Rho GTPases, designated ROPs (Rho-like GTPase of Plants) [15–18]. There is substantial evidence that ROP GTPases are central regulators of tip growth in pollen tubes [15–18] and that they regulate both the tip-focused Ca^{2+} gradient and apical actin cytoskeleton through antagonistic effector pathways [19,20]. Specifically, ROPs mediate, through the actions of immediate downstream effectors, F-actin organization so that actin is present in bundles at the tube, as opposed to the cables present further back in the tube [20,21]. Plasma membrane localization is essential to ROP biological function and is mediated by isoprenylation. Spatial restriction of the biological activity of ROP is also critical to tip-growth, and in common with other GTPases, is regulated by a number of classes of regulatory protein that mediate alternation between GTP-bound biologically active and GDP-bound inactive states, as well as membrane association. Rho guanine exchange factors (RhoGEFs) positively regulate ROP activity and are themselves positively regulated by pollen receptor-like kinases (PRK) [22]). The localization of RhoGEFs is important for spatially restricting activation of ROPs at the tube tip [23,24].

Negative regulation of ROP occurs by stimulation of the intrinsic GTPase activity of these proteins (causing hydrolysis of bound GTP to GDP) by Rho GTPase activating proteins (RhoGAPs), and secondarily by the removal of ROP from the plasma membrane by Rho guanine dissociation inhibitors (RhoGDIs). In pollen, RhoGAPs activate ROP GTPases activity in the pollen tube shank behind the tip, confining biological activity to the tube apex [25]. A RhoGAP spatially coordinates the activity of ROP, acting as a rheostat for ROP signaling in times of increased or decreased expansion [24]. RhoGDI binds preferentially to GDP bound ROP behind the tip, causing its dissociation from the plasma membrane and sequestration in the cytosol [26]. Interestingly, recycling of ROP from its complex with RhoGDI appears to be critical to pollen tube growth, as mutant RhoGDI that binds but cannot release ROP inhibits growth [26]. RhoGDI function has also been implicated in regulating the distribution of cell wall components in pollen tubes, as a triple knockout mutant in *A. thaliana* exhibits an increase in cell wall components at the tube tip, as well as altered ROP activation [27].

Recycling and activation of ROP requires the action of RhoGDI displacement factors (RhoGDFs) that promote dissociation of ROP from RhoGDI and its re-association with the plasma membrane. RhoGDFs have not yet been identified in plants but it has been

speculated that PtdIns(4,5) P_2, which possesses RhoGDF activity in animal cells, may fulfill this function [16,28]. However, this is unlikely to be the sole RhoGDF activity, as in animal cells phosphorylation of Rho GTPase affects its affinity for binding to RhoGDI [29], in addition post-translational modifications of RhoGDI, including phosphorylation by kinases including protein kinase C [30] and p21-activated kinase also influence dissociation of RhoGDI-Rho complexes [31]. Subsequent to plasma membrane recruitment, the biological activity of ROP is activated by Rho guanine exchange factors (RhoGEFs), which promote exchange of the GDP bound by ROP for GTP, and a novel class of plant-specific RhoGEFs has been identified [19,32]. In pollen tubes, RhoGEF interacts with a pollen receptor kinase (PRK) in a manner that leads to the recruitment of RhoGEF to the plasma membrane at the tube apex as well as the release of an intrinsic C-terminal inhibition of RhoGEF activity [32,33]. Three distinct RhoGEFs from *Arabidopsis* interact with PRKs, in some cases forming protein complexes, and these interactions are essential for tube elongation and seed set. The interaction between PRK and RhoGEF leads to an increase in ROP activity, suggesting that RhoGEF becomes activated by this interaction [22,34]. Significantly, this direct link between ROP pathways and a transmembrane receptor provides a mechanism by which pollen tubes may perceive extracellular signals and orient polar growth in response.

We previously reported that the pollen-specific CDPK isoform PiCDPK1 plays a pivotal role in regulating pollen tube growth polarity [10]. As a protein kinase directly regulated by Ca^{2+}, PiCDPK1 is necessarily an effector of this secondary messenger in pollen tubes. How PiCDPK1 activity mediates tip growth is unclear and identification of PiCDPK1 substrates is an important goal in elucidating these processes. Here we report the identification of a RhoGDI from pollen of *Petunia inflata* (designated PiRhoGDI1) as a downstream target of PiCDPK1 using the yeast 2-hybrid system. Several lines of evidence supporting this interaction are presented including in vitro pull-down and phosphorylation assays, and an in vivo rescue of the loss-of-polarity induced by over-expressing PiCDPK1 by co-over-expressing PiRhoGDI1 in pollen tubes of stable transgenic plants of *Nicotiana tabacum*.

2. Results

2.1. Yeast 2-Hybrid Library Screening

In an effort to identify substrates, a pollen tube (yeast 2-hybrid) cDNA library was screened with a bait construct encoding the N-terminal variable and kinase domains of PiCDPK1. DNA sequencing revealed that one class of five independent positive clones identified represented a cDNA encoding a full-length homolog of *AtRhoGDI1* (At3g07880, BLASTP E value = 7×10^{-42}). This cDNA possessed an in-frame 5′ stop codon that theoretically prevented synthesis of a fusion protein with the yeast GAL4 activation domain, however as RhoGDIs regulate ROP GTPases, which, similar to PiCDPK1, have been shown to regulate pollen tube growth polarity [10,15–18], we chose to investigate this class further, naming the gene *P. inflata RhoGDI1* (*PiRhoGDI1*) (GenBank acc. # DQ905960). The coding region of PiRhoGDI1 was re-cloned in the yeast 2-hybrid prey vector to create an in-frame fusion with the GAL4 activation domain. The resulting construct was determined to facilitate yeast growth under histidine selection in the interaction assay when co-transformed with the in-frame PiCDPK1 bait construct (Figure 1a), but neither prey nor bait construct conferred this ability when co-transformed into yeast with the respective empty partner vectors (Figure 1b). These results suggested that PiRhoGDI1 did interact with PiCDPK1 and that neither protein was capable of activating the GAL4 promoter alone. Whether the initial identification of this gene was entirely fortuitous is unclear, an alternative possibility being that the 5′ stop codon in the cDNA of the initial clone identified was removed during RNA processing in yeast. We next sought to confirm, and investigate the nature of, the interaction between PiCDPK1 and PiRhoGDI1 using alternative methodologies.

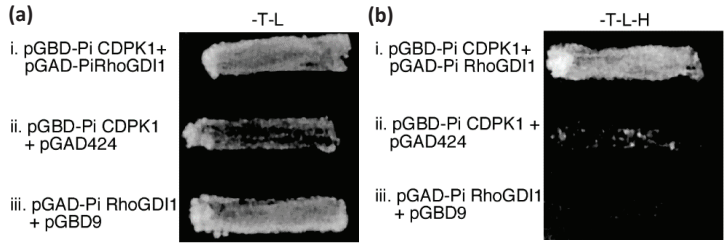

Figure 1. PiRhoGDI1 interacts with PiCDPK1 in vivo. Yeast transformed with bait (pGBD) and prey (pGAD) constructs or empty vectors (as labeled) were grown on (**a**) media lacking tryptophan and leucine (plasmid selection), and (**b**) media lacking trytophan, leucine, and histidine, providing selection for both plasmids and interaction of fusion proteins. Only cells transformed with pGBD-PiCDPK1 and pGAD-PiRhoGDI1 grew well on histidine selection, suggesting these clones encode proteins that interact.

2.2. PiRhoGDI1 Interacts with and Is Phosphorylated by PiCDPK1 In Vitro

In the presence of Ca^{2+}, the calmodulin-like domain of CDPKs binds specifically to phenyl sepharose by hydrophobic interaction [35]. Exploiting this characteristic, we designed an assay using phenyl sepharose resin to selectively pull-down PiCDPK1 and any interacting protein. We employed recombinant His-tagged PiCDPK1 and PiRhoGDI1, allowing detection of both proteins on a single protein blot using an anti-His tag monoclonal antibody. As shown in Figure 2a, PiCDPK1 bound to phenyl sepharose as expected and PiRhoGDI1 was pulled-down only in the presence of PiCDPK1 providing a second line of evidence of protein–protein interaction between PiRhoGDI1 and PiCDPK1.

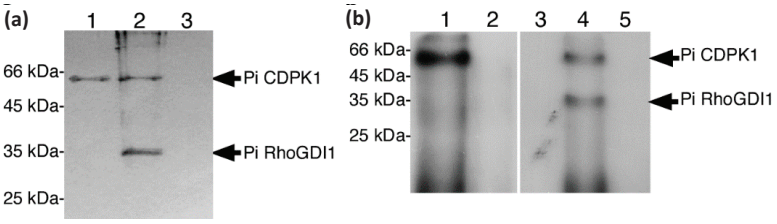

Figure 2. PiCDPK1 interacts with and phosphorylates PiRhoGDI1 in vitro. (**a**) Pull down assay. His-tagged protein samples were incubated with phenyl sepharose resin, washed, separated by SDS-PAGE, and blotted to PVDF membrane. Immuno-detection was performed with anti-His tag monoclonal antibody. Lanes represent the following samples: (1) PiCDPK1 alone, (2) PiCDPK1 and PiRhoGDI1, (3) PiRhoGDI1 alone. PiRhoGDI1 was only detected in combination with PiCDPK1, suggesting that the two proteins interact. (**b**) In vitro phosphorylation assay. Phosphorylation assays were performed in the presence of 50 μM Ca^{2+} to stimulate PiCDPK1 or 1 mM EGTA to inhibit PiCDPK1. Samples were separated by SDS-PAGE and subjected to autoradiography. Lanes: (1) PiCDPK1 + Ca^{2+}, (2) PiCDPK1 + EGTA, (3) PiRhoGDI1 + Ca^{2+}, (4) PiRhoGDI1 + PiCDPK1 + Ca^{2+}, (5) PiRhoGDI1 + EGTA. PiRhoGDI1 was phosphorylated only in the presence of PiCDPK1 and Ca^{2+}.

As physical interaction between a protein with a protein kinase does not necessarily infer phosphorylation, we also assessed whether PiRhoGDI1 was substrate of PiCDPK1 in vitro. Phosphorylation assays were performed in the presence of P^{32} labelled ATP, 50 μM Ca^{2+} or the Ca^{2+} chelator EGTA (1 mM) and with or without addition of PiCDPK1, and the products of reactions analyzed by SDS-PAGE and autoradiography. PiCDPK1 exhibited autophosphorylation only in the presence of Ca^{2+} as expected, and PiRhoGDI1 was found to be phosphorylated in the presence of Ca^{2+} and PiCDPK1, but not in the absence of PiCDPK1 or the presence of 1 mM EGTA and PiCDPK1 (Figure 2b). These results are consistent with PiRhoGDI1 being a PiCDPK1 substrate in vitro and the phosphorylation observed not

being caused by a contaminating protein kinase. Using Michaelis–Menton conditions, we then investigated the kinetics of this reaction and determined an approximate K_m of 2.2 μM and a V_{max} of 1920 pmol min^{-1} mg^{-1}, the latter being similar to the V_{max} of PiCDPK1 phosphorylation of the synthetic CDPK substrate syntide-2 (2042 pmol min^{-1} mg^{-1}) [10].

2.3. Confirmation of the Interaction of PiRhoGDI1 with ROP GTPase

RNA blot analysis indicated that PiRhoGDI1 is predominantly expressed in pollen, being first detectable in anthers from 15–20 mm buds (corresponding to pollen mitosis I), peaking in mature pollen and remaining high in pollen tubes (Figure S1), this expression pattern mimics that of PiCDPK1 [10]. Expression in other tissues was not detected but cannot be excluded in under-represented cell types, notably root hairs, which also grow by tip growth. A RhoGDI isoform from tobacco (Nt*RhoGDI2*) has been demonstrated to interact with ROP GTPase and suppress loss of growth polarity caused by *ROP* over-expression [26]. To confirm that PiRhoGDI1 also interacts with ROP, we cloned a *ROP* GTPase isoform from *P. inflata* pollen (Pi*Rop1*; GenBank acc. # DQ905959), and determined that it exhibited 94% amino acid identity with At*Rop1* (At3g51300). PiRop1 was then cloned into a yeast 2 hybrid vector and the interaction between PiRhoGDI1 and PiRop1 confirmed using the two genes in prey and bait constructs (respectively) in a yeast 2-hybrid interaction assay (Figure S2).

2.4. PiCDPK1 Suppresses the Effect of PiRhoGDI1 Over-Expression In Vivo

RhoGDIs are negative regulators of Rho class GTPases, acting to lock them in a biologically inactive state in cytosolic complexes. RhoGDIs are themselves regulated by RhoGDI-displacement factors (RhoGDFs), which promote the re-association of the GTPases with the plasma membrane, making them accessible for biological re-activation by RhoGEFs [36]. The molecular identities of RhoGDFs are not well understood in plants. Of particular relevance to this study, however, phosphorylation of RhoGDI by kinases is involved in fast recycling of Rho GTPases in animal cells [29]. For example, RhoGDI phosphorylation by protein kinase C [30] and p21-activated kinase [31] stimulates release of the GTPase from the inhibitor complex. This precedent led us to hypothesize that phosphorylation of PiRhoGDI1 by PiCDPK1 may regulate release of ROP GTPase from the RhoGDI complex in pollen tubes and design an experiment to test this hypothesis.

2.5. Co-Expression with PiRhoGDI1 Rescues the PiCDPK1 Overexpression Phenotype

As noted above, over-expression of PiCDPK1 in pollen and pollen tubes causes a loss in growth polarity (ballooning). We reasoned that if PiCDPK1 negatively regulates RhoGDI, over-expressing the two proteins together should at least partially neutralize the effect of excess PiCDPK1 by both titrating kinase activity away from endogenous RhoGDI and by increasing the non-phosphorylated pool of RhoGDI. We chose to use stable transformants to investigate this possibility to facilitate accurate quantification of expression the transgenes. *Nicotiana tabacum* was used for these transgenic experiments to take advantage of its ease of transformation, suitability for pollen tube growth and microscopy assays (large pollen), whilst retaining close phylogenetic proximity to *Petunia*. The strong pollen-specific *Lat52* promoter [37] was chosen to drive the constructs as this promoter was previously used to drive expression of PiCDPK1 in transient pollen transformation assays [10].

The goal of this experiment was to assay the ability of PiRhoGDI1 to rescue the PiCDPK1 over-expression phenotype in pollen tubes. To interpret the results of this experiment it was necessary to be able to accurately assess expression levels of the transgenes. As pollen are haploid it was necessary to generate lines that were homozygous for the transgenes to provide populations of pollen with uniform genotype. Further it was important that rescue lines expressing both transgenes expressed similar expression levels of PiCDPK1 to those expressing PiCDPK1 alone, to improve our chances of achieving this we employed sequential transformations. We first used *Agrobacterium*-mediated transformation of leaf strips to generate stable tobacco lines transformed with *pLat52-PiCDPK1:GFP*.

Pollen of these lines was cultured in vitro and those that exhibited GFP fluorescence in 50% of the pollen (indicating a T-DNA single insertion) identified. The transformed pollen also recapitulated previously reported the loss-of-polarity phenotype [10]. Selected T0 plants were then self-pollinated, and the resultant seed was used to generate T1 progeny. T1 plants homozygous for the transgene were then identified based on 100% of the pollen exhibiting GFP fluorescence and at least some loss-of-polarity (Figure 3C,D). Such plants were self-pollinated and some of the resultant seed was used to grow a T2 population of seedlings homozygous for the T-DNA. In a similar manner transgenic plants homozygous for *pLat52-GFP* were also generated to control for potential effects of expressing high levels of GFP on pollen tube growth (Figure 3G,H). T2 homozygous *pLat52-PiCDPK1:GFP* seedlings were then used as the leaf material for a second round of *Agrobacterium*-mediated transformation with *pLat52-PiRhoGDI1* to generate rescue lines. Primary transformants from this second round were assessed for presence of the *pLat52-PiRhoGDI1* transgene by RT-PCR of pollen cDNA and in vitro pollen tube growth phenotypes assessed.

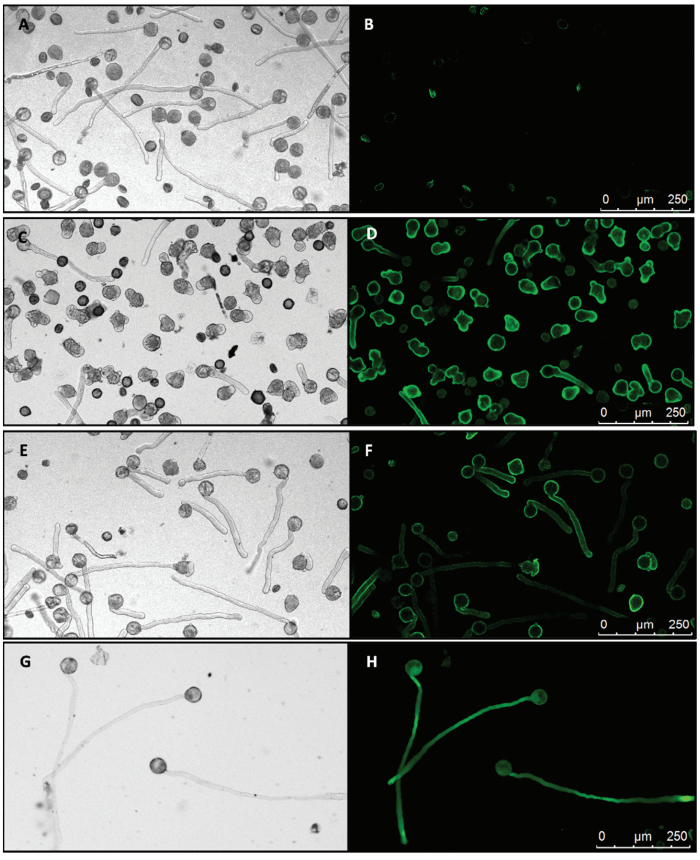

Figure 3. Effect of expressing PiCDPK1 alone and with PiRhoGDI1. Images show pollen cultured in vitro for 4 h at 28–30 °C. Paired images show light micrographs and equivalent fluorescence micrographs (black background). (**A**,**B**), wild type pollen tubes, the slight fluorescence in (**B**) is associated with a low percentage of dead pollen which auto-fluoresces. (**C**,**D**), pollen tubes from line OE1 (homozygous for *Lat52-PiCDPK1-GFP* alone) exhibiting loss of growth polarity (OE1). (**E**,**F**), pollen tubes from line Rescue 2 (homozygous for both *Lat52-PiCDPK1-GFP* and *Lat52-PiRhoGDI1*), these tubes did not lose polarity and resemble wild type pollen tubes. (**G**,**H**) from a homozygous p*Lat52-GFP* transgenic line showing pollen tubes expressing GFP alone.

Transformants expressing PiRhoGDI1 were found to bear pollen 50% of which exhibited loss of polarity and 50% grew in a polar manner, but 100% exhibited PiCDPK1:GFP fluorescence consistent with the *pLat52-PiRhoGDI1* transgene being capable of rescuing loss of polarity caused by PiCDPK1. These plants were self-pollinated, and the resulting seed used to generate a T1 population. From this population, lines were then identified for which 100% of the pollen exhibited both PiCDPK1:GFP fluorescence (indicating homozygosity for *pLat52-PiCDPK1:GFP*) and grew in a polar manner (indicating homozygosity for *pLat52-PiRhoGDI1*) (Figure 3E,F).

Pollen from the various homozygous lines was cultured in vitro for 4 h and the phenotypes assessed. Pollen germination was not significantly different from wild type for any of the transgenic lines (Figure S3), in contrast there were significant differences in pollen tube phenotypes. Pollen expressing GFP alone grew with normal polarity to an average length of 293 μm, 107% of the average wild-type tube length (273.4 μm), the difference between the two was not statistically significant (Student's *t*-test, $p > 0.1$) (Figure 3G,H). In contrast, consistent with previous transient expression studies, overexpression of PiCDPK1:GFP (OE lines) resulted in the majority of the pollen growing short, often almost spherical, pollen tubes (Figure 3G,H) [10]. Pollen from two independent lines over-expressing PiCDPK1:GFP (OE1 and OE2) alone grew to an average tube length of 68.6 μm (OE1) and 49.7 μm (OE2), 25% and 18%, respectively, of the average wild-type tube length (273.4 μm), both lines being significantly decreased in length relative to wild-type (Student's *t*-test, $p < 0.001$). In contrast, lines expressing PiCDPK1:GFP and PiRhoGDI1 (Rescue lines) grew to an average length of 185.9 μm (Rescue 2) and 213 μm (Rescue 3), 68% and 78% respectively, of wild-type (Figure 4a). Both rescue lines exhibited significantly increased tube length compared with the overexpression lines (Student's *t*-test, $p < 0.001$, Figures 3E,F and 4a). Consistent with reduced length resulting from loss-of-polarity, tube width was also affected. Pollen expressing PiCDPK1:GFP alone displayed an average tube width of 25.3 μm (OE1) and 25.4 μm (OE2), 222% and 224% of and significantly different from wild type (11.4 μm) (Student's *t*-test, $p < 0.001$) (Figure 4b). In contrast, rescue lines overexpressing both PiCDPK1:GFP and PiRhoGDI1 pollen grew to average widths of 14.9 μm (Rescue 3) and 12.6 μm (Rescue 2) these widths being significantly decreased relative to the OE lines (Student's *t*-test, $p < 0.001$). Average pollen tube widths from rescue lines were more similar to those of the wild-type tubes, being 111% (OE1) and 131% (IE2) of the average wild-type tube width (Figures 3E,F and 4b).

In this experiment, both transgenes were driven by the pollen-specific promoter *pLat52*. This provided an advantage in that it increased the likelihood of expressing them at similar levels, but raised the possibility that addition of the second transgene could negatively affect the expression of the first. As a result, it was important to verify that phenotypic rescue was not trivially a result of a reduction in PiCDPK1 expression. To this end, qRT-PCR primers were designed to amplify a region spanning the junction of *pLat52* and the 5′ end of the PiCDPK1 or PiRhoGDI1 coding sequences. This minimized the potential of endogenous tobacco transcripts, which share high levels of identity with the transgenes, interfering with assessment of transgene expression. qRT-PCR was then used to assess expression levels of the two transgenes. Expression was normalized to internal *N. tabacum* reference genes, elongation factor 1-alpha (EF1) and ribosomal protein 25 (L25) [38]. As shown in Figure 5, the results of qRT-PCR indicated that expression levels of PiCDPK1 were very similar in the rescue and OE lines. Both rescue lines displayed similar expression of the PiCDPK1 transgene to the OE lines, and there was no significant difference between lines (Student's *t*-test, $p > 0.1$) (Figure 5). No significant qRT-PCR signals were found in wild-type samples, supporting the idea that transgene expression was being measured specifically and endogenous RhoGDI and CDPK1 genes were not interfering with the assays. Overall, these results suggest that expression of PiRhoGDI1 at least partially rescues the effects of over-expression of PiCDPK1, and supports the hypothesis that PiCDPK1 possesses RhoGDF activity in vivo.

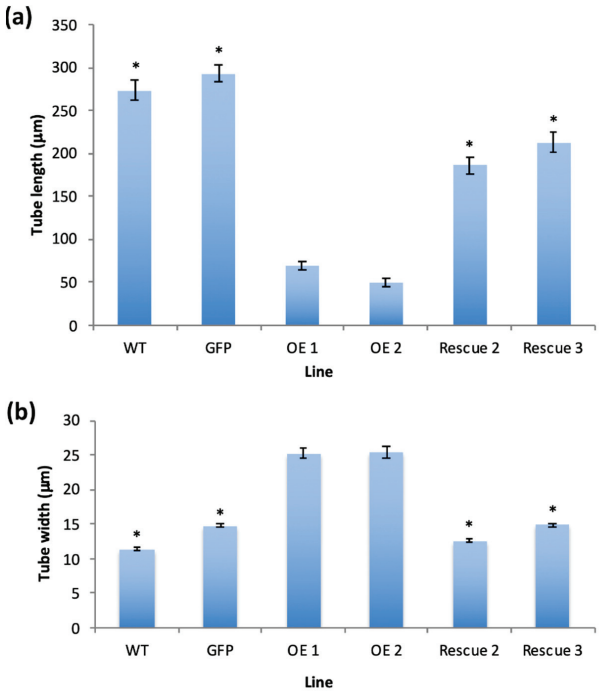

Figure 4. (**a**) Average pollen tube length (µm) and (**b**) average pollen tube width of the transgenic lines (as indicated) after 4 h of incubation at 28–30 °C. Plant lines shown: WT (wild type), GFP (transformant expressing GFP alone), OE1 and OE2 (transgenic lines expressing PiCDPK1-GFP alone), Rescue 2 and Rescue 3 (transgenic lines expressing PiCDPK1-GFP and PiRhoGDI1). Data are presented as means ± SE collected from >100 pollen tubes of each line, asterisks indicate significant differences between the samples labelled and the OE lines (Student's *t*-test, $p < 0.001$).

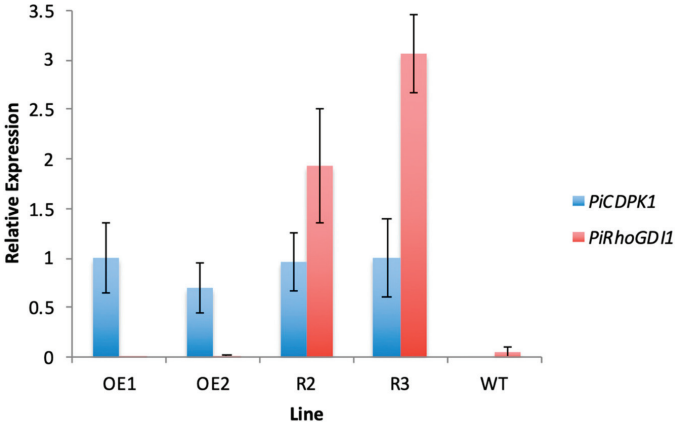

Figure 5. Quantitative PCR results showing relative expression of the PiRhoGDI transgene compared with the PiCDPK1 transgene in pollen from stable transgenic tobacco lines. Plant lines shown: OE1 and OE2 (transgenic lines expressing PiCDPK1-GFP alone), Rescue 2 and Rescue 3 (transgenic lines expressing PiCDPK1-GFP and PiRhoGDI1) and WT (wild type). Results are normalized to the ribosomal protein 25 (L25) internal reference gene and the OE1 line is used as the control (expression level of 1.0). Data are presented as means ± SE from three biological replicates.

3. Discussion

The data presented provide several lines of evidence that PiRhoGDI1 interacts with, and is likely a substrate of, the calmodulin-domain protein kinase PiCDPK1. Though the regulatory site(s) were not identified, PiCDPK1 interacted with and phosphorylated PiRhoGDI1 in vitro. The ability of PiRhoGDI1 to rescue the effect of PiCDPK1 in pollen tubes provides support for this interaction occurring in vivo. The homology based predicted activity of PiRhoGDI1 to bind ROP GTPase was confirmed using the yeast 2-hybrid assay. As RhoGDI is an established regulator of ROP GTPase this suggests that the pathway leading to the PiCDPK1 loss of polarity phenotype involves the activity of ROP GTPase. Combined these results are consistent with PiCDPK1 regulating PiRhoGDI1 by phosphorylation, and that this phosphorylation mediates the ability of PiRhoGDI1 to bind ROP GTPase. The observed phenotypes are consistent with the scenario that when PiCDPK1 alone is over-expressed, the negative regulatory activity of endogenous RhoGDI is neutralized by excess kinase activity, leading to increased recruitment of ROP to the plasma membrane. Co-over expressing PiRhoGDI with PiCDPK1, titrates much of the excess kinase activity away from endogenous RhoGDI reducing ROP membrane recruitment and resulting in a more polar growth phenotype. Extrapolating from these results, and integrating them with the current knowledge of the functioning of RhoGDI's and the regulation of ROP GTPases and Ca^{2+} in tip growth, allows us to propose a model for the integration of these components into a pathway which mediates rapid recycling and regulation of ROP at the pollen tube tip (Figure 6).

In this model, ROP GTPase is held inactive in a cytosolic complex with PiRhoGDI1. Under high cytosolic Ca^{2+} concentrations at the pollen tube tip, PiCDPK1, which is localized to the plasma membrane [10], is activated to phosphorylate PiRhoGDI1. This phosphorylation leads to release of ROP from the complex, exposure of its hydrophobic prenyl side chain and plasma membrane recruitment. At the plasma membrane, ROP is stimulated to exchange GDP for GTP by a GEF and biologically activated to promote polarized growth. As the tube tip extends and secretory vesicles are deposited, biologically active GTPase is progressively carried in a posterior direction by membrane flow. GTPase activating proteins (GAPs) are absent at the tube tip, but present in the plasma membrane in the tube shank (their recruitment to this localization being mediated by a 14:3:3 protein and possibly phosphorylation by phosphoglycerate kinase [39,40]). In the tube shank, where PiCDPK1 is inactive due to lower cytosolic Ca^{2+} concentration, GAPs stimulate the GTPases to hydrolyze GTP to GDP leading to biological inactivation. Non-phosphorylated RhoGDI can now extract the GDP-bound GTPase from the plasma membrane and recycle the GTPase back to the pollen tube tip. As a whole, this pathway facilitates rapid recycling of ROP GTPase to the growing tip, the role of PiCDPK1 being that of a GDF.

In this pathway, Ca^{2+} influx at the growing pollen tube tip provides the spatial information that leads to the plasma membrane recruitment, placing it in position for subsequent activation of ROP. This model is consistent with many previously reported observations. First, though the majority of ROP in pollen tubes is cytosolic, the active fraction localizes to the apical region of the plasma membrane, coincident with the peak of the tip focused Ca^{2+} gradient [17]. This tip region is the only location in pollen tubes that has cytosolic Ca^{2+} levels sufficient for PiCDPK1 activation [10]. As noted above, ROP has been reported to be upstream of cytosolic Ca^{2+} through a pathway involving RIC3 [41]. This being the case, Ca^{2+} and PiCDPK1 act downstream of ROP in addition to regulating its activation and these molecules thus form a positive feedback loop (Figure 6). Such feedback loops are common components of GTPase pathways involved in polarity and exist in pollen tubes [1,10,42,43]. Empirical support for involvement of PiCDPK1 in such a feedback loop is provided by its over-expression not only leading to loss of growth polarity but also dramatic elevation of cytosolic Ca^{2+} within the tube tip [10]. The model proposed is also consistent with a report that mutant ROP, lacking the ability to interact with RhoGDI, accumulates at the plasma membrane in the pollen tube shank and does not exhibit the tip localization of wild type ROP [39]. Lastly, more than 25 years ago it was shown that asymmetric release of caged

Ca^{2+} within a pollen tube tip leads to growth re-orientation, focused to the location of Ca^{2+} release [44]. The model proposed provides a mechanism to explain how this phenomenon occurs.

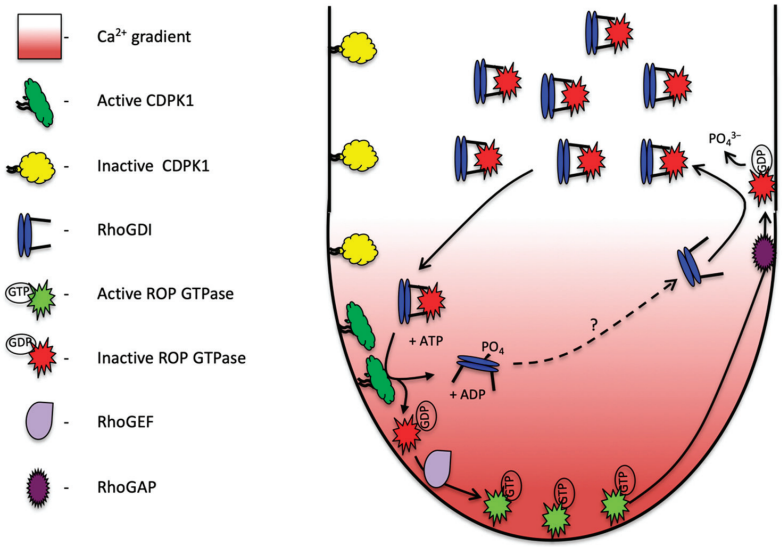

Figure 6. Proposed model of PiCDPK1 regulation of ROP in growing pollen tubes. Calcium-dependent protein kinase (PiCDPK1) is localized to the plasma membrane of the pollen tube. In the cytosol in the tube shank, Rho Guanine Dissociation Inhibitor (RhoGDI) binds to ROP GTPase removing to from the plasma membrane and locking it in an inactive state. At the tube tip, elevated calcium levels activate PiCDPK1, which phosphorylates the cytosolic RhoGDI:ROP GTPase complex. Upon phosphorylation ROP GTPase is released from the protein complex and recruited to the membrane where it is available for biological activation by Rho Guanine Exchange Factor (RhoGEF). Active (GTP bound) ROP GTPase interacts with and mediates the activity of downstream effectors to coordinate growth. As the tube extends, active ROP GTPase is passed back in the membrane until it interacts with ROP GTPase Activating Protein (RhoGAP), activating the enzyme activity of ROP causing it to hydrolyze GTP to GDP and become biologically inactivated. GDP bound ROP can be removed from the membrane by non-phosphorylated RhoGDI and recycled back to the tube tip. The dotted line and question mark indicate the activity of an as yet unidentified phosphatase the activity of which is needed to re-activate RhoGDI.

The signaling pathway proposed facilitates the perpetuation of rapid recruitment of ROP to the plasma membrane at the tip of pollen tubes. Currently missing from this model are potential mechanisms for negative regulation of the feedback loop. One likely mechanism is the dephosphorylation of PiRhoGDI1 by a protein phosphatase behind the tip, reactivating its ability to extract ROP from the plasma membrane (illustrated in Figure 6). In human cancer cells, dephosphorylation of RhoGDI occurs through the activity of a PPM family phosphatase, protein phosphatase 1b (PPM1B), which acts antagonistically and results in suppressed Rho GTPase activity [45]. Consistent with dephosphorylation of RhoGDI playing a similar role in pollen tubes, type 2A protein phosphatase inhibitors induce a phenotype similar to ROP over-expression [46]. Another significant question not included in the model proposed is the nature of mechanism(s) by which polarity is initially established at pollen germination. Establishment of polarity may require additional signaling events, but the simplest scenario does not. Pollen plasma membranes possess stretch-activated Ca^{2+} channels [47–50]. On the stigma surface, stress is likely to be focused on the direction of water uptake, and as a result maximal activation of Ca^{2+} channels may occur proximal to the point of attachment on the stigma. A Ca^{2+} gradient created in this

fashion could potentially activate the feedback loop outlined in Figure 6. Support for this scenario comes from the observation that pollen grains usually germinate from the pollen wall aperture closest to the stigma surface, but in very high humidity they will sometimes germinate in random directions [51]. For simplicity, we omitted the regulation of GEF activation of ROP from this model, but considerable progress has been made in this area. RhoGEF localization in pollen tubes has been shown to be mediated by their phosphorylation by AGC kinases, phosphorylation of the PRONE domain of RhoGEF leading to localization to the apical tip of the pollen tube and loss of this interaction causing ectopic targeting of RhoGEF [23]. Furthermore, tomato RopGEF/KPP interacts with the kinase domain of pollen-specific receptor-like kinases LePRK1 and LePRK2 [31] and studies in *Arabidopsis* have demonstrated that interaction between PRK and RhoGEF results in activation of ROP GTPase [52]. Excitingly, as these receptor-like kinases possess extracellular domains, these interactions provide a mechanism by which ROP GTPase activation can be mediated by external ligands providing a mechanism for the chemotropism exhibited by pollen tubes. Interestingly PiCDPK1 might itself play a direct role in regulating ROP it was recently reported that its' *A. thaliana* homologs CPK17 and -34, phosphorylates At ROP1 at S97, though whether this phosphorylation has any biological relevance is currently unclear [53].

Regulation of RhoGDI by a CDPK isoform has significant implications to our understanding of the regulation of growth polarity in plant cells in general. ROP isoforms have been implicated in polarity in a variety of plant cell types [54], and RhoGDI mutants exhibit defective polar growth in root hairs in *Arabidopsis* [55] hence it is likely that similar pathways employing isoforms of these enzymes are involved in many cell types. For example, a RhoGDI was shown to be critical for nuclear migration in emerging root hair cells [56], and was demonstrated to act in tandem with vesicular trafficking to regulate Rop GTPase signaling in leaf pavement cells [57]. In a broader context, fluctuations of cytosolic Ca^{2+} are associated with most aspects of growth and development, and responses to environmental signals in plants [58–61]. The majority of Ca^{2+}-stimulated kinase activity in plant cells appears to be associated with CDPKs and these molecules are thought to be pivotal to many Ca^{2+} regulated processes [62–66]. Though a considerable number of CDPK isoforms have been identified from multiple plant species, only some have clearly defined biological functions [58,67]. Many processes involving GTPase signaling are associated with Ca^{2+} transients and Ca^{2+}-regulated kinase activity [54,58], and we speculate that CDPK-mediated membrane recruitment of ROP GTPases is likely to be significant to a wide range of cellular processes in plant cells.

4. Materials and Methods

4.1. Yeast 2-Hybrid Library Screening

A pGBD/ΔN-PiCDPK1 bait plasmid was constructed by amplifying PiCDPK1 cDNA clone (Genbank acc. # DQ147913) by PCR using primers: ΔN-PiCDPK1-F, 5′-GGATCCAGG GGCCAACCTAAT-3′ and PiCDPK1-K 5′-GTCGACCTCCTTGATCCAAGG-3′. The amplicon was cloned into the *Bam* H1/*Sal* I sites of pGBD-C1 (20). Yeast strain AH109 was sequentially transformed with pGBD/ΔN-PiCDPK1 and a pollen cDNA library in pGAD424 by the LiAc method. In the first phase of selection (-his) transformants were plated onto synthetic dropout (SD) medium lacking leu, tryp, and his. After 7 days, cells were replica-plated onto SD medium lacking leu, tryp, his, and ade. Plasmid DNA was extracted from positive clones, transformed into *E. coli* and plated on LB agar supplemented with 100 μg/mL ampicillin. Plasmid DNA extracted from *E. coli* was back-transformed into yeast strain AH109 with the bait and cultured on SD medium lacking leu, tryp, his to confirm interactions. To generate an in-frame PiRhoGDI1 bait construct, PiRhoGDI1 was amplified with primers PiRhoGDI1-BH1-F (5′-GGATCCATGTCAGCTATTGTTGA-3′) and PiRhoGDI1-Sal1-R (5′-GTCGACTCAGAGCTGAAGCCA), to add 5′ *Bam* HI and 3′ *Sal* I sites. The amplicon was cloned into the *Bam* HI/*Sal* I sites of pGAD-C1 [68].

4.2. Expression of Recombinant Proteins

pRSET-B vector (Invitrogen, Waltham, MA, USA) was used to express full-length PiCDPK1 and PiRhoGDI1 6X N-terminal His-fusion proteins. Expression of PiCDPK1 was performed as previously reported [10]. The PiRhoGDI1 expression construct was generated by PCR by using PiRhoGDI1-NcoI-5′ (5′-CCATGGTAATGTCAGCTATTGTTGAAC-3′) and PiRhoGDI1-NcoI-3′ (5′-CCATGGCCCAGAGCTGAAGCCA-3′). The amplified fragment was verified by DNA sequencing and cloned into the Nco I site of pRSET-B. Expression and purification of His-tagged-PiRhoGDI1 were performed as previously described [10].

4.3. Pull-Down Assay

Pull-down assays were performed by mixing 2 µg of each 6X His-tag fusion protein with phenyl sepharose beads in 500 µL of binding buffer (20 mM HEPES, pH 7.5, 5 mM $MgCl_2$, 1 mM DTT, and 0.1% Triton X-100) with 1 mM Ca^{2+}. Samples were rotated for 2 h at 4 °C, pelleted, and washed three times with wash buffer (binding buffer supplemented with 0.3 M NaCl). Proteins were eluted in 1X SDS sample buffer, resolved on a 12% SDS-PAGE gel and transferred to Immobilon-P membrane (Millipore, Bedford, MA, USA). Fusion proteins were detected using a monoclonal Anti-polyHISTIDINE Clone HIS-1 antibody (Sigma-Aldrich, St Louis, MO, USA), anti-mouse IgG alkaline phosphatase conjugated 2° antibody (Sigma, St. Louis, MO, USA) and WesternBlue stabilized alkaline phosphatase substrate (BioRad, La Jolla, CA, USA) all following the manufacturers' recommended protocols.

4.4. Phosphorylation Assay

A total of 0.6 µg PiCDPK1-6X His-tag fusion protein was incubated with 0.5 µg PiRhoGDI1-6X His-tag in phosphorylation buffer (50 mM HEPES, pH 7.0, 1 mM $MgCl_2$, 1 mM DTT) with either 50 µM Ca^{2+} or 1 mM EGTA. Reactions were initiated by addition of 10µCi [γ-^{32}P] ATP, incubated for 10 min at room temperature then terminated by adding 5X SDS sample buffer. Samples were electrophoresed on 10% SDS-PAGE gels, blotted to Immobilon-P membrane and exposed to autoradiography.

4.5. Stable Expression in Tobacco

The previously constructed *pLat52-PiCDPK1:GFP* construct [10] subcloned from pBluescript into the plant transformation vector pBI101. This construct was used to generate transgenic *Nicotiana tabacum* using *Agrobacterium*-mediated plant transformation. We generated homozygous lines by identifying transgenic lines displaying GFP fluorescence as well as the PiCDPK1 overexpression phenotype of ballooning pollen tubes. These were self-fertilized and the resultant seed used to generate progeny. Once flowering, the pollen phenotypes of the progeny assess to identify lines with 100% of pollen tubes displaying GFP fluorescence and the PiCDPK1 overexpression phenotype (homozygous lines). A line was selected for re-transformation. For the second transformation we used the plant transformation vector pGreenII 0179 (kindly provided by Dr. Henning Kunz, SBS WSU) to transform *Agrobacterium* strain GV3101 with our gene of interest coding for PiRhoGDI1 driven by the pollen-specific *Lat52* promoter. The common sequencing primers M13 Forward and M13 Reverse were used to amplify the Lat52:PiRhoGDI1:Nos transgene cassette from the pBluescript vector as previously built [10]. PCR reactions were resolved on an agarose gel, excised and recovered using the ZymoClean DNA Gel Recovery Kit according to the manufacturers protocol. DNA fragments were digested with restriction enzymes and subsequently ligated into pGreenII. We then re-transformed the homozygous *N. tabacum* overexpressing PiCDPK1:GFP with the GV3101 *Agrobacterium* containing our PiRhoGDI1 construct and regenerated the plants using tissue culture methods. Plants were screened by RT-PCR to verify expression of PiRhoGDI1 and pollen tube phenotypes assessed. Once plants possessing both transgenes were identified, they were self-pollinated to generate lines homozygous for both transgenes.

4.6. Analysis of Transformed Pollen Tubes

Confocal images were taken with a Leica TCS SP8 confocal laser-scanning microscope (Leica Microsystems, Wetzlar, Germany) at the 514-nm excitation wavelength to image GFP fluorescence. Light micrographs were also taken for each sample and the pollen tubes quantitatively analyzed by measuring tube lengths with the FIJI distribution of ImageJ [69].

4.7. Quantitative RT-PCR

RT-qPCR was performed at the WSU Genomics Core on an ABI 7500 Fast thermocycler (ABI, Vernon, CA, USA) with the ability to perform real time quantification of PCR products. RNA was extracted from pollen using the Trizol reagent (Invitrogen, Carlsbad, CA, USA) according to the manufacturers protocol. cDNA was generated using the SensiFAST cDNA Synthesis Kit (BioLine, London, UK) which was used as the template DNA to perform qPCR using the SensiFAST SYBR Lo-ROX Kit (BioLine, London, UK), both according to the manufacturers' protocol. The forward primer for quantifying both the PiCDPK1 and PiRhoGDI1 transgenes was designed to span the 3′ end of the Lat52 promoter coding sequence: Lat52 F (5′-CACACACAAAGAGAAGGAGCA-3′). Reverse primers were designed to span the 5′ end of the PiCDPK1 coding sequence (5′-GCAGTGCTGATGGATTCTG-3′) and the 5′ end of the PiRhoGDI1 coding sequence (5′-CCTCTTCTTGCTCAATTCCA-3′). Control primers used for normalization were designed to amplify a small 215bp fragment of the tobacco *L25* coding sequence: L25F (5′-CAAGGCTGTCAAGTCAGGA-3′), L25R (5′-AGGGTGTTGTTGTCCTCAATC-3′).

Supplementary Materials: The following supporting information can be downloaded at: https://www.mdpi.com/article/10.3390/plants11030254/s1, Figure S1, RNA blots showing the developmental profile of PiRhoGDI expression, Figure S2, yeast 2-hybrid assay of PiRhoGDI1 and PiRop1 interaction.

Author Contributions: Conceptualization, A.G.M.; methodology, N.S. and G.M.Y.; validation, N.S. and G.M.Y.; investigation, N.S. and G.M.Y.; writing—original draft preparation, N.S.; writing—review and editing, A.G.M.; visualization, N.S. and G.M.Y.; supervision, A.G.M.; funding acquisition, A.G.M. All authors have read and agreed to the published version of the manuscript.

Funding: This research was funded in part by National Science Foundation Grant DOI 05-43922 awarded to A.G.M. Funding to support microscopy performed by N.S. was also provided by a Vincent Franceschi Graduate Research Fellowship in Plant Biology (WSU).

Institutional Review Board Statement: Not applicable.

Informed Consent Statement: Not applicable.

Data Availability Statement: The data presented in this study are available within the article or Supplementary Materials.

Acknowledgments: We would like to thank Chuck Cody for greenhouse support, Callum McCubbin for technical support, Hans-Henning Kunz for providing the pGreenII 0179 vector, and the Franceschi Microscopy and Imaging Center at Washington State University (https://sbs.wsu.edu/facilities/franceschi-microscopy-imaging-center/) (15 January 2022) for technical support with microscopy.

Conflicts of Interest: The authors declare no conflict of interest.

References

1. Gilroy, S.; Swanson, S.J. Tip Growth. *eLS* **2017**, 1–4. [CrossRef]
2. Miller, D.D.; Callaham, D.A.; Gross, D.J.; Hepler, P.K. Free Ca^{2+} gradient in growing pollen tubes of *Lilium*. *J. Cell Sci.* **1992**, *101*, 7–12. [CrossRef]
3. Pierson, E.S.; Miller, D.D.; Callaham, D.A.; Shipley, A.M.; Rivers, B.A.; Cresti, M.; Hepler, P.K. Pollen tube growth 1 s coupled to the extracellular calcium ion flux and the intracellular calcium gradient: Effect of BAPTA-type buffers and hypertonic media. *Plant Cell* **1994**, *6*, 1815–1828.
4. Malho, R.; Trewavas, A.J. Localized apical increases of cytosolic free calcium control pollen tube orientation. *Plant Cell* **1996**, *8*, 1935–1949. [CrossRef]
5. Hepler, P.K. Tip growth in pollen tubes: Calcium leads the way. *Trend Plant Sci.* **1997**, *2*, 79–80. [CrossRef]

6. Messerli, M.; Robinson, K.R. Tip localized Ca^{2+} pulses are coincident with peak pulsatile growth rates in pollen tubes of *Lilium longiflorum*. *J. Cell Sci.* **1997**, *110*, 1269–1278. [CrossRef]
7. Rathore, K.S.; Cork, R.J.; Robinson, K.R. A cytoplasmic gradient of Ca^{2+} is correlated with the growth of lily pollen tubes. *Dev. Biol.* **1991**, *148*, 612–619. [CrossRef]
8. Li, Y.Q.; Zhang, H.Q.; Pierson, E.S.; Huang, F.Y.; Linskens, H.F.; Hepler, P.K.; Cresti, M. Enforced growth-rate fluctuation causes pectin ring formation in the cell wall of *Lilium longiflorum* pollen tubes. *Planta* **1996**, *200*, 41–49. [CrossRef]
9. Zhao, L.-N.; Shen, L.-K.; Zhang, W.-Z.; Zhang, W.; Wang, Y.; Wu, W.-H. Ca^{2+}-dependent protein kinase 11 and 24 modulate the activity of the inward rectifying K+ channels in Arabidopsis pollen tubes. *Plant Cell* **2013**, *25*, 649–661. [CrossRef]
10. Yoon, G.M.; Dowd, P.E.; Gilroy, S.; McCubbin, A.G. Calcium-Dependent Protein Kinase isoforms in Petunia have distinct functions in pollen tube growth, including regulating polarity. *Plant Cell* **2006**, *18*, 867–878. [CrossRef]
11. Myers, C.; Romanowsky, S.M.; Barron, Y.D.; Garg, S.; Azuse, C.L.; Curran, A.; Davis, R.M.; Hatton, J.; Harmon, A.C.; Harper, J.F. Calcium-dependent protein kinases regulate polarized tip growth in pollen tubes. *Plant J.* **2009**, *59*, 528–539. [CrossRef]
12. Di Giorgio, J.A.; Bienert, G.P.; Ayub, N.D.; Yaneff, A.; Barberini, M.L.; Mecchia, M.A.; Amodeo, G.; Soto, G.C.; Muschietti, J.P. Pollen-specific aquaporins NIP4;1 and NIP4;2 are required for pollen development and pollination in *Arabidopsis thaliana*. *Plant Cell* **2016**, *28*, 1053–1077. [CrossRef]
13. Gutermuth, T.; Lassig, R.; Portes, M.-T.; Maierhofer, T.; Romeis, T.; Borst, J.-W.; Hedrich, R.; Feijo, J.A.; Konrad, K.R. Pollen tube growth regulation by free anions depends on the interaction between the anion channel SLAH3 and calcium-dependent protein kinases CPK2 and CPK20. *Plant Cell* **2013**, *25*, 4525–4543. [CrossRef] [PubMed]
14. Gao, Q.-F.; Fei, C.-F.; Dong, J.-Y.; Gu, L.-L.; Wang, Y.-F. Arabidopsis CNGC18 is a Ca^{2+}-permeable channel. *Mol. Plant* **2014**, *7*, 739–743. [CrossRef]
15. Lin, Y.; Yang, Z. Inhibition of pollen tube elongation by microinjected anti-Rop1Ps antibodies suggests a crucial role for Rho type GTPases in the control of tip-growth. *Plant Cell* **1997**, *9*, 1647–1659. [CrossRef] [PubMed]
16. Kost, B.; Lemichez, E.; Spielhofer, P.; Hong, Y.; Tolias, K.; Carpenter, C.; Chua, N.H. Rac homologues and compartmentalized phosphatidylinositol 4,5-bisphosphate act in a common pathway to regulate polar pollen tube growth. *J. Cell Biol.* **1999**, *145*, 317–330. [CrossRef] [PubMed]
17. Li, H.; Lin, Y.; Heath, R.M.; Zhu, M.X.; Yang, Z. Control of pollen tube tip growth by a Rop GTPase–dependent pathway that leads to tip-localized calcium influx. *Plant Cell* **1999**, *11*, 1731–1742. [PubMed]
18. Zheng, Z.-L.; Yang, Z. The Rop GTPase: An emerging signaling switch in plants. *Plant Mol. Biol.* **2000**, *44*, 1–9. [CrossRef] [PubMed]
19. Gu, Y.; Fu, Y.; Dowd, P.; Li, S.; Vernoud, V.; Gilroy, S.; Yang, Z. A Rho family GTPase controls actin dynamics and tip growth via two counteracting downstream pathways in pollen tubes. *J. Cell Biol.* **2005**, *169*, 127–138. [CrossRef]
20. Lee, Y.J.; Szumlanski, A.; Nielsen, E.; Yang, Z. Rho-GTPase-dependent filamentous actin dynamics coordinate vesicle targeting and exocytosis during tip growth. *J. Cell Biol.* **2008**, *181*, 1155–1168. [CrossRef]
21. Zhou, Z.; Shi, H.; Chen, B.; Zhang, R.; Huang, S.; Fun, Y. Arabidopsis RIC1 severs actin filaments at the apex to regulate pollen tube growth. *Plant Cell* **2015**, *27*, 1140–1161. [CrossRef]
22. Chang, F.; Gu, Y.; Ma, H.; Yang, Z. AtPRK2 promotes ROP1 activation via RopGEFs in the control of polarized pollen tube growth. *Mol. Plant* **2013**, *6*, 1187–1201. [CrossRef]
23. Li, E.; Cui, Y.; Ge, F.-R.; Chai, S.; Zhang, W.-T.; Feng, Q.-N.; Jiang, L.; Li, S.; Zhang, Y. AGC1.5 Kinase Phosphorylates RopGEFs to Control Pollen Tube Growth. *Mol. Plant* **2018**, *11*, 1198–1209. [CrossRef]
24. Li, H.; Luo, N.; Wang, W.; Liu, Z.; Chen, J.; Zhao, L.; Tan, L.; Wang, C.; Qin, Y.; Li, C.; et al. The REN4 rheostat dynamically coordinates the apical and lateral domains of Arabidopsis pollen tubes. *Nat. Commun.* **2018**, *9*, 2573. [CrossRef]
25. Zhang, Y.; He, J.; McCormick, S. Two Arabidopsis AGC kinases are critical for the polarized growth of pollen tubes. *Plant J.* **2009**, *58*, 474–484. [CrossRef]
26. Klahre, U.; Becker, C.; Schmitt, A.C.; Kost, B. Nt-RhoGDI2 regulates Rac/Rop signaling and polar cell growth in tobacco pollen tubes. *Plant J.* **2006**, *46*, 1018–1031. [CrossRef] [PubMed]
27. Feng, Q.-N.; Kang, H.; Song, S.-J.; Ge, F.-R.; Zhang, Y.-L.; Li, E.; Li, S.; Zhang, Y. Arabidopsis RhoGDIs are critical for cellular homeostasis of pollen tubes. *Plant Physiol.* **2016**, *170*, 841. [CrossRef] [PubMed]
28. Fauré, J.; Vignais, P.V.; Dagher, M.C. Phosphoinositide-dependent activation of Rho A involves partial opening of the RhoA/Rho-GDI complex. *Eur. J. Biochem.* **1999**, *262*, 879–889. [CrossRef]
29. Garcia-Mata, R.; Boulter, E.; Burridge, K. The 'invisible hand': Regulation of RHO GTPases by RHOGDIs. *Nat. Rev. Mol. Cell Biol.* **2011**, *12*, 493–504. [CrossRef]
30. Mehta, D.; Rahman, A.; Malik, A.B. Protein kinase C signals Rho-guanine nucleotide dissociation inhibitor phosphorylation and Rho activation and regulates the endothelial cell barrier function. *J. Biol. Chem.* **2001**, *276*, 22614–22620. [CrossRef] [PubMed]
31. DerMardirossian, C.; Schnelzer, A.; Bokoch, G.M. Phosphorylation of RhoGDI by Pak1 mediates dissociation of Rac GTPase. *Mol. Cell* **2004**, *15*, 117–127. [CrossRef]
32. Kaothien, P.; Ok, S.H.; Shuai, B.; Wengier, D.; Cotter, R.; Kelley, D.; Kiriakopolos, S.; Muschietti, J.; McCormick, S. Kinase partner protein interacts with the LePRK1 and LePRK2 receptor kinases and plays a role in polarized pollen tube growth. *Plant J.* **2005**, *42*, 492–503. [CrossRef]

33. Zhang, Y.; McCormick, S. A distinct mechanism regulating a pollen-specific guanine nucleotide exchange factor for the small GTPase Rop in Arabidopsis thaliana. *Proc. Natl. Acad. Sci. USA* **2007**, *104*, 18830–18835. [CrossRef]
34. Zhu, L.; Chu, L.-C.; Liang, Y.; Zhang, X.-Q.; Chen, L.-Q.; Ye, D. The Arabidopsis CrRLK1L protein kinases BUPS1 and BUPS2 are required for normal growth of pollen tubes in the pistil. *Plant J.* **2018**, *95*, 474–486. [CrossRef]
35. Battey, N.H.; Venis, M.A. Calcium-dependent hydrophobic interaction chromatography. *Meth. Mol. Biol.* **1992**, *11*, 73–80. [CrossRef]
36. Kost, B. Spatial control of Rho (Rac-Rop) signaling in tip-growing plant cells. *Trends Cell Biol.* **2008**, *18*, 119–127. [CrossRef] [PubMed]
37. Twell, D.; Klein, T.M.; Fromm, M.; McCormick, S. Transient expression of chimeric genes delivered into pollen by microprojectile bombardment. *Plant Physiol.* **1989**, *91*, 1270–1274. [CrossRef] [PubMed]
38. Schmidt, G.W.; Delaney, S.K. Stable internal reference genes for normalization of real-time RT-PCR in tobacco (*Nicotiana tabacum*) during development and abiotic stress. *Mol. Genet. Genom.* **2010**, *283*, 233–241. [CrossRef]
39. Klahre, U.; Kost, B. Tobacco RhoGTPase ACTIVATING PROTEIN1 spatially restricts signaling of RAC/Rop to the apex of pollen tubes. *Plant Cell* **2006**, *18*, 3033–3046. [CrossRef]
40. Chen, W.; Gong, P.; Guo, J.; Li, H.; Li, R.; Xing, W.; Yang, Z.; Guan, Y. Glycolysis regulates pollen tube polarity via Rho GTPase signaling. *PLoS Genet.* **2018**, *14*, e1007373. [CrossRef]
41. Gu, Y.; Li, S.; Lord, E.M.; Yang, Z. Members of a novel class of Arabidopsis Rho guanine nucleotide exchange factors control Rho GTPase-dependent polar growth. *Plant Cell* **2006**, *18*, 366–381. [CrossRef]
42. Hwang, J.U.; Gu, Y.; Lee, Y.J.; Yang, Z. Oscillatory ROP GTPase activation leads the oscillatory polarized growth of pollen tubes. *Mol. Biol. Cell* **2005**, *16*, 5385–5399. [CrossRef]
43. Cole, R.A.; Fowler, J.E. Polarized growth: Maintaining focus on the tip. *Curr. Opin. Plant Biol.* **2006**, *9*, 579–588. [CrossRef] [PubMed]
44. Malhó, R.; Read, N.D.; Pais, M.S.; Trewavas, A.J. Role of cytosolic free calcium in the reorientation of pollen tube growth. *Plant J.* **1994**, *5*, 331–341. [CrossRef]
45. Cho, H.J.; Kim, J.T.; Lee, S.J.; Hwang, Y.S.; Park, S.Y.; Kim, B.Y.; Yoo, J.; Hong, K.S.; Min, J.K.; Lee, C.H.; et al. Protein phosphatase 1B dephosphorylates Rho guanine nucleotide dissociation inhibitor 1 and suppresses cancer cell migration and invasion. *Cancer Lett.* **2018**, *417*, 141–151. [CrossRef]
46. Foissner, I.; Grolig, F.; Obermeyer, G. Reversible protein phosphorylation regulates the dynamic organization of the pollen tube cytoskeleton: Effects of calyculin A and okadaic acid. *Protoplasma* **2002**, *220*, 1–15. [CrossRef] [PubMed]
47. Malhó, R.; Read, N.D.; Trewavas, A.J.; Pais, M.S. Calcium channel activity during pollen tube growth and reorientation. *Plant Cell* **1995**, *7*, 1173–1184. [CrossRef]
48. Dutta, R.; Robinson, K.R. Identification and characterization of stretch-activated ion channels in pollen protoplasts. *Plant Physiol.* **2004**, *135*, 1398–1406. [CrossRef]
49. Hamilton, E.S.; Jensen, G.S.; Maksaev, G.; Katims, A.; Sherp, A.M.; Haswell, E.S. Mechano-sensitive channel MSL8 regulates osmotic forces during pollen hydration and germination. *Science* **2015**, *350*, 438–441. [CrossRef]
50. Hamilton, E.S.; Haswell, E.S. The tension-sensitive ion transport activity of MSL8 is critical for its function in pollen hydration and germination. *Plant Cell Physiol.* **2017**, *58*, 1222–1237. [CrossRef]
51. Lush, W.M.; Grieser, F.; Wolters-Arts, M. Directional guidance of *Nicotiana alata* pollen tubes in vitro and on the stigma. *Plant Physiol.* **1998**, *118*, 733–741. [CrossRef]
52. Yu, Y.; Song, J.; Tian, X.; Zhang, H.; Li, L.; Zhu, H. Arabidopsis PRK6 interacts specifically with AtRopGEF8/12 and induces depolarized growth of pollen tubes when overexpressed. *Sci. China Life Sci.* **2018**, *61*, 100–112. [CrossRef]
53. Ménesi, D.; Klement, É.; Ferenc, G.; Fehér, A. The Arabidopsis Rho of Plants GTPase ROP1 Is a Potential Calcium-Dependent Protein Kinase (CDPK) Substrate. *Plants* **2021**, *10*, 2053. [CrossRef]
54. Li, H.; Shen, J.J.; Zheng, Z.L.; Lin, Y.; Yang, Z. The Rop GTPase switch controls multiple developmental processes in Arabidopsis. *Plant Physiol.* **2001**, *126*, 670–684. [CrossRef] [PubMed]
55. Carol, R.J.; Takeda, S.; Linstead, P.; Durrant, M.C.; Kakesova, H.; Derbyshire, P.; Drea, S.; Zarsky, V.; Dolan, L. A RhoGDP dissociation inhibitor spatially regulates growth in root hair cells. *Nature* **2005**, *438*, 1013–1016. [CrossRef] [PubMed]
56. Nakamura, M.; Claes, A.R.; Grebe, T.; Hermkes, R.; Viotti, C.; Ikeda, Y.; Grebe, M. Auxin and ROP GTPase signaling of polar nuclear migration in root epidermal hair cells. *Plant Physiol.* **2018**, *176*, 378–391. [CrossRef]
57. Ge, F.R.; Chai, S.; Li, S.; Zhang, Y. Targeting and signaling of Rho of plants guanosine triphosphatases require synergistic interaction between guanine nucleotide inhibitor and vesicular trafficking. *J. Integr. Plant. Biol.* **2020**, *62*, 1484–1499. [CrossRef]
58. Harper, J.F.; Harmon, A. Plants, symbiosis and parasites: A calcium signaling connection. *Nat. Rev. Mol. Cell. Biol.* **2005**, *6*, 556–566. [CrossRef]
59. Hetherington, A.M.; Brownlee, C. The generation of Ca^{2+} signals in plants. *Ann. Rev. Plant Biol.* **2004**, *55*, 401–427. [CrossRef]
60. Costa, A.; Navazio, L.; Szabo, I. The contribution of organelles to plant intracellular calcium signaling. *J. Exp. Bot.* **2018**, *69*, 4175–4193. [CrossRef]
61. Kudla, J.; Becker, D.; Grill, E.; Hedrich, R.; Hippler, M.; Kummer, U.; Parniske, M.; Romeis, T.; Schumacher, K. Advances and current challenges in calcium signaling. *New Phytol.* **2018**, *218*, 414–431. [CrossRef]

62. Satterlee, J.S.; Sussman, M.R. Unusual membrane-associated protein kinases in higher plants. *J. Membr. Biol.* **1998**, *164*, 205–213. [CrossRef]
63. Cheng, S.H.; Willmann, M.R.; Chen, H.C.; Sheen, J. Calcium signaling through protein kinases. The Arabidopsis calcium-dependent protein kinase gene family. *Plant Physiol.* **2002**, *129*, 469–485. [CrossRef] [PubMed]
64. Ludwig, A.A.; Romeis, T.; Jones, J.D. CDPK-mediated signaling pathways: Specificity and cross-talk. *J. Exp. Bot.* **2004**, *55*, 181–188. [CrossRef] [PubMed]
65. Harper, J.F.; Breton, G.; Harmon, A. Decoding Ca^{2+} signals through plant protein kinases. *Ann. Rev. Plant Biol.* **2004**, *55*, 263–288. [CrossRef]
66. Shi, S.; Li, S.; Asim, M.; Mao, J.; Xu, D.; Ullah, Z.; Liu, G.; Wang, Q.; Liu, H. The Arabidopsis calcium-dependent protein kinases (CDPKs) and their roles in plant growth regulation and abiotic stress responses. *Int. J. Mol. Sci.* **2018**, *19*, 1900. [CrossRef]
67. Singh, A.; Sagar, S.; Biswas, D.K. Calcium dependent protein kinase, a versatile player in plant stress management and development. *Crit. Rev. Plant Sci.* **2017**, *36*, 336–352. [CrossRef]
68. James, P.; Halladay, J.; Craig, E.A. Genomic libraries and a host strain designed for highly efficient two-hybrid selection in yeast. *Genetics* **1996**, *144*, 1425–1436. [CrossRef]
69. Schindelin, J.; Arganda-Carreras, I.; Frise, E.; Kaynig, V.; Longair, M.; Pietzsch, T.; Preibisch, S.; Rueden, C.; Saalfeld, S.; Schmid, B.; et al. Fiji: An open-source platform for biological-image analysis. *Nat. Methods* **2012**, *9*, 676–682. [CrossRef]

plants

MDPI

Article

Deciphering Molecular Mechanisms Involved in Salinity Tolerance in Guar (*Cyamopsis tetragonoloba* (L.) Taub.) Using Transcriptome Analyses

Biswa R. Acharya [1,2], Devinder Sandhu [1,*], Christian Dueñas [2], Jorge F. S. Ferreira [1] and Kulbhushan K. Grover [3,*]

[1] U.S. Salinity Lab (USDA-ARS), 450 W Big Springs Road, Riverside, CA 92507, USA; biswaa@ucr.edu (B.R.A.); Jorge.ferreira@usda.gov (J.F.S.F.)
[2] College of Natural and Agricultural Sciences, University of California Riverside, 900 University Avenue, Riverside, CA 92521, USA; cduen002@ucr.edu
[3] Department of Plant and Environmental Sciences, New Mexico State University, Las Cruces, NM 88003, USA
* Correspondence: devinder.sandhu@ars.usda.gov (D.S.); kgrover@nmsu.edu (K.K.G.)

Abstract: Guar is a commercially important legume crop known for guar gum. Guar is tolerant to various abiotic stresses, but the mechanisms involved in its salinity tolerance are not well established. This study aimed to understand molecular mechanisms of salinity tolerance in guar. RNA sequencing (RNA-Seq) was employed to study the leaf and root transcriptomes of salt-tolerant (Matador) and salt-sensitive (PI 340261) guar genotypes under control and salinity. Our analyses identified a total of 296,114 unigenes assembled from 527 million clean reads. Transcriptome analysis revealed that the gene expression differences were more pronounced between salinity treatments than between genotypes. Differentially expressed genes associated with stress-signaling pathways, transporters, chromatin remodeling, microRNA biogenesis, and translational machinery play critical roles in guar salinity tolerance. Genes associated with several transporter families that were differentially expressed during salinity included ABC, MFS, GPH, and P-ATPase. Furthermore, genes encoding transcription factors/regulators belonging to several families, including SNF2, C_2H_2, bHLH, C3H, and MYB were differentially expressed in response to salinity. This study revealed the importance of various biological pathways during salinity stress and identified several candidate genes that may be used to develop salt-tolerant guar genotypes that might be suitable for cultivation in marginal soils with moderate to high salinity or using degraded water.

Keywords: guar; gene expression; qRT-PCR; RNA-Seq; salt stress; salt tolerance; stress; transcriptome; salinity

Citation: Acharya, B.R.; Sandhu, D.; Dueñas, C.; Ferreira, J.F.S.; Grover, K.K. Deciphering Molecular Mechanisms Involved in Salinity Tolerance in Guar (*Cyamopsis tetragonoloba* (L.) Taub.) Using Transcriptome Analyses. *Plants* **2022**, *11*, 291. https://doi.org/10.3390/plants11030291

Academic Editors: Milan S. Stankovic, Paula Baptista and Petronia Carillo

Received: 13 December 2021
Accepted: 18 January 2022
Published: 22 January 2022

1. Introduction

Soil salinization is a serious global problem as saline soil severely impacts crop productivity. It has been predicted that problems associated with soil salinity will increase in many parts of the world due to climate change [1]. The effects of soil salinity are aggravated in plants in response to high temperatures due to evapotranspiration, specifically in semiarid and arid regions. Salinity stress affects plants at molecular, biochemical, physiological, morphological, and productivity levels [2]. Although degraded waters negatively affect the productivity of salt-sensitive crops due to their higher salt concentration, they could be a valuable alternative to freshwater to grow salt-tolerant crops.

High concentrations of NaCl in the soil cause a reduction in water potential that in turn leads to reduced availability of water from the soil to the plant, which ultimately induces osmotic stress in plants [3]. Soil ions such as Na^+ and Cl^- enter plants through outer root cells [4]. Then, these ions can be transported to the root xylem and subsequently from roots to shoots. Increasing ions inside plant cells cause an ionic imbalance that leads to immediate osmotic stress followed by ionic toxicity and the production of reactive oxygen

species. A salinity-induced increase in Na^+ in plant cells inhibits the biosyntheses and activities of various metabolic enzymes, induces stomatal closure, and decreases photosynthesis. To prevent the severity of salinity-induced osmotic stress, plants synthesize various compatible solutes and osmoprotectants (betaine, glycine, inositol, mannitol, trehalose, and polyamines) [2,5,6].

The detailed mechanisms by which plants sense salt are not well understood. In plants, salinity stress activates multiple signaling pathways that collectively provide tolerance to salinity [7]. An extracellular salt sensor, monocation-induced $[Ca^{2+}]_i$ increases 1 (MOCA1), senses Na^+ and a few other monovalent cations [8]. Glycosyl inositol phosphorylceramide (GIPC) sphingolipids in the plasma membrane are synthesized by MOCA1. GIPCs can bind monovalent cations, such as Na. It has been proposed that the binding of Na ions to GIPCs causes the depolarization of cell-surface potential that leads to the opening of calcium-influx channels, which increases intracellular Ca^{2+} levels. The salt overly sensitive (SOS) pathway is activated upon the increase in intracellular Ca^{2+} levels. Upon binding with Ca^{2+}, SOS3 interacts with SOS2 and activates its kinase domain [9]. In turn, SOS2 phosphorylates SOS1, which transports Na^+ from inside to outside of the cell [10]. These facts indicate that calcium and SOS signaling pathways play critical roles during salinity stress.

Calcium is a vital secondary messenger in response to salinity stress. The calcium signaling pathway regulates many types of cellular machinery (e.g., transporters) and signaling components (e.g., CIPKs and CBLs) that help in metal uptake regulation and the maintenance of homeostasis of potassium-, magnesium-, and nitrogen-containing homeostasis [11].

Reactive oxygen species (ROS) are secondary messengers in response to various stress signaling pathways, including salinity stress [12]. Excess production of ROS in response to salinity induces oxidative stress that leads to oxidative damage of nucleic acid, proteins, and membrane lipids [13]. Plants also synthesize enzymatic and non-enzymatic antioxidants that protect cellular components and macromolecules from oxidative stress. Enzymatic antioxidants that perform detoxification of ROS, include catalase (CAT), peroxidase (POX), superoxide dismutase (SOD), and enzymes associated with ascorbate (ASC)—glutathione cycle, ASC peroxidase (APX), glutathione reductase (GR), dehydroascorbate reductase (DHAR), and monodehydroascorbate dehydrogenase (MDHAR) [14,15].

Phytohormone signaling pathways play crucial roles in salinity tolerance in plants by regulating development, growth, and adaptation [16]. During salinity stress, plant stress hormones [abscisic acid (ABA), jasmonic acid (JA), salicylic acid (SA), and ethylene] and plant growth hormones [auxin (IAA), gibberellins (GA), and cytokinin] play modulatory roles (positive and negative) with intricate crosstalk that contribute to plant growth adaptation during salinity stress. In response to salinity, differential expression of genes associated with phytohormone biosynthesis, signaling, and transport mechanisms have been reported in different plant species, which could be important determinants for salinity tolerance [17–19].

Membrane transport mechanisms play a vital role in salinity tolerance in plants [20]. Several transporters have been identified in different plants linked to salinity tolerance. For example, proton pumps transport solutes and ions across membranes. Non-selective cation channels are permeable to many monovalent cations, which have been suggested to play roles in an influx of Na^+ across the plasma membrane in root cortical cells [21,22]. Hence, the differential expression of various transporters linked to salinity tolerance is critical, primarily regulated by a specific set of transcription factors.

Transcription factors are key regulators of gene expression in response to various stresses, including salinity stress [23]. Transcription factors regulate the expression of genes that are required for salt sensing, signal transduction, transport, ion homeostasis, and various other genes involved in salinity tolerance [24].

Guar (*Cyamopsis tetragonoloba* (L.) Taub.) is a self-pollinated legume crop mostly grown in resource-deficient conditions in semiarid and arid regions because of its drought

and heat tolerance [25,26]. About 80% of the world guar is produced in Rajasthan, India, as a rain-fed crop from July to early November. The rest is produced the USA, Brazil, South Africa, Malawi, Zaire, Sudan, Australia, and China, with 38% of Indian guar being exported to the US in 2014–2016 (https://agriculture.rajasthan.gov.in/content/dam/agriculture/Rajasthan%20Agricultural%20Competitiveness%20Project/valuechainreport/RACP_VC_Guar.pdf; accessed on 13 January 2022). Recent research efforts focus on the production of guar in the southwest US, which is often affected by high water and soil salinity [27–29].

The endosperm of guar seeds is a rich source of a natural hydrocolloid (galactomannan), popularly known as guar gum. Guar gum is used in various industries, including food, textile, petroleum, natural gas, mining, pharmaceutical, cosmetics, paper, and paint, making guar an important industrial crop [30]. The productivity of guar is negatively affected by salinity [31–33]. Hence, identification and molecular analysis of salt-tolerant genotypes are essential for guar productivity under saline conditions. Transcriptome analysis, combined with phenotypic and physiological characterizations of salt-tolerant vs. salt-sensitive genotypes, will further unveil the importance of different pathways that are critical for salinity tolerance in guar. This understanding may become instrumental in developing new salt-tolerant guar genotypes that could be grown under saline conditions without a significant crop productivity compromise. Successful guar cultivation in the U.S. will reduce the burden of importing guar gum from foreign countries and increase farmers' profitability by efficiently utilizing marginal soils and recycled water for crop cultivation.

A few preliminary studies have been performed to examine the salinity tolerance of different guar genotypes [32–37]. Salinity stress affects guar development, growth, and productivity. Guar seed yield was reduced in response to irrigation-water salinity above 8.8 dS m^{-1}, whereas vegetative growth was reduced above 4.9 dS m^{-1}, with its root system adapted to salinity tolerance [38,39].

Matador is an improved guar cultivar with higher yields than other U.S. guar cultivars due to its prolific branching [27]. A recent field study indicated that the genotype PI 340261 had similar traits as Matador, except for branching [31]. In a previous study, 'Matador' was classified as salt-tolerant and 'PI 340261' as salt-sensitive, based on salt tolerance index (STI) for root length, shoot length, root biomass, shoot biomass, and their tissue Na, and Cl accumulation [31]. This study applied the RNA-Seq approach to study molecular mechanisms of salinity tolerance and salinity-regulated transcriptomes in leaves and roots of the salt-tolerant 'Matador' (genotype '3') and the salt-sensitive 'PI 340261' (genotype '22') under control and salinity conditions.

2. Results

2.1. De Novo Transcript Assembly and Functional Annotation

To understand the molecular mechanism of salinity tolerance of guar at the transcriptome level of the salt-tolerant 'Matador' ('03', hereafter) and salt-sensitive 'PI 340261' ('22', hereafter), a three-factor RNA-Seq experiment was performed with two levels/factors to examine differential gene expression between variables: genotypes (03 and 22), tissue types (root and leaf), and treatment types (control and salt treatment). The experimental samples were named as C03L for Control '03' Leaf, C22L for Control '22' Leaf, T03L for Treatment '03' Leaf, T22L for Treatment '22' Leaf, C03R for Control '03' Root, C22R for Control '22' Root, T03R for Treatment '03' Root, and T22R for Treatment '22' R (Table S1). Our analyses identified a total of 527,407,683 clean reads, consisting of 158 gigabases (Gb) with an average of 6.6 Gb/library (Table S2). A total of 296,167 transcripts ($\geq$200 bp) were identified, with transcript sizes ranging from 200 bp to 19,633 bp, of which 46% had more than 1000 bp. Our data analysis identified a total of 296,114 unigenes, which ranged from 301 bp to 19,363 bp with a mean length of 1494 bp (Figure S1).

To obtain broad functional annotation of all unigenes, seven databases were searched, which revealed substantial sequence similarity in the databases ranging from 90,848 uni-

genes (30.68%) in KO (KEGG ortholog) to 201,592 unigenes (68%) in NR (NCBI non-redundant protein sequences) databases. In addition, our analyses indicated that 228,611 unigenes (77%) were annotated in at least one database, whereas 19,214 (6.4%) unigenes were found to be annotated in all seven databases (Figure S2).

2.2. Differentially Expressed Genes (DEGs) in Response to Salt Stress

To analyze differential gene expression, gene expression levels of all 24 libraries were calculated by mapping reads of each replicate compared to the assembled transcriptome. Of all the reads, 93% were mapped to the assembly (Table S2) with 65,703 DEGs, and 22% of the total identified clusters (296,114) being present at least in one of the comparisons: treatment vs. control, '03' (salt-tolerant) vs. '22' (salt-sensitive), or leaf vs. root (Figure 1 and Supplemental Table S3). The cluster analysis based on gene expression indicated two major groups according to tissue types: root and leaf (Figure 1). Genes of T03R and C03R formed the first subgroup, whereas T22R and C22R formed the second subgroup within the root group. In the leaf group, subgroupings were also based on genotypes, as observed in the root group (Figure 1).

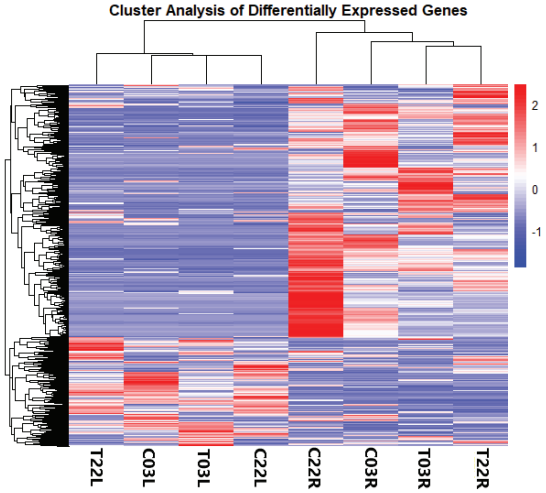

Figure 1. Heatmap-based clustering of differentially expressed genes (DEGs). The heatmap and hierarchical clustering show the status of gene expression and clustering of DEGs (those that were differentially expressed at least in one comparison) across all eight indicated samples in a specific column.

DEGs were identified in treatment vs. control, '03' (salt-tolerant) vs. '22' (salt-sensitive), and leaf vs. root comparisons by gene expression analyses (Figure S3 and Table 1). In treatment vs. control comparisons, 853 (357 upregulated and 496 downregulated), 8283 (1805 upregulated and 6478 downregulated), 1070 (644 upregulated and 426 downregulated), 1006 (511 upregulated and 495 downregulated) DEGs were identified when comparing T03L vs. C03L, T03R vs. C03R, T22L vs. C22L, and T22R vs. C22R, respectively. In salt-tolerant ('03') vs. salt-sensitive ('22') comparisons, 1049, 1355, 1031, and 1727 DEGs were identified in C03L vs. C22L, C03R vs. C22R, T03L vs. T22L, and T03R vs. T22R, respectively. In leaf vs. root comparisons, 41,540, 35,936, 21,383, and 27,383 DEGs were identified in C03L vs. C03R, C22L vs. C22R, T03L vs. T03R, and T22L vs. T22R, respectively (Table 1, Figure S3, and Table S3).

Table 1. Differentially expressed genes (DEGs) identified in different comparisons.

Comparison	Groups	DEGs	Upregulated	Downregulated
Treatment vs. Control	T03L vs. C03L	853	357	496
	T03R vs. C03R	8263	1805	6478
	T22L vs. C22L	1070	644	426
	T22R vs. C22R	1006	511	495
Tolerant vs. Sensitive	C03L vs. C22L	1049	541	508
	C03R vs. C22R	1355	583	772
	T03L vs. T22L	1031	430	601
	T03R vs. T22R	1727	538	1189
Leaf vs. Root	C03L vs. C03R	41,540	10,259	31,281
	C22L vs. C22R	35,936	8978	26,958
	T03L vs. T03R	21,383	8168	13,215
	T22L vs. T22R	27,383	8702	18,681

2.3. Verification of DEGs Using Quantitative Reverse Transcription PCR (qRT-PCR)

RNA-Seq data validation was performed employing the qRT-PCR assay for 33 randomly selected guar gene clusters for different comparisons (Tables S4 and S5). Out of 33 gene clusters, 27 were studied for single comparisons, and three were evaluated for two different comparisons (Figure 2). Comparisons were performed for relative normalized expressions data for all tested genes (clusters) (Figure 2). The general trend of differential expression profiles observed by both qRT-PCR and RNA-Seq methods was similar for most genes (clusters), indicating the validity of the RNA-Seq results.

2.4. Gene Ontology (GO) Enrichment Analysis of DEGs

To examine significant functional enrichment of DEGs in treatment vs. control and salt-tolerant ('03') vs. salt-sensitive ('22') genotypes, GO enrichment analyses were performed for three main categories: biological process (BP), molecular function (MF), and cellular components (CC) (Table S6). In treatment vs. control comparisons, 3, 2, 6, and 7 GO terms were significantly enriched in T03L vs. C03L, T03R vs. C03R, T22L vs. C22L, and T22R vs. C22R, respectively (Table S6). Among these, GTPase activity (GO:0003924) was significantly enriched in the T03R vs. C03R. In salt-tolerant ('03') vs. salt-sensitive ('22') comparisons, two GO terms, including transmembrane transport (GO:0005794), were significantly enriched in T03L vs. T22L (Table S6).

2.5. KEGG Enrichment Analysis of DEGs

KEGG enrichment analyses of DEGs were performed in all pairwise comparisons to identify enriched biological pathways (Supplemental Table S7). In salt treatment vs. control comparisons, 6, 43, 0, and 45 pathways were significantly enriched in T03L vs. C03L, T03R vs. C03R, T22L vs. C22L, and T22R vs. C22R, respectively. Among these, MAPK signaling pathway (ko04011) was enriched in T03L vs. C03L, plant hormone signal transduction (ko04075), and glutathione metabolism (ko00480) pathways were enriched in T03R vs. COR, and brassinosteroid biosynthesis pathway (ko00905) was enriched in T22R vs. C22R. In salt-tolerant (03) vs. salt-sensitive (22) comparisons, 0, 40, 4, and 6 pathways were significantly enriched in C03L vs. C22L, C03R vs. C22R, T03L vs. T22L, and T03R vs. T22R, respectively. Among these pathways, zeatin biosynthesis (ko00908) was enriched in C03R vs. C22R and sphingolipid metabolism (ko00600) in T03L vs. T22L (Table S7).

2.6. DEGs Associated with Stress Pathways

In plants, various pathways contribute to salinity stress signaling. All DEGs were examined to find out their association with phytohormone signaling, calcium signaling, and redox signaling, as these pathways are known to play critical roles in response to salinity stress (Figure 3 and Tables S8–S10).

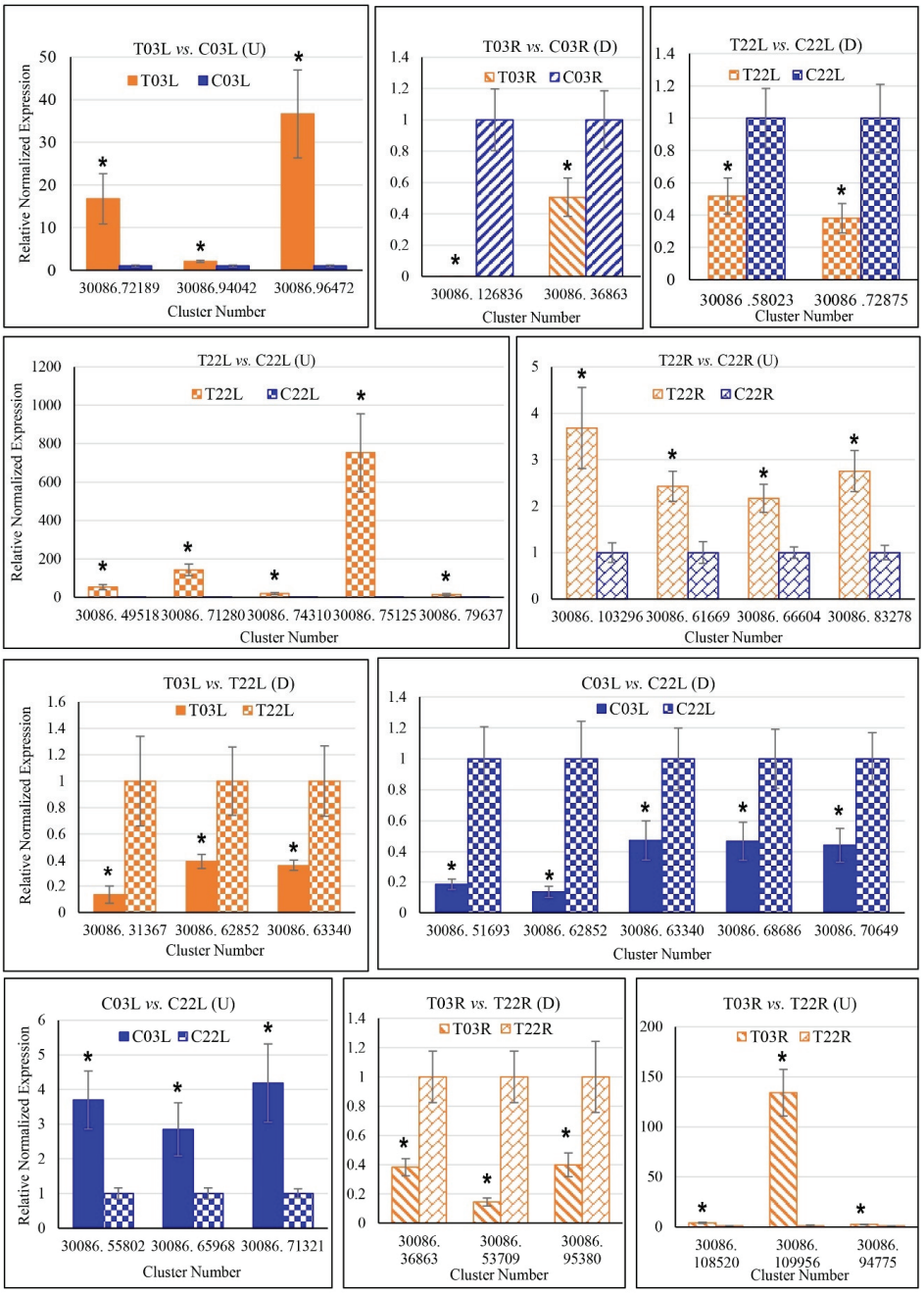

Figure 2. qRT-PCR validation of gene expression observed through RNA-Seq analysis. The *y*-axis indicates relative normalized expression, and the *x*-axis indicates cluster number (gene IDs). Graphs for upregulated (U) and downregulated (D) genes are shown separately. An asterisk (*) indicates a significant difference (t-test at $p \leq 0.05$). T03L, Treatment '03' Leaf; C03L, Control '03' Leaf; T22L, Treatment '22' Leaf; C22L, Control '22' Leaf; T22R, Treatment '22' Root; C22R, Control '22' Root, T03R, treatment '03' Root, and C03R, Control '03' Root.

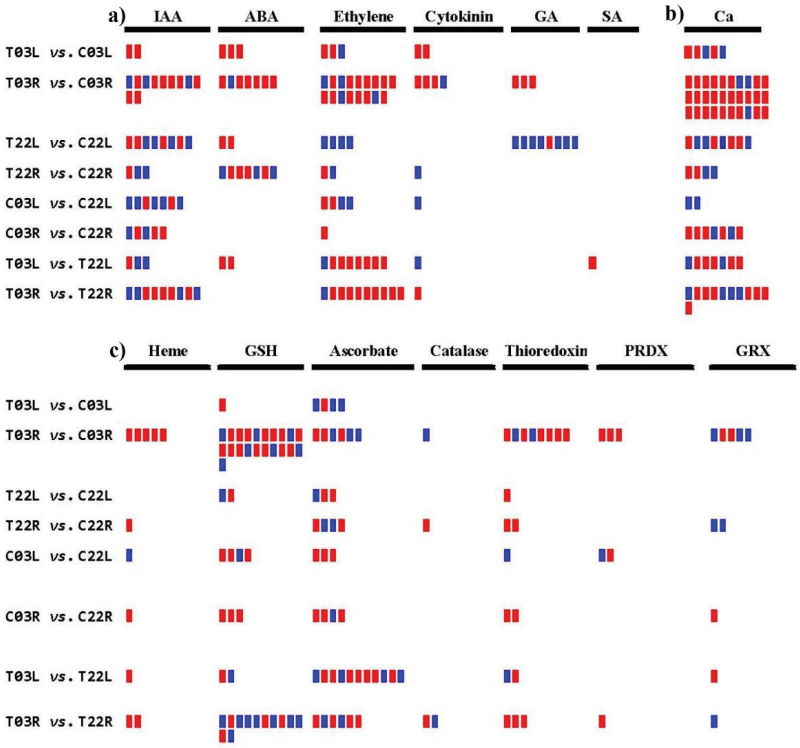

Figure 3. DEGs associated with phytohormone, calcium signaling, and redox pathways. (**a**) DEGs associated with phytohormone pathways (are indicated at the top). (**b**) DEGs associated with calcium signaling (Ca). (**c**) DEGs associated with redox signaling pathways (indicated at the top). The red color indicates downregulated DEGs, and the blue indicates upregulated DEGs. Left-side texts show pairwise comparisons. The top four compared samples indicate treatment vs. control, and the bottom four compared samples indicate salt-sensitive vs. salt-tolerant comparisons. IAA, indole acetic acid (auxin); ABA, abscisic acid; GA, gibberellins; SA, salicylic acid; Ca, calcium; GSH, glutathione; PRDX, peroxiredoxin; GRX, glutaredoxin.

2.6.1. Hormonal Signaling

In treatment vs. control comparisons, 10 DEGs were identified in T03L vs. C03L, two downregulated for IAA, three downregulated for ABA, two downregulated and one upregulated for ethylene, and two downregulated DEGs for cytokinin. In T03R vs. C03R, 11 DEGs were found for IAA (eight downregulated and three upregulated), seven were for ABA (six downregulated and one upregulated), 17 were for ethylene (14 downregulated and 3 upregulated), four were for cytokinin (three downregulated and one upregulated), and three downregulated DEGs were for GA. In T22L vs. C22L, eight DEGs were detected for IAA (four downregulated and four upregulated), two downregulated DEGs for ABA, four upregulated DEGs for ethylene, and eight for GA (one downregulated and seven upregulated). In T22R vs. C22R, 3 DEGs were identified for IAA (one downregulated and two upregulated), seven were for ABA (four downregulated and three upregulated), two were for ethylene (one downregulated and one upregulated), and one upregulated DEG was for cytokinin. When comparing salt-tolerant vs. salt-sensitive groups, 12, 6, 15, and 20 DEGs associated with hormonal signaling were identified in C03L vs. C22L, C03R vs. C22R, T03L vs. T22L, T03R vs. T22R, respectively. We observed that the highest number of DEGs was associated with ethylene signaling, followed by IAA and ABA (Figure 3a and Table S8).

2.6.2. Calcium Signaling

In treatment vs. control comparisons, 5, 30, 8, and 4 DEGs associated with calcium signaling were observed in T03L vs. C03L, T03R vs. C03R, T22L vs. C22L, and T22R vs. C22R, respectively. In salt-tolerant vs. salt-sensitive comparisons, 2, 7, 7, and 11 DEGs related to calcium signaling were identified in C03L vs. C22L, C03R vs. C22R, T03L vs. T22L, and T03R vs. T22R, respectively (Figure 3b and Table S9).

2.6.3. Redox Signaling

In treatment vs. control comparisons, 5, 49, 6, and 10 DEGs associated with redox signaling were identified in T03L vs. C03L, T03R vs. C03R, T22L vs. C22L, and T22R vs. C22R, respectively. In salt-tolerant vs. salt-sensitive comparisons, 11, 11, 17, and 27 DEGs related to redox signaling were identified in C03L vs. C22L, C03R vs. C22R, T03L vs. T22L, and T03R vs. T22R, respectively. Our analysis revealed the highest number of DEGs was associated with GSH, followed by ascorbate and thioredoxin (Figure 3c and Table S10).

2.7. DEGs Associated with Transporters

Transporters are vital for ion distribution and homeostasis throughout the plants. A previous study indicated that in response to salinity stress, guar genotype 03 (Matador) showed a lower accumulation of Na and other ions in comparison to a salt-sensitive genotype 22 (PI 340261), which encouraged us to identify genes encoding transporters [31]. We identified a total of 2764 DEGs encoding transporters in treatment vs. control comparisons and salt-tolerant vs. salt-sensitive comparisons (Figure 4 and Tables S11 and S12).

In treatment vs. control comparisons, 1614 DEGs encoding various families of transporters were identified. In T03L vs. C03L, 48 families of transporters encoded by 168 DEGs were identified, including the monovalent cation: proton antiporter-1 (CPA1) family. In T03R vs. C03R, 1114 DEGs encoding 87 transporter families, including the K^+ uptake permease (KUP) family, were found. In T22L vs. C22L, 228 DEGs encoding 56 transporter families were detected, which included the auxin efflux carrier (AEC) family and the voltage-gated ion channel. In T22R vs. C22 R, 184 DEGs encoding 58 transporter families were found, including the monovalent cation (K^+ or Na^+): proton antiporter-3 (CPA3) family (Tables S11 and S12).

When comparing salt-tolerant vs. salt-sensitive guar cultivars, 1150 DEGs encoding numerous families of transporters were identified. In C03L vs. C22L, 239 DEGs encoding 52 transporter families were detected, including the voltage-gated ion channel (VIC) superfamily and the P-type ATPase superfamily. In C03R vs. C22R, 286 DEGs encoding 55 transporter families were found, including the major intrinsic protein (MIP) family. In T03L vs. T22L, 226 DEGs encoding 47 transporter families were identified, including the ATP-binding cassette (ABC) superfamily. In T03R vs. T22R, 399 DEGs encoding 59 transporter families were recognized, including the ankyrin family transporters (Tables S11 and S12).

2.8. DEGs Associated with Transcription Factors/Regulators

Transcription factors are major regulators of gene expressions during growth, development, and in response to various stresses, including salinity. Thus, we focused on identifying DEGs encoding transcription factors in salt-tolerant '03' and salt-sensitive '22' guar genotypes in response to salinity stress. Our analyses revealed a total of 962 transcription factors/regulators in treatment vs. control and salt-tolerant vs. salt-sensitive comparisons (Tables S13 and S14). In treatment vs. control companions, 69, 394, 69, and 68 transcription factors/regulators were identified in T03L vs. C03L, T03R vs. C03R, T22L vs. C22L, and T22R vs. C22R, respectively. In salt-tolerant vs. salt-sensitive comparisons, 74, 96, 77, and 115 transcription factors/regulators were identified in C03L vs. C22L, C03R vs. C22R, T03L vs. T22L, and T03R vs. T22R, respectively (Tables S13 and S14). Differential expressions of genes encoding transcription factors such as MYB in C03L vs. C22L, GRAS in C03R vs. C22R, bHLH in T03L vs. T22L, and GRAS in T03R vs. C03R were observed (Figure 5 and Table S13).

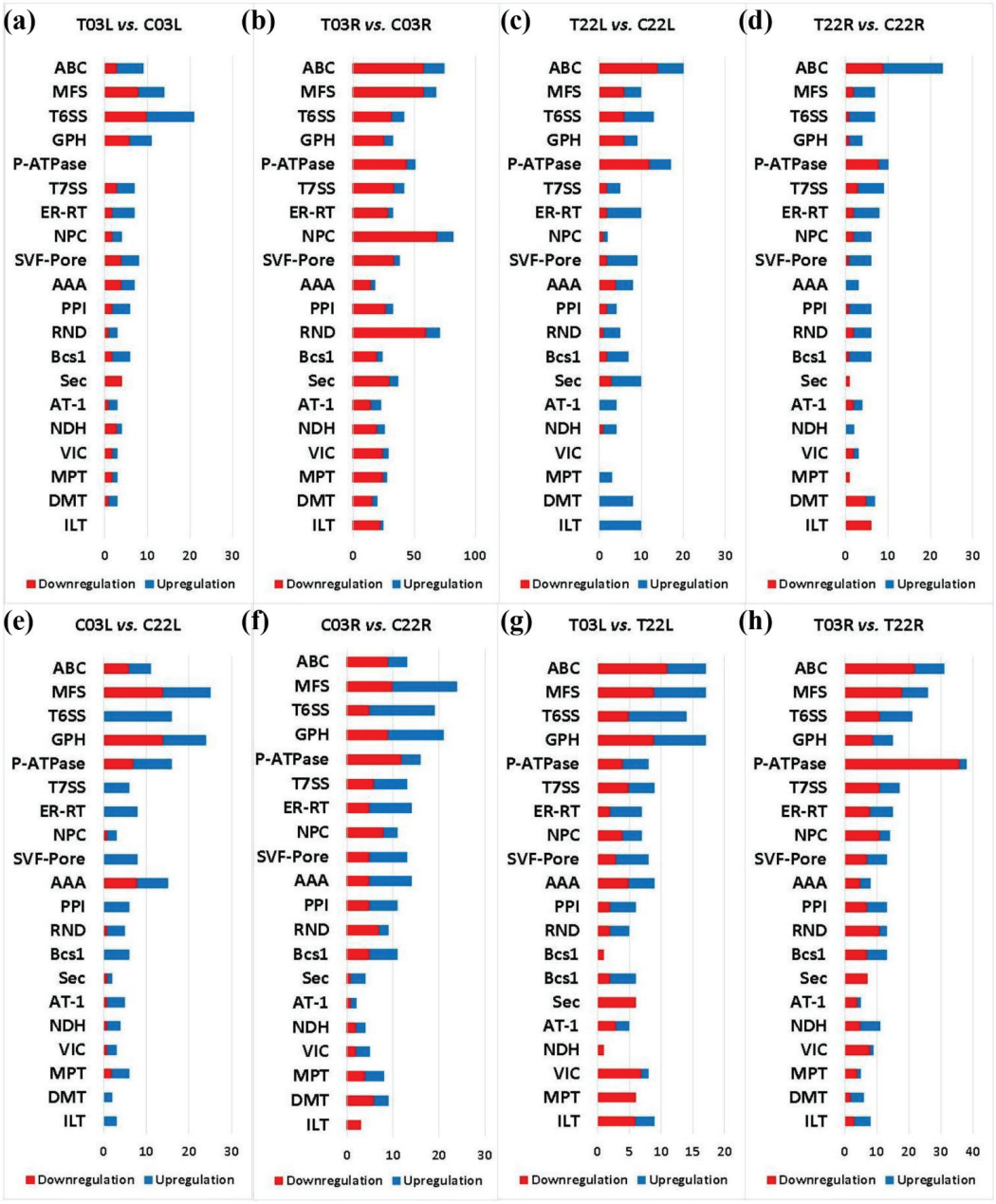

Figure 4. Transporter analysis of DEGs. The *y*-axis indicates transporter superfamilies. The *x*-axis shows gene counts. Salt treatment vs. control comparisons are shown in the top four panels (**a**–**d**). Salt-tolerant vs. salt-sensitive comparisons are shown in the bottom panels (**e**–**h**). The red color indicates downregulated DEGs, and the blue indicates upregulated DEGs. Compared samples are indicated at the top of each panel.

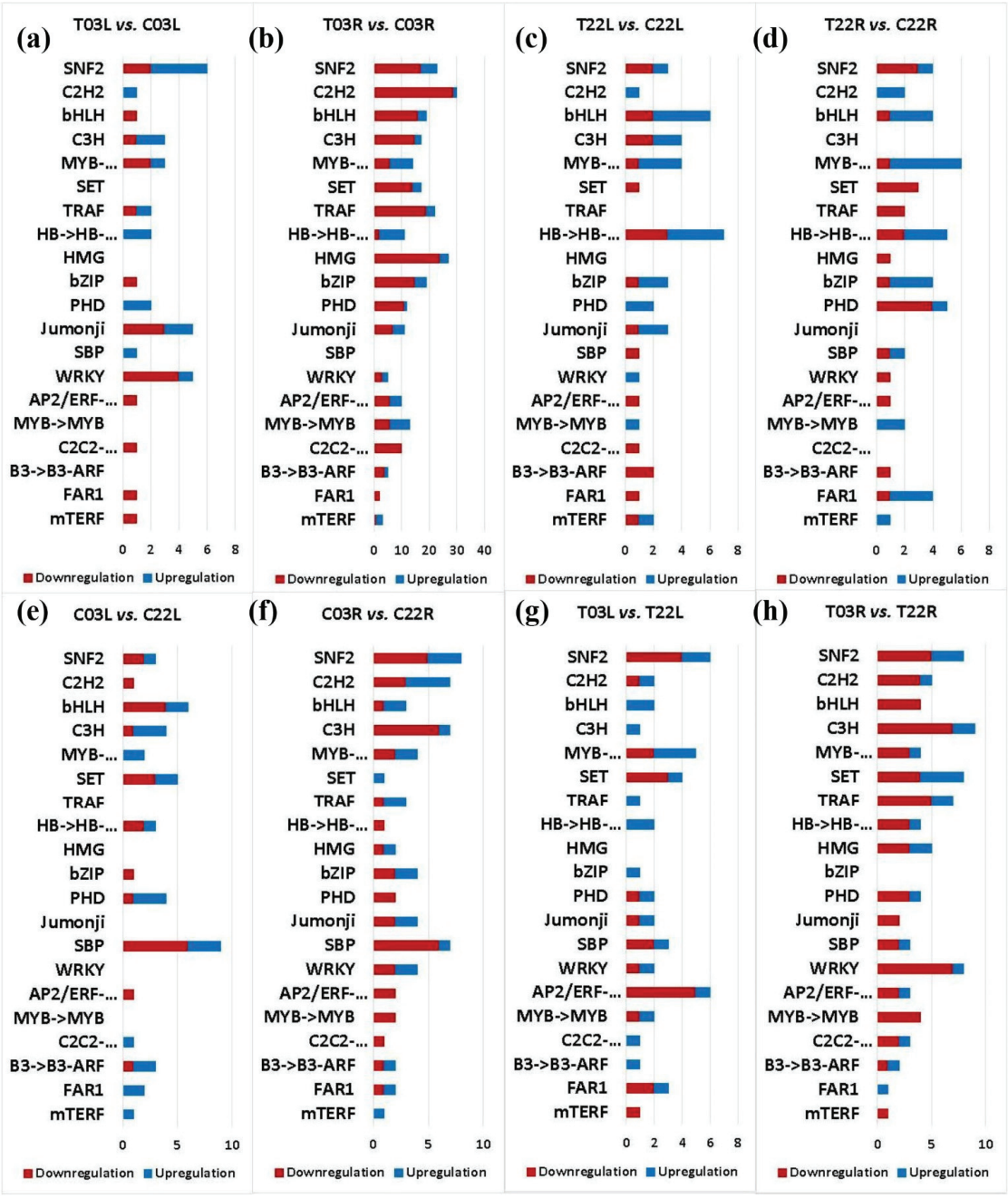

Figure 5. Transcription factor analysis of DEGs. The *y*-axis indicates transcription factor families. The *x*-axis shows gene counts. Salt treatment vs. control comparisons are shown in the top four panels (**a**–**d**). Salt-tolerant vs. salt-sensitive comparisons are shown in the bottom panels (**e**–**h**). The red color indicates downregulated DEGs, and the blue indicates upregulated DEGs. Compared samples are indicated at the top of each panel.

3. Discussion

RNA-Seq is one of the most suitable approaches to study gene expression at the transcriptome level that enables researchers to discover genes that play critical roles in specific tissues, physiological conditions, and metabolic pathways in response to various stresses [26,40–47]. The primary goal of this work was to find molecular mechanisms of salinity tolerance in guar. To achieve this goal, we performed RNA-Seq experiments, using the salt-tolerant guar genotype Matador ('03') and the salt-sensitive genotype PI 340261 ('22'), both previously confirmed for their respective salt tolerance and sensitivity [31].

Comparative transcriptome analyses were performed between '03' and '22' in root and leaf of one-month-old guar plants in response to control irrigation water and saline water with electrical conductivity (EC_{iw}) of 13.65 dS m^{-1} (Table 2). As the guar genome has not been sequenced, guar de novo assembly was constructed from all sequencing libraries. Our analyses revealed a total of 296,114 non-redundant guar unigenes. A few guar transcriptomics studies have been reported previously. RNA-Seq studies of two guar varieties (M-83 and RGC-1066) had reported the identification of 62,146 unigenes for the leaf tissue [40] and 102,479 unigenes for the root tissue [43]. Other guar studies focusing under different environmental conditions revealed 48,007 to 85,395 unigenes [41,44,46]. Variation in the number of unigenes observed in different reports could be due to multiple factors including the number of genotypes used, number of tissues used, number of treatments used, developmental stage of the tissues used, the quality of RNA, the quality of RNA-Seq data, and the stringency used for data analyses.

Table 2. Salt ion composition of control and saline irrigation water treatments. Water pH = 7.4.

	EC_{iw}	Ion Concentration in $Mmol_c$ L^{-1}								
Treatment	dS m^{-1}	NO_3^-	SO_4^{2-}	Cl^-	PO_4^{3-}	CO_3H^-	Ca^{2+}	Mg^{2+}	Na^+	K^+
Control	1.46	5.4	1.44	1.41	1.5	4.2	3.35	2.1	1.88	6.6
Saline	13.65	5.4	27.32	128.4	1.5	3.5	29.6	23	106.9	6.6

Functional annotation analyses of our data showed that 77% of all identified unigenes were protein-coding genes, as they were found in at least one database out of the seven public databases (Figure S2). The remaining 23% of unigenes may not have known protein domains and/or some of these could be non-coding RNA genes.

Differential gene expression analyses revealed a higher number of DEGs in treatment vs. control comparisons than salt-tolerant vs. salt-sensitive comparisons, suggesting that expression differences between salt treatment and control were more pronounced than between the two genotypes. In treatment vs. control comparisons, the highest number of DEGs was observed in the T03R vs. C03R (Table 1). Eight times higher DEGs observed in T03R vs. C03R than T22R vs. C22R indicated that the root of '03' was more responsive to salinity than the root of '22', resulting in better salinity tolerance of '03'. Our analyses revealed that a wide variety of genes contributed toward the salinity tolerance of '03' compared to '22', including negative regulators of the SOS signaling pathway, negative regulators of oxidative stress, metabolic enzymes, pathogen defense signaling, hormonal signaling, calcium signaling, redox signaling, transporters, transcription factors, chromatin remodeling factors, microRNA biogenesis, and translational machinery.

Phytohormones play key roles during salinity stress. A maximum number of DEGs for ethylene signaling followed by IAA and ABA signified the higher importance of these three phytohormones in response to salt stress in guar. More DEGs linked with plant hormone signaling were observed in treatment vs. control comparisons than salt-tolerant vs. salt-sensitive comparisons. In treatment vs. control comparisons, a higher number of DEGs associated with phytohormone was observed in roots than leaves in '03'. In contrast, we observed more DEGs associated with phytohormone in leaves than roots in '22'. These findings indicate that the contrasting tissue-specific expression of genes associated with

phytohormone signaling may be one of the contributing factors for differential salinity tolerance abilities of 03 and 22 guar genotypes (Table S8).

A higher number of DEGs associated with calcium signaling was observed in treatment vs. control comparisons than salt-tolerant vs. salt-sensitive comparisons, indicating that induction or suppression of genes involved in calcium signaling is critical during salinity stress in guar (Figure 3). A higher expression level of a gene encoding calcium-dependent protein kinase 26 (CPK26) was observed in T03L compared to C03L and in T03R compared to C03R (Table S9). Overexpression of *Vitis amurensis CPK26* or *Stipa purpurea CIPK26* in Arabidopsis provided tolerance to salinity [48,49]. A higher expression of a gene encoding *CIPK26* in treatment than control in the leaves and roots of '03' demonstrate its positive regulatory role in salinity tolerance in the genotype 03 (Table S3).

Our redox signaling pathway data identified the highest number of DEGs linked with glutathione followed by ascorbate, suggesting the importance of these genes in redox signaling in response to salinity stress (Figure 3 and Table S10). Additionally, DEGs encoding/associated with catalase were observed, suggesting their roles in ROS homeostasis in guar in response to salinity stress. It is known that E3 ubiquitin ligase PQT3 (PARAQUAT TOLERANCE 3) is a negative regulator of oxidative stress. The loss of function or downregulation of this gene protects plants in response to salinity stress by negatively affecting the severity of salinity-induced oxidative stress that protects plants in response to salinity stress [50]. We observed drastic downregulation of a gene encoding E3 ubiquitin ligase PQT3 (cluster-30086.17545) in T03L compared to C03L, but no differential expression was observed in T22L vs. C22L (Table S3). Our findings suggest that the downregulation of guar *E3 ubiquitin ligase PQT3* in genotype '03' may have contributed to higher salinity tolerance in '03' compared to '22'.

The homeostasis of ions including Na^+ and K^+ is critical for salinity tolerance in plants. In response to salinity, guar genotype 03 accumulates less Na in leaves than genotype 22 [31]. A higher number of DEGs encoding unique transporter families was observed in treatment vs. control comparisons than salt-tolerant vs. salt-sensitive comparisons, indicating inducible/repressible expression of various transporters in response to salinity stress in guar (Table S12).

CPA1 (cation/proton antiporter gene 1) has been implicated in the positive regulation of salinity tolerance [51]. We observed upregulation of various genes encoding CPA1 family in '03' compared to '22' in different comparisons: cluster-30086.145590 in T03L vs. C03L, cluster-30086.113349 in T03R vs. C03R, cluster-30086.145593 in C03L vs. C22L, cluster-30086.82459 in C03R vs. C22R, and cluster-30086.145593 in T03 L vs. T22L (Table S11). Additionally, it is also known that guar *SOS1* (*NHX7*) is upregulated in response to salinity [31]. Our findings suggest that genes encoding CPA family members may have contributed to better salinity tolerance in '03' compared to '22'. GIGANTEA is a flowering time controller that negatively regulates salinity tolerance by inhibiting SOS2 protein kinase, an essential component of the SOS-signaling pathway [52]. We observed downregulation of a gene encoding GIGANTEA (cluster-30086.81200) in T03L vs. C03L but not in T22L vs. C22L (Table S3). The downregulation of poplar *GIGANTEA*-like gene expression has been shown to improve salinity tolerance and enhance biomass under salinity [53]. Our findings suggest that the downregulation of a gene encoding GIGANTEA in genotype 03 may have increased salinity tolerance and biomass in salinity conditions.

Potassium homeostasis is necessary during salinity stress indicating that potassium is a determinant factor for salinity tolerance [54]. Genotype 03 (Matador) showed higher K accumulation than genotype 22 (PI 340261) in root tissues [31]. Our transporter analysis revealed a higher expression of a gene encoding a potassium uptake permease (KUP) family protein (cluster-30086.79861) in T03R compared to C03R. In Arabidopsis, KUP family proteins (also known as HAK/KT) play roles in K translocation and transport [55]. Therefore, the gene (cluster-30086.79861) encoding KUP may have contributed to a higher accumulation of K in '03' in response to salinity stress. Higher expression of a gene encoding

SKD1 (protein suppressor of K^+ transport growth defect 1) in T03L compared to C03L indicates that SKD1 contributes to salinity tolerance in the guar genotype 03 [56].

Differential expressions of various genes encoding transporters in treatment vs. control and salt-tolerant vs. salt-sensitive comparisons may have resulted in differential growth responses in guar. Genes encoding important transporters showed differential expression between salinity treatment vs. control or/and salt-tolerant vs. salt-sensitive comparisons, which included genes encoding ABC transporter family, MFS, T6SS, GPH, and P-ATPase (Figure 4). Our analysis indicated upregulation of a gene (cluster-30086.87927) in T03R compared to C03R (Table S11). The gene (cluster-30086.87927) encoding an ABC transporter C family member may have contributed toward salinity tolerance in '03'. The overexpression of an ABC transporter has been shown to provide tolerance to salinity stress [57].

Genes encoding GPH and P-ATPase showed a higher level of differential expressions in salt-tolerant vs. salt-sensitive comparisons compared to treatment vs. control comparisons, suggesting that these transporters may be critical for genotype-specific differences. We observed upregulation of a gene (cluster-30086.114412) encoding an MFS transporter in T03R compared to T22R. Several transporters that belong to the major facilitator superfamily (MFS) are known to play positive roles in salinity tolerance, which suggests that genes encoding MFS transporters may have contributed toward salinity tolerance in guar [58]. This study identified upregulation of a gene (cluster-30086.54118) encoding for a GPH (glycoside–pentoside–hexuronide) transporter in T03L compared to C03L. The GPH transporter is known as a sucrose:H^+ symporter in plants [59,60]. In Arabidopsis, sucrose transporters play positive regulatory roles in salinity tolerance [61]. These facts suggest that genes encoding GPH/sucrose transporters play positive roles and provide tolerance to salinity in guar. The upregulation of a gene encoding P-ATPase (cluster-30086.493) was observed in T03L compared to T22L (Table S11). P-ATPase facilitates Na^+ extrusion in response to salinity which in turn helps maintain ion homeostasis [62]. These examples suggest that various transporters play critical roles in salinity tolerance in guar.

Various transcription factors regulate gene expression in response to salinity stress. Additionally, several proteins modulate transcriptional processes and are known as transcriptional regulators. For instance, multiple proteins (chromatin remodelers) are associated with chromatin remodeling processes that aid in converting the transcriptionally inactive state of chromatin to active. The most prominent genes encoding transcription factors in our study included C_2H_2, bHLH, C3H, and MYB. We identified the upregulation of a gene (cluster-30086.79202) encoding for the C_2H_2-type zinc finger protein in T03L compared to C03L in response salinity (Figure 5 and Table S13). Higher expression of C_2H_2-type zinc finger proteins has been shown to improve salinity tolerance in plants, indicating that genes encoding C_2H_2-type zinc finger proteins may have contributed to better salinity tolerance in genotype 03 compared to 22 [63]. Higher expression of a gene (cluster-30086.34912) encoding a bHLH transcription factor was observed in T03L compared to T22L (Figure 5 and Table S13). Additionally, the higher expression of a gene encoding transcription factor bHLH112 that was observed in T03L compared to C03L suggests its positive role in salinity tolerance [64]. The positive regulatory roles of bHLH transcription factors have been shown in different plants [65]. Our data analysis revealed higher expression of a gene encoding zinc finger C3H domain-containing protein 53 (cluster-30086.92972) in T03R than T22R (Figure 5 and Table S13), suggesting that this gene might be a contributor to salinity tolerance in guar [66]. We observed upregulation of a gene (cluster-30086.34639) encoding an MYB transcription factor in T03R compared to C03R in response to salinity (Figure 5 and Table S13). It is known that MYB transcription factors contribute to salinity tolerance in plants [67]. Transcriptional regulators play essential roles in transcriptional reprogramming during development, physiological and stress responses. The SNF2 protein is a critical component of the chromatin remodeling complex [68]. The involvement of SNF2 has been shown in response to abiotic stress. Our data revealed upregulation of a gene (cluster-30086.108041) encoding SNF2 in T03L compared to C03L, indicating a possible regulatory role of SNF2 in providing salinity tolerance in guar mediated by chromatin

dynamics (Figure 5 and Table S13). Chromatin remodeling factors alter the structure of chromatin and are vital regulators of eukaryotic gene expression. The Arabidopsis chromatin remodeling factors have been shown to play regulatory roles in response to biotic and abiotic stresses in plants [69,70]. Our data showed higher expression of chromatin remodeling 5-like (cluster-30086.80282) in T03R than T22R, suggesting its role in regulating gene expression in response to salinity (Table S3). Our findings indicate both transcription factors and transcription regulators play critical roles in providing salinity tolerance in guar.

MicroRNAs (miRNA) are a class of non-coding RNA that play critical roles in regulating the expression of genes at the post-transcriptional level, which is important for plant growth, development, and adaptation to various biotic and abiotic stresses, including salinity stress [71]. Our data also showed higher expression of a gene encoding serine-/arginine-rich splicing factor RS41-like isoform X2 (cluster-30086.82952) in T03R than T22R. It has been reported that, in addition to pre-mRNA splicing, RS41 is also involved in miRNA biogenesis along with RNA binding protein HOS5 and serine-/arginine-rich splicing factor RS40 [72]. Our findings suggest that higher expression of serine-/arginine-rich splicing factor RS41-like isoform X2 gene (cluster-30086.82952) in '03' may contribute to salinity tolerance via miRNA-mediated regulation in response to salinity in guar.

The differential expression of genes associated with translational machinery has been shown to be involved in salinity tolerance [73]. For example, in Arabidopsis, elongation factor 1-alpha is a positive regulator in response to salinity stress [73]. Our RNA-Seq data showed higher expression of a gene encoding for an elongation factor 1-alpha (cluster-30086.137964) in T03L than T22L, indicating that guar elongation factor 1-alpha may be a contributor for salinity tolerance in guar genotype 03 (Table S3).

4. Materials and Methods

4.1. Plant Material and Salt Treatment

Seeds of a salt-tolerant genotype 03 (Matador, PI 28699) and a salt-sensitive genotype 22 (PI 340261) were sown in lysimeters at the USDA ARS greenhouse (33.973265 latitude, −117.321158 longitude). Plants were watered two times a day with modified half Hoagland's solution for three weeks to provide macronutrients. Then, plants were treated with saline water, while modified half Hoagland's solution was used as a control (Table 2). The salt concentration was increased incrementally in four days to avoid osmotic shock. Root and leaf samples were collected for RNA isolation after 48 h of full salinity treatment.

4.2. RNA Extraction and Transcript Sequencing

Total RNA isolation from root and leaf tissues was performed using TRIzol reagent (Invitrogen, Carlsbad, CA, USA). Nanodrop was used for the preliminary quantitation of total RNA. Subsequently, Agarose gel electrophoresis was performed to examine RNA degradation and any potential contamination. The 2100 Bioanalyzer (Agilent Technologies, Santa Clara, CA, USA) was used to check the integrity and quantitation of all total RNA samples. Poly-T oligo-attached magnetic beads were used to purify mRNA from total RNA. The mRNA samples fragmented using fragmentation buffer were used for first-strand cDNA synthesis using reverse transcriptase and random hexamers. The product of first-strand synthesis (the cDNA-mRNA hybrid) was used as the template for a nick translation reaction [74]. The second-strand synthesis buffer (Illumina, San Diego, CA, USA), dNTPs, RNase H, and *E. coli* polymerase I were used to generate the second strand. AMPure XP beads were used to purify the cDNA. Then, A-tailing, ligation of sequencing adapters, size selection, and PCR enrichment steps were performed. A Qubit 2.0 fluorometer (Life Technologies, Carlsbad, CA, USA) was used to measure library concentration. An Agilent 2100 was used to check insert size using diluted cDNA library samples (1 ng/μL), and qRT-PCR was also performed to quantify library samples. HiSeq platform (Illumina, San Diego, CA, USA) was used for RNA-Seq (Novogene Corp. Inc., Sacramento, CA, USA).

4.3. De Novo Transcriptome Assembly and Functional Annotation

The raw reads were cleaned by removing reads that had adaptor contamination; more than 10 percent uncertain nucleotides or more than 50 percent of the reads constituted low-quality nucleotides (base quality is less than 5). The rest of the analysis was performed using the cleaned reads. The transcriptome assembly was performed using Trinity [75]. The transcriptome was reconstructed by forming contig assemblies, clustering those assemblies into components, constructing complete de Brujin graphs for each component, and then reconciling the de Brujin graphs to reconstruct distinct isoforms for splice transcripts. The final results were outputted in a FASTA file. Seven databases were used for functional gene annotation. These databases consisted of NR (NCBI non-redundant protein sequences), NT (NCBI nucleotide sequences), PFAM (Protein Family), KOG/COG (euKaryotic Orthologous Groups/Cluster of Orthologous Groups of proteins), Swiss-Prot, KEGG (Kyoto Encyclopedia of Genes and Genome) and GO (Gene Ontology).

4.4. Differential Gene Expression Analysis

The cleaned raw reads were mapped onto the assembled transcriptome. The mapping results returned a read count for each transcript. RSEM (1.2.28) was used to map reads back to the transcriptome, quantify the expression levels, and convert them into Fragments per Kilobase of transcript sequence per million base pairs sequenced (FPKM) [76]. The DESeq2 (1.26.0) R package was then used to normalize the read counts and performed a differential expression analysis based on the negative binomial distribution for its estimation model [77]. To control the false discovery rate (FDR), Benjamini and Hochberg's method was used to calculate adjusted *p*-values. The significance threshold for the adjusted *p*-values was set to $\alpha = 0.05$. Genes deemed significantly differentially expressed needed to satisfy both $p_{adj} \leq 0.05$ and $|\log_2(\text{fold change})| \geq 2$.

Once the differentially expressed genes were gathered, Venn diagrams and a heatmap were constructed. The Venn diagrams were made using the "VennDiagram" R package, and the heatmap was constructed using the pheatmap R package (https://cran.r-project.org/web/packages/pheatmap/index.html; accessed on 12 September 2021) using the top 100 most significant genes [78].

4.5. Gene Ontology Annotation and Enrichment Analysis of DEGs

The GOseq (1.32.0) R package was used to perform a Gene Ontology (GO) analysis of the differentially expressed genes [79]. All three GO terminologies (biological processes, cellular component, molecular function) were considered in the GO distribution. Assuming that all genes have the same probability of being chosen within a category, the Wallenius non-central hypergeometric distribution could perform the GO enrichment test. Over-representation of the DEGs was tested with an adjusted *p*-value threshold of $\alpha = 0.05$. The effect size calculation was performed by taking the *p*-value and performing a $-\log_{10}$ transformation.

4.6. KEGG Pathway Enrichment Analysis of DEGs

The Kyoto Encyclopedia of Genes and Genomes, or KEGG (http://www.genome.jp/kegg/; accessed on 11 September 2021), is an accumulation of databases associated with genomes and biological pathways. The hypergeometric distribution was applied to perform a KEGG enrichment test using the clusterProfiler R package [80,81]. To control the false discovery rate across multiple tests, adjusted *p*-values were computed and used when determining significance.

4.7. Functional Analysis and Visualization

Using the built-in "grep" R function, specific keywords were searched for in the NR descriptions of each comparison. Genes with $\log_2$ fold change greater than zero were colored blue, while genes with $\log_2$ fold change lesser than zero were colored red.

4.8. Transporter Analysis

Mappings to Transporter families were obtained from the Transporter Classification Database (https://tcdb.org/; accessed on 23 September 2021). Protein family (PFam) IDs were used to map the genes to their associated families and superfamilies.

4.9. Transcription Factor and Regulator Analyses

To perform transcription factor and regulator analyses, iTAK and HMMER (3.1) were used to perform an hmmerscan and identity families from the Transcription Factor/Regulator Database. If applicable, differentially expressed genes were mapped to their respective families and sub-families [82,83].

4.10. Quantitative Reverse Transcription PCR (qRT-PCR)

Thirty differentially expressed genes (clusters) were randomly selected for qRT-PCR analyses (Table S4). Phytozome portal (v13) was used for BLAST analyses for each gene (cluster) to identify the *Glycine max* gene with the best sequence homology. To identify the intron-exon boundaries of the guar gene, the genomic sequence of *G. max* gene was compared with the corresponding cluster sequence. In most clusters, a minimum of one primer of each pair was designed from two exons flanking an intron (Table S5).

A previously described method was used qRT-PCR assays [17]. For qRT-PCR assays, same RNA samples were used, which were also used for RNA Seq experiments. All RNA samples were treated with DNase I to remove any DNA contaminations according to the manufacturer's instruction (Thermo Scientific, Waltham, MA, USA). Subsequently, the RNA samples were diluted to 5 ng/µL. All qRT-PCR assays were performed in BioRad CFX96 System using iTaqTM Universal SYBR® Green One-Step Kit (Bio-Rad Laboratories, Hercules, CA, USA). Each qRT-PCR reaction was performed in a 10 µL volume containing 5 µL of 2× one-step SYBR® Green Reaction mix, 10 ng total RNA, 0.75 µM each of forward and reverse primers, and 0.125 µL iScriptTM Reverse Transcriptase. The following conditions were used qRT-PCR: 50 °C for 10 min, 95 °C for 1 min, afterward 40 cycles of 95 °C denaturation for 10 s, 57 °C annealing for 30 s, and 68 °C extension for 30 s. RNA samples from three biological replicates and two technical replicates were used for all assays. Guar *Actin 11* (*Act11*), *elongation factor-1 alpha* (*EF-1a*), and *glyceraldehyde-3-phosphate dehydrogenase* (*GAPDH*) were used as reference genes in expression analyses [84].

5. Conclusions

The transcriptomics approach was employed to study molecular mechanisms of salinity tolerance in two contrasting guar genotypes: Matador ('03'), which is salt tolerant, and PI 340261 ('22'), which is salt sensitive. Thousands of DEGs identified in '03' vs. '22' were linked to several biological pathways, including hormonal signaling, calcium signaling, redox signaling, transcriptional regulation, microRNA biogenesis, and post-transcriptional regulation in guar. This study also revealed upregulated expression of a gene belonging to the cation/proton antiporter 1 (CPA1) family that plays a role in Na^+ homeostasis and a gene encoding *KUP* which contributes to K^+ homeostasis in response to salinity. It also appears that the salt-tolerant '03' has a better ability to suppress the expression of genes that function as negative regulators of salinity tolerance in plants (e.gs. *GIGANTEA* and *E3 ubiquitin ligase PQT3*) than '22'. The reverse genetics approach can be employed to examine the biological roles of some promising genes in response to salinity. Positive functional validation data for different genes would be useful to develop salt-tolerant guar genotypes, which could be cultivated in moderately saline soils or with recycled waters of elevated salinity.

Supplementary Materials: The following are available online at https://www.mdpi.com/article/10.3390/plants11030291/s1, Figure S1. Length distribution of guar transcripts and unigenes. Figure S2. Functional annotation data of Guar transcriptome assembly. Figure S3. Venn diagram analysis of differentially expressed genes (DEGs). Table S1: The experimental arrangement shows leaf and root samples from two guar genotypes 03 (Matador) (salt-tolerant) and 22 (PI 340261) (salt-sensitive) subjected to control and salt treatment. Table S2: Summary of the RNA-Seq reads of 24 libraries of guar. Table S3. Expression comparison and gene ontology annotation of DEGs. Different sheets represent different comparisons. Table S4. List of guar genes (clusters) used for expression analyses by qRT-PCR Assays. Table S5. List of primers used for the qRT-PCR analyses. Table S6. Summary for gene ontology (GO) enrichment analysis of DEGs. Table S7. KEGG enrichment analysis of DEGs. Different sheets represent different comparisons. Table S8. DEGs associated with hormonal signaling. Table S9. Differentially expressed genes (DEGs) involved in calcium signaling. Table S10. Differentially expressed genes (DEGs) involved in Redox signaling. Table S11. Differentially expressed genes (DEGs) involved in transport. Table S12. Number of transporter families identified in different comparisons. Table S13. Differentially expressed genes (DEGs) encoding transcription factors/regulators. Table S14. Number of family members of transcription factors/regulators.

Author Contributions: Conceptualization, B.R.A., D.S. and K.K.G.; methodology, B.R.A., C.D. and D.S.; formal analysis, C.D., B.R.A. and D.S.; resources, D.S. and K.K.G.; writing—original draft preparation, B.R.A.; writing—review and editing, D.S., J.F.S.F. and K.K.G.; supervision, D.S. and K.K.G.; project administration, D.S. and K.K.G.; funding acquisition, D.S. and K.K.G. All authors have read and agreed to the published version of the manuscript.

Funding: This research was funded by the United States Department of Agriculture—Agricultural Research Service, National Program 301: Plant Genetic Resources, Genomics, and Genetic Improvement (project number 2036-13210-012-00-D), NIFA-AFRI CAP Grant # 2017-68005-26867, and from the Agriculture Experiment Station of New Mexico State University.

Institutional Review Board Statement: Not applicable.

Informed Consent Statement: Not applicable.

Data Availability Statement: Illumina HiSeq generated RNA-Seq reads are available in NCBI Sequence Read Archive (SRA) for the Bioproject: PRJNA763938 (https://www.ncbi.nlm.nih.gov/sra/PRJNA763938) (Release date: 1 February 2022). Additional datasets supporting this research are included in the paper and as Supplementary Materials.

Acknowledgments: All authors thank Manju V. Pudussery and Andrew Pallete for qTR-PCR analysis.

Conflicts of Interest: The authors declare no conflict of interest. The funders had no role in the design of the study, data collection, analyses, or interpretation, writing of the manuscript, or in the decision to publish the results.

Disclaimer: The use of trade, firm, or corporation names in this publication is for the information and convenience of the reader. Such use does not constitute an official endorsement or approval by the United States Department of Agriculture or the Agricultural Research Service of any product or service to the exclusion of others that may be suitable.

References

1. Hassani, A.; Azapagic, A.; Shokri, N. Global predictions of primary soil salinization under changing climate in the 21st century. *Nat. Commun.* **2021**, *12*, 6663. [CrossRef]
2. Munns, R.; Tester, M. Mechanisms of salinity tolerance. *Annu. Rev. Plant Biol.* **2008**, *59*, 651–681. [CrossRef]
3. Acosta-Motos, J.R.; Ortuño, M.F.; Bernal-Vicente, A.; Diaz-Vivancos, P.; Sanchez-Blanco, M.J.; Hernandez, J.A. Plant responses to salt stress: Adaptive mechanisms. *Agronomy* **2017**, *7*, 18. [CrossRef]
4. Isayenkov, S.V.; Maathuis, F.J.M. Plant salinity stress: Many unanswered questions remain. *Front. Plant Sci.* **2019**, *10*, 80. [CrossRef]
5. van Zelm, E.; Zhang, Y.; Testerink, C. Salt tolerance mechanisms of plants. *Annu. Rev. Plant Biol.* **2020**, *71*, 403–433. [CrossRef] [PubMed]
6. Park, H.J.; Kim, W.Y.; Yun, D.J. A new insight of salt stress signaling in plant. *Mol. Cells* **2016**, *39*, 447–459. [CrossRef]
7. Acharya, B.R.; Sandhu, D.; Ferreira, J.F.S. Physiological, morphological, biochemical, and genetic responses of alfalfa to salinity. In *The Alfalfa Genome*; Yu, L.-X., Kole, C., Eds.; Springer International Publishing: Cham, Switzerland, 2021; pp. 145–157.
8. Jiang, Z.; Zhou, X.; Tao, M.; Yuan, F.; Liu, L.; Wu, F.; Wu, X.; Xiang, Y.; Niu, Y.; Liu, F.; et al. Plant cell-surface GIPC sphingolipids sense salt to trigger Ca^{2+} influx. *Nature* **2019**, *572*, 341–346. [CrossRef]

9. Zhao, C.; William, D.; Sandhu, D. Isolation and characterization of Salt Overly Sensitive family genes in spinach. *Physiol. Plant.* **2021**, *171*, 520–532. [CrossRef] [PubMed]
10. Quintero, F.J.; Martinez-Atienza, J.; Villalta, I.; Jiang, X.; Kim, W.Y.; Ali, Z.; Fujii, H.; Mendoza, I.; Yun, D.J.; Zhu, J.K.; et al. Activation of the plasma membrane Na/H antiporter Salt-Overly-Sensitive 1 (SOS1) by phosphorylation of an auto-inhibitory C-terminal domain. *Proc. Natl. Acad. Sci. USA* **2011**, *108*, 2611–2616. [CrossRef]
11. Manishankar, P.; Wang, N.; Köster, P.; Alatar, A.A.; Kudla, J. Calcium signaling during salt stress and in the regulation of ion homeostasis. *J. Exp. Bot.* **2018**, *69*, 4215–4226. [CrossRef] [PubMed]
12. Ma, L.; Zhang, H.; Sun, L.; Jiao, Y.; Zhang, G.; Miao, C.; Hao, F. NADPH oxidase AtrbohD and AtrbohF function in ROS-dependent regulation of Na^+/K^+ homeostasis in *Arabidopsis* under salt stress. *J. Exp. Bot.* **2011**, *63*, 305–317. [CrossRef] [PubMed]
13. Hasanuzzaman, M.; Bhuyan, M.; Zulfiqar, F.; Raza, A.; Mohsin, S.M.; Mahmud, J.A.; Fujita, M.; Fotopoulos, V. Reactive oxygen species and antioxidant defense in plants under abiotic stress: Revisiting the crucial role of a universal defense regulator. *Antioxidants* **2020**, *9*, 681. [CrossRef] [PubMed]
14. Foyer, C.H.; Noctor, G. Ascorbate and glutathione: The heart of the redox hub. *Plant Physiol.* **2011**, *155*, 2–18. [CrossRef]
15. Gill, S.S.; Tuteja, N. Reactive oxygen species and antioxidant machinery in abiotic stress tolerance in crop plants. *Plant Physiol. Biochem.* **2010**, *48*, 909–930. [CrossRef]
16. Yu, Z.; Duan, X.; Luo, L.; Dai, S.; Ding, Z.; Xia, G. How plant hormones mediate salt stress responses. *Trends Plant Sci.* **2020**, *25*, 1117–1130. [CrossRef]
17. Kaundal, R.; Duhan, N.; Acharya, B.R.; Pudussery, M.V.; Ferreira, J.F.S.; Suarez, D.L.; Sandhu, D. Transcriptional profiling of two contrasting genotypes uncovers molecular mechanisms underlying salt tolerance in alfalfa. *Sci. Rep.* **2021**, *11*, 5210. [CrossRef]
18. Zhao, C.; Sandhu, D.; Ferreira, J.F.S. Transcript analysis of two spinach cultivars reveals the complexity of salt tolerance mechanisms. *ACS Agric. Sci. Technol.* **2021**, *1*, 64–75. [CrossRef]
19. Acharya, B.; Sandhu, D.; Dueñas, C.; Dueñas, M.; Pudussery, M.; Kaundal, A.; Ferreira, J.F.S.; Suarez, D.; Skaggs, T. Morphological, physiological, biochemical, and transcriptome studies reveal the importance of transporters and stress signaling pathways during salinity stress in *Prunus*. *Sci. Rep.* **2021**. [CrossRef]
20. Brini, F.; Masmoudi, K. Ion transporters and abiotic stress tolerance in Plants. *ISRN Mol. Biol.* **2012**, *2012*, 927436. [CrossRef]
21. Apse, M.P.; Blumwald, E. Na^+ transport in plants. *FEBS Lett.* **2007**, *581*, 2247–2254. [CrossRef] [PubMed]
22. Zhang, J.-L.; Flowers, T.J.; Wang, S.-M. Mechanisms of sodium uptake by roots of higher plants. *Plant Soil* **2009**, *326*, 45. [CrossRef]
23. Golldack, D.; Lüking, I.; Yang, O. Plant tolerance to drought and salinity: Stress regulating transcription factors and their functional significance in the cellular transcriptional network. *Plant Cell Rep.* **2011**, *30*, 1383–1391. [CrossRef] [PubMed]
24. Fernando, V.C.D. Major transcription factor families involved in salinity stress tolerance in plants. In *Transcription Factors for Abiotic Stress Tolerance in Plants*; Wani, S.H., Ed.; Academic Press: Cambridge, MA, USA, 2020; pp. 99–109.
25. Hymowitz, T.; Upadhya, M.D. The Chromosome number of *Cyamopsis serrata*. *Schinz. Curr. Sci.* **1963**, *32*, 427–428.
26. Alshameri, A.; Al-Qurainy, F.; Gaafar, A.R.; Khan, S.; Nadeem, M.; Alansi, S. Identification of heat-responsive genes in guar [*Cyamopsis tetragonoloba* (L.) Taub]. *Int. J. Genom.* **2020**, *2020*, 3126592. [CrossRef]
27. Abidi, N.; Liyanage, S.; Auld, D.; Imel, R.K.; Norman, L.; Grover, K.; Angadi, S.; Singla, S.; Trostle, C. Challenges and opportunities for increasing guar production. In *Hydraulic Fracturing Impacts and Technologies*; Uddameri, V., Morse, A., Tindle, K.J., Eds.; CRC Press: Boca Raton, FL, USA, 2015; pp. 207–226.
28. Adams, C.B.; Boote, K.J.; Shrestha, R.; MacMillan, J.; Hinson, P.O.; Trostle, C. Growth stages and developmental patterns of guar. *Agron. J.* **2020**, *112*, 4990–5001. [CrossRef]
29. Singla, S.; Grover, K.; Angadi, S.V.; Schutte, B.; VanLeeuwen, D. Guar stand establishment, physiology, and yield responses to planting date in southern New Mexico. *Agron. J.* **2016**, *108*, 2289–2300. [CrossRef]
30. Sharma, G.; Sharma, S.; Kumar, A.; Al-Muhtaseb, A.H.; Naushad, M.; Ghfar, A.A.; Mola, G.T.; Stadler, F.J. Guar gum and its composites as potential materials for diverse applications: A review. *Carbohydr. Polym.* **2018**, *199*, 534–545. [CrossRef]
31. Sandhu, D.; Pallete, A.; Pudussery, M.V.; Grover, K.K. Contrasting responses of guar genotypes shed light on multiple component traits of salinity tolerance mechanisms. *Agronomy* **2021**, *11*, 1068. [CrossRef]
32. Suthar, J.D.; Rajpar, I.; Ganjegunte, G.K.; Shah, Z.-U.-H. Evaluation of guar (*Cyamopsis tetragonoloba* L.) genotypes performance under different irrigation water salinity levels: Growth parameters and seed yield. *Ind. Crops Prod.* **2018**, *123*, 247–253. [CrossRef]
33. Suthar, J.D.; Rajpar, I.; Ganjegunte, G.K.; Shah, Z.U.H.; Niu, G.; Grover, K. Germination, growth, and ion uptake of 15 Guar accessions under elevated salinity. *Agrosyst. Geosci. Environ.* **2019**, *2*, 1–9. [CrossRef]
34. Teolis, I.; Liu, W.; Peffley, E.B. Salinity effects on seed germination and plant growth of guar. *Crop Sci.* **2009**, *49*, 637–642. [CrossRef]
35. Khator, K.; Mahawar, L.; Shekhawat, G.S. NaCl induced oxidative stress in legume crops of Indian Thar Desert: An insight in the cytoprotective role of HO_1, NO and antioxidants. *Physiol. Mol. Biol. Plants* **2020**, *26*, 51–62. [CrossRef]
36. Rasheed, M.J.Z.; Ahmad, K.; Ashraf, M.; Qurainy, F.A.; Khan, S.; Athar, H.U.R. Screening of diverse local germplasm of guar (*Cyamposis tetragonoloba* (L.) taub) for salt tolerance: A possible approach to utilize salt-affected soils. *Pak. J. Bot.* **2015**, *47*, 1721–1726.
37. Ghaffarian, M.R.; Yadavi, A.; Movahhedi Dehnavi, M.; Dabbagh Mohammadi Nassab, A.; Salehi, M. Improvement of physiological indices and biological yield by intercropping of Kochia (*Kochia scoparia*), Sesbania (*Sesbania aculeata*) and Guar (*Cyamopsis tetragonoliba*) under the salinity stress of irrigation water. *Physiol. Mol. Biol. Plants* **2020**, *26*, 1319–1330. [CrossRef] [PubMed]

38. Francois, L.E.; Donovan, T.J.; Maas, E.V. Salinity effects on emergence, vegetative growth, and seed yield of guar. *Agron. J.* **1990**, *82*, 587–592. [CrossRef]
39. Ashraf, M.Y.; Akhtar, K.; Sarwar, G.; Ashraf, M. Role of the rooting system in salt tolerance potential of different guar accessions. *Agron. Sustain. Dev.* **2005**, *25*, 243–249. [CrossRef]
40. Tanwar, U.K.; Pruthi, V.; Randhawa, G.S. RNA-Seq of guar (*Cyamopsis tetragonoloba*, L. Taub.) leaves: De novo transcriptome assembly, functional annotation and development of genomic resources. *Front. Plant Sci.* **2017**, *8*, 91. [CrossRef]
41. Rawal, H.C.; Kumar, S.; Mithra, S.V.A.; Solanke, A.U.; Nigam, D.; Saxena, S.; Tyagi, A.; Sureshkumar, V.; Yadav, N.R.; Kalia, P.; et al. High quality unigenes and microsatellite markers from tissue specific transcriptome and development of a database in clusterbean (*Cyamopsis tetragonoloba*, L. Taub). *Genes* **2017**, *8*, 313. [CrossRef] [PubMed]
42. Tyagi, A.; Nigam, D.; Mithra, S.V.A.; Solanke, A.U.; Singh, N.K.; Sharma, T.R.; Gaikwad, K. Genome-wide discovery of tissue-specific miRNAs in clusterbean (*Cyamopsis tetragonoloba*) indicates their association with galactomannan biosynthesis. *Plant Biotechnol. J.* **2018**, *16*, 1241–1257. [CrossRef]
43. Thakur, O.; Randhawa, G.S. Identification and characterization of SSR, SNP and InDel molecular markers from RNA-Seq data of guar (*Cyamopsis tetragonoloba*, L. Taub.) roots. *BMC Genom.* **2018**, *19*, 951. [CrossRef]
44. Al-Qurainy, F.; Alshameri, A.; Gaafar, A.-R.; Khan, S.; Nadeem, M.; Alameri, A.A.; Tarroum, M.; Ashraf, M. Comprehensive stress-based de novo transcriptome assembly and annotation of Guar (*Cyamopsis tetragonoloba* (L.) Taub.): An important industrial and forage crop. *Int. J. Genom.* **2019**, *2019*, 7295859. [CrossRef]
45. Alshameri, A.; Al-Qurainy, F.; Gaafar, A.R.; Khan, S.; Nadeem, M.; Alansi, S.; Shaikhaldein, H.O.; Salih, A.M. Identification of differentially expressed drought-responsive genes in guar [*Cyamopsis tetragonoloba* (L.) Taub]. *Int. J. Genom.* **2020**, *2020*, 4147615. [CrossRef]
46. Hu, H.; Wang, H.; Zhang, Y.; Kan, B.; Ding, Y.; Huang, J. Characterization of genes in guar gum biosynthesis based on quantitative RNA-sequencing in guar bean (*Cyamopsis tetragonoloba*). *Sci. Rep.* **2019**, *9*, 10991. [CrossRef]
47. Rajaprakasam, S.; Rahman, H.; Karunagaran, S.; Bapu, K.; Kulandivelu, G.; Kambale, R.; Ramanathan, V.; Muthurajan, R. Comparative transcriptome and metabolome profiling in the maturing seeds of contrasting cluster bean (*Cyamopsis tetragonoloba* L. Taub) cultivars identified key molecular variations leading to increased gum accumulation. *Gene* **2021**, *791*, 145727. [CrossRef] [PubMed]
48. Dubrovina, A.S.; Kiselev, K.V. The role of calcium-dependent protein kinase genes *VaCPK1* and *VaCPK26* in the response of *Vitis amurensis* (in vitro) and *Arabidopsis thaliana* (in vivo) to abiotic Stresses. *Russ. J. Genet.* **2019**, *55*, 319–329. [CrossRef]
49. Zhou, Y.; Sun, X.; Yang, Y.; Li, X.; Cheng, Y.; Yang, Y. Expression of *Stipa purpurea SpCIPK26* in *Arabidopsis thaliana* enhances salt and drought tolerance and regulates abscisic acid signaling. *Int. J. Mol. Sci.* **2016**, *17*, 966. [CrossRef] [PubMed]
50. Luo, C.; Cai, X.T.; Du, J.; Zhao, T.L.; Wang, P.F.; Zhao, P.X.; Liu, R.; Xie, Q.; Cao, X.F.; Xiang, C.B. PARAQUAT TOLERANCE3 is an E3 ligase that switches off activated oxidative response by targeting histone-modifying protein methyltransferase4b. *PLoS Genet.* **2016**, *12*, e1006332. [CrossRef] [PubMed]
51. Ma, Y.C.; Augé, R.M.; Dong, C.; Cheng, Z.M. Increased salt tolerance with overexpression of cation/proton antiporter 1 genes: A meta-analysis. *Plant Biotechnol. J.* **2017**, *15*, 162–173. [CrossRef]
52. Kim, W.Y.; Ali, Z.; Park, H.J.; Park, S.J.; Cha, J.Y.; Perez-Hormaeche, J.; Quintero, F.J.; Shin, G.; Kim, M.R.; Qiang, Z.; et al. Release of SOS2 kinase from sequestration with GIGANTEA determines salt tolerance in *Arabidopsis*. *Nat. Commun.* **2013**, *4*, 1352. [CrossRef]
53. Ke, Q.; Kim, H.S.; Wang, Z.; Ji, C.Y.; Jeong, J.C.; Lee, H.-S.; Choi, Y.-I.; Xu, B.; Deng, X.; Yun, D.-J.; et al. Down-regulation of *GIGANTEA-like* genes increases plant growth and salt stress tolerance in poplar. *Plant Biotechnol. J.* **2017**, *15*, 331–343. [CrossRef] [PubMed]
54. Kumari, S.; Chhillar, H.; Chopra, P.; Khanna, R.R.; Khan, M.I.R. Potassium: A track to develop salinity tolerant plants. *Plant Physiol. Biochem.* **2021**, *167*, 1011–1023. [CrossRef]
55. Ahn, S.J.; Shin, R.; Schachtman, D.P. Expression of *KT/KUP* genes in Arabidopsis and the role of root hairs in K^+ uptake. *Plant Physiol.* **2004**, *134*, 1135–1145. [CrossRef]
56. Xia, Z.; Wei, Y.; Sun, K.; Wu, J.; Wang, Y.; Wu, K. The maize AAA-type protein SKD1 confers enhanced salt and drought stress tolerance in transgenic tobacco by interacting with Lyst-interacting protein 5. *PLoS ONE* **2013**, *8*, e69787. [CrossRef] [PubMed]
57. Kim, D.Y.; Jin, J.Y.; Alejandro, S.; Martinoia, E.; Lee, Y. Overexpression of AtABCG36 improves drought and salt stress resistance in *Arabidopsis*. *Physiol. Plant.* **2010**, *139*, 170–180. [CrossRef]
58. Niño-González, M.; Novo-Uzal, E.; Richardson, D.N.; Barros, P.M.; Duque, P. More transporters, more substrates: The *Arabidopsis* Major Facilitator Superfamily revisited. *Mol. Plant* **2019**, *12*, 1182–1202. [CrossRef] [PubMed]
59. Reinders, A.; Ward, J.M. Functional characterization of the alpha-glucoside transporter Sut1p from *Schizosaccharomyces pombe*, the first fungal homologue of plant sucrose transporters. *Mol. Microbiol.* **2001**, *39*, 445–454. [CrossRef]
60. Schulz, A.; Beyhl, D.; Marten, I.; Wormit, A.; Neuhaus, E.; Poschet, G.; Büttner, M.; Schneider, S.; Sauer, N.; Hedrich, R. Proton-driven sucrose symport and antiport are provided by the vacuolar transporters SUC4 and TMT1/2. *Plant J.* **2011**, *68*, 129–136. [CrossRef]
61. Gong, X.; Liu, M.; Zhang, L.; Ruan, Y.; Ding, R.; Ji, Y.; Zhang, N.; Zhang, S.; Farmer, J.; Wang, C. Arabidopsis *AtSUC2* and *AtSUC4*, encoding sucrose transporters, are required for abiotic stress tolerance in an ABA-dependent pathway. *Physiol. Plant.* **2015**, *153*, 119–136. [CrossRef]

62. Blumwald, E.; Aharon, G.S.; Apse, M.P. Sodium transport in plant cells. *Biochim. Biophys. Acta* **2000**, *1465*, 140–151. [CrossRef]
63. Han, G.; Lu, C.; Guo, J.; Qiao, Z.; Sui, N.; Qiu, N.; Wang, B. C2H2 zinc finger proteins: Master regulators of abiotic stress responses in plants. *Front. Plant Sci.* **2020**, *11*, 115. [CrossRef] [PubMed]
64. Liu, Y.; Ji, X.; Nie, X.; Qu, M.; Zheng, L.; Tan, Z.; Zhao, H.; Huo, L.; Liu, S.; Zhang, B.; et al. Arabidopsis AtbHLH112 regulates the expression of genes involved in abiotic stress tolerance by binding to their E-box and GCG-box motifs. *New Phytol.* **2015**, *207*, 692–709. [CrossRef]
65. Qian, Y.; Zhang, T.; Yu, Y.; Gou, L.; Yang, J.; Xu, J.; Pi, E. Regulatory mechanisms of bHLH transcription factors in plant adaptive responses to various abiotic stresses. *Front. Plant Sci.* **2021**, *12*, 677611. [CrossRef]
66. Han, G.; Qiao, Z.; Li, Y.; Wang, C.; Wang, B. The roles of CCCH zinc-finger proteins in plant abiotic stress tolerance. *Int. J. Mol. Sci.* **2021**, *22*, 8327. [CrossRef]
67. Li, J.; Han, G.; Sun, C.; Sui, N. Research advances of MYB transcription factors in plant stress resistance and breeding. *Plant Signal. Behav.* **2019**, *14*, 1613131. [CrossRef]
68. Thouly, C.; Le Masson, M.; Lai, X.; Carles, C.C.; Vachon, G. Unwinding BRAHMA functions in plants. *Genes* **2020**, *11*, 90. [CrossRef] [PubMed]
69. Yang, R.; Hong, Y.; Ren, Z.; Tang, K.; Zhang, H.; Zhu, J.-K.; Zhao, C. A role for PICKLE in the regulation of cold and salt stress tolerance in Arabidopsis. *Front. Plant Sci.* **2019**, *10*, 900. [CrossRef] [PubMed]
70. Zou, B.; Sun, Q.; Zhang, W.; Ding, Y.; Yang, D.L.; Shi, Z.; Hua, J. The Arabidopsis chromatin-remodeling factor CHR5 regulates plant immune responses and nucleosome occupancy. *Plant Cell Physiol.* **2017**, *58*, 2202–2216. [CrossRef] [PubMed]
71. Xu, T.; Zhang, L.; Yang, Z.; Wei, Y.; Dong, T. Identification and functional characterization of plant miRNA under salt stress shed light on salinity resistance improvement through miRNA manipulation in crops. *Front. Plant Sci.* **2021**, *12*, 665439. [CrossRef]
72. Chen, T.; Cui, P.; Xiong, L. The RNA-binding protein HOS5 and serine/arginine-rich proteins RS40 and RS41 participate in miRNA biogenesis in Arabidopsis. *Nucleic Acids Res.* **2015**, *43*, 8283–8298. [CrossRef]
73. Shin, D.; Moon, S.-J.; Park, S.R.; Kim, B.-G.; Byun, M.-O. Elongation factor 1α from *A. thaliana* functions as molecular chaperone and confers resistance to salt stress in yeast and plants. *Plant Sci.* **2009**, *177*, 156–160. [CrossRef]
74. Synthesis of complementary DNA. *Nat. Methods* **2005**, *2*, 151–152. [CrossRef]
75. Grabherr, M.G.; Haas, B.J.; Yassour, M.; Levin, J.Z.; Thompson, D.A.; Amit, I.; Adiconis, X.; Fan, L.; Raychowdhury, R.; Zeng, Q.; et al. Full-length transcriptome assembly from RNA-Seq data without a reference genome. *Nat. Biotechnol.* **2011**, *29*, 644–652. [CrossRef]
76. Li, B.; Dewey, C.N. RSEM: Accurate transcript quantification from RNA-Seq data with or without a reference genome. *BMC Bioinform.* **2011**, *12*, 323. [CrossRef]
77. Anders, S.; Huber, W. Differential expression analysis for sequence count data. *Genome Biol.* **2010**, *11*, R106. [CrossRef] [PubMed]
78. Chen, H.; Boutros, P.C. VennDiagram: A package for the generation of highly-customizable venn and euler diagrams in R. *BMC Bioinform.* **2011**, *12*, 35. [CrossRef] [PubMed]
79. Young, M.D.; Wakefield, M.J.; Smyth, G.K.; Oshlack, A. Gene ontology analysis for RNA-seq: Accounting for selection bias. *Genome Biol.* **2010**, *11*, R14. [CrossRef]
80. Kanehisa, M.; Araki, M.; Goto, S.; Hattori, M.; Hirakawa, M.; Itoh, M.; Katayama, T.; Kawashima, S.; Okuda, S.; Tokimatsu, T.; et al. KEGG for linking genomes to life and the environment. *Nucleic Acids Res.* **2008**, *36*, D480–D484. [CrossRef]
81. Mao, X.; Cai, T.; Olyarchuk, J.G.; Wei, L. Automated genome annotation and pathway identification using the KEGG Orthology (KO) as a controlled vocabulary. *Bioinformatics* **2005**, *21*, 3787–3793. [CrossRef] [PubMed]
82. Perez-Rodriguez, P.; Riano-Pachon, D.M.; Correa, L.G.; Rensing, S.A.; Kersten, B.; Mueller-Roeber, B. PlnTFDB: Updated content and new features of the plant transcription factor database. *Nucleic Acids Res.* **2010**, *38*, D822–D827. [CrossRef]
83. Jin, J.; Tian, F.; Yang, D.C.; Meng, Y.Q.; Kong, L.; Luo, J.; Gao, G. PlantTFDB 4.0: Toward a central hub for transcription factors and regulatory interactions in plants. *Nucleic Acids Res.* **2017**, *45*, D1040–D1045. [CrossRef]
84. Jaiswal, P.S.; Kaur, N.; Randhawa, G.S. Identification of reference genes for qRT-PCR gene expression studies during seed development and under abiotic stresses in *Cyamopsis tetragonoloba*. *Crop Sci.* **2019**, *59*, 252–265. [CrossRef]

plants

MDPI

Article

D-Tagatose-Based Product Triggers Sweet Immunity and Resistance of Grapevine to Downy Mildew, but Not to Gray Mold Disease

Nikola Mijailovic [1,2], Nicola Richet [1], Sandra Villaume [1], Andrea Nesler [2], Michele Perazzolli [3,4], Essaid Aït Barka [1] and Aziz Aziz [1,*]

[1] Induced Resistance and Plant Bioprotection, USC INRAE 1488, University of Reims, UFR Sciences, CEDEX 02, 51687 Reims, France; nikola.mijailovic@univ-reims.fr (N.M.); nicolas.richet@univ-reims.fr (N.R.); sandra.villaume@univ-reims.fr (S.V.); ea.barka@univ-reims.fr (E.A.B.)
[2] Bi-PA NV, 1840 Londerzeel, Belgium; andrea.nesler@bi-pa.com
[3] Research and Innovation Centre, Fondazione Edmund Mach, Via E. Mach 1, 38098 San Michele all'Adige, Italy; michele.perazzolli@unitn.it
[4] Centre Agriculture, Food and the Environment (C3A), University of Trento, Via E. Mach 1, 38098 San Michele all'Adige, Italy
* Correspondence: aziz.aziz@univ-reims.fr; Tel.: +33-326-918-525

Abstract: The use of natural bio-based compounds becomes an eco-friendly strategy to control plant diseases. Rare sugars would be promising compounds as inducers of plant "sweet immunity". The present study aimed to investigate the induced resistance of grapevine leaves against *Plasmopara viticola* and *Botrytis cinerea* by a rare sugar-based product (IFP48) and its active ingredient D-tagatose (TAG), in order to elucidate molecular mechanism involved in defense-related metabolic regulations before and after pathogen challenge. Data showed that spraying leaves with IFP48 and TAG lead to a significant reduction of downy mildew, but not of gray mold disease. The induced protection against *P. viticola* relies on IFP48's and to a lesser extent TAG's ability to potentiate the activation of salicylic acid- and jasmonic acid/ethylene-responsive genes and stilbene phytoalexin accumulation. Most of defense responses remained upregulated in IFP48-treated plants after infection with *P. viticola*, but inconsistent following challenge with *B. cinerea*. The beneficial effects of IFP48 were associated with an enhanced accumulation of tagatose inside leaf tissues compared to TAG treatment. Meanwhile, the amounts of sugars, glucose, fructose, maltose, galactose and trehalose remained unchanged or decreased in IFP48-treated leaves after *P. viticola* infection, although only a few genes involved in sugar transport and metabolism showed transcriptional regulation. This suggests a contribution of sugar homeostasis to the IFP48-induced sweet immune response and priming plants for enhanced resistance to *P. viticola*, but not to *B. cinerea*.

Keywords: D-tagatose; IFP48; induced resistance; sweet immunity; sugar-enhanced defense; *Plasmopara viticola*; *Botrytis cinerea*; *Vitis vinifera*

Citation: Mijailovic, N.; Richet, N.; Villaume, S.; Nesler, A.; Perazzolli, M.; Aït Barka, E.; Aziz, A. D-Tagatose-Based Product Triggers Sweet Immunity and Resistance of Grapevine to Downy Mildew, but Not to Gray Mold Disease. *Plants* **2022**, *11*, 296. https://doi.org/10.3390/plants11030296

Academic Editors: Milan S. Stankovic, Paula Baptista and Petronia Carillo

Received: 31 December 2021
Accepted: 21 January 2022
Published: 23 January 2022

Publisher's Note: MDPI stays neutral with regard to jurisdictional claims in published maps and institutional affiliations.

1. Introduction

The cultivated grapevine (*Vitis vinifera* L.) is highly susceptible to a large number of economically devastating diseases, including downy mildew, caused by the oomycete *Plasmopora viticola*, and gray mold, caused by the fungus *Botrytis cinerea* [1]. *P. viticola* is an obligate biotroph that invades grapevine through the stomata, forms a long-term feeding relationship and acquires nutrients via haustoria which are formed within mesophyll cells [1]. However, the necrotrophic *B. cinerea* first kills the host cell with toxins and hydrolytic enzymes, and then uses the macerating plant tissues as food [2]. These diseases are mainly controlled by chemical fungicides, which cause negative impacts on human health and environment, as well as the appearance of resistant pathogen strains [3–5]. The

challenge for a sustainable viticulture is to reduce chemical inputs by the implementation of new innovative and eco-friendly strategies aiming at inducing plant resistance and inhibiting pathogen development. In this context, promising outcomes have been achieved using natural bio-based elicitors or resistance inducers of different nature, capable of triggering plant innate immunity [3–11].

Most resistance inducers characterized so far are bio-based compounds containing sugar repeat units [3–11]. They include microbe-associated molecular patterns (MAMPs), derived from fungi, bacteria or oomycetes such as β-glucans, oligochitosaccharides or glycolipids [6–9], and damage-associated molecular patterns (DAMPs) derived from the host cell wall, such as oligogalacturonides from pectin [10], cellodextrins from cellulose [3], or xyloglucans from hemicellulose [11]. Their ability to induce resistance in plants seems to be dependent not only on their backbone structure, but also on plant cultivars, pathogen lifestyle and environmental conditions [3,4,8]. The successfully induced plant resistance depends on the recognition of MAMPs or DAMPs, which trigger a cascade of early responses and a transcriptional reprogramming, characteristic of MAMP-triggered immunity (MTI). Phytohormones, jasmonic acid (JA), ethylene (ET) and salicylic acid (SA) are also produced to different levels depending on the perceived MAMPs/DAMPs, and are also involved in the regulation of MTI to ensure plant resistance to pathogens [12,13].

Increasing attention has been paid to the role of endogenous sugars in mediating plant immune response and counteracting pathogen attack [14–17], resulting in the concept of "sweet immunity" or "sugar-enhanced defense" [14,15]. Sugars are energy sources for both plants and pathogens for which they compete, and sugar transporters are the molecular actors involved in this competition and probably in the fate of the interaction. Sugars also function as signaling molecules to regulate defense gene expression and plant metabolism [16,17]. Another way that sugar signaling could mediate resistance is through modulation of the ability of pathogens to produce effector molecules in the host [18]. Plants also respond to the PAMP signals with induction of hexose/H^+ symporters, that may limit apoplastic sugar accumulation, thus affecting pathogen virulence directly [19]. Plants can use monosaccharide transporters to quickly resorb sugars upon pathogen invasion [20,21]. By using hexose/H^+ symporters, plants may also counteract the SWEET-mediated secretion and thus retrieve apoplastic sugars, causing pathogen starvation [21,22]. It has also been proposed that sugars may function as priming molecules leading to MTI in plants [15,22]. This concept of "sweet priming" predicts specific key roles to sugars in perceiving, mediating and counteracting pathogen attack [15].

In recent years, some rare monosaccharides and their derivatives have shown potential functional and ecological properties in controlling plant pathogens [23–36]. Their availability has been achieved through the implementation of new enzymatic and microbial processes, making their use effective in food and agricultural sectors [25,30]. D-tagatose, as a ketohexose, is among rare sugars found at low concentrations in many foods and generally recognized as safe by the Food and Drug Administration [30]. D-tagatose was shown to inhibit the growth of various plant pathogens, such as *Phytophthora infestans* causing late blight [24], *Oidium violae* causing powdery mildew in tomato [33], *Plasmopara viticola* (downy mildew) and *Erysiphe necator* (powdery mildew) in grapevine [32,33] and *Hyaloperonospora parasitica* (downy mildew) in Chinese cabbage [31]. It has been reported that D-tagatose acted directly on the pathogen by inhibiting essential enzymes leading to impairment of the whole metabolism [31]. In particular, D-tagatose inhibited fructose metabolizing enzymes (for e.g., fructokinase and phosphomannose isomerase) leading to inhibition of glycolysis and cell wall synthesis [31].

Rare sugars can also play a role in fulfilling "sweet immunity" processes and triggering plant defense [15]. It is speculated that after being exogenously applied, some rare sugars could penetrate into plant cells [37], alter the sucrose-to-hexose ratio, differentially influencing glucose [38], fructose [39] and sucrose signaling pathways [40], and thereby inducing plant immune responses [15,30]. Furthermore, exogenous application of rare sugars could be sensed through hexokinase-dependent or -independent pathways [41],

thus producing an elicitor-like effect [42,43]. It is also likely that a coordinated interaction of sugar and hormonal pathways in plants leads to effective induction of defense responses [15]. Although the effectiveness of tagatose against some fungal and oomycete pathogens was reported [25,26,31,35], the molecular mechanisms involved in grapevine protection against downy mildew and gray mold remained to be elucidated.

In this study, we first investigated the ability of foliar applied D-tagatose-based product (IFP48) and pure tagatose (TAG) as active ingredient to protect grapevine leaves against *P. viticola* and *B. cinerea*. We then explored molecular mechanisms underpinning induced protection before and after pathogen challenge. We especially targeted the expression of defense hormonal-responsive genes and the synthesis of stilbene phytoalexins. We further investigated weather IFP48 and TAG could induce change in the expression of genes encoding sugar transporters and vacuolar invertase. The relationship between the efficiency of IFP48 and TAG and the accumulation of D-tagatose, as well as of endogenous sugars in leaf tissues was also assessed before and after *P. viticola* inoculation. We showed that IFP48 triggers sweet immune response and priming plants for enhanced resistance to *P. viticola*, but not to *B. cinerea*. The induced resistance against *P. viticola* relies on the accumulation of tagatose in leaf tissues and the potentiation of SA and JA/ET-dependent responses with the contribution of sugar homeostasis upon pathogen challenge.

2. Results

2.1. IFP48 and TAG Confer Leaf Protection against P. viticola, but Not B. cinerea

The capacity of IFP48 and TAG to protect grapevine leaves was assessed by foliar spraying of both products at 5 g/L, as an optimal concentration previously optimized in the lab conditions. Two days post treatment (dpt), leaves were detached from water-(control), IFP48- and TAG-treated plants, washed with Tween 80 at 0.001%, and infected with *P. viticola* and *B. cinerea*. Disease symptoms were monitored by quantifying sporulation of *P. viticola* at 7 days post inoculation (dpi) and measuring necrotic lesions of *B. cinerea* at 5 dpi and 14 dpi. Data showed that leaves from control plants were heavily colonized by *P. viticola*, while IFP48 and TAG reduced sporulation density by about 50 and 35%, respectively (Figure 1A). However, neither IFP48 nor TAG was able to reduce the severity of gray mold disease (Figure 1B,C). Most leaves developed the same symptoms as the control at both 5 dpi (Figure 1B) and 14 dpi (Figure 1C).

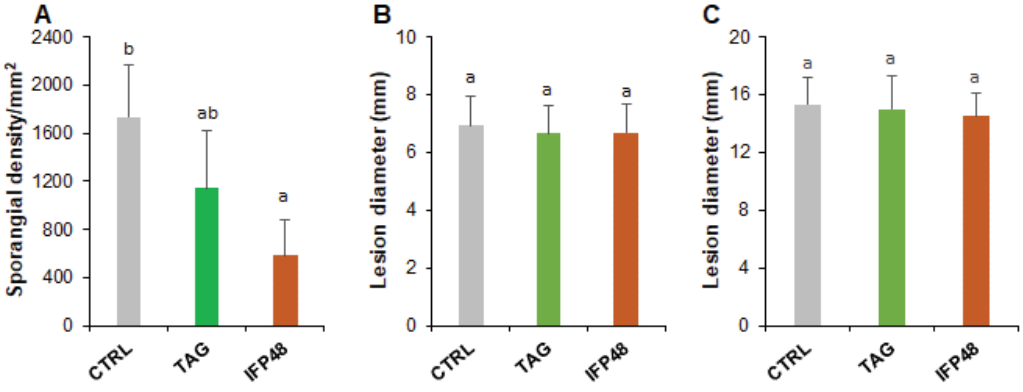

Figure 1. Downy mildew and gray mold diseases in grapevine leaves after treatment with IFP48 and TAG. Plants were sprayed with IFP48 or TAG at 5 g/L or water as control (CTRL). After two days of treatment (dpt), leaves were detached, washed and inoculated with *P. viticola* (**A**) or *B. cinerea* (**B**,**C**), then disease was evaluated by counting the *P. viticola* sporangia at 7 dpi (**A**), and by measuring the *B. cinerea* necrosis size at 5 dpi (**B**) and 14 dpi (**C**). Data are means ± SD from three independent experiments and different letters indicate significant differences according to the One-way ANOVA and Tukey's test ($p \leq 0.05$).

2.2. IFP48 and TAG Potentiate the Expression of SA- and JA/ET-Responsive Genes

The expression of defense genes responsive to SA (*PR1* and *PR2*), JA/ET (*PR3c*, lipoxygenase 9 (*LOX9*), 1-aminocyclopropane carboxylic acid oxidase (*ACO*), ET-response factor (*ERF1*)), and ABA (*NCED2*) was evaluated by RT-qPCR in treated leaves before and after pathogen infection (Figure 2).

A

2dpt	ACO	ERF1	LOX9	PR1	PR2	PR3c	NCED2
Ctrl	0.97	0.82	0.99	2.05	0.94	0.92	0.88
TAG	1.11	3.18	1.16	5.15	1.01	1.97	1.20
IFP48	1.18	2.73	0.99	13.00	1.83	4.79	1.32

B

2dpt+24hpi		ACO	ERF1	LOX9	PR1	PR2	PR3c	NCED2
Ctrl	Ni	0.94	1.76	0.90	0.78	1.90	1.57	0.93
	Pv	1.39	1.03	0.86	3.11	1.95	1.50	1.00
	Bc	1.37	1.30	1.14	0.63	5.10	5.56	0.85
TAG	Ni	1.44	1.56	1.02	1.33	2.15	1.46	1.04
	Pv	1.38	1.58	1.09	1.27	1.57	1.74	1.08
	Bc	1.70	2.61	1.49	2.88	4.78	5.25	0.86
IFP48	Ni	1.35	2.17	0.90	10.44	3.67	3.20	1.27
	Pv	1.77	1.28	1.08	2.52	3.27	4.05	1.03
	Bc	1.46	1.92	1.26	0.42	5.06	5.85	1.05

C

2dpt	HT1	HT3	SWEET2a	SWEET4	GIN1
Ctrl	0.89	0.94	0.96	0.87	3.12
TAG	1.03	1.02	1.22	3.11	0.56
IFP48	0.88	0.87	1.02	2.01	1.07

D

2dpt+24hpi		HT1	HT3	SWEET2a	SWEET4	GIN1
Ctrl	Ni	0.84	0.89	0.89	0.79	0.85
	Pv	1.02	1.20	0.92	2.54	1.24
	Bc	1.23	1.34	0.97	0.90	0.90
TAG	Ni	1.06	1.26	0.76	0.41	1.34
	Pv	0.86	1.27	0.73	0.85	1.31
	Bc	0.80	1.43	0.97	0.84	0.99
IFP48	Ni	1.27	1.34	0.81	0.80	1.48
	Pv	1.13	1.32	1.20	2.08	1.67
	Bc	1.37	1.64	0.88	1.25	0.94

Figure 2. Relative expression of defense- and sugar-related genes in grapevine leaves after treatment with IFP48 and TAG (**A**,**C**) and inoculation with *P. viticola* and *B. cinerea* (**B**,**D**). Plants were treated with IFP48 and TAG at 5 g/L or water (control, Ctrl), 2 days post treatment (dpt) samples were inoculated with *P. viticola*, *B. cinerea* or mock (non-infected, Ni) and collected before (**A**,**C**) and after 24 h of inoculation (2 dpt + 24 hpi) (**B**,**D**). Data are means from three independent experiments. Ctrl, control; Ni, non-infected; Pv, *P. viticola*; Bc, *B. cinerea*. Heatmaps represent changes in transcript expression levels as indicated by the color legend.

The expression of *ERF1*, *PR1* and *PR3c* was upregulated in leaf tissues at 2 dpt with TAG and IFP48 compared to control (Figure 2A). The expression of *PR1* increased by approximately 5- and 13-fold, respectively. Those of *ERF1* and *PR3c* reached 3 and 4-fold, while *PR2* was slightly upregulated by IFP48. However, no consistent changes were observed in the expression of *ACO*, *LOX9* and *NCED2* in response to TAG and IFP48.

The expression of *PR-1* was increased after *P. viticola* inoculation compared to mock inoculated leaves, while it was downregulated after *B. cinerea* inoculation (Figure 2B). The *PR1* expression remained elevated in IFP48-treated plants following *P. viticola* inoculation, but it downregulated after *B. cinerea* inoculation, compared to the inoculated mocks. TAG had only slight effect on the *PR1* level, especially after *B. cinerea* challenge. The expression of *PR2* increased more following infection with *B. cinerea* than with *P. viticola*. Interestingly, *PR2* expression slightly increased in IFP48-treated leaves following *P. viticola* inoculation, but remained constant after *B. cinerea* inoculation. The pathogen infection did not affect *ERF1* expression, except in TAG- and IFP48-treated leaves inoculated with *B. cinerea*. Following *P. viticola* inoculation, the expression of *PR-3c* remained low, while it increased after *B. cinerea* inoculation. However, compared to the inoculated mocks, IFP48 treatment resulted in an enhanced expression of *PR3c* upon *P. viticola* inoculation, while *PR3c* expression remained constant after *B. cinerea* inoculation. No significant change was observed at the transcriptional level of *NCED2* involved in ABA synthesis, in response to both IFP48 and TAG (Figure 2A), and even after pathogen inoculation (Figure 2B).

2.3. IFP48 and TAG Induce Slight Changes in the Expression of Sugar Transport-Related Genes

Considering the importance of sugar resources in the outcome of the plant-pathogen interaction, we investigated the possible contribution of sugar transport and cleavage

processes in grapevine response to TAG and IFP48 treatment before and after pathogen infection. We monitored the expression of two genes which encode high affinity hexose transporters of the plasma membrane (VvHT1 and VvHT3), two genes encoding sugar transporters of the SWEET (Sugar Will be Eventually Exported Transporters) family (Sweet2a and Sweet4), and GIN1 gene which encodes vacuolar invertase 1. Data showed that both VvHT1 and VvHT3 did not show any significant transcriptional regulation after TAG and IFP48 treatment (Figure 2C) and after *P. viticola* or *B. cinerea* inoculation (Figure 2D). The expression of Sweet2a was not affected by both treatments, while that of Sweet4 was upregulated at 2 dpt with both IFP48 and TAG (Figure 2C). At 24 hpi with *B. cinerea*, the expression level of Sweet4 remained low as in water-treated plants (Figure 2D). However, after infection with *P. viticola*, Sweet4 was upregulated. The TAG-treated leaves showed a low expression of Sweet4 after pathogen inoculation, while in IFP48-treated leaves the expression of Sweet4 remained high following *P. viticola* infection, but not *B. cinerea* (Figure 2D). The expression of vacuolar invertase gene GIN1 decreased in response to IFP48, and more drastically following TAG treatment, compared to control (Figure 2C). However, after pathogen challenge GIN expression did not show any relevant modification among treatments (Figure 2D).

2.4. IFP48 and TAG Enhance Stilbene Phytoalexin Accumulation

IFP48 exhibited a stronger effect on the biosynthesis of stilbenes than TAG (Figure 3). This was especially noticeable at 2 dpt, in case of resveratrol (Figure 3A). The amount of resveratrol reached approximately 5.5 μg per gram fresh weight, which was 46 folds higher than control. At 2 dpt, the amount of resveratrol was also slightly induced by TAG, reaching approximately 3.5 folds compared to control (Figure 3A). After *P. viticola* inoculation, the amount of resveratrol was slightly induced in both IFP48- and to a lesser extent in TAG-treated plants at both 1 dpi and 2 dpi (Figure 3B). A slight increase of resveratrol content was also observed after *B. cinerea* inoculation in IFP48-treated leaves (Figure 3C).

Both IFP48 and TAG had almost the same effect on the amount of ε-viniferin (a resveratrol dehydrodimer) as on resveratrol before and after leaf inoculation with *P. viticola*. The amount of ε-viniferin peaked at 2 dpt in response to IFP48, reaching approximately 3 μg per gram fresh (15 folds higher than control treatment) (Figure 3D). As for resveratrol, the early induction of ε-viniferin was followed by a sudden drop at 3 dpt and 4 dpt, while keeping the statistical significance over the control. Following *P. viticola* inoculation, ε-viniferin was slightly higher in IFP48-treated plants compared to water control (Figure 3E). After *B. cinerea* inoculation, a slight increase of ε-viniferin amount was detected at 1 dpi, but not at 2 dpi (Figure 3F).

The content of δ-viniferin increased in IFP48- and TAG-treated plants compared to control before pathogen inoculation (Figure 3G). δ-viniferin was accumulated later compared to resveratrol and ε-viniferin. At 3 and 4 dpt, the amount of δ-viniferin increased in response to IFP48 compared to water and TAG treatments. After pathogen inoculation, the pattern of δ-viniferin was very similar to that of ε-viniferin (Figure 3H,I). The amount of δ-viniferin was higher in IFP48-treated leaves at 2 dpi with *P. viticola*, but no significant change was observed in TAG-treated plants (Figure 3H). In both TAG and IFP48-treated leaves, the level of δ-viniferin was comparable among treatments after infection with *B. cinerea* (Figure 3I).

The amount of piceid, a glycosylated form of resveratrol, increased over time of treatment with TAG and IFP48 (Figure 3J). The level of piceid remained high after pathogen infection and it was higher in IFP48-treated plants compared to water-treated plants at 1 dpi with *P. viticola* (Figure 3K). However, no significant differences were observed between treatments in the amount of piceid after *B. cinerea* inoculation (Figure 3L).

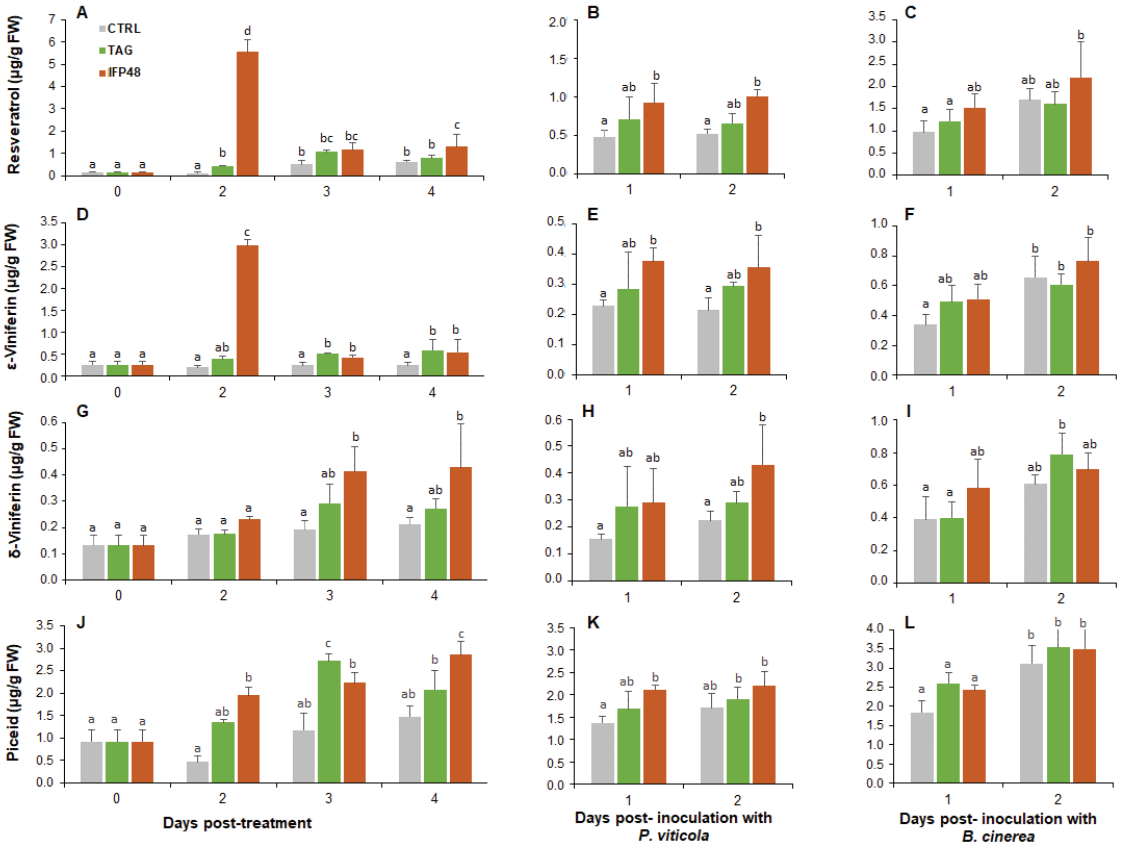

Figure 3. Stilbene accumulation in grapevine leaves after treatment with IFP48 and TAG and inoculation with *P. viticola* and *B. cinerea*. Plants were treated during four days with IFP48 and TAG at 5 g/L, or water (**A**,**D**,**G**,**J**), or treated for 2 days then infected with *P. viticola* (**B**,**E**,**H**,**K**) or *B. cinerea* (**C**,**F**,**I**,**L**). Data are means from three independent experiments and different letters indicate significant differences according to the One-way ANOVA and Tukey's test ($p \leq 0.05$).

2.5. IFP48 and TAG Induce Differential Change in Tagatose and Endogenous Sugar Amounts in Leaf Tissues before and after P. viticola Challenge

The modulation of sugar content in plants is considered to function as a signal to prime immune response. In this study we investigated whether the level of tagatose (derived from IFP48 and TAG) accumulated inside the leaf tissues and the changes in endogenous sugars in association to plant resistance against *P. viticola*. Grapevine leaves accumulated a high and similar amount of D-tagatose at 2 dpt with IFP48 and TAG, reaching approximately 1800 µg/g FW, while control leaves contained less than 1 µg/g FW (Figure 4A). However, at 3 dpt the accumulated D-tagatose level decreased by about 80% in IFP48-treated leaves and by 95% in TAG-treated leaves, compared to D-tagatose quantified at 2 dpt. After *P. viticola* inoculation, the amount of D-tagatose was higher in IFP48-treated plants compared to control plants (Figure 4B).

Plants treated with IFP48 and TAG did not show any significant change in the amounts of endogenous D-glucose, D-ribose, D-fructose, D-mannose and D-galactose (Figure 4C). The amounts of D-maltose and D-trehalose were reduced at 2 dpt in IFP48- and TAG-treated plants compared to control plants. After *P. viticola* inoculation, the amounts of D-glucose, D-fructose and D-maltose decreased, while those of D-galactose and D-trehalose increased, compared to mock plants (Figure 4D). No changes were observed in the levels of D-ribose

and D-mannose after pathogen infection. The amounts of D-glucose, D-fructose and D-maltose remained constant in both TAG and IFP48-treated plants after *P. viticola* inoculation, compared to control-infected plants (Figure 4D). However, D-galactose and D-trehalose contents were reduced by both treatments after pathogen inoculation. The amount of D-trehalose was reduced by approximately 3- and 2-fold in IFP48- and TAG-treated plants in comparison to water-treated plants, respectively (Figure 4D).

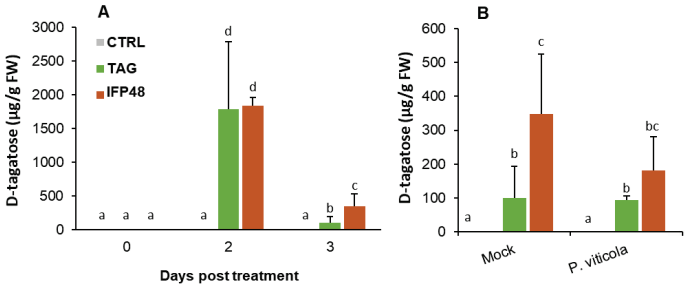

C

2 dpt	D-glucose	D-ribose	D-fructose	D-mannose	D-galactose	D-maltose	D-trehalose
CTRL	4624 a	21 b	5533 a	33 b	948 b	78 c	55 b
TAG	3968 a	24 b	4975 a	29 b	1057 b	36 b	20 a
IFP48	4045 a	27 b	5155 a	28 b	1098 b	37 b	42 ab

D

2 dpt + 1 dpi		D-glucose	D-ribose	D-fructose	D-mannose	D-galactose	D-maltose	D-trehalose
CTRL	Mock	5673 b	17 a	6039 b	19 a	820 a	24 ab	23 a
	P. viticola	4325 a	19 a	4955 a	16 a	995 b	13 a	55 b
TAG	Mock	5065 a	17 a	5491 a	18 a	882 ab	20 ab	31 ab
	P. viticola	4160 a	16 a	5000 a	19 a	844 a	13 a	31 ab
IFP48	Mock	4123 a	17 a	5052 a	17 a	733 a	14 a	30 ab
	P. viticola	3508 a	19 a	4181 a	18 a	805 a	11 a	18 a

Figure 4. Amounts of D-tagatose and endogenous sugars in grapevine leaf tissues after treatment with IFP48 and TAG and inoculation with *P. viticola*. Plants were treated during three days with IFP48 and TAG at 5 g/L, or water (**A**,**C**), or treated for 2 days then infected with *P. viticola* (**B**,**D**). D-tagatose (**A**,**B**), D-glucose, D-ribose, D-fructose, D-mannose, D-galactose, D-maltose and D-trehalose (**C**,**D**) were quantified. Data are means from three independent experiments and different letters indicate significant differences according to the One-way ANOVA and Tukey's test ($p \leq 0.05$).

3. Discussion

3.1. IFP48 Induces Grapevine Resistance against P. viticola, but Not B. cinerea, by Modulating the Expression SA, JA/ET-Responsive Defense Genes and Potentiating Phytoalexin Accumulation

Rare sugars have been shown to reduce severity of various plant diseases and their effectiveness depends on the pathogen lifestyle [25,28–31]. For instance, D-tagatose was more effective against biotroph oomycetes including grapevine downy mildew, than necrotrophs like *B. cinerea* [31–34]. However, molecular mechanisms underlying the efficiency of D-tagatose or D-tagatose-based products against grapevine diseases are not understood. The broader effectiveness of D-tagatose was shown to be linked to its direct action on the pathogen, rather than its capacity to activate plant defense mechanisms [31,32]. In this study, we showed that foliar applications of TAG-based product IFP48 and pure TAG reduce *P. viticola* infection, but not *B. cinerea*, in the susceptible cv. Chardonnay under greenhouse conditions. The TAG-based product (IFP48) was more effective than the TAG itself, suggesting a potential contribution of co-formulants, which would also be related to

the bioavailability or the fate of D-tagatose in plant tissues. Given that grapevine leaves were Tween80-washed before pathogen inoculation, it can be inferred that protective effects triggered by IFP48 and TAG might rely at least in part on the induced grapevine resistance.

Our data provided evidence that the induced protection against *P. viticola* is associated to the IFP48's and to a lesser extent TAG's ability to induce a sweet immune response (before pathogen infection) and to potentiate the activation of various defense-related genes and stilbene phytoalexin accumulation upon pathogen challenge. It is noteworthy that most of defense responses remained highly upregulated in IFP48-treated plants after infection with *P. viticola*, but inconsistent following challenge with *B. cinerea*. The induced resistance to *P. viticola* is correlated to a strong activation of SA- and JA/ET-dependent defense pathways by IFP48 and to a lesser extent by TAG before *P. viticola* inoculation, as emphasized by an upregulation of *PR1* and *PR2* (markers of SA), *ERF1* and *PR3c* genes (markers of JA/ET), and stilbene phytoalexin accumulation in the absence of pathogen infection. In most cases, some SA-dependent defenses and viniferin accumulation were highly upregulated in response to IFP48 compared to TAG treatment, and even maintained to some extent after *P. viticola*, but not *B. cinerea* infection. This indicates that IFP48-mediated resistance against *P. viticola* is at least to some extent dependent on the ability of IFP48 to elicit grapevine defenses, but also to prime the plants for enhanced SA-dependent immune reactions upon *P. viticola* challenge. Data are in agreement with previous research showing that enhanced resistance to downy mildew involves SA- and to some extent JA/ET-responsive immune defenses, such as in the case for glucan-based elicitors [3,5,8,44] or β-amino-butyric acid (BABA) [45]. The interplay between SA and JA/ET signaling pathways seems to play a key role in the effective resistance against *P. viticola* [46]. This is in line with the TAG-induced weaker resistance compared to IFP48, since despite a priming effect of TAG for enhanced expression of *PR1*, the expression of JA/ET responsive genes was not affected. Another assumption would be that TAG could be easily used, in absence of appropriate co-formulant, as a nutrient source by phyllospheric microorganisms as reported in the greenhouse [35], or by the pathogen itself, thus reducing its efficiency against the disease.

It is likely that the ineffectiveness of IFP48 or TAG against *B. cinerea* could also be due to weak induction of JA/ET pathways or to the ability of *B. cinerea* to overcome SA-dependent defenses. Our data are, at least in part in agreement with other reports [36] showing that foliar treatment of tomato with D-allose primed plants for enhanced expression of *PR-1* (SA-pathway), leading to a slight reduction of the gray mold symptoms (by approximately 15%). Although resistance to necrotrophs is generally associated to JA/ET pathways [1,13], which were activated by IFP48 and to a lesser extent by TAG, no significant protection against *B. cinerea* was conferred by both treatments. It has been reported that D-allose treatment of riceinduced systemic acquired resistance (SAR)-like necrotic symptoms and the upregulation of *PR-1* gene [29]. Such plant responses are frequently related to hypersensitive reaction (HR) [44,47], which could even facilitate plant infection by the necrotrophic pathogen like *B. cinerea* [4,48].

Data also showed that *NCED2* gene, involved in ABA biosynthesis, did not respond to TAG or IFP48 treatments either before or after pathogen inoculation. This suggests that TAG- or IFP48-activated immune response is independent on ABA. These results are in contrast to the D-allose effect in rice, which induced a strong and transient accumulation of ABA and upregulation of ABA biosynthetic genes, including *NCED2* [49]. It is likely that D-tagatose uses a different route than D-allose retarding defense induction. Nevertheless, it seems that *NCED2* is rather developmentally regulated, while *NCED1* might be linked to ABA biosynthesis under stress conditions [50]. Thus, further research is needed to understand whether ABA can be involved in the induced resistance against *P. viticola*.

Increasing the synthesis of stilbenes is among the arsenal of defense response implemented by grapevine plants against various pathogens, including *B. cinerea* and *P. viticola* [6,51,52]. IFP48 and TAG induced a significant accumulation of stilbenes, which remained high even after pathogen inoculation. This was especially important in the case of resveratrol dimers, trans-*ε*-viniferin and trans-*δ*-viniferin, which are known to display

antifungal activity and reduce the release and mobility of *P. viticola* zoospores [51–54]. However, upon *B. cinerea* challenge only resveratrol content remained high in the IFP48-treated plants, while trans-piceid amount was unchanged. These results are in line with other research [54] showing that resveratrol and piceid have little or no toxic activity against *P. viticola*, whereas viniferins are highly toxic and can be considered important markers of grapevine resistance to downy mildew.

3.2. IFP48 and TAG Induce Changes in Sugar-Related Gene Expression and Sugar Amounts

IFP48 and TAG treatments did not induce any consistent change in the expression of genes encoding hexose transporters (*VvHT1* and *VvHT3*), even after pathogen inoculation. Among the two *VvSweet* (Sugar Will be Eventually Exported Transporters) genes tested, only *VvSweet4* was slightly upregulated at 2 dpt with IFP48 (and to a lesser extent with TAG) before the pathogen challenge. The enhanced expression of *VvSweet4* was correlated with the increased level of D-tagatose inside the leaf tissues. It has been reported that the expression of *VvSweet4* in grapevine hairy roots mediates increase in sugar levels and facilitates the expression of phenylpropanoid-related genes [55]. Thus, it becomes tempting to assume that the upregulation of *VvSweet4* could play a significant role in sugar homeostasis into the cells, thereby contributing to IFP48-induced resistance against *P. viticola*. *VvSweet4* could also be involved in the accumulation of exogenous D-tagatose into the cells, counteracting the infection structures of *P. viticola* [31]. *VvGIN1*, encoding a vacuolar invertase, was downregulated by IFP48 and to the lesser extent by TAG, especially after pathogen inoculation. The *VvGIN1* regulation seems to correlate with the observed influx of D-tagatose, as abundant hexose, into leaf tissues. Plant invertases are known to hydrolyze sucrose into glucose and fructose moieties [56,57], thus shifting apoplastic sucrose/hexose ratio in favor of hexoses. It is suggested that the newly accumulated D-tagatose, due to IFP48 or TAG treatment, could reduce the expression *VvGIN1*.

Some differences between IFP48 and TAG treatments were also observed regarding the amount of D-tagatose accumulated in leaf tissues, which remained slightly higher in IFP48-treated leaves (3.5-fold) compared to the TAG treatment. This is consistent with the efficiency of IFP48 in inducing resistance against *P. viticola*. Similar results have been reported in a recent study [26], showing higher level (3 to 4-fold) of D-tagatose in cucumber leaves following root treatment with IFP48 compared to pure TAG. This indicates that co-formulant in IFP48 can facilitate D-tagatose influx into leaf tissues or protected it from the consumption by phyllospheric microbes [35], thereby improving grapevine resistance against *P. viticola*. Although co-formulant included in IFP48 is protected by industrial secret and cannot be tested separately, the characterization of IFP48 clarified the mechanism of action of the formulated D-tagatose against *P. viticola*. Further experiments with different D-tagatose formulations are necessary to understand the exact contribution of co-formulants in D-tagatose efficacy against *P. viticola*.

IFP48 and TAG did not induce major changes in sugar content, except the amounts of D-maltose and D-trehalose which showed a significant decrease. This suggests possible triggered sugar-specific singling events resulting in the induction of immune responses. The slight reduction of glucose and fructose content in inoculated leaves of the IFP48- and TAG-treated plants could be linked to the observed downregulation of *VvGIN*. A direct connection between D-tagatose and D-glucose metabolism has been reported in the oomycete *P. infestans* [27]. D-glucose may also be redirected to the phenylpropanoid pathway for the synthesis of phytoalexins, resulting in enhanced resistance [58]. Structural similarity of D-tagatose with common sugars is probably a crucial factor contributing to its effect. D-fructose (a D-tagatose epimer) have been shown to hinder the efficacy of D-tagatose against *P. infestans* [27], *Streptococcus mutans* [59], and grapevine downy mildew [34]. This suggests that D-tagatose can interact with the fructose metabolism in an antagonistic manner. However, IFP48 and TAG did not induce any significant change in the amount of mannose and ribose, probably due to their relative structural dissimilarity. Yet, D-tagatose was reported to interfere with D-mannose metabolism in *Hyaloperonospora*

arabidopsidis [31] and reduce the amount of D-mannose in *P. infestans* [27], leading to the inhibition of both oomycetes. The slight reduction of D-maltose might indicate possible impairment of starch breakdown or to enhanced transglucosidase activity, using maltose as a donor to transfer one glucose moiety to a polysaccharide [60]. The amounts of galactose (monosaccharide) and trehalose (a non-reducing disaccharide composed of two glucose units) were significantly reduced in IFP48- and TAG-treated grapevine plants and after *P. viticola* infection. Although trehalose is considered as an important signal that regulates defense response [61], it may also affect the biology of the pathogen by upregulating the expression of virulence genes, or by activating its metabolism and promoting its development within the host [62]. Galactose may also contribute to the biosynthesis of pectin in the plant primary cell wall [63]. This suggests that the reduction of trehalose and galactose in IFP48-treated plants could contribute to the reduction of downy mildew disease.

In conclusion, foliar application of a D-tagatose-based product can increase grapevine resistance to *P. viticola*, but not to *B. cinerea*. IFP48 can enhance SA- and to some extent JA/ET-dependent immune responses and viniferin accumulation in grapevine leaves upon *P. viticola* infection. IFP48 also improves the accumulation of D-tagatose in the leaf tissues, which seems to interact with endogenous sugar contents, thereby enhancing its eliciting defense activity. Further studies with different D-tagatose formulations are necessary to clarify the contribution of co-formulants in D-tagatose efficacy.

4. Materials and Methods

4.1. Plant Material and Growth Conditions

Cuttings were collected from ten-year-old grapevine plants (*Vitis vinifera* L., cv. Chardonnay) and placed in the cold chamber at 4 °C. After a two-month period, cuttings were surface-sterilized for 4 h with 0.05% cryptonol (8-hydroxyquinoline sulfate), washed with distilled water and right away placed back in the cold chamber for another week in darkness. Afterwards, cuttings were hydrated in the distilled water bath for 16 h at 25 °C and potted in the 5 L pot (three cuttings per pot) containing horticultural soil (Sorexto M4600, Grenoble, France). Pots were placed in a greenhouse (25 °C day/night, 60% relative humidity, and 16 h photoperiod using natural daylight or artificial lamps). Plants were watered with tap water twice per week and grown for 8 weeks.

4.2. Preparation of Rare Sugar and Treatment

D-tagatose-based product (IFP48, wettable powder containing 80% D-tagatose w/w; Lot: 17F-5786) and pure D-tagatose (TAG) were provided by Bi-PA (Biological Products for Agriculture, Londerzeel, Belgium). IFP48 and TAG were diluted in sterile ultra-pure water, filtered through syringe filters with sterile membranes (0.45 µm pore size) (VWR International) and prepared at 5 g/L as an optimal concentration. Plants were treated with IFP48, TAG and water (control) by using the hand sprayer until the homogenous coverage of axial and abaxial leaf sides was reached. Plants were left in the greenhouse for two additional days after treatment before pathogen inoculation.

4.3. Pathogen Growth Conditions and Inoculum Preparation

Plasmopara viticola isolate was purified as a fresh single spore from infected leaves of the susceptible Chardonnay in vitro plantlets [64]. Pathogen was maintained on the leaves of *V. vinifera* cv. Chardonnay cuttings and subcultured every week for the fresh inoculum supply [44]. To obtain sporangia for the inoculum, leaves with oil spot symptoms were put in the dew chamber (100% RH, 25 °C) overnight. After the sporulation was promoted, lesions were washed with sterile distilled water and the concentration of sporangia in the suspension was adjusted to 1×10^5 with Malassez hemocytometer.

Botrytis cinerea strain 630 was grown on potato dextrose agar (PDA) medium for 14 days at 22 °C under continuous light for sporulation. Conidia were scratched and suspended in 10 mL sterile water as described in Aziz et al. [44]. To eliminate the mycelium,

the obtained suspension was filtered through sterile filter paper. Then, concentration of conidia was measured with Malassez hemocytometer and adjusted to 1×10^6 conidia/mL.

4.4. Pathogen Inoculation

At two days post-treatment (dpt) with IFP48, TAG and water, 2 leaves per plant (3rd and 4th leaves from the top) were detached and washed three times with 0.001% Tween80 to remove external IFP48 and TAG, which could directly affect the pathogen growth. Leaves were then placed in glass Petri dishes on wet Whatman paper and inoculated in two different ways: (i) For the purposes of disease severity assessment, leaves were inoculated by placing five 20-µL drops of a fresh suspension of *P. viticola* (1×10^5 sporangia/mL) and three 5-µL drops of conidial suspension of *B. cinerea* (1×10^6 conidia/mL) on their abaxial side. (ii) For the purposes of analyzing the expression of targeted defense responses and sugar accumulation inside the leaf tissues, abaxial side of the leaves was inoculated by spraying 1×10^5 sporangia/mL or 1×10^6 conidia/mL of fresh suspensions of *P. viticola* and *B. cinerea*, respectively, using the hand sprayer. Mock was inoculated by spraying distilled water.

4.5. Disease Severity Assessment

In case of *B. cinerea,* disease severity was measured at 5 and 14 dpi by measuring the diameter of necrotic lesions as described by Aziz et al. [44]. In case of *P. viticola*, disease severity was determined by measuring sporangial density by using leaf discs of 18-mm diameter (10 leaf discs per plant). At 7 dpi leaf discs were randomly pooled in the groups of 5 leaf discs (each group consisted of 5 leaf discs from different plants that underwent the same treatment), placed in a falcon tube 50 mL, and covered with 1 mL sterile distilled water. After 1 h shaking time, suspended sporangia were counted under the light microscope using a Malassez hemocytometer. Each *B. cinerea* and *P. viticola* experiment was performed with 12 leaves (derived from 6 plants) per treatment, and experiments were repeated three times.

4.6. RNA Extraction and Analysis of Gene Expression by RT-qPCR

Sampling was done at zero-, 2-dpt with IFP48, TAG and water, and at 1 dpi and 2 dpi with *P. viticola*, *B. cinerea* or mock inoculation. Total RNA was extracted from 50 mg of leaf powder using PlantRNA (Invitrogen, Thermo Fisher Scientific, Waltham, MA, USA). Complementary DNA was synthesized from 1 µg of total RNA. Reverse transcription was done with Verso cDNA Synthesis Kit (Thermo Fisher Scientific, Inc., Waltham, MA, USA) according to the manufacturer's instructions. Using CFX 96TM Real Time System (Bio-Rad, Marnes-la-Coquette, France) and Absolute qPCR Mix, SYBR Green, ROX (Thermo Fisher Scientific), with qPCR, we assessed the expression profiles of genes markers of SA pathway including pathogenesis related protein-1 (*PR-1*) and 1,3-glucanase (*PR-2*) [48]; JA pathway: 9-lipoxygenase (*LOX9*) [45] and acidic class IV chitinase (*PR-3*) [48,65]; ET: 1-aminocyclopropane carboxylic acid oxidase (*ACO*) and Ethylene response factor 1 (*ERF1*) (transcription factor in both JA/ET signaling) [48]; ABA: 9-cis-epoxycarotenoid dioxygenase 2 (*NCED2*); genes encoding for vacuolar invertase *VvGIN1* and sugar transporters such as *VvHT1, VvHT3, VvSweet2a and VvSweet4*. The specific primers listed in Supplementary Table S1 were designed by Primer 3.0 software (Applied Biosystems) [48]. PCR reactions were set at 95 °C for 10 s (denaturation) and 60 °C for 45 s (annealing/extension) for 42 cycles as described in Lakkis et al. [64]. After the evaluation with Bio-Rad CFX MANAGER software v.3.0, that expression of Elongation factor 1-alpha (*EFα1*) and 60S ribosomal protein (*60SRP*) remained unchanged in all tested conditions, therefore, they were selected as reference genes. Transcript levels of target genes were quantified using the standard curve method. Normalization was done against *EFα1* and *60SRP* as internal controls. Water control at 0 hpt was considered as reference sample (1× expression level). For each experimental condition, PCR reactions were performed in duplicate. Twelve leaves from 6 plants were used for each condition. Three independent experiments were performed.

4.7. Phytoalexins Extraction and Analysis

Leaf samples were collected at zero and 2-dpt with IFP48, TAG and water, and at 1 dpi and 2 dpi with *P. viticola*, *B. cinerea* or mock inoculation. Stilbene phytoalexins were extracted from 200 mg of leaf powder prepared in liquid Nitrogen. In the first step, 2 mL of methanol-to-water 85 % *v*/*v* was added to each tube containing the plant material. Samples were shaken at 800 rpm for 2 h in darkness at the room temperature, then centrifuged for 15 min at 15,000 rpm and 4 °C. Supernatants were collected, protected from the light and stored in the fridge. For the second step, pellets were resuspended in 1 mL of pure methanol, shaken at 800 rpm for 1 h in the darkness, and centrifuged for 15 min (15,000 rpm and 4 °C). Supernatants were collected and pooled together with supernatants obtained in the first step, then dried with the speed vacuum at 45 °C (Speed-Vac, Eppendorf France SAS, Montesson, France). Residues were re-solubilized with 1 mL of pure methanol, filtered through 0.22 µm PTFE filters and stored into 2 mL amber vials for UPLC analysis. Transpiceid, resveratrols, ε- and δ-viniferins were analysed using ACQUITY™ UPLC system (Waters Corporation, USA) with Acquity^{TM} UPLC BEH C18 1.7 µm 2.1×100 mm column heated at 40 °C. Water and acetonitrile with 0.1% phosphoric acid were used to elute stilbenes at the flow rate of 0.5 mL min^{-1} over 7 min [64]. Detection of phytoalexins was performed with an Acquity fluorimeter (Waters Corporation, Milford, MA 01757, USA) with an excitation/emission wavelength of 330/375 nm and phytoalexins were quantified with reference to retention time and calibrated with external standards. Twelve leaves from 6 plants were used for each condition, and experiments were repeated three times.

4.8. Sugar Quantification

Leaf samples were collected at 2 dpt with IFP48, TAG and water before infection and after one day of *P. viticola* or mock inoculation. Leaves were collected from each plant, washed three times with 0.001% Tween80 to remove external IFP48 and TAG and immediately frozen in liquid nitrogen for subsequent quantification of sugars inside the leaf tissues. The amount of D-tagatose, D-glucose, D-ribose, D-fructose, D-mannose, D-galactose, D-maltose and D-trehalose in ground leaf samples was assessed by ion chromatography [66]. Briefly, samples were dissolved in ultrapure water, filtered through a 0.45 µm PTFE membrane (Sartorius, Goettingen, Germany) and analysed with an ionic chromatograph ICS 5000 (Dionex-Thermo Scientific, Waltham, MA, USA), equipped with an autosampler, a quaternary gradient pump, a column oven and a pulsed amperometric detector with a gold working electrode and a palladium counter electrode. The separation was obtained by injecting 5 µL of diluted sample onto a CarboPac PA200 3 × 250 mm analytical column (Dionex-Thermo Scientific, Waltham, MA, USA), preceded by a CarboPac PA200 3 × 50 mm guard column (Dionex-Thermo Scientific), with a KOH gradient (from 1 to 100 mM) at 0.4 mL/min flow rate. Sugar content was expressed in µg per g fresh weight leaf material by using a calibration curve of each pure sugar (Sigma-Aldrich, Merc, Kenilworth, NJ, USA) dissolved in ultrapure water within a range between 0.2 and 40 µg/mL.

4.9. Statistical Analysis

Quantification of *P. viticola* sporangia was repeated three times. Data were analyzed with R software version 3.6.0, and One-way ANOVA statistical test with pairwise comparisons and Student's t-test were used to detect significant differences ($p \leq 0.05$). In case of disease severity caused by *B. cinerea*, quantification of sugars in leaf tissues, phytoalexin and gene expression analyses, experiments were carried out three times. Data analysis was performed with R software version 3.6.0. One-way ANOVA statistical test was used with SPSS 20 software with post-hoc Tukey's test HSD (Honestly Significant Difference) to detect significant differences ($p \leq 0.05$) between treatments.

Supplementary Materials: The following supporting information can be downloaded at: https://www.mdpi.com/article/10.3390/plants11030296/s1, Table S1: Primers used in this study.

Author Contributions: Conceptualization, N.M, E.A.B. and A.A.; methodology, N.M., S.V., N.R., E.A.B. and A.A.; validation, A.N., M.P., E.A.B. and A.A.; formal analysis, N.M., S.V., N.R., A.N., M.P., E.A.B. and A.A.; resources, A.N., A.A. and E.A.B.; data curation, N.M., S.V., N.R., A.N., M.P., E.A.B. and A.A.; writing—original draft preparation, N.M., E.A.B. and A.A.; writing—review and editing, N.M., A.N., M.P., E.A.B. and A.A.; supervision, A.N., A.A. and E.A.B.; project administration, A.A. and E.A.B.; funding acquisition, A.N., A.A. and E.A.B.; All authors have read and agreed to the published version of the manuscript.

Funding: This project has received funding from the European Union's Horizon 2020 research and innovation program under the Marie Skłodowska-Curie grant agreement no. 722642 (project INTERFUTURE).

Institutional Review Board Statement: Not applicable.

Informed Consent Statement: Not applicable.

Acknowledgments: We thank Jean-François Guise from the RIBP Unit at University of Reims (France) for assistance with plant material and plant growth in greenhouse. We also thank the Chemistry Unit at Fondazione Edmund Mach (Italy) for sugar analysis by ion chromatography.

Conflicts of Interest: N.M. and A.N. were employed by Bi-PA nv. The remaining authors declare that the research was conducted in the absence of any commercial or financial relationships that could be construed as a potential conflict of interest.

References

1. Armijo, G.; Schlechter, R.; Agurto, M.; Muñoz, D.; Nuñez, C.; Arce-Johnson, P. Grapevine pathogenic microorganisms: Understanding infection strategies and host response scenarios. *Front. Plant Sci.* **2016**, *7*, 382. [CrossRef] [PubMed]
2. van Kan, J.A.L. Licensed to kill: The lifestyle of a necrotrophic plant pathogen. *Trends Plant Sci.* **2006**, *11*, 247–253. [CrossRef] [PubMed]
3. Aziz, A.; Gauthier, A.; Bezier, A.; Poinssot, B.; Joubert, J.-M.; Pugin, A.; Heyraud, A.; Baillieul, F. Elicitor and resistance-inducing activities of β-1,4 cellodextrins in grapevine, comparison with β-1,3 glucans and β-1,4 oligogalacturonides. *J. Exp. Bot.* **2007**, *58*, 1463–1472. [CrossRef] [PubMed]
4. Delaunois, B.; Farace, G.; Jeandet, P.; Clément, C.; Baillieul, F.; Dorey, S.; Cordelier, S. Elicitors as alternative strategy to pesticides in grapevine? Current knowledge on their mode of action from controlled conditions to vineyard. *Environ. Sci. Pollut. Res.* **2014**, *21*, 4837–4846. [CrossRef]
5. Héloir, M.C.; Adrian, M.; Brulé, D.; Claverie, J.; Cordelier, S.; Daire, X.; Dorey, S.; Gauthier, A.; Lemaître-Guillier, C.; Negrel, J.; et al. Recognition of elicitors in grapevine: From MAMP and DAMP perception to induced resistance. *Front. Plant Sci.* **2019**, *10*, 1117. [CrossRef] [PubMed]
6. Aziz, A.; Trotel-Aziz, P.; Dhuicq, L.; Jeandet, P.; Couderchet, M.; Vernet, G. Chitosan oligomers and copper sulfate induce grapevine defense reactions and resistance to gray mold and downy mildew. *Phytopathology* **2006**, *96*, 1188–1194. [CrossRef]
7. Brulé, D.; Villano, C.; Davies, L.J.; Trdá, L.; Claverie, J.; Héloir, M.C.; Chiltz, A.; Adrian, M.; Darblade, B.; Tornero, P.; et al. The grapevine (*Vitis vinifera*) LysM receptor kinases VvLYK1-1 and VvLYK1-2 mediate chitooligosaccharide-triggered immunity. *Plant Biotechnol. J.* **2019**, *17*, 812–825. [CrossRef]
8. Gauthier, A.; Trouvelot, S.; Kelloniemi, J.; Frettinger, P.; Wendehenne, D.; Daire, X.; Joubert, J.-M.; Ferrarini, A.; Delledonne, M.; Flors, V.; et al. The sulfated laminarin triggers a stress transcriptome before priming the SA- and ROS-dependent defenses during grapevine's induced resistance against *Plasmopara viticola*. *PLoS ONE* **2014**, *9*, e88145. [CrossRef]
9. Varnier, A.L.; Sanchez, L.; Vatsa, P.; Boudesocque, L.; Garcia-Brugger, A.; Rabenoelina, F.; Sorokin, A.; Renault, J.H.; Kauffmann, S.; Pugin, A.; et al. Bacterial rhamnolipids are novel MAMPs conferring resistance to *Botrytis cinerea* in grapevine. *Plant Cell Environ.* **2009**, *32*, 178–193. [CrossRef]
10. Aziz, A.; Heyraud, A.; Lambert, B. Oligogalacturonide signal transduction, induction of defense-related responses and protection of grapevine against *Botrytis cinerea*. *Planta* **2004**, *218*, 767–774. [CrossRef]
11. Claverie, J.; Balacey, S.; Lemaître-Guillier, C.; Brulé, D.; Chiltz, A.; Granet, L.; Noirot, E.; Daire, X.; Darblade, B.; Héloir, M.-C.; et al. The cell wall-derived xyloglucan is a new DAMP triggering plant immunity in *Vitis vinifera* and *Arabidopsis thaliana*. *Front. Plant Sci.* **2018**, *9*, 1725. [CrossRef] [PubMed]
12. Liu, L.; Sonbol, F.M.; Huot, B.; Gu, Y.; Withers, J.; Mwimba, M.; Yao, J.; He, S.Y.; Dong, X. Salicylic acid receptors activate jasmonic acid signalling through a non-canonical pathway to promote effector-triggered immunity. *Nat. Commun.* **2016**, *7*, 1–10. [CrossRef] [PubMed]
13. Pieterse, C.M.J.; Van Der Does, D.; Zamioudis, C.; Leon-Reyes, A.; Van Wees, S.C.M. Hormonal modulation of plant immunity. *Annu. Rev. Cell Dev. Biol.* **2012**, *28*, 489–521. [CrossRef] [PubMed]
14. Ceusters, N.; Van den Ende, W.; Ceusters, J. Exploration of sweet immunity to enhance abiotic stress tolerance in plants: Lessons from CAM. *Prog. Bot.* **2016**, *78*, 145–166. [CrossRef]

15. Moghaddam, M.R.B.; Van Den Ende, W. Sugars and plant innate immunity. *J. Exp. Bot.* **2012**, *63*, 3989–3998. [CrossRef]
16. Trouvelot, S.; Héloir, M.C.; Poinssot, B.; Gauthier, A.; Paris, F.; Guillier, C.; Combier, M.; Trdá, L.; Daire, X.; Adrian, M. Carbohydrates in plant immunity and plant protection: Roles and potential application as foliar sprays. *Front. Plant Sci.* **2014**, *5*, 592. [CrossRef]
17. Gebauer, P.; Korn, M.; Engelsdorf, T.; Sonnewald, U.; Koch, C.; Voll, L.M. Sugar Accumulation in leaves of Arabidopsis sweet11/sweet12 double mutants enhances priming of the salicylic acid-mediated defense response. *Front. Plant Sci.* **2017**, *8*, 1378. [CrossRef]
18. Stauber, J.L.; Loginicheva, E.; Schechter, L.M. Carbon source and cell density-dependent regulation of type III secretion system gene expression in *Pseudomonas syringae* pathovar tomato DC3000. *Res. Microbiol.* **2012**, *163*, 531–539. [CrossRef]
19. Yamada, K.; Saijo, Y.; Nakagami, H.; Takano, Y. Regulation of sugar transporter activity for antibacterial defense in Arabidopsis. *Science* **2016**, *354*, 1427–1430. [CrossRef]
20. Slewinski, T.L. Diverse functional roles of monosaccharide transporters and their homologs in vascular plants: A physiological perspective. *Mol. Plant* **2011**, *4*, 641–662. [CrossRef]
21. Bezrutczyk, M.; Yang, J.; Eom, J.-S.; Prior, M.; Sosso, D.; Hartwig, T.; Szurek, B.; Oliva, R.; Vera-Cruz, C.; White, F.F.; et al. Sugar flux and signaling in plant-microbe interactions. *Plant J.* **2018**, *93*, 675–685. [CrossRef] [PubMed]
22. Gómez-Ariza, J.; Campo, S.; Rufat, M.; Estopà, M.; Messeguer, J.; San Segundo, B.; Coca, M. Sucrose-mediated priming of plant defense responses and broad-spectrum disease resistance by overexpression of the maize pathogenesis-related PRms protein in rice plants. *Mol. Plant-Microbe Interact.* **2007**, *20*, 832–842. [CrossRef] [PubMed]
23. Akimitsu, K.; Tsukuda, S.; Suzuku, N.; Ichii, M.; Tajima, S. An elicitor effect of D-psicose for induction of plant defense gene transcriptions. In Proceedings of the International Society of Rare Sugars: Creating a Novel Bio-World with Rare Sugars, Kagawa, Japan, 3 April 2008; pp. 163–168.
24. Chahed, A.; Lazazzara, V.; Moretto, M.; Nesler, A.; Corneo, P.E.; Barka, E.A.; Pertot, I.; Puopolo, G.; Perazzolli, M. The differential growth inhibition of *Phytophthora* spp. caused by the rare sugar tagatose is associated with species-specific metabolic and transcriptional changes. *Front. Microbiol.* **2021**, *12*, 711545. [CrossRef] [PubMed]
25. Chahed, A.; Nesler, A.; Aziz, A.; Barka, E.A.; Pertot, I.; Perazzolli, M. A review of knowledge on the mechanisms of action of the rare sugar d-tagatose against phytopathogenic oomycetes. *Plant Pathol.* **2021**, *70*, 1979–1986. [CrossRef]
26. Corneo, P.E.; Jermini, M.; Nadalini, S.; Giovannini, O.; Nesler, A.; Perazzolli, M.; Pertot, I. Foliar and root applications of the rare sugar tagatose control powdery mildew in soilless grown cucumbers. *Crop Prot.* **2021**, *149*, 105753. [CrossRef]
27. Corneo, P.E.; Nesler, A.; Lotti, C.; Chahed, A.; Vrhovsek, U.; Pertot, I.; Perazzolli, M. Interactions of tagatose with the sugar metabolism are responsible for *Phytophthora infestans* growth inhibition. *Microbiol. Res.* **2021**, *247*, 126724. [CrossRef]
28. Kano, A.; Gomi, K.; Yamasaki-Kokudo, Y.; Satoh, M.; Fukumoto, T.; Ohtani, K.; Tajima, S.; Izumori, K.; Tanaka, K.; Ishida, Y.; et al. A rare sugar, D-allose, confers resistance to rice bacterial blight with upregulation of defense-related genes in *Oryza sativa*. *Phytopathology* **2010**, *100*, 85–90. [CrossRef]
29. Kano, A.; Fukumoto, T.; Ohtani, K.; Yoshihara, A.; Ohara, T.; Tajima, S.; Izumori, K.; Tanaka, K.; Ohkouchi, T.; Ishida, Y.; et al. The rare sugar d-allose acts as a triggering molecule of rice defence via ROS generation. *J. Exp. Bot.* **2013**, *64*, 4939–4951. [CrossRef]
30. Mijailovic, N.; Nesler, A.; Perazzolli, M.; Aït Barka, E.; Aziz, A. Rare sugars: Recent advances and their potential role in sustainable crop protection. *Molecules* **2021**, *26*, 1720. [CrossRef]
31. Mochizuki, S.; Fukumoto, T.; Ohara, T.; Ohtani, K.; Yoshihara, A.; Shigematsu, Y.; Tanaka, K.; Ebihara, K.; Tajima, S.; Gomi, K.; et al. The rare sugar d-tagatose protects plants from downy mildews and is a safe fungicidal agrochemical. *Commun. Biol.* **2020**, *3*, 1–15. [CrossRef]
32. Ohara, T.; Ishida, Y.; Kudou, R.; Kakibuchi, K.; Akimitsu, K.; Izumori, K.; Tajima, S. Plant Disease Control agent Comprising D-tagatose as Active Ingredient, and Plant Disease Control Method. U.S. Patent 9,125,409-B2, 18 August 2008.
33. Ohara, T. Effect of D-tagatose on plant disease; downy mildew and powdery mildew. In Proceedings of the 5th Symposium of International Society of Rare Sugars, Takamatsu and Miki, Kagawa, Japan, 9–12 November 2011.
34. Ohara, T.; Tanaka, K.; Ishizaki, S.; Kato, S.; Akimitsu, K.; Izumori, K. Composition for Enhancing Plant Disease Control Effect of Monosaccharides. U.S. Patent 10, 638,752, 5 May 2020.
35. Perazzolli, M.; Nesler, A.; Giovannini, O.; Antonielli, L.; Puopolo, G.; Pertot, I. Ecological impact of a rare sugar on grapevine phyllosphere microbial communities. *Microbiol. Res.* **2020**, *232*, 126387. [CrossRef] [PubMed]
36. Zhang, H.; Jiang, M.; Song, F. D-allose is a critical regulator of inducible plant immunity in tomato. *Physiol. Mol. Plant Pathol.* **2020**, *111*, 101507. [CrossRef]
37. Müller, J.; Aeschbacher, R.A.; Sprenger, N.; Boller, T.; Wiemken, A. Disaccharide-mediated regulation of sucrose:fructan-6-fructosyltransferase, a key enzyme of fructan synthesis in barley leaves. *Plant Physiol.* **2000**, *123*, 265–273. [CrossRef] [PubMed]
38. Moore, B.; Zhou, L.; Rolland, F.; Hall, Q.; Cheng, W.H.; Liu, Y.X.; Hwang, I.; Jones, T.; Sheen, J. Role of the Arabidopsis glucose sensor HXK1 in nutrient, light, and hormonal signaling. *Science* **2003**, *300*, 332–336. [CrossRef] [PubMed]
39. Li, P.; Wind, J.J.; Shi, X.; Zhang, H.; Hanson, J.; Smeekens, S.C.; Teng, S. Fructose sensitivity is suppressed in Arabidopsis by the transcription factor ANAC089 lacking the membrane-bound domain. *Proc. Natl. Acad. Sci. USA* **2011**, *108*, 3436–3441. [CrossRef]
40. Smeekens, S.; Ma, J.; Hanson, J.; Rolland, F. Sugar signals and molecular networks controlling plant growth. *Curr. Opin. Plant Biol.* **2010**, *13*, 273–278. [CrossRef]

41. Kano, A.; Hosotani, K.; Gomi, K.; Yamasaki-Kokudo, Y.; Shirakawa, C.; Fukumoto, T.; Ohtani, K.; Tajima, S.; Izumori, K.; Tanaka, K.; et al. D-Psicose induces upregulation of defense-related genes and resistance in rice against bacterial blight. *J. Plant Physiol.* **2011**, *168*, 1852–1857. [CrossRef]
42. Sinha, A.K.; Hofmann, M.G.; Römer, U.; Köckenberger, W.; Elling, L.; Roitsch, T. Metabolizable and non-metabolizable sugars activate different signal transduction pathways in tomato. *Plant Physiol.* **2002**, *128*, 1480–1489. [CrossRef]
43. Harm, A.; Kassemeyer, H.H.; Seibicke, T.; Regner, F. Evaluation of chemical and natural resistance inducers against downy mildew (*Plasmopara viticola*) in grapevine. *Am. J. Enol. Vitic.* **2011**, *62*, 184–192. [CrossRef]
44. Aziz, A.; Poinssot, B.; Daire, X.; Adrian, M.; Bézier, A.; Lambert, B.; Joubert, J.M.; Pugin, A. Laminarin elicits defense responses in grapevine and induces protection against *Botrytis cinerea* and *Plasmopara viticola*. *Mol. Plant-Microbe Interact.* **2003**, *16*, 1118–1128. [CrossRef]
45. Hamiduzzaman, M.M.; Jakab, G.; Barnavon, L.; Neuhaus, J.M.; Mauch-Mani, B. β-Aminobutyric acid-induced resistance against downy mildew in grapevine acts through the potentiation of callose formation and jasmonic acid signaling. *Mol. Plant-Microbe Interact.* **2005**, *18*, 819–829. [CrossRef] [PubMed]
46. Figueiredo, A.; Monteiro, F.; Sebastiana, M. First clues on a jasmonic acid role in grapevine resistance against the biotrophic fungus *Plasmopara viticola*. *Eur. J. Plant Pathol.* **2015**, *142*, 645–652. [CrossRef]
47. Alvarez, M.E.; Pennell, R.I.; Meijer, P.J.; Ishikawa, A.; Dixon, R.A.; Lamb, C. Reactive oxygen intermediates mediate a systemic signal network in the establishment of plant immunity. *Cell* **1998**, *92*, 773–784. [CrossRef]
48. Gruau, C.; Trotel-Aziz, P.; Villaume, S.; Rabenoelina, F.; Clement, C.; Baillieul, F.; Aziz, A. *Pseudomonas fluorescens* PTA-CT2 triggers local and systemic immune response against *Botrytis cinerea* in grapevine. *Mol. Plant-Microbe Interact.* **2015**, *28*, 1117–1129. [CrossRef] [PubMed]
49. Fukumoto, T.; Kano, A.; Ohtani, K.; Inoue, M.; Yoshihara, A.; Izumori, K.; Tajima, S.; Shigematsu, Y.; Tanaka, K.; Ohkouchi, T.; et al. Phosphorylation of d-allose by hexokinase involved in regulation of *OsABF1* expression for growth inhibition in *Oryza sativa* L. *Planta* **2013**, *237*, 1379–1391. [CrossRef] [PubMed]
50. Soar, C.J.; Speirs, J.; Maffei, S.M.; Loveys, B.R. Gradients in stomatal conductance, xylem sap ABA and bulk leaf ABA along canes of *Vitis vinifera cv. Shiraz*: Molecular and physiological studies investigating their source. *Funct. Plant Biol.* **2004**, *31*, 659–669. [CrossRef]
51. Jeandet, P.; Hébrard, C.; Deville, M.-A.; Cordelier, S.; Dorey, S.; Aziz, A.; Crouzet, J. Deciphering the role of phytoalexins in plant-microorganism interactions and human health. *Molecules* **2014**, *19*, 18033–18056. [CrossRef]
52. Aziz, A.; Verhagen, B.; Magnin-Robert, M.; Couderchet, M.; Clément, C.; Jeandet, P.; Trotel-Aziz, P. Effectiveness of beneficial bacteria to promote systemic resistance of grapevine to gray mold as related to phytoalexin production in vineyards. *Plant Soil* **2016**, *405*, 141–153. [CrossRef]
53. Dercks, W.; Creasy, L.L. The significance of stilbene phytoalexins in the *Plasmopara viticola*-grapevine interaction. *Physiol. Mol. Plant Pathol.* **1989**, *34*, 189–202. [CrossRef]
54. Pezet, R.; Gindro, K.; Viret, O.; Richter, H. Effects of resveratrol, viniferins and pterostilbene on *Plasmopara viticola* zoospore mobility and disease development. *Vitis-Geilweilerhof* **2004**, *43*, 45–148.
55. Meteier, E.; La Camera, S.; Goddard, M.-L.; Laloue, H.; Mestre, P.; Chong, J. Overexpression of the *VvSWEET4* transporter in grapevine hairy roots increases sugar transport and contents and enhances resistance to *Pythium irregulare*, a soilborne pathogen. *Front. Plant Sci.* **2019**, *10*, 884. [CrossRef] [PubMed]
56. Lemoine, R.; La Camera, S.; Atanassova, R.; Dédaldéchamp, F.; Allario, T.; Pourtau, N.; Bonnemain, J.L.; Laloi, M.; Coutos-Thévenot, P.; Maurousset, L.; et al. Source-to-sink transport of sugar and regulation by environmental factors. *Front. Plant Sci.* **2013**, *4*, 272. [CrossRef] [PubMed]
57. Essmann, J.; Bones, P.; Weis, E.; Scharte, J. Leaf carbohydrate metabolism during defense. *Plant Signal. Behav.* **2008**, *3*, 885–887. [CrossRef] [PubMed]
58. Li, C.; Wang, K.; Lei, C.; Cao, S.; Huang, Y.; Ji, N.; Xu, F.; Zheng, Y. Alterations in sucrose and phenylpropanoid metabolism affected by BABA-primed defense in postharvest grapes and the associated transcriptional mechanism. *Mol. Plant-Microbe Interact.* **2021**, *33*, 1250–1266. [CrossRef] [PubMed]
59. Hasibul, K.; Nakayama-Imaohji, H.; Hashimoto, M.; Yamasaki, H.; Ogawa, T.; Waki, J.; Tada, A.; Yoneda, S.; Tokuda, M.; Miyake, M.; et al. D-Tagatose inhibits the growth and biofilm formation of *Streptococcus mutans*. *Mol. Med. Rep.* **2018**, *17*, 843–851. [CrossRef]
60. Fan, J.; Chen, C.; Brlansky, R.H.; Gmitter, F.G.; Li, Z.G. Changes in carbohydrate metabolism in *Citrus sinensis* infected with '*Candidatus Liberibacter asiaticus*'. *Plant Pathol.* **2010**, *59*, 1037–1043. [CrossRef]
61. Reignault, P.; Cogan, A.; Muchembled, J.; Lounes-Hadj Sahraoui, A.; Durand, R.; Sancholle, M. Trehalose induces resistance to powdery mildew in wheat. *New Phytol.* **2001**, *149*, 519–529. [CrossRef]
62. Djonović, S.; Urbach, J.M.; Drenkard, E.; Bush, J.; Feinbaum, R.; Ausubel, J.L.; Traficante, D.; Risech, M.; Kocks, C.; Fischbach, M.A.; et al. Trehalose biosynthesis promotes *Pseudomonas aeruginosa* pathogenicity in plants. *PLoS Pathog.* **2013**, *9*, e1003217. [CrossRef]
63. Burton, R.A.; Gidley, M.J.; Fincher, G.B. Heterogeneity in the chemistry, structure and function of plant cell walls. *Nat. Chem. Biol.* **2010**, *6*, 724–732. [CrossRef]

64. Lakkis, S.; Trotel-Aziz, P.; Rabenoelina, F.; Schwarzenberg, A.; Nguema-Ona, E.; Clément, C.; Aziz, A. Strengthening grapevine resistance by *Pseudomonas fluorescens* PTA-CT2 relies on distinct defense pathways in susceptible and partially resistant genotypes to downy mildew and gray mold diseases. *Front. Plant Sci.* **2019**, *10*, 1112. [CrossRef]
65. Trotel-Aziz, P.; Abou-Mansour, E.; Courteaux, B.; Rabenoelina, F.; Clément, C.; Fontaine, F.; Aziz, A. *Bacillus subtilis* PTA-271 counteracts Botryosphaeria dieback in grapevine, triggering immune responses and detoxification of fungal phytotoxins. *Front. Plant Sci.* **2019**, *24*, 25. [CrossRef] [PubMed]
66. Cataldi, T.R.I.; Campa, C.; De Benedetto, G.E. Carbohydrate analysis by high-performance anion-exchange chromatography with pulsed amperometric detection: The potential is still growing. *Fresenius' J. Anal. Chem.* **2000**, *368*, 739–758. [CrossRef] [PubMed]

plants

MDPI

Article

Characterization of Ingredients Incorporated in the Traditional Mixed-Salad of the Capuchin Monks

Laura Cornara [1,*], Gabriele Ambu [1], Alex Alberto [1], Domenico Trombetta [2] and Antonella Smeriglio [2,*]

[1] Department of Earth, Environment and Life Sciences, University of Genova, C.so Europa 26, 16132 Genova, Italy; gabrieleambu1976@gmail.com (G.A.); alex.universita.12@gmail.com (A.A.)
[2] Department of Chemical, Biological, Pharmaceutical and Environmental Sciences, University of Messina, Viale Ferdinando Stagno d'Alcontres 31, 98166 Messina, Italy; dtrombetta@unime.it
* Correspondence: laura.cornara@unige.it (L.C.); asmeriglio@unime.it (A.S.)

Abstract: Recipes on the composition of the "salad of the monks" (Capuchin monks) have been reported in Italy since the 17th century. Different wild edible plants were highly regarded as an important ingredient of this mixed salad. Among these, some species played a key role for both their taste and nutritional properties: *Plantago coronopus* L. (PC), *Rumex acetosa* L., *Cichorium intybus* L., and *Artemisia dracunculus* L. In the present study, the micromorphological and phytochemical features as well as the antioxidant and anti-inflammatory properties of extracts of these fresh and blanched leaves, were investigated. The extracts obtained by blanched leaves, according to the traditionally used cooking method, showed the highest content of bioactive compounds (total phenols 1202.31–10,751.88 mg GAE/100 g DW; flavonoids 2921.38–61,141.83 mg QE/100 g DW; flavanols 17.47–685.52 mg CE/100 g DW; proanthocyanidins 2.83–16.33 mg CyE/100 g DW; total chlorophyll 0.84–1.09 mg/g FW; carbohydrates 0.14–1.92 g/100 g FW) and possess the most marked antioxidant (IC_{50} 0.30–425.20 µg/mL) and anti-inflammatory activity (IC_{50} 240.20–970.02 µg/mL). Considering this, our results indicate that increased consumption of the investigated plants, in particular of PC, raw or cooked briefly, could provide a healthy food source in the modern diet by the recovery and enhancement of ancient ingredients.

Keywords: human diet; edible wild plants; *Plantago coronopus* L.; *Rumex acetosa* L.; *Cichorium intybus* L.; *Artemisia dracunculus* L.; phytochemistry; antioxidant activity; anti-inflammatory properties

Citation: Cornara, L.; Ambu, G.; Alberto, A.; Trombetta, D.; Smeriglio, A. Characterization of Ingredients Incorporated in the Traditional Mixed-Salad of the Capuchin Monks. *Plants* **2022**, *11*, 301. https://doi.org/10.3390/plants11030301

Academic Editors: Milan S. Stankovic, Paula Baptista and Petronia Carillo

Received: 31 December 2021
Accepted: 21 January 2022
Published: 24 January 2022

Publisher's Note: MDPI stays neutral with regard to jurisdictional claims in published maps and institutional affiliations.

1. Introduction

Since ancient time, humans have learned to recognize and use wild edible plant species (WEPs) as an important source of supplementary food [1]. Although agricultural production has more than tripled from 1960 to today, also thanks to the technologies of the Green Revolution, widespread hunger and malnutrition still persist in many countries of the world (FAO, 2017).

In this context, the WEPs play a pivotal role in human nutrition, especially in the developing countries, and also represent important components of the Mediterranean Diet today [2,3]. Recent studies have shown a renewed interest in the use of wild plant resources and in the deepening the relationship between plants used as food and their medicinal values [4,5].

Traditional knowledge related to the use of WEPs has been handed down for centuries both orally and in writing in those cultures with a rich literary tradition such as Europe, India, and China [6]. In Europe, from the Middle Ages to the Renaissance, this knowledge was documented, codified, and protected, mainly by monastic communities, within their vegetable gardens (*horti*) [7–11].

The 16th century was a period of progress in European medical knowledge, with renewed interest in healthy foods, such as those vegetables and salads, that until then were considered food of the lower social strata [12].

The Franciscan Order of Capuchin monks (ca 1530) is placed in this cultural context [13–15] and Father Zaccaria Boverio in his text *De sacris ritibus* (1626) described an interesting traditional recipe for a mixed salad of wild edible leaves. It was known as "insalatina dei frati" (salad of monks) or "misticanza", widely used in Liguria and Lazio. According to what was later reported by Father Vincenzo Celesia in *Selva Botanica* (1892), this tradition was still in use at the time among the Ligurian Capuchin monks, who brought this type of healthy salad to their benefactors as a sign of gratitude.

In the present study, we have selected, from this recipe, four species that played a key role for both their taste and nutritional properties, *Plantago coronopus* L. (PC), *Rumex acetosa* L. (RA), *Cichorium intybus* L. (CI), and *Artemisia dracunculus* L. (AD).

Plantago coronopus L. (PC), although it is normally considered a weed, has been cultivated for centuries in various traditional contexts for its food and medicinal value, especially from the sixteenth century. Its leaves are cooked as a vegetable in Balkan traditional cuisine, in France and Italy are mixed with other species to prepare salads, with a particular taste and crunchiness. In addition, PC is used in traditional medicine for its analgesic, anti-inflammatory, antipyretic, anticancer and emollient properties, as well as to treat respiratory problems [16,17]. In Liguria PC leaves were in the past the main ingredient of Capuchin monks' salad, as reported by Father Vincenzo Celesia.

Rumex acetosa L. (RA) has been used and cultivated for thousands of years as a medicinal plant, as food and as a dye. Archaeobotanical remains of this plant have been found in Neolithic and Mesolithic settlement sites throughout Europe, where it is still today a very popular vegetable, widely used in traditional cuisine [18,19]. RA is used in folk medicine for its health properties: diaphoretic, diuretic, anti-septic, antipyretic, anti-inflammatory, antioxidant, antimicrobial, anti-hypersensitive, analgesic and antiviral [19–21]. In Liguria, still today, the leaves and flowers of RA ("erba agretta") are chewed against stomatitis [22].

Cichorium intybus L. (CI) has been considered a sacred plant and used for its medicinal properties since ancient times [23]. Egyptians, Romans, and Greeks ate chicory root as a useful remedy for liver, digestive, metabolic, and heart ailments. In the Middle Ages, chicory was used to treat jaundice and malaria and its use in European folk medicine has continued until recent times. Chicory root is a traditional remedy for digestive and hepatobiliary diseases, kidney and rheumatic disorders, as well as gout. The aerial parts are mainly used for their diuretic, analgesic, diaphoretic, and antipyretic properties [24–26]. In Liguria, leaves of CI are still today consumed as a fresh salad, and briefly boiled as a side dish or to prepare vegetable pies and stuffing of "ravioli". A decoction of leaves is used for its depurative value [22,27].

Artemisia dracunculus L. (AD), native to Siberia and Mongolia, has been introduced in Europe probably since around the XV-XVI centuries, and became a popular spice in culinary tradition for the aromatic taste of its leaves [28,29]. AD has long been used also in traditional medicine as an anti-inflammatory and anti-pyretic, in the treatment of gastrointestinal diseases, and as an anaesthetic, hypnotic and anti-epileptic agent [30,31]. In northern Italy, a still current use of this plant has been reported as a flavouring for making a traditional cheese, called *saurnschotte* [28].

In recent decades, some studies have been conducted on the phytochemical profile of PC, RA, CI, and AD, and their nutritional properties, but much remains to be explored on the antioxidant and anti-inflammatory properties of their extracts, in particular derived from fresh and cooked plants. Nowadays, nutraceutical science shows a growing interest in the recovery and enhancement of ancient ingredients, such as many monastic and conventual wild plants that can be a source of healthy food in the modern diet [32]. Therefore, we carried out the present study, analysing the macro- and micromorphological features and phytochemistry of these species. We also investigated the antioxidant and anti-inflammatory properties of the selected fresh and cooked plant extracts in order to compare their health properties and establish whether the commonly cooking method used affects them, positively or negatively.

2. Results and Discussion

2.1. Macro- and Micromorphological Characterization

Recently, the new trend of being green and environmentally friendly has led many people to search for wild edible plants (WEPs), but often this tendency is accompanied by a misidentification between edible and toxic plants, causing poisonings [33,34]. Many WEPs have useful antioxidant and anti-inflammatory properties and are rich in nutritional principles, but their consumption cannot be separated from the correct identification, in order to avoid health risks. Many examples of misidentifications have been reported, such as leaves of *Rumex acetosella* and *R. acetosa* confused with those of *Arum maculatum* or *R. crispus* [35]. Fresh salads are a frequent source of food contamination and poisoning, e.g., *Datura stramonium* accidentally used as ingredient of traditional meals [36], *Digitalis purpurea* and *Mandragora autumnalis* confused with *Borago officinalis* [33,34], and *Veratrum album* mistaken for *Allium ursinum* [37].

Factors contributing to poisoning due to misidentification are often related to the difficulties of identifying the plants in raw mixtures, as well as chopped and processed herbs [38].

The edible leaves of the species considered in our study have a significant intraspecific morphological variability as a plastic response to different environmental conditions [19,29,39,40]. Therefore, macromorphological analysis combined with scanning electron microscopy (SEM) (Table 1 and Figures 1–3) allowed one to highlight some anatomical details of PC, RA, CI, and AD, that can be used for the taxonomic determination of the plant material, even when the leaves are mixed in salad, frozen, or processed. In particular, different typical features of the epidermal surfaces of each species were pointed out, including the shape of the epidermal cells, the type of trichomes, and the stomatal apparatus.

Table 1. Macro- and micromorphological features of the leaves of the selected species (PC, RA, CI and AD).

Species	Leaf Macromorphological Features	Leaf Micromorphological Features
Plantago coronopus L. (PC) Buck's-horn plantain (Figure 1a)	Pubescent, toothed at the tip, slightly fleshy; narrow and pinnately lobed, arranged in a dense ascending rosette at the apex of a short stem [41].	Figure 2a–c *Epidermal cells*: rectangular with almost straight cell walls. *Stomata apparatus*: diacytic-type. *Trichomes*: two non-glandular types: bottle-like and larger, long stalked, multicellular trichomes [42]. Rarely, secretory trichomes could be observed [41].
Rumex acetosa L. (RA) Common sorrel (Figure 1b)	Large, ovate, hairless, fleshy; the lobes of basal leaves are pointed, and the petiole elongated; the stem leaves are almost stalkless [18].	Figure 2d–f *Epidermal cells*: irregularly shaped, with slightly undulating cell walls. *Stomata apparatus*: anisocytic and paracytic types. *Trichomes*: non-glandular trichomes lacking; glandular trichomes peltate, normally showing four-celled secretory heads [43].
Cichorium intybus L. (CI) Chicory (Figure 1c)	Hairy, arranged in an ascending rosette; oblong lanceolate, pinnate shape; basal leaves oblanceolate, toothed, with short petiole; cauline leaves smaller and sessile [24].	Figure 3a–c *Epidermal cells*: undulating cell walls. *Stomata apparatus*: anomocytic-type [44]. *Trichomes*: mutiseriate glandular trichomes on abaxial surface; multiseriate non-glandular trichomes with non-projecting cell apices on both surfaces [45].
Artemisia dracunculus L. (AD) Wild tarragon (Figure 1d)	Sessile, arranged alternately along the stem, with a sharp tip and entire leaf margins; lower leaves tripartite at the apex, the middle and upper leaves are lanceolate [30].	Figure 3d–f *Epidermal cells*: highly undulating cell walls. *Stomata apparatus*: anomocytic-type. *Trichomes*: stellate non-glandular trichomes and biseriate glandular trichomes with a subcuticular space filled with secondary compounds [46].

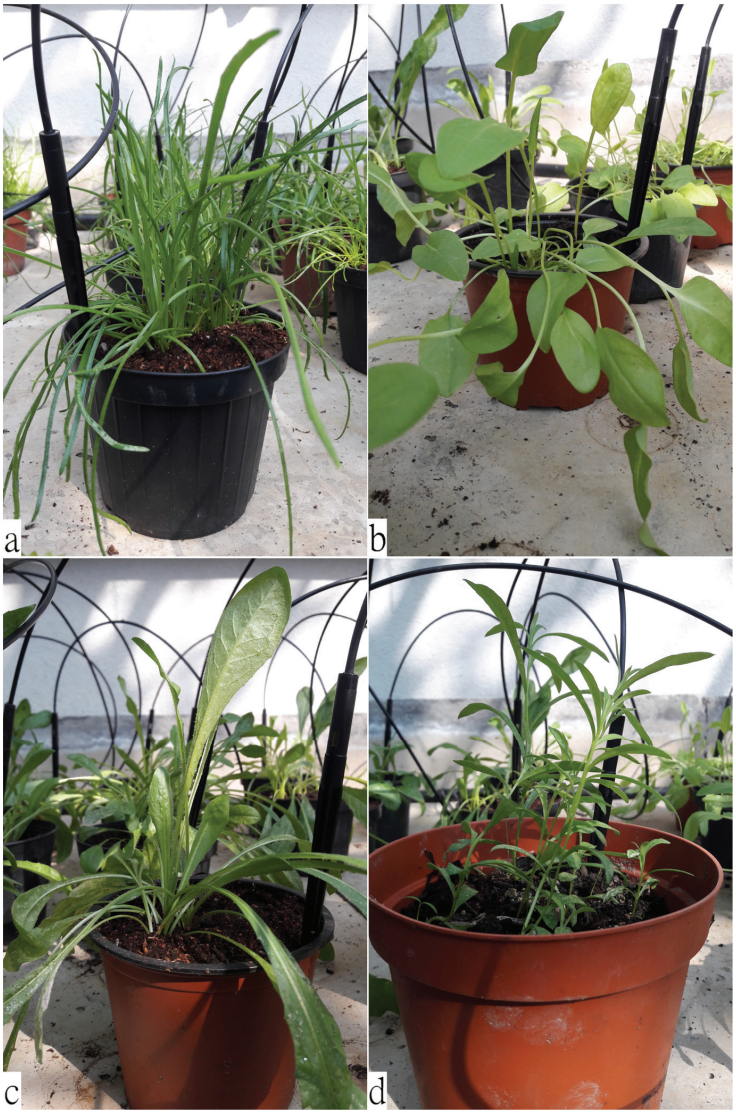

Figure 1. Representative pictures of the four selected plant species: (**a**) *Plantago coronopus* L.; (**b**) *Rumex acetosa* L.; (**c**) *Cichorium intybus* L.; (**d**) *Artemisia dracunculus* L.

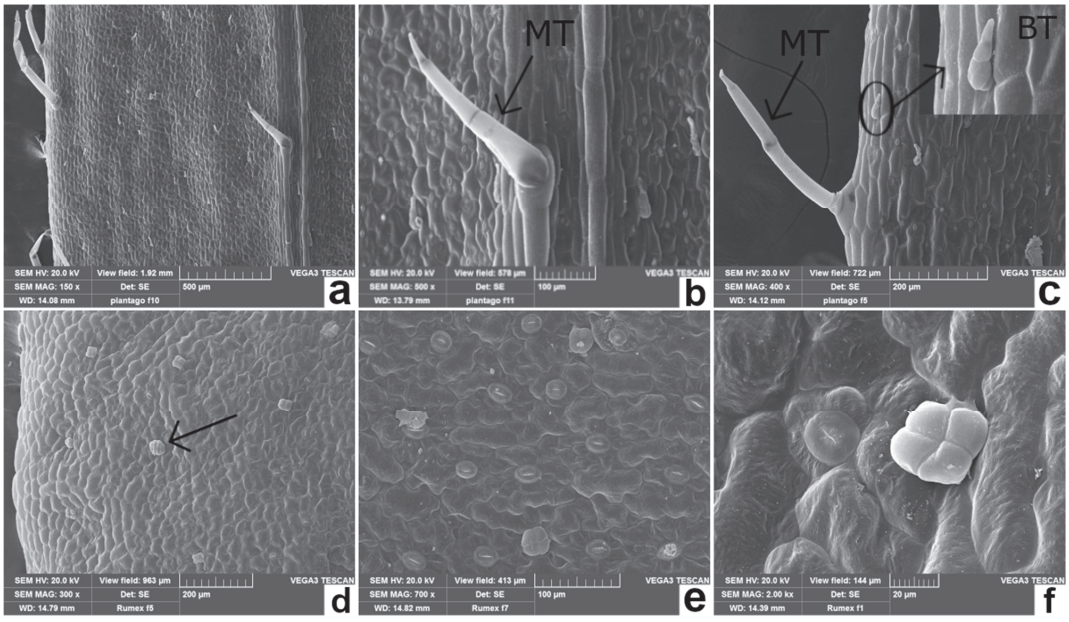

Figure 2. Scanning electron microscopic view of leaves from PC (**a**–**c**) and RA (**d**–**f**). (**a**) Abaxial surface showing epidermal cells, trichomes and stomata; (**b**) abaxial surface showing a non-glandular multicellular trichome (MT) on the leaf midrib; (**c**) adaxial surface showing two types of non-glandular trichomes: bottle-like trichomes (BT) and long stalked MT; (**d**) on the adaxial surface are visible anisocytic and paracytic stomata, and peltate glandular trichomes (the arrow points an abnormal glandular trichome); (**e**) abaxial surface with glandular trichomes and anisocytic and paracytic stomata; (**f**) close-up view of a peltate glandular trichome on the adaxial surface.

2.2. Phytchemical Investigations

The edible leaves of the selected plants, once characterized from the micromorphological point of view, were processed, partly fresh and partly blanched, by pulverization with liquid nitrogen and extraction by sonication. These treatments allowed one to obtain high extractive yields, between 1.40% and 4.10%, without modifying the native phytochemical profile of the investigated plants, by exhaustively extracting the bioactive compounds. The phytochemical screening carried out made it possible to quantify the total phenols, flavonoids, flavanols (vanillic index) and proanthocyanidins present in the four plant species of interest, also allowing to calculate the polymerization index, i.e., the preponderance of monomeric/polymeric molecules in each extract. Moreover, since it is well known that pigments, especially chlorophyll and carbohydrates, can contribute to the biological properties of these matrices and may, more or less, be affected by the cooking method used [47], even the latter have been determined on the starting matrices, as they are and after blanching

As reported in Table 2, all extracts analyzed showed a very interesting phytochemical profile, being very rich in bioactive compounds.

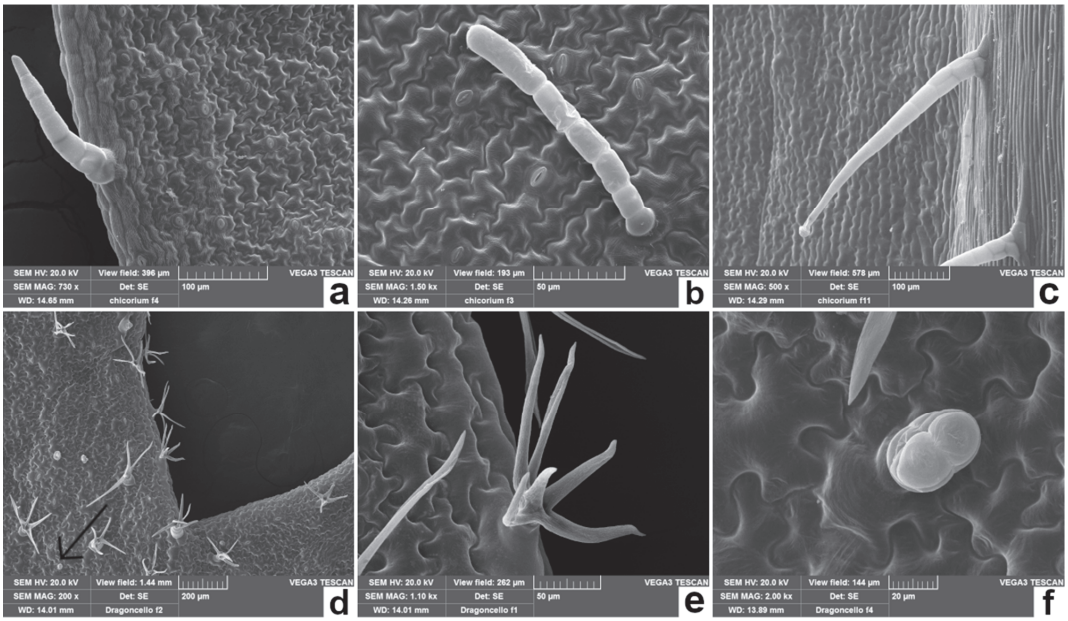

Figure 3. Scanning electron microscopic view of leaves from CI (**a**–**c**) and AD (**d**–**f**). (**a**) Adaxial surface showing a non-glandular multiseriate trichome on the leaf margin; (**b**) adaxial surface showing another type of non-glandular multiseriate trichome and characteristic undulating epidermal cell walls; (**c**) abaxial surface showing multiseriate glandular trichomes along the midrib; (**d**) abaxial surface showing stellate non-glandular trichomes and biseriate glandular trichomes (arrow); (**e**) close-up view of a stellate non-glandular trichome; (**f**) close-up view of a biseriate glandular trichome.

Table 2. Comparison between the phytochemical profiles of fresh (F) and cooked (C) leaf extracts of the traditional mixed-green salad of the Capuchin monks: *Plantago coronopus* L. (PC), *Rumex acetosa* L. (RA), *Cichorium intybus* L. (CI), and *Artemisia dracunculus* L. (AD). Results, which represent the average ± S.D. of three independent experiments in triplicate (n = 3), were expressed as mg of reference compound (gallic acid, quercetin, catechin and cyanidin for total phenols, flavonoids, vanillin index and proanthocyanidins, respectively) equivalents/100 g of dry extract (DE). Total chlorophyll and carbohydrates content were expressed as mg/g and g/100 g of fresh weight (FW), respectively.

Plant Extracts	Total Phenols	Flavonoids	Vanillin Index	Proanthocyanidins	Total Chlorophyll	Carbohydrates
PCF	1704.00 ± 93.22 [a,d]	8594.25 ± 43.49 [a,d]	446.96 ± 35.67 [a,d]	1.27 ± 0.01 [a,d]	0.93 ± 0.02 [a]	0.60 ± 0.02 [a,d]
RAF	644.71 ± 25.28 [b,e]	2364.09 ± 7.01 [b,e]	53.74 ± 3.88 [b]	6.00 ± 0.25 [b,e]	1.04 ± 0.03 [b,e]	0.39 ± 0.01 [b,e]
CIF	1025.83 ± 95.63 [f]	3613.59 ± 68.05 [c,f]	10.75 ± 0.67 [c,f]	3.73 ± 0.17 [c,f]	1.14 ± 0.02 [f]	0.54 ± 0.02 [c,f]
ADF	1170.29 ± 101.90	1567.33 ± 95.21 [g]	134.36 ± 5.24 [g]	0.07 ± 0.00 [g]	1.13 ± 0.01	0.48 ± 0.01
PCC	0.88 ± 686.37 [a]	0.83 ± 1002.87 [a]	557.38 ± 10.34 [a]	16.33 ± 0.58 [a]	0.94 ± 0.02 [a]	1.92 ± 0.03 [a]
RAC	1202.31 ± 50.21 [b]	2921.38 ± 83.13 [b]	60.65 ± 3.94 [b]	2.83 ± 0.05 [b]	0.84 ± 0.01 [b]	0.14 ± 0.00 [b]
CIC	1476.96 ± 61.66 [c]	6355.65 ± 93.30 [c]	17.47 ± 0.49 [c]	9.55 ± 0.12 [c]	1.05 ± 0.03	0.21 ± 0.00 [c]
ADC	1298.73 ± 84.36	8767.83 ± 430.86	685.52 ± 5.23	13.13 ± 0.24	1.09 ± 0.04	0.48 ± 0.01

[a] $p < 0.05$ vs. RAF or RAC, CIF or CIC, and ADF or ADC, between fresh and cooked extracts, respectively; [b] $p < 0.05$ vs. CIF or CIC, and ADF or ADC, between fresh and cooked extracts, respectively; [c] $p < 0.05$ vs. ADF or ADC, between fresh and cooked extracts, respectively; [d] $p < 0.05$ vs. PCC; [e] $p < 0.05$ vs. RAC; [f] $p < 0.05$ vs. CIC; [g] $p < 0.05$ vs. ADC.

Specifically, the results obtained with the fresh extracts and those obtained with the blanched extracts were compared with each other, and then the results obtained with each fresh extract was compared to the corresponding blanched extract.

Already in the extracts obtained from fresh leaves, important differences were found. PCF, in particular, showed the highest content of total phenols, flavonoids, flavanols and carbohydrates with statistically significant results ($p < 0.05$) compared to all other plant species investigated (Table 2). The total phenols content, in particular, is about double with respect to that previously reported by Janković et al. [48], who observed a total phenols content for *P. coronopus* equal to 925 mg GAE/100 g DE.

The other plants, on the contrary, showed a very variable trend depending on the class of bioactive compound investigated. With respect to the total phenols content, ADF resulted as the richest one, followed by CIF and RAF, while it was the poorest in terms of flavonoids after RAF and CIF. However, examining the class of flavanols, it appears again as the richest one after PCF, RAF and CIF. Finally, in terms of proatocyanidins, RAF was found to be the richest extract, followed by CIF, PCF and ADF.

On the contrary, CIF and ADF represent the richest source of chlorophyll without any statistically significant difference between them, followed by RAF and PCF ($p < 0.05$). Moreover, CIF contains the highest content of carbohydrates after PCF ($p < 0.05$), followed by ADF and RAF ($p < 0.05$) (Table 2).

Surprisingly, the leaf blanching statistically, and significantly, increased ($p < 0.05$) the bioactive compounds content in all the extracts investigated, with the exception of the total phenols, chlorophyll and carbohydrates content in ADF, which showed comparable amounts. The same trend was observed also for PCF, but only for chlorophyll content (Table 2).

Indeed, apart from the total chlorophyll and carbohydrate content of RAC and CIC, whose decreased in a statistically significant manner after blanching with respect to RAF and CIF ($p < 0.05$), and ADC, which remained unchanged, in all other cases, the blanched leaf extracts showed a bioactive compounds content from 1.2 to 13 times higher than the fresh leaf extracts (Table 2).

These results are in accordance with previous studies, which highlighted that the blanching process resulted in a significant increase in total phenols and flavonoids as result of their easily extraction by plant cell membrane disruption [49–52]. Similar observations, in particular, were reported also for coriander and majorana leaves [51,53]. During blanching, indeed, exposure to high-temperature steam can cause tissue disruption and the release of polyphenols from the vacuole or other cellular structures. However, this phenomenon, and consequently the extent of tissue damage, is strictly related to the plant's heat tolerance [54]. Furthermore, the degree to which phytochemicals change during processing depends on their structure and, consequently, by the sensitivity of the compound to the heat-induced modification or degradation [55]. The only decrease was recorded in terms of the proanthocyanidins content in RAC. It must be said, however, that RAF, the corresponding fresh leaf extract, showed the highest proanthocyanidins content, compounds well known to give depolymerization after heating leading to an increase in terms of monomeric polyphenols [56].

This phenomenon appears even more evident calculating the polymerization index (vanillin index/proanthocyanidins). Indeed, the extracts obtained from fresh leaves have a significantly higher polymerization index ($p < 0.05$) than the corresponding extracts obtained from blanched leaves (350.62 vs. 34.13 for PCF and PCC, respectively; 8.96 vs. 4.62 for RAF and RAC, respectively; 2.89 vs. 1.83 for CIF and CIC, respectively; 2028.95 vs. 242.15 for ADF and ADC, respectively) having a much higher flavanols content than proanthocyanidins. However, after blanching, this index is significantly reduced as a result of a substantial increase in the proanthocyanidins content and a more restrained flavanol content, leading to a greater presence of monomeric molecules. These results are in accordance with White et al. [50], who observed a significant increase in both proanthocyanidins oligomers and polymers after blanching.

From the calculation of the polymerization index, it is possible to deduce also that AD is the plant characterized by the greatest number of polymeric molecules, followed by PC, RA and CI.

The plant species investigated showed a comparable amount of carbohydrates with respect to previous studies carried out on fresh salads [57], and a higher content of total chlorophyll with respect to previous investigations (1.04 and 0.93 mg/g vs. 0.56 and 0.76 mg/g for RA and PC, respectively; 1.14 mg/g vs. 0.30 mg/g for CI; 1.13 mg/g vs. 0.89 mg/g for AD) [58–60] that could be attributed to the freshness and young leaves used in the present study, as well as also by the speed with which they were processed after collection.

Even in the case of chlorophyll and carbohydrates, the results reflect those reported in the literature, which state that rapid blanching does not influence or has very little influence on the content of these substances, with a sometimes-significant increase in the same after cooking, which allows an increase in the biological activity observed [61,62].

To conclude, after blanching, all plant leaves investigated, showed a higher content of bioactive compounds, albeit with substantial differences in some cases in terms of the phytochemical profile. However, among the investigated species, PC continues to be the extract that shows the highest content of total phenols, flavonoids, flavanols, chlorophyll and carbohydrates, certainly proving to be the most interesting plant in terms of phytochemical profile, becoming also the richest one in proanthocyanidins following cooking.

2.3. Health Properties

The extracts obtained by fresh and blanched plant leaves were also characterized from a biological point of view using a battery of antioxidant and anti-inflammatory tests based on different environments and reaction mechanisms. This is very important, since, given the complexity of a plant extract in terms of phytochemicals, it is impossible to evaluate its antioxidant and anti-inflammatory activity with a single method [52]. Considering this, four different antioxidant assays based on electron transfer (FRAP), electrons' and hydrogen atoms' transfer (TEAC), hydrogen atom transfer (ORAC) and iron-chelating activity, were carried out. Regarding anti-inflammatory activity, the heat-induced BSA denaturation assay (BDA) and the protease inhibitory activity test (APA), were carried out. The first one is based on the sample's ability to protect endogenous proteins against denaturation, whereas the second one is based on the sample's ability to inhibit directly the protease, an enzyme well-known to be involved in several inflammatory-based diseases [63].

The results of the health properties of the extracts under examination, expressed as IC_{50} (μg/mL) with the respective C.L., are shown in Table 3. Additionally, in this case, the results obtained for the fresh extracts, as well as those obtained from the blanched extracts were compared between them. Furthermore, the results of each fresh extract were compared with those obtained with the extract of the respective blanched leaves.

All the samples showed a marked and concentration-dependent antioxidant and anti-inflammatory activity (Figures 4 and 5, respectively), although there are important and statistically significant differences between the different extracts investigated, both as fresh and blanched extracts (Table 3).

First of all, when comparing the results of the extracts obtained from fresh leaves, the same order of activity appears evident, with PCF, which showed the strongest antioxidant activity, followed by ADF, CIF and RAF, both in the TEAC and FRAP test (Table 3 and Figure 4). The situation changes radically instead in the ORAC test, where ADF shows the highest antioxidant activity, followed by CIF, PCF and RAF, which holds the last position (Table 3 and Figure 4). On the contrary, RAF exhibits the strongest iron-chelating activity, followed by CIF, ADF and PCF (Table 3 and Figure 4). This order of potency positively correlates with the total phenols and flavonoids content, and the slight differences found in terms of activity between the extracts under study can be attributed to the greater or lesser expression of some secondary metabolites, as seen in Table 2, as well as from the specific chemical structures of the polyphenols present [51].

Table 3. Comparison between the health properties of fresh (F) and cooked (C) leaf extracts of the traditional mixed-green salad of the Capuchin monks: *Plantago coronopus* L. (PC), *Rumex acetosa* L. (RC), *Cichorium intybus* L. (CI), and *Artemisia dracunculus* L. (AD). Results, which represent the average of three independent experiments in triplicate (n = 3), were expressed as half maximal inhibitory concentration (IC_{50}, μg/mL) with confident limits (C.L.) at 95%.

Plant Extracts	TEAC	FRAP	ORAC	ICA	BDA	APA
PCF	230.20 (190.47–278.22) [a,d]	244.38 (171.30–348.57) [a,d]	2.41 (1.94–2.50) [d,g]	22.66 (19.28–26.62) [a,d]	970.22 (405.66–2330.12)	701.55 (350.55–1430.22)
RAF	1111.82 (831.15–1487.27) [b,e]	1970.96 (1493.70–2600.70) [b,e]	5.67 (4.60–6.98) [b,e]	6.63 (5.79–7.60) [c]	910.11 (762.33–1092.11)	1141.22 (891.99–1480.21) [b]
CIF	510.96 (419.14–622.89) [f]	841.48 (709.86–997.51) [c,f]	1.89 (1.50–2.38) [f]	7.80 (6.53–9.33)	1020.31 (862.05–1224.58)	540.34 (462.22–640.12)
ADF	331.66 (258.54–425.47)	546.40 (444.0–672.0)	1.36 (0.95–1.96)	9.85 (8.10–11.97)	980.08 (842.34–1162.66)	441.22 (380.05–510.11)
PCC	31.89 (27.06–37.59) [a]	31.35 (26.51–37.09) [a]	0.30 (0.25–0.37) [a]	9.05 (7.49–10.95)	760.25 (650.22–890.27)	440.04 (190.10–992.90)
RAC	377.70 (296.34–481.39)	383.59 (322.90–455.69)	1.94 (1.58–2.39) [f]	6.52 (5.76–7.38)	861.33 (731.22–1020.66)	871.22 (730.22–044.10) [b]
CIC	273.80 (228.12–328.63)	396.67 (331.67–474.40)	1.10 (0.89–1.36)	7.64 (6.47–9.02)	970.02 (812.49–1151.08)	371.02 (142.04–960.07)
ADC	278.10 (220.15–353.57)	425.20 (343.0–527.0)	1.22 (0.93–1.60)	7.11 (6.06–8.35)	812.42 (692.77–951.55)	240.20 (212.33–298.99) [c]
Standard	3.28 (2.44–3.89) [h]	3.88 (1.62–5.78) [h]	0.79 (0.39–1.65) [i]	6.48 (5.22–7.68) [l]	31.82 (26.58–38.10) [h]	32.88 (25.22–39.13) [h]

* Standard: trolox for TEAC, ORAC and FRAP assays, EDTA for iron-chelating activity (ICA), diclofenac sodium for BSA denaturation assay (BDA) and anti-protease activity (APA). [a] $p < 0.05$ vs. RAF or RAC, CIF or CIC, and ADF or ADC, between fresh and cooked extracts, respectively; [b] $p < 0.05$ vs. CIF or CIC, and ADF or ADC between fresh and cooked extracts, respectively; [c] $p < 0.05$ vs. ADF; [d] $p < 0.05$ vs. PCC; [e] $p < 0.05$ vs. RAC; [f] $p < 0.05$ vs. CIC; [g] $p < 0.05$ vs. RAF; [h] $p < 0.05$ vs. all extracts investigated; [i] $p < 0.05$ vs. PCF and RAF; [l] $p < 0.05$ vs. PCF and ADF.

What is certain, however, is that the marked iron-chelating activity found in RAF is attributable to the high proanthocyanidins content found in this extract. Indeed, it has been shown, both in vitro and in vivo, that proanthocyanidins, thanks to their strong iron-chelating activity, act as antimicrobial agents [64] and protect against oxidative renal damage induced by iron overload in rats [65].

Despite that no statistically significant difference was found between the extracts under examination, in terms of the inhibition of heat-induced protein denaturation (BDA) (Table 3), also in this case, the proanthocyanidins content seems to play a pivotal role in the activity of RAF extract, which shows the lowest IC_{50} value and, therefore, the most marked anti-inflammatory activity, followed by PCF, CIF and ADF. The activity found, attributable to an anti-peroxidase activity of the extract under study, has been previously observed for other proanthocyanidins-rich extracts [66].

On the contrary, the strong anti-tryptic activity was recorded for ADF, followed by CIF, PCF and RAF. However, specifically, a statistically significant difference was found only between RAF, CIF and ADF (Table 3 and Figure 5). This activity seems to correlate mainly with the total content of phenols and flavanols, although what makes the difference is the structure of the main polyphenols present in the extracts under examination, rather than the class of compounds. Indeed, being an enzymatic activity, it implies a direct interaction of the bioactive compound/s at the enzyme level.

Finally, it is interesting to note that, in accordance with what has been observed for the phytochemical characterization, the extracts obtained from blanched leaves show a much more pronounced free-radical scavenging (TEAC, FRAP and ORAC assay) than the extracts obtained from fresh leaves, with statistically significant results for all tested extracts except ADC ($p < 0.05$). On the contrary, no statistically significant difference was found as regards the iron-chelating activity and the anti-inflammatory activity, in which the extracts obtained from the cooked leaves did not show a statistically significant difference compared to the corresponding extracts obtained from the fresh leaves.

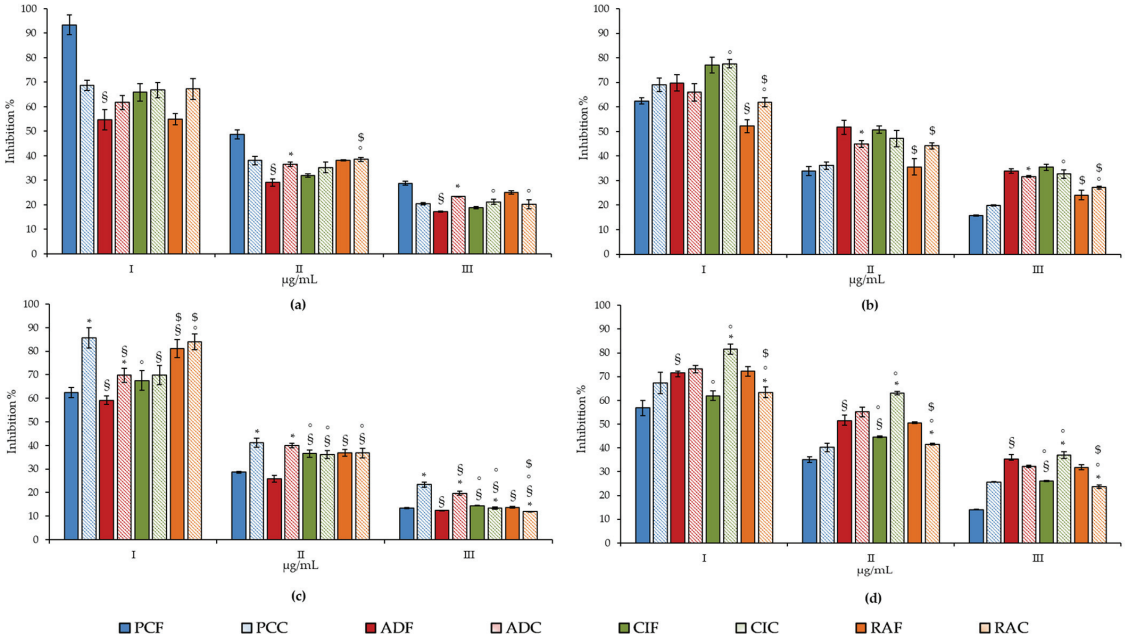

Figure 4. Antioxidant and free radical-scavenging activity of fresh (F) and cooked (C) leaf extracts of the traditional wild salad of the Capuchin monks: *Plantago coronopus* L. (PC), *Rumex acetosa* L. (RC), *Cichorium intybus* L. (CI), and *Artemisia dracunculus* L. (AD). Results were expressed as mean inhibition percentage (%) ± standard deviation of three independent experiments (n = 3). (**a**) FRAP, concentration ranges (I–III): 12.5–50.0 µg/mL for PCC; 150.0–600.0 µg/mL for PCF, RAC, CIC, ADF and ADC; 300.0–1200.0 µg/mL for CIF; 600–2400.0 µg/mL for RAF; (**b**) TEAC, concentration ranges (I-III): 12.5–50.0 µg/mL for PCC; 80.0–320.0 µg/mL for PCF; 150.0–600.0 µg/mL for ADC, ADF, CIC and RAC; 300.0–1200.0 µg/mL CIF and RAF; (**c**) Ferrozine, concentration ranges (I–III): 3.0–12.0 µg/mL for PCF, RAF, RAC, CIF, CIC, ADF and ADC; 12.0–48.0 µg/mL for PCC; (**d**) ORAC, concentration ranges (I–III): 0.12–0.50 µg/mL for PCC; 0.5–4.0 µg/mL for PCF, CIF, CIC, ADF, ADC and RAC; 1.5–12.0 µg/mL for RAF. * $p < 0.05$ vs. fresh extract; § $p < 0.05$ vs. PCF or PCC; $^{\circ}$ $p < 0.05$ vs. ADF or ADC; $^{\$}$ $p < 0.05$ vs. CIF or CIC.

The increase or retention of total phenols, flavonoids and proanthocyanidins content, as well as of the antioxidant and anti-inflammatory activity of plant extracts during blanching, may be mainly ascribed to the increase of individual polyphenols or to their thermal degradation through, for example, deglycosylation or hydrolysis processes, which contribute differently, with respect to the parent compounds, to the health properties investigated [50]. Although an in-depth phytochemical characterization is outside the topic of this manuscript, comparing completely different plant species from a phytochemical point of view, recent studies have shown that the plants subject to this study are particularly rich in complex polyphenols, mostly glycosylated and esterified. In particular, *P. coronopus* is characterized by the iridoid glucosides, aucubin and catalpol, as well as the phenylpropanoid glycoside, acteoside. Among flavonoids, luteolin- and apigenin-7-*O*-glucoside represent the most abundant compounds [48]. The phytochemical profile of *R. acetosa* includes anthraquinones, polyphenols and a high level of oxalic acid, which seems to be reduced to a negligible amount during cooking. The main phenolic compounds present include resveratrol, vanillic and sinapic acid and catechin. The leaves contain also β-carotene, but not in a significant amount for human health [18]. The phytochemical profile of *A. dracunculus* showed, apart from the characteristic lactones, artemisinin, dihydroartemisinin and artemether, several flavonoids among which the most abundant are rutin, luteolin,

naringenin and chrysin [67]. Regarding *C. intybus*, other than some simple phenolics such as malic, caffeic, quinic, caftaric and chlorogenic acid, all identified components were in the glycosylated or ester form. Among these, the most abundant are the glycosylated derivatives of cyanidin, delphinidin, quercetin, kaempferol, isorhamnetin and apigenin. Furthermore, acetyl and malonyl derivatives were also found [68,69].

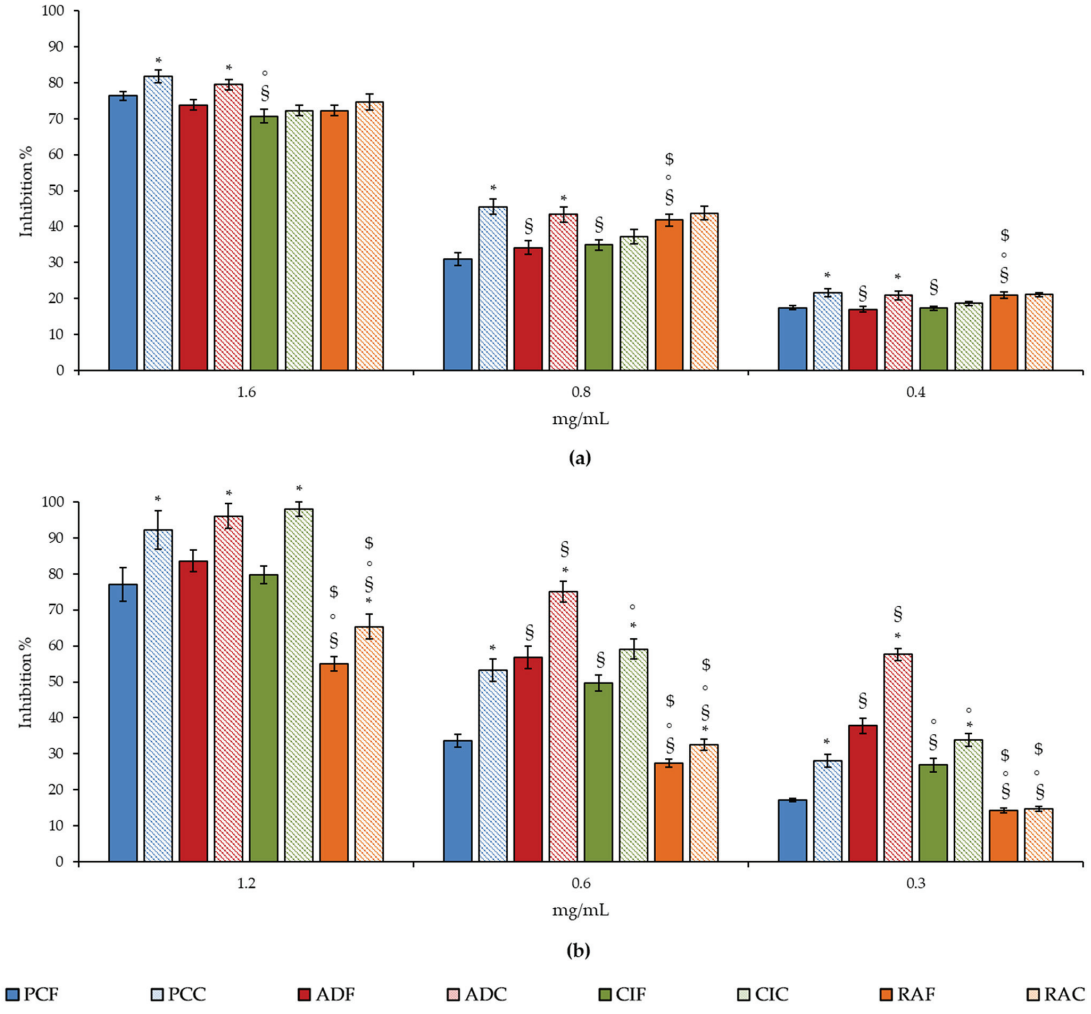

Figure 5. Anti-inflammatory activity of fresh (F) and cooked (C) leaf extracts of the traditional wild salad of the Capuchin monks: *Plantago coronopus* L. (PC), *Rumex acetosa* L. (RC), *Cichorium intybus L.* (CI), and *Artemisia dracunculus* L. (AD) towards BSA denaturation assay (**a**) and protease inhibition assay (**b**). Results were expressed as mean inhibition percentage (%) ± standard deviation of three independent experiments ($n = 3$). * $p < 0.05$ vs. fresh extract; § $p < 0.05$ vs. PCF or PCC; $^{\circ}$ $p < 0.05$ vs. ADF or ADC; $^{\$}$ $p < 0.05$ vs. CIF or CIC.

In addition, the contribution of non-phenolic substances such as sugars or ascorbic acid must not be neglected, because they can contribute in particular to the reducing ability of the plant extracts. Finally, synergistic and additive effects of polyphenols may enhance the biological activity observed [51].

3. Materials and Methods

3.1. Plant Material and Growth Conditions

Seeds of PC, RA, CI, and AD were purchased from Fratelli Ingegnoli Spa (Milano, Italy) and sown according to Poorter et al. [70].

Briefly, they were sown in plastic plug within a greenhouse located in San Barnaba convent (Genova, Italy, 190masl; 44°25′26″ N 8°55′42″ E, https://goo.gl/maps/UaN9eCS9cWtQvcT56, accessed on 22 January 2022) (Figure 6a,b) and equipped with additional UV artificial lighting to ensure constant daily irradiation and fine-textured shade-nets to attenuate the excessive solar overheating according to Lenka et al. [71].

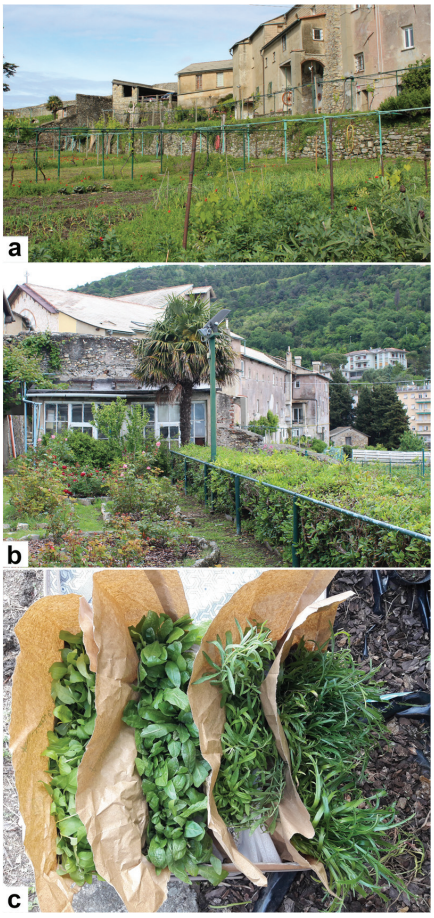

Figure 6. (**a**,**b**) San Barnaba Convent vegetable garden and greenhouses (Genova, Italy); (**c**) plants collected after 60 days for carrying out laboratory analyses.

Plastic plug trays were filled with Irish peat (Vigorplant Italia Srl) and after fifteen days 1 g/L NPK 20-10-20 water soluble fertilizer (Vialca Srl) was added once a week. In the first two weeks, plants were watered (about 180 mL) twice a day for three days a week (Monday, Wednesday, Friday). Subsequently, they were watered once a day, only on Monday and Friday.

After two months, the plant leaves were collected (Figure 6c) and immediately sent to the laboratory, where they were suitably processed for micromorphological, phytochemical and biological analyses.

3.2. Scanning Electron Microscopy (SEM) Analysis

Plant leaves were cut, using a razor blade, into small pieces (15–20 mm^2). Such dimensions have allowed to have sufficient surfaces of both leaf pages to analyze the distinctive characters of the selected species. Samples were fixed in FineFIX working solution (Milestone s.r.L., Bergamo, Italy) with 70% ethanol, and left overnight at 4 °C [72]. The next day, samples were serially dehydrated in ethanol (80, 90, 95 and 100%) for 1 h, and then in CO_2 using a Critical Point Drier processor (K850 CPD 2M Strumenti S.r.l., Roma, Italy).

Dried specimens were mounted on stubs using double stick tape and coated with 10 nm gold. SEM analysis was carried out using a Vega3 Tescan LMU (Tescan USA Inc., Cranberry Twp, PA, USA) at an accelerating voltage of 20 kV.

3.3. Mixed Salad Traditional Recipe

The plants analyzed in this study are part of the recipe of a mixed salad reported by Zaccaria Boverio in 1626 [73]. These plants were also cited in other contemporary texts dealing with salads, such as *Archidipno* by Salvatore Massonio (1627) [74]. According to Zaccaria Boverio, the plants used in the Capuchin monks mixed salad were: Coronopum (*Plantago coronopus* L.), Intubum (*Cichorium intybus* L.), Oxalim (*Rumex acetosa* L.), Draconculum (*Artemisia dracunculus* L.), Pimpinellam (*Poterium sanguisorba* L.), Lactucas crispas (*Lactuca sativa* L. var. crispa), Lactucas laconicas (*Lactuca sativa* L. var. capitata), Nasturcium (Nasturtium officinale W.T. Aiton), Rapa sylvestria (*Brassica rapa* L. subsp. sylvestris (L.) Janch.) and Mentam (*Mentha* spp.). This mixed salad was known as "insalatina dei frati".

One of the most frequently reported cooking methods throughout history has been represented by a short boiling or blanching. This method is still commonly mentioned in ethnobotanical studies concerning the use of WEPs in Mediterranean area [75]. In addition, it is used both at domestic level and in the food industry to inactivate enzyme activity and to preserve vegetables [76].

3.4. Chemicals

All reagents and solvents were of analytical grade and, as well as trolox, were purchased from Merck (Darmstadt, Germany). Standard compounds (gallic acid, quercetin, catechin, cyanidin chloride) were purchased from Extrasynthese (Genay, France).

3.5. Sample Processing and Extract Preparation

For each plant species collected (PC, RA, CI, and AD), leaves were cut, gently cleaned with paper and weighed (50 g). In order to obtain the fresh extracts (PCF, RAF, CIF, and ADF), the leaves were added directly in a blade mill pulverization chamber (A11, IKA®-Werke GmbH & Co. KG, Staufen, Germany) to which was added liquid nitrogen during powdering, in order to preserve the nutritional and chemical features by blocking enzymatic activities. For cooked plant extracts (PCC, RAC, CIC, and ADC), leaves, before powdering according to the above protocol, were added to boiling water and blanched for 1 min in compliance with the most traditionally used cooking method.

Thereafter, powdered raw or cooked leaves (10 g for each plant species) were added with 100 mL 70% ethanol, mixed for 3 min and then sonicated in ice-cold bath for 5 min using a 3 mm titanium probe set to 200 W and 30% amplitude (Vibra Cell™ Sonics Materials, Inc., Danbury, CT, USA). Samples were centrifuged at 3000× *g* for 15 min at 4 °C and the supernatants were evaporated to dryness by a rotary evaporator at RT. The extraction procedure was repeated 3 times. Dry extracts (DE) were stored for 24 h in a vacuum desiccator in the dark on anhydrous sodium sulphate and subsequently stored at −20 °C until the subsequent analyses, which were carried out solubilizing and appropriately diluting the dry extracts in the extraction solvent (70% ethanol).

3.6. Phytochemical Screening

3.6.1. Total Phenols

Total phenols were quantified according to Bazzicalupo et al. [77] using the Folin–Ciocalteu reagent, by mixing each extract solution (6.0–24.0 mg/mL for PCF, RAF, RAC, CIF, CIC, ADF and ADC; 0.5–2.0 mg/mL for PCC) with deionized water and Folin–Ciocalteu reagent in the following ratio: 1:9:10, *v*/*v*/*v*. After 3 min, 10% sodium carbonate (1:2, *v*/*v*) was added and samples were incubated for 60 min in the dark at RT, mixing every 10 min. The absorbance was recorded at 785 nm with a UV-VIS spectrophotometer (Shimadzu UV-1601, Kyoto, Japan). Gallic acid was used as reference compound (0.075–0.60 mg/mL) and results, which represent the average of three independent experiments in triplicate (n = 3), were expressed as mg of gallic acid equivalents (GAE)/100 g DE.

3.6.2. Flavonoids

The flavonoid content was quantified according to Smeriglio et al. [78]. Briefly, 200 µL of each extract solution (3–12.0 mg/mL for PCF, RAF, CIF, CIC and ADF; 6.0–24.0 mg/mL for ADC and RAC; 0.20–0.80 mg/mL for PCC) were added to 2 mg/mL $AlCl_3$ (1:1, *v*/*v*), and brought up to 1.6 mL with 50 mg/mL sodium acetate. After 2.5 h, the absorbance was recorded at 440 nm using an UV–Vis spectrophotometer (Shimadzu UV-1601, Kyoto, Japan). Quercetin was used as reference compound (0.25–1.0 mg/mL) and results, which represent the average of three independent experiments in triplicate (n = 3), were expressed as mg of quercetin equivalents (QE)/100 g DE.

3.6.3. Vanillin Index

The flavanols content was evaluated according to Boudjelal et al. [79] by vanillin index test. Briefly, 2.0 mL of sample solution, diluted in 0.5 M H_2SO_4 in order to reach an absorbance ranging from 0.2 to 0.4 (1.75 mg/mL for ADC; 3.5 mg/mL for PCF, PCC and ADF; 6.25 mg/mL for RAC, CIF and CIC; 12.5 mg/mL for RAF), were loaded onto a conditioned Sep-Pak C18 cartridge (Waters, Milan, Italy). The column was activated by 2.0 mL of 5.0 mM H_2SO_4 and then air-purged. Samples were slowly eluted by adding 5.0 mL of methanol. Six millilitres of a 4% vanillin methanol solution were added to 1 mL of sample eluate, incubating in a water bath at 20 °C for 10 min. After this, 3 mL of HCl was added and after 15 min, the absorbance was recorded at 500 nm with a UV-VIS spectrophotometer (Model UV-1601, Shimadzu, Kyoto, Japan) against a blank consisting of the same sample solvent. Catechin was used as reference compound (0.125–0.50 mg/mL). Results, which represent the average of three independent experiments in triplicate (n = 3), were expressed as g of cathechin equivalents (CE)/100 g DE.

3.6.4. Proanthocyanidins

The proanthocyanidin content was evaluated according to Baali et al. [80]. Briefly, 2.0 mL of sample solution diluted with 0.05 M H_2SO_4 (0.75 mg/mL for PCC; 5 mg/mL for PCF, PCC, ADF and ADC; 10 mg/mL for RAC and CIF; 20 mg/mL for RAF), was loaded onto a Sep-Pak C18 cartridge (Waters, Milan, Italy) preconditioned with 5 mM H_2SO_4 (2.0 mL), and purged with air. Samples were eluted with methanol (3.0 mL) and collected in a 100 mL flask shielded from light, containing 9.5 mL of absolute ethanol. After that, 12.5 mL of $FeSO_4 \cdot 7H_2O$ solubilized in 37% HCl (300 mg/L) was added to the reaction mixture and placed to reflux for 50 min. After cooling by immersion in cold water (20 °C) for ten min, the absorbance was read at 550 nm with an UV-VIS spectrophotometer (Model UV-1601, Shimadzu, Kyoto, Japan) against a blank consisting of the same sample solvent. The basal anthocyanins content of samples was determined detracting the absorbance of samples prepared under the same conditions reported above, without the reflux process. Proanthocyanidins content was expressed as 5 times the amount of cyanidin formed by means of a cyanidin chloride (ε = 34,700) calibration curve. Results, which represent the average of three independent experiments in triplicate (n = 3), were expressed as mg of cyanidin equivalents (CyE)/100 g DE.

3.6.5. Chlorophyll Determination

The total chlorophyll content (chlorophyll a + chlorophyll b) was evaluated according to Porra et al. [81]. Briefly, 0.2 g of leaves of fresh and blanched PC, RA, CI and AD were homogenized in an ice-cold mortar with quartz sand by adding 1 mL of 80% acetone for three times. Samples were then poured in a screw cap glass tube, washing with 1 mL of acetone, and centrifuged at 3000× *g* for 10 min, 4 °C. The supernatants were recovered with a glass Pasteur pipette and stored in a graduated glass cylinder in the dark. The sample pellets were resuspended with 2 mL of 80% acetone and centrifuged as described above. This procedure was repeated until exhaustive extraction. Finally, the supernatants were pooled in the cylinder and the volume noted to calculate the dilution factor. The absorbance was recorded at 663 nm to quantify chlorophyll *a*, and at 648 nm to quantify chlorophyll *b* content, according to the following equations:

$$Chlorophyll\ a\ (\mu g/mL) = 12.25 \times ABS(663\ nm) - 2.55 \times ABS\ (648\ nm)$$

$$Chlorophyll\ b\ (\mu g/mL) = 20.31 \times ABS(648\ nm) - 4.91 \times ABS\ (663\ nm)$$

Results, which represent the average of three independent experiments in triplicate (n = 3), were expressed as mg/g of fresh weight (FW).

3.6.6. Carbohydrates

The carbohydrates content was determined according to Bazzicalupo et al. [77]. Briefly, 10 mg of fresh and blanched PC, RA, CI and AD were placed in a glass test tube with screw cap, together with 0.5 mL of 2.5 mol/L HCl, and the mixture was incubated in a water bath at 100 °C for 3 h. After cooling, samples were neutralized with sodium carbonate and brought up to 10 mL with distilled water. After centrifugation at 3500× *g* for 5 min, 20 µL of each sample, blank (distilled water) or reference standard (glucose 5–100 µg/mL), were brought up to 200 µL with distilled water. Two-hundred microliters of 5% phenolic solution and 1 mL of 96% H_2SO_4 were added and the reaction mixture was stirred for 10 min and incubated in a water bath at 30 °C for 20 min. The absorbance was recorded at 490 nm and results, which represent the average of three independent experiments in triplicate (n = 3), were expressed as g/100 g of fresh weight (FW).

3.7. Evaluation of Health Properties: Antioxidant and Anti-Inflammatory Activity

The health properties of fresh and cooked extracts were evaluated by several colorimetric in vitro cell-free assays based on different reaction mechanisms and environments. Absorbance and fluorescence data, acquired by a UV-VIS (Multiskan GO; Thermo Scientific, MA, USA) and a fluorescence plate reader (Fluostar Omega, BMG labtech, Ortenberg, Germany), respectively, were recorded against a blank consisting of samples' extraction solvent (70% ethanol). Results, which represent the average of three independent experiments in triplicate (n = 3), were expressed as half-maximal inhibitory concentration (IC_{50}, µg/mL) with confident limits (CLs.) at 95%, calculated by the Litchfield and Wilcoxon test, using PHARM/PCS software version 4 (MCS Consulting, Wynnewood, PA, USA). Sample and reference compound concentration ranges reported below refer to the final concentrations into the reaction mixture, which did not show any interference at the characteristic wavelengths of the tests carried out.

3.7.1. Antioxidant Activity

Trolox Equivalent Antioxidant Capacity (TEAC) Assay

The TEAC test was performed according to the method described by Smeriglio et al. [82], with some modifications. Briefly, the reagent solution consisting of 1.7 mM ABTS and 4.3 mM $(NH_4)_2S_2O_8$ was incubated in the dark at RT for 12 h, diluted with deionized water until an absorbance of 0.7 ± 0.02 at 734 nm, and used within 4 h. Five microliters (5 µL) of each sample solution (12.5–50.0 µg/mL for PCC; 80.0–320.0 µg/mL for PCF; 150.0–600.0 µg/mL for ADC, ADF, CIC and RAC; 300.0–1200.0 µg/mL CIF and RAF)

were added to 100 µL of the reagent solution, mixed and incubated in the dark for 6 min at RT. The absorbance was recorded at 734 nm using trolox (1.0–4.0 µg/mL) as reference compound.

Ferric Reducing Antioxidant Power (FRAP) Assay

The FRAP test was carried out according to Muscarà et al. [83], with some modifications by using a fresh pre-warmed (37 °C) reagent consisting of 300 mM buffer acetate (pH 3.6), 10 mM 2,4,6-Tris (2-pyridyl)-s-triazine (TPTZ)-40 mM HCl, and 20 mM $FeCl_3$. Briefly, 5 µL of each sample solution (12.5–50.0 µg/mL for PCC; 150.0–600.0 µg/mL for PCF, RAC, CIC, ADF and ADC; 300.0–1200.0 µg/mL for CIF; 600.0–2400.0 µg/mL for RAF) were incubated for 4 min with 100 µL of the above reagent and the absorbance was recorded at 593 nm by using trolox (1.0–4.0 µg/mL) as reference compound.

Oxygen Radical Absorbance Capacity (ORAC) Assay

The ORAC test was carried out according to Smeriglio et al. [84]. Twenty microliters of sample solution (0.12–0.5 µg/mL for PCC; 1.0–4.0 µg/mL for PCF, CIF, CIC, ADF, ADC and RAC; 3.0–12.0 µg/mL for RAF) diluted in 75 mM phosphate buffer (pH 7.4), were mixed with 117 nM fresh fluorescein solution (120 µL) and incubated for 15 min at 37 °C, before adding 40 mM fresh AAPH solution (60 µL) to start the reaction. The probe decay was monitored for 90 min by recording the fuorescence intensity every 30 s using the following excitation and emission wavelengths: λ_{ex} 485 nm and λ_{em} 520 nm. Trolox (0.25–1.0 µg/mL) was used as reference compound.

Iron-Chelating Activity

Iron-chelating activity was evaluated by ferrozine assay according to Muscarà et al. [85], with some modifications. Five microliters of each sample solution (3.0–2.0 µg/mL for PCF, RAF, RAC, CIF, CIC, ADF and ADC; 12.0–48.0 µg/mL for PCC), ethylenediaminetetraacetic acid (EDTA) as reference standard (3.0–12.0 µg/mL), or blank (70% ethanol), were added to 2.5 µL of 2 mM $FeCl_2 \cdot 4\ H_2O$ and incubated at RT for 5 min. After that, 5 µL of 5 mM ferrozine and 137.5 µL of deionized water were added to the reaction mixture. The absorbance was recorded after 10 min at 562 nm.

3.7.2. Anti-Inflammatory Activity

Bovine Serum Albumin (BSA) Denaturation Assay

The BSA denaturation assay was carried out according to Denaro et al. [86]. Briefly, 80 µL of each sample solution (0.075–0.60 mg/mL for CIF and CIC; 0.15–1.20 mg/mL for ADF, ADC, RAC, PCF and PCC; 1.2–9.60 mg/mL for RAF) were added to 100 µL of 0.4% BSA fatty acid-free solution and 20 µL of phosphate-buffered saline (PBS, pH 5.3). The absorbance was recorded at 595 nm at the starting time (T_0) and after incubation for 30 min at 70 °C in order to measure the samples' ability to counteract the heat-induced BSA denaturation. Diclofenac sodium (15.63–62.50 µg/mL) was used as a reference compound.

Protease Inhibition Assay

The anti-tryptic activity was evaluated according to Smeriglio et al. [87]. Briefly, 200 µL of each sample solution (0.20–1.60 mg/mL for PCF, PCC, ADF, ADC, CIF, CIC, RAF and RAC) was added to the reaction mixture consisting of 12 µL trypsin (10 µg/mL) and 188 µL Tris-HCl buffer (25 mM, pH 7.5). After that, 200 µL of 0.8% casein was added to the reaction mixture, starting the incubation time (20 min, 37 °C). Reaction was stopped by adding 400 µL perchloric acid, which allowed the protein precipitation, leading to a cloudy suspension, which was centrifuged at 3500× *g* for 10 min. The absorbance of the supernatant was recorded at 280 nm. Diclofenac sodium (15.63–62.50 µg/mL) was used as reference compound.

3.8. Statistical Analysis

Results, which represent the average of three independent experiments in triplicate ($n = 3$), were expressed as mean ± standard deviation (S.D.) for phytochemical analyses, and as IC_{50} with CLs. at 95% for health properties evaluation. Data were analysed by one-way analysis of variance (ANOVA) followed by Dunnett's test for antioxidant and anti-inflammatory assays, and Tukey's test for phytochemical screening by SigmaPlot 12.0 software (Systat Software Inc., San Jose, CA, USA). Results were considered statistically significant for $p < 0.05$.

4. Conclusions

In conclusion, the investigated ingredients of the Capuchin monks' mixed salad represent a good source of polyphenols with interesting antioxidant and anti-inflammatory properties if consumed both raw or briefly cooked. Blanching affects the bioactive compounds content, both as class and individual phytochemicals and, consequently, influences the health properties of the plant extracts differently, according to the matrix's features. However, this traditional cooking method for the Capuchin monks' salads proved to be a suitable method regarding the retention of phytochemicals and their health properties, unlike extended boiling, which resulted in compounds' leaching into the blanching water.

Considering this, our results indicate that increased consumption of the investigated plants, even more if cooked according to the tradition, could provide a healthy food source in the modern diet by the recovery and enhancement of ancient ingredients.

In particular, *P. coronopus*, which resulted the most interesting plant species from this point of view, is an unconventional food plant, little known for its organoleptic and nutritional properties, which is until today little known and appreciated for its organoleptic and nutritional properties, that could be an excellent candidate to be exploited for new crops and new gastronomic uses.

Author Contributions: Conceptualization, L.C. and A.S.; methodology, L.C., A.S., D.T., G.A. and A.A.; software, D.T. and A.A.; validation, L.C., A.S. and D.T.; formal analysis, A.S., L.C., G.A. and A.A.; investigation, D.T., L.C. and A.S.; resources, L.C. and D.T.; data curation, L.C., D.T., A.S., G.A. and A.A.; all authors contribute in writing, review and editing; visualization, L.C. and A.S.; supervision, L.C., A.S. and D.T.; project administration, L.C. and A.S. All authors have read and agreed to the published version of the manuscript.

Funding: This research received no external funding.

Institutional Review Board Statement: Not applicable.

Informed Consent Statement: Not applicable.

Data Availability Statement: The data presented in this study are available on request from the corresponding author.

Acknowledgments: We wish to thank the Provincia di Genova dei Frati Minori Cappuccini for the kind consultation of the ancient texts: Vincenzo Celesia, Selva Botanica, Genova 1892 (1MANOSSXX-64) and Zaccaria Boverio, De sacris ritibus . . . , Napoli 1626 (ISIL: IT-GE0039). We also thank Elena Mora (DISTAV Botanical Garden) for her technical help during plant cultivation.

Conflicts of Interest: The authors declare no conflict of interest.

References

1. Łuczaj, Ł. Ethnobotanical Review of Wild Edible Plants of Slovakia. *Acta Soc. Bot. Pol.* **2012**, *81*, 245–255. [CrossRef]
2. Savo, V.; Salomone, F.; Mattoni, E.; Tofani, D.; Caneva, G. Traditional Salads and Soups with Wild Plants as a Source of Antioxidants: A Comparative Chemical Analysis of Five Species Growing in Central Italy. *Evid.-Based Complement. Altern. Med.* **2019**, *2019*, 6782472. [CrossRef]
3. Guarrera, P.M.; Savo, V. Wild Food Plants Used in Traditional Vegetable Mixtures in Italy. *J. Ethnopharmacol.* **2016**, *185*, 202–234. [CrossRef]
4. Motti, R.; Bonanomi, G.; Lanzotti, V.; Sacchi, R. The Contribution of Wild Edible Plants to the Mediterranean Diet: An Ethnobotanical Case Study Along the Coast of Campania (Southern Italy). *Econ. Bot.* **2020**, *74*, 249–272. [CrossRef]

5. Pieroni, A.; Nebel, S.; Quave, C.; Münz, H.; Heinrich, M. Ethnopharmacology of Liakra: Traditional Weedy Vegetables of the Arbëreshë of the Vulture Area in Southern Italy. *J. Ethnopharmacol.* **2002**, *81*, 165–185. [CrossRef]
6. Leonti, M. The Future Is Written: Impact of Scripts on the Cognition, Selection, Knowledge and Transmission of Medicinal Plant Use and Its Implications for Ethnobotany and Ethnopharmacology. *J. Ethnopharmacol.* **2011**, *134*, 542–555. [CrossRef]
7. Watson, S. *On Hospitals. Welfare, Law, and Christianity in Western Europe*; Oxford University Press: Oxford, UK, 2020.
8. Mądra-Gackowska, K.; Gackowski, M.; Główczewska-Siedlecka, E. Medications of Medieval Monastery Medicine Assessment of Nutritional Status of Geriatric Patients View Project. *J. Educ. Health Sport* **2018**, *8*, 1667–1674. [CrossRef]
9. Jotischky, A. *A Hermit's Cookbook. Monks, Food and Fasting in the Middle Ages*; Continuum International Publishing Group: London, UK, 2011.
10. Ubrizsy, A. Funzione Degli Orti Botanici Nella Scuola Medica Dal XVI al XVIII Secolo in Italia. In *La Formazione del Medico in età Moderna (secc. XVIXVIII), Atti della XXXVIII Tornata di Studi Storici dell'Arte Medica e della Scienza, Fermo, Italy, 20–22 maggio 2010*; Sani, R., Zurlini, F., Eds.; EUM: Macerata, Italy, 2012; p. 37.
11. Åsen, P.A. Plants of possible monastic origin, growing in the past or present, at medieval monastery grounds in Norway, Plants and Culture: Seeds of the cultural heritage of Europe. In *Plants and Culture: Seeds of the Cultural Heritage of Europe*; Morel, J.P., Mercuri, A.M., Eds.; Edipuglia: Bari, Italy, 2009; pp. 227–238.
12. Giannetti, L. Italian Renaissance Food-Fashioning or the Triumph of Greens. *Calif. Ital. Stud.* **2010**, *1*, 1–16. [CrossRef]
13. Cesarini, G. II convento dei Cappuccini di Viterbo: Un esempio di organico sviluppo territoriale. *Bibl. Società* **2008**, *61*, 24–26.
14. Kiser, L.J. The Garden of St. Francis: Plants, Landscape, and Economy in Thirteenth-Century Italy. *Environ. Hist.* **2003**, *8*, 229–245. [CrossRef]
15. Cassiano da Langasco. *Un Pizzico di Misticanza. La Presa di Tabacco*; Sorriso Francescano: Genova, Italy, 1990.
16. Pereira, C.G.; Custódio, L.; Rodrigues, M.J.; Neng, N.R.; Nogueira, J.M.F.; Carlier, J.; Costa, M.C.; Varela, J.; Barreira, L. Avaliação Do Potencial Antioxidante e Perfil Fitoquímico Do *Plantago coronopus*. *Braz. J. Biol.* **2017**, *77*, 632–641. [CrossRef] [PubMed]
17. Gonçalves, S.; Romano, A. The Medicinal Potential of Plants from the Genus *Plantago* (Plantaginaceae). *Ind. Crops Prod.* **2016**, *83*, 213–226. [CrossRef]
18. Bello, O.M.; Fasinu, P.S.; Bello, O.E.; Ogbesejana, A.B.; Adetunji, C.O.; Dada, A.O.; Ibitoye, O.S.; Aloko, S.; Oguntoye, O.S. Wild Vegetable *Rumex acetosa* Linn.: Its Ethnobotany, Pharmacology and Phytochemistry—A Review. *S. Afr. J. Bot.* **2019**, *125*, 149–160. [CrossRef]
19. Korpelainen, H.; Pietiläinen, M. Sorrel (*Rumex acetosa* L.): Not Only a Weed but a Promising Vegetable and Medicinal Plant. *Bot. Rev.* **2020**, *86*, 234–246. [CrossRef]
20. Hussain, M.; Raza, S.M.; Janbaz, K.H. Pharmacologically Mechanistic Basis for the Traditional Uses of *Rumex acetosa* in Gut Motility Disorders and Emesis. *Bangladesh J. Pharmacol.* **2015**, *10*, 548–554. [CrossRef]
21. Vasas, A.; Orbán-Gyapai, O.; Hohmann, J. The Genus Rumex: Review of Traditional Uses, Phytochemistry and Pharmacology. *J. Ethnopharmacol.* **2015**, *175*, 198–228. [CrossRef]
22. Cornara, L.; la Rocca, A.; Terrizzano, L.; Dente, F.; Mariotti, M.G. Ethnobotanical and Phytomedical Knowledge in the North-Western Ligurian Alps. *J. Ethnopharmacol.* **2014**, *155*, 463–484. [CrossRef]
23. Storl, W.D. *A Curious History of Vegetables: Aphrodisiacal and Healing Properties, Folk Tales, Garden Tips, and Recipes*; North Atlantic Books: Berkeley, CA, USA, 2016.
24. Janda, K.; Gutowska, I.; Geszke-Moritz, M.; Jakubczyk, K. The Common Cichory (*Cichorium intybus* L.) as a Source of Extracts with Health-Promoting Properties—A Review. *Molecules* **2021**, *26*, 1814. [CrossRef]
25. Bahmani, M.; Rafieian-Kopaei, M.; Saki, K. Chicory: A Review on Ethnobotanical Effects of *Cichorium intybus* L. Microbiologi View Project Melatonin and Human Mitochondrial Diseases View Project. *J. Chem. Pharm. Sci.* **2015**, *8*, 672–682.
26. Street, R.A.; Sidana, J.; Prinsloo, G. *Cichorium intybus*: Traditional Uses, Phytochemistry, Pharmacology, and Toxicology. *Evid.-Based Complement. Altern. Med.* **2013**, *2013*, 579319. [CrossRef]
27. Cornara, L.; la Rocca, A.; Marsili, S.; Mariotti, M.G. Traditional Uses of Plants in the Eastern Riviera (Liguria, Italy). *J. Ethnopharmacol.* **2009**, *125*, 16–30. [CrossRef] [PubMed]
28. Manfrinato, C.; Canella, M.; Ardenghi, N.M.; Guzzon, F. Traditional Use of Tarragon/Pèrschtròmm (*Artemisia dracunculus* L., Asteraceae) in the Linguistic Island of Sappada/Plodn (European Alps, Northern Italy). *Ethnobot. Res. Appl.* **2019**, *18*, 1–9. [CrossRef]
29. Obolskiy, D.; Pischel, I.; Feistel, B.; Glotov, N.; Heinrich, M. *Artemisia dracunculus* L. (Tarragon): A Critical Review of Its Traditional Use, Chemical Composition, Pharmacology, and Safety. *J. Agric. Food Chem.* **2011**, *59*, 11367–11384. [CrossRef] [PubMed]
30. Ekiert, H.; Świątkowska, J.; Knut, E.; Klin, P.; Rzepiela, A.; Tomczyk, M.; Szopa, A. *Artemisia dracunculus* (Tarragon): A Review of Its Traditional Uses, Phytochemistry and Pharmacology. *Front. Pharmacol.* **2021**, *12*, 653993. [CrossRef]
31. Wang, J.; Fernández, A.E.; Tiano, S.; Huang, J.; Floyd, E.; Poulev, A.; Ribnicky, D.; Pasinetti, G.M. An Extract of *Artemisia dracunculus* L. Promotes Psychological Resilience in a Mouse Model of Depression. *Oxidative Med. Cell. Longev.* **2018**, *2018*, 7418681. [CrossRef]
32. D'Ambrosio, A. II Potere Degli Erbaggi Salutiferi. Influenze Leonardiane e Mensa Fitoterapica Nei Secoli XVI-XVII. *L'Idomeneo* **2019**, *28*, 165–190. [CrossRef]

33. Cornara, L.; Smeriglio, A.; Frigerio, J.; Labra, M.; di Gristina, E.; Denaro, M.; Mora, E.; Trombetta, D. The Problem of Misidentification between Edible and Poisonous Wild Plants: Reports from the Mediterranean Area. *Food Chem. Toxicol.* **2018**, *119*, 112–121. [CrossRef]
34. Colombo, M.L.; Assisi, F.; della Puppa, T.; Moro, P.; Sesana, F.M.; Bissoli, M.; Borghini, R.; Perego, S.; Galasso, G.; Banfi, E.; et al. Most Commonly Plant Exposures and Intoxications from Outdoor Toxic Plants. *J. Pharm. Sci. Res.* **2010**, *2*, 417.
35. Chelsea Physic Garden. *The Herb Almanac: A Seasonal Guide to Medicinal Plants*; Aster: Hachette, UK, 2021; p. 160.
36. Rana Disel, N.; Yilmaz, M.; Kekec, Z.; Karanlik, M. Poisoned after Dinner: Dolma with Datura Stramonium. *Turk. J. Emerg. Med.* **2015**, *15*, 51–55. [CrossRef]
37. Gilotta, I.; Brvar, M. Accidental Poisoning with *Veratrum album* Mistaken for Wild Garlic (*Allium ursinum*). *Clin. Toxicol.* **2010**, *48*, 949–952. [CrossRef]
38. Huxtable, R.J. The Harmful Potential of Herbal and Other Plant Products. *Drug Saf.* **1990**, *5*, 126–136. [CrossRef] [PubMed]
39. Smekens, M.J.; van Tienderen, P.H. Genetic Variation and Plasticity of *Plantago coronopus* under Saline Conditions. *Acta Oecologica* **2001**, *22*, 187–200. [CrossRef]
40. Gemeinholzer, B.; Bachmann, K. Examining Morphological and Molecular Diagnostic Character States of *Cichorium intybus* L. (Asteraceae) and *C. spinosum* L. *Plant Syst. Evol.* **2005**, *253*, 105–123. [CrossRef]
41. Ianovici, N. *Histoanatomical Studies on Some Halophytes from Romania-Plantago coronopus. Biomonitoring in Urban Environment View Project COST Action FA 1203-Sustainable Management of Ambrosia artemisiifolia in Europe (SMARTER)*; 2013–2017 View Project; West University of Timişoara: Timişoara, Romania, 2010.
42. Andrzejewska-Golec, E. Hair morphology in *Plantago* sect. Coronopus (Plantaginaceae). *Plant Syst. Evol.* **1992**, *179*, 107–113. [CrossRef]
43. Yasmin, Y.G.; Khan, K.M.A.; Shaheen, S.N. Micromorphological Investigation of Foliar Anatomy of Fagopyrum Mill., and Rumex L. of Polygonaceae. *Pak. J. Bot.* **2010**, *42*, 47–57.
44. El-Alfy, E.T.; El-Askary, E.H.; El-Tawab, E.S.; MKamel, M.S. A Pharmacognostical Study of *Cichorium intybus* L. Herb Growing in Egypt. *Bull. Fac. Pharm. Cairo Univ.* **2009**, *47*, 77–99.
45. Krak, K.; Mráz, P. Trichomes in the Tribe Lactuceae (Asteraceae)—Taxonomic Implications. *Biologia* **2008**, *63*, 616–630. [CrossRef]
46. Ivashchenko, I.V.; Rakhmetov, D.B.; Ivanenko, G.F. Anatomical Features of Leaf Blade of *Artemisia dracunculus* L. (Asteraceae) during Introduction in Zhytomyr Polissya. *Mod. Phytomorphol.* **2015**, *8*, 123–130. [CrossRef]
47. Yilmaz, C.; Gökmen, V. Chlorophyll. In *Encyclopedia of Food and Health*; Caballero, B., Finglas, P.M., Toldrá, F., Eds.; Academic Press: Cambridge, MA, USA, 2016; pp. 37–41.
48. Janković, T.; Zdunić, G.; Beara, I.; Balog, K.; Pljevljakušić, D.; Stešević, D.; Šavikin, K. Comparative Study of Some Polyphenols in *Plantago* Species. *Biochem. Syst. Ecol.* **2012**, *42*, 69–74. [CrossRef]
49. Chukwumah, Y.; Walker, L.; Vogler, B.; Verghese, M. Changes in the Phytochemical Composition and Profile of Raw, Boiled, and Roasted Peanuts. *J. Agric. Food Chem.* **2007**, *55*, 9266–9273. [CrossRef]
50. White, B.L.; Howard, L.R.; Prior, R.L. Impact of Different Stages of Juice Processing on the Anthocyanin, Flavonol, and Procyanidin Contents of Cranberries. *J. Agric. Food Chem.* **2011**, *59*, 4692–4698. [CrossRef] [PubMed]
51. Kaiser, A.; Kammerer, D.R.; Carle, R. Impact of Blanching on Polyphenol Stability and Antioxidant Capacity of Innovative Coriander (*Coriandrum sativum* L.) Pastes. *Food Chem.* **2013**, *140*, 332–339. [CrossRef] [PubMed]
52. Ma, T.; Tian, C.; Luo, J.; Zhou, R.; Sun, X.; Ma, J. Influence of Technical Processing Units on Polyphenols and Antioxidant Capacity of Carrot (*Daucus carrot* L.) Juice. *Food Chem.* **2013**, *141*, 1637–1644. [CrossRef] [PubMed]
53. Kaiser, A.; Carle, R.; Kammerer, D.R. Effects of Blanching on Polyphenol Stability of Innovative Paste-like Parsley (*Petroselinum crispum* (Mill.) Nym Ex A. W. Hill) and Marjoram (*Origanum majorana* L.) Products. *Food Chem.* **2013**, *138*, 1648–1656. [CrossRef] [PubMed]
54. Sablani, S.S.; Andrews, P.K.; Davies, N.M.; Walters, T.; Saez, H.; Syamaladevi, R.M.; Mohekar, P.R. Effect of Thermal Treatments on Phytochemicals in Conventionally and Organically Grown Berries. *J. Sci. Food Agric.* **2010**, *90*, 769–778. [CrossRef]
55. Bernaert, N.; de Loose, M.; van Bockstaele, E.; van Droogenbroeck, B. Antioxidant Changes during Domestic Food Processing of the White Shaft and Green Leaves of Leek (*Allium ampeloprasum* Var. Porrum). *J. Sci. Food Agric.* **2014**, *94*, 1168–1174. [CrossRef]
56. Ku, C.S.; Mun, S.P.; Jang, J.P. Effects of Water Extraction Temperatures on the Yield, Molecular Weight, and Antioxidant Activity of Proanthocyanidins Extracted from Pinus Radiata Bark. *For. Prod. J.* **2011**, *61*, 321–325. [CrossRef]
57. CREA. Linee Guida per una sana Alimentazione 2018. Available online: https://www.crea.gov.it/documents/59764/0/LINEE-GUIDA+DEFINITIVO.pdf/28670db4-154c-0ecc-d187-1ee9db3b1c65?t=1576850671654 (accessed on 16 January 2022).
58. Puccinelli, M.; Pezzarossa, B.; Pintimalli, L.; Malorgio, F. Selenium Biofortification of Three Wild Species, *Rumex acetosa* L., *Plantago coronopus* L., and *Portulaca oleracea* L., Grown as Microgreens. *Agronomy* **2021**, *11*, 1155. [CrossRef]
59. Jan, G.; Kahan, M.; Ahmad, M.; Iqbal, Z.; Afzal, A.; Afzal, M.; Shah, G.M.; Majid, A.; Fiaz, M.; Zafar, M.; et al. Nutritional analysis, micronutrients and chlorophyll contents of *Cichorium intybus* L. *J. Med. Plants Res.* **2011**, *5*, 2452–2456.
60. Liopa-Tsakalidi, A.; Chalikiopoulos, D.; Papasavvas, A. Effect of chitin on growth and chlorophyll content of two medicinal plants. *J. Med. Plants Res.* **2010**, *4*, 499–508.
61. Nartnampong, A.K.W.; Porasuphatana, S. Blanching process increases health promoting phytochemicals in green leafy Thai vegetables. *Int. Food Res. J.* **2016**, *23*, 2426–2435.

62. Xiao, H.W.; Pan, Z.; Deng, L.-Z.; El-Mashad, H.M.; Yang, X.-H.; Mujumdar, A.S.; Gao, Z.-J.; Zhang, Q. Recent developments and trends in thermal blanching—A comprehensive review. *IPA* **2017**, *4*, 101–127. [CrossRef]
63. Smeriglio, A.; de Francesco, C.; Denaro, M.; Trombetta, D. Prickly Pear Betalain-Rich Extracts as New Promising Strategy for Intestinal Inflammation: Plant Complex vs. Main Isolated Bioactive Compounds. *Front. Pharmacol.* **2021**, *12*, 2067. [CrossRef]
64. Lin, B.; Johnson, B.J.; Rubin, R.A.; Malanoski, A.P.; Ligler, F.S. Iron Chelation by Cranberry Juice and Its Impact on *Escherichia coli* Growth. *BioFactors* **2011**, *37*, 121–130. [CrossRef]
65. Yun, S.; Chu, D.; He, X.; Zhang, W.; Feng, C. Protective Effects of Grape Seed Proanthocyanidins against Iron Overload-Induced Renal Oxidative Damage in Rats. *J. Trace Elem. Med. Biol.* **2020**, *57*, 126407. [CrossRef]
66. Maffei Facino, R.; Carini, M.; Aldini, G.; Bombardelli, E.; Morazzoni, P.; Morelli, R. Free radicals scavenging action and anti-enzyme activities of procyanidines from Vitis vinifera. A mechanism for their capillary protective action. *Arzneimittelforschung* **1994**, *44*, 592–601.
67. Singh, P.; Bajpai, V.; Khandelwal, N.; Varshney, S.; Gaikwad, A.N.; Srivastava, M.; Singh, B.; Kumar, B. Determination of Bioactive Compounds of Artemisia Spp. Plant Extracts by LC–MS/MS Technique and Their in-Vitro Anti-Adipogenic Activity Screening. *J. Pharm. Biomed. Anal.* **2021**, *193*, 113707. [CrossRef]
68. Bergantin, C.; Maietti, A.; Cavazzini, A.; Pasti, L.; Tedeschi, P.; Brandolini, V.; Marchetti, N. Bioaccessibility and HPLC-MS/MS Chemical Characterization of Phenolic Antioxidants in Red Chicory (*Cichorium intybus*). *J. Funct. Foods* **2017**, *33*, 94–102. [CrossRef]
69. Ferrare, K.; Bidel, L.P.R.; Awwad, A.; Poucheret, P.; Cazals, G.; Lazennec, F.; Azay-Milhau, J.; Tournier, M.; Lajoix, A.-D.; Tousch, D. Increase in Insulin Sensitivity by the Association of Chicoric Acid and Chlorogenic Acid Contained in a Natural Chicoric Acid Extract (NCRAE) of Chicory (*Cichorium intybus* L.) for an Antidiabetic Effect. *J. Ethnopharmacol.* **2018**, *215*, 241–248. [CrossRef]
70. Poorter, H.; Fiorani, F.; Stitt, M.; Schurr, U.; Finck, A.; Gibon, Y.; Usadel, B.; Munns, R.; Atkin, O.K.; Tardieu, F.; et al. The Art of Growing Plants for Experimental Purposes: A Practical Guide for the Plant Biologist. *Funct. Plant Biol.* **2012**, *39*, 821–838. [CrossRef]
71. Lenka, S.K. Cultivation of Crops under Shade-Net Greenhouse. In *Protected Cultivation and Smart Agriculture*; New Delhi Publishers: New Delhi, India, 2020.
72. Chieco, C.; Rotondi, A.; Morrone, L.; Rapparini, F.; Baraldi, R. An Ethanol-Based Fixation Method for Anatomical and Micro-Morphological Characterization of Leaves of Various Tree Species. *Biotech. Histochem.* **2013**, *88*, 109–119. [CrossRef]
73. Boverio, Z. *De Sacris Ritibus iuxta Romanam Regulam vsui Fratrum Minorum S. Francisci, qui vulgo Capuccini nuncupantur accommodatis*; Typis Scorigianis: Napoli, Italy, 1626.
74. Massonio, S. *Archidipno Overo Dell'insalata e Dell'uso di Es*; Marcantonio Brogiollo: Venezia, Italy, 1990.
75. Cucinotta, F.; Pieroni, A. "If You Want to Get Married, You Have to Collect Virdura": The Vanishing Custom of Gathering and Cooking Wild Food Plants on Vulcano, Aeolian Islands, Sicily. *Food Cult. Soc.* **2018**, *21*, 539–567. [CrossRef]
76. Sicari, V.; Loizzo, M.R.; Sanches Silva, A.; Romeo, R.; Spampinato, G.; Tundis, R.; Leporini, M.; Musarella, C.M. The Effect of Blanching on Phytochemical Content and Bioactivity of *Hypochaeris* and *Hyoseris* Species (Asteraceae), Vegetables Traditionally Used in Southern Italy. *Foods* **2021**, *10*, 32. [CrossRef]
77. Bazzicalupo, M.; Cornara, L.; Burlando, B.; Cascini, A.; Denaro, M.; Smeriglio, A.; Trombetta, D. *Carpobrotus edulis* (L.) N.E.Br. Extract as a Skin Preserving Agent: From Traditional Medicine to Scientific Validation. *J. Integr. Med.* **2021**, *19*, 526–536. [CrossRef] [PubMed]
78. Smeriglio, A.; Denaro, M.; Trombetta, D.; Ragusa, S.; Circosta, C. New Insights on *Euphorbia dendroides* L. (Euphorbiaceae): Polyphenol Profile and Biological Properties of Hydroalcoholic Extracts from Aerial Parts. *Plants* **2021**, *10*, 1621. [CrossRef]
79. Boudjelal, A.; Smeriglio, A.; Ginestra, G.; Denaro, M.; Trombetta, D. Phytochemical Profile, Safety Assessment and Wound Healing Activity of *Artemisia absinthium* L. *Plants* **2020**, *9*, 1744. [CrossRef]
80. Baali, F.; Boumerfeg, S.; Boudjelal, A.; Denaro, M.; Ginestra, G.; Baghiani, A.; Righi, N.; Deghima, A.; Benbacha, F.; Smeriglio, A.; et al. Wound-Healing Activity of Algerian *Lavandula stoechas* and *Mentha pulegium* Extracts: From Traditional Use to Scientific Validation. *Plant Biosyst.-Int. J. Deal. All Asp. Plant Biol.* **2021**, 1–13. [CrossRef]
81. Porra, R.J.; Thompson, W.A.; Kriedemann, E. Determination of accurate extinction coefficients and simultaneous equations for assaying chlorophylls a and b extracted with four different solvents: Verification of the concentration of chlorophyll standards by atomic absorption spectroscopy. *Biochim. Biophys. Acta* **1989**, *975*, 384–394. [CrossRef]
82. Smeriglio, A.; Denaro, M.; di Gristina, E.; Mastracci, L.; Grillo, F.; Cornara, L.; Trombetta, D. Pharmacognostic Approach to Evaluate the Micromorphological, Phytochemical and Biological Features of *Citrus lumia* Seeds. *Food Chem.* **2022**, *375*, 131855. [CrossRef]
83. Muscarà, C.; Smeriglio, A.; Trombetta, D.; Mandalari, G.; la Camera, E.; Grassi, G.; Circosta, C. Phytochemical characterization and biological properties of two standardized extracts from a non-psychotropic *Cannabis sativa* L. cannabidiol (CBD)-chemotype. *Phytother. Res.* **2021**, *35*, 5269–5281. [CrossRef]
84. Smeriglio, A.; Bonasera, S.; Germanò, M.P.; D'Angelo, V.; Barreca, D.; Denaro, M.; Monforte, M.T.; Galati, E.M.; Trombetta, D. *Opuntia ficus-indica* (L.) Mill. Fruit as Source of Betalains with Antioxidant, Cytoprotective, and Anti-angiogenic Properties. *Phytother. Res.* **2019**, *33*, 1526–1537. [CrossRef] [PubMed]
85. Muscarà, C.; Smeriglio, A.; Trombetta, D.; Mandalari, G.; la Camera, E.; Occhiuto, C.; Grassi, G.; Circosta, C. Antioxidant and antimicrobial activity of two standardized extracts from a new Chinese accession of non-psychotropic *Cannabis sativa* L. *Phytother. Res.* **2021**, *35*, 1099–1112. [CrossRef] [PubMed]

86. Denaro, M.; Smeriglio, A.; Trombetta, D. Antioxidant and Anti-Inflammatory Activity of *Citrus* Flavanones Mix and Its Stability after In Vitro Simulated Digestion. *Antioxidants* **2021**, *10*, 140. [CrossRef] [PubMed]
87. Smeriglio, A.; Denaro, M.; D'Angelo, V.; Germanò, M.P.; Trombetta, D. Antioxidant, Anti-Inflammatory and Anti-Angiogenic Properties of *Citrus lumia* Juice. *Front. Pharmacol.* **2020**, *11*, 2033. [CrossRef] [PubMed]

plants

MDPI

Article

No Evidence for Light-Induced Embolism Repair in Cut Stems of Drought-Resistant Mediterranean Species under Soaking

Martina Tomasella [1], Sara Natale [1], Francesco Petruzzellis [1,2], Sara Di Bert [1], Lorenzo D'Amico [3,4], Giuliana Tromba [3] and Andrea Nardini [1,*]

[1] Dipartimento di Scienze della Vita, Università di Trieste, Via L. Giorgieri 10, 34127 Trieste, Italy; martina.tomasella@units.it (M.T.); sara.natale@phd.units.it (S.N.); fpetruzzellis@units.it (F.P.); sara.dibert@studenti.units.it (S.D.B.)
[2] Dipartimento di Scienze Agroalimentari, Ambientali e Animali, Università di Udine, Via delle Scienze 91, 33100 Udine, Italy
[3] Elettra-Sincrotrone Trieste, Area Science Park, 34149 Basovizza, Italy; LORENZO.D'AMICO@studenti.units.it (L.D.); giuliana.tromba@elettra.eu (G.T.)
[4] Dipartimento di Fisica, Università di Trieste, Via A. Valerio 2, 34127 Trieste, Italy
* Correspondence: nardini@units.it

Abstract: (1) Recent studies suggested that stem photosynthesis could favor bark water uptake and embolism recovery when stem segments are soaked in water under light conditions, but evidence for this phenomenon in drought-resistant Mediterranean species with photosynthetic stems is missing. (2) Embolism recovery upon immersion in water for 2 h–4 h under light was assessed (i) via a classical hydraulic method in leafless *Fraxinus ornus* and *Olea europaea* branch segments stressed to xylem water potentials (Ψ_{xyl}) inducing ca. 50% loss of hydraulic conductivity (PLC) and (ii) via X-ray micro-CT imaging of the stem segments of drought-stressed potted *F. ornus* saplings. Hydraulic recovery was also assessed in vivo in intact drought-stressed *F. ornus* saplings upon soil re-irrigation. (3) Intact *F. ornus* plants recovered hydraulic function through root water uptake. Conversely, the soaked stem segments of both species did not refill embolized conduits, although Ψ_{xyl} recovered to pre-stress levels (between −0.5 MPa and −0.2 MPa). (4) We hypothesize that xylem embolism recovery through bark water uptake, even in light conditions, may not be a common phenomenon in woody plants and/or that wounds caused by cutting short stem segments might inhibit the refilling process upon soaking.

Keywords: stem photosynthesis; hydraulic recovery; soaking; X-ray micro-CT; bark water uptake; embolism

Citation: Tomasella, M.; Natale, S.; Petruzzellis, F.; Di Bert, S.; D'Amico, L.; Tromba, G.; Nardini, A. No Evidence for Light-Induced Embolism Repair in Cut Stems of Drought-Resistant Mediterranean Species under Soaking. *Plants* **2022**, *11*, 307. https://doi.org/10.3390/plants11030307

Academic Editors: Milan S. Stankovic, Paula Baptista and Petronia Carillo

Received: 20 December 2021
Accepted: 21 January 2022
Published: 24 January 2022

1. Introduction

Most terrestrial plants rely on root-level water absorption to maintain their hydration status. However, water can also be absorbed from the surface of aboveground plant organs under particular biophysical conditions, i.e., when liquid water is wetting plant surfaces or the water potential of the surrounding atmospheric boundary layer is higher than that of cells [1]. This occurs when water vapor pressure in the air is at (or close to) saturation and, most importantly, when liquid water forms or falls on a plant surface due to fog, rain or snow melting, allowing local rehydration and partial xylem tension relief, especially when plants are experiencing a soil water deficit [2].

Water uptake through leaves has been widely observed in many plant lineages [3,4]. Leaf trichomes, depending on their density, composition and structure, are the major media for water absorption in a Mediterranean (*Quercus ilex*) and a temperate (*Fagus sylvatica*) species [5,6]. In addition, in two species without leaf trichomes or hydathodes, open stomata have been observed to play a major role in water uptake over cuticles when exposed to fog [7]. Leaf water absorption can also be involved in the recovery of leaf [8] and stem [9,10] hydraulic functions after drought- or frost-induced xylem embolism.

The stems of woody plants, even when covered with suberized tissue, are also able to absorb water when the bark becomes wet, allowing partial xylem tension relief [11]. There is some evidence that leafless dehydrated branches soaked in water for at least some hours partially recover their xylem hydraulic function in a conifer (*Sequoia sempervirens*, [12]) and in an angiosperm (*Salix matsudana*, [13]). Xylem hydraulic recovery would require radial water movement from the phloem to the xylem through parenchyma rays, as proven in a dying experiment on wetted stems [11]. Liu et al. [13] soaked short *S. matsudana* stem segments in water and observed faster embolism repair (within 2 h) when under light conditions compared to dark conditions, where partial refilling nevertheless occurred. The enhanced refilling effect under light was ascribed to the sugars produced by stem photosynthesis, which provide the driving (osmotic) force for the process. In fact, embolism repair can occur as the result of a water potential gradient between the xylem apoplast, where sugars are accumulated, and parenchyma cells surrounding the conduits [14–16]. Independently of the mechanisms involved in the process, such soaking experiments on short leafless stem segments on other woody species performing stem photosynthesis are underrepresented, and they might constitute an interesting experimental model to investigate the biology of post-drought hydraulic recovery.

In the past decade, some methodological issues have arisen regarding stem hydraulic vulnerability assessment and the study of embolism recovery via classic hydraulic methods due to the possible overestimation of embolism rates, which may be generated when cutting xylem under tension [17]. At the same time, prolonged xylem relaxation prior to hydraulic measurements, which is suggested to avoid artefactual embolism appearance, can favor refilling, leading to the underestimation of embolism levels [18]. In well-established sample preparation procedures for hydraulic measurements, stems are often kept under water prior to hydraulic measurements, even for long time intervals, based on the principle that the very low pressure head upon immersion would avoid embolism dissolution [19]. However, the above-mentioned soaking experiments in short leafless branch segments [12,13] indicated that the active accumulation of solutes at the wood parenchyma–conduit interface drives water into the apoplast and might refill the conduits under soaking. If this happens, soaking stems for a prolonged period would induce overestimation of xylem hydraulic conductivity.

These controversies can be overcome using X-ray micro-computed tomography (micro-CT), an important tool to visualize embolized xylem conduits at a proper resolution and to quantify in vivo xylem vulnerability, as well as possible hydraulic recovery in intact plants [20,21]. Therefore, this method has been exploited to validate destructive hydraulic methods (e.g., [22,23]) and related sample preparation procedures [24].

In this study, we hypothesized that bark water uptake in the presence of light would induce the recovery of hydraulic function in two embolism-resistant Mediterranean angiosperm species performing stem photosynthesis, namely, *Fraxinus ornus* and *Olea europaea*. We tested this hypothesis both with a classical hydraulic method in dehydrated leafless cut branches of adult plants of both species, and in vivo through X-ray micro-CT imaging of segments of drought-stressed potted young saplings of *F. ornus*. There is evidence suggesting that *O. europaea* is capable of partial hydraulic recovery following drought-induced xylem embolism [18], making this species a good candidate to investigate the eventual process of conduit refilling under soaking conditions. Similarly, intact *F. ornus* plants have already been reported to recover hydraulic function when the soil is re-watered after substantial drought-induced loss of xylem hydraulic conductivity [25], but in vivo evidence is missing. For this reason, we additionally tested the hydraulic recovery capability of this species through root water uptake via micro-CT imaging of intact potted plants.

2. Results

The stem segments used for the soaking experiments, i.e., 2-year-old *F. ornus* and 1-year-old *O. europaea* branch portions, as well as the 1-year-old stem portions of *F. ornus* saplings, showed a relatively high capability of performing photosynthesis (Figure 1). In particular, the maximum quantum yield of PSII (F_v/F_m) in the outer bark was about 0.8 in

all three different samples. Similar values were also measured in the outer wood and in the longitudinal section of the wood (sapwood + pith) of the 1-year-old branch and stem segments of both species. Lower (but still relatively high) F_v/F_m values were measured in the outer wood (0.65) and in the longitudinal section of the wood (0.49) of *F. ornus* 2-year-old branch portions.

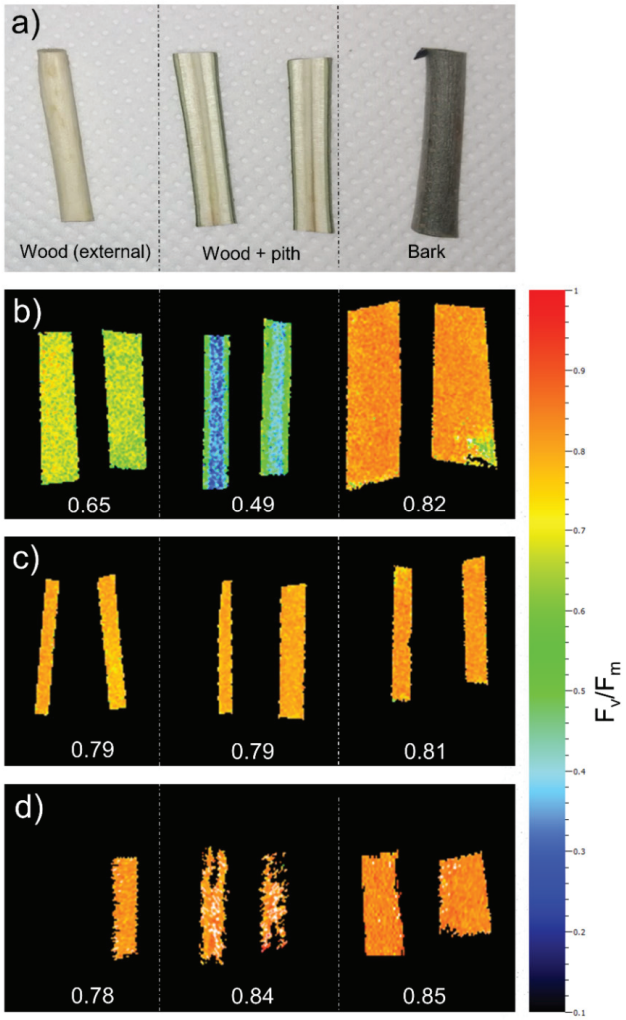

Figure 1. Maximum quantum yield of PSII (F_v/F_m) measured in branch/stems used for the experiment. Wood (exposing the side next to the vascular cambium), wood + pith (exposing the cut side) and bark were analyzed separately (**a**). Measurements were performed on 2-year old *F. ornus* branch segments (**b**), in 1-year old *O. europaea* branch segments (**c**) and in 1-year old stems of *F. ornus* saplings (**d**). Values in b–c are the average value of the sample.

2.1. Hydraulic Measurements

Some native embolism was detected in the hydrated branches of *F. ornus* and *O. europaea* (H samples), with PLC averaging 17% and 5%, respectively (Figure 2). After dehydration on the bench, PLC at the target Ψ_{xyl} (−3.7 MPa and −4.4 MPa in *F. ornus* and *O. europaea*, respectively) significantly increased to 56 ± 4% in *F. ornus* and to 54 ± 10% in *O. europaea*. After the soaking treatment in distilled water for 2 h (S_{2h} samples), Ψ_{xyl} increased to pre-

stress levels, averaging −0.46 MPa in *F. ornus* and −0.33 MPa in *O. europaea*, but stem PLC did not recover in either species. Moreover, prolonged immersion in water (four hours, S_{4h} stems) did not induce xylem hydraulic recovery in *F. ornus*, albeit xylem tension further and significantly decreased with respect to the S_{2h} samples (Ψ_{xyl} = −0.19 ± 0.06 MPa, $p < 0.05$).

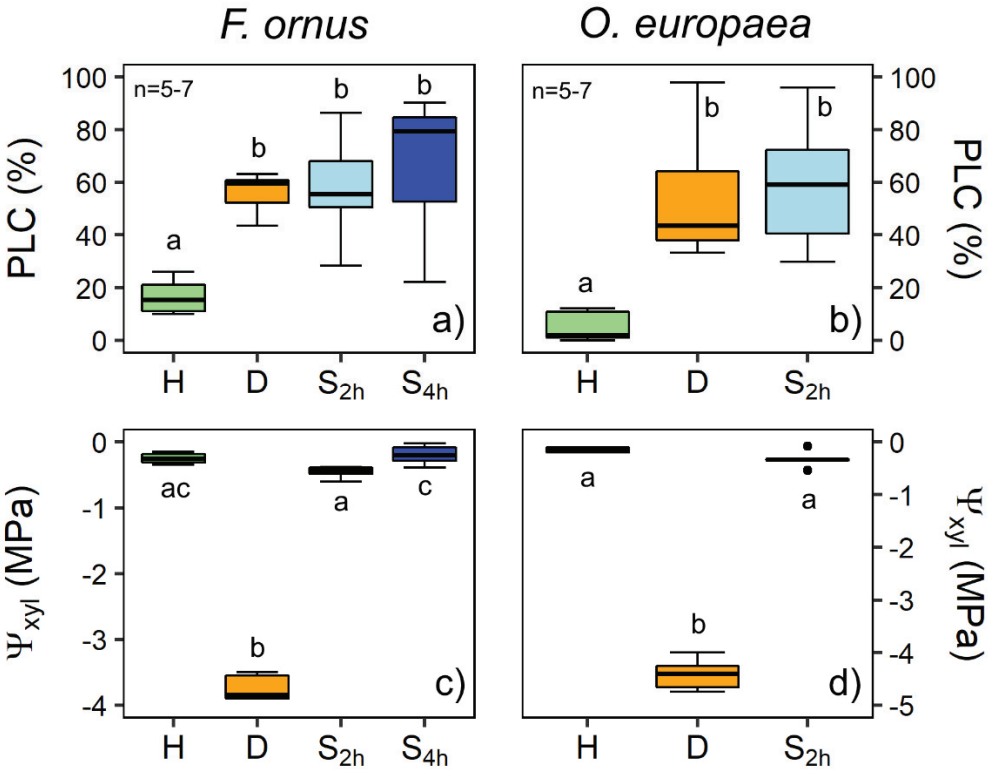

Figure 2. Percentage loss of xylem hydraulic conductivity (PLC, (**a**,**b**)) and xylem water potential (Ψ_{xyl}, (**c**,**d**)) measured in *F. ornus* (**a**,**c**) and *O. europaea* (**b**,**d**) in hydrated (H, $n = 5$), drought-stressed (D, $n = 5$–6) and soaked (for 2 and 4 h, S_{2h} and S_{4h}, respectively, $n = 6$–7) stems. Note the different scales for Ψ_{xyl} between the two species. The 4 h soaking treatment was performed only for *F. ornus*. Different letters denote statistically significant differences among groups ($p < 0.05$).

2.2. Micro-CT Analyses

The micro-CT experiment on the potted plants of *F. ornus* proved the capability of xylem hydraulic recovery in intact plants through root water uptake 24 h after soil rehydration to field capacity. In fact, the embolized vessel area (EVA) was around 40–50% in drought-stressed (D_{pot}) plants, which reached Ψ_{xyl} of −3.50 MPa, and it was restored to pre-stress control (C_{pot}) values in the two re-irrigated (R_{pot}) plants (6% and 21% in the two scanned plants, Figure 3), which relieved Ψ_{xyl} to −0.25 MPa and −0.70 MPa.

The consecutive micro-CT scans performed on the 2-year-old *F. ornus* drought-stressed (D) plants after each progressive sample preparation step are shown in Figure S1. The first cut at the base of the stem did not significantly increase the embolized sapwood area (A_{embol}) or EVA. However, the second cut made to obtain the final D segment significantly increased EVA from 44 ± 7% (measured in the shoots cut at the base) to 63 ± 11%, with an overall increase of 27% compared to the intact plant (Figure S2).

The stem segments did not refill their embolized conduits after the 2 h soaking treatment under light, as the values of A_{embol} and EVA (1.07 ± 0.06% and 58 ± 1%, respectively) were similar to those calculated for D stem segments ($p > 0.05$; Figure 4 and Figure S3).

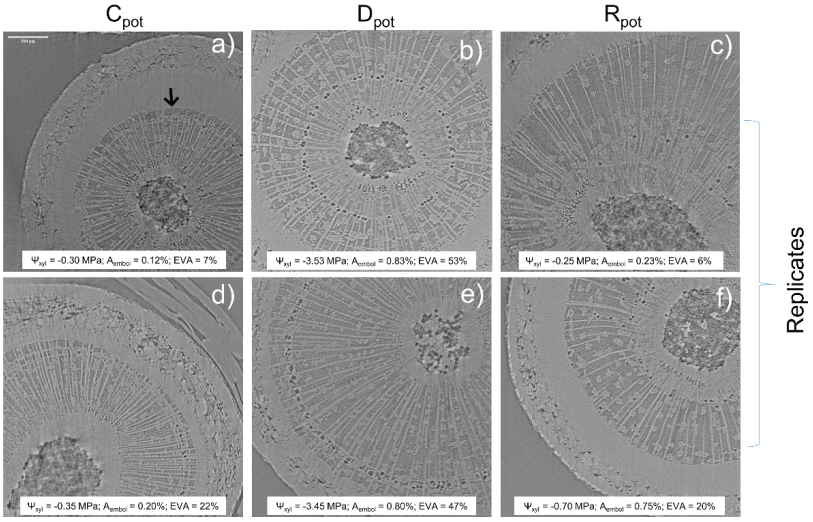

Figure 3. Transverse reconstructed images of the 1-year-old stem portion obtained with X-ray micro-CT in well-hydrated (C_{pot}, (**a**,**d**)), drought-stressed (D_{pot}, (**b**,**e**)) and re-irrigated (R_{pot}, (**c**,**f**)) intact *F. ornus* plants. Ψ_{xyl} = xylem water potential, A_{embol} = percentage of embolized sapwood area, EVA = percentage of embolized vessel area; all calculated excluding the immature sapwood close to the cambium (see arrow delimiting mature/immature sapwood in (**a**)).

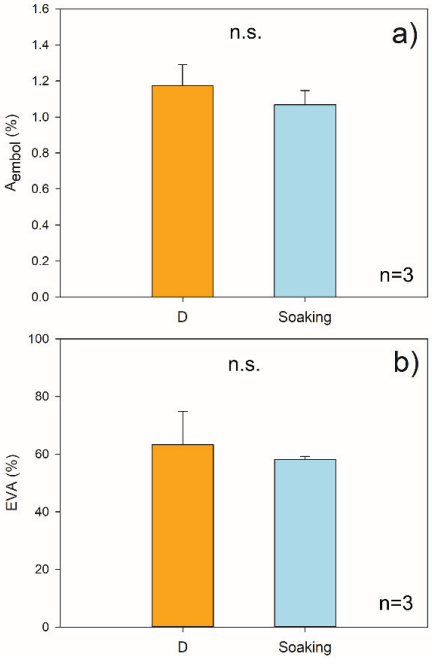

Figure 4. Percentage of embolized sapwood area (A_{embol}, (**a**)) and percentage of embolized vessel area (EVA, (**b**)) measured in micro-CT transverse reconstructed images of *F. ornus* stem segments. D = segments of drought-stressed plants (n = 3). Soaking = segments of additional D plants scanned upon soaking in water for 2 h (n = 3). Values are means ± SE. n.s. = difference not significant among groups.

3. Discussion

No Evidence for Hydraulic Recovery in Stem Segments upon Soaking

The in vivo micro-CT analyses showed that *F. ornus* plants can recover xylem hydraulic function through root water uptake after experiencing substantial embolism levels under drought, confirming the previous classical hydraulic measurements of cut stems [25]. In addition, embolism recovery occurred even though plants were still experiencing overall negative xylem pressure, supporting previous observations. However, the leafless stem segments of *F. ornus* and *O. europaea* that reached about 50% PLC (i.e., the same target PLC used in the pot re-irrigation experiment) did not recover xylem hydraulics after immersion in water under light conditions (Figure 2). This outcome was additionally validated by the micro-CT scans of the *F. ornus* cut stems, obtained from the drought-stressed potted saplings (Figure 4 and Figure S2).

The hydraulic measurements of *F. ornus* branches (Figure 2) were in agreement with the micro-CT measurements of intact plants (Figure 3), confirming the lack of cutting artifacts. Likewise, the PLC values obtained in our study for *O. europaea* at the target Ψ_{xyl} were consistent with the vulnerability curves obtained for the same species both via hydraulic measurements and X-ray micro-CT scans [26,27], making us confident that sample preparation artefacts were avoided. However, with the methodological test performed at the micro-CT beamline on the dehydrated saplings of *F. ornus*, we aimed to examine if the sample preparation procedure used to obtain the final stem segments for soaking would induce additional non-native embolism. The progressive cuts made on the stem of the potted saplings increased the embolized vessel area (Figure S1 and Figure S2). In this test, we first made a cut underwater at the base of the shoot, and then a second cut was made at a distal position (ca. 20 cm from the previous one) to obtain a stem segment in the basal part of the stem. Given that the maximum vessel length of the saplings (40 cm on average) was higher than the obtained stem segment, it is likely that air entry upon cutting under substantial xylem tension induced embolism in the stem portion where the micro-CT scans were made (at 8 cm–9 cm from the first cut). Given that we aimed to perform the soaking experiment on the lower 1-year-old stem portion and that the plants were relatively small, we were forced to obtain the stem segment in that proximal stem region. With this simple test, we underline that experiments with in vivo imaging techniques should be further exploited to better identify the possible artefacts of sample preparation. However, the results of our cutting test do not influence the outcome of the soaking experiment because the samples scanned prior (D) or after (Soaking) immersion in water (Figure 4) were prepared with the same procedure.

The results of the soaking experiments contradict those obtained for *S. matsudana* stem segments soaked in water under light conditions, where bark water uptake contributed to refill about 75% of the previously embolized vessels after 2 h of immersion [13]. Here, we also showed that *F. ornus* and *O. europaea* stems can perform photosynthesis both at wood and bark levels (Figure 1), which should provide additional sugars to enhance the process of water uptake by generating an osmotic gradient.

There is evidence that local xylem tension relief is important to refill xylem conduits [28,29]. In *S. sempervirens*, partial hydraulic recovery was observed upon soaking when branch water potential slightly increased with respect to dehydrated conditions, but it was still quite negative (ca. −4 MPa, [12]). Similarly, recovery under substantial tension occurred in *Picea glauca* leafy twigs exposed to fog [10], suggesting possible localized hydraulic isolation in the xylem. Xylem tension in our two study species was even relaxed to Ψ_{xyl} above −0.5 MPa (Figure 2). These values are comparable to those measured in the intact potted plants of *F. ornus*, which recovered xylem hydraulics when re-irrigated in pots (Figure 3). Therefore, we note that the residual xylem tension of the cut stems was comparable to that of intact plants, and it was expected to promote the refilling of conduits through bark water uptake.

Earles et al. [12] suggested that tall trees, such as redwoods, which, due to their height, must develop low Ψ_{xyl} even under well-hydrated conditions, may profit from bark water

uptake during prolonged fog periods to partially restore xylem functionality. It is suggested that trees adapted to climates with prolonged periods of rain and/or fog [30] and trees at the timberline with crowns covered with snow that melts in spring [9,31] may have evolved bark characteristics that favor water uptake and subsequent hydraulic recovery. Indeed, radial water uptake may depend on outer (rhytidome) and/or inner (phloem) bark characteristics. For example, bark porosity and density influence hygroscopicity [32], while the hydrophobicity of cork cells in the outer bark limits water absorption [33,34]. It is possible that species adapted to Mediterranean climates, commonly not exposed to prolonged fogs/rainy periods, may not have evolved such bark characteristics that would favor radial water uptake. However, we might rule out this hypothesis because, although we did not directly measure bark water uptake, the marked Ψ_{xyl} relief upon soaking indicated substantial stem rehydration (Figure 2b). Alternatively, sample preparation/experimental conditions could have been responsible for the lack of hydraulic recovery. Previous experiments have highlighted the role of phloem in xylem hydraulic recovery [35]. In particular, stem girdling in *O. europaea* prevented embolism refilling upon branch rehydration, while hydraulic recovery was observed in samples with intact phloem [18]. Hence, it is possible that the wounds caused by the preparation of stem segments for soaking had similar inhibitory effects on the refilling process. Tests on different species could help improve our understanding as to whether refilling through bark water uptake might be species specific, as well as the possible limits of the soaking method when applied to cut stem segments.

4. Materials and Methods

4.1. Plant Material

The experiment was carried out on two Mediterranean tree species, namely, manna ash (*Fraxinus ornus* L.) and olive (*Olea europaea* L.), between mid-June and the end of July 2021. In order to test the hydraulic recovery capability upon soaking under light conditions, embolism was measured both with a classical hydraulic conductivity apparatus and in vivo via micro-CT, but on different plant material. Hydraulic measurements were performed on sun-exposed branches taken from several *F. ornus* trees and one *O. europaea* tree growing in the Botanical Garden of the University of Trieste (Italy, 45°39′40.9″ N, 13°47′40.1″ E). For micro-CT experiments, 2-year-old and 1-year-old *F. ornus* saplings provided by a local public nursery (Vivai Pascul, Regional Forestry Service, Tarcento, Italy) were transplanted in 3.4 L and 1 L pots in March 2020 and 2021, respectively. Pots were filled with a lightweight substrate for green roof installations (for the 2-year-old plants) or with red soil (for the 2-year-old plants) sampled from a vineyard in the Italian Karst (Duino-Aurisina, Italy). Plants were grown in a greenhouse of the University of Trieste, supplied with tap water twice a day to soil field capacity through a clock irrigation system.

To check the capability of the study species to perform bark and wood photosynthesis, some stem segments were analyzed with an imaging PAM chlorophyll fluorometer (Photon Systems Instruments, Brno, Czech Republic) to obtain the maximum quantum yield of PSII (Fv/Fm). Stem segments of approx. 2 cm length were dark adapted for 1 h, longitudinally sectioned and positioned on a plate with a layer of paper towels, keeping them hydrated through partial immersion in a film of water. Outer bark, outer xylem and xylem longitudinal section (sapwood + pith) were measured (see Figure 1a).

4.2. Hydraulic Measurements

F. ornus and *O. europaea* branches were collected in the late afternoon and rehydrated overnight while covered with a black plastic bag after cutting the basal 5 cm underwater. In the early morning, full hydration was checked to ensure that xylem water potential (Ψ_{xyl}) was above −0.3 MPa. A group of hydrated branches was used for hydraulic measurements to check possible residual embolism (hydrated group, H, $n = 5$). The remaining branches were dehydrated on the bench, covering several leaves with cling film and aluminum foil to stop transpiration and favor equilibration between leaf and stem xylem in order to measure Ψ_{xyl} with a pressure chamber (mod. 1505D, PMS Instrument Co., Albany, OR, USA). For

olive, before bench dehydration, about 15 cm of the 2-year-old stem portions selected for hydraulic measurements and soaking treatment were deprived of leaf blades by cutting them at the insertion point at the petiole and sealing the cut section with impermeable glue (Super Attack, Loctite). Branches were dehydrated until reaching the target Ψ_{xyl}, fixed to -(3.5–3.9) MPa for *F. ornus* and to -(4.2–4.7) MPa for *O. Europaea,* based on preliminary assessments. At that point, a group of branches was immediately processed for hydraulic conductivity measurements (dehydration group, D, n = 5–6), while a third group was subjected to the soaking treatment as follows. Stem segments, obtained as described below, were sealed at the cut ends with wax tape (Parafilm® M), kept under water and then immersed in a white rectangular bowl containing distilled water, lying horizontally 1 cm below the water level. Stems were rotated by 180° every hour to allow whole stem light exposure. A LED panel (red/blue 96/24) was mounted above the bowl to produce a photosynthetic photon flux density (PPFD) at the water level of about 400 μmol m^{-2} s^{-1}. According to Liu et al. [13], most of the embolized vessels of *S. matsudana* refilled already 2 h after branch segment immersion in light conditions. Therefore, duration of soaking was fixed to 2 h for both species (S_{2h} group, n = 6). For *F. ornus*, a second set of branches was immersed for 4 h to check if longer rehydration times were needed for hydraulic recovery (S_{4h} group, n = 7). After soaking, branch segments were prepared for hydraulic measurements as described below, while a 3 cm adjacent stem segment was taken for Ψ_{xyl} measurements, performed with a dew point hygrometer (WP4-C, Meter Group, Inc., Pullman, WA, USA). To this aim, the segment was quickly wiped with paper towel, cut longitudinally in half, placed in a sample holder and measured upon Ψ_{xyl} stabilization (reached in 30 min–40 min).

Measurements were performed on 3 cm–4 cm long segments of H, D, S_{2h} and S_{4h} stems. For all samples, the base of the branch was trimmed under clean tap water at a distance higher than the maximum vessel length. Maximum vessel length, determined with the "air method" described by Wang et al. [36], averaged 29 cm and 45 cm in *F. ornus* and *O. europaea* branches, respectively. Then, a selected ~15 cm long segment was cut and kept under water. S_{2h} and S_{4h} segments were sealed at both ends with Parafilm and soaked as described above. For hydraulic conductivity measurements, a shorter segment was obtained; the bark was removed from both cut ends, and several thin sharp slides were made with a razorblade at both ends to obtain a 3 cm–4 cm long segment; and the basal end was inserted in a hydraulic apparatus (see [25]).

Xylem hydraulic conductance was measured gravimetrically under a water head of 3.5 kPa, perfusing stems with filtered (0.45 μm) and degassed mineral water added with 10 mM KCl [37]. Hydraulic conductance was measured before (initial hydraulic conductance, k_i) and after (maximum hydraulic conductance, k_{max}), flushing the sample at high pressure (0.15 MPa) for 3 min to remove xylem embolism. Xylem hydraulic conductivity (K) was calculated as

$$K = k \times L/A \quad (1)$$

where L is the length of the segment, and A is the sapwood area, calculated as the average sapwood areas measured at the cut ends of the sample.

Percentage loss of hydraulic conductivity (PLC) was then calculated as

$$PLC = 100 \times [1 - (k_i\ {k_{max}}^{-1})] \quad (2)$$

4.3. Micro-CT Scans and Image Processing

Micro-CT scans were performed at the SYRMEP beamline of the Elettra Synchrotron light source (Trieste, Italy).

To check the capability of *F. ornus* to recover xylem embolism after soil rewetting, four 3-year-old saplings were dehydrated in pots to reach the target Ψ_{xyl} (−3.5 MPa) on 17–21 July 2020. The 2-year-old stem portion of two plants was scanned right after reaching the target Ψ_{xyl} (D_{pot} plants), while the other two were scanned 24 h after re-irrigation to soil

field capacity (recovery, R_{pot} plants). Two additional well-watered plants were measured as controls (C_{pot}). In all plants, Ψ_{xyl} was measured prior to scanning.

The soaking experiment was performed on potted *F. ornus* saplings on 1 August 2021. All plants were dehydrated by withholding irrigation for about 5 days. Three of them were scanned to detect the embolism level at the target Ψ_{xyl} (D plants). These plants were also used to tests the sample preparation effect on embolism formation, scanning the stem at the same point in three different steps: (i) the intact plant, (ii) the plant cut underwater right above the root collar after immersing the pot (sealed in a plastic bag) in water and (iii) the final stem segment obtained by cutting the stem 14 cm–21 cm above the previous cut, keeping the sample underwater. The length of the segment depended on the length of the 2-year-old stem segment portion, while the scan was always 8 cm–9 cm above the basal cut. After every cut, the cut surface was tightly sealed underwater with Parafilm. An additional scan was performed after cutting the stem segment a few mm above the scanned region in order to observe the fully embolized xylem.

The remaining three plants were prepared in the same way as the D plants, but they were only scanned after soaking the stem segment (obtained at step iii) in water for 2 h (S_{2h} samples) as described above for branches measured with the hydraulic apparatus. This was carried out to avoid the possibility of multiple scans inhibiting cellular activity and possible related processes involved in water uptake and hydraulic recovery [38].

Before micro-CT scanning, all samples were quickly wrapped in cling film and Parafilm to avoid water loss and fixed to the sample holder. The CT studies were performed in propagation-based phase contrast modality using an Orca Flash 4.0 SCMOS, coupled with a 17 μm GGG scintillator, as a detector. The sample was placed 15 cm from the detector, and the pixel size was set at 2.1 μm. The experiment was performed in white beam mode, and 1.0 mm of silica was applied, resulting in a mean X-ray energy of about 22 keV. For each scan, 1800 projections were acquired during the sample rotation over 180°.

The slice reconstructions were performed using SYRMEP Tomo Project (STP) software [39]. A phase retrieval pre-processing algorithm [40] was applied prior to the conventional filtered back-projection algorithm to increase the image contrast.

Reconstructed images were processed using ImageJ (https://imagej.nih.gov/ij/, accessed on 30 November 2021). Due to the larger diameter of the stems compared to the field of view (ca. 4 mm × 4 mm), analyses were conducted on about one-quarter of the stem section, excluding the immature xylem next to the vascular cambium (see Figure 3, Figure 4, Figure S1 and Figure S2). The embolized sapwood area (A_{embol}) was calculated by dividing the embolized pixel area by the analyzed sapwood area, expressed as percentage. The embolized vessel area (EVA) was calculated by dividing A_{embol} by the A_{embol} after the final cut above the scanned region (representing the percentage of sapwood area occupied by conduits), expressed as percentage.

4.4. Statistics

Statistical analyses were carried out with R (R Core Team, 2017). Boxplot panels were obtained with the "ggplot2" package in R. Bar charts were prepared with SigmaPlot (v. 12.0, Systat Software Inc., Berkshire, UK). For PLC and Ψ_{xyl}, the one-way ANOVA test (response variable ~f(treatment)) through the *aov* function was applied, followed by Tukey's HSD post hoc test (only for significant ANOVA, $p < 0.05$) through the *TukeyHSD* function in the "stats" package after checking for normality of residuals and homogeneity of variances. When homogeneity of variance assumption was violated, generalized least squares (GLS) models were calculated with the *gls* function, including a "varIdent" variance structure, in the "nlme" R package [41], followed by Tukey's HSD post hoc analysis (for significant tests), with *p*-values adjusted using the Bonferroni–Holm method. The effect of progressive cuttings on A_{embol} and EVA in the micro-CT test experiment was tested using linear mixed models (LMMs) through the *lme* function. Specifically, one LMM was fitted by separately setting A_{embol} or EVA as the response variable and by setting the cutting stage as the

explanatory one, with the plant replicate as the random effect. Pairwise comparisons were performed through *lsmeans* function in R package "emmeans" [42].

5. Conclusions

In this work, we tested the hypothesis that the immersion of photosynthesizing stem segments in distilled water for some hours in the presence of light would induce hydraulic recovery through bark water uptake in the embolized branches of two drought-resistant Mediterranean tree species (*F. ornus* and *O. europaea*). Hydraulic recovery was previously reported for the soaked stem segments of *S. matsudana*, and it was related to the generation of an osmotic gradient [13]. However, for the two species analyzed in this study, which are known to be capable of hydraulic repair under moderate tension (additionally demonstrated here by an in vivo micro-CT analysis of the potted saplings of *F. ornus*), refilling by bark water uptake did not occur. Our data suggest that refilling does not commonly occur in cut stems soaked under water, thus suggesting that this common procedure in hydraulic measurements is not likely to produce artefactual results. Clearly, further soaking studies under light conditions should be performed on photosynthesizing stems of other species to better understand both the potential and the limits of this process, as well as the possible consequences in terms of the accuracy of hydraulic measurements of xylem embolism.

Supplementary Materials: The following are available online at https://www.mdpi.com/article/10.3390/plants11030307/s1, Figure S1: X-ray micro-CT transverse images of stems of drought-stressed 2-year-old *F. ornus* saplings, Figure S2: Cutting effect on embolism formation in *F. ornus* potted saplings visualized with micro-CT. Figure S3: X-ray micro-CT transverse images of 2-year-old *F. ornus* stem segments after the soaking treatment (S_{2h}).

Author Contributions: Conceptualization and experimental design, A.N., M.T. and S.N.; methodology, M.T., S.N. and A.N.; formal analysis, M.T. and S.N.; investigation, M.T., S.N., F.P., S.D.B., L.D. and G.T.; data curation, M.T.; visualization, M.T.; writing—original draft preparation, M.T. and A.N.; writing—review and editing, A.N.; supervision, A.N. All authors have read and agreed to the published version of the manuscript.

Funding: The beamtime access to the SYRMEP beamline was granted by Elettra Sincrotrone Trieste (proposal no. 20195384 and no. 20210284).

Institutional Review Board Statement: Not applicable.

Informed Consent Statement: Not applicable.

Data Availability Statement: The data presented in this study are available in the Supplementary Materials.

Acknowledgments: We thank the "Direzione centrale risorse agroalimentari, forestali e ittiche–area foreste e territorio" of the "Regione autonoma Friuli Venezia Giulia" and the public nursery Vivai Pascul (Tarcento, Italy) for providing us with the potted plant material.

Conflicts of Interest: The authors declare no conflict of interest.

References

1. Berry, Z.C.; Emery, N.C.; Gotsch, S.G.; Goldsmith, G.R. Foliar Water Uptake: Processes, Pathways, and Integration into Plant Water Budgets. *Plant Cell Environ.* **2019**, *42*, 410–423. [CrossRef] [PubMed]
2. Breshears, D.D.; McDowell, N.G.; Goddard, K.L.; Dayem, K.E.; Martens, S.N.; Meyer, C.W.; Brown, K.M. Foliar absorption of intercepted rainfall improves woody plant water status most during drought. *Ecology* **2008**, *89*, 41–47. [CrossRef] [PubMed]
3. Dawson, T.E.; Goldsmith, G.R. The Value of Wet Leaves. *New Phytol.* **2018**, *219*, 1156–1169. [CrossRef]
4. Carmichael, M.J.; White, J.C.; Cory, S.T.; Berry, Z.C.; Smith, W.K. Foliar Water Uptake of Fog Confers Ecophysiological Benefits to Four Common Tree Species of Southeastern Freshwater Forested Wetlands. *Ecohydrology* **2020**, *13*, e2240. [CrossRef]
5. Fernández, V.; Sancho-Knapik, D.; Guzmán, P.; Peguero-Pina, J.J.; Gil, L.; Karabourniotis, G.; Khayet, M.; Fasseas, C.; Heredia-Guerrero, J.A.; Heredia, A.; et al. Wettability, Polarity, and Water Absorption of Holm Oak Leaves: Effect of Leaf Side and Age. *Plant Physiol.* **2014**, *166*, 168–180. [CrossRef] [PubMed]
6. Schreel, J.D.M.; Leroux, O.; Goossens, W.; Brodersen, C.; Rubinstein, A.; Steppe, K. Identifying the Pathways for Foliar Water Uptake in Beech (*Fagus Sylvatica* L.): A Major Role for Trichomes. *Plant J.* **2020**, *103*, 769–780. [CrossRef]

7. Guzmán-Delgado, P.; Laca, E.; Zwieniecki, M.A. Unravelling Foliar Water Uptake Pathways: The Contribution of Stomata and the Cuticle. *Plant Cell Environ.* **2021**, *44*, 1728–1740. [CrossRef] [PubMed]
8. Fuenzalida, T.I.; Bryant, C.J.; Ovington, L.I.; Yoon, H.; Oliveira, R.S.; Sack, L.; Ball, M.C. Shoot Surface Water Uptake Enables Leaf Hydraulic Recovery in *Avicennia Marina*. *New Phytol.* **2019**, *224*, 1504–1511. [CrossRef]
9. Mayr, S.; Schmid, P.; Laur, J.; Rosner, S.; Charra-Vaskou, K.; Dämon, B.; Hacke, U.G. Uptake of Water via Branches Helps Timberline Conifers Refill Embolized Xylem in Late Winter. *Plant Physiol.* **2014**, *164*, 1731–1740. [CrossRef]
10. Laur, J.; Hacke, U.G. Exploring *Picea Glauca* Aquaporins in the Context of Needle Water Uptake and Xylem Refilling. *New Phytol.* **2014**, *203*, 388–400. [CrossRef]
11. Katz, C.; Oren, R.; Schulze, E.-D.; Milburn, J.A. Uptake of Water and Solutes through Twigs of *Picea Abies* (L.) Karst. *Trees* **1989**, *3*, 33–37. [CrossRef]
12. Mason Earles, J.; Sperling, O.; Silva, L.C.; McElrone, A.J.; Brodersen, C.R.; North, M.P.; Zwieniecki, M.A. Bark Water Uptake Promotes Localized Hydraulic Recovery in Coastal Redwood Crown. *Plant Cell Environ.* **2016**, *39*, 320–328. [CrossRef] [PubMed]
13. Liu, J.; Gu, L.; Yu, Y.; Huang, P.; Wu, Z.; Zhang, Q.; Qian, Y.; Wan, X.; Sun, Z. Corticular Photosynthesis Drives Bark Water Uptake to Refill Embolized Vessels in Dehydrated Branches of *Salix Matsudana*. *Plant Cell Environ.* **2019**, *42*, 2584–2596. [CrossRef]
14. Salleo, S.; Lo Gullo, M.A.; Trifilo, P.; Nardini, A. New Evidence for a Role of Vessel-Associated Cells and Phloem in the Rapid Xylem Refilling of Cavitated Stems of *Laurus Nobilis* L. *Plant Cell Environ.* **2004**, *27*, 1065–1076. [CrossRef]
15. Zwieniecki, M.A.; Holbrook, N.M. Confronting Maxwell's Demon: Biophysics of Xylem Embolism Repair. *Trends Plant Sci.* **2009**, *14*, 530–534. [CrossRef] [PubMed]
16. Secchi, F.; Pagliarani, C.; Zwieniecki, M.A. The Functional Role of Xylem Parenchyma Cells and Aquaporins during Recovery from Severe Water Stress: Response of Xylem Parenchyma Cells to Embolism. *Plant Cell Environ.* **2017**, *40*, 858–871. [CrossRef]
17. Wheeler, J.K.; Huggett, B.A.; Tofte, A.N.; Rockwell, F.E.; Holbrook, N.M. Cutting Xylem under Tension or Supersaturated with Gas Can Generate PLC and the Appearance of Rapid Recovery from Embolism. *Plant Cell Environ.* **2013**, *36*, 1938–1949. [CrossRef]
18. Trifilò, P.; Raimondo, F.; Lo Gullo, M.A.; Barbera, P.M.; Salleo, S.; Nardini, A. Relax and Refill: Xylem Rehydration Prior to Hydraulic Measurements Favours Embolism Repair in Stems and Generates Artificially Low PLC Values. *Plant Cell Environ.* **2014**, *37*, 2491–2499. [CrossRef]
19. Sperry, J.S.; Donnelly, J.R.; Tyree, M.T. A Method for Measuring Hydraulic Conductivity and Embolism in Xylem. *Plant Cell Environ* **1988**, *11*, 35–40. [CrossRef]
20. Brodersen, C.R.; McElrone, A.J.; Choat, B.; Matthews, M.A.; Shackel, K.A. The Dynamics of Embolism Repair in Xylem: In Vivo Visualizations Using High-Resolution Computed Tomography. *Plant Physiol.* **2010**, *154*, 1088–1095. [CrossRef]
21. Secchi, F.; Pagliarani, C.; Cavalletto, S.; Petruzzellis, F.; Tonel, G.; Savi, T.; Tromba, G.; Obertino, M.M.; Lovisolo, C.; Nardini, A.; et al. Chemical Inhibition of Xylem Cellular Activity Impedes the Removal of Drought-induced Embolisms in Poplar Stems—New Insights from Micro-CT Analysis. *New Phytol.* **2020**, *229*, 820–830. [CrossRef] [PubMed]
22. Savi, T.; Miotto, A.; Petruzzellis, F.; Losso, A.; Pacilè, S.; Tromba, G.; Mayr, S.; Nardini, A. Drought-Induced Embolism in Stems of Sunflower: A Comparison of in Vivo Micro-CT Observations and Destructive Hydraulic Measurements. *Plant Physiol. Biochem.* **2017**, *120*, 24–29. [CrossRef] [PubMed]
23. Venturas, M.D.; Pratt, R.B.; Jacobsen, A.L.; Castro, V.; Fickle, J.C.; Hacke, U.G. Direct Comparison of Four Methods to Construct Xylem Vulnerability Curves: Differences among Techniques Are Linked to Vessel Network Characteristics. *Plant Cell Environ.* **2019**, *42*, 2422–2436. [CrossRef] [PubMed]
24. Torres-Ruiz, J.M.; Jansen, S.; Choat, B.; McElrone, A.J.; Cochard, H.; Brodribb, T.J.; Badel, E.; Burlett, R.; Bouche, P.S.; Brodersen, C.R.; et al. Direct X-Ray Microtomography Observation Confirms the Induction of Embolism upon Xylem Cutting under Tension. *Plant Physiol.* **2015**, *167*, 40–43. [CrossRef]
25. Tomasella, M.; Casolo, V.; Aichner, N.; Petruzzellis, F.; Savi, T.; Trifilò, P.; Nardini, A. Non-Structural Carbohydrate and Hydraulic Dynamics during Drought and Recovery in *Fraxinus Ornus* and *Ostrya Carpinifolia* Saplings. *Plant Physiol. Biochem.* **2019**, *145*, 1–9. [CrossRef] [PubMed]
26. Torres-Ruiz, J.M.; Cochard, H.; Mayr, S.; Beikircher, B.; Diaz-Espejo, A.; Rodriguez-Dominguez, C.M.; Badel, E.; Fernández, J.E. Vulnerability to Cavitation in *Olea Europaea* Current-Year Shoots: Further Evidence of an Open-Vessel Artifact Associated with Centrifuge and Air-Injection Techniques. *Physiol. Plant.* **2014**, *152*, 465–474. [CrossRef]
27. Torres-Ruiz, J.M.; Cochard, H.; Choat, B.; Jansen, S.; López, R.; Tomášková, I.; Padilla-Díaz, C.M.; Badel, E.; Burlett, R.; King, A.; et al. Xylem Resistance to Embolism: Presenting a Simple Diagnostic Test for the Open Vessel Artefact. *New Phytol.* **2017**, *215*, 489–499. [CrossRef]
28. Zwieniecki, M.A.; Holbrook, N.M. Bordered Pit Structure and Vessel Wall Surface Properties. Implications for Embolism Repair. *Plant Physiol.* **2000**, *123*, 1015–1020. [CrossRef]
29. Secchi, F.; Zwieniecki, M.A. Accumulation of Sugars in the Xylem Apoplast Observed under Water Stress Conditions Is Controlled by Xylem PH. *Plant Cell Environ.* **2016**, *39*, 2350–2360. [CrossRef]
30. Burgess, S.S.O.; Dawson, T.E. The Contribution of Fog to the Water Relations of Sequoia Sempervirens (D. Don): Foliar Uptake and Prevention of Dehydration. *Plant Cell Environ.* **2004**, *27*, 1023–1034. [CrossRef]
31. Losso, A.; Bär, A.; Unterholzner, L.; Bahn, M.; Mayr, S. Branch Water Uptake and Redistribution in Two Conifers at the Alpine Treeline. *Sci. Rep.* **2021**, *11*, 22560. [CrossRef] [PubMed]

32. Ilek, A.; Siegert, C.M.; Wade, A. Hygroscopic Contributions to Bark Water Storage and Controls Exerted by Internal Bark Structure over Water Vapor Absorption. *Trees* **2021**, *35*, 831–843. [CrossRef]
33. Schönherr, J.; Ziegler, H. Water Permeability of Betula Periderm. *Planta* **1980**, *147*, 345–354. [CrossRef] [PubMed]
34. Groh, B.; Hübner, C.; Lendzian, K. Water and Oxygen Permeance of Phellems Isolated from Trees: The Role of Waxes and Lenticels. *Planta* **2002**, *215*, 794–801. [CrossRef] [PubMed]
35. Nardini, A.; Lo Gullo, M.A.; Salleo, S. Refilling Embolized Xylem Conduits: Is It a Matter of Phloem Unloading? *Plant Sci.* **2011**, *180*, 604–611. [CrossRef]
36. Wang, R.; Zhang, L.; Zhang, S.; Cai, J.; Tyree, M.T. Water Relations of R*Obinia Pseudoacacia* L.: Do Vessels Cavitate and Refill Diurnally or Are R-shaped Curves Invalid in *Robinia*? *Plant Cell Environ.* **2014**, *37*, 2667–2678. [CrossRef]
37. Nardini, A.; Gasco, A.; Trifilo, P.; Lo Gullo, M.A.; Salleo, S. Ion-Mediated Enhancement of Xylem Hydraulic Conductivity Is Not Always Suppressed by the Presence of Ca^{2+} in the Sap. *J. Exp. Bot.* **2007**, *58*, 2609–2615. [CrossRef]
38. Petruzzellis, F.; Pagliarani, C.; Savi, T.; Losso, A.; Cavalletto, S.; Tromba, G.; Dullin, C.; Bär, A.; Ganthaler, A.; Miotto, A.; et al. The Pitfalls of in Vivo Imaging Techniques: Evidence for Cellular Damage Caused by Synchrotron X-ray Computed Micro-Tomography. *New Phytol.* **2018**, *220*, 104–110. [CrossRef]
39. Brun, F.; Pacilè, S.; Accardo, A.; Kourousias, G.; Dreossi, D.; Mancini, L.; Tromba, G.; Pugliese, R. Enhanced and Flexible Software Tools for X-ray Computed Tomography at the Italian Synchrotron Radiation Facility Elettra. *Fundam. Informaticae* **2015**, *141*, 233–243. [CrossRef]
40. Paganin, D.; Mayo, S.C.; Gureyev, T.E.; Miller, P.R.; Wilkins, S.W. Simultaneous phase and amplitude extraction from a single defocused image of a homogeneous object. *J. Microsc.* **2002**, *206*, 33–40. [CrossRef]
41. Pinheiro, J.; Bates, D.; DebRoy, S.; Sarkar, D.; R Core Team. Nlme: Linear and Nonlinear Mixed Effects Models. 2019. Available online: https://CRAN.R-project.org/package=nlme (accessed on 30 November 2021).
42. Lenth, R.V. Emmeans: Estimated Marginal Means, Aka Least-Squares Means. R Package Version 1.5.0. 2020. Available online: https://CRAN.R-project.org/package=emmeans (accessed on 30 November 2021).

plants

MDPI

Article

The INRAE Centre for Vegetable Germplasm: Geographically and Phenotypically Diverse Collections and Their Use in Genetics and Plant Breeding

Jérémy Salinier †, Véronique Lefebvre, Didier Besombes, Hélène Burck, Mathilde Causse , Marie-Christine Daunay, Catherine Dogimont , Juliette Goussopoulos, Christophe Gros, Brigitte Maisonneuve, Louis McLeod, Fatiha Tobal and Rebecca Stevens *

Unité de Génétique et Amélioration des Fruits et Légumes, INRAE, 84140 Montfavet, France; Jeremy.Salinier@cirad.fr (J.S.); veronique.lefebvre@inrae.fr (V.L.); didier.besombes@inrae.fr (D.B.); helene.burck@inrae.fr (H.B.); mathilde.causse@inrae.fr (M.C.); Marie-christine.brand-daunay@inrae.fr (M.-C.D.); catherine.dogimont@inrae.fr (C.D.); juliette.goussopoulos@inrae.fr (J.G.); Christophe.gros@inrae.fr (C.G.); brigitte.maisonneuve@inrae.fr (B.M.); louis.mcleod@inrae.fr (L.M.); fatiha.tobal@inrae.fr (F.T.)

* Correspondence: rebecca.stevens@inrae.fr

† Current address: Unité Mixte de Recherche Peuplements Végétaux et Bioagresseurs en Milieu Tropical, CIRAD, 97410 Saint-Pierre, France.

Abstract: The French National Research Institute for Agriculture, Food and the Environment (INRAE) conserves and distributes five vegetable collections as seeds: the aubergine* (in this article the word aubergine refers to eggplant), pepper, tomato, melon and lettuce collections, together with their wild or cultivated relatives, are conserved in Avignon, France. Accessions from the collections have geographically diverse origins, are generally well-described and fixed for traits of agronomic or scientific interest and have available passport data. In addition to currently conserving over 10,000 accessions (between 900 and 3000 accessions per crop), the centre maintains scientific collections such as core collections and bi- or multi-parental populations, which have also been genotyped with SNP markers. Each collection has its own merits and highlights, which are discussed in this review: the aubergine collection is a rich source of crop wild relatives of *Solanum*; the pepper, melon and lettuce collections have been screened for resistance to plant pathogens, including viruses, fungi, oomycetes and insects; and the tomato collection has been at the heart of genome-wide association studies for fruit quality traits and environmental stress tolerance.

Keywords: genetic resources; Solanaceae; *Cucumis*; *Lactuca*; diversity; vegetables; genebank

Citation: Salinier, J.; Lefebvre, V.; Besombes, D.; Burck, H.; Causse, M.; Daunay, M.-C.; Dogimont, C.; Goussopoulos, J.; Gros, C.; Maisonneuve, B.; et al. The INRAE Centre for Vegetable Germplasm: Geographically and Phenotypically Diverse Collections and Their Use in Genetics and Plant Breeding. *Plants* **2022**, *11*, 347. https://doi.org/10.3390/plants11030347

Academic Editors: Milan S. Stankovic, Paula Baptista and Petronia Carillo

Received: 6 December 2021
Accepted: 21 January 2022
Published: 27 January 2022

1. Introduction

The evolutionary history of vegetable crops is fascinating because it coincides with the birth and development of agriculture and the world history of human migrations and land discovery. For example, the wild ancestor of aubergine (eggplant), *Solanum insanum*, originated in Asia after ancestral species spread from Northeastern Africa two million years ago [1]. Domesticated chili pepper, *Capsicum annuum*, originated in Central–East Mexico more than 6500 years ago [2] and the process of tomato domestication started in Ecuador and Peru with *Solanum pimpinellifolium* before finishing with modern-sized fruit in Mexico [3]. Melon, *Cucumis melo*, was domesticated in both Africa and Asia before arriving in Europe [4,5]. The ancestor of lettuce was domesticated in Southwest Asia, and then some primitive forms were identified in Egypt around 4500 BC. With the Greek and Roman civilisations, lettuce spread rapidly through the Mediterranean, then Western Europe, and became known in America from the late fifteenth century [6–8]. Today's fruit and vegetables bear little resemblance to their undomesticated wild relatives: for example, the *Lactuca* ancestors of lettuce resemble a weed, with spines under the leaves, bitterness

and small seeds [9]. The domestication process for the five crops has changed the size of the edible part, total yield and also fruit shape and colour, ripening and plant architecture [10].

The domestication of plants has been at the expense of the plant's resistance to abiotic and biotic stresses [11] and latterly selection has also changed the organoleptic quality of the product [12]. The conservation of crop wild relatives (CWR) and knowledge of the evolutionary history of species mean that sources of genes for quality, resistance to pests and pathogens or adaptation to environmental conditions can be fully or partially restored by plant breeders, and knowledge at the genomic level facilitates their use. However, the accessibility and exchange of genetic resources is increasingly complicated, being regulated by international laws: exchange or collection of live material can no longer occur spontaneously. This means that ex-situ conservation is necessary, along with clear documentation (including phytosanitary documents, passport data and material transfer agreements) relating to the stored germplasm, particularly since the ITPGRFA (International Treaty on Plant Genetic Resources for Food and Agriculture) and the Nagoya protocol, adopted in 2010 for fair and equitable sharing of genetic resources [13]. These facts explain the importance of vegetable genebanks as a means of conserving and characterising phytogenetic resources.

Vegetable genebanks from around the world, a non-exhaustive list of which is included in Supplementary Table S1, conserve part of the diversity found in species of local and international importance. In France, a network called 'RARe' regroups the French Biological Resource Centres for agricultural, environmental and life sciences (https://www.agrobrc-rare.org/ (accessed on 5 December 2021)). The vegetable genebank situated in Avignon in the south east of France, the INRAE Centre for Vegetable Germplasm—or Centre de Ressources Biologiques Légumes in French—conserves seeds for five vegetable crops. Three of these are from the Solanaceae family: aubergine is a staple food for much of Africa and Asia, pepper is an important crop worldwide, used fresh or dried as a spice, and tomato is one of the world's most produced fruit vegetables and used fresh or transformed in sauces and conserves. Melon (from the Cucurbitaceae family), grown worldwide in a diversity of forms and consumed as a sweet or non-sweet fruit or vegetable, and lettuce (from the Asteraceae family) complete the list of species conserved and are important for nutritional diversification [14]. More generally, vegetables are an essential part of a balanced diet and the collections are witness to progress in the domestication of vegetable crops and their adaptation to the environment. The need for plants to suit new environmental or agricultural conditions is proof of their value.

The aim of this paper is to unite the information on the five collections conserved by the INRAE Centre for Vegetable Germplasm in a single article, which has not been accomplished previously. The collections are at the heart of much of the research carried out within the Genetics and Breeding of Fruit and Vegetables research unit and form the basis of many collaborations with both research institutes and plant breeders. We will include the history of the genebank's constitution, the characteristics of the material now present, the methods of conservation, the descriptors used, current databases and finally a spotlight on how the material has been used in different research programmes.

2. Overview and Origins of the Five Collections

Each collection has developed independently over different periods, having been built up by individual researchers working on different research programmes. Generally, the collections started in the 1960s and 1970s and grew rapidly at the end of the last century; introductions have mostly slowed since 2010 (Figure 1). The origins of accessions seen in Figure 2 are closely linked with the domestication/diversification centres for each crop.

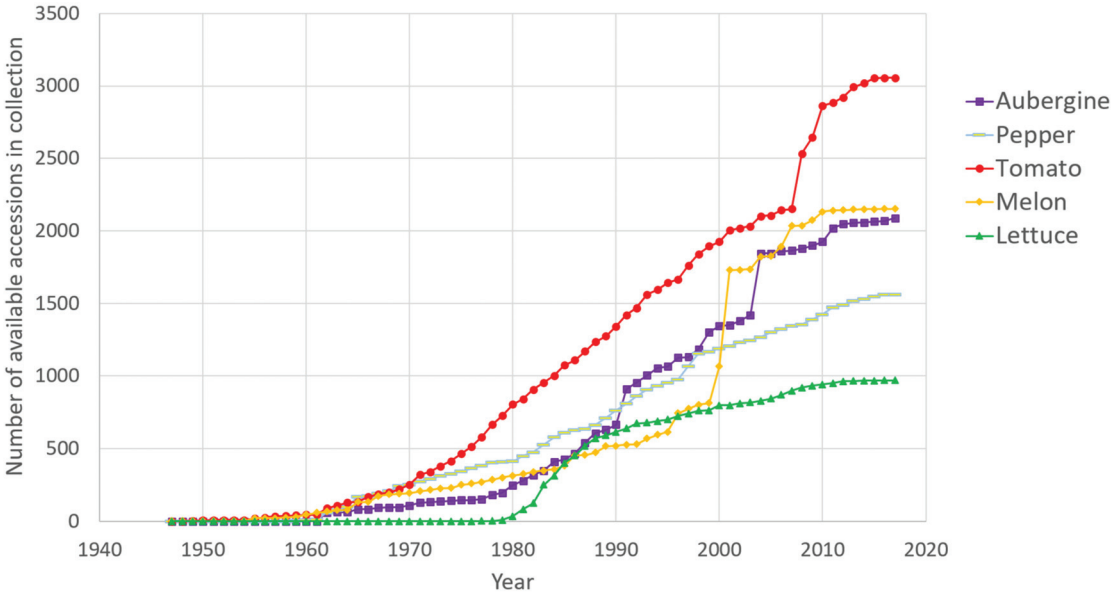

Figure 1. Number of available accessions for each collection by year of introduction: each crop appears with a different colour (see legend). Note that the introduced accessions that have since been 'lost' do not appear.

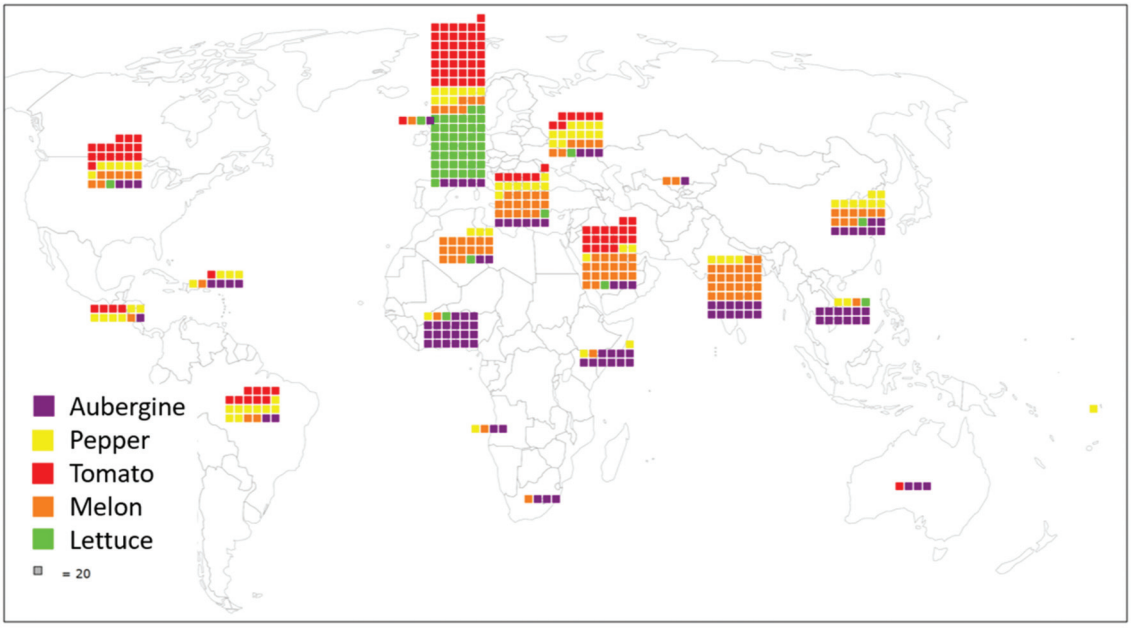

Figure 2. Supposed geographic M49 region of origin or of breeding of the accessions using the colour code shown in the legend. Each square corresponds to 20 accessions. Note that sometimes the recorded origin is that of the collection, even if the accession comes from a foreign country.

Table 1 shows the number of accessions by geographic region of origin based on the M49 regions of the United Nations Statistics Division (standard country or area codes for statistical use) and Supplementary Figure S1 shows the number of accessions by precise country of origin and by continent. There are two points of note on the origin of an accession: firstly, the origin can correspond to the donating genebank's origin when historical passport data are not available, and, secondly, some accessions resulting from breeding programmes mixing parents of different origins are listed as being of unknown origin, which was seen as preferable to using the local geographic origin: this is the case for both aubergine and lettuce.

Table 1. Number of accessions originating from the different regions of the United Nations Statistical Division. Note that sometimes the recorded origin is that of the original collection, even if the accession was introduced from a foreign country. The colour scale ranges from dark (most represented region) to light (least represented region).

Geographic Region	Aubergine	Pepper	Tomato	Melon	Lettuce [1]
Australia and New Zealand	59		4		
Melanesia		2			
Polynesia	1				
Caribbean	75	79	26	18	
Central America	9	115	97	4	
Northern America	45	102	354	140	5
South America	29	170	208	21	2
Central Asia	4	3		36	5
Eastern Asia	150	151	39	175	9
Southeastern Asia	237	52	4	19	1
Southern Asia	230	69	14	518	
Western Asia	51	57	378	370	18
Eastern Africa	195	50	6	7	
Middle Africa	34	22		12	
Northern Africa	33	85	6	285	3
Southern Africa	60		4	3	
Western Africa	406	41	20	8	1
Eastern Europe	53	222	175	109	1
Northern Europe	3		53	13	5
Southern Europe	106	160	145	303	37
Western Europe	97	165	913	122	224

[1] Not applicable for modern commercial cultivars (600 cultivated lettuces) because, for a given cultivar, breeding can be carried out in different countries.

The collections are rich in phenotypic diversity: many lines have been fixed for morphological characteristics often related to fruit size, shape or colour. Some of the visual diversity of a selection of our collections is shown in Figure 3 and includes wild or other cultivated species. The morphological diversity can be used to classify the collection into groups based on morphological data such as fruit colour and shape (Supplementary Figure S2), which is useful in certain cases—for example, for breeding or for comparing with genotyping data.

Table 2 summarises the number of accessions for the main individual species and the number of crop wild relatives, and Supplementary Figure S3 provides extra information on the number of accessions present in the collections for individual species.

Figure 3. Illustrations of examples of the phenotypic diversity present in the five collections. (**Top**) aubergine collection, from left to right—MM 01560: KOPEK PUTIH/TS58/X452; MM 00133: DE BUKAREST = BUCA; MM 00500: ZEBRINA LONGUE; MM 01737: AUBERGINE LOCAL OP10 (ABIDJAN); MM 00662: BIRM/S.0657; MM 01192: DIEGO ANTSINANARA (MARCHE). (**Second from top**) pepper collection, from left to right—PM0235: CHILI ICONO; PM0802: SAFI; PM0658: BOTIJILLO TINTO; PM1216: EX HD(YWx702)11; PM0611: MULATO ROQUE; PM1409: VANIA; PM0225: PEPERONE DI LUCCA. (**Middle line**) tomato collection, from left to right—T300077: LA1274 *S. peruvianum*; T300165: LA1447: *S. cheesmanii*; T101431: Marmande Jaune; T101560: Poivron des Andes; T102434: EA2679; T102446: EA2751. (**Second from bottom**) melon collection, from left to right—Unknown; ME0857: MR-1; ME2343: ACEM; ME2369: DAMIAN GUA; ME1038: SVI 0024; wild African accession. (**Bottom**) lettuce collection, from left to right—LC0251: butterhead cv Grosse brune têtue; LC0152: Batavia, cv craquante d'Ecully; LC0206: oak leaf, cv Feuille de chêne espagnole; Production of seed in insect-proof tunnel; LC0858: *L. virosa*, LS360.

Table 2. Summary of taxonomy of the collections for the accessions whose taxonomy has been identified.

Collection	Species/Crop Wild Relatives	Number of Species	Number of Accessions
Aubergine	*Solanum melongena*		1211
	S. aethiopicum		335
	S. macrocarpon		91
	Crop wild relatives—Solanum	109	609
	Other Solanaceae genus (8)	17	24
Pepper	*Capsicum annuum*		1683
	C. baccatum		129
	C. chinense		159
	C. frutescens		86
	C. pubescens		28
	Crop wild relatives	6	24
Tomato	*Solanum lycopersicum*		3095
	Crop wild relatives	9	285
Melon	*Cucumis melo* [1]		2359
Lettuce	*Lactuca sativa*		712
	Crop wild relatives—*Lactuca*	10	225
	Crop wild relatives—other genus	3	15

[1] includes 91 *Cucumis melo* subsp. agrestis (wild melon).

3. Summary of the Individual Collections

Each collection is described in detail below with information on geographic diversity, taxonomy and scientific resources available: core collections are available for aubergine,

pepper and tomato [15,16]. Many mapping progenies have been created for research purposes and are available for collaborative projects.

(i). **The aubergine collection** (**2388 accessions**) contains two introductory peaks: one from 1991, which corresponds to the scientific collaboration with the taxonomist Richard N. Lester of the University of Birmingham, UK, and the second in 2004, when the collection of *Solanum* species related to aubergine were transferred from the University of Birmingham to INRAE [17]. More recently, we have introduced new aubergine accessions from the H2020 G2P-SOL project (http://www.g2p-sol.eu/ (accessed on 5 December 2021)). Most of the aubergine accessions originate from Africa and Asia. The aubergine collection is notable amongst the five collections because it includes a large proportion of crop wild relatives (26%). This number of CWR is rare in other germplasm centres, mostly because of the difficulties in maintaining them. The collection includes more than 1000 accessions principally from Africa (related cultivated species including *Solanum macrocarpon* L., *Solanum aethiopicum* L., *Solanum scabrum Mill.).* These species are indigenous African leafy vegetables and/or fruits: *S. aethiopicum* and *S. macrocarpon* provide a usable secondary gene pool for the improvement of *S. melongena.* Approximately 500 accessions, representing over a hundred wild species, the majority related to cultivated aubergine, complete the collection, as well as accessions of other Solanaceae of interest (*Atropa*, *Datura*, *Lycium*, *Nicandra*, *Physalis* and *Withania*) [18]. A word of caution must be added about the taxonomy of *Solanum* species. The taxonomic classification of aubergine dates back to the work of RN Lester in the 1990s; the nomenclature has evolved since the early 2000s and the taxonomic status of several taxa is unclear [19,20].

The aubergine scientific collection contains five double-haploid populations and F1, F2 and backcrosses of six biparental progenies. A total of 706 aubergine accessions from our collection were supplied to the G2P-SOL project, of which 106 are included in the final core collection from the project. The project has and will supply low- and high-density genotyping data, which extends the knowledge available on the whole collection.

(ii). **The pepper collection** (**2188 accessions**) is representative of domestication centres (South and Central America). In pepper, the collection focuses on *Capsicum annuum* (76% of accessions), with a large collection, rich in phenotypic and geographic variability, that is easily exploited in breeding programmes. Eleven species of *Capsicum* are available in the collection, including the five cultivated species (C. *annuum*, *C. frutescens*, *C. chinense*, *C. baccatum* and C. *pubescens*) [21]. Recombinant inbred lines in pepper [22] have allowed the evaluation of fruit traits [23] and resistance to *Phytophthora* species [24,25]. Similarly to aubergine, 912 INRAE accessions (889 cultivated) were included in the G2P-SOL project, of which 59 are included in the final core collection [26]. The genotypic diversity in pepper from the G2P-SOL core collection maximises the diversity of around 10,000 accessions from 10 genebanks and research institutes from around the world in a collection of 423 mostly *C. annuum* accessions [26]. INRAE is the official distributor of the G2P-SOL pepper core collection. Another core collection of over 280 accessions has been constructed with INRAE material [27].

(iii). **The tomato collection** (**3410 accessions**) is representative of its domestication centre (South and Central America). In tomato, the number of wild-relative species is lower than in the other collections but a good diversity of *S. pimpinellifolium* is available. For tomato, *S. peruvianum* has been separated into four species, including two new species, *S. arcanum* and *S. huaylasense*, which requires database information to be corrected: taxonomic identification is therefore an ongoing process [28]. More than 500 accessions have been genotyped with the SolCap Illumina array and a core collection of 160 accessions constructed and amply characterised (see below) [29]. The tomato scientific resources include progenies of recombinant inbred lines [30], advanced backcrosses, intra- and interspecific progenies and multi-parent progenies (MAGIC) [31] representing more than 1000 accessions.

(iv). **The melon collection** (**2359 accessions**) comes from all around the world, particularly Africa and Asia, and includes around 100 genotypes of wild *C. melo* (mostly from the agrestis cultigroup), which are compatible for crossing with cultivated melons. Recombinant inbred lines obtained by crossing distant melon lines have been created and studied for many segregating agronomic traits and for monogenic as well as quantitative pest and disease resistance [32–37]. A mutant melon collection obtained by chemical EMS mutagenesis of an INRAE Charentais melon line includes more than 7000 M2 families and is useful for the functional validation of genes or for generating new diversity [38–41].

(v). **The lettuce collection** (**948 accessions**) comes essentially from Europe. For cultivated lettuce, the introduction year is unknown for 151 cultivars received before 1980; for wild *Lactuca* species, 64% of the wild accessions (mainly of *L. serriola*) were collected directly by INRAE, mainly in France in the 1980s. Out of the 479 introduced wild accessions, 343 collected accessions and 136 received from other laboratories, only 248 are still present with seed stock in the 2020s: seed for many accessions arriving in the 1970s was lost because the storage at room temperature before 1984 was inadequate for long-term conservation in *Lactuca*. In lettuce, the 704 cultivated accessions are *L. sativa*, with many modern cultivars cultivated in Western Europe over the last 40 years. For wild lettuce, the precise collection site is known for 92% of the INRAE accessions. There are 11 *Lactuca* species, including the three species mainly used by breeders: *L. serriola*, *L. saligna* and *L. virosa*. The lettuce collection is completed by 15 accessions from other genera of the Asteraceae family (*Chondrilla*, *Mycelis*, *Sonchus*). The lettuce collection contains a few lines with resistance to potyviruses or *Bremia lactuca* identified in *L. virosa* and introgressed into a cultivated background [42–44].

4. Collection Management

The genebank follows typical procedures for seed storage, multiplication and distribution [45]. An overview of the processes and procedures is provided in Figure 4, with an indication given regarding the number of accessions or samples concerned by each process for a typical year. These figures are specific to the INRAE Centre for Vegetable Germplasm.

(i). Conservation of seed stocks

The genebank focuses on medium- and long-term storage (4 °C and 50% relative humidity for ~15 years or −20 °C and 50% relative humidity for >30 years [46]) with procedures for checking germination rates following long-term storage (after one year and then every 5 or 10 years depending on the results). Safety duplicates are held at a genebank centre based in Montpellier, France.

(ii). Regeneration of seed stocks

Regeneration by seed multiplication is performed mostly by controlled self-pollination in insect-proof greenhouses (three plants per accession, two for lettuce). For accessions that are regenerated as wild populations, i.e., those accessions that were harvested from a mixed genepool that potentially contains many rare alleles and/or accessions that are self-incompatible, we use isolation fields with natural pollinators. We aim for a minimum of 600 seeds per accession. Twenty seeds are used in germination tests.

The management of a collection of wild relatives of *Solanum* is complex: problems arise at numerous levels—for example, difficulty in obtaining accessions, misidentification, poor germination, physiological problems with flowering, pollination and fruit set [47]. Many wild accessions missing from the collection are endangered because of the eradication of their natural habitat, notably in East Africa [48]. Many species cannot be regenerated in the short culture periods available in the greenhouses or fields in Avignon; this is particularly true for the majority of *Solanum* species native to Australia and many species of tropical origin. New culture conditions for those species that are difficult to regenerate have been investigated in a recent project (https://www6.paca.inrae.fr/gafl_eng/Partnerships-and-Projects/Closed-Projects/SESAM (accessed on 5 December 2021)) in which we have

varied the photoperiod, growing season or watering regime to obtain success in saving some accessions.

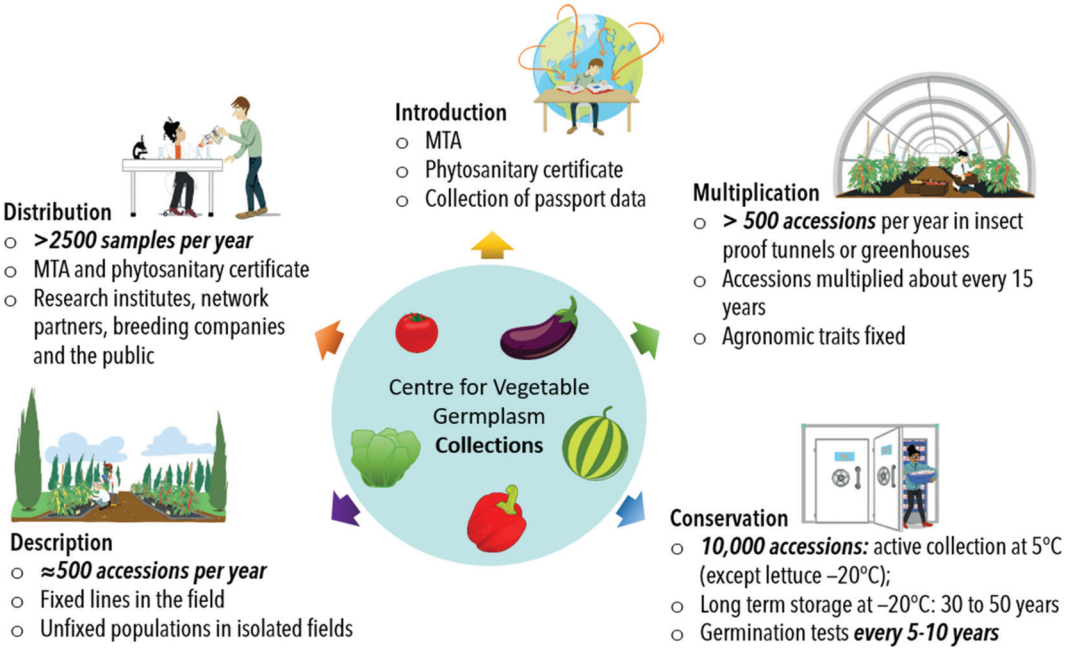

Figure 4. Current procedures for management of the collections at the INRAE Vegetable Germplasm Centre, including the major missions of introduction, multiplication, description, conservation and distribution and with an estimation of the number of samples or accessions involved. The multiplications are mostly carried out by self-pollination. Illustrations Camille Ulrich—Copyright INRAE.

(iii). Descriptions

Collections are systematically characterised using botanic and primary descriptors (fruit, flower, plant and leaf characteristics). A large percentage of the collections has been described using descriptors from either the International Plant Genetic Resources Institute, the International Union for the Protection of New Varieties in Plants or with in-house descriptors. The supplementary dataset includes the list of descriptors used for each collection (Supplementary Figure S4) and the proportion of accessions that have been described. Fruit diversity and colour are a particular focus for descriptions [23,26,49–51] and we are now establishing techniques for phenotyping root system architecture [52]. Specific ways of describing wild lettuce and aubergine, which have characteristics quite different to the cultivated species, have also been put into place (Supplementary Figure S4). Cultivated lettuce has been described for bolting and flowering characteristics; the heading characters were scored on progeny, either in the field for cultivars bred for outdoor culture, or under plastic tunnels for cultivars bred for protected cultures (Supplementary Figure S4). For the five collections, secondary descriptors include criteria such as pest and pathogen resistance (Supplementary Figure S4). Fixing of traits of agronomic interest (for example, fruit colour or shape) has been carried out for most of the accessions when possible, in order to complete phenotypic gaps in the collections.

(iv). Networks and sub-collections

Each INRAE collection is wholly or partially regenerated and/or described in partnership with private breeding companies, the French organisation 'Variety and Seed Study and Control Group' (GEVES) and the CIRAD. With the INRAE Centre for Vegetable Germplasm,

a different subset of these partners forms three national networks: (i) the Fruit Solanaceae network (created in 1996), (ii) the melon network (since 1997) and (iii) the *Lactuca* network (created in 2020). Each network partner not only contributes to the network by multiplying seeds and describing accessions each year but also shares extra varieties or accessions with the network's members. The French national collection (approximately 100 accessions of patrimonial value) is defined by the network members and includes accessions from INRAE and the network's collections. The national collection is freely available to all parties and the public and appears in the databases (see below). In addition, the aubergine national collection has been submitted to the International Treaty on Plant Genetic Resources for Food and Agriculture (ITPGRFA), to encourage the open exchange of plant genetic resources for food use.

(v). Seed and data sharing

Online local databases are used for storing passport data, descriptions and information on seeds (seed batch date, seed quantity, exchange, storage conditions and germination rate). Our local databases are linked to national or European databases where part of the collections are found (for the moment often only the national collection). These databases contain accession names and passport data as a minimum and currently include Siregal (https://urgi.versailles.inra.fr/siregal/siregal/grc.do (accessed on 5 December 2021)), where phenotyping data are also available, Florilège (http://florilege.arcad-project.org/fr (accessed on 5 December 2021)), ECPGR (https://www.ecpgr.cgiar.org/ (accessed on 5 December 2021)) and Eurisco (https://eurisco.ipk-gatersleben.de/ (accessed on 5 December 2021)). As many changes are occurring in the management of these databases and the links between them, we have provided a list of our accessions and passport data in Supplementary Table S2. This includes the national, network and INRAE collections. Please contact us for the distribution conditions specific to each accession.

Seeds can be ordered via our local website: https://www6.paca.inrae.fr/gafl_eng/Vegetable-Germplasm-Centre/Use-our-genetic-resources (accessed on 5 December 2021). A charge is made for sending accessions, which are provided with a phytosanitary passport or certificate and MTA as necessary.

We estimate that approximately 2000–3000 samples are sent annually to partners outside the research unit, of which around 50% are for private research companies, nearly 20% are for international and national research laboratories and around 5% go to members of the general public, associations and amateurs. The remaining 25% of samples are supplied to other INRAE laboratories.

5. The Collections as Material for Scientific Study

The genetic resources are used by INRAE, research institutes, universities and breeding companies. The collections are currently used or studied for the following themes.

(i). Domestication and structure of the collections

Solanaceae genetic resources conserved at INRAE have been used to investigate domestication scenarios by analysing transcriptome data from aubergine, pepper and tomato with their close wild relatives to show both common and species-specific demographic changes, the latter being particularly true for aubergine [53]. Geographic isolation has played a role in determining the genetic structure of aubergine populations; there is also evidence for outcrossing in aubergine between wild and cultivated gene pools [20,54–56].

In pepper, 1352 accessions of our collection, representing 11 *Capsicum* species with wide geographic diversity, were genotyped using 28 microsatellite markers. This collection was assigned to six clusters, with three clusters for *C. annuum* and three additional clusters separating the other main species, including the cultivated species and wild relatives, according to their taxonomic classification (*C. frutescens*/*C. chinense*, *C. baccatum*, *C. pubescens*). The three *C. annuum* clusters were significantly distinct for plant and fruit descriptors corresponding to cultivar types, showing that the genetic structure of cultivated pepper has been affected by human selection in primary as well as secondary diversification centres [21]. A

total of 869 accessions from our collection, together with more than 9000 accessions from nine other collections worldwide, were genotyped with more than 26,000 GBS-derived SNPs in the G2P-SOL project. This study revealed a reticulate interbreeding history in *C. annuum* and a differentiation between two major genepools (i.e., European and Central American/Asian). It also demonstrated that approximately 80% of the accessions we maintain at INRAE are not represented in the main world collections [26].

In tomato, where the phenotypic effects of domestication have been well documented [57,58], it has been shown that domestication has affected gene expression within gene regulatory networks: changes in gene co-expression levels were associated with lower nucleotide diversity, often because of the fixation of useful mutations during domestication [53,59]. Tomato also appears to have been domesticated in a two-step process: first in South America and then in Mesoamerica [60]. A similar reduction in nucleotide diversity has been seen in candidate genes involved in meristem development in cultivated compared to wild tomato: around half the genes analysed revealed footprints of selection and polymorphisms putatively involved in fruit size variation by showing negative Tajima's D and a reduction in nucleotide diversity in cultivated tomato [61,62].

Genotyping of 713 melon accessions has given information on the collection's genetic subdivisions and led to the hypothesis that melon has probably been domesticated at least twice [63]. More recently, one hundred accessions of our collection, together with more than 1000 accessions worldwide, have been re-sequenced: the data confirmed the two domestications in Africa and Asia and suggested the occurrence of a third domestication event in India [5]. Iconographical and textual sources suggest the presence of melon in the Mediterranean basin dating back to antiquity and are illustrated by two melon types in Italy in the late medieval times: melons of the Chate group, the likely ancestor of our sweet melons, and elongated and unsweet snake melons, still appreciated in East and North Africa [64]. Complementary studies have shown the genetic diversity available within melon cultigroups [65,66] and the phenotypic diversity, which is greater in cultivated melon than wild melon [51].

(ii). Resistance to plant pests and pathogens

In aubergine, the collections are of particular interest in screening for *Ralstonia solanacearum* resistance and mapping populations have been created to this end: *R. solanacearum* (bacterial wilt, southern wilt or potato brown rot) causes major yield losses in the tropics and subtropics but is also a threat in temperate climates [67–69]. Numerous strains or phylotypes exist, and, whereas one aubergine variety may be resistant or partially resistant to one strain, it is often not resistant to all strains. The aubergine collection is a source of resistance genes against *Ralstonia*: from a subset of 10 genotypes, none controlled all strains but some are able to control the most virulent strains (six accessions were totally resistant to six strains) [70–73]. Crosses between resistant and susceptible parents have generated recombinant inbred lines [72] for QTL mapping related to resistance in different environments; a major resistance gene, *ERs1*, has been identified. Further sequencing and QTL mapping for resistance have shown that both broad-spectrum and strain-specific QTLs exist and that, by combining three or more QTLs, large-spectrum resistance could be obtained [74,75]. Remarkably, aubergine accession Ceylan SM 164 was resistant to all six strains. Aubergine accessions SM6, Surya and AG91-25, as well as pepper accessions CA8 and MC4, were moderately to highly resistant to all six strains [76].

The pepper germplasm has been shown to include a diversity of genetic backgrounds favourable to resistance durability to pests and pathogens. In the case of potato virus Y, the evaluation of a core collection of *Capsicum annuum* landraces showed breakdown frequencies of given resistance alleles that varied from 0 to 53% [15]. In the same core collection, genome-wide association studies detected SNPs associated with the presence of the virus at inoculation and/or systemically [27]. Screening of 1179 accessions of the pepper collection for quantitative resistance to *P. capsici* revealed 26 new sources of resistance [77] and furthermore a key conserved QTL cluster has been shown to exhibit broad-spectrum resistance to *P. capsici* [78]. In a similar way, double-haploid lines obtained from the F1

hybrid of a resistant accession (H3) crossed with a susceptible accession (Vania) revealed QTLs for resistance to powdery mildew due to *Leveillula taurica* [79]. Other double-haploid progenies have been used to study the genetics of resistance to viruses such as potato virus Y, tobacco mosaic virus, tomato spotted wilt virus, cucumber mosaic virus and pepper veinal mottle virus [80–84], and *P. capsici* [85]. Within the G2P-SOL project, the final core collection is to be phenotyped for agronomic traits and biotic stress resistance, including to *Phytophthora capsici*, *Leveillula taurica*, cucumber mosaic virus and *Meloidogyne incognita* by INRAE and *Verticilium dahliae*, pepper mild mottle virus, *Fusarium oxysporum* and tomato spotted wilt virus by other partners.

The melon collection has been extensively evaluated for resistance to pests and pathogens, including several viruses (cucumber mosaic virus; potyviruses such as the zucchini yellow mosaic virus; and the whitefly-transmitted begomoviruses, melon chlorotic mosaic virus, tomato leaf curl New Delhi virus and watermelon chlorotic stunt virus); fungi such as Fusarium wilt and downy and powdery mildew, and also insects [86–91]. QTLs have been detected for both whitefly and aphid resistance in a biparental population: a major QTL affecting aphid behaviour and biotic potential co-localises with the *Vat* gene, although resistance is polygenic [32,92–95]. In melon, an example of a success story is the cloning of the *Vat* gene, which was shown to be a CC-NBS-LRR gene mediating both resistance to aphid infestation and virus infection using *Aphis gossypii* as a vector [94,96].

The lettuce collection in particular has been a target for screening for resistance to plant diseases including viruses, oomycetes, bacteria, nematodes and fungi (summarised in Table 3) [42,97–100]. Breeding for resistance in lettuce is a priority and many resistance gene sources have been reported, particularly in wild lettuce species, for potyvirus, *B. lactucae* and *Meloidogyne incognita* [100–102]. When resistance is found in wild species, the compatibility with *L. sativa* determines the success of breeding programmes: several species are compatible with *L. sativa* (*L. serriola*, *L. saligna* and *L. virosa*) and can therefore be used, but the crosses are only straightforward with *L. serriola*. The hybrids with *L. virosa* are sterile and often show physiological disorders such as necrosis or stunted plants, which are difficult to eliminate in any progenies that are obtained [101]. Resistant genes from *L. virosa* have been introgressed into a butterhead background to produce lines with new resistance to *Bremia* [103] and two potyviruses [43,44]. More than 400 lettuce accessions have also been tested with three stimulators of plant defences; some interesting protection against *B. lactucae* was obtained with a few cultivars [104].

(iii). Floral biology and crossing compatibility

The outcrossing potential of aubergine was investigated using 23 populations of wild weedy aubergine [54]. Controlled crosses with cultivated aubergine resulted in seed set and viable F1 progeny. The exerted stigmas of wild aubergines are likely to promote outcrossing under natural conditions, highlighting the risk of growing Bt transgenic plants in Southern India, where wild and cultivated aubergines coexist.

Variability in the melon germplasm collection (497 accessions of *C. melo*) has been used to validate a locus controlling sex determination in melon: within C. melo, most plants are monoecious (single sex flowers) or andromonoecious (male and hermaphrodite flowers). This trait is under the control of a recessive locus and a single-nucleotide polymorphism in the CmACS7 gene, which co-segregates with the sex determination phenotype of the flowers [53]. The insertion of a transposon, which epigenetically controls the expression of the CmWIP1 transcription factor, was shown to co-segregate with the gynoecious (female flowers only) phenotype [41]. Together with advances in the understanding of sex determination in plants, these studies have provided markers of interest for breeders, facilitating F1 seed production in melon.

The crossing potential of seven accessions of *L. virosa* with 10 lettuce cultivars was compared by using in vitro cultures of immature embryos or harvesting mature seeds. Few F1 progenies were obtained but, after backcrossing to lettuce and self-pollination, some lines with virus resistance were obtained [106].

Table 3. Screening of the lettuce collection for resistance to pests and pathogens.

Plant Disease	Number of Accessions	Comment
Bremia lactucae	400 and 66 accessions within the European Evaluation Network project	EVA projet (2019–2023) https://www.ecpgr.cgiar.org/european-evaluation-network-eva/eva-networks/lettuce/ (accessed on 5 December 2021)
Reactive cultivars to stimulator of plant defences (SDP) for *Bremia* protection	402 cultivars tested with 3 SDP	Some reactive cultivars with good protection against *Bremia* [104]
Potyvirus lettuce mosaic virus	231 (116 cultivated and 115 wild)	*L. virosa* PIVT1398 resistant to all lettuce mosaic virus strains [42].
Potyvirus lettuce Italian necrotic virus	20 (11 cultivated and 9 wild)	One resistant: PIVT1398 [97] Same *Mo3* locus, introgressed from *L. virosa*, confers resistance to LMV and to LINV [43]
Xanthomonas campestris	986 (789 cultivated and 197 wild)	Few genitors in cultivars [99] QTL analysis in RIL population [105]
Meloidogyne incognita	569 (409 cultivated and 160 wild)	Resistance found in *L. sativa* and *L. serriola* [100]

(iv). Fruit quality and abiotic stress tolerance

In pepper, the collections have been used to show that the gene encoding Capsanthin Capsorubin Synthase is responsible for the yellow colour in pepper [50]. Following work on sensory traits in an intraspecific RIL population [49], several core collections of tomato have been used to evaluate the genetics of fruit quality traits [16,107–110]. An example is the genetics of fruit metabolite content—including sugars, vitamin C, amino acids and volatiles. These traits, using two different genotyped core collections, one composed mostly of cherry tomato accessions and the other including breeding material, have been shown to be heritable and under the control of multiple QTLs. The studies also pinpointed candidate genes for traits such as fruit malate content and phenylpropanoid volatile production [16,108]. The GWAS studies have paved the way towards predictive genomic selection, which can be used on crops such as tomato: this could be particularly useful for polygenic traits such as fruit quality [111]. The tomato scientific collections have also been evaluated for potential adaptation to environmental stress—in particular, under conditions of limited water [107,112], elevated temperature [113] and, for the MAGIC population, multiple stress conditions [114], revealing candidate genes involved in stress responses.

(v). Selection and breeding

The creation of new vegetable varieties has mostly stopped at INRAE and is now the domain of private plant breeders. However, some of our past creations are well known. Crosses of certain aubergine introductions combined with INRAE breeding in traditional populations allowed the creation of the first French F1 hybrids, registered in the official catalogue in 1973: F1 Bonica with purple globular fruits and F1 Baluroi with medium-length purple fruits. In aubergine, crop wild relatives offer numerous possibilities for the improvement of *S. melongena* [48], including providing resistance to pests and pathogens: the challenge is creating interspecific hybrids (sexual or somatic) and research has been dedicated to this area over recent decades [115–118].

Crop wild relatives are also particularly good as rootstocks [119]. The Solanaceae family contains many candidates that can be used as rootstocks for cultivated aubergine

and tomato. Part of the collection has been screened to find species having a good grafting affinity with aubergine and a number of candidates identified [120,121].

In pepper, our best-known varieties are Lamuyo F1 hybrid (the first pepper hybrid in the world) and Alby (cumulating five resistance genes) as well as the F1 sweet pepper hybrid Ulysse. In tomato, Montfavet H63-5 is an F1 hybrid widely grown in France, and elsewhere, in the 1970s. Recent tomato varieties include Garance and Jouvance (good colour and flavour, firm, eight disease resistance genes) and Terradou (processing tomato, high soluble solids).

The Margot (1988) melon was the first variety to integrate the *Vat* gene for aphid resistance, and breeders have incorporated the resistance into many varieties, currently including more than 50% of Charentais varieties. Our genetic resources are still used for breeding through our private/public networks and particularly the melon network: only the genetic diversity within the species *C. melo* is usable—there are currently no inter-specific crosses.

For lettuce breeding, resistance to Lettuce mosaic virus (LMV), identified in *L. virosa* PIVT1398 [42], was introduced into butterhead lines by INRAE [101]. The NILs with the *Mo3* locus were also resistant to another potyvirus: lettuce Italian necrotic virus (LINV) [44]. Some NILs with the *Mo3* resistance gene have been made available for research and breeding [43].

6. Conclusions and Perspectives

An overview of the highlights of each of the five collections with the scientific data and resources that have been produced is presented in Figure 5. The availability of genotyping data and phenotypic data has enhanced the usefulness and long-term perspectives of the collections, although phenotyping is still to be carried out on the collections: for example, root descriptors are mostly absent and little information is available on the adaptation of the collections to the environment. Projects including phenotyping or genotyping also allow us to improve the collections by eliminating duplicates or by using introductions to cover gaps. We mainly aim at being complementary to other collections in the world, but there is a need to know which accessions are complementary, and this shows the importance of having an inventory of genetic resources (passport data and descriptors) or genotyping data of collections, which also presents several advantages:

- Allows the study of allelic diversity for genes of interest for mining allelic diversity;
- Facilitates the determination of the "uniqueness" of an accession and better identification of duplicates;
- Gives an idea of the phenomenon of introgression between species;
- Can help in the study of core- and pan-genomes.

For the longer-term perspectives for our genetic resource collections at a local level, we can list as priorities:

- Increasing the duration between multiplication cycles by improved conservation;
- Mobile applications for management of collections (seed harvest, descriptions in the field, etc.) and their direct link to databases for improved traceability and quality standards with the aim of obtaining ISO 9001 certification;
- More complete and quantifiable phenotyping by use of image analysis to measure size, shape and colour of plant organs.

We are continuing our efforts to reduce the cost of conservation, guarantee the long-term preservation of crop resources and increase the knowledge on these resources to facilitate their use in research and breeding projects.

	Total number of accessions	Research highlights	Screening data available	Scientific resources available
	2388	Large collection of CWR; inter-crossing compatibility	Ralstonia resistance and rootstocks	RILs, DH lines, genotyped core collections: G2P-SOL and local
	2188	*C. annuum* collection rich in phenotypic variability; studies on polygenic resistance	PVY, CMV, TMV Phytophthora resistance	RILs, DH lines, genotyped core collections: G2P-SOL and local
	3410	Large *S. lycopersicum* collection; studies on quality traits	Drought stress, fruit metabolites and fruit volatiles	RILs, MAGIC, genotyped cherry tomato core collection
	2359	Large collection of *C. melo*; studies on sex determination and pest resistance	Resistance to virus, fungi and insects	RILs, EMS mutant collection
	948	CWR collected from France; several genitors of disease resistance	Resistances: *Bremia lactucae*, several viruses, *Xanthomonas campestris*, *Meloidogyne*	Progenies from interspecific crosses: (NILs with potyvirus resistance, lines with *Bremia* resistance) and NILs with Ms7

Figure 5. Collection highlights, total number of accessions, screening data and scientific resources available for each of the five collections.

Supplementary Materials: The following are available online at https://www.mdpi.com/article/10.3390/plants11030347/s1, Figure S1: Number of accessions and their origins by country; Figure S2: Morphological groups (aubergine—fruit colour; pepper—fruit shape, colour and pungency; tomato—fruit shape and colour; melon—cultigroups; and lettuce—cultigroups); Figure S3: Number of accessions and their taxa or species; Figure S4: Qualitative and quantitative descriptor lists used for each of the five crops and the proportion of accessions that have been described. Table S1: Non-exhaustive list of vegetable genebanks worldwide; Table S2: List of the accessions for each collection with passport data (Excel file).

Author Contributions: Conceptualisation, V.L., M.C., M.-C.D., C.D., B.M. and R.S.; analysis, J.S.; resources, D.B., H.B., J.G., C.G., L.M. and F.T.; data curation, J.S., J.G. and B.M.; writing—original draft preparation, J.S. and R.S.; writing—coordination of review and editing, R.S. All authors have read and agreed to the published version of the manuscript.

Funding: This research was in part funded by grants received from IBiSA (Infrastructures en Biologie Santé et Agronomie). The SESAM project was funded by a grant received from the French 'Ministère de l'Agriculture et de l'Alimentation' and the French 'Groupement national interprofessionnel des semences et plants'.

Institutional Review Board Statement: Not applicable.

Informed Consent Statement: Not applicable.

Data Availability Statement: Not applicable.

Acknowledgments: The authors would like to thank all those who have participated in the building-up, conservation, maintenance and characterisation of these collections over the years and those who have generously donated or shared material.

Conflicts of Interest: The authors declare no conflict of interest.

References

1. Aubriot, X.; Knapp, S.; Syfert, M.M.; Poczai, P.; Buerki, S. Shedding New Light on the Origin and Spread of the Brinjal Eggplant (*Solanum melongena* L.) and Its Wild Relatives. *Am. J. Bot.* **2018**, *105*, 1175–1187. [CrossRef]
2. Kraft, K.H.; Brown, C.H.; Nabhan, G.P.; Luedeling, E.; De Luna Ruiz, J.J.; Coppens d'Eeckenbrugge, G.; Hijmans, R.J.; Gepts, P. Multiple Lines of Evidence for the Origin of Domesticated Chili Pepper, *Capsicum annuum*, in Mexico. *Proc. Natl. Acad. Sci. USA* **2014**, *111*, 6165–6170. [CrossRef]
3. Razifard, H.; Ramos, A.; Della Valle, A.L.; Bodary, C.; Goetz, E.; Manser, E.J.; Li, X.; Zhang, L.; Visa, S.; Tieman, D.; et al. Genomic Evidence for Complex Domestication History of the Cultivated Tomato in Latin America. *Mol. Biol. Evol.* **2020**, *37*, 1118–1132. [CrossRef]
4. Endl, J.; Achigan-Dako, E.G.; Pandey, A.K.; Monforte, A.J.; Pico, B.; Schaefer, H. Repeated Domestication of Melon (*Cucumis melo*) in Africa and Asia and a New Close Relative from India. *Am. J. Bot.* **2018**, *105*, 1662–1671. [CrossRef]
5. Zhao, G.; Lian, Q.; Zhang, Z.; Fu, Q.; He, Y.; Ma, S.; Ruggieri, V.; Monforte, A.; Wang, P.; Julca, I.; et al. A Comprehensive Genome Variation Map of Melon Identifies Multiple Domestication Events and Loci Influencing Agronomic Traits. *Nat. Genet.* **2019**, *51*, 1607–1615. [CrossRef]
6. Wei, T.; Van Treuren, R.; Liu, X.; Zhang, Z.; Chen, J.; Liu, Y.; Dong, S.; Sun, P.; Yang, T.; Lan, T.; et al. Whole-Genome Resequencing of 445 *Lactuca* Accessions Reveals the Domestication History of Cultivated Lettuce. *Nat. Genet.* **2021**, *53*, 752–760. [CrossRef]
7. De Vries, I.M. Origin and Domestication of *Lactuca sativa* L. *Genet. Resour. Crop. Evol.* **1997**, *44*, 165–174. [CrossRef]
8. Lebeda, A.; Ryder, E.J.; Grube, R.; Dolezalova, I.; Kristova, E. Lettuce (Asteraceae; Lactuca Spp.). In *Genetic Resources, Chromosome Engineering, and Crop Improvement. Vegetable Crops; Genetic Resources, Chromosome Engineering, and Crop Improvement Series*; CRC Press: Boca Raton, FL, USA; Taylor & Francis Group: Oxford, UK, 2007; pp. 377–472. ISBN 978-0-8493-9646-5.
9. Mou, B. Lettuce. Vegetables 1: "Asteraceae", "Brassicaceae", "Chenopodicaceae", and "Cucurbitaceae". In *Handbook of Plant Breeding*; Springer: New York, NY, USA, 2008; pp. 73–114. ISBN 978-0-387-30443-4.
10. Paran, I.; Van der Knaap, E. Genetic and Molecular Regulation of Fruit and Plant Domestication Traits in Tomato and Pepper. *J. Exp. Bot.* **2007**, *58*, 3841–3852. [CrossRef]
11. Herms, D.A.; Mattson, W.J. The Dilemma of Plants: To Grow or Defend. *Q. Rev. Biol.* **1992**, *67*, 283–335. [CrossRef]
12. Bai, Y.; Lindhout, P. Domestication and Breeding of Tomatoes: What Have We Gained and What Can We Gain in the Future? *Ann. Bot.* **2007**, *100*, 1085–1094. [CrossRef]
13. Biosafety Unit About the Nagoya Protocol. Available online: https://www.cbd.int/abs/about/ (accessed on 5 December 2021).
14. Tontisirin, K.; Nantel, G.; Bhattacharjee, L. Food-Based Strategies to Meet the Challenges of Micronutrient Malnutrition in the Developing World. *Proc. Nutr. Soc.* **2002**, *61*, 243–250. [CrossRef]
15. Quenouille, J.; Saint-Felix, L.; Moury, B.; Palloix, A. Diversity of Genetic Backgrounds Modulating the Durability of a Major Resistance Gene. Analysis of a Core Collection of Pepper Landraces Resistant to Potato Virus Y. *Mol. Plant Pathol.* **2016**, *17*, 296–302. [CrossRef]
16. Sauvage, C.; Segura, V.; Bauchet, G.; Stevens, R.; Do, P.T.; Nikoloski, Z.; Fernie, A.R.; Causse, M. Genome-Wide Association in Tomato Reveals 44 Candidate Loci for Fruit Metabolic Traits. *Plant Physiol.* **2014**, *165*, 1120–1132. [CrossRef]
17. Lester, R.N.; Hawkes, J.G.; Marsh, S.; Daunay, M.C.; Van der Weerden, G.; Barendse, G. The Sources, Successes and Successors of the Birmingham University Solanaceae Collection (1964–2000). In *Solanaceae V, Advances in Taxonomy and Utilization*; Nijmegen University Press: Nijmegen, The Netherlands, 2001; pp. 391–412. ISBN 978-90-373-0580-7.
18. Salinier, J.; Brand-Daunay, M.-C.; Goussopoulos, J.; Gros, C.; Lefebvre, V. The Fascinating Diversity of Pepper and Eggplant Collections Held at the INRA Centre for Vegetable Germplasm. In Proceedings of the Eucarpia Meeting on Genetics and Breeding of Capsicum and Eggplant, Avignon, France, 11–13 September 2019.
19. Daunay, M.C.; Lester, R.N.; Van der Weerden, G. La taxinomie des Solanacées. Ce qu'il faut savoir et les pièges à éviter. In *Virus des Solanacées: Du Génome Viral à la Protection des Cultures*; Synthèses; Éd. Quae: Versailles, France, 2008; pp. 3–10. ISBN 978-2-7592-0076-4.
20. Aubriot, X.; Daunay, M.-C. Eggplants and Relatives: From Exploring Their Diversity and Phylogenetic Relationships to Conservation Challenges. In *The Eggplant Genome; Compendium of Plant Genomes*; Chapman, M.A., Ed.; Springer International Publishing: Berlin/Heidelberg, Germany, 2019; pp. 91–134. ISBN 978-3-319-99207-5.
21. Nicolaï, M.; Cantet, M.; Lefebvre, V.; Sage-Palloix, A.-M.; Palloix, A. Genotyping a Large Collection of Pepper (*Capsicum* Spp.) with SSR Loci Brings New Evidence for the Wild Origin of Cultivated C. Annuum and the Structuring of Genetic Diversity by Human Selection of Cultivar Types. *Genet. Resour. Crop. Evol.* **2013**, *60*, 2375–2390. [CrossRef]
22. Barchi, L.; Bonnet, J.; Boudet, C.; Signoret, P.; Nagy, I.; Lanteri, S.; Palloix, A.; Lefebvre, V. A High-Resolution, Intraspecific Linkage Map of Pepper (*Capsicum annuum* L.) and Selection of Reduced Recombinant Inbred Line Subsets for Fast Mapping. *Genome* **2007**, *50*, 51–60. [CrossRef]
23. Barchi, L.; Lefebvre, V.; Sage-Palloix, A.-M.; Lanteri, S.; Palloix, A. QTL Analysis of Plant Development and Fruit Traits in Pepper and Performance of Selective Phenotyping. *Theor. Appl. Genet.* **2009**, *118*, 1157–1171. [CrossRef]
24. Bonnet, J.; Danan, S.; Boudet, C.; Barchi, L.; Sage-Palloix, A.-M.; Caromel, B.; Palloix, A.; Lefebvre, V. Are the Polygenic Architectures of Resistance to *Phytophthora capsici* and *P. parasitica* Independent in Pepper? *Theor. Appl. Genet.* **2007**, *115*, 253–264. [CrossRef]

25. Thabuis, A.; Palloix, A.; Pflieger, S.; Daubèze, A.-M.; Caranta, C.; Lefebvre, V. Comparative Mapping of *Phytophthora* Resistance Loci in Pepper Germplasm: Evidence for Conserved Resistance Loci across Solanaceae and for a Large Genetic Diversity. *Theor. Appl. Genet.* **2003**, *106*, 1473–1485. [CrossRef]
26. Tripodi, P.; Rabanus-Wallace, M.T.; Barchi, L.; Kale, S.; Esposito, S.; Acquadro, A.; Schafleitner, R.; Van Zonneveld, M.; Prohens, J.; Diez, M.J.; et al. Global Range Expansion History of Pepper (*Capsicum* Spp.) Revealed by over 10,000 Genebank Accessions. *Proc. Natl. Acad. Sci. USA* **2021**, *118*, e2104315118. [CrossRef]
27. Tamisier, L.; Szadkowski, M.; Nemouchi, G.; Lefebvre, V.; Szadkowski, E.; Duboscq, R.; Santoni, S.; Sarah, G.; Sauvage, C.; Palloix, A.; et al. Genome-Wide Association Mapping of QTLs Implied in Potato Virus Y Population Sizes in Pepper: Evidence for Widespread Resistance QTL Pyramiding. *Mol. Plant Pathol.* **2020**, *21*, 3–16. [CrossRef]
28. Peralta, I.E.; Knapp, S.; Spooner, D.M. New Species of Wild Tomatoes (*Solanum lycopersicon*: Solanaceae) from Northern Peru. *Syst. Bot.* **2005**, *30*, 424–434. [CrossRef]
29. Sim, S.-C.; Durstewitz, G.; Plieske, J.; Wieseke, R.; Ganal, M.W.; Van Deynze, A.; Hamilton, J.P.; Buell, C.R.; Causse, M.; Wijeratne, S.; et al. Development of a Large SNP Genotyping Array and Generation of High-Density Genetic Maps in Tomato. *PLoS ONE* **2012**, *7*, e40563. [CrossRef] [PubMed]
30. Saliba-Colombani, V.; Causse, M.; Langlois, D.; Philouze, J.; Buret, M. Genetic Analysis of Organoleptic Quality in Fresh Market Tomato. 1. Mapping QTLs for Physical and Chemical Traits. *Theor. Appl. Genet.* **2001**, *102*, 259–272. [CrossRef]
31. Pascual, L.; Desplat, N.; Huang, B.E.; Desgroux, A.; Bruguier, L.; Bouchet, J.-P.; Le, Q.H.; Chauchard, B.; Verschave, P.; Causse, M. Potential of a Tomato MAGIC Population to Decipher the Genetic Control of Quantitative Traits and Detect Causal Variants in the Resequencing Era. *Plant Biotechnol. J.* **2015**, *13*, 565–577. [CrossRef]
32. Boissot, N.; Thomas, S.; Sauvion, N.; Marchal, C.; Pavis, C.; Dogimont, C. Mapping and Validation of QTLs for Resistance to Aphids and Whiteflies in Melon. *Theor. Appl. Genet.* **2010**, *121*, 9–20. [CrossRef]
33. Diaz, A.; Fergany, M.; Formisano, G.; Ziarsolo, P.; Blanca, J.; Fei, Z.; Staub, J.E.; Zalapa, J.E.; Cuevas, H.E.; Dace, G.; et al. A Consensus Linkage Map for Molecular Markers and Quantitative Trait Loci Associated with Economically Important Traits in Melon (*Cucumis melo* L.). *BMC Plant Biol.* **2011**, *11*, 111. [CrossRef]
34. Perchepied, L.; Dogimont, C.; Pitrat, M. Strain-Specific and Recessive QTLs Involved in the Control of Partial Resistance to *Fusarium oxysporum* f. Sp. Melonis Race 1.2 in a Recombinant Inbred Line Population of Melon. *Theor. Appl. Genet.* **2005**, *111*, 65–74. [CrossRef]
35. Périn, C.; Hagen, S.; De Conto, V.; Katzir, N.; Danin-Poleg, Y.; Portnoy, V.; Baudracco-Arnas, S.; Chadoeuf, J.; Dogimont, C.; Pitrat, M. A Reference Map of *Cucumis melo* Based on Two Recombinant Inbred Line Populations. *Theor. Appl. Genet.* **2002**, *104*, 1017–1034. [CrossRef]
36. Périn, C.; Hagen, L.S.; Giovinazzo, N.; Besombes, D.; Dogimont, C.; Pitrat, M. Genetic Control of Fruit Shape Acts Prior to Anthesis in Melon (*Cucumis melo* L.). *Mol. Genet. Genom.* **2002**, *266*, 933–941. [CrossRef]
37. Périn, C.; Gomez-Jimenez, M.; Hagen, L.; Dogimont, C.; Pech, J.-C.; Latché, A.; Pitrat, M.; Lelièvre, J.-M. Molecular and Genetic Characterization of a Non-Climacteric Phenotype in Melon Reveals Two Loci Conferring Altered Ethylene Response in Fruit. *Plant Physiol.* **2002**, *129*, 300–309. [CrossRef]
38. Boualem, A.; Fergany, M.; Fernandez, R.; Troadec, C.; Martin, A.; Morin, H.; Sari, M.-A.; Collin, F.; Flowers, J.M.; Pitrat, M.; et al. A Conserved Mutation in an Ethylene Biosynthesis Enzyme Leads to Andromonoecy in Melons. *Science* **2008**, *321*, 836–838. [CrossRef]
39. Boualem, A.; Lemhemdi, A.; Sari, M.-A.; Pignoly, S.; Troadec, C.; Abou Choucha, F.; Solmaz, I.; Sari, N.; Dogimont, C.; Bendahmane, A. The Andromonoecious Sex Determination Gene Predates the Separation of *Cucumis* and *Citrullus* Genera. *PLoS ONE* **2016**, *11*, e0155444. [CrossRef]
40. Dahmani-Mardas, F.; Troadec, C.; Boualem, A.; Lévêque, S.; Alsadon, A.A.; Aldoss, A.A.; Dogimont, C.; Bendahmane, A. Engineering Melon Plants with Improved Fruit Shelf Life Using the TILLING Approach. *PLoS ONE* **2010**, *5*, e15776. [CrossRef]
41. Martin, A.; Troadec, C.; Boualem, A.; Rajab, M.; Fernandez, R.; Morin, H.; Pitrat, M.; Dogimont, C.; Bendahmane, A. A Transposon-Induced Epigenetic Change Leads to Sex Determination in Melon. *Nature* **2009**, *461*, 1135–1138. [CrossRef]
42. Maisonneuve, B.B.; Bellec, Y.; Souche, S.; Lot, H. New Resistance against Downy Mildew and Lettuce Mosaic Potyvirus in Wild Lactuca Spp. In Proceedings of the Eucarpia Leafy Vegetables 99, European Association for Research on Plant Breeding, Olomouc, Czech Republic, 8–11 June 1999.
43. Maisonneuve, B.; Bellec, Y.; Martin, E.; Lot, H.; Gognalon, P.; Moury, B. Lettuce Lines with Potyvirus Resistance: Differential Set for Study of Strains and New Genitors of Resistance. In Proceedings of the Abstracts Eucarpia Leafy Vegetables 2019, Olomouc, Czech Republic, 24–28 June 2019; pp. 86–87.
44. Maisonneuve, B.; Pitrat, M.; Gognalons, P.; Moury, B. Growth Stage-Dependent Resistance to the Potyviruses Lettuce Italian Necrotic Virus and Lettuce Mosaic Virus Displayed by Lactuca Sativa Introgression Lines Carrying the *Mo3* Locus from L. Virosa. *Plant Pathol.* **2018**, *67*, 2013–2018. [CrossRef]
45. Plant Production and Protection Division. *Genebank Standards for Plant Genetic Resources for Food and Agriculture*; FAO: Rome, Italy, 2016; ISBN 978-92-5-109528-7.
46. Nanduri, K.; Hanson, J.; Dulloo, M.; Ghosh, K.; Nowell, D.; Larinde, M. *Handbooks for Genebanks No. 8 Seed Handling in Genebanks*; Bioversity International: Rome, Italy, 2006. Available online: https://www.bioversityinternational.org/e-library/publications/detail/manual-of-seed-handling-in-genebanks/ (accessed on 5 December 2021).

47. Daunay, M.C.; Dalmon, A.; Lester, R.N. Management of a Collection of Solanum Species for Eggplant (*Solanum melongena*) Breeding Purposes. In *Solanaceae IV: Advances in Biology and Utilization*; Royal Botanic Gardens: Kew, UK, 1999; pp. 369–383. ISBN 978-1-900347-90-7.
48. Syfert, M.M.; Castañeda-Álvarez, N.P.; Khoury, C.K.; Särkinen, T.; Sosa, C.C.; Achicanoy, H.A.; Bernau, V.; Prohens, J.; Daunay, M.-C.; Knapp, S. Crop Wild Relatives of the Brinjal Eggplant (*Solanum melongena*): Poorly Represented in Genebanks and Many Species at Risk of Extinction. *Am. J. Bot.* **2016**, *103*, 635–651. [CrossRef]
49. Causse, M.; Saliba-Colombani, V.; Lecomte, L.; Duffe, P.; Rousselle, P.; Buret, M. QTL Analysis of Fruit Quality in Fresh Market Tomato: A Few Chromosome Regions Control the Variation of Sensory and Instrumental Traits. *J. Exp. Bot.* **2002**, *53*, 2089–2098. [CrossRef]
50. Lefebvre, V.; Kuntz, M.; Camara, B.; Palloix, A. The Capsanthin-Capsorubin Synthase Gene: A Candidate Gene for the y Locus Controlling the Red Fruit Colour in Pepper. *Plant Mol. Biol.* **1998**, *36*, 785–789. [CrossRef]
51. Pitrat, M. Phenotypic Diversity in Wild and Cultivated Melons (*Cucumis melo*). *Plant Biotechnol.* **2013**, *30*, 273–278. [CrossRef]
52. Salinier, J.; Daunay, M.C.; Talmot, V.; Lecarpentier, C.; Pagès, L.; Bardel, A.; Fournier, C.; Torres, M.; Stevens, R. Root Architectural Trait Diversity in Aubergine (*Solanum melongena* L.) and Related Species and Correlations with Plant Biomass. *Crop. Breed. Genet. Genom.* **2019**, *1*, e190011. [CrossRef]
53. Arnoux, S.; Fraïsse, C.; Sauvage, C. Genomic Inference of Complex Domestication Histories in Three Solanaceae Species. *J. Evol. Biol.* **2021**, *34*, 270–283. [CrossRef]
54. Davidar, P.; Snow, A.A.; Rajkumar, M.; Pasquet, R.; Daunay, M.-C.; Mutegi, E. The Potential for Crop to Wild Hybridization in Eggplant (*Solanum melongena*; Solanaceae) in Southern India. *Am. J. Bot.* **2015**, *102*, 129–139. [CrossRef]
55. Mutegi, E.; Snow, A.A.; Rajkumar, M.; Pasquet, R.; Ponniah, H.; Daunay, M.-C.; Davidar, P. Genetic Diversity and Population Structure of Wild/Weedy Eggplant (*Solanum insanum*, Solanaceae) in Southern India: Implications for Conservation. *Am. J. Bot.* **2015**, *102*, 140–148. [CrossRef]
56. Page, A.; Gibson, J.; Meyer, R.S.; Chapman, M.A. Eggplant Domestication: Pervasive Gene Flow, Feralization, and Transcriptomic Divergence. *Mol. Biol. Evol.* **2019**, *36*, 1359–1372. [CrossRef]
57. Chakrabarti, M.; Zhang, N.; Sauvage, C.; Munos, S.; Blanca, J.; Canizares, J.; Diez, M.J.; Schneider, R.; Mazourek, M.; McClead, J.; et al. A Cytochrome P450 Regulates a Domestication Trait in Cultivated Tomato. *Proc. Natl. Acad. Sci. USA* **2013**, *110*, 17125–17130. [CrossRef]
58. Frary, A.; Nesbitt, T.C.; Grandillo, S.; Knaap, E.; Cong, B.; Liu, J.; Meller, J.; Elber, R.; Alpert, K.B.; Tanksley, S.D. Fw2.2: A Quantitative Trait Locus Key to the Evolution of Tomato Fruit Size. *Science* **2000**, *289*, 85–88. [CrossRef]
59. Sauvage, C.; Rau, A.; Aichholz, C.; Chadoeuf, J.; Sarah, G.; Ruiz, M.; Santoni, S.; Causse, M.; David, J.; Glémin, S. Domestication Rewired Gene Expression and Nucleotide Diversity Patterns in Tomato. *Plant J.* **2017**, *91*, 631–645. [CrossRef]
60. Blanca, J.; Montero-Pau, J.; Sauvage, C.; Bauchet, G.; Illa, E.; Díez, M.J.; Francis, D.; Causse, M.; Van der Knaap, E.; Cañizares, J. Genomic Variation in Tomato, from Wild Ancestors to Contemporary Breeding Accessions. *BMC Genom.* **2015**, *16*, 257. [CrossRef]
61. Bauchet, G.; Munos, S.; Sauvage, C.; Bonnet, J.; Grivet, L.; Causse, M. Genes Involved in Floral Meristem in Tomato Exhibit Drastically Reduced Genetic Diversity and Signature of Selection. *BMC Plant Biol.* **2014**, *14*, 279. [CrossRef]
62. Lin, T.; Zhu, G.; Zhang, J.; Xu, X.; Yu, Q.; Zheng, Z.; Zhang, Z.; Lun, Y.; Li, S.; Wang, X.; et al. Genomic Analyses Provide Insights into the History of Tomato Breeding. *Nat. Genet.* **2014**, *46*, 1220–1226. [CrossRef]
63. Serres-Giardi, L.; Dogimont, C. How Microsatellite Diversity Helps to Understand the Domestication History of Melon. In Proceedings of the Xth EUCARPIA Meeting on Genetics and Breeding of Cucurbitaceae, Antalya, Turkey, 15–18 October 2012; pp. 254–263.
64. Paris, H.S.; Janick, J.; Daunay, M.-C. Medieval Herbal Iconography and Lexicography of *Cucumis* (Cucumber and Melon, Cucurbitaceae) in the Occident, 1300–1458. *Ann. Bot.* **2011**, *108*, 471–484. [CrossRef]
65. Dhillon, N.P.S.; Ranjana, R.; Singh, K.; Eduardo, I.; Monforte, A.J.; Pitrat, M.; Dhillon, N.K.; Singh, P.P. Diversity among Landraces of Indian Snapmelon (*Cucumis melo* Var. Momordica). *Genet. Resour. Crop. Evol.* **2007**, *54*, 1267–1283. [CrossRef]
66. Fergany, M.; Kaur, B.; Monforte, A.J.; Pitrat, M.; Rys, C.; Lecoq, H.; Dhillon, N.P.S.; Dhaliwal, S.S. Variation in Melon (*Cucumis melo*) Landraces Adapted to the Humid Tropics of Southern India. *Genet. Resour. Crop. Evol.* **2011**, *58*, 225–243. [CrossRef]
67. Huet, G. Breeding for Resistances to *Ralstonia solanacearum*. *Front. Plant Sci.* **2014**, *5*, 715. [CrossRef]
68. Mansfield, J.; Genin, S.; Magori, S.; Citovsky, V.; Sriariyanum, M.; Ronald, P.; Dow, M.; Verdier, V.; Beer, S.V.; Machado, M.A.; et al. Top 10 Plant Pathogenic Bacteria in Molecular Plant Pathology. *Mol. Plant Pathol.* **2012**, *13*, 614–629. [CrossRef]
69. Xue, H.; Lozano-Durán, R.; Macho, A.P. Insights into the Root Invasion by the Plant Pathogenic Bacterium *Ralstonia solanacearum*. *Plants* **2020**, *9*, 516. [CrossRef]
70. Clarke, C.R.; Studholme, D.J.; Hayes, B.; Runde, B.; Weisberg, A.; Cai, R.; Wroblewski, T.; Daunay, M.-C.; Wicker, E.; Castillo, J.A.; et al. Genome-Enabled Phylogeographic Investigation of the Quarantine Pathogen *Ralstonia solanacearum* Race 3 Biovar 2 and Screening for Sources of Resistance Against Its Core Effectors. *Phytopathology®* **2015**, *105*, 597–607. [CrossRef]
71. Lebeau, A.; Daunay, M.-C.; Frary, A.; Palloix, A.; Wang, J.-F.; Dintinger, J.; Chiroleu, F.; Wicker, E.; Prior, P. Bacterial Wilt Resistance in Tomato, Pepper, and Eggplant: Genetic Resources Respond to Diverse Strains in the *Ralstonia solanacearum* Species Complex. *Phytopathology* **2011**, *101*, 154–165. [CrossRef]
72. Lebeau, A.; Gouy, M.; Daunay, M.C.; Wicker, E.; Chiroleu, F.; Prior, P.; Frary, A.; Dintinger, J. Genetic Mapping of a Major Dominant Gene for Resistance to *Ralstonia solanacearum* in Eggplant. *Theor. Appl. Genet.* **2013**, *126*, 143–158. [CrossRef]

73. Pensec, F.; Lebeau, A.; Daunay, M.C.; Chiroleu, F.; Guidot, A.; Wicker, E. Towards the Identification of Type III Effectors Associated with *Ralstonia Solanacearum* Virulence on Tomato and Eggplant. *Phytopathology®* **2015**, *105*, 1529–1544. [CrossRef]
74. Salgon, S.; Jourda, C.; Sauvage, C.; Daunay, M.-C.; Reynaud, B.; Wicker, E.; Dintinger, J. Eggplant Resistance to the *Ralstonia solanacearum* Species Complex Involves Both Broad-Spectrum and Strain-Specific Quantitative Trait Loci. *Front. Plant Sci.* **2017**, *8*, 828. [CrossRef]
75. Salgon, S.; Raynal, M.; Lebon, S.; Baptiste, J.-M.; Daunay, M.-C.; Dintinger, J.; Jourda, C. Genotyping by Sequencing Highlights a Polygenic Resistance to *Ralstonia pseudosolanacearum* in Eggplant (*Solanum melongena* L.). *IJMS* **2018**, *19*, 357. [CrossRef] [PubMed]
76. Ivey, M.L.; Madrid, A.J.; Daunay, M.-C.; Shah, D. Evaluation of Tomato, Eggplant and Pepper Accessions for Resistance to *Ralstonia solanacearum* Species Complex (RSSC) Strains from Louisiana. *Eur. J. Plant Pathol.* **2021**, *159*, 279. [CrossRef]
77. Cantet, M. Variation Phénotypique de La Résistance Quantitative à *Phytophthora capsici* Dans La Diversité Naturelle Du Piment, et Diversité Moléculaire et Profil d'évolution Du QTL Majeur Pc5.1. Ph.D. Thesis, Institut National d'Etudes Supérieures Agronomiques de Montpellier, Montpellier, France, 12 April 2013.
78. Mallard, S.; Cantet, M.; Massire, A.; Bachellez, A.; Ewert, S.; Lefebvre, V. A Key QTL Cluster Is Conserved among Accessions and Exhibits Broad-Spectrum Resistance to *Phytophthora capsici*: A Valuable Locus for Pepper Breeding. *Mol. Breed.* **2013**, *32*, 349–364. [CrossRef]
79. Lefebvre, V.; Daubèze, A.-M.; Van der Voort, J.R.; Peleman, J.; Bardin, M.; Palloix, A. QTLs for Resistance to Powdery Mildew in Pepper under Natural and Artificial Infections. *Theor. Appl. Genet.* **2003**, *107*, 661–666. [CrossRef]
80. Moury, B.; Pflieger, S.; Blattes, A.; Lefebvre, V.; Palloix, A. A CAPS Marker to Assist Selection of Tomato Spotted Wilt Virus (TSWV) Resistance in Pepper. *Genome* **2000**, *43*, 137–142. [CrossRef]
81. Lefebvre, V.; Palloix, A.; Caranta, C.; Pochard, E. Construction of an Intraspecific Integrated Linkage Map of Pepper Using Molecular Markers and Doubled-Haploid Progenies. *Genome* **1995**, *38*, 112–121. [CrossRef]
82. Caranta, C.; Pflieger, S.; Lefebvre, V.; Daubèze, A.M.; Thabuis, A.; Palloix, A. QTLs Involved in the Restriction of Cucumber Mosaic Virus (CMV) Long-Distance Movement in Pepper. *Theor. Appl. Genet.* **2002**, *104*, 586–591. [CrossRef]
83. Caranta, C.; Palloix, A.; Lefebvre, V.; Daubèze, A.M. QTLs for a Component of Partial Resistance to Cucumber Mosaic Virus in Pepper: Restriction of Virus Installation in Host-Cells. *Theor. Appl. Genet.* **1997**, *94*, 431–438. [CrossRef]
84. Caranta, C.; Lefebvre, V.; Palloix, A. Polygenic Resistance of Pepper to Potyviruses Consists of a Combination of Isolate-Specific and Broad-Spectrum Quantitative Trait Loci. *MPMI* **1997**, *10*, 872–878. [CrossRef]
85. Lefebvre, V.; Palloix, A. Both Epistatic and Additive Effects of QTLs Are Involved in Polygenic Induced Resistance to Disease: A Case Study, the Interaction Pepper—*Phytophthora capsici* Leonian. *Theor. Appl. Genet.* **1996**, *93*, 503–511. [CrossRef] [PubMed]
86. Caranta, C.; Dogimont, C. Plant Resistance to Viruses: Natural Resistance Associated with Recessive Genes. In *Encyclopedia of Virology*; Elsevier: Amsterdam, The Netherlands, 2008; pp. 177–186. ISBN 978-0-12-374410-4.
87. Pitrat, M. Melon Genetic Resources: Phenotypic Diversity and Horticultural Taxonomy. In *Genetics and Genomics of Cucurbitaceae; Plant Genetics and Genomics: Crops and Models*; Springer International Publishing: Berlin/Heidelberg, Germany, 2016; Volume 20, 340p.
88. Romay, G.; Pitrat, M.; Lecoq, H.; Wipf-Scheibel, C.; Millot, P.; Girardot, G.; Desbiez, C. Resistance Against Melon Chlorotic Mosaic Virus and Tomato Leaf Curl New Delhi Virus in Melon. *Plant Dis.* **2019**, *103*, 2913–2919. [CrossRef] [PubMed]
89. Solmaz, I.; Sari, N.; Dogimont, C.; Pitrat, M. Evaluation of Turkish Melon Accessions for Resistance to Fusarium Wilt, Downy Mildew, Powdery Mildew, *Cucumber mosaic virus* and *Zucchini yellow mosaic virus*. *Acta Hortic.* **2016**, 133–140. [CrossRef]
90. Villeneuve, F.; Latour, F.; Théry, T.; Steinberg, C.; Edel-Hermann, V.; Pitrat, M.; Daunay, M.-C. The Control of Soil-Borne Vascular Diseases: Limits of Genetic Resistance of Cultivars and Rootstocks for Controlling *Fusarium oxysporum* F. Sp. Melonis (Melon) and Verticillium Sp. (Eggplant). *Acta Hortic.* **2014**, 57–65. [CrossRef]
91. Yousif, M.T.; Kheyr-Pour, A.; Gronenborn, B.; Pitrat, M.; Dogimont, C. Sources of Resistance to Watermelon Chlorotic Stunt Virus in Melon. *Plant Breed.* **2007**, *126*, 422–427. [CrossRef]
92. Dogimont, C.; Boissot, N. Insect Resistance in Melon and Its Modification by Molecular Breeding. In *Functional Genomics and Biotechnology in Solanaceae and Cucurbitaceae Crops*; Springer: Berlin/Heidelberg, Germany, 2016; pp. 199–219. ISBN 978-3-662-48535-4.
93. Dogimont, C.; Bendahmane, A.; Chovelon, V.; Boissot, N. Host Plant Resistance to Aphids in Cultivated Crops: Genetic and Molecular Bases, and Interactions with Aphid Populations. *Comptes Rendus Biol.* **2010**, *333*, 566–573. [CrossRef] [PubMed]
94. Dogimont, C.; Chovelon, V.; Pauquet, J.; Boualem, A.; Bendahmane, A. The Vat Locus Encodes for a CC-NBS-LRR Protein That Confers Resistance to *Aphis gossypii* Infestation and A. Gossypii-Mediated Virus Resistance. *Plant J.* **2014**, *80*, 993–1004. [CrossRef]
95. Thomas, S.; Dogimont, C.; Boissot, N. Association between *Aphis gossypii* Genotype and Phenotype on Melon Accessions. *Arthropod-Plant Interact.* **2012**, *6*, 93–101. [CrossRef]
96. Boissot, N.; Schoeny, A.; Vanlerberghe-Masutti, F. Vat, an Amazing Gene Conferring Resistance to Aphids and Viruses They Carry: From Molecular Structure to Field Effects. *Front. Plant Sci.* **2016**, *7*, 1420. [CrossRef]
97. Desbiez, C.; Schoeny, A.; Maisonneuve, B.; Berthier, K.; Bornard, I.; Chandeysson, C.; Fabre, F.; Girardot, G.; Gognalons, P.; Lecoq, H.; et al. Molecular and Biological Characterization of Two Potyviruses Infecting Lettuce in Southeastern France. *Plant Pathol.* **2017**, *66*, 970–979. [CrossRef]
98. Parra, L.; Maisonneuve, B.; Lebeda, A.; Schut, J.; Christopoulou, M.; Jeuken, M.; McHale, L.; Truco, M.-J.; Crute, I.; Michelmore, R. Rationalization of Genes for Resistance to *Bremia lactucae* in Lettuce. *Euphytica* **2016**, *210*, 309–326. [CrossRef]

99. Maisonneuve, B.; Chassagne, C.; Gautheron, E.; Glaux, C.; Morris, C.E. Screening of Genetic Resources for Resistance to *Xanthomonas axonopodis* Pv. Vitians. In Proceedings of the Eucarpia Leafy Vegetables Conference, Warwick, UK, 18–20 April 2007.
100. Maisonneuve, B.; Jouan, C.; Gard, B.; Gimenez, S.; Goillon, C.; Jean, L.; Trottin, Y.; Védie, H.; Pitrat, M. LACTUMEL–Des Résistances Aux Nématodes à Galles Du Genre Meloidogyne Dans Le Genre Lactuca: Espoir Pour La Sélection de La Laitue. *Innov. Agron.* **2021**, *84*, 11–23. [CrossRef]
101. Maisonneuve, B. Lactuca Virosa, a Source of Disease Resistance Genes for Lettuce Breeding: Results and Difficulties for Gene Introgression. In Proceedings of the EUCARPIA Meeting on Leafy Vegetables Genetics and Breeding, Noordwijkerhout, The Netherlands, 19–21 March 2003; pp. 61–67.
102. Maisonneuve, B.; Bellec, Y.; Anderson, P.; Michelmore, R.W. Rapid Mapping of Two Genes for Resistance to Downy Mildew from *Lactuca serriola* to Existing Clusters of Resistance Genes. *Theor. Appl. Genet.* **1994**, *89*, 96–104. [CrossRef]
103. Wood, K.J.; Nur, M.; Gil, J.; Fletcher, K.; Lakeman, K.; Gann, D.; Gothberg, A.; Khuu, T.; Kopetzky, J.; Naqvi, S.; et al. Effector Prediction and Characterization in the Oomycete Pathogen *Bremia lactucae* Reveal Host-Recognized WY Domain Proteins That Lack the Canonical RXLR Motif. *PLoS Pathog.* **2020**, *16*, e1009012. [CrossRef] [PubMed]
104. Maisonneuve, B.; Allen-Aubouard, C.; Pitrat, M. Effect of Plant Genotype on the Efficacy of Stimulators of Plant Defences in Two Horticultural Pathosystems. *IOBC WPRS Bull.* **2013**, *89*, 327–331.
105. Sandoya, G.V.; Maisonneuve, B.; Truco, M.J.; Bull, C.T.; Simko, I.; Trent, M.; Hayes, R.J.; Michelmore, R.W. Genetic Analysis of Resistance to Bacterial Leaf Spot in the Heirloom Lettuce Cultivar Reine Des Glaces. *Mol. Breed.* **2019**, *39*, 160. [CrossRef]
106. Maisonneuve, B.B.; Chupeau, M.C.; Bellec, Y.; Chupeau, Y.Y. Sexual and Somatic Hybridization in the Genus Lactuca. *Euphytica* **1995**, *85*, 281–285. [CrossRef]
107. Albert, E.; Segura, V.; Gricourt, J.; Bonnefoi, J.; Derivot, L.; Causse, M. Association Mapping Reveals the Genetic Architecture of Tomato Response to Water Deficit: Focus on Major Fruit Quality Traits. *J. Exp. Bot.* **2016**, *67*, 6413–6430. [CrossRef]
108. Bauchet, G.; Grenier, S.; Samson, N.; Segura, V.; Kende, A.; Beekwilder, J.; Cankar, K.; Gallois, J.; Gricourt, J.; Bonnet, J.; et al. Identification of Major Loci and Genomic Regions Controlling Acid and Volatile Content in Tomato Fruit: Implications for Flavor Improvement. *New Phytol.* **2017**, *215*, 624–641. [CrossRef]
109. Bauchet, G.; Grenier, S.; Samson, N.; Bonnet, J.; Grivet, L.; Causse, M. Use of Modern Tomato Breeding Germplasm for Deciphering the Genetic Control of Agronomical Traits by Genome Wide Association Study. *Theor. Appl. Genet.* **2017**, *130*, 875–889. [CrossRef]
110. Xu, J.; Ranc, N.; Muños, S.; Rolland, S.; Bouchet, J.-P.; Desplat, N.; Le Paslier, M.-C.; Liang, Y.; Brunel, D.; Causse, M. Phenotypic Diversity and Association Mapping for Fruit Quality Traits in Cultivated Tomato and Related Species. *Theor. Appl. Genet.* **2013**, *126*, 567–581. [CrossRef] [PubMed]
111. Duangjit, J.; Causse, M.; Sauvage, C. Efficiency of Genomic Selection for Tomato Fruit Quality. *Mol. Breed.* **2016**, *36*, 29. [CrossRef]
112. Albert, E.; Gricourt, J.; Bertin, N.; Bonnefoi, J.; Pateyron, S.; Tamby, J.-P.; Bitton, F.; Causse, M. Genotype by Watering Regime Interaction in Cultivated Tomato: Lessons from Linkage Mapping and Gene Expression. *Theor. Appl. Genet.* **2016**, *129*, 395–418. [CrossRef] [PubMed]
113. Bineau, E.; Diouf, I.; Carretero, Y.; Duboscq, R.; Bitton, F.; Djari, A.; Zouine, M.; Causse, M. Genetic Diversity of Tomato Response to Heat Stress at the QTL and Transcriptome Levels. *Plant J.* **2021**, *107*, 1213–1227. [CrossRef]
114. Diouf, I.; Derivot, L.; Koussevitzky, S.; Carretero, Y.; Bitton, F.; Moreau, L.; Causse, M. Genetic Basis of Phenotypic Plasticity and Genotype × Environment Interactions in a Multi-Parental Tomato Population. *J. Exp. Bot.* **2020**, *71*, 5365–5376. [CrossRef]
115. Daunay, M.C.; Lester, R.N.; Dalmon, A.; Ferri, M.; Kapilima, W.; Poveda-Aguilar, M.M.; Jullian, E. The Use of Wild Genetic Resources for Eggplant (*Solanum melongena* L.) Breeding. II Crossability and Fertility of Interspecific Hybrids. In Proceedings of the Xth Meeting on Genetics and Breeding of Capsicum and Eggplant, Avignon, France, 7–11 September 1998; INRA: Paris, France, 1998; pp. 19–24, ISBN 978-2-7380-0830-5.
116. Daunay, M.C. Eggplant. In *Vegetables II: Fabaceae, Liliaceae, Solanaceae, and Umbelliferae; Handbook of Plant Breeding*; Springer: New York, NY, USA, 2008; pp. 163–220. ISBN 978-0-387-74108-6.
117. Daunay, M.C.; Lester, R.N.; Laterrot, H. The Use of Wild Species for the Genetic Improvement of Brinjal Eggplant (*Solanum melongena*) and Tomato (*Lycopersicon esculentum*). In *Solanaceae III: Taxonomy, Chemistry, Evolution; [Based on Papers Read at the Third International Solanaceae Congress, held in Bogotá, Columbia from July 25 to 30, 1988]*; The Royal Botanic Gardens: Kew, UK, 1991; pp. 389–412. ISBN 978-0-947643-31-7.
118. Daunay, M.C.; Lester, R.N.; Gebhardt, C.; Hennart, J.W.; Jahn, M.; Frary, A.; Doganlar, S. Genetic Resources of Eggplant (*Solanum melongena* L.) and Allied Species: A New Challenge for Molecular Geneticists and Eggplant Breeders. In *Solanaceae V: Advances in Taxonomy and Utilization*; Nijmegen University Press: Nijmegen, The Netherlands, 2001; pp. 251–274. ISBN 978-90-373-0580-7.
119. Lanteri, S.; Rotino, G.L. *Breakthroughs in the Genetics and Breeding of Capsicum and Eggplant: Proceedings of the XV EUCARPIA Meeting on Genetics and Breeding of Capsicum and Eggplant: 2–4 September 2013, Torino-Italy*; FA, Università degli Studi di Torino: Torino, Italy, 2013; ISBN 978-88-97239-16-1.
120. Villeneuve, F.; Latour, F.; Théry, T.; Steinberg, C.; Edel-Hermann, V.; Brand-Daunay, M.-C. Greenhouse Eggplant Production in France: Success and Failures of Grafting for Controlling *Verticillium* sp. In Proceedings of the 16. Eucarpia Capsicum and Eggplant Meeting, Kecskemét, Hungary, 12–14 September 2016; p. 6.
121. Villeneuve, F.; Latour, F.; Théry, T.; Erard, P.; Fournier, C.; Daunay, M.C. Screening of Solanaceous Wild Relatives for Graft Affinity with Eggplant (*Solanum melongena* L.). In Proceedings of the 16. Eucarpia Capsicum and Eggplant Meeting, Kecskemét, Hungary, 12–14 September 2016; pp. 152–160.

plants

MDPI

Article

The Anti-Inflammatory Response of *Lavandula luisieri* and *Lavandula pedunculata* Essential Oils

Monica Zuzarte [1,2,3,*], Cátia Sousa [2,4,5], Carlos Cavaleiro [4,6], Maria Teresa Cruz [2,4,5] and Lígia Salgueiro [4,6]

[1] Coimbra Institute for Clinical and Biomedical Research (iCBR), Faculty of Medicine, University of Coimbra, 3000-548 Coimbra, Portugal
[2] Center for Innovative Biomedicine and Biotechnology (CIBB), University of Coimbra, 3000-548 Coimbra, Portugal; uc45185@uc.pt (C.S.); trosete@ff.uc.pt (M.T.C.)
[3] Clinical Academic Centre of Coimbra (CACC), 3000-548 Coimbra, Portugal
[4] Faculty of Pharmacy, University of Coimbra, 3000-548 Coimbra, Portugal; cavaleir@ff.uc.pt (C.C.); ligia@ff.uc.pt (L.S.)
[5] Centre for Neuroscience and Cell Biology (CNC), University of Coimbra, 3000-548 Coimbra, Portugal
[6] Chemical Process Engineering and Forest Products Research Centre (CIEPQPF), Department of Chemical Engineering, Faculty of Sciences and Technology, University of Coimbra, 3030-790 Coimbra, Portugal
* Correspondence: mzuzarte@uc.pt; Tel.: +351-239-480-220

Abstract: Portuguese lavenders remain undervalued in global markets due to the lack of high-quality end-products and scarcity of scientific-based studies validating their bioactive potential. Moreover, chemical variability is frequent in these species, and can compromise both safety and efficacy. In the present study, the anti-inflammatory potential of *L. luisieri* and *L. pedunculata*, two highly prevalent species in Portugal, was assessed and correlated with their chemical variability. Representative samples with distinct chemical profiles were selected to assess the anti-inflammatory effect on LPS-stimulated macrophages. *L. luisieri* essential oil with low quantities of necrodane derivatives was the most potent at inhibiting NO production. Interestingly, the essential oil was more effective than its main compounds (1,8-cineole and fenchone), assessed alone or in combination. Our results also demonstrated a significant effect of the oil on the expression of the inflammatory proteins (iNOS and pro-IL-1β) and on the NF-κB pathway. Overall, this study highlights the impact of chemical variability on oils' efficacy by showing distinct effects among the chemotypes. We also identify *L. luisieri* essential oil, with low quantities of necrodane derivatives, as the most promising in the mitigation of the inflammatory response, thus corroborating its traditional uses and paving the way for the development of herbal medicinal products.

Keywords: essential oil; iNOS; interleukin; lavenders; NF-κB

Citation: Zuzarte, M.; Sousa, C.; Cavaleiro, C.; Cruz, M.T.; Salgueiro, L. The Anti-Inflammatory Response of *Lavandula luisieri* and *Lavandula pedunculata* Essential Oils. *Plants* **2022**, *11*, 370. https://doi.org/10.3390/plants11030370

Academic Editors: Milan S. Stankovic, Paula Baptista and Petronia Carillo

Received: 31 December 2021
Accepted: 26 January 2022
Published: 29 January 2022

1. Introduction

In recent years, there has been a growing demand for natural products, with the global market impact of aromatic and medicinal plants increasing mainly in the health sector [1]. Several industries have perceived this trend and are searching for bioactive and biodegradable products that concomitantly present a safe profile to humans and animals [2]. Lamiaceae is among the families that comprise a higher number of aromatic plants with commercial interest [3]. For example, several lavender products, such as essential oils, fresh or dried flowers, and landscape plants, mainly from four *Lavandula* species, namely *L. stoechas*, *L. angustifolia*, *L. latifolia*, and *L.* x *intermedia* (a hybrid between the two last species), are highly appreciated. These species are extremely valuable and recognized in global markets and, in some cases, regulated by international ISO standards [4,5]. Nevertheless, the genus comprises many other species that remain undervalued and have no commercial value. For example, the Portuguese lavenders *L. luisieri* and *L. pedunculata* remain unbranded despite their economic potential, high prevalence, and popularity among

local communities [6]. A lack of both scientific-based studies validating their traditional applications and high-quality end-products is partially responsible for this scenario. Indeed, the chemical variability of lavenders is high [7–9] and compromises their bioactive potential. Therefore, a well-defined chemical profile and validated bioactive potential are necessary to fulfil the requirements of competitive markets and guarantee efficacy and safety profiles.

L. luisieri has been traditionally used as a expectorant, stimulant, spasmolytic, and laxative, for relieving headaches and migraines, and for its disinfectant properties [7,10]. In addition, *L. pedunculata* has been applied to treat bronchitis, cough, asthma, headaches, anxiety, insomnia, strokes, and dyspepsia, and as an analgesic [11–13]. Several of these conditions are associated with an inflammatory response and their relief or even treatment may be related to the anti-inflammatory properties of these aromatic plants. Although the anti-inflammatory potential of other lavender species, namely *L. angustifolia*, *L. stoechas*, *L. multifida* and *L. viridis* [14–18], is known, information on *L. luisieri* and *L. pedunculata* essential oils is sparse. Only two studies were carried out on *L. luisieri* essential oils, one showing its effect on primary human chondrocytes and the intestinal cell line [19], and another highlighting its potential to reduce cytokines and chemokines in human acute monocytic leukemia cells (THP-1) [20]. Taking this into account, and the fact that chronic inflammation has been associated with aging and related diseases [21–23] that greatly impact the quality of life, it is imperative to search for effective and safe anti-inflammatory therapeutic strategies. Therefore, using an *in vitro* model of lipopolysaccharide (LPS)-stimulated macrophages, the present study aimed to evaluate the anti-inflammatory potential of these essential oils with distinct chemical profiles. For the most promising oil, the effect of the main compounds, alone or in combination, was also investigated, and its mechanism of action underlying the pharmacological effects, namely the nuclear factor kappa B (NF-κB) signaling pathway, was further explored. Our results demonstrate relevant anti-inflammatory properties for the chemotype of *L. luisieri* essential oil with low quantities of necrodane derivatives, thus paving the way for the development of new plant-based anti-inflammatory therapeutics.

2. Results

2.1. Essential Oil Characterization

Samples of *L. luisieri* and *L. pedunculata* were collected throughout Portugal and their essential oils were further analyzed. The main chemical compounds present in the different samples allowed the identification of two chemotypes for *L. luisieri* and three for *L. pedunculata*. *L. luisieri* chemotypes were distinguished by the amounts of necrodane derivatives, with some samples presenting low concentrations of these compounds (6.9 ± 4.6%) and others showing high amounts (24.9 ± 2.4%). For *L. pedunculata*, differences occurred in the concentrations of three main compounds, with samples rich in fenchone (36.0% ± 12.9), 1,8-cineol (32.9% ± 8.3) or camphor (37.5% ± 8.1). The main compounds of representative samples of the identified chemotypes are listed in Table 1. Overall, the essential oils from both species were obtained with a yield of 0.8–1.10% and were characterized by high contents of oxygen-containing monoterpenes (54.9–80.3%). Regarding *L. luisieri*, the concentrations of 1,8-cineole, fenchone and necrodane derivatives differed among samples, with sample A1 characterized by low amounts of necrodane derivatives and high amounts of 1,8-cineole and fenchone, whereas in sample A2, necrodane derivatives occurred in higher amounts. For *L. pedunculata*, three main compounds (1,8-cineole, fenchone and camphor) were always identified, but their concentrations differed significantly between samples, with B1 rich in 1,8-cineole, B2 in fenchone, and B3 in camphor.

Table 1. Main compounds of *Lavandula luisieri* and *Lavandula pedunculata* essential oils.

			Lavandula luisieri		*Lavandula pedunculata*		
RI SPB-1	RI SW 10	Compound	A1	A2	B1	B2	B3
930	1030	α-pinene	1.1	3.2	2.5	3.9	3.8
942	1075	camphene	0.5	-	0.8	1.8	6.1
969	1116	β-pinene	0.7	1.6	9.0	0.2	1.4
1020	1215	1,8-cineole	33.9	6.4	34.3	12	25.1
1065	1400	fenchone	18.2	-	7.6	49.5	6.2
1082	1542	linalool	3.0	6.2	3.8	2.4	1.2
1118	1514	camphor	2.2	2.5	9.9	15	34.0
1121	1645	*cis*-verbenol	-	0.2	2.8	0.3	0.2
1125	1669	*trans*-verbenol	-	-	1.1	0.4	2
1130	1657	*trans*-α-necrodol	4.5	7.1	-	-	-
1146	1692	borneol	-	-	3.4	0.3	0.6
1154	1712	1,1,2,3-tetramethyl-4-hidroximethyl-2-cyclopentane	1.1	2.0	-	-	-
1159	1645	2,3,4,4-tetramethyl-5-methylene-cyclopent-2-enone	0.3	2.8	-	-	-
1165	1621	myrtenal	-	0.3	2.4	0.4	0.8
1265	1590	*trans*-α-necrodyl acetate	3.2	17.4	-	-	-
1269	1602	lavandulyl acetate	2.2	7.6	-	-	-
1269	1657	lyratyl acetate	0.3	2.4	-	-	-
1301	1683	myrtenyl acetate	2.0	-	-	-	-
1571	2068	viridiflorol	1.4	2.1	-	-	-
1628	2218	α-cadinol	-	0.7	3.1	0.2	0.2
Monoterpene hydrocarbons			2.3	4.5	12.3	5.9	11.3
Oxygen containing monoterpenes (including necrodane derivatives)			72.3	54.9	65.3	80.3	70.1
Oxygen containing sesquiterpenes			1.4	2.8	3.1	0.2	0.2

Compounds listed in order of elution from the SPB-1 column. RI SPB-1: GC-retention indices relative to C9–C23 n-alkanes on the SPB-1 column. RI SW 10: GC-retention indices relative to C9–C23 n-alkanes on the SupelcoWax-10 column. A1 and A2—representative samples of *L. luisieri* chemotypes; B1–B3—representative samples of *L. pedunculata* chemotypes. (-)—not detected.

2.2. Nitric Oxide Scavenging Potential of Lavandula luisieri and Lavandula pedunculata Essential Oils

The antioxidant potential of the essential oils towards reactive nitrogen species (RNS) was assessed using an *in chemico* nitrite-scavenging assay. Overall, the essential oils were ineffective and no nitric oxide (NO) scavenging effect was observed for all the tested concentrations (Figure 1). Indeed, nitrite values remained very similar to those of the NO donor, SNAP, in both *L. luisieri* (Figure 1A,B) and *L. pedunculata* (Figure 1C–E) chemotypes.

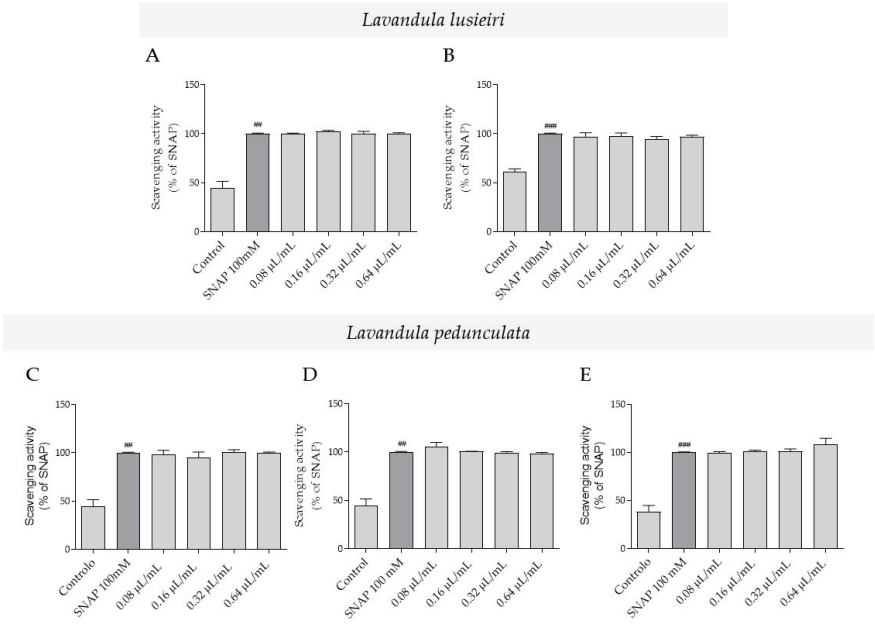

Figure 1. NO scavenging potential of *Lavandula* spp. essential oils. Effect of *L. luisieri* essential oil with (**A**) low (sample A1) or (**B**) high (sample A2) amounts of necrodane derivatives and *L. pedunculata* rich in (**C**) 1,8-cineole (sample B1), (**D**) fenchone (sample B2) and (**E**) camphor (sample B3). Different concentrations of essential oils (0.08–0.64 µL/mL) were incubated with the NO donor, SNAP (100 mM), in culture medium for 3 h. Results are expressed as percentage of NO release triggered by SNAP (positive control, dark grey bars). Each value represents the mean ± SEM of three experiments, performed in duplicate (## $p < 0.01$, ### $p < 0.001$, compared to control).

2.3. Effect of Lavandula luisieri and Lavandula pedunculata Essential Oils on Macrophages' Viability

To evaluate the anti-inflammatory activity of the essential oils, we first evaluated their effect on cell viability of murine macrophages stimulated with LPS (Figure 2), in order to select non-toxic concentrations. For all the essential oils, a range of concentrations varying from 0.08 to 0.64 µL/mL was tested. Overall, the essential oils were devoid of toxicity, except for the highest concentration of *L. luisieri* essential oil rich in necrodane derivatives (sample A2), which decreased cell viability by more than 70% compared to LPS-treated cells (Figure 2B). The vehicle, DMSO, did not interfere with macrophages' viability compared to control cells (Figure S1A).

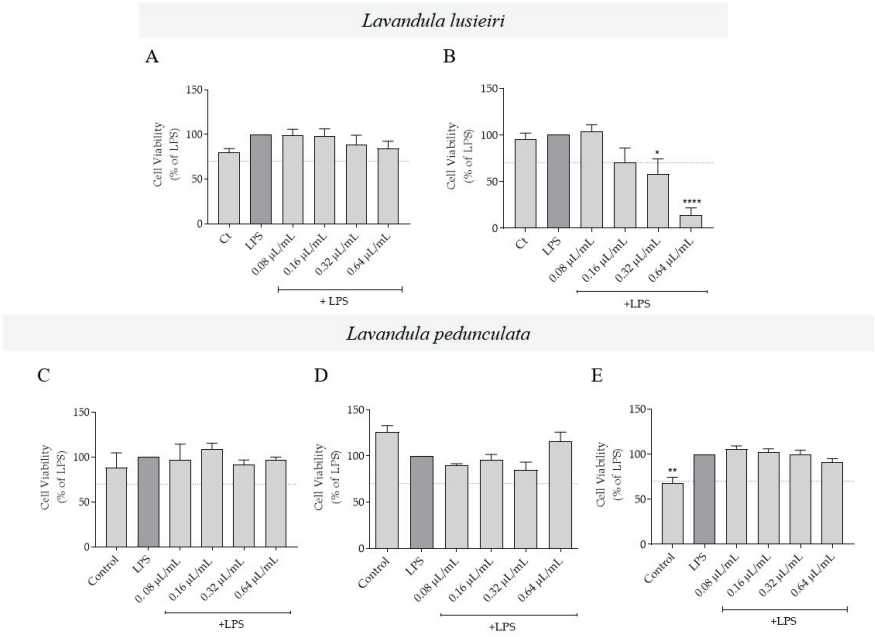

Figure 2. The effect of *Lavandula* spp. essential oils on cell viability. Effect of *L. luisieri* essential oil with (**A**) low (sample A1) or (**B**) high (sample A2) amounts of necrodane derivatives and *L. pedunculata* rich in (**C**) 1,8-cineole (sample B1), (**D**) fenchone (sample B2) and (**E**) camphor (sample B3) on macrophages' viability. Cells were maintained in culture medium (control), or incubated with 1 µg/mL LPS or with LPS in the presence of different concentrations of the oil (0.08–0.64 µL/mL), for 24 h. Results are expressed as percentage of MTT reduction by cells treated with LPS. Each value represents the mean ± SEM of three experiments, performed in duplicate (* $p < 0.05$, ** $p < 0.01$ and **** $p < 0.0001$, compared to LPS). The dotted line represents the threshold (70% of maximal viability) below which cytotoxicity is recognized, in agreement with standard ISO 10993-5 [24].

2.4. Effect of Lavandula luisieri and Lavandula pedunculata Essential Oils on NO Production

Using an *in vitro* model of LPS-stimulated macrophages referred to previously, the non-toxic concentrations of the essential oils determined in the previous section were used to assess the effect of the oils with distinct chemical profiles on LPS-induced NO production. Macrophages produce residual levels of nitrites (stable metabolite of NO). However, when stimulated with LPS, NO production increases considerably when compared to control. *L. luisieri* essential oils having both low amounts of necrodane derivatives (sample A1) and high amounts of necrodane derivatives (sample A2), significantly decreased LPS-induced NO production in a concentration-dependent manner (Figure 3A,B, respectively). However, sample A1 was much more effective in decreasing NO production (Figure 3A) than sample A2 (Figure 3B) at the concentrations tested without compromising cell viability (Figure 2A). Regarding *L. pedunculata* essential oils, the samples with high amounts of 1,8-cineole (B1; Figure 3C) and high amounts of camphor (B3; Figure 3E) were able to inhibit NO production induced by LPS, in a concentration-dependent manner, with the latter being more active at the lower concentration tested. By comparison, the sample with high amounts of fenchone (B2; Figure 3D) significantly inhibited NO production, but only at the higher concentrations tested (0.32 and 0.64 µL/mL). The vehicle, DMSO, did not interfere with LPS-induced NO production when compared to LPS-treated cells (Figure S1B).

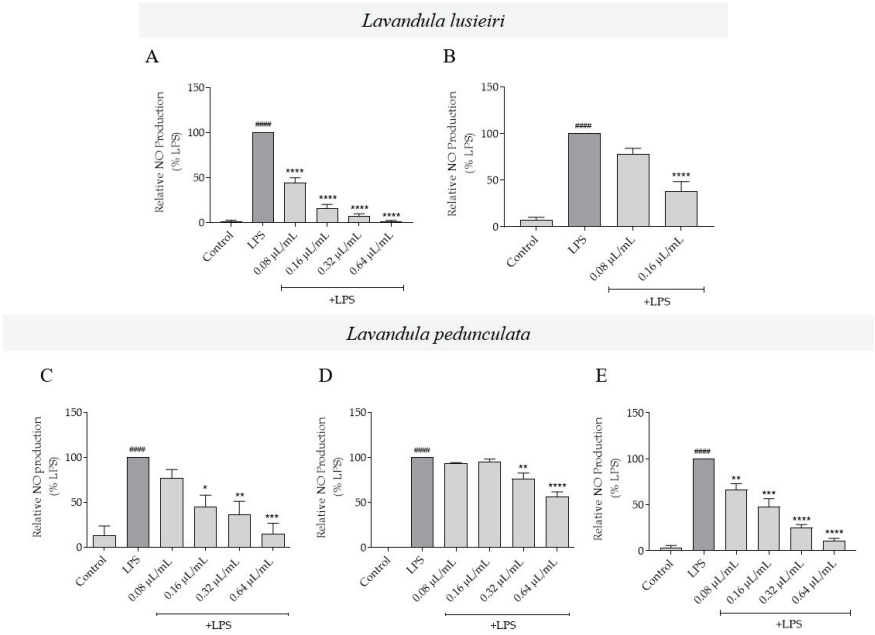

Figure 3. Inhibition of NO production by *Lavandula* spp. essential oils. Effect of *L. luisieri* essential oil with (**A**) low (sample A1) or (**B**) high (sample A2) amounts of necrodane derivatives and *L. pedunculata* rich in (**C**) 1,8-cineole (sample B1), (**D**) fenchone (sample B2) and (**E**) camphor (sample B3) on NO production induced by LPS in macrophages. Cells were maintained in culture medium (control), or incubated with 1 µg/mL LPS, or with LPS in the presence of different concentrations of the oil (0.08–0.64 µL/mL), for 24 h. Nitrite concentration was determined from a sodium nitrite standard curve and the results are expressed as a percentage of NO production by cells treated with LPS. Each value represents the mean ± SEM of three independent experiments, performed in duplicate (#### $p < 0.0001$, compared to control; * $p < 0.05$, ** $p < 0.01$ and *** $p < 0.001$ and **** $p < 0.0001$, compared to LPS).

Overall, regarding the ability of the essential oils to inhibit NO production, *L. luisieri* essential oil with low amounts of necrodane derivatives (sample A1) was the most potent (IC_{50} = 0.07 µL/mL; concentration range within the 95% confidence interval: 0.06 to 0.08 µL/mL).

2.5. Effect of 1,8-Cineole and Fenchone on NO Production

As *L. luisieri* essential oil with low amounts of necrodane derivatives (sample A1) was the most potent in inhibiting NO production induced by LPS in macrophages, its main compounds (1,8-cineole and fenchone) were also assessed to determine if the observed effect was due to these compounds. Our results showed that 1,8-cineole was not able to decrease LPS-induced NO production at non-toxic concentrations (Figure 4B,C). By comparison, fenchone significantly decreased NO production at the highest non-toxic concentrations tested (Figure 4E,F). Strikingly, when both compounds were combined in the same proportions as they occurred in the essential oil (33.9% 1,8-cineole and 18.2% fenchone), no effect was observed in LPS-induced NO production at non-toxic concentrations (Figure 4G,H). Notably, the effective concentrations for 1,8-cineole, fenchone, and the mixture were higher ($\geq$0.64 µL/mL) in comparison to those tested for *L. luisieri* essential oil (sample A1), which suggests that other compounds are responsible for the bioactive potential of this essential oil, or that synergisms may occur between compounds.

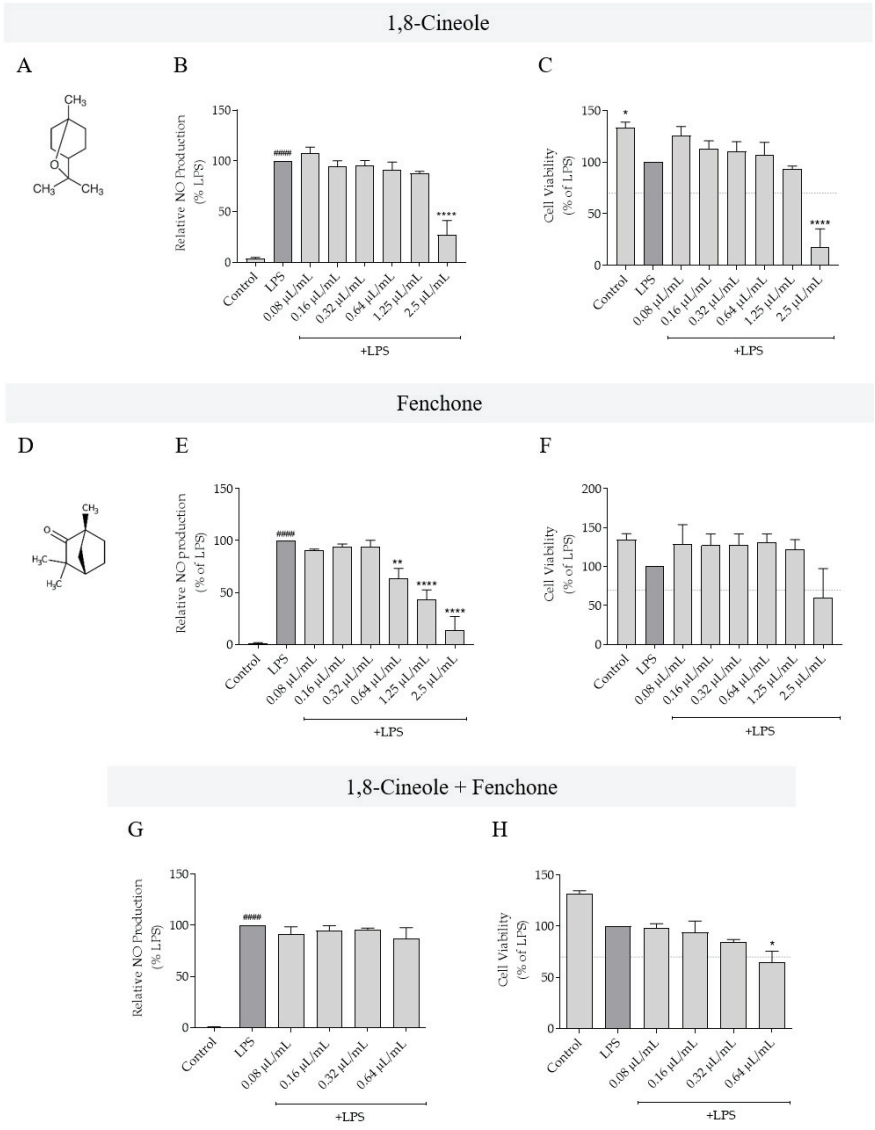

Figure 4. Effect of 1,8-cineole, fenchone, and their mixture on NO production. Chemical structure of (**A**) 1,8-cineole and (**D**) fenchone. Effect of 1,8-cineole (**B**,**C**), fenchone (**E**,**F**) and 1,8-cineole combined with fenchone (**G**,**H**) on NO production and cell viability, respectively. Cells were maintained in culture medium (control), or incubated with 1 µg/mL LPS, or with LPS in the presence of different concentrations of the compounds (0.08– 2.5 µL/mL), for 24 h. Nitrite concentration was determined from a sodium nitrite standard curve and the results are expressed as a percentage of NO production by cells treated with LPS. Cell viability results are expressed as percentage of MTT reduction by cells treated with LPS. Each value represents the mean ± SEM of three experiments, performed in duplicate (#### $p < 0.0001$, compared to control; * $p < 0.05$, ** $p < 0.01$ and **** $p < 0.0001$, compared to LPS). The dotted line in cell viability graphs represents the threshold (70% of maximal viability) below which cytotoxicity is recognized, in agreement with standard ISO 10993-5 [24].

2.6. Effect of Lavandula luisieri Essential on the Expression of Inflammatory Mediators

As *L. luisieri* rich in 1,8-cineole and fenchone was the most potent essential oil tested and was more active than its major compounds assessed alone or in combination, we sought to confirm its anti-inflammatory potential. Thus, the effect on the levels of inflammatory proteins, namely inducible nitric oxide synthase (iNOS), ciclooxigenase-2 (COX-2), and the immature form of interleukin—1β (pro-IL-1β), was assessed.

In untreated cells (control) and in cells treated with the essential oil, without LPS stimulation, iNOS, COX-2 and pro-IL-1β were not detected or were slightly expressed (Figure 5). However, after LPS stimulation for 24 h, the levels of these mediators significantly increased (Figure 5). Nevertheless, when macrophages were concomitantly treated with LPS and *L. luisieri* essential oil (0.32 µL/mL), iNOS levels significantly decreased compared to LPS-treated cells (Figure 5A,B), corroborating the previous results demonstrating NO inhibition (Figure 3A). However, *L. luisieri* essential oil did not interfere with LPS-induced COX-2 levels (Figure 5A,C). Interestingly, the essential oil significantly increased the levels of pro-IL-1β induced by LPS (Figure 5A,D), thus suggesting that the conversion of pro-IL-1β into its mature form IL-1β may be inhibited.

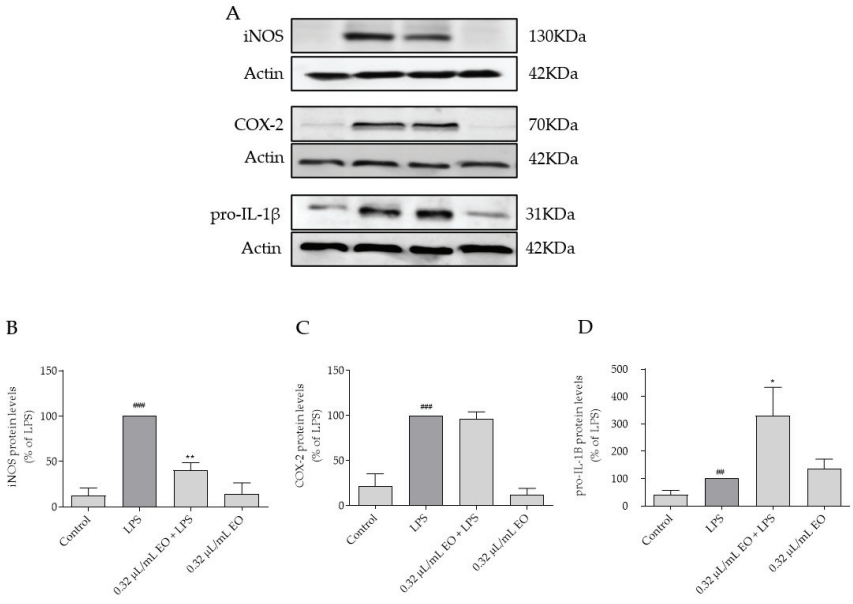

Figure 5. Inhibitory effect of *Lavandula luisieri* essential oil (EO) on LPS-induced inflammatory proteins. (**A**) Representative Western blots of iNOS, COX-2 and pro-IL-1β. Quantification of (**B**) iNOS, (**C**) COX-2 and (**D**) pro-IL-1β protein levels. Cells were maintained in culture medium (control), or incubated with 1 µg/mL LPS, or incubated with the essential oil (0.32 µL/mL) alone or simultaneously with 1 µg/mL LPS, for 24 h. Results are expressed as percentage of protein levels relative to LPS. Each value represents the mean ± SEM from at least 3 experiments (## $p < 0.01$; ### $p < 0.001$, compared to control; * $p < 0.05$, ** $p < 0.01$, compared to LPS). Each value represents the mean ± SEM from three experiments.

2.7. Effect of L. luisieri Essential Oil on NF-κB/p65 Nuclear Translocation

A complex network of intracellular signaling pathways and transcription factors tightly regulate the expression of pro-inflammatory molecules. Among the signaling cascades, the NF-κB assumes a decisive role during inflammation. In basal conditions, NF-κB is retained in the cytoplasm by its inhibitor, IκB. Upon a specific stimulus, phosphorylation and, consequently, proteasomal degradation of IκB occurs. Then, free NF-κB dimers, com-

posed of p65 and p50, rapidly translocate into the nucleus where transcription of target genes, such as *NOS2* and *COX-2*, is promoted [25]. To assess the effect of the oil on this signaling pathway, immunocytochemistry for the NF-κB subunit, p65, was performed. As expected, in untreated cells, immunoreactivity for NF-κB/p65 was exclusively located in the cytoplasm (Figure 6). However, after LPS treatment, NF-κB/p65 immunoreactivity was mostly observed in the nucleus (Figure 6). Treatment with *L. luisieri* essential oil (0.32 µL/mL) clearly impaired nuclear translocation of NF-κB/p65, as shown in Figure 6. Moreover, pre-treatment with MG-132 (10 µM), a synthetic proteasome inhibitor peptide, fully inhibited NF-κB/p65 nuclear translocation, as immunoreactivity is only visible in the cytoplasm (Figure 6). The vehicle (DMSO) did not interfere with NF-κB/p65 nuclear translocation when compared to control cells (data not shown). These results suggest that *L. luisieri* essential oil decreased iNOS protein levels by interfering with NF-κB/p65 nuclear translocation.

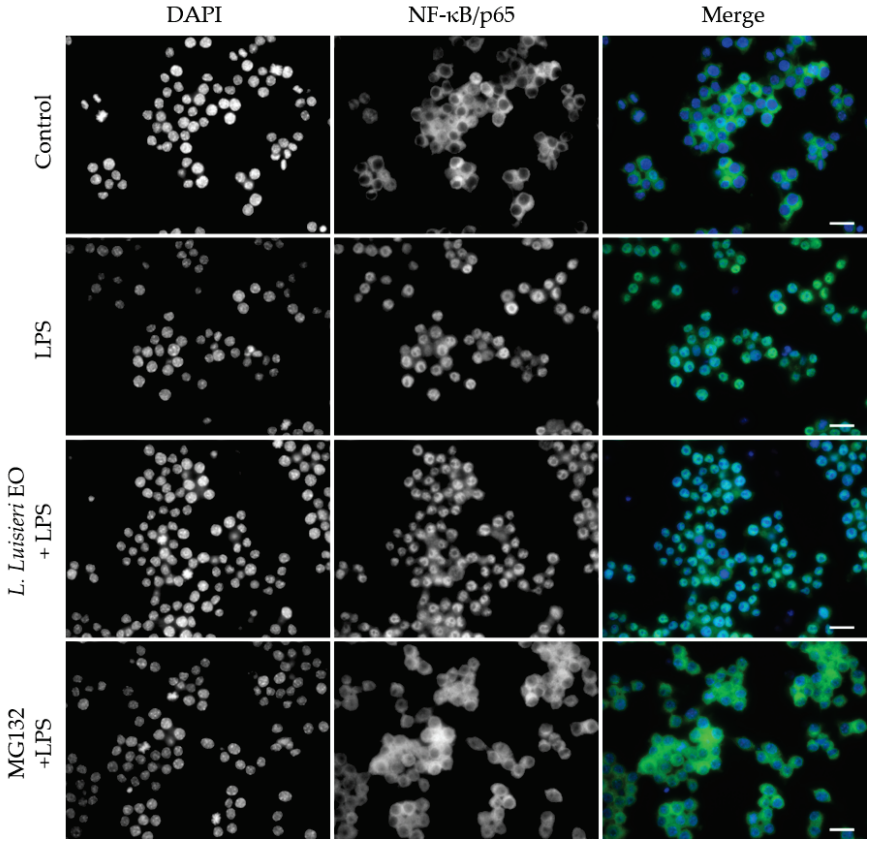

Figure 6. Inhibitory effect of *Lavandula luisieri* essential oil (EO) on NF-κB/p65 nuclear translocation. Macrophages were incubated on µ-slides and pre-treated with MG-132 (10 µM) for 1 h and, then, treated with 1 µg/mL LPS for 20 min, alone or in combination with the essential oil (0.32 µL/mL) or MG-132. Control cells (Ctrl) were left untreated. Immunofluorescence staining of NF-κB/p65 (green) was performed as detailed in the Materials and Methods section and DAPI (blue) was used as a counter stain. Representative images of each condition are shown. Scale bar: 20 µm.

3. Discussion

The Lamiaceae family comprises a high number of aromatic and medicinal plants with commercial interest. Among these species, lavenders stand out due to their high essential oil yield and pleasant odor, which are both important features for industrial applications. Indeed, the typical lavender scent is globally recognized and is included in many home and bath-care products. Lavender essential oil is considered a valuable raw-material in cosmetics and perfumes, and for flavoring [3,26]. Although the *Lavandula* genus comprises 39 wild essential oil bearing species, only four are commercially valued [3]. Nevertheless, some of the remaining species have economic potential mainly due to their bioactive properties. In fact, *L. luisieri* and *L. pedunculata* are widely used in traditional medicine by local communities, but scientific information validating these uses remains sparse. Moreover, local communities use these plants but are unaware of their chemical variability, which can compromise both safety and efficacy. Indeed, *L. luisieri* essential oils have a peculiar chemical composition due to the presence of necrodane derivatives that do not occur in other species [7,27–31] and, although these compounds are always present, significant variations among samples can occur [7]. Therefore, in the present work, two samples, one with low and another with high amounts of these compounds, were studied. Regarding *L. pedunculata*, the chemical composition of the essential oils from Portugal showed similarities with that reported for *L. stoechas* from other Mediterranean countries, namely from Spain [27], Greece [32] and Turkey [33]. Although *L. pedunculata* and *L. stoechas* are morphologically distinct, their essential oils present a similar chemical profile. This is interesting because *L. stoechas* is one of the four species with commercial value, thus suggesting that *L. pedunculata* can be used for the same purposes. Both species present the same major compounds, namely 1,8-cineole, fenchone and camphor, and the amount of these compounds can vary considerably. Therefore, three representative samples, with high amounts of each one of these compounds, were also selected.

As *L. luisieri* and *L. pedunculata* are used in traditional medicine to treat several conditions that share an inflammatory component, the present study aimed to validate the anti-inflammatory potential of these species considering their high chemical variability [7,8], which can affect oil quality and compromise both safety and bioactivity profiles. Inflammation is considered an important mechanism that maintains homeostasis, regardless of whether the insult is exogenous, as in the case of infections, or endogenous, as occurs, for instance, in metabolic disorders [34]. During this process, the first line of defense is provided by macrophages, which in the presence of a Toll-like receptor agonist such as microbial LPS, produce several pro-inflammatory mediators, including NO, COX-2, prostaglandins and cytokines, such as IL-1β [35]. Under normal conditions, the release of these pro-inflammatory mediators for a short period of time is of utmost importance, and aims to eradicate the harmful stimuli. However, the abnormal and sustained production of these mediators may result in damage to the host tissue, leading to a vicious circle that, if maintained over a long period, may evolve to chronic inflammation that has been associated with several aged-related diseases. One of the most important players in this process is the transcription factor NF-κB. Therefore, inhibition of NF-κB transcriptional activity, and its downstream mediators, represents a valuable therapeutic strategy for intervention in inflammation-based pathologies. In this context, the knowledge of phytochemicals' molecular mechanisms is a good strategy in the search for novel anti-inflammatory compounds. Taking into consideration the above, in this work we performed an initial screening assay using an *in vitro* inflammation model, specifically macrophages stimulated with LPS. Under these experimental conditions, LPS activates the pro-inflammatory transcription factor NF-κB/p65, which rapidly translocates into the nucleus to trigger the transcription of its target genes, such as *NOS2*, *COX-2* and *Il1*. Overall, the results achieved demonstrated that *L. luisieri* and *L. pedunculata* essential oils display anti-inflammatory potential, nonetheless presenting distinct efficacies and safety profiles depending on their chemical composition. In fact, *L. luisieri* essential oil with low amounts of necrodane derivatives was the most potent in mitigating the anti-inflammatory response, as assessed by the inhibition of NO

production evoked by LPS. Interestingly, the main compounds of the oil, namely 1,8-cineole and fenchone, were not the only compounds responsible for the observed effect, because they were much less effective than the oil, both alone and in combination, thus indicating that other minor compounds are responsible for the effect of the oil, or that synergistic effects among compounds may occur. In addition, the results achieved demonstrated that the observed anti-inflammatory effect was not related to a scavenging effect of the oil; therefore, the putative mechanism underlying the anti-inflammatory potential was further explored by addressing the effect of the oil on the expression of relevant inflammatory proteins. Our results clearly demonstrated that the anti-inflammatory potential ascribed to *L. luisieri* essential oil (with low amounts of necrodane derivatives) was achieved through inhibition of nuclear translocation of NF-κB/p65, which consequently leads to a decrease in iNOS protein levels and NO production. Interestingly, the essential oil also significantly increased the LPS induced expression of pro-IL-1β, the precursor of the potent pro-inflammatory cytokine IL-1β. It would be expected that pro-IL-1β levels were decreased because the essential oil compromised the nuclear translocation of NF-κB/p65. Nevertheless, we hypothesize that the observed accumulation indicates that pro-IL-1β is not being converted into IL-1β, thus suggesting an effect of the oil on the inflammasome, a proteolytic complex responsible for the maturation and secretion of the inflammatory and pyrogenic IL-1β. However, further studies should be performed to prove this hypothesis.

The results presented herein were corroborated by previous studies describing the anti-inflammatory potential of *L. luisieri* essential oil in both primary human chondrocytes and in an intestinal cell line [19], and in THP-1 cells [20]. The first study showed a decrease in iNOS levels and, consequently, in NO production, and reported that the effect was due to the inhibition of IκB phosphorylation and degradation, thus blocking NF-κB activation [19]. The latter pointed out a reduction in the cytokine tumor necrosis factor-α (TNFα) and the chemokine (C-C motif) ligand 2 (CCL2), following LPS stimulation. Regarding other lavender species, studies on *L. angustifolia* have frequently reported inhibitory effects on carrageenan-induced paw oedema [15], croton oil-induced ear oedema, and dextran-induced paw oedema models [36]. Moreover, decreases in the levels of TNF-α and IL-1β, and increases in IL-10, were also shown in a rat model of myocardial infarction [37]. *L. stoechas* also showed strong lipoxygenase inhibitory effects [14] and our group previously reported the ability of *L. viridis* essential oil to inhibit LPS-induced NO production through down-modulation of NF-κB-dependent *Nos2* transcription and, consequently, iNOS protein expression, in addition to a decrease in proteasomal activity, inhibition of *Il1b* and *Il6* transcription, and down-regulation of COX-2 levels [18]. Overall, these previous studies highlight the anti-inflammatory potential of lavender species, and the current study contributes by providing additional scientific information regarding less recognized species.

To conclude, our results indicate potent anti-inflammatory activity of *L. luisieri* essential oil via down-modulation of the NF-κB pathway, with significant inhibitions in major inflammatory mediators. In addition, the importance of well-defined chemical products is highlighted, because chemical variability compromises essential oils' quality and, consequently, their safety profile and efficacy. Moreover, our findings corroborate the traditional uses ascribed to these species and indicate that *L. luisieri*, with low amounts of necrodane derivatives, is the most promising for the development of safe anti-inflammatory agents, thus contributing to its industrial valorization.

4. Materials and Methods

4.1. Plant Material

Flowering parts of representative samples of *L. luisieri* (Rozeira) Rivas Mart. and *L. pedunculata* (Mill.) Cav. (Table 2) were collected. Voucher specimens were included in the Herbarium of the University of Coimbra (COI). Species authenticity was confirmed by Dr. Jorge Paiva, a taxonomist at the University of Coimbra, and plant names were checked at http://www.theplantlist.org accessed on 20 December 2021.

Table 2. Site of collection of *Lavandula* spp.

Species	Region	Site of Collection	Sample
L. luisieri	Coimbra	Piódão	A1
	Algarve	Cabo de São Vicente	A2
L. pedunculata	Guarda	Celorico da Beira	B1
	Bragança	Serra da Nogueira	B2
	Coimbra	Foz de Arouce	B3

A1 and A2—representaive samples of *L. lusieri*; B1–B3—representative samples of *L. pedunculata.*

4.2. Essential Oil Isolation and Analysis

Flowering aerial parts of *L. luisieri* and *L. pedunculata* were submitted to hydrodistillation for 3 h in a Clevenger-type apparatus [38]. Essential oils were analyzed by gas chromatography (GC) on a Hewlett Packard 6890 gas chromatograph (Agilent Technologies, Palo Alto, CA, USA) with a HP GC ChemStation Rev. A.05.04 data handling system, equipped with a single injector and two flame ionization detectors (FID). A graphpak divider (Agilent Technologies, Part Number 5021-7148) was used for simultaneous sampling in two Supelco (Supelco Inc., Bellefont, PA, USA) fused silica capillary columns with different stationary phases: SPB-1 (polydimethylsiloxane; 30 m × 0.20 mm i.d., film thickness 0.20 μm), and SupelcoWax 10 (polyethylene glycol; 30 m × 0.20 mm i.d., film thickness 0.20 μm). The oven temperature program was: 70–220 °C (3 °C/min), 220 °C (15 min); injector temperature: 250 °C; detector carrier gas: He, adjusted to a linear velocity of 30 cm/s; splitting ratio 1:40; detector temperature: 250 °C. Gas chromatography-mass spectrometry (GC/MS) analyses were performed on a Hewlett Packard 6890 gas chromatograph fitted with a HP1 fused silica column (polydimethylsiloxane; 30 m × 0.25 mm i.d., film thickness 0.25 μm), interfaced with an Hewlett Packard Mass Selective Detector 5973 (Agilent Technologies, Palo Alto, CA, USA) operated by HP Enhanced ChemStation software, version A.03.00. GC parameters were as above; interface temperature: 250 °C; MS source temperature: 230 °C; MS quadrupole temperature: 150 °C; ionization energy: 70 eV; ionization current: 60 μA; scan range: 35–350 u; scans/s: 4.51. Retention indices (RIs) and mass spectra were used to identify volatile compounds. RIs were calculated by linear interpolation relative to retention times of a series of n-alkanes, and compared with those of authenticated samples from the database of the Laboratory of Pharmacognosy, Faculty of Pharmacy, University of Coimbra. Mass spectra were compared with reference spectra from a home-made library or from literature data [39,40]. Relative amounts of individual components were calculated based on GC peak areas without FID response factor correction.

4.3. Nitric Oxide Scavenging Potential

The essential oils' NO scavenging potential was evaluated using S-nitroso-N-acetyl-DL-penicillamine (SNAP) as a NO donor. NO production was measured using Griess reaction. Briefly, in 48-well plates, 300 μL of culture medium alone (control) or with different concentrations of the essential oils and 300 μM of SNAP were incubated for 3 h at 37 °C. After this period, equal volumes of the supernatants and Griess reagent [1% (*w*/*v*) sulphanilamide in 2.5% (*v*/*v*) phosphoric acid and 0.1% (*w*/*v*) naphthylethylenediamine dihydrochloride] were mixed and incubated in the dark, for 30 min, at room temperature. The absorbance was then read at 550 nm using a Biotek Synergy HT plate reader (Biotek, CA, USA). The concentration of nitrites accumulated in supernatants was calculated by interpolation of the absorbance of each sample in a standard curve of sodium nitrite. All experiments were performed in triplicate.

4.4. Cell Culture and Treatments

The mouse leukemic macrophage cell line, RAW 264.7 (ATCC—TIB-71), was cultured in Dulbecco's Modified Eagle Medium supplemented with 10% (*v*/*v*) non-inactivated Fetal Bovine Serum, 100 μg/mL streptomycin and 100 U/mL penicillin. The cell line was maintained at 37 °C, in a humidified atmosphere of 95% air and 5% CO_2, and used after reaching 80–90% confluence. Cells were plated at 3×10^5 cells/well and left to stabilize for 12 h.

For cell treatments, essential oils, 1,8-cineol (extra pure; Merck, Darmstadt, Germany) and fenchone (99.9% purity; Fluka AG, Buchs, Switzerland) were initially diluted in dimethyl sulfoxide (DMSO; Sigma-Aldrich Co., St. Louis, Mo, USA) at a 1:1 proportion and, then, serial dilutions were performed in culture medium. MG-132 (Z-Leu-Leu-Leu-CHO, Boston Biochem, Cambridge, MA, USA) was also dissolved in DMSO (Sigma-Aldrich Co). In both cases, the final concentration of DMSO did not exceed 0.1% (*v*/*v*). LPS from *Escherichia coli* 026:B6 (Sigma-Aldrich Co.) was dissolved in phosphate buffered saline (PBS). The concentrations of the essential oils, 1,8-cineol, fenchone, MG-132 and LPS, and the experimental treatment periods, are indicated in figures and/or figure legends.

4.5. Cell Viability

Assessment of cell viability was performed using the 3-(4,5-dimethylthiazol-2-yl)-2,5-diphenyl tetrazolium bromide (MTT) assay. After the treatment period, a MTT solution (final concentration 0.5 mg/mL; Sigma-Aldrich Co.) was added to each well and further incubated at 37 °C for 15 min in a humidified atmosphere of 95% air and 5% CO_2. Acidified isopropanol (0.04 N HCl in isopropanol) was added to each cell to dissolve formazan crystals and quantification was carried out using an Biotek Synergy HT plate reader (Biotek) at 570 and 620 nm (reference wavelength). A cell-free control was performed in order to exclude non-specific effects of the essential oils, 1,8-cineol and fenchone on MTT (data not shown). All experiments were performed in triplicate.

4.6. Nitric Oxide Production

NO production was measured as the amount of nitrite accumulation in the culture supernatants using the Griess reaction described in Section 4.3.

4.7. Western Blotting

Total cell extracts were obtained using RIPA buffer (50 mM Tris-HCL, pH 8.0, 1% Nonidet P-40, 150 mM NaCl, 0.5% sodium deoxycholate, 0.1% sodium dodecyl sulphate (SDS) and 2 mM ethylenediaminetetraacetic acid) freshly supplemented with 1 mM dithiothreitol (DTT), protease (Complete Mini, Roche Diagnostics, Mannheim, Germany) and phosphatase (PhosSTOP, Roche Diagnostics, Mannheim, Germany) inhibitor cocktails. The cell lysates were then sonicated (4 times, 40 μm peak to peak) in a Vibra Cell sonicator (Sonica and Material INC) and centrifuged for 10 min at 4 °C to remove nuclei and cell debris. Protein concentration in the total lysates was determined using the bicinchoninic acid kit (Sigma-Aldrich Co.) and cell lysates were denatured in sample buffer [0.125 mM Tris pH 6.8, 2% (*w*/*v*) SDS, 100 mM DTT, 10% glycerol and bromophenol blue] at 95 °C for 5 min. Equal amounts of proteins were then separated by SDS-PAGE and electrotransferred onto PDVF membranes. After blocking with 5% (*w*/*v*) non-fat milk in Tris-Buffered saline (TBS)-Tween 20 (0.1%) for 1 h, membranes were incubated overnight at 4 °C with the primary antibodies indicated in Table 3 and then with anti-rabbit (dilution 1:20,000; NIF1317, GE Healthcare, Chalfont St. Giles, UK) or anti-mouse (dilution 1:20,000; NIF1316, GE Healthcare, Chalfont St. Giles, UK) alkaline phosphatase-conjugated secondary antibodies. Immune complexes were detected with Enhanced ChemiFluorescent reagent (GE Healthcare) in the Typhoon™ FLA 9000 imaging system. Mouse anti-actin was used as loading control. Image analysis was performed with Image Quant TL software.

Table 3. List of primary antibodies used in Western blot assays.

Protein	Source	Clonality	Dilution	Supplier	Catalogue Number
COX-2	rabbit	polyclonal	1:10,000	Abcam, Cambridge, UK	ab6665
IL-1β	rabbit	polyclonal	1:1000	Abcam	ab9722
iNOS	mouse	monoclonal	1:1000	R&D Systems, Minneapolis, MN, USA	MAB9502
Actin	mouse	monoclonal	1:20,000	Sigma-Aldrich Co.	MAB1501

4.8. Immunocytochemistry

To evaluate NF-κB/p65 nuclear translocation, immunocytochemistry was performed as previously described [41]. Briefly, at the end of the treatment period, cells were washed with ice-cold PBS pH = 7.4 and, then, fixed in 4% paraformaldehyde at room temperature, for 15 min. After fixing, cells were blocked with 5% Goat Serum, 0.3% Triton in PBS, pH = 7.4 for 1 h at room temperature. Then, slides were incubated with a rabbit monoclonal anti-NF-κB p65 (D14E12) XP® antibody (dilution 1:400; #8242, Cell Signaling Technology, Inc.) in 1% Bovine Serum Albumin in PBS (pH = 7.4) overnight at 4 °C and then incubated with anti-rabbit IgG (H+L) CF™488A (dilution 1:400; SAB4600165, Biothium, Inc., Fremont, CA, USA) for 1 h at room temperature in the dark. The cells were counterstained with DAPI (dilution 1:1,000; Sigma-Aldrich D9542) to stain the nuclei. Specificity was confirmed in negative controls set up by omitting the primary antibody. Fluorescence images were obtained in a widefield fluorescence microscope (Axio Observer.Z1; Carl Zeiss, Germany) and images were acquired using Zen Black 2010 software.

4.9. Statistical Analysis

Results are expressed as mean ± SEM. Statistical analysis was performed with GraphPad Prism version 9 (GraphPad Software, San Diego, CA, USA), using a two-sided unpaired t-test for comparisons between a control and treated group or using one-way ANOVA with Dunnett's post-test for multiple comparisons to a control group. Results were considered statistically significant at $p < 0.05$.

Supplementary Materials: The following supporting information can be downloaded at: https://www.mdpi.com/article/10.3390/plants11030370/s1, Figure S1: Effect of DMSO on macrophages viability and NO production.

Author Contributions: Conceptualization, M.Z., M.T.C. and L.S.; methodology, M.Z., C.S. and C.C.; validation, M.Z. and C.S.; formal analysis, M.Z., C.C. and C.S.; investigation, M.Z. and C.S.; resources, M.T.C. and L.S.; writing—original draft preparation, M.Z.; writing—review and editing, C.S., C.C., M.T.C. and L.S.; visualization, M.Z.; supervision, M.T.C. and L.S.; project administration, M.Z. and L.S.; funding acquisition, M.T.C. and L.S. All authors have read and agreed to the published version of the manuscript.

Funding: This work was financed by the European Regional Development Fund (ERDF), through the Centro 2020 Regional Operational Programme, under project CENTRO-01-0145-FEDER-000012 (HealthyAging2020).

Institutional Review Board Statement: Not applicable.

Informed Consent Statement: Not applicable.

Data Availability Statement: The data presented in this study are available on request from the corresponding author.

Acknowledgments: The authors thank Otília Vieira (CEDOC, NOVA Medical School, Portugal) for the kind gift of the mouse macrophage-like cell line Raw 264.7.

Conflicts of Interest: The authors declare no conflict of interest.

References

1. Inoue, M.; Hayashi, S.; Craker, L.E. Role of Medicinal and Aromatic Plants: Past, Present, and Future. *Pharmacogn. Med. Plants* **2019**. [CrossRef]
2. Barreca, S.; La Bella, S.; Maggio, A.; Licata, M.; Buscemi, S.; Leto, C.; Pace, A.; Tuttolomondo, T. Flavouring extra-virgin olive oil with aromatic and medicinal plants essential oils stabilizes oleic acid composition during photo-oxidative stress. *Agriculture* **2021**, *11*, 266. [CrossRef]
3. Upson, T.; Andrews, S. *The Genus Lavandula. Kew: Royal Botanic Gardens*; Kew Publishing: London, UK, 2004.
4. *ISO TC 54-ISO/CD 8902*; Oil of Lavandin Grosso [*Lavandula angustifolia* Miller × *Lavandula latifolia* (L. f) Medikus]. French Type, ISO: Geneva, Switzerland, 2007.
5. *ISO TC 54 N-ISO/WD 4719*; Oil of Spike Lavender [*Lavandula latifolia* (L.F.) Medikus]. Spanish Type, ISO: Geneva, Switzerland, 2009.
6. Vairinhos, J.; Miguel, M.G. Essential oils of spontaneous species of the genus *Lavandula* from Portugal: A brief review. *Zeitschrift Für Naturforsch. C* **2020**, *75*, 233–245. [CrossRef] [PubMed]
7. Zuzarte, M.; Gonçalves, M.; Cruz, M.; Cavaleiro, C.; Canhoto, J.; Vaz, S.; Pinto, E.; Salgueiro, L. *Lavandula luisieri* essential oil as a source of antifungal drugs. *Food Chem.* **2012**, *135*, 1505–1510. [CrossRef]
8. Zuzarte, M.; Gonçalves, M.J.; Cavaleiro, C.; Dinis, A.M.; Canhoto, J.M.; Salgueiro, L.R. Chemical composition and antifungal activity of the essential oils of *Lavandula pedunculata* (Miller) Cav. *Chem. Biodivers.* **2009**, *6*, 1283–1292. [CrossRef]
9. Aprotosoaie, A.C.; Gille, E.; Trifan, A.; Luca, V.S.; Miron, A. Essential oils of *Lavandula* genus: A systematic review of their chemistry. *Phytochem. Rev.* **2017**, *16*, 761–799. [CrossRef]
10. Tavares, A.C.; Zuzarte, M.R.; Salgueiro, L.R. *Plantas Aromáticas e Medicinais: Escola Médica do Jardim Botânico da Universidade de Coimbra*; Imprensa da Universidade de Coimbra: Coimbra, Portugal, 2010. [CrossRef]
11. Neves, J.; Matos, C.; Moutinho, C.; Queiroz, G.; Gomes, L.R. Ethnopharmacological notes about ancient uses of medicinal plants in Trás-os-Montes (northern of Portugal). *J. Ethnopharmacol.* **2009**, *124*, 270–283. [CrossRef]
12. Rivera, D.; Obón, C. The ethnopharmacology of Madeira and Porto Santo Islands, a review. *J. Ethnopharmacol.* **1995**, *46*, 73–93. [CrossRef]
13. Ferreira, A.; Proença, C.; Serralheiro, M.L.; Araújo, M. The *in vitro* screening for acetylcholinesterase inhibition and antioxidant activity of medicinal plants from Portugal. *J. Ethnopharmacol.* **2006**, *108*, 31–37. [CrossRef]
14. Amira, S.; Dade, M.; Schinella, G.; Ríos, J.-L. Anti-inflammatory, anti-oxidant, and apoptotic activities of four plant species used in folk medicine in the Mediterranean basin. *Pak. J. Pharm. Sci.* **2012**, *25*, 65–72.
15. Hajhashemi, V.; Ghannadi, A.; Sharif, B. Anti-inflammatory and analgesic properties of the leaf extracts and essential oil of *Lavandula angustifolia* Mill. *J. Ethnopharmacol.* **2003**, *89*, 67–71. [CrossRef]
16. Wei, A.; Shibamoto, T. Antioxidant/lipoxygenase inhibitory activities and chemical compositions of selected essential oils. *J. Agric. Food Chem.* **2010**, *58*, 7218–7225. [CrossRef] [PubMed]
17. Sosa, S.; Altinier, G.; Politi, M.; Braca, A.; Morelli, I.; Della Loggia, R. Extracts and constituents of *Lavandula multifida* with topical anti-inflammatory activity. *Phytomedicine* **2005**, *12*, 271–277. [CrossRef] [PubMed]
18. Zuzarte, M.; Francisco, V.; Neves, B.M.; Liberal, J.; Cavaleiro, C.; Canhoto, J.M.; Salgueiro, L.; Cruz, M.T. *Lavandula viridis* essential oil inhibits the inflammatory response in macrophages through blockade of NF-KB signaling cascade. *Front. Pharmacol.* **2022**, *12*, 695911. [CrossRef]
19. Rufino, A.T.; Ferreira, I.; Judas, F.; Salgueiro, L.; Lopes, M.C.; Cavaleiro, C.; Mendes, A.F. Differential effects of the essential oils of *Lavandula luisieri* and *Eryngium duriaei* subsp. *juresianum* in cell models of two chronic inflammatory diseases. *Pharm. Biol.* **2015**, *53*, 1220–1230. [CrossRef]
20. Miguel, M.G.; Da Silva, C.I.; Farah, L.; Braga, F.C.; Figueiredo, A.C. Effect of essential oils on the release of TNF-a and CCL2 by LPS-stimulated THP-1 cells. *Plants* **2020**, *10*, 50. [CrossRef]
21. Coussens, L.M.; Werb, Z. Inflammation and cancer. *Nature* **2002**, *420*, 860–867. [CrossRef]
22. Zatterale, F.; Longo, M.; Naderi, J.; Raciti, G.A.; Desiderio, A.; Miele, C.; Beguinot, F. Chronic adipose tissue inflammation linking obesity to insulin resistance and type 2 diabetes. *Front. Physiol.* **2020**, *10*, 1607. [CrossRef]
23. Hunter, J.D.; Doddi, M. Sepsis and the heart. *Br. J. Anaesth.* **2010**, *104*, 3–11. [CrossRef]
24. Standardization, I.O.f. *Biological Evaluation of Medical Devices. Part 5 Tests Vitro Cytotoxicity*; HIS: Geneva, Switzerland, 2009; pp. 1–34.
25. Mulero, M.C.; Huxford, T.; Ghosh, G. NF-κB, IκB, and IKK: Integral components of immune system signaling. *Struct. Immunol.* **2019**, *1172*, 207–226. [CrossRef]
26. Cavanagh, H.M.A.; Wilkinson, J.M. Lavender essential oil: A review. *Aust. Infect. Control.* **2005**, *10*, 35–37. [CrossRef]
27. Garcia Vallejo, M.I. *Aceites Esenciales de las Lavandulas Ibéricas-Ensayo de la Quimiotaxonomia*; Universidad Complutense de Madrid: Madrid, Spain, 1992.
28. Lavoine-Hanneguelle, S.; Casabianca, H. New Compounds from the essential oil and absolute of *Lavandula luisieri* L. *J. Essent. Oil Res.* **2004**, *16*, 445–448. [CrossRef]
29. Sanz, J.; Soria, A.C.; García-Vallejo, M. Analysis of volatile components of *Lavandula luisieri* L. by direct thermal desorption–gas chromatography–mass spectrometry. *J. Chromatogr. A* **2004**, *1024*, 139–146. [CrossRef] [PubMed]

30. Baldovini, N.; Lavoine-Hanneguelle, S.; Ferrando, G.; Dusart, G.; Lizzani-Cuvelier, L. Necrodane monoterpenoids from *Lavandula luisieri*. *Phytochemistry* **2005**, *66*, 1651–1655. [CrossRef]
31. González-Coloma, A.; Delgado, F.; Rodilla, J.M.; Silva, L.; Sanz, J.; Burillo, J. Chemical and biological profiles of *Lavandula luisieri* essential oils from western Iberia Peninsula populations. *Biochem. Syst. Ecol.* **2011**, *39*, 1–8. [CrossRef]
32. Skoula, M.; Abidi, C.; Kokkalou, E. Essential oil variation of *Lavandula stoechas* L. ssp. stoechas growing wild in crete (Greece). *Biochem. Syst. Ecol.* **1996**, *24*, 255–260. [CrossRef]
33. Dadalioğlu, I.; Evrendilek, G.A. Chemical compositions and antibacterial effects of essential oils of Turkish oregano (*Origanum minutiflorum*), bay laurel (*Laurus nobilis*), Spanish lavender (*Lavandula stoechas* L.), and fennel (*Foeniculum vulgare*) on common foodborne pathogens. *J. Agric. Food Chem.* **2004**, *52*, 8255–8260. [CrossRef]
34. Antonelli, M.; Kushner, I. It's time to redefine inflammation. *FASEB J.* **2017**, *31*, 1787–1791. [CrossRef]
35. Medzhitov, R. Origin and physiological roles of inflammation. *Nature* **2008**, *454*, 428–435. [CrossRef]
36. Cardia, G.F.E.; Silva-Filho, S.E.; Silva, E.L.; Uchida, N.S.; Cavalcante, H.A.O.; Cassarotti, L.L.; Salvadego, V.E.C.; Spironello, R.A.; Bersani-Amado, C.A.; Cuman, R.K.N. Effect of Lavender (*Lavandula angustifolia*) essential oil on acute inflammatory response. *Evidence-Based Complement. Altern. Med.* **2018**, *2018*, 1–10. [CrossRef]
37. Souri, F.; Rakhshan, K.; Erfani, S.; Azizi, Y.; Maleki, S.N.; Aboutaleb, N. Natural lavender oil (*Lavandula angustifolia*) exerts cardioprotective effects against myocardial infarction by targeting inflammation and oxidative stress. *Inflammopharmacology* **2019**, *27*, 799–807. [CrossRef] [PubMed]
38. Council of Europe. *European Pharmacopoeia, 9th ed*; Council of Europe: Strasbourg, France, 2016.
39. Joulain, D.; König, W.A. *The Atlas of Spectral Data of Sesquiterpene Hydrocarbons*; E.B.-Verlag: Hamburg, Germany, 1998.
40. Adams, R.P. *Identification of Essential Oil Components by Gas Chromatography/Mass Spectroscopy*; Allured Publishing Corporation: Carol Stream, IL, USA, 2007.
41. Sousa, C.; Neves, B.; Leitão, A.; Mendes, A. Elucidation of the mechanism underlying the anti-inflammatory properties of (S)-(+)-carvone identifies a novel class of sirtuin-1 activators in a murine macrophage cell line. *Biomedicines* **2021**, *9*, 777. [CrossRef] [PubMed]

plants

MDPI

Review

Critical Determinants in ER-Golgi Trafficking of Enzymes Involved in Glycosylation

Ning Zhang and Olga A. Zabotina *

Roy J. Carver Department of Biochemistry, Biophysics, and Molecular Biology, Iowa State University, Ames, IA 50011, USA; ningz@iastate.edu
* Correspondence: zabotina@iastate.edu

Abstract: All living cells generate structurally complex and compositionally diverse spectra of glycans and glycoconjugates, critical for organismal evolution, development, functioning, defense, and survival. Glycosyltransferases (GTs) catalyze the glycosylation reaction between activated sugar and acceptor substrate to synthesize a wide variety of glycans. GTs are distributed among more than 130 gene families and are involved in metabolic processes, signal pathways, cell wall polysaccharide biosynthesis, cell development, and growth. Glycosylation mainly takes place in the endoplasmic reticulum (ER) and Golgi, where GTs and glycosidases involved in this process are distributed to different locations of these compartments and sequentially add or cleave various sugars to synthesize the final products of glycosylation. Therefore, delivery of these enzymes to the proper locations, the glycosylation sites, in the cell is essential and involves numerous secretory pathway components. This review presents the current state of knowledge about the mechanisms of protein trafficking between ER and Golgi. It describes what is known about the primary components of protein sorting machinery and trafficking, which are recognition sites on the proteins that are important for their interaction with the critical components of this machinery.

Keywords: glycosyltransferases; ER-Golgi trafficking; mechanism of protein sorting; COPI and COPII complexes; sequences and motifs involved in trafficking

Citation: Zhang, N.; Zabotina, O.A. Critical Determinants in ER-Golgi Trafficking of Enzymes Involved in Glycosylation. *Plants* **2022**, *11*, 428. https://doi.org/10.3390/plants11030428

Academic Editors: Milan S. Stankovic, Paula Baptista and Petronia Carillo

Received: 6 December 2021
Accepted: 1 February 2022
Published: 4 February 2022

1. Introduction

All living cells generate structurally complex and compositionally diverse spectra of glycans and glycoconjugates, critical for organismal evolution, development, functioning, defense, and survival. The glycans attached to proteins and lipids determine their activity, solubility, subcellular localization, and structural organization in cells during normal and stressed conditions. Glycan-rich cell walls control cell growth and morphogenesis and protect them against environmental stresses. Glycosylation is the reaction that forms glycosidic linkages between activated sugar (donor substrate) and acceptor substrate (protein, lipid, polysaccharide, etc.). This reaction is performed by a large group of specialized enzymes, called glycosyltransferases, and broadly takes place in most organisms, such as yeast, humans, plants, etc. Because of the diversity of sugars and acceptor substrates, the resulting products of glycosylation present high variability and complexity in structures and functions.

Glycosyltransferases (GTs) are distributed among more than 130 gene families [1]. Most GTs are type II transmembrane proteins with several distinct domains: a short *N*-terminal cytosolic tail, transmembrane domain (TMD), flexible stem region, and large catalytic domain. Another group of GTs comprises integral membrane proteins with multiple TMDs and a large catalytic domain frequently localized on the cytosolic side of the membrane. Based on the type of catalytic domain folds, the GTs are grouped into GT-A, GT-B, and GT-C [2,3]. Two tight β/α/β Rossmann domains form a central *β*-sheet in GT-A folding, and mostly GT-A type proteins contain DxD catalytic motifs that cooperate with

metal. Instead of being tightly associated, the two β/α/β Rossmann domains in GT-B are separate and form a cleft. GT-C proteins are predicted and found based on sequence and structure research and contain multiple hydrophobic helices. In addition, it was also found that the structure of the peptidoglycan glycosyltransferase of Aquifex aeolicus contains a lysozyme-like domain [4].

The primary types of glycosylation in various glycoconjugates are *N*-glycosylation and *O*-glycosylation. *N*-glycosylation is the formation of the glycosidic linkage between the amino group of an asparagine residue and the first sugar of the glycan. Asparagine in the Asn-X-Ser/Thr consensus sequence is the candidate for *N*-glycosylation, although not all Asn residues are glycosylated [5]. *N*-glycosylation is essential and usually impacts protein solubility, structure, and folding. It is also essential for protein localization and interactions with glycan-binding proteins. The glycan oligosaccharides in *N*-glycosylated proteins share the core sugar sequence and structure-Manα1-6(Manα1–3)Manβ1-4GlcNAcβ1-4GlcNAcβ1-Asn [6], which can be further branched with different sugars depending on the type of mature glycan synthesized. The *N*-glycosylation reactions take place in the endoplasmic reticulum (ER) and Golgi. The initiation of *N*-glycosylation occurs in the ER with the biosynthesis of the precursor oligosaccharide [7], which is later transferred to the peptide's Asn by the oligosaccharyltransferase (OST) complex.

At the end of the multistep process, the glycoprotein is transported to cis-Golgi, and the next steps of *N*-glycan processing continue in different Golgi cisternae. The GTs, such as medial-Golgi-localized *N*-acetylglucosaminyltransferase I (GnTI) [8,9], GnTII [10,11], trans-Golgi-localized Galactose-1-phosphate uridylyltransferase l (GALT) [12], *β*-galactoside-α2,6-sialyltransferase l (ST6Gal-l) [13–15], and *β*-galactoside-α2,3-sialyltransferase-III (ST3Gal-lII) [16,17] are localized in distinct Golgi cisternae and responsible for subsequent steps of the synthesis of final glycan structures. It was demonstrated that most of these GTs form homo- and heterocomplexes, most likely to support the error-proof synthesis [14,18,19].

The *O*-glycosylation process is different in plant and mammalian cells. In mammalian type *O*-glycosylation, the glycan is attached to the hydroxyl group of the serine or threonine residue in a glycoprotein. *O*-glycosylation primarily occurs in Golgi and is also found in the cytoplasm and nucleus [20–22]. The first sugar, *N*-acetylgalactosamine (GalNAc), links to serine and threonine residues in Golgi and is called *O*-GalNAc. Multiple core sugar sequences are found in *O*-GalNAc-type glycosylation, and different biosynthesis steps are involved [6,23]. In plants, the main *O*-glycoproteins are the hydroxyproline-rich glycoprotein (HRGP) superfamily, including arabinogalactan proteins (AGPs), extensions (EXTs), and the repetitive Pro-rich proteins (PRPs) [24]. The type II arabino-3,6-galactans (AGs) get attached to noncontiguous Hyp residues in AGPs in Golgi [24]. In *A.thaliana*, eight Hyp-galactosyltransferases added the Gal to Hyp residues as the initiation steps of *O*-glycosylation of AGPs [24,25]. The variation of AGPs depends on the complexity of galactan side chains attached to Hyp residues [24]. The *β* 1-6 galactosyltransferases are involved in the elongation of the side-chain backbone; other GTs, such as arabinosyltransferases, rhamnosyltransferases, and xylosyltransferases, further branch this galactan backbone [24]. The Ser residues and three to five contiguous Hyp residues are the candidate sites of *O*-glycosylation in EXTs. The *β* 1-3-arabinosyltransferase attaches the first arabinofuranose reside to Hyp [24]. The Reduced Residual Arabinose 1–3 (RRA1-RRA3), Xyloglucanase 113 (XEG113), and Extensin Arabinose Deficient (ExAD) add the second, third and fourth Araf residues sequentially [24].

Cell-wall polysaccharides are synthesized in two locations: the Golgi and the plasma membrane. On the plasma membrane, most GTs involved in synthesizing polysaccharides are integral membrane proteins with multiple TMDs. For example, in plants, cellulose synthases (CESA) [3,26–28] are organized in multiprotein cellulose synthase complexes (CSCs) and synthesize cellulose microfibrils. These complexes are assembled in Golgi and delivered to the plasma membrane via cargo carriers. Multiple isoforms of CESA are identified: in primary plant cell wall synthesis, CESA1, CESA2, CESA3, CESA5, CESA6, and CESA9 assemble CSCs in Golgi [28,29]. At the same time, CESA4, CESA7, and CESA8

are involved in the biosynthesis of the secondary plant cell wall [28,29]. Other plant cell wall polysaccharides representing pectins and hemicelluloses are synthesized in Golgi by Golgi-localized GTs [3]. The latest studies suggest that Golgi-localized GTs are also organized in multiprotein complexes to synthesize polysaccharides. For example, β -1,4-xylosyltransferase (IRX) 9, IRX10, and IRX14 are xylosyltransferases and form the protein complex to synthesize the backbone of xylan [30–32]. The other seven GTs (cellulose synthase-like C4; xyloglucan xylosyltransferases XXT1, XXT2, and XXT5; galactosyltransferases XLT2 and MUR3 and fucosyltransferase FUT1) involved in xyloglucan biosynthesis were also shown to form heterocomplexes [3,33,34]. The homogalacturonan synthesizing galacturonosyltransferase (GAUT) 1 and GAUT7 proteins form a heterocomplex required to anchor catalytically active GAUT1 to Golgi [35].

2. Main Components of the Secretory Pathway

The trafficking of enzymes involved in glycosylation is essential for their proper delivery to the sites of their functioning in the cell, but it is still poorly understood. However, the information about trafficking processes available for various other proteins can also be applied to GTs. More information has recently become available concerning the primary components and routes of secretory pathways. The GTs and glycosidases involved in glycosylation, the focus of this review, most likely follow a similar secretory pathway and therefore are subjected to similar sorting mechanisms like other membrane proteins.

Thus, it has become clear that the coat protein complex I (COPI) -coated cargo carriers and the coat protein complex II (COPII)-coated cargo carriers mediate the trafficking path between the ER and the Golgi (Figure 1). One part of this trafficking pathway is the sorting signal in the protein sequence of GTs, which is recognized by the cargo receptor or COP coatomer to trigger the trafficking of proteins. The transmembrane region and *N*-terminal cytoplasmic domain of lipid phosphatase Sac1 are essential in the retention mechanism of phosphatidylinositol-3-phosphatase (Sac1) in Golgi [36]. The core components of the COPI-coated cargo carriers are the α-COP, β-COP, β'-COP, γ-COP, δ-COP, ε-COP, and ζ-COP subunit. The activation of the GTPase ADP-ribosylation factor 1 (Arf1) is a prerequisite for the assembly of the COPI coat [37–39]. Guanine nucleotide-exchange factors (GEFs) stimulate the GTPase Arf1 activation by exchanging GDP to GTP; then, the activated GTPase Arf1 embeds into the lipid membrane by using a myristoylated α-helix [40,41]. In turn, GTPase Arf1 recruits the coatomer complex with an inner coat and outer coat to transport protein and lipid cargo from the Golgi to the ER and between the Golgi cisternae [42,43]. COPII-coated cargo carriers deliver the cargo proteins from the ER to the Golgi, with the inner and outer layers of the protein lattice acting as the core component of COPII-coated cargo carriers [44–47]. The activation of the Ras-like small COPII coat Sar1 GTPase is the prerequisite of the assembly of the COPII coat [48]. Guanine nucleotide-exchange factor Sec12 assists the exchange of the GDP to the GTP on Sar1 to recruit the coat protein Sec23-Sec24 inner layer of the protein lattice, and the heterotetramers of coat protein Sec13 and Sec31 as the outer layer of the protein lattice is recruited to continue the assembly of the COPII coat [44–47].

There are some differences in COPI and COPII transportation in plants compared to animals and yeast. In plant cells, the COPII and COPI-coated cargo carriers' transportation impacts plant growth, stress response, and protein transportation. In *A.thaliana*, multiple paralogs of COPI components have been discovered [49,50]. The silencing of the β1/2-COP gene enhanced the sensitivity of *A.thaliana* to salt stress [49,51]. Double mutant of β1/2-COP and a single mutant of α2-COP were dwarfed compared to *Col-0* [49,52], and the silencing of β1/2-COP or α2-COP or p24 protein altered the structure of the Golgi [49,52,53]. The knockout of α1-COP, γ-COP, and ε-COP resulted in a reduction in seed production due to altered pollen grain adherence and pollen tube germination [54]. The β'-, γ-, and δ-COP proteins were shown to interact with each other and were localized in Golgi [55]. The β'-, γ-, and δ-COP proteins were required to support the Golgi structure, and the silence of these genes caused the plant cell death [55]. The maintenance of the Golgi structure also

requires the recruitment of Arf1 [56] and multiple paralogs of the cargo receptor p24 family protein [53]. The multiple paralogs of the p24 family proteins are involved in the trafficking of GPI-anchored proteins to the plasma membrane. For example, it was shown that these paralogs could interact with GPI-anchored protein arabinogalactan protein 4 [50]. In the *Arabidopsis p24δ3δ4δ5δ6* quadruple mutant, ER lumen protein-retaining receptor A(ERD2a), as the K/HDEL receptor, accumulated in Golgi and, as a result, the expression of *Sec31* gene was upregulated [53]. The p24 family protein affected the ERD2a trafficking by direct interaction with ERD2a via luminal GOLD domain, and their interaction showed pH-dependence [57,58].

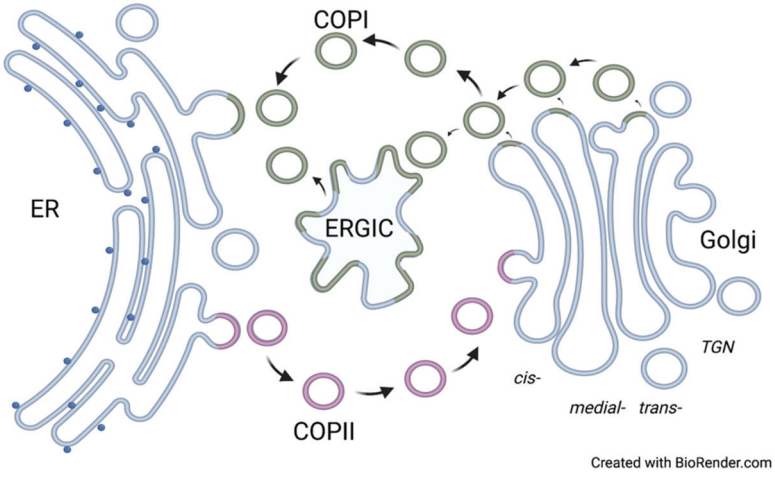

Figure 1. The cargo transportation between ER and Golgi via COP-coated cargo carriers. ER: endoplasmic reticulum; COPI: coat protein complex I; COPII: coat protein complex II; ERGIC: ER-Golgi intermediate compartment. Note that the ERGIC compartment has not been demonstrated in plant and yeast cells.

The Multiple paralogs of COPII protein components were also discovered in plants [59]. The expression pattern, subcellular localization, and function of the COPII protein paralogs showed a significant difference [60–63]. SEC23A/SEC23D [64], SEC31A/B [61,65] and Sar1B/C [62] had been reported to be required in pollen development. In *Physcomitrium patens*, Sec23D is localized in the presumptive ER-exit sites [60]. The knockout of the *Sec23d* gene suppressed the protein transportation between ER and Golgi and protein secretion in the mutant plants, leading to ER morphology defects and ER stress [60]. In *A.thaliana*, Sar1A is also localized in ER-exit sites [63]. The residue Cys84 in the Sar1A is crucial for its specific interaction with AtSec23A, essential for the ER-export process [63]. The mutation of this residue disturbed their interaction resulting in the suppression of the ER-export process of vacuolar protein [63]. In *A.thaliana*, the formation of unusually giant COPII vesicles, which modulated the transport of channel proteins and transporters, was observed in response to stress conditions [66]. Even though the importance of COPII components in plant growth and development has been demonstrated, the existence of COPII-coated cargo carriers in plant cells is still disputed [67,68]. The notion that the Golgi entry core compartments can work independently from COPII-coated cargo carriers formation has been proposed [69].

The cargo sorting during COPI and COPII coat assembly is essential. The sorting signal in the cargo protein plays a dominant role in the direct or indirect interaction between cargo proteins and components in the coat. The Sec24 subunit in the COPII complex is involved in cargo sorting and directly binds with the cargo protein [70–72]. The diverse cargo binding sites in the Sec24 protein recognize different cargo sorting signal motifs in cargo proteins, and multiple isoforms of Sec24 are involved in diverse cargo sorting [71–73].

For example, the ER-exit signal DxE [74,75], LxxLE [75,76], YxxNPF [77], triple arginine (RRR) motif [78], and ΦXΦXΦ motif of bovine anion exchanger 1 (AE1) [79] are recognized by Sec24. Sar1 also participates in cargo sorting and directly interacts with cargo sorting signal motifs. Sar1A directly interacts with the polybasic motif of planar cell polarity protein Frizzled-6 to adjust the cargo packaging into coated cargo carriers [80]. The RNKR motif of Drosophila type I transmembrane protein Crumbs is the ER-exit signal interacting with Sar1 [81]. Cargo transportation via COPII-coated cargo carriers also requires the protein–protein interaction between cargo sorting motifs and COPI coatomers or cargo receptors. The KXD/E motif of *A.thaliana* endomembrane protein 12 binds with COPI coatomers [82]. α- COP, β'-COP, and γ-COP bind with diverse motifs to assemble the COPI-coated cargo carriers. For example, α- COP and β'-COP directly bind di-lysine motifs [83], and γ-COP recognizes the FFxxBB(x)n of the P24 protein [38] and directly binds with human ER α-1, 2-mannosidase [84].

Besides the direct interaction between the cargo protein and COP complex, the cargo receptors mediate the cargo sorting. In mammalian cells, the ER-Golgi intermediate compartment (ERGIC) ERGIC-53 protein [85] and p24 protein families [76,77,86] are known as the cargo receptors for the soluble cargo proteins, and Erv29 proteins are involved in COPII vesicles assembly with the GFP-HDEL and glycosylated pro–α-factor (gpαf) cargo proteins [87–89]. Transmembrane proteins Erv14 [90,91] and Erv26 [72] work as the cargo receptors for the membrane proteins via their direct interaction with Sec24 and cargo proteins. It has been shown that KDEL receptors recognize ER-retrieval signal KDEL and directly interact with the KDEL motif. At the same time, the strength of interaction and release of cargo protein is regulated by the difference of pH in the ER and the Golgi [72]. The Arg residues in the KDEL receptor anchored the KDEL peptides via salt bridge interactions, whereas the Glu residues formed a hydrogen bond with tryptophan in the KDEL receptor [92]. The Glu residues hydrogen bonding with histidine in the KDEL receptor was shown to be pH-sensitive [92]. The cargo receptor Rer1 binds to the KKXX motif in the ER membrane proteins [93] and the polar residue in the TMDs [94]. The positively charged amino acids in the cytosolic tail, such as the di-arginine motif (RXR) and di-lysine motif (KK or KXKXX), have proven to play essential roles in the trafficking of type I membrane proteins [38]. In addition, so-called kin recognition has also been proposed. The interactions between kin oligomers and GTs and glycosidases occur in specific Golgi cisternae and prevent their entry into transportation carriers and their forward movement to later cisternae [95].

3. Specific Sequence Motifs Involved in GTs and Glycosidases Sorting and Trafficking

The mechanism of trafficking GTs and glycosidases between the ER and the Golgi is somewhat similar to the mechanism of diverse protein sorting in the Golgi and ER. The transportation and localization of GTs and glycosidases rely on the presence of a single amino acid (e.g., arginine, lysine, leucine, and phenylalanine residues) in the cytosolic tails of GTs, or several amino acids together determine the localization of GTs. In yeast, the consensus sequence of (F/L)-(L/I/V)-X-X-(R/K) is broadly found in many GTs and has been shown to interact with the cargo receptor Vps74p protein in the assembly of COPI-coated cargo carriers (Figure 2A) [96]. The single mutation of F4 or L5 and the double mutation of K7 and R8 in the FLSKR motif in the cytosolic tail of α 1,2-mannosyltransferase (Kre2p) impaired the protein interaction between vacuolar protein sorting-associated protein 74 (Vsp74) and Kre2p. Thus, the presence of the F4, L5, K7, and R8 residues is required in the Kre2p cargo transportation via the coat complex COPI-coated cargo carriers [96]. In plants, the localization of *A.thaliana* ER-α-mannosidase I (MNS3) depends on the four amino acid sorting signal. MNS3 typically localizes in the early Golgi, and the LPYS Golgi-targeting signal motif in the cytosolic tail of MNS3 is believed to be involved in the retaining mechanism [97]. The fusion protein MNS3-GFP-HDEL contained the GFP and ER-targeting signal HDEL at the C terminal of MNS3 and was primarily localized in the Golgi and weakly in the ER [97]. This indicated that the retrieval function of the ER-target signal HDEL is

inhibited in this fusion protein, and the LPYS Golgi-target signal drives the localization of MNS3. However, the deletion of the LPYS Golgi-target signal and, specifically, the mutation of leucine in the LPYS motif recruited fusion protein, MNS3-GFP-HDEL, to the ER [97], which demonstrates the LPYS Golgi-target signal and primarily the leucine residue is essential for localization of MNS3.

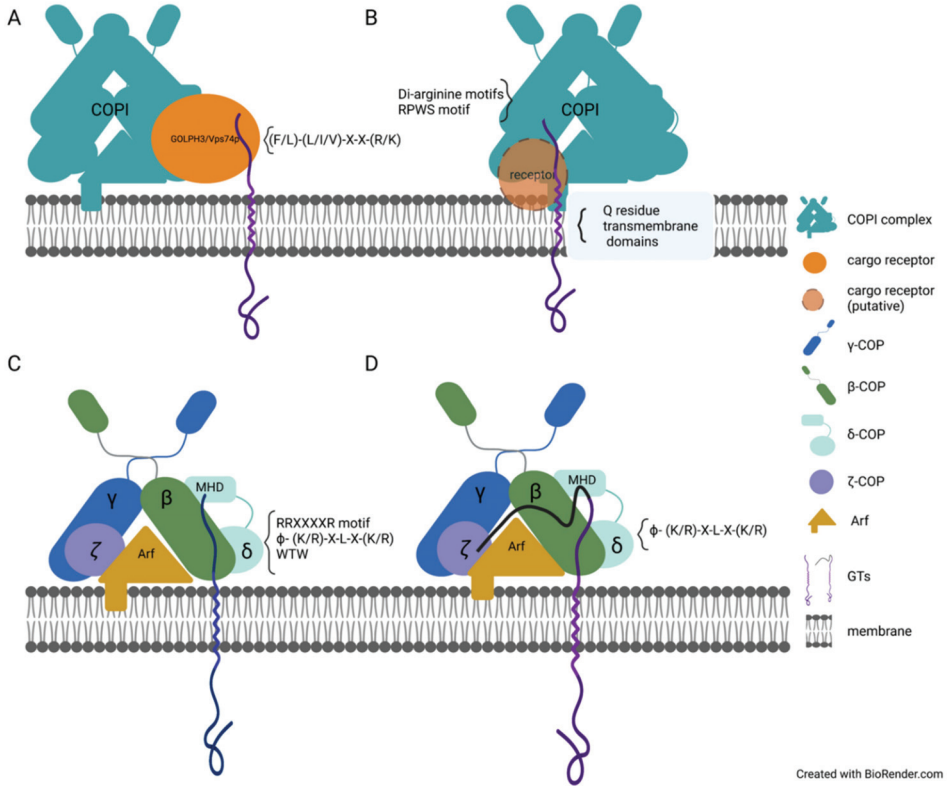

Figure 2. The protein–protein interaction between cargo sorting signal motifs in the GTs and COPI coatomers or cargo receptors. (**A**): The cargo sorting signal motifs in the cytosolic tail of GTs interact with cargo receptors (e.g., Vps74p and GOLPH3). (**B**): The GTs interact with putative cargo receptors or directly interact with the COPI complex via cargo sorting signal motifs in the cytosolic tail and/or TMDs. (**C**): The cargo sorting signal motifs in the cytosolic tail of GTs interact with the MHD domain of *δ*-COP and *β*-COP. (**D**): The cargo sorting signal motifs in the cytosolic tail of GTs interact with the MHD domain of *δ*-COP, *ζ*-COP, and *β*-COP. The figures are created in BioRender.com.

The arginine and lysine residues also play a dominant role in the transportation of GTs in plants and animals. Di-arginine motifs (RR, RXR, or RXXR) are other ER-retaining signals in plants [98]. The first 90 amino acids have been proved to be sufficient to localize *A.thaliana* glucosidase I (AtGCSI) to the ER [99]. The di-arginine motifs (R6R7SAR10GR12) were found in the cytosolic tail of AtGCSI, and the mutation of all four arginine residues altered its ER-localization to the Golgi. In contrast, preserving only one of these di-arginine motifs was sufficient for retaining the AtGCSI protein in the ER and punctate structures [98]. In animals, three isoforms of GM3 synthase (SAT-I), a GT involved in ganglio-series ganglioside synthesis, were discovered and named M1-SAT-I, M2-SAT-I, and M3-SAT-I. Surprisingly, these three isoforms showed different localizations: M2-SAT-I and M3-SAT-I were localized in the Golgi, and M1-SAT-I was found in the ER [100]. The arginine-rich motif RRXXXXR

has proven critical for M1-SAT-I retention in the ER. The single mutation of any arginine in this motif could not change the ER-localization of M1-SAT-I. However, the mutation of any two arginine residues in this arginine-rich motif held M1-SAT-I in the Golgi [100].

In addition to being essential for the ER retention of GTs, the arginine and lysine residues are also involved in the Golgi-targeting of GT and glycosidases in both plant and animal cells. In *N. tabacum*, two arginine residues were found in the cytosolic tail (MR2GYK5FCCDFR11) of Golgi-localized *N. tabacum* GnTI [101]. The mutation of R11 and K5 resulted in GnTI being localized in the ER and the Golgi, while the mutation of R11, K5, and R2 held GnTI predominantly in the ER. However, the mutation of K5 and R2 resulted in GnTI being localized only in the Golgi [101]. These results demonstrate that the arginine residues (R11) proximal to the TMD are essential for retaining GnTI in the Golgi [101]. The lysine residues in the cytosolic tail (MPRKRTLVVN) of *A. thaliana* a-mannosidase II (GMII) are required for Golgi-localization. In contrast, the arginine and lysine residues in the cytosolic tail (MSKRNPKILK) of *A. thaliana* glycosyltransferase XylT are essential for this protein localization in the Golgi [101].

In mammalian cells, the [RK](X)[RK] sequence, as an ER-exit signal, is found in the cytosolic tail of Golgi-localized β-1,3-galactosyltransferase (GalT2) [102]. GalT2 was localized in the ER when the RR motif was mutated [102]. Meanwhile, the replacement of RR to RAR/KAK/KK also held GalT2 in the Golgi, which indicates that the motifs with similar [RK](X)[RK] properties have similar functions [102]. The mutations in the [RK](X)[RK] sequence in the cytosolic tails of β-1,4-*N*-acetyl-galactosaminyltransferase (GalNAcT), GM3 sialyltransferase (Sial-T2), and β1,4Galactosyltransferase (β1,4GT) also altered their Golgi-localization [102]. Meanwhile, there are two [RK](X)[RK] motifs in the cytosolic tail of Golgi-localized Sial-T2, and the mutation of any [RK](X)[RK] motif resulted in the ER-localization of Sial-T2 [102]. The mutation of R7R8 held Sial-T2 in dual localization—the majority of the Sial-T2 proteins localized in Golgi and partial Sial-T2 protein localized in the ER. In contrast, the mutation of R23R25 held Sial-T2 mostly in ER and partially in the Golgi [102]. This indicated that the contribution of the [RK](X)[RK] motif to localization could differ. The conserved sequence "ϕ-K4LLQR8" was critical for the Golgi-localization of GlcNAc-1-phosphotransferase (Ptase). The localization of mutant proteins with the single mutations of the K4/R8/S15 residues did not overlap with the Golgi marker, GOLPH4 [103]. The Golgi-retention signal motif RPWS, which is in the cytosolic tail of UbiA prenyltransferase (UBIAD1), determines the protein localization in the Golgi, and the RPWS signal is highly conserved in its orthologs in different species [104]. The UBIAD1 protein with a mutation of the arginine residue in its RPWS motif failed to retain UBIAD1 in the Golgi [104]. The positive charge and branched structure of the arginine and lysine residues may be significant in the trafficking of GTs. Hence, the sorting signal in the cytosolic tail of GTs determines the localization of GTs.

Arginine-based motifs are broadly involved in the trafficking of GTs and retaining them either in the Golgi or ER. Therefore, the mechanism of recognizing arginine-based motifs as specific to ER or Golgi-target signals is unclear. The distance between the arginine-based motif and lipid bilayer and the distance between the arginine/lysine residues within the motif can affect the function of arginine-based motifs. For example, the ER-localized M1-SAT-I proteins changed localization primarily to Golgi when the amino acids 28-55 on its *N*-terminus were deleted. Such deletion shortened the distance between the ER-target signal RRXXXXR and membrane from 53 amino acids to 25 amino acids, indicating that the function of ER-target signal RRXXXXR in localization of M1-SAT-I requires a long enough functional distance [100]. The change in the distance between the arginine residues within motifs can also alter the localization of plant and mammalian GTs. For instance, increasing the distance between two arginine residues in the cytosolic tail of ER-localized *A.thaliana* AtGCSI recruited this protein to the Golgi or partial Golgi [98]. In addition, shortening or elongating the distance between K4 and R8 in the cytosolic tail of Ptase switched normal Golgi-localization of the Ptase to ER-localization [103].

4. Other Protein Domains Essential for the Trafficking of Enzymes Involved in Glycosylation

Although the cytosolic tail of GTs and glycosidases is critical for their localization [98,101,102], the transmembrane and luminal domains also impact the plant GTs localization. For example, the lumen domain of *A.thaliana* AtGCSI, as well as its di-arginine motifs in the cytosolic tail, affects the ER-localization of AtGCSI; the shortening of the AtGCSI lumen domain results in a switch from its ER-localization to Golgi-localization when the di-arginine motifs are deleted [98], which indicates the di-arginine motifs in the cytosolic tail and lumen domain independently affect the localization of AtGCSI. The *N*-terminus protein sequence of two proteins, Golgi-localized GnTI from *N. benthamiana* and trans-Golgi marker a–2,6-sialyltransferase (ST), are grouped into three parts: the cytosolic tail, the TMD, and the stem region. To study the function of the cytosolic tail, the TMD, and stem region in localization of GnTI and ST, three parts of sequences of two proteins were switched in different types of recombination [105]. The GnTI-ST-GnTI fusion protein generated by swapping the TMD of GnTI with the TMD of ST was mislocalized and unable to function correctly. Conversely, the switching of the cytosolic tail and stem region of GnTI to the cytosolic tail and stem region of ST did not impact the localization of the fusion proteins in the Golgi [105], indicating that the TMD is more critical for the correct localization of GnTI (Figure 2B). The highly conserved sequence (FIYIQ) in the TMD of NtGnTI is responsible for the protein localization in the cis/medial-Golgi [106]. The Q residue in the FIYIQ sequence is conserved, and the mutation of Q25 altered the cis/medial-Golgi localization of NtGnTI to trans-Golgi. In addition, the NtGnTI-Q25A-GFP was detected in the vacuole and occasionally in the apoplast, indicating the secretion of full-length NtGnTI-Q25A or a degradation product [106]. It was also observed that the mutation of Q25 impacted the formation of the homodimer of NtGnTI [106]. In *A.thaliana* GnTI, the Q residue has a similar function. The AtGnTI protein with a mutation on Q23 failed to restore the process of complex *N*-glycans synthesis in the *gntI* mutant plants and was mislocalized to apoplast instead of Golgi [106]. Furthermore, AtGnTI-Q23A-GFP protein was hardly detected on the immunoblot, while its transcript level was comparable with the level of wild-type mRNA. It was also estimated that the half-life of the AtGnTI-Q23A mutant protein was much shorter in comparison with wild-type protein, indicating that AtGnTI-Q23A-GFP is not stable and degrades more quickly [106]. To investigate how the Q residue affects the localization of AtGnTI, the Q23 residue was replaced by either His, Leu, Glu, Tyr, Val, or Ser residues. Only AtGnTI-Q23H was localized in Golgi and showed a result similar to that of the wild-type AtGnTI function when expressed in mutant *A.thaliana gntI* plants [106]. It was determined that the stem region of GnTI contributed predominately to homomeric and heteromeric protein complex formation [105].

In some cases, either the cytosolic tail, TMD, or lumen domain alone cannot determine the localization of GTs, and the cooperation of two domains is frequently required. The cooperation of several GTs domains to determine their localization is broadly reported in mammalian cells, but not much is known about such cooperation in plants. Therefore, below, we describe what is currently known in animals. The polypeptide *N*-acetylgalactosaminyltransferases (GalNAc-T) are type II transmembrane proteins localized in the Golgi. Although GalNAc-T1, GalNAc-T2, GalNAc-T7, and GalNAc-T10 belong to the same GT family, the mechanism that supports their Golgi-localization is different [107]. For example, neither cytosolic tail, TMD, or luminal stem domain could determine the Golgi-localization of Gal-NAc-Ts. It has been shown that GalNAc-T1 and GalNAc-T2 proteins share a similar mechanism where the cooperation of their cytosolic tail and TMD are required to determine their localization. The cytosolic tail or luminal stem together with TMD recruit GalNAc-T7 to the Golgi, whereas the luminal stem and TMD are necessary for the Golgi-localization of GalNAc-T10 [107].

The *N*-acetylglucosamine-1-phosphotransferase (PT) complex is involved in the biosynthesis of mannose 6-phosphate; α-, β-, and γ -subunits are the essential components of the Golgi-localized PT complex [108]. The maturation of α/β-subunits requires cleavage

of the precursor protein. Both versions of the α/β -subunits, precursor and cleaved, were detected in the Golgi. The cleavage of the precursor protein in the Golgi is necessary for the assembly of the PT complex, and the ER-export of the precursor protein of α/β -subunit is a prerequisite of cleavage of α/β -subunit in the Golgi [108]. Thus, the trafficking of precursor protein to the Golgi considerably affects the proper function of the PT complex in the biosynthesis of mannose 6-phosphate. There are four potential ER-export signals in the α/β -subunit precursor protein: di-leucine motif (L5L6) in the *N*-terminus and [RK]X[RK] motifs (K1236RK1238, R1242RR1244, and R1253IR1255) in the *C*-terminus. The double mutation of L5L6 to AA and R1253IR1255 to AAA caused the precursor protein to be recruited to the ER [108], indicating that the ER-export of α/β -subunit precursor protein requires two ER-export signals on its *N*- and C-termini. UBIAD1 is involved in the biosynthesis of vitamin K and CoQ10, and UBIAD1 has eight putative TMDs. The UBIAD1 *N*-terminal domain contains the Golgi-retention signal RPWS, which, together with the first two TMDs, is required for its Golgi-localization [104].

5. Recycling of Glycosyltransferase and Glycosidases Involved in Glycosylation

The transport cargo carriers (i.e., the COPI and COPII complexes) are critical for GTs recycling. It was shown in plants when the *N*-terminal domain of GnTI and Sar1p were co-expressed in *N. benthamiana* leaf epidermal cells, both proteins were co-localized in the punctate structure at ER-exit sites (ERES) [101]. However, a mutant version of GnTI, where basic amino acids within its cytoplasmic tail were mutated, was not able to recruit Sar1 to ERES, indicating that COPII proteins are involved in GnTI transport. Even though the studies about the transport of the plant GTs via the COPI and COPII complexes are limited, the results indicate that the mechanism of membrane proteins transport in plant and mammalian cells are similar. For example, the LxxLE motif functions as the ER-export signal in animals and plants [75,76,109]. Hence, the advanced knowledge about trafficking of GTs via COPI and COPII-coated cargo carriers in animal cells might offer some clues to the GTs transport via COPI and COPII complexes in plants. For example, the silencing of the coatomer subunits δCOP or εCOP results in the mislocalization of the Golgi-resident *A.thaliana* MNS3-GFP protein [97]. During the formation of the COPI and COPII-coated cargo carriers harboring GTs as cargo, indirect or direct interactions between GTs and COPI/COPII complex proteins were observed. For example, the Vps74p protein was detected as the intermediate protein in interaction with the COPI complex in yeast, and the knockout of Vps74p impacted the localization of Kre2p, Mnn2, Mnn9, and Ktr6 [96]. Vps74p was shown to bind to Sec26p (β-COP) and Ret2p (δ-COP) in in vitro experiments (Figure 2A) [96].

In animal cells, the Vps74p ortholog protein GOLPH3 functions similarly to Vps74p in yeast. GOLPH3 binds to C2GnT and SiaTI in vitro, and all three proteins, GOLPH3, C2GnT, and SiaTI, were detected in COPI vesicles [110]. Meanwhile, the knockout of GOLPH3 triggered the mislocalization of C2GnT and SiaTI from ER/Golgi to Golgi only. At the same time, the content of C2GnT and SiaTI in COPI vesicles was significantly decreased [110]. In recent studies, GOLPH3 was proved to interact with not only the LxxR motif but the positively charged amino acids upstream of the LxxR motif, [111], which further confirmed the function of GOLPH3/ Vps74p in retaining the cargo protein in the Golgi cisternae and preventing cargo from leaving to the TGN [111,112]. The protein was transported to lysosomes when it escaped the GOLPH3-mediated cisternal inter-conversion mechanism. This indicated that GOLPH3/ Vps74p controls the lysosomal degradation of the protein [111,112]. The ER-target signal, R11R12XXXXR, in the cytosolic tail of M1-SAT-I has been proven to interact with β-COP or δ-COP (Figure 2C), while the mutation, M1-SAT-I-R11/12S, interrupted this interaction [100]. This indicates that the RR residues may directly bind to β-COP or δ-COP (Figure 2C). The Golgi protein GlcNAc-1-phosphotransferase (Ptase) synthesizes the mannose 6-phosphate recognition marker. The utilization of the recently developed BioID2 assay revealed the interactions among the Ptase, δ-, and ζ-COP subunit proteins [103]. The direct interaction between δ-/ζ-COP and Ptase was confirmed

by pull-down assay, which also detected traces of β-COP and γ-COP (Figure 2D) [103]. It has been shown that Ptase directly binds to the highly reserved sequence, VRFSTE, in the MHD domain of δ-COP [103]. The mutations of K4 to Q, R8 to G, and S15 to Y in the cytosolic tail of Ptase impaired and weakened its interaction with δ-/ζ-COP [103]. The ϕ- (K/R)-X-L-X-(K/R) sequence is also found in the cytosolic tail of other GTs, such as C2GNT1, GALNT3, GALNT6, and GALNT8 [103]. C2GNT1, GALNT3, and GALNT8 directly bind to β-COP, ζ-COP, and the MHD domain of δ-COP (Figure 2D); GALNT6 interacts with β-COP and the MHD domain of δ-COP (Figure 2C) [103]. The arginine residues in the R3TLLR7R8R9 sequence in the cytosolic tail of C2GNT1 are essential for recruiting C2GNT1 to the Golgi. The mutation of arginine residues impaired the interaction between C2GNT1 and ζ-COP protein, and the interaction between C2GNT1 and the MHD domain of δ-COP (Figure 2D) [103]. In previous studies on CHO-K1 cells, C2GNT1 was shown to interact with GOLPH3 and later with COPI subunits [110]. However, in HeLa cells, the knockout of GOLPH3 did not affect the localization of C2GNT1 [103]. UBIAD1 is localized in the Golgi in L02 cells, but UBIAD1 is localized in the ER and the Golgi in both HEK293 and T24 cells [104], which indicates that the mechanism of trafficking of GTs might vary for different cell types. Although there is no ϕ- (K/R)-X-L-X-(K/R) sequence in the cytosolic tail of GALNT4, the WTW motif was found to be responsible for its interaction with the MHD domain of δ-COP and β-COP (Figure 2C) [103]. In addition, the Sar1 protein has been proven to interact with GTs directly. Synthetic cytosolic tails with RR motifs of GalNAcT and GalT2 interacted with Sar1 in vitro. The mutation of RR to AA impaired the interaction between Sar1 and GalT2 or GalNAcT (Figure 3) [102]. The cytosolic tails of GalNAcT and GalT2 bond to Sec23p in vitro, and the presence of active Sar1 increased interaction between GalNAcT or GalT2 with Sec23p [102].

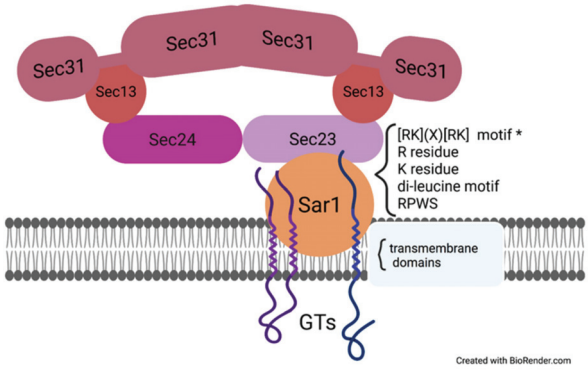

Figure 3. The protein–protein interaction between cargo sorting signal motifs in GTs and COPII coatomers.

In addition to Vps74p and GOLPH3 being shown to affect GT-localization via direct interaction with the COPI complex, other proteins are involved in determining the localization of GTs. The Golgi-localized STELLO1 and STELLO2 proteins (STL1 and STL2) from *A.thaliana*, which contain the glycosyltransferase-like domain, were shown to alter the CesA distribution and assembly via direct interaction with the latter [113]. The genes encoding the STL1 and STL2 proteins were co-expressed together with CesA genes in the *A.thaliana stl1stl2* mutant recovering the cellulose content that was reduced in the *stl1stl2* mutant [113]. In animal cells, the GlcNAcT-I inhibitory protein (GnT1IP) shares a similar protein sequence with GlcNAcT-IV glycosyltransferases and inhibits GlcNAcT-I activity [114]. Two GnT1IP transcripts were named GnT1IP-L and GnT1IP-S, and the GnT1IP-L protein was shown to be the type II membrane protein [114]. GnT1IP-L can interact directly with GlcNAcT-I, causing its mislocalization from the medial-Golgi to the ER, ERGIC, and cis-Golgi [114]. Golgi-resident GRASP55 regulated the subcellular localization of glycosylation protein

involved in glycosphingolipid biosynthesis by direct interaction [115]. The L95LGV98 sequence in the GRASP domain of GRASP55 interacted with the cytosolic tail of GlcCer synthase (GCS), which catalyzes the critical step in glycosphingolipid biosynthesis [115]. The direct binding with GRASP55 promoted the correct subcellular localization of GCS by preventing GCS from entering in the retrograde transportation [115]. The GTP exchange factor GBF1 facilitated the phosphorylation of Arf1-GDP, and the Src tyrosine kinase (Src) played an essential role in the ARF GTP formation [116]. Src phosphorylated the Y876 and Y898 in the GEF domain C-terminus of GBF1, further increasing the binding between GBF1 and Arf1 and the GALNT relocation [116].

6. Protein–Protein Interactions Contribute to GT Trafficking

It was proposed that the protein–protein interactions between plant GTs are required for the ER-export of protein complexes. GAUT1 and GAUT7 are involved in plant cell wall pectin biosynthesis and form a protein complex in the Golgi [35]. The TMD of GAUT1 becomes post-translationally cleaved and, thus, the GAUT1-recruitments to the Golgi require its interaction with GAUT7 [35]. Proteomic analyses of wheat glycosyltransferases involved in the xylan synthesis [117] showed the network of protein–protein interactions among the glycosyltransferases TaGT43-4 and TaGT47-1, mutases TaGT75-3 and TaGT75-4, and the TaVER2 and TaGLP proteins. The protein–protein interactions among TaGT43-4, TaGT47-13, TaGT75-3, and TaGT75-4 were confirmed, and a single complex was detected via immunoblot analysis. TaGT43-4, TaVER2, and TaGLP were localized in the ER when transiently expressed in tobacco leaves, while TaGT47-13 was localized in trans-Golgi, overlapping with ST-GFP trans-Golgi maker [117]. Meanwhile, TaGT43-4 interacted with TaGT47-1, TaGLP, TaVER2, and TaGT75-4 to form heterodimers in the ER, and co-expression with TaGT47-13 recruited these heterodimers to trans-Golgi [117]. Thus, it is proposed that TaGT43-4 functions as a scaffold protein, assisting in forming a xylan biosynthesis complex in the ER [117]. It was proposed that the interaction between TaGT43-4 and TaGT47-13 was required for the xylan-synthesizing protein exportation from the ER to trans-Golgi [117].

In *Asparagus officinalis*, AoIRX14A and AoIRX10 proteins with catalytic DxD motifs are involved in xylan biosynthesis. AoIRX9, AoIRX14A, and AoIRX10 were detected within a single multiprotein complex via the GFP-trap approach [30]. When AoIRX9, AoIRX10, or AoIRX14A were individually expressed in *N.benthamiana* leaves, AoIRX9, and AoIRX10 localized in ER, while AoIRX14A localized in the ER and Golgi [30]. When AoIRX9, AoIRX14A, and AoIRX10 were co-expressed, the signal of AoIRX9-VENUS or AoIRX10-VENUS was detected in the Golgi, and direct protein interactions between AoIRX9 and AoIRX14A were confirmed [30]. These studies strongly suggest that AoIRX9, AoIRX10, and AoIRX14A function as components of the xylan-synthesizing complex, and the protein–protein interaction among these GTs is required for their ER-export.

It is also proposed that ER and Golgi acidic environments impact protein–protein interactions of GTs and, specifically, the formation of homo- and heterocomplexes. For example, the GnT-I, GnT-II, GalT-I, ST3Gal-III, and ST6Gal-I proteins form the homodimers in the ER, and no heterodimers among these GTs have been detected in the ER [118]. Meanwhile, the heterodimers among GTs were detected in Golgi, and the formation of heteromeric GT complexes inhibited the formation of homomers in the Golgi [118]. In the study by Antti Hassinen [119], treatment with chloroquine (CQ) altered the pH in the observed cells, thereby inhibiting the formation of heteromers. The increase in pH by 0.4 in the Golgi inhibited the formation of heteromers and facilitated the formation of homomers. Thus, the difference in pH between the ER and Golgi alters the probability of forming either heteromers or homomers [118].

7. Conclusions

The common mechanism of GTs and glycosidases trafficking between the ER and Golgi involves the motifs or specific amino acids in their cytosolic tails, their TMDs, and catalytic domains. These different factors can act either independently or cooperatively via

directly or indirectly interacting with COP coatomer proteins, ultimately affecting the localization and transportation of GTs and glycosidases (Table 1). The common mechanism of GTs and glycosidases trafficking is similar to the trafficking mechanism of other proteins. Thus, the studies of other protein trafficking mechanisms can offer clues to investigate the potential mechanism for GTs and glycosidases trafficking. Arginine and Lysine residues are commonly found in most GTs and glycosidases and can directly interact with cargo receptors and COP coatomers. The positive charge and branched structure of the arginine and lysine residues are critical in the protein–protein interactions with the cargo receptors and COP coatomers. Some motifs are the ER-retrieval signal and Golgi-retrieval signal, but the mechanism of recognizing and distinguishing these two signaling sequences remains unclear. One possible mechanism might depend on the different positions of these motifs in the structure of GTs and glycosidases, determining the specific type of the retrieval signal. Different isoforms of COP coatomers and cargo receptors recognize these motifs at various positions. For the GTs that lack the motifs and specific amino acids recognized by COP coatomers, the protein–protein interaction with other GTs or cargo proteins is critical to their proper localization. These protein complexes work as a unit of cargo in COP-coated cargo carriers. In addition, the localization and transportation of GTs are regulated by various inhibitors and environmental conditions in the ER/Golgi. The altered distribution of GTs influences the outcome of glycosylation in the ER and Golgi, and ultimately, signal diverse pathways, affecting cell development and growth. In different types of cells, the mechanism for trafficking the identical or homologous GTs can be numerous, affecting the cell differentiation and function differently. As a whole, the proper localization and effective trafficking of GTs and glycosidases are the prerequisites of their proper and efficient functioning. They require broader and intensive investigation to advance our knowledge in this significant field of research.

Table 1. The cargo sorting signals of GTs and glycosidases in their trafficking via COP-dependent transportation.

COPI-Dependent Transportation					
Motif	**Species**	**Interaction with**	**Position**	**GTs**	**Ref.**
(F/L)-(L/I/V)-X-X-(R/K)	Yeast	Vps74p	Cytosolic tail	Kre2, Mnn5, Mnn9, Mnn2, Ktr6	[96]
RRXXXXR	Mouse	β-and/or δ-COP (data not shown)	Cytosolic tail	M1-SAT-I	[100]
Di-arginine motifs/lumen domain	*A.thaliana*	Receptor (putative)	Cytosolic tail/ lumen domain	AtGCSI	[98]
ϕ- (K/R)-X-L-X-(K/R)	Human	β -, ζ-COP and MHD domain of δ-COP	Cytosolic tail	Ptase, C2GNT1, GALNT3, GALNT8	[103]
ϕ- (K/R)-X-L-X-(K/R)	Human	β -COP and MHD domain of δ-COP	Cytosolic tail	GALNT6	[103]
WTW	Human	β -COP and MHD domain of δ-COP	Cytosolic tail	GALNT4	[103]
Q residue	*N. benthamiana*/ *A.thaliana*		TMD	GnTI	[105,106]
	Human	GOLPH3		SiaTI, C2GnT	[110]

Table 1. *Cont.*

COPII-Dependent Transportation					
Motif	Species	Interaction with	Position	GTs	Ref.
RPWS/ first two TMDs	Human	Sar1 (putative)	Cytosolic tail/ TMDs	UBIAD1	[104]
[RK](X)[RK]	Mouse/ Human	Sar1 Sec23p	Cytosolic tail	GalT2, GalNAcT	[102]
RLR	Rat		Cytosolic tail	β1,4GT	[102]
RR, RTR	Chicken		Cytosolic tail	Sial-T2	[102]
R and K residues	*N. tabacum/A.thaliana*		Cytosolic tail	GnTI, XylT, GMII	[101]
Di-leucine motif /[RK]X[RK] motifs	Human		*N*-terminus/C-terminus	Precursor protein of α/β-subunit of PT complex	[108]
Others					
Motif	Species	Interaction with	Position	GTs	Ref.
LPYS	*A.thaliana*		Cytosolic tail	MNS3	[97]
Cytosolic tail or luminal stem and TMDs	Human			GalNAc-T7	[107]
Luminal stem and TMDs	Human			GalNAc-T10	[107]
Cytosolic tail and TMDs	Human			GalNAc-T1, GalNAc-T2	[107]

Author Contributions: N.Z. and O.A.Z. wrote the review. All authors have read and agreed to the published version of the manuscript.

Funding: This research was funded by grants from the National Science Foundation (NSF), grant number NSF-MCB #1856477 (2019-2023) and NSF-PGRP #1951819 (2020–2023).

Institutional Review Board Statement: Not applicable.

Informed Consent Statement: Not applicable.

Data Availability Statement: Not applicable.

Acknowledgments: I would like to thank the support from BioRender.com for helping to create the figures.

Conflicts of Interest: The funders had no role in the design of the study; in the collection, analyses, or interpretation of data; in the writing of the manuscript; or in the decision to publish the results.

References

1. Cantarel, B.L.; Coutinho, P.M.; Rancurel, C.; Bernard, T.; Lombard, V.; Henrissat, B. The Carbohydrate-Active EnZymes database (CAZy): An expert resource for Glycogenomics. *Nucleic Acids Res.* **2009**, *37*, D233–D238. [CrossRef] [PubMed]
2. Lairson, L.L.; Henrissat, B.; Davies, G.J.; Withers, S.G. Glycosyltransferases: Structures, functions, and mechanisms. *Annu. Rev. Biochem.* **2008**, *77*, 521–555. [CrossRef] [PubMed]
3. Zabotina, O.A.; Zhang, N.; Weerts, R. Polysaccharide Biosynthesis: Glycosyltransferases and Their Complexes. [published correction appears in *Front. Plant Sci.* **2021**, *12*, 720709]. *Front. Plant Sci.* **2021**, *12*, 625307. [CrossRef]
4. Yuan, Y.; Barrett, D.; Zhang, Y.; Kahne, D.; Sliz, P.; Walker, S. Crystal structure of a peptidoglycan glycosyltransferase suggests a model for processive glycan chain synthesis. *Proc. Natl. Acad. Sci. USA* **2007**, *104*, 5348–5353. [CrossRef]
5. Nagashima, Y.; von Schaewen, A.; Koiwa, H. Function of N-glycosylation in plants. *Plant Sci.* **2018**, *274*, 70–79. [CrossRef] [PubMed]
6. Varki, A.; Cummings, R.D.; Esko, J.D.; Stanley, P.; Hart, G.W.; Aebi, M.; Darvill, A.G.; Kinoshita, T.; Packer, N.H.; Prestegard, H.H. (Eds.) *Essentials of Glycobiology*, 3rd ed.; Cold Spring Harbor Laboratory Press: Cold Spring Harbor, NY, USA, 2015.

7. Aebi, M. N-linked protein glycosylation in the ER. *Biochim. Biophys. Acta* **2013**, *1833*, 2430–2437. [CrossRef]
8. Li, Y.; Liu, Y.; Zhu, H.; Chen, X.; Tian, M.; Wei, Y.; Gong, Y.; Jiang, J. N-acetylglucosaminyltransferase I promotes glioma cell proliferation and migration through increasing the stability of the glucose transporter GLUT1. *FEBS Lett.* **2020**, *594*, 358–366. [CrossRef]
9. Vanier, G.; Lucas, P.L.; Loutelier-Bourhis, C.; Vanier, J.; Plasson, C.; Walet-Balieu, M.-L.; Tchi-Song, P.C.; Remy-Jouet, I.; Richard, V.; Bernard, S.; et al. Heterologous expression of the N-acetylglucosaminyltransferase I dictates a reinvestigation of the N-glycosylation pathway in Chlamydomonas reinhardtii. *Sci. Rep.* **2017**, *7*, 10156. [CrossRef]
10. Yoo, J.Y.; Ko, K.S.; Vu, B.N.; Lee, Y.E.; Yoon, S.H.; Pham, T.T.; Kim, J.-T.; Lim, J.-M.; Kang, Y.J.; Hong, J.C.; et al. N-acetylglucosaminyltransferase II Is Involved in Plant Growth and Development under Stress Conditions. *Front. Plant Sci.* **2021**, *12*, 761064. [CrossRef]
11. Kadirvelraj, R.; Yang, J.-Y.; Sanders, J.H.; Liu, L.; Ramiah, A.; Prabhakar, P.K.; Boons, G.-J.; Wood, Z.A.; Moremen, K.W. Human N-acetylglucosaminyltransferase II substrate recognition uses a modular architecture that includes a convergent exosite. *Proc. Natl. Acad. Sci. USA* **2018**, *115*, 4637–4642. [CrossRef]
12. Wong, L.-J.; Sheu, K.-F.R.; Lee, S.-L.; Frey, P.A. Galactose-1-phosphate uridylyltransferase: Isolation and properties of a uridylyl-enzyme intermediate. *Biochemistry* **1977**, *16*, 1010–1016. [CrossRef] [PubMed]
13. Garnham, R.; Scott, E.; Livermore, K.E.; Munkley, J. ST6GAL1: A key player in cancer (Review). *Oncol. Lett.* **2019**, *18*, 983–989. [CrossRef] [PubMed]
14. Khoder-Agha, F.; Harrus, D.; Brysbaert, G.; Lensink, M.F.; Harduin-Lepers, A.; Glumoff, T.; Kellokumpu, S. Assembly of B4GALT1/ST6GAL1 heteromers in the Golgi membranes involves lateral interactions via highly charged surface domains. *J. Biol. Chem.* **2019**, *294*, 14383–14393. [CrossRef] [PubMed]
15. Huang, G.; Li, Z.; Li, Y.; Liu, G.; Sun, S.; Gu, J.; Kameyama, A.; Li, W.; Dong, W. Loss of core fucosylation in both ST6GAL1 and its substrate enhances glycoprotein sialylation in mice. *Biochem. J.* **2020**, *477*, 1179–1201. [CrossRef] [PubMed]
16. Yu, M.; Wang, H.; Liu, J.; Qin, H.; Liu, S.; Yan, Q. The sialyltransferase ST3Gal3 facilitates the receptivity of the uterine endometrium in vitro and in vivo. *FEBS Lett.* **2018**, *592*, 3696–3707. [CrossRef] [PubMed]
17. Zhang, X.; Yang, X.; Chen, M.; Zheng, S.; Li, J.; Lin, S.; Wang, X. ST3Gal3 confers paclitaxel-mediated chemoresistance in ovarian cancer cells by attenuating caspase-8/3 signaling. *Mol. Med. Rep.* **2019**, *20*, 4499–4506. [CrossRef] [PubMed]
18. Khoder-Agha, F.; Sosicka, P.; Escriva Conde, M.; Hassinen, A.; Glumoff, T.; Olczak, M.; Kellokumpu, S. N-acetylglucosaminyltransferases and nucleotide sugar transporters form multi-enzyme-multi-transporter assemblies in golgi membranes in vivo. *Cell. Mol. Life Sci.* **2019**, *76*, 1821–1832. [CrossRef]
19. Kellokumpu, S.; Hassinen, A.; Glumoff, T. Glycosyltransferase complexes in eukaryotes: Long-known, prevalent but still unrecognized. *Cell. Mol. Life Sci.* **2016**, *73*, 305–325. [CrossRef]
20. van Tol, W.; Wessels, H.; Lefeber, D.J. O-glycosylation disorders pave the road for understanding the complex human O-glycosylation machinery. *Curr. Opin. Struct. Biol.* **2019**, *56*, 107–118. [CrossRef]
21. Van den Steen, P.; Rudd, P.M.; Dwek, R.A.; Opdenakker, G. Concepts and Principles of O-Linked Glycosylation. *Crit. Rev. Biochem. Mol. Biol.* **1998**, *33*, 151–208. [CrossRef]
22. Joshi, H.J.; Narimatsu, Y.; Schjoldager, K.T.; Tytgat, H.; Aebi, M.; Clausen, H.; Halim, A. SnapShot: O-Glycosylation Pathways across Kingdoms. *Cell* **2018**, *172*, 632. [CrossRef] [PubMed]
23. Yang, W.; Song, A.; Ao, M.; Xu, Y.; Zhang, H. Large-scale site-specific mapping of the O-GalNAc glycoproteome. *Nat. Protoc.* **2020**, *15*, 2589–2610. [CrossRef] [PubMed]
24. Strasser, R.; Seifert, G.; Doblin, M.S.; Johnson, K.L.; Ruprecht, C.; Pfrengle, F.; Bacic, A.; Estevez, J.M. Cracking the "Sugar Code": A Snapshot of N- and O-Glycosylation Pathways and Functions in Plants Cells. *Front. Plant Sci.* **2021**, *12*, 640919. [CrossRef] [PubMed]
25. Lombard, V.; Golaconda Ramulu, H.; Drula, E.; Coutinho, P.M.; Henrissat, B. Arabidopsis β-COP Function Affects Golgi Structure, Plant Growth and Tolerance to Salt. *Nucleic Acids Res.* **2014**, *42*, D490–D495. [CrossRef] [PubMed]
26. Polko, J.K.; Kieber, J.J. The Regulation of Cellulose Biosynthesis in Plants. *Plant Cell* **2019**, *31*, 282–296. [CrossRef]
27. Kumar, M.; Turner, S. Plant cellulose synthesis: CESA proteins crossing kingdoms. *Phytochemistry* **2015**, *112*, 91–99. [CrossRef]
28. Kumar, M.; Mishra, L.; Carr, P.; Pilling, M.; Gardner, P.; Mansfield, S.D.; Turner, S. Exploiting Cellulose Synthase (CESA) Class Specificity to Probe Cellulose Microfibril Biosynthesis. *Plant Physiol.* **2018**, *177*, 151–167. [CrossRef]
29. Speicher, T.L.; Li, P.Z.; Wallace, I.S. Phosphoregulation of the Plant Cellulose Synthase Complex and Cellulose Synthase-Like Proteins. *Plants* **2018**, *7*, 52. [CrossRef]
30. Zeng, W.; Lampugnani, E.R.; Picard, K.; Song, L.; Wu, A.; Farion, I.M.; Zhao, J.; Ford, K.; Doblin, M.S.; Bacic, A. Asparagus IRX9, IRX10, and IRX14A Are Components of an Active Xylan Backbone Synthase Complex that Forms in the Golgi Apparatus. *Plant Physiol.* **2016**, *171*, 93–109. [CrossRef]
31. Wu, A.-M.; Hörnblad, E.; Voxeur, A.; Gerber, L.; Rihouey, C.; Lerouge, P.; Marchant, A. Analysis of the Arabidopsis IRX9/IRX9-L and IRX14/IRX14-L Pairs of Glycosyltransferase Genes Reveals Critical Contributions to Biosynthesis of the Hemicellulose Glucuronoxylan. *Plant Physiol.* **2010**, *153*, 542–554. [CrossRef]
32. Urbanowicz, B.R.; Peña, M.J.; Moniz, H.A.; Moremen, K.W.; York, W.S. Two Arabidopsis proteins synthesize acetylated xylan in vitro. *Plant J.* **2014**, *80*, 197–206. [CrossRef] [PubMed]

33. Culbertson, A.T.; Ehrlich, J.J.; Choe, J.Y.; Honzatko, R.B.; Zabotina, O.A. Structure of xyloglucan xylosyltransferase 1 reveals simple steric rules that define biological patterns of xyloglucan polymers. *Proc. Natl. Acad. Sci. USA* **2018**, *115*, 6064–6069. [CrossRef] [PubMed]
34. Chou, Y.H.; Pogorelko, G.; Zabotina, O.A. Xyloglucan xylosyltransferases XXT1, XXT2, and XXT5 and the glucan synthase CSLC4 form Golgi-localized multiprotein complexes. *Plant Physiol.* **2012**, *159*, 1355–1366. [CrossRef] [PubMed]
35. Atmodjo, M.A.; Sakuragi, Y.; Zhu, X.; Burrell, A.J.; Mohanty, S.S.; Atwood, J.A.; Orlando, R.; Scheller, H.; Mohnen, D. Galacturonosyltransferase (GAUT)1 and GAUT7 are the core of a plant cell wall pectin biosynthetic homogalacturonan:galacturonosyltransferase complex. *Proc. Natl. Acad. Sci. USA* **2011**, *108*, 20225–20230. [CrossRef]
36. Wang, J.; Chen, J.; Enns, C.A.; Mayinger, P. The First Transmembrane Domain of Lipid Phosphatase SAC1 Promotes Golgi Localization. *PLoS ONE* **2013**, *8*, e71112. [CrossRef]
37. Béthune, J.; Wieland, F.T. Assembly of COPI and COPII Vesicular Coat Proteins on Membranes. *Annu. Rev. Biophys.* **2018**, *47*, 63–83. [CrossRef]
38. Arakel, E.C.; Schwappach, B. Formation of COPI-coated vesicles at a glance. [published correction appears in *J. Cell Sci.* **2018**, *131*]. 37073 Göttingen, Germany. *J. Cell Sci.* **2018**, *131*, jcs209890. [CrossRef]
39. Luo, P.M.; Boyce, M. Directing Traffic: Regulation of COPI Transport by Post-translational Modifications. *Front. Cell Dev. Biol.* **2019**, *7*, 190. [CrossRef]
40. Sager, G.; Szul, T.; Lee, E.; Kawai, R.; Presley, J.F.; Sztul, E. Modeling the dynamic behaviors of the COPI vesicle formation regulators, the small GTPase Arf1 and its activating Sec7 guanine nucleotide exchange factor GBF1 on Golgi membranes. *Mol. Biol. Cell* **2021**, *32*, 446–459. [CrossRef]
41. Bui, Q.T.; Golinelli-Cohen, M.P.; Jackson, C.L. Large Arf1 guanine nucleotide exchange factors: Evolution, domain structure, and roles in membrane trafficking and human disease. *Mol. Genet. Genom.* **2009**, *282*, 329–350. [CrossRef]
42. Beck, R.; Adolf, F.; Weimer, C.; Bruegger, B.; Wieland, F.T. ArfGAP1 activity and COPI vesicle biogenesis. *Traffic* **2009**, *10*, 307–315. [CrossRef] [PubMed]
43. Shiba, Y.; Luo, R.; Hinshaw, J.E.; Szul, T.; Hayashi, R.; Sztul, E.; Nagashima, K.; Baxa, U.; Randazzo, P.A. ArfGAP1 promotes COPI vesicle formation by facilitating coatomer polymerization. *Cell. Logist.* **2011**, *1*, 139–154. [CrossRef] [PubMed]
44. Stagg, S.M.; LaPointe, P.; Razvi, A.; Gurkan, C.; Potter, C.S.; Carragher, B.; Balch, W.E. Structural Basis for Cargo Regulation of COPII Coat Assembly. *Cell* **2008**, *134*, 474–484. [CrossRef] [PubMed]
45. Peotter, J.; Kasberg, W.; Pustova, I.; Audhya, A. COPII-mediated trafficking at the ER/ERGIC interface. *Traffic* **2019**, *20*, 491–503. [CrossRef] [PubMed]
46. Fath, S.; Mancias, J.D.; Bi, X.; Goldberg, J. Structure and Organization of Coat Proteins in the COPII Cage. *Cell* **2007**, *129*, 1325–1336. [CrossRef]
47. McCaughey, J.; Stephens, D.J. COPII-dependent ER export in animal cells: Adaptation and control for diverse cargo. *Histochem. Cell Biol.* **2018**, *150*, 119–131. [CrossRef]
48. Melville, D.B.; Studer, S.; Schekman, R. Small sequence variations between two mammalian paralogs of the small GTPase SAR1 underlie functional differences in coat protein complex II assembly. *J. Biol. Chem.* **2020**, *295*, 8401–8412. [CrossRef]
49. Sánchez-Simarro, J.; Bernat-Silvestre, C.; Gimeno-Ferrer, F.; Selvi-Martínez, P.; Montero-Pau, J.; Aniento, F.; Marcote, M.J. Loss of Arabidopsis β-COP Function Affects Golgi Structure, Plant Growth and Tolerance to Salt Stress. *Front. Plant Sci.* **2020**, *11*, 430. [CrossRef]
50. Bernat-Silvestre, C.; De Sousa Vieira, V.; Sanchez-Simarro, J.; Pastor-Cantizano, N.; Hawes, C.; Marcote, M.J.; Aniento, F. p24 Family Proteins Are Involved in Transport to the Plasma Membrane of GPI-Anchored Proteins in Plants. *Plant Physiol.* **2020**, *184*, 1333–1347. [CrossRef]
51. Sánchez-Simarro, J.; Bernat-Silvestre, C.; Aniento, F.; Marcote, M.J. ß-COP mutants show specific high sensitivity to chloride ions. *Plant Signal. Behav.* **2021**, *16*, 1858629. [CrossRef]
52. Gimeno-Ferrer, F.; Pastor-Cantizano, N.; Bernat-Silvestre, C.; Selvi-Martínez, P.; Vera-Sirera, F.; Gao, C.; Perez-Amador, M.A.; Jiang, L.; Aniento, F.; Marcote, M.J. α2-COP is involved in early secretory traffic in Arabidopsis and is required for plant growth. *J. Exp. Bot.* **2017**, *68*, 391–401. [CrossRef] [PubMed]
53. Pastor-Cantizano, N.; Bernat-Silvestre, C.; Marcote, M.J.; Aniento, F. Loss of Arabidopsis p24 function affects ERD2 trafficking and Golgi structure, and activates the unfolded protein response. *J. Cell Sci.* **2018**, *131*, jcs203802. [CrossRef] [PubMed]
54. Cabada Gomez, D.A.; Chavez, M.I.; Cobos, A.N.; Gross, R.J.; Yescas, J.A.; Balogh, M.A.; Indriolo, E. COPI complex isoforms are required for the early acceptance of compatible pollen grains in Arabidopsis thaliana. *Plant Reprod.* **2020**, *33*, 97–110. [CrossRef] [PubMed]
55. Ahn, H.K.; Kang, Y.W.; Lim, H.M.; Hwang, I.; Pai, H.S. Physiological Functions of the COPI Complex in Higher Plants. *Mol. Cells* **2015**, *38*, 866–875. [CrossRef] [PubMed]
56. Min, M.K.; Jang, M.; Lee, M.; Lee, J.; Song, K.; Lee, Y.; Choi, K.Y.; Robinson, D.G.; Hwang, I. Recruitment of Arf1-GDP to Golgi by Glo3p-type ArfGAPs is crucial for golgi maintenance and plant growth. *Plant Physiol.* **2013**, *161*, 676–691. [CrossRef]
57. Pastor-Cantizano, N.; García-Murria, M.J.; Bernat-Silvestre, C.; Marcote, M.J.; Mingarro, I.; Aniento, F. N-Linked Glycosylation of the p24 Family Protein p24δ5 Modulates Retrograde Golgi-to-ER Transport of K/HDEL Ligands in Arabidopsis. *Mol. Plant* **2017**, *10*, 1095–1106. [CrossRef]

58. Montesinos, J.C.; Pastor-Cantizano, N.; Robinson, D.G.; Marcote, M.J.; Aniento, F. Arabidopsis p24δ5 and p24δ9 facilitate Coat Protein I-dependent transport of the K/HDEL receptor ERD2 from the Golgi to the endoplasmic reticulum. *Plant J.* **2014**, *80*, 1014–1030. [CrossRef]
59. Chung, K.P.; Zeng, Y.; Jiang, L. COPII Paralogs in Plants: Functional Redundancy or Diversity? *Trends Plant Sci.* **2016**, *21*, 758–769. [CrossRef]
60. Chang, M.; Wu, S.Z.; Ryken, S.E.; O'Sullivan, J.E.; Bezanilla, M. COPII Sec23 proteins form isoform-specific endoplasmic reticulum exit sites with differential effects on polarized growth. *Plant Cell* **2022**, *34*, 333–350. [CrossRef]
61. Liu, X.; Tong, M.; Zhang, A.; Liu, M.; Zhao, B.; Liu, Z.; Li, Z.; Zhu, X.; Guo, Y.; Li, R. COPII genes SEC31A/B are essential for gametogenesis and interchangeable in pollen development in Arabidopsis. *Plant J.* **2021**, *105*, 1600–1614. [CrossRef]
62. Liang, X.; Li, S.W.; Gong, L.M.; Li, S.; Zhang, Y. COPII Components Sar1b and Sar1c Play Distinct yet Interchangeable Roles in Pollen Development. *Plant Physiol.* **2020**, *183*, 974–985. [CrossRef] [PubMed]
63. Zeng, Y.; Chung, K.P.; Li, B.; Lai, C.M.; Lam, S.K.; Wang, X.; Cui, Y.; Gao, C.; Luo, M.; Wong, K.-B.; et al. Unique COPII component AtSar1a/AtSec23a pair is required for the distinct function of protein ER export in Arabidopsis thaliana. *Proc. Natl. Acad. Sci. USA* **2015**, *112*, 14360–14365. [CrossRef] [PubMed]
64. Aboulela, M.; Nakagawa, T.; Oshima, A.; Nishimura, K.; Tanaka, Y. The Arabidopsis COPII components, AtSEC23A and AtSEC23D, are essential for pollen wall development and exine patterning. *J. Exp. Bot.* **2018**, *69*, 1615–1633. [CrossRef] [PubMed]
65. Zhao, B.; Shi, H.; Wang, W.; Liu, X.; Gao, H.; Wang, X.; Zhang, Y.; Yang, M.; Li, R.; Guo, Y. Secretory COPII Protein SEC31B Is Required for Pollen Wall Development. *Plant Physiol.* **2016**, *172*, 1625–1642. [CrossRef]
66. Li, B.; Zeng, Y.; Cao, W.; Zhang, W.; Cheng, L.; Yin, H.; Wu, Q.; Wang, X.; Huang, Y.; Lau, W.C.Y.; et al. A distinct giant coat protein complex II vesicle population in Arabidopsis thaliana. *Nat. Plants* **2021**, *7*, 1335–1346. [CrossRef] [PubMed]
67. Robinson, D.G.; Brandizzi, F.; Hawes, C.; Nakano, A. Vesicles versus Tubes: Is Endoplasmic Reticulum-Golgi Transport in Plants Fundamentally Different from Other Eukaryotes? *Plant Physiol.* **2015**, *168*, 393–406. [CrossRef] [PubMed]
68. Mironov, A.A. ER-Golgi transport could occur in the absence of COPII vesicles. *Nat. Rev. Mol. Cell Biol.* **2014**, *15*, 1. [CrossRef] [PubMed]
69. Ito, Y.; Uemura, T.; Nakano, A. The Golgi entry core compartment functions as a COPII-independent scaffold for ER-to-Golgi transport in plant cells. *J. Cell Sci.* **2018**, *131*, jcs203893. [CrossRef]
70. Pagant, S.; Wu, A.; Edwards, S.; Diehl, F.; Miller, E.A. Sec24 is a coincidence detector that simultaneously binds two signals to drive ER export. *Curr. Biol.* **2015**, *25*, 403–412. [CrossRef]
71. Chatterjee, S.; Choi, A.J.; Frankel, G. A systematic review of Sec24 cargo interactome. *Traffic* **2021**, *22*, 412–424. [CrossRef]
72. Gomez-Navarro, N.; Miller, E. Protein sorting at the ER-Golgi interface. *J. Cell Biol.* **2016**, *215*, 769–778. [CrossRef] [PubMed]
73. Geva, Y.; Schuldiner, M. The back and forth of cargo exit from the endoplasmic reticulum. *Curr. Biol.* **2014**, *24*, R130–R136. [CrossRef] [PubMed]
74. Sieben, C.; Mikosch, M.; Brandizzi, F.; Homann, U. Interaction of the K(+)-channel KAT1 with the coat protein complex II coat component Sec24 depends on a di-acidic endoplasmic reticulum export motif. *Plant J.* **2008**, *56*, 997–1006. [CrossRef]
75. Mancias, J.D.; Goldberg, J. Structural basis of cargo membrane protein discrimination by the human COPII coat machinery. *EMBO J.* **2008**, *27*, 2918–2928. [CrossRef]
76. Dancourt, J.; Barlowe, C. Protein sorting receptors in the early secretory pathway. *Annu. Rev. Biochem.* **2010**, *79*, 777–802. [CrossRef] [PubMed]
77. Barlowe, C.K.; Miller, E.A. Secretory protein biogenesis and traffic in the early secretory pathway. *Genetics* **2013**, *193*, 383–410. [CrossRef] [PubMed]
78. Dong, C.; Nichols, C.D.; Guo, J.; Huang, W.; Lambert, N.A.; Wu, G. A triple arg motif mediates α(2B)-adrenergic receptor interaction with Sec24C/D and export. *Traffic* **2012**, *13*, 857–868. [CrossRef] [PubMed]
79. Otsu, W.; Kurooka, T.; Otsuka, Y.; Sato, K.; Inaba, M. A new class of endoplasmic reticulum export signal PhiXPhiXPhi for transmembrane proteins and its selective interaction with Sec24C. *J. Biol. Chem.* **2013**, *288*, 18521–18532. [CrossRef]
80. Tang, X.; Zhang, L.; Ma, T.; Wang, M.; Li, B.; Jiang, L.; Yan, Y.; Guo, Y. Molecular mechanisms that regulate export of the planar cell-polarity protein Frizzled-6 out of the endoplasmic reticulum. *J. Biol. Chem.* **2020**, *295*, 8972–8987. [CrossRef]
81. Kumichel, A.; Kapp, K.; Knust, E. A Conserved Di-Basic Motif of Drosophila Crumbs Contributes to Efficient ER Export. *Traffic* **2015**, *16*, 604–616. [CrossRef]
82. Woo, C.H.; Gao, C.; Yu, P.; Tu, L.; Meng, Z.; Banfield, D.K.; Yao, X.; Jiang, L. Conserved function of the lysine-based KXD/E motif in Golgi retention for endomembrane proteins among different organisms. *Mol. Biol. Cell* **2015**, *26*, 4280–4293. [CrossRef] [PubMed]
83. Jackson, L.P.; Lewis, M.; Kent, H.M.; Edeling, M.A.; Evans, P.R.; Duden, R.; Owen, D.J. Molecular Basis for Recognition of Dilysine Trafficking Motifs by COPI. *Dev. Cell* **2012**, *23*, 1255–1262. [CrossRef] [PubMed]
84. Pan, S.; Cheng, X.; Sifers, R.N. Golgi-situated endoplasmic reticulum α-1, 2-mannosidase contributes to the retrieval of ERAD substrates through a direct interaction with γ-COP. *Mol. Biol. Cell* **2013**, *24*, 1111–1121. [CrossRef]
85. Kappeler, F.; Klopfenstein, D.R.; Foguet, M.; Paccaud, J.P.; Hauri, H.P. The recycling of ERGIC-53 in the early secretory pathway. ERGIC-53 carries a cytosolic endoplasmic reticulum-exit determinant interacting with COPII. *J. Biol. Chem.* **1997**, *272*, 31801–31808. [CrossRef] [PubMed]

86. Manzano-Lopez, J.; Perez-Linero, A.M.; Aguilera-Romero, A.; Martin, M.E.; Okano, T.; Silva, D.V.; Seeberger, P.H.; Riezman, H.; Funato, K.; Goder, V.; et al. COPII coat composition is actively regulated by luminal cargo maturation. *Curr. Biol.* **2015**, *25*, 152–162. [CrossRef]
87. Malkus, P.; Jiang, F.; Schekman, R. Concentrative sorting of secretory cargo proteins into COPII-coated vesicles. *J. Cell Biol.* **2002**, *159*, 915–921. [CrossRef]
88. Caldwell, S.R.; Hill, K.J.; Cooper, A.A. Degradation of endoplasmic reticulum (ER) quality control substrates requires transport between the ER and Golgi. *J. Biol. Chem.* **2001**, *276*, 23296–23303. [CrossRef]
89. Belden, W.J.; Barlowe, C. Role of Erv29p in collecting soluble secretory proteins into ER-derived transport vesicles. *Science* **2001**, *294*, 1528–1531. [CrossRef]
90. Barlowe, C.; Helenius, A. Cargo Capture and Bulk Flow in the Early Secretory Pathway. *Annu. Rev. Cell Dev. Biol.* **2016**, *32*, 197–222. [CrossRef]
91. Herzig, Y.; Sharpe, H.J.; Elbaz, Y.; Munro, S.; Schuldiner, M. A systematic approach to pair secretory cargo receptors with their cargo suggests a mechanism for cargo selection by Erv14. *PLoS Biol.* **2012**, *10*, e1001329. [CrossRef]
92. Bräuer, P.; Parker, J.L.; Gerondopoulos, A.; Zimmermann, I.; Seeger, M.A.; Barr, F.A.; Newstead, S. Structural basis for pH-dependent retrieval of ER proteins from the Golgi by the KDEL receptor. *Science* **2019**, *363*, 1103–1107. [CrossRef] [PubMed]
93. Sato, K.; Sato, M.; Nakano, A. Rer1p as common machinery for the endoplasmic reticulum localization of membrane proteins. *Proc. Natl. Acad. Sci. USA* **1997**, *94*, 9693–9698. [CrossRef] [PubMed]
94. Sato, K.; Sato, M.; Nakano, A. Rer1p, a retrieval receptor for ER membrane proteins, recognizes transmembrane domains in multiple modes. *Mol. Biol. Cell* **2003**, *14*, 3605–3616. [CrossRef] [PubMed]
95. Nilsson, T.; Hoe, M.H.; Slusarewicz, P.; Rabouille, C.; Watson, R.; Hunte, F.; Watzele, G.; Berger, E.G.; Warren, G. Kin recognition between medial Golgi enzymes in HeLa cells. *EMBO J.* **1994**, *13*, 562–574. [CrossRef] [PubMed]
96. Tu, L.; Tai, W.C.; Chen, L.; Banfield, D.K. Signal-mediated dynamic retention of glycosyltransferases in the Golgi. *Science* **2008**, *321*, 404–407. [CrossRef] [PubMed]
97. Schoberer, J.; König, J.; Veit, C.; Vavra, U.; Liebminger, E.; Botchway, S.W.; Altmann, F.; Kriechbaumer, V.; Hawes, C.; Strasser, R. A signal motif retains Arabidopsis ER-α-mannosidase I in the cis-Golgi and prevents enhanced glycoprotein ERAD. *Nat. Commun.* **2019**, *10*, 3701. [CrossRef]
98. Boulaflous, A.; Saint-Jore-Dupas, C.; Herranz-Gordo, M.-C.; Pagny-Salehabadi, S.; Plasson, C.; Garidou, F.; Kiefer-Meyer, M.-C.; Ritzenthaler, C.; Faye, L.; Gomord, V. Cytosolic N-terminal arginine-based signals together with a luminal signal target a type II membrane protein to the plant ER. *BMC Plant Biol.* **2009**, *9*, 144. [CrossRef]
99. Saint-Jore-Dupas, C.; Nebenführ, A.; Boulaflous, A.; Follet-Gueye, M.-L.; Plasson, C.; Hawes, C.; Driouich, A.; Faye, L.; Gomord, V. PlantN-Glycan Processing Enzymes Employ Different Targeting Mechanisms for Their Spatial Arrangement along the Secretory Pathway. *Plant Cell* **2006**, *18*, 3182–3200. [CrossRef]
100. Uemura, S.; Yoshida, S.; Shishido, F.; Inokuchi, J. The cytoplasmic tail of GM3 synthase defines its subcellular localization, stability, and in vivo activity. *Mol. Biol. Cell* **2009**, *20*, 3088–3100. [CrossRef]
101. Schoberer, J.; Vavra, U.; Stadlmann, J.; Hawes, C.; Mach, L.; Steinkellner, H.; Strasser, R. Arginine/lysine residues in the cytoplasmic tail promote ER export of plant glycosylation enzymes. *Traffic* **2009**, *10*, 101–115. [CrossRef]
102. Giraudo, C.G.; Maccioni, H.J. Endoplasmic reticulum export of glycosyltransferases depends on interaction of a cytoplasmic dibasic motif with Sar1. *Mol. Biol. Cell* **2003**, *14*, 3753–3766. [CrossRef] [PubMed]
103. Liu, L.; Doray, B.; Kornfeld, S. Recycling of Golgi glycosyltransferases requires direct binding to coatomer. *Proc. Natl. Acad. Sci. USA* **2018**, *115*, 8984–8989. [CrossRef] [PubMed]
104. Wang, X.; Wang, D.; Jing, P.; Wu, Y.; Xia, Y.; Chen, M.; Hong, L. A Novel Golgi Retention Signal RPWS for Tumor Suppressor UBIAD1. *PLoS ONE* **2013**, *8*, e72015. [CrossRef] [PubMed]
105. Schoberer, J.; Liebminger, E.; Vavra, U.; Veit, C.; Castilho, A.; Dicker, M.; Maresch, D.; Altmann, F.; Hawes, C.; Botchway, S.W.; et al. The transmembrane domain of N -acetylglucosaminyltransferase I is the key determinant for its Golgi subcompartmentation. *Plant J.* **2014**, *80*, 809–822. [CrossRef] [PubMed]
106. Schoberer, J.; Liebminger, E.; Vavra, U.; Veit, C.; Grünwald-Gruber, C.; Altmann, F.; Botchway, S.W.; Strasser, R. The Golgi Localization of GnTI Requires a Polar Amino Acid Residue within Its Transmembrane Domain. *Plant Physiol.* **2019**, *180*, 859–873. [CrossRef] [PubMed]
107. Becker, J.L.; Tran, D.T.; Tabak, L.A. Members of the GalNAc-T family of enzymes utilize distinct Golgi localization mechanisms. *Glycobiology* **2018**, *28*, 841–848. [CrossRef]
108. Franke, M.; Braulke, T.; Storch, S. Transport of the GlcNAc-1-phosphotransferase α/β-Subunit Precursor Protein to the Golgi Apparatus Requires a Combinatorial Sorting Motif. *J. Biol. Chem.* **2013**, *288*, 1238–1249. [CrossRef] [PubMed]
109. Chung, K.P.; Zeng, Y.; Li, Y.; Ji, C.; Xia, Y.; Jiang, L. Signal motif-dependent ER export of the Qc-SNARE BET12 interacts with MEMB12 and affects PR1 trafficking in Arabidopsis. *J. Cell Sci.* **2018**, *131*, jcs202838. [CrossRef]
110. Eckert, E.S.; Reckmann, I.; Hellwig, A.; Röhling, S.; El-Battari, A.; Wieland, F.T.; Popoff, V. Golgi Phosphoprotein 3 Triggers Signal-mediated Incorporation of Glycosyltransferases into Coatomer-coated (COPI) Vesicles. *J. Biol. Chem.* **2014**, *289*, 31319–31329. [CrossRef]

111. Rizzo, R.; Russo, D.; Kurokawa, K.; Sahu, P.; Lombardi, B.; Supino, D.; A Zhukovsky, M.; Vocat, A.; Pothukuchi, P.; Kunnathully, V.; et al. Golgi maturation-dependent glycoenzyme recycling controls glycosphingolipid biosynthesis and cell growth via GOLPH3. *EMBO J.* **2021**, *40*, e107238. [CrossRef]
112. Welch, L.G.; Peak-Chew, S.Y.; Begum, F.; Stevens, T.J.; Munro, S. GOLPH3 and GOLPH3L are broad-spectrum COPI adaptors for sorting into intra-Golgi transport vesicles. *J. Cell Biol.* **2021**, *220*, e202106115. [CrossRef] [PubMed]
113. Zhang, Y.; Nikolovski, N.; Sorieul, M.; Vellosillo, T.; McFarlane, H.E.; DuPree, R.; Kesten, C.; Schneider, R.; Driemeier, C.; Lathe, R.; et al. Golgi-localized STELLO proteins regulate the assembly and trafficking of cellulose synthase complexes in Arabidopsis. *Nat. Commun.* **2016**, *7*, 11656. [CrossRef]
114. Huang, H.H.; Stanley, P. A testis-specific regulator of complex and hybrid N-glycan synthesis. *J. Cell Biol.* **2010**, *190*, 893–910. [CrossRef] [PubMed]
115. Pothukuchi, P.; Agliarulo, I.; Pirozzi, M.; Rizzo, R.; Russo, D.; Turacchio, G.; Nüchel, J.; Yang, J.; Gehin, C.; Capolupo, L.; et al. GRASP55 regulates intra-Golgi localization of glycosylation enzymes to control glycosphingolipid biosynthesis. *EMBO J.* **2021**, *40*, e107766. [CrossRef] [PubMed]
116. Chia, J.; Wang, S.C.; Wee, S.; Gill, D.J.; Tay, F.; Kannan, S.; Verma, C.S.; Gunaratne, J.; Bard, F.A. Src activates retrograde membrane traffic through phosphorylation of GBF1. *eLife* **2021**, *10*, e68678. [CrossRef] [PubMed]
117. Jiang, N.; Wiemels, R.E.; Soya, A.; Whitley, R.; Held, M.; Faik, A. Composition, Assembly, and Trafficking of a Wheat Xylan Synthase Complex. *Plant Physiol.* **2016**, *170*, 1999–2023. [CrossRef]
118. Hassinen, A.; Kellokumpu, S. Organizational interplay of Golgi N-glycosyltransferases involves organelle microenvironment-dependent transitions between enzyme homo- and heteromers. *J. Biol. Chem.* **2014**, *289*, 26937–26948. [CrossRef]
119. Hassinen, A.; Pujol, F.M.; Kokkonen, N.; Pieters, C.; Kihlström, M.; Korhonen, K.; Kellokumpu, S. Functional organization of Golgi N- and O-glycosylation pathways involves pH-dependent complex formation that is impaired in cancer cells. *J. Biol. Chem.* **2011**, *286*, 38329–38340. [CrossRef]

plants

MDPI

Communication

Functional Antagonism of WRI1 and TCP20 Modulates *GH3.3* Expression to Maintain Auxin Homeostasis in Roots

Que Kong [1], Pui Man Low [1], Audrey R. Q. Lim [1], Yuzhou Yang [1], Ling Yuan [2] and Wei Ma [1,*]

[1] School of Biological Sciences, Nanyang Technological University, Singapore 637551, Singapore; quekong@ntu.edu.sg (Q.K.); puiman001@e.ntu.edu.sg (P.M.L.); limr0029@e.ntu.edu.sg (A.R.Q.L.); yuzhou001@e.ntu.edu.sg (Y.Y.)

[2] Kentucky Tobacco Research and Development Center, Department of Plant and Soil Sciences, University of Kentucky, Lexington, KY 40546, USA; lyuan3@uky.edu

* Correspondence: weima@ntu.edu.sg

Abstract: Auxin is a well-studied phytohormone, vital for diverse plant developmental processes. The *GH3* genes are one of the major auxin responsive genes, whose expression changes lead to modulation of plant development and auxin homeostasis. However, the transcriptional regulation of these *GH3* genes remains largely unknown. WRI1 is an essential transcriptional regulator governing plant fatty acid biosynthesis. Recently, we identified that the expression of *GH3.3* is increased in the roots of *wri1-1* mutant. Nevertheless, in this study we found that AtWRI1 did not activate or repress the promoter of *GH3.3* (*proGH3.3*) despite of its binding to *proGH3.3*. Cross-family transcription factor interactions play pivotal roles in plant gene regulatory networks. To explore the molecular mechanism by which WRI1 controls *GH3.3* expression, we screened an Arabidopsis transcription factor library and identified TCP20 as a novel AtWRI1-interacting regulator. The interaction between AtWRI1 and TCP20 was further verified by several approaches. Importantly, we found that TCP20 directly regulates *GH3.3* expression via binding to TCP binding element. Furthermore, AtWRI1 repressed the TCP20-mediated transactivation of *proGH3.3*. EMSAs demonstrated that AtWRI1 antagonized TCP20 from binding to *proGH3.3*. Collectively, we provide new insights that WRI1 attenuates *GH3.3* expression through interaction with TCP20, highlighting a new mechanism that contributes to fine-tuning auxin homeostasis.

Keywords: Arabidopsis; gene regulation; protein-protein interaction; transcription factor; WRI1; TCP20

Citation: Kong, Q.; Low, P.M.; Lim, A.R.Q.; Yang, Y.; Yuan, L.; Ma, W. Functional Antagonism of WRI1 and TCP20 Modulates *GH3.3* Expression to Maintain Auxin Homeostasis in Roots. *Plants* **2022**, *11*, 454. https://doi.org/10.3390/plants11030454

Academic Editors: Milan S. Stankovic, Paula Baptista and Petronia Carillo

Received: 11 January 2022
Accepted: 4 February 2022
Published: 7 February 2022

1. Introduction

The phytohormone auxin (indole-3-acetic acid; IAA) plays a pivotal role in plant developmental processes, such as embryogenesis, organogenesis, shoot and root growth, and organ patterning [1–3]. The *Aux/IAA* (AUXIN/INDOLE-3-ACETIC ACID), *SAUR* (small, auxin-induced RNA), and *GH3* (Gretchen Hagen 3) are the major auxin responsive genes [2,4,5]. Changes in *GH3* gene expression affect the plant developmental processes, such as the growth of hypocotyl, root, and shoot [6–9]. The *GH3* gene family in Arabidopsis comprises 20 members [9]. Several *GH3* genes control the formation of IAA-amino acid conjugates which play roles in storing, transporting, compartmentalizing, and metabolizing auxins [7,10]. These findings suggest that GH3s are essential for mediating auxin homeostasis and auxin-associated growth responses [11,12]. A majority of the *GH3* gene promoters have been found to contain *cis*-acting auxin responsive elements (AuxREs) that are recognized by auxin response factors (ARFs) [2,4,13]. In addition, bZIP transcription factors (e.g., Arabidopsis bZIP11) have been found to bind the G-box-related element (GRE) in the *GH3* promoter to activate *GH3* expression [11,14].

2. Results and Discussion

We recently found that the *GH3.3* gene is upregulated in the roots of Arabidopsis *WRINKLED1* (*AtWRI1*) loss-of-function mutant (*wri1-1*) [15]. WRI1 is a member of APETALA2 (AP2) transcription factor family, well known for transcriptional regulation of plant oil accumulation [16,17]. WRI1 functions as a transcriptional activator of genes involved in oil biosynthetic pathways [18–21]. However, how AtWRI1 regulates the expression of *GH3.3* is unclear. *AtWRI1* is differentially expressed in Arabidopsis embryo over other vegetative tissues. *AtWRI1* also displays significant expression in roots [15,16]. Interestingly, although AtWRI1 is able to bind to *proGH3.3* [15], our dual-luciferase (LUC) transactivation assay showed that AtWRI1 did not activate or repress the promoter of *GH3.3* (*proGH3.3*) (Supplementary Figure S1). We hence hypothesized that AtWRI1 regulates the expression of *GH3.3* through the coordination with an alternative transcriptional regulator. To investigate the molecular mechanism by which WRI1 controls *GH3.3* expression, we performed yeast-two-hybrid (Y2H) assay to screen an Arabidopsis transcription factor library [22], using truncated AtWRI1 variants (AtWRI1$^{1\text{-}306}$ and AtWRI1$^{58\text{-}240}$) as baits. The truncated AtWRI1 variants as baits are necessary to avoid high transactivation activity mediated by the C-terminus of AtWRI1 [23]. We identified a class I TEOSINTE BRANCHED1/CYCLOIDEA/ PROLIFERATING CELL FACTOR (TCP) family transcription factor TCP20 as a previously unknown interacting partner of AtWRI1. We confirmed that AtWRI1 physically interacts with TCP20 in yeast cells (Figure 1A). In the pull-down assays, His-tagged TCP20 was pulled down by the GST agarose-coupled AtWRI1 (Figure 1B), providing further evidence for the interaction between AtWRI1 and TCP20. To further validate the AtWRI1-TCP20 interaction in vivo, we conducted bimolecular fluorescence complementation (BiFC) assays by co-producing the split YFP fusions of the two proteins, nYFP-AtWRI1 and cYFP-TCP20, in *Nicotiana benthamiana* leaves. We detected YFP fluorescence in leaf samples that co-produced nYFP-AtWRI1 and cYFP-TCP20 (Figure 1C). Taken together, our results verified the physical interaction between AtWRI1 and TCP20.

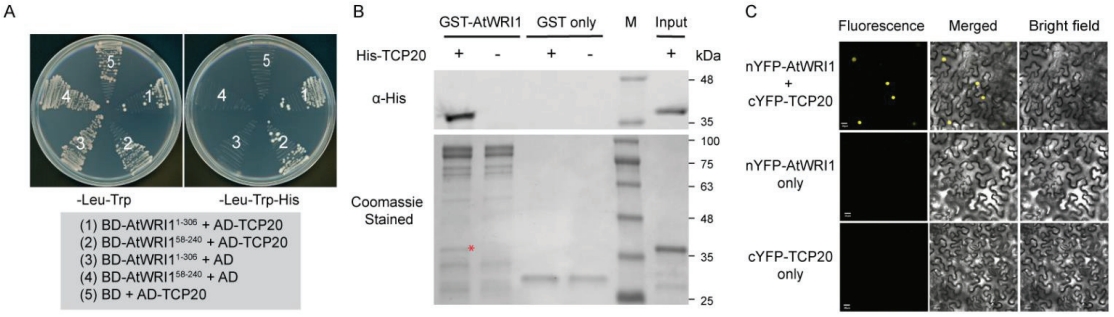

Figure 1. Physical interaction of AtWRI1 with TCP20. (**A**) TCP20 interacts with AtWRI1 variants in yeast cells. Yeast growth on either permissive (-Leu/-Trp) or stringent selective (-Leu/-Trp/-His) medium was shown. The numbers in the plates indicate the co-expression of DNA binding domain (BD) fusions of AtWRI1 with varied amino acid length and activation domain (AD)-TCP20 fusion (indicated in shaded box). (**B**) GST pull-down assay showing the interaction of TCP20 with AtWRI1. The bottom panel shows Coomassie blue stained SDS-PAGE gel of GST pull-down using *E. coli* expressed protein. Red asterisk indicates the pull-down product of His-TCP20 that has identical molecular mass as the purified His-TCP20 in the far-right lane. The upper panel shows the immunoblotting of the pull-down products using anti-His antibody, verifying the presence of the His-TCP20. (**C**) A BiFC assay showing the physical interaction of AtWRI1 with TCP20 in plant cells. Confocal images show *N. benthamiana* epidermal cells transiently co-producing nYFP-AtWRI1 and cYFP-TCP20. Scale bar is 20 μM.

Previous studies show that TCP20 is highly expressed in Arabidopsis roots to regulate numerous genes that are important for plant development and signaling pathways [24–26]. However, the molecular mechanism underlying TCP20 working with AtWRI1 to regulate *GH3.3* expression remains unknown. We thus analyzed *proGH3.3* and found four putative TCP binding motifs in the promoter (Supplementary Figure S2). To test whether TCP20 binds to *proGH3.3*, we synthesized four DNA probes (Probe 1–4), each containing an individual putative TCP binding motif with flanking sequences on both sides (Figure 2A and Supplementary Figure S2) and performed electrophoretic mobility shift assay (EMSA) using TCP20 protein. Our result showed that TCP20 bound to all four DNA probes (probe 1–4; Figure 2A); however, TCP20 failed to bind to the DNA probes with nucleotide mutations at the TCP20 binding element (probe 1M–4M; Figure 2A), implying the binding specificity to the TCP motifs in the *proGH3.3*. To explore the transcriptional regulation of *GH3.3* by TCP20, we subsequently characterized two homozygous Arabidopsis *tcp20* T-DNA insertional lines (*tcp20-2* (SALK_088460) and *tcp20-4* (SALK_041906)). We examined the expression of *GH3.3* in roots of *tcp20* loss-of-function mutants and found significant downregulation of *GH3.3* in both lines compared to wild-type (WT) (Figure 2B). We also examined the transactivation of TCP20 on *proGH3.3* using dual-LUC transient expression assay in *N. benthamiana* leaves (Figure 2C). TCP20 significantly activated the *LUC* expression driven by *proGH3.3* in the transient assay (Figure 2D). Taken together, these results indicate that TCP20 directly regulates *GH3.3* expression through binding to the TCP binding motifs in its promoter.

We next examined whether the transactivation activity of TCP20 on *proGH3.3* is attenuated by interaction with AtWRI1. The reporter vector, in which the *LUC* gene expression is driven by *proGH3.3*, was transformed into *N. benthamiana* leaves, alone or in combination with the effectors in which *TCP20* or *AtWRI1* is controlled by the *CaMV* 35S promoter (Figure 3A). While TCP20 significantly activated *proGH3.3*, the activation was greatly reduced when *AtWRI1* was co-expressed (Figure 3B), suggesting that AtWRI1 antagonizes TCP20 upon the interaction. We also conducted a promoter deletion assay to identify the regions in *proGH3.3* critical for TCP20-AtWRI1 mediated expression. We generated three 5′-deletions in *proGH3.3-LUC* (Supplementary Figure S3). The full-length and truncated *proGH3.3-LUC* were transformed into *N. benthamiana* leaves alone, with *AtWRI1*, or with *AtWRI1* and *TCP20*. The 1 kb deletion (from −1940 to −941 bp including one TCP binding motif) caused a significant reduction of LUC activity compared to the full-length promoter (Supplementary Figure S3). The 1.5 kb deletion (from −1940 to −441 bp) did not result in additional loss of activity compared to the 1 kb deletion. When all TCP binding motifs were deleted (−80 bp), less than 10% of the activity remained compared to the full-length promoter. In all cases except the −80 deletion, co-expression of *TCP20* and *AtWRI1* significantly reduced the transactivation of *proGH3.3* by TCP20 (Supplementary Figure S3). These results indicated that the deletion of motif 4 resulted in approximately 70% reduction of TCP20 activation, although the activation of the promoter fragment containing motifs 1–3 was still 15-fold higher than the reporter-alone control. Further removal of motifs 1–3 greatly reduced the activation and abolished the antagonizing effect of AtWRI1. Therefore, while motif 4 contributes most to the TCP20-mediated activation, all four TCP binding motifs contribute to the TCP20 regulation of *proGH3.3*. This conclusion is consistent with the EMSA results showing TCP20 binding to all four TCP binding motifs (Figure 2A).

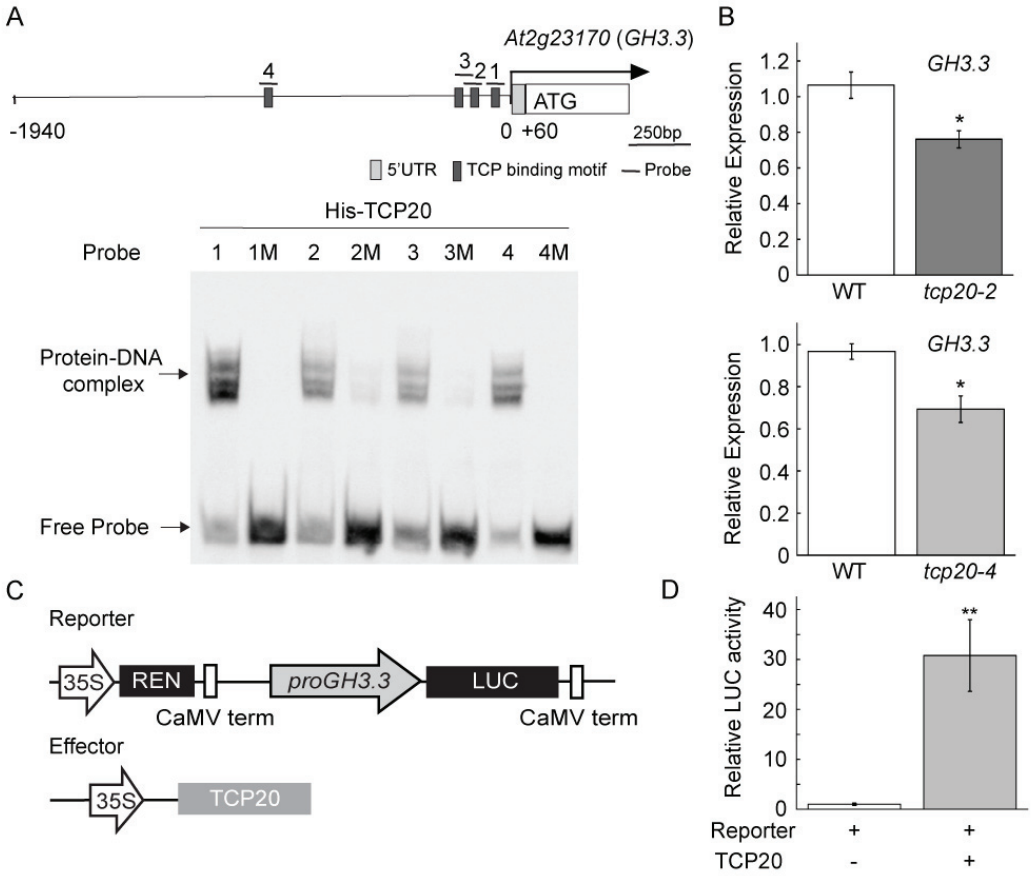

Figure 2. Direct promoter binding and regulation of *GH3.3* by TCP20. (**A**) EMSA showing TCP20 binding to the TCP binding motifs in the *GH3.3* promoter (*proGH3.3*). As indicated in the schematic representation of *proGH3.3*, four biotin-labelled DNA probes (dark boxes indicated by underlined numbers 1–4), containing consensus TCP binding motifs, and their corresponding mutant (M) probes (Supplementary Figure S2) were used for EMSA experiments to test the interaction with purified His-TCP20 protein. The shifted DNA-protein complexes are indicated by an arrow. (**B**) Quantitative real-time PCR (qRT-PCR) analysis of *GH3.3* transcript in the roots of wild-type (WT), *tcp20-2* (SALK_088460), and *tcp20-4* (SALK_041906) mutants. Results are shown as means ± SE (n = 3). "*" indicates a significant difference ($p < 0.05$, Student's t-test) compared with WT. (**C**) Schematic representation of the constructs used in a transient expression assay in *N. benthamiana* leaves. The *LUC* reporter gene was driven by a 2kb *proGH3.3*. The *Renilla* luciferase (*REN*) reporter gene was controlled by the *CaMV* 35S promoter. (**D**) Transactivation of the *LUC* reporter by TCP20 in *N. benthamiana* leaves. Relative reporter activity in *N. benthamiana*, infiltrated either using the reporter alone or in combination with the effector, was shown. The LUC activity was normalized to the REN activity. Results are shown as means ± SE (n = 5–6). "**" indicates a significant difference ($p < 0.01$, one-way ANOVA) between reporter alone and co-transformation of TCP20 and reporter.

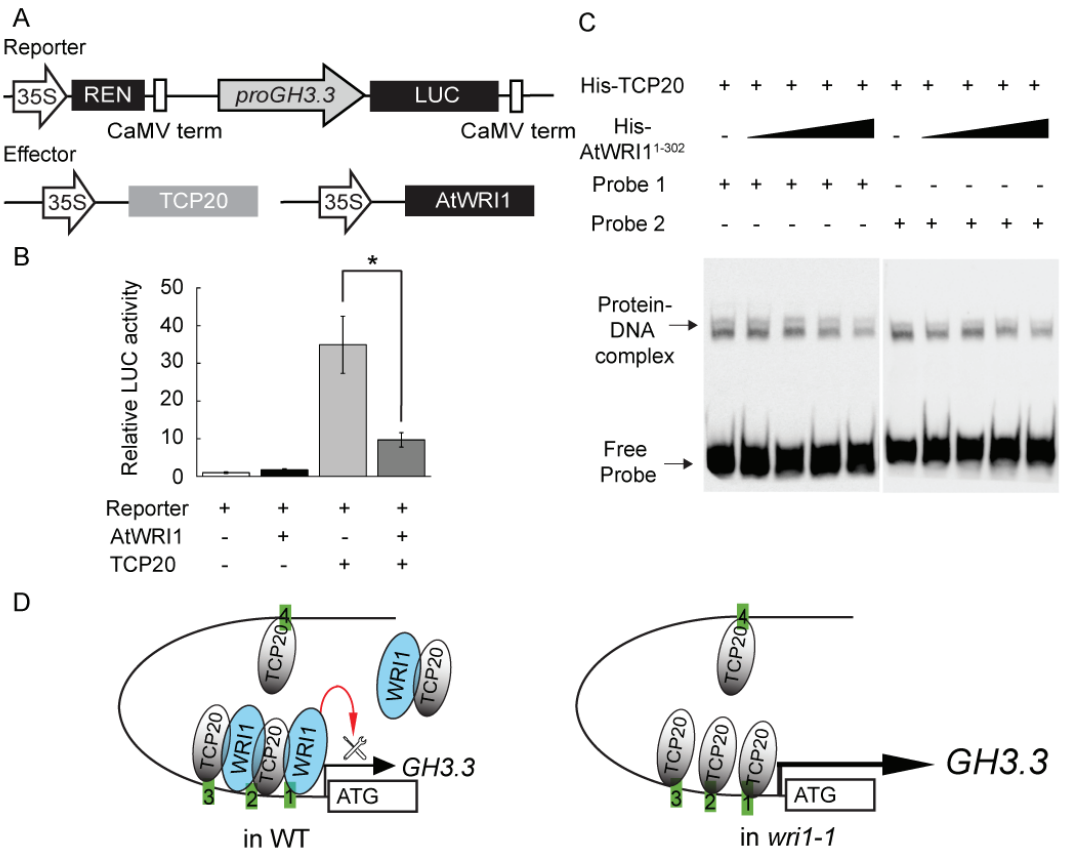

Figure 3. Interference of TCP20 binding to *proGH3.3* by AtWRI1. (**A**) Schematic representation of the constructs used in a transient expression assay in *N. benthamiana*. (**B**) Co-expression of *AtWRI1* with *TCP20* repressed the transactivation activity of TCP20 on *proGH3.3*. Results are shown as means ± SE (n = 5–6). "*" indicates a significant difference ($p < 0.05$, Student's t-test) between sole expression of *TCP20* and co-expression of *AtWRI1* with *TCP20* as indicated. (**C**) EMSA demonstrated the TCP20 binding to *proGH3.3* fragments (probe 1 and 2; also see Supplementary Figure S2) in the presence of increasing amount of AtWRI1$^{1-302}$ (0.53, 0.71, 1.06, and 2.12 pmol, respectively). The decreasing amount of the protein-DNA complex is indicated by an arrow. (**D**) A proposed model for co-regulation of *GH3.3* expression by TCP20 and WRI1. TCP20 activates *GH3.3* expression by direct binding to *proGH3.3*; however, the activation is attenuated by WRI1 through 1) co-occupation of the promoter and 2) formation of a possible non-DNA binding heterodimer. In any case, the TCP20-AtWRI1 complex exhibits reduced TCP20 target transactivation activity because of the TCP20-AtWRI1 interaction. Hence, in WT, WRI1 fine-tunes TCP20 activation of *GH3.3*, whereas in *wri1-1* that lacks WRI1, TCP20 exhibits stronger activation of *GH3.3* (represented by thicker arrow and increased size of *GH3.3*) compared to WT.

We demonstrated AtWRI1 attenuating the TCP20 activity on *proGH3.3* possibly by interacting sequestering TCP20. Our previous work shows the binding of AtWRI1 to *proGH3.3*. Additionally, WRI1 did not activate or repress *proGH3.3* in a transactivation assay suggesting that WRI1 likely requires a partner to function [15]. We therefore investigated whether AtWRI1 antagonizes TCP20 from binding to *proGH3.3* in EMSA. The results revealed that AtWRI1 bound to probes 1, 2, and 3 in a TCP binding site-independent manner, as AtWRI1 bound the mutant probes (1M, 2M, and 3M) with equal affinity as the

WT probes (Supplementary Figure S4). Since there is no recognizable WRI1 binding motif AW-box found in probes 1–3, AtWRI1 likely recognizes cryptic motifs that are close to the TCP binding motifs. Moreover, upon the addition of an increasing amount of AtWRI1$^{1\text{-}302}$, we detected reduced binding of TCP20 to probe 1 and 2 (Figure 3C), but not probe 3 and 4 (Supplementary Figure S5A), in a dose-dependent manner (Supplementary Figure S5B). We therefore speculate that AtWRI1 antagonizes the function of TCP20 through two potential mechanisms: 1) both transcription factors co-occupy *proGH3.3*, resulting in reduced activity of TCP20, and 2) the AtWRI1-TCP20 heterodimer reduces the amount of free TCP20 to activate *proGH3.3* (Figure 3D). In the absence of AtWRI1, e.g., in *wri1-1* mutant, *GH3.3* is significantly upregulated (Figure 3D), leading to the increased production of IAA-Asp conjugates.

TCP20 is known to be involved in cell division, immunity, jasmonic acid biosynthesis, and nitrate foraging [27–29]. The regulation of auxin-responsive gene expression in this study defines a new role for TCP20 in Arabidopsis. Prior to this work, it was unclear how AtWRI1 affected auxin homeostasis through regulation of *GH3.3* expression. By demonstration of the direct binding of both AtWRI1 and TCP20 to *proGH3.3* and the protein-protein interaction of the two factors, we elucidate a previously unknown mechanism by which AtWRI1 antagonized the activity of TCP20 on *GH3.3* to modulate auxin homeostasis.

3. Materials and Methods

3.1. Plant Materials

Arabidopsis and *N. benthamiana* plants were grown in a growth chamber at 23 °C with a photoperiod of 16 h light (100–150 μmol m^{-2} s^{-1} illumination)/8 h dark. Arabidopsis wild-type (Columbia ecotype) was used in this work. Seeds of the *tcp20-2* (SALK_088460) and *tcp20-4* (SALK_041906) mutants, which have been previously described [26], were obtained from the Arabidopsis Biological Resource Center (ABRC). Genotyping assay was conducted to confirm the homozygosity of *tcp20-2* and *tcp20-4* mutants. Reverse transcription-polymerase chain reaction assay was subsequently conducted to verify that the *TCP20* expression was disrupted in *tcp20-2* and *tcp20-4* mutants. Seed sterilization and germination were performed as previously described [30].

3.2. Bioinformatic Analysis

In silico analysis of TCP binding sites was performed using AthaMap [31].

3.3. Plasmid Construction

Entry constructs subcloning and recombination with destination vectors [Y2H vectors, BiFC vectors (pSITE-nEYFP-C1 and pSITE-cEYFP-C1 [32]), and pEarleyGate binary vectors [33] were via Gateway LR reactions (Life Technologies, Waltham, MA, USA). To generate constructs for epitope-tagged recombinant protein production in *E. coli*, the full-length *AtWRI1* and *TCP20* were sub-cloned into pET41a-GST and pET41a-6×His vectors, respectively, [34]. *AtWRI1*$^{1\text{-}302}$ was sub-cloned into pNIC28-Bsa4 to produce an N-terminal 6×His-tagged protein (Protein Production Platform, Nanyang Technological University). To generate *proGH3.3:LUC* reporter constructs, various lengths of PCR amplified *proGH3.3* were subcloned into the pGreenII 0800-LUC vector [35]. A list of the primers used for plasmid construction in this study is provided in Table S1.

3.4. Yeast Two-Hybrid Assay (Y2H)

For screening Arabidopsis transcription factor library, transcription factors were sub-cloned into the pDEST22 vector (prey) and transformed into yeast strain Y187 (Clontech, San Jose, CA, USA). *AtWRI1* (*AtWRI1*$^{1\text{-}306}$ and *AtWRI1*$^{58\text{-}240}$) variants were sub-cloned into pDEST32 vector (bait) and introduced into yeast strain AH109. The prey and bait were mated and spotted on permissive (-Leu/-Trp) medium. After 3 days, the colonies were streaked onto stringent selective (-Leu/-Trp/-His) medium to screen positive interactions. *TCP20* was subcloned into pDEST22 as the prey and *AtWRI1* variants were subcloned into

pDEST32 as the bait. The prey and bait constructs were transformed into Y187 and AH109, respectively. Then the prey and bait were mated and plated on -Leu/-Trp medium. To evaluate the interaction, transformants were streaked onto stringent selective (-Leu/-Trp/-His) medium.

3.5. Transient Expression in N. benthamiana, BiFC, and Confocal Microscopy

For BiFC assay, *Agrobacterium tumefaciens* cells carrying the nYFP and cYFP fusion constructs were resuspended in MMA medium (10 mM $MgCl_2$, 10 mM MES, 100 μM acetosyringone) to an OD_{600} of 1.2 and adjusted to an OD_{600} of 0.4 before infiltration into *N. benthamiana* leaves. The plasmid pEAQ HT producing the P19 protein was co-infiltrated with other constructs to maintain high expression in *N. benthamiana* leaves [36]. Healthy leaves of *N. benthamiana* plants were infiltrated with *A. tumefaciens* suspensions carrying nYFP and cYFP fusion constructs using a 1 mL blunt-end syringe. After agroinfiltration, plants were placed in a growth chamber. YFP fluorescence signals were detected by a confocal microscope 2–3 days post agroinfiltration.

3.6. Recombinant Protein Production, In Vitro Pull-Down Assays, and EMSA

Recombinant proteins, including the GST-AtWRI1 variants and His-TCP20, were produced in *E coli* strain BL21 (DE3). Protein induction, extraction and purification were conducted as described previously [23,34]. For in vitro pull-down assay, purified His-TCP20 protein was incubated with GST beads coupled with purified GST-AtWRI1 or GST protein in binding buffer [20 mM Tris-HCl (pH 7.4), 150 mM NaCl, 1 mM DTT, 0.1 mM EDTA (pH 8.0), 0.1% IGEPAL CA-630] at 4 °C overnight, followed by washing for 5 times with washing buffer (same as binding buffer). Then the samples were boiled in SDS-PAGE sample buffer at 95 °C for 5 min, followed by SDS-PAGE. The proteins were detected by immunoblot probed with anti-His antibody (Proteintech, Rosemont, IL, USA). EMSA was performed as described previously [34]. In brief, the 5′end biotin-labeled WT probes (1–4) and mutated probes (1M–4M) were used for EMSA. The standard binding reaction (20 μL) contained 0.05 μg/μL poly(dI-dC), 15 mM HEPES-KOH (pH 7.5), 7.5 mM KCl, 0.5 mM EDTA, 5% glycerol, 2 mM dithiothreitol, 1 μg/μL BSA, 2 fmol/μL of the hot DNA probe and ~1 pmol of His-TCP20. The binding competition assays were performed using ~1 pmol of His-TCP20 with addition of His-AtWRI1$^{1\text{-}302}$ as described in the figure legend. The reaction mixture was incubated at room temperature for 30 min. The DNA-protein complexes were resolved on 5% (*w*/*v*) non-denaturing polyacrylamide gels and subsequently transferred to nylon membranes. The band shifts were detected by a chemiluminescent nucleic acid detection module (Thermo Fisher Scientific, Waltham, MA, USA).

3.7. RNA Extraction, Quantitative Real-Time PCR (qRT-PCR)

Roots from 1-week-old Arabidopsis seedlings grown vertically on the regular growth medium were harvested, immediately frozen in liquid nitrogen, and stored at −80 °C freezer until use for RNA extraction. Total RNA was extracted using the Monarch Total RNA Miniprep Kit (New England Biolabs, Ipswich, MA, USA) following the supplier's instructions. First-strand cDNA was synthesized using the qScript cDNA Synthesis Kit (Quantabio, Beverly, MA, USA). Quantitative real-time PCR (qRT-PCR) was conducted using Luna Universal qPCR Master Mix (New England Biolabs, Ipswich, MA, USA) according to the supplier's instructions. *Isopentenyl pyrophosphate:dimethylallyl pyrophosphate isomerase 2 (IPP2)* gene was used as an internal control to normalize the gene expression. The primers used for qRT-PCR is provided in Table S2.

3.8. Transient Dual-Luciferase (Dual-LUC) Assays

Transient dual-LUC assays in *N. benthamiana* were conducted as described previously [37,38], with minor modifications. After agroinfiltration, plants were placed in a plant growth chamber, and leaf samples were harvested 3 d after infiltration for the dual-LUC assay using Dual-Luciferase Reporter 1000 Assay System (Promega, Madison, WI, USA).

In brief, three leaf discs at agroinfiltration areas (5–6 mm in diameter) were excised and ground in liquid nitrogen to fine powder and homogenized in 100 µL Passive Lysis buffer (Promega, Madison, WI, USA). Subsequently, 5 µL of the extract was mixed with 40 µL Luciferase Assay Buffer, and the firefly LUC activity was measured by a cell imaging multi-mode plate reader (BioTek Cytation 5, Santa Clara, CA, USA). The reaction was stopped by addition of 40 µL Stop and Glo Buffer (Promega, Madison, WI, USA), and the Renilla (REN) LUC activity was measured. The firefly LUC activity was normalized to the REN LUC activity.

3.9. Accession Numbers

Accession numbers are as following: WRI1 (AT3G54320), TCP20 (AT3G27010), GH3.3 (AT2G23170).

Supplementary Materials: The following supporting information can be downloaded at: https://www.mdpi.com/article/10.3390/plants11030454/s1. Figure S1. Transactivation of the firefly luciferase (LUC) reporter by AtWRI1. Figure S2. In silico analysis of TCP binding sites in *proGH3.3*. Figure S3. The transactivation activity of TCP20 on the *proGH3.3* deletion fragments in *N. benthamiana* leaves. Figure S4. Examination of AtWRI1 binding to *proGH3.3* fragments that are also recognized by TCP20. Figure S5. Effects of AtWRI1 on TCP20 binding to *proGH3.3*. Table S1. Primers used for plasmid construction in this study. Table S2. Primers used for quantitative real-time PCR (qRT-PCR) in this study.

Author Contributions: Q.K. and W.M. conceived and designed the experiments. Q.K., P.M.L., A.R.Q.L. and Y.Y. performed the experiments. Q.K., L.Y. and W.M. analyzed the data. Q.K., L.Y. and W.M. wrote the manuscript. All authors have read and agreed to the published version of the manuscript.

Funding: This work was supported by a Nanyang Technological University Startup grant to W.M. and a Ministry of Education (MOE) of Singapore Tier 1 to W.M. (grant number: RG140/18).

Data Availability Statement: All data supporting the findings of this study are available within the paper and within its Supplementary Materials published online.

Acknowledgments: We thank Michael Thomashow (Michigan State University) for the Arabidopsis transcription factor library, Hao Yu and Chengxiang Li (National University of Singapore) for the vector of dual-luciferase assay, and Sitakanta Pattanaik (University of Kentucky) for critical reading of the manuscript. We also thank the NTU Protein Production Platform for His-AtWRI1$^{1\text{-}302}$ protein expression and purification for the EMSA experiment.

Conflicts of Interest: The authors declare no conflict of interest.

References

1. Zhao, Y. Auxin biosynthesis and its role in plant development. *Annu. Rev. Plant Biol.* **2010**, *61*, 49–64. [CrossRef] [PubMed]
2. Woodward, A.W.; Bartel, B. Auxin: Regulation, action, and interaction. *Ann. Bot.* **2005**, *95*, 707–735. [CrossRef] [PubMed]
3. Lavy, M.; Estelle, M. Mechanisms of auxin signaling. *Development* **2016**, *143*, 3226–3229. [CrossRef] [PubMed]
4. Hagen, G.; Guilfoyle, T. Auxin-responsive gene expression: Genes, promoters and regulatory factors. *Plant Mol. Biol.* **2002**, *49*, 373–385. [CrossRef]
5. Paponov, I.A.; Paponov, M.; Teale, W.; Menges, M.; Chakrabortee, S.; Murray, J.A.; Palme, K. Comprehensive transcriptome analysis of auxin responses in Arabidopsis. *Mol. Plant* **2008**, *1*, 321–337. [CrossRef]
6. Nakazawa, M.; Yabe, N.; Ichikawa, T.; Yamamoto, Y.Y.; Yoshizumi, T.; Hasunuma, K.; Matsui, M. DFL1, an auxin-responsive GH3 gene homologue, negatively regulates shoot cell elongation and lateral root formation, and positively regulates the light response of hypocotyl length. *Plant J.* **2001**, *25*, 213–221. [CrossRef]
7. Park, J.E.; Park, J.Y.; Kim, Y.S.; Staswick, P.E.; Jeon, J.; Yun, J.; Kim, S.Y.; Kim, J.; Lee, Y.H.; Park, C.M. GH3-mediated auxin homeostasis links growth regulation with stress adaptation response in Arabidopsis. *J. Biol. Chem.* **2007**, *282*, 10036–10046. [CrossRef]
8. Khan, S.; Stone, J.M. Arabidopsis thaliana GH3.9 influences primary root growth. *Planta* **2007**, *226*, 21–34. [CrossRef]
9. Takase, T.; Nakazawa, M.; Ishikawa, A.; Manabe, K.; Matsui, M. DFL2, a new member of the Arabidopsis GH3 gene family, is involved in red light-specific hypocotyl elongation. *Plant Cell Physiol.* **2003**, *44*, 1071–1080. [CrossRef]
10. Staswick, P.E.; Serban, B.; Rowe, M.; Tiryaki, I.; Maldonado, M.T.; Maldonado, M.C.; Suza, W. Characterization of an Arabidopsis enzyme family that conjugates amino acids to indole-3-acetic acid. *Plant Cell* **2005**, *17*, 616–627. [CrossRef]

11. Weiste, C.; Droge-Laser, W. The Arabidopsis transcription factor bZIP11 activates auxin-mediated transcription by recruiting the histone acetylation machinery. *Nat. Commun.* **2014**, *5*, 3883. [CrossRef] [PubMed]
12. Chapman, E.J.; Estelle, M. Mechanism of auxin-regulated gene expression in plants. *Annu. Rev. Genet.* **2009**, *43*, 265–285. [CrossRef] [PubMed]
13. Guilfoyle, T.J.; Hagen, G. Auxin response factors. *Curr. Opin. Plant Biol.* **2007**, *10*, 453–460. [CrossRef] [PubMed]
14. Heinekamp, T.; Strathmann, A.; Kuhlmann, M.; Froissard, M.; Muller, A.; Perrot-Rechenmann, C.; Droge-Laser, W. The tobacco bZIP transcription factor BZI-1 binds the GH3 promoter in vivo and modulates auxin-induced transcription. *Plant J.* **2004**, *38*, 298–309. [CrossRef]
15. Kong, Q.; Ma, W.; Yang, H.; Ma, G.; Mantyla, J.J.; Benning, C. The Arabidopsis WRINKLED1 transcription factor affects auxin homeostasis in roots. *J. Exp. Bot.* **2017**, *68*, 4627–4634. [CrossRef] [PubMed]
16. Cernac, A.; Benning, C. WRINKLED1 encodes an AP2/EREB domain protein involved in the control of storage compound biosynthesis in Arabidopsis. *Plant J.* **2004**, *40*, 575–585. [CrossRef] [PubMed]
17. Kong, Q.; Ma, W. WRINKLED1 transcription factor: How much do we know about its regulatory mechanism? *Plant Sci.* **2018**, *272*, 153–156. [CrossRef]
18. Maeo, K.; Tokuda, T.; Ayame, A.; Mitsui, N.; Kawai, T.; Tsukagoshi, H.; Ishiguro, S.; Nakamura, K. An AP2-type transcription factor, WRINKLED1, of Arabidopsis thaliana binds to the AW-box sequence conserved among proximal upstream regions of genes involved in fatty acid synthesis. *Plant J.* **2009**, *60*, 476–487. [CrossRef]
19. Kong, Q.; Singh, S.K.; Mantyla, J.J.; Pattanaik, S.; Guo, L.; Yuan, L.; Benning, C.; Ma, W. TEOSINTE BRANCHED1/CYCLOIDEA/PROLIFERATING CELL FACTOR4 Interacts with WRINKLED1 to Mediate Seed Oil Biosynthesis. *Plant Physiol.* **2020**, *184*, 658–665. [CrossRef]
20. Baud, S.; Mendoza, M.S.; To, A.; Harscoet, E.; Lepiniec, L.; Dubreucq, B. WRINKLED1 specifies the regulatory action of LEAFY COTYLEDON2 towards fatty acid metabolism during seed maturation in Arabidopsis. *Plant J.* **2007**, *50*, 825–838. [CrossRef]
21. Kong, Q.; Yuan, L.; Ma, W. WRINKLED1, a "Master Regulator" in Transcriptional Control of Plant Oil Biosynthesis. *Plants* **2019**, *8*, 238. [CrossRef] [PubMed]
22. Kim, W.C.; Reca, I.B.; Kim, Y.; Park, S.; Thomashow, M.F.; Keegstra, K.; Han, K.H. Transcription factors that directly regulate the expression of CSLA9 encoding mannan synthase in Arabidopsis thaliana. *Plant Mol. Biol.* **2014**, *84*, 577–587. [CrossRef] [PubMed]
23. Ma, W.; Kong, Q.; Grix, M.; Mantyla, J.J.; Yang, Y.; Benning, C.; Ohlrogge, J.B. Deletion of a C-terminal intrinsically disordered region of WRINKLED1 affects its stability and enhances oil accumulation in Arabidopsis. *Plant J.* **2015**, *83*, 864–874. [CrossRef] [PubMed]
24. Herve, C.; Dabos, P.; Bardet, C.; Jauneau, A.; Auriac, M.C.; Ramboer, A.; Lacout, F.; Tremousaygue, D. In vivo interference with AtTCP20 function induces severe plant growth alterations and deregulates the expression of many genes important for development. *Plant Physiol.* **2009**, *149*, 1462–1477. [CrossRef]
25. Guan, P.; Ripoll, J.J.; Wang, R.; Vuong, L.; Bailey-Steinitz, L.J.; Ye, D.; Crawford, N.M. Interacting TCP and NLP transcription factors control plant responses to nitrate availability. *Proc. Natl. Acad. Sci. USA* **2017**, *114*, 2419–2424. [CrossRef] [PubMed]
26. Guan, P.; Wang, R.; Nacry, P.; Breton, G.; Kay, S.A.; Pruneda-Paz, J.L.; Davani, A.; Crawford, N.M. Nitrate foraging by Arabidopsis roots is mediated by the transcription factor TCP20 through the systemic signaling pathway. *Proc. Natl. Acad. Sci. USA* **2014**, *111*, 15267–15272. [CrossRef]
27. Lopez, J.A.; Sun, Y.; Blair, P.B.; Mukhtar, M.S. TCP three-way handshake: Linking developmental processes with plant immunity. *Trends Plant Sci.* **2015**, *20*, 238–245. [CrossRef]
28. Li, S. The Arabidopsis thaliana TCP transcription factors: A broadening horizon beyond development. *Plant Signal. Behav.* **2015**, *10*, e1044192. [CrossRef]
29. Danisman, S. TCP Transcription Factors at the Interface between Environmental Challenges and the Plant's Growth Responses. *Front. Plant Sci.* **2016**, *7*, 1930. [CrossRef]
30. Ma, W.; Kong, Q.; Arondel, V.; Kilaru, A.; Bates, P.D.; Thrower, N.A.; Benning, C.; Ohlrogge, J.B. Wrinkled1, a ubiquitous regulator in oil accumulating tissues from Arabidopsis embryos to oil palm mesocarp. *PLoS ONE* **2013**, *8*, e68887. [CrossRef]
31. Steffens, N.O.; Galuschka, C.; Schindler, M.; Bulow, L.; Hehl, R. AthaMap web tools for database-assisted identification of combinatorial cis-regulatory elements and the display of highly conserved transcription factor binding sites in Arabidopsis thaliana. *Nucleic Acids Res.* **2005**, *33*, W397–W402. [CrossRef] [PubMed]
32. Martin, K.; Kopperud, K.; Chakrabarty, R.; Banerjee, R.; Brooks, R.; Goodin, M.M. Transient expression in Nicotiana benthamiana fluorescent marker lines provides enhanced definition of protein localization, movement and interactions in planta. *Plant J.* **2009**, *59*, 150–162. [CrossRef] [PubMed]
33. Earley, K.W.; Haag, J.R.; Pontes, O.; Opper, K.; Juehne, T.; Song, K.; Pikaard, C.S. Gateway-compatible vectors for plant functional genomics and proteomics. *Plant J.* **2006**, *45*, 616–629. [CrossRef] [PubMed]
34. Kong, Q.; Pattanaik, S.; Feller, A.; Werkman, J.R.; Chai, C.; Wang, Y.; Grotewold, E.; Yuan, L. Regulatory switch enforced by basic helix-loop-helix and ACT-domain mediated dimerizations of the maize transcription factor R. *Proc. Natl. Acad. Sci. USA* **2012**, *109*, E2091–E2097. [CrossRef] [PubMed]
35. Hellens, R.P.; Allan, A.C.; Friel, E.N.; Bolitho, K.; Grafton, K.; Templeton, M.D.; Karunairetnam, S.; Gleave, A.P.; Laing, W.A. Transient expression vectors for functional genomics, quantification of promoter activity and RNA silencing in plants. *Plant Methods* **2005**, *1*, 13. [CrossRef] [PubMed]

36. Sainsbury, F.; Thuenemann, E.C.; Lomonossoff, G.P. pEAQ: Versatile expression vectors for easy and quick transient expression of heterologous proteins in plants. *Plant Biotechnol. J.* **2009**, *7*, 682–693. [CrossRef] [PubMed]
37. Li, J.; Li, G.; Gao, S.; Martinez, C.; He, G.; Zhou, Z.; Huang, X.; Lee, J.H.; Zhang, H.; Shen, Y.; et al. Arabidopsis transcription factor ELONGATED HYPOCOTYL5 plays a role in the feedback regulation of phytochrome A signaling. *Plant Cell* **2010**, *22*, 3634–3649. [CrossRef]
38. Liu, H.; Yu, X.; Li, K.; Klejnot, J.; Yang, H.; Lisiero, D.; Lin, C. Photoexcited CRY2 interacts with CIB1 to regulate transcription and floral initiation in Arabidopsis. *Science* **2008**, *322*, 1535–1539. [CrossRef]

plants

MDPI

Review

Plant GDSL Esterases/Lipases: Evolutionary, Physiological and Molecular Functions in Plant Development

Gaodian Shen, Wenli Sun, Zican Chen, Lei Shi, Jun Hong and Jianxin Shi *

Joint International Research Laboratory of Metabolic and Developmental Sciences, School of Life Sciences and Biotechnology, Shanghai Jiao Tong University, Shanghai 200240, China; shengaodian@sjtu.edu.cn (G.S.); sunwenli@sjtu.edu.cn (W.S.); czcqbqmx@163.com (Z.C.); shileilei@sjtu.edu.cn (L.S.); m13605151497@163.com (J.H.)
* Correspondence: jianxin.shi@sjtu.edu.cn; Tel.: +86-021-34207174

Abstract: GDSL esterases/lipases (GELPs), present throughout all living organisms, have been a very attractive research subject in plant science due mainly to constantly emerging properties and functions in plant growth and development under both normal and stressful conditions. This review summarizes the advances in research on plant GELPs in several model plants and crops, including Arabidopsis, rice, maize and tomato, while focusing on the roles of GELPs in regulating plant development and plant–environment interactions. In addition, the possible regulatory network and mechanisms of GELPs have been discussed.

Keywords: lipases; lipid metabolism; plant-environment interactions; reproductive development; vegetative development

Citation: Shen, G.; Sun, W.; Chen, Z.; Shi, L.; Hong, J.; Shi, J. Plant GDSL Esterases/Lipases: Evolutionary, Physiological and Molecular Functions in Plant Development. *Plants* **2022**, *11*, 468. https://doi.org/10.3390/plants11040468

Academic Editors: Wei Ma and José Manuel Martínez-Rivas

Received: 25 November 2021
Accepted: 4 February 2022
Published: 9 February 2022

Publisher's Note: MDPI stays neutral with regard to jurisdictional claims in published maps and institutional affiliations.

1. Introduction

GDSL esterase/lipases (GELPs) represent a variety of lipolytic enzymes that hydrolyze diverse lipidic substrates including thioesters, aryl esters, and phospholipids [1]. GELPs contain a unique and conserved GDSL motif GDSxxDxG at their N-terminus that distinguish them from classic lipolytic enzymes that harbor a conserved motif GxSxG [1]. GELPs are widely distributed in microbes, animals and plants, playing vital roles in growth, development and stress responses [2,3].

Compared with bacteria and animals, plants retain substantial amounts of GELPs that are composed of three subfamilies [2,3], indicating that GELPs have acquired essential physiological functions in plants. To date, genome wide identification of GELPs has been carried out in various plant species (Table 1), including *Arabidopsis thaliana* [4], *Oryza sativa* [5], *Brassica rapa* [6], *Vitis vinifera* [7], *Zea mays* [8], *Glycine max* [2,9], and Rosaceae (such as *Fragaria vesca*, *Prunus persica*, *P. avium*, *P. mume*, Pyrus *bretschneideri*, and *Malus domestica*) [10]. However, the enzymatic or biological functions of most of GELPs have not been characterized *in planta* [2,3].

The classical lipolytic enzymes have a catalytic Ser residue while GELPs have four invariant catalytic residues—Ser, Gly, Asn, and His—that play important roles in enzyme catalysis [1]. Therefore, GDSLs are also known as SGNH lipases. Unlike other lipolytic enzymes, GELPs are more flexible in structure with more flexible active sites, broadly diverse substrates and multifunctional properties [1–5]. In addition, while other lipolytic enzymes hydrolyze lipids, GELPs can hydrolyze sulfur, aryl vinegar and amino acids, in addition to lipids [1]. Understanding physiological and molecular functionalities of plant GDSL lipases will not only facilitate functional characterization of these fascinating lipolytic enzymes, but also the possible application in plant breeding for resilient crops with multiple resistant/tolerant traits to environmental changes, to secure food supply under changing climate conditions. In this review, we have focused on new, recent information on plant GELPs and their roles in plant growth and development.

Table 1. Numbers of plant GELPs predicted through whole genome identification.

Species	Numbers	Reference
Arabidopsis thaliana	105	[4]
Brassica rapa	121	[6]
Fragaria vesca	96	[10]
Glycine max	194	[2,9]
Malus domestica	150	[10]
Oryza sativa	114	[5]
Prunus avium	70	[10]
Prunus mume	90	[10]
Prunus persica	97	[10]
Pyrus bretschneideri	94	[10]
Vitis vinifera	83	[7]
Zea mays	103	[8]

2. Roles of GELP in Plant Land Colonization

One important evolutionary feature of plant land colonization was the formation of the cuticle approximately 450 million years ago [11], which was together with the formation of a cell wall before the first colonization of true land plants [12]. Cuticle formation, particularly cutin and suberin, involves many proteins and enzymes including GELPs that play important roles in the polymerization. GELPs are found across all land plants [13], including anciently conserved spermatophytes and bryophytes such as *Selaginella moellendorffii* and *Physcomitrella patens* [14]. In addition, GELPs emerged as early as in *Penium margaritaceum* charophytes, the last common ancestor of the Zygnematophyceae and land plants [15]. These results highlight important roles of GELPs in plant land colonization. In addition, GELPs expand significantly in an ancient lycophyte (*Selaginella moellendorffi*) that diverged shortly after land plants had evolved vascular tissues, which also indicates a role for GELPs in the early evolution of vascular plants [3]. Evolutionarily, the emergence of GELPs in charophytes is supposed to contribute to plant land colonization by providing biological services including the conservation of water in a desiccating environment [11] and biological interactions between cuticle and other cell wall components [12]. Nevertheless, more comparative genomic and molecular studies are needed to better understand the exact roles of GELPs in plant land colonization.

3. Roles of GELPs in Plant Development and Plant Metabolism

GELPs have been suggested to play crucial roles in almost all aspects of plant growth and development [2,4,9,16]. Increasing studies confirmed their functions in both vegetative and reproductive development, and plant metabolism as well. The exploration of metabolic and physiological functions of GELPs will provide new routes for redesigning the regulatory networks of plant growth and development.

3.1. Vegetative Development

3.1.1. Seed Germination

In germinating seeds, the hydrolysis of stored lipids by lipases plays a crucial role in the initial stage of seed germination. A study investigated the expression of 110 *GELP* genes over three time points during rice seed germination, and found that most of them are expressed during germination, and about one third of them are highly expressed across all three germination stages [17], indicating an important role for GELPs in seed germination. Nevertheless, none of them have been experimentally validated. In *Brassica napus*, BnSCE3/BnLIP2, a sinapine esterase, catalyzed the hydrolysis of sinapine during early seed germination, and overexpression of *BnSCE3/BnLIP2* slightly enhanced seed germination rate and seedling development [18]; however, its function in seed germination has not been confirmed using loss-of-function mutant. In Arabidopsis, *LIP1*, whose expression is highly induced by GA and repressed by DELLAs during seed imbibition, controls embryo axis

elongation before germination, implying its involvement in seed germination [19]; however, no functional analysis has been performed. The function of GELPs in seed germination remains to be determined in more plant species.

3.1.2. Coleoptile Elongation

Plant coleoptile elongation is influenced by various genetic and environmental factors. The regulatory mechanisms underlying this process and particularly the involvement of GELP are poorly understood. Rice *GER1* (*GDSL containing enzyme rice 1*) is the only *GELP* that has been reported in this area. GER1 was inducible by jasmonic acid (JA) and light (both red and far-red light), and negatively regulated coleoptile elongation in rice [20].

3.1.3. Lateral Root Development

Suberin plasticity is highly associated with plant lateral root development, and GELPs have recently been found to be involved this auxin signaling-mediated process, in which different sets of auxin responsive *GELPs* modulate both suberine deposition and degradation in the cell walls of endodermal cells overlying the lateral root primordium to facilitate the lateral root development [21]. Auxin repressible *GELP22*, *GELP38*, *GELP49*, *GELP51* and *GELP96* were needed for suberin polymerization in the apoplast while auxin inducible *GELP72*, *GELP73* and *GELP81* were required for suberin degradation during lateral root emergence [21]. Single loss-of-function mutants of five suberin-biosynthetic GELPs did not show defectiveness in lateral root development, while lateral root emergences in triple mutants of suberin-degrading GELPs were all delayed [21]. Additionally, loss-of-function mutants of *GLIP2* were more sensitive to auxin with increased expression of auxin signaling genes, such as *IAA1* and *IAA2*, and increased numbers of lateral roots [22]. Notably, although Arabidopsis *CDEF1* was expressed in the zone of lateral root emergence, loss-of-function mutants of *CDEF1* did not show any defects in lateral root emergence [23], likely due to redundancy among *GELPs*. The involvement of GELPs in lateral root development in other plants remains unknown.

3.1.4. Root Development

Exogenous ethylene restricts root growth. A recent study provided novel mechanistic insights into ethylene signaling in rice, in which the ER localized GELP MHZ11 (mao huzi 11) was necessary for ethylene signal transduction, and the overexpression of *MHZ11* resulted in shorter roots in the presence of air or ethylene [24]. Loss-of-function of *MHZ11* did not alter coleoptile and root growth in the presence of air under dark, but significantly altered the ethylene sensitivity in rice primary roots, in which wild type root growth was drastically repressed while *mhz11* root growth was barely inhibited [24]. In response to ethylene, MHZ11 lipase inhibited *OsCTR2* phosphorylation and ethylene signaling by maintaining low sterol levels on the ER membrane [24], thus activating ethylene response in root growth. The detailed network of GELPs in the ethylene signal-mediated root development merits further investigations.

3.1.5. Plant Height

The epidermis is one of the multiple regulatory factors of plant height, an important agronomic trait [25]. Theoretically, epidermal apoplast localized GELPs are expected to influence plant height. Indeed, DR (drooping leaf), a rice GELP without localization information, and WDL1 (wilted dwarf and lethal 1), an ER localized Arabidopsis GELP, were reported to affect plant height. *DR* was required for leaf silica deposition; *dr* mutant exhibited drooping leaves with small midrib, shorter panicle, and reduced plant height [26]. Notably, silica is deposited in the epidermis just beneath the cuticle layer. *WDL1* was involved in cutin patterning in the epidermis; *wdl1* mutant was dwarf and died soon after the seedling establishment due to over loss of water [26]. These studies indicated that GELP-mediated cuticle and silica metabolism affects plant height, although the exact mechanisms have not been resolved.

3.1.6. Stomata Development

Epidermal cell patterning is closely associated with stomata development and plays key roles in plant–environment interactions. Two studies demonstrated the involvement of GELPs in stomata development. Arabidopsis *wdl1* mutant exhibited smaller stomatal and pavement cells but more stomatal and pavement cells per unit area [27]. Arabidopsis OSP1 (occlusion of stomatal pore 1), an ER and lipid droplet localized GELP, was reported to be involved in the early wax biosynthesis and stomatal cuticular ledge formation [28]. Almost half of the mature stomata in *osp1* were occluded with reduced stomata conductance, due to the fully covered cuticular layer formed between the edges of two guard cells surrounding the pore [28]. It seems that disrupting *GELP* mediated-epidermal cell patterning affects stomata development.

3.2. Reproductive Development

3.2.1. Flower Development

Up to date, several GELPs have been reported to be involved in flower development. DAD1 (defective in anther dehiscence1) in Arabidopsis was reported to catalyze the initial step of JA biosynthesis and coordinates JA-dependent flower development [29]. *dad1* mutant was defective in anther dehiscence, pollen maturation, and flower opening [29]. *CUS2* (*cutin synthase 2*), an orthologue of tomato *CD1/CUS1* [14,30] in Arabidopsis was found to be not required for initial formation but required for maintenance of cuticular ridge on sepal epidermis [31]. At early stages, *cus2* mutant sepals showed similar cuticular ridge distributions and patterns similar to WT sepals. At mature stage, *cus2* mutant sepal epidermis lacked cuticular ridges. Thus, mutant flowers were found to be more permeable to toluidine blue dye although the morphology of sepals and petals were normal [31]. Our previous study found that expression levels of two Arabidopsis GELP genes, *GELP15* and *GELP39*, are significantly down-regulated in *hsp70-16* mutant sepals grown under normal and mild heat stress conditions [32], which was found to be concomitant with fused lateral sepals and abnormal flower opening [33].

3.2.2. Anther and Pollen Development

Lipid metabolism is critical for the building of the anther cuticle and the pollen wall, and mutants of genes associated with lipid metabolism often show male sterility [34,35]. It is reported that, about 10% of predicted oilseed rape GELPs are specifically expressed in fertile but not in male-sterile buds, implying their functions in pollen development [6]. Mutants of some *GELPs* displayed similar male sterility phenotypes in different plant species, indicating conservative roles for *GELPs* in plant male fertility.

Besides *DAD1*, which functioned in anther dehiscence and pollen maturation, more *GELPs* have been reported to be involved in anther and pollen development in Arabidopsis. *RVMS* (*reversible male sterile*) was found to encode a GELP with lipase activity that localizes especially in microspore mother cells, meiotic cells and microspores, and participates in pollen development [36]. *rvms* mutant displayed defective nexine formation, degenerated microspore cytoplasm, and complete male sterility [36]. Notably, *rvms* was fertile at low temperatures [36]. In addition, *GELP77* was reported to be necessary for pollen fertility and pollen dissociation. *gelp77* pollen grains lacked well-organized reticulate surface structure; they were shrunken and stuck to each other that could not be released from mature anthers [37]. Furthermore, a pollen coat protein encoding the gene *EXL6* (extracellular lipase 6), the target of a key Arabidopsis pollen development regulator AMS (aborted microspores) [38], was reported to be highly expressed at stage corresponding to microspore pollen development. Knockdown mutants of *EXL6* exhibited defective pollen grains due to cytoplasmic degradation after the tetrad stage [6].

In rice, *RMS2* (*rice male sterility 2*) encodes an ER-localized GELP with esterase activity that is required for male fertility. *rms2* displayed complete male sterility with defective middle layer and tapetum degradation, abnormal cuticle and exine formation, and irregular central vacuole development [39]. In addition, the ER localized OSGELP34 [40,41]

and peroxisome localized OsGELP110/OsGELP115 [40] were found to catalyze different compounds for pollen exine development. *OsGELP34* was primarily expressed in anthers during pollen exine formation; *osgelp34* mutant showed abnormal exine and altered expression of many key pollen development genes, their anthers were light yellow and smaller with nonviable pollens [40,41]. *OsGELP110* is the most homologous to *OsGELP115*; both are dominantly expressed in anthers with similar patterns. The single mutant of either *OsGELP110* or *OsGELP115* did not affect male fertility, but double mutants were male sterile, harboring smaller and light yellow anther with aborted pollen grains [40]. Notably, compared with *osgelp34*, anthers in *osgelp110osgelp115* were more prominent with un-degenerated swollen tapetum and endothecium layer, and the foot layer in *osgelp110osgelp115* mutant was continuous without obvious intermission [40].

In maize, *IPE2* (*irregular pollen exine 2*), encoding an ER localized GELP, is specifically expressed in developing anthers. *ipe2* mutants, exhibiting irregular anther cuticle and pollen nexine, delayed degeneration of tapetum and middle layer, were male sterile [42]. *ZmMs30* encodes an ER localized GELP, and is specifically expressed in maize anthers similar to IPE2. *ms30* mutant exhibited a defective anther cuticle, an irregular foot layer of pollen exine, and complete male sterility [8]. Importantly, male sterility in *ms30* was stable in different inbred lines with diverse genetic backgrounds, without any penalty on maize heterosis and production, providing a valuable male-sterility system for the hybrid breeding maize [8]. Notably, *IPE2* phylogenetically is distant from *MS30* [42].

3.2.3. Pollen-Stigma Interaction and Pollinator Attraction

For successful pollination, the stigma cuticle has to be destroyed by lipases-like cutinase. The identification of such plant cutinases is indispensable for elucidating the molecular mechanisms of pollen–stigma interaction. Arabidopsis *CDEF1* was found to be expressed in pollen and pollen tubes, and to be associated with pollen-stigma interaction [23], however, its function *in planta* remains unknown. Pollination begins with the hydration in which lipids and proteins are important. Arabidopsis *EXL4* alone was reported to be required for the hydration on the stigma, the initial step of pollination. *EXL4* also functioned together with *GRP17* to promote the initiation of hydration. *exl4* mutant exhibited a delayed pollen hydration [43].

Attraction of pollinators is a unique feature for pollination in plants. A study in the tropical tree *Jacaranda mimosifolia* demonstrated a role for GELPs in this process. JNP1 (jacaranda nectar protein 1) is an extracellular GELP protein present in the nectar of *J. mimosifolia* that displays lipase/esterase activities. Because of the fact that *J. mimosifolia* nectar contains lipophilic particles and accumulates large amount of free fatty acids within the nectar, JNP1 was supposed to release fatty acids from lipid particles to attract pollinators [44]. In addition, a tomato GELP, Sl-LIP8, was reported to be involved in the production of fatty acid-derived organic compounds [45]. Based on the above reports, GELPs are supposed to be functional in pollinator attraction.

3.2.4. Fruit Development

A bioinformatics study of GELPs in Rosaceae genomes indicated that a set of GELPs likely participated in fruit development [10]. Nevertheless, except for increasing the glossy of the fruit surface, the mutation of *GDSL1* [46], *SlGDSL2* [47], *CUS1/CD1* [14,30] in tomato did not affect fruit size. The involvement of GELPs in the development of other fruits is rarely reported.

3.2.5. Seed Development

Seed development is promoted significantly in transgenic plants overexpressing the *GLIP* genes. Expression of a *Brassica napus GLIP* gene *BnSCE3/BnLIP2* under a seed-specific promoter in oilseed rape resulted in enhanced weight and size of the transgenic seeds [18]. Ectopic expressing of a cotton *GhGLIP* in Arabidopsis increased seed size and weight [48]. Arabidopsis *RGE1* (*retarded growth of embryo 1*) is a nucleus localized bHLH transcription

factor that controls embryo development from the endosperm; *rge* mutants displayed smaller and shriveled seeds, in which the expression of two *GELP* genes was especially suppressed [49]. However, the single mutant of either of *GELP* gene did not show any defectiveness in seeds due to possible functional redundancy [49].

3.3. Plant Metabolism

3.3.1. Lipid Metabolism

GELPs possess extensive hydrolytic activity, such as thioesterase, protease, phospholipase, and arylesterase activity, making the identification of their substrates and biochemical functions in vivo a great challenge, especially in plants. Generally, their primary functions are predicted to be related to lipid metabolism to produce storage oil in seeds, cuticular lipids to cover and decorate organ surfaces, oxylipins, and other signaling molecules [1–3,9–11]. Indeed, lipolytic activity of plant GELPs has been confirmed using p-nitrophenyl butyrate as a common substrate. Those GELPs include CaGLIP1 [50], SFAR4 (seed fatty acid reducer 4) [51], GLIP2 [22], CDEF1 [23], OsGLIP1 [52], OsGLIP2 [52], ZmMs30 [8], EXL4 [43], JNP1 [44], and RMS2 [39]. Among them, cell wall or aqueous apoplast localized GELPs often acted as esterases or hydrolases, such as CDEF1 (cuticle destructing factor 1) in Arabidopsis and CUS1 in tomato. CDEF1 functioned as a cutinase disrupting pollen cuticle [23] while CUS1 was reported to be essential for cutin deposition on fruit epidermis via catalyzing the esterification of both primary and secondary alcohol groups [30]. In addition, PLIP1 (plastid lipase 1), a plastid phospholipase, contributed to seed oil biosynthesis; *plip1* mutant seeds contain 10% less oil while overexpressive mutant seeds contain 40–50% more seed oils [53].

3.3.2. Cell Wall Metabolism

So far, only three GELPs have been reported to be involved in cell wall patterning. The first two are Golgi-localized GELPs in rice [54,55]. Rice BS1 (brittle leaf sheath1) deacetylated hemicellulose xylan and maintains acetylation homeostasis of the xylan backbone that is vital for secondary cell wall development. *bs1* mutants showed reduced plant height, smaller panicle, reduced tiller, and significantly decreased yield and grain weight [55]. Rice DARX1 (deacetylase on arabinosyl sidechain of xylan1) deacetylated arabinosyl residues of xylan and modulates the arabinoxylan acetylation profiles that is important for secondary wall formation. *darx1* mutants showed lower contents of cellulose, disrupted secondary wall formation and patterning, reduced mechanical strength such as easily broken internodes and drooping leaves, and slightly decreased plant height [54]. The third one is a cotton *GhGDSL*, which exhibited secondary cell wall stage-specific expression during cotton fiber development, and a 194 bp region in the 5′ of *GhGDSL* controls its expression, playing an important role in the secondary cell wall formation during fiber development [56].

3.3.3. Secondary Metabolism

However, many GELPs can catalyze other reactions, showing additional transferase activities. Extracellular space localized GELPs often acted as acyltransferases, for example, SlCD1 (cutin defective 1) [57] GDSL1 in tomato [46]. CD1 catalyzed polymerization of cutin by transferring the hydroxyacyl group from its substrate 2-mono(10,16-dihydroxyhexadecanoyl)glycerol to the growing cutin polymer, GDSL1 catalyzed the multiple crosslinks present in the cuticular matrix via this transesterification activity. A novel allelic mutant of *SlCD1*, *slgdsl2*, lacked intact fruit epidermal cutin, confirming the role for *SlCD1/SlGDSL2* in cutin polymerization [47]. In addition, TcGLIP in *Tanacetum cinerariifolium* harbored transferase activity in vivo and esterase activity in vitro, which is involved in pyrethrins biosynthesis [58]. Tomato SlCGT (chlorogenate: glucarate caffeoyltransferase), the first GELP that lost hydrolytic activity but acquired acyltransferase activity, was found to participate in the synthesis of hydroxycinnamate esters by employing amino acid residues [59]. Another tomato GELP Sl-LIP8 cleaved glycerolipids to produce

short chain fatty acid derived volatile organic compounds (FA-VOCs), *sl-lip8* mutant exhibited significantly reduced contents of several C5 and C6 FA-VOCs [45]. Supportively, comparative metabolomics studies between wild type and *rms2* mutant anthers demonstrated that, in addition to lipid metabolism, *RMS2* functions in other metabolic processes such as plant hormone biosynthesis and signaling and secondary metabolism [39].

Interestingly, a recent study revealed that *dr*—another allelic mutation of *BS1* in the Nipponbare background—lacks an intact silica layer in its leaf epidermis [26], implying a novel function of *GELP* in silica accumulation to maintain erect leaf morphology in rice. Nevertheless, *bs1* [55] and *dr* [26] showed different phenotypes, indicating that functions of the same GELP are controlled by different alleles and different genomic backgrounds, which merit further validations. In addition, an apoplast localized GELP in wheat, XAT (xanthophyll acyltransferase), was reported to catalyze the esterification of lutein for the synthesis of xanthophyll esters. Notably, XAT possesses esterase and lipase activity [60].

4. Roles of GELPs in Plant-Environment Interactions

Extensive studies have demonstrated that multiple GELPs are inducible by various abiotic and biotic stresses in some species, suggesting their defensive roles in both biotic and abiotic stresses [9,17]. Elucidation of precise roles for GELPs in synchronizing plant responses to both abiotic and biotic stresses would benefit breeding for more resilient crops to deal with changing climates.

4.1. Plant-Abiotic Stress Interaction

Rapid water loss is one of the important features of cuticle defective mutants; it is particularly true in mutants of GELPs with cutinase or transferase activity. Compared with wild type, mutants of rice *WDL1* [27] and tomato *GDSL1* [46], *SlGDSL2/CD1* [47,57] all showed an increased transpiration rate. Nevertheless, the water permeance of the isolated enzyme-treated cuticle from *slcus1* was found to be similar to wild type [30]; suggesting that the levels of cutin cross-linking do not affect water permeance, in agreement with reports that waxes are major determinants of cuticle permeability. On the other hand, *osp1* mutant in Arabidopsis displayed lower transpiration rate and enhanced drought tolerance [28]. In addition, overexpression plants of *CaGLIP1* [50] and *GmGELP28* [9] were highly tolerant to drought; their exact functions in drought tolerance are not yet confirmed genetically.

Several GELPs are associated with salt stress or ABA-mediated abiotic stress. *gelp*^{quint} suberin-biosynthetic mutants [21] were more sensitive to salt stress while *GmGELP28* overexpression [9] plants were highly tolerant to salt. Both *PLIP2* and *PLIP3* contributed to ABA-induced JA accumulation, participating in ABA-mediated abiotic stress responses [61], while overexpression of *SFAR4* [51] and *CaGLIP1* [50] enhanced tolerance to osmotic and oxidative stress, respectively.

Nevertheless, the involvement of GELPs in plant–abiotic stress interaction is obtained mainly from bioinformatics prediction and overexpression studies. More and more evidence, particularly regarding the mechanisms behind and from mutant analyses are needed for potentially breeding abiotic tolerant plants via genetic engineering.

4.2. Plant-Biotic Stress Interaction

Most plant–biotic stress interaction studies have been carried out in Arabidopsis and rice with mutant analyses, which indicate an important role of GELPs-mediated lipid metabolism and hormone signaling in plant immunity.

In Arabidopsis, GELPs are essential for ethylene-associated systemic resistance. The SA-inducible *GLIP1* was known to be involved in the plant resistance to necrotrophic pathogen, the fungus (*Alternaria brassicicola*). *glip1* plants were significantly susceptible to pathogen infection [62]. *GLIP1* regulated resistance by direct disruption of the structure of fungal spore cell wall or membrane [62], and by positively and negatively feedback regulation of ethylene signaling [62,63]. In addition, *GLIP2* was reported to be inducible by JA, SA and ethylene; *glip2* mutants were more sensitive to auxin and more susceptible to

necrotrophic bacteria *Erwinia carotovora* [22]. *GLIP2* was found to function in pathogenic responses through down-regulation of auxin signaling [22]. In rice, *OsGLIP1* and *OsGLIP2* negatively regulated plant's resistance to both bacterial and fungal pathogens via modulating lipid metabolism; simultaneous down-regulation of both of them enhanced the resistance to both bacterial and fungal pathogens while the overexpression of either of them compromises tolerance [52]. In addition, expressions of 5 *GELP* genes in rice infected with *Fusarium verticillioides* was accompanied with impaired mobilization of lipids [17].

Furthermore, sporadic relevant reports could be found in pepper and sunflower; however, none of them has been confirmed with loss-of-function mutants. Transcripts of *CaGLIP1* accumulated in response to multiple defense hormones, such as SA, JA, and ethylene, and to infection with virulent and avirulent strains of *Xanthomonas campestris pv. vesicatoria*, while *CaGLIP1* overexpression plants were hypersensitive to infection of *Pseudomonas. syringae pv. tomato* [50]. In sunflower, a pan-genome analysis indicated the contribution of introgressions from wild species to downy mildew resistance, in which a GELP sits within the genomic region associated with resistance [64].

5. Possible Regulatory Factors and Networks

Very few studies have explored the regulatory aspects of GELPs, although bioinformatics predication of putative cis-elements has been done in many plant species [5,9,19,48]. It seems from the available information that GELPs are direct targets of multiple transcription factors and are essential elements in the signaling pathways of several phytohormones. Unearthing such regulatory networks is of importance in better understanding GELPs for potential application in breeding.

So far, several transcription factors have been reported to regulate the expression of *GELPs* directly or indirectly. First, SHN transcription factors were known regulators of cuticle deposition [65,66]. In Arabidopsis, *GELP60* and *GELP95* were targeted by SHN for cutin deposition and flower organ surface patterning [66]. In tomato, expression levels of *SlGDSL1* and *SlGDSLa* were downregulated in tomato *SHN3RNAi* mutant [67]. Second, ATML1 and PDF2, two epidermis specification regulators, targeted Arabidopsis *LIP1* at the L1 box promoter sequence that is conserved in promoter regions of epidermis-specific genes. *LIP1* expressed specifically in the epidermis and its L1 box sequence mediated GA-induced transcription in seed germination [19]. Third, UDT1 (Undeveloped Tapetum1) [68] and PTC1 (Persistent Tapetal Cell1) [69], two important early anther development regulators in rice, both targeted and regulated expression of *RMS2* [70], regulating early anther development. Fourth, MYB transcription factors were known to play important roles in almost all aspects of plant development. A cotton MYB transcription factor, GhMYB1, targeted *GhGDSL* at the MYB1AT sequence, regulating the expression of *GhGDSL* during fiber development [56].

Other factors have also been found to regulate *GELP* during plant development and response to the environment. Arabidopsis *OSP1* acted upstream of *MAH1* or *CER1* to regulate epidermal permeability and OCL formation and drought tolerance [28]. Furthermore, Arabidopsis *GELP15* and *GELP39*, two sepal expressed *GELPs*, participated in a *HSP70-16* mediated transcription regulatory network that maintains metabolic homeostasis for flower opening [32].

Regarding signaling pathways, besides the involvement of Arabidopsis *LIP1* in GA signaling, rice *MHZ11* was found to be involved in ethylene signaling, which acts upstream of *OsCTR2* in the ethylene signaling pathway, reducing sterol levels to disrupt receptor-*OsCTR2* interactions and *OsCTR2* phosphorylation for initiating ethylene signaling, thus regulating root growth [24]. Recently, two studies highlighted the participation of GELPs in plant immunity signaling. When overexpressing *Hrip1*, an elicitor isolated from necrotrophic fungus *Alternaria tenuissima*, the expression levels of two *GELPs* (*GLIP1* and *GLIP4*) were upregulated, which was associated with enhanced resistance to insect *Spodoptera exigua* [71], indicating the involvement of *GELPs* in *Hrip1* triggered insect resistant responses. In addition, two pathogen-responsive MAPKs, MPK3 and MPK6, regulated

expression of *GLIP1*, *GLIP3* and *GLIP4*, contributing resistance to *Botrytis cinerea*, independent of JA and ethylene [72].

6. Concluding Remarks and Future Prospects

The GELP family is diverse but conserved in land plants; their isozymes differ in activity, substrate specificity, and product formation. GELPs and their hydrolyzing products play multiple roles in plant growth and development and responses to biotic and abiotic stresses. Our review provides contemporary information for the plant GELPs (Figure 1). Over the past two decades, bioinformatics has predicted the presence of GELPs in various plants including several important crop plants (Table 1), and a number of GELPs have been successfully characterized, primarily in Arabidopsis, rice and tomato (Table 2). Even with this, our understanding regarding their functions in plants, the mechanisms underlined and the regulatory aspects, is unable to meet the need for maintaining sustainable agriculture in changing climates. Natural variations in GELP genes provide valuable genetic resources for better understanding their physiological and evolutional importance in plant adaption. To better understand the exact roles of GELPs in plant development and stress response and to facilitate breeding for resilient crops to effectively secure food supply, combined genomics with genetic, biochemical and molecular approaches are needed.

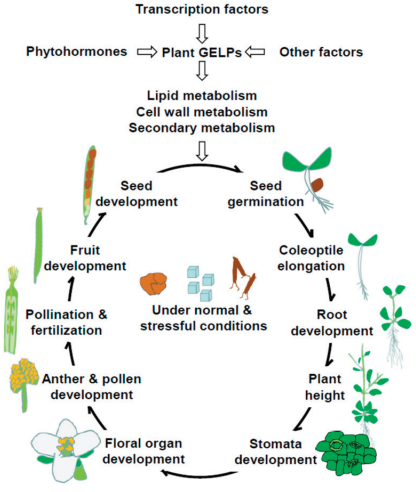

Figure 1. Roles and possible regulatory networks for plant GELPs in plant development and plant-environment interaction.

Table 2. Functional summary of plant GELPs.

Crop Species	Reported GELPs	Process of Development	Reference
Arabidopsis thaliana	CDEF1	Lateral root development (auxin signaling-mediated); Pollen-stigma interaction and pollinator attraction; Lipid metabolism	[23]
	CUS2	Flower development	[31]
	DAD1	Flower development; Anther and pollen development	[29]
	EXL4	Pollen-stigma interaction and pollinator attraction; Lipid metabolism	[43]
	EXL6	Anther and pollen development	[6,38]
	GELP15, GELP39	Flower development	[32,33]

Table 2. *Cont.*

Crop Species	Reported GELPs	Process of Development	Reference
	GELP22, GELP38, GELP49, GELP51 and GELP96 GELP12, DELP55, GELP72, GELP73 and GELP81	Lateral root development (auxin signaling-mediated)	[21]
	GELP77	Anther and pollen development	[37]
	GER1	Coleoptile elongation; Lateral root development (auxin signaling-mediated)	[20,22]
	GLIP1	Plant-biotic stress interaction	[62]
	GLIP2	Lipid metabolism; Plant-biotic stress interaction	[22]
	LIP1	Seed germination	[19]
	OSP1	Plant-abiotic stress interaction; Stomata development	[28]
	PLIP2, PLIP3	Plant-abiotic stress interaction	[61]
	RVMS	Anther and pollen development	[36]
	SFAR4	Lipid metabolism; Plant-abiotic stress interaction	[51]
	WDL1	Plant height; Stomata development	[26]
Brassica napus	BnSCE3, BnLIP2	Seed germination; Seed development	[18]
Capsicum annuum	CaGLIP1	Plant-abiotic/biotic stress interaction; Lipid metabolism	[50]
Glycine max	GmGELP28	Plant-abiotic stress interaction	[9]
Gossypium hirsutum	GhGDSL	Cell wall metabolism	[56]
	GhGLIP	Seed development	[48]
Jacaranda mimosifolia	JNP1	Pollen-stigma interaction and pollinator attraction; Lipid metabolism	[44]
Oraza sativa	BS1	Cell wall metabolism	[55]
	DARX1	Cell wall metabolism	[54]
	DR	Plant height	[26]
	MHZ11	Root development	[24]
	OSGELP34, OsGELP110, OsGELP115	Anther and pollen development	[40,41]
	OsGLIP1, OsGLIP2	Plant-biotic stress interaction; Lipid metabolism	[52]
	RMS2	Anther and pollen development; Lipid metabolism; Secondary metabolism	[39]
	WDL1	Plant-abiotic stress interaction	[27]
Solanum lycopersicum	CD1	Secondary metabolism; Flower development; Fruit development; Plant-abiotic stress interaction	[14,30,47,57]
	CUS1	Flower development; Fruit development	[14,30]
	GDSL1	Fruit development; Plant-abiotic stress interaction; Secondary metabolism	[46]
	SlCGT	Secondary metabolism	[59]
	SlGDSL2/SlCD1	Fruit development; Plant-abiotic stress interaction	[47,57]
	Sl-LIP8	Pollen-stigma interaction and pollinator attraction; Lipid metabolism	[45]

Table 2. *Cont.*

Crop Species	Reported GELPs	Process of Development	Reference
Tanacetum cinerariifolium	TcGLIP	Secondary metabolism	[58]
Zea mays	IPE2	Anther and pollen development	[42]
	ZmMs30	Anther and pollen development; Lipid metabolism	[8]

Author Contributions: Conceptualization, J.S.; information collection and discussion, G.S., W.S., Z.C., L.S. and J.H.; writing—original draft preparation, G.S. and J.S.; writing—review and editing, J.S.; funding acquisition, J.S. All authors have read and agreed to the published version of the manuscript.

Funding: This research was funded in part by the National Natural Science Foundation of China (Grant No. 31971907, 31671511 and 31461143001), and the SJTU JiRLMDS Joint Research Fund (MDS-JF-2019B02).

Institutional Review Board Statement: Not applicable.

Informed Consent Statement: Not applicable

Data Availability Statement: Data is contained within the article.

Conflicts of Interest: The authors declare no conflict of interest.

References

1. Ding, L.N.; Wang, W.J.; Cao, J.; Wang, Z.; Zhu, K.M.; Yang, Y.H.; Li, Y.L.; Tan, X.L. Advances in plant GDSL lipases: From sequences to functional mechanisms. *Acta Physiol. Plant.* **2019**, *41*, 151. [CrossRef]
2. Volokita, M.; Rosilio-Brami, T.; Rivkin, N.; Zik, M. Combining comparative sequence and genomic data to ascertain phylogenetic relationships and explore the evolution of the large GDSL-lipase family in land plants. *Mol. Biol. Evol.* **2011**, *28*, 551–565. [CrossRef]
3. Vujaklija, I.; Bielen, A.; Paradzik, T.; Bidin, S.; Goldstein, P.; Vujaklija, D. An effective approach for annotation of protein families with low sequence similarity and conserved motifs: Identifying GDSL hydrolases across the plant kingdom. *BMC Bioinform.* **2016**, *17*, 91. [CrossRef] [PubMed]
4. Lai, C.P.; Huang, L.M.; Chen, L.O.; Chan, M.T.; Shaw, J.F. Genome-wide analysis of GDSL-type esterases/lipases in Arabidopsis. *Plant Mol. Biol.* **2017**, *95*, 181–197. [CrossRef]
5. Chepyshko, H.; Lai, C.P.; Huang, L.M.; Liu, J.H.; Shaw, J.F. Multifunctionality and diversity of GDSL esterase/lipase gene family in rice (*Oryza sativa* L. *japonica*) genome: New insights from bioinformatics analysis. *BMC Genom.* **2012**, *13*, 309. [CrossRef] [PubMed]
6. Dong, X.; Yi, H.; Han, C.T.; Nou, I.S.; Hur, Y. GDSL esterase/lipase genes in *Brassica rapa* L.: Genome-wide identification and expression analysis. *Mol. Genet. Genom.* **2016**, *291*, 531–542. [CrossRef]
7. Ni, P.Y.; Ji, X.R.; Guo, D.L. Genome-wide identification, characterization, and expression analysis of GDSL-type esterases/lipases gene family in relation to grape berry ripening. *Sci. Hortic.* **2020**, *264*, 109162. [CrossRef]
8. An, X.L.; Dong, Z.Y.; Tian, Y.H.; Xie, K.; Wu, S.W.; Zhu, T.T.; Zhang, D.F.; Zhou, Y.; Niu, C.F.; Ma, B.; et al. ZmMs30 encoding a novel GDSL lipase is essential for male fertility and valuable for hybrid breeding in maize. *Mol. Plant* **2019**, *12*, 343–359. [CrossRef]
9. Su, H.G.; Zhang, X.H.; Wang, T.T.; Wei, W.L.; Wang, Y.X.; Chen, J.; Zhou, Y.B.; Chen, M.; Ma, Y.Z.; Xu, Z.S.; et al. Genome-wide identification, evolution, and expression of GDSL-type esterase/lipase gene family in soybean. *Front. Plant Sci.* **2020**, *11*, 726. [CrossRef]
10. Cao, Y.; Han, Y.; Meng, D.; Abdullah, M.; Yu, J.; Li, D.; Jin, Q.; Lin, Y.; Cai, Y. Expansion and evolutionary patterns of GDSL-type esterases/lipases in Rosaceae genomes. *Funct. Integr. Genom.* **2018**, *18*, 673–684. [CrossRef]
11. Niklas, K.J.; Cobb, E.D.; Matas, A.J. The evolution of hydrophobic cell wall biopolymers: From algae to angiosperms. *J. Exp. Bot.* **2017**, *68*, 5261–5269. [CrossRef]
12. Philippe, G.; Sorensen, I.; Jiao, C.; Sun, X.; Fei, Z.; Domozych, D.S.; Rose, J.K. Cutin and suberin: Assembly and origins of specialized lipidic cell wall scaffolds. *Curr. Opin. Plant Biol.* **2020**, *55*, 11–20. [CrossRef] [PubMed]
13. Smyth, D.R. Wrinkles on sepals: Cuticular ridges form when cuticle production outpaces epidermal cell expansion. *Mol. Plant* **2017**, *10*, 540–541. [CrossRef] [PubMed]
14. Yeats, T.H.; Huang, W.; Chatterjee, S.; Viart, H.M.; Clausen, M.H.; Stark, R.E.; Rose, J.K. Tomato Cutin Deficient 1 (CD1) and putative orthologs comprise an ancient family of cutin synthase-like (CUS) proteins that are conserved among land plants. *Plant J.* **2014**, *77*, 667–675. [CrossRef] [PubMed]

15. Kong, L.; Liu, Y.; Zhi, P.; Wang, X.; Xu, B.; Gong, Z.; Chang, C. Origins and evolution of cuticle biosynthetic machinery in land plants. *Plant Physiol.* **2020**, *184*, 1998–2010. [CrossRef] [PubMed]
16. Jiang, Y.Y.; Chen, R.J.; Dong, J.L.; Xu, Z.J.; Gao, X.L. Analysis of GDSL lipase (GLIP) family genes in rice (*Oryza sativa*). *Plant Omics* **2012**, *5*, 351–358.
17. Dolui, A.K.; Vijayaraj, P. Functional omics identifies serine hydrolases that mobilize storage lipids during rice seed germination. *Plant Physiol.* **2020**, *184*, 693–708. [CrossRef] [PubMed]
18. Clauss, K.; von Roepenack-Lahaye, E.; Bottcher, C.; Roth, M.R.; Welti, R.; Erban, A.; Kopka, J.; Scheel, D.; Milkowski, C.; Strack, D. Overexpression of sinapine esterase BnSCE3 in oilseed rape seeds triggers global changes in seed metabolism. *Plant Physiol.* **2011**, *155*, 1127–1145. [CrossRef]
19. Rombola-Caldentey, B.; Rueda-Romero, P.; Iglesias-Fernandez, R.; Carbonero, P.; Onate-Sanchez, L. Arabidopsis DELLA and two HD-ZIP transcription factors regulate GA signaling in the epidermis through the L1 Box cis-element. *Plant Cell* **2014**, *26*, 2905–2919. [CrossRef]
20. Riemann, M.; Gutjahr, C.; Korte, A.; Riemann, M.; Danger, B.; Muramatsu, T.; Bayer, U.; Waller, F.; Furuya, M.; Nick, P. GER1, a GDSL motif-encoding gene from rice is a novel early light- and jasmonate-induced gene. *Plant Biol.* **2007**, *9*, 32–40. [CrossRef]
21. Ursache, R.; De Jesus Vieira Teixeira, C.; Denervaud Tendon, V.; Gully, K.; De Bellis, D.; Schmid-Siegert, E.; Grube Andersen, T.; Shekhar, V.; Calderon, S.; Pradervand, S.; et al. GDSL-domain proteins have key roles in suberin polymerization and degradation. *Nat. Plants* **2021**, *7*, 353–364. [CrossRef] [PubMed]
22. Lee, D.S.; Kim, B.K.; Kwon, S.J.; Jin, H.C.; Park, O.K. Arabidopsis GDSL lipase 2 plays a role in pathogen defense via negative regulation of auxin signaling. *Biochem. Biophys. Res. Commun.* **2009**, *379*, 1038–1042. [CrossRef] [PubMed]
23. Takahashi, K.; Shimada, T.; Kondo, M.; Tamai, A.; Mori, M.; Nishimura, M.; Hara-Nishimura, I. Ectopic expression of an esterase, which is a candidate for the unidentified plant cutinase, causes cuticular defects in *Arabidopsis thaliana*. *Plant Cell Physiol.* **2010**, *51*, 123–131. [CrossRef] [PubMed]
24. Zhao, H.; Ma, B.; Duan, K.X.; Li, X.K.; Lu, X.; Yin, C.C.; Tao, J.J.; Wei, W.; Zhang, W.K.; Xin, P.Y.; et al. The GDSL lipase MHZ11 modulates ethylene signaling in rice roots. *Plant Cell* **2020**, *32*, 1626–1643. [CrossRef] [PubMed]
25. Savaldi-Goldstein, S.; Peto, C.; Chory, J. The epidermis both drives and restricts plant shoot growth. *Nature* **2007**, *446*, 199–202. [CrossRef] [PubMed]
26. Yu, Y.; Woo, M.O.; Rihua, P.; Koh, H.J. The DROOPING LEAF (DR) gene encoding GDSL esterase is involved in silica deposition in rice (*Oryza sativa* L.). *PLoS ONE* **2020**, *15*, e0238887. [CrossRef] [PubMed]
27. Park, J.J.; Jin, P.; Yoon, J.; Yang, J.I.; Jeong, H.J.; Ranathunge, K.; Schreiber, L.; Franke, R.; Lee, I.J.; An, G. Mutation in Wilted Dwarf and Lethal 1 (WDL1) causes abnormal cuticle formation and rapid water loss in rice. *Plant Mol. Biol.* **2010**, *74*, 91–103. [CrossRef]
28. Tang, J.; Yang, X.P.; Xiao, C.L.; Li, J.Y.; Chen, Y.Q.; Li, R.Y.; Li, S.P.; Lu, S.Y.; Hu, H.H. GDSL lipase occluded stomatal pore 1 is required for wax biosynthesis and stomatal cuticular ledge formation. *New Phytol.* **2020**, *228*, 1880–1896. [CrossRef]
29. Ishiguro, S.; Kawai-Oda, A.; Ueda, J.; Nishida, I.; Okada, K. The defective in anther dehiscence1 gene encodes a novel phospholipase A1 catalyzing the initial step of jasmonic acid biosynthesis, which synchronizes pollen maturation, anther dehiscence, and flower opening in Arabidopsis. *Plant Cell* **2001**, *13*, 2191–2209. [CrossRef]
30. Philippe, G.; Gaillard, C.; Petit, J.; Geneix, N.; Dalgalarrondo, M.; Bres, C.; Mauxion, J.P.; Franke, R.; Rothan, C.; Schreiber, L.; et al. Ester cross-link profiling of the cutin polymer of wild-type and cutin synthase tomato mutants highlights different mechanisms of polymerization. *Plant Physiol.* **2016**, *170*, 807–820. [CrossRef]
31. Hong, L.L.; Brown, J.; Segerson, N.A.; Rose, J.K.C.; Roeder, A.H.K. CUTIN SYNTHASE 2 maintains progressively Developing cuticular ridges in Arabidopsis sepals. *Mol. Plant* **2017**, *10*, 560–574. [CrossRef]
32. Ran, X.R.; Chen, X.; Shi, L.; Ashraf, M.; Yan, F.Z.; Chen, Y.Q.; Xu, J.; Shi, J.X. Transcriptomic insights into the roles of HSP70-16 in sepal's responses to developmental and mild heat stress signals. *Environ. Exp. Bot.* **2020**, *179*, 104225. [CrossRef]
33. Chen, X.; Shi, L.; Chen, Y.Q.; Zhu, L.; Zhang, D.S.; Xiao, S.; Aharoni, A.; Shi, J.X.; Xu, J. Arabidopsis HSP70-16 is required for flower opening under normal or mild heat stress temperatures. *Plant Cell Environ.* **2019**, *42*, 1190–1204. [CrossRef] [PubMed]
34. Zhang, D.; Shi, J.; Yang, X. Role of lipid metabolism in plant pollen exine development. In *Lipids in Plant and Algae Development*; Nakamura, Y., Li-Beisson, Y., Eds.; Springer: Cham, Switzerland, 2016; Volume 86, pp. 315–337, ISBN 978-3-319-25979-6.
35. Shi, J.; Cui, M.; Yang, L.; Kim, Y.J.; Zhang, D. Genetic and biochemical mechanisms of pollen wall development. *Trends Plant Sci.* **2015**, *20*, 741–753. [CrossRef] [PubMed]
36. Zhu, J.; Lou, Y.; Shi, Q.S.; Zhang, S.; Zhou, W.T.; Yang, J.; Zhang, C.; Yao, X.Z.; Xu, T.; Liu, J.L.; et al. Slowing development restores the fertility of thermo-sensitive male-sterile plant lines. *Nat. Plants* **2020**, *6*, 360–367. [CrossRef] [PubMed]
37. Tsugama, D.; Fujino, K.; Liu, S.; Takano, T. A GDSL-type esterase/lipase gene, GELP77, is necessary for pollen dissociation and fertility in Arabidopsis. *Biochem. Biophys. Res. Commun.* **2020**, *526*, 1036–1041. [CrossRef]
38. Xu, J.; Ding, Z.W.; Vizcay-Barrena, G.; Shi, J.X.; Liang, W.Q.; Yuan, Z.; Werck-Reichhart, D.; Schreiber, L.; Wilson, Z.A.; Zhang, D.B. ABORTED MICROSPORES acts as a master regulator of pollen wall formation in Arabidopsis. *Plant Cell* **2014**, *26*, 1544–1556. [CrossRef]
39. Zhao, J.; Long, T.; Wang, Y.F.; Tong, X.H.; Tang, J.; Li, J.L.; Wang, H.M.; Tang, L.Q.; Li, Z.Y.; Shu, Y.Z.; et al. RMS2 encoding a GDSL lipase mediates lipid homeostasis in anthers to determine rice male fertility. *Plant Physiol.* **2020**, *182*, 2047–2064. [CrossRef]

40. Zhang, H.H.; Wang, M.L.; Li, Y.Q.; Yan, W.; Chang, Z.Y.; Ni, H.L.; Chen, Z.F.; Wu, J.X.; Xu, C.J.; Deng, X.W.; et al. GDSL esterase/lipases OsGELP34 and OsGELP110/OsGELP115 are essential for rice pollen development. *J. Integr. Plant Biol.* **2020**, *62*, 1574–1593. [CrossRef]
41. Yuan, G.Q.; Zou, T.; Zhang, X.; Liu, M.M.; Luo, T.T.; He, Z.Y.; Tao, Y.; Zhou, D.; Zhao, H.F.; Liu, S.J.; et al. A rice GDSL esterase/lipase protein (GELP) is required for anther and pollen development. *Mol. Breed.* **2020**, *40*, 90. [CrossRef]
42. Huo, Y.Q.; Pei, Y.R.; Tian, Y.H.; Zhang, Z.G.; Li, K.; Liu, J.; Xiao, S.L.; Chen, H.B.; Liu, J. IRREGULAR POLLEN EXINE2 encodes a GDSL lipase essential for male fertility in maize. *Plant Physiol.* **2020**, *184*, 1438–1454. [CrossRef] [PubMed]
43. Updegraff, E.P.; Zhao, F.; Preuss, D. The extracellular lipase EXL4 is required for efficient hydration of Arabidopsis pollen. *Sex. Plant Reprod.* **2009**, *22*, 197–204. [CrossRef] [PubMed]
44. Kram, B.W.; Bainbridge, E.A.; Perera, M.A.D.N.; Carter, C. Identification, cloning and characterization of a GDSL lipase secreted into the nectar of *Jacaranda mimosifolia*. *Plant Mol. Biol.* **2008**, *68*, 173–183. [CrossRef] [PubMed]
45. Li, X.; Tieman, D.; Liu, Z.M.; Chen, K.S.; Klee, H.J. Identification of a lipase gene with a role in tomato fruit short-chain fatty acid-derived flavor volatiles by genome-wide association. *Plant J.* **2020**, *104*, 631–644. [CrossRef]
46. Girard, A.L.; Mounet, F.; Lemaire-Chamley, M.; Gaillard, C.; Elmorjani, K.; Vivancos, J.; Runavot, J.L.; Quemener, B.; Petit, J.; Germain, V.; et al. Tomato GDSL1 is required for cutin deposition in the fruit cuticle. *Plant Cell* **2012**, *24*, 3119–3134. [CrossRef]
47. Petit, J.; Bres, C.; Just, D.; Garcia, V.; Mauxion, J.P.; Marion, D.; Bakan, B.; Joubes, J.; Domergue, F.; Rothan, C. Analyses of tomatoFfruit brightness mutants uncover both cutin-deficient and cutin-abundant mutants and a new hypomorphic allele of GDSL lipase. *Plant Physiol.* **2014**, *164*, 888–906. [CrossRef]
48. Ma, R.D.; Yuan, H.L.; An, J.; Hao, X.Y.; Li, H.B. A Gossypium hirsutum GDSL lipase/hydrolase gene (GhGLIP) appears to be involved in promoting seed growth in Arabidopsis. *PLoS ONE* **2018**, *13*, e0195556. [CrossRef]
49. Kondou, Y.; Nakazawa, M.; Kawashima, M.; Ichikawa, T.; Yoshizumi, T.; Suzuki, K.; Ishikawa, A.; Koshi, T.; Matsui, R.; Muto, S.; et al. RETARDED GROWTH OF EMBRYO1, a new basic helix-loop-helix protein, expresses in endosperm to control embryo growth. *Plant Physiol.* **2008**, *147*, 1924–1935. [CrossRef]
50. Hong, J.K.; Choi, H.W.; Hwang, I.S.; Kim, D.S.; Kim, N.H.; Choi, D.S.; Kim, Y.J.; Hwang, B.K. Function of a novel GDSL-type pepper lipase gene, CaGLIP1, in disease susceptibility and abiotic stress tolerance. *Planta* **2008**, *227*, 539–558. [CrossRef]
51. Huang, L.M.; Lai, C.P.; Chen, L.F.O.; Chan, M.T.; Shaw, J.F. Arabidopsis SFAR4 is a novel GDSL-type esterase involved in fatty acid degradation and glucose tolerance. *Bot. Stud.* **2015**, *56*, 33. [CrossRef]
52. Gao, M.J.; Yi, X.; Yang, W.B.; Lam, S.M.; Tong, X.H.; Liu, J.Y.; Wang, X.; Li, Q.; Shui, G.H.; He, Z.H. GDSL lipases modulate immunity through lipid homeostasis in rice. *PLoS Pathog.* **2017**, *13*, e1006724. [CrossRef] [PubMed]
53. Wang, K.; Froehlich, J.E.; Zienkiewicz, A.; Hersh, H.L.; Benning, C. A Plastid phosphatidylglycerol lipase contributes to the export of acyl groups from plastids for seed oil biosynthesis. *Plant Cell* **2017**, *29*, 1678–1696. [CrossRef] [PubMed]
54. Zhang, L.J.; Gao, C.X.; Mentink-Vigier, F.; Tang, L.; Zhang, D.M.; Wang, S.G.; Cao, S.X.; Xu, Z.P.; Liu, X.L.; Wang, T.; et al. Arabinosyl deacetylase modulates the arabinoxylan acetylation profile and secondary wall formation. *Plant Cell* **2019**, *31*, 1113–1126. [CrossRef]
55. Zhang, B.; Zhang, L.; Li, F.; Zhang, D.; Liu, X.; Wang, H.; Xu, Z.; Chu, C.; Zhou, Y. Control of secondary cell wall patterning involves xylan deacetylation by a GDSL esterase. *Nat. Plants* **2017**, *3*, 17017. [CrossRef] [PubMed]
56. Yadav, V.K.; Yadav, V.K.; Pant, P.; Singh, S.P.; Maurya, R.; Sable, A.; Sawant, S.V. GhMYB1 regulates SCW stage-specific expression of the GhGDSL promoter in the fibres of *Gossypium hirsutum* L. *Plant Biotechnol. J.* **2017**, *15*, 1163–1174. [CrossRef] [PubMed]
57. Yeats, T.H.; Martin, L.B.; Viart, H.M.; Isaacson, T.; He, Y.; Zhao, L.; Matas, A.J.; Buda, G.J.; Domozych, D.S.; Clausen, M.H.; et al. The identification of cutin synthase: Formation of the plant polyester cutin. *Nat. Chem. Biol.* **2012**, *8*, 609–611. [CrossRef]
58. Kikuta, Y.; Ueda, H.; Takahashi, M.; Mitsumori, T.; Yamada, G.; Sakamori, K.; Takeda, K.; Furutani, S.; Nakayama, K.; Katsuda, Y.; et al. Identification and characterization of a GDSL lipase-like protein that catalyzes the ester-forming reaction for pyrethrin biosynthesis in *Tanacetum cinerariifolium*- a new target for plant protection. *Plant J.* **2012**, *71*, 183–193. [CrossRef]
59. Teutschbein, J.; Gross, W.; Nimtz, M.; Milkowski, C.; Hause, B.; Strack, D. Identification and localization of a lipase-like acyltransferase in phenylpropanoid metabolism of tomato (*Solanum lycopersicum*). *J. Biol. Chem.* **2010**, *285*, 38374–38381. [CrossRef]
60. Watkins, J.L.; Li, M.; McQuinn, R.P.; Chan, K.X.; McFarlane, H.E.; Ermakova, M.; Furbank, R.T.; Mares, D.; Dong, C.M.; Chalmers, K.J.; et al. A GDSL esterase/lipase catalyzes the esterification of lutein in bread wheat. *Plant Cell* **2019**, *31*, 3092–3112. [CrossRef]
61. Wang, K.; Guo, Q.; Froehlich, J.E.; Hersh, H.L.; Zienkiewicz, A.; Howe, G.A.; Benning, C. Two abscisic acid-responsive plastid lipase genes involved in jasmonic acid biosynthesis in *Arabidopsis thaliana*. *Plant Cell* **2018**, *30*, 1006–1022. [CrossRef]
62. Oh, I.S.; Park, A.R.; Bae, M.S.; Kwon, S.J.; Kim, Y.S.; Lee, J.E.; Kang, N.Y.; Lee, S.M.; Cheong, H.; Park, O.K. Secretome analysis reveals an Arabidopsis lipase involved in defense against *Alternaria brassicicola*. *Plant Cell* **2005**, *17*, 2832–2847. [CrossRef] [PubMed]
63. Kim, H.G.; Kwon, S.J.; Jang, Y.J.; Nam, M.H.; Chung, J.H.; Na, Y.C.; Guo, H.W.; Park, O.K. GDSL LIPASE1 modulates plant immunity through feedback regulation of ethylene signaling. *Plant Physiol.* **2013**, *163*, 1776–1791. [CrossRef] [PubMed]
64. Hubner, S.; Bercovich, N.; Todesco, M.; Mandel, J.R.; Odenheimer, J.; Ziegler, E.; Lee, J.S.; Baute, G.J.; Owens, G.L.; Grassa, C.J.; et al. Sunflower pan-genome analysis shows that hybridization altered gene content and disease resistance. *Nat. Plants* **2019**, *5*, 54–62. [CrossRef] [PubMed]

65. Aharoni, A.; Dixit, S.; Jetter, R.; Thoenes, E.; van Arkel, G.; Pereira, A. The SHINE clade of AP2 domain transcription factors activates wax biosynthesis, alters cuticle properties, and confers drought tolerance when overexpressed in Arabidopsis. *Plant Cell* **2004**, *16*, 2463–2480. [CrossRef]
66. Shi, J.X.; Malitsky, S.; De Oliveira, S.; Branigan, C.; Franke, R.B.; Schreiber, L.; Aharoni, A. SHINE transcription factors act redundantly to pattern the archetypal surface of Arabidopsis flower organs. *PLoS Genet.* **2011**, *7*, e1001388. [CrossRef] [PubMed]
67. Shi, J.X.; Adato, A.; Alkan, N.; He, Y.H.; Lashbrooke, J.; Matas, A.J.; Meir, S.; Malitsky, S.; Isaacson, T.; Prusky, D.; et al. The tomato SlSHINE3 transcription factor regulates fruit cuticle formation and epidermal patterning. *New Phytol.* **2013**, *197*, 468–480. [CrossRef]
68. Jung, K.H.; Han, M.J.; Lee, Y.S.; Kim, Y.W.; Hwang, I.W.; Kim, M.J.; Kim, Y.K.; Nahm, B.H.; An, G.H. Rice Undeveloped Tapetum1 is a major regulator of early tapetum development. *Plant Cell* **2005**, *17*, 2705–2722. [CrossRef]
69. Li, H.; Yuan, Z.; Vizcay-Barrena, G.; Yang, C.Y.; Liang, W.Q.; Zong, J.; Wilson, Z.A.; Zhang, D.B. PERSISTENT TAPETAL CELL1 encodes a PHD-finger protein that is required for tapetal cell death and pollen development in rice. *Plant Physiol.* **2011**, *156*, 615–630. [CrossRef]
70. Zhang, W. A GDSL lipase is required for anther and pollen development. *Plant Physiol.* **2020**, *182*, 1810–1811. [CrossRef]
71. Miao, X.Y.; Qu, H.P.; Han, Y.L.; He, C.F.; Qiu, D.W.; Cheng, Z.W. The protein elicitor Hrip1 enhances resistance to insects and early bolting and flowering in *Arabidopsis thaliana*. *PLoS ONE* **2019**, *14*, e0216082. [CrossRef]
72. Han, X.F.; Li, S.; Zhang, M.; Yang, L.Y.; Liu, Y.D.; Xu, J.; Zhang, S.Q. Regulation of GDSL lipase gene expression by the MPK3/MPK6 cascade and its downstream WRKY transcription factors in Arabidopsis immunity. *Mol. Plant Microbe* **2019**, *32*, 673–684. [CrossRef] [PubMed]

plants

MDPI

Review

Nettle Cultivation Practices—From Open Field to Modern Hydroponics: A Case Study of Specialized Metabolites

Nevena Opačić [1], Sanja Radman [1,*], Sanja Fabek Uher [1], Božidar Benko [1], Sandra Voća [2] and Jana Šic Žlabur [2]

[1] Department of Vegetable Crops, University of Zagreb Faculty of Agriculture, Svetošimunska Cesta 25, 10000 Zagreb, Croatia; nopacic@agr.hr (N.O.); sfabek@agr.hr (S.F.U.); bbenko@agr.hr (B.B.)
[2] Department of Agricultural Technology, Storage and Transport, University of Zagreb Faculty of Agriculture, Svetošimunska Cesta 25, 10000 Zagreb, Croatia; svoca@agr.hr (S.V.); jszlabur@agr.hr (J.Š.Ž.)
* Correspondence: sradman@agr.hr

Abstract: Conventional agricultural production faces numerous challenges due to the pronounced effects of climate change, particularly global warming, and drought more than ever before in history, with the primary concern being to produce adequate yields and high-quality, nutritious plant material. Likewise, people are increasingly looking for new sources of food and are becoming aware of the importance of a varied diet and its connection to health. In this sense, stinging nettle (*Urtica dioica* L.) stands out as a valuable species that is neglected as a food source, as it has a significant content of specialized metabolites, and thus has an extremely high potential for use both nutritionally and pharmacologically, but is still traditionally collected from natural habitats, so it can be of questionable quality and undefined chemical composition. Therefore, sustainable agricultural practices are increasingly shifting to modern hydroponic cultivation methods in greenhouses. The advantage lies in the easier management and control of a number of factors during cultivation (air temperature and relative humidity, balanced and rational fertilization, minimization of nitrate uptake, etc.), ensuring better conditions for the growth and development of nettle according to its needs. The aim of this review is to give an overview of the technology of stinging nettle cultivation in the field and to show the possibilities of cultivation with modern hydroponic techniques to obtain a final product of consistent and uniform quality, high content of specialized metabolites and significant nutritional value. Research on this topic is still sparse but will certainly increase in the future. Therefore, this review provides all the necessary data for such future studies.

Keywords: *Urtica dioica*; soilless systems; bioactive compounds; cultivated nettle; stress factors; functional properties

Citation: Opačić, N.; Radman, S.; Fabek Uher, S.; Benko, B.; Voća, S.; Šic Žlabur, J. Nettle Cultivation Practices—From Open Field to Modern Hydroponics: A Case Study of Specialized Metabolites. *Plants* **2022**, *11*, 483. https://doi.org/10.3390/plants11040483

Academic Editors: Milan S. Stankovic, Paula Baptista and Petronia Carillo

Received: 26 December 2021
Accepted: 9 February 2022
Published: 11 February 2022

1. Introduction

The current trend among consumers is to pay more attention to a balanced diet and the consumption of wild leafy plants, as they are recognized as a source of a high content of phytonutrients [1–4], which play an important role in the prevention of many chronic diseases [5]. One of these wild edible species is stinging nettle (*Urtica dioica* L.), which has been known since ancient times for its medicinal value as a herbal remedy for the treatment of numerous health problems [3,6–8]. Nettle is perhaps one of the most widely distributed wild plants, found in all regions of the temperate zones and growing in all seasons [3]. Although it is consumed as a green vegetable in some parts of the world, it is often considered a weed and neglected despite its high nutritional value [8–11]. All parts of the plant (flowers, stems, leaves and roots) can be used in the food, cosmetic and pharmaceutical industries for their health-promoting properties [8,12,13], as nettle is rich in various biologically active compounds and specialized metabolites (SM) [10]. The phytochemical profile of nettle leaves can be divided into several categories: terpenoids,

chlorophylls and carotenoids, fatty acids, polyphenolic acids and compounds, essential amino acids, vitamins, tannins, carbohydrates, sterols, polysaccharides, isolectins and minerals [10,14,15]. According to various studies [1–3,16,17], the presence of chemical components in plants is variable, of inconsistent quality and depends on many abiotic, biotic and anthropological factors as well as on the conditions of raw material storage. Phytochemicals, i.e., SM are products of various metabolic pathways whose synthesis is directly influenced by these factors.

Most nettle herb is wild harvested [9], but it is challenging and even expensive to control the quality standards of wild collected plants and obtain a standardized product with a high content of SM [6]. Large differences are observed in genotype-environment interactions so that the same species has large differences in the availability of SM under different environmental conditions and habitats [18]. Therefore, cultivation is recommended, but often open field cultivation does not allow complete control over the growing conditions and consequently the SM content of the plants. There is a need for alternative systems for the production of medicinal plants, which could be an effective means to overcome the increased risk associated with open field cultivation [6,19].

Hydroponics, soilless techniques, are suitable for the cultivation of many vegetable species, but hydroponic cultivation of medicinal and aromatic plants is also attracting great interest [20–22]. These techniques allow for more efficient use of water and nutrients, resulting in accelerated plant growth, earlier and multiple harvests, more production cycles as crops can be grown throughout the year, and higher biomass production, ultimately leading to higher yields [21,23]. Previous research on hydroponic techniques was based on leafy vegetables with short vegetation [21,24–29], but there are few studies on hydroponic cultivation of perennial deciduous species, such as stinging nettle.

Based on the literature reviewed, which supports the fact that stinging nettle is a mesophilic, nitrophilic species and a phytoremediator that can retrovegetate during a growing season, it is our hypothesis that stinging nettle could reach its full biological potential through greenhouse cultivation using modern hydroponic techniques. Through the appropriate management of some hydroponic techniques (e.g., induction of water stress in the ebb and flow system), it is possible to create positive stress conditions that help increase SM and the nutritional value of the plant material.

Therefore, the aim of this study was to provide a detailed overview of the nutritional and functional aspects of stinging nettle, the possibilities of growing stinging nettle in the open field, and a detailed overview of hydroponic cultivation techniques for growing stinging nettle in greenhouses, such as the nutrient film technique, floating hydroponics, ebb and flow, and the aeroponic system as the best options for stinging nettle growing.

2. Nutritional Aspects of Nettle

Stinging nettle is a plant with great nutritional value, containing biologically significant classes of chemical compounds. Nettle leaves contain 4–7% carbohydrates, 6% dietary fiber, 0.6–9% fat, and 0.4–4% protein [30,31], while Zeipiņa et al. [32] stated that proteins from *Urtica* leaves are of better quality compared to proteins from other leafy vegetables. Among the most abundant fatty acids in nettle, palmitic acid and linoleic acid stand out [4,7,9,33,34]. It is a valuable source of vitamins A, B group vitamins, C, D, E, and K, and minerals [7,8,11,13–16,31,32,35–38], especially P, Ca, Mg, and Fe, the values of which are listed in Table 1 according to various authors.

Table 1. The content of the main minerals in nettle depends on the habitats and the part of the plant analyzed.

Mineral	Content	Method Used	Cultivation or Wild Harvest Location	Plant Part	Reference
Ca	28,605 µg/g	US EPA, 1994	wild harvested (Serbia)	dried leaves	[7]
	853–1050 mg/100 g	unknown	unknown	whole plant	[9]
	3.43%	Nowosielski, 1988	open field (Poland)	leaves	[16]
	2.15–3.09%	AOAC, 1995	floating hydroponics (Croatia)	leaves	[17]
	168.77 mg/100 g	AOAC, 2005	wild harvested (Nepal)	dry leaves powder	[31]
	278–788 mg/100 g	AOAC, 2000	open field (USA)	shoots before flowering	[33]
	323 mg/100 g	AACC Int., 2000	open field (South Africa)	leaves	[37]
	3.04%	71/250/EEC	open field (Lithuania)	leaves	[38]
	2.63–5.09%	AOAC, 1995	wild harvested (Macedonia)	leaves	[39]
	5.21%	AOAC, 1995	open field (Croatia)	leaves before flowering	[40]
Fe	150.97 µg/g	US EPA, 1994	wild harvested (Serbia)	dried leaves	[7]
	227.89 mg/100 g	unknown	unknown	leaf powder	[8]
	2–200 mg/100 g	unknown	unknown	whole plant	[9]
	79.20–89.50 mg/kg	AOAC, 1995	floating hydroponics (Croatia)	leaves	[17]
	886–3651 mg/kg	AOAC, 1995	open field (Croatia)	leaves	[28]
	227.89 mg/100 g	AOAC, 2005	wild harvested (Nepal)	dry leaves powder	[31]
	1.2–3.4 mg/100 g	AOAC, 2000	open field (USA)	shoots before flowering	[33]
	2.5 mg/100 g	AACC Int., 2000	open field (South Africa)	leaves	[37]
	224.78 mg/kg	73/46/EEC	open field, (Lithuania)	leaves	[38]
	2765 ppm	AOAC, 1995	open field (Croatia)	leaves before flowering	[40]
	145–2717 mg/kg	AOAC, 1995	open field (Croatia)	leaves before flowering	[41]
Mg	8699.76 µg/g	US EPA, 1994	wild harvested (Serbia)	dried leaves	[7]
	0.34%	Nowosielski, 1988	open field (Poland)	leaves	[16]
	0.23–0.48%	AOAC, 1995	floating hydroponics (Croatia)	leaves	[17]
	104 mg/100 g	AACC Int., 2000	open field (South Africa)	leaves	[37]
	0.61%	73/46/EEC	open field, (Lithuania)	leaves	[38]
	2.51–3.56%	AOAC, 1995	wild harvested (Macedonia)	leaves	[39]
P	50–265 mg/100 g	unknown	unknown	whole plant	[9]
	0.39%	Nowosielski, 1988	open field (Poland)	leaves	[16]
	0.41–0.49%	AOAC, 1995	floating hydroponics (Croatia)	leaves	[17]
	82.6 mg/100 g	AACC Int., 2000	open field (South Africa)	leaves	[37]
	0.82%	71/393/EEC	open field (Lithuania)	leaves	[38]

Table 2 lists the content of some SM in stinging nettle identified in various studies. In addition to the SM listed in the table, nettle also contains essential amino acids, tannins, various flavonoids [3,7,11,13,14,34,35,37,42], volatile compounds [3,11,16,36], essential oils with carvacrol, carvone and naphthalene as major constituents [7,35,36], phytosterols, saponins [36], coumarins [14,38], amines, glucokinins [11] and terpenoids [7–9,12,38]. Nine carotenoids are present in stinging nettle, the most important of which are β-carotene, violaxanthin, xanthophylls, zeaxanthin, luteoxanthin, and lutein epoxide [8,10,32,38]. Nettle also contains caffeic acid, hydroxybenzoic acid, vanillic acid, coumaric acid, and quinic acid, among others, as well as many caffeic acid and quinic acid derivatives [9,12,36,42]. It is important to emphasize that the amounts of these chemical compounds vary greatly from author to author. This is because their amount depends on the origin of the plant material, the plant part, the phenological stage, and the analytical method used for their determination. Many authors emphasize the antioxidant properties of nettle, which are

determined by phenols, vitamins, pigments, and other compounds [38]. The values of antioxidant capacity of nettle leaves are also listed in Table 2.

Table 2. The content of SM and antioxidant capacity in nettle depends on the habitats and the part of the plant analyzed.

Specialized Metabolite	Content	Method Used	Cultivation or Wild Harvest Location	Plant Part	Reference
Total carotenoids	1.62 mg/g	spectrophotometry	wild harvested (Latvia)	leaves (ethanol extract)	[1]
	51.4–74.8 µg/g	Wills et al., 1988	wild harvested (Spain)	leaves	[4]
	5.47 mg/g	Wellburn, 1994; Dere et al., 1998; Pavlić et al., 2016	wild harvested (Serbia)	dried leaves (96% ethanol extract)	[7]
	2.95–8 mg/100 g	unknown	unknown	whole plant	[9]
	33.03 mg/100 g	Castro– Puyana et al. (2017)	wild harvested (Croatia)	leaves and stalks	[13]
	1.31 mg/g	Rumińska et al., 1985	open field (Poland)	leaves	[16]
	3496.67 µg/g, db	Ranganna (2001)	wild harvested (Nepal)	dry leaves powder	[31]
	0.55 mg/g	spectrophotometry	wild harvested (Latvia)	shoots	[32]
	0.216–0.323 mg/g	Holm, 1954 and Van Wattstein, 1957	wild harvested (Bosnia and Herzegovina)	leaves	[35]
	15.36 mg/100 g	Strumite et al., 2015	open field (Lithuania)	leaves	[38]
	0.81–1.01 mg/g	Porra et al., 1989	open field (Poland)	leaves	[43]
β-carotene	3.8–5.6 µg/g	Wills et al., 1988	wild harvested (Spain)	leaves	[4]
	5035–7860 IU/100 g	colorimetry	open field (USA)	shoots before flowering	[33]
	58,059 µg/100 g	colorimetry	open field (South Africa)	leaves	[37]
Total chlorophyll	24.13 mg/g	Wellburn, 1994; Dere et al., 1998; Pavlić et al., 2016	wild harvested (Serbia)	dried leaves (96% ethanol extract)	[7]
	4.8 mg/g	unknown	wild harvested	leaves	[8]
	611.19 mg/100 g	Castro–Puyana et al. (2017)	wild harvested (Croatia)	leaves and stalks	[13]
	9.66 mg/g	Rumińska et al., 1985	open field (Poland)	leaves	[16]
	1.02–1.174 mg/g	Holm, 1954 and Van Wattstein, 1957	wild harvested (Bosnia and Herzegovina)	leaves	[35]
	2.17 mg/g	spectrophotometry	wild harvested (Latvia)	shoots	[32]
	8.03–9.45 mg/g	Porra et al., 1989	open field (Poland)	leaves	[43]
Chlorophyll a	5.56 mg/g	spectrophotometer	wild harvested (Latvia)	leaves (ethanol extract)	[1]
	16.55 mg/g	Wellburn, 1994; Dere et al., 1998; Pavlić et al., 2016	wild harvested (Serbia)	dried leaves (96% ethanol extract)	[7]
	0.698–0.882 mg/g	Holm, 1954 and Van Wattstein, 1957	wild harvested (Bosnia and Herzegovina)	leaves	[35]
	67.29 mg/100 g	Strumite et al., 2015	open field (Lithuania)	leaves	[38]
Chlorophyll b	1.84 mg/100 g	spectrophotometer	wild harvested (Latvia)	leaves (ethanol extract)	[1]
	7.58 mg/g	Wellburn, 1994; Dere et al., 1998; Pavlić et al., 2016	wild harvested (Serbia)	dried leaves (96% ethanol extract)	[7]
	0.285–0.320 mg/g	Holm, 1954 and Van Wattstein, 1957	wild harvested (Bosnia and Herzegovina)	leaves	[35]
	29.14 mg/100 g	Strumite et al., 2015	open field (Lithuania)	leaves	[38]
Total phenolics	128.75 mg GAE/g	unknown	unknown	leaf powder	[8]
	380.90 mg/100 g	Repajić et al., 2020	wild harvested (Croatia)	leaves and stalks	[13]
	14.47 mg/g	Slinghart et al., 1977	open field (Poland)	leaves	[16]
	140 mg GAE/g	Folin–Ciocalteu	wild harvested (Italy)	leaves	[12]
	450.81–539.27 mg GAE/g	Folin–Ciocalteu	unknown (Serbia)	dried leaves (different extraction methods)	[14]
	128.75 mg GAE/g	Ranganna, 2001	wild harvested (Nepal)	dry leaves powder	[31]
	26.78 mg GAE/g	unknown	wild harvested (Turkey)	USB extract	[34]
	208.37 mg GAE/g	Folin–Ciocalteu	wild harvested (Bosnia and Herzegovina)	leaves	[35]
	118.4 mg GAE/g	Folin–Ciocalteu	open field (South Africa)	leaves	[37]
	8.87 mg GAE/g	Folin–Ciocalteu	open field (Lithuania)	leaves	[38]
	732.49 mg GAE/100 g	Ough and Amerine, 1988	open field (Croatia)	leaves before flowering	[40]
	22.01–24.94 mg/g	Folin–Ciocalteu	open field (Poland)	leaves	[43]
	7.9 g/100 g	Folin–Ciocalteu	wild harvested (Portugal)	dry aerial parts during flowering	[44]
	28.42 µg/g	Orčić et al., 2014	wild harvested (Serbia)	herb	[45]

Table 2. *Cont.*

Specialized Metabolite	Content	Method Used	Cultivation or Wild Harvest Location	Plant Part	Reference
Vitamin C	20–60 mg/100 g	unknown	unknown	whole plant	[9]
	8.4 mg/g	Kampfenkel et al., 1995	wild harvested (Italy)	leaves	[12]
	0.5–1.1 mg/100 g	AOAC, 2000	open field (USA	shoots before flowering	[33]
	14.2 mg/100 g	HPLC	open field (South Africa)	leaves	[37]
	8.53 mg/100 g	Latimer, 2016	open field (Lithuania)	leaves	[38]
	63.75 mg/100 g	AOAC, 2002	open field (Croatia)	leaves before flowering	[40]
Antioxidant capacity	60 mg TEAC/g	Brand-Williams et al., 1995	wild harvested (Italy)	leaves	[12]
	26.5 µM Trolox/g	Re et al., 1999	open field (Poland)	leaves	[16]
	66.3% DPPH	Nuengchamnong et al., 2009	wild harvested (Nepal)	dry leaves powder	[31]
	0.85% DPPH	DPPH	wild harvested (Bosnia and Herzegovina)	leaves (ethanol extract)	[35]
	65.1% DPPH	Brand-Williams et al., 1995	open field (South Africa)	leaves	[37]
	70.37% DPPH	Zeipina et al., 2015	open field (Lithuania)	leaves	[38]
	1936.58 mM Trolox/L	Miller et al., 1993; Re et al., 1999	open field (Croatia)	leaves before flowering	[40]
	10.95–11.80 µM Trolox/g	Re et al., 1999	open field (Poland)	leaves	[43]

3. Functional Properties and Use of Nettle

Nettle, like other plants, was and is used as a general remedy, both in traditional folk medicine and in industrially manufactured products [46]. Cancer, emphysema, cirrhosis of the liver, atherosclerosis, atheroma, hypertension, neoplasms, and arthritis are all associated with oxidative damage, but foods rich in antioxidants can help the human body reduce oxidative damage from free radicals and active oxygen [16,46]. According to various studies [4,7,8,10,12–16,36,43,47], all parts of the nettle plant possess anti-radical and antioxidant, anti-inflammatory, antimicrobial, antifungal, antiviral, anti-ulcer, anti-rheumatic, and anti-cancer properties due to their rich phytochemical composition. The beneficial pharmacological effects of nettle leaves are probably due to the content of flavanol glycosides, phenolic and amino acids, tannins, vitamins, and carotenoids [48,49].

Fresh nettle has been used since Roman times to treat urticaria, to stimulate blood circulation and warm the joints and extremities [7,32] and to help with rheumatism and arthritis [3,14,45,46,48–51]. The aqueous and alcoholic extracts of nettle are used to treat rhinitis [9,10] and lung diseases [3,16,32,51], while it is reported that dried nettle is good for treating allergies [14,43]. It is also used as a moderate diuretic and for ailments related to urinary and renal problems [3,8,13,14,16,32,42,43,45,46,48,49], cardiovascular problems [9,10,43,45,48,52], diabetes [48], gout [8,10,13], eczema [10,32,46,48], and liver cirrhosis [16,50]. Chemotherapeutic agents from nettle are being developed for the treatment of cancer patients [32,51].

Nettle is traditionally used as a green leafy vegetable in many Mediterranean and Eastern European countries [7,9,10,14,53]. Young leaves and shoots are usually collected in spring before flowering [3,32,53], as older plants may contain higher amounts of cystolytes, which can irritate the kidneys [8]. Because of its very similar taste and texture, cooked nettle is often used as a spinach substitute [8]. It is also used in the preparation of various dishes, such as salads, soups, vegetable cakes [3,8,10,13,45,53] or rice and pasta dishes [3,53]. Very often, the herb is used to prepare tea, which can be a nutrient-rich substitute for water [8–10,13], in the UK it is used to prepare drinks similar to ginger beer [3,8], or it can be used for cocktails and herbal liqueurs [3,53]. Increasingly, nettle is used as livestock feed and improves the quality of meat, eggs, and dairy products [32,53]. The food industry uses nettle to produce milk curd and to extract chlorophyll (as used as green dye E140) or yellow dye from its roots. It is also used in the medical, pharmaceutical, and cosmetic industries for the production of hair shampoos and tonics [3,7,13,32,47,53]. Other traditional uses of stinging nettle include the textile industry, where it is used for light and resistant fibers from its stems [47], and the production of biopesticides [53].

4. Cultivation of Nettle—From Open Field to Hydroponics

Due to the high nutritional value and functional properties, as well as the wide use of stinging nettle described in Sections 2 and 3, the demand for its fresh biomass is increasing. Nettle is traditionally collected from the wild for various purposes (organic fertilizer, food, pharmacological and cosmetic products), but this type of plant material is often of questionable quality and inconsistent chemical composition and even unsuitable for human consumption. In fact, nettle is also mentioned as a hyperaccumulating plant that has a strong tendency to collect heavy metals (Pb, Cd, Zn, As) from the soil in leaves and shoots, so wild harvested plant material may be contaminated. This ability to accumulate heavy metals and nutrients, such as nitrogen and phosphorus is sometimes used to purify the soil, which is why nettle is considered a phytoremediation plant [54,55]. Moreover, stinging nettle is a nitrophilous plant species that prefers to grow in soils rich in nitrogen and organic matter, which can lead to the accumulation of potentially harmful nitrates in plant material [40]. All this indicates the need to introduce nettle into agricultural production, but the technology of nettle cultivation is still unknown and insufficiently researched [19].

Since most research studies analyze the chemical composition of wild-collected nettles, it is important to emphasize that it is difficult to find detailed information on both appropriate cultivation techniques (field or greenhouse) and the nutrient quality or SM content of the cultivated plant material. Literature indicates that nettle can be propagated both generatively and vegetatively, by direct seeding, by seedlings, or by planting underground stems (rhizomes) [10,41]. In generative propagation by seeds, it should be noted that nettle seeds are quite small, and their absolute weight is about 0.15 g (Figure 1). Therefore, when sowing in the field, it is important to prepare the sowing layer adequately (fine preparation of the soil surface) and not to sow deeper than 1 cm. Since nettle seeds have a hard seed coat, which makes germination difficult, sowing in autumn (but before the late autumn frosts) is more favorable than sowing in spring. In this case, the dormancy of the seed is canceled, and the seeds germinate the following spring.

Figure 1. *Urtica dioica* seeds.

The distance between rows is 20 cm and it is recommended to sow about 1000 seeds/m^2. However, it is known that seed germination is affected by numerous abiotic (humidity, heat, light, and substrate) and biotic (seed size and type, seed coat thickness and permeability, dormancy) factors, which may result in lower seed germination (20–23% under controlled conditions in the climate chamber; [56]), longer germination time, and uneven planting density. It takes a long time for seeds to germinate and some time for them to reach a favorable plant density, so weeds can also be a potential problem in field cultivation. Radman et al. [28,40] concluded that although direct seeding is a faster and cheaper method of nettle propagation, it is not used in practice because of the many limiting factors mentioned above. Vegetative propagation by rhizomes is also relatively cheap (the cost of producing and procuring planting material is eliminated), but it is a more demanding propagation method, especially for intensive production, because it requires a lot of physical labor. Rhizomes are taken from the existing planting in late fall, removing above-ground, rotten and dead parts. Then the cleaned rhizomes are separated and cut to a length of 25–30 cm. It is important to coordinate the removal with planting to keep the rhizomes out of the soil as short as possible to avoid desiccation. Another risk of this propagation technique is that the age of the rhizome and the number of dormant buds cannot be determined at the time of removal [57].

In view of all this, it is recommended to grow nettles from seedlings sown in greenhouses in early spring and planted outdoors after about 40 days, but the optimal cultivation technique is not yet well defined or researched [16,41].

Seedlings (Figure 2a) should be grown under controlled conditions in a greenhouse at a temperature of 15 or 20 °C and a relative humidity of 60%. Stepanović et al. [57] state that the optimal conditions for germination of nettle seeds are light or a 12-h light and dark period at a temperature of 15–20 °C. Temperatures of 20–25 °C are recommended for herb growth and development (Figure 2b) [30,56].

(**a**) (**b**)

Figure 2. (**a**) Nettle seedlings in polystyrene containers; (**b**) Nettle herb growing in the open field.

Considering that in nature nettle prefers moist sites at forest edges and along springs or rivers, the lack of precipitation during certain growth stages of the plant can be a serious problem in field cultivation [8]. Therefore, irrigation must be provided, especially in dry and semi-arid areas.

In cultivation, it is important to provide the plants with the necessary nutrients, through an appropriate and, above all, balanced fertilization. Nettle requires various nutrients for its growth and development, especially nitrogen, which is why it is considered

a very nitrophilous plant species [41,57]. On the other hand, as mentioned earlier, in the cultivation of leafy vegetables, a higher nitrogen supply can lead to excessive accumulation of nitrates and negatively affect crop quality and groundwater contamination. Nitrate itself is relatively nontoxic, but its metabolites can lead to a number of health problems, such as methemoglobinemia in young children. The European Union prescribes maximum allowable levels for nitrate in lettuce and spinach in Regulation 563/2002 [58], but there are no regulations for other types of leafy vegetables [24,28]. For these reasons, the balanced application of nitrogen fertilizers is of paramount importance to enable the availability of high-quality plant material [28]. For optimum yields and high content of SM in the plant material, it is recommended to apply 100 kg/ha of nitrogen fertilizer (KAN) at several intervals during growth, depending on the amount of available nutrients in the soil and the planned number of harvests. Nettle is also rich in minerals (Table 1), such as P, Ca, Mg and Fe [28,33,40,59], which means that the soil must be supplied with these nutrients in a form in which the plant can absorb them because the uptake of nutrients by the root system of the plant depends on a number of its physicochemical properties [41].

Nettle is characterized by its ability to retrovegetate, so it can be harvested several times during the growing season (Figure 3). The stage at which it is harvested depends on the objective of cultivation, e.g., intensive growth of the plant before flowering when the objective of cultivation is a fresh leaf for human consumption. Harvesting is carried out above the first two nodules to allow the plant to regenerate [9,41].

Figure 3. Harvesting nettle in open field.

5. Possibilities and Challenges of Hydroponic Nettle Cultivation

In general, the quality of plants grown outdoors varies from year to year due to fluctuating environmental conditions (early or late frost, hail, extreme temperature changes) and it is difficult or even impossible to obtain fully standardized plant material [19].

Cultivation under controlled conditions in a greenhouse provides the opportunity to increase and equalize the quality of the raw material by monitoring and managing abiotic factors during plant growth [21]. New strategies and cultivation technologies are constantly being developed to address specific constraints during production and, more importantly, to reduce the negative impact of environmental factors (climate-related floods, wildfires,

drought, and heatwaves, and in some cases, hurricanes) and adapt to new market demands and consumer needs [30].

Hydroponic cultivation techniques, i.e., cultivation in nutrient solution with or without substrates, is a successful alternative to traditional agriculture. Hydroponic cultivation eliminates potential problems caused by soil contamination with heavy metals and pesticide residues or by complex soil-nutrient relationships, allows lower water consumption, and precise and balanced plant nutrition according to the needs of the cultivated species to ensure high yields and nutrient-rich raw material [23,60–62].

Hydroponics takes advantage of the fact that plants can synthesize all necessary metabolic products from inorganic ions, water and CO_2 using solar energy. All nutrients are provided in their inorganic form by the water solution according to the average requirement of a particular crop during cultivation, but some organic compounds, such as iron chelates, may also be present [63]. Hydroponic cultivation can have high efficiency in water use and fertilization and low environmental impact [24]. According to Nicola et al. [21] and Resh [64], hydroponic systems allow the reuse of the nutrient solution through recirculation, where the spent solution is collected and returned to the system after sterilization. This system is called closed and is suitable for environmentally sensitive areas to protect soil and groundwater. If the nutrient solution is used only once, it is an open system. In an open system, environmental impacts can also be reduced by minimizing water and nutrient losses through the use of sensing technologies and nutrient solution delivery strategies, with the goal of minimizing solution runoff from the system [65].

However, hydroponic techniques require a larger initial investment in greenhouse and equipment, but on the other hand have long-term and multiple benefits. For successful modern hydroponic production of nettles, it is very important to have appropriate tools and equipment to adjust the vegetation factors (light, heat, humidity and composition) to the optimal value.

Light is a vegetation factor needed for the basic process in plants—photosynthesis. Cultivation under controlled conditions allows plant material to be available in the market throughout the year, for example, in winter when sunlight is absent or when the change in the spectrum causes undesirable stretching of plants, resulting in uneven growth [66]. Therefore, additional lighting must be used during a part of the year when there is not enough light. Supplemental lighting in the form of LED diodes is common practice. Different wavelengths of LEDs or their combination can increase the SM content (vitamin C, anthocyanins, and total phenols) of leafy vegetables, and thus also in nettles. However, this is species-specific, so the combinations and duration of light treatments for each species need further research [67]. Although moderate light treatments can have a positive effect on the content of the plant SM, on the other hand, an excessive amount of light is associated with a reduction in the amount of chlorophyll. Therefore, it is common practice to install shade curtains in greenhouses to protect plants during seasons with strong sunlight. However, photoselective nets of different colors and shading efficiencies can also be used to stimulate SM production [68]. For example, stinging nettle is a mesophilic species that, according to its biological requirements, does not have a great need for light and heat, and therefore, requires shaded places without direct sunlight [57].

Because of the greenhouse effect in the warm months (June to September in temperate climates), ventilation is required. Usually, there is an automatic system controlled by a computer. When a certain temperature is reached, the sidewalls and part of the roof are opened to allow the warmer air to leave the greenhouse with the help of fans. In the colder months, the shade curtain is often used as an energy curtain along with a heater to minimize heat loss. The heater is accompanied by fans that drive warm air through the greenhouse to distribute heat more evenly.

The ability to hold water vapor in the air is determined by the air temperature. The proper balance of humidity and temperature in the greenhouse is critical to the health and success of plant production. This is usually balanced by a ventilation system, sometimes in combination with misting [69].

The composition of the air in the greenhouse is also very important; carbon dioxide (CO_2) is necessary for plant photosynthesis. On a cold, sunny day when the ventilation is not open, the concentration in the greenhouse can drop to only half of that outside. The atmosphere contains about 340 ppm (0.03%) CO_2. Increasing CO_2 by 3 to 4 times accelerates photosynthesis, but should be performed with caution, as plant organs can be damaged if there is not enough light, heat, water, and plant nutrients. Pure CO_2 (bottled, compressed, dry ice) is mainly used for research purposes [70].

Depending on the hydroponic technique to be used, the greenhouse must be equipped with a system of tanks, pumps, and pipes for preparing and transporting the nutrient solution to the plants (Figure 4).

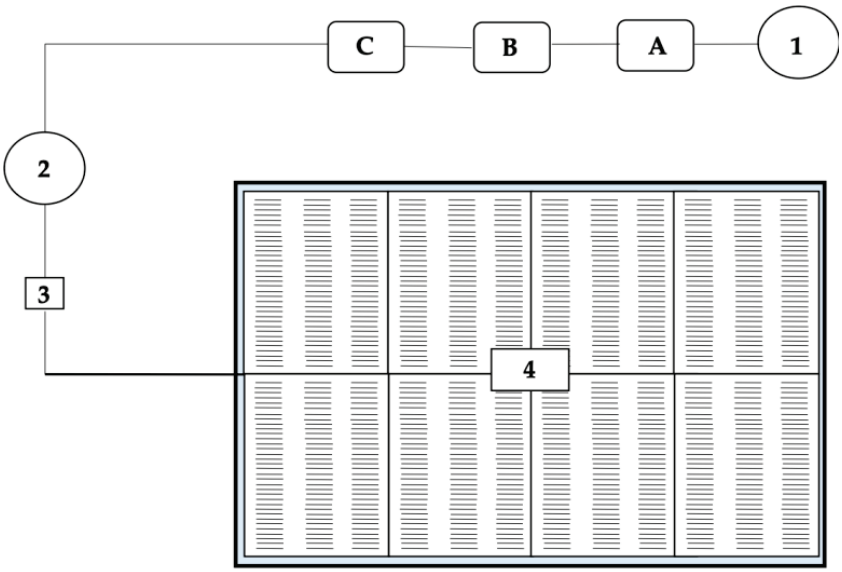

Figure 4. Graphical scheme of floating hydroponics cultivation. 1—water; A, B, C—tanks for concentrated nutrient solutions and injectors; 2—tank for standard nutrient solution; 3—pump; 4—basin with polystyrene containers or boards.

5.1. Nutrient Solution Management

In hydroponic cultivation with water, nutrients and salt ions are needed to produce the nutrient solution. The advantage of nutrient salts is that they are highly pure chemical compounds consisting of two to three elements, i.e., nutrients. All nutrient solutions used in hydroponic growing are essentially derived from the original protocol developed by Hoagland and Arnon in 1938. A standardized solution consists of the following macronutrients: nitrogen (N), potassium (K), phosphorus (P), calcium (Ca), magnesium (Mg) and sulfur (S); and trace elements: the soluble form of iron (Fe), boron (B), copper (Cu), manganese (Mn), zinc (Zn), molybdenum (Mo) and chlorine (Cl). Sometimes silicon (Si) and selenium (Se) are also added to the solution, although they are not biogenic elements. However, they are considered useful for plants because they increase stress tolerance, vegetative growth, and seed production [71]. It is also important to emphasize that the availability of certain biogenic elements, especially nitrogen, can negatively affect certain SMs, such as polyphenolic compounds [40], so growing SM rich plant material is very often a trade-off between a high yield and the content of SM in the harvested product [9].

According to Sonneveld and Voogt [72], it is necessary to perform a chemical analysis of the water to be used before preparing the nutrient solution. For the preparation of the nutrient solution, fewer salts are added to the solution, which contains ions that are

also present in the water (most commonly Ca^{2+}, Mg^{2+} and SO_4^{2-}). When a significant concentration of these ions is present, the pH of the nutrient solution easily becomes too high due to the alkaline buffering capacity of the carbonate. Regardless of the hydroponic technique, the finished nutrient solution is made from 100-fold concentrated solutions, based on the concentration of a solution supplied to each plant through a fertigation system. Therefore, in each hydroponic production, there are at least three containers for the concentrated solution (Figure 4).

The salts are prepared in two concentrated base solutions in two separate containers (A and B). Because of the chemical reactions and the possible sinking of the compounds formed, the calcium salts must be separated from the sulfates and phosphates. The third container I contains a solution of nitric or phosphoric acid, which serves to regulate the pH of the solution (Figure 3). Although the HCO_3 ion is not a plant nutrient, it must be considered in the preparation of the nutrient solution. Its accumulation greatly increases the pH of the solution, which can have a negative effect on nutrient uptake. The availability of P and Mn is strongly influenced by pH. At values > 6.5, the concentration may be low regardless of the concentration supplied with irrigation, because these elements are less soluble at high pH values. Therefore, acids are used to neutralize it and achieve the desired pH [72,73].

Plant species grown using hydroponic techniques can differ significantly in the uptake of individual nutrients, which is influenced by many abiotic (temperature and humidity, pH, oxygen content of the nutrient solution, amount of light, and CO_2 concentration) and biotic factors (stage of growth and development, presence of harmful organisms). Therefore, during cultivation, it is necessary to monitor the above parameters of the nutrient solution on a daily basis and correct them if necessary [74]. The same assertion is made by Tomasi et al. [60], pointing out that the management of the cultivation conditions and, in particular, the concentration of the nutrient solution is one of the most important aspects for successful hydroponic production. The same authors note that electrical conductivity (EC, dS/m), the chemical form of the elements (e.g., in hydroponics, N is usually supplied as NO^{3-} because the NH_4^+ form is not immediately available to the plant), temperature, and pH of the solution can affect growth, quality, and plant health, so it is necessary to monitor and correct the solution throughout the growing season. EC indicates the amount of soluble salts in the solution, and optimal values can vary widely among different crops [75].

The optimum pH of the final nutrient solution for hydroponic vegetable species ranges from 5.8 to 6.5, the optimum EC values of the nutrient solution are 1.5–3 dS/m, while the optimum amount of dissolved oxygen in the nutrient solution is 2–4 mg/L [76]. According to Nguyen et al. [63], plant roots require a constant supply of oxygen. If the roots become anoxic, they can no longer absorb nutrients and transport. In hydroponics, there are different solutions for this depending on the growing technique, but in cases where the roots are in constant contact with the nutrient solution, there is usually a pump system that oxygenates the solution to a satisfactory level (above 1 mg/L).

In modern hydroponic growing systems, the amount of oxygen, EC and the pH of the solution, as well as the dilution of the concentrated solution, are automatically controlled by a computer system that uses special sensors. The software sets the target pH and EC of the nutrient solution. The device for mixing concentrated solutions with water measures the set factors of the diluted solution and independently corrects the volumes of concentrated solutions (A and B) and acI(C) until the set values are reached. In floating hydroponics, there are also probes that are immersed in the nutrient solution in basins with plants. The data is transmitted in real time to the cloud, from where it can be read at any time via a mobile app or computer. In this way, a faster response is possible when the parameters of the nutrient solution need to be corrected, which undoubtedly has a positive effect on the success of the cultivation [77].

It can be concluded that the nutrient solItion is certainly one of thI most important factors in the quality and yield of the plant material, as it allows direct control of the amount of each biogenic element, avoids nutrient antagonism, and ensures optimal plant

nutrition [78]. To obtain a high content of SM and an adequate yield, it is necessary to determine for each species the optimal composition of the nutrient solution, the seeding density and the appropriate assortment depending on the growing period and the intended use of the final product [72]. To date, a few studies [6,17] have been conducted on nutrient solutions suitable for hydroponic nettle cultivation.

5.2. Suitable Hydroponics Techniques for Nettle Cultivation

In general, hydroponic systems for the production of green leafy vegetables can be divided into two groups according to Resh [64]. Hydroponic systems in which the root of the plant is submerged, i.e., in constant contact with the nutrient solution (nutrient film technique, floating hydroponics and aeroponic system). Systems in which the inert substrates in which the plants are rooted are soaked at intervals (ebb and flow system). The following text is a brief description of the rare studies on hydroponic stinging nettle cultivation and the factors tested, which provide valuable results and the basis for future research.

Most research to date has been conducted using the floating hydroponic system. In floating hydroponics, plants are grown on an aerated nutrient solution in tanks 20 to 25 cm deep (Figure 5). Plants are grown in Styrofoam containers or boards that float on the nutrient solution. This is an ideal technique for growing leafy vegetables, such as lettuce, gentian, dill, arugula, radicchio, spinach, and basil, which features a shorter production cycle and higher growing density [21,60].

Radman et al. [6] studied the effects of three seeding densities (0.2, 0.5 and 0.9 g/m^2) and two substrates (perlite, vermiculite) on nettle yield and number of harvests. Floating hydroponics proved to be a good cultivation technique for nettles. High yields and a greater number of harvests were obtained in the months when the nettle rested in the open field. The highest yields (1.41 kg/m^2 and 1.22 kg/m^2) were obtained in the spring growing season in combination with perlite $\times$ 0.2 g/m^2 and vermiculite $\times$ 0.2 g/m^2 seeding density.

The objective of the study by Radman et al. [17] was to determine the effect of two standard nutrient solutions for leafy vegetables on the yield and mineral content of nettle in multiple harvests (Figure 5a–d). The first nutrient solution was prepared according to Tesi with slightly lower EC values (2.3 dS/m) and the second according to Osvald (2.5 dS/m). Both nutrient solutions proved to be adequate for growing nettles in the floating system, but the Tesi solution had higher values for most of the observed traits (dry matter, N, P, K, Fe).

In the aeroponic system, plants are placed in lattice pots in holes in Styrofoam panels placed horizontally or at an angle of 45 to 60 degrees (A-frames). The roots of the plants hang in a closed chamber and are exposed to the air. The nutrient solution is sprayed every few minutes for about 15 s so that the root system is in constant contact with it [64,79]. In the study by Hayden [23], stinging nettle was grown in an aeroponic A-frame system, with no information on the nutrient solution used. The control group was grown in a soilless potting mix. The aeroponic nettle produced the same biomass in the air, but lower biomass on the ground compared to the control group.

In a study by Pagliarulo et al. [20], two nutrient solutions modified from Resh (1998) with different phosphorus and potassium contents were tested on nettles grown in hydroponic systems (aeroponic and soilless systems in controlled environments). The change in PK ratio had no significant effect on yield, but the soilless medium treatments produced greater root biomass and the same shoot biomass compared to aeroponics.

Figure 5. (**a**) Placing of polystyrene boards in floating hydroponics basins after initial germination of nettle seeds (**b**) Beginning of herb growth; (**c**) Nettle plants before flowering, ready for harvest; (**d**) Harvest above plants first two nodules to allow retrovegetation.

Most research has addressed the cultivation of nettles in floating hydroponics [6,17] and in aeroponic systems [20,23], but considering the techniques and nettle as a species, it shows great potential for cultivation with both nutrient films and ebb and flow techniques. The potential of cultivation with the aforementioned techniques comes from the rational use of nutrients, which results in less nitrate accumulation, and the ability of stinging nettle to retrovegetate, which allows for multiple harvests. In addition, the controlled management and control of stressors through the use of these techniques (especially in the ebb and flow system) can influence the increase of specialized metabolites.

In the NFT nutrient film technique, an aerated nutrient solution up to 1 cm high flows continuously in shallow channels containing growing containers with a relatively small amount of substrate and plants. Because the solution is constantly in motion, the ion concentration in the root zone does not increase. NFT maximizes water use efficiency by recycling a nutrient solution that is sterilized before being returned to the system [64,80].

The ebb and flow system (a"so c'lled flood and drain) works on the principle of the time intervals between the availability of nutrient solutions and dry periods (water stress) to which plants are exposed. The benches on which the containers with the plants are placed are soaked with a nutrient solution. After a certain time, interval (programmed

according to the plant grown), the nutrient solution drains from the bench. The system is closed, and the solution is recycled [23,64]. The use of ebb and flow systems and the regulation of the time interval between two irrigations with nutrient solution (which cause water stress) can affect the morphological and nutritional characteristics of plants [81]. Water stress can have a positive or negative effect on the chemical composition of plants, depending mainly on the length of the stress period, the genetic characteristics of the plant material, and the phenological phase of the plant. Water stress was shown to have a negative effect on the uptake of phosphorus and calcium in arugula and of phosphorus and magnesium in spinach. On the other hand, water stress had a positive effect on the content of bioactive compounds: vitamin C, total phenols, non-flavonoids and glucosinolates [82].

As you can see from the described chapter, research on hydroponic stinging nettle cultivation is scarce, but it provides valuable guidance for the selection of appropriate hydroponic techniques and also for their appropriate management to induce positive stress in stinging nettle cultivation, which increases the content of SM.

5.3. Management of Hydroponic Techniques Affecting SM in Plants

The induction of positive stress by the cultivation method and the application of agrotechnical measures at different stages of plant development can influence the content of SM [82]. For example, Šic Žlabur et al. [66] proved that induced mechanical stress by brushing is a good method for growing basil, the application of which provides high quality plant material with high nutritional potential and a significantly higher content of antioxidants and phytochemicals important for human health. Hydroponic growing techniques also offer the possibility of positively affecting stress in plants in various ways, which can lead to plant material with a richer SM composition and thus higher nutrient quality [68]. Indeed, in plants exposed to stress, the total content of flavonoids, phenols and polyphenols, vitamins C and E, carotenoids, and antioxidant enzymes, i.e., all compounds of secondary metabolism responsible for the defense mechanism of plants, increases [66,83,84].

According to Hayden [23] and Maggini et al. [19], it is possible to improve the synthesis and accumulation of SM in medicinal plants by manipulating the nutrient solution for certain SM provoking stress conditions. According to Maggini et al. [19], the content of basil SM, rosmarinic acid, can be increased when plants are exposed to moderate NaCl salt stress, moderate hypoxia conditions, or altered nitrogen supply. More specifically, when the nutrient solution was manipulated with NO_3^- concentration, it was found that rosmarinic acid content was higher when NO_3^- was decreased. In general, plants SM, such as β-carotene, vitamins, flavanols, lycopene and phenols are stimulated under N deficiency conditions. This can be very interesting for controlling the amount of nitrate in the plant material by changing the concentration and composition of the nutrient solution to improve the SM content while reducing the accumulation of undesirable compounds [68]. Leafy vegetables and nettles tend to accumulate nitrate, so reducing nitrate levels is an important aspect of vegetable production. Nitrate accumulation in plants is influenced by many factors, including fertilization, soil properties, growth stage, air temperature, light intensity, and harvest time [21]. The same authors state that nitrate content in leafy vegetables grown in hydroponics can be reduced by stopping fertilization a few days before harvest. Radman et al. [85] also indicate the possibility of reducing nitrate content in lamb's lettuce (*Valerianella locusta* L.) by replacing the nutrient solution with water 3 days before harvest. However, the authors indicate that this process resulted in a lower amount of dry matter and minerals in the plant material. Gonnella et al. [24] state that replacing the nutrient solution with water 3 days before harvest of lamb's lettuce had no effect on yield and organoleptic characteristics.

Increasing the potassium or magnesium content in the nutrient solution can also have a positive effect on the SM content of the plants. However, it is advisable to handle this with caution, as nutrient antagonism may occur [68].

The ebb-and-flow method is best suited for studying the effects of water stress on SM content in plants. The dry period, i.e., lack of water (water/drought stress), sig-

nificantly affects the content and profile of SM. During this period, the plant begins to accumulate a greater amount of SM in response to its defense mechanism [86]. According to Yadav et al. [84], De Abreu and Mazzafera [87], Selmar and Kleinwächter [88], and Bloem et al. [89], it is possible to increase the content of SM in medicinal and aromatic plants by causing moderate water stress during cultivation. It is of great importance to set an appropriate time interval for irrigation so that plants are sufficiently stressed to produce larger amounts of SM, but this stress does not lead to wilting or irreversible damage to plant tissues.

Since even moderate stress can cause yield loss, it is important in agricultural production to find the right balance between generated stress, which gives the plant material a richer SM content, and a satisfactory yield [88,90].

6. Conclusions

Considering the peculiarities of nettle as a wild plant, such as the possibility of revegetation, the tendency to accumulate nitrates and heavy metals in the soil, resulting in a variable composition of various specialized metabolites, it is necessary to control the nutritional properties of this plant material. Cultivation allows easier control of chemical properties, which is a necessity in the case of stinging nettle. Cultivation of stinging nettle in the open field proves to be a suitable option. However, as it is not possible to fully control some important abiotic factors, such as temperature, light and humidity, this method of cultivation faces many challenges, especially in the face of increasingly volatile climate change and the increasing occurrence of extreme weather events. The cultivation of nettles using modern hydroponic techniques in greenhouses offers itself as a suitable solution to overcome the above challenges. The literature review has revealed numerous advantages of using certain techniques of modern hydroponic cultivation for stinging nettle. These include the ability to control and manage abiotic factors for both the greenhouse and the nutrient solution, balanced and rational fertilization, optimized water management and supply, and most importantly, the production of plant material with adequate yields and high levels of specialized metabolites. With the ebb and flow system, it is even possible to induce water stress, the optimized application of which can be successfully used to stimulate the synthesis and accumulation of secondary plant compounds, such as polyphenols. After all, the floating hydroponics and the ebb and flow system prove to be optimal hydroponic techniques for greenhouse cultivation of nettles, ultimately resulting in uniform plant material with consistent chemical composition, high yields and a high content of specific metabolites.

Author Contributions: Conceptualization, N.O., J.Š.Ž. and S.R.; methodology, J.Š.Ž., S.R. and N.O.; software, S.R. and S.F.U.; data curation, N.O.; writing—original draft preparation, N.O.; writing–review and editing, J.Š.Ž., S.R. and B.B.; visualization, S.V. All authors have read and agreed to the published version of the manuscript.

Funding: The publication was supported by the Open Access Publication Fund of the University of Zagreb Faculty of Agriculture.

Institutional Review Board Statement: Not applicable.

Informed Consent Statement: Not applicable.

Data Availability Statement: Not applicable.

Acknowledgments: This research was funded by Croatian Science Foundation (Hrvatska zaklada za znanost—www.hrzz.hr) under the project IP-2019-04-3325 URTICA-BioFuture—Nutritional and functional value of nettle (*Urtica dioica* L.) by application of modern hydroponic cultivation techniques.

Conflicts of Interest: The authors declare no conflict of interest.

References

1. Ozola, B.; Augspole, I.; Duma, M. Pigments content in different processed edible wild plants. In Proceedings of the 13th Baltic Conference on Food Science and Technology "Food, Nutrition, Well-Being", Jelgava, Latvia, 2–3 May 2019; pp. 204–209. [CrossRef]
2. Demir, E.; Turfan, N.; Özer, H.; Üstün, N.Ş.; Pekşen, A. Nutrient and bioactive substance contents of edible plants grown naturally in Salipazari (Samsun). *Acta Sci. Pol.-Hortorum Cultus* **2020**, *19*, 151–160. [CrossRef]
3. Grauso, L.; De Falco, B.; Lanzotti, V.; Motti, R. Stinging nettle, *Urtica dioica* L.: Botanical, phytochemical and pharmacological overview. *Phytochem. Rev.* **2020**, *19*, 1341–1377. [CrossRef]
4. Guil-Guerrero, J.L.; Torija-Isasa, M.E. Fatty acid profiles of Mediterranean wild edible plants. In *Mediterranean Wild Edible Plants*, 1st ed.; Sánchez-Mata, M.C., Tardío, J., Eds.; Springer: New York, NY, USA, 2016; pp. 173–186. [CrossRef]
5. Bergquist, S.Å.; Gertsson, U.E.; Knuthsen, P.; Olsson, M.E. Flavonoids in baby spinach (*Spinacia oleracea* L.): Changes during plant growth and storage. *J. Agric. Food Chem.* **2005**, *53*, 9459–9464. [CrossRef] [PubMed]
6. Radman, S.; Fabek, S.; Žutić, I.; Benko, B.; Toth, N. Stinging nettle cultivation in floating hydropon. *Contemp. Agric.* **2014**, *63*, 215–223.
7. Đurović, S.; Pavlić, B.; Šorgić, S.; Popov, S.; Savić, S.; Petronijević, M.; Radojković, M.; Cvetanović, A.; Zeković, Z. Chemical composition of stinging nettle leaves obtained by different analytical approaches. *J. Funct. Foods* **2017**, *32*, 18–26. [CrossRef]
8. Kregiel, D.; Pawlikowska, E.; Antolak, H. *Urtica* spp.: Ordinary plants with extraordinary properties. *Molecules* **2018**, *23*, 1664. [CrossRef]
9. Upton, R. Stinging nettles leaf (*Urtica dioica* L.): Extraordinary vegetable medicine. *J. Herb. Med.* **2013**, *3*, 9–38. [CrossRef]
10. Di Virgilio, N.; Papazoglou, E.G.; Jankauskiene, Z.; Di Lonardo, S.; Praczyk, M.; Wielgusz, K. The potential of stinging nettle (*Urtica dioica* L.) as a crop with multiple uses. *Ind. Crops Prod.* **2015**, *68*, 42–49. [CrossRef]
11. De Vico, G.; Guida, V.; Carella, F. *Urtica dioica* (Stinging Nettle): A neglected plant with emerging growth promoter/immunostimulant properties for farmed fish. *Front. Physiol.* **2018**, *9*, 285. [CrossRef]
12. Garcìa, L.M.; Ceccanti, C.; Negro, C.; De Bellis, L.; Incrocci, L.; Pardossi, A.; Guidi, L. Effect of Drying Methods on Phenolic Compounds and Antioxidant Activity of Urtica dioica L. Leaves. *Horticulturae* **2021**, *7*, 10. [CrossRef]
13. Repajić, M.; Cegledi, E.; Zorić, Z.; Pedisić, S.; Elez Garofulić, I.; Radman, S.; Palčić, I.; Dragović-Uzelac, V. Bioactive Compounds in Wild Nettle (*Urtica dioica* L.) Leaves and Stalks: Polyphenols and Pigments upon Seasonal and Habitat Variations. *Foods* **2021**, *10*, 190. [CrossRef] [PubMed]
14. Stanojević, L.P.; Stanković, M.Z.; Cvetković, D.J.; Cakić, M.D.; Ilić, D.P.; Nikolić, V.D.; Stanojević, J.S. The effect of extraction techniques on yield, extraction kinetics, and antioxidant activity of aqueous-methanolic extracts from nettle (*Urtica dioica* L.) leaves. *Sep. Sci. Technol.* **2016**, *51*, 1817–1829. [CrossRef]
15. Đurović, S.; Zeković, Z.; Šorgić, S.; Popov, S.; Vujanović, M.; Radojković, M. Fatty acid profile of stinging nettle leaves: Application of modern analytical procedures for sample preparation and analysis. *Anal. Methods* **2018**, *10*, 1080–1087. [CrossRef]
16. Biesiada, A.; Kucharska, A.; Sokół-Łętowska, A.; Kuś, A. Effect of the Age of Plantation and Harvest Term on Chemical Composition and Antioxidant Avctivity of Stinging Nettle (*Urtica dioica* L.). *Ecol. Chem. Eng. A* **2010**, *17*, 1061–1068.
17. Radman, S.; Javornik, M.; Žutić, I.; Opačić, N.; Benko, B. Impact of different nutrient solution composition on stinging nettle growth and mineral content. In Proceedings of the VIII South-Eastern Europe Symposium on Vegetables and Potatoes 1320, Ohrid, North Macedonia, 24–26 September 2021; Acta Horticulturae: Leuven, Belgium, 2021; pp. 157–166. [CrossRef]
18. Basu, A.; Basu, S.K.; Sengupta, R.; Asif, M.; Li, X.; Li, Y.; Hirani, A.; Zandi, P.; Sajad, M.; Solorio-Sánchez, F.; et al. Important Plant-Based Phytonutrients. *Phytonutr. Improv. Crops* **2017**, *1*, 1–82.
19. Maggini, R.; Kiferle, C.; Pardossi, A. Hydroponic production of medicinal plants. In *Medicinal Plants: Antioxidant Properties, Traditional Uses and Conservation Strategies*; Pereira, A.D.M., Ed.; Nova Science Publishers, Inc.: Hauppauge, NY, USA, 2014; pp. 91–116.
20. Pagliarulo, C.L.; Hayden, A.L.; Giacomelli, G.A. Potential for greenhouse aeroponic cultivation of *Urtica dioica*. In Proceedings of the VII International Symposium on Protected Cultivation in Mild Winter Climates: Production, Pest Management and Global Competition 659, Acta Horticulturae 2004, Kissimmee, FL, USA, 25 November 2004; pp. 61–66. [CrossRef]
21. Nicola, S.; Hoeberechts, J.; Fontana, E. Ebb-and-flow and floating systems to grow leafy vegetables: A review for rocket, corn salad, garden cress and purslane. In Proceedings of the VIII International Symposium on Protected Cultivation in Mild Winter Climates: Advances in Soil and Soilless Cultivation under 747, Acta Horticulturae 2006, Agadir, Morocco, 31 August 2007; pp. 585–593. [CrossRef]
22. Honary, H.; Vasundhara, M.; Nuthan, D. Hydroponics and aeroponics as alternative production systems for high-value medicinal and aromatic crops: Present scenario and future prospects. *J. Med. Aromat. Plant Sci.* **2011**, *33*, 397–403.
23. Hayden, A.L. Aeroponic and hydroponic systems for medicinal herb, rhizome, and root crops. *HortScience* **2016**, *41*, 536–538. [CrossRef]
24. Gonnella, M.; Serio, F.; Conversa, G.; Santamaria, P. Production and nitrate content in lamb's lettuce grown in floating system. *Acta Hort.* **2004**, *644*, 61–68. [CrossRef]
25. Toth, N.; Borošić, J.; Fabek, S.; Benko, B.; Novak, B. Leafy vegetables grown in floating system. In Proceedings of the Book of abstracts of 43rd Croatian and 3rd International Symposium on Agriculture, Opatija, Croatia, 18–21 February 2008; p. 132.

26. Petrazzini, L.L.; Souza, G.A.; Rodas, C.L.; Emrich, E.B.; Carvalho, J.G.; Souza, R.J. Nutritional deficiency in crisphead lettuce grown in hydroponics. *Hortic. Bras.* **2014**, *32*, 310–313. [CrossRef]
27. Kowalczyk, K.; Niedzińska, M.; Przybył, J.; Metera, A.; Cetner, M.D. The effect of nutrient solution on yield, its quality and the reaction of photosynthetic apparatus of endive (*Cichorium endivia*) grown in hydroponics. In Proceedings of the VI Balkan Symposium on Vegetables and Potatoes 1142, Acta Horticulturae 2016, Zagreb, Croatia, 31 October 2016; pp. 335–342. [CrossRef]
28. Radman, S.; Žutić, I.; Fabek, S.; Toth, N.; Benko, B.; Čoga, L. Influence of propagation method and fertilization on chemical composition and yield of stinging nettle. In Proceedings of the 51st Croatian & 11th International Symposium on Agriculture, Opatija, Hrvatska, 15–18 February 2016; pp. 192–196.
29. Conversa, G.; Bonasia, A.; Lazzizera, C.; Elia, A. Soilless Cultivation System, Electrical Conductivity of Nutrient Solution, and Growing Season on Yield and Quality of Baby-Leaf Oak-Leaf Lettuce. *Agronomy* **2021**, *11*, 1220. [CrossRef]
30. Rutto, L.K.; Ansari, M.S.; Brandt, M. Biomass yield and dry matter partitioning in greenhouse-grown stinging nettle under different fertilization regimes. *HortTechnology* **2012**, *22*, 751–756. [CrossRef]
31. Adhikari, B.M.; Bajracharya, A.; Shrestha, A.K. Comparison of nutritional properties of Stinging nettle (*Urtica dioica*) flour with wheat and barley flours. *Food Sci. Nutr.* **2016**, *4*, 119–124. [CrossRef] [PubMed]
32. Zeipiņa, S.; Alsiņa, I.; Lepse, L. Stinging nettle–the source of biologically active compounds as sustainable daily diet supplement. *Res. Rural Dev.* **2014**, *20*, 34–38.
33. Rutto, L.K.; Xu, Y.; Ramirez, E.; Brandt, M. Mineral properties and dietary value of raw and processed stinging nettle (*Urtica dioica* L.). *Int. J. Food Sci.* **2013**, *2013*, 857120. [CrossRef]
34. Çolak, S.; Çömlekcioğlu, N.; Aygan, A. Investigation of antioxidant and antimicrobial activities of *Urtica dioica* plant extracts. In Proceedings of the 3rd International Eurasian Conference on Biological and Chemical Sciences (EurasianBioChem 2020), Ankara, Turkey, 19–20 March 2020; p. 137.
35. Kukrić, Z.Z.; Topalić-Trivunović, L.N.; Kukavica, B.M.; Matoš, S.B.; Pavičić, S.S.; Boroja, M.M.; Savić, A.V. Characterization of antioxidant and antimicrobial activities of nettle leaves (*Urtica dioica* L.). *Acta Period. Technol.* **2012**, *43*, 257–272. [CrossRef]
36. Joshi, B.C.; Mukhija, M.; Kalia, A.N. Pharmacognostical review of *Urtica dioica* L. *Int. J. Green Pharm.* **2014**, *8*, 201. [CrossRef]
37. Shonte, T.T.; Duodu, K.G.; De Kock, H.L. Effect of drying methods on chemical composition and antioxidant activity of underutilized stinging nettle leaves. *Heliyon* **2020**, *6*, e03938. [CrossRef]
38. Paulauskienė, A.; Tarasevičienė, Ž.; Laukagalis, V. Influence of Harvesting Time on the Chemical Composition of Wild Stinging Nettle (*Urtica dioica* L.). *Plants* **2021**, *10*, 686. [CrossRef]
39. Rafajlovska, V.; Kavrakovski, Z.; Simonovska, J.; Srbinoska, M. Determination of protein and mineral contents in stinging nettle. *Qual. Life* **2013**, *7*, 7. [CrossRef]
40. Radman, S.; Žutić, I.; Fabek, S.; Žlabur, J.Š.; Benko, B.; Toth, N.; Čoga, L. Influence of nitrogen fertilization on chemical composition of cultivated nettle. *Emir. J. Food Agric.* **2015**, *27*, 889–896. [CrossRef]
41. Radman, S. Influence of Nitrogen Fertilization and Cultivation Methods on the Chemical Composition of Stinging Nettle (*Urtica dioica* L.). Ph.D. Thesis, Faculty of Agriculture, University of Zagreb, Zagreb, Croatia, 2015.
42. Chrubasik, J.E.; Roufogalis, B.D.; Wagner, H.; Chrubasik, S.A. A comprehensive review on nettle effect and efficacy profiles, Part I: Herba urticae. *Phytomedicine* **2007**, *14*, 423–435. [CrossRef] [PubMed]
43. Biesiada, A.; Wołoszczak, E.; Sokół-Łętowska, A.; Kucharska, A.Z.; Nawirska-Olszańska, A. The effect of nitrogen form and dose on yield, chemical composition and antioxidant activity of stinging nettle (*Urtica dioica* L.). *Herba Pol.* **2009**, *55*, 84–93.
44. Carvalho, A.R.; Costa, G.; Figueirinha, A.; Liberal, J.; Prior, J.A.; Lopes, M.C.; Batista, M.T. *Urtica* spp.: Phenolic composition, safety, antioxidant and anti-inflammatory activities. *Food Res. Int.* **2017**, *99*, 485–494. [CrossRef] [PubMed]
45. Francišković, M.; Gonzalez-Pérez, R.; Orčić, D.; Sanchez de Medina, F.; Martínez-Augustin, O.; Svirčev, E.; Mimica-Dukić, N. Chemical Composition and Immuno-Modulatory Effects of *Urtica dioica* L.(Stinging Nettle) Extracts. *Phytother. Res.* **2017**, *31*, 1183–1191. [CrossRef]
46. Gül, S.; Demirci, B.; Başer, K.H.C.; Akpulat, H.A.; Aksu, P. Chemical composition and in vitro cytotoxic, genotoxic effects of essential oil from *Urtica dioica* L. *Bull. Environ. Contam. Toxicol.* **2012**, *88*, 666–671. [CrossRef]
47. Otles, S.; Yalcin, B. Phenolic compounds analysis of root, stalk, and leaves of nettle. *Sci. World J.* **2012**, *2012*, 564367. [CrossRef]
48. Grevsen, K.; Fretté, X.; Christensen, L.P. Concentration and composition of flavonol glycosides and phenolic acids in aerial parts of stinging nettle (*Urtica dioica* L.) are affected by high nitrogen fertilization and by harvest time. *Eur. J. Hortic. Sci.* **2008**, *73*, 20–27.
49. AlShuwayeb, M.H.; Al-Khatib, A.J. Molecular and chemical therapeutic features of *Urtica* species. *Eur. Sci. J.* **2013**, *9*, 253–261.
50. Gülçin, I.; Küfrevioğlu, Ö.İ.; Oktay, M.; Büyükokuroğlu, M.E. Antioxidant, antimicrobial, antiulcer and analgesic activities of nettle (*Urtica dioica* L.). *J. Ethnopharmacol.* **2004**, *90*, 205–215. [CrossRef]
51. Modarresi-Chahardehi, A.; Ibrahim, D.; Fariza-Sulaiman, S.; Mousavi, L. Screening antimicrobial activity of various extracts of *Urtica dioica*. *Rev. Biol. Trop.* **2012**, *60*, 1567–1576. [CrossRef]
52. Di Venere, D.; Gatto, M.A.; Ippolito, A.; Bianco, V.V. Antimicrobial potential of wild edible herbaceous species. In *Mediterranean Wild Edible Plants*, 1st ed.; Sánchez-Mata, M.C., Tardío, J., Eds.; Springer: New York, NY, USA, 2016; pp. 233–252. [CrossRef]
53. Tardío, J.; de Cortes Sánchez-Mata, M.; Morales, R.; Molina, M.; García-Herrera, P.; Morales, P.; Boussalah, N. *Ethnobotanical and Food Composition Monographs of Selected Mediterranean Wild Edible Plants*, 1st ed.; Sánchez-Mata, M.C., Tardío, J., Eds.; Springer: New York, NY, USA, 2016; pp. 273–470. [CrossRef]

54. Petrović, J.V.; Alagić, S.Č.; Tošić, S.B.; Šteharnik, M.M.; Bugarin, M.M.; Stevanović, Z.O. The content of heavy metals in the aerial parts of the common nettle and sun spurge from Oštrelj (municipality of Bor): A contribution to the examinations of plant biomonitoring and phytoremediation potentials. *Zaštita Mater.* **2019**, *60*, 105–111. [CrossRef]
55. Viktorova, J.; Jandova, Z.; Madlenakova, M.; Prouzova, P.; Bartunek, V.; Vrchotova, B.; Lovecka, P.; Musilova, L.; Macek, T. Native phytoremediation potential of *Urtica dioica* for removal of PCBs and heavy metals can be improved by genetic manipulations using constitutive CaMV 35S promoter. *PLoS ONE* **2016**, *11*, e0167927. [CrossRef] [PubMed]
56. Radman, S.; Žutić, I.; Fabek, S.; Frkin, A.; Benko, B.; Toth, N. Utjecaj temperature i svjetla na klijavost sjemena koprive. In Proceedings of the 50th Croatian & 10th International Symposium on Agriculture, Opatija, Croatia, 16–20 February 2015; p. 271.
57. Stepanović, B.; Radanović, D.; Turšić, I.; Nemčević, N.; Ivanec, J. *Uzgoj Ljekovitog i Aromatičnog Bilja*; Jan-Spider: Pitomača, Croatia, 2009; pp. 243–245.
58. An Official Website of the European Union. Available online: https://eur-lex.europa.eu/legal-content/EN/ALL/?uri=CELEX%3A32002R0563 (accessed on 20 December 2021).
59. Başgel, S.; Erdemoğlu, S.B. Determination of mineral and trace elements in some medicinal herbs and their infusions consumed in Turkey. *Sci. Total Environ.* **2006**, *359*, 82–89. [CrossRef] [PubMed]
60. Tomasi, N.; Pinton, R.; Dalla Costa, L.; Cortella, G.; Terzano, R.; Mimmo, T.; Scampicchio, M.; Cesco, S. New 'solutions' for floating cultivation system of ready-to-eat salad: A review. *Trends Food Sci. Technol.* **2015**, *46*, 267–276. [CrossRef]
61. Fernández, J.A.; Orsini, F.; Baeza, E.; Oztekin, G.B.; Muñoz, P.; Contreras, J.; Montero, J.I. Current trends in protected cultivation in Mediterranean climates. *Eur. J. Hortic. Sci.* **2018**, *83*, 294–305. [CrossRef]
62. Savvas, D.; Gruda, N. Application of soiless culture techologies in the modern greenhouse industry—A review. *Eur. Hortic. Sci.* **2018**, *83*, 280–293. [CrossRef]
63. Nguyen, N.T.; McInturf, S.A.; Mendoza-Cózatl, D.G. Hydroponics: A versatile system to study nutrient allocation and plant responses to nutrient availability and exposure to toxic elements. *J. Vis. Exp. JoVE* **2016**, *113*, e54317. [CrossRef]
64. Resh, H.M. *Hydroponic Food Production: A Definitive Guidebook for the Advanced Home Gardner and the Commercial Hydroponic Grower*, 7th ed.; CRC Press: Boca Raton, FL, USA, 2013.
65. Massa, D.; Magán, J.J.; Montesano, F.F.; Tzortzakis, N. Minimizing water and nutrient losses from soilless cropping in southern Europe. *Agric. Water Manag.* **2020**, *241*, 106395. [CrossRef]
66. Šic Žlabur, J.; Radman, S.; Fabek Uher, S.; Opačić, N.; Benko, B.; Galić, A.; Samirić, P.; Voća, S. Plant Response to Mechanically-Induced Stress: A Case Study on Specialized Metabolites of Leafy Vegetables. *Plants* **2021**, *10*, 2650. [CrossRef]
67. Hasan, M.; Bashir, T.; Ghosh, R.; Lee, S.K.; Bae, H. An overview of LEDs' effects on the production of bioactive compounds and crop quality. *Molecules* **2017**, *22*, 1420. [CrossRef]
68. Rouphael, Y.; Kyriacou, M.C.; Petropoulos, S.A.; De Pascale, S.; Colla, G. Improving vegetable quality in controlled environments. *Sci. Hortic.* **2018**, *234*, 275–289. [CrossRef]
69. Körner, O.; Challa, H. Process-based humidity control regime for greenhouse crops. *Comput. Electron. Agric.* **2003**, *39*, 173–192. [CrossRef]
70. Vox, G.; Teitel, M.; Pardossi, A.; Minuto, A.; Tinivella, F.; Schettini, E. Sustainable greenhouse systems. In *Sustainable Agriculture: Technology, Planning and Management*; Nova Publishers: New York, NY, USA, 2010; pp. 1–79.
71. Shavrukov, Y.; Genc, Y.; Hayes, J. The use of hydroponics in abiotic stress tolerance research. In *Hydroponics—A Standard Methodology for Plant Biological Researches*, 1st ed.; Toshiki, A., Ed.; InTech: Rijeka, Croatia, 2012; pp. 39–66. [CrossRef]
72. Sonneveld, C.; Voogt, W. Plant nutrition in future greenhouse production. In *Plant Nutrition of Greenhouse Crops*; Springer: Dordrecht, The Netherlands, 2009; pp. 393–403.
73. Benton Jones, J., Jr. *Complete Guide for Growing Plants Hydroponically*; CRC Press: Boca Raton, FL, USA, 2014. [CrossRef]
74. Marschner, P. *Marschner's Mineral Nutrition of Higher Plants*, 3rd ed.; Academic Press Elsevier: London, UK; Waltham, MA, USA; San Diego, CA, USA, 2012.
75. Van Delden, S.H.; Nazarideljou, M.J.; Marcelis, L.F. Nutrient solutions for Arabidopsis thaliana: A study on nutrient solution composition in hydroponics systems. *Plant Methods* **2020**, *16*, 72. [CrossRef]
76. Toth, N.; Fabek, S.; Benko, B.; Žutić, I.; Stubljar, S.; Zeher, S. Učinak abiotskih čimbenika, gustoće sjetve i višekratne berbe na prinos rige u plutajućem hidroponu. *Glas. Zaštite Bilja* **2012**, *35*, 24–34.
77. Cafuta, D.; Dodig, I.; Cesar, I.; Kramberger, T. Developing a Modern Greenhouse Scientific Research Facility—A Case Study. *Sensors* **2021**, *21*, 2575. [CrossRef]
78. Trejo-Téllez, L.I.; Gómez-Merino, F.C. Nutrient solutions for hydroponic systems. In *Hydroponics—A Standard Methodology for Plant Biological Researches*; IntechOpen: London, UK, 2012; pp. 1–22.
79. AlShrouf, A. Hydroponics, aeroponic and aquaponic as compared with conventional farming. *Am. Sci. Res. J. Eng. Technol. Sci. (ASRJETS)* **2017**, *27*, 247–255.
80. Putra, P.A.; Yuliando, H. Soilless culture system to support water use efficiency and product quality: A review. *Agric. Agric. Sci. Procedia* **2015**, *3*, 283–288. [CrossRef]
81. Erken, O.; Oztokat Kuzucu, C.; Cakir, R. Impact of different water supply levels on yield and biochemical ingridients in broccoli. *Bulg. J. Agric. Sci.* **2013**, *19*, 1009–1017.

82. Cukrov, M.; Jerončić, L.; Prelogović, L. *Utjecaj Kontroliranog Vodnog Stresa na Sadržaj Bioaktivnih Spojeva u Hidroponskom Uzgoju Rikole (Eruca Sativa Mill.) i Špinata (Spinacia oleracea L.)*; Graduate Paper Awarded with Rector Award; Faculty of Agronomy, University of Zagreb: Zagreb, Croatia, 2017.
83. Waraich, E.A.; Ahmad, R.; Ashraf, M.Y. Role of mineral nutrition in alleviation of drought stress in plants. *Aust. J. Crop Sci.* **2011**, *5*, 764–777.
84. Yadav, B.; Jogawat, A.; Rahman, M.D.; Narayan, O. Secondary metabolites in the drought stress tolerance of crop plants: A review. *Gene Rep.* **2021**, *23*, 101040. [CrossRef]
85. Radman, S.; Ćurko, J.; Toth, N.; Fabek, S.; Čoga, L.; Žutić, I.; Benko, B. Lamb's lettuce mineral content in floating system. *Acta Hortic.* **2016**, *1142*, 343–348. [CrossRef]
86. Sharma, A.; Kumar, V.; Shahzad, B.; Ramakrishnan, M.; Sidhu, G.P.S.; Bali, A.S.; Handa, N.; Kapoor, D.; Yadav, P.; Khanna, K.; et al. Photosynthetic Response of Plants Under Different Abiotic Stresses: A Review. *J. Plant Growth Regul.* **2020**, *39*, 509–531. [CrossRef]
87. De Abreu, I.N.; Mazzafera, P. Effect of water and temperature stress on the content of active constituents of *Hypericum brasiliense* Choisy. *Plant Physiol. Biochem.* **2005**, *43*, 241–248. [CrossRef] [PubMed]
88. Selmar, D.; Kleinwächter, M. Influencing the product quality by deliberately applying drought stress during the cultivation of medicinal plants. *Ind. Crops Prod.* **2013**, *42*, 558–566. [CrossRef]
89. Bloem, E.; Haneklaus, S.; Kleinwächter, M.; Paulsen, J.; Schnug, E.; Selmar, D. Stress-induced changes of bioactive compounds in *Tropaeolum majus* L. *Ind. Crops Prod.* **2014**, *60*, 349–359. [CrossRef]
90. Ahanger, M.A.; Tomar, N.S.; Tittal, M.; Argal, S.; Agarwal, R.M. Plant growth under water/salt stress: ROS production; antioxidants and significance of added potassium under such conditions. *Physiol. Mol. Biol. Plants* **2017**, *23*, 731–744. [CrossRef]

plants

MDPI

Review

Exploring Breakthroughs in Three Traits Belonging to Seed Life

Angel J. Matilla

Departamento de Biología Funcional (Área Fisiología Vegetal), Facultad de Farmacia, Universidad de Santiago de Compostela, 15782 Santiago de Compostela, Spain; angeljesus.matilla@usc.es; Tel.: +34-981-563-100

Abstract: Based on prior knowledge and with the support of new methodology, solid progress in the understanding of seed life has taken place over the few last years. This update reflects recent advances in three key traits of seed life (i.e., preharvest sprouting, genomic imprinting, and stored-mRNA). The first breakthrough refers to cloning of the mitogen-activated protein kinase-kinase 3 (MKK3) gene in barley and wheat. MKK3, in cooperation with ABA signaling, controls seed dormancy. This advance has been determinant in producing improved varieties that are resistant to preharvest sprouting. The second advance concerns to uniparental gene expression (i.e., imprinting). Genomic imprinting primarily occurs in the endosperm. Although great advances have taken place in the last decade, there is still a long way to go to complete the puzzle regarding the role of genomic imprinting in seed development. This trait is probably one of the most important epigenetic facets of developing endosperm. An example of imprinting regulation is polycomb repressive complex 2 (PRC2). The mechanism of PRC2 recruitment to target endosperm with specific genes is, at present, robustly studied. Further progress in the knowledge of recruitment of PRC2 epigenetic machinery is considered in this review. The third breakthrough referred to in this update involves stored mRNA. The role of the population of this mRNA in germination is far from known. Its relations to seed aging, processing bodies (P bodies), and RNA binding proteins (RBPs), and how the stored mRNA is targeted to monosomes, are aspects considered here. Perhaps this third trait is the one that will require greater experimental dedication in the future. In order to make progress, herein are included some questions that are needed to be answered.

Keywords: preharvest sprouting; MKK3; maternal and paternal expressed genes; imprinted genes; polycomb repressive complex 2; mRNA processing bodies; ribonucleic binding proteins; monosomes

Citation: Matilla, A.J. Exploring Breakthroughs in Three Traits Belonging to Seed Life. *Plants* **2022**, *11*, 490. https://doi.org/10.3390/plants11040490

Academic Editors: Milan S. Stankovic, Paula Baptista and Petronia Carillo

Received: 4 January 2022
Accepted: 9 February 2022
Published: 11 February 2022

1. Starting: Key Biological Traits about Seed Dormancy and Germination Mechanisms

The seed stage is a key life-cycle stage for many plants. Higher plants use the seeds for their perpetuation through successive generations. Mature seeds are highly resistant entities favoring plant dispersal. Seeds constitute also the basis of agriculture, and genes affecting seed dormancy and germination are among those under the strongest selection. The switch-off of translation between seed maturation and seed germination makes seeds a unique system to study developmentally regulated translation. Accordingly, seed germination is the first critical step of the plant life cycle and the foundation of agricultural production. The decision to germinate gravitates in a complex network of developmental and environmental signals to ensure seedling survival. The in-depth study of the seed's life is being carried out under different scientific approaches, justified by the following molecular and genetic findings: (i) the endosperm (i.e., triploid nutritive support tissue with a 2:1 maternal-to-paternal genome ratio) is essential to repress dormant seed germination by releasing abscisic acid (ABA), which blocks embryonic growth. Although the interaction between endosperm–embryo is largely elusive, the flow of nutrients from mother to embryo is essentially unidirectional during the whole process of seed-life. Thus, early seedling growth is supported by catabolism of stored reserves of protein, oil, or starch accumulated in stored tissues during seed maturation [1–4]. (ii) Germination on the mother plant

(preharvest sprouting, PHS), can also occur in crops, which is an agronomically and industrially undesired trait that compromises yield, nutritional and processing quality. Annual losses due to PHS are likely to approach $1 billion US dollars worldwide. Orthodox seeds acquire dormancy by thus avoiding PHS [5–7]. (iii) Orthodox and viable dry seeds are alive because they have acquired desiccation resistance, a feature accomplished together with longevity (storability) at the beginning of maturation [8–11]. (iv) Interestingly, dry and viable seeds store a multitude of transcripts to be used at the beginning of the germination process [12,13]. (v) Reactive oxygen species (ROS) and nitric oxide (NO) play fundamental roles in seed-life [14–17]. (vi) All the above vital events that occur in seeds are coordinated by transcription factors (TFs) such as ABI3, ABI4, and ABI5 [18–23], and phytohormones, being the regulatory mechanisms underlying abscisic acid (ABA) and gibberellins (GAs) crosstalk, intensively documented during seed dormancy and germination. However, identification of the ABA and GAs synthesis/degradation pathways, their feedbacks, and their impact on the regulation of dormancy and germination is far from clarified [23–26]. On the other hand, the involvement of ethylene in the regulation of seed dormancy and germination was recently updated and discussed [27–30]; and (vii) the life of this propagule is strongly influenced by external signals (e.g., light, nitrate, humidity, temperature) [31–35]. Taken together, all the events previously referred occur, among other instances, in human-used seeds. That is, in agronomically important crops that are therefore related to the world economy. Finally, the seeds of several species are used as biological systems in order to advance knowledge of the complex puzzle that constitutes the seed life and perpetuation of these entities that have been key in the colonization of dry land [36]. This update summarizes recent breakthroughs in our knowledge of some aspects highly involved in the life of orthodox seeds.

2. Preharvest Sprouting: Recent Progress and Economical Repercussions

Seed dormancy, a key quantitative trait for the prevention of PHS, has essential repercussion in plant survival and crop production. PHS is a complex trait influenced by genetic and environmental factors [37–40]. However, the intensity of this trait decreases during plant domestication to ensure that crops successfully germinate in the field. This is true in the case of wild and cultivated barley (*Hordeum vulgare*) [41]. If the rain comes before harvest, the mature seeds can germinate (i.e., PHS or vivipary) on the mother plant, causing substantial damages and crop losses. Considering that PHS broadly constitutes the opposite process to primary dormancy, at an experimental level, the natural phenomenon of PHS can be used to collaborate in the study the dormancy mechanisms. On the other hand, it seems logical to understand that achieving tolerance to PHS (i.e., breeding PHS-resistant varieties) is one of the goals of actual seed research. Consequently, it is not surprising that the focus of PHS research in recent years has been on identifying individual genes impacting seed dormancy. *Osaba1* was the first PHS-related mutant to be identified in rice [42]. This mutant harbors a point mutation in the zeaxanthin epoxidase gene, is strongly viviparous with wilty phenotype, and displays a low ABA level with almost no further increase in its levels upon drought.

PHS is a trait controlled by multiple QTLs [39]. In rice, an important cereal crop, more than 165 QTLs associated with seed dormancy or PHS resistance and located on different chromosomes have been identified. Similar to rice, several research groups identified causal genes for the major dormancy QTL in other cereals such as barley and wheat (*Triticum aestivum*). Dormancy QTLs have been found on all chromosomes in both crops [43]. However, although PHS-associated QTL or genes have been reported and cloned, the PHS molecular mechanism remains little-known. Since two major dormancy QTLs (*SD1* and *SD2*) have been detected in barley grains at the beginning of the present century, the PHS process has been extensively investigated and new advances are constantly emerging. In the past few years, it was eventually revealed that alanine aminotransferase (*AlaAT*) is the causal gene for the major grain dormancy QTL *Qsd1* (*SD1*) in barley [44], and that mitogen-activated protein kinase–kinase 3 (*MKK3*) is the causal gene for the

major grain dormancy QTLs *Qsd2-AK* (*SD2*) in barley and *Phs1* in wheat [41,45]. *MKK3* was found to control seed dormancy in wheat and barley using a map-based cloning method [41,45]. *Phs1* in wheat is an ortholog of *SD2* in barley [45]. *Qsd2-AK* at *SD2* acts as a single major determinant explaining the difference in seed dormancy between the dormant cultivar "Azumamugi" (Az) and the nondormant cultivar "Kanto Nakate Gold" (KNG) [41]. QTL *Qsd2-AK* (*SD2*) is a component of the MAPK cascade (i.e., MKKK, MKK, and MAPK) which is evolutionarily conserved in photosynthetic eukaryotes, including Arabidopsis [41]. In summary, Nakamura's group provided for the first time the key to finding plants refractory to PHS. Therefore, cloning of the *MKK3* wheat gene (*TaMKK3*) has been essential to produce improved varieties that are resistant to PHS. Thus, transformation with the *TaMKK3* susceptible allele caused a large increase in PHS susceptibility in dormant backgrounds [41]. The N(asparragine) 260 T(threonine) mutation reduces TaMKK3 kinase activity [41]. Accordingly, the N260T-substituted dormant *MKK3* recessive allele cannot efficiently transmit phosphorylation signals in the MAPK module for germination, delaying germination and conferring the hyperdormant phenotype. Introducing the N260T mutation into all of the functional wheat homologs of MKK3 will be a novel way to increase seed dormancy in wheat. On the other hand, a more recent update provides unique insight into the genetic mechanisms governing PHS in bread wheat [46]. It is important to emphasize that these recent advances can be directly applied in breeding programs to improve PHS tolerance in studied species. Thus, causal genes are now available for marker-assisted selection to improve PHS tolerance in barley and wheat [47].

Together with other map kinases, MKK3 also works in ABA signaling and seed dormancy in Arabidopsis, and loss of *AtMKK3* function has led to ABA-hypersensitive seed germination [48–50]. In 2019, a solid advance occurred in seeds of rice. Thus, the overexpression of *MKKK62* in the embryo and endosperm significantly decreased seed dormancy levels, while the overexpression in the testa and husk did not. *MKKK62*-overexpressing rice lines lost seed dormancy, increased PHS and ABA sensitivity was decreased. High levels of MKKK62-mRNAs were found at the late stage of rice-seed maturation, suggesting that *MKKK62* affected seed traits. MKKK62 (rice has 75 *MKKK*s) interacted with MKK3, while MKK3 interacted with MAPK7 and MAPK14 (from in yeast two-hybrid experiments) [51]. Knock-out experiments confirmed that *MKKK62*, *MKK3*, *MAPK7,* and *MAPK14* (i.e., the entire rice MAPK module) were involved in the regulation of seed dormancy in rice. In other words, protein modification by phosphorylation plays a key role in controlling rice seed dormancy. Interestingly, the results from [51] also indicated that regulation of seed dormancy by *MKKK62* is a common phenomenon among cereals. On the other hand, at least five MKKKs (AtMKKK14/15/16/17/18) are able to activate AtMKK3 in Arabidopsis; but none of these five genes affect seed dormancy when they are overexpressed [52]. The results from [51] also prove that seed dormancy in rice is negatively regulated by *MKKK62* and insinuate that the regulation of seed dormancy distinguish between *Arabidopsis* and rice. Very recently, the ENHANCED RESPONSE TO ABA8 (ERA8) mutant increases seed dormancy and, consequently, PHS tolerance in the soft white wheat 'Zak' [53]. This work suggests that the ERA8 phenotype results from the MKK3-A-G1093A mutation and for that reason, is being used to introgress ERA8 into soft white winter wheat to improve PHS tolerance by increasing ABA sensitivity. An in-depth study of the relationship between MKK3 and ABA will produce a great scientific step not only in breeding programs, but also in model systems such as Arabidopsis or *Medicago truncatula*. Referring to this, two genes in the Raf subfamily of MKKK genes, *Raf10* and *Raf11,* were found to positively regulate seed dormancy in *Arabidopsis* [54]. The functions of these genes are still unknown in crop species like rice. But an influence on seed dormancy should not be ruled out.

Apart from the study of QTLs involved in seed dormancy, other approaches are currently underway for understanding of molecular mechanisms underlying PSH. There is a lot of evidence indicating that ABA and sugars participate in the regulation of seed dormancy and germination [55,56]. Data presented in [57] strongly support that the sugar accumulation is the essential cause of PHS in rice *phs8* T-DNA insertion mutant and the

ABA level is lower in the mutant than in the wild type. The alterations in the content of free monosaccharides and oligosaccharides were more notable in the endosperm of *phs8*. It is of interest to note that the *OsABI3* and *OsABI5* transcripts decreased in mutant seeds, and that overexpression of *OsABI3* and *OsABI5* could partially rescue PHS in the *phs8* mutant. Interestingly, both glucose and sucrose suppressed the expression of *ABI3* and *ABI5*, suggesting that sugar is sufficient to suppress the ABA signaling pathway (see Figure 6 from [57]). Curiously, PHS8 is located in seed-dormancy-related QTLs, which leads us to suppose that any natural variation of *PHS8* may affect seed dormancy. More recently, another T-DNA insertion dominant mutant (*phs9-D*) was characterized in rice. The authors conclude that PHS9 plays an important role in PHS regulation through the integration of ROS and ABA signalings [58]. However, the role of ROS in PHS control requires much more investigation [16]. On the other hand, it is well-known that the expression of *ABI5*, the ortholog of *VP1*, is regulated by *ABI3*, expression of which is required for appropriate *ABI5* expression. ABI3 and ABI5 control the seed sensitivity to ABA [23]. ABI5-binding protein (AFP) induces ABI5 degradation [24,59]. In order to understand the mechanisms underlying seed dormancy or PHS tolerance in common wheat (*Triticum aestivum*), the possible role of TaAFP in seed dormancy was developed, concluding that TaAFP is a negative regulator in seed dormancy [60]. Likewise, this magnificent work concludes that TaAFP-B had a 4-bp InDel in the 5′UTR, which affected the mRNA stability, mRNA transcription expression level, and GUS activity and was significantly associated with PHS tolerance. Finally, QTL-seq analysis was recently performed to identify for the first time QTLs associated with PHS in cucumber (*Cucumis sativus*) using an F2-segregating population, and two QTLs were detected and two candidate genes (*Csa4G622760* and *Csa4G622800*) were proposed [61]. Taking into account the remarkable research on PHS carried out in the last decade, we should be hopeful regarding the avoidance of the great losses produced by PHS in cereal crops. Although a number of QTL or genes related to PHS have been reported in cereals, the molecular mechanism underlying PHS remains largely elusive.

3. Endosperm–Embryo Relationships: Imprinted Gene Expression

In angiosperms, reproduction occurs by double fertilization whereby one of the two sperm cells in the pollen grain fertilizes the egg cell to produce the embryo; while the other one fertilizes the binucleate central cell to generate the triploid (3n) endosperm, which nourishes the embryo. Although with very few exceptions, the endosperm and embryo have essentially the same genotype and markedly different developmental programs. However, the endosperm has two maternal doses of the genome, whereas the embryo has one paternal dose [1,62]. The endosperm does not contribute with genetic material to the next generation, but controls a good number of key processes for the development of the embryo (e.g., providing genetic and molecular signals [63]) and it is an important site of genomic imprinting in higher plants [64].

Genomic imprinting (i.e., uniparental gene expression) is an epigenetic phenomenon in higher plants whereby genetically identical alleles (i.e., parental alleles) have unequal expression depending upon their parental origin [65,66]. The first imprinted gene was discovered in the maize endosperm 51 years ago by phenotypic identification [67]. Maize is also among the several plant species in which gene imprinting has been studied most comprehensively in recent years [68,69]. *Arabidopsis thaliana* has been reported to display genomic imprinting on at least 436 genes in its seed endosperm. In mammals, approximately 80% of the imprinted genes are clustered on chromosomes; but in plants, the majority of the imprinted genes are scattered on chromosomes. At present, and unlike in mammals, a wide debate exists regarding the conservation of the imprinted status in plants (for update see [70]). That is, in developing the seeds of higher plants, some genes show biased gene expression of the allele descended from a particular parent [71]. For this reason, the imprinted genes are classified into maternal expressed genes (*MEG*s) and paternal expressed genes (*PEG*s). Probably *PEG* and *MEG* are subject to different selec-

tive pressures. In mammals, approximately 80% of the imprinted genes are clustered on chromosomes, and in plants most of the imprinted genes are scattered on chromosomes. Recently, *PEG* and *MEG* genes identified under positive selection are involved in processes such as auxin biosynthesis (e.g., *YUCCA10*, *TAR1*) [72]. On the other hand, the number of *PEG*s was much lower than the number of *MEG*s in species as *A. thaliana*, maize, *B. napus*, sorghum and *A. lyrata*. The unbalanced *MEG*s and *PEG*s in plants agreed with the maternal-offspring co-adaptation theory, indicating that the maternal genes were more favored during natural selection [70]. In the present year, a work on the genomic imprinted genes of dicot *B. napus* endosperm provided 297 imprinted genes, including 283 *MEG*s and 14 *PEG*s. More specifically, (i) 36 of 297 imprinted genes were continuously imprinted during endosperm development; (ii) only 26 imprinted genes were specifically expressed in endosperm, while other genes were also expressed in other tissues of *B. napus*, rather than specifically in endosperm; and (iii) a total of 109 imprinted genes were clustered on rapeseed chromosomes [73]. Recently, imprinting status in two closely related dicot species, Arabidopsis and *Capsella rubella*, was analyzed, revealing that less than one-third of orthologous genes are imprinted in both species, and that genomic imprinting is a highly dynamic process [74]. On the other hand, in dicot *Ricinus communis* were identified 209 genes in reciprocal endosperms with potential parent-of-origin specific expression, including 200 and 9 maternally and paternally expressed genes, respectively. More information on *MEG*s and *PEG*s in mono- and dicot species can be reviewed [1]. Likewise, increasingly imprinted genes have been identified and characterized in plant species (for reviews see [64,75]). Although many imprinted genes have been identified in plants, the functional significance of the majority of them remains unknown both in seed life and in other plant organs, which constitutes a strong weakness of this remarkable breakthrough in development biology. Functional studies are necessary to unravel relevant imprinted characterized genes (reviewed in [76]). However, a positive aspect of the study of the imprinting phenomenon is the conclusion that the genes subjected to imprinting are largely conserved across kingdoms [65,77,78]. In contrast to *B. rapa*, genomic imprinting in diploid (*Aegilops* spp.), tatraploid, and hexaploid wheat (*Triticum* spp.), showed evolutionary conserved nature of imprinting status during polyploidization [78].

During the present century, it was evidenced that epigenetic modifications play notable functions in developing seeds [79]. Interestingly, the endosperm has a significant level of hypomethylated DNA in maternal alleles and a looser chromatin structure. As in plant genome methylation, Arabidopsis and rice endosperm is hypomethylated at short transposable elements and related sequences that reside near genes [76,80]. *A. thaliana* has been reported to display genomic imprinting on at least 436 genes in its seed endosperm. Maize, sorghum, and rice endosperm DNA are also hypomethylated [81,82]. Conversely, the embryos are hypermethylated [81]. DNA methylation is essential for the repression of transposable elements and the regulation of gene expression. At present, there is no direct evidence for how dynamic DNA methylation and differentially methylated genes regulate seed development. Curiously, the expression of the imprinted genes was not tightly linked to DNA methylation in castor bean [83]. It is noteworthy that imprinted genes expressed in the endosperm of *A. thaliana* are rapidly evolving due to positive selection; such positive selection is preferentially associated with imprinted paternally expressed genes [72].

DNA methylation is a crucial epigenetic modification involved in many biological processes, including genomic imprinting [84]. The imprinting process includes trimethylation of histone (i.e., H3K27me3) and DNA methylation without altering the genetic sequence [69,85]. In angiosperms, H3K27me3 predominantly marks the maternally imprinted alleles of paternally expressed genes, whereas DNA methylation predominantly marks paternally imprinted alleles of maternally expressed gene [76]. As summary, in mammals and higher plants imprinted genes, likely established prior to fertilization, are silenced through cytosine methylation, histone modifications or both. However, in mammals the epigenetic modifications at imprinted loci are deleted and re-established in each generation (i.e., imprinted alleles are targeted for silencing), while in plants most of the evidence so far

is that pre-existing methylation present on both alleles in the parent plant is specifically removed during gametogenesis from the allele destined to be active in endosperm [86]. In higher plants, DNA methylation is maintained by the maintenance methyltransferase enzyme (MET1 in Arabidopsis) and is essential for propagating methylation marks on imprinted genes. However, in mammals, de novo methylation is also required to place the marks, while in Arabidopsis there is no evidence so far that de novo methylation has a role in imprinting. On the other hand, the evolution of imprinting in animals and higher plants still has many gaps. The characterization of the dynamic DNA methylome will be of the great help [87]. Imprinting is an evolutionary puzzle, as it bears the costs of diploidization without its advantages, namely, protection from recessive mutations. A recent review helps to clarify the complexity of this epigenetic puzzle [88].

The reason for the importance of imprinting is that the chemical modification produced in the DNA, which is transmitted to the offspring, changes the gene expression or the function of the gene product. Interestingly, for complex traits (e.g., rice grain size), some QTLs may also exhibit imprinting effects (i.e., manifesting different genotypic values between reciprocal heterozygotes) and hence are termed imprinted QTLs (iQTLs) [65]. Genomic imprinting primarily occurs in the endosperm [76,89]. As a possibility, the endosperm growth is suitable when *PEG*s (presumably promoting growth) and *MEG*s (presumably repressing growth) are jointly expressed with appropriate dosages. That is: do imprinted genes interact? Although *PEG*s and *MEG*s may be physically and functionally linked, they are possibly regulated by different mechanisms [90]. Although the main functions of imprinting in the endosperm are not fully understood, experiments in *A. thaliana* have demonstrated that imprinting defects in the endosperm may cause seeds to abort [80,90]. Conversely, few embryo processes were linked to genomic imprinting [69,91,92]. Several lines of evidence indicate that the endosperm and embryo exist in distinct transcriptional and chromatin states immediately after fertilization [93]. Summarizing the information to date, endosperm plays an active role in promoting embryo development and its epigenetic regulation could have consequences for embryo developmental programs. Unfortunately, little is known about gene imprinting in dicotyledons.

Given the interest in imprinting in higher plants, numerous updates have been published recently [69,70,80,94–96]. By using: (i) the rapid development of modern technologies (e.g., CRISPR/Cas9, protein-DNA interactions by CUT&RUN, high-throughput transcriptome sequencing, and single-cell RNA sequencing, among others), together with yeast two-hybrid tests; and (ii) the F1 hybrid seeds derived from reciprocal crosses of plants with different ploidy levels to provide different dosages of the parental genomes, a direct genome-wide survey of imprinted genes at the transcription level has become possible. Furthermore, the studies of imprinting in diverse plant species, especially in several important crops, have intensified [75,97]. In biological terms, paternal-excess crosses strongly promote seed development and big seeds; whereas maternal-excess crosses dramatically inhibit endosperm growth and the production of small seeds. These features indicate that an adequate balance between maternally and paternally derived genomes is responsible for both embryo and endosperm development.

Although the progress about genetical properties of imprinted genes is unquestionable (see above), aspects regarding the biological relevance of genomic imprinting still remain to be answered. The increased understanding of the role of PRC2 (polycomb repressive complex 2) in different plant species should be of great value to addressing many of the unanswered questions. PRC2, a subset of the PcG proteins, possesses an evolutionarily conserved epigenetic histone methyltransferase, is a major chromatin-modifying multisubunity complex that catalyzes H3K27me3, and plays a role in safeguarding cellular identity [98], among other functions. H3K27me3 is a repressive epigenetic mark that results in compaction of chromatin, and is associated with genes with low expression levels and high tissue specificity (e.g., endosperm) (Figure 1). Plants lacking PRC2 components do not show severe embryonic phenotypes and most produce viable offspring [99]. The mechanism of recruitment of PRC2 to endosperm target genes is an intense and actual

area of study. Therefore, how PRC2 epigenetic machinery is recruited to specific targets in plants remains largely unclear. However, some progress has occurred recently: (i) seed-coat initiation is controlled by an epigenetic regulator commonly used in developmental transitions [100]. This feature hints that recruitment of polycomb-group protein FERTILIZATION INDEPENDENT ENDOSPERM (FIE), acts as an epigenetic switch that may have been key to the evolution of the seed coat (revised in [1]); (ii) in lateral roots of *A. thaliana*, BASIC PENTACYSTEINS (BPCs) recruit PRC2 to the ABI4 (ABA INSENSITIVE 4) locus and repress ABI4 expression epigenetically by catalyzing the H3K27me3. That is, BPCs bind to the ABI4 promotor, repress ABI4 expression and physically interact with PRC2 [101]. It will be important to demonstrate all these facts in seed development. (iii) Interestingly, the PRC2 recruitment in Arabidopsis relies in large part on binding of trans-acting factors to cis-localized DNA sequence motifs [102]; and (iv) a short time ago, it was shown that SDG711-mediated H3K27me3 changed significantly in genes related to endosperm development, and that SDG711, a histone transmethylase, can directly bind to the gene body region of several starch-synthesis and amylase genes, respectively [103]. For more information on how PRC2 is involved in development and identification of its direct target genes, see [104].

In *Arabidopsis*, DNA methylation and some maternally expressed components of PRC2 are involved in the regulation of some imprinted loci in the endosperm [69]. PRC2 represses endosperm development both before and after fertilization. In other words, some components of PRC2 are maternally expressed and involved in the control of endosperm development [105]. However, the role of PRC2 in endosperm development in monocot is still unclear. Recent results provide strong evidence that rice PRC2 represses central cell proliferation and endosperm formation before fertilization [106,107]. PRC2 core components are broadly conserved and essential for the H3K27 trimethyltransferase activity of the complex [108]. Plants possess several different PRC2 complexes, such as FIS-PRC2 (FIS2), which is specifically involved in female gametophyte reproduction, and endosperm and seed development [109]. Endosperm development prior to fertilization is inhibited by FIS2, which acts in the female gametophyte and during endosperm development (for extension, see the update from [100]). On the other hand, the protein–protein interactions of each PRC2 component are important determinants of the activity of the PRC2 complex. Seeds inheriting maternal mutant alleles of these FIS-class genes abort due to a failure in endosperm cellularization and embryonic arrest, regardless of the paternal genotype. This maternal effect is observed because FIS2 is regulated by epigenetic genomic imprinting.

In conclusion, although great advances have taken place in this decade, there is still a long way to go to complete the puzzle regarding the role of genomic imprinting in seed development. Future investigations will refine the interplay between transcriptional, hormonal, signaling, and epigenetic controls operating in the regulation of endosperm growth. Thus, the interaction between PEGs and MEGs must be definitively confirmed in higher plants. Once it has been demonstrated that PRC1 and PRC2 directly interact, it is important to clarify the role of PRC1 in the functioning of PRC2 in the endosperm and demonstrate whether imprinting always preferentially affects the endosperm. Evolutionarily speaking, it is necessary to investigate if imprinting takes place in organisms other characterized [110–112]. Finally, it is worth knowing how PRC2 epigenetic machinery is recruited to specific targets in endosperm. This aspect is probably one of the most important epigenetic facets of developing endosperm.

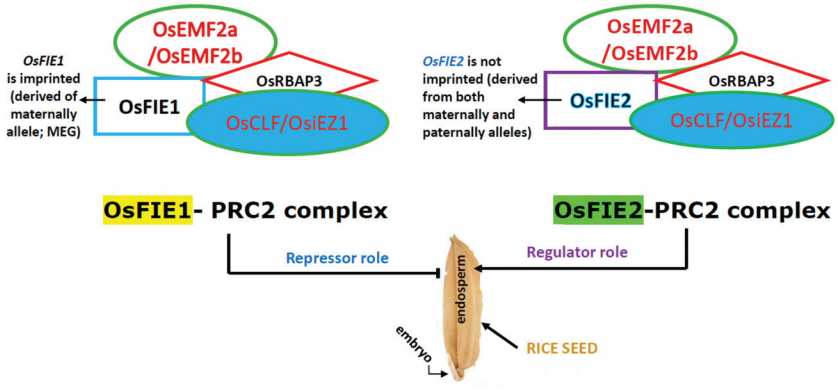

Figure 1. The role of polycomb repressive complex (PRC2) in rice endosperm. PRC2 is an evolutionarily conserved multimeric protein complex that has methyltransferase activity for Lys27 of histone H3 (H3K27), repressing gene expression. Mutation of the imprinted gene *OsEMF2a* induces autonomous endosperm development [108]. FIE: fertilization independent endosperm; EMF2: embryonic flower 2; RBPA3: WD-repeat protein; CLF and iEZ1: enhancer of zeste-like homologs. Adapted from [107,108].

4. The Stored mRNA: A Surprising Singularity in the Seed Life

Excepting dry, viable seeds, molecules of mRNA are generally short-lived. Different mRNAs transcribed during the last phase of development are stored in dry seeds of many species [113]. Seed-stored mRNA can survive for long periods. Some of these stored mRNAs are called 'long-lived mRNAs' because they remain active for a long time, the great majority being selectively translatable at the onset of germination [114], and the others are degraded. Although mRNA decay regulates mRNA levels, the regulation of stored-mRNA decay machinery remains still elusive in seeds. Dry rice and Arabidopsis seeds contain >17,000 and >12,000 stored mRNAs, respectively [115–117]. The seed-stored mRNAs encode many proteins of diverse physiological processes and cues [13]. However, not all of these mRNAs are considered 'long-lived mRNAs' because the temporality of translation is different between members of this population. In addition to mRNAs, dry seeds accumulate a large amount functional proteins involved in metabolism, transcription, and translation. Before the onset of desiccation and triggering of dormancy, embryos transcribe and store 'long-lived mRNAs' involved in the germination process (e.g., ABA catabolism-related enzymes, phospholipids, and calcium ion signaling-related proteins) [118]. The evidence that seeds translate stored mRNA during germination using stored ribosomes has been amply demonstrated [114]. However, ribosomes are inactive in dry seeds, and must be reactivated in order to germination process takes place. A task for 'long-lived mRNAs' once demonstrated that germination is not inhibited in the presence of transcription inhibitors; but it does when translational inhibitors were added to the medium [119,120]. One of the existing gaps is deciphering if the population of stored 'long-lived mRNAs' is sufficient to initiate germination. Anyway, the population of stored mRNA within dry seeds can sustain germination completion in several species [121]. The authors of [121] suggest that the classes of 'long-lived mRNAs' are highly conserved between dicot and monocot seeds. To clarify the distinct roles of proteins translated from long-lived mRNAs and de novo transcribed mRNAs, a proteome analysis was recently performed in germinating rice seeds. This leading work proposes that long-lived mRNAs support an initial energy production (e.g., glycolysis-related proteins) and activation of the translational machinery upon imbibition, whereas the de novo transcriptions accelerate the energy production after glycolysis [122].

So far, it has been unknown how fragmentation of seed-stored mRNA affects germination once rehydration occurred. However, there is no doubt that the cellular redox state affects RNA fragmentation by altering several key processes of seed life [16,123]. It seems

also clear that the seed does not have mechanisms that resolve the mRNA fragmentation. Therefore, seed viability and aging are affected by fragmentation, and sometimes death occurs. Seed aging is a convoluted biological trait in which several interconnected molecular, biochemical, physiological, and metabolic events are involved. The seed-aging process is usually associated with the oxidation of macromolecules. Recently, Fleming et al. (2018) observed fragmentation of seed-stored mRNAs in soybean embryonic axis by transcriptomic analysis, and suggested that mRNA breakage occurs at random positions [124]. Later, Zhao et al. (2020) elegantly showed in Arabidopsis that the degradation of seed-stored mRNA is greatly correlated with seed-aging time. Stored mRNA of almost all the ubiquitination-related and heat-shock protein (HSP) genes analyzed decreased gradually in aged seeds. In addition, enzymes related to energy production and structural proteins of the cytoskeleton are also involved in this seed-stored mRNA degradation process [125]. Interestingly, the data from [125] also indicate that the majority of Arabidopsis seed-stored mRNA have a similar and constant rate of degradation (i.e., the time for the mRNA level to decrease by 50% is constant) during seed aging. These findings were ratified in canola and wheat, two valuable agricultural species [126]. This and previous work indicate that the damage or degradation of stored mRNA occurred randomly along the length of this RNA, and also propose that stored mRNA degradation during seed aging is a general phenomenon for seeds [124,125]. On the other hand, the degradation of ribosomal RNA is widely described during seed aging [127–129].

Although many physiological properties of stored mRNA are known, the cellular conservation, stability, transcription, and translation of these molecules is not entirely clear yet [12,130]. Degradation of mRNA is a key process in the regulation of gene expression and elimination of defective mRNAs. The processing bodies (P bodies) are equipped with machinery for RNA degradation (Figure 2). These cytoplasmic bodies are RNA membraneless granules (i.e., liquid–liquid phase separation), constituted by ribonucleoproteins associated with both mRNA decay and translation repression. Plant P bodies share many protein components with yeast and mammalian P bodies and are conserved in eukaryotes. It is worth highlighting that P bodies possess targets of the mRNA decapping machinery (e.g., *ASL9*; [131]) and can also serve as translationally repressed mRNA reservoirs in regulating the homeostasis of mRNA translation [132–134]. Interestingly, the mRNA decay machinery directly targets *ASL9* transcripts for decay to balance cytokinin/auxin responses during developmental reprogramming [131]. In other words, P bodies are often considered to be the site for mRNA decay due to their content of decapping complexes (i.e., proteins related to mRNA decay), de-adenylation factors, 5′ to 3′ exoribonuclease, Argonaute 1 (key protein gene silencing), and factors involved in nonsense-mediated mRNA decay [135–137]. Therefore, it is not surprising that plants deficient in P-body components display severe developmental perturbations [132]. However, little is known about how decapping contributes to plant development. Recently, it was reported that mRNA decay is required to unlock cellular states during development [131]. On the other hand, mRNA may be sequestered in P bodies for degradation, or re-enter polysomal translation complexes, which may be related to the use of dry seed-stored mRNA during onset germination. However, this assumption still needs to be proved and generalized in angiosperms. Interestingly, P bodies are highly mobile and connected to actin filament and myosins via interaction with DECAPPING PROTEIN1 (DCP1) [138]. Decapping enzymes DCP1/2 present their genes in a single copy in the Arabidopsis genome, and together with VARICOSE (VCS) are part of the conserved components among eukaryotes' decapping complex located in P bodies. The mRNA turnover carried out in this decapping complex is essential for postembryonic development in Arabidopsis. DCP2 form a complex catalyzing the removal of m7GDP caps from mRNAs [132,139]. Importantly, components of the cytoplasmic 5′-3′ mRNA decapping pathway (i.e., DCP1/2/5, VCS, PAT1 (which accumulates in P bodies) and exoribonuclease XRN4) [140] contribute to ABA signaling in Arabidopsis [141]. Other types of RNA granules together with P bodies may also be involved in controlling the translation in seeds [142].

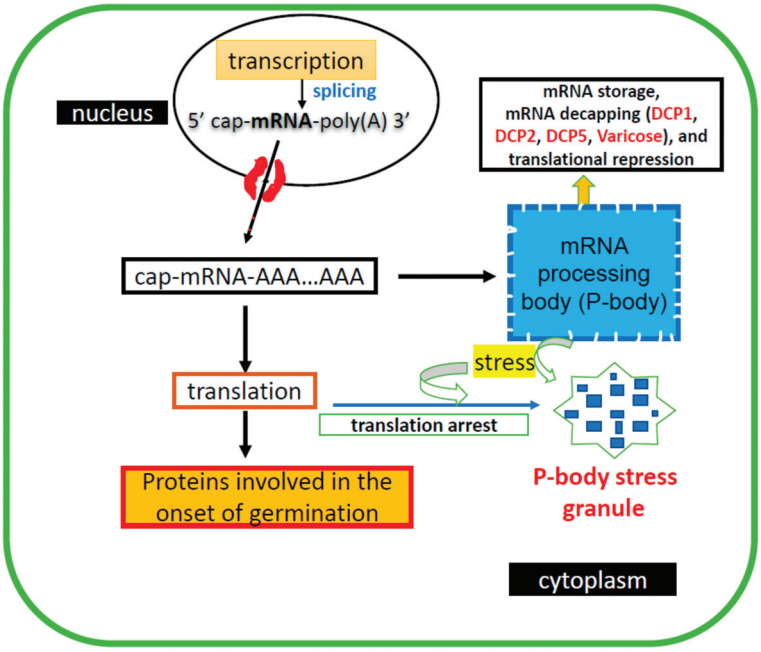

Figure 2. The stored mRNA, once in the cytoplasm, can be sent to P bodies located in the ER for processing; or, alternatively, included in the translation machinery. What controls this mRNA distribution is not known. Under stress, P bodies are agglutinated in granules and their translation is reduced. DCP (decapping enzyme), ER (endoplasmic reticulum).

On the other hand, P bodies can contain several RNA-binding proteins (RBPs), which stabilize and/or modulate the translation of target mRNAs for decay [136,143]. Importantly, binding of RBPs' sequence elements in mRNA can both promote and repress translation [137]. RBPs are tightly bound RNAs that through one or multiple globular RNA-binding domains form ribonucleoprotein complexes that dynamically regulate the RNA's fate and function. Thus, RBPs are versatile key players in the posttranscriptional control of mRNAs and candidates for regulating translation during seed germination [144–146]. However, few RBPs have been functionally explored in the seed world. Knowledge of the functional roles of RBPs in plants is lagging far behind regarding those in other organisms. Recent findings in the field have been collected and commented on [147]. Suggestively, some studies clearly indicate that many RBPs harboring RNA chaperone activity play essential roles in the regulation of RNA metabolism during plant growth and development (for more information, see [144]). Some RBPs as RZ-1A and glycine-rich (GR)-RBP (GRP1A), have been detected in rice seeds by proteomic analysis [148]. In 2013, it was demonstrated that RZ-1A and GRP1A are solid RBP candidates involved in seed desiccation while also preserving the stability of "long-lived mRNAs" [149]. In 2020, a solid experimental work was reported in *A. thaliana* leaves. This protocol developed the RNA interactome capture to identify proteins that interact with RNAs-poly(A) in living cells [150,151]. The use of this methodology in seeds will provide an outstanding breakthrough in the study of RBPs. In a recent and detailed work carried out in *A. thaliana*, the Bentsink group smartly identified 30 seed-specific RBPs and 22 dynamic RBPs from testa rupture to radicle protrusion period [152]. These authors argue, in a well-built discussion, the possible role of RBPs in the germination process. A major task in the seed world is to identify RNA targets and to understand how RBPs recognize substrate RNAs and how they interact with

other protein factors to regulate posttranscriptional RNA metabolism during plant growth and development.

The Arabidopsis genome harbors hundreds of mRNA binding proteins, of which a large majority do not yet have an assigned function (see comments from Bai et al., 2017 [114]). Since it is known that monosomes are very abundant in Arabidopsis dry seeds, a complicated protocol was started to demonstrate if any protein of monosomes was bound to the seed-stored mRNA. Thus, Bai et al. (2020) proved that seed-stored mRNA can bind to monosome proteins (i.e., 50% of seed-stored mRNAs are bound to 80S ribosomes, mostly monosomes, whereas the other 50% are free-stored mRNA). In other words, transcripts that are associated with ribosome complexes in the dry state are translated (associated with polysomes) upon seed imbibition (see Tables 1 and 2 from [153]). On the other hand, a determined monosome population in dry seeds is enriched with proteins related to protection against oxidative stress. This feature suggests that specific mRNAs are preserved from oxidation until the translation machinery begins with the seed hydration. But the way to choose theses specific mRNAs is, at present, noteless. Chantarachot and Bailly-Serres (2018) suggested several possibilities for it [137]. Moreover, these authors also suggested that the conserved eukaryotic decapping VCS, a protein associated with monosomes and polysomes, can be involved in the degradation of seed stored-mRNAs not compromised in the germination process. However, how specific mRNAs are targeted to monosome complexes and are specifically translated during imbibition is at present unknown.

The complexity of the involvement of stored mRNA in the seed-germination machinery is considerable. Further analyses are required to identify and characterize which mechanisms are used by the seed to benefit from some of the mRNAs transcribed during the maturation period. The following questions, among others, will need to be answered in order to make progress. Thus:

(i) Is the population of stored-mRNA sufficient to initiate the germination process? Are the stored-transcripts encoding ribosomal proteins involved in the onset germination?
(ii) Since selective mRNA translation is a key feature of the seed germination process, which mRNAs are exclusively for that process, and how are they selected from among stored mRNAs?
(iii) Are the chosen mRNAs epigenetically marked?
(iv) Is the signaling network involved in germination compromised in the choice of mRNAs?
(v) What is the mechanism for the spatio-temporal choice of each transcript during maturation and onset germination? That is, how do the cells of imbibed seeds discriminate between stored mRNAs to be utilized in germination and those to be destroyed?
(vi) Do differences exist among stored-mRNAs in terms of the rate of degradation?
(vii) The future challenge, therefore, will be to understand how these multiple noted components are integrated.

Funding: This research received no external funding.

Institutional Review Board Statement: Not applicable.

Informed Consent Statement: Not applicable.

Data Availability Statement: Not applicable.

Acknowledgments: I thank J. Barrero, G. Bassel, L. Bentsink, R. Iglesias-Fernández, S. Pollmann and N. Sano for his valuable help in scrutinizing along the recent milestones in the world of seed life. Also, I thank you for sending manuscripts and, where appropriate, the constructive comments.

Conflicts of Interest: The author declares no conflict of interest.

References

1. Baroux, C.; Grossniklaus, U. Seeds-An evolutionary innovation underlying reproductive success in flowering plants. *Curr. Top. Dev. Biol.* **2019**, *131*, 605–642.
2. Song, J.; Xie, X.; Cui, Y.; Zou, J. Endosperm-embryo communications: Recent advances and perspectives. *Plants* **2021**, *10*, 2511. [CrossRef]
3. An, L.; Tao, Y.; Chen, H.; He, M.; Xiao, F.; Li, G.; Ding, Y.; Liu, Z. Embryo-endosperm interaction and its agronomic relevance to rice quality. *Front. Plant Sci.* **2020**, *11*, 587641. [CrossRef] [PubMed]
4. Dai, D.; Ma, Z.; Song, R. Maize endosperm development. *J. Integr. Plant Biol.* **2021**, *63*, 613–627. [CrossRef]
5. Rodríguez, M.V.; Barrero, J.M.; Corbineau, F.; Gubler, F.; Benech-Arnold, R.L. Dormancy in cereals (not too much, not so little): About the mechanisms behind this trait. *Seed Sci. Res.* **2015**, *25*, 99–119. [CrossRef]
6. Chahtane, H.; Kim, W.; López-Molina, L. Primary seed dormancy: A temporally multilayered riddle waiting to be unlocked. *J. Exp. Bot.* **2017**, *68*, 857–869. [CrossRef] [PubMed]
7. Nonogaki, H. Seed germination and dormancy: The classic story, new puzzles, and evolution. *J. Integr. Plant Biol.* **2019**, *61*, 541–563. [CrossRef] [PubMed]
8. Sano, N.; Rajjou, L.; North, H.M.; Debeaujon, I.; Marion-Poll, A.; Seo, M. Staying alive: Molecular aspects of seed longevity. *Plant Cell Physiol.* **2016**, *57*, 660–674. [CrossRef] [PubMed]
9. Pereira-Lima, J.J.; Buitink, J.; Lalanne, D.; Rossi, R.F.; Pelletier, S.; da Silva, E.A.A.; Leprince, O. Molecular characterization of the acquisition of longevity during seed maturation in soybean. *PLoS ONE* **2017**, *12*, e0180282. [CrossRef]
10. Kijak, H.; Ratajczak, E. What do we know about the genetic basis of seed desiccation tolerance and longevity? *Int. J. Mol. Sci.* **2020**, *21*, 3612. [CrossRef]
11. Matilla, A.J. The orthodox dry seeds are alive: A clear example of desiccation tolerance. *Plants* **2022**, *11*, 20. [CrossRef] [PubMed]
12. Sajeev, N.; Bai, B.; Bentsink, L. Seeds: A unique system to study translational regulation. *Trends Plant Sci.* **2019**, *24*, 487–495. [CrossRef] [PubMed]
13. Sano, N.; Rajjou, L.; North, H.M. Lost in translation: Physiological roles of stored mRNAs in seed germination. *Plants* **2020**, *9*, 347. [CrossRef] [PubMed]
14. El-Maarouf-Bouteau, H. The seed and the metabolism regulation. *Biology* **2022**, *11*, 168. [CrossRef]
15. Signorelli, S.; Considine, M.J. Nitric oxide enables germination by a four-pronged attack on ABA-induced seed dormancy. *Front. Plant Sci.* **2018**, *9*, 296. [CrossRef]
16. Bailly, C. The signalling role of ROS on the regulation of seed germination and dormancy. *Biochem. J.* **2019**, *476*, 3019–3032. [CrossRef]
17. Katsuya-Gaviria, K.; Caro, E.; Carrillo-Barral, N.; Iglesias-Fernández, R. ROS and nucleic acids modifications during seed dormancy. *Plants* **2020**, *9*, 679. [CrossRef]
18. Ali, F.; Qanmber, G.; Li, F.; Wang, Z. Updated role of ABA in seed maturation, dormancy, and germination. *J. Adv. Res.* **2022**, *35*, 199–214. [CrossRef]
19. Skuback, A.; Daszkowska-Golek, A.; Szarejko, J. The role and regulation of ABI5 (ABA-Insensitive 5) in plant development, abiotic stress responses and phytohormone crosstalk. *Front. Plant Sci.* **2016**, *7*, 1884.
20. Carbonero, P.; Iglesias-Fernández, R.; Vicente-Carbajosa, J. The AFL subfamily of B3 transcription factors: Evolution and function in angiosperms seeds. *J. Exp. Bot.* **2017**, *68*, 871–880. [CrossRef]
21. Chandrasekaran, U.; Luo, X.; Zhou, W.; Shu, K. Multifaceted signaling networks mediated by abscisic acid insensitive 4 (ABI4). *Plant Commun.* **2020**, *1*, 100040. [CrossRef] [PubMed]
22. Tian, R.; Wang, F.; Zheng, Q.; Niza, V.; Downie, A.B.; Perry, S.E. Direct and indirect targets of the Arabidopsis seed transcription factor ABSCISIC ACID INSENSITIVE3. *Plant J.* **2020**, *103*, 1679–1694. [CrossRef] [PubMed]
23. Sano, A.; Marion-Poll, A. ABA metabolism and homeostasis in seed dormancy and germination. *Int. J. Mol. Sci.* **2021**, *22*, 5069. [CrossRef] [PubMed]
24. Smolikova, G.; Strygina, K.; Krylova, E.; Leonova, T.; Frolov, A.; Khlestkina, E.; Medvedev, S. Transition from seeds to seedlings: Hormonal and epigenetic aspects. *Plants* **2021**, *10*, 1884. [CrossRef]
25. Yan, A.; Chen, Z. The pivotal role of abscisic acid signaling during transition from seed maturation to germination. *Plant Cell Rep.* **2017**, *36*, 689–703. [CrossRef]
26. Tuan, P.A.; Kumar, R.; Real, P.K.; Toora, P.K.; Ayele, B. Molecular mechanisms underlying abscisic acid/gibberellin balance in the control of seed dormancy and germination in cereals. *Front. Plant Sci.* **2018**, *9*, 668. [CrossRef]
27. Corbineau, F.; Xia, Q.; Bailly, C.; El-Maarouf-Bouteau, H. Ethylene, a key factor in the regulation of seed dormancy. *Front. Plant Sci.* **2014**, *5*, 539. [CrossRef]
28. Bogatek, R.; Gniazdowska, A. Ethylene in seed development, dormancy and germination. *Ann. Plant Rev.* **2018**, *44*, 189–218.
29. Zhao, H.; Yin, C.-C.; Ma, B.; Chen, S.-Y.; Zhang, J.-S. Ethylene signaling in rice and Arabidopsis: New regulators and mechanisms. *J. Integr. Plant Biol.* **2021**, *63*, 102–125. [CrossRef]
30. Wang, X.; Maraya Gomes, M.; Bailly, C.; Corbineau, F.J. Role of ethylene and proteolytic N-degron pathway in the regulation of *Arabidopsis* seed dormancy. *Integr. Plant Biol.* **2021**, *63*, 2110–2122. [CrossRef]
31. Basbouss-Serhal, I.; Leymarie, J.; Bailly, C. Fluctuation of *Arabidopsis* seed dormancy with relative humidity and temperature during dry storage. *J. Exp. Bot.* **2016**, *67*, 119–130. [CrossRef]

32. Finch-Savage, W.E.; Footitt, S. Seed dormancy cycling and the regulation of dormancy mechanisms to time germination in variable field environments. *J. Exp. Bot.* **2017**, *68*, 843–856. [CrossRef] [PubMed]
33. Gu, D.; Ji, R.; He, C.; Peng, T.; Zhang, M.; Duan, J.; Xiong, C.; Liu, X. *Arabidopsis* histone methyltransferase SUVH5 is a positive regulator of light-mediated seed germination. *Front. Plant Sci.* **2019**, *10*, 841. [CrossRef] [PubMed]
34. Yan, A.; Chen, Z. The control of seed dormancy and germination by temperature, light and nitrate. *Bot. Rew.* **2020**, *86*, 39–75. [CrossRef]
35. Yang, L.; Liu, S.; Lin, R. The role of light in regulating seed dormancy and germination. *J. Integr. Plant Biol.* **2020**, *62*, 1310–1326. [CrossRef]
36. Harrison, C.J. Development and genetics in the evolution of land plant body plants. *Philos. Trans. R. Soc. Lond. Biol. Sci.* **2017**, *372*, 20150490. [CrossRef] [PubMed]
37. Barrero, J.M.; Cavanagh, C.; Verbyla, K.L.; Tibbits, J.F.G.; Verbyla, A.P.; Huang, B.E.; Rosewame, G.M.; Stephen, S.; Wang, P.; Whan, A.; et al. Transcriptomic analysis of wheat near-isogenic lines identifies PM19-A1 and A2 as candidates for a major dormancy QTL. *Genome Biol.* **2015**, *16*, 93. [CrossRef] [PubMed]
38. Wang, X.; Liu, H.; Liu, G.; Mia, M.S.; Siddique, K.H.M.; Yan, G. Phenotypic and genotypic characterization of near-isogenic lines targeting a major 4BL QTL responsible for pre-harvest sprouting in wheat. *BMC Plant Biol.* **2019**, *19*, 348. [CrossRef] [PubMed]
39. Tai, L.; Wang, H.J.; Xu, X.J.; Sun, W.H.; Ju, L.; Liu, W.T.; Li, W.Q.; Sun, J.; Chen, K.M. Pre-harvest sprouting in cereals: Genetic and biochemical mechanisms. *J. Exp. Bot.* **2021**, *72*, 2857–2876. [CrossRef]
40. Li, L.; Zhang, Y.; Zhang, Y.; Li, M.; Xu, D.; Tian, X.; Song, J.; Luo, X.; Xie, L.; Wang, D.; et al. Genome-wide linkage mapping for preharvest sprouting resistance in wheat using 15K single-nucleotide polymorphism arrays. *Front. Plant Sci.* **2021**, *21*, 749206. [CrossRef]
41. Nakamura, S.; Pourkheirandish, M.; Morishige, H.; Kubo, Y.; Nakamura, M.; Ichimura, K.; Seo, S.; Kanamori, H.; Wu, J.; Ando, T.; et al. Mitogen-activated protein kinase kinase 3 (MKK3) regulates seed dormancy in barley. *Curr. Biol.* **2016**, *26*, 775–781. [CrossRef] [PubMed]
42. Tian, C.; Zuo, Z.; Qiu, J.-L. Identification and characterization of ABA responsive microRNAs in rice. *J. Genet. Genom.* **2015**, *42*, 393–402. [CrossRef] [PubMed]
43. Nakamura, S.; Pourkheirandhish, M.; Morishige, H.; Sameri, M.; Sato, K.; Komatsuda, T. Quantitative trait loci and maternal effects affecting the strong grain dormancy of wild barley (*Hordeum vulgare* ssp. *spontaneum*). *Front. Plant Sci.* **2017**, *8*, 1840. [CrossRef]
44. Sato, K.; Yamane, M.; Yamaji, N.; Kanamori, H.; Tagiri, A.; Schwerdt, J.G.; Fincher, G.B.; Matsumoto, T.; Takeda, K.; Komatsuda, T. Alanine aminotransferase controls seed dormancy in barley. *Nat. Commun.* **2016**, *7*, 11625. [CrossRef] [PubMed]
45. Torada, A.; Koike, M.; Ogawa, T.; Takenouchi, Y.; Tadamura, K.; Wu, J.; Matsumoto, T.; Kawaura, K.; Ogihara, Y. A causal gene for seed dormancy on wheat chromosome 4A encodes a MAP kinase kinase. *Curr. Biol.* **2016**, *26*, 782–787. [CrossRef]
46. Vetcha, J.M.; Stougaarda, R.N.; Martina, J.M.; Giroux, M.J. Review: Revealing the genetic mechanisms of pre-harvest sprouting in hexaploid wheat (*Triticum aestivum* L.). *Plant Sci.* **2019**, *281*, 180–185. [CrossRef]
47. Nakamura, S. Grain dormancy genes responsible for preventing pre-harvest sprouting in barley and wheat. *Breed. Sci.* **2018**, *68*, 295–304. [CrossRef]
48. Danquah, A.; de Zélicourt, A.; Boudsocq, M.; Neubauer, J.; Frei dit Frey, N.; Leonhardt, N.; Pateyron, S.; Gwinner, F.; Tamby, J.; Ortiz-Masia, D.; et al. Identification and characterization of an ABA-activated MAP kinase cascade in *Arabidopsis thaliana*. *Plant J.* **2015**, *82*, 232–244. [CrossRef]
49. Jin, D.; Wu, M.; Li, B.; Bücker, B.; Keil, P.; Zhang, S.; Li, J.; Kang, D.; Liu, J.; Dong, J.; et al. The COP9 signalosome regulates seed germination by facilitating protein degradation of RGL2 and ABI5. *PLoS Genet.* **2018**, *14*, e1007237. [CrossRef]
50. Qin, N.; Xu, D.; Li, J.; Deng, X.W. COP9 signalosome: Discovery, conservation, activity, and function. *J. Integr. Plant Biol.* **2020**, *62*, 90–103. [CrossRef]
51. Mao, X.; Zhang, J.; Liu, W.; Yang, S.; Liu, Q.; Fu, H.; Zhao, J.; Huang, W.; Dong, J.; Zhang, S.; et al. The MKKK62-MKK3-MAPK7/14 module negatively regulates seed dormancy in rice. *Rice* **2019**, *12*, 2. [CrossRef] [PubMed]
52. Choi, S.; Lee, S.; Na, Y.; Jeung, S.; Kim, S.Y. *Arabidopsis* MAP3K16 and other salt-inducible MAP3Ks regulate ABA response redundantly. *Mol. Cells* **2017**, *40*, 230–242. [PubMed]
53. Martínez, S.A.; Shorinola, O.; Conselman, S.; See, D.; Skinner, D.Z.; Uauy, C.; Steber, C.M. Exome sequencing of bulked segregants identified a novel TaMKK3-A allele linked to the wheat ERA8 ABA-hypersensitive germination phenotype. *Theor. Appl. Genet.* **2020**, *133*, 719–736. [CrossRef]
54. Lee, S.J.; Lee, M.H.; Kim, J.I.; Kim, S.Y. Arabidopsis putative MAP kinase kinase kinases Raf10 and Raf11 are positive regulators of seed dormancy and ABA response. *Plant Cell Physiol* **2015**, *56*, 84–97. [CrossRef]
55. Zhu, G.; Ye, N.; Zhang, J. Glucose-induced delay of seed germination in rice is mediated by the suppression of ABA catabolism rather than an enhancement of ABA biosynthesis. *Plant Cell Physiol.* **2009**, *50*, 644–651. [CrossRef] [PubMed]
56. Howard, T.P.; Fahy, B.; Craggs, A.; Mumford, R.; Leigh, F.; Howell, P.; Greenland, A.; Smith, A.M. Barley mutants with low rates of endosperm starch synthesis have low grain dormancy and high susceptibility to preharvest sprouting. *New Phytol.* **2012**, *194*, 158–167. [CrossRef]
57. Du, L.; Xu, F.; Fang, J.; Gao, S.; Tang, J.; Fang, S.; Wang, H.; Tong, H.; Zhang, F.; Chu, J.; et al. Endosperm sugar accumulation caused by mutation of PHS8/ISA1 leads to pre-harvest sprouting in rice. *Plant J.* **2018**, *95*, 545–556. [CrossRef]

58. Xu, F.; Tang, J.; Gao, S.; Cheng, X.; Du, L.; Chu, C. Control of rice pre-harvest sprouting by glutaredoxin-mediated abscisic acid signaling. *Plant J.* **2019**, *5*, 1036–1051. [CrossRef]
59. López-Molina, L.; Mongrand, S.; McLachlin, D.T.; Chait, B.T.; Chua, N.H. ABI5 acts downstream of ABI3 to execute an ABA-dependent growth arrest during germination. *Plant J.* **2002**, *32*, 1–12. [CrossRef]
60. Feng, Y.; Liu, M.; Wang, Z.; Zhao, X.; Han, B.; Xing, Y.; Wang, M.; Yang, Y. A 4-bp deletion in the 5′UTR of TaAFP-B is associated with seed dormancy in common wheat (*Triticum aestivum* L.). *BMC Plant Biol.* **2019**, *19*, 349. [CrossRef]
61. Cao, M.; Li, S.; Deng, Q.; Wang, H.; Yang, R. Identification of a major-effect QTL associated with pre-harvest sprouting in cucumber (*Cucumis sativus* L.) using the QTL-seq method. *BMC Genom.* **2021**, *22*, 249. [CrossRef]
62. Zhou, L.Z.; Dresslhaus, T. Friend or foe: Signaling mechanisms during double fertilization in flowering seed plants. *Curr. Top. Dev. Biol.* **2019**, *131*, 453–496. [PubMed]
63. Sato, H.; Santos-González, J.; Köhler, C. Combinations of maternal-specific repressive epigenetic marks in the endosperm control seed dormancy. *eLife* **2021**, *10*, e64593. [CrossRef] [PubMed]
64. Liu, Y.; Jing, X.; Zhang, H.; Xiong, J.; Qiao, Y. Identification of imprinted genes based on homology: An example of *Fragaria vesca*. *Genes* **2021**, *12*, 380. [CrossRef]
65. Yuan, J.; Chen, S.; Jiao, W.; Wang, L.; Wang, L.; Ye, W.; Lu, J.; Hong, D.; You, S.; Cheng, Z.; et al. Both maternally and paternally imprinted genes regulate seed development in rice. *New Phytol.* **2017**, *216*, 373–387. [CrossRef] [PubMed]
66. Lafon-Placette, C.; Hatorangan, M.R.; Steige, K.A.; Cornille, A.; Lascoux, M.; Slotte, T.; Köhler, C. Paternally expressed imprinted genes associate with hybridization barriers in *Capsella*. *Nat. Plants* **2018**, *4*, 352–357. [CrossRef]
67. Kermicle, J.L. Dependence of the R-mottled aleurone phenotype in maize on mode of sexual transmission. *Genetics* **1970**, *66*, 69–85. [CrossRef]
68. Li, G.; Wang, D.; Yang, R.; Logan, K.; Chen, H.; Zhang, S.; Skaggs, M.I.; Lloyd, A.; Burnett, W.J.; Laurie, J.D.; et al. Temporal patterns of gene expression in developing maize endosperm identified through transcriptome sequencing. *Proc. Natl. Acad. Sci. USA* **2014**, *111*, 7582–7587. [CrossRef]
69. Batista, R.A.; Köhler, C. Genomic imprinting in plants-revisiting existing models. *Genes Dev.* **2020**, *34*, 24–36. [CrossRef]
70. Mongomery, S.A.; Berger, F. The evolution of imprinting in plants: Beyond the seed. *Plant Reprod.* **2021**, *34*, 373–383. [CrossRef]
71. Köhler, C.; Wolff, P.; Spillane, C. Epigenetic mechanisms underlying genomic imprinting in plants. *Annu. Rev. Plant Biol.* **2012**, *63*, 331–352. [CrossRef] [PubMed]
72. Tuteja, R.; McKeown, P.C.; Ryan, P.; Claire, C.; Morgan, C.C.; Donoghue, M.T.A.; Downing, T.; O'Connell, M.J.; Spillane, C. Paternally expressed imprinted genes under positive Darwinian selection in A. thaliana. *Mol. Biol. Evol.* **2019**, *36*, 1239–1253. [CrossRef] [PubMed]
73. Rong, H.; Yang, W.; Zhu, H.; Jiang, B.; Jian, J.; Wang, Y. Genomic imprinted genes in reciprocal hybrid endosperm of Brassica napus. *BMC Plant Biol.* **2021**, *21*, 140. [CrossRef]
74. Hatorangan, M.R.; Laenen, B.; Steige, K.A.; Slotte, T.; Köhler, C. Rapid evolution of genomic imprinting in two species of the Brassicaceae. *Plant Cell* **2016**, *28*, 1815–1827. [CrossRef] [PubMed]
75. Picard, C.L.; Gehring, M. Identification and comparison of imprinted genes across plant species. In *Plant Epigenetics and Epigenomics*, 2nd ed.; Spillane, C., McKeown, P., Eds.; Methods in Molecular Biology: New York, NY, USA, 2020; Volume 2093, pp. 173–201.
76. Gehring, M.; Satyaki, P.R. Endosperm and imprinting, inextricably linked. *Plant Physiol.* **2017**, *173*, 143–154. [CrossRef] [PubMed]
77. Klosinska, M.; Picard, C.L.; Gehring, M. Conserved imprinting associated with unique epigenetic signatures in the *Arabidopsis* genus. *Nat. Plants* **2016**, *2*, 16145. [CrossRef]
78. Yang, G.; Liu, Z.; Gao, L.; Yu, K.; Feng, M.; Yao, Y.; Peng, H.; Hu, Z.; Sun, Q.; Ni, Z.; et al. Genomic imprinting was evolutionarily conserved during wheat polyploidization. *Plant Cell* **2018**, *30*, 37–47. [CrossRef]
79. O'Brien, E.K.; Wolf, J.B. The coadaptation theory for genomic imprinting. *Evol. Lett.* **2017**, *1*, 49–59. [CrossRef]
80. Satyaki, P.R.; Gehring, M. DNA methylation and imprinting in plants: Machinary and mechanisms. *Crit. Rev. Biochem. Mol. Biol.* **2017**, *52*, 163–175. [CrossRef]
81. Feng, S.; Cokus, S.J.; Zhang, X.; Chen, P.Y.; Bostick, M.; Goll, M.G.; Hetzel, J.; Jain, J.; Strauss, S.H.; Halpern, M.E.; et al. Conservation and divergence of methylation patterning in plants and animals. *Proc. Natl. Acad. Sci. USA* **2010**, *107*, 8689–8694. [CrossRef]
82. Xu, G.; Lyu, J.; Li, Q.; Liu, H.; Wang, D.; Zhang, M.; Springer, N.M.; Ross-Ibarra, J.; Yang, J. Evolutionary and functional genomics of DNA methylation in maize domestication and improvement. *Nat. Commun.* **2020**, *11*, 5539. [CrossRef] [PubMed]
83. Xu, W.; Dai, M.; Li, F.; Liu, A. Genomic imprinting, methylation and parent-of-origin effects in reciprocal hybrid endosperm of castor vean. *Nucl. Acid. Res.* **2014**, *42*, 6987–6998. [CrossRef] [PubMed]
84. Pei, L.; Zhang, L.; Li, J.; Shen, C.; Qiu, P.; Tu, L.; Zhang, X.; Wang, M. Tracing the origin and evolution history of methylation-related genes in plants. *BMC Plant Biol.* **2019**, *19*, 307. [CrossRef] [PubMed]
85. Mozgova, I.; Hennig, L. The polycomb group protein regulatory network. *Ann. Rev. Plant Biol.* **2015**, *66*, 269–296. [CrossRef] [PubMed]
86. Zhang, M.; Li, N.; He, W.; Zhang, H.; Yang, W.; Liu, B. Genome-wide screen of genes imprinted in sorghum endosperm, and the roles of allelic differential cytosine methylation. *Plant J.* **2016**, *85*, 424–436. [CrossRef]

87. Xing, M.-Q.; Zhang, Y.-J.; Zhou, S.-R.; Hu, W.-Y.; Wu, X.-T.; Ye, Y.-J.; Wu, X.-X.; Xiao, Y.-P.; Li, X.; Xue , H.W.; et al. Global analysis reveals the crucial roles of DNA methylation during rice seed development. *Plant Phys.* **2015**, *168*, 1417–1432. [CrossRef]
88. Sazhenova, E.A.; Lebedev, I.N. Evolutionary aspects of genomic imprinting molecular. *Mol. Biol.* **2021**, *55*, 1–15. [CrossRef]
89. Xu, X.; Zhiguo, E.; Zhang, D.; Yung, Q.; Zhou, Y.; Niu, B.; Chen, C. OsYUC11-mediated auxin biosynthesis es essential for endosperm development of rice. *Plant Physiol.* **2021**, *185*, 934–950. [CrossRef]
90. Roth, M.; Florez-Rueda, A.M.; Griesser, S.; Paris, M.; Städler, T. Incidence and developmental timing of endosperm failure in post-zygotic isolation between wild tomato lineages. *Ann. Bot.* **2018**, *121*, 107–118. [CrossRef]
91. Raissig, M.T.; Bemer, M.; Baroux, C.; Grossniklaus, U. Genomic imprinting in the *Arabidopsis* embryo is partly regulated by PRC2. *PLoS Genet.* **2013**, *9*, e1003862. [CrossRef]
92. Meng, D.; Zhao, J.; Zhao, C.; Luo, H.; Xie, M.; Liu, R.; Lai, J.; Zhang, X.; Jin, W. Sequential gene activation and gene imprinting during early embryo development in maize. *Plant J.* **2017**, *93*, 445–459. [CrossRef] [PubMed]
93. Pillot, M.; Baroux, C.; Vázquez, M.A.; Autran, D.; Leblanc, O.; Vielle-Calzada, J.-P.; Grossniklaus, U.; Grimanelli, D. Embryo and endosperm inherit distinct chromatin and transcriptional states from the female gametes in Arabidopsis. *Plant Cell* **2010**, *22*, 307–320. [CrossRef] [PubMed]
94. Bay, F.; Settles, A.M. Imprinting in plants as a mechanism to generate seed phenotypic diversity. *Front. Plant Sci.* **2015**, *5*, 780. [CrossRef]
95. Köhler, C.; Lafon-Placette, C. Evolution and function of epigenetic processes in the endosperm. *Front. Plant Sci.* **2015**, *6*, 130. [CrossRef] [PubMed]
96. Hugues, A.; Jacobs, C.S.; Roudier, F. Mitotic inheritance of PRC2-mediated silencing: Mechanistic insights and developmental perspectives. *Front. Plant Sci.* **2020**, *11*, 262. [CrossRef] [PubMed]
97. Colette, L.; Picard, R.; Povilus, A.; Ben, P.W.; Gehring, M. Transcriptional and imprinting complexity in *Arabidopsis* seeds at single-nucleus resolution. *Nat. Plants* **2021**, *7*, 730–738.
98. Xiao, J.; Warner, D. Polycomb repression in the regulation of growth and development in *Arabidopsis*. *Curr. Opin. Plant Biol.* **2015**, *23*, 15–24. [CrossRef]
99. Bouyer, D.; Roudier, F.; Hesse, M.; Andersen, E.D.; Gey, D.; Nowack, M.K.; Goodrich, J.; Renou, J.P.; Grini, P.E.; Colot, V.; et al. Polycomb repressive complex 2 controls the embryo-to-seedling phase transition. *PLoS Genet.* **2011**, *7*, e1002014. [CrossRef]
100. Xiao, J.; Jin, R.; Warner, D. Developmental transitions: Integrating environmental cues with hormonal signaling in the chromatin landscape in plants. *Genome Biol.* **2017**, *18*, 88. [CrossRef]
101. Mu, Y.; Zou, M.; Sun, X.; He, B.; Xu, X.; Liu, Y.; Zhang, L.; Chi, W. BASIC PENTACYSTEINE proteins repress ABSCISIC ACID INSENSITIVE4 expression via direct recruitment of the Polycomb-repressive complex 2 in *Arabidopsis* root development. *Plant Cell Physiol.* **2017**, *58*, 607–621. [CrossRef]
102. Xiao, J.; Jin, R.; Yu, X.; Shen, M.; Wagner, J.D.; Pai, A.; Song, C.; Zhuang, M.; Klasfeld, S.; He, C.; et al. Cis and trans determinants of epigenetic silencing by Polycomb repressive complex 2 in Arabidopsis. *Nat Genet.* **2017**, *49*, 1546–1552. [CrossRef] [PubMed]
103. Liu, X.; Luo, J.; Li, T.; Yang, H.; Wang, P.; Su, L.; Zheng, Y.; Bao, C.; Zhou, C. SDG711 is involved in rice seed development through regulation of starch metabolism gene expression in coordination with other histone modifications. *Rice* **2021**, *14*, 25. [CrossRef] [PubMed]
104. Baile, F.; Merini, W.; Hidalgo, I.; Calonje, M. EAR domain-containing transcription factors trigger PRC2-mediated chromatin marking in Arabidopsis. *Plant Cell* **2021**, *33*, 2701–2715. [CrossRef] [PubMed]
105. Gehring, M. Genomic imprinting: Insights from plants. *Annu. Rev. Genet.* **2013**, *47*, 187–208. [CrossRef]
106. Tonosaki, K.; Kinoshita, T. Possible roles for polycomb repressive complex 2 in cereal endosperm. *Front. Plant Sci.* **2015**, *12*, 144. [CrossRef]
107. Tonosaki, K.; Ono, A.; Kunisada, M.; Nishino, M.; Nagata, H.; Sakamoto, S.; Kijima, S.T.; Furuumi, H.; Nonomura, K.-I.; Sato, Y.; et al. Mutation of the imprinted gene OsEMF2a induces autonomous endosperm development and delayed cellularization in rice. *Plant Cell* **2021**, *85*, 103.
108. Bieluszewski, T.; Xiao, J.; Yang, Y.; Wagner, D. PRC2 activity, recruitment, and silencing: A comparative perspective. *Trends Plant Sci.* **2021**, *26*, 1186–1198. [CrossRef]
109. Grossniklaus, U.; Paro, R. Transcriptional silencing by polycomb-group proteins. *Cold Spring Harb. Perspect. Biol.* **2014**, *6*, a019331. [CrossRef]
110. Povilus, R.A.; DaCosta, J.M.; Grassa, C.; Satyaki, P.R.V. Water lily (*Nymphaea thermarum*) genome reveals variable genomic signatures of ancient vascular cambium losses. *Proc. Natl. Acad. Sci. USA* **2020**, *117*, 8649–8656. [CrossRef]
111. Li, F.; Nishiyama, T.; Waller, M.; Frangedakis, E.; Keller, J.; Li, Z.; Fernandez-Pozo, N.; Barker, M.S.; Bennett, T.; Blázquez, M.A.; et al. Anthoceros genomes illuminate the origin of land plants and the unique biology of hornworts. *Nat. Plants* **2020**, *6*, 259–272. [CrossRef]
112. Carey, S.B.; Jenkins, J.; Lovell, J.T.; Maumus, F.; Sreedasyam, A.; Payton, A.C.; Shu, S.; Tiley, G.P.; Fernandez-Pozo, N.; Barry, K.; et al. The Ceratodon purpureus genome uncovers structurally complex, gene rich sex chromosomes. *bioRxiv* **2020**. [CrossRef]
113. Matilla, A.J.; Nicolás, G.; Vicente, O.; Sierra, J.M. Preformed mRNA in cotyledons of ungerminated seeds of *Cicer arietinum* L. *Plant Phys.* **1980**, *65*, 1128–1132. [CrossRef] [PubMed]
114. Bai, B.; Peviani, A.; van der Horst, S.; Gamm, M.; Snel, B.; Bentsink, L.; Hanson, J. Extensive translational regulation during seed germination revealed by polysomal profiling. *New Phytol.* **2017**, *214*, 233–244. [CrossRef]

115. Nakabayashi, K.; Okamoto, M.; Koshiba, T.; Kamiya, Y.; Nambara, E. Genome-wide profiling of stored mRNA in *Arabidopsis thaliana* seed germination: Epigenetic and genetic regulation of transcription in seed. *Plant J.* **2005**, *41*, 697–709. [CrossRef] [PubMed]
116. Howell, K.A.; Narsai, R.; Carroll, A.; Ivanova, A.; Lohse, M.; Usadel, B.; Millar, A.H.; Whelan, J. Mapping metabolic and transcript temporal switches during germination in rice highlights specific transcription factors and the role of RNA instability in the germination process. *Plant Phys.* **2009**, *149*, 961–980. [CrossRef] [PubMed]
117. Kimura, M.; Nambara, E. Stored and neosynthesized mRNA in *Arabidopsis* seeds: Effects of cycloheximide and controlled deterioration treatment on the resumption of transcription during imbibition. *Plant Mol. Biol.* **2010**, *73*, 119–129. [CrossRef]
118. Sano, N.; Ono, H.; Murata, K.; Yamada, T.; Hirasawa, T.; Kanekatsu, M. Accumulation of long-lived mRNAs associated with germination in embryos during seed development of rice. *J. Exp. Bot.* **2015**, *66*, 4035–4046. [CrossRef]
119. Rajjou, L.; Gallardo, K.; Debeaujon, I.; Vandekerckhove, J.; Job, C.; Job, D. The effect of alpha-amanitin on the *Arabidopsis* seed proteome highlights the distinct roles of stored and neosynthesized mRNAs during germination. *Plant Physiol.* **2004**, *134*, 1598–1613. [CrossRef]
120. Sano, N.; Permana, H.; Kumada, R.; Shinozaki, Y.; Tanabata, T.; Yamada, T.; Hirasawa, T.; Kanekatsu, M. Proteomic analysis of embryonic proteins synthesized from long-lived mRNAs during germination of rice seeds. *Plant Cell Physiol.* **2012**, *53*, 687–698. [CrossRef]
121. Rajjou, L.; Duval, M.; Gallardo, K.; Catusse, J.; Bally, J.; Job, C.; Job, D. Seed germination and vigor. *Ann. Rev. Plant Biol.* **2012**, *63*, 507–533. [CrossRef]
122. Sano, N.; Takebayshi, Y.; To, A.; Mhiri, C.; Rajjou, L.; Nakagami, H.; Kanekatsu, M. Shotgun proteomic analysis highlights the roles of long-lived mRNAs and de novo transcribed mRNAs in rice seeds upon imbibition. *Plant Cell Physiol.* **2019**, *60*, 2584–2596. [CrossRef] [PubMed]
123. El-Maarouf-Bouteau, H.; Meimoun, P.; Job, C.; Job, D.; Bailly, C. Role of protein and mRNA oxidation in seed dormancy and germination. *Front. Plant Sci.* **2013**, *4*, 77. [CrossRef] [PubMed]
124. Fleming, M.B.; Patterson, E.L.; Reeves, P.A.; Richards, C.M.; Gaines, T.A.; Walters, C. Exploring the fate of mRNA in aging seeds: Protection, destruction, or slow decay? *J. Exp. Bot.* **2018**, *69*, 4309–4321. [CrossRef] [PubMed]
125. Zhao, Z.; Wang, S.; Fu, Y.-B.; Wang, H. *Arabidopsis* seed stored mRNAs are degraded constantly over aging time, as revealed by new quantification methods. *Front. Plant Sci.* **2020**, *10*, 1764. [CrossRef] [PubMed]
126. Zhao, Z.; Wang, S.; Fu, Y.-B. Analysis of stored mRNA degradation in acceleratedly aged seeds of wheat and canola in comparison to Arabidopsis. *Plants* **2020**, *9*, 1707. [CrossRef]
127. Kranner, I.; Chen, H.Y.; Pritchard, H.W.; Pearce, S.R.; Birtic, S. Internucleosomal DNA fragmentation and loss of RNA integrity during seed ageing. *Plant Growth Regul.* **2011**, *63*, 63–72. [CrossRef]
128. Fleming, M.B.; Hill, L.M.; Walters, C. The kinetics of ageing in drystored seeds: A comparison of viability loss and RNA degradation in unique legacy seed collections. *Ann. Bot.* **2018**, *123*, 1133–1146. [CrossRef]
129. Sharma, S.N.; Maheshwari, A.; Sharma, C.; Shukla, N. Gene expression patterns regulating the seed metabolism in relation to deterioration/ageing of primed mung bean (*Vigna radiata* L.) seeds. *Plant Physiol. Biochem.* **2018**, *124*, 40–49. [CrossRef]
130. Saighani, K.; Kondo, D.; Sano, N.; Murata, K.; Yamada, T.; Kanekatsu, M. Correlation between seed longevity and RNA integrity in the embryos of rice seeds. *Plant Biotechnol.* **2021**, *38*, 277–283. [CrossRef]
131. Zuo, Z.; Roux, M.E.; Chevalier, J.R.; Dagdas, Y.F.; Yamashino, T.; Højgaard, S.D.; Knight, E.; Østergaard, L.; Petersen, M. mRNA decapping machinery targets LBD3/ASL9 transcripts to authorize developmental reprogramming in Arabidopsis. *bioRxiv* **2020**, 834465. [CrossRef]
132. Xu, J.; Chua, N.H. Processing bodies and plant development. *Curr. Opin. Plant Biol.* **2011**, *14*, 88–93. [CrossRef] [PubMed]
133. Hubstenberger, A.; Courel, M.; Benard, M.; Souquere, S.; Ernoult-Lange, M.; Chouaib, R.; Yi, Z.; Morlot, J.B.; Munier, A.; Fradet, M.; et al. P-body purification reveals the condensation of repressed mRNA regulons. *Mol. Cell* **2017**, *68*, e145. [CrossRef] [PubMed]
134. Jang, G.J.; Jang, J.C.; Wu, S.H. Dynamics and functions of stress granules and processing bodies in plants. *Plants* **2020**, *9*, 1122. [CrossRef] [PubMed]
135. Sheth, U.; Parker, R. Decapping and decay of messenger RNA occur in cytoplasmic processing bodies. *Science* **2003**, *300*, 805–808. [CrossRef]
136. Maldonado-Bonilla, L.D. Composition and function of P bodies in *Arabidopsis thaliana*. *Front. Plant Sci.* **2014**, *5*, 201. [CrossRef]
137. Chantarachot, T.; Bailey-Serres, J. Polysomes, stress granules, and processing bodies: A dynamic triumvirate controlling cytoplasmic mRNA fate and function. *Plant Phys.* **2018**, *176*, 254–269. [CrossRef]
138. Steffens, A.; Jaegle, B.; Tresch, A.; Hülskamp, M.; Jakoby, M. Processing-body movement in *Arabidopsis* depends on an interaction between myosins and DECAPPING PROTEIN1. *Plant Physiol.* **2014**, *164*, 1879–1892. [CrossRef] [PubMed]
139. Xu, J.; Yang, J.Y.; Niu, Q.W.; Chua, N.H. *Arabidopsis* DCP2, DCP1, and VARICOSE form a decapping complex required for postembryonic development. *Plant Cell* **2006**, *18*, 3386–3398. [CrossRef]
140. Roux, M.E.; Rasmunssen, M.W.; Palma, K.; Lolle, S.; Regué, A.M.; Bethke, G.; Glazebrook, J.; Zhang, W.; Sierbuth, L.; Larsen, M.R.; et al. The mRNA decay factor PAT1 functions in a pathway including MAP kinase 4 and immune receptor SUMM2. *EMBO J.* **2015**, *34*, 593–608. [CrossRef]

141. Wawer, I.; Golisz, A.; Sulkowska, A.; Kawa, D.; Kulik, A.; Kufel, J. mRNA decapping and 5′-3′ decay contribute to the regulation of ABA signaling in *Arabidopsis thaliana*. *Front. Plant Sci.* **2018**, *9*, 312. [CrossRef]
142. Tian, S.; Curnutte, H.A.; Trcek, T. RNA Granules: A view from the RNA perspective. *Molecules* **2020**, *25*, 3130. [CrossRef] [PubMed]
143. Perea-Resa, C.; Carrasco-López, C.; Catala, R.; Tureckova, V.; Novak, O.; Zhang, W.P.; Sieburth, L.; Jiménez-Gómez, J.M.; Salinas, J. The LSM1-7 complex differentially regulates Arabidopsis tolerance to abiotic stress conditions by promoting selective mRNA decapping. *Plant Cell* **2016**, *28*, 505–520. [CrossRef] [PubMed]
144. Lee, K.; Kang, H. Emerging roles of RNA-binding proteins in plant growth, development, and stress responses. *Mol. Cells* **2016**, *39*, 179–185. [PubMed]
145. Dedow, L.K.; Bailey-Serres, J. Searching for a match: Structure, function, and application of sequence-specific RNA-binding proteins. *Plant Cell Physiol.* **2019**, *60*, 1927–1938. [CrossRef] [PubMed]
146. Lou, L.; Ding, L.; Wang, T.; Xiang, Y. Emerging roles of RNA-binding proteins in seed development and performance. *Int. J. Mol. Sci.* **2020**, *21*, 6822. [CrossRef]
147. Cho, H.; Cho, H.S.; Hwang, I. Emerging roles of RNA-binding proteins in plant development. *Curr. Opin. Plant Biol.* **2019**, *51*, 51–57. [CrossRef]
148. Masaki, S.; Yamada, T.; Hirasawa, T.; Todaka, D.; Kanekatsu, M. Proteomic analysis of RNA-binding proteins in dry seeds of rice after fractionation by ssDNA affinity column chromatography. *Biotechnol. Lett.* **2008**, *30*, 955–960. [CrossRef]
149. Sano, N.; Masaki, S.; Tanabata, T.; Yamada, T.; Hirasawa, T.; Kashiwagi, M.; Kanekatsu, M. RNA-binding proteins associated with desiccation during seed development in rice. *Biotechnol. Lett.* **2013**, *35*, 1945–1952. [CrossRef]
150. Hentze, M.W.; Castello, A.; Schwarz, T.; Preis, T. A brave new world of RNA-binding proteins. *Nat. Rev. Nat. Cell Biol.* **2018**, *19*, 327–341. [CrossRef]
151. Bach-Pages, M.; Homma, F.; Kourelis, J.; Kaschani, F.; Mohammed, S.; Kaiser, M.; van der Hoorn, R.A.L.; Castello, A.; Preston, G.M. Discovering the RNA-binding proteome of plant leaves with an improved RNA interactome capture method. *Biomolecules* **2020**, *10*, 661. [CrossRef]
152. Sajeev, N.; Baral, A.; America, A.H.P.; Willems, L.A.H.; Merret, R.; Bentsink, L. The mRNA-binding proteome of a critical phase transition during *Arabidopsis* seed germination. *New Phytol.* **2022**, *233*, 251–264. [CrossRef] [PubMed]
153. Bai, B.; van der Horst, S.; Cordewener, J.H.G.; America, T.A.H.P.; Hanson, J.; Bentsink, L. Seed-stored mRNAs that are specifically associated to monosomes are translationally regulated during germination. *Plant Phys.* **2020**, *182*, 378–392. [CrossRef] [PubMed]

plants

MDPI

Article

Photoactivated TiO_2 Nanocomposite Delays the Postharvest Ripening Phenomenon through Ethylene Metabolism and Related Physiological Changes in *Capsicum* Fruit

Arijit Ghosh [1], Indraneel Saha [1], Masayuki Fujita [2,*], Subhas Chandra Debnath [3], Alok Kumar Hazra [4], Malay Kumar Adak [1,*] and Mirza Hasanuzzaman [5,*]

[1] Plant Physiology and Plant Molecular Biology Research Unit, Department of Botany, University of Kalyani, Kalyani, Nadia 741235, West Bengal, India; arijitgo625@gmail.com (A.G.); indraneelsaha92@gmail.com (I.S.)
[2] Laboratory of Plant Stress Responses, Faculty of Agriculture, Kagawa University, Miki-cho, Kita-gun, Kagawa 761-0795, Japan
[3] Department of Chemistry, University of Kalyani, Kalyani, Nadia 741235, West Bengal, India; subhasd81@gmail.com
[4] IRDM Faculty Centre, Ramakrishna Mission Vivekananda Educational, Research Centre (RKMVERI), Ramakrishna Mission Ashrama, Narendrapur, Kolkata 700103, West Bengal, India; alokhazra8@gmail.com
[5] Department of Agronomy, Faculty of Agriculture, Sher-e-Bangla Agricultural University, Dhaka 1207, Bangladesh
* Correspondence: fujita@ag.kagawa-u.ac.jp (M.F.); mkadak09@gmail.com (M.K.A.); mhzsauag@yahoo.com (M.H.)

Citation: Ghosh, A.; Saha, I.; Fujita, M.; Debnath, S.C.; Hazra, A.K.; Adak, M.K.; Hasanuzzaman, M. Photoactivated TiO_2 Nanocomposite Delays the Postharvest Ripening Phenomenon through Ethylene Metabolism and Related Physiological Changes in *Capsicum* Fruit. *Plants* **2022**, *11*, 513. https://doi.org/10.3390/plants11040513

Academic Editors: Milan S. Stankovic, Paula Baptista, Petronia Carillo and Paul K. Boss

Received: 22 December 2021
Accepted: 8 February 2022
Published: 14 February 2022

Abstract: Capsicum is one of the most perishable fruit which undergo rapid loss of commercial value during postharvest storage. In this experiment our aim is to evaluate the effect of photoactivated TiO_2 nano-particle complexed with chitosan or TiO_2-nanocomposite (TiO_2-NC) on extension self-life of *Capsicum* fruit and its effect on related morphological, physiological and molecular attributes at room temperature (25 °C). Initially, TiO_2-NC coated fruits recorded superior maintenance of total soluble solids accumulation along with retention of firmness, cellular integrity, hydration, color etc. On the extended period of storage, fruit recorded a lower bioaccumulation of TiO_2 in comparison to metallic silver over the control. On the level of gene expression for ethylene biosynthetic and signaling the TiO_2-NC had more regulation, however, discretely to moderate the ripening. Thus, ACC synthase and oxidase recorded a significantly better downregulation as studied from fruit pulp under TiO_2-NC than silver. On the signaling path, the transcripts for Ca*ETR1* and Ca*ETR2* were less abundant in fruit under both the treatment when studied against control for 7 d. The reactive oxygen species (ROS) was also correlated to retard the oxidative lysis of polyamine oxidation by diamine and polyamine oxidase activity. The gene expression for hydrolytic activity as non-specific esterase had corroborated the development of essential oil constituents with few of those recorded in significant abundance. Therefore, TiO_2-NC would be reliable to induce those metabolites modulating ripening behavior in favor of delayed ripening. From gas chromatography-mass spectrometry (GC-MS) analysis profile of all tested essential oil constituents suggesting positive impact of TiO_2-NC on shelf-life extension of *Capsicum* fruit. Our results indicated the potentiality of TiO_2-NC in postharvest storage those may connect ethylene signaling and ROS metabolism in suppression of specific ripening attributes.

Keywords: ethylene; elicitors; fruit ripening; ACC synthase/oxidase; GC-MS; polyamines

1. Introduction

Fruit ripening is a unique process in plant biology where differential gene expression leads to a set of cellular and biochemical events, mostly catabolic in nature. Those are regulated throughout the ripening period with some metabolic fluxes under coverage of growth regulators such as auxin, ethylene (ET), gibberellin, abscisic acid and kinetins [1]. Ethylene, the key hormone is responsible for respiratory burst accompanying other cellular

changes hastening the ripening of fleshy fruit. The changes during ripening essentially include hydrolysis of storage polysaccharides, turnover of proteins, conversion of pigments, de-acidification into organic acids, hydrolysis of esters leading to softening of pulp tissues [2]. Regardless of climacteric and non-climacteric types ET evokes several signaling cascades for fruit senescence through gene expression. Mostly those govern catabolic processes of biomolecules which may expedite ripening within postharvest storage [3,4]. Therefore, ET-mediated cellular reactions have principally been in quest for identification of specific gene(s) to alter metabolic functions for enhanced shelf life [5]. Likewise, key biosynthetic genes, viz. ACC synthase and ACC oxidase are targeted by synthetic residues to inhibit their activity to reduce postharvest losses. The metallic silver (Ag) has been a choice for biosynthesis and functional inhibition for ET activities [6]. At the cellular level, ET mediated signaling in ripening fruit are also blocked the ET receptors: *ETR1*, *EIN3*, *CTR1*, etc. In downstream of ET signaling identification of specific transcription factors (*AP2/ERF*) to their corresponding *cis*-elements is another point of approach for delayed senescence/ripening under storage [7]. Ethylene regulated such genes are diverse, still, principally falls under wall hydrolyzing/depolymerization (softening of texture), sugar-acid interconversion (changes in taste), secondary metabolite turnover (for aroma) related genes. In the background of ET sensitivity, the climacteric and non-climacteric types are characteristically differed with the presence or absence of auto-catalytic ET generation [8]. Moreover, the regulation of ET also governs the changes of metabolic flux that correspondingly contribute to the sensory character of ripening. Despite this, in postharvest biology, exogenous application of ET might be aligned to several cellular responses for softening of non-climacteric fruit also [9]. The major focus has been paid on cell wall depolymerization, ET generation and pigment biosynthetic enzymes as responsive genes were identified from non-climacteric fruit such as pepper [10].

The commercial practices to retard the postharvest softening are materialized by regulation of the ripening specific pathways. Ethylene would be the key one in a system to avoid direct exposure to fruit or minimization ET induced ripening phenomenon in the tissues [11]. Many approaches are established to down regulate ripening of the fruit by synthetic inhibitors, action inhibitors of ET such as 1-amino vinyl glycine, Ag^+ ion, respectively, are the most common. The other physical and chemical treatments through oxidation, decomposition and adsorption of gas are not bio-compatible for the corrosive nature of chemicals used [12,13]. The adsorption technologies with activated carbon in various forms as powder/granular, fibers, zeolite, silica gel, electron-deficient based compounds such as dienes and trienes are very time consuming as well as complicated device-based in application [14]. So, any system qualified for ET scavenging if proves non-toxic, less absorbing, biocompatible for fruit quality must be in pursuit for postharvest storage. In the modern state-of-art the exercise of nanocomposite with metallics is important to scavenge ET by complete oxidation [15]. In an application of TiO_2-NP under UV radiation observed a significant removal of gas in in vitro system. This metal oxide produces superoxide and hydroxyl radicals and other reactive oxygen species (ROS) under UV excitation on its nano-surface. The produced ROS is more effective to oxidize ET into CO_2, H_2O, regardless of room/low temperature, high humidity and no other specific environments. It is also noteworthy that TiO_2 within nano ranges varies ROS generation with surface bridging $OH^{\bullet}$. Moreover, there recorded an intrinsic correlation for ROS activation under UV illumination for TiO_2 nanocomposite with oxidation of ET [16]. So, ROS generation and its involvement in the ripening process is expected to be modulated by TiO_2 in nano forms.

Many investigations have been carried out on effect of bulk TiO_2 as well as TiO_2-NC on postharvest shelf life of fruit such as mango, tomato, cucumber etc. [17,18]. On the other hand, chitosan/TiO_2-NP composite also can effectively protect grapes from fruit rotting micro-organism [19]. Although TiO_2-NC have been used studies in various fruit and vegetable, there is almost no data regarding its effect on quality of *Capsicum* fruit during postharvest storage.

In this paper, we focused on effects of TiO_2-NC coating on quality indices, physiochemical properties and molecular characteristics of *Capsicum* fruit during postharvest storage at 25 °C for 7 d. In this investigation, we have evaluated the effectivity of TiO_2-NC for ROS generation, polyamine metabolism, wall loosening enzyme, volatile substances and gene expression for ET metabolism on delayed ripening during postharvest storage.

2. Materials and Methods

2.1. Plant Material and Treatments

Chilli or *Capsicum* fruits of Tejaswani cultivar were brought in mature green stage from a local agricultural farm, then checked for any deformity, infection, damage and disinfected with 1% sodium hypochlorite solution followed by a repeated wash with deionized water. Treatment sets for the fruits are as follows: control (treated with distilled water), treated with 2 mg mL^{-1} silver solution (silver), coated with 1% chitosan solution containing 10 g L^{-1} TiO_2-nanoparticle or TiO_2 nanocomposite (TiO_2-NC). Samples were kept inside separate quartz bottles equipped with airtight cap containing rubber septa with 3 replicates per treatment and 30 fruits in each replicate. All the beakers are kept under UV-A (365 nm) led light for 7 d at 25 °C. Sampling was carried out after 7 d taking at least three replicates per treatment and stored in −80 °C for further analysis. All results are expressed on fresh weight (FW) basis.

2.2. Study of Fruit Surface Morphology through Scanning Electron Microscopy (SEM)

Fresh samples from each treatment were cut into manageable pieces followed by dehydration through critical point drying method with K850 (Quarum Technologies, Switzerland). After drying samples were placed on metallic stubs and coated with 30 nm thick gold with plasma sputter coater (MNT-JS1600, MNT, Canada). Finally, surface morphology of the coated samples was analyzed through SEM (GeminiSEM 450, Zeiss, Oberkochen, Germany) according to [20].

2.3. Quality Parameters

2.3.1. Firmness of Fruit Coat

The firmness of fruit coat was measured by handheld penetrometer (GY-1, Wenzhou Tripod Instrument Manufacturing Ltd., China) with 8 mm wide stainless-steel plunger and measurements were carried out at 3 different points on fruit surface opposite to each other and the average value was expressed in N.

2.3.2. Color of Fruit Coat

Fruit from each treatment 3 replicates were taken and the color of each fruit at 3 different points was measured by chroma meter (CR-400, Konica Minolta, Osaka, Japan). The color was reported as hue angle (°).

2.3.3. Percentage of Water Loss

This was measured in gravimetric method comparing total water content (difference of weight of the fruit before and after drying in hot air oven at 50 °C for 48 h) and the difference in weight of fruit at initial day and after 7 d of treatment taking 3 replicates from each treatment according to Scalisi and O'Connell [21].

2.3.4. Total Soluble Solid Content

Five g of fruit from each replicate was taken, and fruit juice was extracted from pericarp region by pressing. The total soluble solid content was measured using refractometer (RHB-32ATC MCP, Japan) by putting a few drops of fruit juice on the detection surface.

2.3.5. Quantification of Ti in Fruit

One g of fruit pericarp was digested with 10 mL tri acid mixture (H_2SO_4:HNO_3:$HClO_4$ = 3:3:1) and cooled. After cooling the concentrated acid mixture was diluted in 90 mL of ddH_2O

and Ti content was measured with ICP-MS (Agilent 7800, Agilent Technologies Inc., Santa Clara, CA, USA) against known standard according to Ghosh et al. [6].

2.4. Ethylene Measurement

One mL of gas sample from each replicate were drawn using as GC syringe from the head space of each vail containing rubber septum and the ET was quantified with a flame ionization detector gas chromatograph (GC-8A, Shimadzu, Japan) equipped with an active aluminum column T.R. Ethylene content was expressed in nM kg^{-1} s^{-1}.

2.5. Preparation of RNA

One g of fresh pericarp tissue of fruit was frozen with liquid nitrogen and frozen tissue was crushed to powder with mortar and pastel. RNA was isolated from about 50 mg frozen powdered tissue using trizol (Trizin, GCC Biotech, West Bengal, India) RNA extraction method according to the manufacturer's protocol. For removal genomic DNA isolated RNA was digested with DNase I (Qiagen) according to manufacturer's instructions. Quantification of RNA was carried out by nano-drop spectrophotometer (Thermo Fisher Scientific, Wilmington, NC, USA) and integrity RNA samples were analyzed by electrophoresis in 1.5% agarose gel.

2.6. Semi-Quantitative PCR

For semi-quantitative PCR analysis, total RNA samples were reverse transcribed into cDNA using cDNA synthesis kit (GCC Biotech, India) following the manufacturer's protocol in triplicate. cDNA samples are amplified by step one PCR system using PCR master mix (GCC Biotech, India) with specific primers. Gene-specific primer for *ACCS*, *ACCO*, *ETR1*, *ETR2* and *GAPDH* used according to [22] where *GPDH* gene used as control. The temperature for the PCR reaction was: initial denaturation 95 °C for 5 min, 35 × (denaturation at 95 °C 30 s, annealing at 55 °C for 30 s and extension at 72 °C for 30 s), final extension at 72 °C for 5 min. 2 uL of PCR product from each sample was run in 2% agarose gel and photographed for using Gel Doc system. Densitometry scanning was carried out using GelAnalyzer 19.1 (www.gelanalyzer.com, accessed on 11 December 2022) software.

2.7. Quantification of ROS

2.7.1. Quantification of H_2O_2

One g of the sample from each treatment were crushed 0.01 M phosphate buffer (pH 7.0). After that the homogenate is centrifuged at 12,000× *g* for 15 min and obtained supernatant was mixed with chromate reagent [19]. The mixture was then kept inside a boiling water bath until the development of greenish color and quantification of H_2O_2 was carried out spectrophotometrically at 570 nm according to Ghosh et al. [23]. The result was expressed as μmol g^{-1} FW.

2.7.2. $O_2^{\bullet -}$ Content

For detection of $O_2^{\bullet -}$ fresh samples were thoroughly crushed in a 65 mM phosphate buffer pH 6.5. The homogenate was centrifuged at 12,000× *g* for 15 min at 4 °C and obtained supernatant was mixed with 65 mM phosphate buffer pH 7.8. The diluted supernatant was then mixed with 10 mM hydroxylamine hydrochloride and incubated 30 min at 25 °C. After that 7 mM alfa-napthylamine and 10 mM sulfanilamide were added and kept at 37 °C for 20 min. From mixture $O_2^{\bullet -}$ was quantified according to Ghosh et al. [23].

2.8. Quantification of Total Capsaicin Content

In this case, 500 mg of dried fruits from each replicate crushed into fine powder and extracted with 10 mL of acetone for 5 h. Then all samples centrifuged at 10,000× *g* and supernatant collected. 4 mL of supernatant for each sample were taken into separate test tube and the capsaicin content was determined at 660 nm according to Sadasivam and Manickam [24]. Capsaicin content is expressed in μg capsaicin g^{-1} dry weight (μg g^{-1} DW).

2.9. Quantification of Polyamine and TLC Separation

500 mg of fruit tissue was crushed in 10% perchloric acid and homogenates were reacted with dansylchloride and run through silica TLC plate and quantified according to Wettlaufer and Weinstein [25].

2.10. Enzyme Activity Assay

2.10.1. Esterase (EC 3.1.1.1) Activity

One g of fruit pericarp tissues was frozen in liquid N_2 and ground into fine powder. From the powdered tissue, esterase activity was measured according to Kumar et al. [26].

2.10.2. Polyamine Oxidase Activity and Diamine Oxidase Activity

Fruit samples were frozen with liquid N_2 and crushed into powder for enzyme extraction. The enzyme extraction and activity were determined for polyamine oxidase activity (PAO; EC 1.5.3.11) and diamine oxidase activity (DAO; 1.4.3.22) according to Moschou (2018), respectively.

2.11. Extraction of Essential Oil

Fifty grams of fruit from each treatment including control were chopped into manageable pieces and gone through hydro distillation by clevenger type apparatus [27]. Then essential oil was extracted by dichloromethane (DCM) and condensed with a rotatory evaporator. Before GC MS analysis DCM fraction of essential oil was dehydrated over anhydrous sodium sulphate.

2.12. GC-MS Analysis of Essential Oil

GC-MS analysis was carried out using Agilent 7000 (Agilent Technologies Inc., Cheadle, UK) and compounds were separated using Agilent 122-5532 DB–5MS column. Helium was used as a carrier gas with a flow rate of 1 mL min^{-1} and injection volume was 2 µL and slit injection was used with ratio of 10:1. The inlet temperature was 250 °C and the ion source temperature 230 °C. Total run time was 60 min and the range of mass scanned was 50 to 550 amu GC-MS data were analyzed with Chem-Station (Agilent Technologies Inc., Cheadle, UK) following identification of compounds from retention index and custom mass spectra with NIST, 2014 library. Retention indices were calculated using n-alkane series C7 to C40 under sample operating parameter. Experiment was carried out with two replicates.

2.13. Characterization of TiO_2-NP

The morphology, size and atomic composition of TiO_2-NP was determined by SEM (GeminiSEM 450, Zeiss, Oberkochen, Germany) equipped with Energy Dispersive X-ray (EDX) module according to Femi-Adepoju et al. [28]. Determination of functional group was carried out Fourier transform infrared spectroscopy (FTIR, Agilent Cary 630, Agilent Technologies India Pvt Ltd, Delhi, India) analysis with spectral scan od 450–4000 cm^{-1} at a resolution of 4 cm^{-1} [29].

2.14. Statistical Analysis

All the acquired data were analyzed by Student's *t*-test (SPSS, IBM, Armonk, New York, NY, USA) for analysis of the difference between treatments. The statistically significant differences were considered at $p \leq 0.05$. The obtained data were presented at mean ± standard error (SE). The correlation figure was created through software.

3. Results

3.1. Firmness, Color, Turgidity and Total Soluble Solids of Fruit on TiO_2-NC Treatment

Developmental changes in fruit 7 d of ripening period under storage recorded significant morphological variations (Figure 1). The changes in color, texture, fruit coat firmness was notably affected with treatments such as silver or TiO_2-NC (Figure 2). The surface morphology as critically analyzed by SEM studies for fruit coat which recorded a distinct

variation through the treatments (Figure 1). Interestingly, the surface was significantly affected with 7 d on postharvest storage indicating the changes through ripening activities including loss of water. This pledges a possible relationship with other qualitative characters for ripening on fruit. This exclusively shows distinct crack and crevices on the cell wall that might ooze out cell sap and odor as a mark of ripening, however, in general. This feature was almost erased when fruit were observed from either silver or TiO_2-NC, still maximum for the latter. Remarkably, the changes on cell surface nearly exist in parallel with variations in fruit color through the days of storage. Therefore, a possibility may arise on recovery of any cellular lysis of fruit coat being quite usual as usual for ripening under the aid of TiO_2-NC.

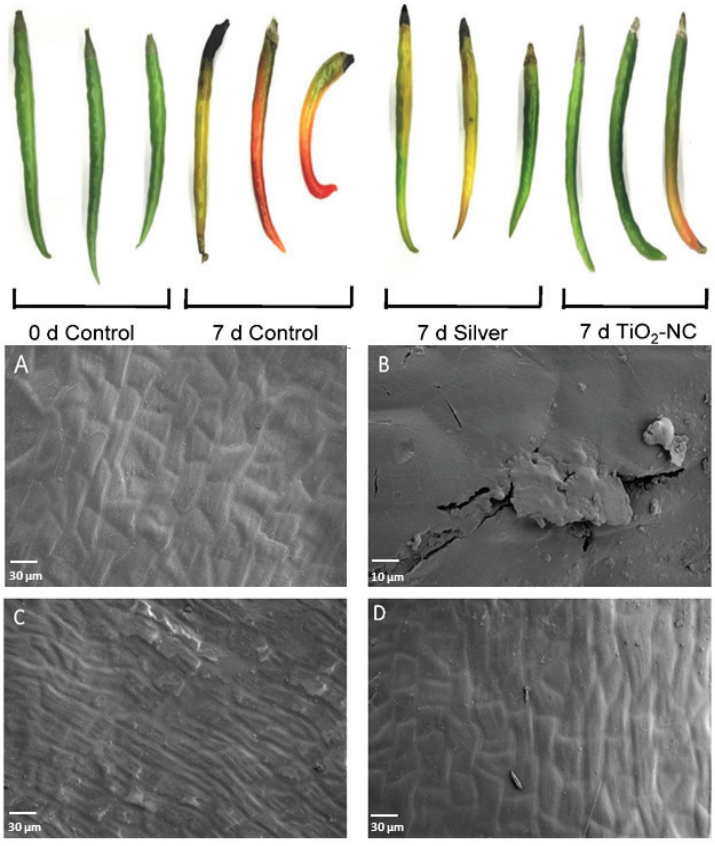

Figure 1. Changes in morphology and changes in fruit coat surface as revealed through scanning electron micrograph (SEM) in *Capsicum* fruit. The SEM images revealed the microscopic cracks and crevices on fruit coat surfaces and their variations on 7 d (**B**) postharvest storage over 0 d control (**A**). The 7d silver (**C**) and 7d TiO_2-NC treatments (**D**) had their respective impacts on the possible repair of cell wall lysis.

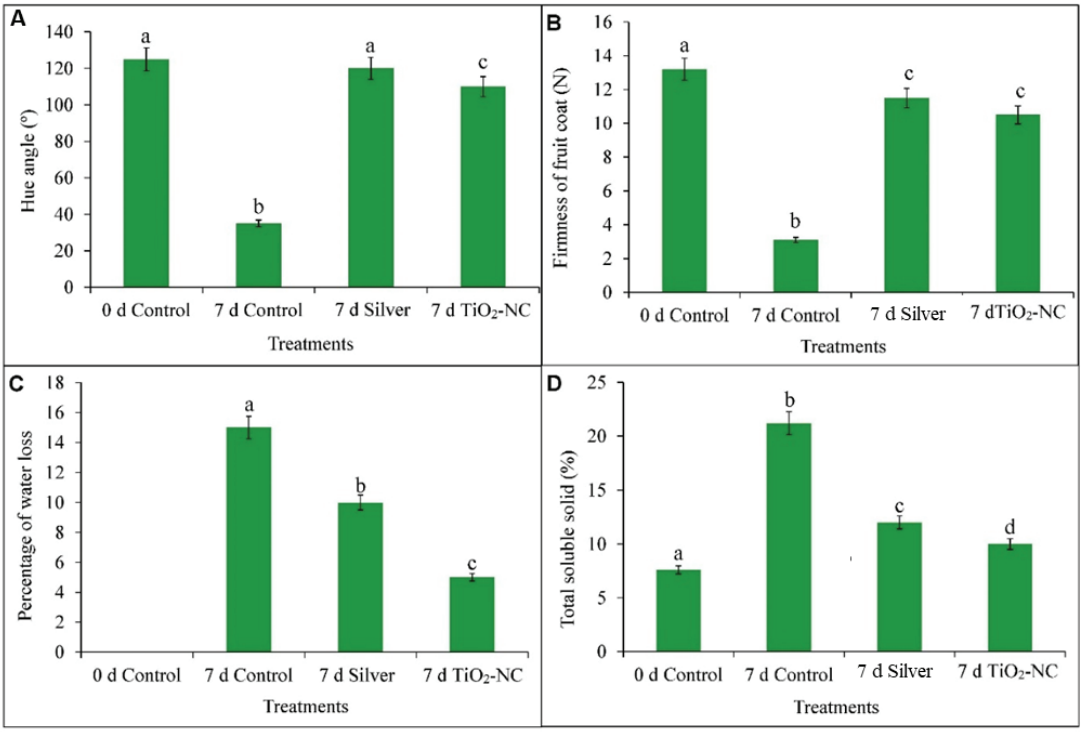

Figure 2. Hue angle (**A**), fruit firmness (**B**), percentage of water loss (**C**) and total soluble solid (**D**) of *Capsicum* fruit recorded under silver and TiO_2-NC with respect to control during 0 d and 7 d of postharvest storage at 25 °C. Vertical bars showing SE± 1 ($n = 3$) on each column and letters above bars indicate statistical variations between treatments based on One Way ANOVA ($p \leq 0.05$).

The changes in fruit color as measured by hue angle had significant variation under both treatments (Silver and TiO_2-NC) compared to control at 7 d of storage. Both silver and TiO_2-NC maintained the color with only 4 and 12% decrease in hue angle compared to 72% in 7 d control over control at 0 d (Figure 2A). The firmness of fruit in the pressure unit (N) reveals the integrity of *Capsicum* fruit coat when observed under different treatments. A significant ($p \leq 0.05$) reduction by 76% was recorded from fruit on 7th d of storage as compared to the initial day (Figure 2B). Interestingly, silver and TiO_2-NC maintained firmness with only 13 and 20% reduction with respect to control at 0 d. The individual interaction of silver and TiO_2-NC showed no significant ($p \leq 0.05$) variations infirmness of fruit at 7 d.

With the duration of storage time fruit also observed gradual dehydration or loss of seeming freshness. This was documented with the percentage of water loss by gravimetric method and maximum loss of water was recorded in 7 d control by 15% compared to 0 d control (Figure 2C). Whereas, both silver and TiO_2-NC had proportionately reduced water loss by 50 and 100%, respectively, over control at 7 d. On the other hand, fruit accumulated soluble solid that varied significantly through the treatments. (Figure 2D). The maximum amount of TSS was recorded in 7 d control which accounts 76% increase over 7 d silver. The treatment such as silver and TiO_2-NC significantly ($p \leq 0.05$) reduced TSS accumulation in respective to 7 d control. Still, TiO_2-NC had reduced the content by 47% over control (7 d) and thus suggested more effectiveness in delayed ripening with a negative correlation value ($r = -0.97$) with the firmness of the fruit coat.

3.2. Absorption of Ti and Release of Ethylene from Fruit Tissues

The biosorption of the Ti within the fruit tissues was interesting when observed after 7 d of TiO_2-NC treatment compared to control (untreated). In one of those groups treated (TiO_2-NC) fruit, metal content was directly measured (Ti) without any washing and these samples recorded 4.17 mg kg^{-1} DW which was only 0.14 mg kg^{-1} DW in untreated control (Figure 3). In another group, samples were thoroughly washed, dried and measured the metal content show a significantly ($p \leq 0.05$) lower values, an almost negligible increase of 0.22 mg kg^{-1} DW over control. Thus, as on a comparative basis, it accounted for 91% reduction of Ti over TiO_2-NC before washing. This implies a significant low absorbing trend of Ti within the fruit tissues when applied with chitosan amalgamation as TiO_2-NC. Therefore, the application of TiO_2-NC may involve the phenomenon of biosorption of metal rather than bioaccumulation which may have entered into the fruit tissue through opening present is pedicel region of fruit. This may recommend TiO_2-NC would be a safe residue to be applied as a postharvest preservative for its non-invasive nature.

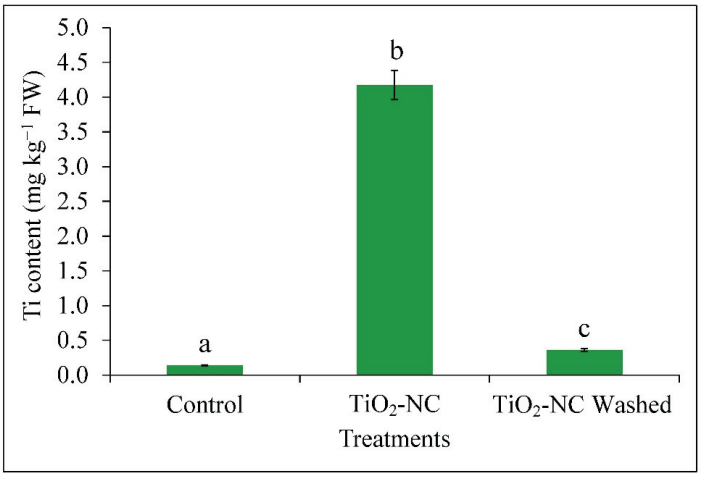

Figure 3. Absorption of Ti in *Capsicum* fruit recorded from 7 d TiO_2-NC treatment and 7 d TiO_2-NC washed with respect to control on 7 d storage under 25 °C. Vertical bars showing SE ± 1 (n = 3) on each column and letters above bars indicate statistical variations between treatments based on one way ANOVA ($p \leq 0.05$).

Endogenous ET in the fruit tissues was recorded in varying concentrations from different treatments. Thus, control fruit at 7 d recorded significant upregulation of ET generation against 0 d control and measured 5.4 nmol kg^{-1} s^{-1} compared to 0 d control 2.1 nmol kg^{-1} s^{-1} (Figure 4). The treatments such as silver or TiO_2-NC had significant variations in ET content as expected over the control. So, the release of endogenous ET was maximized under silver treatment with 83% increase from 7 d TiO_2-NC but not with significant variation against 7 d control (Figure 4). On the contrary, the ET content was downregulated by 36% under the same condition when fruit were treated with TiO_2-NC (Figure 4). The changes in ET concentration were significantly impacted on quality characters TSS (r = 0.75), firmness (r = −0.62), hue angle (r = −0.54) with as evident from the correlation matrix (Supplementary Materials Table S1).

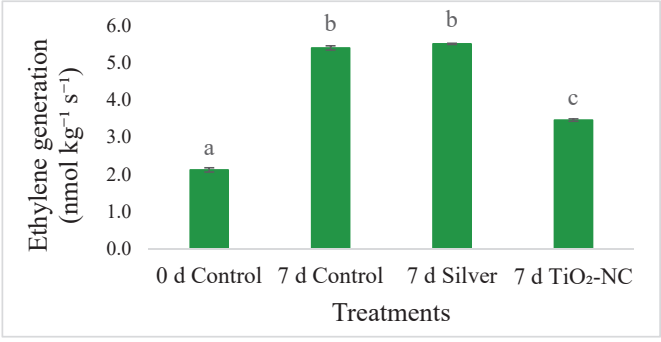

Figure 4. Changes in ET evolution of *Capsicum* fruit under silver and TiO_2-NC with respect to control during 0 d and 7 d of postharvest storage at 25 °C. Vertical bars showing SE ± 1 (n = 3) on each column and letters above bars indicate statistical variations between treatments based on one way ANOVA ($p \leq 0.05$).

3.3. Expression of Genes for Ethylene Biosynthesis and Signaling

Expression levels of the targeted homologs for transcripts for ET biosynthesis and signaling genes, viz., Ca*ACC synthase*, Ca*ACC oxidase* and Ca*ETR1* and Ca*ETR2* were checked. Through the semi-quantitative RT-PCR technique, the transcripts were evaluated against Ca*GAPDH* (as internal control) and those revealed about downregulation for *ACC synthase* under TiO_2-NC against 0 d control. During storage of 7 d, the expression changed under the same treatment which was significantly ($p \leq 0.05$) higher than silver (Figure 5). Meanwhile, silver had changed the expression of a gene compared to respective 0 and 7 d control. For conversion of ACC to ET the gene involved as Ca*ACC oxidase* had inclined a similar pattern of expression. However, for both the treatments such as silver and TiO_2-NC expression was more pronounced by distinct suppression respective genes (Figure 5). Contrarily, signaling pathways of ET governed by different genes: Ca*ETR1* and Ca*ETR2* had distinct variations in expression under treatment concerned. Interestingly, for *ETR1* expression was quite abundant by transcript densities of 7 d control less than TiO_2-NC under same duration (Figure 5). Thereafter, the variations were more pronounced by 25% downregulation under silver and upregulation under TiO_2-NC over the 0 d control. For other genes such as Ca*ETR2*, the relative expression recorded a steady fall from ongoing days of storage under 7 d control (Figure 5). Interestingly, TiO_2-NC had retrieved the expression of *CaETR2* as compared to silver. Still, silver was not able to upregulate *ETR2* as TiO_2-NC rather subdued the expression on completion of storage i.e., after 7 d.

3.4. Accumulation of ROS (H_2O_2 and $O_2^{\bullet-}$) in Fruit Tissues under Storage

H_2O_2 and $O_2^{\bullet-}$ followed almost a similar pattern in control and treatments up to the completion of the storage period. In the case of H_2O_2, the maximum accumulation occurred (17% over 7 d control) in fruit tissue when observed from silver treatment. Conversely, TiO_2-NC reduced the content on 7 d storage which recorded 63% less than 7 d control (Figure 6A). TiO_2-NC had suppressed $O_2^{\bullet-}$ accumulation by 69% over the silver under the same condition (Figure 6B). Fruit proceeding through storage period recorded 0.67 μmol g^{-1} increase in $O_2^{\bullet-}$ content, however, under control condition. Furthermore, treatments such as silver had the impact on ripening to accumulate $O_2^{\bullet-}$ by 0.87 μmol g^{-1} over 0 d control. On the contrary, TiO_2-NC rather reduced the ROS ($O_2^{\bullet-}$) significantly ($p \leq 0.05$) by 53% in contrast with silver as compared to 7 d control.

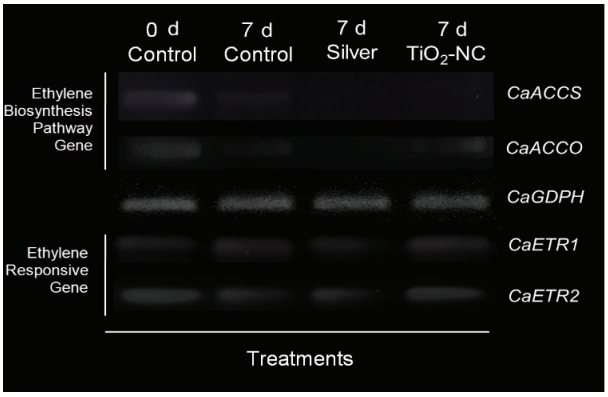

Figure 5. Expression of *CaACCS*, *CaACCO*, *CaETR1*, *CaETR2* genes as compared to *CaGAPDH* as control gene in *Capsicum* fruit under silver and TiO_2-NC with respect to control during 0 d and 7 d of postharvest storage at 25 °C.

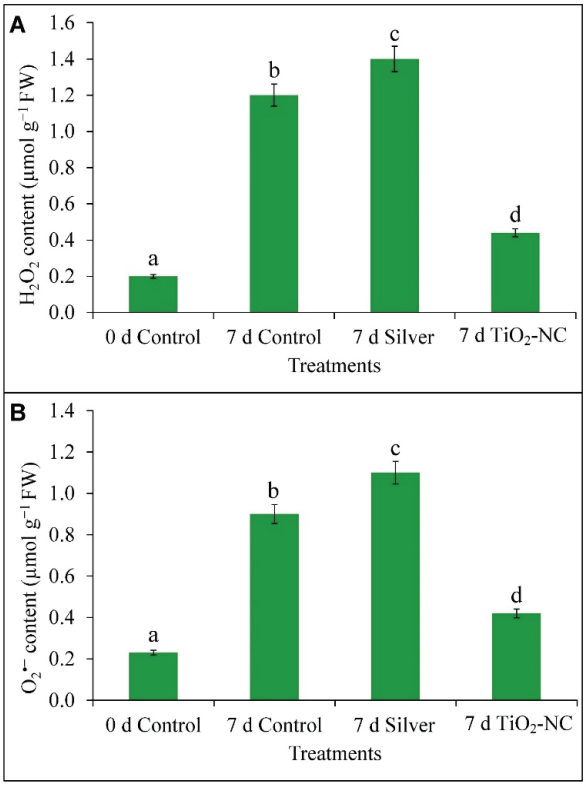

Figure 6. H_2O_2 content (**A**) and $O_2^{\bullet-}$ content (**B**) of *Capsicum* fruit recorded under silver and TiO_2-NC with respect to control during 0 d and 7 d of postharvest storage at 25 °C. Vertical bars showing SE ± 1 (n = 3) on each column and letters (a, b, c and d) above bars indicate statistical variations between treatments based on one way ANOVA ($p \leq 0.05$).

3.5. Catabolism of Polyamine during Ripening on Storage

Ripening of fruit with many physiological effects by ET intervention are antagonized by polyamines. As Figure 7 shows the total polyamine content gradually decreased during the ongoing storage period. This decrease was maximum at TiO_2-NC which shows 27% decrease with respect to 0 d control at 7 d. Increased polyamine often supports fruit firmness, redox maintenance, sugar metabolism those all for the prevention of ripening. Therefore, turnover of polyamines is likely to be hastening the fruit senescence, specifically through ROS generation under storage conditions.

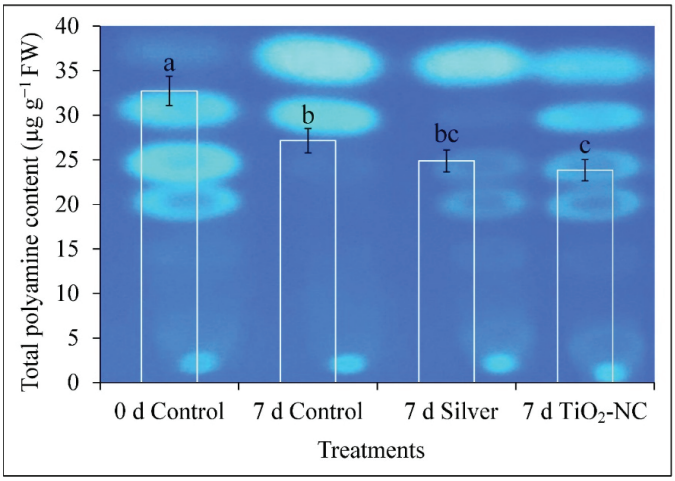

Figure 7. Separation and identification of total polyamine from *Capsicum* fruit on TLC plate and resolved under UV illumination under silver and TiO_2-NC with respect to control during 0 d and 7 d of postharvest storage at 25 °C. Vertical bars showing SE ± 1 (n = 3) on each column and letters above bars indicate statistical variations between treatments based on one way ANOVA ($p \leq 0.05$).

On this notion, we checked the catabolism of polyamines by enzymatic lysis with polyamine oxidase activities. This is more to predict the correlation ($p \leq 0.05$, $r = -0.99$) of ROS (H_2O_2) generated by polyamine oxidation and its contribution to the peroxidation of fruit. Thus, the activity of DAO enzyme had the downregulation through 7 d storage, however, under control by 11% over the initial (Figure 8B). Treatment such as silver or TiO_2-NC had their respective effects on DAO activity. Thus, under silver treatment, the subdued activity recorded 11% less over control whereas, it was upregulated by 33% for TiO_2-NC (Figure 8B). An almost similar or compatible trend was noticed for PAO also where fruit attained a peak activity at 0 d control. Two treatments such as silver and TiO_2-NC were more capable to minimize the activities of the enzymes where 64 and 14% fall in values over the 0 d control were recorded during storage (Figure 8A). Although PAO activity is higher in TiO_2-NC with respect to other treatments at 7 d, lower polyamine content in fruit tissue may have minimized its impact on fruit ripening.

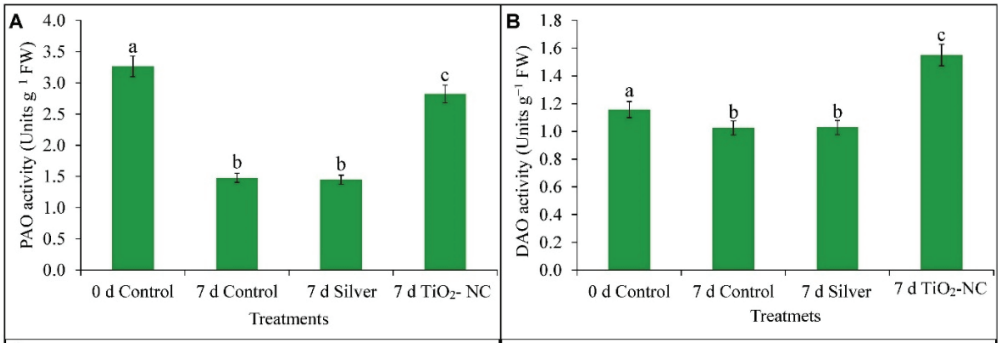

Figure 8. Activity of PAO (**A**), DAO (**B**) from pulp tissues of *Capsicum* on tissues under silver and TiO_2-NC treatments with respect to control (0 d) and 7 d storage of postharvest at 25 °C. Vertical bars showing SE ± 1 (n = 3) on each column and letters (a, b, c and d) above bars indicate statistical variations between treatments based on one way ANOVA ($p \leq 0.05$).

3.6. Esterase Activity and Its Polymorphic Expression on Fruit Softness

Changes in the functioning of various cell-wall bound or cytosolic hydrolases including esterases are important in fruit softening. Ongoing days of postharvest storage *Capsicum* fruit recorded a distinct variation of esterase activity in 7 d silver and 7 d TiO_2-NC treated fruits with respect to 7 d control. From the initial (0 d) period of ripening fruit showed a sharp rise of esterase activity by 10 units reaching at 7 d, however, at control. Still, on the activity of silver and TiO_2-NC the activity of esterase reduced by 56 and 96% over control (Figure 9). Interestingly, the activity of esterase under those treatments had an impact on fruit firmness with a significant ($p \leq 0.05$) effect as reading correlation matrix. The influence of TiO_2-NC for its altered activity had also been accompanied by polymorphic expression of esterase at the gene level. Thus, esterase profile may set as a possible biomarker as *Capsicum* fruit attained the delayed ripening under silver or TiO_2-NC.

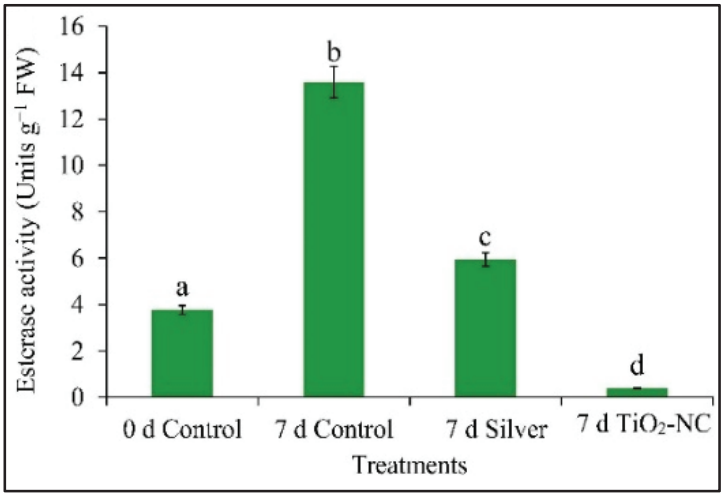

Figure 9. Activity of esterase from pulp tissues of *Capsicum* on tissues under silver and TiO_2-NC treatments with respect to control (0 d) and 7 d storage of postharvest at 25 °C. Vertical bars showing SE ± 1 (n = 3) on each column and letters above bars indicate statistical variations between treatments based on one way ANOVA ($p \leq 0.05$).

3.7. Changes in Essential Oil Contributing Major Metabolites in Ripening

The major metabolites were separated, resolved their identification and relative concentration were determined with GC-MS studies. From overall 52 identified metabolites, it was only 13 had significant up/downregulation in the content through the storage period which includes alkane, ester, fatty acid and alcohol etc. (Table 1). It is quite clear from the Figure 10 constituents of essential oil follow a pattern which indicated ongoing ripening process. On specific constituent of essential oil such as C1 (Cuben-11-ol), C2 (Spiroether) and C6 (1,3-dihydroxypropane-2-ylhexadecanoate) it exhibited sharp decrease concentration by 30, 12 and 0.4% at 7 d storage, whereas, it is only 16, 6 and 0.13%, respectively, under influence of TiO_2-NC over the 0 d control (Figure 10). Contrarily, alkanes such as C9 (Heptacosane), C11(Triacontane), C12 (Hentriacontane) recorded significant increase at 7 d control by 10, 7 and 3.21%, respectively over 0 d control. On the other hand, TiO_2-NC treatment recoded just 44 and 21% increase C9, C11, respectively, and C12 decrease by 0.09% compared to control (Table 1).

3.8. Capsaicin Content

Capsaicin content was quantified spectrophotometrically which is main contributing factor for pungency. It has been observed that capsaicin content increase as the fruit ripening during storage (Figure 11). Likewise, capsaicin content increased by 1312 μg kg^{-1} at 7 d control with over 0 d control. On the other hand, capsaicin content of 7 d silver and 7 d TiO_2-NC increase by 15 and 59% over control at initial day. Changes in the capsaicin content showed positive correlation with ET content and negative strong correlation with hue angle and firmness of fruit.

Table 1. Major composition of essential oil in *C. annuum* fruit under various treatments.

No.	Name of Compound	Calculated KI	Reported KI	Concentration (%)		
				0 d Control	7 d Control	TiO_2-NC
C1	Cuben-11-ol	1595	1595	34.02	4.12	17.66
C2	Spiroether	1880	1879	14.22	1.78	7.94
C3	1,3-dihydroxypropan-2-ylhexadecanoate	2289	2289	3.15	2.79	3.02
C4	Methyl labdanolate	2382	2381	2.83	9.36	9.11
C5	Tetracosane	2388	2400	4.67	5.39	5.40
C6	Pentacosane	2488	2500	4.74	8.32	4.88
C7	Hexacosane	2588	2600	4.36	11.30	5.50
C8	Nonacosanoicacid	2673	2674	3.95	3.08	5.65
C9	Heptacosane	2745	2700	3.41	13.79	4.90
C10	Pentatriacontane-2-one	2873	2873	2.85	0.40	4.31
C11	Triacontane	2985	3000	2.50	9.31	3.10
C12	Hentriacontane	3084	3100	2.55	6.26	2.46
C13	Dotriacontane	3183	3200	1.84	4.02	2.02
Total percentage				85.10	79.93	75.94

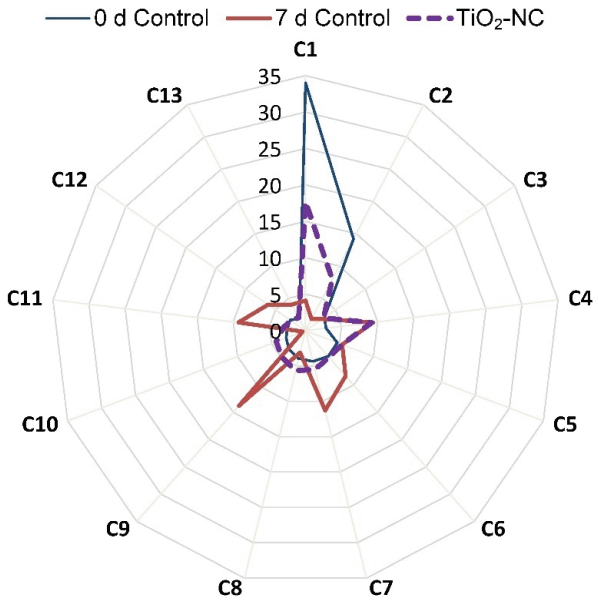

Figure 10. Radar plot showing the pattern of changes in concentration of major constituents of essential oil under TiO_2-NC treatments with respect to control at 0 d and 7 d storage of postharvest at 25 °C.

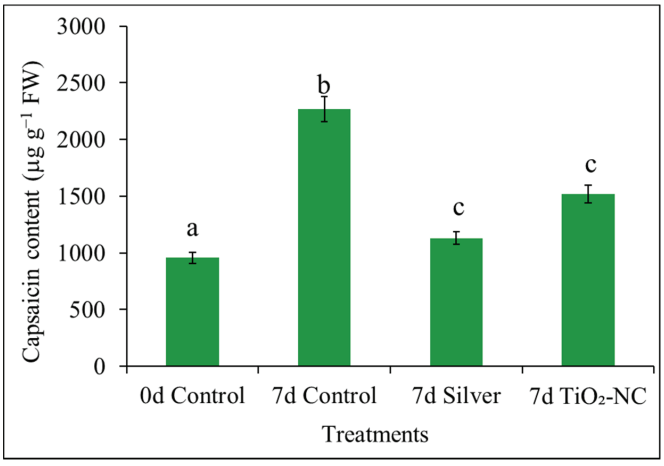

Figure 11. Capsaicin content of *Capsicum* fruit recorded under silver and TiO_2-NC with respect to control during 0 d and 7 d of postharvest storage at 25 °C. Vertical bars showing SE ± 1 (n = 3) on each column and letters above bars indicate statistical variations between treatments based on one way ANOVA ($p \leq 0.05$).

3.9. TiO_2-NP and Its Opto-Physico-Chemical Characterizations

As described earlier molecular nature of TiO_2-NP was confirmed by different physico-optical properties. This assumed the uniform sizes of particles as bearing conformity with earlier description [29]. Preliminarily, FE-SEM study was carried out for the shape and size of nanomaterial. This revealed diameter of NP ranges between 15–30 nm which was within the limit of ≤100 nm size as resolved in SEM image and appeared spherical to the

globular unit (Figure 12A). From the SEM EDAX the presence of Ti in the NP has been verified which is represented as green dots in Figure 12B and it also shows a sharp pick of Ti in Figure 12C which confirms the presence of Ti in NP. The FTIR spectroscopy finally revealed the associated bond energy changes (cm^{-1}) from projected varying functional groups of TiO_2-NP (Figure 12D) [30]. Largest pick was observed at 726.96 cm^{-1} along with another small pick at 482 cm^{-1} which confirms presence of characteristic O-Ti-O bond in TiO_2-NP. Other picks at 3402.82 cm^{-1} and 1624.96 cm^{-1} indicated surface absorbed water and hydroxyl bonds, respectively (Figure 12D).

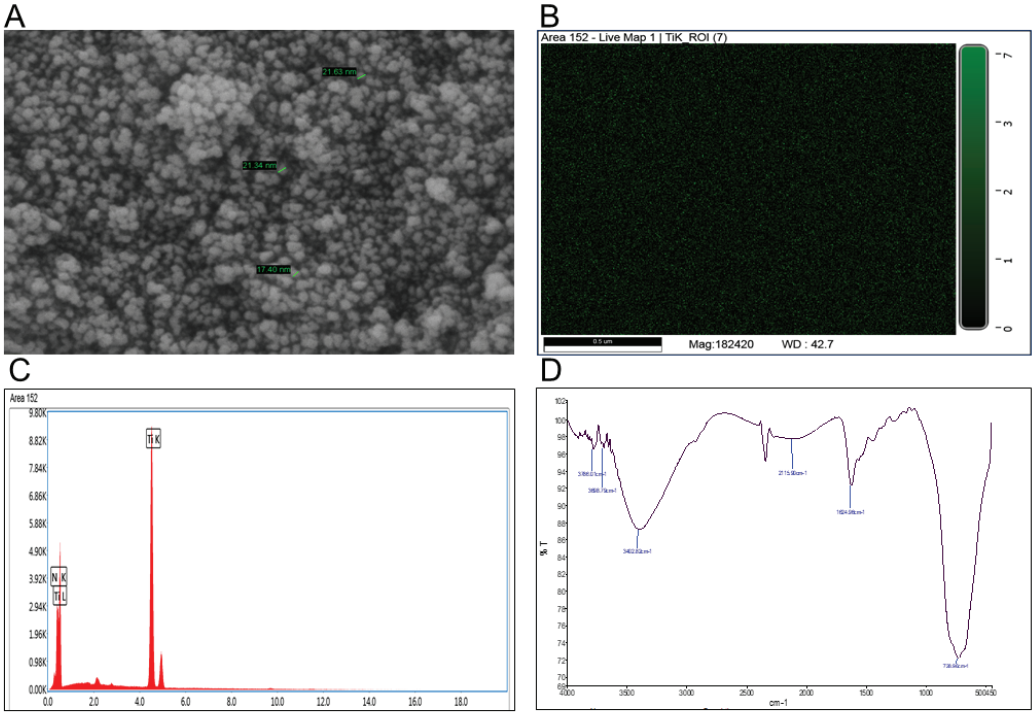

Figure 12. SEM image showing size dstribution of TiO_2-NPs (**A**), EDAX map TiO_2-NPs to confirmtion the presence of Ti (**B**), quantification of Ti by EDAX in the TiO_2-NP (**C**) and FTIR showing distribution of different bonds present in TiO_2-NPs (**D**).

3.10. Correlation among the Parameters

From the Pearson's correlation matrix, it comes in a note that physiological and cellular attributes in ripening are quite variable in contribution and more in a complex manner. Ripening of *Capsicum* fruit involves oxidative reactions, so ROS metabolism influencing ripening specific traits found significant, however, variably regulated under different treatment. Thus, initially changes in ROS (H_2O_2 and $O_2^{\bullet -}$) related positively with ripening parameters such as TSS but negatively with firmness. Similarly, total polyamine content had a significant ($p \leq 0.05$) negative correlation with ROS (Figure 13). The ROS-producing activity polyamine oxidation had a variable influence on ripening. Thus, DAO and PAO had an indirect contribution with ROS by the generation of H_2O_2 but not with others. On the other hand, ET accumulation with *ACC synthase* and oxidase had their respective values but not always directly contributed to ripening characters such as TSS, color, firmness etc. Contrarily, ET receptors, specifically *ETR2* had regulated negatively the ET accumulation thereby showing an indirect feedback on ripening. Moreover, signaling through *ETR2* had impacted in suppression of ROS such as both $O_2^{\bullet -}$ and H_2O_2 content as observed through

negative correlation values (Figure 13). So, ROS intervention in ripening phenomena is not simple but complex and discriminatorily in collusion with related physiological characters.

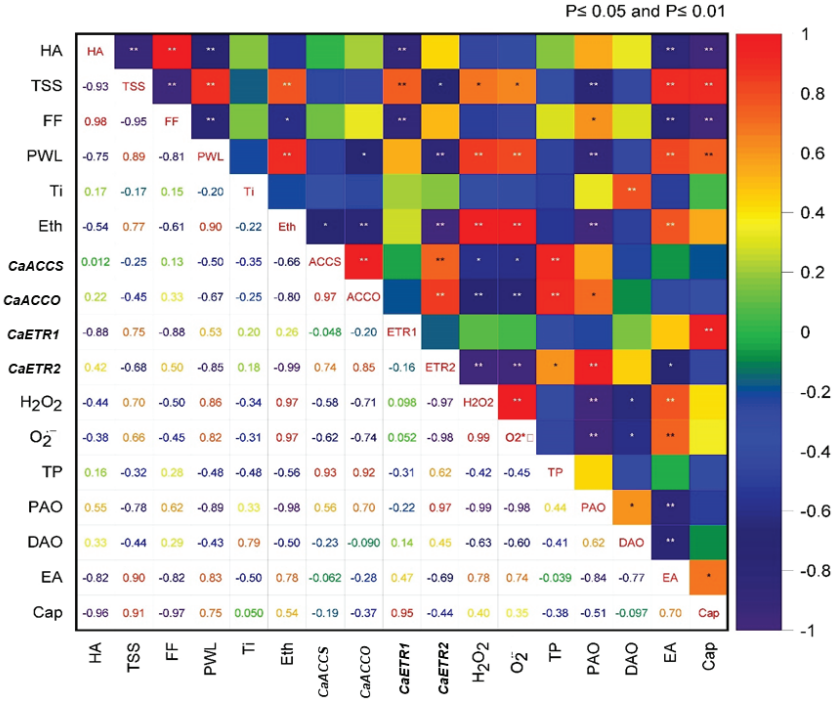

Figure 13. Correlation matrix heatmap of significant attributes in modulation ripening process under treatments. Here, lower triangle represents correlation values and upper triangle represents the significance levels (* and ** represent significance level at $p \leq 0.05$ and $p \leq 0.01$, respectively) between different parameters. HA-Color in hue angle, TSS-Total Soluble Solid Content, FF-Firmness of fruit coat, PWL-Percentage of water loss, Ti-Titanium accumulation, Eth-Ethelene content, ACCS-expression of *ACC Synthase*, ACCO-Expression of *ACC oxidase*, ETR1-Expression of *ETR1*, ETR2-expression of *ETR2*, H_2O_2-Hydrogen peroxide content, $O_2^{\bullet -}$-superoxide content, TP-Total Polyamine Content, PAO-Activity of PAO, DAO-Activity of DAO, EA-Activity of Esterase, Cap-Capsaicin content.

4. Discussion

4.1. Modulation of Quality Characters for Ripening under TiO_2 Nanocomposite

Nanoparticles of titanium (TiO_2-NPs) are less frequent in use but focus exclusively on their photocatalytic properties. Thus, TiO_2-NPs in plants are exercised as a photocatalytic agent for ET with strong reducing activity under UV irradiation [31,32]. In postharvest storage of fruit and vegetables, the application of such an ET scavenger is thus entrusted more with its non-toxicity as well as less invasiveness within the fruit coats [33]. This have got evident in our experiment when *Capsicum* recorded a less bioaccumulation of Ti in the fruit pulp over the control. This is more realistic when we used the chitosan coating in the retention of hydration to support freshness during the storage of *Capsicum* fruit. Chitosan being semi-permeable in nature could modify the fruit tissue atmosphere, more specifically increasing hydration vis-a-vis regulating transpiration loss [23]. This makes it prudent for ET and its role in initiation, modulation and coordination of gene expression related to ripening. Therefore, initially for sensory characters such as color, firmness, relative water content etc. were more significantly bothered under treatment of TiO_2-NP with chitosan (TiO_2-NC) over silver treated samples. Stimulatingly, the experiment became optimistic in

the delay of the ripening process when the TiO_2-NC treatment sustained more firmness and color of the fruit through ongoing days of storage. This may be caused by combinational effect of chitosan (caused by inhibition of transpersonal loss of water and maintenance of fruit coat integrity) and TiO_2-NP which reduce the ET accumulation by photocatalytic reductor process which cause delay in ET induced ripening responses such as turnover of pigments [34]. This assumes the possible suppression of ET in delaying of ripening process through other changes in the structural and functional integrity of fruit undergoing maturation. One of the most import characters of *Capsicum* is pungency which is mainly due to capsaicin, one of main metabolite in capsinoids family [35]. During postharvest storage capsaicin content becomes increased, which is an indication of progress of fruit ripening [36]. In this experiment TiO_2-NC effectively decreased accumulation of capsaicin with respect to untreated control which is an indication of delayed ripening during postharvest storage. Interestingly, the TiO_2-NC treatment was more lenient to maintain the fruit coat intactness as no significant rupture/scars were observed by SEM images as compared to silver-treated fruit. This ensures the acceptability of NC as ecofriendly chemical residues owing to non-invasive features. This is quite in agreement with previous cases where suppression of ET by 1-MCP had secured the firmness of fruit coat with a decrease in soluble solid content during storage [37]. The changes in soluble solid content are important for characterizing the ripening metabolism. Soluble solids cover heterogenous complex organic residues which in combination with titrable acidity make a reliable ripening index [38]. So, a decline or subdued of soluble solid concentration may serve the characteristics of delayed ripening. Thus, TiO_2-NC would be reliable for maintaining the soluble solid throughout the postharvest circumvents the paths of retarded senescence. So, from the biosafety purpose *Capsicum* fruit in our experiment might acknowledge the efficacy of TiO_2-NC in retention of firmness, color over refereed toxic of chemicals such as silver. Loss of water otherwise deducing the reduction of hydration or freshness of the fruit during postharvest storage had more success with TiO_2-NC than silver. In general, chitosan, basically a cationic polymer of *N*-acetyl-d-glucosamine is served with an admirable film coating surface with hydrophilic activity. In addition to the hydrophilic activity of chitosan through semi-permeable film, it can control the tissue atmosphere decreasing the transpiration or vapor loss [19]. So, from fruit quality aspect application of chitosan with the combination of nanomaterial would be successful. Chitosan steeping with additional residues such as Ca^{2+} on fruit coat had impacted on key metabolites pool such as organic acid and its turn over governing moderation of shelf life in other fruit [39].

4.2. Transcript Dynamics of Ethylene Biosynthesis and Signaling Paths

Available information has emphasized the bioaccumulation of ET and its regulation is a key element for the moderation of postharvest ripening. Inhibitors such as 1-MCP not only played in the suppression of ET biosynthesis but also delay the fruit senescence through the accumulation of different antioxidants [40]. The latter in turn suppresses the membrane permeability as well as lipid peroxidation of the fruit coat. Herein also *Capsicum* fruit had significantly moderated under treatment of TiO_2-NC as compared to standard ET action inhibitor such as metallic silver. The differential ET accumulation on storage is quite consistent for the expression of ripening specific genes such as Ca*ACC synthase* and Ca*ACC oxidase* [41]. This is quite satisfactory to receive a good regulation for both of those transcripts and their relative abundance under TiO_2-NC. The transcriptional upregulation for ACC conversion would sensitize not only the ET accumulation but also induces gene cascade linked to other metabolites web. Therefore, ACC metabolism contributing ET moderation under any treatments would suffice the sustenance of greenness on storage where TiO_2-NC might efficaciously qualify. ACC metabolic genes in nexus with anti-oxidation paths and their upregulation have maximum affinity when treated with blue LED irradiation as recoded in citrus [42]. This could be accounted in the present case when TiO_2-NC with its s intrinsic property to be energized with UV irradiation which photocatalytic degrade ET. Inhibition of ET on the biosynthetic pool for delayed senescence

a level of regulation exists with its downstream signaling for ripening genes. It is well agreed that ET signaling cascade is active in normal condition and binding of ET to its receptors facilitated autocatalytic degradation of certain regulatory elements of ET by feedback regulation. This contemplates for silver treatment is no longer with any inhibition for ET synthesis but may act as an inhibitor of the signaling pathway of ET sensitivity is based on activation of receptors such as *ETR2* and *EIN2* which at specific domain is occupied by silver in a competitive manner such as 1-MCP [41]. Ongoing days of ripening for *Capsicum* where TiO_2-NC upregulated the transcriptional dynamics of *ETR1* and *ETR2* significantly over silver when compared to 0 d control. This establishes no regulation of TiO_2-NC on action or functioning level besides exclusively for the subdued synthesis of ET by the compatible trend of *ACC synthase* and *ACC oxidase* expression. This is well consistent with the revealed fact from others' studies in tomato, apple where treated fruit with 1-MCP had delayed the ripening both in terms of reduced ET biogenesis corresponding to the decrease in gene expression. However, non-inhibitory nature of TiO_2-NC in ET signaling is otherwise advantageous over silver, however, in a different way. In fact, induction of Ca*ETR1* and Ca*ETR2* is otherwise involved for significant expression of related gene cascade of ET signaling. The latter includes the antioxidation-related gene in lysis of ROS; reduces peroxidation, carbonylation reactions and accelerates senescence, otherwise hastens ripening process. So, TiO_2-NC may be more privileged over silver, 1-MCP such as conventional agents in the application for dual roles: to reduce the endogenous ET concentration and induce antioxidation activities to retards ripening in postharvest storage.

4.3. ROS Metabolism Is Related to Polyamine Oxidation in Progress of Fruit Ripening at Storage

Ripening being on penultimate stages of senescence characterized by hydrolysis and diverse peroxidative reactions on macromolecules with the generation of ROS [42]. It is with well evidential support that an active metabolism of ROS is involved in various species such as sweet pepper, tomato, guava, mango, grape etc. [43]. Consistently, the ROS metabolism and its antioxidation by nonenzymatic as well enzymatic paths characterize the changes in quality characters of fruit such as softening, color, odor. However, in-built antioxidation system or its improvisation by exogenous elicitors accommodated to regulate the ripening behavior within postharvest storage. Understanding the hastening of senescence by the advent of ROS fruit tissues in our experiment realized a significant moderation superoxide ($O_2^{\bullet -}$), peroxide (H_2O_2) under TiO_2-NC. ROS has its dual functionalities in ripening incident of fruit mostly with peroxidative lysis and activation of conserved ripening-related genes regardless of non-climacteric and climacteric types [44]. It is mostly the metabolism within mitochondrial energy-dependent paths and oxidation of few biomolecules connecting between ET production and respiratory during the ripening. The availability of ROS may also be circumvented by oxidation of residues polyamine being predominant. Polyamine, a ubiquitous polycationic straight-chain hydrocarbon residue with characteristics of few $-NH_2$ functional groups with varied unsaturation exists in various cell fractions. This molecule undergoes protonated at biological pH and being nucleophilic in nature can bind most of the positively charged bioresidues in cells. This facilitates rendering a shielding effect from oxidation by ROS or free radicals under abiotic stress in plants [5]. In ripening fruit roles of polyamines are based on two facts: one, antagonizing the ET biosynthetic paths and shielding the biomolecules from peroxidative degradation by ROS developed from various catabolic reactions [45]. Polyamines use a common precursor (such as arginine) and biosynthetic paths with ET. This may be diverged depending on plants' cellular demand from an intermediate such as ACC and directed either into polyamine or ET. Postharvest period triggering more ET biosynthesis than polyamine is obvious to expedite the fruit senescence. A consistent inverse interrelationship has been common in many cases between ET and polyamine metabolism in ripening fruit. Thereby, a depletion of polyamine on 7 d of storage in *Capsicum* fruit might link the increased activities of DAO and PAO under treatment of silver and TiO_2-NC in favor of more ROS such as H_2O_2 [46]. H_2O_2, however, within a threshold concentration, in turn, be

inductive of several antioxidation cascade-like activities of class III peroxidase to reduce the oxidative damages of fruit tissues and thereby impeding the ripening process.

4.4. Metabolites Profiling: The Abundance of Essential Oils Induced by Nanocomposite

The ripening is highly regulated by abundance of specific metabolites influencing quality characters. Instead of a single one metabolite collection of different metabolites have wide coverage through ripening period as well as proportionate contribution to agronomic values [47]. In *Capsicum* the development of essential oils with ripening progress happens to be a good correlative index with few characters (Supplementary Materials Table S1). This finding would be important and contested for ripening specificity of fruit where mostly alkane group of residues were synchronously increased [48]. On contrary the alcohols and esters were also documented in a negative manner for contribution on ripening specific changes. Therefore, conclusively essential oil constituents with special reference to alkane residues can be considered as screening indices for delayed ripening *vis-à-vis* extended shelf life of fruit on postharvest storage. Those such as color, texture, softness etc. necessarily indicative of ripening stages by significant changes with up/downregulation. Essential oils its constituent residues are associated with capsinoids in support of hot favor and intense burning sensation for pepper consumption. Factually, *Capsicum* fruit from many cultivars have been frequently in more exercise for its essential oils and adjoining compounds (phenolics, terpenoids, steroids) than that of capsinoids also. In the contribution of specific aroma pepper fruit with their volatile oils, however, relatively low in concentration may vary depending on harvest stages and supplementation of agronomic inputs [49]. The chief constituents of pepper oil and related residues cover esters, small chain fatty acid, alcohol, ketones, unsaturated hydrocarbons, benzene and naphthalene derivatives, sulfur residues etc. This is interesting to note that *Capsicum* fruit are well responsive to TiO_2-NC in upregulation of essential oils, however, few of those. This would be more imperative having a significant correlation with any ripening-related phenomena, particularly, in the contribution of quality characteristics. Identification of several hundred constituents in essential oils as percentage varied from dry and fresh fruit categorically grouped into aldehyde, terpenoid, hydrocarbon. Additionally, ketone, alcohol, unsaturated/saturated fatty acids, esters are adjoining to complement the physicochemical properties of essential oil [50].

Contextually, metabolites flux as studied in GC-MS analysis in the *Capsicum* fruit and its comparative allocation through ongoing days of ripening in the present experiment is interesting. As compared to initial days of ripening fruit recorded a significant metabolites allocation variably with silver and TiO_2-NC. In general fruit ripening being a penultimate stage of senescence is characteristically experienced with both re-synthesis and turn of metabolites. Maximum accessible research has been attentive on analyzing the organic acids, secondary metabolites, sugar residues, volatile compounds and changes of their anabolic and catabolic paths. However, in pepper fruit residues are in different proportions as principle depending on stages of maturity [51]. It also identifies terpene(s), esters, ketones, naphthalene, phenolics, hydrocarbon, aromatic volatiles etc. This may establish the metabolic imprint that necessarily validates the role(s) of specific compounds satisfying paths of ripening under TiO_2-NC. Expectedly, this makes it prudent to suffice the biomarker concept through the exhibition of ripening specific residues matching with existing GC-MS library attributing regulation of postharvest shelf life of *Capsicum*. Identified residues in essential oils varied under TiO_2-NC may not be any exceptions in quality but in quantity as compared to control. The changes in content according to storage would be rather significant otherwise. It would be overbearing to focus any specific residues if expressed in parallel to definite any quality characters for in moderation of ripening. It offers a selective pressure for *Capsicum* fruit for delayed senescence based on such a metabolomic profile of essential oil. In pursuit of overexpression of such a metabolite(s), identification of key/regulatory gene(s) for its biosynthetic paths, would be the target in better postharvest management.

5. Conclusions

This work is first time report on effect of TiO_2-NC for its biocompatibility and moderation of ripening phenomena on postharvest storage at 25 °C. The exercise of a bio safe and non-toxic TiO_2-NC (since its concentration is insignificant in fruit tissues) in our experiment with *Capsicum* fruit had evident it to be potential. This is proved exclusively in ripening stipulated cellular responses attributing ET metabolism as studied herein. The spotlight of the experiment on photocatalytic break down of endogenous ET and changes signaling by TiO_2-NC had verified the potentials of ripening postpone by ROS metabolism. It moderated the ET biosynthetic (*CaACCS* and *CaACCO*) as well as signaling regulatory (*CaETR1* and *CaETR2*) genes in parallel to changes the sensory characters in fruit. The moderation of ET signaling had carry forwarded in the upregulation of polyamine-mediated ROS generation during storage. The enzymatic oxidation of polyamines by DAO and PAO and changes had fairly characterized ripening during storage. TiO_2-NP had received attention in the identification of metabolite flux contributing to the moderation of any ripening volatile residues. A distinct variation of those constituents under influence of TiO_2-NC is a pertinent feature for any change in ripening under treatments. This generation of metabolites could serve as a biomarker in support of delayed senescence, however, directly or indirectly. As a whole, this study verified the nature of biological interaction for TiO_2-NC on *Capsicum* fruit for alteration of ripening during postharvest storage. Still, it awaits deep insights for underlying mechanism or reactivity in favor of TiO_2-NC perception to peruse other specific paths of ripening of fruit.

Supplementary Materials: The following supporting information can be downloaded at: https://www.mdpi.com/article/10.3390/plants11040513/s1, Figure S1: *CaERT1* and *CaETR2* gene expression bands under different treatments with 100bp DNA marker; Table S1: Correlation matrix of significant constituents of essential oil and quality indices in modulation ripening process under treatments; Table S2: Primer used in the PCR reaction.

Author Contributions: Conceptualization, M.F. and M.K.A.; methodology, S.C.D., A.K.H. and M.K.A.; validation, I.S. and M.K.A.; formal analysis, I.S. and M.H.; investigation, A.G., S.C.D., A.K.H. and M.K.A.; resources, M.K.A.; data curation, M.K.A.; writing—original draft preparation, A.G. and M.K.A.; writing—review and editing, M.F., M.K.A. and M.H.; visualization, M.H.; supervision, M.K.A.; project administration, M.K.A.; funding acquisition, M.K.A. All authors have read and agreed to the published version of the manuscript.

Funding: This work is financially supported by DST PURSE II (Department of Science and Technology-Promotion of the University Research and Scientific Excellence) program, DST, Govt. of India allocated to the university of Kalyani and we are thankful to University Grant Commission for providing UGC-SRF fellowship to A.G. (I.D:341842).

Institutional Review Board Statement: Not applicable.

Informed Consent Statement: Not applicable.

Data Availability Statement: All data are available in this manuscript.

Acknowledgments: We are also thankful to the sophisticated instrument facility of Envirocheck (North 24 Paraganas, West Bengal, India) for providing all the support during GC and GC-MC analysis.

Conflicts of Interest: The authors declare no conflict of interest.

References

1. Fuentes, L.; Figueroa, C.R.; Valdenegro, M. Recent advances in hormonal regulation and cross-talk during non-climacteric fruit development and ripening. *Horticulturae* **2019**, *5*, 45. [CrossRef]
2. Prasanna, V.; Prabha, T.N.; Tharanathan, R.N. Fruit ripening phenomena–An overview. *Crit. Rev. Food Sci. Nutr.* **2007**, *47*, 1–19. [CrossRef] [PubMed]
3. Chen, Y.; Grimplet, J.; David, K.; Castellarin, S.D.; Terol, J.; Wong, D.C.; Luo, Z.; Schaffer, R.; Celton, J.M.; Talon, M.; et al. Ethylene receptors and related proteins in climacteric and non-climacteric fruits. *Plant Sci.* **2018**, *276*, 63–72. [CrossRef] [PubMed]

4. Siebeneichler, T.J.; Crizel, R.L.; Camozatto, G.H.; Paim, B.T.; da Silva Messias, R.; Rombaldi, C.V.; Galli, V. The postharvest ripening of strawberry fruits induced by abscisic acid and sucrose differs from their *in vivo* ripening. *Food Chem.* **2020**, *317*, 126407. [CrossRef]
5. Yan, S.C.; Chen, J.Y.; Yu, W.M.; Kuang, J.F.; Chen, W.X.; Li, X.P.; Lu, W.J. Expression of genes associated with ethylene-signalling pathway in harvested banana fruit in response to temperature and 1-MCP treatment. *J. Sci. Food Agric.* **2011**, *91*, 650–657. [CrossRef]
6. Ghosh, A.; Saha, I.; Dolui, D.; De, A.K.; Sarkar, B.; Adak, M.K. Silver can induce oxidative stress in parallel to other chemical elicitors to modulate the ripening of chili cultivars. *Plants* **2020**, *9*, 238. [CrossRef]
7. Li, X.; Zhu, X.; Mao, J.; Zou, Y.; Fu, D.; Chen, W.; Lu, W. Isolation and characterization of ethylene response factor family genes during development, ethylene regulation and stress treatments in papaya fruit. *Plant Physiol. Biochem.* **2013**, *70*, 81–92. [CrossRef] [PubMed]
8. Giné-Bordonaba, J.; Echeverria, G.; Duaigües, E.; Bobo, G.; Larrigaudière, C. A comprehensive study on the main physiological and biochemical changes occurring during growth and on-tree ripening of two apple varieties with different postharvest behaviour. *Plant Physiol. Biochem.* **2019**, *135*, 601–610. [CrossRef]
9. Farcuh, M.; Rivero, R.M.; Sadka, A.; Blumwald, E. Ethylene regulation of sugar metabolism in climacteric and non-climacteric plums. *Postharvest Biol. Technol.* **2018**, *139*, 20–30. [CrossRef]
10. Dubey, M.; Jaiswal, V.; Rawoof, A.; Kumar, A.; Nitin, M.; Chhapekar, S.S.; Kumar, N.; Ahmad, I.; Islam, K.; Brahma, V.; et al. Identification of genes involved in fruit development/ripening in *Capsicum* and development of functional markers. *Genomics* **2019**, *111*, 1913–1922. [CrossRef]
11. Cisneros, L.; Gao, F.; Corma, A. Silver nanocluster in zeolites. Adsorption of ethylene traces for fruit preservation. *Microporous Mesoporous Mater.* **2019**, *283*, 25–30. [CrossRef]
12. Strano, A.; Falcone, G.; Nicolò, B.F.; Stillitano, T.; De Luca, A.I.; Nesci, F.S.; Gulisano, G. Eco-profiles and economic performances of a high-value fruit crop in southern Italy: A case study of bergamot (*Citrus bergamia* Risso). *Agroecol. Sustain. Food Syst.* **2017**, *41*, 1124–1145.
13. Ntsoane, M.L.; Jalali, A.; Römer, J.; Duewel, K.; Göller, C.; Kühn, R.; Mähne, K.; Geyer, M.; Sivakumar, D.; Mahajan, P.V. Performance evaluation of silica gel-water adsorption based cooling system for mango fruit storage in Sub-Saharan Africa. *Postharvest Biol. Technol.* **2019**, *149*, 195–199. [CrossRef]
14. Bailén, G.; Guillén, F.; Castillo, S.; Serrano, M.; Valero, D.; Martínez-Romero, D. Use of activated carbon inside modified atmosphere packages to maintain tomato fruit quality during cold storage. *J. Agric. Food Chem.* **2006**, *54*, 2229–2235. [CrossRef] [PubMed]
15. Pathak, N.; Caleb, O.J.; Geyer, M.; Herppich, W.B.; Rauh, C.; Mahajan, P.V. Photocatalytic and photochemical oxidation of ethylene: Potential for storage of fresh produce—A review. *Food Bioproc. Technol.* **2017**, *10*, 982–1001. [CrossRef]
16. Geng, Q.; Lin, X.; Si, R.; Chen, X.; Dai, W.; Fu, X.; Wang, X. The correlation between the ethylene response and its oxidation over TiO_2 under UV irradiation. *Sens. Actuators B Chem.* **2012**, *174*, 449–457. [CrossRef]
17. Xing, Y.; Yang, H.; Guo, X.; Bi, X.; Liu, X.; Xu, Q.; Wang, Q.; Li, W.; Li, X.; Shui, Y.; et al. Effect of chitosan/Nano-TiO_2 composite coatings on the postharvest quality and physicochemical characteristics of mango fruits. *Sci. Hortic.* **2020**, *263*, 109135. [CrossRef]
18. Helal, M.; Sami, R.; Khojah, E.; Elhakem, A.; Benajiba, N.; Al-Mushhin, A.A.; Fouda, N. Evaluating the coating process of titanium dioxide nanoparticles and sodium tripolyphosphate on cucumbers under chilling condition to extend the shelf-life. *Sci. Rep.* **2021**, *11*, 20312. [CrossRef]
19. de Matos Fonseca, J.; dos Santos Alves, M.J.; Soares, L.S.; Moreira, R.D.F.P.M.; Valencia, G.A.; Monteiro, A.R. A review on TiO2-based photocatalytic systems applied in fruit postharvest: Set-ups and perspectives. *Food Res. Int.* **2021**, *144*, 110378. [CrossRef]
20. Wonglom, P.; Daengsuwan, W.; Ito, S.I.; Sunpapao, A. Biological control of *Sclerotium* fruit rot of snake fruit and stem rot of lettuce by *Trichoderma* sp. T76-12/2 and the mechanisms involved. *Physiol. Mol. Plant Pathol.* **2019**, *107*, 1–7. [CrossRef]
21. Scalisi, A.; O'Connell, M.G. Application of Visible/NIR spectroscopy for the estimation of soluble solids, dry matter and flesh firmness in stone fruits. *J. Sci. Food Agric.* **2021**, *101*, 2100–2107. [CrossRef] [PubMed]
22. Aizat, W.M.; Able, J.A.; Stangoulis, J.C.; Able, A.J. Characterisation of ethylene pathway components in non-climacteric capsicum. *BMC Plant Biol.* **2013**, *13*, 191. [CrossRef] [PubMed]
23. Ghosh, A.; Saha, I.; Debnath, S.C.; Hasanuzzaman, M.; Adak, M.K. Chitosan and putrescine modulate reactive oxygen species metabolism and physiological responses during chili fruit ripening. *Plant Physiol. Biochem.* **2021**, *163*, 55–67. [CrossRef] [PubMed]
24. Sadasivam, S.; Manickam, A. *Biochemical Methods*, 3rd ed.; New Age International Publishers: New Delhi, India, 2008; pp. 209–210.
25. Wettlaufer, S.H.; Weinstein, L.H. Quantitation of polyamines using thin-layer chromatography and image analysis. *J. Chromatogr. A* **1988**, *441*, 361–366. [CrossRef]
26. Kumar, D.; Behal, S.; Bhattacharyya, R.; Banerjee, D. Fast blue B produces a light background on the gel surface. *Indian J. Clin. Biochem.* **2020**, *16*, 124–125. [CrossRef] [PubMed]
27. Navarro-Rocha, J.; Andrés, M.F.; Díaz, C.E.; Burillo, J.; González-Coloma, A. Composition and biocidal properties of essential oil from pre-domesticated Spanish *Satureja Montana*. *Ind. Crops Prod.* **2020**, *145*, 111958. [CrossRef]
28. Femi-Adepoju, A.G.; Dada, A.O.; Otun, K.O.; Adepoju, A.O.; Fatoba, O.P. Green synthesis of silver nanoparticles using terrestrial fern (*Gleichenia Pectinata* (Willd.) C. Presl.): Characterization and antimicrobial studies. *Heliyon* **2019**, *5*, e01543. [CrossRef]
29. Wang, Z.; Liu, S.; Cao, X.; Wu, S.; Liu, C.; Li, G.; Jiang, W.; Wang, H.; Wang, N.; Ding, W. Preparation and characterization of TiO_2 nanoparticles by two different precipitation methods. *Ceram. Int.* **2020**, *46*, 15333–15341. [CrossRef]

30. Bagheri, S.; Shameli, K.; Abd Hamid, S.B. Synthesis and characterization of anatase titanium dioxide nanoparticles using egg white solution via Sol-Gel method. *J. Chem.* **2013**, *1*, 848205. [CrossRef]
31. Lyu, S.; Wei, X.; Chen, J.; Wang, C.; Wang, X.; Pan, D. Titanium as a beneficial element for crop production. *Front. Plant Sci.* **2017**, *8*, 597. [CrossRef]
32. Ji, Y.; Zhou, Y.; Ma, C.; Feng, Y.; Hao, Y.; Rui, Y.; Wu, W.; Gui, X.; Han, Y.; Wang, Y.; et al. Jointed toxicity of TiO_2 NPs and Cd to rice seedlings: NPs alleviated Cd toxicity and Cd promoted NPs uptake. *Plant Physiol. Biochem.* **2017**, *110*, 82–93. [CrossRef] [PubMed]
33. Jaimun, R.; Sangsuwan, J. Efficacy of chitosan-coated paper incorporated with vanillin and ethylene adsorbents on the control of anthracnose and the quality of Nam Dok Mai mango fruit. *Packag. Technol. Sci.* **2019**, *32*, 383–394. [CrossRef]
34. Xing, Y.; Yang, S.; Xu, Q.; Xu, L.; Zhu, D.; Li, X.; Shui, Y.; Liu, X.; Bi, X. Effect of chitosan/nano-TiO_2 composite coating on the postharvest quality of blueberry fruit. *Coatings* **2021**, *11*, 512. [CrossRef]
35. Jang, S.; Park, M.; Lee, D.G.; Lim, J.H.; Jung, J.W.; Kang, B.C. Breeding *Capsicum chinense* lines with high levels of capsaicinoids and capsinoids in the fruit. *Agriculture* **2021**, *11*, 819. [CrossRef]
36. Samira, A.; Woldetsadik, K.; Workneh, T.S. Postharvest quality and shelf life of some hot pepper varieties. *J. Food Sci. Technol.* **2013**, *50*, 842–855. [CrossRef]
37. Zou, J.; Chen, J.; Tang, N.; Gao, Y.; Hong, M.; Wei, W.; Cao, H.; Jian, W.; Li, N.; Deng, W.; et al. Transcriptome analysis of aroma volatile metabolism change in tomato (*Solanum lycopersicum*) fruit under different storage temperatures and 1-MCP treatment. *Postharvest Biol. Technol.* **2018**, *135*, 57–67. [CrossRef]
38. Steelheart, C.; Alegre, M.L.; Bahima, J.V.; Senn, M.E.; Simontacchi, M.; Bartoli, C.G.; Grozeff, G.E. Nitric oxide improves the effect of 1-methylcyclopropene extending the tomato (*Lycopersicum esculentum* L.) fruit postharvest life. *Sci. Hortic.* **2019**, *255*, 193–201. [CrossRef]
39. Kumarihami, H.M.; Kim, J.G.; Kim, Y.H.; Lee, M.; Lee, Y.S.; Kwack, Y.B.; Kim, J. Preharvest application of chitosan improves the postharvest life of 'Garmrok' kiwifruit through the modulation of genes related to ethylene biosynthesis, cell wall modification, and lignin metabolism. *Foods* **2021**, *10*, 373. [CrossRef]
40. Massolo, J.F.; Forte, L.G.; Concellón, A.; Viña, S.Z.; Vicente, A.R. Effects of ethylene and 1-MCP on quality maintenance of fresh cut celery. *Postharvest Biol. Technol.* **2019**, *148*, 176–183. [CrossRef]
41. Li, S.; Chen, K.; Grierson, D. A critical evaluation of the role of ethylene and MADS transcription factors in the network controlling fleshy fruit ripening. *New Phytol.* **2019**, *221*, 1724–1741. [CrossRef]
42. Pérez-Ambrocio, A.; Guerrero-Beltrán, J.A.; Aparicio-Fernández, X.; Ávila-Sosa, R.; Hernández-Carranza, P.; Cid-Pérez, S.; Ochoa-Velasco, C.E. Effect of blue and ultraviolet-C light irradiation on bioactive compounds and antioxidant capacity of habanero pepper (*Capsicum chinense*) during refrigeration storage. *Postharvest Biol. Technol.* **2018**, *135*, 19–26. [CrossRef]
43. Rodríguez-Ruiz, M.; González-Gordo, S.; Cañas, A.; Campos, M.J.; Paradela, A.; Corpas, F.J.; Palma, J.M. Sweet pepper (*Capsicum annuum* L.) fruits contain an atypical peroxisomal catalase that is modulated by reactive oxygen and nitrogen species. *Antioxidants* **2019**, *8*, 374. [CrossRef] [PubMed]
44. Shakya, R.; Singh, N.; Bhatla, S.C. Iron homeostasis regulates maturation of tomato (climacteric) and capsicum (non-climacteric) fruits. *J. Plant Biochem. Biotechnol.* **2021**, *30*, 392–395. [CrossRef]
45. Sharma, S.; Pareek, S.; Sagar, N.A.; Valero, D.; Serrano, M. Modulatory effects of exogenously applied polyamines on postharvest physiology, antioxidant system and shelf life of fruits: A review. *Int. J. Mol. Sci.* **2017**, *18*, 1789. [CrossRef] [PubMed]
46. Sánchez-Rodríguez, E.; Romero, L.; Ruiz, J.M. Accumulation of free polyamines enhances the antioxidant response in fruits of grafted tomato plants under water stress. *J. Plant Physiol.* **2016**, *190*, 72–78. [CrossRef]
47. Zamljen, T.; Zupanc, V.; Slatnar, A. Influence of irrigation on yield and primary and secondary metabolites in two chilies species, *Capsicum annuum* L. and *Capsicum chinense* Jacq. *Agric. Water Manag.* **2020**, *234*, 106104. [CrossRef]
48. Romero, P.; Lafuente, M.T. Abscisic acid deficiency alters epicuticular wax metabolism and morphology that leads to increased cuticle permeability during sweet orange (*Citrus sinensis*) fruit ripening. *Front. Plant Sci.* **2020**, *11*, 1914. [CrossRef]
49. Spadafora, N.D.; Cocetta, G.; Cavaiuolo, M.; Bulgari, R.; Dhorajiwala, R.; Ferrante, A.; Spinardi, A.; Rogers, H.J.; Müller, C.T. A complex interaction between pre-harvest and post-harvest factors determines fresh-cut melon quality and aroma. *Sci. Rep.* **2019**, *9*, 2745. [CrossRef]
50. Taheri, A.; Behnamian, M.; Dezhsetan, S.; Karimirad, R. Shelf life extension of bell pepper by application of chitosan nanoparticles containing *Heracleum persicum* fruit essential oil. *Postharvest Biol. Technol.* **2020**, *170*, 111313. [CrossRef]
51. Korkmaz, A.; Atasoy, A.F.; Hayaloglu, A.A. Changes in volatile compounds, sugars and organic acids of different spices of peppers (*Capsicum annuum* L.) during storage. *Food Chem.* **2020**, *311*, 125910. [CrossRef]

plants

MDPI

Review

Revisiting the Domestication Process of African *Vigna* Species (Fabaceae): Background, Perspectives and Challenges

Davide Panzeri [1,*], Werther Guidi Nissim [1,2], Massimo Labra [1] and Fabrizio Grassi [1,*]

[1] Department of Biotechnology and Bioscience, University of Milan-Bicocca, Piazza della Scienza 2, 20126 Milano, Italy; werther.guidi.nissim@gmail.com (W.G.N.); massimo.labra@unimib.it (M.L.)
[2] Department of Agriculture, Food, Environment and Forestry (DAGRI), University of Florence, Viale delle Idee 30, 50019 Sesto Fiorentino, Italy
* Correspondence: davide.panzeri@unimib.it (D.P.); fabrizio.grassi@unimib.it (F.G.)

Abstract: Legumes are one of the most economically important and biodiverse families in plants recognised as the basis to develop functional foods. Among these, the *Vigna* genus stands out as a good representative because of its relatively recent African origin as well as its outstanding potential. Africa is a great biodiversity centre in which a great number of species are spread, but only three of them, *Vigna unguiculata*, *Vigna subterranea* and *Vigna vexillata*, were successfully domesticated. This review aims at analysing and valorising these species by considering the perspective of human activity and what effects it exerts. For each species, we revised the origin history and gave a focus on where, when and how many times domestication occurred. We provided a brief summary of bioactive compounds naturally occurring in these species that are fundamental for human wellbeing. The great number of wild lineages is a key point to improve landraces since the domestication process caused a loss of gene diversity. Their genomes hide a precious gene pool yet mostly unexplored, and genes lost during human activity can be recovered from the wild lineages and reintroduced in cultivated forms through modern technologies. Finally, we describe how all this information is game-changing to the design of future crops by domesticating *de novo*.

Keywords: *Vigna* genus; introgression; hybridisation; phylogeny; *de novo* domestication; feralisation; bioactive compounds

Citation: Panzeri, D.; Guidi Nissim, W.; Labra, M.; Grassi, F. Revisiting the Domestication Process of African *Vigna* Species (Fabaceae): Background, Perspectives and Challenges. *Plants* **2022**, *11*, 532. https://doi.org/10.3390/plants11040532

Academic Editors: Milan S. Stankovic, Paula Baptista and Petronia Carillo

Received: 25 January 2022
Accepted: 13 February 2022
Published: 16 February 2022

1. Introduction

Legumes (Fabaceae) are considered one of the most important families of plants for human nutrition, especially considering the rapid growth rate of the world population [1]. However, almost all the efforts and resources invested in agriculture during the last century were focused on improving the yield, resistance and quality of a few specific staple crops. Neglected landraces are regarded as having interesting potential, and recent studies have demonstrated that some wild legumes can be an important target to develop modern functional foods because they possess various bioactive molecules that interact positively with human health [2–5]. Among these, members of the *Vigna* genus show a growing social and economic importance in several African regions, especially where the local population is not able to afford animal proteins [6–8]. Their seeds are rich in essential amino acids and contain a high concentration of minerals, lipids and vitamins [9,10].

The genus *Vigna* (Savi, 1824), which belongs to the tribe Phaseoleae of the family Fabaceae, includes over 100 species [11] distributed in the tropical and subtropical areas of the world [12] grouped in five subgenera: *Vigna*, *Ceratotropis*, *Plectotropis*, *Lasiosporon* and *Haydonia* [13–15]. Phylogenetic findings propose the age of split between *Phaseolus* and *Vigna* genera at about 8–10 million years (Mya) and the age of split between *Ceratotropis* and *Vigna* subgenera at about 3–4 Mya [13–17], but the genetic relationships between subgenera are particularly complex and far from being completely solved. Although most domesticated or semi-domesticated species are distributed in Asia, the greatest diversity

of the *Vigna* genus is located in Sub-Saharan Africa [14,18]. *Vigna* subgenus, distributed in Africa, includes about 40 wild and 2 domesticated species, namely cowpea (also called black-eyed peas, chawli and kunde) (*Vigna unguiculata* L.) and Bambara groundnut (*V. subterranea* L.) [19] while *Ceratotropis* (Piper) Verdc., distributed in Asia, contains 21 wild and 7 domesticated species used widely for food and forage, namely mungbean or green gram (*V. radiata* L. Wilczek), black gram (*V. mungo* L. Hepper), moth bean (*V. aconitifolia* Jacq. Maréchal), rice bean (*V. umbellata* Thunb. Ohwi and Ohashi), adzuki bean (*V. angularis* L. Ohwi and Ohashi), creole bean (*V. reflexo-pilosa* Hayata), jungli bean (*V. trilobata* L. Verdc.). [15,20–22]. Moreover, three species belonging to *Plectrotropis* (Schumach.) are distributed in Africa, including tuber cowpea (*V. vexillata* L.) [23]. Most of the African *Vigna* germplasm is based on wild plants and neglected or underutilized landraces, and many of these lineages are declining with a high risk of extinction. The recovery of wild accessions and research devoted to the phylogeny of the genus is therefore essential to prevent genetic erosion and the loss of *Vigna* diversity.

Plant domestication is widely recognised as an accelerated evolutionary process driven by a synergistic impact of human and natural selection, occurring in geographically restricted areas from wild progenitors. In legumes, the main modification is the loss of seed pod dehiscence or shattering [24,25]. The split at the dorsal and ventral sutures of the dry pod and successive release of the seeds occurs due to the desiccation of lignified cells in the pods [26]. The shattering habit is related to environmental aridity and persists in many varieties of domesticated *Vigna* species, thereby determining severe yield losses [27,28]. Additional implementations in *Vigna* domesticated species include an increase in seed or fruit size, change in seed colour, loss of seed dormancy, apical dominance and change in flowering timing [29–33]. These modifications were inherited more or less effectively in the various vine species currently cultivated, and this is the basis of the agrobiodiversity of this genus.

Generally, the current existing crops show lower resistance to biotic and abiotic stress compared to wild relatives, and often they have reached their full yield. The selection of desirable traits and breeding processes to improve crop productivity have caused the depletion of diversity and the increase in the frequency of deleterious genetic variants that are fixed in the genomes of crops [34–36]. These constraints have a serious impact on agriculture, limiting the possibility to grow such crops under more extreme environmental conditions. Thanks to this residual genetic diversity and also to studies performed on *Vigna* species, most of the accessions are well adapted to a wide range of extreme environmental conditions, such as sandy beaches, arid lands and wetlands, harbouring tolerance and resistance genes towards biotic and abiotic stresses. These genetic traits are used for developing new stress-tolerant crops [37–43]. By contrast, less is known about the effects of domestication on the nutritional value of seeds [7] even if recent studies have reported that cultivated legumes show a lower carotenoid and protein content in seeds compared with the wild relatives [44,45]. Where, when and how many times the domestication process of African *Vigna* crops occurred continues to be debated among researchers. Although archaeological remains of *Vigna* indicate that the domestication process in Africa was started recently compared to other field crops [46,47]. Modern evolutionary models proposed for other crops suggest that the predomestication phase may have lasted several thousands of years [48,49]. Generally, the centres of origin are also recognized as centres of diversity, and thus these areas require special precautionary measures of conservation [50]. Although for many crops the single-origin model is usually the most parsimonious, the hypothesis that provides multiple origins starting from independent founder lineages seems well suited for the crops of *Vigna* originated in Africa [51,52]. Moreover, despite whether and to what extent introgression influences the domestication process is still underexplored, some studies already show that gene flow between cowpea and its wild relatives may occur. Pervasive introgression can also intensify the feralisation process, promoting the crops to return to a wild environment and causing serious problems for the conservation of biodiversity [53].

In this review, we re-examine the available scientific information on the domestication process of three African *Vigna* crops and discuss the future perspectives and challenges in the light of modern technologies in the time of climate change and new parading of conservative agriculture strategies. Another crucial point in exploring natural biodiversity is not only a matter of sustainability but also a matter of human health. A balanced diet gives extreme benefits to people's wellbeing by properly assuming the correct amount of micro and macro nutrients as well as useful, healthy bioactive compounds. Finding and characterising these compounds is an ambitious challenge for researchers thus we briefly summarise the bioactivity of some compounds, and we discuss how human activity and breeding has impacted the variability of molecules.

Although recent genetic studies have led to a deeper understanding of these crops, the continuation of investigating the domestication process through a multidisciplinary approach which includes genomic, transcriptomic, metabolomic and epigenomic analyses is needed to highlight the wide agronomic opportunities related to these species. Moreover, recent techniques of gene editing have opened new and crucial ways to redesign modern crops because traditional genetic improvement is generally limited by the cross-compatibility between species. Thus, because the *de novo* domestication process may represent a turn toward more modern and sustainable agriculture, further efforts are needed to explore the genome diversity of wild germplasm.

2. *Vigna unguiculata* (L.) Walp.

V. unguiculata, which was considered an orphan crop for several decades, has recently become one of the most important legumes in the world. Its name derives from Latin and means "with a small claw", referring to the size of the claw of the petals [54] or commonly named as "cowpea" because of its use as fodder for cows [55] and black-eyed pea/bean for the black hilum. This crop is largely cultivated, especially in semiarid regions of Africa and Asia where other crops fail to grow [10]. Currently, on a global scale, about 15 million hectares are dedicated to *V. unguiculata*, with an annual production of 7 million Mg and an average yield of 0.6 Mg ha^{-1} [56]. The most interesting environmental traits of this species are represented by the generalized low agrochemical input requirements. In fact, this crop shows relatively high adaptation to drought, especially in comparison to other legumes [57] and can fix up to 200 kg N ha^{-1} [58] with a positive soil N balance of up to 92 kg ha^{-1} [59]. Nevertheless, several abiotic and biotic constraints (i.e., low soil fertility, pests, diseases, parasitic weeds, and nematodes) limit the yield [43,60,61]. Moreover, low productivity is often associated with the use of traditional and unimproved varieties, still widely cultivated in Africa [62]. This crop has a fundamental role in human nutrition, showing seeds rich in proteins and essential amino acids (i.e., tryptophan and lysine), carbohydrates, folic acid and minerals. Recent studies carried on a large sampling have shown high variability in protein and mineral concentrations, suggesting that some lineages could be potential sources of genes useful to produce new varieties [63–66].

The high number of wild subspecies found exclusively in Africa strongly supports the idea of an African origin. However, intraspecies phylogeny remains far from being completely elucidated [67]. The centre of origin of the species is probably located in the southernmost regions of Africa, where most subspecies are found and where most genetic diversity could be still hidden [68]. Several taxonomic revisions based on morphological and molecular traits permitted to identify 10 perennial and 1 annual subspecies, the latter split into two varieties: ssp. *unguiculata* var. *unguiculata* (domesticated cowpea) and ssp. *unguiculata* var. *spontanea* (Schweinf.) Pasquet., also known as subsp. *dekindtiana* sensu Verdcourt non Harms [69–76]. Besides the domesticated cowpea, the *dekindtiana* group includes some obligate short-day wild forms, well adapted to arid environments. While the var. *spontanea* grows especially around cultivated fields and roadsides, and it is recognized as the progenitor of domesticated cowpea [75,77–79], the subspecies *alba*, *pubescens*, *tenuis*, *stenophylla* and *dekindtiana* are perennial plants [75,76]. The development of new molecular tools to discriminate among wild, weedy, and cultivated accessions is considered a modern

and fundamental target, particularly needed for disentangling the complex taxonomic relationships among subspecies and to discriminate between true wild plants and ferals.

Although little is known about the domestication process, some scientists have hypothesized that ancient cowpea progenitors, such as the modern wild forms, were adapted to dry habitats and grew spontaneously south of the Sahara Desert [80]. These plants were gathered, cultivated and dispersed by men near the villages, but they were unsuited for cultivation. Although they did not show high yield, the wild lineages were spread in the humid zones thanks to their pods that remained closed for the humid atmosphere. Through several generations of cultivation, new mutants have arisen, showing interesting domestic traits, including resistance to shattering. Subsequently, humans have selected and helped spread these landraces by exchange and trade activities. Since the oldest archaeological records of domesticated forms found in central Ghana are dated around 1500 BC, the domestication process likely started before that period (Figure 1) [47,81]. However, the precise origin is widely debated, and two independent domestication centres in West and East Africa are proposed by different authors [68,74,79,82–86].

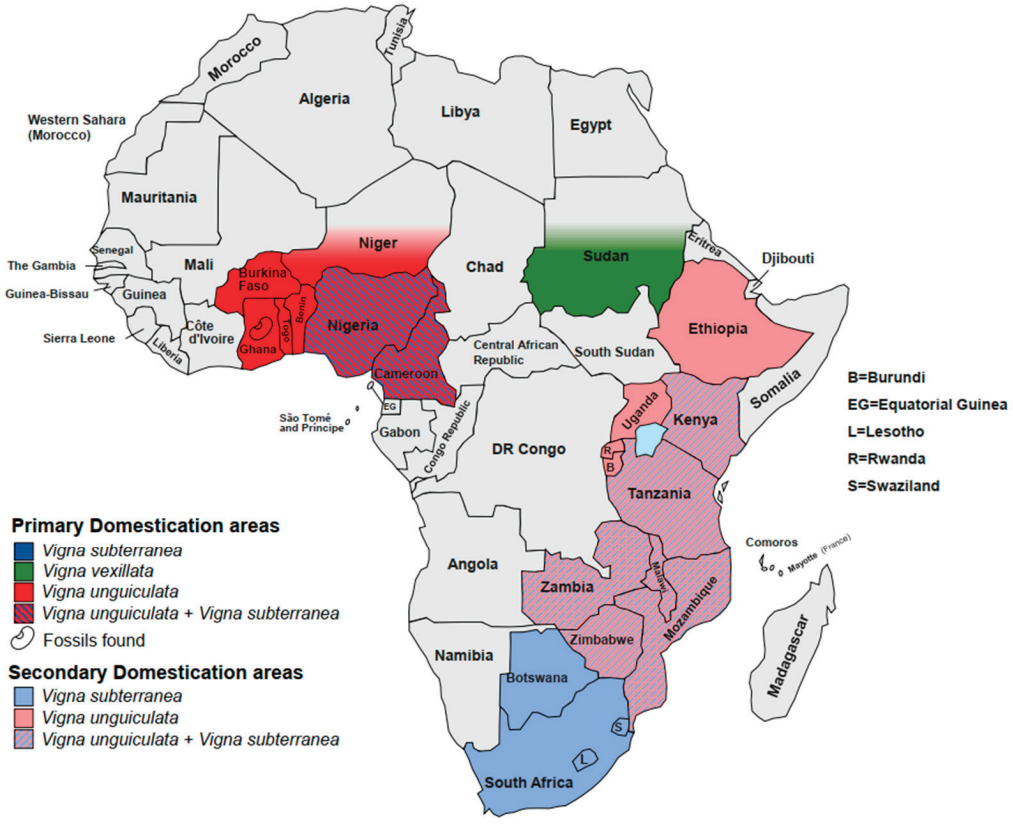

Figure 1. Primary and secondary domestication sites in Africa.

Morphological and DNA markers support the idea that domestication occurred only once, but analyses on whole genomes provide evidence for more independent domestication events in Africa and diversification events out of Africa [51,87]. Analyses of genetic variability are generally applied to identify the origin of species and the groups of accessions that show high variability in certain geographic areas and are interpreted as the most ancient populations. Although cowpea from West Africa showed a high genetic

variability [88], cultivated accessions grown in East and West Africa were shown to be most closely related to the respective local wild lineages [52,89], thereby indicating that domestication could have occurred in both regions. Outside Africa, cultivated cowpea was exposed to different ecological conditions, including new biotic and abiotic stresses that probably have contributed to shaping the genetic structure of landraces. When cowpea moved through Asian regions (especially in Thailand, China, the Philippines and India), it encountered environments with more humidity and less brightness where the drying of pots and grains was hindered. Some accessions were selected for the use of the immature pods to produce a peculiar form of vegetable called yardlong bean (*V. unguiculata* ssp. *unguiculata* cv. *sesquipedalis*) [51,90,91]. Although Chinese accessions show lower genetic diversity compared to African cowpea, signals of genetic bottlenecks lead to the conclusion that a limited number of relatively recent selection events occurred;however, where the selection process arose is still unknown [92]. Moreover, other cultivar groups (e.g., 'Textilis', 'Biflora' or 'Cylindrica', 'Melanophthalmus') are classified by morphological traits [75,93]. Still, additional genomic analyses should be performed to confirm the genetic relationships and understand how and where these accessions originated [67,85,88,94,95].

3. *Vigna subterranea* (L.) Verdc.

Vigna subterranea, also named Bambara groundnut, is an indigenous African grain legume. Its common name derives from the groundnut (*Arachis hypogaea* L.) due to the hypogean pods' growth, whereas the "Bambara" name is derived from a Malian tribe [96]. Despite its potential in terms of nutritional value and resistance to biotic and abiotic stresses [97,98], Bambara is cultivated mainly in small farms or in families as a subsistence crop [99], and naturally grows in semi-arid regions in Africa. Regarding the origin of the species itself, the domesticated or semi-domesticated *Vigna subterranea* var. *subterranea* was most likely generated from its wild counterpart *Vigna subterranea* var. *spontanea* using both morphological and isozyme data [100,101].

The origin of this species is hypothesised to be in Mali, in the Timbuktu region [102], but the precise centre of origin is still unknown. In fact, there is no evidence of wild lineages in Mali [103]. Dalziel, Begemann and Goli [104–106] analysed a lot of morphologic traits such as seed morphology, seed pattern diversity and other diversity indices (number of days to maturity, pod length, number of stems per plant and internode length). They found that the most diversity is located in an area that spans from Jos Plateau and Yola Adamawa (Nigeria) to Garoua (Cameroon). Somta and Olukolu [107,108] evaluated the phylogeography of several accessions spread in Africa. The markers used (i.e., SSR and DaRT) showed a cluster with higher diversity in the area between Nigeria and Cameroon. The authors confirm the area of origin while suggesting a possible subsequent introduction of Western domesticated accessions in East Africa (Figure 1). In contrast, Aliyu et al. [97], in an overview of the past two decades of genetic diversity analysis, also proposed that the Southern African region could constitute a divergent time-spaced domestication event. However, the authors suggest that these hypotheses need further examination.

In terms of genetic diversity, Bambara has a peculiar behaviour. In fact, many authors studied Bambara's genetics with different techniques to clarify how wide the genetic pool is and how homogeneous the single landraces are. Molosiwa et al. [109] evaluated genetic distances between 24 landraces with phenotypic and genetic markers (i.e., SSR and DaRT). The main results report that landraces are different to each other, suggesting the existence of great allelic diversity among the various populations. At the same time, though, single landraces tend to be very homogeneous, and in three generations of inbreeding became pure lines. This is due mainly to its self-pollinating nature [110] but also small farmers, who, by breeding the same landraces, also acted as selection drivers [111,112]. Molosiwa [113] selected 12 SSR markers and 5 Bambara accessions to evaluate the potential for creating pure lines, finding that these accessions at the second cycle of selection completely have lost the heterozygosity.

All these findings suggest that Bambara has incredible genetic potential. The genetic screening through the different lineages and the consequent discovery of peculiar sites of interest could be the basis for an improvement of crop programs. Moreover, the use of pure lines in agriculture is fundamental not only for the optimisation and standardisation of agricultural practices but also for the development of breeding programs. Currently, to the best of our knowledge, there are no reports of ongoing improvement or breeding programs for this species. The extremely wide pool of wild and domesticated accessions can be used to create ideal crops that can better withstand climate change as well as being able to grow with low agronomic inputs.

4. *Vigna vexillata* (L.) A. Rich.

Widely distributed in Africa, Asia, America and Australia, *V. vexillata* (Zombi pea) is one the least known and underutilized *Vigna* crops. Likewise, *V. unguiculata*, Zombi pea shows a high morphological diversity probably determined by geological, ecological, climatic and anthropomorphic constraints that also determined exceptional patterns of genetic variability [19,71]. Eight varieties including *vexillata*, *angustifolia*, *ovata*, *dolichomena*, *yunnanensis*, *plurifora*, *lobatifloria* and *macrosperma* are recognized [12,19,23,114,115]. Var. *macrosperma* shows typical traits associated with domestication syndrome such as bush-like habit, early flowering and higher seed yield [116,117]. Moreover, loss of seed dormancy and various degrees of pod shattering were detected in different crop accessions while the wild seeds remained intrinsically dormant [118,119]. Several authors reported that two forms were domesticated independently (i.e., seed type and tuber type), and some evidence lines suggest that the seed type was domesticated in Sudan, whereas the tuber type was domesticated in India (Figure 1) [120–124]. However, molecular analyses were performed on a limited number of accessions and loci [124], and the phylogenetic intra-specific delimitation has resulted in much more complexity than that of other *Vigna* crops [125]. Thus, modern genomic analyses are needed to resolve the genetic relationships and confirm the origin of the two forms.

Several studies have also shown that the Zombi pea is the result of a long adaptation process to different environmental stress, including acid, alkaline, saline, drought and wet soils [115,117,126–128]. Moreover, since some accessions were found to be resistant to different viral diseases and parasite insects, widely recognized as major pests of cowpea, this species is an important harbour of resistances to various biotic stresses, particularly useful to improve modern *Vigna* crops [129–134].

5. Healthy Natural Compounds for Designing Sustainable Crops

The process of domestication was selected during the early millennia due to all the characteristics that made a species very productive or easier to harvest. Nowadays, a lot of crops varieties that have a great yield and high contents of macronutrients exist, such as carbohydrates or proteins. However, bioactive compounds that are naturally present in the *Vigna* genus were never taken into account. In a world where the main concern is no more denutrition but instead malnutrition, the adoption of crops with high-value nutraceutical compounds becomes a challenge for the next generation. The *Vigna* genus is a great source of small proteins and secondary metabolites with nutraceutical roles in everyday diet.

Often agricultural practices themselves could stimulate the production of these compounds, such as hydric stress or no tillage with cover crops fields. However, they could not be sufficient to enhance the output of bioactive molecules. In this perspective, *de novo* domestication programs should consider these compounds to develop future healthy crops. In the next paragraph, we listed and discussed some of these molecules based on the nutraceutical activity they exert against three great world concerns.

5.1. Antioxidant and Anti-Inflammatory Activity

Nowadays, inflammation and oxidative stress are becoming great concerns due to detrimental effects on human health, and diet is a powerful way to protect cells from the

rise of reactive oxygen species (ROS) as well as inflammatory processes. In this view, seeds of cowpea contain different phenols, and other pigments present in the seed coat [135] are able to promote antioxidant action; among these, quercetin and flavonols are very well represented [136]. Different works [137,138] demonstrated a clear correlation between antioxidant properties and the colour of the seed coat in different accessions of *Vigna vexillata* and *Vigna subterranea*. Sowndhararajan and Leu [139,140] identified that *Vigna vexillata* extracts three molecules with strong antioxidant properties. Daidzein, abscisic acid and quercetin were highly active and displayed a pivotal capacity to deny the inflammation pathway.

Studies performed on protein extracts of *Vigna subterranea* suggest that different protein fractions exert crucial properties against ROS relevant in cellular metabolism [141]. Furthermore, a review by Quan et al. [142] summarised how polyphenols and proteins naturally interact, providing a higher antioxidant and anti-inflammatory capacity as a result.

The presence of antioxidant compounds is clearly a good starting point for the bioprospecting approach. The research could start from accessions already studied and kept in germplasm banks, with the aim of breeding the most promising ones (e.g., more colourful, thicker coat or better nutrient profile) with domesticated landraces to create variants that are, at the same time, easy to cultivate but with the most interesting characteristics found from the available natural pool. In addition, this could lead to new experiments to understand better the synergic role of the phenolic fraction with bioactive proteins.

5.2. Anti-Tumor Compounds

Concerning the anti-cancer activity, Bowman–Birk inhibitors (BBI), present exclusively in the Fabaceae family and some cereals [143], have proven anticancer effects [144,145]. Panzeri et al. [146] demonstrated that aqueous extracts from boiled seeds containing BBI are, as expected, effective against some colorectal cancer cell lines, but the healthy line was not hit by the treatment. Mehdad et al. [147] proved its activity on breast cancer lines, and they were the first to discover a potential intracellular target, the proteasome 20S. Furthermore, they demonstrated cytostatic activity and increased apoptosis in cancer lines, but BBI was ineffective on the healthy mammary epithelial line. It is important to underline that this protein is kept by evolution due to its defensive role; in fact, it inhibits herbivores' digestion by interacting negatively with trypsin and chymotrypsin. Preliminary results obtained via the alignment of sequences downloaded from genebanks (NCBI) showed a high variability of BBI gene in some cowpea accessions, confirming the greatness of natural biodiversity. Unfortunately, little is known about the impact of domestication on the variability of the BBI gene. The domestication process can have acted as a strong constraint causing a bottleneck in the gene pool and reducing the variability of genes and exchange of alleles between cultivated and wild accessions. However, the exploration of haplotypes by sequencing several accessions is needed to verify the effective impact of human activity on gene diversity. Moreover, methods of ancestral sequence reconstruction (ASR) based on phylogenetic inference can predict the existence of stable, soluble, and active variants of proteins. The comparison of the structure of modern proteins with the corresponding ancestral intermediates can highlight functionally important substitutions within proteins and consequently drive the protein engineers to design variants that confer novel or more efficient activities (Figure 2). While different case studies are discussed in the literature where ancestral reconstructions were applied in eukaryotes, few instances are available in plants. Since ASR can be used to explore the remote evolutionary past as well as to investigate molecular evolution on shorter timescales, we argue that the proteins expressed in different genera of legumes are particularly well suited for ancestral reconstruction studies.

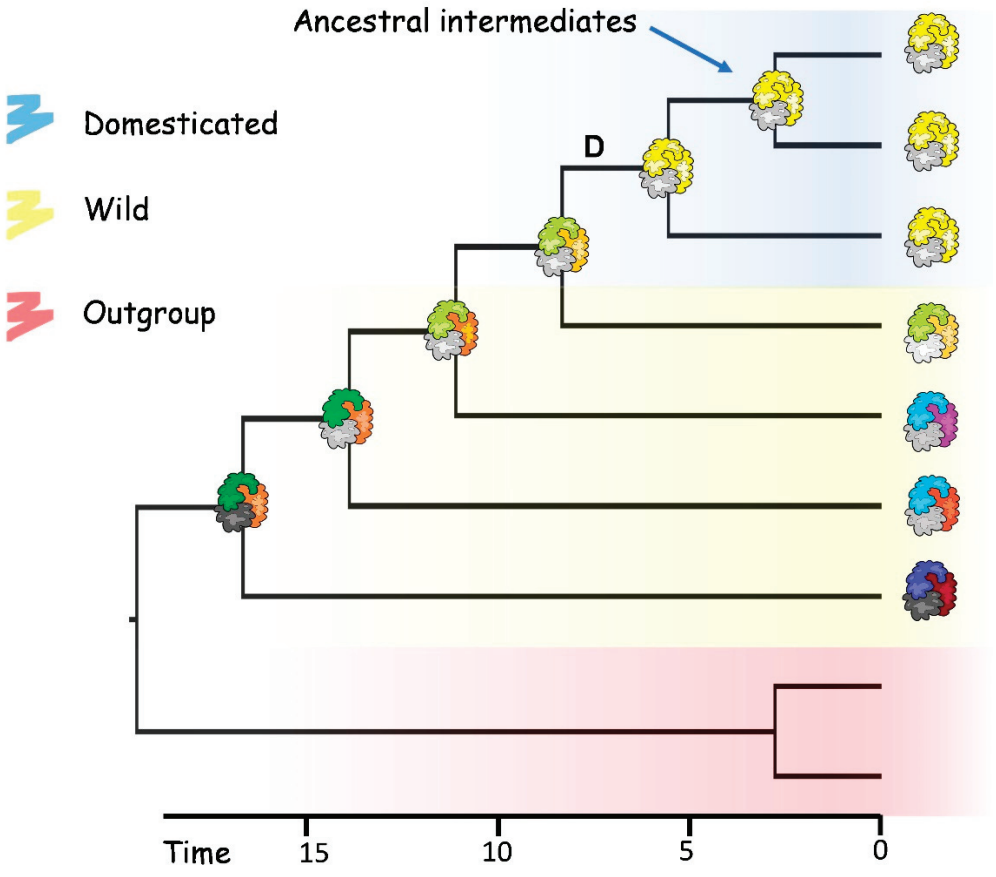

Figure 2. An example of reconstruction of putative ancestral intermediates by inferring the phylogenetic relationship between modern homologs. ASR studies can explore biodiversity to infer the historical evolution of natural proteins. Statistical models of amino acid substitution can be applied to calculate the sequences at internal nodes. Although domestication (D) has produced bottlenecks and reduced the genetic variability, ASR analyses can be applied to wild crop relatives.

Phenolic acids (e.g., gallic acid, ferulic acid, caffeic acid and chlorogenic acid) and flavonols (catechins, kaempferols and quercetins) are groups of molecules that are very active against cancer. Teixera-Guedes et al. [148] found some of these molecules in the phenolic fraction of cowpea sprouts. Sprouting is an alternative method to consume food, especially seeds, grains and pulses. As a matter of fact, sprouting refers activating the metabolism of the dormant seeds and this way, complex reserve molecules are degraded into simpler ones, releasing other molecules and secondary metabolites [149]. The authors demonstrated at first the efficacy of the extracts against CRC cell lines; then combined it with 5-Fluorouracil (5-FU). This drug is potent but is susceptible to the occurrence of resistance by the tumour mass [150]. Among all these compounds, quercetin is one of the most common, was found to be the main representative of extracts and is well known to be active against different cancer lines [151–153].

The capacity to exert different kinds of bioactivities appoints phenolics and small proteins as very potential phyto complexes with an extreme wideness of possible applications. In this paragraph, the fact that extracts can be much more effective than single drugs is underlined. The use of a mixture of bioactive compounds in addition to the chosen drug could help in the treatment of many diseases.

5.3. Anti Hypercholesterolemic

One of the major world concerns is the role of the diet for healthy living. In particular, the main problem is malnutrition, 1.9 billion adults are overweight, and 452 million are underweight [154]. These numbers are going to increase during the next few years, so a healthy diet must become a worldwide topic. One way to prevent obesity is to find food or molecules that can lower LDL cholesterol concentration or production. Legumes are known to have a good nutritional profile and possess some interesting anti hypercholesterolemic capacities. For example, in the work of Tan et al. [155], *Vigna subterranea* was the object of study to create a powdered drink mix. The authors managed to characterise the extracts and proved the ability to lower the total cholesterol content in a population of rats. The observed effects were comparable to those given by the commercial drug simvastatin, demonstrating a potential commercial formulation usable in everyday life. In addition, Bambara powder fat content was lower than the soybean, while it had more proteins. Regarding *Vigna unguiculata*, Kanetro [156] studied the hypocholesterolemic feature of protein extracts from the sprouts. The tests were performed on rats that mimicked a diabetic condition. This kind of extract established the potential of *Vigna unguiculata* in fighting high cholesterol concentrations. *Vigna unguiculata* was also studied in rabbit models by Janeesh and Abraham [157]. Rabbits received a rich fraction polyphenols and flavonoids extracted from the leaves that showed antioxidant capacity, hypolipidemic and anti-atherogenic properties in ill animals. The road opened by the studies reported here is encouraging and already tending to practical applications usable worldwide by combining the natural nutritive features to bioactive compounds present in the seeds.

Although many important bioactivities are reported in this paragraph, the actual knowledge is still incomplete. Small proteins and polyphenols were objects of these studies, and their versatility in terms of the panel of bioactivities exerted was highlighted and valorised over and over. A topic that we would like to stress more and encourage research on is the variability of seed coat colours. In fact, human activity has selected a wide range of shapes, textures and pigments in coats (including eye shapes and sizes), allowing us to clearly distinguish seeds of domestication accessions from unattractive seeds of wild lineages. The seed colours are correlated to the presence of tannins and flavonoids [158,159], and phenolic profiles showed that seed coats contain up to 10 times more flavonoids if compared to whole seeds [160]. The seed coat pattern is a fundamental aspect of consumer preference, but in different regions, only some patterns are preferred. On the other hand, local landraces contain a great variability of colours, selected through centuries by human activity, but often this richness remains undervalued [135,137,161]. Our suggestion is to use this kind of information to correlate the colours of seed coats with the proper chemical characterisation regarding previously mentioned bioactivities. Moreover, modern experimental planes should include wild accessions/species and underused landraces because these mostly unexplored taxa could hide important micronutrients. Finally, we underline that the introduction of new dishes based on a mix of seeds that show different colours could be a new way to assimilate a great variety of nutrients into the diet.

6. Introgression and Feralisation Processes

Through the domestication process, one or more populations that showed desirable traits are selected by humans producing new independent lineages. Farmers have strongly influenced the survival of these cultivated lineages that continued to diverge from wild ancestors because they were affected by different selective pressures. However, crops and their wild relatives can exchange genetic information spontaneously or through human activity. Generally, wild relatives of legumes show undesirable traits, but their genomes can hide a precious gene pool that is mostly untapped that can be recovered and reintroduced in cultivated forms.

Introgression of useful genes remains a fundamental way to improve the cultivar [162], and successful crosses mediated by humans were acquired, especially in cowpea [163]. Although domesticated cowpea is known as an inbred crop, outcrossing is reported sug-

gesting that frequency and distance can vary depending on the environment, climate, subspecies, genotype and insect involved [73,164,165]. In *Vigna unguiculata,* spontaneous introgressive events between wild perennial subspecies of the *dekindtiana* group, including accessions of var. *spontanea*, are widely described observing different morphological traits [71,84,166–168]. Molecular analysis using AFLP [74] and internal transcribed spacers [53,169,170] have confirmed the natural propensity to hybridisation between subspecies and have revealed intricate intraspecies phylogenetic relationships. Intragenomic 5S rRNA repeat unit heterogeneity was interpreted as the consequence of extensive hybridisation events [170], and recently, plastid DNA sequences have confirmed chloroplast capture events [76].

In recent decades, several researchers have tried to produce introgressive lineages obtaining interesting results and showing that the most important gene pool for breeding programs could be harboured in wild subspecies. Intraspecific hybrids obtained crossing ssp. *unguiculata* with ssp. *pubescens* and cv. *sesquipedalis* with ssp. *tenuis* have shown vigorous growth and partial fertility [171–173]. Some authors attributed the incomplete success to chromosomal disturbances that ensue in endosperms and embryos during early seed development when crosses between wild perennial accessions and domesticated cowpeas are performed [174]. However, different accessions showed diverse propensity to hybridize, and a recent study suggests that temperature and humidity also have a prevalent role in increasing the success of hybridisation [175]. A wild lineage of cowpea (TVNu-1158) collected in the Republic of Congo showed resistance to *Aphis craccivora,* surviving long after infestation [176], and was successively crossed with cowpea to produce new lineages [177]. Moreover, resistance to *Maruca vitrata* was observed in the wild lineage of ssp. *dekindtiana* (Tvnu 863) from Zimbabwe andresistance to *Clavigralla tomentosicollis* was observed in ssp. *dekindtiana* (TVnu 151) from Ghana; however, literature about their use to produce new cultivars is missing [178,179].

Limited information is available about the intraspecific introgression of *V. subterranea* and *V. vexillata*. The success of the artificial cross of Bambara is constrained by scarce pollen viability, the small size of the flower and the reduced stigma–anther separation, which improves the transfer of pollen to the stigma but at the same time complicate the emasculation process [180–183]. However, F1 and F2 lines were obtained by crossing *Vigna subterranea* var. *spontanea* (Harms) Pasquet and *Vigna subterranean* var. *subterranea* (L.) Verdc. varieties, allowing us to identify that the main morphological traits to distinguish the two forms (internode length and stems per plant) are regulated by relatively limited numbers of genes [184]. Intraspecific introgression success was also obtained by James and Lawn [185] who crossed African and Australian accessions of *V. vexillata* with the aim to explain the resistance to mottle carmovirus (CPMoV). Recently, modern hybridisation techniques were applied to cross var. *macrosperma* cultivated and wild accessions obtaining encouraging results [186,187]. Unfortunately, scarce findings are achieved by interspecific hybridisation. Differently from Asian taxa, where the compatibility was confirmed in different studies, the African taxa show a cross incompatibility barrier that has so far prevented the introgression of useful genes (e.g., *V. vexillata* × *V. unguiculata*) [168,188–190].

In recent years, advances in sequencing technologies have allowed the generation of a large number of genomic resources that, if combined with approaches that estimate the rate of gene flow, enable us to detect which lineages are prone to hybridisation. Screening the level of introgression already existing in nature is an important opportunity that can help us to obtain advanced information useful in breeding activity. For example, natural hybrid zones harbour genetic variance and, pervasive and occasional introgressive events are identified in several crops such as kiwi, common bean, soybean, sunflower and grape [191–196]. Differently from neutral introgression, which could be lost during successions of generations, adaptive introgression events are maintained by selection, and foreign gene variants introduced by gene flow can increase the fitness of receiver populations as observed in potato, rice and millet [197–199].

African *Vigna* species have a potential for introgression that today remains mostly unexplored. *V. unguiculata* and *V. vexillata* show an elevated number of wild lineages that probably have diverged well before the Pleistocene due to climate changes [71,125]. Several subspecies are adapted to different environments, and Padulosi and Ng [68] proposed that the southernmost region of Africa is presumably the origin center for *V. unguiculata* where most subspecies grow, while Pasquet [71] indicated that some lineages from Namibia to Zimbabwe are the result of spontaneous introgression events. However, genomic studies are needed to confirm these hypotheses, including in the analyses of populations spread at the margins of species distribution that could hide local adaptation to extreme conditions. Principal component analysis, Bayesian clustering methods (e.g., NEWHYBRIDS, STRUCTURE and ADMIXTURE) and divergence statistics such as FST are used to explore patterns of divergence in *Vigna* species, but they manifest shortness to provide the effective migration rate. To overcome this limitation, different probabilistic approaches recently developed are able to identify recent and ancient signals of introgression such as tree-based methods (e.g., Treemix), coalescent-with-introgression simulations (e.g., MSci model implemented in BPP), composite-likelihood test (e.g., VolcanoFinder), site frequency spectrum to explicitly model migrations (e.g., ∂a∂i), gene genealogies (e.g., Twisst) and ABBA–BABA statistics [200–204]. Moreover, only some genomic regions could be involved in gene flow, and thus introgression might be localised in specific chromosomes [205]. Since alleles shared through incomplete lineage sorting remain complex to distinguish from alleles shared through introgression and none of the measures described above is without simplifying assumptions, we suggest that different methods should be applied to ascertain the origin of introgression.

Although introgression from wild to crops has important economic consequences and many attempts are made to understand the evolutionary dynamics, in recent years, attention to the gene flow from crop to wild is rapidly increasing. Introgression of domesticated alleles can stimulate the evolution of weeds or increase the risk of extinction of wild populations with dramatic evolutionary consequences, as demonstrated in several annual and perennial plants [206–211]. Moreover, under specific circumstances, the spread of ferals escaped from cultivation and adapted to wild environments can hardly be contained. Although several authors consider feralisation the opposite process of domestication, few population genomics studies show how these genetic changes occurred in plants [212]. Some authors show that multiple de-domestication events have occurred in rice, highlighting that some crops are exceptionally prone to feralisation [213,214]. The introgression process is probably improved when the wild forms grow along the road margins, villages and fields where domesticated forms are cultivated. To date, few studies have investigated the introgression effects on the wild populations of African *Vigna* species. Some researchers have proposed that alleles from cowpea may be incorporated into wild forms especially improved by their cohabitation, replacing the original alleles and making new lineages well adapted to wild environments [215]. A molecular study based on analysis of isozyme loci showed that outcrossing rates in West Africa range from 1% to 9.5%, confirming possibilities of gene flow from domesticated cowpea to var. *spontanea* [216]. The distinction between feral and truly wild lineages is ever more complicated because introgression produces fertile offspring and the small seed-size typical of wild forms is dominant to large seed size [76,217]. Moreover, var. *spontanea* is represented by both annual and perennial plants, and it is acknowledged that while the annual and inbred habit is an adaptive strategy in dry and warm environments (e.g., in warm tropical savannas), perennials tend to grow in mountainous regions where the environment is often cooler and wetter [76]. Annual inbred plants produce more seeds and show a competitive advantage on perennials when they are sympatric in environments. Although few data about introgression are available, we cannot exclude that perennial outcrossed subspecies can be fertilized by cowpea pollen, and consequently, domesticated alleles can be introgressed. Moreover, feralisation can involve adaptive changes in genes related to flowering timing, dormancy and metabolic pathways, which are also unknown. Therefore, several aspects of the feralisation process, including the

ability to spread domesticated alleles accross long distances by seeds and pollen through mammals or birds and the predisposition to invade territories where perennial subspecies grow, should be further explored.

7. Domestication-Related Traits and *De Novo* Domestication

As described by Darwin [218], most plants subjected to intensive domestication have lost the ability to survive in the wild environment for more than a few generations. Traits selected by humans allow us to clearly distinguish a domesticated plant from its wild progenitor, and several studies were recently proposed to highlight the genes at the base of these changes. In recent years, modern genomic techniques were applied to *Vigna* germplasm, accelerating research activity and opening new avenues to identify domestication-related traits [33,161,219–221].

Among the main domesticated traits in legumes, the loss of pod shattering and increase of organ size are most relevant for breeding. In cowpea, two main quantitative trait loci (QTLs) were identified for pod shattering, whereas QTLs identified for seed weight, leaf length, leaf width and pod length were located in the same region, suggesting a potential pleiotropy that controls the organ size [177]. Lonardi et al., 2019 [222] managed to obtain the entire genome sequence in order to analyse and identify the eventual putative syntelog for organ gigantism. They found a region containing a cluster of QTLs controlling pod length, seed size, leaf length and leaf width (CPodl8, CSw8, CLl8, CLw8). Similar results were also observed in *V. vexillata* where the main domestication traits, including seed size, pod size and leaf size, were controlled only by one or a major QTL and some minor QTLs [33,90,124]. More complex is the control of seed dormancy, which is generally managed by water-impermeable layers of cells of the seed coat. In yardlong bean, a vegetable crop that has experienced divergent domestication from cowpea, six QTLs were detected for seed dormancy-related traits [90]. The seed coat pattern is an essential trait in cowpea, intensely selected by human preferences that change in the different areas of Africa. For example, pigmentation displays high variability of colours, including varied eye shapes and sizes. Recent studies show that the colour and position of the pigmentation can be defined by expression patterns, and some genes that encode for proteins involved in the flavonoid biosynthesis pathway were identified [161]. Moreover, phenotypic observations show that a lack of pigment in flowers is often correlated with a lack of pigment in the seed coat, and a gene was recently proposed to have a dual function in cowpea controlling the colour in both organs [177]. As observed for several species, the flower was involved intensely in the domestication process, and it has a fundamental trait that allows us to distinguish domesticated cowpea from their wild relatives. Recently, innovative studies focused on exploring the genetic basis of floral scent. A group of five O-methyltransferase genes involved in the biosynthesis of melatonin and located within the floral scent QTL region was identified [221]. Melatonin is recognized as an essential molecule in several plants used to interact with pollinators. Flowering timing undoubtedly plays a key role in plant adaptation and diffusion of crops because several agronomic traits such as grain quality, plant growth and plant height are directly influenced by this characteristic [223]. However, how the domestication process has affected the timing of flowering in legumes is unclear [224]. Flowering timing is a complex trait generally regulated by genetic networks. While in *Arabidopsis thaliana* L., the existence of up to 80 loci [225] was shown, in a cowpea genome-wide association study (GWAS) seven reliable SNPs were revealed that explained phenotypic variance [220]. Important agronomic implications are expected because the candidate genes could be transferred by hybridisation in crops. Early flowering accessions can mature earlier, avoiding periods of drought stress, whereas late-flowering accessions can mature later and extend the vegetative period, thereby increasing biomass production.

It is widely recognized that the study of domestication-related traits is a fundamental step that enables us to understand how to design ideal crops for the future. Throughout the process of domestication and successive breeding phases, the genetic diversity of crops was significantly reduced, and this homogeneity is becoming a serious threat. The increase

of disease and inability of adaptation to environmental changes that consequently cause an increased use of pesticides and water with a severe impact on the environment are the main issues that affect the sustainability of modern agriculture. Fernie and Yan [226] emphasized that wild species contain less deleterious allelic variants than their crops, and Smykal et al. [227], in a recent review, reported that modern cultivars have lower levels of key vitamins and micronutrients, suggesting that several wild and semi-wild African species should be *de novo* domesticated.

Unfortunately, few studies of re-domestication are available, but recent advances in gene editing combined with the decryption of pan-genomes are opening new perspectives of manipulation of genes for the creation of modern crops [228,229]. Gene editing is used to modify the function of genes already existing, incorporate new genes and delete short or large DNA fragments [230,231]. For instance, undesirable traits can be reduced or removed by intervening in genes that regulate the content of secondary metabolites, accelerating the process of domestication. Otherwise, the life cycle of cowpea could be shifted coming back from annual to perennial, as occurred for *Triticum aestivum* L. [232]. Perennial cowpea crop would show deep roots, higher water and nutrients efficiency and would not need to be sown every year.

Modern techniques such as CRISPR/Cas9 are applied successfully in several staple food crops. In *Oryza sativa* L., mutations on three yield-related genes have produced more and larger grains and erect panicles [233], whereas, in *Solanum pimpinellifolium* L., eight genes were targeted improving architectural traits, day-length insensitivity, the size and shape of fruits and content of vitamins [234,235]. Moreover, the CRISPR-Cas9 system was also used in cowpea to disrupt the symbiotic nitrogen fixation by the modification of a symbiosis receptor-like kinase (SYMRK) gene, thereby demonstrating that gene editing can be applied to the *Vigna* genus [236]. However, this technique requires that the genome is sequenced to identify the ortholog gene that controls the domestication trait [237].

African *Vigna* species are an ideal group of plants on which to apply gene-editing techniques and to produce modern crops. A great number of wild species, besides showing resistance to pests and diseases and having high nutritional values, are well adapted to diverse environmental conditions [9]. Only Angola, with 28 native *Vigna* species documented, is recognized as one of the most important sources of germplasm in the world [238]. *V. monantha* occurs in permanently dry conditions [42], whereas *V. marina* and *V. luteola* grow well in saline lands [9]. In particular, seedlings of *V. marina* can survive for several weeks in flooded conditions and high NaCl concentration [39], accumulating high levels of salt in leaves, roots and stem [41].

However, few farmers currently use these plants because of low yield and strong pod-shattering behaviour, which requires high labour during the harvest. Adaptation to extreme environments often involves multiple genes, whereas domestication-related traits are due to mutations of a single locus that affects the loss of a function. Previously reported domestication-related traits in *Vigna* seem to be controlled by a restricted number of QTLs. Thus, introducing domestication-related mutations into wild species might be preferred rather than modifying multiple genes related to complex adaptation traits. For example, the first steps of re-domestication were achieved by Takahashi [4], starting from the accessions of *Vigna stipulacea* (Lam.) Kuntze originated in Asia. The authors obtained one mutant with reduced pod shattering and three mutants with reduced seed dormancy, characterizing the respective SNPs in the candidate genes. *V. stipulacea* was selected for their fast growth, edible seeds andbroad resistance to pests and diseases. Thus, *de novo* crops can be designed to preserve several traits that nature has selected in millions of years. Moreover, in the next few years, the pan-genomes of several economically important crops will be available. The investigation by sequencing multiple individuals, including wild and domesticated accessions, will allow us to acquire full knowledge of variations at the genome level. Since it is widely accepted that the use of few reference genomes is limiting, the pan-genome of the *Vigna* species should be achieved in a short time [239,240]. Consequently, given the

large diversity of wild *Vigna* germplasm spread in Africa and the modern techniques of gene editing, great margins of genetic improvement are expected in the near future.

Author Contributions: Conceptualization, D.P., F.G., W.G.N. and M.L.; investigation, D.P. and F.G.; writing—original draft preparation, D.P. and F.G.; writing—review and editing, D.P., F.G., W.G.N. and M.L.; visualization, D.P.; supervision, F.G. and M.L. All authors have read and agreed to the published version of the manuscript.

Funding: This research received no external funding.

Data Availability Statement: Not applicable.

Conflicts of Interest: The authors declare no conflict of interest.

References

1. Kahane, R.; Hodgkin, T.; Jaenicke, H.; Hoogendoorn, C.; Hermann, M.; d'Arros Hughes, J.; Padulosi, S.; Looney, N. Agrobiodiversity for Food Security, Health and Income. *Agron. Sustain. Dev.* **2013**, *33*, 671–693. [CrossRef]
2. Hu, X.-R.; Chou, G.-X.; Zhang, C.-G. Flavonoids, Alkaloids from the Seeds of Crotalaria Pallida and Their Cytotoxicity and Anti-Inflammatory Activities. *Phytochemistry* **2017**, *143*, 64–71. [CrossRef]
3. Lam, S.-H.; Li, Y.-C.; Kuo, P.-C.; Hwang, T.-L.; Yang, M.-L.; Wang, C.-C.; Tzen, J.T. Chemical Constituents of *Vigna luteola* and Their Anti-Inflammatory Bioactivity. *Molecules* **2019**, *24*, 1371. [CrossRef]
4. Takahashi, Y.; Sakai, H.; Yoshitsu, Y.; Muto, C.; Anai, T.; Pandiyan, M.; Senthil, N.; Tomooka, N.; Naito, K. Domesticating *Vigna stipulacea*: A Potential Legume Crop with Broad Resistance to Biotic Stresses. *Front. Plant Sci.* **2019**, *10*, 1607. [CrossRef]
5. Ku, Y.-S.; Contador, C.A.; Ng, M.-S.; Yu, J.; Chung, G.; Lam, H.-M. The Effects of Domestication on Secondary Metabolite Composition in Legumes. *Front. Genet.* **2020**, *11*, 581357. [CrossRef] [PubMed]
6. Marconi, E.; Ruggeri, S.; Carnovale, E. Chemical Evaluation of Wild Under-Exploited *Vigna* spp. Seeds. *Food Chem.* **1997**, *59*, 203–212. [CrossRef]
7. Duranti, M. Grain Legume Proteins and Nutraceutical Properties. *Fitoterapia* **2006**, *77*, 67–82. [CrossRef] [PubMed]
8. Tomooka, N.; Naito, K.; Kaga, A.; Sakai, H.; Isemura, T.; Ogiso-Tanaka, E.; Iseki, K.; Takahashi, Y. Evolution, Domestication and Neo-Domestication of the Genus *Vigna*. *Plant Genet. Resour.* **2014**, *12*, S168–S171. [CrossRef]
9. Harouna, D.V.; Venkataramana, P.B.; Ndakidemi, P.A.; Matemu, A.O. Under-Exploited Wild *Vigna* Species Potentials in Human and Animal Nutrition: A Review. *Glob. Food Secur.* **2018**, *18*, 1–11. [CrossRef]
10. Boukar, O.; Belko, N.; Chamarthi, S.; Togola, A.; Batieno, J.; Owusu, E.; Haruna, M.; Diallo, S.; Umar, M.L.; Olufajo, O. Cowpea (*Vigna unguiculata*): Genetics, Genomics and Breeding. *Plant Breed.* **2019**, *138*, 415–424. [CrossRef]
11. Vigna Savi | Plants of the World Online | Kew Science. Available online: http://powo.science.kew.org/taxon/urn:lsid:ipni.org:names:325971-2 (accessed on 17 January 2022).
12. Maréchal, R. Etude Taxonomique d'un Groupe Complexe d'espèces Des Genres *Phaseolus* et *Vigna* (Papilionaceae) Sur La Base de Données Morphologiques et Polliniques, Traitées Par l'analyse Informatique. *Boissiera* **1978**, *28*, 1–273.
13. Thulin, M.; Lavin, M.; Pasquet, R.; Delgado-Salinas, A. Phylogeny and Biogeography of *Wajira* (Leguminosae): A Monophyletic Segregate of *Vigna* Centered in the Horn of Africa Region. *Syst. Bot.* **2004**, *29*, 903–920. [CrossRef]
14. Javadi, F.; Tun, Y.T.; Kawase, M.; Guan, K.; Yamaguchi, H. Molecular Phylogeny of the Subgenus *Ceratotropis* (Genus Vigna, Leguminosae) Reveals Three Eco-Geographical Groups and Late Pliocene–Pleistocene Diversification: Evidence from Four Plastid DNA Region Sequences. *Ann. Bot.* **2011**, *108*, 367–380. [CrossRef] [PubMed]
15. Delgado-Salinas, A.; Thulin, M.; Pasquet, R.; Weeden, N.; Lavin, M. *Vigna* (Leguminosae) Sensu Lato: The Names and Identities of the American Segregate Genera. *Am. J. Bot.* **2011**, *98*, 1694–1715. [CrossRef] [PubMed]
16. Lavin, M.; Herendeen, P.S.; Wojciechowski, M.F. Evolutionary Rates Analysis of Leguminosae Implicates a Rapid Diversification of Lineages during the Tertiary. *Syst. Biol.* **2005**, *54*, 575–594. [PubMed]
17. Li, H.; Wang, W.; Lin, L.; Zhu, X.; Zhu, X.; Li, J.; Chen, Z. Diversification of the Phaseoloid Legumes: Effects of Climate Change, Range Expansion and Habit Shift. *Front. Plant Sci.* **2013**, *4*, 386. [CrossRef] [PubMed]
18. Singh, B. *Cowpea: The Food Legume of the 21st Century*; John Wiley & Sons: Hoboken, NJ, USA, 2020; Volume 164.
19. Maxted, N.; Mabuza-Diamini, P.; Moss, H.; Padulosi, S.; Jarvis, A.; Guarino, L. *An Ecogeographic Study African Vigna*; International Plant Genetic Resources Institute (IPGRI): Rome, Italy, 2004; ISBN 978-92-9043-637-9.
20. Tateishi, Y. Systematics of the Species of Vigna Subgenus Ceratotropis. *Mungbean Germplasm Collect. Util. Breed. Program.* **1996**, 9–24.
21. Tomooka, N.; Maxted, N.; Thavarasook, C.; Jayasuriya, A.H.M. Two New Species, Sectional Designations and New Combinations in *Vigna* Subgenus Ceratotropis (Piper) Verdc. (Leguminosae, Phaseoleae). *Kew Bull.* **2002**, *57*, 613–624. [CrossRef]
22. Tomooka, N.; Yoon, M.S.; Doi, K.; Kaga, A.; Vaughan, D. AFLP Analysis of Diploid Species in the Genus *Vigna* Subgenus *Ceratotropis*. *Genet. Resour. Crop. Evol.* **2002**, *49*, 521–530. [CrossRef]
23. Pienaar, B.J. The *Vigna vexillata* Complex (Fabaceae) in Southern Africa. *South Afr. J. Bot.* **1991**, *57*, 236–245. [CrossRef]
24. Ladizinsky, G. Seed Dispersal in Relation to the Domestication of Middle East Legumes. *Econ. Bot.* **1979**, *33*, 284–289. [CrossRef]

25. Takahashi, Y.; Kongjaimun, A.; Muto, C.; Kobayashi, Y.; Kumagai, M.; Sakai, H.; Satou, K.; Teruya, K.; Shiroma, A.; Shimoji, M. Same Locus for Non-Shattering Seed Pod in Two Independently Domesticated Legumes, *Vigna angularis* and *Vigna unguiculata*. *Front. Genet.* **2020**, *11*, 748. [CrossRef] [PubMed]
26. Roberts, J.A.; Elliott, K.A.; Gonzalez-Carranza, Z.H. Abscission, Dehiscence, and Other Cell Separation Processes. *Annu. Rev. Plant Biol.* **2002**, *53*, 131–158. [CrossRef] [PubMed]
27. Lo, S.; Parker, T.; Muñoz-Amatriaín, M.; Berny-Mier y Teran, J.C.; Jernstedt, J.; Close, T.J.; Gepts, P. Genetic, Anatomical, and Environmental Patterns Related to Pod Shattering Resistance in Domesticated Cowpea (*Vigna unguiculata* [L.] Walp.). *J. Exp. Bot.* **2021**, *72*, 6219–6229. [CrossRef] [PubMed]
28. Parker, T.A.; Berny Mier y Teran, J.C.; Palkovic, A.; Jernstedt, J.; Gepts, P. Pod Indehiscence Is a Domestication and Aridity Resilience Trait in Common Bean. *New Phytol.* **2020**, *225*, 558–570. [CrossRef]
29. Meyer, R.S.; Purugganan, M.D. Evolution of Crop Species: Genetics of Domestication and Diversification. *Nat. Rev. Genet.* **2013**, *14*, 840–852. [CrossRef]
30. Herniter, I.A.; Muñoz-Amatriaín, M.; Lo, S.; Guo, Y.-N.; Close, T.J. Identification of Candidate Genes Controlling Black Seed Coat and Pod Tip Color in Cowpea (*Vigna unguiculata* [L.] Walp.). *G3 Genes Genomes Genet.* **2018**, *8*, 3347–3355. [CrossRef]
31. Lo, S.; Muñoz-Amatriaín, M.; Hokin, S.A.; Cisse, N.; Roberts, P.A.; Farmer, A.D.; Xu, S.; Close, T.J. A Genome-Wide Association and Meta-Analysis Reveal Regions Associated with Seed Size in Cowpea [*Vigna unguiculata* (L.) Walp.]. *Theor. Appl. Genet.* **2019**, *132*, 3079–3087. [CrossRef]
32. Seo, E.; Kim, K.; Kang, R.; Kim, G.; Park, A.; Kim, W.J.; Sun, H.; Ha, B.-K. Genome-Wide Association Study for Flowering Time in Korean Cowpea Germplasm. *Plant Breed. Biotechnol.* **2020**, *8*, 413–425. [CrossRef]
33. Amkul, K.; Somta, P.; Laosatit, K.; Wang, L. Identification of QTLs for Domestication-Related Traits in Zombi Pea [*Vigna vexillata* (L.) A. Rich.], a Lost Crop of Africa. *Front. Genet.* **2020**, *11*, 803. [CrossRef]
34. Lu, J.; Tang, T.; Tang, H.; Huang, J.; Shi, S.; Wu, C.-I. The Accumulation of Deleterious Mutations in Rice Genomes: A Hypothesis on the Cost of Domestication. *Trends Genet.* **2006**, *22*, 126–131. [CrossRef] [PubMed]
35. Zhang, H.; Mittal, N.; Leamy, L.J.; Barazani, O.; Song, B.-H. Back into the Wild—Apply Untapped Genetic Diversity of Wild Relatives for Crop Improvement. *Evol. Appl.* **2017**, *10*, 5–24. [CrossRef] [PubMed]
36. Liu, Q.; Zhou, Y.; Morrell, P.L.; Gaut, B.S. Deleterious Variants in Asian Rice and the Potential Cost of Domestication. *Mol. Biol. Evol.* **2017**, *34*, 908–924. [CrossRef] [PubMed]
37. Yokoyama, T.; Tomooka, N.; Okabayashi, M.; Kaga, A.; Boonkerd, N.; Vaughan, D.A. Variation in the Nod Gene RFLPs, Nucleotide Sequences of 16S RRNA Genes, Nod Factors, and Nodulation Abilities of Bradyrhizobium Strains Isolated from Thai *Vigna* Plants. *Can. J. Microbiol.* **2006**, *52*, 31–46. [CrossRef] [PubMed]
38. Chankaew, S.; Isemura, T.; Naito, K.; Ogiso-Tanaka, E.; Tomooka, N.; Somta, P.; Kaga, A.; Vaughan, D.A.; Srinives, P. QTL Mapping for Salt Tolerance and Domestication-Related Traits in *Vigna marina* subsp. *oblonga*, a Halophytic Species. *Theor. Appl. Genet.* **2014**, *127*, 691–702. [CrossRef]
39. Tomooka, N.; Kaga, A.; Isemura, T.; Vaughan, D.V. *Wild Crop Relatives: Genomic and Breeding Resources: Legume Crops and Forages*; Kole, C., Ed.; Springer: Berlin/Heidelberg, Germany, 2011.
40. Takahashi, Y.; Somta, P.; Muto, C.; Iseki, K.; Naito, K.; Pandiyan, M.; Natesan, S.; Tomooka, N. Novel Genetic Resources in the Genus *Vigna* Unveiled from Gene Bank Accessions. *PLoS ONE* **2016**, *11*, e0147568.
41. Yoshida, J.; Tomooka, N.; Yee Khaing, T.; Shantha, P.S.; Naito, H.; Matsuda, Y.; Ehara, H. Unique Responses of Three Highly Salt-Tolerant Wild *Vigna* Species against Salt Stress. *Plant Prod. Sci.* **2020**, *23*, 114–128. [CrossRef]
42. van Zonneveld, M.; Rakha, M.; Tan, S.y.; Chou, Y.-Y.; Chang, C.-H.; Yen, J.-Y.; Schafleitner, R.; Nair, R.; Naito, K.; Solberg, S.Ø. Mapping Patterns of Abiotic and Biotic Stress Resilience Uncovers Conservation Gaps and Breeding Potential of *Vigna* Wild Relatives. *Sci. Rep.* **2020**, *10*, 1–11.
43. Carvalho, M.d.; Halecki, W. Modeling of Cowpea (*Vigna unguiculata*) Yield and Control Insecticide Exposure in a Semi-Arid Region. *Plants* **2021**, *10*, 1074. [CrossRef]
44. Peña-Valdivia, C.B.; García-Nava, J.R.; Aguirre R, J.R.; Ybarra-Moncada, M.C.; López H, M. Variation in Physical and Chemical Characteristics of Common Bean (*Phaseolus vulgaris* L.) Grain along a Domestication Gradient. *Chem. Biodivers.* **2011**, *8*, 2211–2225. [CrossRef] [PubMed]
45. Fernández-Marín, B.; Milla, R.; Martín-Robles, N.; Arc, E.; Kranner, I.; Becerril, J.M.; García-Plazaola, J.I. Side-Effects of Domestication: Cultivated Legume Seeds Contain Similar Tocopherols and Fatty Acids but Less Carotenoids than Their Wild Counterparts. *BMC Plant Biol.* **2014**, *14*, 1–11. [CrossRef] [PubMed]
46. Larson, G.; Piperno, D.R.; Allaby, R.G.; Purugganan, M.D.; Andersson, L.; Arroyo-Kalin, M.; Barton, L.; Vigueira, C.C.; Denham, T.; Dobney, K. Current Perspectives and the Future of Domestication Studies. *Proc. Natl. Acad. Sci. USA* **2014**, *111*, 6139–6146. [CrossRef] [PubMed]
47. D'Andrea, A.C.; Kahlheber, S.; Logan, A.L.; Watson, D.J. Early Domesticated Cowpea (*Vigna unguiculata*) from Central Ghana. *Antiquity* **2007**, *81*, 686–698. [CrossRef]
48. Allaby, R.G.; Fuller, D.Q.; Brown, T.A. The Genetic Expectations of a Protracted Model for the Origins of Domesticated Crops. *Proc. Natl. Acad. Sci. USA* **2008**, *105*, 13982–13986. [CrossRef] [PubMed]
49. Purugganan, M.D.; Fuller, D.Q. Archaeological Data Reveal Slow Rates of Evolution during Plant Domestication. *Evol. Int. J. Org. Evol.* **2011**, *65*, 171–183. [CrossRef] [PubMed]

50. Engels, J.M.M.; Ebert, A.W.; Thormann, I.; De Vicente, M.C. Centres of Crop Diversity and/or Origin, Genetically Modified Crops and Implications for Plant Genetic Resources Conservation. *Genet. Resour. Crop. Evol.* **2006**, *53*, 1675–1688. [CrossRef]
51. Huynh, B.; Close, T.J.; Roberts, P.A.; Hu, Z.; Wanamaker, S.; Lucas, M.R.; Chiulele, R.; Cissé, N.; David, A.; Hearne, S. Gene Pools and the Genetic Architecture of Domesticated Cowpea. *Plant Genome* **2013**, *6*, 1–8. [CrossRef]
52. Herniter, I.A.; Muñoz-Amatriaín, M.; Close, T.J. Genetic, Textual, and Archeological Evidence of the Historical Global Spread of Cowpea (*Vigna unguiculata* [L.] Walp.). *Legume Sci.* **2020**, *2*, e57. [CrossRef]
53. Vijaykumar, A.; Saini, A.; Jawali, N. Assessment of Hybridization among Wild and Cultivated *Vigna unguiculata* Subspecies Revealed by Arbitrarily Primed Polymerase Chain Reaction Analysis. *AoB Plants* **2012**, *2012*, pls012. [CrossRef]
54. Small, E. *Top 100 Food Plants: The World's Most Important Culinary Crops*; NRC Research Press: Ottawa, ON, Canada, 2009.
55. Timko, M.P.; Ehlers, J.D.; Roberts, P.A. Cowpea. In *Pulses, Sugar and Tuber Crops*; Springer: Berlin/Heidelberg, Germany, 2007; pp. 49–67.
56. FAOSTAT. Available online: https://www.fao.org/faostat/en/#home (accessed on 17 January 2022).
57. Smith, M.R.; Veneklaas, E.; Polania, J.; Rao, I.M.; Beebe, S.E.; Merchant, A. Field Drought Conditions Impact Yield but Not Nutritional Quality of the Seed in Common Bean (*Phaseolus vulgaris* L.). *PLoS ONE* **2019**, *14*, e0217099. [CrossRef]
58. Adjei-Nsiah, S.; Kuyper, T.W.; Leeuwis, C.; Abekoe, M.K.; Cobbinah, J.; Sakyi-Dawson, O.; Giller, K.E. Farmers' Agronomic and Social Evaluation of Productivity, Yield and N 2-Fixation in Different Cowpea Varieties and Their Subsequent Residual N Effects on a Succeeding Maize Crop. *Nutr. Cycl. Agroecosyst.* **2008**, *80*, 199–209. [CrossRef]
59. Chikowo, R.; Mapfumo, P.; Nyamugafata, P.; Giller, K.E. Woody Legume Fallow Productivity, Biological N_2-Fixation and Residual Benefits to Two Successive Maize Crops in Zimbabwe. *Plant Soil* **2004**, *262*, 303–315. [CrossRef]
60. Singh, B.B.; Sharma, B. Restructuring Cowpea for Higher Yield. *Indian J. Genet.* **1996**, *56*, 389–405.
61. Boukar, O.; Fatokun, C.A.; Huynh, B.-L.; Roberts, P.A.; Close, T.J. Genomic Tools in Cowpea Breeding Programs: Status and Perspectives. *Front. Plant Sci.* **2016**, *7*, 757. [CrossRef]
62. Horn, L.; Shimelis, H.; Laing, M. Participatory Appraisal of Production Constraints, Preferred Traits and Farming System of Cowpea in the Northern Namibia: Implications for Breeding. *Legume Res. Int. J.* **2015**, *38*, 691–700. [CrossRef]
63. Boukar, O.; Massawe, F.; Muranaka, S.; Franco, J.; Maziya-Dixon, B.; Singh, B.; Fatokun, C. Evaluation of Cowpea Germplasm Lines for Protein and Mineral Concentrations in Grains. *Plant Genet. Resour.* **2011**, *9*, 515–522. [CrossRef]
64. Abadassi, J. Cowpea (*Vigna unguiculata* (L.) Walp.) Agronomic Traits Needed in Tropical Zone. *Int. J. Pure Appl. Biosci.* **2015**, *3*, 158–165.
65. Dakora, F.D.; Belane, A.K. Evaluation of Protein and Micronutrient Levels in Edible Cowpea (*Vigna unguiculata* L. Walp.) Leaves and Seeds. *Front. Sustain. Food Syst.* **2019**, *3*, 70. [CrossRef]
66. Weng, Y.; Shi, A.; Ravelombola, W.S.; Yang, W.; Qin, J.; Motes, D.; Moseley, D.O.; Chen, P. A Rapid Method for Measuring Seed Protein Content in Cowpea (*Vigna unguiculata* (L.) Walp.). *Am. J. Plant Sci.* **2017**, *8*, 2387. [CrossRef]
67. Zuluaga, D.L.; Lioi, L.; Delvento, C.; Pavan, S.; Sonnante, G. Genotyping-by-Sequencing in *Vigna unguiculata* Landraces and Its Utility for Assessing Taxonomic Relationships. *Plants* **2021**, *10*, 509. [CrossRef]
68. Padulosi, S.; Ng, N.Q. Origin, Taxonomy, and Morphology of *Vigna unguiculata* (L.) Walp. *Adv. Cowpea Res.* **1997**, 1–12.
69. Padulosi, S. Genetic Diversity, Taxonomy and Ecogeographic Survey of the Wild Relatives of Cowpea (*Vigna unguiculata* (L.) Walpers). Ph.D. Thesis, University of Louvain La Neuve, Ottignies-Louvain-la-Neuve, Belgium, 1993.
70. Pasquet, R.S. Classification Infraspécifique des Formes Spontanées de *Vigna unguiculata* (L.) Walp. (Fabaceae) à Partir de Données Morphologiques. *Bull. Du Jard. Bot. Natl. Belg. Bull. Natl. Plantentuin Van Belg.* **1993**, *62*, 127–173. [CrossRef]
71. Pasquet, R.S. Wild Cowpea (*Vigna unguiculata*) Evolution. *Adv. Legume Syst.* **1996**, *8*, 95–100.
72. Pasquet, R. A New Subspecies of *Vigna unguiculata* (Leguminosae: Papilionoideae). *Kew Bull.* **1997**, *52*, 840. [CrossRef]
73. Pasquet, R.S. Genetic Relationships among Subspecies of *Vigna unguiculata* (L.) Walp. Based on Allozyme Variation. *Theor. Appl. Genet.* **1999**, *98*, 1104–1119. [CrossRef]
74. Coulibaly, S.; Pasquet, R.S.; Papa, R.; Gepts, P. AFLP Analysis of the Phenetic Organization and Genetic Diversity of *Vigna unguiculata* L. Walp. Reveals Extensive Gene Flow between Wild and Domesticated Types. *Theor. Appl. Genet.* **2002**, *104*, 358–366. [CrossRef]
75. Pasquet, R. Genus *Vigna* and Cowpea (*V. unguiculata* [L.] Walp.) Taxonomy: Current Status and Prospects. In Proceedings of the Fifth World Cowpea Conference on Improving Livelihoods in the Cowpea Value Chain through Advancement in Science, Dakar, Senegal, 27 September–1 October 2010.
76. Pasquet, R.S.; Feleke, Y.; Gepts, P. Cowpea [*Vigna unguiculata* (L.) Walp.] Maternal Lineages, Chloroplast Captures, and Wild Cowpea Evolution. *Genet. Resour. Crop. Evol.* **2021**, *68*, 2799–2812. [CrossRef]
77. Lush, W.M.; Evans, L.T.; Wien, H.C. Environmental Adaptation of Wild and Domesticated Cowpeas (*Vigna unguiculata* (L.) Walp.). *Field Crop. Res.* **1980**, *3*, 173–187. [CrossRef]
78. Faris, D.G. The Origin and Evolution of the Cultivated Forms of *Vigna sinensis*. *Can. J. Genet. Cytol.* **1965**, *7*, 433–452. [CrossRef]
79. Vaillancourt, R.E.; Weeden, N.F. Chloroplast DNA Polymorphism Suggests Nigerian Center of Domestication for the Cowpea, *Vigna unguiculata* (Leguminosae). *Am. J. Bot.* **1992**, *79*, 1194–1199. [CrossRef]
80. Lush, W.M.; Evans, L.T. The Domestication and Improvement of Cowpeas (*Vigna unguiculata* (L.) W Alp.). *Euphytica* **1981**, *30*, 579–587. [CrossRef]

81. Champion, L.; Fuller, D.Q.; Ozainne, S.; Huysecom, É.; Mayor, A. Agricultural Diversification in West Africa: An Archaeobotanical Study of the Site of Sadia (Dogon Country, Mali). *Archaeol. Anthropol. Sci.* **2021**, *13*, 60. [CrossRef] [PubMed]
82. Vavilov, N.I. Centers of Origin of Cultivated Plants. In *Origin and Geography of Cultivated Plants*; Cambridge University Press: Cambridge, UK, 1926.
83. Faris, D.G. *Evidence for the West African Origin of* Vigna sinensis *(L.) Savi*; University of California: Davis, CA, USA, 1963.
84. Rawal, K.M. Natural Hybridization among Wild, Weedy and Cultivated *Vigna unguiculata* (L.) Walp. *Euphytica* **1975**, *24*, 699–707. [CrossRef]
85. Ba, F.S.; Pasquet, R.S.; Gepts, P. Genetic Diversity in Cowpea [*Vigna unguiculata* (L.) Walp.] as Revealed by RAPD Markers. *Genet. Resour. Crop. Evol.* **2004**, *51*, 539–550. [CrossRef]
86. Fang, J.; Chao, C.-C.T.; Roberts, P.A.; Ehlers, J.D. Genetic Diversity of Cowpea [*Vigna unguiculata* (L.) Walp.] in Four West African and USA Breeding Programs as Determined by AFLP Analysis. *Genet. Resour. Crop. Evol.* **2007**, *54*, 1197–1209. [CrossRef]
87. Xiong, H.; Shi, A.; Mou, B.; Qin, J.; Motes, D.; Lu, W.; Ma, J.; Weng, Y.; Yang, W.; Wu, D. Genetic Diversity and Population Structure of Cowpea (*Vigna unguiculata* L. Walp.). *PLoS ONE* **2016**, *11*, e0160941. [CrossRef]
88. Muñoz-Amatriaín, M.; Lo, S.; Herniter, I.; Boukar, O.; Fatokun, C.; Carvalho, E.; Castro, I.; Guo, Y.; Huynh, B.; Roberts, P.A. The UCR Minicore: A Valuable Resource for Cowpea Research and Breeding. *Legume Sci.* **2021**, *3*, e95. [CrossRef]
89. Sarr, A.; Bodian, A.; Gbedevi, K.M.; Ndir, K.N.; Ajewole, O.O.; Gueye, B.; Foncéka, D.; Diop, E.A.; Diop, B.M.; Cissé, N. Genetic Diversity and Population Structure Analyses of Wild Relatives and Cultivated Cowpea (*Vigna unguiculata* (L.) Walp.) from Senegal Using Simple Sequence Repeat Markers. *Plant Mol. Biol. Rep.* **2021**, *39*, 112–124. [CrossRef]
90. Kongjaimun, A.; Kaga, A.; Tomooka, N.; Somta, P.; Vaughan, D.A.; Srinives, P. The Genetics of Domestication of Yardlong Bean, *Vigna unguiculata* (L.) Walp. ssp. *unguiculata* Cv.-Gr. *sesquipedalis*. *Ann. Bot.* **2012**, *109*, 1185–1200. [CrossRef]
91. Xu, P.; Wu, X.; Wang, B.; Luo, J.; Liu, Y.; Ehlers, J.D.; Close, T.J.; Roberts, P.A.; Lu, Z.; Wang, S. Genome Wide Linkage Disequilibrium in Chinese Asparagus Bean (*Vigna unguiculata* ssp. *sesquipedialis*) Germplasm: Implications for Domestication History and Genome Wide Association Studies. *Heredity* **2012**, *109*, 34–40. [CrossRef]
92. Xu, P.; Wu, X.; Wang, B.; Liu, Y.; Qin, D.; Ehlers, J.D.; Close, T.J.; Hu, T.; Lu, Z.; Li, G. Development and Polymorphism of Vigna Unguiculata ssp. Unguiculata Microsatellite Markers Used for Phylogenetic Analysis in Asparagus Bean (*Vigna unguiculata* ssp. *sesquipedialis* (L.) Verdc.). *Mol. Breed.* **2010**, *25*, 675–684. [CrossRef]
93. Pasquet, R.S. Morphological Study of Cultivated Cowpea *Vigna unguiculata* (L.) Walp. Importance of Ovule Number and Definition of Cv Gr Melanophthalmus. *Agronomie* **1998**, *18*, 61–70. [CrossRef]
94. Pasquet, R.S. Allozyme Diversity of Cultivated Cowpea *Vigna unguiculata* (L.) Walp. *Theor. Appl. Genet.* **2000**, *101*, 211–219. [CrossRef]
95. Kongjaimun, A.; Kaga, A.; Tomooka, N.; Somta, P.; Shimizu, T.; Shu, Y.; Isemura, T.; Vaughan, D.A.; Srinives, P. An SSR-Based Linkage Map of Yardlong Bean (*Vigna unguiculata* (L.) Walp. subsp. *unguiculata* Sesquipedalis Group) and QTL Analysis of Pod Length. *Genome* **2012**, *55*, 81–92. [CrossRef] [PubMed]
96. Mubaiwa, J.; Fogliano, V.; Chidewe, C.; Linnemann, A.R. Hard-to-Cook Phenomenon in Bambara Groundnut (*Vigna subterranea* (L.) Verdc.) Processing: Options to Improve Its Role in Providing Food Security. *Food Rev. Int.* **2017**, *33*, 167–194. [CrossRef]
97. Aliyu, S.; Massawe, F.; Mayes, S. Genetic Diversity and Population Structure of Bambara Groundnut (*Vigna subterranea* (L.) Verdc.): Synopsis of the Past Two Decades of Analysis and Implications for Crop Improvement Programmes. *Genet. Resour. Crop. Evol.* **2016**, *63*, 925–943. [CrossRef]
98. Olayide, O.E.; Donkoh, S.A.; Ansah, I.G.K.; Adzawla, W.; O'Reilly, P.J.; Mayes, S.; Feldman, A.; Halimi, R.A.; Nyarko, G.; Ilori, C.O. *Assessing Socioeconomic Factors Influencing Production and Commercialization of Bambara Groundnut as an Indigenous Climate Resilient Crop in Nigeria*; Springer Nature: Cham, Switzerland, 2018.
99. Azam-Ali, S.; Azam-Ali, S.N.; Aguilar-Manjarrez, J.; Bannayan-Avval, M. *A Global Mapping System for Bambara Groundnut Production*; Food and Agriculture Organization: Rome, Italy, 2001; Volume 1.
100. Pasquet, R.S.; Schwedes, S.; Gepts, P. Isozyme Diversity in Bambara Groundnut. *Crop. Sci.* **1999**, *39*, 1228–1236. [CrossRef]
101. Doku, E.V.; Karikari, S.K. Operational Selection in Wild Bambara Groundnuts. *Ghana J. Sci.* **1971**, *11*, 45–56.
102. Majola, N.G.; Gerrano, A.S.; Shimelis, H. Bambara Groundnut (*Vigna subterranea* [L.] Verdc.) Production, Utilisation and Genetic Improvement in Sub-Saharan Africa. *Agronomy* **2021**, *11*, 1345. [CrossRef]
103. Mohammed, S.M. Pre-Breeding of Bambara Groundnut (*Vigna subterranea* [L.] Verdc.). Ph.D. Thesis, Abubakar Tafawa Balewa University, Bauchi, Nigeria, 2014.
104. Dalziel, J.M. *The Useful Plants of West Tropical Africa*; Royal Botanic Gardens: London, UK, 1937.
105. Begemann, F. *Ecogeographic Differentiation of Bambarra Groundnut (Vigna subterranea) in the Collection of the International Institute of Tropical Agriculture (IITA)*; Wissenschaftlicher Fachverlag; Wissenschaftlicher Fachverlag: Berlin, Germany, 1988.
106. Goli, A.E.; Begemann, F.; Ng, N.Q. *Characterisation and Evaluation of IITA'S Bambara Groundnut (Vigna subterranea (L) Verdc). Promoting the Conservation and Use of Underutilized and Neglected Crops*; International Plant Genetic Resources Institute: Rome, Italy, 1997; Volume 9, pp. 101–118.
107. Somta, P.; Chankaew, S.; Rungnoi, O.; Srinives, P. Genetic Diversity of the Bambara Groundnut (*Vigna subterranea* (L.) Verdc.) as Assessed by SSR Markers. *Genome* **2011**, *54*, 898–910. [CrossRef]

108. Olukolu, B.A.; Mayes, S.; Stadler, F.; Ng, N.Q.; Fawole, I.; Dominique, D.; Azam-Ali, S.N.; Abbott, A.G.; Kole, C. Genetic Diversity in Bambara Groundnut (*Vigna subterranea* (L.) Verdc.) as Revealed by Phenotypic Descriptors and DArT Marker Analysis. *Genet. Resour. Crop. Evol.* **2012**, *59*, 347–358. [CrossRef]
109. Molosiwa, O.O.; Aliyu, S.; Stadler, F.; Mayes, K.; Massawe, F.; Kilian, A.; Mayes, S. SSR Marker Development, Genetic Diversity and Population Structure Analysis of Bambara Groundnut [*Vigna subterranea* (L.) Verdc.] Landraces. *Genet. Resour. Crop. Evol.* **2015**, *62*, 1225–1243. [CrossRef]
110. Tanimu, B.; Aliyu, L. Bambara Groundnut, *Vigna subterranea* (L.) verdc. In Proceedings of the Workshop on Conservation and Improvement of Bambara Groundnut, Harare, Zimbabwe, 14–16 November 1995; Country Report: Northern Nigeria; Promoting the Conservation and Use of Underutilized and Neglected Crops. International Plant Genetic Resources Institute: Rome, Italy, 1997.
111. Muhammad, I.; Rafii, M.Y.; Ramlee, S.I.; Nazli, M.H.; Harun, A.R.; Oladosu, Y.; Musa, I.; Arolu, F.; Chukwu, S.C.; Sani Haliru, B. Exploration of Bambara Groundnut (*Vigna subterranea* (L.) Verdc.), an Underutilized Crop, to Aid Global Food Security: Varietal Improvement, Genetic Diversity and Processing. *Agronomy* **2020**, *10*, 766. [CrossRef]
112. Molosiwa, O.; Basu, S.M.; Stadler, F.; Azam-Ali, S.; Mayes, S. Assessment of Genetic Variability of Bambara Groundnut (*Vigna subterranean* (L.) Verdc.) Accessions Using Morphological Traits and Molecular Markers. In Proceedings of the II International Symposium on Underutilized Plant Species: Crops for the Future-Beyond Food Security 979, Kuala Lumpur, Malaysia, 27 June1 July 2011; pp. 779–790.
113. Molosiwa, O.O. Genetic Diversity and Population Structure Analysis of Bambara Groundnuts (*Vigna subterranea* (L.) Verdc.) Landraces Using Morpho-Agronomic Characters and SSR Markers. Ph.D. Thesis, University of Nottingham, Nottingham, UK, 2012.
114. Verdcourt, B. Studies in the Leguminosae-Papilionoïdeae for the'Flora of Tropical East Africa': III. *Kew Bull.* **1970**, *24*, 379–447. [CrossRef]
115. Vanderborght, T. Some Observations on Seedlings of *Vigna vexillata* (L.) A. Rich. (Fabaceae). *Bull. Du Jard. Bot. Natl. Belg. Bull. Natl. Plantentuin Belg.* **1989**, *59*, 179–187. [CrossRef]
116. Damayanti, F.; Lawn, R.J.; Bielig, L.M. Genotypic Variation in Domesticated and Wild Accessions of the Tropical Tuberous Legume *Vigna vexillata* (L.) A. Rich. *Crop. Pasture Sci.* **2010**, *61*, 771–784. [CrossRef]
117. Dachapak, S.; Somta, P.; Poonchaivilaisak, S.; Yimram, T.; Srinives, P. Genetic Diversity and Structure of the Zombi Pea (*Vigna vexillata* (L.) A. Rich.) Gene Pool Based on SSR Marker Analysis. *Genetica* **2017**, *145*, 189–200. [CrossRef]
118. Cosmas, P.; Agathar, K.; Ronald, M.; John, C.T.; Simon, M. Preliminary Evaluation of Different Seed Dormancy Breaking Methods In Wild Tuber Cowpea (*Vigna vexillata*). *Can. J. Agric. Crop.* **2019**, *4*, 33–40. [CrossRef]
119. Tripathi, K.; Gore, P.G.; Pandey, A.; Nayar, E.R.; Gayacharan, C.; Pamarthi, R.K.; Bhardwaj, R.; Kumar, A. Morphological and Nutritional Assessment of Vigna Vexillata (L.) A. Rich.: A Potential Tuberous Legume of India. *Genet. Resour. Crop. Evol.* **2021**, *68*, 397–408. [CrossRef]
120. Ferguson, H. *The Food Crops of the Sudan and Their Relationship to Environment*; McCorquodale & Co., Ltd.: London, UK, 1954.
121. Bhattacharyya, P.K.; Ghosh, A.K.; Sanyal, B.; Deb Ray, G. Grow *Vigna vexillata* for Protein-Rich Tuber-Cum-Pulse Crop in North-Eastern Hill Region. *Seeds Farms* **1984**, *10*, 33–36.
122. Wong, K.C. *Vigna vexillata* (L.) A. Richard. PROSEA, Plant Resources of South-East Asia. *Aux. Plants* **1997**, *11*, 261–263.
123. Asati, B.S.; Yadav, D.S. Diversity of Horticultural Crops in North Eastern Region. *ENVIS Bull. Himal. Ecol.* **2004**, *12*, 1.
124. Dachapak, S.; Tomooka, N.; Somta, P.; Naito, K.; Kaga, A.; Srinives, P. QTL Analysis of Domestication Syndrome in Zombi Pea (*Vigna vexillata*), an Underutilized Legume Crop. *PLoS ONE* **2018**, *13*, e0200116. [CrossRef] [PubMed]
125. Garba, M.; Pasquet, R.S. Isozyme Diversity in *Vigna vexillata* (L.) A. Rich. (Fabaceae) Complex. *S. Afr. J. Bot.* **1998**, *64*, 163–175. [CrossRef]
126. Lawn, R.J.; Watkinson, A.R. Habitats, Morphological Diversity, and Distribution of the Genus *Vigna* Savi in Australia. *Aust. J. Agric. Res.* **2002**, *53*, 1305–1316. [CrossRef]
127. Karuniawan, A.; Iswandi, A.; Kale, P.R.; Heinzemann, J.; Grüneberg, W.J. *Vigna vexillata* (L.) A. Rich. Cultivated as a Root Crop in Bali and Timor. *Genet. Resour. Crop. Evol.* **2006**, *53*, 213–217. [CrossRef]
128. Butsayawarapat, P.; Juntawong, P.; Khamsuk, O.; Somta, P. Comparative Transcriptome Analysis of Waterlogging-Sensitive and Tolerant Zombi Pea (*Vigna vexillata*) Reveals Energy Conservation and Root Plasticity Controlling Waterlogging Tolerance. *Plants* **2019**, *8*, 264. [CrossRef]
129. Chiang, H.S.; Singh, S.R. Pod Hairs as a Factor in *Vigna vexillata* Resistance to the Pod-Sucking Bug, *Clavigralla tomentosicollis*. *Entomol. Exp. Et Appl.* **1988**, *47*, 195–199. [CrossRef]
130. Jackai, L.E.N.; Oghiakhe, S. Pod Wall Trichomes and Resistance of Two Wild Cowpea, *Vigna vexillata*, Accessions to *Maruca testualis* (Geyer) (Lepidoptera: Pyralidae) and *Clavigralla tomentosicollis* Stål (Hemiptera: Coreidae). *Bull. Entomol. Res.* **1989**, *79*, 595–605. [CrossRef]
131. Thottappilly, G.; Ng, N.Q.; Rossel, H.W. Screening Germplasm of *Vigna vexillata* for Resistance to Cowpea Mottle Virus. *Int. J. Trop. Plant Dis.* **1994**, *12*, 75–80.
132. Ogundiwin, E.A.; Thottappilly, G.; AkenOva, M.E.; Ekpo, E.J.A.; Fatokun, C.A. Resistance to Cowpea Mottle Carmovirus in *Vigna vexillata*. *Plant Breed.* **2002**, *121*, 517–520. [CrossRef]

133. Amkul, K.; Wang, L.; Somta, P.; Wang, S.; Cheng, X. Construction of a High Density Linkage Map and Genome Dissection of Bruchid Resistance in Zombi Pea (*Vigna vexillata* (L.) A. Rich.). *Sci. Rep.* **2019**, *9*, 1–10. [CrossRef] [PubMed]
134. Sodedji, F.A.K.; Agbahoungba, S.; Nguetta, S.-P.A.; Agoyi, E.E.; Ayenan, M.A.T.; Sossou, S.H.; Mamadou, C.; Assogbadjo, A.E.; Kone, D. Resistance to Legume Pod Borer (*Maruca vitrata* Fabricius) in Cowpea: Genetic Advances, Challenges, and Future Prospects. *J. Crop. Improv.* **2020**, *34*, 238–267. [CrossRef]
135. Ojwang, L.O.; Dykes, L.; Awika, J.M. Ultra Performance Liquid Chromatography–Tandem Quadrupole Mass Spectrometry Profiling of Anthocyanins and Flavonols in Cowpea (*Vigna unguiculata*) of Varying Genotypes. *J. Agric. Food Chem.* **2012**, *60*, 3735–3744. [CrossRef]
136. González, R.; Ballester, I.; López-Posadas, R.; Suárez, M.D.; Zarzuelo, A.; Martinez-Augustin, O.; Medina, F.S.D. Effects of Flavonoids and Other Polyphenols on Inflammation. *Crit. Rev. Food Sci. Nutr.* **2011**, *51*, 331–362. [CrossRef]
137. Sombié, P.A.E.D.; Compaoré, M.; Coulibaly, A.Y.; Ouédraogo, J.T.; Tignégré, J.-B.D.L.S.; Kiendrébéogo, M. Antioxidant and Phytochemical Studies of 31 Cowpeas (*Vigna unguiculata* (L. Walp.)) Genotypes from Burkina Faso. *Foods* **2018**, *7*, 143. [CrossRef]
138. Adedayo, B.C.; Anyasi, T.A.; Taylor, M.J.; Rautenbauch, F.; Roes-Hill, L.; Jideani, V.A. Phytochemical Composition and Antioxidant Properties of Methanolic Extracts of Whole and Dehulled Bambara Groundnut (*Vigna subterranea*) Seeds. *Sci. Rep.* **2021**, *11*, 14116. [CrossRef]
139. Sowndhararajan, K.; Siddhuraju, P.; Manian, S. Antioxidant and Free Radical Scavenging Capacity of the Underutilized Legume, *Vigna vexillata* (L.) A. Rich. *J. Food Compos. Anal.* **2011**, *24*, 160–165. [CrossRef]
140. Leu, Y.-L.; Hwang, T.-L.; Kuo, P.-C.; Liou, K.-P.; Huang, B.-S.; Chen, G.-F. Constituents from *Vigna vexillata* and Their Anti-Inflammatory Activity. *Int. J. Mol. Sci.* **2012**, *13*, 9754–9768. [CrossRef] [PubMed]
141. Arise, A.K.; Alashi, A.M.; Nwachukwu, I.D.; Ijabadeniyi, O.A.; Aluko, R.E.; Amonsou, E.O. Antioxidant Activities of Bambara Groundnut (*Vigna subterranea*) Protein Hydrolysates and Their Membrane Ultrafiltration Fractions. *Food Funct.* **2016**, *7*, 2431–2437. [CrossRef]
142. Quan, T.H.; Benjakul, S.; Sae-leaw, T.; Balange, A.K.; Maqsood, S. Protein–Polyphenol Conjugates: Antioxidant Property, Functionalities and Their Applications. *Trends Food Sci. Technol.* **2019**, *91*, 507–517. [CrossRef]
143. James, A.M. Evolutionary Insights into Two Plant Protein Families: Bowman-Birk Inhibitors and Asparaginyl Endopeptidases. Ph.D. Thesis, University of Victoria, Victoria, BC, Canada, 2017.
144. Clemente, A.; del Carmen Arques, M. Bowman-Birk Inhibitors from Legumes as Colorectal Chemopreventive Agents. *World J. Gastroenterol. WJG* **2014**, *20*, 10305. [CrossRef]
145. Clemente, A.; Olias, R. Beneficial Effects of Legumes in Gut Health. *Curr. Opin. Food Sci.* **2017**, *14*, 32–36. [CrossRef]
146. Panzeri, D.; Guzzetti, L.; Sacco, G.; Tedeschi, G.; Nonnis, S.; Airoldi, C.; Labra, M.; Fusi, P.; Forcella, M.; Regonesi, M.E. Effectiveness of *Vigna unguiculata* Seed Extracts in Preventing Colorectal Cancer. *Food Funct.* **2020**, *11*, 5853–5865. [CrossRef]
147. Mehdad, A.; Brumana, G.; Souza, A.A.; Barbosa, J.; Ventura, M.M.; De Freitas, S. A Bowman–Birk Inhibitor Induces Apoptosis in Human Breast Adenocarcinoma through Mitochondrial Impairment and Oxidative Damage Following Proteasome 20S Inhibition. *Cell Death Discov.* **2016**, *2*, 1–10. [CrossRef]
148. Teixeira-Guedes, C.I.; Oppolzer, D.; Barros, A.I.; Pereira-Wilson, C. Phenolic Rich Extracts from Cowpea Sprouts Decrease Cell Proliferation and Enhance 5-Fluorouracil Effect in Human Colorectal Cancer Cell Lines. *J. Funct. Foods* **2019**, *60*, 103452. [CrossRef]
149. Guo, X.; Li, T.; Tang, K.; Liu, R.H. Effect of Germination on Phytochemical Profiles and Antioxidant Activity of Mung Bean Sprouts (*Vigna radiata*). *J. Agric. Food Chem.* **2012**, *60*, 11050–11055. [CrossRef]
150. Rejhová, A.; Opattová, A.; Čumová, A.; Slíva, D.; Vodička, P. Natural Compounds and Combination Therapy in Colorectal Cancer Treatment. *Eur. J. Med. Chem.* **2018**, *144*, 582–594. [CrossRef]
151. Xavier, C.P.; Lima, C.F.; Preto, A.; Seruca, R.; Fernandes-Ferreira, M.; Pereira-Wilson, C. Luteolin, Quercetin and Ursolic Acid Are Potent Inhibitors of Proliferation and Inducers of Apoptosis in Both KRAS and BRAF Mutated Human Colorectal Cancer Cells. *Cancer Lett.* **2009**, *281*, 162–170. [CrossRef]
152. Yang, L.; Liu, Y.; Wang, M.; Qian, Y.; Dong, X.; Gu, H.; Wang, H.; Guo, S.; Hisamitsu, T. Quercetin-Induced Apoptosis of HT-29 Colon Cancer Cells via Inhibition of the Akt-CSN6-Myc Signaling Axis. *Mol. Med. Rep.* **2016**, *14*, 4559–4566. [CrossRef]
153. Reyes-Farias, M.; Carrasco-Pozo, C. The Anti-Cancer Effect of Quercetin: Molecular Implications in Cancer Metabolism. *Int. J. Mol. Sci.* **2019**, *20*, 3177. [CrossRef]
154. Fact Sheets—Malnutrition. Available online: https://www.who.int/news-room/fact-sheets/detail/malnutrition (accessed on 17 January 2022).
155. Tan, W.-C.; Tan, C.-H.; Nyam, K.-L.; Tan, C.-P.; Julkifle, A. Nutritive Bambara Groundnut Powdered Drink Mix: Characterization and in-Vivo Assessment of the Cholesterol-Lowering Effect. *J. Food Sci. Technol.* **2021**, *58*, 2992–3000. [CrossRef]
156. Kanetro, B. Hypocholesterolemic Properties of Protein Isolate from Cowpeas (*Vigna unguiculata*) Sprout in Normal and Diabetic Rats. *Procedia Food Sci.* **2015**, *3*, 112–118. [CrossRef]
157. Janeesh, P.A.; Abraham, A. Amelioration of Cholesterol Induced Atherosclerosis by Normalizing Gene Expression, Cholesterol Profile and Antioxidant Enzymes by *Vigna unguiculata*. *Plant Foods Hum. Nutr.* **2013**, *68*, 118–123. [CrossRef]
158. Lattanzio, V.; Cardinali, A.; Linsalata, V.; Perrino, P.; Ng, N.Q. A Chemosystematic Study of the Flavonoids of *Vigna*. *Genet. Resour. Crop. Evol.* **1996**, *43*, 493–504. [CrossRef]
159. Lattanzio, V.; Terzano, R.; Cicco, N.; Cardinali, A.; Venere, D.D.; Linsalata, V. Seed Coat Tannins and Bruchid Resistance in Stored Cowpea Seeds. *J. Sci. Food Agric.* **2005**, *85*, 839–846. [CrossRef]

160. Gutiérrez-Uribe, J.A.; Romo-Lopez, I.; Serna-Saldívar, S.O. Phenolic Composition and Mammary Cancer Cell Inhibition of Extracts of Whole Cowpeas (*Vigna unguiculata*) and Its Anatomical Parts. *J. Funct. Foods* **2011**, *3*, 290–297. [CrossRef]
161. Herniter, I.A.; Lo, R.; Muñoz-Amatriaín, M.; Lo, S.; Guo, Y.-N.; Huynh, B.-L.; Lucas, M.; Jia, Z.; Roberts, P.A.; Lonardi, S. Seed Coat Pattern QTL and Development in Cowpea (*Vigna unguiculata* [L.] Walp.). *Front. Plant Sci.* **2019**, *10*, 1346. [CrossRef]
162. Gaiero, P.; Speranza, P.; de Jong, H. Introgressive Hybridization in Potato Revealed by Novel Cytogenetic and Genomic Technologies. *Am. J. Potato Res.* **2018**, *95*, 607–621. [CrossRef]
163. Aliyu, B. Crossability of *Vigna rhomboidea* Burtt. Davy with Cowpea (*V. unguiculata* (L.) Walp.). *Genet. Resour. Crop. Evol.* **2005**, *52*, 447–453. [CrossRef]
164. Fatokun, C.A.; Ng, Q. Outcrossing in Cowpea. *J. Food Agric. Environ.* **2007**, *5*, 334–338.
165. Pasquet, R.S.; Peltier, A.; Hufford, M.B.; Oudin, E.; Saulnier, J.; Paul, L.; Knudsen, J.T.; Herren, H.R.; Gepts, P. Long-Distance Pollen Flow Assessment through Evaluation of Pollinator Foraging Range Suggests Transgene Escape Distances. *Proc. Natl. Acad. Sci. USA* **2008**, *105*, 13456–13461. [CrossRef]
166. Sakupwanya, S.; Mithen, R.; Mutangandura-Mhlanga, T. *Studies on the African Vigna Genepool. II. Hybridization Studies with Vigna unguiculata var. tenuis and var. stenophylla. Bulletin des Ressources Genetiques Vegetales (CIRP/FAO)*; Noticiario de Recursos Geneticos Vegetales (CIRF/FAO): Roma, Italy, 1989.
167. Mithen, R.; Kibblewhite, H. Taxonomy and ecology of *Vigna unguiculata* (Leguminosae—Papilionoideae) in south-central africa. *Kirkia* **1993**, *14*, 100–113.
168. Fatokun, C.A. Wide Hybridization in Cowpea: Problems and Prospects. *Euphytica* **1991**, *54*, 137–140. [CrossRef]
169. Vijaykumar, A.; Saini, A.; Jawali, N. Phylogenetic Analysis of Subgenus *Vigna* Species Using Nuclear Ribosomal RNA ITS: Evidence of Hybridization among *Vigna unguiculata* Subspecies. *J. Hered.* **2010**, *101*, 177–188. [CrossRef]
170. Vijaykumar, A.; Saini, A.; Jawali, N. Molecular Characterization of Intergenic Spacer Region of 5S Ribosomal RNA Genes in Subgenus Vigna: Extensive Hybridization among V. Unguiculata Subspecies. *Plant Syst. Evol.* **2011**, *294*, 39–55. [CrossRef]
171. Fatokun, C.A.; Singh, B.B. Interspecific Hybridization between *Vigna pubescens* and *V. unguiculata* (L.) Walp. through Embryo Rescue. *Plant Cell Tissue Organ Cult.* **1987**, *9*, 229–233. [CrossRef]
172. Fatokun, C.A.; Perrino, P.; Ng, N.Q. Wide Crossing in African *Vigna* Species. *Adv. Cowpea Res.* **1997**, 50–57.
173. Mohammed, M.S.; Russom, Z.; Abdul, S.D. Inheritance of Hairiness and Pod Shattering, Heritability and Correlation Studies in Crosses between Cultivated Cowpea (*Vigna unguiculata* (L.) Walp.) and Its Wild (var. *pubescens*) Relative. *Euphytica* **2010**, *171*, 397–407. [CrossRef]
174. Lelou, B.; Diawata, M.; Van Damme, P. A Study of Intraspecific Hybrid Lines Derived from the Reciprocal Crosses between Wild Accessions and Cultivated Cowpeas (*Vigna unguiculata* (L.) Walp.). *Afr. J. Plant Sci.* **2011**, *5*, 337–348.
175. Amusa, O.D.; Ogunkanmi, L.A.; Adetumbi, J.A.; Akinyosoye, S.T.; Bolarinwa, K.A.; Ogundipe, O.T. Intraspecific-Cross Compatibility in Cowpea (*Vigna unguiculata* (L.) Walp.). *J. Crop. Improv.* **2021**, *19*, 100–119. [CrossRef]
176. Souleymane, A.; Aken'Ova, M.E.; Fatokun, C.A.; Alabi, O.Y. Screening for Resistance to Cowpea Aphid (*Aphis craccivora* Koch) in Wild and Cultivated Cowpea (*Vigna unguiculata* L. Walp.) Accessions. *Int. J. Sci. Environ. Technol.* **2013**, *2*, 611–621.
177. Lo, S.; Muñoz-Amatriaín, M.; Boukar, O.; Herniter, I.; Cisse, N.; Guo, Y.-N.; Roberts, P.A.; Xu, S.; Fatokun, C.; Close, T.J. Identification of QTL Controlling Domestication-Related Traits in Cowpea (*Vigna unguiculata* L. Walp.). *Sci. Rep.* **2018**, *8*, 1–9. [CrossRef] [PubMed]
178. Oigiangbe, O.N.; Jackai, L.E.N.; Ewete, F.K.; Hughes, J.d.A.; Lajide, L. Reduced Consumption and Use of Pods of *Vigna* Species (Leguminosae) by *Maruca vitrata* (Lepidoptera: Pyralidae). *Afr. Entomol.* **2002**, *10*, 333–340.
179. Koona, P.; Osisanya, E.O.; Jackai, L.E.N.; Tamo, M.; Markham, R.H. Resistance in Accessions of Cowpea to the Coreid Pod-Bug *Clavigralla tomentosicollis* (Hemiptera: Coreidae). *J. Econ. Entomol.* **2002**, *95*, 1281–1288. [CrossRef]
180. Massawe, F.J.; Schenkel, W.; Basu, S.; Temba, E.M. Artificial Hybridisation in Bambara Groundnut (*Vigna subterranea* (L.) Verdc.). In Proceedings of the International Symposium on Bambara Groundnut, Botswana College of Agriculture, Gaborone, Botswana, 8–12 September 2003; pp. 8–12.
181. Suwanprasert, J.; Toojinda, T.; Srinives, P.; Chanprame, S. Hybridization Technique for Bambara Groundnut. *Breed. Sci.* **2006**, *56*, 125–129. [CrossRef]
182. Oyiga, B.C.; Uguru, M.I.; Aruah, C.B. Studies on the Floral Traits and Their Implications on Pod and Seed Yields in Bambara Groundnut [*Vigna subterrenea* (L.) Verdc]. *Aust. J. Crop. Sci.* **2010**, *4*, 91–97.
183. Onwubiko, N.I.C.; Odum, O.B.; Utazi, C.O.; Poly-Mbah, P.C. Studies on the Adaptation of Bambara Groundnut [*Vigna subterranea* (L.) Verdc] in Owerri Southeastern Nigeria. *N. Y. Sci. J.* **2011**, *4*, 60–67. [CrossRef]
184. Basu, S.; Mayes, S.; Davey, M.; Roberts, J.A.; Azam-Ali, S.N.; Mithen, R.; Pasquet, R.S. Inheritance of 'Domestication'Traits in Bambara Groundnut (*Vigna subterranea* (L.) Verdc.). *Euphytica* **2007**, *157*, 59–68. [CrossRef]
185. James, A.T.; Lawn, R.J. Inheritance of Selected Traits in Accessions of *Vigna vexillata* (L) a Rich of Australian and African Origin. *Aust. J. Bot.* **1991**, *39*, 415–429. [CrossRef]
186. Damayanti, F.; Lawn, R.J.; Bielig, L.M. Genetic Compatibility among Domesticated and Wild Accessions of the Tropical Tuberous Legume *Vigna vexillata* (L.) A. Rich. *Crop. Pasture Sci.* **2010**, *61*, 785–797. [CrossRef]
187. Damayanti, F.; Lawn, R.J.; Bielig, L.M. Expression of Qualitative and Quantitative Traits in Hybrids between Domesticated and Wild Accessions of the Tropical Tuberous Legume *Vigna vexillata* (L.) A. Rich. *Crop. Pasture Sci.* **2010**, *61*, 798–811. [CrossRef]

188. Barone, A.; Del Giudice, A.; Ng, N.Q. Barriers to Interspecific Hybridization between *Vigna unguiculata* and *Vigna vexillata*. *Sex. Plant Reprod.* **1992**, *5*, 195–200. [CrossRef]
189. Gomathinayagam, P.; Rathnaswamy, R.; Ramaswamy, N.M. Interspecific Hybridization between *Vigna unguiculata* (L.) Walp. and *V. vexillata* (L.) A. Rich. through in Vitro Embryo Culture. *Euphytica* **1998**, *102*, 203–209. [CrossRef]
190. Boukar, O.; Abberton, M.; Oyatomi, O.; Togola, A.; Tripathi, L.; Fatokun, C. Introgression Breeding in Cowpea [*Vigna Unguiculata* (L.) Walp.]. *Front. Plant Sci.* **2020**, *11*, 567425. [CrossRef]
191. Lexer, C.; Heinze, B.; Alia, R.; Rieseberg, L.H. Hybrid Zones as a Tool for Identifying Adaptive Genetic Variation in Outbreeding Forest Trees: Lessons from Wild Annual Sunflowers (*Helianthus* spp.). *For. Ecol. Manag.* **2004**, *197*, 49–64. [CrossRef]
192. Huang, H.; Liu, Y. Natural Hybridization, Introgression Breeding, and Cultivar Improvement in the Genus *Actinidia*. *Tree Genet. Genomes* **2014**, *10*, 1113–1122. [CrossRef]
193. Janzen, G.M.; Wang, L.; Hufford, M.B. The Extent of Adaptive Wild Introgression in Crops. *New Phytol.* **2019**, *221*, 1279–1288. [CrossRef]
194. Wang, X.; Chen, L.; Ma, J. Genomic Introgression through Interspecific Hybridization Counteracts Genetic Bottleneck during Soybean Domestication. *Genome Biol.* **2019**, *20*, 1–15. [CrossRef]
195. Zecca, G.; Labra, M.; Grassi, F. Untangling the Evolution of American Wild Grapes: Admixed Species and How to Find Them. *Front. Plant Sci.* **2020**, *10*, 1814. [CrossRef]
196. Chacón-Sánchez, M.I.; Martínez-Castillo, J.; Duitama, J.; Debouck, D.G. Gene Flow in *Phaseolus* Beans and Its Role as a Plausible Driver of Ecological Fitness and Expansion of Cultigens. *Front. Ecol. Evol.* **2021**, *9*, 312. [CrossRef]
197. Kovach, M.J.; Calingacion, M.N.; Fitzgerald, M.A.; McCouch, S.R. The Origin and Evolution of Fragrance in Rice (*Oryza sativa* L.). *Proc. Natl. Acad. Sci. USA* **2009**, *106*, 14444–14449. [CrossRef]
198. Hardigan, M.A.; Laimbeer, F.P.E.; Newton, L.; Crisovan, E.; Hamilton, J.P.; Vaillancourt, B.; Wiegert-Rininger, K.; Wood, J.C.; Douches, D.S.; Farré, E.M. Genome Diversity of Tuber-Bearing *Solanum* Uncovers Complex Evolutionary History and Targets of Domestication in the Cultivated Potato. *Proc. Natl. Acad. Sci. USA* **2017**, *114*, E9999–E10008. [CrossRef]
199. Burgarella, C.; Barnaud, A.; Kane, N.A.; Jankowski, F.; Scarcelli, N.; Billot, C.; Vigouroux, Y.; Berthouly-Salazar, C. Adaptive Introgression: An Untapped Evolutionary Mechanism for Crop Adaptation. *Front. Plant Sci.* **2019**, *10*, 4. [CrossRef]
200. Pickrell, J.; Pritchard, J. Inference of Population Splits and Mixtures from Genome-Wide Allele Frequency Data. *Nat. Preced.* **2012**, *8*, e1002967. [CrossRef]
201. Martin, S.H.; Davey, J.W.; Jiggins, C.D. Evaluating the Use of ABBA–BABA Statistics to Locate Introgressed Loci. *Mol. Biol. Evol.* **2015**, *32*, 244–257. [CrossRef]
202. Martin, S.H.; Van Belleghem, S.M. Exploring Evolutionary Relationships across the Genome Using Topology Weighting. *Genetics* **2017**, *206*, 429–438. [CrossRef]
203. Flouri, T.; Jiao, X.; Rannala, B.; Yang, Z. A Bayesian Implementation of the Multispecies Coalescent Model with Introgression for Phylogenomic Analysis. *Mol. Biol. Evol.* **2020**, *37*, 1211–1223. [CrossRef]
204. Setter, D.; Mousset, S.; Cheng, X.; Nielsen, R.; DeGiorgio, M.; Hermisson, J. VolcanoFinder: Genomic Scans for Adaptive Introgression. *PLoS Genet.* **2020**, *16*, e1008867. [CrossRef]
205. Hellenthal, G.; Busby, G.B.; Band, G.; Wilson, J.F.; Capelli, C.; Falush, D.; Myers, S. A Genetic Atlas of Human Admixture History. *Science* **2014**, *343*, 747–751. [CrossRef]
206. Ellstrand, N.C.; Meirmans, P.; Rong, J.; Bartsch, D.; Ghosh, A.; De Jong, T.J.; Haccou, P.; Lu, B.-R.; Snow, A.A.; Neal Stewart Jr, C. Introgression of Crop Alleles into Wild or Weedy Populations. *Annu. Rev. Ecol. Evol. Syst.* **2013**, *44*, 325–345. [CrossRef]
207. Heredia, S.M.; Ellstrand, N.C. Novel Seed Protection in the Recently Evolved Invasive, California Wild Radish, a Hybrid *Raphanus* sp. (Brassicaceae). *Am. J. Bot.* **2014**, *101*, 2043–2051. [CrossRef]
208. Page, A.M.; Daunay, M.-C.; Aubriot, X.; Chapman, M.A. Domestication of Eggplants: A Phenotypic and Genomic Insight. In *The Eggplant Genome*; Springer: Berlin/Heidelberg, Germany, 2019; pp. 193–212.
209. Grimm, A.; Sahi, V.P.; Amann, M.; Vidotto, F.; Fogliatto, S.; Devos, K.M.; Ferrero, A.; Nick, P. Italian Weedy Rice—A Case of de-Domestication? *Ecol. Evol.* **2020**, *10*, 8449–8464. [CrossRef] [PubMed]
210. Grassi, F.; De Lorenzis, G. Back to the Origins: Background and Perspectives of Grapevine Domestication. *Int. J. Mol. Sci.* **2021**, *22*, 4518. [CrossRef]
211. McAlvay, A.C.; Ragsdale, A.P.; Mabry, M.E.; Qi, X.; Bird, K.; Velasco, P.; An, H.; Pires, C.; Emshwiller, E. Brassica Rapa Domestication: Untangling Wild and Feral Forms and Convergence of Crop Morphotypes. *bioRxiv* **2021**. [CrossRef]
212. Scossa, F.; Fernie, A.R. When a Crop Goes Back to the Wild: Feralization. *Trends Plant Sci.* **2021**, *26*, 543–545. [CrossRef]
213. Cao, Q.; Lu, B.-R.; Xia, H.U.I.; Rong, J.; Sala, F.; Spada, A.; Grassi, F. Genetic Diversity and Origin of Weedy Rice (*Oryza sativa* f. *spontanea*) Populations Found in North-Eastern China Revealed by Simple Sequence Repeat (SSR) Markers. *Ann. Bot.* **2006**, *98*, 1241–1252. [CrossRef]
214. Gering, E.; Incorvaia, D.; Henriksen, R.; Conner, J.; Getty, T.; Wright, D. Getting Back to Nature: Feralization in Animals and Plants. *Trends Ecol. Evol.* **2019**, *34*, 1137–1151. [CrossRef] [PubMed]
215. Feleke, Y.; Pasquet, R.S.; Gepts, P. Development of PCR-Based Chloroplast DNA Markers That Characterize Domesticated Cowpea (*Vigna unguiculata* ssp. *unguiculata* var. *unguiculata*) and Highlight Its Crop-Weed Complex. *Plant Syst. Evol.* **2006**, *262*, 75–87. [CrossRef]

216. Kouam, E.B.; Pasquet, R.S.; Campagne, P.; Tignegre, J.-B.; Thoen, K.; Gaudin, R.; Ouedraogo, J.T.; Salifu, A.B.; Muluvi, G.M.; Gepts, P. Genetic Structure and Mating System of Wild Cowpea Populations in West Africa. *BMC Plant Biol.* **2012**, *12*, 113. [CrossRef]
217. Kouadio, D.; Echikh, N.; Toussaint, A.; Pasquet, R.S.; Baudoin, J.-P. Organization of the Gene Pool of *Vigna unguiculata* (L.) Walp.: Crosses between the Wild and Cultivated Forms of Cowpea. *Biotechnol. Agron. Soc. Environ.* **2007**, *11*, 47–57.
218. Darwin's, C. *On the Origin of Species*; John Murray: London, UK, 1859.
219. Ho, W.K.; Chai, H.H.; Kendabie, P.; Ahmad, N.S.; Jani, J.; Massawe, F.; Kilian, A.; Mayes, S. Integrating Genetic Maps in Bambara Groundnut [*Vigna subterranea* (L) Verdc.] and Their Syntenic Relationships among Closely Related Legumes. *BMC Genom.* **2017**, *18*, 1–9. [CrossRef] [PubMed]
220. Paudel, D.; Dareus, R.; Rosenwald, J.; Munoz-Amatriain, M.; Rios, E. Genome-Wide Association Study Reveals Candidate Genes for Flowering Time in Cowpea (*Vigna unguiculata* [L.] Walp.). *bioRxiv* **2021**, *12*, 667038. [CrossRef] [PubMed]
221. Lo, S.; Fatokun, C.; Boukar, O.; Gepts, P.; Close, T.J.; Muñoz-Amatriaín, M. Identification of QTL for Perenniality and Floral Scent in Cowpea (*Vigna unguiculata* [L.] Walp.). *PLoS ONE* **2020**, *15*, e0229167. [CrossRef] [PubMed]
222. Lonardi, S.; Muñoz-Amatriaín, M.; Liang, Q.; Shu, S.; Wanamaker, S.I.; Lo, S.; Tanskanen, J.; Schulman, A.H.; Zhu, T.; Luo, M.-C. The Genome of Cowpea (*Vigna unguiculata* [L.] Walp.). *Plant J.* **2019**, *98*, 767–782. [CrossRef]
223. González, A.M.; Yuste-Lisbona, F.J.; Saburido, S.; Bretones, S.; De Ron, A.M.; Lozano, R.; Santalla, M. Major Contribution of Flowering Time and Vegetative Growth to Plant Production in Common Bean as Deduced from a Comparative Genetic Mapping. *Front. Plant Sci.* **2016**, *7*, 1940. [CrossRef]
224. Gong, Z. Flowering Phenology as a Core Domestication Trait in Soybean. *J. Integr. Plant Biol.* **2020**, *62*, 546–549. [CrossRef]
225. Levy, Y.Y.; Dean, C. Control of Flowering Time. *Curr. Opin. Plant Biol.* **1998**, *1*, 49–54. [CrossRef]
226. Fernie, A.R.; Yan, J. *De Novo* Domestication: An Alternative Route toward New Crops for the Future. *Mol. Plant* **2019**, *12*, 615–631. [CrossRef]
227. Smỳkal, P.; Nelson, M.N.; Berger, J.D.; Von Wettberg, E.J. The Impact of Genetic Changes during Crop Domestication. *Agronomy* **2018**, *8*, 119. [CrossRef]
228. Khan, A.W.; Garg, V.; Roorkiwal, M.; Golicz, A.A.; Edwards, D.; Varshney, R.K. Super-Pangenome by Integrating the Wild Side of a Species for Accelerated Crop Improvement. *Trends Plant Sci.* **2020**, *25*, 148–158. [CrossRef] [PubMed]
229. Della Coletta, R.; Qiu, Y.; Ou, S.; Hufford, M.B.; Hirsch, C.N. How the Pan-Genome Is Changing Crop Genomics and Improvement. *Genome Biol.* **2021**, *22*, 1–19. [CrossRef] [PubMed]
230. Rodríguez-Leal, D.; Lemmon, Z.H.; Man, J.; Bartlett, M.E.; Lippman, Z.B. Engineering Quantitative Trait Variation for Crop Improvement by Genome Editing. *Cell* **2017**, *171*, 470–480. [CrossRef] [PubMed]
231. Xiao, A.; Wang, Z.; Hu, Y.; Wu, Y.; Luo, Z.; Yang, Z.; Zu, Y.; Li, W.; Huang, P.; Tong, X. Chromosomal Deletions and Inversions Mediated by TALENs and CRISPR/Cas in Zebrafish. *Nucleic Acids Res.* **2013**, *41*, e141. [CrossRef]
232. DeHaan, L.; Larson, S.; López-Marqués, R.L.; Wenkel, S.; Gao, C.; Palmgren, M. Roadmap for Accelerated Domestication of an Emerging Perennial Grain Crop. *Trends Plant Sci.* **2020**, *25*, 525–537. [CrossRef]
233. Li, M.; Li, X.; Zhou, Z.; Wu, P.; Fang, M.; Pan, X.; Lin, Q.; Luo, W.; Wu, G.; Li, H. Reassessment of the Four Yield-Related Genes Gn1a, DEP1, GS3, and IPA1 in Rice Using a CRISPR/Cas9 System. *Front. Plant Sci.* **2016**, *7*, 377. [CrossRef]
234. Zsögön, A.; Čermák, T.; Naves, E.R.; Notini, M.M.; Edel, K.H.; Weinl, S.; Freschi, L.; Voytas, D.F.; Kudla, J.; Peres, L.E.P. *De Novo* Domestication of Wild Tomato Using Genome Editing. *Nat. Biotechnol.* **2018**, *36*, 1211–1216. [CrossRef]
235. Li, T.; Yang, X.; Yu, Y.; Si, X.; Zhai, X.; Zhang, H.; Dong, W.; Gao, C.; Xu, C. Domestication of Wild Tomato Is Accelerated by Genome Editing. *Nat. Biotechnol.* **2018**, *36*, 1160–1163. [CrossRef]
236. Ji, J.; Zhang, C.; Sun, Z.; Wang, L.; Duanmu, D.; Fan, Q. Genome Editing in Cowpea *Vigna unguiculata* Using CRISPR-Cas9. *Int. J. Mol. Sci.* **2019**, *20*, 2471. [CrossRef]
237. Østerberg, J.T.; Xiang, W.; Olsen, L.I.; Edenbrandt, A.K.; Vedel, S.E.; Christiansen, A.; Landes, X.; Andersen, M.M.; Pagh, P.; Sandøe, P. Accelerating the Domestication of New Crops: Feasibility and Approaches. *Trends Plant Sci.* **2017**, *22*, 373–384. [CrossRef]
238. Catarino, S.; Rangel, J.; Darbyshire, I.; Costa, E.; Duarte, M.C.; Romeiras, M.M. Conservation Priorities for African *Vigna* Species: Unveiling Angola's Diversity Hotspots. *Glob. Ecol. Conserv.* **2021**, *25*, e01415. [CrossRef]
239. Tettelin, H.; Masignani, V.; Cieslewicz, M.J.; Donati, C.; Medini, D.; Ward, N.L.; Angiuoli, S.V.; Crabtree, J.; Jones, A.L.; Durkin, A.S. Genome Analysis of Multiple Pathogenic Isolates of *Streptococcus agalactiae*: Implications for the Microbial "Pan-Genome". *Proc. Natl. Acad. Sci. USA* **2005**, *102*, 13950–13955. [CrossRef] [PubMed]
240. Bayer, P.E.; Golicz, A.A.; Scheben, A.; Batley, J.; Edwards, D. Plant Pan-Genomes Are the New Reference. *Nat. Plants* **2020**, *6*, 914–920. [CrossRef] [PubMed]

plants

MDPI

Article

Ecological Networks in Urban Forest Fragments Reveal Species Associations between Native and Invasive Plant Communities

Sonali Chauhan [1,2], Gitanjali Yadav [3,*] and Suresh Babu [1,2,*]

[1] School of Human Ecology, Ambedkar University Delhi, Delhi 110006, India; sonalichauhan@aud.ac.in
[2] Centre for Urban Ecology and Sustainability (CUES), Ambedkar University Delhi, Delhi 110006, India
[3] National Institute of Plant Genome Research, New Delhi 110067, India
* Correspondence: gy@nipgr.ac.in (G.Y.); suresh@aud.ac.in (S.B.)

Abstract: Forest fragments are characteristic features of many megacities that have survived the urbanisation process and are often represented by unique assemblages of flora and fauna. Such woodlands are representations of nature in the city—often dominated by non-native and invasive species that coexist with resilient native congeners and purposefully introduced flora. These forest fragments also provide significant ecosystem services to urban society and therefore, understanding their compositional patterns is of considerable importance for conservation and management. In this work, we use a complex network approach to investigate species assemblages across six distinct urban forest fragments in the South Delhi Ridge area of the National Capital Territory, India. We generate bipartite ecological networks using conventional vegetation sampling datasets, followed by network partitioning to identify multiple cliques across the six forest fragments. Our results show that urban woodlands primarily form invasive–native associations, and that major invasive species, such as *Prosopis juliflora* and *Lantana camara* exclude each other while forming cliques. Our findings have implications for the conservation of these urban forests and highlight the importance of using network approaches in vegetation analysis.

Keywords: novel ecosystems; complex networks; tree communities; *Lantana camara*; *Prosopis juliflora*

Citation: Chauhan, S.; Yadav, G.; Babu, S. Ecological Networks in Urban Forest Fragments Reveal Species Associations between Native and Invasive Plant Communities. *Plants* **2022**, *11*, 541. https://doi.org/10.3390/plants11040541

Academic Editors: Milan S. Stankovic, Paula Baptista and Petronia Carillo

Received: 26 December 2021
Accepted: 13 February 2022
Published: 17 February 2022

Publisher's Note: MDPI stays neutral with regard to jurisdictional claims in published maps and institutional affiliations.

1. Introduction

The city of Delhi (National Capital Territory) in North India is constructed over 1100 square kilometres of erstwhile Dry Thorn Scrub Aravalli vegetation, which comprises agricultural lands and the wetlands of the Yamuna river [1]. Over the past 500 years, Delhi has been built and rebuilt several times with major changes in the landscape during the Mughal and British periods. Among these changes were general beautification efforts and the creation of parks. The Delhi Ridge Forest consists of sections known as the Northern, Central, South-Central and the Southern Delhi Ridge, all of which are fragments of the erstwhile Aravalli vegetation that survived these transformations. The 'Delhi Ridge' (as these forest fragments are referred to) thus includes remnants of the Aravalli woodlands that have survived urbanisation. The contemporary literature on ecology refers to such urban ecosystems as 'novel ecosystems' [2], in that they represent unique formations that are not fully understood by ecosystem ecologists and pose challenges to the general principles of community ecology. The Delhi Ridge Forest is known to have been overrun by invasive species such as *Prosopis juliflora* and *Lantana camara*, and much of the vegetation now consists of a combination of invasive species, exotics or agricultural escapes, apart from native Aravalli species.

Prosopis juliflora was first introduced in Delhi around the 1900s by William R. Mustoe, an expert gardener during the colonial afforestation program of Delhi [3,4]. Even post-independence, it remained an important part of greening efforts [5]. Owing to its drought tolerance and rapid growth, this species was widely introduced in several Indian states including Gujarat, Madhya Pradesh, Rajasthan and Delhi. Later on, it invaded agricultural

fields, pasturelands and forest areas [6,7]. Today it is amongst the most aggressive plant invaders and is considered a nuisance in several arid and semi-arid areas of Asia, Africa and North America. It has been reported that *Prosopis juliflora* changes the physicochemical and nutrient profiles of soils, and has allelopathic characteristics that lead to suppression of understory vegetation [8–11]. In Delhi Ridge, *Prosopis juliflora* has been cited as the main reason for the disappearance of native tree species such as *Prosopis cineraria* [11].

The history of the arrival and ecological impacts of *Lantana camara* in Delhi have not been well studied, despite this species being amongst the top 100 most invasive plants in the world [12]. It is estimated to have been introduced in the 1800s as an ornamental plant in India due to its showy flowers [13]. It is a fast-growing shrub, produces many seeds and can also propagate vegetatively. *Lantana camara* forms dense thickets that crowd out seedlings of native species, has a wide environmental tolerance range and is reported to have the allelopathic potential [14,15]. It has been reported as the most invasive weed in national parks and nature reserves of India, wherein it colonises forest gaps, periphery and other disturbed areas [14]. Urban forests and woodlands tend to be much smaller in size and have a high degree of internal fragmentation compared to the more protected reserves of non-urban regions. Accordingly, urban forests become ideal hotspots for the colonisation and spread of invasive species such as *Lantana camara*. Species distribution maps of both *Lantana camara* and *Prosopis juliflora*, with data presented on a temporal scale are publicly available in the GBIF (the Global Biodiversity Information Facility) database and interested readers can find interactive temporal distribution maps at these URLs [16,17].

Urban forests are particularly prone to invasion due to fragmentation, changes in environmental conditions, heavy pollutant load and the constant inflow of non-native species [18–20]. There is increasing evidence that urban nature plays a significant role in modulating the microclimate, and enhancing the quality of life in cities [21–23]. The actual relationship between these species however, is less known, and several questions remain unanswered. For instance, do invasive species decimate native vegetation? If so, do the present forest patches consist of singular stands of invasives? How do native species respond to the propagule pressure of invasive species? In short, this work was undertaken with the aim of understanding what kind of species associations form as a result of the combined impact of urbanisation, biological invasions and active use by local communities.

In the context of network theory, a complex network is a graph (network) with non-trivial topological features that are often associated with robust or real-world systems such as computer networks, disease networks, technological networks, climate networks and social networks [24].The use of network approaches in ecological studies has increased over the past decade but these are largely focused on mutualistic networks (plant–pollinator) of species or the stability of ecological networks in which species' interactions are already known [25–28].The novelty of this work lies in making use of a network approach to supplement traditional multivariate analyses in plant ecology for the visualisation of special assemblages. Since the early 20th century, the identification of plant communities and the patterns of their organisation have been some of the core research areas in vegetation ecology [29,30]. Ordination methods are commonly used for the identification of communities and vegetation–environment correlates using techniques such as cluster analysis, principal component analysis (PCA), non-metric multidimensional scaling (NMDS), correspondence analysis (CA), etc. These techniques are sensitive to species abundances, some of which are biased towards rare species, or species-rich areas while others are based on the assumption of linearity or appropriate for unimodal distribution. Each of these techniques has advantages and disadvantages and requires careful consideration of the various algorithms used based on the type of data; compute-intensive nature and software availability. Biplots produced by ordination techniques may be efficient in visualising community structure, but these are cumbersome in projecting large species associations and individual interactions [31–33].

In this work, we propose a novel approach of adding graph theoretical methods to detect and visualise ecological communities, and we use this approach to explore species

associations across six distinct urban forest fragments of the South Delhi Ridge. We then use network partitioning methods to identify and compare topologically significant 'cliques' formed by native and/or invasive species in these forests. Our results provide new insights into competitive exclusion apart from identifying emergent invasive species that are likely to become established in these urban ecosystems. Taken together, our work offers a new and parallel method of simultaneously investigating patterns at the level of both community and individual species.

2. Results

2.1. Study Area Networks

We identified over 5500 associations among 57 native, introduced and invasive plant species spread across the six study sites in the urban forests of the South Delhi ridge, New Delhi. These six sites have been identified as described in the Methods section and are depicted on the Delhi NCT map in Figure 1. The plants were categorised into 50 native, four invasive and three introduced (non-native) species, all of which were named and assigned short codes as listed in the Table S1. The four invasive species, along with their codes, are *Lantana camara* (LC), *Prosopis juliflora* (PJ), *Opuntia* (OP), and *Leucaena leucocephala* (LL). The three non-native introduced species include *Morus alba* (MOA; Mulberry), *Cassia tora* (CT) and *Azadirachta indica* (AI or Neem).

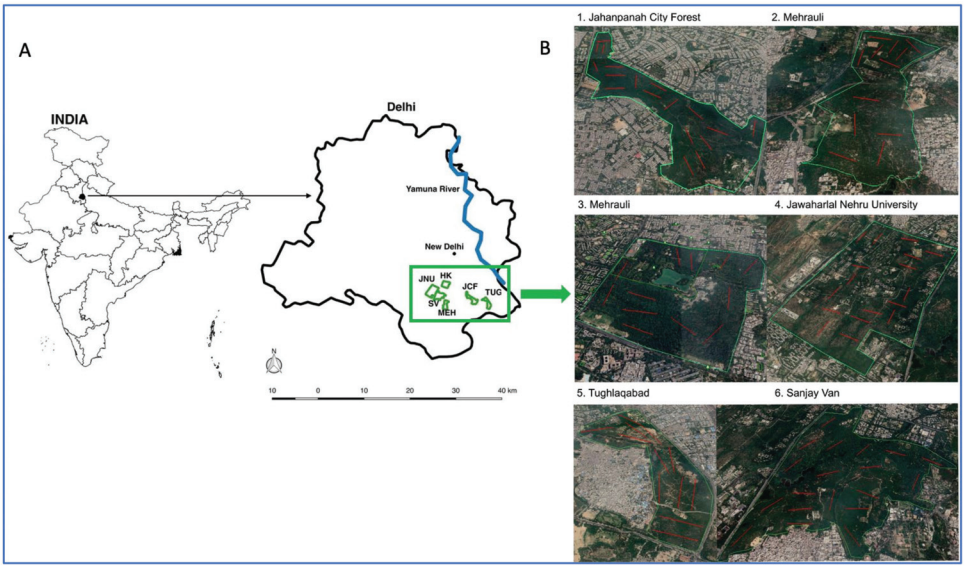

Figure 1. Study area map indicating the six urban forest fragments investigated in this work, in terms of (**A**) location and (**B**) landscape topology. Red lines in (**B**) indicate line transects placed in each sampling site using Google Earth Pro.

Each study site represents a distinct ecological community as established by a rarefaction test, and relative abundance was measured across these communities. The six graphs in Figure 2 depict ranked abundance patterns, indicating the extent to which invasive species appear to dominate each sampling site, as compared to native or introduced species. For example, one or more of the top three species in each community are invariably invasive, with three study sites (TUQ, HK and JNU) having invasive *Lantana camara* or *Prosopis juliflora* as the most abundant species in the community. In case of SV, HK and JCF, both invasive species (LC and PJ) are among the most abundant. The three introduced species are generally low in abundance, although at least one of these appears among the top five most abundant species in the TUQ, HK and MEH communities. A UPGMA-based cluster

analysis of the communities across the six sites revealed these to be roughly divisible into two groups, namely, SV-(TUQ-HK) and JCF-(JNU-MEH). These relationships are depicted as a dendrogram in Figure 3 using the Bray Curtis dissimilarity index as described in Methods. The dendrogram in Figure 3 reveals greater compositional overlap between TUQ and HK as compared to JNU and MEH, although their most abundant invasive species are distinct (TUQ forest fragment is predominated by *Prosopis juliflora* while the HK forest fragment has *Lantana camara* as the major invasive). The two remaining communities, namely, JCF and SV, are distinct in the dendrogram, but these also stand out among the other four communities, in terms of having high abundance of both *Prosopis juliflora* and *Lantana camara* as can be seen in Figure 2.

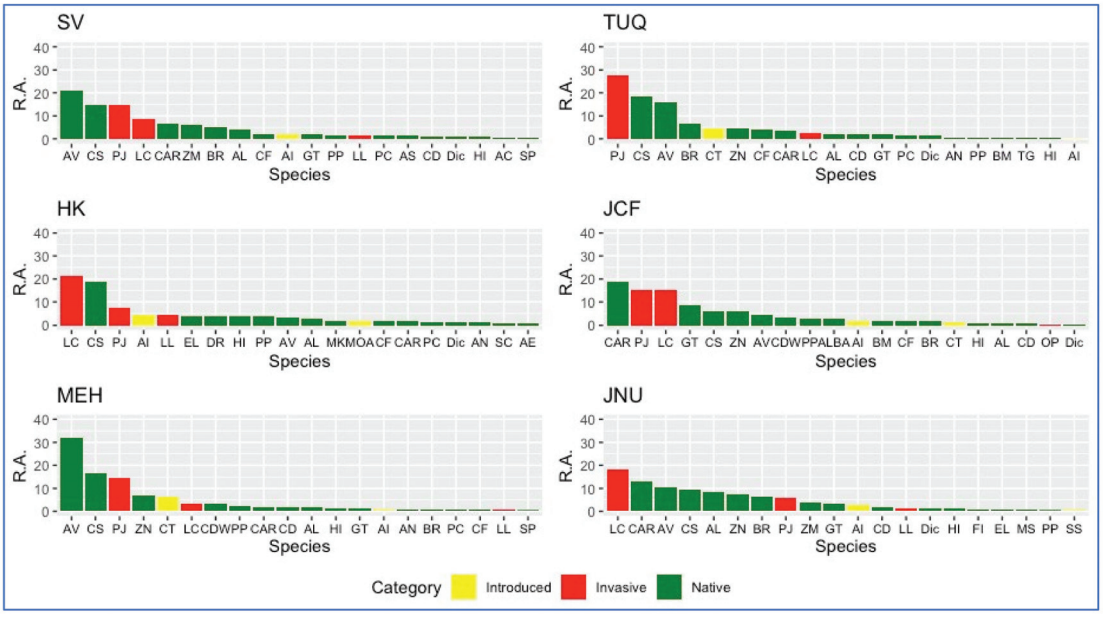

Figure 2. Ranked abundance of native (green), invasive (red) and yellow (introduced) species in each study site. For species codes, see Table S1.

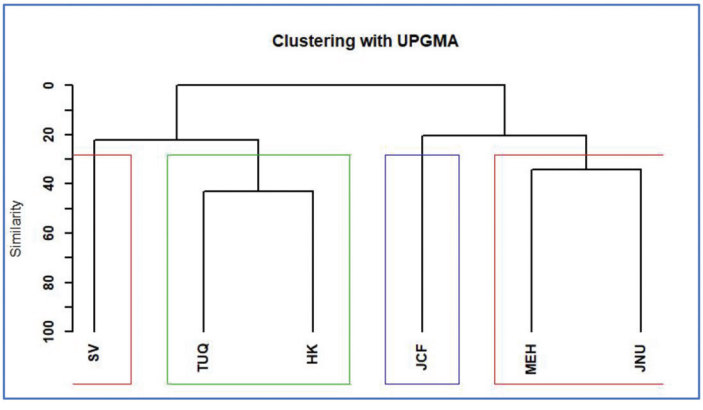

Figure 3. Cluster analysis between sampling sites using Bray Curtis dissimilarity index.

In order to understand the six forest fragments in terms of their native and invasive plant communities, we generated six bipartite species association networks, one for each forest fragment, as described in Methods. Nodes in these networks represent one of two independent sets or 'partites', namely, plants and transects, in order to retain both location and species identity. Accordingly, any two species found on a given transect were considered 'associated' in the bipartite networks, as shown in Figure 4, the study area network of Hauz Khas ridge forest (HK). As can be seen in this network, the HK forest fragment has 256 edges or associations between 49 species identified across 12 transects. Each edge in these bipartite (two-mode) networks ties a plant (green) to the location (brown) where it was found. Each node is either a transect labelled by the forest code (i.e., HK1 to HK12 in case of HK) or a woodland species that has been assigned a short code (two to four letters) based on its species and genus names (Table S1).

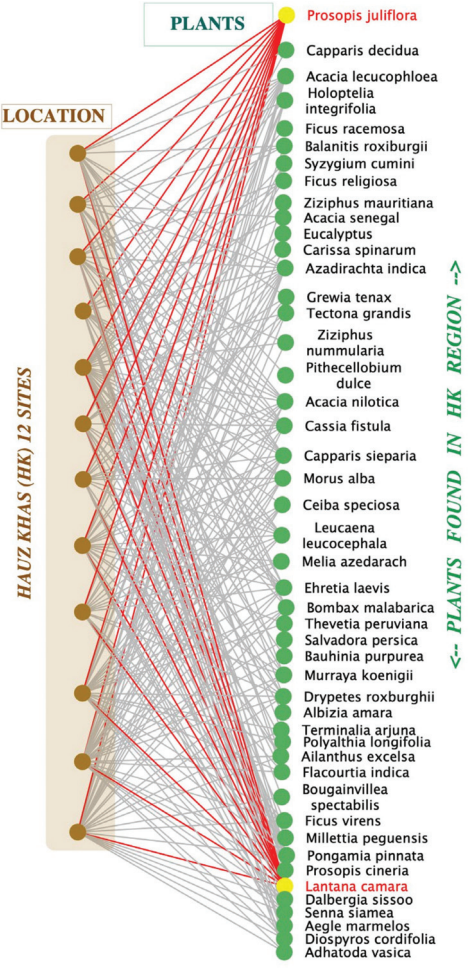

Figure 4. Bipartite species association network of Hauz Khas (HK) Forest fragment. Circles (nodes) represent plants (green) or location/transects (brown), and lines (edges) connect plants found at a location. This network has 256 associations (edges) between 49 plant species located across 12 transects of 200 m each, in the HK Ridge Forest. Note how the invasive species (yellow highlighted nodes) *Lantana camara* and *Prosopis juliflora* are present in all transects (red edges) of this forest fragment.

In general, invasive species were found to be present extensively in each forest fragment, as evidenced by their occurrence across transects. For instance, note how the invasive shrub *Lantana camara* (highlighted in yellow) is present in each of the 12 HK transects (red edges) in Figure 4. Similarly, *Prosopis juliflora* was also present in all transects investigated. In contrast, other native species such as *Acacia nilotica* (AN) or naturalised species like *Cassia tora* (CT) are often present in low numbers as evident from the relative abundance of these species across the study sites (Figure 2). This pattern holds true in each of the six forest fragments investigated and supports the theory of local decline and displacement of native species in urban forest fragments. However, the coexistence of native and invasive species needs to be investigated further to understand their associations and to explore patterns across different sites. The next section addresses this aspect to understand the nature and extent of native species displacement across the forest fragments investigated.

2.2. Distinct Native–Invasive Communities

Community detection was performed as described in Methods and we found about 25 species-specific community cliques across the six urban forest sites. Three to six distinct cliques were found in each forest fragment based on the Glay partitioning algorithm, as can be seen in Table 1. Each 'clique' is identified as a set of densely connected nodes in the network, which in turn represents woodland species comprising various combinations of native, introduced and invasive plants. Interestingly, all forest fragments in the South Delhi ridge have cliques with dominant invasive members, with two sampling sites (SV and HK) having each of the three invasive species forming their own cliques. Some native trees form communities without any invasive species, but such 'native–native' communities are few, and they tend to have fewer species than the native–invasive cliques. Another significant pattern among these species associations, in terms of invasives, is that the two most aggressive plant invaders of this region, namely, *Lantana camara* and *Prosopis juliflora* always occur in distinct communities, never together in the same clique. The correlation was tested as described in Methods and is depicted in Figure 5, revealing a significant negative association between *Lantana camara* and *Prosopis juliflora*, reaffirming that these two major invasive species of the region exclude each other, which supports the competitive exclusion theory.

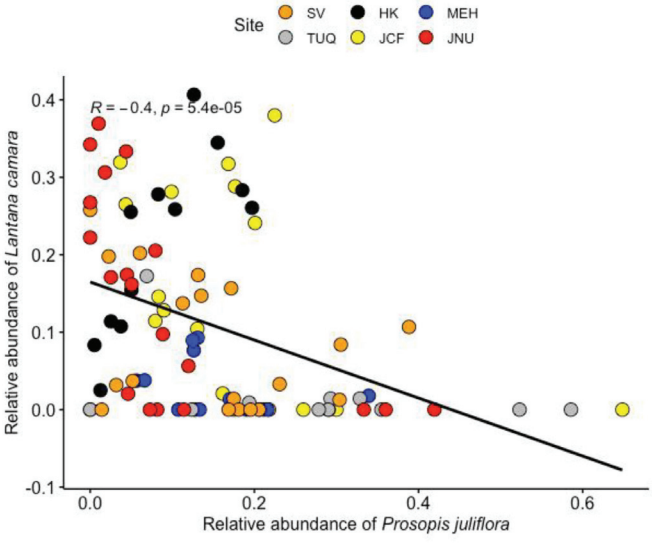

Figure 5. Correlation between the relative abundance of *Prosopis juliflora* and *Lantana camara* reveal a significant negative relationship.

Table 1. Distinct communities within urban forests show distinct 'native–invasive' and 'native–native' cliques. Invasive species are marked in bold letters.

Site	# Species	Clique	(Hub) Species in Each Community/Clique
SV	42	1	***Leucaena leucocephala***, *Cassia fistula*, *Pongamia pinnata*, *Ailanthus excelsa*, *Carissa spinarum*
		2	*Azadirachta indica*, ***Lantana camara***, *Grewia tenax*, *Holoptelea integrifolia*, *Dalbergia sissoo*
		3	*Adhatoda vasica*, *Capparis sepiaria*, *Balanites roxiburgii*
		4	*Capparis decidua*, ***Prosopis juliflora***, *Diospyros cordifolia*, *Maytenus senegalensis*
		5	*Tectona grandis*, *Acacia senegal*, *Ziziphus mauritiana*, *Prosopis cineria*
TUQ	31	1	*Balanites roxiburgii*, ***Prosopis juliflora***, *Capparis sepiaria*
		2	*Acacia nilotica*, *Cassia fistula*, *Acacia lecucophloea*, *Prosopis cineraria*
		3	*Grewia tenax*, *Holoptelea integrifolia*, *Pongamia pinnata*, *Ziziphus nummularia*, *Diospyros cordifolia*
		4	*Azadirachta indica*, *Capparis decidua*, *Adhatoda vasica*
			Lantana camara, *Bougainvillea spectabilis*
HK	50	1	*Senna siamea*, *Pongamia pinnata*, *Capparis sepiaria*, *Ehretia laevis*
		2	***Leucaena leucocephala***, *Morus alba*, *Adhatoda vasica*, *Acacia nilotica*, *Dalbergia sissoo*
		3	***Lantana camara***, *Diospyros cordifolia*, *Ziziphus nummularia*, *Azadirachta indica*
		4	*Prosopis cineraria*, *Cassia fistula*, *Grewia tenax*, *Capparis decidua*, *Murraya koenigii*, *Drypetes roxburghii*
		5	***Prosopis juliflora***, *Bombax malabarica*, *Milletia peguensis*, *Ailanthus excelsa*, *Terminalia arjuna*
JCF	49	1	*Prosopis juliflora*, *Capparis sepiaria*, *Carissa spinarum*, *Azadirachta indica*
		2	*Holoptelea integrifolia*, *Pongamia pinnata*, *Albizia amara*, *Cassia fistula*, *Senna siamea*, *Tectona grandis*, *Prosopis cineraria*
		3	***Lantana camara***, *Ziziphus nummularia*, *Bombax malabarica*
MEH	37	1	***Lantana camara***, *Adhatoda vasica*, *Acacia nilotica*, *Holoptelea integrifolia*, *Pongamia pinnata*, *Cassia fistula*
		2	*Cassia tora*, *Ziziphus nimmularia*, *Acacia lecucophloea*, *Grewia tenax*
		3	*Abutilon*, *Capparis sepiaria*, *Capparis decidua*
		4	*Azadirachta indica*, ***Prosopis juliflora***
JNU	42	1	*Balanites roxiburgii*, ***Lantana camara***, *Ziziphus nummularia*, *Ziziphus mauritiana*
		2	*Capparis decidua*, *Adhatoda vasica*, *Azadirachta indica*, *Acacia lecucophloea*
		3	***Prosopis juliflora***, *Capparis sepiaria*, *Diospyros cordifolia*

As a case study, Figure 6 shows the six species association cliques identified in the SV forest fragment, and this is one of the communities with the largest number of cliques. Of the six cliques in the SV region, three (cliques 1, 2 and 4) have a dominant invasive member. The remaining three cliques are composed of native–native species associations but the number and size of such communities that have remained invasion-free are often small, and this may have a bearing on the stability and robustness of each of the six forest fragments. In order to be able to compare the six forest fragments, and to identify ecologically meaningful species associations, each of the six partitioned networks was standardised for community analysis. Before performing any community analysis, the Cytoscape 'Glay' plugin transforms the input network into a simplified model, with edge directionality, duplication and self-looping removed. This enables network standardisation, making the resultant community structures from different community detection algorithms comparable. This was followed by identification of keynote species or hub species by using the graph theoretical clustering algorithm, MCODE, based on vertex weighting by local neighbourhood density and outward traversal from a locally dense seed node to isolate the dense regions according to given parameters. The top-ranking cliques of this forest, along with their respective hub species are listed in Table 1, with invasives highlighted in bold font. Thus, dominant species for each clique identified as 'hubs' represent trees/shrubs that tend to co-occur more often than by random chance. A pattern can be observed among the 25 cliques listed in Table 1, (as well as other smaller cliques), indicating that the two major invasives tend to avoid each other and form exclusive groups with native species. The next section addresses the specificity, if any, of such invasive–native associations.

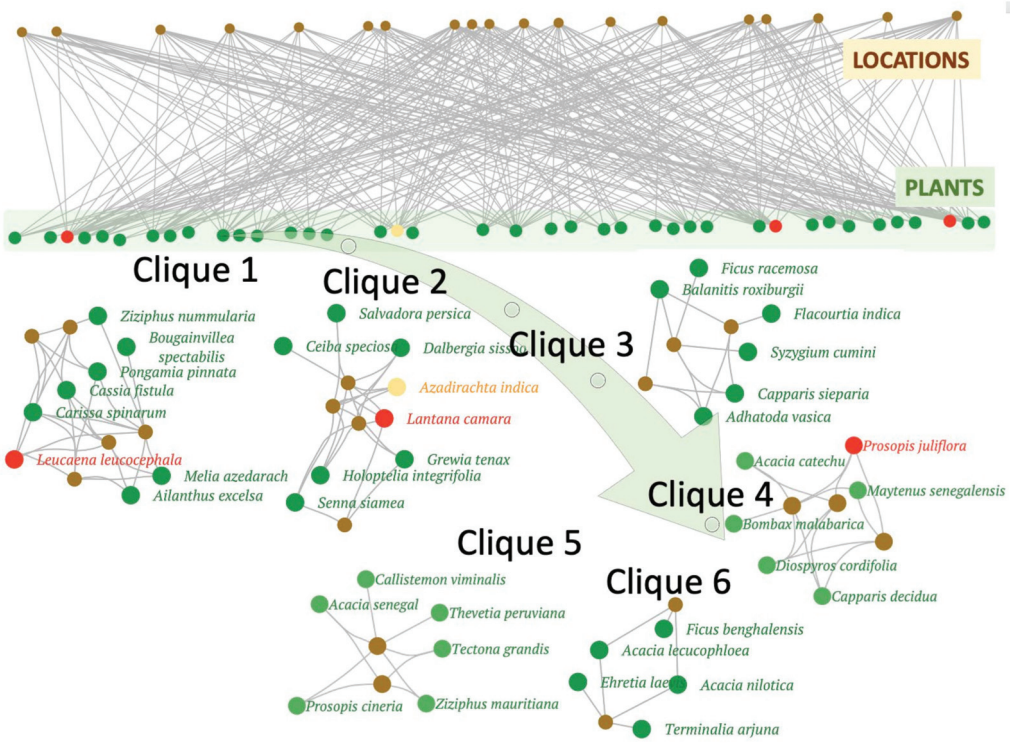

Figure 6. Community detection in the Sanjay Van (SV) Forest fragment. The upper panel depicts the complete bipartite species association network with 277 edges (grey lines) among 42 plant species (green circles) found across 19 transects (brown nodes). The lower panel depicts the six distinct cliques derived from the topology of this forest fragment, of which three are dominated by invasive (red) species *Leucaena leucocephala* (LL), *Lantana camara* (LC) and *Prosopis juliflora* (PJ).

2.3. Patterns in Species Association

Table 1 and Figure 6 in the previous section indicate how native species in urban forest fragments form distinct communities, some of which are dominated by 'hubs' that may comprise at most, one invasive species. From a management point of view, it would be interesting to understand the preference for native species, if any. The species association networks and the identified cliques of the six forest fragments enabled us to perform this analysis for each plant invader. Towards this, all 25 study area network cliques (listed in Table 1) were superimposed and the pairwise species associations of *Lantana camara* (LC) and *Prosopis juliflora* (PJ) were extracted from each community. This data was then visualised jointly in order to estimate the overlap between native species found to be associated with the two major invasives, as shown in Figure 7. Two main types of assemblages are discernible in this figure depicted in yellow and blue-shaded modules, respectively, of which the former represents the shared associations between LC and PJ, while the latter (blue) modules represent the assemblages unique to either LC or PJ. Furthermore, the nodes or species in the shared (yellow) module have lower edge weights as compared to the species in the non-shared or exclusive (blue) modules. Species that form common or shared associations include *Grewia tenax* (Gre), *Acacia leucophloea* (AL) *Acacia nilotica* (AN), as well as the three introduced species *Morus alba* (MOA; Mulberry), *Cassia tora* (CT) and *Azadirachta indica* (AI or Neem). However, it may be noted that these common woodland species are never found with 'both' LC and PJ, in the 'same' location/forest fragment.

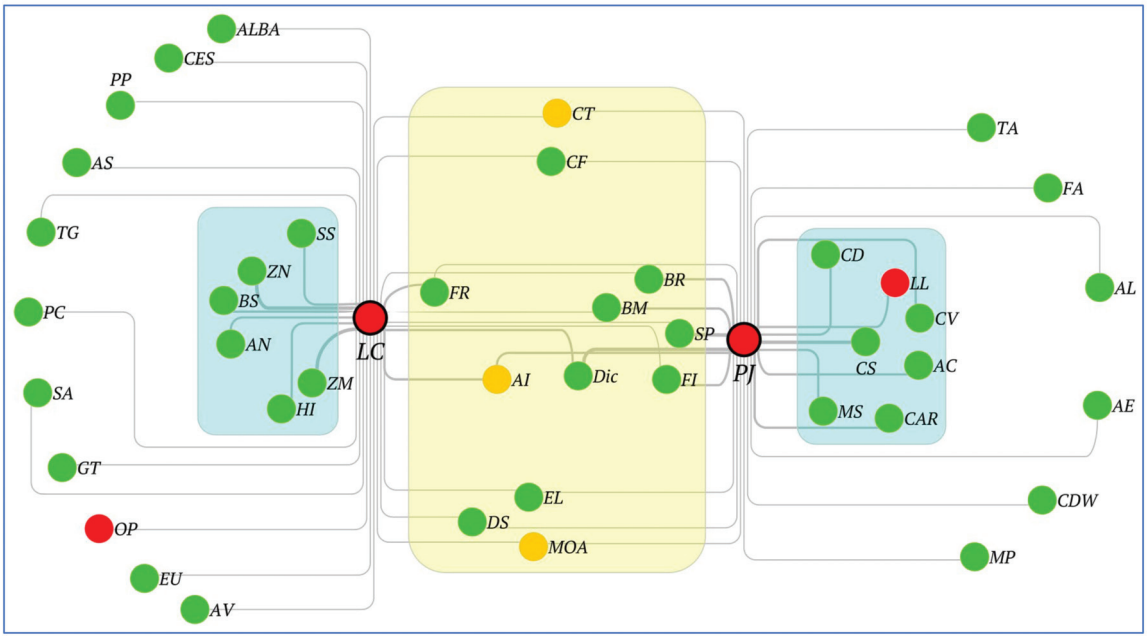

Figure 7. Distinct species associations of the two most aggressive invasives *Lantana camara* (LC) and *Prosopis juliflora* (PJ), both depicted as large red nodes with black borders. The two invasives have shared associations (yellow cluster) as well as distinct species associations with native (green), introduced (orange) species across the six investigated forest fragments. Edge weights represent the number of times a given association was observed.

Species in the blue modules of Figure 7 represent two exclusive sets of plants, preferred by *Lantana camara* and *Prosopis juliflora*, that are not shared with each other, such as for example *Carissa* (CAR) for PJ and *Tectona grandis* (Teak) for LC. Similarly, *Acacia leucophloea* is preferentially associated with *Prosopis juliflora* while *Acacia nilotica* forms species associations with *Lantana camara*. Interestingly, the invasive *Leucaena leucocephala (LL)* is present in the blue module of *Prosopis juliflora*, suggesting an invasive–invasive association that was not observed earlier in the individual study area networks. A comparison of the relative strengths of each of these two sets of associations, reveals that the blue (exclusive) modules are stronger than the shared (yellow) assemblages in terms of both module size and edge weights. This observation implies that shared associations may be transient or weak in nature, as compared to the exclusive associations formed by either *Lantana camara* or *Prosopis juliflora* in urban forests.

Looking closely at the preferential associations of these two invasive species (Figure 7) reveals some interesting insights. Firstly, the distinct sets of congeners for each invasive can further be divided into two subsets; one that is more preferred (blue module), as compared to the outer, more peripheral (white region) species with smaller edge weights, as these associations are detected less frequently. When compared with Table 1, the species in blue modules were often found among hubs in the 25 cliques. However, as noted earlier, there is not a single native species that is preferentially associated (thick edges) with both invasive species, providing further evidence for competitive exclusion, and this is discussed further in the next section. Another notable pattern from Figure 7 is that the invasive shrub *Lantana camara* tends to exclude other native shrub species and is only preferentially associated with one native shrub, i.e., *Ziziphus nummularia* (a berry). *Lantana camara* tends to form associations with small and medium-size tree species such as *Pongamia pinnata (PP)*, *Holoptelea integrifolia (HI)*, *Ziziphus mauritiana (ZM)*. On the other hand, the

invasive tree species *Prosopis juliflora* forms large groups with several native trees and shrubs and it is preferentially associated with non-native species (*Thevetia*). *Prosopis juliflora* is preferentially associated with several native trees such as *Ehretia laevis*, *Salvadora persica*, *Balanites roxburghii* and *Acacia leucophloea*. *Prosopis juliflora* forms associations with native shrubs *Capparis sepiaria*, *Adhatoda vasica*, *Carissa*. It may be noted that while *Prosopis juliflora* and *Lantana camara* exclude each other mutually, they are found to co-exist with other invasive species such as *Opuntia* (OP; cactus) or *Leucaena leucocephala* (LL), thus forming potential invasive–invasive cliques. However, OP and LL have not yet been identified as fully invasive in these habitats, and a closer look at Table 1 suggests that LL is likely to become a more aggressive invader in this region, as it was identified as the dominant invasive in at least two communities, namely, the SV and HK forest fragments. In two other cliques, it was identified as a non-hub member of PJ-associated cliques. On the other hand, OP was found in very few cliques, and may be considered as a borderline non-native species that is more likely to become naturalised in this region. In summary, the native species common to both invasives are either (a) preferentially associated with one invasive (blue boxes in Figure 7), or (b) equally rarely observed for both invasives (yellow box in Figure 7, but these are weaker edges).

3. Discussion

Urban flora is known to be largely composed of migrants or non-native species that become part of urban ecosystems as escapes from horticulture, forestry, agriculture sectors or enter through transport networks [34–37]. These species further form associations in different habitats types that range from being complete man-made (gardens, roadsides, parks, etc.) to semi-wild such as urban forests [38–40]. The urban forest fragments of South Delhi ridge are the key source of ecosystem services to the city but are constantly at risk of being converted to homogenised, species-poor habitats dominated by invasive species. This observation was supported in the present study in Section 2.1 (Figures 2 and 3), where each sampling unit was found to be dominated by one or more invasive species, and overall, *Prosopis juliflora* and *Lantana camara* were identified as the most dominating invasive species in all six study sites. These observations reveal that the process of plant invasion is much more complex in urban forests, as there are multiple invasive species involved.

Further investigation and partitioning of study area networks in Section 2.2 (Table 1 and Figure 6) revealed that the two dominant invaders *Lantana camara* and *Prosopis juliflora* exclude each other and form distinct native–invasive, native–native and native–non-native species associations. This competitive exclusion between the two invaders could be a result of the difference in their habitat requirements. *Lantana camara* is a light-demanding understory shrub, that requires moisture and thick soil, while, *Prosopis juliflora* is a tree species known for its drought tolerance and ability to grow in rocky terrain, both species are also known to have allelopathic characteristics. These distinct high-fidelity native–invasive cliques suggest that plant invasion alters community composition by forming novel assemblages instead of wiping out the native flora, thereby acting at the community level by altering species associations. *Prosopis juliflora* is already known to have a differential impact on native species, altering community composition by forming associations with few 'weedy' native species [9,41,42]. *Prosopis juliflora* has a more detrimental effect on annual species than perennials and forms associations with species of 'disturbed forests', and has been reported to negatively affect 'higher order seral' species [41,42]. Our results also affirm this ecological alliance between native and invasive species. *Prosopis juliflora* is a nitrogen-fixing tree legume, capable of altering soil characteristics, thereby having a competitive advantage [43]. In addition, it is reported to have higher soil microbial biomass and mycorrhization intensity as compared to native tree species [44]. It alters community composition by forming associations with few native species and it has been suggested that in the Delhi Ridge, *Prosopis juliflora* is the main reason for the disappearance of native tree species [9,11]. On the other hand, *Lantana camara* forms a dense canopy that once established, not only limits native tree seedling recruitment but also inhibits the

growth of other understory vegetation, forming small groups in comparison with *Prosopis juliflora*. *Lantana* is a gregarious shrub known for negatively affecting native species by outcompeting them for scarce resources and possessing allelopathic attributes. It forms impenetrable thickets, thus crowding out seedling recruitments. This light-loving plant often begins colonisation in forest edges and gaps, and takes advantage of disturbance events as it can quickly regenerate following fires as well as chopping or cutting [15]. Thus, in comparison to *Prosopis juliflora*, *Lantana camara* was observed to form smaller native–invasive cliques with almost no association with native shrubs. When an invasive species enters the ecosystem, it gradually takes over the assemblages and reduces the number of species in those clusters. The continuous inflow of non-native species and changing environmental conditions diverts historical assemblages to new associations, significantly influencing ecosystem structure and function [45–47]

Recent research on urban ecology often categorises these new associations as novel and views them as an opportunity to study ecosystem change. Thus, these 'novel ecosystems' usually describe an assemblage of non-native and native species that never existed before in an ecosystem. Novel ecosystems are composed of a non-historical species configuration that arises due to anthropogenic environmental change, land conversion, species invasion or a combination of the three. They are created as a consequence of human activity but do not depend on human intervention for their maintenance [46]. Under the framework, green spaces can be categorised into three categories, i.e., historical, hybrid and novel ecosystems. A hybrid ecosystem is similar to a historical system based on its function and species composition, while a novel ecosystem is defined as a system that has crossed a threshold beyond which ecological and social processes stops it from returning to its historical state. Novel ecosystem frameworks argue that the focus of ecologists should shift from patterns to processes and conservation practices should not focus on 'fossilising nature' but rather work towards restoring ecosystem function [46]. While it is too early to categorise the Delhi Ridge as a hybrid or novel ecosystem, such a framework can help provide more achievable targets in terms of species conservation in an urban context, keeping in mind the social, political and ecological conditions amidst which these forests are located. Many case studies have pointed out that some invasive species act as transformers to establish positive feedback loops by way of increased biomass, nitrogen fixation, etc. that may move an ecosystem to an alternate stable state wherein maintaining diversity becomes a near-impossible task [46,47]. Studies of interspecies association can prove effective in tracking ecosystem change as in the case of naturalised species that have been reported to generate positive influences, both natural-ecological and socio-cultural, and some of these benefits have been quantified [48].

However, in case of invasives, studies like ours can also provide opportunities for interventions before the establishment of permanent feedback loops. For example, at the time of data collection, another species with high invasive potential, *Leucaena leucocephala* was found to have a limited but significant impact; it was identified as the dominant invasive in at least two cliques (see Table 1), while loosely forming associations with *Prosopis juliflora* in other communities as a non-hub species (see Figure 7). Although it is not possible to say whether the invasive–invasive cliques it forms with PJ are more recent, or whether it has evolved into a more aggressive invader by forming its own dominant invasive cliques, we hypothesise that in few years it will break the present association, reduce the number of species, and may create a new clade of its own. The strength of the overall associations emerging from Table 1 and Figure 6 in Section 2.2 reflect mutual exclusion, as a form of association, among the invasive species, whereas Figure 7 (Section 2.3) reflects the extent of shared associations between invasive cliques. It should be recalled that the data presented in Section 2.2 only reflects individual locations whereas Section 2.3 combines all cliques across all locations, and therefore it brings out generic patterns that were not discernible in individual study sites. Competitive exclusion, particularly between invasive species is well reported in the literature where one invasive is shown to suppress another invasive species [49–51]. Some studies also indicate invasive meltdowns where a swarm of invasives

can completely overtake native communities over a period of time [52]. However, in this study, we observed that while PJ and LC form exclusive cliques in individual study sites (Section 2.2), in the overall combined data presented in Section 2.3 we observed that there is a cohort of species that form transient associations shared by these two strong invaders (yellow-shaded region in Figure 7) and invasive exclusion is moderated by the presence of these transient associations. However, in terms of network topological properties such as module size and edge weights, it is quite evident that the invasive-specific associations (blue-shaded region in Figure 7) are stronger than the shared transient (yellow) associations. This observation could inform conservation planning as the existence of invasive-specific associations indicates that (a) some species clusters or locations are vulnerable and thus more likely to be colonised by invasives, and (b) once such associations have formed, it could also be harder to eradicate the invasives and restore native vegetation.

To understand or predict urban forest fragment communities and identify key species of concern, it is first essential to identify major groups of species that exist together or exclude each other as has been done in this study. However, the present work is cross-sectional, a single slice in time. Furthermore, the present investigation is focused on compositional patterns identifying cliques and associations between species, and we hope to pave the way for investigations into causal elements that lead to the formation of these communities. Therefore, there is a need to extend this study to understand the underlying processes that drive the formation of these assemblages—particularly plant functional traits that significantly affect the outcomes of competitive trade-offs between native and invasive plants. Further work is also needed to delineate the relative importance of landscape features at fine scales and competitive interactions in driving these assemblages in the urban context. This forms part of our ongoing work on Delhi Ridge and we are in the process of investigating the role played by landscape heterogeneity in explaining the associations.

In summary, we present a novel approach that uses complex network analyses to detect communities and explore associations between different species of plants more specifically to identify clusters formed by invasive species. From a management perspective, although we do find evidence for interventions to contain emergent invasives such as *Leucaena leucocephala* before they become more established in the ecosystems, a more extensive temporal analysis on similar lines needs to be performed in order to identify patterns that may assist in containing the spread of established invasives such as *Lantana camara* and *Prosopis juliflora*. This study is part of a long-term vegetation monitoring programme, and the early results on vegetation associations have been presented here. Further work on the interaction between different biotic and abiotic filters would provide insights into community assembly in the urban context.

4. Material and Methods

4.1. Site Selection

The South Delhi Ridge consists of multiple forest fragments that represent residual woodlands of Aravalli vegetation in the urban cosmopolitan city of New Delhi, namely, the National Capitol Territory (NCT), Delhi, India. For this study, all forest fragments >1 sqkm were included, leading to the identification of six study sites, as depicted in Figure 1. The first panel (Figure 1A) shows the map of New Delhi indicating each of these six study areas, namely, Hauz Khas (HK), Jahanpanah City Forest (JCF), Mehrauli Forest (MED), Tughlaqabad Forest (TUQ), Sanjay Van (SV), and Jawaharlal Nehru University (JNU). The climatic conditions of all six study areas are similar with rocky terrain (Pahari zone/Denudational Hills) and same soil type of Aravalli Quartzitic origin [53]. All forest fragments have the same nationally classified Forest Type, i.e., Northern Tropical Thorn Forests.

4.2. Vegetation Sampling

The primary vegetation survey data for this study was collected from a standardised ecological survey of six forest fragments in the South Delhi region, using the plotless

sampling technique, i.e., line transect [54,55]. Line transects of 250 metres each were placed systematically inside each of the six identified study sites with an a priori design using Google Earth Pro. The transects were placed with a minimum distance of 100 m from each other, and from boundary walls or jogging tracks to minimise pseudo-replication and edge effects, respectively, as shown in Figure 1B. The alignment of the transects was opportunistic to avoid unscalable obstacles and geographic features. Transects that were found to be in modified landscape features, such as gardens, lawns, nurseries, buildings and other similar sites, were removed. All remaining transects were treated as sampling units, these were geo-referenced and subsequently used as a sampling guide for the entire vegetation survey. The number of transects varied depending upon the size of the patch and the area with built-up structures in each location. The starting points and bearing for each transect were accessed using a handheld GPS and the transect length was measured with the help of a Pedometer with a 3D motion sensor with predefined stride length.

4.3. Species Identification

For each site, the name of the species, number of individuals, girth at breast height (GBH) and canopy cover was recorded. It is important to point out here that some of the species names have changed during and after this study was conducted but to avoid confusion across all the published literature, nomenclature as per *Flora of Delhi* (1963) was followed [56]. Native and introduced species were categorised by referring to this key floral text. The categorisation of invasive species was done based on a list of alien invasive species of India published by the National Biodiversity Authority of India, under the Ministry of Environment Forests and Climate Change, Government of India [57]. Reference collections were made and herbarium samples were deposited in the Ecology Laboratory at the Ambedkar University Delhi for follow-up in case of difficulties with identification. In all, the data include presence/absence and abundance information from 57 woodland plant species, based on their representation in a total of 94 transects of 250 metres each.

4.4. Multivariate Data Analyses

Species richness was measured across the six sampling sites using rarefaction techniques followed by construction of distance dendrograms for each site, using the *vegan* package (version 2.5–7) in R-studio (Version 1.3.959). The Bray Curtis dissimilarity index along with a linkage method, the unweighted pair group method (UPGMA) was used for performing cluster analyses [49]. Species association and exclusion patterns were tested by Pearson correlation test (alpha = 0.05) between the relative abundance of both invasive species using *ggpubr* library in R-studio (Version 1.3.959) [58]

4.5. Network Analyses

Species presence–absence matrices were converted to structured information file (SIF) files using our in-house webserver NEXCADE [59]. Thus, each study area network dataset was comprised of an unweighted edge list. An edge list is a data structure used to represent a graph as a list of its edges. Unweighted edge lists are therefore two column matrices that directly connect nodes for each edge. In this case, each row in the edge list represented the physical location (or transect ID) and the name of the identified species, respectively. The SIF edge lists were exported for visualisation in Cytoscape version 3.9 [60]. Community detection was performed by parsing each study area network through algorithms that identify densely connected regions using topological parameters. For this, we used the MCODE and GLay network partitioning algorithms, which enable versatile community structure identification as well as graph layout functions for network clustering and structured visualisation [61,62]. For each of the six forest community networks, this led to the identification of node clusters, which we called 'cliques'. The species with the highest degree in each clique were treated as 'hubs' or key species of each clique and all study area networks were compared in terms of clique composition. Finally, all the cliques comprising the two major invasive species (*Lantana camara* and *Prosopis juliflora*) were superimposed in

order to explore and assess the extent of the fidelity of species associations formed by these invasives. This was done using the Markov cluster algorithm or MCL, an unsupervised cluster algorithm for networks based on the simulation of (stochastic) flow in graphs [63].

5. Conclusions

There has been considerable interest in the last two decades in understanding the ecology of urban ecosystems that were previously understood to be degraded as they were poor representations of the original vegetation. While these urban ecosystems are dominated by non-native and invasive species, there is renewed interest in these modified or 'novel ecosystems' as they continue to provide ecosystem services and value to the city. Urban woodlands and forest remnants in Delhi consist of a combination of species that range from species native to the Aravalli, to those that were introduced to Delhi purposefully during the urbanisation, to species that have escaped from cultivation. Of all these groups, invasive species are seen to be a significant challenge for conservation efforts because they are known to displace natives or cause declines in native species populations. Using a network approach in this study, we identified distinct communities of plants among the vegetation survey data from six urban forest fragments in the South Delhi Ridge of the Aravalli region. Species that were found to occur together significantly more often than by random chance, represent co-occurrence patterns. In contrast, species that were not found to grow together on the same-line transects reflected a tendency to consistently avoid each other, thereby suggesting a pattern of exclusion.

Importantly, we identified co-occurrence as well as exclusion patterns among species across the six urban forest communities. Despite overlaps, these communities constitute invasive–invasive, invasive–native and native–native associations in each of the woodland patches investigated. We found that the invasive species *Lantana camara* and *Prosopis juliflora* form species assemblages or 'cliques' that are mutually exclusive across all sites, in the sense that these two major invaders do not form associations with each other. As such, these two major invasive species form invasive–native and invasive–invasive associations that seem consistent across different forests, indicating the formation of new stable associations in Delhi's woodlands, and supporting the widely held notion of novel ecosystems in urban ecology. This work indicates that community identification algorithms can find applications in pattern analysis in vegetation ecology and may provide an altogether new way of investigating species associations using networks. In summary, our findings have implications in the conservation of these urban forests and this work highlights a new application of network approach for identifying species associations and visualisations that could be explored further for its efficacy in vegetation analysis.

Supplementary Materials: The following supporting information can be downloaded at: https://www.mdpi.com/article/10.3390/plants11040541/s1, Table S1: Species Name Codes.

Author Contributions: Conceptualisation, G.Y. and S.B.; Data curation, S.C.; Formal analysis, S.C. and G.Y.; Funding acquisition, S.B.; Methodology, S.C.; Project administration, S.B.; Software, G.Y.; Supervision, S.B.; Visualisation, G.Y.; Writing—original draft, S.C. and S.B.; Writing—review & editing, S.C., G.Y. and S.B. All authors have read and agreed to the published version of the manuscript.

Funding: This work was funded by an Extramural Research Grant to G.Y. by the Science and Engineering Research Board (SERB) of the Govt of India (Grant ID EMR/2016/006486). S.C. is supported by a CUES research grant by AUD. The funding bodies provided the equipment required for the collection, analysis, and interpretation of data in this study.

Informed Consent Statement: Not Applicable.

Data Availability Statement: The data is available from the authors upon request.

Acknowledgments: G.Y. thanks the Director, NIPGR for their support. S.B. thanks AUD for supporting the fieldwork at the Centre for Urban Ecology and Sustainability (CUES).

Conflicts of Interest: The authors declare no conflict of interest.

References

1. Champion, S.H.G.; Seth, S.K. *A Revised Survey of the Forest Types of India*; The Manager of Publications: Delhi, India, 1968.
2. Hobbs, R.J.; Higgs, E.; Harris, J.A. Novel ecosystems: Implications for conservation and restoration. *Trends Ecol. Evol.* **2009**, *24*, 599–605. [CrossRef] [PubMed]
3. Mann, M.; Sehrawat, S. A City With a View: The Afforestation of the Delhi Ridge, 1883–1913. *Mod. Asian Stud.* **2009**, *43*, 543–570. [CrossRef]
4. Bowe, P. the Genius of an Artist': William R. Mustoe and the Planting of the City of New Delhi and Its Gardens. *Gard. Hist. Soc.* **2009**, *37*, 68–79.
5. Sud, M. *Political Ecology of the Ridge: The Establishment and Contestation of Urban Forest Conservation in Delhi*; Franz Steiner Verlag: Stuttgart, Germany, 2015.
6. Pasha, S.V.; Satish, K.V.; Reddy, C.S.; Rao, P.P.; Jha, C.S. Satellite image based quantification of invasion and patch dynamics of mesquite (Prosopis juliflora) in Great Rann of Kachchh, Kachchh Biosphere Reserve, Gujarat, India. *J. Earth Syst. Sci.* **2014**, *123*, 1481–1490. [CrossRef]
7. Robbins, P. Tracking Invasive Land Covers in India, or Why Our Landscapes Have Never Been Modern. *Annals of the Association of American Geographers.* **2001**, *91*, 637–659. [CrossRef]
8. Kaur, R.; Gonzáles, W.L.; Llambi, L.D.; Soriano, P.J.; Callaway, R.M.; Rout, M.E.; Gallaher, T.J. Inderjit. Community Impacts of Prosopis juliflora Invasion: Biogeographic and Congeneric Comparisons. *PLoS ONE* **2012**, *7*, e44966. [CrossRef]
9. Dakshini, K.M.M. Vegetation of Delhi State: Mehrauli Region. *Proc. Natl. Inst. Sci. India Biol. Sci.* **1966**, *34*, 127–133.
10. Robbins, P. Comparing Invasive Networks: Cultural and Political Biographies of Invasive Species. *Geogr. Rev.* **2004**, *94*, 139–156. [CrossRef]
11. Sharma, R.; Dakshini, K.M.M. A Comparative Assessment of the Ecological Effects of *Prosopis cineraria* and *P. juliflora* on the Soil of Revegetated Spaces. *Vegetio* **1991**, *96*, 87–96. [CrossRef]
12. Lowe, S.; Browne, M.; Boudjelas, S.; De Poor, M. 100 of the World's Worst Invasive Alien Species A selection from the Global Invasive Species Database.The Invasive Species Specialist Group (ISSG) a specialist group of the Species Survival Commission (SSC) of the World Conservation Union (IUCN). 2000. Available online: http://www.issg.org/pdf/publications/worst_100/english_100_worst.pdf (accessed on 20 December 2021).
13. Babu, S.; Love, A.; Babu, C.R. Ecological Restoration of Lantana-Invaded Landscapes in Corbett Tiger Reserve, India. *Ecol. Restorration* **2009**, *27*, 467–477. [CrossRef]
14. Love, A.; Babu, S.; Babu, C.R. Management of Lantana, an invasive alien weed, in forest ecosystems of India. *Curr. Sci.* **2009**, *97*, 1421–1429.
15. Sundaram, B.; Hiremath, A.J.; Krishnaswamy, J. Factors influencing the local scale colonisation and change in density of a widespread invasive plant species, Lantana camara, in South India. *NeoBiota* **2015**, *25*, 27–46. [CrossRef]
16. "*Lantana camara* L." GBIF Secretariat. GBIF Backbone Taxonomy. 2021. Available online: https://www.gbif.org/species/2925303 (accessed on 31 January 2022).
17. "*Prosopis juliflora* (Sw.) DC." GBIF Secretariat. GBIF Backbone Taxonomy. 2021. Available online: https://www.gbif.org/species/5358460 (accessed on 31 January 2022).
18. Sukopp, H. Urban Ecology-Scientific and Practical Aspects. In *Urban Ecology*; Breuste, J.U.O., Feldmann, H., Eds.; Springer: Berlin/Heidelberg, Germany, 1998.
19. Rowntree, R.A. Ecology Of The Urban Forest-Introduction To Part I. *Urban Ecol.* **1984**, *8*, 1–11. [CrossRef]
20. Labatore, A.C.; Spiering, D.J.; Potts, D.L.; Warren, R.J. Canopy trees in an urban landscape—viable forests or long-lived gardens? *Urban Ecosyst.* **2017**, *20*, 393–401. [CrossRef]
21. Barton, J.; Pretty, J. Urban Ecology. In *Urban Ecology*; Gaston, K., Ed.; Cambridge University Press: Cambridge, UK, 2013; pp. 202–229.
22. Bolund, P.; Hunhammar, S. Ecosystem services in urban areas. *Ecol. Econ.* **1999**, *29*, 293–301. [CrossRef]
23. Cox, D.T.C.; Shanahan, D.F.; Hudson, H.L.; Fuller, R.A.; Gaston, K.J. The impact of urbanisation on nature dose and the implications for human health. *Landsc. Urban Plan.* **2018**, *179*, 72–80. [CrossRef]
24. Albert, R.; Barabási, A.L. Statistical mechanics of complex networks. *Rev. Mod. Phys.* **2002**, *74*, 47–97. [CrossRef]
25. Bascompte, J.; Jordano, P. Plant-animal mutualistic networks: The architecture of biodiversity. *Annu. Rev. Ecol. Evol. Syst.* **2007**, *38*, 567–593. [CrossRef]
26. Qu, X.; Peng, W.; Liu, Y.; Zhang, M.; Ren, Z.; Wu, N.; Liu, X. Networks and ordination analyses reveal the stream community structures of fish, macroinvertebrate and benthic algae, and their responses to nutrient enrichment. *Ecol. Indic.* **2019**, *101*, 501–511. [CrossRef]
27. Ramaswami, G.; Somnath, P.; Quader, S. Plant-disperser mutualisms in a semi-arid habitat invaded by *Lantana camara* L. *Plant Ecol.* **2017**, *218*, 935–946. [CrossRef]
28. Lusseau, D. Evidence for social role in a dolphin social network. *Evol. Ecol.* **2007**, *21*, 357–366. [CrossRef]
29. Ellenberg, H.; Mueller-Dombois, D. *Aims and Methods of Vegetation Ecology*; Wiley: New York, NY, USA, 1974.
30. Tansley, A.G. The Use and Abuse of Vegetational Concepts and Terms. *Ecology* **1935**, *16*, 284–307. [CrossRef]
31. Ter Braak, C.J.F. Ordination. In *Data Analysis in Community and Landscape Ecology*; Cambridge University Press: Cambridge, UK, 1995; pp. 91–173.

32. McCune, B.; Grace, J.B.; Urban, D.L. *Analysis of Ecological Communities*; MjM Software Design: Gleneden Beach, OR, USA, 2002; Volume 28.
33. Podani, J. Multivariate exploratory analysis of ordinal data in ecology: Pitfalls, problems and solutions. *J. Veg. Sci.* **2005**, *16*, 497–510. [CrossRef]
34. Aronson, M.F.J.; Handel, S.N.; la Puma, I.P.; Clemants, S.E. Urbanization promotes non-native woody species and diverse plant assemblages in the New York metropolitan region. *Urban Ecosyst.* **2015**, *18*, 31–45. [CrossRef]
35. Rebelle, F. Urban Ecology and Special Features of Urban Ecosystems. *Glob. Ecol. Biogeogr. Lett.* **1994**, *4*, 173–187. [CrossRef]
36. Reshi, Z.A.; Dar, P.A.; Bhat, M.S.; Shah, M.A.; Andrabi, S.M. Urbanization and Its Impact on Biodiversity in the Kashmir Himalaya. In *Biodiversity of the Himalaya: Jammu and Kashmir State*; Topics in Biodiversity and Conservation; Dar, G.K.A., Ed.; Springer: Singapore, 2020; pp. 1011–1028.
37. Von Der Lippe, M.; Kowarik, I. Long-distance dispersal of plants by vehicles as a driver of plant invasions. *Conserv. Biol.* **2007**, *21*, 986–996. [CrossRef] [PubMed]
38. Kent, M.; Stevens, R.A.; Zhang, L. Urban plant ecology patterns and processes: A case study of the flora of the City of Plymouth, Devon, UK. *J. Biogeogr.* **1999**, *26*, 1281–1298. [CrossRef]
39. Niemelä, J. Ecology and urban planning. *Biodivers. Conserv.* **1999**, *8*, 119–131. [CrossRef]
40. Kowarik, I. Cities and Wilderness-A New Perspective. *Int. J. Wilderness* **2013**, *19*, 32–36.
41. El-Keblawy, A.; Al-Rawai, A. Impacts of the invasive exotic Prosopis juliflora (Sw.) D.C. on the native flora and soils of the UAE. *Plant Ecol.* **2007**, *190*, 23–35. [CrossRef]
42. Kumar, S.; Mathur, M. Impact of invasion by Prosopis juliflora on plant communities in arid grazing lands. *Trop. Ecol.* **2014**, *55*, 33–46.
43. Pasiecznik, N.; Felker, P.; Harris, P.; Harsh, L.; Cruz, G.; Tewari, J.; Cadoret, K.; Maldonado, L. *The Prosopis Juliflora-Prosopis Pallida Complex: A Monograph*; HDRA: Conventery, UK, 2002; Volume 12, p. 229. ISBN 0-905343-30-1.
44. Mosbah, M.; Taieb, T.; Habib, K. Invasive character of Prosopis juliflora facilitated by its Allelopathy and a wide Mutualistic interaction with soil microorganisms. *J. Biol. Sci.* **2018**, *18*, 115–123. [CrossRef]
45. Gaertner, M.; Wilson, J.R.U.; Cadotte, M.W.; MacIvor, J.S.; Zenni, R.D.; Richardson, D.M. Non-native species in urban environments: Patterns, processes, impacts and challenges. *Biol. Invasions* **2017**, *19*, 3461–3469. [CrossRef]
46. *Novel Ecosystems: Intervening in the New Ecological World Order*; Wiley Online Books; Hobbs, R.J.; Higgs, E.S.; Hall, C.M. (Eds.) Wiley-Blackwell: Hoboken, NJ, USA, 2013; ISBN 9781118354186.
47. Richardson, D.M.; Ricciardi, A. Misleading criticisms of invasion science: A field guide. *Divers. Distrib.* **2013**, *19*, 1461–1467. [CrossRef]
48. Lee, L.S.H.; Zhang, H.; Jim, C.Y. Serviceable tree volume: An alternative tool to assess ecosystem services provided by ornamental trees in urban forests. *Urban For. Urban Green.* **2021**, *59*, 127003. [CrossRef]
49. Vila, M.; Weiner, J. Are invasive plant species better competitors than native plant species?–evidence from pair-wise experiments. *Oikos* **2004**, *105*, 229–238. [CrossRef]
50. Richardson, D.M.; Ek, P.P.Y.S.; Rejmánek, M.; Barbour, M.G.; Panetta, F.D.; West, C.J. Naturalization and invasion of alien plants: Concepts and definitions. *Divers. Distrib.* **2000**, *6*, 93–107. [CrossRef]
51. McKinney, M.L. Urbanization as a major cause of biotic homogenization. *Biol. Conserv.* **2006**, *127*, 247–260. [CrossRef]
52. Simberloff, D.; Von Holle, B. Positive interactions of nonindigenous species: Invasional meltdown? *Biol. Invasions* **1999**, *1*, 21–32. [CrossRef]
53. Geological Survey of India. Copyright Government of India.Geological, Geomorphological and Mineral Map of Delhi. 2000. 30, 16. Available online: https://www.indiawaterportal.org/sites/default/files/iwp2/Map_Delhi_State_Geology_and_Mineral_Maps_Geological_Survey_of_India.pdf (accessed on 20 December 2021).
54. Chauhan, S. Analysis of Woody Species in Delhi Ridge: Community Dynamics in Urban Context. Master's Thesis, School of Human Ecology, Ambedkar University Delhi, Delhi, India, 2013.
55. Krebs, C.J. Ecological Methodology. In *Ecological Methodology*, 2nd ed.; A. Wesley Longman: New York, NY, USA, 1999; pp. 157–168.
56. Maheshwari, J.K. *Flora of Delhi*; Council of Scientific and Industrial Research: New Delhi, India, 1963.
57. Sandilyan, S. *Invasive Species of India Report*; National Biodiversity Authority, Ministry of Environment Forests and Climate Change Government of India: Chennai, India, 2005; Available online: http://nbaindia.org/uploaded/pdf/Iaslist.pdf (accessed on 20 December 2021).
58. Kassambara, A. *Package 'ggpubr'*; 2017; pp. 37–40. Available online: https://rpkgs.datanovia.com/ggpubr/ (accessed on 20 December 2021).
59. Yadav, G.; Babu, S. Nexcade: Perturbation analysis for complex networks. *PLoS ONE* **2012**, *7*, e41827. [CrossRef]
60. Shannon, P.; Markiel, A.; Ozier, O.; Baliga, N.S.; Wang, J.T.; Ramage, D.; Amin, N.; Schwikowski, B.; Ideker, T. Cytoscape: A Software Environment for Integrated Models of Biomolecular Interaction Networks. *Genome Res.* **1971**, *13*, 426. [CrossRef] [PubMed]
61. Pruitt, K.D.; Hogue, C.W.; Groll, M.; Hartmann, C.; Huber, R.; Fields, S. An automated method for finding molecular complexes in large protein interaction networks. *Nucleic Acids Res.* **2001**, *29*, 137–140. [CrossRef] [PubMed]

62. Su, G.; Kuchinsky, A.; Morris, J.H.; States, D.J.; Meng, F. GLay: Community structure analysis of biological networks. *Bioinformatics* **2010**, *26*, 3135–3137. [CrossRef] [PubMed]
63. Dongen, S.V.A.N. Graph Clustering Via a Discrete Uncoupling Process. *SIAM J. Matrix Anal. Appl.* **2008**, *30*, 121–141. [CrossRef]

plants

MDPI

Article

Metabolomic Fingerprinting and Molecular Characterization of the Rock Samphire Germplasm Collection from the Balkan Botanic Garden of Kroussia, Northern Greece

Kalliopi Kadoglidou [1,*], Maria Irakli [1], Anastasia Boutsika [1], Ifigeneia Mellidou [1], Nikolas Maninis [1], Eirini Sarrou [1], Vasiliki Georgiadou [1], Nikolaos Tourvas [1], Nikos Krigas [1], Theodoros Moysiadis [1,2], Katerina Grigoriadou [1], Eleni Maloupa [1], Aliki Xanthopoulou [1] and Ioannis Ganopoulos [1,*]

[1] Institute of Plant Breeding and Genetic Resources, ELGO-DIMITRA, Thermi, GR-57001 Thessaloniki, Greece; irakli@cerealinstitute.gr (M.I.); bouanastasia@outlook.gr (A.B.); ifimellidou@gmail.com (I.M.); nikolasmaninis@gmail.com (N.M.); esarroy@gmail.com (E.S.); vaso.geo@gmail.com (V.G.); nikostourvas@gmail.com (N.T.); nikoskrigas@gmail.com (N.K.); moysiadis.t@unic.ac.cy (T.M.); kgrigoriadou@ipgrb.gr (K.G.); maloupa@bbgk.gr (E.M.); aliki.xanthopoulou@gmail.com (A.X.)

[2] Department of Computer Science, School of Sciences and Engineering, University of Nicosia, Nicosia 2417, Cyprus

* Correspondence: kadoglidou@ipgrb.gr (K.K.); giannis.ganopoulos@gmail.com (I.G.)

Abstract: The traditionally edible aerial parts of rock samphire (*Crithmum maritimum* L.) could be a valuable functional food or feed ingredient due to their high antioxidant capacity, ascorbic acid content, and rich content in secondary metabolites such as phenolics and flavonoids. The first objective of this study was to evaluate eighteen genotypes derived from different regions of Greece regarding the phytochemical contents of their soluble extracts in total phenolics, total flavonoids, and individual polyphenols as determined by LC-MS analysis, as well as ascorbic acid content and their antioxidant capacity as determined by different assays, including ABTS (2,2-azino-bis-3-ethylbenzothiazoline-6-sulfonic acid), DPPH (2,2-diphenyl-1-picrylhydrazyl radical scavenging activity), and FRAP (ferric reducing antioxidant power) assays. The second objective of the study was the molecular characterization of native Greek *C. maritimum* genotypes. Great variation among genotypes was observed in terms of the antioxidant capacity, ascorbic acid content, and phenolic compounds (total phenolic content and total flavonoid content), as well as in caffeolquinic acids and flavonoids. The principal component analysis highlighted genotypes with a higher potential in antioxidants and polyphenolics. The most promising genotypes were G9 from Kefalonia, followed by G4 from Ikaria, where both clearly exhibited a similar response with high values of evaluated traits. The molecular characterization of genotypes revealed low variability and low to moderate genetic diversity between populations. Our data indicated that the rock samphire germplasm collection from the Balkan Botanic Garden of Kroussia could serve as an important source of documented genetic material and, thus, it is suggested for further investigation to provide insight regarding cultivation and agro-processing aspects, artificial selection, or plant breeding aimed at developing *C. maritimum* genotypes of high-bioactive value.

Keywords: *Crithmum maritimum*; phenolics; ascorbic acid; antioxidant capacity; genetic diversity; molecular markers

Citation: Kadoglidou, K.; Irakli, M.; Boutsika, A.; Mellidou, I.; Maninis, N.; Sarrou, E.; Georgiadou, V.; Tourvas, N.; Krigas, N.; Moysiadis, T.; et al. Metabolomic Fingerprinting and Molecular Characterization of the Rock Samphire Germplasm Collection from the Balkan Botanic Garden of Kroussia, Northern Greece. *Plants* **2022**, *11*, 573. https://doi.org/10.3390/plants11040573

Academic Editors: Milan S. Stankovic, Paula Baptista and Petronia Carillo

Received: 31 December 2021
Accepted: 17 February 2022
Published: 21 February 2022

Publisher's Note: MDPI stays neutral with regard to jurisdictional claims in published maps and institutional affiliations.

1. Introduction

Crithmum maritimum L., also known as rock samphire or sea fennel, is a native Greek, wild-growing plant of the Apiaceae family. It is a perennial, medicinal-aromatic plant with fleshy leaves that are traditionally edible [1]. Rock samphire naturally thrives on rocky crevices as a chasmophyte (rock-dweller) and in sandy substrates as a halophyte [2]. *C. maritimum* has a Euri-Mediterranean native distribution, extending to the Atlantic European coastline and the British Isles as well as along parts of the Black Sea coastline [3,4]. At

the beginning of the twentieth century, *C. maritimum* has also been established as an alien plant along the coasts of Belgium and the Netherlands, mainly in disturbed man-made environments such as harbors and dikes [5].

Rock samphire attracts considerable scientific interest, mainly due to its properties. Rock samphire is used as a food ingredient in several traditional recipes [6] and it is known for its good sensory traits due to its high essential oil content [7]. Moreover, as a food ingredient, it is associated with positive health effects [8] due to its richness in biologically active compounds in the leaves, such as vitamin C, iodine, carotenoids, flavonoids, minerals (mainly calcium), organic acids, and phenolics [9,10], whereas the seeds are beneficial for human consumption as they are rich in essential fatty acids [11]. The most commonly detected phenolic compounds of rock samphire are phenolic acids such as chlorogenic, neochlorogenic, cryptochlorogenic, ferulic, and caffeoylquinic acids and its derivatives [12]. This edible halophyte also contains interesting amounts of gallic, caffeic, vanillic, rosmarinic, and *p*-coumaric acids, while small amounts of trans-2-hydroxycinnamic and trans-cinnamic acids have also been reported [12]. Moreover, flavonoids such as rutin, apigenin, quercetin-3-galactoside, epicatechin, epigallocatechin, catechin, pyrocatechol, and 4-hydroxybenzaidehyde (polyphenols) are also present in *C. maritimum*, but in rather low amounts [13,14].

Innovation-wise, the encapsulation of rock samphire's essential oil is reported as a promising alternative for the control of insects causing human diseases (e.g., the dengue vector *Aedes aegypti*) and crop pests (e.g., the cotton leafworm *Spodoptera litura*) [15]. Additionally, rock samphire may be an alternative for both horticultural and industrial crops in the case of low soil quality and/or irrigation water with high electrical conductivity [6], whereas, at the same time, methods for its production with compost-based substrates has recently been investigated [10].

A survey of the literature makes evident that the primary focus of most previous investigations mainly concern the phytochemical profile and the biological activities of *C. maritimum* e.g., [16–18], as well as the growing techniques of rock samphire e.g., [10,19,20]. Nevertheless, to the best of our knowledge, comparative studies are scarce regarding the bioactive compounds, the antioxidant capacity, the metabolomic analysis, and the genetic identification of different rock samphire genotypes/ecotypes, and this research field remains almost unexplored e.g., [5,21,22]. Generally, the identification of genetic variation could be based on the changes accrued on nucleotide sequences of DNA stands during the process of genome proliferation. Various techniques have been developed to identify the species diversity at the molecular level, such as genetic markers. These markers are necessary tools for the investigation of the intraspecific genetic diversity across the geographical distribution of plant species. In general, these markers mainly differ in their application requirements, sensitivity, and the degree of reliability [23]. A highly reproducible polymorphic DNA fingerprinting technique based on polymerase chain reaction (PCR) is the Amplified Fragment Length Polymorphism (AFLP) [24]. The AFLP has been applied for the discrimination of genetic diversity in various species [25,26]. The Inter-Simple Sequence Repeat (ISSR) is another molecular marker that involves PCR amplifications of DNA [27]. It has proven to be a rapid, simple, and inexpensive technique to analyze the structure and genetic diversity of species, as well as to analyze the genetic relationships among cultivars [28]. With respect to rock samphire, previous studies [5] have developed nuclear microsatellite loci by using 454 pyrosequencing, and they have shown a strictly coastal geographical distribution with high levels of genetic differentiation (FST = 0.3) and a genetic structure typical of a mostly selfing species [unbiased fixation index (FIS) ranging from 0.16 to 0.58].

Taking all of this information into account, the aim of this study was to provide insight through a comparative analysis of the genetic diversity, the polyphenolic profile, and the antioxidant capacity of native Greek rock samphire genotypes.

2. Results and Discussion

A total of 18 rock samphire accessions with geographic origin from 8 different and representative regions of Greece are presented with relative information in Table 1.

Table 1. Origin of the 18 native Greek rock samphire genotypes studied, with their IPEN (International Plant Exchange Network) accession numbers and their abbreviations.

a/a	IPEN Accession Number	Genotype Abbreviation	Origin in Greece
1	GR-1-BBGK-17,6006	G1	Karavostamo, Ikaria Island
2	GR-1-BBGK-16,5963	G2	Kalamaki, Tymbaki, Heraklion, Crete
3	GR-1-BBGK-12,5685_A	G3	Karavostamo, Ikaria Island
4	GR-1-BBGK-12,5685_B	G4	Karavostamo, Ikaria Island
5	GR-1-BBGK-12,5685_C	G5	Karavostamo, Ikaria Island
6	GR-1-BBGK-16,5962	G6	Heraklion city, Crete
7	GR-1-BBGK-16,5961	G7	Vatopedi, Agio Oros, Chalkidiki
8	GR-1-BBGK-16,5964	G8	Rethimno city, Crete
9	GR-1-BBGK-17,5972	G9	Kefalonia, Ionian Islands
10	GR-1-BBGK-16,5965	G10	Kalamata, Peloponnese
11	GR-1-BBGK-05,3041	G11	Kefalonia, Ionian Islands
12	GR-1-BBGK-97,719_A	G12	Agio Oros, Chalkidiki
13	GR-1-BBGK-97,719	G13	Agio Oros, Chalkidiki
14	GR-1-BBGK-14,5800	G14	Pantana, Heraklion, Crete
15	GR-1-BBGK-15_5902_A	G15	Ikaria Island
16	GR-1-BBGK-15,5902	G16	Ikaria Island
17	GR-1-BBGK-05,3001	G17	Chania city, Crete
18	GR-1-BBGK-10,5458	G18	Vokaria, Chios Island

2.1. Antioxidant Activity, Ascorbic Acid Content, Total Phenolic Content, and Total Flavonoid Content

An analysis of variance (ANOVA) applied to data obtained from antioxidant capacity determined with three different assays [2′-azinobis-(3-ethylbenzothiazoline-6-sulfonate) radical scavenging activity (ABTS), 2,2-diphenylpicrylhydrazyl radical scavenging activity (DPPH), and ferric reducing antioxidant power assay (FRAP)], as well as on ascorbic acid (AsA) content, showed a significant effect due to tested genotype of rock samphire as source of variation (Table 2).

Table 2. Results of an analysis of variance applied on the evaluated bioactive compounds, antioxidant capacity parameters, and phenolic groups identified by an LC-MS analysis of the aboveground portion of 18 native Greek rock samphire genotypes. F-ratios' significance is given for the effects exerted by replication and rock samphire genotype.

		Significance of *F*-Ratio									
								Determined by LC-MS			
Variation Source	**df** [z]	**ABTS**	**DPPH**	**FRAP**	**AsA**	**TPC**	**TFC**	**CQAs**	**OPAs**	**FLAs**	**Total**
Replication	2	NS	NS	NS	NS	NS	NS	NS	NS	NS	NS
Genotype	17	***	***	***	***	***	***	***	***	***	***
CV%		8.68	9.49	10.35	17.5	5.63	7.80	4.58	5.82	5.96	4.14

[z] df, degrees of freedom; ABTS, 2,2-azino-bis-(3-ethylbenzothiazoline-6-sulfonic acid); DPPH, 2,2-diphenyl-1-picrylhydrazyl radical scavenging activity; FRAP, ferric reducing antioxidant power; AsA, ascorbic acid content; TPC, total phenolic content; TFC, total flavonoid content; CQAs, caffeolquinic acids; OPAs, other phenolic acids; FLAs, flavonoids; Total, total phenolics; CV, coefficient of variance; ***, significance at $p < 0.001$; NS, non-significant.

Comparing the various genotypes, the G9 genotype clearly presented the highest antioxidant capacity, with nearly 1.8-fold higher values for all three assays than the general average value of the other genotypes (Figure 1a–c). More specifically, ABTS values ranged between 4.32 to 20.88 mg of trolox equivalant (TE)/g of dry weight (dw) basis (Figure 1a). The ABTS activity of G9 (20.88 mg TE/g dw) did not differ from the corresponding value for the G14 genotype, whereas the rest of genotypes–with the exception of G13 and G16–had

values ranging from 8.95–15.96 mg/g. Other studies reported ABTS activity of *C. maritimum* of about 0.43 mg TE/mL [29] and 0.095–0.418 mg/mL, expressed as IC_{50} [14].

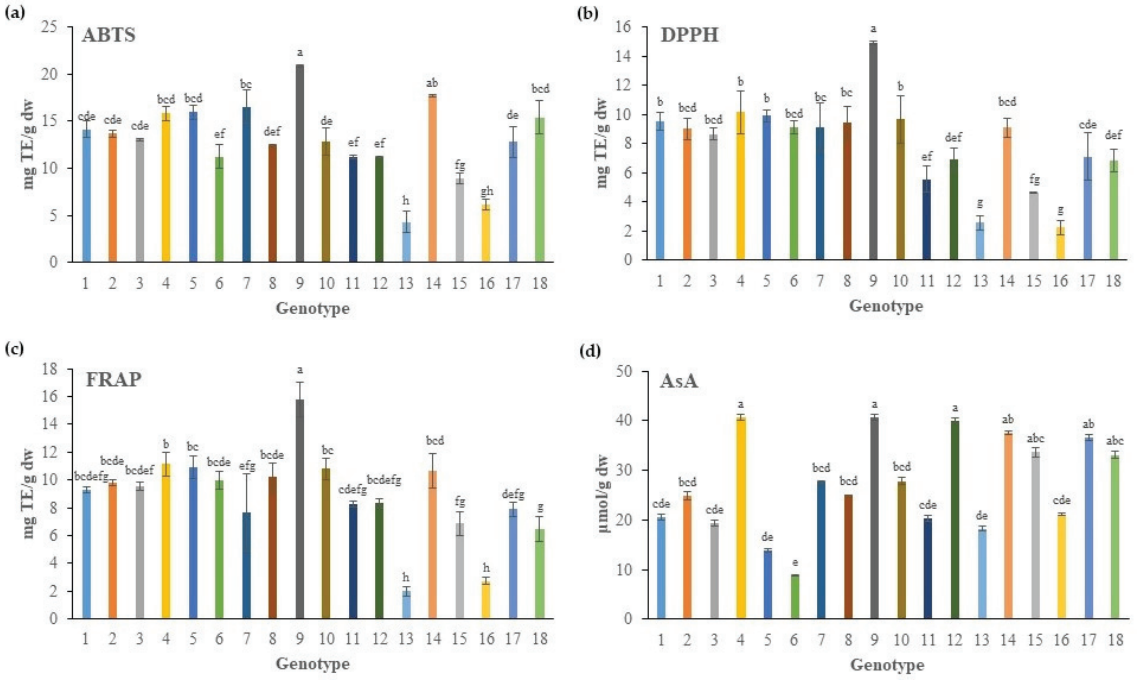

Figure 1. Overview of the antioxidant capacity of extracts derived from the aboveground portion of 18 native Greek rock samphire genotypes (Table 1) determined as 2,2-azino-bis-(3-ethylbenzothiazoline-6-sulfonic acid) radical scavenging activity (ABTS) (**a**); 2,2-diphenyl-1-picrylhydrazyl radical scavenging activity (DPPH) (**b**); and ferric reducing antioxidant power (FRAP) (**c**); all values are expressed as mg of trolox equivalent (TE) per g of dry weight (dw). The content of ascorbic acid (AsA), expressed as µmol of AsA per g of dw, is also shown (**d**). Data represent the mean values ± standard deviation. Different letters on the bars characterize significant differences among genotypes according to Tukey's test for $p \leq 0.05$.

In the same way, DPPH ranged from 2.24 to 14.92 mg of TE/g dw in different genotypes of *C. maritimum*, exhibiting the following descending order: G14 > the majority of genotypes > G13 and G16 (Figure 1b). Generally, DPPH values in native Greek genotypes of *C. maritimum* presented an average value of 8.0 mg of TE/g dw, which is in accordance with those of Sousa et al. [30], who found a value of 7.3 mg of TE/g dw. Previous studies in the literature presented a DPPH scavenging activity of *C. maritimum*, expressed as IC_{50}, of around 7.6 mg/mL [29], or ranged from 0.15 to 1.21 mg/mL [14].

In agreement with the abovementioned results obtained for ABTS and DPPH were those obtained by the FRAP assay, which presented the same trend (Figure 1c).

The AsA content of native Greek *C. maritimum* showed a mean value of 27.23 µmol/g of dw basis, ranging from 8.83 to 40.70 µmol/g (Figure 1d). Specifically, the genotype G4 from Ikaria Island and G9 from Kefalonia Island had, numerically, the greater AsA content of 40.70 µmol/g, a value that did not differ from the respective values of the other studied genotypes (G12, G14, G15, G17, and G18). However, the AsA content was significantly lower in several native Greek genotypes such as G6, G5, G13, G3, G1, and G16.

An ANOVA on data obtained from the evaluated parameters of bioactive compounds [total phenolic content (TPC) and total flavonoid content (TFC)] showed significant effects

due to genotype of 18 native Greek rock samphire as a source of variation (Table 2). The TPC of genotypes ranged from 2.55 to 10.84 mg gallic acid equivalents (GAE)/g of dw basis (Figure 2a). Specifically, genotype G9, derived from Kefalonia Island, had the greater TPC value of 10.84 mg GAE/g dw, followed by the majority of genotypes, with the exception of G13 and the G16, which showed the lowest values for TPC. Generally, the rest of the studied germplasm presented small or ameliorated TPC differences, ranging from 4.89 mg/g in G14 from Heraklion, Crete to 7.30 mg/g in G4 from Ikaria Island. Comparing the results with that found in the literature, a previous report [29] presented the TPC of rock samphire extracts to be about 47 mg GAE/g dw, a value that is eight-fold higher than the mean value of 6.18 mg/g dw found in the present study. Recently, other researchers [31] stated that *C. maritimum* leaves contained 31.7 mg/g dw of TPC, or a similar level of 23–33 mg/g dw depending of the season (spring-summer) [14]. Conversely, Sánchez-Faure et al. [18] found a TPC of rock samphire of about 8.6 mg/g dw, a value closer to the one found in the current study harvested before flowering, in the middle of July. Moreover, another study [32] reported a value of 2.3 mg/g dw for TPC in the aerial parts of rock samphire, a content similar to the lower values found in the present study.

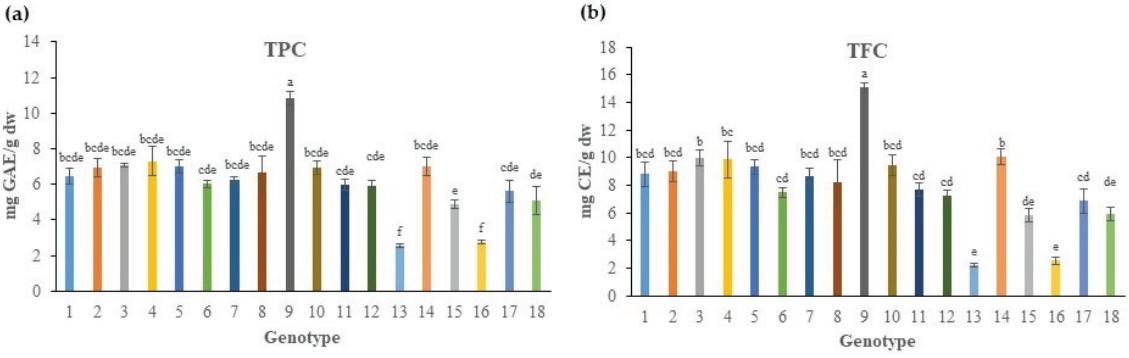

Figure 2. The content of total phenolic compounds (TPC) (**a**), expressed as mg of gallic acid equivalents (GAE) per g of dry weight (dw), and total flavonoid compounds (TPC) (**b**), expressed as mg of catechin equivalents (CE) per g of dw in the extracts of aboveground portion of 18 native Greek rock samphire genotypes. Data represent the mean values ± standard deviation. Different letters on the bars characterize significant differences among genotypes according to Tukey's test for $p \leq 0.05$.

Generally, the TPC content presents a wide variation of 0.5 to 132 mg GAE/g dw among the different halophytes from the Mediterranean area [33], whereas it occurs at a level of about 6 mg/g dw in different vegetables [34]. In the current study, the majority of the tested genotypes of *C. maritimum* had about 6.0–7.3 mg/g dw of TPC, a content slightly higher than that of other vegetables. Recently, Martins-Noguerol et al. [35] found that the TPC content of rock samphire under optimum conditions was 6.1 mg/g dw, even though plants under field conditions exhibited a high phenolic content of 30.2–48.0 mg/g dw regardless of the variability of the contrasting habitats.

Moreover, Zhou and Yu [36] reported that some vegetables, such as spinach and broccoli, had TPC contents of 13 and 10.84 mg/g dw, respectively. Notably, in our results, G9 had a comparable level of TPC to the values reported for spinach and broccoli.

The TFC content of the various genotypes ranged from 2.25 to 15.08 mg of catechin equivalents (CE)/g dw (Figure 2b). Similar to the TPC content, the highest TFC value was observed in G9, followed by the majority of genotypes, while the lowest values were found in G13 and G16 genotypes of *C. maritimum*, which is in line with the TPC results. More precisely, most of the genotypes contained TFC in the 5.82–10.02 CE/g dw range. Rock samphire derived from different climatic areas exhibited contrasting TFC contents. For example, Nabet et al. [29] reported that the TFC content of rock samphire extracts from

Algeria was 17 mg/g dw, a value near the maximum of TFC content that we found in G14, whereas another study [32] reported a content of 2.3 mg/g dw of TFC in aerial parts of rock samphire from the Croatian Adriatic coast, a value similar to the lower value found in two native Greek genotypes in the present study. On the other hand, Souid et al. [31] found that *C. maritimum* leaves from the French Atlantic coast contained 25.6 mg/g of TFC. In addition, previous researchers [37] stated that the TFC content of infusions and decoctions of different above-ground organs of rock samphire from the Portugeuse Atlantic coast ranged from 25 (in stems) to 55 (in leaves) mg rutin equivalents/200 mL (a cup of tea).

2.2. Identification and Quantification of Phenolic Compounds

The chromatographic profile of the native Greek rock samphire's extracts identified by liquid chromatography-mass spectrometry (LC-MS) analysis is shown in Figure 3. The LC-MS analysis allowed the identification of 18 main phenolic compounds, which were separated and characterized regarding their retention time, UV, and MS spectra data (Table 3). Eleven of them belong mainly to quinic acid derivatives (peaks 1, 2, 3, 5, 6, 8, 10, 11, 16, 17, and 18), four of them are characterized as flavones (peaks 7, 12, 13, and 14)–mainly quercetin derivatives–, two of them are classified as hydroxycinnamic acids (peaks 9 and 15), and one of them as hydroxybenzoic acid (peak 4). All of the detected peaks were identified by the use of reference standards; however, the peaks 8, 10, and 11 were identified based on data from the literature. Four peaks (peaks 2, 3, 5, and 6) appeared at 4.01, 4.34, 5.65, and 5.85 min, respectively, with pseudo-molecular ion $[M\text{-}H]^-$ at m/z = 353 and UV maximum at 325 nm corresponds to 1-caffeoyl-quinic acid (1-CQA), 5-O-caffeoylquinic acid (5-CQA or neochlorogenic acid), 3-O-caffeoylquinic acid (3-CQA or chlorogenic acid), and 4-O-caffeoylquinic acid (4-CQA or cryptochlorogenic acid), respectively. The peaks 16, 17, and 18 that appeared at 10.45, 10.95, and 10.61 min, respectively, with pseudo-molecular ion $[M\text{-}H]^-$ at m/z = 515 and UV maximum at 327 nm were assigned to dicaffeoyl quinic acids as 3,4-dicaffeoyl-quinic acid (3,4-DCQA), 3,5-dicaffeoyl-quinic acid (3,5-DCQA), and 4,5-dicaffeoyl quinic acid (4,5-DCQA), respectively. Four peaks appearing at 6.36, 9.21, 9.63, and 9.78 min were characterized as flavonoids, e.g., vicenin-2 (VIC), quercetin-3-O-rutinoside (QURU or rutin), quercetin-3-O-glucoside (QUGL), and quercetin-3-O-galactoside (QUGA or hyperoside), respectively. Three minor peaks detected at 5.01, 7.61, and 9.98 min presenting $[M\text{-}H]^-$ at m/z = 137, 179 and 163 were identified as protocatechuic acid (PRCA), caffeic acid (CA), and *p*-coumaric acid (pCA), respectively.

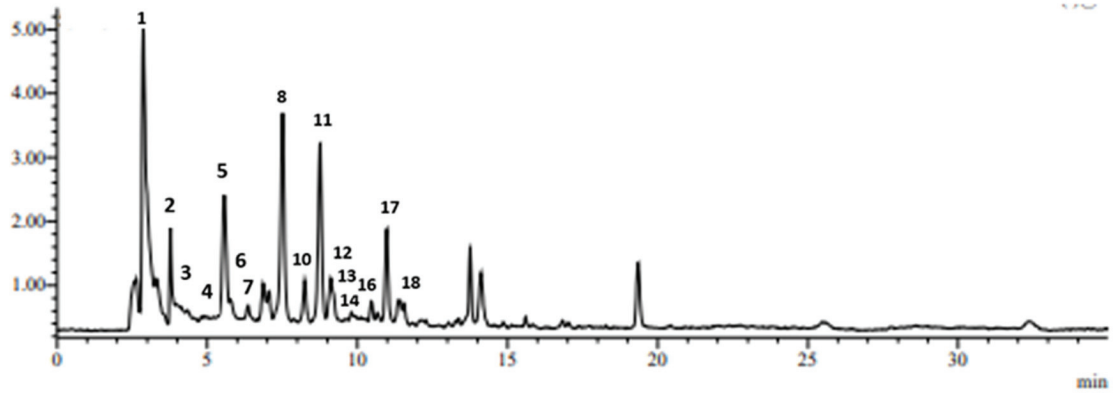

Figure 3. Representative total ion current chromatographic (TIC) profile of rock samphire extract (genotype G16) obtained by HPLC-MS.

Table 3. Eighteen main phenolic compounds with their abbreviations, identified by HPLC-DAD-MS in methanolic extracts of native Greek rock samphire genotypes.

Peak	R_t (Min)	λ_{max} (nm)	$[M-H]^-$ (m/z)	Attempt to Identify	Abbreviation
1	2.78	330	191	Quinic acid	QNA
2	4.01	325	353	1-caffeoyl-quinic acid	1-CQA
3	4.34	325	353	5-O-caffeoylquinic acid	5-CQA
4	5.01	260	153	Protocatechuic acid	PRCA
5	5.65	325	353	3-O-caffeoylquinic acid	3-CQA
6	5.85	325	353	4-O-caffeoylquinic acid	4-CQA
7	6.36	270, 335	593	Vicenin-2	VIC
8	7.51	311	337	5-coumaroyl-quinic acid	5-cQA
9	7.61	320	179	Caffeic acid	CA
10	8.24	297, 325	367	5-feruloy-quinic acid	5-fQA
11	8.84	311	337	5-coumaroyl-quinic acid isomer	5-cQA
12	9.21	256, 354	609	Quercetin-3-O-rutinoside	QURU
13	9.63	260, 36	463	Quercetin-3-O-glucoside	QUGL
14	9.78	260, 36	463	Quercetin-3-O-galactoside	QUGA
15	9.98	309	163	*p*-coumaric acid	pCA
16	10.45	327	515	3,4-dicaffeoyl-quinic acid	3,4-DCQA
17	10.95	327	515	3,5-dicaffeoyl-quinic acid	3,5-DCQA
18	11.61	327	515	4,5-dicaffeoul quinic acid	4,5-DCQA

The peaks 8 and 11 at 7.51 and 8.84 min, respectively, showing pseudo-molecular ion $[M-H]^-$ at m/z = 337 and UV maximum at 311 nm were attributed to a coumaroyl quinic acid isomers (5-cQA) [29,38]. Similarly, peak 10 detected at 8.24 min having UV maxima at 297 and 325 nm and pseudo-molecular ion $[M-H]^-$ at m/z 367 was attributed to a feruloyl quinic acid (5-fQA) derivative.

An ANOVA applied to the 18 major phenolic compounds derived from 18 native Greek rock samphire genotypes revealed significant differences among genotypes (Table 2). Generally, caffeoylquinic acids (CQAs) were the major phenolic compounds quantified by LC-MS, ranging from 414 to 1547.3 mg/100 g dw, with a mean value of 1089.4 mg/100 g dw (Table 4). The predominant CQAs quantified were 5-cQA, followed by 3-CQA (or CLA), 3,5-DCQA, 1-CQA, and 5-fQA, presenting mean values of 369.2 (sum of isomers/peaks 8 and 11), 258.7, 211.1, 109.3, and 74.6 mg/100 g dw, respectively (Table 4).

Table 4. Content (mg/100 g of dw) of main caffeolquinic acids (CQAs) of 18 native Greek rock samphire genotypes (for abbreviations and origin, see Table 1). Different letters in the same column characterize significant differences among genotypes according to Tukey's test for $p \leq 0.05$.

Genotype	CQAs																	
	1-CQA		5-CQA		3-CQA		4-CQA		5-cQA		5-fQA		3,4-DCQA		3,5-DCQA		4,5-DCQA		Total	
G1	112.70	defg	16.02	ef	310.05	bc	45.95	a	474.79	abc	87.41	abcd	15.39	fghi	259.54	bc	12.83	d	1334.68	b
G2	125.33	cde	44.01	a	298.60	bc	31.43	b	488.84	ab	71.21	defg	15.10	fghi	259.25	bc	10.57	de	1344.34	b
G3	147.06	abc	14.99	ef	315.45	bc	22.97	e	361.85	efg	85.82	abcd	17.75	cdef	282.04	ab	13.03	d	1260.96	b
G4	130.28	bcd	37.23	b	286.16	bcd	32.45	b	358.99	efg	91.66	abcd	24.00	a	227.95	cde	19.71	ab	1208.43	bcd
G5	148.05	abc	26.88	c	296.71	bc	26.07	d	399.60	def	83.76	abcde	19.38	bcde	218.75	de	17.36	bc	1236.56	bc
G6	112.43	defg	37.01	b	251.24	def	23.42	e	346.02	fgh	81.30	bcdef	16.82	efg	208.85	ef	7.89	f	1084.98	cde
G7	137.09	bcd	13.05	fgh	299.81	bc	28.87	c	446.51	bcd	72.80	cdefg	16.11	fgh	226.85	de	12.02	d	1253.11	b
G8	61.90	h	20.30	de	305.51	bc	18.41	f	488.46	ab	88.77	abc	20.19	bcd	241.27	cd	16.30	c	1261.11	b
G9	171.86	abc	25.18	cd	372.65	a	24.61	de	520.49	a	100.96	a	22.46	ab	291.40	a	17.68	abc	1547.29	a
G10	157.01	abc	24.39	cd	288.83	bcd	26.82	cd	416.57	cde	83.43	bcdef	20.79	abc	223.18	dc	17.60	bc	1258.62	b
G11	121.41	cdef	7.79	hi	277.11	cde	17.30	fg	329.62	gh	63.90	fg	12.42	i	231.55	cde	8.65	ef	1069.75	de
G12	110.66	defg	14.63	efg	227.57	f	15.32	g	280.56	hi	79.34	bcdefg	12.28	i	165.20	g	7.26	f	912.82	f
G13	25.83	i	3.61	i	83.97	g	5.58	j	208.54	j	26.58	h	3.08	k	55.15	h	1.75	g	414.09	g
G14	92.32	g	11.32	fgh	236.84	f	18.07	f	278.14	hi	70.94	defg	17.24	def	239.49	cde	20.14	a	984.50	ef
G15	91.24	g	7.58	hi	230.40	f	9.83	i	287.10	hi	67.70	efg	8.86	j	179.57	fg	6.75	f	889.03	f
G16	28.13	i	3.59	i	79.20	g	3.20	j	233.39	ij	28.92	h	3.51	k	60.91	h	3.13	g	443.98	g
G17	100.80	efg	11.99	fgh	251.39	def	22.33	e	367.18	efg	93.84	ab	13.47	hi	213.77	de	7.69	f	1082.46	cde
G18	93.83	fg	9.03	ghi	245.66	ef	12.22	h	358.03	efg	63.66	g	13.84	ghi	214.09	de	12.53	d	1022.89	ef
Mean value	109.32		18.26		258.73		21.38		369.15		74.56		15.15		211.05		11.83		1089.42	

Other minor CQAs quantified in rock samphire's genotypes were 4-CQA (cryptochlorogenic acid), 5-CQA (neochlorogenic acid), 3,4-DCQA, and 4,5-DCQA, with mean values of 21.4, 18.3, 15.1, and 11.9 mg/100 g dw, respectively. Regarding the flavonoid class, QURU and VIC were the major compounds detected (20.3 and 14.2 mg/100 g dw, respectively), along with QUGL and QUGA as the most abundant flavone derivatives (Table 5). Finally, among other phenolic acids (OPAs), which are summarized in Table 6, only QNA was found with 82.8 mg/100 g dw, whereas the concentrations of PRCA, CA, and pCA was negligible. Concerning the rock samphire's phenolics identification by LC-MS, our results resemble those of other researchers [39], who identified three caffeoylquinic acid isomers (3-CQA, 4-CQA, and 5-CQA) and three dicaffeoylquinic acids (3,4-DCQA, 3,5-DCQA, and 4,5-DCQA), which were also presented in the current work.

Table 5. Content (mg/100 g of dw) of flavonoids (FLAs) of 18 native Greek rock samphire genotypes (for abbreviations and origin, see Table 1). Different letters in the same column characterize significant differences among genotypes according to Tukey's test for $p \leq 0.05$.

Genotype	FLAs									
	VIC		QURU		QUGL		QUGA		Total	
G1	13.97	f	29.21	bc	0.82	fgh	2.71	def	46.71	bcd
G2	20.59	bc	33.68	ab	7.88	b	4.81	abc	66.96	a
G3	14.40	f	22.57	def	1.46	fg	3.55	bcde	41.98	de
G4	25.32	a	35.08	ab	2.97	cd	5.88	a	69.25	a
G5	19.28	bcd	28.58	bc	1.05	fgh	4.46	abc	53.37	b
G6	21.94	b	23.85	cde	2.88	cd	3.29	cde	51.96	b
G7	13.41	f	18.97	efg	2.99	cd	2.38	efg	37.75	ef
G8	21.80	bv	17.44	fg	1.79	ef	2.62	efg	43.65	cde
G9	16.06	ef	25.70	cde	18.27	a	5.11	abc	65.14	a
G10	18.92	cde	24.95	cde	3.87	c	3.36	cde	51.1	bc
G11	8.21	g	10.38	ij	2.54	de	1.26	fg	22.39	hi
G12	2.53	h	10.14	ij	1.06	fgh	1.15	fg	14.88	ij
G13	4.14	h	5.77	j	0.47	gh	1.01	g	11.39	j
G14	8.28	g	14.58	ghi	2.50	de	2.73	def	28.09	gh
G15	10.27	g	10.51	hij	0.62	gh	1.41	fg	22.81	h
G16	17.49	de	16.10	ghi	0.18	h	3.73	bcde	37.5	ef
G17	8.84	g	20.11	defg	0.88	fgh	4.00	bcde	33.83	fg
G18	9.62	g	18.10	fg	0.75	gh	4.34	abcd	32.81	fg
Mean value	14.17		20.32		2.94		3.21		40.64	

Table 6. Content (mg/100 g of dw) of other phenolic acids (OPAs) of 18 native Greek rock samphire genotypes (for abbreviations and origin, see Table 1). Different letters in the same column characterize significant differences among genotypes according to Tukey's test for $p \leq 0.05$.

Genotype	OPAs									
	QNA		PRCA		CA		pCA		Total	
G1	105.75	a	0.42	de	0.61	fg	0.06	g	106.84	a
G2	74.48	efghi	0.41	def	0.72	defg	0.12	efg	75.73	defgh
G3	73.33	fghi	0.60	bc	0.63	efg	0.07	fg	74.63	defgh
G4	86.76	cdefg	0.41	def	0.86	cdef	0.08	fg	88.11	bcde
G5	80.64	defgh	0.47	cd	0.88	cdef	0.20	cde	82.19	cdef
G6	71.51	ghij	0.51	bcd	0.99	bc	0.32	b	73.33	efgh
G7	101.27	abcd	0.57	bc	0.69	defg	0.09	fg	102.62	ab
G8	60.73	ij	0.63	b	0.79	cdefg	0.30	b	62.45	gh
G9	89.57	bcde	0.50	bcd	1.49	a	0.24	bcd	91.8	abc
G10	104.90	ab	0.77	a	0.88	cde	0.16	def	106.71	a
G11	95.72	abcd	0.60	bc	1.15	bc	0.13	efg	97.6	ab
G12	92.03	abcd	0.31	ef	1.01	bc	0.07	fg	93.42	abc
G13	74.32	efghij	0.85	a	0.65	defg	0.56	a	76.38	defg
G14	70.92	hij	0.50	bcd	0.63	efg	0.08	fg	72.13	fgh
G15	88.16	cdefg	0.28	f	0.90	bcd	0.29	bcd	89.63	bcd
G16	90.47	abcd	0.46	cd	0.59	g	0.53	a	92.05	abc
G17	59.02	j	0.50	bcd	1.01	bc	0.31	b	60.84	h
G18	71.44	ghij	0.39	def	0.72	defg	0.10	efg	72.65	fgh
Mean value	82.83		0.51		0.84		0.21		84.40	

It should be noted that, as mentioned above, 5-CQA, 3-CQA, and 4-CQA are the neochlorogenic, chlorogenic, and cryptochlorogenic acid, respectively, whereas, generally, quinic acid is a component of a chlorogenic acid moiety [9]. According to previous research [9], rock samphire is among the richest phenolic-containing species within the Apiaceae family, with caffeoylquinic acid derivatives being the sole class of phenolics [40]. In agreement with our results, Mekinić et al. [41] reported that 3-CQA ranged from 5.65 to 7.48 mg/g dw, while it was 16.28 mg/g dw at an April harvest.

Moreover, a previous study [1] reported that, among seventeen constituents identified, the main phenolics were 3-CQA, 4-CQA, 5-CQA, and 1.5-dicaffeoylquinic acid. Our results are in accordance with the findings of that study [1] concerning the concentrations of 4-CQA and 5-CQA; nevertheless, they are in contrast in the case of 3-CQA and 1-CQA. More specifically, we found over fifteen-fold more 3-CQA and over two-fold more 1-CQA concentrations (averaged over genotype) compared with the respective values reported by Sarrou et al. [1]. These differences may be partially attributed to the different initial material used in the two studies, as, in the current work, the whole edible above-ground part was used at a ratio of leaves:stems 1:1 (w:w), whereas in Sarrou et al. [1], a ratio of 2:1 was used. Moreover, our results are comparable with those of Nabet et al. [29], who revealed that hydroxycinnamic acids were among the main phenolic compounds of rock samphire from Algeria according the following order of importance: 5-CQA (636 mg/100 g dw) > 3,5-DCQA (164 mg/100 g dw) > 5-cQA and 5-fQA (104 mg/100 g dw) > 1-CQA and 4,5-DCQA (each one of 103 mg/100 g dw). In the current work, 5-CQA was more than thirty times lower (18.26 mg/100 g dw), but 5-cQA content was about three times higher (369 mg/100 g dw) than in those results [29]. Concerning the 3-CQA (chlorogenic acid) content, other researchers [9] found huge concentrations of 1880–2790 mg/100 g dw in rock samphire growing in sand and 300–1000 mg/100 g dw in plants growing on cliffs, compared to the 258.73 mg/100 g dw found in the current study.

Genotypes of native Greek rock samphire were rich in quinic and chlorogenic acids, despite the fact that halophytic species are usually pure in these compounds. However, quinate and/or chlorogenate were detected in several members of the Apiaceae family, including carrot [42,43], fennel [44], and celery [45]. Based on the aforementioned knowledge, Meot Duros and Magné [20] stated that these two molecules could play a chemotaxonomic role in the Apiaceae family. In any case, rock samphire, similar to fennel and greater than carrot, can be considered among the 3-CQA (or CLA)-richest Apiaceae members, with concentrations up to 259 mg/100 g dw [44].

Contrary to a previous study [13], other phenolic compounds such as catechins, vanillic, and rosmarinic acids were undetectable in the present work. Nevertheless, it should be not disregarded that differences in the ranges of estimated parameters among the results of the current study and similar studies could be attributed to factors such as climatic conditions, harvesting time, and extraction method (solvent, temperature, time, etc.).

Altogether, the eighteen components of native Greek rock samphire's extracts had a total polyphenol content of 1214.4 mg/100 g dw, a half-reduced value compared with the 2503 mg/100 g dw reported by a previous study [31].

Regarding the differences among genotypes, the G9 genotype from Kefalonia Island had cumulatively CQAs of 1547.3 mg/100 g dw, followed by G1-G5, G7, G8, and G10, while G13 and G16 had the lowest content (Table 4). It is remarkable that the genotypes G1, G3, G4, and G5 exhibited high CQAs values originating from the same island, namely Ikaria. Concerning the major quinic acids, it seems that G9, G8, and G2 contained more 5-cQA than the others, whereas G9 and G3 had more 3,5-DCQA (Table 4). Similarly, G9 had the highest 1-CQA concentration, although not statistically different than the respective values of several other genotypes (such as G2–G5, G7, and G10). With regard to chlorogenic acids, the G9 genotype had the highest content, even though the majority of genotypes had also high contents (Table 4). In addition, G9, G2, and G4 had the highest total concentration of FLAs (Table 5).

2.3. Correlation Coefficients among Bioactive Compounds, Antioxidant Capacity, and Phenolic Groups

The correlation Pearson coefficient (r) analysis was used to evaluate the relationship between bioactive compounds, antioxidant capacity, and phenolic groups. Significant positive correlations ($p \leq 0.001$) were observed between the vast majority of traits (Table 7), which indicated that when selection or breeding are applied for one of these traits, an indirect improvement could also be observed in other traits [46]. Clearly, TPC was strongly correlated with TFC, ABTS, DPPH, FRAP, CQAs, and FLAs (r = 0.65–0.99, $p \leq 0.001$), but it had no significant correlation with OPAs (r = 0.102, $p > 0.05$) and no correlation with AsA (r = 0.332, $p > 0.05$).

Table 7. Correlation matrix (r coefficients) between bioactive compounds, antioxidant capacity, and phenolic groups identified by LC-MS and AsA content in 18 native Greek rock samphire genotypes.

Parameters	TPC [z]	TFC	ABTS	DPPH	FRAP	CQAs	OPAs	FLAs	AsA
TPC	1	0.992 ***	0.868 ***	0.955 ***	0.977 ***	0.897 ***	0.102	0.649 ***	0.332
TFC		1	0.880 ***	0.949 ***	0.964 ***	0.892 ***	0.141	0.633 ***	0.317
ABTS			1	0.882 ***	0.828 ***	0.815 ***	0.051	0.559 *	0.420
DPPH				1	0.949 ***	0.907 ***	0.066	0.727 ***	0.241
FRAP					1	0.879 ***	0.057	0.670 **	0.277
CQAs						1	0.113	0.691 **	0.150
OPAs							1	0.047	0.027
FLAs								1	−0.019
AsA									1

[z] TPC, total phenolic content; TFC, total flavonoid content; ABTS, 2,2-azino-bis-(3-ethylbenzothiazoline-6-sulfonic acid); DPPH, 2,2-diphenyl-1-picrylhydrazyl radical scavenging activity; FRAP, ferric reducing antioxidant power; CQAs, caffeolquinic acids; OPAs, other phenolic acids; FLAs, flavonoids; AsA, Ascorbic acid. Asteriks, *** indicate significant at $p \leq 0.001$, ** at $p \leq 0.01$, and * at $p \leq 0.05$.

Similarly, TFC was highly correlated with all the other traits (r = 0.633–0.964, $p \leq 0.001$), except from the case of OPAs and AsA, where no significant correlation was observed (r = 0.141, $p > 0.05$ and r = 0.317, $p > 0.05$, respectively). ABTS was very strongly correlated with DPPH, FRAP, and CQAs (r = 0.815–0.882, $p \leq 0.001$), highly correlated with FLAs (r = 0.559 $p \leq 0.001$), but it was not correlated with OPAs (r = 0.066, $p > 0.05$) and AsA (r = 0.420, $p > 0.05$). The same trend was observed for the rest of the traits, except for the cases of OPAs and AsA, where no correlation with any other trait was detected.

These findings clearly show that TPC and TFC contribute, to a high extent, to the antioxidant activity of rock samphire's native Greek genotypes. Moreover, the phenolic groups were identified successfully by LC-MS in the current study and they corresponded, to a great extent, to the determined TPC and TFC, as well as to antioxidant capacity, whereas our findings are in agreement with earlier reports [47,48]. Indeed, Xu et al. [47] reported that CQA isomers (specifically 3-CQA, 4-CQA, and 5-CQA) and DCQA isomers (specifically 3,5-DCQA, 3,4-DCQA, and 4,5-DCQA) exhibit antioxidant activities and DNA damage protective effects to various extents. In the same direction, Kooti et al. [48] have reported that the major phenolic compounds, such as CQAs, of fennel seed extracts show important antioxidant activity.

2.4. Principal Component Analysis and Hierarchical Clustering

In total, 23 determined variables (3 bioactive compounds, 3 antioxidant capacity assays, and 17 phenolic compounds identified by LC-MS) of 18 rock samphire genotypes were subjected to a principal component analysis (PCA). Based on an eigenvalue > 1, we extracted a total of two PCs with a cumulative distribution of 68.0%, (specifically 57.5% for the first component and 10.5% for the second one) (Figure 4a). Generally, native Greek rock samphire genotypes formed four distinct groups, where the majority of genotypes were placed in the center of the PCA, mainly in the lower left (group 2) and in the upper right quarter (group 3). Interestingly, G9 from Kefalonia Island was identified alone and it was located in group 4, close to the positive side of PC1, presenting a rather similar response with high values at most evaluated parameters. Additionally, the genotypes G5, G4, G3, and G1, all originating from Ikaria Island, were included in group 3 and they were

ordinated to the positive side of PC1 and PC2 in the upper right quadrant, indicating a tendency for high values in most evaluated traits. Notably, among them, G4 from Ikaria Island was separated from the rest by the higher positive loadings on PC1. Conversely, the genotypes of group 2 presented values of phytochemical and antioxidant capacity below the mean value, and were thus grouped at the lower left quarter. Moreover, G13 and G16 genotypes–the only members of group 1 lined with the green color in Figure 4 and located at the left side–presented the most distinct and significant reduced values for the evaluated parameters.

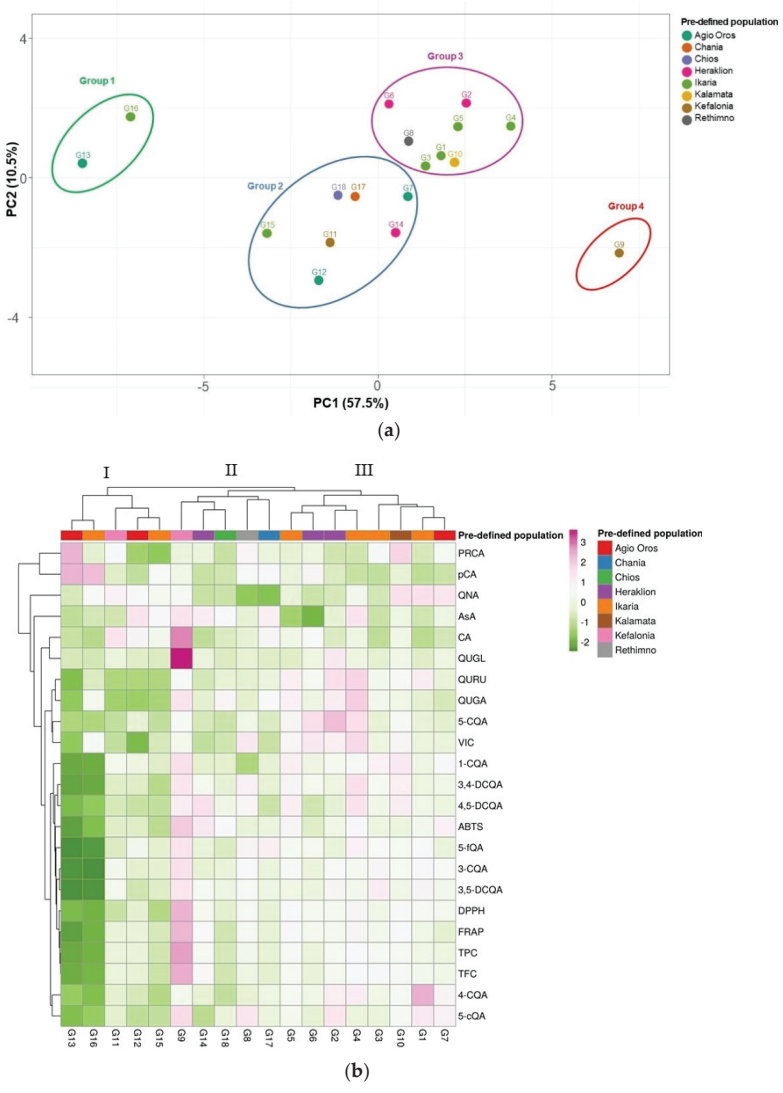

Figure 4. Two-D PCA plot of the first two components of 18 native Greek rock samphire genotypes (see Table 1) based on 23 determined traits related to bioactive compounds and antioxidant activity (**a**), and a heat map showing fold changes of the same traits of the 18 rock samphire genotypes (**b**). Columns are centered; unit variance scaling is applied to columns. Columns are clustered using Euclidean distance and Ward linkage (23 rows, 18 columns).

Stepping forward to investigate the differences on rock samphire genotypes, an agglomerative hierarchical clustering (AHC, heatmap) analysis on the bioactive content, antioxidant capacity, and main phenolics was employed to enable the grouping of genotypes into clusters of similar responses based on calculations of the Euclidean distance (Figure 4b). The resulting dendrogram using the Ward's method for agglomeration, revealed three distinct groups: Group I and Group II, which were comprised of five genotypes each, and Group III, which contained eight genotypes. More specifically, the heatmap analysis identified a subgroup of genotypes G13 and G16 within Cluster I based on the lower values in the vast majority of traits. The genotypes G11, G12, and G15 were grouped in the same Cluster I. A subgroup of Cluster II contained only the G9 genotype from Kefalonia Island, exhibiting high values for most of the parameters, which is highlighted with a strong pink color in Figure 4b. The same Cluster II contained the genotypes G14, G8, and G17 from Heraklion, Rethimno, and Chania (Crete), respectively, and G18 from Chios Island. Additionally, Cluster III presented fluctuating responses in different estimated variables, whereas half of the included genotypes originated from Ikaria Island. Specifically, a subgroup consisting of G2 and G6 from Heraklion and G5 and G4 from Ikaria presented medium to high values in most estimated traits. Notably, G4 from Ikaria presented impressively high values on most estimated variables and is thus indicated with different shades of pink color in Figure 4b. A different subgroup of Group III, comprised of the G1, G3, G9, and G7 genotypes, presented small fluctuations around the mean values of estimated variables. Finally, results from the AHC are in accordance with the PCA.

2.5. Genetic Diversity and Molecular Characterization

Concerning the GenAlEx analysis for allelic patterns of the examined samples from *C. maritimum* native Greek populations, i.e., Agio Oros (3 genotypes), Chania (1), Chios (1), Heraklion (3), Ikaria (6), Kalamata (1), Kefalonia (2), and Rethimno (1), the results showed that the mean number of different alleles (Na) was 5.500, while the mean number of different alleles with a frequency $\geq$5% was 4.375. Moreover, the number of effective alleles (Ne) was 3.131, Shanon's information Index (I) was 1.181, and the unbiased expected heterozygosity (uHe) was 0.577 (Table 8). The combined probability of identity (PI) was 1.5×10^{-6}, while the combined value for PIsibs was 4.8×10^{-3}. The results, according to a PCoA analysis, classified the genotypes into three groups. Most of the genotypes were concentrated on the left side of the plot. G2, G6, and G8 formed another group in the right part of the plot. A third cluster is detected in the bottom left quadrant, consisting of G4 and G5. According to the percentage of explained variance (%), which is used to measure the discrepancy between a model and actual data, a small variance between genotypes was revealed, while the percentage of this variance was below 60% (Figure 5a).

Table 8. Diversity statistics for the 18 native Greek rock samphire genotypes based on GenAlEx analysis for allelic patterns.

Locus	Na	Ne	I	Ho	uHe	PI	PIsibs	PIC
CM14	3.000	2.249	0.907	0.529	0.572	0.282	0.543	0.469
CM15	7.000	5.635	1.833	0.722	0.846	0.055	0.352	0.8
CM33	6.000	3.846	1.559	1.000	0.766	0.098	0.405	0.714
CM34	2.000	1.117	0.215	0.111	0.108	0.807	0.899	0.099
CM03	3.000	1.476	0.572	0.278	0.332	0.496	0.713	0.285
CM04	6.000	1.846	0.999	0.389	0.471	0.315	0.599	0.437
CM11	7.000	2.769	1.359	0.667	0.657	0.164	0.472	0.605
CM12	10.000	6.113	2.004	0.611	0.860	0.046	0.343	0.817
Mean	5.500	3.131	1.181	0.538	0.577	0.283	0.541	0.528

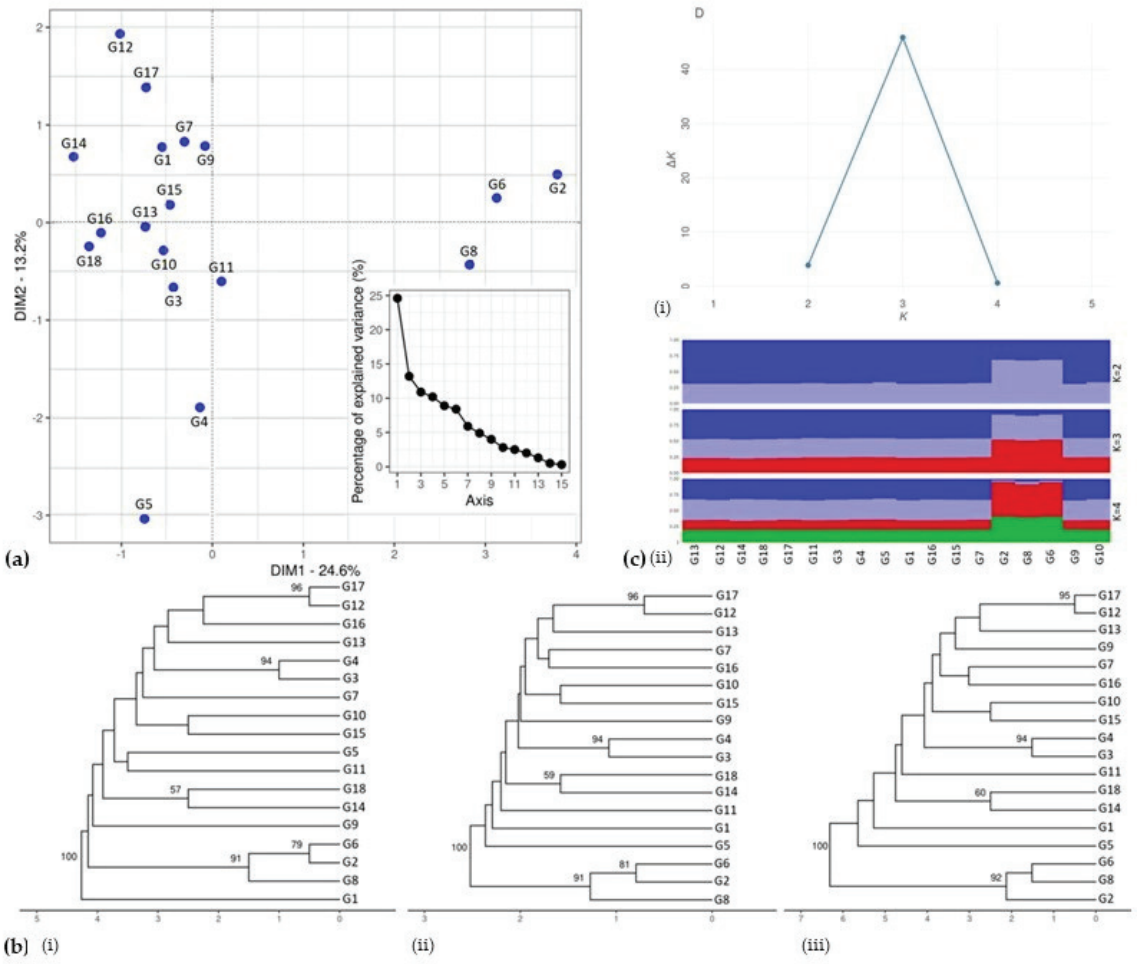

Figure 5. (**a**) Principal Coordinate Analysis (PCoA) plot of 18 native Greek rock samphire genotypes (Table 1) with the percentage of the explained variance (%) demonstrated on the right side of the figure. (**b**) UPGMA dendrogram computed by using three distance measures, i.e., (**i**) Relative dissimilarity matrix, (ii) Euclidean Distance, and (**iii**) Smouse and Peakall distance. (**c**) Distribution of 18 rock samphire genotypes according to molecular data of 8 SSR loci in the Structure software with (**i**) values of Evanno's ΔK statistic indicating the most probable genetic structure model and (**ii**) genetic assignment based on STRUCTURE. The individuals are represented by vertical bars; the colors were assigned according to the group formed in the Structure software (three groups, K = 3).

The three unweighted pair group method with arithmetic average (UPGMA) dendrograms were in concordance with each other, with two main clusters appearing in all of them. According to the first dendrogram using the relative dissimilarity matrix, a large cluster included the majority of genotypes, while a second cluster consisted of G2, G6, and G8. G1 was clustered separately from all the other genotypes [Figure 5(bi)]. The following two dendrograms using the Euclidean Distance and the genetic distance of Smouse and Peakall, respectively, seemed to support the same pattern, forming two clusters with the main one comprising most genotypes and the second one including three genotypes (G2, G8, and G6) [Figure 5(bii,biii)].

To gain further insight, a STRUCTURE analysis was also conducted. In this analysis, K = 3 was deemed as optimal according to the ΔK statistic of Evanno [49]. However, K = 2 also produced a solution that could have biological relevance. For K = 3, the first group assembled all accessions, except from genotypes G2, G8, and G6 which formed a second cluster [Figure 5(ci)]. A similar result was obtained for K = 2 in concordance with the corresponding dendrogram [Figure 5(cii)].

Lately, there has been an escalation in phylogeographical studies regarding coastal and halophytic plants, not only in the Mediterranean Basin, but also along the European coasts [50]. Numerous hypotheses have been suggested to explain the present genetic structure and natural distribution of halophytic species. Understanding the evolutionary history of populations that have emerged from various complex events is challenging work. Hence, researchers should be able to examine different molecular markers from different genomes to comprehend the differences in evolution between species [51]. In contrast to other types of molecular markers, microsatellites, or simple sequence repeats (SSRs), have many advantages, such as simplicity, effectiveness, abundance, hypervariability, reproducibility, co–dominant inheritance, and extensive genomic coverage [52]. The SSRs markers have become one of the most useful molecular markers for cultivar fingerprinting and genetic diversity assessments, molecular mapping, positional cloning, phylogenetic analyses, and marker-assisted breeding [53]. They have successfully been used for many plant species, such as rice (*Oryza sativa*), maize (*Zea mays*), barley (*Hordeum vulgare*), and sorghum (*Sorghum bicolor*) [54–57].

Halophytic plants are ideal models for studying the colonization routes of species because of their simple linear distributions across the coastlines. Thus, a couple of studies have been carried out using SSR molecular markers to analyze the phylogenetic relationships between species and populations of halophytes. In 2010, Escudero et al. [58], made a successful attempt to examine the evolutionary history of 24 populations of the halophyte *Carex extensa*, analyzing its genetic structure with the aim of understanding the heterogeneity of closely related halophytic species. The results indicated that *C. extensa*, together with the South American *Carex vixdentata* and the southern African *Carex ecklonii*, form a monophyletic group of halophytic species [58]. Another study [59] investigated *Nitraria sibirica*'s chloroplast genome to provide insights into comparative genome analysis, and to understand the phylogenetic relationships within the Sapindales. This evolutionary analysis showed that *N. sibirica* belongs to the order Sapindales, providing valuable information about halophytes in general [59]. Evolutionary studies have been performed at the genome level to untangle the conserved features of *Oryza coarctata* within the genus *Oryza*, and to uncover its similarity with other halophytic species and differences from the AA, BB, and FF genome types present in members of the genus *Oryza* [60]. Further phylogenetic analysis, based on the single copy genes among *Oryza* species, pointed to the existence of the *O. coarctata* genome somewhere between the divergence of the FF and BB genomes from the AA genome [60]. In addition, another study identified a number of genic SSR markers from the transcriptomic dataset, providing valuable resources for future ecological and evolutionary studies of *Phragmites karka* [61]. Regarding *C. maritinum*, few studies have been performed to date to investigate and comprehend the phylogenetic relationships between closely related species and populations. Two studies presented in 2005 using an Amplified Fragment Length Polymorphism (AFLP) marker have shown several incipient geographical lineages in the Mediterranean and European coastal regions for *C. maritimum*, but without any noteworthy support, indicating, however, that its colonization happened after the Last Glacial Maximum [21,62].

The results herein indicated a conformity between the analyses from GenAlEx, UPGMA, and STUCTURE software. As evident from the PCoA plot, most native Greek genotypes have similarities to each other, forming a group on the left part of the plot, comprised of genotypes from Kalamata, Chania, Agio Oros, Kefalonia, Ikaria, Chios, and Heraklion. A little further away from these genotypes, there are G2 and G6, 2 genotypes from Heraklion, and G8 from Rethimno. According to the GenAlEx analysis, the results

showed low to moderate diversity between native Greek populations, while the expected heterozygosity (He) was 0.560, and the unbiased expected heterozygosity (uHe) was 0.577. Moreover, Shanon's information Index was quite low in the amount of 1.131. The number of different alleles was 5.500 and the number of effective alleles was 3.131, also pointing to a low diversity pattern. In addition, the low levels of the percentage of the explained variance (under 60%) also indicate the low variability detected between Greek populations of *C. maritimum*.

A genetic structure of a population can generally be interpreted by the amount and distribution of genetic variation within and between populations. According to STUCTURE software, one main group is formed comprised of most of the genotypes and excluding only three of them (G2, G6, and G8) from Heraklion and Rethimno. Therefore, a resemblance between genotypes can be inferred, without significant divergence.

The method of unweighted average binding among clusters, better known as UPGMA, has been used most frequently in ecology and systematics [63], as well as in numerical taxonomy [64]. Regarding the results obtained in this study, we can notice once more the two formed groups on the dendrograms below, which are in agreement with the PCoA and STRUCTURE analysis, excluding genotypes G2, G6, and G8 from Heraklion and Rethimno.

Genetic diversity is crucial for a population to allow for adaptation to changing environments. Gene flow within a population could increase genetic variation, with numerous factors affecting it. Gene duplication, mutation, or other physical processes are some factors leading to this increment. In addition, new variations could be created when a population has high reproduction levels. On the other hand, small populations are more likely to undergo diversity loss gradually, by random chance, via genetic drift. Factors that cause genetic drift might be the unlike number of offspring by different members of a population, such that specific genes increase or decrease in number over generations free of selection, the unexpected immigration or emigration of individuals, resulting in changing genes, etc. Besides genetic drift, gene flow is supposed to be lower in species that have a small distribution range or low adaptability, that arise in fragmented environments, where populations are geographically distant, and the population sizes are small. Overall, it is argued in this study that many island populations of *C. maritimum* in Greece might have low rates of gene flow and thus suffer high genetic drift due to geographic isolation and small population sizes, with the latter being so isolated that the lack of gene flow may lead to high rates of inbreeding.

3. Materials and Methods

3.1. Reagents

Analytical standards of quinic acid (QNA), 3-O-caffeoylquinic acid (3-CQA), 4-O-caffeoylquinic acid (4-CQA), 5-O-caffeoylquinic acid (5-CQA), quercetin-3-O-rutinoside (QURU), quercetin-3-O-glucoside (QUGL), and quercetin-3-O-galactoside (QUGA) were purchased from Extrasynthese (Genay Cedex, France), whereas protocatechuic acid (PRCA), gallic acid (GA), caffeic acid (CA), and *p*-coumaric acid (pCA) were obtained from Sigma-Aldrich (Steinheim, Germany). 1-caffeoylquinic acid (1-CQA), 3,5-dicaffeoylquinic acid (3,5-DCQA), 3,4-dicaffeoylquinic acid (3,4-DCQA), 4,5-dicaffeoylquinic acid (4,5-DCQA), and vicenin-2 were obtained from Carbosynth (Berkshire, UK). All other reagents were of HPLC or LC-MS grade.

3.2. Plant Material

The plant material used in this study is part of the *C. maritimum* germplasm collection maintained ex situ at the grounds of the Balkan Botanic Garden of Kroussia in Northern Greece (Pontokerasia: 41°05′24″ N, 23°06′43″ E and Thermi: 40°32′08.7″ N, 23°00′06.4″ E). All plant materials of *C. maritimum* have been collected directly from wild-growing populations based on sustainable plant exploitation strategies. The collections were conducted using a special permit to the Institute of Plant Breeding and Phytogenetic Resources, Hellenic Agricultural Organization–Dimitra issued by the Greek Ministry of Environment and

Energy, which is renewed annually after a detailed report (for the last two years Permit 82336/879 of 18 May 2019 & 26895/1527 of 21 April 2021). Each genotype after taxonomic identification is allocated a unique IPEN (International Plant Exchange Network) accession number given by the Balkan Botanic Garden of Kroussia (BBGK), Institute of Plant Breeding and Genetic Resources (IPB & GR), Hellenic Agricultural Organization-Dimitra. A total of 18 rock samphire accessions with geographic origin from 8 different and representative regions of Greece were selected for further study and they are presented with relative information in Table 1 and Figure 6.

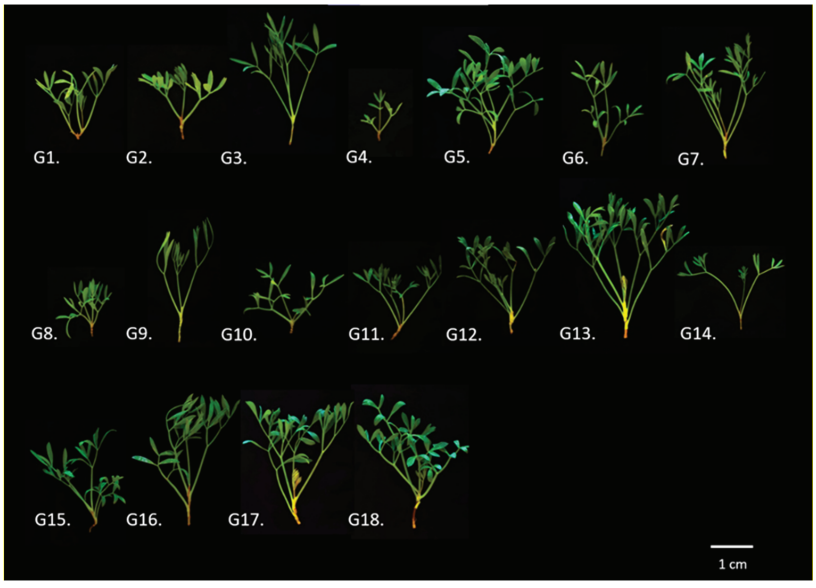

Figure 6. Indicative visual phenotype of the 18 native Greek rock samphire genotypes studied. Explanations for the abbreviations G1–G18 are given in Table 1.

3.3. Sample Preparation

From each of the rock samphire genotypes grown under the same ex situ conditions, 500 g of fresh aerial parts was collected in the stage before flowering in the middle of July, when the plants reached their maximum foliage. Samples were collected and put in sterile polyethylene carrier bags and transported to the laboratory in a portable refrigerator (3–4 °C) not more than one hour after their collection. The fresh samples were divided into leaves and stems and then they were weighed on a digital balance with an accuracy to 0.01 g to calculate their ratio and to avoid tissue-specific differential content in samples. Separated tissue samples were put in plastic bags and were freeze-dried for 72 h with a lyophilizer (Freeze-dryer Alpha 1–2 LD plus, Christ, Osterode, Germany) until they obtained their dw. Afterwards, samples were grounded in a laboratory mill (ZM 1000, Retsch GmbH, Haan, Germany) to pass through a 0.50 mm sieve, and then they were stored at −20 °C until analysis.

3.4. Evaluated Parameters

Several indicators regarding the antioxidant potential of *C. maritimum* (expressed as ABTS and DPPH radical scavenging activity, as well as a FRAP assay), the AsA content, and the bioactive profile (as TPC and TFC) were determined, along with the main phenolic compounds identified and quantified by LC-MS (all described below).

3.4.1. Sample Extraction

To extract each sample, 400 mg of freeze-dried and powdered sample derived of equal portions of leaves and stems of *C. maritimum* were transferred to glass vials containing 4.5 mL of methanol/water (70:30, v/v). The suspension was vortexed for 1 min and then incubated in an ultrasound bath (model FB15051, Thermo Fisher Scientific Inc. Loughborough, UK) for 20 min. Afterwards, the crude extract was centrifuged at 4000× *g* for 10 min, the supernatant was collected, and the pellet was re-extracted as described above. Each extraction was triplicated and all analyses were performed in three replications.

3.4.2. Antioxidant Capacity Determination

For a valid assessment of antioxidant capacity, a combination of methods was important [65]. For this reason, the antioxidant capacity was determined according ABTS and DPPH reactive oxygen species scavenging assays and a FRAP redox potential-based assay. Specifically, ABTS and DPPH scavenging assays are based on electron donation of antioxidants to neutralize ABTS and DPPH radical cations, whereas the FRAP assay is a typical, single electron transfer-based method that measures the reduction of a ferric ion (Fe^{3+})–ligand complex to the intensely blue-colored ferrous (Fe^{2+}) complex by antioxidants in acidic media.

ABTS Radical Scavenging Activity

The radical scavenging activity of rock samphire's extracts against the ABTS radical cation was evaluated according to the protocol of Re et al. [66], which was appropriately adjusted. Briefly, 100 µL of the sample extract was added to 3.9 mL of diluted $ABTS^+$ solution and the absorbance was measured at 734 nm after 4 min against a blank (methanol). The results were expressed as mg trolox equivalents (TE) per g of dried sample (mg TE/g dw).

DPPH Radical Scavenging Activity

The DPPH radical scavenging activity of rock samphire's extracts against the DPPH radical cation was evaluated according to the protocol of Yen and Chen [67], with some modifications. Briefly, 150 mL of the extract was reacted with 2.85 mL of a 0.1 mM methanolic solution of DPPH. After 5 min, the absorbance at 516 nm was recorded, with methanol being used as the blank. The percentage of scavenging effect was calculated by using the following equation: DPPH radical scavenging capacity (%) = $(A_0 - A_s)/A_0 \times 100$, where A_0 and A_s are the absorbance of the blank and the sample, respectively. Results were expressed as mg of TE per g of dried sample (mg TE/g dw).

FRAP Assay

The FRAP assay was carried out according to Benzie and Strain [68], with slight modifications. Briefly, the fresh FRAP reagent consisted of 20 mM ferric chloride solution, 10 mM TPTZ (2,4,6-tripyridyl-s-triazine) solution in 40 mM HCl, and 0.3 mM acetate buffer pH 3.6 in a proportion of 1:1:10, respectively. An aliquot of 100 µL of sample extract was reacted with 3 mL of the FRAP reagent at 37 °C for 4 min under dark conditions, and the absorbance was recorded at 593 nm against a blank (methanol). Results were expressed as mg of TE per g of dried sample (mg TE/g dw).

3.4.3. Ascorbic Acid Determination

The AsA content was determined spectrophotometrically using the ascorbate oxidase (AO) enzyme as previously described [69]. Briefly, 1 g of frozen tissue (*C. maritimum* stems and leaves, 1:1) were ground to a powder using liquid nitrogen, and were extracted using 1 M $HClO_4$. After centrifugation, supernatants were neutralized to pH 5.6 using K_2CO_3. Calculations were based upon the difference in absorbance at 265 nm before, and 3 min after the addition of 1 U/µL AO (Sigma Chemical Co., St Louis, MO, USA) to a 200 µL aliquot of extract in 200 mM sodium phosphate buffer (pH 5.6). Absorbance values were evaluated against a standard curve constructed using L-ascorbic acid (Merck KgaA, Darmstadt, Germany) in the range of 0–100 nmol and expressed as µmol/g of dw.

3.4.4. TPC Determination

The analyses of TPC were performed using the Folin–Ciocalteu's method according to Singleton et al. [70], with some modifications. Briefly, 0.2 mL of sample extract was mixed with 0.8 mL of the Folin–Ciocalteu reagent. After incubation for 2 min, 2 mL of sodium carbonate (7.5% w/v) solution was added to the reaction mixture and the volume was adjusted to 10 mL with distilled water. The mixture was allowed to stand for 60 min in a dark place, and then the absorbance at 725 nm was recorded [71]. The results were expressed as mg of gallic acid equivalent (GAE) per g of sample on a dw basis (mg GAE/g dw).

3.4.5. TFC Determination

The TFC of the sample extracts obtained as described above were evaluated by the $AlCl_3$ reagent method of Bao et al. [72], with slight modifications. An aliquot of 0.3 mL of extract was pipetted into a test tube containing 2 mL of distilled H_2O and mixed with 0.225 mL of 5% $NaNO_2$. After 5 min, 0.225 mL of 10% $AlCl_3 \cdot 6H_2O$ solution was added, the mixture was allowed to stand for another 5 min, and then 0.750 mL of 2 M NaOH was added. The reaction solution was well mixed, kept for 30 min in the dark, and the absorbance was determined at 510 nm. The results were expressed as mg of catechin equivalents (CE) per g of sample on a dw basis (mg CE/g dw).

3.4.6. LC-MS Identification and Quantitation of Metabolomics (Phenolic Compounds)

Identification and quantitation of the phenolic profile from rock samphire extracts was performed according Irakli et al. [46] on a Shimadzu Nexera HPLC system (Kyoto, Japan) consisting of two pumps, a degasser, a column oven, an auto injector, a diode array detector (DAD), and a single quadrupole mass spectrometer combined with an electrospray ionization (ESI) interface. A Poroshell 120 EC-C_{18} column (4.6 × 150 mm, 4 μm) was used for the separation of phenolic compounds and was thermostated at 35 °C, and the flow rate was set at 800 μL/min. Each extract was filtered (pore size 0.2 μm), then an aliquot of 10 μL was injected while the gradient was 0–5 min (15–25% B), 5–10 min (25–35% B), 10–28 min (35–60% B), 28–28.01 min (60–15% B), and an isocratic elution until 35 min. Mobile phase A was 0.1% formic acid in water and mobile phase B was acetonitrile.

The DAD acquisition ranged from 190 to 400 nm. The mass spectrometer was equipped with an ESI source recorded on a negative ionization mode under the following conditions: interface voltage, +4.5 kV; curved desolvation line (CDL) voltage, 20 V; nebulizing gas (nitrogen) flow, 1.5 L/min; drying gas flow, 15 L/min; block heater temperature, 200 °C; CDL temperature, 250 °C. Mass acquisitions were performed in full scan mode (100–1000 m/z) and selective ion monitoring mode (SIM). Data acquisition and processing was done using Lab Solutions LC-MS software (Shimadzu, Kyoto, Japan).

The identification of all constituents was performed by LC-DAD-MS analysis by comparing the retention time, as well as the UV and MS spectra of the peaks in the extracts with those of authentic reference samples. The method of internal standard (salicylic acid) was applied to quantify the phenolic compounds of *C. maritimum*. Quantification was carried out at SIM mode, constructing calibrations curves of corresponding standard solutions at five concentration levels within the linear range of 0.01 to 4 μg/mL. Correlation coefficients (r^2) from calibration curves for all the compounds were between 0.9969 and 0.9999. The limit of detection was in the range of 0.007–0.093 ng/mL and the limit of quantification was from 0.021 to 0.282 μg/mL The results of intra-day and inter-day precision was less than 6.1% and 10.6%, respectively. The quantification of coumaroyl-quinic and feruoyl-quinic acids was based on standard curves generated by the 3-CQA due to the lack of commercial standards. Analyses were carried out in triplicate and the results were expressed as mg per 100 g of sample.

3.5. DNA Isolation

Isolation of DNA from leaves was performed with the NucleoSpin Plant kit (Macherey–Nagel, Düren, Germany), according to the manufacturer's instructions. DNA quantity

(concentration) was estimated in a NanoDrop™ One/OneC Microvolume UV-Vis Spectrophotometer, by Thermo Fisher Scientific, by determining the absorbance at 260 nm, while DNA quality was determined by 1% agarose gel electrophoresis using MIDORI Green Direct by Nippon Genetics. Samples were then diluted to 25 ng/μL to form working solutions.

3.6. Multiplex Polymerase Chain Reaction (PCR) and Capillary Electrophoresis (CE)

Samples were genotyped with eight simple sequence repeat (SSRs) markers (CM03, CM04, CM11, CM12, CM14, CM15, CM33, and CM34). The forward primers were labeled with FAM, HEX, and ROX fluorescent dyes. Multiplex PCR was performed using KAPA2G Fast Multiplex PCR Kit (KAPA Biosystems, Wilmington, MA, USA)). The 2× Multiplex Mix contains KAPA2G Fast HotStart DNA Polymerase (1 U per 25 μL reaction), KAPA2G Buffer A (1.5× at 1×), dNTPs (0.2 mM each dNTP at 1×), MgCl2 (3.0 mM at 1×), and stabilizers. Amplifications were performed in a reaction volume of 25 μL containing 2× KAPA2G Fast Multiplex Mix (12.5 μL), 10 μM Forward Primer (0.5 μL each), 10 μM Reverse Primer (0.5 μL each), DNA (0.5 μL), and PCR-grade Water (up to 25 μL). The PCR was performed in the following thermocycling conditions: 1 cycle of initial denaturation at 95 °C for 3 min, followed by 35 cycles of denaturation at 95 °C for 15 s, annealing at 60 °C for 30 s, extension at 72 °C for 30 s, and 1 cycle of final extension at 72 °C for 1 min. The resulting PCR products were first visualized by 2% agarose gel electrophoresis and then loaded into an SeqStudio Genetic Analyzer, a fluorescence-based capillary electrophoresis system, for fragment analysis (Applied Biosystems, Foster City, CA, USA). SSR fragments were scored via GeneMapper v6 software using the internal size standard GS 600 LIZ (Applied Biosystems, Foster City, CA, USA).

3.7. Data Analysis and Cluster Analysis

ANOVA was carried out using the computer software MSTAT-C version 1.41 (Michigan State University, East Lansing, MI, USA). Data of TPC, TFC, ABTS, and DPPH radical scavenging activity, as well as of the FRAP assay, were subjected to an ANOVA by using the experiment model number 7 of one factor (rock samphire genotype) randomized complete block design. Tukey's multiple comparison procedures were used to detect and separate the eighteen means differences at $p < 0.05$. Pearson's correlation coefficient was used for the determination of the relationships between the variables by using SPSS Statistics 21.0 software (SPSS Inc., Chicago, IL, USA). The web tool Clustvis [73] was used for the visualization of clustering on multivariate data using PCA and AHC. The construction of two-dimensional (2-D) plots was based on the first two principal components (PCs). The AHC analysis was performed using Euclidean distance and Ward's method for agglomeration to systematically analyze the combined bioactive compounds and antioxidant capacity per *C. maritimum* genotype.

Principal Coordinate Analysis (PCoA), which is used when variables are qualitative or discrete, thus offering a unique analytical solution, was applied for molecular data. PCoA based on Euclidean distance was performed using the cmdscale function in R 4.1.0 [74]. For the identification of unique genotypes of *C. maritimum*, all possible pairwise comparisons between two genotypes were attempted. The number of alleles per locus (Na) and the observed (Ho) and expected (He) heterozygosity (assuming Hardy–Weinberg equilibrium) were calculated using GenAlEx software [75]. The probability that two individuals will, by chance, have the same multilocus genotype was investigated by estimates for Probability of Identity (PI) and Probability of Identity between siblings (PIsibs), which were also inferred with the same software. Polymorphic Information Content (PIC) for each genetic marker employed was estimated by the polysat R package [76], whereas UPGMA dendrograms were constructed. Three different genetic distances, namely relative dissimilarity, Euclidean distance, and the individual genetic distance measure of Smouse and Peakall were used [77].

Possible population structure was analyzed to examine how geographical distribution affects the genotype similarity in genetically homogenous populations using a model-based Bayesian procedure implemented in the STRUCTURE v.2.3.4 software [78,79]. Genotypes

were divided into genetic clusters using the "admixture" model along with the "uncorrelated allele frequencies" model. Analyses were run with 500,000 burn-in iterations followed by 1,000,000 iterations for Markov chain Monte Carlo in 20 independent runs for each number of clusters (K) from 1 to 5. The most likely K was determined by employing the Evanno method [49] and visualizations were made using the pophelper v2.3.1 R package [80].

4. Conclusions

In summary, the present work constitutes the first characterization of native Greek rock samphire germplasm in terms of metabolomic and molecular fingerprinting. The wide variation observed in the bioactive compounds and the antioxidant capacity, as well as the low variability and the low to moderate diversity observed in the genetic profile of Greek rock samphire genotypes, revealed that the germplasm collection conserved in the Balkan Botanic Garden of Kroussia in Northern Greece could serve as an important source of genetic material for artificial selection and future plant breeding. Interestingly, the most remarkable and distinctive genotype genotypes were G9 from Kefalonia Island, followed by G4 from Ikaria Island; both clearly exhibited a rather similar response with high values in the evaluated traits. Based on the reported outcomes here, these *C. maritimum* genotypes stand out as well-documented, and therefore they can be prioritized for large scale cultivation. Additionally, these genotypes can be the springboard for the development of new *C. maritimum* cultivars with desirable traits with respect to polyphenolic content and/or antioxidant potential.

Author Contributions: Conceptualization, I.G. and K.K.; methodology, K.K., M.I., A.B., I.M., N.M., E.S., N.K., K.G., E.M., A.X. and I.G.; formal analysis, K.K., N.T. and V.G.; investigation, K.K., A.B., N.M., T.M. and M.I.; data curation, K.K. and N.M.; writing—original draft preparation, K.K. and A.B.; review and editing, M.I., I.M., E.S., V.G., N.T., N.K., K.G., E.M., A.X. and I.G.; supervision, K.K. and I.G. All authors have read and agreed to the published version of the manuscript.

Funding: This research did not receive any specific grant from funding agencies in the public, commercial, or not-for-profit sectors. This investigation has been financially supported by the Hellenic Agricultural Organization-Dimitra.

Institutional Review Board Statement: Not applicable.

Informed Consent Statement: Not applicable.

Data Availability Statement: The data is available from the authors upon request.

Conflicts of Interest: The authors declare that they have no known competing financial interests or personal relationships that could have appeared to influence the work reported in this paper.

References

1. Sarrou, E.; Siomos, A.S.; Riccadona, S.; Aktsoglou, D.-C.; Tsouvaltzis, P.; Angeli, A.; Franceschi, P.; Chatzopoulou, P.; Vrhovsek, U.; Martens, S. Improvement of sea fennel (*Crithmum maritimum* L.) nutritional value through iodine biofortification in a hydroponic floating system. *Food Chem.* **2019**, *296*, 150–159. [CrossRef] [PubMed]
2. Pateira, L.; Nogueira, T.; Antunes, A.; Venâncio, F.; Tavares, R.; Capelo, J. Two chemotypes of *Crithmum maritimum* L. from Portugal. *Flavour Fragr. J.* **1999**, *14*, 333–343. [CrossRef]
3. Atia, A.; Barhoumi, Z.; Mokded, R.; Abdelly, C.; Smaoui, A. Environmental eco-physiology and economical potential of the halophyte *Crithmum maritimum* L. (Apiaceae). *J. Med. Plants Res.* **2011**, *5*, 3564–3571.
4. Hamed, K.B.; Debez, A.; Chibani, F.; Abdelly, C. Salt response of *Crithmum maritimum*, an oleaginous halophyte. *Trop. Ecol.* **2004**, *45*, 151–159.
5. Latron, M.; Arnaud, J.F.; Ferla, H.; Godé, C.; Duputié, A. Polymorphic nuclear markers for coastal plant species with dynamic geographic distributions, the rock samphire (*Crithmum maritimum*) and the vulnerable dune pansy (*Viola tricolor* subsp. *curtisii). Mol. Biol. Rep.* **2018**, *45*, 203–209. [CrossRef] [PubMed]
6. Renna, M. Reviewing the prospects of sea fennel (*Crithmum maritimum* L.) as emerging vegetable crop. *Plants* **2018**, *7*, 92. [CrossRef] [PubMed]
7. Özcan, M.; Akgül, A.; Başcr, K.H.C.; Özck, T.; Tabanca, N. Essential oil composition of sea fennel (*Crithmum maritimum*) form Turkey. *Nahrung Food* **2001**, *45*, 353–356. [CrossRef]

8. Pereira, A.G.; Fraga-Corral, M.; García-Oliveira, P.; Jimenez-Lopez, C.; Lourenço-Lopes, C.; Carpena, M.; Otero, P.; Gullón, P.; Prieto, M.A.; Simal-Gandara, J. Culinary and nutritional value of edible wild plants from northern Spain rich in phenolic compounds with potential health benefits. *Food Funct.* **2020**, *11*, 8493–8515. [CrossRef]
9. Giungato, P.; Renna, M.; Rana, R.; Licen, S.; Barbieri, P. Characterization of dried and freeze-dried sea fennel (*Crithmum maritimum* L.) samples with headspace gas-chromatography/mass spectrometry and evaluation of an electronic nose discrimination potential. *Food Res. Int.* **2019**, *115*, 65–72. [CrossRef]
10. Montesano, F.F.; Gattullo, C.E.; Parente, A.; Terzano, R.; Renna, M. Cultivation of potted sea fennel, an emerging Mediterranean halophyte, using a renewable seaweed-based material as a peat substitute. *Agriculture* **2018**, *8*, 96. [CrossRef]
11. Zarrouk, M.; El Almi, H.; Ben Youssef, N.; Sleimi, N.; BenMiled, D.; Smaoui, A.; Abdelly, C. Lipid composition of seeds of local halophytes: *Cakile maritima*, *Zygophyllum album* and *Crithmum maritimum*. In *Cash Crop Halophytes: Recent Studies*; Lieth, H., Ed.; Springer: Dordrecht, The Netherlands, 2003; pp. 121–122.
12. Jallali, I.; Megdiche, W.; M'Hamdi, B.; Queslati, S.; Smaoui, A.; Abdelly, C.; Ksouri, R. Changes in phenolic composition and antioxidant activities of the edible halophyte *Crithmum maritimum* L. with physiological stage and extraction method. *Acta Physiol Plant* **2012**, *34*, 1451–1459. [CrossRef]
13. Jallali, I.; Zaouali, Y.; Missaoui, I.; Smeoui, A.; Abdelly, C.; Ksouri, R. Variability of antioxidant and antibacterial effects of essential oils and acetonic extracts of two edible halophytes: *Crithmum maritimum* L. and *Inula crithmoïdes* L. *Food Chem.* **2014**, *145*, 1031–1038. [CrossRef] [PubMed]
14. Meot-Duros, L.; Magné, C. Antioxidant activity and phenol content of *Crithmum maritimum* L. leaves. *Plant Physiol. Biochem.* **2009**, *47*, 37–41. [CrossRef] [PubMed]
15. Suresh, U.; Murugan, K.; Panneerselvam, C.; Aziz Al, T.; Cianfaglione, K.; Wang, L.; Maggi, F. Encapsulation of sea fennel (*Crithmum maritimum*) essential oil in nanoemulsion and SiO_2 nanoparticles for treatment of the crop pest *Spodoptera litura* and the dengue vector *Aedes aegypti*. *Ind. Crops Prod.* **2020**, *158*, 113033. [CrossRef]
16. Mekinić, G.I.; Blažević, I.; Mudnić, I.; Burčul, F.; Grga, M.; Skroza, D.; Jerčić, I.; Ljubenkov, I.; Boban, M.; Miloš, M.; et al. Sea fennel (*Crithmum maritimum* L.): Phytochemical profile, antioxidative, cholinesterase inhibitory and vasodilatory activity. *J. Food Sci. Technol.* **2016**, *53*, 3104–3112. [CrossRef]
17. Burczyk, J.; Wierzchowska-Renke, K.; Głowniak, K.; Głowniak, P.; Marek, D. Geographic and environmental influences on the variation of essential oil and coumarins in *Crithmum maritimum* L. *J. Herbs Spices Med. Plants* **2002**, *9*, 305–311. [CrossRef]
18. Sánchez-Faure, A.; Calvo, M.M.; Pérez-Jiménez, J.; Martín-Diana, A.B.; Rico, D.; Montero, M.P.; Gómez-Guillén, M.C.; López-Caballero, M.E.; Martínez-Alvarez, O. Exploring the potential of common iceplant, seaside arrowgrass and sea fennel as edible halophytic plants. *Food Res. Int.* **2020**, *137*, 109613. [CrossRef]
19. Grigoriadou, K.; Maloupa, E. Micropropagation and salt tolerance of in vitro grown *Crithmum maritimum* L. *Plant Cell Tissue Organ Cult.* **2008**, *94*, 209–217. [CrossRef]
20. Meot-Duros, L.; Magné, C. Effect of salinity and chemical factors on seed germination in the halophyte *Crithmum maritimum* L. *Plant Soil* **2008**, *313*, 83–87. [CrossRef]
21. Kadereit, J.; Arafeh, R.; Somogyi, G.; Westberg, E. Terrestrial growth and marine dispersal? Comparative phylogeography of five coastal plant species at a European scale. *Taxon* **2005**, *54*, 861–876. [CrossRef]
22. Arafeh, R.M. Molecular Phylogeography of the European Coastal Plants *Crithmum maritimum* L., *Halimione portulacoides* (L.) Aellen, *Salsola kali* L. and *Calystegia soldanella* (L.) R.Br. Ph.D. Thesis, Am Fachbereich Biologie der Johannes Gutenberg-Uni-versität, Mainz, Germany, 2005.
23. Xanthopoulou, A.; Ganopoulos, I.; Kalivas, A.; Nianiou-Obeidat, I.; Ralli, P.; Moysiadis, T.; Tsaftaris, A.; Madesis, P. Comparative analysis of genetic diversity in Greek Genebank collection of summer squash (*'Cucurbita pepo'*) landraces using start codon targeted (SCoT) polymorphism and ISSR markers [online]. *Aust. J. Crop Sci.* **2015**, *9*, 14–21.
24. Vos, P.; Hogers, R.; Bleeker, M.; Reijans, M.; van de Lee, T.; Hornes, M.; Friters, A.; Pot, J.; Paleman, J.; Kuiper, M.; et al. AFLP: A new technique for DNA fingerprinting. *Nucleic Acids Res.* **1995**, *23*, 4407–4414. [CrossRef] [PubMed]
25. Roncallo, P.F.; Beaufort, V.; Larsen, A.O.; Dreisigacker, S.; Echenique, V. Genetic diversity and linkage disequilibrium using SNP (KASP) and AFLP markers in a worldwide durum wheat (*Triticum turgidum* L. var. *durum*) collection. *PLoS ONE* **2019**, *14*, e0218562. [CrossRef] [PubMed]
26. Stathi, E.; Kougioumoutzis, K.; Abraham, E.M.; Trigas, P.; Ganopoulos, I.; Avramidou, E.V.; Tani, E. Population genetic variability and distribution of the endangered Greek endemic *Cicer graecum* under climate change scenarios. *AoB Plants* **2020**, *12*, plaa007. [CrossRef] [PubMed]
27. Zietkiewicz, E.; Rafalski, J.; Labuda, D. Genome fingerprinting by simple sequence repeat (SSR)-anchored polymerase chain reaction amplification. *Genomics* **1994**, *20*, 176–183. [CrossRef] [PubMed]
28. Ganopoulos, I.; Merkouropoulos, G.; Pantazis, S.; Tsipouridis, C.; Tsaftaris, A. Assessing molecular and morpho-agronomical diversity and identification of ISSR markers associated with fruit traits in quince (*Cydonia oblonga*). *Gen. Mol. Res.* **2011**, *10*, 2729–2746. [CrossRef] [PubMed]
29. Nabet, N.; Boudries, H.; Chougui, N.; Loupassaki, S.; Souagui, S.; Burló, F.; Hernández, F.; Carbonell-Barrachina, Á.A.; Madani, K.; Larbat, R. Biological activities and secondary compound composition from *Crithmum maritimum* aerial parts. *Int. J. Food Prop.* **2017**, *20*, 1843–1855. [CrossRef]

30. Sousa, G.; Alves, M.I.; Neves, M.; Tecelão, C.; Ferreira-Dias, S. Enrichment of sunflower oil with ultrasound-assisted extracted bioactive compounds from *Crithmum maritimum* L. *Foods* **2022**, *11*, 439. [CrossRef] [PubMed]
31. Souid, A.; Della Croce, C.M.; Frassinetti, S.; Gabriele, M.; Pozzo, L.; Ciardi, M.; Abdelly, C.; Hamed, K.B.; Magné, C.; Longo, V. Nutraceutical potential of leaf hydro-ethanolic extract of the edible halophyte *Crithmum maritimum* L. *Molecules* **2021**, *26*, 5380. [CrossRef] [PubMed]
32. Males, Z.; Zuntar, I.; Nigovic, B.; Plazibat, M.; Vundać, V.B. Quantitative analysis of the polyphenols of the aerial parts of rock samphire-*Crithmum maritimum* L. *Acta Pharm.* **2003**, *53*, 139–144. [PubMed]
33. Petropoulos, S.A.; Karkanis, A.; Martins, N.; Ferreira, I.C. Edible halophytes of the Mediterranean basin: Potential candidates for novel food products. *Trends Food Sci. Technol.* **2018**, *74*, 69–84. [CrossRef]
34. Chu, Y.F.; Sun, J.; Wu, X.; Liu, R.H. Antioxidant and antiproliferative activities of common vegetables. *J. Agric. Food Chem.* **2002**, *50*, 6910–6916. [CrossRef] [PubMed]
35. Martins-Noguerol, R.; Matías, L.; Pérez-Ramos, I.M.; Moreira, X.; Muñoz-Vallés, S.; Mancilla-Leytón, J.M.; Francisco, M.; García-González, A.; DeAndrés-Gil, C.; Martínez-Force, E.; et al. Differences in nutrient composition of sea fennel (*Crithmum maritimum*) grown in different habitats and optimally controlled growing conditions. *J. Food Compos. Anal.* **2022**, *106*, 104266. [CrossRef]
36. Zhou, K.; Yu, L. Total phenolic contents and antioxidant properties of commonly consumed vegetables grown in Colorado. *LWT-Food Sci. Technol.* **2006**, *39*, 1155–1162.
37. Pereira, C.G.; Barreira, L.; da Rosa Neng, N.; Nogueira, J.M.F.; Marques, C.; Santos, T.F.; Varela, J.; Custódio, L. Searching for new sources of innovative products for the food industry within halophyte aromatic plants: In vitro antioxidant activity and phenolic and mineral contents of infusions and decoctions of *Crithmum maritimum* L. *Food Chem. Toxicol.* **2017**, *107*, 581–589. [CrossRef]
38. Zafeiropoulou, V.; Tomou, E.M.; Ioannidou, O.; Karioti, A.; Skaltsa, H. Sea fennel: Phytochemical analysis of Greek wild and cultivated *Crithmum maritimum* L. populations, based on HPLC-PDA-MS and NMR methods. *J. Pharmacogn. Phytochem.* **2020**, *9*, 998–1004.
39. Alves-Silva, J.M.; Guerra, I.; Gonçalves, M.J.; Cavaleiro, C.; Cruz, M.T.; Figueirinha, A.; Salgueiro, L. Chemical composition of *Crithmum maritimum* L. essential oil and hydrodistillation residual water by GC-MS and HPLC-DAD-MS/MS, and their biological activities. *Ind. Crops Prod.* **2020**, *149*, 112329. [CrossRef]
40. Siracusa, L.; Kulisic-Bilusic, T.; Politeo, O.; Krause, I.; Dejanovic, B.; Ruberto, G. Phenolic cmposition and antioxidant activity of aqueous infusions from *Capparis spinosa* L. and *Crithmum maritimum* L. before and after submission to a two-step in vitro digestion model. *J. Agric. Food Chem.* **2011**, *59*, 12453–12459. [CrossRef]
41. Mekinić, I.G.; Šimat, V.; Ljubenkov, I.; Burčul, F.; Grga, M.; Mihajlovski, M.; Lončar, R.; Katalinić, V.; Skroza, D. Influence of the vegetation period on sea fennel, *Crithmum maritimum* L. (Apiaceae), phenolic composition, antioxidant and anticholinesterase activities. *Ind. Crops Prod.* **2018**, *124*, 947–953. [CrossRef]
42. Schaller, R.G.; Schnitzler, W.H. Nitrogen nutrition and flavour compounds of carrots (*Daucus carota* L.) cultivated in Mitscherlich pots. *J. Sci. Food Agric.* **2000**, *80*, 49–56. [CrossRef]
43. Brooks, J.S.; Feeny, P. Seasonal variation in *Daucus carota* leaf-surface and leaf tissue chemical profile. *Biochem. Syst. Ecol.* **2004**, *32*, 769–782. [CrossRef]
44. Krizman, M.; Baricevic, D.; Prosek, M. Determination of phenolic compounds in fennel by HPLC and HPLC-MS using a monolithic reversed-phase column. *J. Pharm. Biomed. Anal.* **2007**, *43*, 481–485. [CrossRef] [PubMed]
45. Vina, S.Z.; Chaves, A.R. Antioxidant responses in minimally processed celery during refrigerated storage. *Food Chem.* **2006**, *94*, 68–74. [CrossRef]
46. Irakli, M.; Skendi, A.; Bouloumpasi, E.; Chatzopoulou, P.; Biliaderis, C.G. LC-MS identification and quantification of phenolic compounds in solid residues from the essential oil industry. *Antioxidants* **2021**, *10*, 2016. [CrossRef]
47. Xu, J.G.; Hu, Q.P.; Liu, Y. Antioxidant and DNA-protective activities of chlorogenic acid isomers. *J. Agric. Food Chem.* **2012**, *60*, 11625–11630. [CrossRef]
48. Kooti, W.; Moradi, M.; Ali-Akbari, S.; Sharafi-Ahvazi, N.; Asadi-Samani, M.; Ashtary-Larky, D. Therapeutic and pharmacological potential of *Foeniculum vulgare* Mill: A review. *J. Herbmed Pharmacol.* **2015**, *4*, 1–9.
49. Evanno, G.; Regnaut, S.; Goudet, J. Detecting the number of clusters of individuals using the software Structure: A simulation study. *Mol. Ecol.* **2005**, *14*, 2611–2620. [CrossRef]
50. Weising, K.; Freitag, H. Phylogeography of halophytes from European coastal and inland habitats. *Zool. Anz.* **2007**, *246*, 279–292. [CrossRef]
51. Templeton, A.R. Genetics and recent human evolution. *Evolution* **2007**, *61*, 1507–1519. [CrossRef]
52. Garcia, A.A.F.; Benchimol, L.L.; Barbosa, A.M.M.; Geraldi, I.O.; Souza, C.L.; de Souza, A.P. Comparison of RAPD, RFLP, AFLP and SSR markers for diversity studies in tropical maize inbred lines. *Genet. Mol. Biol.* **2004**, *27*, 579–588. [CrossRef]
53. Saha, M.C.; Mian, M.A.R.; Eujayl, I.; Zwonitzer, J.C.; Wang, L.; May, G.D. Tall fescue EST-SSR markers with transferability across several grass species. *TAG* **2004**, *109*, 783–791. [CrossRef] [PubMed]
54. Rani, J.; RaShmi, K.; Sinha, S.; Sahay, S.; Mandal, S.S.; Singh, B. Molecular diversity of babycorn (*Zea mays*) inbred lines by rice SSR Marker. *Indian J. Agric. Sci.* **2020**, *90*, 1212–1215.
55. Sara, S.M.; Said, W.M.; Abdel-Tawab, F.M.; Kamal, L.M.; Mahmoud Shata, S. Phylogenetic relationships of some barley (*Hordeum vulgare* L.) accessions in Egypt. *EJGC* **2021**, *50*, 41–63.

56. Song, Y.; Chen, Y.; Lv, J.; Xu, J.; Zhu, S.; Li, M. Comparative chloroplast genomes of *Sorghum* Species: Sequence divergence and phylogenetic relationships. *Biomed Res. Int.* **2019**, *2019*, 5046958. [CrossRef]
57. Tripathi, S.; Singh, S.K.; Srivashtav, V.; Khaire, A.R.; Vennela, P.; Singh, D.K. Molecular diversity analysis in rice (*Oryza sativa* L.) using SSR markers. *Electron. J. Plant Breed.* **2020**, *11*, 776–782.
58. Escudero, M.; Vargas, P.; Arens, P.; Ouborg, N.J.; LuceÑo, M. The east-west-north colonization history of the Mediterranean and Europe by the coastal plant *Carex extensa* (Cyperaceae). *Mol. Ecol.* **2010**, *19*, 352–370. [CrossRef]
59. Lu, L.; Li, X.; Hao, Z.; Yang, L.; Zhang, J.; Peng, Y.; Xu, H.; Lu, Y.; Zhang, J.; Shi, J.; et al. Phylogenetic studies and comparative chloroplast genome analyses elucidate the basal position of halophyte *Nitraria sibirica* (Nitrariaceae) in the Sapindales. *DNA Mapp. Seq. Anal.* **2017**, *29*, 745–755. [CrossRef]
60. Mondal, T.K.; Rawal, H.C.; Chowrasia, S.; Varshney, D.; Panda, A.K.; Mazumdar, A.; Kaur, H.; Gaikwad, K.; Sharma, T.R.; Singh, N.K. Draft genome sequence of first monocot-halophytic species *Oryza coarctata* reveals stress-specific genes. *Sci. Rep.* **2018**, *8*, 13698. [CrossRef]
61. Nayak, S.S.; Pradhan, S.; Sahoo, D.; Parida, A. De novo transcriptome assembly and analysis of *Phragmites karka*, an invasive halophyte, to study the mechanism of salinity stress tolerance. *Sci. Reps.* **2020**, *10*, 5192. [CrossRef]
62. Kadereit, J.W.; Westberg, E. Phylogeographic structure of seven coastal species. Determinants of phylogeographic structure: A comparative study of seven coastal flowering plant species across their European range. *Watsonia* **2007**, *26*, 229–238.
63. James, F.C.; Mcculloch, C.E. Multivariate analysis in ecology and systematics: Panacea or pandora's box? *Annu. Rev. Ecol. Sys.* **1990**, *21*, 129–166. [CrossRef]
64. Schlee, D.; Sneath, P.H.A.; Sokal, R.R.; Freeman, W.H. Numerical taxonomy. The principles and practice of numerical classification. *Syst. Zool.* **1975**, *24*, 263. [CrossRef]
65. Frankel, E.N.; Meyer, A.S. The problems of using one-dimensional methods to evaluate multifunctional food and biological antioxidants. *J. Sci. Food Agric.* **2000**, *80*, 1925–1941. [CrossRef]
66. Re, R.; Pellegrini, N.; Proteggente, A.; Pannala, A.; Yang, M.; Rice-Evans, C. Antioxidant activity applying an improved ABTS radical cation decolorization assay. *Free Radic. Biol. Med.* **1999**, *26*, 1231–1237. [CrossRef]
67. Yen, G.C.; Chen, H.Y. Antioxidant activity of various tea extracts in relation to their antimutagenicity. *J. Agric. Food Chem.* **1995**, *43*, 27–32. [CrossRef]
68. Benzie, F.; Strain, J. Ferric reducing/antioxidant power assay: Direct measure of total antioxidant activity of biological fluids and modified version for simultaneous measurement of total antioxidant power and ascorbic acid concentration. *Methods Enzymol.* **1999**, *299*, 15–23.
69. Pateraki, I.; Sanmartin, M.; Kalamaki, M.S.; Gerasopoulos, D.; Kanellis, A.K. Molecular characterization and expression studies during melon fruit development and ripening of L-galactono-1,4-lactone dehydrogenase. *J. Exp. Bot.* **2004**, *55*, 1623–1633. [CrossRef]
70. Singleton, V.L.; Orthofer, R.; Lamuela-Raventós, R.M. Analysis of total phenols and other oxidation substrates and antioxidants by means of Folin-Ciocalteu reagent. *Meth. Enzymol.* **1999**, *299*, 152–178.
71. Irakli, M.N.; Samanidou, V.F.; Biliaderis, C.G.; Papadoyannis, I.N. Development and validation of an HPLC-method for determination of free and bound phenolic acids in cereals after solid-phase extraction. *Food Chem.* **2012**, *134*, 624–1632. [CrossRef]
72. Bao, S.; Cai, Y.; Sun, M.; Wang, G.Y.; Corke, H. Anthocyanins, flavonols, and free radical scavenging activity of Chinese bayberry (*Myrica rubra*) extracts and their color properties and stability. *J. Agric. Food Chem.* **2005**, *53*, 2327–2332. [CrossRef]
73. Metsalu, T.; Vilo, J. ClustVis: A web tool for visualizing clustering of multivariate data using Principal Component Analysis and heatmap. *Nucleic Acids Res.* **2015**, *43*, W566–W570. [CrossRef] [PubMed]
74. R Core Team. *R: A Language and Environment for Statistical Computing*; R Foundation for Statistical Computing: Vienna, Austria, 2021.
75. Peakall, R.; Smouse, P.E. GenAlEx 6.5: Genetic analysis in Excel. Population genetic software for teaching and research—An update. *Bioinformatics* **2012**, *28*, 2537. [CrossRef] [PubMed]
76. Clark, L.V.; Jasieniuk, M. Polysat: An R package for polyploid microsatellite analysis. *Mol. Ecol. Resour.* **2011**, *11*, 562–566. [CrossRef] [PubMed]
77. Smouse, P.E.; Peakall, R. Spatial autocorrelation analysis of individual multiallele and multilocus genetic structure. *Heredity* **1999**, *82*, 561–573. [CrossRef] [PubMed]
78. Baldoni, L.; Tosti, N.; Ricciolini, C.; Belaj, A.; Arcioni, S.; Pannelli, G.; Germana, M.A.; Mulas, M.; Porceddu, A. Genetic structure of wild and cultivated olives in the Central Mediterranean Basin. *Ann. Bot.* **2006**, *98*, 935–942. [CrossRef]
79. Rosenberg, N.A.; Pritchard, J.K.; Weber, J.L.; Cann, H.M.; Kidd, K.K.; Zhivotovsky, L.A.; Feldman, M.W. Genetic structure of human populations. *Science* **2002**, *298*, 2381–2385. [CrossRef]
80. Francis, R.M. Pophelper: An R package and web app to analyse and visualize population structure. *Mol. Ecol. Resour.* **2017**, *17*, 27–32. [CrossRef]

plants

MDPI

Article

Assessment of the Fertilization Capacity of the Aquaculture Sediment for Wheat Grass as Sustainable Alternative Use

Marian Burducea [1,*], Andrei Lobiuc [2], Lenuta Dirvariu [1], Eugen Oprea [1], Stefan Mihaita Olaru [3], Gabriel-Ciprian Teliban [4], Vasile Stoleru [4], Vlad Andrei Poghirc [5], Irina Gabriela Cara [5], Manuela Filip [5], Mariana Rusu [5], Valtcho D. Zheljazkov [6] and Cristian-Alin Barbacariu [1]

[1] Research and Development Station for Aquaculture and Aquatic Ecology, "Alexandru Ioan Cuza" University, Carol I, 20A, 700505 Iasi, Romania; dirvariu.lenuta@gmail.com (L.D.); eugen.oprea@uaic.ro (E.O.); alin.barbacariu@uaic.ro (C.-A.B.)
[2] Human Health and Development Department, "Stefan Cel Mare" University, Strada Universitatii, 720229 Suceava, Romania; andrei.lobiuc@usm.ro
[3] Faculty of Biology, "Alexandru Ioan Cuza" University, Carol I, 20A, 700505 Iasi, Romania; stefan.olaru93@gmail.com
[4] Faculty of Horticulture, "Ion Ionescu de la Brad" Iasi University of Life Sciences, Aleea Mihail Sadoveanu 3, 700490 Iasi, Romania; gabrielteliban@uaiasi.ro (G.-C.T.); vstoleru@uaiasi.ro (V.S.)
[5] Research Institute for Agriculture and Environment, "Ion Ionescu de la Brad" Iasi University of Life Sciences, 9 Mihail Sadoveanu Alley, 700789 Iasi, Romania; vlad.poghirc@uaiasi.ro (V.A.P.); carairina@uaiasi.ro (I.G.C.); filipmanuela@yahoo.com (M.F.); rusumariana910@yahoo.com (M.R.)
[6] Crop and Soil Science Department, Oregon State University, 109 Crop Science Building, 3050 SW Campus Way, Corvallis, OR 97331, USA; valtcho.jeliazkov@oregonstate.edu
* Correspondence: marian.burducea@uaic.ro

Citation: Burducea, M.; Lobiuc, A.; Dirvariu, L.; Oprea, E.; Olaru, S.M.; Teliban, G.-C.; Stoleru, V.; Poghirc, V.A.; Cara, I.G.; Filip, M.; et al. Assessment of the Fertilization Capacity of the Aquaculture Sediment for Wheat Grass as Sustainable Alternative Use. *Plants* **2022**, *11*, 634. https://doi.org/10.3390/plants11050634

Academic Editors: Milan S. Stankovic, Paula Baptista and Petronia Carillo

Received: 10 February 2022
Accepted: 24 February 2022
Published: 25 February 2022

Abstract: Periodic removal of sediment from aquaculture ponds is practiced to maintain their productivity and animal welfare. The recovery of sediment as a plant fertilizer could alleviate the costs of sediment removal. The objective of this study was to test the effects of a dried sediment, extracted from an aquaculture pond used for common carp cultivation, on the growth and physiology of potted wheat grass and the quality of the juice obtained from wheat grass. The results showed that sediment application did not produce significant morphological changes, although the values for plant height (16.94–19.22 cm), leaf area (19.67–139.21 mm^2), and biomass (3.39–4.26 g/plant) were higher in sediment-grown plants. However, at a physiological level, the effect was negative, decreasing photosynthesis (0.82–1.66 μmol CO_2 m^2s^{-1}), fluorescence ΦPSII (0.737–0.782), and chlorophyll content (1.40–1.83 CCI). The juice yield was reduced in the sediment treatments (46–58 g/100 g), while the quality was improved by increasing the content of phenols (2.55–3.39 μg/mL gallic acid equivalent), flavonoids (1.41–1.85 μg/mL quercetin equivalent), and antioxidant activity (47.99–62.7% inhibition of; 2,2-diphenyl-1-picrylhydrazyl). The positive results obtained in this study can be attributed to the moderate nutrient content of the sediment and a negligible concentration of heavy metals.

Keywords: aquaculture pond sediment; recovery; *Triticum aestivum*; photosynthesis; heavy metals; chlorophyll fluorescence; wheat grass juice quality

1. Introduction

Aquaculture pond sediment is a mixture of uneaten feed and fish feces, with decaying plant, animal, and microorganisms remains. The accumulation of large amounts of sediment has negative effects on aquaculture economic efficiency, as well as on fish health, mainly because of the reduction of pond depth and living space for fish. Moreover, the accumulation of sediment causes a decrease in the concentration of dissolved oxygen due to its consumption by nitrifying bacteria, as well as the production of toxic compounds, such as H_2S and NO_2 [1]. Therefore, periodic clearing of the aquaculture ponds is needed in order to avoid these issues. Depending on the type of aquaculture, cleaning of pond

sediments can take place several times a year as is the case in organic aquaculture or once every several years, as is the case of aquaculture practiced in natural water bodies [2].

Estimates show that the world aquaculture production will increase by 32% by 2030 [3], thus the continuous development of the aquaculture sector determines a high sediment production. For this reason, there is a need for efficient fish pond sediment management strategies that include both their removal and recovery [4]. This is especially important as uncontrolled spreading of sediment on the field, a widespread practice, can lead to soil pollution with nitrates and water eutrophication [5]. Moreover, leachate can reach groundwater and drinking water sources, threatening human health [6,7].

The aquaculture sediment reuse in agriculture has multiple benefits. The use of sediment in agriculture to fertilize crops and improve soil quality is possible due to the high content of nutrients and organic matter [8]. Previous studies demonstrated the usefulness of sediment application in agriculture [9–11]. For example, sediment from pangasius (*Pangasianodon hypophthalmus*) mixed with organic amendments from rice straw could be a good fertilizer for cucumbers (*Cucumis sativus* L.) [11], while fish sediments from organic aquaculture have been shown to be beneficial for white beans [2]. However, when considering the use of sediment in agriculture, physico-chemical analyses must be performed due to the fact that their composition varies depending on the type of aquaculture, the cultivated fish species and its age, the feed used, etc. [12]. According to Dróżdż et al. 2020 [1], the pH of aquaculture sediments can vary between 4 and 7, the humus content between 0.76 and 3.2 T/ha, N between 1.08 and 7.03 g/kg, *p* between 0.22–2.07 g/kg, and K between 0.62–2.25 g/kg.

Commune carp (*Cyprinus carpio*) is a very popular species in Eastern Europe and Asia, being cultivated mainly in natural fresh water bodies or in constructed ponds. According to the Romanian National Strategy for the Fishing Sector 2014–2020, aquaculture is practiced on a total area of 89,615.23 ha of production farms and 8617.55 ha of nurseries. The structure by species is dominated by Asian cyprinids, 32%, and Romanian carp, 31.8%, followed by crucian at 12.56%, trout at 20.45%, and pike, perch, catfish, and sturgeon at 3.19% [13–15]. Pond aquaculture generates large amounts of sediments, and their recovery as a plant fertilizer source can be a sustainable solution, in accordance with the new environmental policies, such as the Green Deal [16].

Wheat plants *Triticum aestivum* Linn. are generally used as a model plant to test the effect of different substrates or pollutants [17]. Moreover, wheat grass is used to produce wheat grass juice (WGJ), which is an extract made from young (10–15 cm) wheat plants [18]. The WGJ is a solution with a complex chemical composition, rich in minerals, enzymes, vitamins, phenolics, and chlorophylls, with considerable bioactivities [19]. In general, the use of sediments for plant fertilization has positive effects due to the rich content of nutrients and organic matter. However, depending on their origin, they can cause physiological disturbances, such as decreased photosynthesis, which can reduce plant growth rate and can even cause plant death if the content of heavy metals or pathogens are too high [20]. Under these conditions, when sediment is used in agriculture, its quality must meet certain requirements. The objective of this study was to evaluate the potential recovery of sediment from a commune carp pond aquaculture as a growing substrate for wheat, by assessing the effects on wheat grass production and physiology and the quality of wheat grass juice. Furthermore, the quality of the leachate in terms of nitrogen compounds was evaluated to determine the impact of the use of sediment on the environment.

2. Results

2.1. Sediment Composition

This study assessed the potential use of aquaculture sediment as a nutrient substrate for wheat grass. The chemical characterization of the sediment is presented in Table 1. Sun-dried sediment had a slightly alkaline pH (7.67–8.06). In terms of nutrients, humus and total N were significantly higher in CS3, while the content of organic matter, *p* and K are significantly higher in CS1 ($p < 0.05$). The concentrations of heavy metals were below

the maximum allowable limit for use in agriculture according to the Romanian legislation OM 344/2004 (Cu 500 mg/kg, Zn 2000 mg/kg, Pb 300 mg/kg, and Cd 10 mg/kg). The total coliforms ranged from 760 cfu/g to 1536 cfu/g while *E. coli* was not detected.

Table 1. The chemical and microbiological composition of the commune carp pond sediments.

Sampling Station	Collection Station 1	Collection Station 2	Collection Station 3
pH	8.06 ^{a} ± 0.05	7.68 ^{b} ± 0.05	7.67 ^{b} ± 0.04
Humus%	3.31 ^{a,b} ± 0.04	3.16 ^{b} ± 0.1	3.62 ^{a} ± 0.07
Organic matter%	6.43 ^{a} ± 0.01	5.57 ^{c} ± 0.02	6.26 ^{b} ± 0.03
N total%	0.16 ^{b} ± 0	0.16 ^{b} ± 0.00	0.19 ^{a} ± 0.00
P mg/kg	118.67 ^{a} ± 3.28	64.33 ^{b} ± 2.03	66.33 ^{b} ± 1.33
K mg/kg	276.33 ^{a} ± 2.6	235.67 ^{c} ± 1.76	250.67 ^{b} ± 2.03
Cu mg/kg	28.27 ^{ns} ± 0.05	27.29 ^{ns} ± 0.05	28.13 ^{ns} ± 0.05
Fe mg/kg	33,695.62 ^{ns} ± 0.05	33,083.57 ^{ns} ± 0.05	34,609.12 ^{ns} ± 0.05
Mn mg/kg	455.92 ^{ns} ± 0.05	448.52 ^{ns} ± 0.05	449.53 ^{ns} ± 0.05
Zn mg/kg	82.67 ^{ns} ± 0.05	81.41 ^{ns} ± 0.05	84.11 ^{ns} ± 0.05
Pb mg/kg	10.89 ^{ns} ± 0.05	10.58 ^{ns} ± 0.05	11.04 ^{ns} ± 0.05
Cd mg/kg	bdl	bdl	bdl
Total coliforms cfu/g	1020	1536	760
E. coli cfu/g	nd	nd	nd

The values represent the mean ± standard error. The lowercase letters represent a statistically significant difference (Tukey Test, $p < 0.05$). bdl: below detection limit, nd: not detected, ns: not significant.

2.2. Morphology of Wheat Grass and Yield of Wheat Grass Juice

In this study, mixtures (v/v) of sediment from the three collection stations (CS1, CS2, and CS3) with commercial peat (CP) were performed, resulting in 10 treatments: V1 (CP 100%, control); V2 (CS1 50% + CP 50%); V3 (CS1 75% + CP 25%); V4 (CS1 100%); V5 (CS2 50% + CP 50%); V6 (CS2 75% + CP 25%); V7 (CS2 100%); V8 (CS3 50% + CP 50%); V9 (CS3 75% + CP 25%); and V10 (CS3 100%).

The morphological parameters of wheat grass and the yield of wheat grass juice grown on aquaculture sediment are shown in Table 2. In general, wheat plants have grown uniformly in all treatments, with values of plant height between 16.9 cm and 19.2 cm, and the highest increase compared with the control being in the V4 variant. Leaf area and plant biomass increased the most in the V6 variant compared to V1 (control) (2.6% and 8%, respectively), however without statistical significance. In contrast, in all variants wheat grass juice yield decreased significantly ($p < 0.05$) up to 20% at V10 compared with V1.

Table 2. Morphology of wheat grass and yield of wheat grass juice cultivated on pond sediment.

Treatment	Plant Height (cm)	Leaf Area (mm^2)	Plant Biomass (g/Plant)	Wheat Grass Juice Yield (g/100 g)
V1	17.53 ^{ns} ± 0.61	135.61 ^{ns} ± 7.31	3.93 ^{ns} ± 0.19	58.00 ^{b} ± 1.16
V2	18.06 ^{ns} ± 0.44	121.12 ^{ns} ± 10.88	3.39 ^{ns} ± 0.31	50.14 ^{b,c,d} ± 1.04
V3	18.72 ^{ns} ± 0.48	128.32 ^{ns} ± 2.15	3.82 ^{ns} ± 0.01	48.34 ^{c,d} ± 0.88
V4	19.22 ^{ns} ± 0.43	129.17 ^{ns} ± 2.34	3.97 ^{ns} ± 0.07	55.54 ^{a,b,c} ± 1.08
V5	18.06 ^{ns} ± 0.57	116.93 ^{ns} ± 14.35	3.57 ^{ns} ± 0.42	50.00 ^{b,c,d} ± 1.16
V6	18.06 ^{ns} ± 0.49	139.21 ^{ns} ± 3.19	4.26 ^{ns} ± 0.07	54.00 ^{a,b,c} ± 1.16
V7	17.38 ^{ns} ± 0.42	116.44 ^{ns} ± 5.78	3.55 ^{ns} ± 0.20	56.80 ^{a,b} ± 1.34
V8	19.03 ^{ns} ± 0.69	126.86 ^{ns} ± 12.02	3.83 ^{ns} ± 0.12	52.34 ^{a,b,c,d} ± 0.88
V9	18.81 ^{ns} ± 0.56	110.26 ^{ns} ± 8.83	3.51 ^{ns} ± 0.27	56.34 ^{a,b} ± 1.46
V10	16.94 ^{ns} ± 0.44	109.67 ^{ns} ± 4.10	3.47 ^{ns} ± 0.09	46.00 ^{d} ± 3.06

The values represent the mean ± standard error. The lowercase letters represent a statistically significant difference (Tukey Test, $p < 0.05$), ns: not significant.

2.3. Color of Wheat Grass

The color of wheat grass is presented in Table 3. The parameters L (lightness) and b (yellowness) did not vary significantly. The a (greenness) parameter was significantly

higher in V7 and V10 than in V4, which means that V4 had a more pronounced green color. There were no significant differences between the V1 (control) variant and the rest of the variants.

Table 3. Color of wheat grass cultivated on pond sediment.

Treatment	L	a	b
V1	$37.81^{ns} \pm 0.84$	$-9.11^{a,b} \pm 0.2$	$18.11^{ns} \pm 0.87$
V2	$34.75^{ns} \pm 1.26$	$-8.59^{a,b} \pm 0.19$	$17.19^{ns} \pm 0.44$
V3	$36.62^{ns} \pm 0.45$	$-8.64^{a,b} \pm 0.08$	$16.89^{ns} \pm 0.28$
V4	$38.56^{ns} \pm 0.74$	$-9.27^{b} \pm 0.05$	$18.91^{ns} \pm 0.09$
V5	$37.33^{ns} \pm 0.41$	$-9.03^{a,b} \pm 0.07$	$18.49^{ns} \pm 0.27$
V6	$38.47^{ns} \pm 0.49$	$-9.04^{a,b} \pm 0.05$	$17.96^{ns} \pm 0.39$
V7	$35.06^{ns} \pm 0.43$	$-8.48^{a} \pm 0.07$	$17.09^{ns} \pm 0.19$
V8	$36.7^{ns} \pm 1.21$	$-8.8^{a,b} \pm 0.22$	$17.37^{ns} \pm 0.93$
V9	$36.86^{ns} \pm 0.35$	$-8.79^{a,b} \pm 0.09$	$17.23^{ns} \pm 0.13$
V10	$35.97^{ns} \pm 1.18$	$-8.43^{a} \pm 0.22$	$16.44^{ns} \pm 0.95$

The values represent the mean ± standard error. The lowercase letters represent a statistically significant difference (Tukey Test, $p < 0.05$), ns: not significant. L: lightness—darkness, a: redness—greenness, and b: yellowness—blueness.

2.4. Physiology of Wheat Grass

The gas exchange and total chlorophyll parameters are presented in Table 4. Physiological parameters were most affected in V10 (CS3 100%). The Ci dropped significantly in all variants except V2 (CS1 50% + CP 50%) and V4 (CS1 100%). Transpiration (E) and Gs increased significantly at V6 (CS2 75% + CP 25%) compared to V1 (control) by 62% and 30%. Photosynthesis (A) was the highest at V6, however without a significant difference compared with V1, while at V10 it decreased by 40% compared with the control variant. Regarding the chlorophyll content, there were no significant differences between the variants. Regarding chlorophyll fluorescence (Figure 1), ΦPSII parameter (quantum yield of PSII of light adapted leaves) decreased significantly in all variants compared with the control variant.

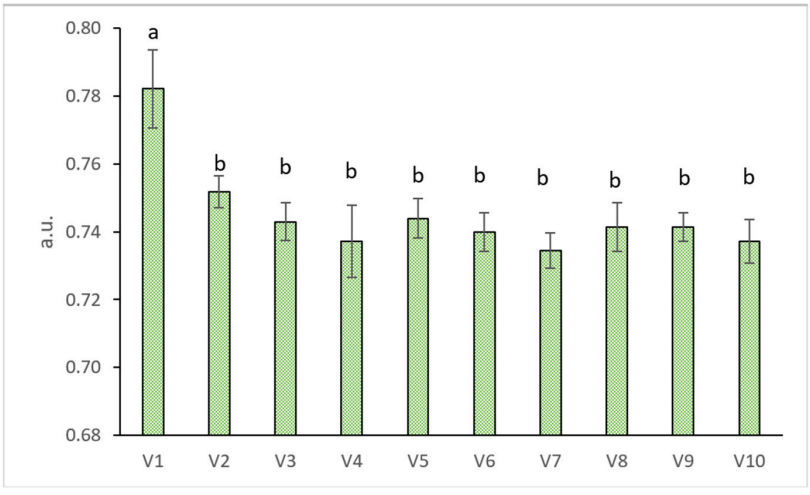

Figure 1. Chlorophyll fluorescence (ΦPSII—quantum yield of PSII of light adapted leaves) of wheat grass cultivated on pond sediment. The values represent the mean ± standard error. The lowercase letters represent a statistically significant difference (Tukey Test, $p < 0.05$). a.u.: arbitrary units.

Table 4. Gas exchange parameters and total chlorophyll content of wheat grass cultivated on pond sediment.

Treatment	Ci	E	Gs	A	CCI
V1	378.97 ^{a} ± 1.66	1.35 ^{b,c} ± 0.03	0.10 ^{a,b,c} ± 0.00	1.47 ^{a} ± 0.07	1.54 ^{ns} ± 0.14
V2	373.13 ^{a} ± 1.46	1.11 ^{b,c} ± 0.02	0.07 ^{b,c} ± 0.00	1.29 ^{a} ± 0.06	1.53 ^{ns} ± 0.20
V3	356.13 ^{b,c} ± 1.47	1.64 ^{b} ± 0.03	0.11 ^{a,b} ± 0.00	1.42 ^{a} ± 0.09	1.48 ^{ns} ± 0.09
V4	371.27 ^{a,b} ± 1.07	1.47 ^{b,c} ± 0.02	0.09 ^{a,b,c} ± 0.00	1.54 ^{a} ± 0.05	1.83 ^{ns} ± 0.23
V5	344.77 ^{c} ± 2.81	0.98 ^{c} ± 0.03	0.05 ^{c,d} ± 0.00	1.44 ^{a} ± 0.11	1.6 ^{ns} ± 0.17
V6	349.9 ^{c} ± 2.18	2.19 ^{a} ± 0.18	0.13 ^{a} ± 0.03	1.66 ^{a} ± 0.11	1.57 ^{ns} ± 0.16
V7	351.43 ^{c} ± 3.30	1.38 ^{b,c} ± 0.02	0.07 ^{b,c} ± 0.00	1.28 ^{a} ± 0.10	1.53 ^{ns} ± 0.14
V8	344.13 ^{c} ± 3.14	1.58 ^{b} ± 0.30	0.05 ^{c,d} ± 0.00	1.36 ^{a} ± 0.14	1.43 ^{ns} ± 0.08
V9	344.97 ^{c} ± 3.71	1.52 ^{b,c} ± 0.15	0.09 ^{a,b,c} ± 0.02	1.38 ^{a} ± 0.13	1.42 ^{ns} ± 0.08
V10	316.63 ^{d} ± 8.27	0.36 ^{d} ± 0.01	0.02 ^{d} ± 0.00	0.82 ^{b} ± 0.09	1.4 ^{ns} ± 0.05

The values represent the mean ± standard error. The lowercase letters represent a statistically significant difference (Tukey Test, $p < 0.05$), ns: not significant. Ci: sub-stomatal CO_2 concentration—µmol mol−1; E: transpiration—mmol H_2O m^2s^{-1}; Gs: stomatal conductance—mole CO_2 m^2s^{-1}, A: photosynthesis—µmol CO_2 m^2s^{-1}; and total chlorophyll content—CCI.

2.5. Wheat Grass Juice Quality

To evaluate the quality of wheat grass juice depending on the sediment application, the total content of phenols and flavonoids and the antioxidant activity were quantified (Table 5). The total phenol content increased significantly in variants V7 (CS2 100%) and V8 (CS3 50% + CP 50%) compared to variant V1 (control) by 14% and 10%, respectively, and decreased in V3 (CS1 75% + CP 25%) and V9 (CS3 75% + CP 25%) by 9% and 14%, respectively. The flavonoid content decreased significantly in V2 (CS1 50% + CP 25%) and V3 by 19% and 20%, respectively. The highest flavonoid content was recorded in V7, however the difference from V1 was not significant. In terms of antioxidant activity, it increased in V4 (CS1 100%), V5 (CS2 50% + CP 50%), V6 (CS2 75% + CP 25%), and V7 and decreased in V2, V3, and V9 compared to V1.

Table 5. Quality of wheat grass juice.

Treatment	Total Phenols Galic Acid µg/mL	Total Flavonoids Quercitin µg/mL	Antioxidant Activity DPPH % Inhibition
V1	2.97 ^{c} ± 0.10	1.77 ^{a,b} ± 0.11	53.35 ^{c} ± 1.49
V2	2.94 ^{c,d} ± 0.10	1.42 ^{c} ± 0.13	47.99 ^{e} ± 0.42
V3	2.69 ^{d,e} ± 0.22	1.41 ^{c} ± 0.11	35.48 ^{f} ± 0.42
V4	3.06 ^{b,c} ± 0.02	1.71 ^{a,b} ± 0.12	60.26 ^{a,b} ± 0.34
V5	2.87 ^{c,d} ± 0.12	1.78 ^{a,b} ± 0.06	60.52 ^{a,b} ± 0.08
V6	2.80 ^{c,d,e} ± 0.05	1.63 ^{a,b,c} ± 0.13	58.04 ^{b} ± 0.23
V7	3.39 ^{a} ± 0.03	1.85 ^{a} ± 0.04	62.70 ^{a} ± 0.51
V8	3.28 ^{a,b} ± 0.02	1.7 ^{a,b} ± 0.02	52.37 ^{c,d} ± 1.64
V9	2.55 ^{e} ± 0.03	1.52 ^{b,c} ± 0.06	48.2 ^{d,e} ± 0.66
V10	2.80 ^{c,d,e} ± 0.04	1.61 ^{a,b,c} ± 0.06	52.88 ^{c} ± 1.11

The values represent the mean ± standard error. The lowercase letters represent a statistically significant difference (Tukey Test, $p < 0.05$), ns: not significant.

The chlorophyll content of wheatgrass juice is shown in Figure 2. No significant differences were recorded in the content of chlorophyll a. However, chlorophyll b, increased significantly with 32% in V3 (CS1 75% + CP 25%) compared with V1 (control). This variant also registered a significant decrease of carotenoid content at 52%.

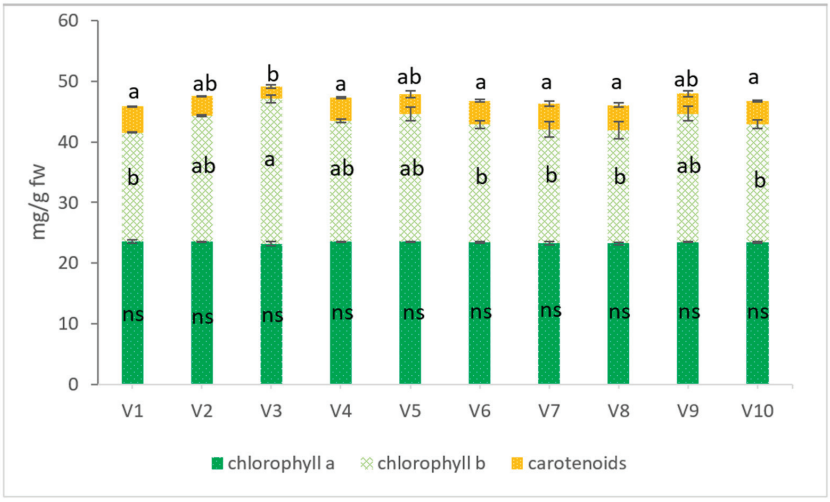

Figure 2. Chlorophyll a, chlorophyll b, and carotenoids in wheatgrass juice. The values represent the mean ± standard error. The lowercase letters represent statistically significant differences according to the Tukey Test, $p < 0.05$. ns: not significant.

2.6. Chemical Composition of Leachate

The chemical composition of the leachate resulting from the pots used in the experiment is shown in Table 6. In general, the pH was alkaline, with values between 7.73 and 8.37. The nitrate content of the leachate decreased by up to 60% at V3 (CS1 75% + CP 25%) and V4 (CS1 100%), however, the nitrate content increased significantly ($p < 0.05$) with up to 225% at V9 (CS3 75% + CP 25%. The lowest NO_2 content was recorded in control, while the highest value was obtained at V8 (CS3 50% + CP 50%). The NH_3 content was low, ranging from 0.02 in V3 and V10 (CS3 100%) to 0.14 in V8.

Table 6. Chemical composition of leachate.

Treatment	pH	NO_3 (mg/L)	NO_2 (mg/L)	NH_3 (mg/L)
V1	$7.90^{b,c,d} \pm 0.06$	$20.20^{c} \pm 1.33$	$0.27^{d} \pm 0.01$	$0.03^{b} \pm 0.00$
V2	$7.97^{b} \pm 0.03$	$19.03^{d} \pm 1.48$	$1.19^{b} \pm 0.00$	$0.04^{a,b} \pm 0.00$
V3	$7.93^{b,c} \pm 0.03$	$8.77^{e} \pm 0.03$	$0.73^{c} \pm 0.00$	$0.02^{b} \pm 0.00$
V4	$7.97^{b} \pm 0.03$	$8.77^{e} \pm 0.03$	$0.28^{d} \pm 0.01$	$0.03^{b} \pm 0.00$
V5	$7.97^{b} \pm 0.03$	$36.63^{b,c} \pm 1.48$	$1.19^{b} \pm 0.00$	$0.05^{a,b} \pm 0.00$
V6	$7.73^{c,d} \pm 0.03$	$35.2^{b,c} \pm 2.54$	$1.17^{b} \pm 0.02$	$0.05^{a,b} \pm 0.00$
V7	$7.77^{c,d} \pm 0.03$	$52.77^{a,b} \pm 4.38$	$1.33^{a} \pm 0.00$	$0.05^{a,b} \pm 0.00$
V8	$8.37^{a} \pm 0.03$	$52.47^{a,b} \pm 8.97$	$1.37^{a} \pm 0.02$	$0.14^{a} \pm 0.06$
V9	$7.77^{c,d} \pm 0.03$	$65.97^{a} \pm 4.38$	$1.15^{b} \pm 0.02$	$0.05^{a,b} \pm 0.00$
V10	$7.87^{b,c,d} \pm 0.03$	$33.67^{c} \pm 2.92$	$1.35^{a} \pm 0.02$	$0.02^{b} \pm 0.00$

The values represent the mean ± standard error. The lowercase letters represent statistically significant differences according to the Tukey Test, $p < 0.05$.

3. Discussion

The objective of this study was to test the effects of a dried aquaculture sediment, from a common carp cultivation pond, on the growth and physiology of potted wheat grass and the quality of the juice obtained from wheat grass. Cypriniculture (cultivation of common carp) occupation is about 8000 years old and is now widespread globally [21]. The traditional ponds used for carp aquaculture represent aquatic ecosystems in which, besides the species of interest in—the carp, there are other populations of plants, animals, and microorganisms, with functions as producers, consumers, and decomposers,

between which trophic relations had been established [22]. Sediments from aquaculture consists mainly of fish feces, uneaten food, organic matter, and mineral elements resulting from the decomposition of aquatic organisms [23]. Depending on the type of production, such as aquaculture in ponds or recirculating systems, the physicochemical composition of sediments can vary greatly [24]. In this study, the sun-dried sediments from a carp (*Cyprinus carpio*) growing pond were tested as a nutrient source for wheatgrass production. Physico-chemical analyzes of pond sediments showed an alkaline pH, which is higher compared to other studies, while the organic matter content was relatively low. The pH of sediments can be influenced by numerous factors, such as the quality of the water and the geological substrate, season, the feed used, the productivity of the pond, etc. [25]. Due to the fact that the oxygen content is low in the sediment because of the lack of air spaces, organic material tends to accumulate [1]. The organic matter content was between 5.5 and 6.4%, which are relatively low values compared with the values reported in previous studies [1,2]. This may be due to the sun drying treatment, which may speed up the transformation of organic material into humus (3.16–3.62) and N (0.16–0.19). Regarding the content of P and K, average values were registered (64–118 and 235–276, respectively), while the content of heavy metals was low compared to other studies [2]. Moreover, the Cd concentration in the sediment was below the detection limit of the AAS instrument. These elements come mainly from unconsumed feed and feces, however also from the remains of vegetation and other decomposed organisms as well as from the geological substrate.

The total coliform content in sediment was between 760 and 1536 cfu/g. Sediments, unlike water, ensure a more favorable climate for the development of coliforms due to the presence of organic matter and shelter from predators. The content of coliforms in sediments can vary spatio-temporally, which is why their monitoring is necessary when sediments are used as fertilizers. Harbi (2003) [26], identified a higher content of total coliforms (3.2×10^5–2.88×10^7) in sediments from hybrid tilapia culture compared to this study.

In this study, wheat plants had a relative uniform growth, with no significant differences in plant height, leaf area, and plant fresh production depending on the sediment application rates. However, wheatgrass juice production was highest in the control and decreased by up to 20% at V10. The sediments in the carp growing pond have a moderate content of macronutrients (N, P, and K) and organic matter, which led to normal plant growth in most variants. Small decreases in plant height, leaf area, and juice production were recorded at variant V10 (CS3 100% pond sediment). In general, the sediments have a high density and are free of porosity, which could negatively influence the growth of the plants as in V10 [1]. For this reason, sediments are generally used in a mixture with different materials such as compost, to improve their physical and chemical properties and subsequently to ensure optimal plant growth [11].

Regarding the effect of sediments on wheat physiology, a decrease of up to 40% in photosynthesis at V10 compared with V1 (control) was found, concomitantly with decreases in the transpiration rate, substomatal carbon dioxide, and the stomatal conductance. The gas exchange parameters enumerated above were lower at the same variant (V10) in which the morphological and production parameters decreased compared with the control. The pigment content and green color (a) were lower in V10 compared with those in the control. Moreover, the chlorophyll fluorescence decreased in all variants compared with that in the control. These variations could be caused by the physico-chemical properties of the sediments, which was the only source of nutrients [8].

From a biochemical point of view, wheat grass juice is a complex solution with proven nutritional and therapeutic properties. Fortuna et al. (2018) [19] highlighted rich mineral content in wheatgrass juice (C, N, O, Na, Mg, Si, Cl, K, and Ca) and different types of chlorophyll (pheophytin a, hydroxychlorophyll a, chlorophyll a, and chlorophyll b). Moreover, the same study showed that the content of phenols can vary from 706 to 818 mg/mL of gallic acid and that of flavonoids from 346 to 809 mg/mL of quercetin, and the antioxidant activity can be between 30% and 48% (DPPH) [19]. However, the nutritional and therapeu-

tic value of plants can vary depending on the species and variety [27]. The sediments used in this study as a nutrient source for wheat influenced the quality of wheatgrass juice. For instance, the content of total phenols, flavonoids, and antioxidant activity increased the most in V7 (CS2 100% pond sediment) compared with the control variant, while in other variants these metabolites decreased. Phenols and flavonoids are products of secondary metabolism and are defensive plant chemicals against ultraviolet radiation and herbivores. Thus, plants synthesize these compounds in larger quantities especially when under stress conditions [28,29]. Another factor that influences the synthesis of these compounds is the chemical composition of the substrate. For example, in the case of a soils with low organic matter content, the rosmarinic acid content increased considerably compared to the plants grown on municipal sewage sludge [30]. Wheat grass juice did not show major variations in the content of chlorophyll a, instead it had a significant increase in the content of chlorophyll b at V3 (CS1 75% + CP 25%) and a decrease in carotenoids at the same variant. Chlorophyll plays an essential role in photosynthesis, its synthesis being directly dependent on the N content of the substrate [31]. In general, the sediments used in this study had a relatively high content of organic matter and N, allowing the growth of wheat in good conditions as well as increased chlorophyll synthesis. Carotenoids on the other hand have a role in protecting plants against oxidative stress [32], and the lower content of V3 is correlated with a lower value of antioxidant activity in the same variant.

In this study, the leachate obtained from the studied substrates had an alkaline pH between 7.73 and 8.37. Regarding the nitrate content, the lowest values were recorded at V3 and V4 (CS1 100% pond sediment), 60% lower than in the control. At the same time, at V7, V8 (CS3 50% + CP 50%), and V9 (CS3 75% + CP 25%), values exceeding the maximum limit of 50 mg/L according to Directive 91/271/EEC were registered. Relatively low values were recorded for NO_2 and NH_3 content. In general, the content of nitrites and nitrates in groundwater can vary from 1 to 150 mg/L. Pollution with N compounds can cause serious environmental problems such as eutrophication of water or contamination of surface or groundwater causing health problems because compounds such as nitrates and nitrites are known to be carcinogenic [33]. In general, this type of pollution is caused by runoff from intensive field crops and animal farms, or from some industrial activities. Improper storage of sediment or sludge can also contribute to this type of pollution [34]. In this context, it is important to monitor these compounds when sediments are used for plant cultivation to avoid environmental contamination.

Considering that sediment removal is costly, $20,000/ha [35], and potting soil cost is 1–5$ (10 L), the sale of the sediment as a growing substrate for plants demonstrates that this residue can be transformed into a value-added product.

4. Materials and Methods

4.1. Sediment Collection

The sediment was collected from a commune carp growing pond, which belongs to the Research and Development Station for Aquaculture and Aquatic Ecology, Alexandru Ioan Cuza University, Iasi, Romania. The pond is 25 m wide and 100 m long. The pond was emptied of water and allowed to dry for 30 days. Then, the pond was divided into three collection stations along the length of the basin (CS1—1 m from the shore, CS2—6.25 m from the shore, and CS3—12.5 m from the shore) and five large samples of pond sediment were collected from each station. The sun dried pond sediment collected from three collection stations (CS1, CS2, and CS3) was crushed through a 0.5-cm mesh sieve and used to prepare the mixtures (v/v) with commercial peat (CP) for the cultivation of wheat resulting in 10 treatments: (V1) CP 100% (control); (V2) CS1 50% + CP 50%; (V3) CS1 75% + CP 25%; (V4) CS1 100%; (V5) CS2 50% + CP 50%; (V6) CS2 75% + CP 25%; (V7) CS2 100%; (V8) CS3 50% + CP 50%; (V9) CS3 75% + CP 25%; and (V10) CS3 100%.

4.2. Sediment Analysis

The pond sediment samples were air dried and passed through a 2-mm sieve to obtain the fraction used for each analysis and then stored at 4 °C. Sediment pH was determined in water using an electronic pH meter with a glass electrode (WTW pH 3320, GmbH, Weilheim, Germany). Organic matter was determined according to the wet oxidation method (Walkley and Black); the available N was measured by the Kjeldahl method; while for *p*, the Olsen extractant method was used, following the standard methods according to Soil Studies Development Methodology delivered by the National Institute of Research and Development in Soil Science, Agrochemistry, and Environment [36]. Available K (extracted with neutral 1N NH4OAc) was determined using a high-resolution continuum source, atomic adsorption spectrometer (ContrAA 700, Analytik, Jena, Germany) equipped with a xenon short lamp with a UV arc in hot spot mode and a high-resolution echelle grating monochromator. The flame was generated using an air-acetylene mixture with 99.95% purity.

4.3. Elemental Analysis of Sediment

The analysis of minerals was performed at the National Research and Development Institute for Animal Biology and Nutrition IBNA Balotesti. The concentration of the chemical elements was determined according to the atomic absorption spectroscopy method presented in Regulation (EC) no. 152/2009/SR EN ISO 6869: 2002 (Cu, Fe, Mn, Zn), and SR EN 15550: 2008 (Pb and Cd). In brief, the sample was mixed with 65% HNO_3: 30% H_2O_2 (5:2, *v*/*v*) and digested under pressure using a microwave oven (8 min: 130 °C, 5 min: 155 °C, 12 min: 170 °C, 800 W); the solution of the sample was aspirated in the flame of an atomic absorption spectrophotometer with double beam and background correction and the radiation absorption was measured at the wavelength specific to the analyzed element (SOLAAR M6 Dual Zeeman Comfort, Thermo Electron Corp., Cambridge, UK) [37].

4.4. Microbiological Analysis of Sediment

Total coliforms and *E. coli* were determined at a National Research and Development Institute for Animal Biology and Nutrition IBNA Balotesti according to the methods SR EN ISO 4831/2006 UFC/g 1020, 1536, 760 E coli SR EN ISO 7251/2006.

The chemical and microbiological characterization of the sediment is presented in Table 1.

4.5. Chemical Composition of Sediment Leachate

The pH was measured with Hach HQ11d (Hach Company, Loveland, CO, USA) portable multiparameter, while ammonia, nitrites, and nitrates were assessed with Hanna Iris HI801 Spectrophotometer and Hanna reagent kits (Hanna Instruments, Salaj, Romania).

4.6. Cultivation of Wheat Grass

Wheat (*Triticum aestivum*) seeds of Glosa cultivar were germinated and grown directly in black plastic pots with a volume of 1 L, filled with the investigated substrates, each pot containing 100 wheat seeds. For each experimental variant, 9 pots were used. The plants were germinated in the dark for 3 days after which they were taken to natural light and grown for 15 days. Natural light was supplemented with fluorescent tubes (4800 K) 12 h/day. The pots were watered daily with distilled water at 250 mL/pot. The average temperature day/night during the growing period was 27/20 °C.

4.7. Fresh Yield and Morphological Parameters of Wheat Grass

At the end of the experiment, fresh biomass was assessed by weighing each plant at an analytical balance and expressed in g. The height of the plants was measured with a ruler and expressed in cm. For each treatment, 10 plants per pot from three pots were measured.

4.8. Leaf Area of Wheat Grass

Leaf area was measured with LI-3100C Area Meter, LI-COR, (Lincoln, NE, USA), and expressed in mm^2. For each treatment, 10 plants per pot from three pots were measured.

4.9. The Color of Wheatgrass

Color was measured with the MiniScan XE Plus colorimeter (HunterLab, Reston, VA, USA). The device was calibrated with black and white tiles and the parameters L, a, and b were determined.

L * (lightness to darkness, 100 to 0), a * (redness to greenness, 0 to 100 = red; −80 to 0 = green), and b* (yellowness and blueness, 0 to 70 = yellow; −100 to 0 = blue). L * (lightness—darkness), a * (redness—greenness), and b * (yellowness—blueness).

4.10. Total Chlorophyll Content of Wheat Grass

Total chlorophyll content was measured with CCM 200 (chlorophyll content meter), a non-destructive portable device produced by ADC Bioscientific Ltd., Hoddesdon, UK, which measures total chlorophyll and expresses it in CCI units (Chlorophyll Content Index) [38].

4.11. Gas Exchange Measurement of Wheat Grass

The gas exchange parameters, photosynthesis, and transpiration were measured with a portable compact system LCI Bioscientific UK Ltd., with a Narrow Leaf Chamber, with an area of 5.8 cm^2, between 9–10 a.m. [38].

4.12. Chlorophyll Fluorescence of Wheat Grass

A chlorophyll meter FMS2, Hansa Tech Ltd., Hoddesdon, UK was used to measure ΦPSII—quantum yield of PSII of light adapted leaves [39].

4.13. Wheat Grass Juice Extraction

The plants were cut 1 cm above the substrate, weighed, and the juice was extracted with a juicer by cold pressing.

4.14. Chlorophyll Content in Wheat Grass Juice

Assimilatory pigments were extracted in acetone (80%) from ground leaves (0.1 g) and the optical density was read at 470, 646, and 663 nm. Pigment content was calculated using equations described in Wellburn (1994) [40].

4.15. Total Phenolic, Total Flavonoid, and Antioxidant Activity of Wheat Grass Juice

The total phenolic and flavonoid content was determined according to Lobiuc et al. (2017) [41]. Extracts (5% *w*/*v*) were prepared from wheat grass juice in methanol (80%) for 24 h at room temperature. Results were expressed as the gallic acid equivalent per ml of fresh weight (μg/mL GAE f.w.) for total phenolic content, and in quercetin equivalent per ml of fresh weight (μg QE f.w.).

Antioxidant activity of WGJ extracts was determined according to Teliban et al. (2020) [42] by the discoloration of DPPH (2.2-diphenyl-1-picrylhydrazyl, Sigma, Schnelldorf, Germany). Results were expressed as % inhibition of DPPH.

4.16. Statistical Analyses of Data

The software used for data processing was IBM SPSS v20 (IBM Corp, Armonk, NY, USA), and results were presented as means ± standard errors. The differences between variants were tested by ANOVA ($p < 0.05$) followed by a Levene test for homogeneity of variances and a Tukey multiple comparison post hoc test [43].

5. Conclusions

In this study, the effects of sediments from the carp pond on wheat grass production and physiology and the quality of wheat grass juice were tested. The sediments had a slightly alkaline pH, and a relatively rich content of nutrients. The content of heavy metals was below the maximum allowed for use in agriculture and the content of total coliforms was relatively low. The growth of the wheat grass on the pond sediment was relatively uniform. The morphological parameters had values close to the control variant while production increased in some variants. Some physiological parameters were affected. The addition of pond sediment to the growth medium had a negative effect on wheat grass juice yield. Wheat grass juice had a rich content of flavonoids, phenols, and chlorophyll and increased antioxidant activity. We can conclude that the dried pond sediment in combination with peat could be safely used for the cultivation of wheat grass. This study demonstrates that the aquaculture sediment could be transformed into a value-added product and the results are relevant for the sustainable management of this residue.

Author Contributions: Conceptualization, M.B.; software, M.B.; methodology, C.-A.B., V.S., G.-C.T., V.D.Z., A.L., L.D., E.O., S.M.O., V.A.P., I.G.C., M.F. and M.R.; formal analysis, C.-A.B., V.S., G.-C.T., V.D.Z., A.L., L.D., E.O., S.M.O., V.A.P., I.G.C., M.F. and M.R.; investigation, C.-A.B., V.S., G.-C.T., A.L., L.D., E.O., S.M.O., V.A.P., I.G.C., M.F. and M.R.; writing—original draft preparation, M.B.; writing—review and editing, V.D.Z.; supervision, V.S. and V.D.Z.; project administration, M.B.; funding acquisition, M.B. All authors have read and agreed to the published version of the manuscript.

Funding: Autorii mulțumesc Ministerului Cercetării, Inovării și Digitalizării, prin Programul 1—Dezvoltarea sistemului național de cercetare-dezvoltare, Subprogram 1.2—Performanță instituțională- Proiecte de finanțare a excelenței în CDI, Contract nr. 11PFE/30 December 2021 pentru suportul financiar The authors are thankful to the Romanian Ministry of Research, Innovation, and Digitization, within Program 1—Development of the national RD system, Subprogram 1.2—Institutional Performance—RDI excellence funding projects, Contract no.11PFE/30 December 2021, for their financial support.

Data Availability Statement: Not applicable.

Conflicts of Interest: The authors declare no conflict of interest.

References

1. Dróżdż, D.; Malińska, K.; Mazurkiewicz, J.; Kacprzak, M.; Mrowiec, M.; Szczypiór, A.; Postawa, P.; Stachowiak, T. Fish pond sediment from aquaculture production—Current practices and the potential for nutrient recovery: A Review. *Int. Agrophys.* **2020**, *34*, 33–41. [CrossRef]
2. Dróżdż, D.; Malińska, K.; Kacprzak, M.; Mrowiec, M.; Szczypiór, A.; Postawa, P.; Stachowiak, T. Potential of Fish Pond Sediments Composts as Organic Fertilizers. *Waste Biomass Valoriz.* **2020**, *11*, 5151–5163. [CrossRef]
3. FAO. *The State of World Fisheries and Aquaculture (SOFIA)*; FAO: Rome, Italy, 2020; ISBN 978-92-5-132692-3.
4. Mizanur, R.; Yakupitiyage, A.; Ranamukhaarachchi, S.L. Agricultural use of fishpond sediment for environmental amelioration. *Thammasat Int. J. Sci. Technol.* **2004**, *9*, 1–12.
5. Junejo, S.H.; Baig, J.A.; Kazi, T.G.; Afridi, H.I. Cadmium and Lead Hazardous Impact Assessment of Pond Fish Species. *Biol. Trace Elem. Res.* **2019**, *191*, 502–511. [CrossRef] [PubMed]
6. Vaverková, M.D.; Elbl, J.; Koda, E.; Adamcová, D.; Bilgin, A.; Lukas, V.; Podlasek, A.; Kintl, A.; Wdowska, M.; Brtnický, M.; et al. Chemical Composition and Hazardous Effects of Leachate from the Active Municipal Solid Waste Landfill Surrounded by Farmlands. *Sustainability* **2020**, *12*, 4531. [CrossRef]
7. Negi, P.; Mor, S.; Ravindra, K. Impact of landfill leachate on the groundwater quality in three cities of North India and health risk assessment. *Environ. Dev. Sustain.* **2020**, *22*, 1455–1474. [CrossRef]
8. Burducea, M.; Lobiuc, A.; Asandulesa, M.; Zaltariov, M.-F.; Burducea, I.; Popescu, S.M.; Zheljazkov, V.D. Effects of Sewage Sludge Amendments on the Growth and Physiology of Sweet Basil. *Agronomy* **2019**, *9*, 548. [CrossRef]
9. Marval, S.; Hejduk, T.; Zajíček, A. An Analysis of Sediment Quality from the Perspective of Land Use in the Catchment and Pond Management. *Soil Sediment Contam. Int. J.* **2020**, *29*, 397–420. [CrossRef]
10. Brigham, R. *Assessing the Effects of Lake Dredged Sediments on Soil Health: Agricultural and Environmental Implications on Midwest Ohio*; Bowling Green State University: Bowling Green, OH, USA, 2020.
11. Thi Da, C.; Anh Tu, P.; Livsey, J.; Tang, V.T.; Berg, H.; Manzoni, S. Improving Productivity in Integrated Fish-Vegetable Farming Systems with Recycled Fish Pond Sediments. *Agronomy* **2020**, *10*, 1025. [CrossRef]

12. Haque, M.B.; Belton, B.; Alam, M.A.; Ahmed, A.G.; Alam, M.R. Reuse of fish pond sediments as fertilizer for fodder grass production in Bangladesh: Potential for sustainable intensification and improved nutrition. *Agric. Ecosyst. Environ.* **2016**, *216*, 226–236. [CrossRef]
13. Neculita, M.; Moga, M.L. Analysis of Romanian fisheries and aquaculture in regional context. *USV Ann. Econ. Public Adm.* **2015**, *15*, 127–132.
14. Bostock, J.; Lane, A.; Hough, C.; Yamamato, K. An assessment of the economic contribution of EU aquaculture production and the influence of policies for its sustainable development. *Aquacult. Int.* **2016**, *24*, 699–733. [CrossRef]
15. National Strategy of the Fisheries Sector 2014–2020. Ministry of Environment and Climate Change, Ministry of Agriculture and Rural Development (Romanian). pp. 1–62. Available online: https://www.madr.ro/docs/fep/programare-2014-2020/Strategia-Nationala-a-Sectorului-Pescaresc-2014-2020-update-apr2014.pdf (accessed on 1 October 2021).
16. Brodny, J.; Tutak, M. Analyzing Similarities between the European Union Countries in Terms of the Structure and Volume of Energy Production from Renewable Energy Sources. *Energies* **2020**, *13*, 913. [CrossRef]
17. Jităreanu, A.; Caba, I.C.; Trifan, A.; Pădureanu, S.; Agoroaei, L. *Triticum aestivum* Assay—A Useful Tool for Environmental Monitoring and Toxicity Assessment. *Not. Bot. Horti Agrobot. Cluj-Napoca* **2019**, *47*, 1005–1018. [CrossRef]
18. Dumitru, G.; Dirvariu, L.; Barbacariu, C.A.; Miron, I.; Sandu, I.; Todirascu Ciornea, E. The Effect of Wheatgrass Juice Administration on Physiological State and Oxidative Stress in Carp. *Rev. Chim.* **2018**, *69*, 4046–4051. [CrossRef]
19. Fortună, M.E.; Vasilache, V.; Ignat, M.; Silion, M.; Vicol, T.; Patras, X.; Miron, I.; Lobiuc, A. Elemental and macromolecular modifications in *Triticum aestivum* L. plantlets under different cultivation conditions. *PLoS ONE* **2018**, *13*, e0202441. [CrossRef] [PubMed]
20. Urbaniak, M.; Lee, S.; Takazawa, M.; Mierzejewska, E.; Baran, A.; Kannan, K. Effects of soil amendment with PCB-contaminated sediment on the growth of two cucurbit species. *Environ. Sci. Pollut. Res.* **2020**, *27*, 8872–8884. [CrossRef]
21. Nakajima, T.; Hudson, M.J.; Uchiyama, J.; Makibayashi, K.; Zhang, J. Common carp aquaculture in Neolithic China dates back 8000 years. *Nat. Ecol. Evol.* **2019**, *3*, 1415–1418. [CrossRef]
22. Wezel, A.; Robin, J.; Guerin, M.; Arthaud, F.; Vallod, D. Management effects on water quality, sediments and fish production in extensive fish ponds in the Dombes region, France. *Limnologica* **2013**, *43*, 210–218. [CrossRef]
23. Avnimelech, Y.; Ritvo, G. Shrimp and fish pond soils: Processes and management. *Aquaculture* **2003**, *220*, 549–567. [CrossRef]
24. Verdegem, M.C.J. Nutrient discharge from aquaculture operations in function of system design and production environment. *Rev. Aquac.* **2013**, *5*, 158–171. [CrossRef]
25. Silburn, B.; Kröger, S.; Parker, E.R.; Sivyer, D.B.; Hicks, N.; Powell, C.F.; Johnson, M.; Greenwood, N. Benthic pH gradients across a range of shelf sea sediment types linked to sediment characteristics and seasonal variability. *Biogeochemistry* **2017**, *135*, 69–88. [CrossRef] [PubMed]
26. Harbi, A.H. Faecal coliforms in pond water, sediments and hybrid tilapia *Oreochromis niloticus* × *Oreochromis aureus* in Saudi Arabia. *Aquac. Res.* **2003**, *34*, 517–524. [CrossRef]
27. Golubkina, N.; Kharchenko, V.; Moldovan, A.; Zayachkovsky, V.; Stepanov, V.; Pivovarov, V.; Sekara, A.; Tallarita, A.; Caruso, G. Nutritional Value of Apiaceae Seeds as Affected by 11 Species and 43 cultivars. *Horticulturae* **2021**, *7*, 57. [CrossRef]
28. Tanase, C.; Coșarcă, S.; Muntean, D.-L. A Critical Review of Phenolic Compounds Extracted from the Bark of Woody Vascular Plants and Their Potential Biological Activity. *Molecules* **2019**, *24*, 1182. [CrossRef] [PubMed]
29. Stoleru, V.; Slabu, C.; Vitanescu, M.; Peres, C.; Cojocaru, A.; Covasa, M.; Mihalache, G. Tolerance of Three Quinoa Cultivars (*Chenopodium quinoa* Willd.) to Salinity and Alkalinity Stress During Germination Stage. *Agronomy* **2019**, *9*, 287. [CrossRef]
30. Burducea, M.; Zheljazkov, V.; Lobiuc, A.; Pintilie, C.; Vîrgolici, M.; Silion, M.; Asandulesa, M.; Burducea, I.; Zamfirache, M. Biosolids application improves mineral composition and phenolic profile of basil cultivated on eroded soil. *Sci. Hortic.* **2019**, *249*, 407–418. [CrossRef]
31. Monostori, I.; Árendás, T.; Hoffman, B.; Galiba, G.; Gierczik, K.; Szira, F.; Vágújfalvi, A. Relationship between SPAD value and grain yield can be affected by cultivar, environment and soil nitrogen content in wheat. *Euphytica* **2016**, *211*, 103–112. [CrossRef]
32. Young, A.J.; Lowe, G.L. Carotenoids—Antioxidant Properties. *Antioxidants* **2018**, *7*, 28. [CrossRef]
33. Kuen-Song, L.; Ni-Bin, C.; Tien-Deng, C. Fine structure characterization of zero-valent iron nanoparticles for decontamination of nitrites and nitrates in wastewater and groundwater. *Sci. Technol. Adv. Mater.* **2008**, *9*, 025015. [CrossRef]
34. Fernández-Nava, Y.; Marañón, E.; Soons, J.; Castrillón, L. Denitrification of wastewater containing high nitrate and calcium concentrations. *Bioresour. Technol.* **2008**, *99*, 7976–7981. [CrossRef] [PubMed]
35. Lembi, C.A. 24—CONTROL OF NUISANCE ALGAE. In *Aquatic Ecology, Freshwater Algae of North America*; Wehr, J.D., Sheath, R.G., Eds.; Academic Press: Amsterdam, The Netherlands, 2003; pp. 805–834. [CrossRef]
36. Florea, N.; Balaceanu, V.; Rauta, C.; Canarache, A. Soil studies development methodology. *Incdpapm-ICPA* **1987**, *1*, 20.
37. Untea, A.; Criste, R.D.; Vladescu, L. Development and validation of a microwave digestion—FAAS procedure for Cu, Mn and Zn determination in liver. *Rev. Chim.* **2012**, *63*, 341–346.
38. Teliban, G.-C.; Burducea, M.; Zheljazkov, V.D.; Dincheva, I.; Badjakov, I.; Munteanu, N.; Mihalache, G.; Cojocaru, A.; Popa, L.-D.; Stoleru, V. The Effect of Myco-Biocontrol Based Formulates on Yield, Physiology and Secondary Products of Organically Grown Basil. *Agriculture* **2021**, *11*, 180. [CrossRef]
39. Burducea, M.; Zheljazkov, V.D.; Dincheva, I.; Lobiuc, A.; Teliban, G.C.; Stoleru, V.; Zamfirache, M.M. Fertilization modifies the essential oil and physiology of basil varieties. *Ind. Crop. Prod.* **2018**, *121*, 282–293. [CrossRef]

40. Wellburn, A.R. The spectral determination of chlorophyll a and b, as well as total carotenoids, using various solvents with spectrophotometers of different resolution. *J. Plant Physiol.* **1994**, *144*, 307–313. [CrossRef]
41. Lobiuc, A.; Vasilache, V.; Oroian, M.; Stoleru, T.; Burducea, M.; Pintilie, O.; Zamfirache, M.M. Blue and red LED illumination improves growth and bioactive compounds contents in acyanic and cyanic *Ocimum basilicum* L. Microgreens. *Molecules* **2017**, *22*, 2111. [CrossRef]
42. Teliban, G.-C.; Stoleru, V.; Burducea, M.; Lobiuc, A.; Munteanu, N.; Popa, L.-D.; Caruso, G. Biochemical, Physiological and Yield Characteristics of Red Basil as Affected by Cultivar and Fertilization. *Agriculture* **2020**, *10*, 48. [CrossRef]
43. Cojocaru, A.; Vlase, L.; Munteanu, N.; Stan, T.; Teliban, G.C.; Burducea, M.; Stoleru, V. Dynamic of Phenolic Compounds, Antioxidant Activity, and Yield of Rhubarb under Chemical, Organic and Biological Fertilization. *Plants* **2020**, *9*, 355. [CrossRef]

plants

MDPI

Article

Chemical Profiling of Two Italian *Olea europaea* (L.) Varieties Subjected to UV-B Stress

Chiara Piccini [1,2,*], Claudio Cantini [2], Giampiero Cai [1], Diana C. G. A. Pinto [3], Artur M. S. Silva [3], Marco Romi [1] and Maria Celeste Dias [3,4]

[1] Department of Life Sciences, University of Siena, Via Mattioli 4, 53100 Siena, Italy; cai@unisi.it (G.C.); marco.romi@unisi.it (M.R.)
[2] Institute for BioEconomy, National Research Council of Italy, 58022 Follonica, Italy; claudio.cantini@ibe.cnr.it
[3] LAQV-REQUIMTE, Department of Chemistry, University of Aveiro, 3810-193 Aveiro, Portugal; diana@ua.pt (D.C.G.A.P.); artur.silva@ua.pt (A.M.S.S.); celeste.dias@uc.pt (M.C.D.)
[4] Centre for Functional Ecology, Department of Life Sciences, University of Coimbra, Calçada Martim de Freitas, 3000-456 Coimbra, Portugal
* Correspondence: piccini3@student.unisi.it; Tel.: +39-05772-32856; Fax: +39-05772-32861

Abstract: The depletion of the stratospheric ozone layer due to natural and/or anthropogenic causes decreases the amount of UV-B radiation filtered, and consequently increases the risk of potential damage to organisms. In the Mediterranean region, high UV-B indices are frequent. Even for species typical of this region, such as the olive tree, the progressive increase in UV-B radiation represents a threat. This work aimed to understand how high UV-B radiation modulates the phenolic and lipophilic profile of olive varieties, and identify metabolites that enhance olive stress tolerance. Two Italian olive varieties were subjected to chronic UV-B stress, and leaves were analyzed by gas and liquid chromatography. The results indicated that the most representative phenolic and lipophilic compounds of Giarraffa and Olivastra Seggianese were readjusted in response to UV-B stress. The Giarraffa variety seemed better suited to prolonged UV-B stress, possibly due to the higher availability of flavonoids that could help control oxidative damage, and the accumulation of hydroxycinnamic acid derivatives that could provide strong UV-B shield protection. In addition, this variety contained higher levels of fatty acids (e.g., palmitic, α-linolenic, and stearic acids), which can help to maintain membrane integrity and accumulate more sorbitol (which may serve as an osmoprotectant or act a free-radical scavenger), terpenes, and long-chain alkanes, providing higher protection against UV-B stress.

Keywords: UV-B radiation; olive tree; metabolomic; phenolic profile; lipophilic profile

Citation: Piccini, C.; Cantini, C.; Cai, G.; Pinto, D.C.G.A.; Silva, A.M.S.; Romi, M.; Dias, M.C. Chemical Profiling of Two Italian *Olea europaea* (L.) Varieties Subjected to UV-B Stress. *Plants* **2022**, *11*, 680. https://doi.org/10.3390/plants11050680

Academic Editors: Milan S. Stankovic, Paula Baptista and Petronia Carillo

Received: 10 January 2022
Accepted: 27 February 2022
Published: 2 March 2022

1. Introduction

The stratospheric ozone layer is deteriorating due to natural and anthropogenic origin factors that decrease the amount of UV-B radiation filtered and consequently increase the damage to living organisms [1]. Although measures have been implemented to reduce the amount of chemicals released into the atmosphere and damage the ozone layer, the intensity of ultraviolet B (UV-B) radiation reaching the Earth's surface is estimated to increase until the mid-21st century [2]. Excessive exposure to UV-B radiation has diverse negative impacts that include a wide range of morphological, physiological, and reproductive aspects in plants and animals, as well as humans. In addition, it can alter biogeochemical cycles, and act synergistically with other environmental problems (such as global warming, ocean acidification, and pollution), thereby deeply impacting ecosystems [1]. Concerning plants, although UV-B radiation represents only a small fraction of the solar radiation that reaches the Earth's surface, it induces a photobiological effect relevant to the anatomy, morphology, physiology, and biochemistry of plants [3,4]. Sunlight provides the energy needed for plant growth, but intense light radiation (particularly in the UV-B spectrum) can induce

stress responses that potentially can lead to severe damage to DNA, proteins, membrane lipids, and other cellular components [5]. Although plants have developed several repair mechanisms over time, the damage caused by UV radiation is still considerable [6].

The Mediterranean region is frequently exposed to high irradiance accompanied by elevated UV-B indices, particularly during the spring and summer seasons [7]. The olive tree (*Olea europaea* L.) is a typical species of the Mediterranean region with high socioeconomic importance. This species is well adapted to the harsh climatic conditions of this region, and its tolerance to drought has been extensively studied [8]. However, there is a lack of comprehensive knowledge about the metabolic changes involved in the tolerance strategies of olive trees to UV-B stress. It remains unclear how UV-B radiation can modulate the metabolome and which metabolic changes enhance olive trees' tolerance [9]. Functional changes that occur during stress are closely linked to metabolic network adjustments that, with the emergence of new metabolomic approaches, are beginning to be unraveled [10,11]. Indeed, the study of metabolomics has helped identify the most sensitive networks related to physiological adaptations in different species and find key stress metabolites [12]. In addition to studies on the model species Arabidopsis [13], a few crops have been studied for metabolome changes in response to UV-B, such as *Zea mays* [14] and *Lactuca sativa* [15]. In recent years, several studies have employed a metabolomic approach, allowing the identification of several groups of metabolites involved in the abiotic stress response (e.g., to UV-B, drought, and heat), such as epicuticular wax components (alkanes, terpenes, and fatty acids), membrane fatty acids, polyphenols, and terpenes [9,16–21]. However, much remains to be studied to fully understand the mechanisms of plant response to increased UV radiation and to determine its impact on other metabolic pathways [17].

Metabolomic studies in olive plants are scarce, and were mainly focused on the impact of abiotic stresses on central key pathways. These studies unraveled adjustments in important phenolic compounds (e.g., secoiridoids, flavonoids, and hydroxycinnamic acid derivatives), carbohydrates, and lipophilic metabolites related to cuticle wax (e.g., long-chain alkanes and terpenes), and identified some metabolites related to ROS scavenger action (e.g., thymol glycosides) and maintenance of membrane integrity (e.g., fatty acids and steroids) [9,16,17,22]. In previous works [23,24], we analyzed the physiological and biochemical responses of two economically important Italian olive varieties to UV-B stress. In the present study, the integration of metabolomics with these previous data allowed a deeper understanding of metabolite dynamics and their connection in a more extensive network of pathways involved in stress response. Thus, we hypothesized that UV-B radiation would promote changes in metabolic pathways, particularly in protective lipophilic and phenolic metabolites that may play an essential role in protection against UV-B stress. Therefore, gas chromatography–mass spectrometry (GC–MS) and ultrahigh-performance liquid chromatography–mass spectrometry (UHPLC–MS) analyses were undertaken in *O. europaea* leaves (Giarraffa and Olivastra Seggianese varieties) exposed to chronic UV-B stress (14 h per day for eight weeks).

2. Results

2.1. Phenolic Profile

The phenolic profile was evaluated in olive leaves (Giarraffa and Olivastra Seggianese varieties) of control plants and subjected to UV-B stress, sampled at the 2nd, 4th, 6th, and 8th week after the onset of stress. In the Giarraffa variety (Table 1), a total of 16 compounds were identified and quantified: 13 flavonoids, one secoiridoid, and two hydroxycinnamic acid derivatives. In the Olivastra Seggianese variety (Table 2), a total of 12 compounds were identified and quantified: 11 flavonoids and one secoiridoid.

Table 1. Phenolic profile (mg kg^{-1} DW) of *Olea europaea* leaves (Giarraffa variety) under control (C) and UV-B conditions sampled at the 2nd (T2), 4th (T4), 6th (T6), and 8th (T8) week after the onset of stress. Values are mean ± standard deviation (n = 3–4). Rt—retention time; Nd—not detected; is.—isomer. ANOVA showed that most of chemical components were significantly affected by the main factors and their interactions.

Rt (min)	Compound	$[M-H]^-$ (m/z)	MS^2 (m/z) Fragments	T2		T4		T6		T8	
				C	UV-B	C	UV-B	C	UV-B	C	UV-B
	Flavonoids										
9.8	Apigenin 6,8-di-C-glucoside	593	353/383/503/575	169.9 ± 15.3	297.6 ± 31.6	174.3 ± 8.49	329.4 ± 10.3	179.6 ± 7.2	443.8 ± 15.0	175.9 ± 4.6	493.4 ± 9.8
11.9	Luteolin-7-*O*-rutinoside is. 1	593	285/447	175.1 ± 15.5	Nd	183.0 ± 9.65	Nd	57.3 ± 10.1	Nd	87.1 ± 11.6	Nd
12.2	Dihydroquercetin	303	125/177/285	181.2 ± 18.8	309.1 ± 31.5	196.5 ± 12.1	335.6 ± 10.8	201.9 ± 18.3	445.9 ± 15.6	351.0 ± 36.7	503.9 ± 23.7
12.5	Quercetin-3-*O*-glucoside	463	301	170.3 ± 15.0	337.7 ± 39.3	174.5 ± 8.41	346.2 ± 10.9	180.1 ± 7.3	Nd	180.5 ± 4.9	519.9 ± 48.8
12.9	Apigenin-7-*O*-rutinoside	577	269	185.4 ± 17.8	392.2 ± 43.3	189.2 ± 10.5	379.6 ± 11.3	225.7 ± 35.6	473.7 ± 27.1	269.6 ± 24.0	531.4 ± 61.5
13.1	Luteolin 7-*O*-rutinoside is. 2	593	285/447	179.6 ± 18.2	342.8 ± 36.6	184.4 ± 9.71	347.7 ± 10.9	64.9 ± 18.2	450.6 ± 17.0	81.0 ± 16.9	523.1 ± 50.1
13.5	Luteolin-4′-methyl ether	607	284/299	188.1 ± 18.2	331.1 ± 35.2	194.8 ± 11.5	343.2 ± 10.8	74.3 ± 24.3	453.6 ± 19.1	130.8 ± 19.2	535.0 ± 67.6
13.6	Luteolin-7-*O*-glucoside	447	289	173.8 ± 15.9	Nd	180.0 ± 9.13	Nd	51.8 ± 7.1	Nd	70.0 ± 6.6	Nd
15.9	Luteolin	285		211.6 ± 21.4	563.4 ± 66.2	227.0 ± 19.0	522.7 ± 14.6	165.4 ± 75.7	514.8 ± 46.5	253.1 ± 36.8	606.9 ± 171.6
16.7	Diosmetin is. 1	299	284	171.3 ± 15.5	318.4 ± 34.4	174.9 ± 8.52	335.2 ± 10.9	183.2 ± 7.2	445.6 ± 15.8	174.9 ± 4.7	501.1 ± 18.4
17.6	Apigenin	269	149	176.3 ± 16.4	432.8 ± 39.7	179.2 ± 9.15	391.3 ± 11.2	196.5 ± 14.7	463.3 ± 23.2	202.4 ± 6.9	541.9 ± 77.2
17.9	Diosmetin is. 2	299	284	182.7 ± 15.2	368.1 ± 38.6	187.7 ± 10.4	373.5 ± 11.0	224.7 ± 33.8	465.8 ± 24.6	237.9 ± 17.9	575.5 ± 124.9
20.1	Diosmetin is. 3	299	284	169.7 ± 15.2	349.1 ± 35.5	174.1 ± 8.38	350.0 ± 10.8	179.9 ± 7.2	449.0 ± 17.1	178.2 ± 4.8	533.8 ± 66.6
	Secoiridoid										
11.3	Decarboxymethyl oleuropein aglycone	319	183	175.2 ± 16.0	Nd	181.6 ± 9.58	Nd	96.5 ± 40.1	Nd	52.8 ± 6.0	Nd
	Hydroxycinnamic Acid Derivatives										
10.6	β-Hydroxyverbascoside is. 1	639	529/621	177.0 ± 16.5	295.3 ± 31.7	195.2 ± 11.8	327.4 ± 9.6	72.2 ± 5.5	447.0 ± 16.1	104.7 ± 7.3	490.6 ± 7.6
10.7	β-Hydroxyverbascoside is. 2	639	529/621	181.7 ± 17.4	296.5 ± 31.9	204.5 ± 13.9	328.7 ± 10.1	76.7 ± 9.6	448.3 ± 16.8	119.9 ± 10.4	492.0 ± 8.9

Table 2. Phenolic profile (mg kg^{-1} DW) of *Olea europaea* leaves (Olivastra Seggianese variety) under control (C) and UV-B conditions sampled at the 2nd (T2), 4th (T4), 6th (T6), and 8th (T8) week after the onset of stress. Values are mean ± standard deviation (n = 3–4). Rt—Retention time; is.—isomer. ANOVA showed that most of chemical components were significantly affected by the main factors and their interactions.

Rt (min)	Compound	$[M-H]^-$ (m/z)	MS^2 (m/z) Fragments	T2		T4		T6		T8	
				C	UV-B	C	UV-B	C	UV-B	C	UV-B
	Flavonoids										
9.8	Apigenin 6,8-di-*C*-glucoside	593	353/383/503/575	217.0 ± 13.0	225.6 ± 7.6	207.5 ± 18.4	245.3 ± 3.6	203.1 ± 1.4	271.4 ± 15.4	215.5 ± 6.2	357.0 ± 1.2
11.6	Quercetin-3-*O*-rutinoside	609	301	216.1 ± 12.5	222.4 ± 7.0	213.0 ± 12.9	244.6 ± 3.3	199.2 ± 1.1	269.7 ± 14.8	210.9 ± 6.9	360.2 ± 1.1
11.9	Luteolin-7-*O*-rutinoside is. 1	593	285	224.1 ± 16.8	225.1 ± 8.3	238.4 ± 4.0	248.4 ± 4.4	217.8 ± 5.5	279.1 ± 16.5	236.3 ± 10.8	380.5 ± 4.3
12.1	Luteolin-7-*O*-rutinoside is. 2	593	285/447	229.6 ± 20.6	226.1 ± 7.9	251.4 ± 8.0	257.7 ± 5.2	246.7 ± 19.4	292.7 ± 19.7	277.0 ± 22.2	460.9 ± 19.5
12.8	Apigenin-7-*O*-rutinoside	577	269	229.3 ± 20.4	252.9 ± 13.7	248.7 ± 10.8	297.1 ± 10.8	256.0 ± 7.7	356.5 ± 35.1	288.6 ± 19.1	427.3 ± 13.3
13.1	Luteolin-4′-methyl ether	607	299/284	225.5 ± 17.8	239.5 ± 11.2	230.4 ± 6.1	274.3 ± 14.1	225.8 ± 3.0	339.6 ± 46.8	247.9 ± 8.5	414.6 ± 14.4
13.4	Luteolin-7-*O*-glucoside	447	285	246.8 ± 33.5	250.7 ± 15.5	282.4 ± 16.1	278.0 ± 4.6	315.6 ± 22.0	321.0 ± 27.9	353.3 ± 30.2	501.1 ± 29.2
15.8	Luteolin	285		342.0 ± 112.1	299.7 ± 29.5	489.8 ± 96.0	449.7 ± 22.7	543.1 ± 104.2	493.9 ± 77.3	471.4 ± 51.2	702.8 ± 47.9
17.5	Apigenin	269	225/149/201	228.0 ± 19.7	258.3 ± 15.7	234.8 ± 5.9	304.8 ± 14.9	228.5 ± 7.4	340.4 ± 31.2	243.5 ± 9.2	410.8 ± 9.2
17.8	Diosmetin is. 1	299	284	270.0 ± 52.5	294.7 ± 24.8	317.2 ± 33.6	319.3 ± 18.7	359.4 ± 34.9	383.5 ± 37.4	389.1 ± 28.5	519.9 ± 27.1
20.1	Diosmetin is. 2	299	284	221.4 ± 15.7	251.2 ± 14.6	226.9 ± 7.7	292.0 ± 13.8	224.9 ± 2.2	306.4 ± 24.6	241.7 ± 11.3	399.1 ± 12.5
	Secoiridoid										
12.5	Caffeoyl-6′-secologanoside	551	507/341/389/281	220.3 ± 14.5	232.2 ± 8.6	223.0 ± 8.5	260.8 ± 5.6	215.1 ± 1.7	315.4 ± 24.7	234.4 ± 10.6	388.3 ± 5.7

ANOVA was able to underline a significant interaction between the factors of treatment and variety (Table S1) for apigenin 6,8-di-*C*-glucoside, apigenin, luteolin-7-*O*-rutinoside, luteolin-4′-methyl ether, luteolin-7-*O*-glucoside, luteolin, quercetin-3-*O*-glucoside, and diosmetin isomers 1 and 2. The stressed plants of both varieties present the highest ($p \leq 0.01$) levels of these compounds (except for luteolin-7-*O*-rutinoside is. 1 and luteolin-7-*O*-glucoside not detected in stressed plants of the Giarraffa, and luteolin for Olivastra Seggianese). Moreover, the stressed plants of the Giarraffa variety show an increase in these compounds higher than the stressed plants of the Seggianese variety.

As regards dihydroquercetin, diosmetin isomer 3, and the two derivatives of hydroxycinnamic acids, these compounds were detected only in plants of the Giarraffa variety. An interaction between the factors of treatment and variety was also observed for these compounds, and they presented the highest ($p \leq 0.01$) levels in stressed plants. Concerning caffeoyl-6′-secologanoside, it was detected only in the Olivastra Seggianese variety plants, and an interaction between the factors of treatment and variety was observed. The stressed plants presented the highest ($p \leq 0.01$) levels of caffeoyl-6′-secologanoside.

Concerning the factors of treatment and sampling time, an interaction of these two factors was observed for all phenolic compounds identified (except for the oleuropein derivative, which was only present in control plants of Giarrafa; (Table S1). For apigenin 6,8-di-*C*-glucoside, luteolin-7-*O*-rutinoside (isomer 1 was not present in UV-B Giarrafa), luteolin-4′-methyl ether, luteolin-7-*O*-glucoside (not present in UV-B Giarrafa), luteolin, apigenin, and diosmetin isomers 1 and 2, the UV-B plants at T8 showed the highest levels. In Giarrafa, the UV-B plants at T8 also showed the highest levels of β-hydroxy-verbascoside, dihydroquercetin, quercetin-3-*O*-glucoside, and diosmetin isomer 3. For the Olivastra Seggianese, the highest levels of caffeoyl-6′-secologanoside and quercetin-3-*O*-rutinoside were found in UV-B plants at T8.

Figure 1 shows the fold changes in phenolic metabolites of the Giarraffa (A) and Olivastra Seggianese (B) after UV-B treatment in the different sampling times (T2, T4, T6, and T8). In general, for the Olivastra Seggianese variety (Figure 1B), the profiles of the response of phenolic compounds progressively increased as stress progressed (except for the diosmetin isomer 1, luteolin, and luteolin 7-*O*-glucoside); while in the Giarraffa variety (Figure 1A), a more heterogenic profile of response was observed, with a progressive increase in some metabolites with the progress of stress, such as apigenin 6,8-di-*C*-glucoside, quercetin-3-*O*-glucoside, diosmetin isomers, and apigenin. In other phenolic metabolites, such as luteolin 7-*O*-rutinoside isomer 2, luteolin-4′-methyl ether, and β-hydroxyverbascoside isomers, the response was more intense in the T6 and T8.

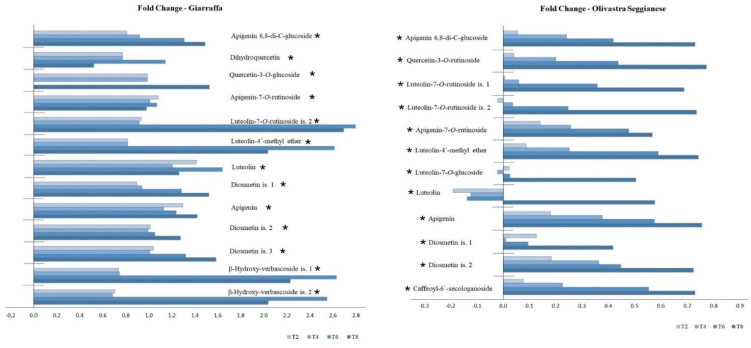

(**A**) (**B**)

Figure 1. Fold changes ($\log_2$ (UV-B/control)) in phenolic metabolites of the Giarraffa (**A**) and Olivastra Seggianese (**B**) varieties after UV-B treatment sampled at the 2nd (T2), 4th (T4), 6th (T6), and 8th (T8) week after the onset of stress. ANOVA showed that most of chemical components were significantly affected by the main factors and their interactions. An asterisk (*) indicates a significant interaction between treatment vs. variety and treatment vs. sampling time.

2.2. Lipophilic Profile

The lipophilic profile was evaluated in olive leaves (Giarraffa and Olivastra Seggianese varieties) of control and UV-B stressed plants, sampled at the 2nd, 4th, 6th and 8th week after the onset of stress (Tables 3 and 4). In the Giarraffa variety (Table 3), a total of 17 compounds were quantified: five terpenes, three carbohydrates, four fatty acids, and five alkanes. In the Olivastra Seggianese variety (Table 4), a total of 18 compounds were quantified: five terpenes, three carbohydrates, four fatty acids, five alkanes, and one sterol.

ANOVA showed (Table S2) a significant interaction between the factors of treatment and variety only for the lupeol derivative, with the plants of the Giarraffa variety under control and UV-B stress treatment presenting the highest levels of this terpene, followed by the Olivastra Seggianese UV-B-stressed plants. For the other lipophilic compounds (except the oleic acid derivative), an effect of the factor of treatment (control vs. UV-B stress) was observed, and the olive plants exposed to UV-B stress showed a level of these compounds significantly ($p \leq 0.05$) higher than controls. In addition, an effect of the factor variety (Olivastra Seggianese vs. Giarraffa) also was observed for the compounds neophytadiene; palmitic and α-linolenic acids; long-chain alkanes 1, 2, 3, and 4; β-amyrin; and oleic acid derivative. Regarding the neophytadiene, Olivastra Seggianese had a significantly ($p \leq 0.05$) higher compound content than Giarraffa. For the other compounds, Giarraffa had a significantly ($p \leq 0.05$) higher content than Olivastra Seggianese.

Concerning the factors of treatment and sampling time, an interaction of these two factors was observed for all lipophilic compounds identified (Table S2). For the cases of neophytadiene, lupeol derivative, oleic acid derivative, and stigmast-5-en (only present in Giarraffa), the UV-B plants at T6 showed the highest levels, and for the other remaining compounds, they were more abundant in the UV-B plants at T8.

Figure 2 shows the rate of change in lipophilic metabolites of Giarraffa (A) and Olivastra Seggianese (B) after UV-B treatment at different sampling times (T2, T4, T6, and T8). In the Olivastra Seggianese variety (Figure 2B), the response profiles of some lipophilic metabolites progressively increased as stress progressed: phytol, ursolic acid, α-D-mannopyranose, D-sorbitol, α-D-thalopyranose, α-linolenic acid, and long-chain alkane 4. Other metabolites, however, did not show a progressive increase, but had peaks at T4 or T6 or both time points, as in the cases of neophytadiene; β-amyrin; lupeol derivative; long-chain alkanes 1, 2, and 3; and stigmast-5-ene. Others, such as palmitic and oleic acids, had peaks at T4 and T8. In addition, the stearic acid response intensity decreased progressively from T2 to T6 and then increased again slightly at T8, whereas the long-chain alkane 5 response intensity decreased with progressing stress from T2 to T8. In the Giarraffa variety (Figure 2A), the response profiles of some lipophilic metabolites increased progressively with stress: α-D-mannopyranose, α-D-thalopyranose, and D-sorbitol. Other metabolites, however, did not show a progressive increase, but had peaks at T4 and T8, such as phytol; β-amyrin; ursolic, palmitic, β-linolenic, and stearic acids; and long-chain alkanes 1, 2, 3, 4, and 5. For some lipophilic metabolites, such as f lupeol derivative and oleic acid derivative, a steady decrease, albeit with fluctuations, was observed in stressed samples compared to controls.

Table 3. Lipophilic profile (g kg^{-1} DW) of *Olea europaea* leaves (Giarraffa variety) under control (C) and UV-B conditions sampled at the 2nd (T2), 4th (T4), 6th (T6), and 8th (T8) week after the onset of stress. Values are mean ± standard deviation (n = 3). Rt—Retention time. ANOVA showed that most of chemical components were significantly affected by the main factors and their interactions.

Rt (min)	Compound	T2		T4		T6		T8	
		C	UV-B	C	UV-B	C	UV-B	C	UV-B
	Terpenes								
34.1	Neophytadiene	0.463 ± 0.013	0.340 ± 0.000	0.451 ± 0.004	0.554 ± 0.002	0.421 ± 0.006	0.546 ± 0.003	0.500 ± 0.021	0.623 ± 0.002
42.1	Phytol	0.361 ± 0.001	0.324 ± 0.000	0.358 ± 0.001	0.459 ± 0.001	0.323 ± 0.000	0.397 ± 0.000	0.396 ± 0.001	0.493 ± 0.001
67.9	β-Amyrin	0.633 ± 0.003	0.594 ± 0.003	0.630 ± 0.004	0.862 ± 0.005	0.570 ± 0.005	0.719 ± 0.007	0.697 ± 0.010	0.959 ± 0.012
71.7	Lupeol derivative	1.777 ± 0.004	1.084 ± 0.005	1.763 ± 0.024	1.888 ± 0.036	1.604 ± 0.034	2.202 ± 0.029	1.936 ± 0.033	1.826 ± 0.014
73.3	Ursolic acid	1.167 ± 0.009	1.194 ± 0.003	1.163 ± 0.010	1.564 ± 0.015	1.072 ± 0.049	1.366 ± 0.013	1.284 ± 0.018	2.005 ± 0.002
	Carbohydrates								
35.4	α-D-Mannopyranose	0.103 ± 0.003	0.092 ± 0.000	0.101 ± 0.002	0.122 ± 0.003	0.090 ± 0.000	0.118 ± 0.000	0.113 ± 0.004	0.280 ± 0.008
36.3	D-Sorbitol	0.130 ± 0.000	0.109 ± 0.001	0.129 ± 0.001	0.135 ± 0.001	0.117 ± 0.000	0.152 ± 0.001	0.143 ± 0.000	0.572 ± 0.001
37.7	α-D-Talopyranose	0.111 ± 0.000	0.099 ± 0.001	0.110 ± 0.000	0.123 ± 0.001	0.100 ± 0.000	0.132 ± 0.000	0.122 ± 0.000	0.348 ± 0.003
	Fatty acids								
39.2	Palmitic acid	3.017 ± 0.008	2.978 ± 0.006	2.992 ± 0.008	4.439 ± 0.008	2.731 ± 0.001	3.406 ± 0.003	3.347 ± 0.010	4.742 ± 0.008
43.0	β-Linolenic acid	3.284 ± 0.002	3.151 ± 0.005	3.252 ± 0.008	4.815 ± 0.014	2.946 ± 0.002	3.669 ± 0.008	3.618 ± 0.005	5.042 ± 0.023
43.7	Stearic acid	2.664 ± 0.002	2.792 ± 0.002	2.640 ± 0.001	4.046 ± 0.002	2.423 ± 0.001	2.968 ± 0.000	2.977 ± 0.002	4.255 ± 0.004
72.7	Oleic acid derivative	1.490 ± 0.213	0.829 ± 0.036	1.593 ± 0.226	1.335 ± 0.014	1.578 ± 0.042	2.232 ± 0.034	1.771 ± 0.248	1.014 ± 0.019
	Alkanes								
57.9	Long-chain alkane 1	1.341 ± 0.003	1.075 ± 0.007	1.331 ± 0.003	1.780 ± 0.006	1.217 ± 0.008	1.326 ± 0.004	1.491 ± 0.012	2.418 ± 0.021
62.4	Long-chain alkane 2	1.888 ± 0.001	1.534 ± 0.014	1.879 ± 0.010	2.683 ± 0.018	1.717 ± 0.025	2.117 ± 0.009	2.106 ± 0.018	3.644 ± 0.040
67.6	Long-chain alkane 3	2.694 ± 0.007	2.001 ± 0.008	2.676 ± 0.013	3.540 ± 0.031	2.418 ± 0.028	2.965 ± 0.012	2.970 ± 0.032	4.623 ± 0.034
70.2	Long-chain alkane 4	0.741 ± 0.011	0.685 ± 0.006	0.750 ± 0.041	1.059 ± 0.006	0.692 ± 0.014	0.894 ± 0.005	0.838 ± 0.003	1.266 ± 0.009
72.8	Long-chain alkane 5	0.566 ± 0.004	1.008 ± 0.059	0.568 ± 0.004	1.742 ± 0.030	0.526 ± 0.021	0.704 ± 0.017	0.632 ± 0.006	2.468 ± 0.064

Table 4. Lipophilic profile (g kg^{-1} DW) of *Olea europaea* leaves (Olivastra Seggianese variety) under control (C) and UV-B conditions sampled at the 2nd (T2), 4th (T4), 6th (T6), and 8th (T8) week after the onset of stress. Values are mean ± standard deviation (n = 3). Rt—Retention time. ANOVA showed that most of chemical components were significantly affected by the main factors and their interactions.

Rt (min)	Compound	T2		T4		T6		T8	
		C	UV-B	C	UV-B	C	UV-B	C	UV-B
	Terpene								
34.1	Neophytadiene	0.533 ± 0.002	0.487 ± 0.006	0.530 ± 0.003	0.586 ± 0.006	0.578 ± 0.008	0.700 ± 0.003	0.483 ± 0.008	0.534 ± 0.007
42.1	Phytol	0.344 ± 0.001	0.361 ± 0.001	0.333 ± 0.001	0.395 ± 0.000	0.355 ± 0.002	0.424 ± 0.002	0.336 ± 0.002	0.444 ± 0.001
67.9	β-Amyrin	0.357 ± 0.001	0.492 ± 0.001	0.363 ± 0.008	0.621 ± 0.006	0.385 ± 0.015	0.629 ± 0.004	0.353 ± 0.001	0.551 ± 0.005
71.7	Lupeol derivative	1.290 ± 0.012	1.591 ± 0.046	1.281 ± 0.007	1.873 ± 0.009	1.378 ± 0.021	1.794 ± 0.017	1.143 ± 0.003	1.490 ± 0.026
73.3	Ursolic acid	1.007 ± 0.010	1.297 ± 0.064	1.083 ± 0.006	0.586 ± 0.015	0.578 ± 0.0008	1.647 ± 0.028	0.975 ± 0.006	1.626 ± 0.036
	Carbohydrates								
35.5	α-D-Mannopyranose	0.120 ± 0.001	0.111 ± 0.000	0.117 ± 0.004	0.131 ± 0.001	0.121 ± 0.000	0.157 ± 0.001	0.116 ± 0.000	0.191 ± 0.004
36.3	D-Sorbitol	0.127 ± 0.000	0.119 ± 0.000	0.126 ± 0.000	0.159 ± 0.001	0.135 ± 0.000	0.209 ± 0.002	0.124 ± 0.000	0.209 ± 0.004
37.7	α-D-Talopyranose	0.134 ± 0.001	0.119 ± 0.000	0.133 ± 0.000	0.153 ± 0.001	0.141 ± 0.001	0.192 ± 0.001	0.131 ± 0.001	0.219 ± 0.002
	Fatty acids								
39.2	Palmitic acid	2.777 ± 0.010	3.411 ± 0.003	2.766 ± 0.005	3.433 ± 0.009	2.946 ± 0.004	3.551 ± 0.015	2.961 ± 0.004	3.868 ± 0.013
43.0	β-Linolenic acid	2.870 ± 0.014	3.463 ± 0.003	2.834 ± 0.006	3.556 ± 0.004	3.024 ± 0.005	3.819 ± 0.005	2.949 ± 0.005	3.980 ± 0.015
43.7	Stearic acid	2.530 ± 0.005	3.202 ± 0.001	2.529 ± 0.001	3.144 ± 0.001	2.695 ± 0.002	3.145 ± 0.002	2.782 ± 0.002	3.592 ± 0.003
72.6	Oleic acid derivative	1.253 ± 0.004	1.167 ± 0.009	1.252 ± 0.003	1.380 ± 0.247	1.059 ± 0.024	1.114 ± 0.041	0.883 ± 0.006	1.046 ± 0.031
	Alkanes								
52.9	Long-chain alkane 1	0.478 ± 0.001	0.621 ± 0.001	0.471 ± 0.001	0.681 ± 0.002	0.503 ± 0.001	0.709 ± 0.001	0.492 ± 0.001	0.681 ± 0.001
57.5	Long-chain alkane 2	0.689 ± 0.005	1.125 ± 0.007	0.684 ± 0.002	1.310 ± 0.003	0.732 ± 0.002	1.409 ± 0.009	0.670 ± 0.001	0.967 ± 0.006
62.4	Long-chain alkane 3	1.034 ± 0.009	1.632 ± 0.007	1.041 ± 0.008	1.890 ± 0.008	1.117 ± 0.010	1.983 ± 0.019	0.992 ± 0.008	1.407 ± 0.020
70.2	Long-chain alkane 4	0.607 ± 0.001	0.770 ± 0.001	0.607 ± 0.003	0.850 ± 0.002	0.647 ± 0.002	0.913 ± 0.007	0.622 ± 0.001	0.899 ± 0.004
72.8	Long-chain alkane 5	0.530 ± 0.002	1.146 ± 0.058	0.531 ± 0.010	1.067 ± 0.0322	0.905 ± 0.049	1.645 ± 0.038	0.894 ± 0.008	1.402 ± 0.005
	Sterol								
67.6	Stigmast-5-ene	1.192 ± 0.008	2.344 ± 0.039	1.198 ± 0.008	2.725 ± 0.004	2.030 ± 0.039	3.188 ± 0.014	1.761 ± 0.009	1.686 ± 0.038

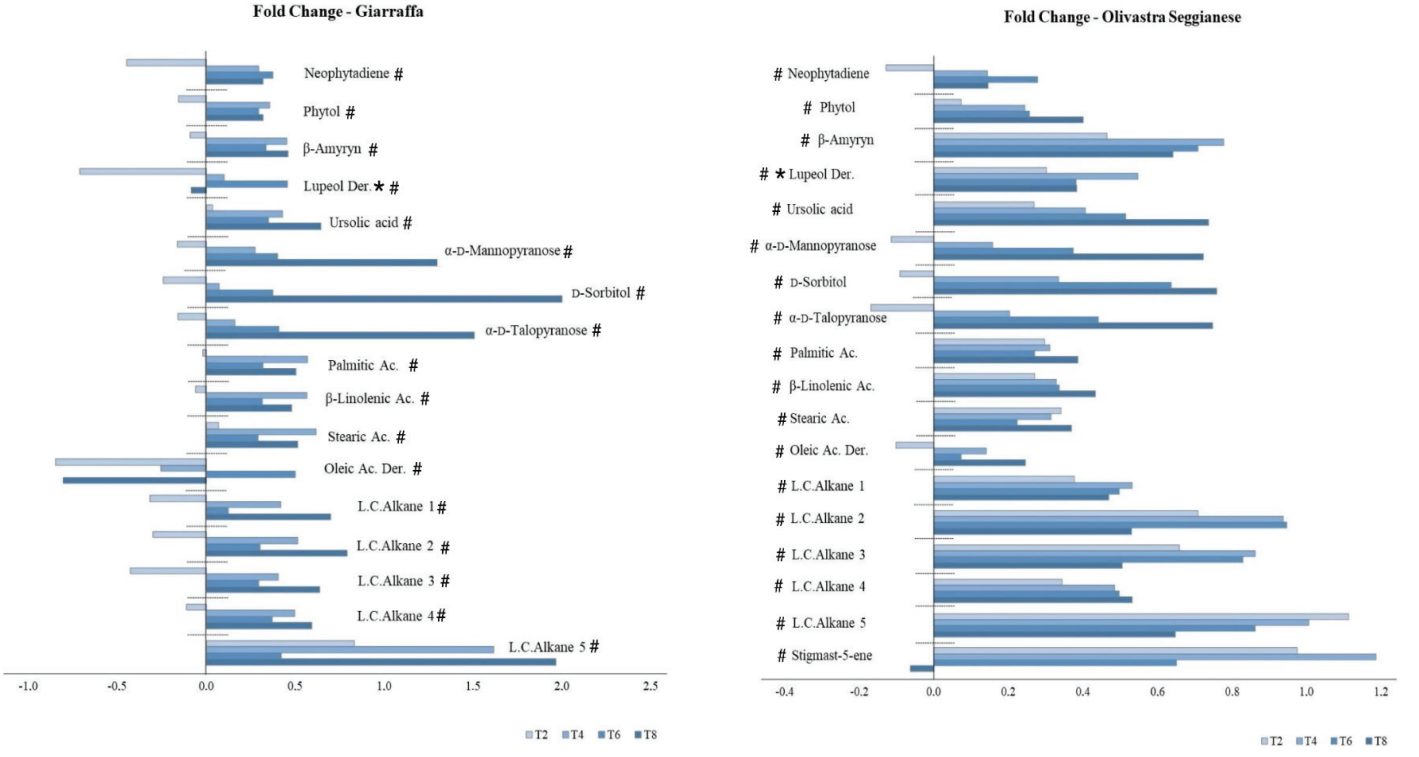

Figure 2. Fold changes (log_2 (UV-B/control)) in lipophilic metabolites of the Giarraffa (**A**) and Olivastra Seggianese (**B**) varieties after UV-B treatment sampled at the 2nd (T2), 4th (T4), 6th (T6), and 8th (T8) week after the onset of stress. ANOVA showed that most of chemical components were significantly affected by the main factors and their interactions. An asterisk (*) indicates a significant interaction between treatment vs. variety; a hashtag (#) indicates a significant interaction between treatment vs. sampling time.

3. Discussion

3.1. Olive Plant UHPLC–MS Metabolite Profile

The metabolomic approach provided information on how the content of phenolic metabolites changed in response to UV-B stress, and identified specific compounds that appeared relevant to the olive response. Concerning the profile, some qualitative differences between the two varieties were detected. However, the flavonoids, secoiridoids, and hydroxycinnamic acids identified were already similar to those described for other olive varieties [25].

In the Olivastra Seggianese and Giarraffa varieties, flavonoids were the main phenolic compounds present in leaves. The flavonoid family is a vast group of compounds with different structures and roles [26]. Flavonoids are the principal phenols that contribute to the overall leaf antioxidant potency through ROS scavenging [27]. Some previous studies suggested that *o*-dihydroxy B-ring (catechol)-substituted flavonoids had a greater antioxidant capacity [28], and they could be found in several cell compartments near the centers of ROS generation or be transported from their sites of biosynthesis to these compartments [26,28]. Flavonoids can also prevent oxygen radical formation by inhibiting the activity of the enzymes involved in their generation [29]. In the Giarraffa variety, except for the luteolin-7-*O*-rutinoside isomer 1, luteolin-7-*O*-glucoside, and the oleuropein derivative, which were not detected in UV-B-stressed leaves, all the other flavonoids accumulated in response to the UV-B stress. These levels were, in general, higher than those found in Olivastra Seggianesse stressed plants. In turn, the Olivastra Seggianese variety showed a more heterogenic response to UV-B, but with a progressive increase in the majority of the flavonoids. The flavonoids, luteolin 7-*O*-rutinoside isomer 2, luteolin 7-*O*-glucoside, and luteolin in this variety, despite some fluctuations during the stress, achieved positive values at the end of the UV-B treatment (higher than those of the respective control). All these data suggested that both varieties responded to stress by increasing flavonoids pools, which represented a higher capacity to deal with the stress, particularly in the variety Giarraffa.

Some olive varieties are rich in luteolin-7-*O*-glucoside, a catechol B-ring-substituted flavonoid, which could be related to this species' high tolerance to stress [16]. However, in others, the luteolin methylated forms (e.g., 4′-methoxyluteolin and 4′- or 3′-methoxyluteolin glucoside) seemed more responsive to stress, particularly the UV-B stress, decreasing their levels possibly due to their use in the neutralization of ROS [30], or due to the inactivation of the enzymes involved in the conversion of luteolin in their methylated forms [31]. In the present study, luteolin methylated forms were also found in both varieties, but their levels were consistently higher in stressed plants.

In general, the profiles of responses of flavonoids to UV-B obtained here for the two olive varieties were in line with those obtained in our previous studies, which also highlighted the accumulation of total flavonoids in response to UV-B radiation [23].

Another class of phenolic compounds identified as the secoiridoids. This family of compounds plays a crucial protective role in olive plants against drought, salt [32,33], and UV-B stress [17], suggesting some involvement in plant stress-defense mechanisms. Contrary to other studies with other olive varieties, only two secoiridoids were identified [17,34,35]. The decarboxymethyl oleuropein aglycone was only identified in the control plants of the Giarraffa variety. This compound is a derivative of oleuropein, which is one of the main phenolic compounds present in olive leaves [16]. Some studies reported the vital role of oleuropein in plant stress response, including to UV-B [17,25]. In turn, the other secoiridoid, caffeoyl-6-secologanoside, was only identified in Olivastra Seggianese, and UV-B plants showed a progressive increase in this metabolite compared to controls. In response to abiotic stresses, an accumulation of caffeoyl-6-secologanoside was also found in Cordovil of Castelo Branco olives [36], suggesting a possible protective stress role of this secoiridoid.

The last phenolic compound class identified was the hydroxycinnamic acid derivatives (HCAds). Hydroxycinnamic acids are predominantly involved in UV-B screening and

accumulate mainly in the leaf epidermal cells, screening UV-B radiation that can reach photosynthetic tissues [27,37]. Moreover, they can also act as antioxidants through the scavenging of ROS, such as $O_2^{\bullet -}$, $OH^{\bullet}$, and $^1O_2$ [27]. In the present study, the HCAd β-hydroxyverbascoside was detected only in the leaves of the Giarraffa variety, and UV-B stress stimulated the production of this compound, which may provide extra UV-B shield protection [17]. These results suggested that the accumulation of β-hydroxyverbascoside in stressed plants allowed the Giarraffa variety to cope better with UV-B stress when compared with the Olivastra Seggianese. This was also in line with our previous work [23], in which Giarrafa showed a better performance (e.g., a higher photosynthetic efficiency) under prolonged UV-B stress. The β-hydroxyverbascoside was also identified in olive leaves from several other olive varieties [38].

3.2. Olive Plant GC–MS Metabolite Profile

The qualitative lipophilic profiles found in Olivastra Seggianese and Giarraffa were very similar. In Olivastra Seggianese leaves, the sterol stigmast-5-ene was also present in relatively high amounts, but was not in Giarraffa. Moreover, similar compounds were found in other varieties, and the fatty acids and long-chain alkanes were the most representative compounds found in olive leaves [9,16,35].

Regarding fatty acids, UV-B stress stimulated the production of palmitic, α-linolenic, and stearic acids in both varieties. Furthermore, stressed plants of Giarraffa produced more palmitic, α-linolenic, and stearic acids than the stressed plants of Olivastra Seggianese. This suggested that the UV-B stress response was weaker in Olivastra Seggianese, and it is possible this variety was unable to engage the same defense mechanisms as Giarraffa, based on readjustments of the levels of the fatty acids. These results aligned with our previous work, in which lipid peroxidation was only noticeable in the Olivastra Seggianese variety (particularly from T2 to T8) [24]. The absence of variations in lipid peroxidation [24] in stressed Giarraffa plants could be related to the higher palmitic, α-linolenic, and stearic acid contents found in these plants. Indeed, fatty acids have been described as constitutive elements of complex lipids, but several studies also suggested their direct involvement in abiotic and biotic responses to stress in plants [39,40]. Complex lipids, in turn, play an essential role in the structure and functions of cells by maintaining the integrity of cells and organelles [41].

Mannitol is one of the main polyols usually found in olive leaves [42]. In the present work, we identified sorbitol, an isomer of mannitol, and the UV-B stress induced by the accumulation of this polyol in both varieties. This response profile aligned with our previous work, particularly for the Giarrafa variety, in which mannitol levels increased after UV-B stress [23]. Olive trees are well adapted to regions with high irradiance (particularly UV). Maintaining high levels of polyols may be essential to cope with this stress, since these compounds provide more efficient use of carbon, act as osmolytes, and defend against photo-oxidative damage [23,42]. Besides mannitol, UV-B stress also induced an accumulation of the carbohydrates α-D-mannopyranose and α-D-talopyranose up to T4 in stressed plants of both varieties. Carbohydrates are involved in several stress-protective mechanisms, and their increase following stress is a typical response of olive trees, particularly under drought [35]. An accumulation in the sugar pool can increase carbon and energy availability to cope with stressful conditions or decrease sugar use for growth [43].

UV-B treatment also induced adjustments in the levels of triterpenes (neophytadiene, phytol, β-amyrin, lupeol derivative, and ursolic acid) and long-chain alkanes in both varieties. Considering that the main components of olive leaf cuticular wax are triterpenes (e.g., ursolic acid and α– and β–amyrin), long-chain alkanes, alcohols, aldehydes, and fatty acids [20,44,45], we hypothesized that olive plants invested (increased the levels) in these compounds to strengthen the cuticle structure. This improvement provided a protective barrier against UV radiation, increased light reflectance, decreased UV radiation penetration into the mesophyll, and reduced membrane damages [9,46,47]. In addition, morphoanatomical studies performed in olive leaves showed an increase in cuticle thickness

in response to a long period of UV-B exposure [48]. Furthermore, Giarraffa stressed plants produced more β-amyrin, lupeol derivative, and long-chain alkanes (1–4) than Olivastra Seggianese stressed plants. In particular, long-chain alkanes in Giarraffa stressed plants showed values two times higher than those found in Olivastra Seggianese stressed plants. This suggested that the higher content of terpenes and long-chain alkanes may have allowed Giarraffa stressed plants to tolerate the UV-B radiation better than the Olivastra Seggianese stressed plants.

4. Materials and Methods

4.1. Plant Growth Conditions and Application of UV-B Treatment

Olive trees (*Olea europaea* L.) that were 18 months old (both Olivastra Seggianese and Giarraffa varieties) were taken from the nursery of the Società Pesciatina di Orticoltura (Pescia, PT, Italy). Subsequently, plants were transferred to climatic cells with the following environmental conditions: temperature of 21 °C; relative humidity (RH) of 60%; photoperiod of 14 light h, 10 dark h [49]; light intensity of 500 μmol m^{-2} s^{-1}; watering with 400 mL of water for each plant once a week; and commercial substrate type "Vigor Plant Soil" (Vigorplant Italia Srl, Fombio, Italy) [23]. Ultraviolet radiation was provided by two TL20W/12 lamps (Philips, Milano, Italy) that emitted in the wavelength of UV-B rays, and that had already been widely used and described in the literature; lamps were used exactly according to the protocol of Allen et al. [49]. Plants (n = 16 for each variety) were positioned under UV-B lamps in the climatic cell. Every day, the homogeneity of UV-B radiation emitted by lamps was verified using a Power Meter 840 with an 818-UV sensor (Newport Optical, Newport Beach, CA, USA). The UV-B biologically effective dose (BED), 25 kJ m^{-2} d^{-1}, was calculated according to Correia et al. [50]. Control plants (n = 16 for each variety), present in the same climatic cell, were carefully separated from those treated by means of a plasterboard panel that shielded most of the UV radiation (BED of 1 kJ m^{-2} d^{-1}). The UV-B treatment corresponded to a high UV-B dose, but within the natural values already reported on the earth's surface [51]. The UV-B treatment was carried out for a period of 8 weeks for 14 h a day. During the treatment, eight time points were established: the first one before the onset of UV-B treatment (T0); and after 1, 2, 3, 4, 5, 6, 7, and 8 weeks of UV-B treatment (respectively indicated as T1, T2, T3, T4, T5, T6, T7, and T8) [23]. Leaf samples were collected at four representative sampling times (T2, T4, T6 and T8), immediately frozen in liquid nitrogen, and stored at −80 °C.

4.2. Preparation of Leaf Extracts

Frozen olive leaves were macerated and mixed with *n*-hexane (5 g of leaves for 50 mL of extraction solvent) at room temperature with magnetic stirring for 48 h. The *n*-hexane was removed, and a new extraction cycle of 24 h was performed with the addition of new *n*-hexane in the same volume. The *n*-hexane from the two extraction cycles was placed in a glass balloon, and the *n*-hexane was evaporated to dryness at low pressure in a rotatory evaporator. The extracts obtained were left to dry for one week. The pellet obtained was also left to dry, and then mixed with 50 mL of methanol to extract phenolic compounds. After a first extraction cycle of 48 h at room temperature with magnetic stirring, the methanol was removed, and new methanol was added for a second extraction cycle. This last cycle lasted 24 h. The methanol obtained from both extraction cycles was put together in a glass balloon and evaporated to dryness at low pressure in a rotatory evaporator. The extract was left to dry for two weeks.

4.3. Gas Chromatography−Mass Spectrometry

The extracts obtained from the *n*-hexane extraction were weighted and prepared for silylation. In a glass tube, 200 μL of the extract was mixed with 200 μL of tetracosane 0.5 mg mL^{-1}, 250 μL of pyridine, 250 μL of *N*,*O*-bis(trimethylsilyl)trifluoroacetamide, and 50 μL of trimethylsilyl chloride and incubated at 70 °C for 40 min. A sample (1 μL) of the silylated extract was injected into the gas chromatography−mass spectrometry

(GC−MS) device (QP2010 Ultra Shimadzu). The chromatography conditions were set as described in Dias et al. (2019). For the identification of the lipophilic compounds, the peaks obtained in the chromatograms were compared with the library entries of the mass spectra database (NIST14 Mass Spectral Library and Wiley Registry® of Mass Spectral Data) or compared with the mass spectra and retention times of pure compounds analyzed and prepared similarly to the samples. Calibration curves were prepared for quantification with standard compounds representing the main families presented in the extracts (maltose for carbohydrates, palmitic acid for fatty acids, octadecane for alkanes, and cholesterol for terpenes) and obtained by injection of known concentrations of these standard compounds. For maltose, the concentrations ranged from 0.06 to 11 mg/mL ($y = 0.042x + 0.013$ and $r^2 = 0.99$); for palmitic acid, they ranged from 0.3 to 9 mg/mL ($y = 0.095x + 0.447$ and $r^2 = 0.99$); for octadecane, they ranged from 0.08 to 8 mg/mL ($y = 0.092x + 0.082$ and $r^2 = 0.98$); and for cholesterol, they ranged from 0.04 to 0.7 mg/mL ($y = 0.060x + 0.048$ and $r^2 = 0.99$). The results obtained are expressed in g/Kg DW and presented as mean ± standard deviation of three independent analyses.

4.4. Ultrahigh-Performance Liquid Chromatography–Mass Spectrometry

The dry methanolic extract was weighted, and 50 mg were collected and dissolved in 1 mL of methanol. Samples with a concentration of 10 mg mL^{-1} were filtered through a 0.2 mL nylon membrane (Whatman, Medstone, UK) and injected in the ultrahigh-performance liquid chromatography–mass spectrometry (UHPLC–MS) device (Thermo Scientific Ultimate 3000RSLC Dionex, Waltham, MA, USA). The chromatography analysis was performed as described by Dias et al. [16]. The UHPLC–MS equipment contained a Dionex UltiMate 3000 RS diode array detector coupled to a mass spectrometer, and a Thermo Scientific Hypersil GOLD column (1000 mm × 2.1 mm) with a particle size of 1.9 µm and a temperature adjusted to 30 °C. The mobile phase was composed of degassed and filtered acetonitrile and 0.1% formic acid (v/v) at a flow rate of 0.2 mL min^{-1}. During the first 14 min, the gradient of the solvent was 5% acetonitrile, followed by 40% formic acid for 2 min, 100% for 7 min, and 5% for the last 10 min. Then, 1 µL of the sample was injected into the UHPLC–MS device. UV–vis spectral data were collected between 250 and 500 nm wavelengths, and the chromatograms were recorded at 280 nm. The equipment contained a mass spectrometer (LTQ XL Linear Ion Trap 2D) with an orthogonal electrospray ion source (ESI) that operated in negative-ion mode with an electrospray ionization source of 5.00 kV (ESI capillarity temperature of 275 °C). It covered a mass range of 50.00 to 2000.00 m/z, and collision-induced dissociation MS/MS and MS^n experiments were performed for precursor ions. The retention times, UV–vis spectra, and spectral data were compared with those of standard compounds to identify the phenolic compounds. Semiquantification was performed by peak integration through the standard external method, using the closest standard compound. The detection and quantification limits (LOD and LOQ, respectively) were determined using calibration curves prepared with standard compounds (each family: quercetin and luteolin for flavonoids, and caffeic acid for secoiridoid and hydroxycinnamic acid derivatives). Calibration curves were obtained by injection of known concentrations (ranging from 5µg to 0.5 mg/mL) of these standard compounds: quercetin ($y = 3 \times 10^{-7}x + 0.0951$ and $r^2 = 0.99$), luteolin ($y = 2 \times 10^{-7}x + 0.0236$ and $r^2 = 0.98$), and caffeic acid ($y = 9 \times 10^{-8}x + 0.0358$ and $r^2 = 0.99$). The results obtained are expressed in g/Kg DW and presented as the mean ± standard deviation of four independent analyses.

4.5. Statistical Analysis

Statistical analysis was performed using the Systat 11 statistical package (Systat Software Inc., Richmond, CA, USA). Data were checked for normality distribution by the Shapiro–Wilk test before a repeated-measures ANOVA analysis to test the significance of each of the three factors: treatment, variety, and time, as well as their interactions. When ANOVA presented $p \leq 0.01$ or 0.05, a post hoc test was performed, and the content of each

dependent variable in the control and treated plants was discussed in relation to the variety and date.

5. Conclusions

This study characterized the most representative phenolic and lipophilic compounds in Giarraffa and Olivastra Seggianese leaves. We demonstrated how the levels of some compounds were modulated by UV-B stress and that, in general, UV-B plants at the end of the experiment (T8) contained higher levels of phenolic and lipophilic compounds. The Giarraffa variety seemed better suited to prolonged UV-B stress, possibly due to the higher availability of flavonoids that neutralized ROS and radicals, and the accumulation of HCAds that provided extra UV-B shield protection. Besides phenolic compounds, this variety also stood out due to the high levels of fatty acids (e.g., palmitic, α-linolenic, and stearic acids), which could help to maintain membrane integrity; accumulation of sorbitol, which may have osmoprotective and antagonistic functions against free radicals and increases in some terpenes; and long-chain alkanes, which could provide better protection from UV-B radiation. The investment in the synthesis of these phenolic and lipophilic compounds to cope with the UV-B stress may occur at the expenses of other processes. Besides the lipophilic and phenolic metabolite profiles, the expression and/or activity of key enzymes involved in the biosynthesis of these metabolites (e.g., phenylalanine ammonia lyase, chalcone-synthase, and acetyl-CoA carboxylase) deserve further studies to understand their roles in *O. europaea* response to and tolerance of UV-B stress.

Supplementary Materials: The following are available online at https://www.mdpi.com/article/10.3390/plants11050680/s1, Table S1: ANOVA table produced with experimental data of UV treated olive plants belonging to two different varieties compared to the control and analysed in four different dates. When a chemical component was not detected in both varieties in every date only the variables treatment and date were used with a lost in degrees of freedom into the ANOVA and consequent missing data in the table., Table S2: ANOVA table produced with experimental data of UV treated olive plants belonging to two different varieties compared to the control and analysed in four different dates.

Author Contributions: Conceptualization, C.P., C.C., G.C. and M.C.D.; analysis, C.P., M.R., D.C.G.A.P. and A.M.S.S.; data curation, C.P., G.C., C.C. and M.C.D.; writing—original draft preparation, C.P.; writing—review and editing C.P., G.C., C.C., D.C.G.A.P., A.M.S.S. and M.C.D. All authors have read and agreed to the published version of the manuscript.

Funding: This research received no external funding.

Institutional Review Board Statement: No institutional statement required.

Informed Consent Statement: Not applicable.

Data Availability Statement: Data are available upon request due to restrictions.

Acknowledgments: We thank the Tuscany Region for supporting a Ph.D. grant to C.P. in the framework of the 'Pegaso'-POR FSE TOSCANA 2014–2020 Program GiovaniSì. We also thank the Società Pesciatina di Orticultura (Pescia, PT, Italy) for kindly providing the olive plants used in the present work. The Foundation for Science and Technology (FCT, Portugal) and Ministério da Educação e Ciência (MEC) supported this work through national funds and cofunding with the FEDER within the PT2020 Partnership Agreement and COMPETE 2010 within the projects of the research units CEF (UI0183–UID/BIA/04004/2020) and LAQV-REQUIMTE (UIDB/50006/2020). M.C.D. (SFRH/BPD/100865/2014) acknowledges the FCT and MEC for the support.

Conflicts of Interest: The authors declare no conflict of interest.

References

1. Abbasi, S.A.; Abbasi, T. Impacts of Ozone Hole. In *Ozone Hole*; Springer: Berlin/Heidelberg, Germany, 2017; pp. 51–99. [CrossRef]
2. McKenzie, R.; Bodeker, G.; Scott, G.; Slusser, J.; Lantz, K. Geographical differences in erythemally-weighted UV measured at mid-latitude USDA sites. *Photochem. Photobiol. Sci.* **2006**, *5*, 343–352. [CrossRef] [PubMed]

3. Kakani, V.; Reddy, K.; Zhao, D.; Sailaja, K. Field crop responses to ultraviolet-B radiation: A review. *Agric. For. Meteorol.* **2003**, *120*, 191–218. [CrossRef]
4. Searles, P.S.; Flint, S.D.; Caldwell, M.M. A meta-analysis of plant field studies simulating stratospheric ozone depletion. *Oecologia* **2001**, *127*, 1–10. [CrossRef] [PubMed]
5. Müller-Xing, R.; Xing, Q.; Goodrich, J. Footprints of the sun: Memory of UV and light stress in plants. *Front. Plant Sci.* **2014**, *5*, 474. [CrossRef] [PubMed]
6. Hollósy, F. Effects of ultraviolet radiation on plant cells. *Micron* **2002**, *33*, 179–197. [CrossRef]
7. Martínez-Lüscher, J.; Morales, F.; Delrot, S.; Sánchez-Díaz, M.; Gomès, E.; Aguirreolea, J.; Pascual, I. Characterization of the adaptive response of grapevine (cv. Tempranillo) to UV-B radiation under water deficit conditions. *Plant Sci.* **2015**, *232*, 13–22. [CrossRef]
8. Brito, C.; Dinis, L.-T.; Moutinho-Pereira, J.; Correia, C.M. Drought Stress Effects and Olive Tree Acclimation under a Changing Climate. *Plants* **2019**, *8*, 232. [CrossRef]
9. Dias, M.C.; Pinto, D.C.G.A.; Correia, C.; Moutinho-Pereira, J.; Oliveira, H.; Freitas, H.; Silva, A.M.S.; Santos, C. UV-B radiation modulates physiology and lipophilic metabolite profile in Olea europaea. *J. Plant Physiol.* **2018**, *222*, 39–50. [CrossRef]
10. Schwachtje, J.; Whitcomb, S.J.; Firmino, A.A.P.; Zuther, E.; Hincha, D.K.; Kopka, J. Induced, imprinted, and primed responses to changing environments: Does metabolism store and process information? *Front. Plant Sci.* **2019**, *10*, 106. [CrossRef]
11. Bueno, P.C.P.; Lopes, N.P. Metabolomics to Characterize Adaptive and Signaling Responses in Legume Crops under Abiotic Stresses. *ACS Omega* **2020**, *5*, 1752–1763. [CrossRef]
12. Rodziewicz, P.; Swarcewicz, B.; Chmielewska, K.; Wojakowska, A.; Stobiecki, M. Influence of abiotic stresses on plant proteome and metabolome changes. *Acta Physiol. Plant.* **2014**, *36*, 1–19. [CrossRef]
13. Kusano, M.; Tohge, T.; Fukushima, A.; Kobayashi, M.; Hayashi, N.; Otsuki, H.; Kondou, Y.; Goto, H.; Kawashima, M.; Matsuda, F.; et al. Metabolomics reveals comprehensive reprogramming involving two independent metabolic responses of Arabidopsis to UV-B light. *Plant J.* **2011**, *67*, 354–369. [CrossRef] [PubMed]
14. Casati, P.; Campi, M.; Morrow, D.J.; Fernandes, J.F.; Walbot, V. Transcriptomic, proteomic and metabolomic analysis of UV-B signaling in maize. *BMC Genom.* **2011**, *12*, 321. [CrossRef] [PubMed]
15. Wargent, J.J.; Nelson, B.C.W.; Mcghie, T.K.; Barnes, P.W. Acclimation to UV-B radiation and visible light in Lactuca sativa involves up-regulation of photosynthetic performance and orchestration of metabolome-wide responses. *Plant Cell Environ.* **2015**, *38*, 929–940. [CrossRef] [PubMed]
16. Dias, M.C.; Figueiredo, C.; Pinto, D.C.G.A.; Freitas, H.; Santos, C.; Silva, A.M.S. Heat shock and UV-B episodes modulate olive leaves lipophilic and phenolic metabolite profiles. *Ind. Crops Prod.* **2019**, *133*, 269–275. [CrossRef]
17. Dias, M.C.; Pinto, D.C.G.A.; Freitas, H.; Santos, C.; Silva, A.M.S. The antioxidant system in Olea europaea to enhanced UV-B radiation also depends on flavonoids and secoiridoids. *Phytochemistry* **2020**, *170*, 112199. [CrossRef]
18. Gil, M.; Pontin, M.; Berli, F.; Bottini, R.; Piccoli, P. Metabolism of terpenes in the response of grape (*Vitis vinifera* L.) leaf tissues to UV-B radiation. *Phytochemistry* **2012**, *77*, 89–98. [CrossRef]
19. Lytovchenko, A.; Beleggia, R.; Schauer, N.; Isaacson, T.; Leuendorf, J.E.; Hellmann, H.; Rose, J.K.; Fernie, A.R. Application of GC-MS for the detection of lipophilic compounds in diverse plant tissues. *Plant Methods* **2009**, *5*, 4. [CrossRef]
20. Mihailova, A.; Abbado, D.; Pedentchouk, N. Differences in n -alkane profiles between olives and olive leaves as potential indicators for the assessment of olive leaf presence in virgin olive oils. *Eur. J. Lipid Sci. Technol.* **2015**, *117*, 1480–1485. [CrossRef]
21. Wenzel, A.; Frank, T.; Reichenberger, G.; Herz, M.; Engel, K.-H. Impact of induced drought stress on the metabolite profiles of barley grain. *Metabolomics* **2015**, *11*, 454–467. [CrossRef]
22. Liakopoulos, G.; Stavrianakou, S.; Karabourniotis, G. Trichome layers versus dehaired lamina of *Olea europaea* leaves: Differences in flavonoid distribution, UV-absorbing capacity, and wax yield. *Environ. Exp. Bot.* **2006**, *55*, 294–304. [CrossRef]
23. Piccini, C.; Cai, G.; Dias, M.C.; Romi, M.; Longo, R.; Cantini, C. UV-B radiation affects photosynthesis-related processes of two Italian *Olea europaea* (L.) varieties differently. *Plants* **2020**, *9*, 1712. [CrossRef]
24. Piccini, C.; Cai, G.; Dias, M.C.; Araújo, M.; Parri, S.; Romi, M.; Faleri, C.; Cantini, C. Olive Varieties under UV-B Stress Show Distinct Responses in Terms of Antioxidant Machinery and Isoform/Activity of RubisCO. *Int. J. Mol. Sci.* **2021**, *22*, 11214. [CrossRef]
25. Talhaoui, N.; Taamalli, A.; Gómez-Caravaca, A.M.; Fernández-Gutiérrez, A.; Segura-Carretero, A. Phenolic compounds in olive leaves: Analytical determination, biotic and abiotic influence, and health benefits. *Food Res. Int.* **2015**, *77*, 92–108. [CrossRef]
26. Agati, G.; Azzarello, E.; Pollastri, S.; Tattini, M. Flavonoids as antioxidants in plants: Location and functional significance. *Plant Sci.* **2012**, *196*, 67–76. [CrossRef] [PubMed]
27. Luengo Escobar, A.; Alberdi, M.; Acevedo, P.; Machado, M.; Nunes-Nesi, A.; Inostroza-Blancheteau, C.; Reyes-Díaz, M. Distinct physiological and metabolic reprogramming by highbush blueberry (*Vaccinium corymbosum*) cultivars revealed during long-term UV-B radiation. *Physiol. Plant.* **2017**, *160*, 46–64. [CrossRef]
28. Brunetti, C.; Di Ferdinando, M.; Fini, A.; Pollastri, S.; Tattini, M. Flavonoids as Antioxidants and Developmental Regulators: Relative Significance in Plants and Humans. *Int. J. Mol. Sci.* **2013**, *14*, 3540–3555. [CrossRef] [PubMed]
29. Mierziak, J.; Kostyn, K.; Kulma, A. Flavonoids as Important Molecules of Plant Interactions with the Environment. *Molecules* **2014**, *19*, 16240–16265. [CrossRef]

30. Agati, G.; Biricolti, S.; Guidi, L.; Ferrini, F.; Fini, A.; Tattini, M. The biosynthesis of flavonoids is enhanced similarly by UV radiation and root zone salinity in L. vulgare leaves. *J. Plant Physiol.* **2011**, *168*, 204–212. [CrossRef]
31. Grignon-Dubois, M.; Rezzonico, B. First Phytochemical Evidence of Chemotypes for the Seagrass *Zostera noltii*. *Plants* **2012**, *1*, 27–38. [CrossRef]
32. Petridis, A.; Therios, I.; Samouris, G.; Koundouras, S.; Giannakoula, A. Effect of water deficit on leaf phenolic composition, gas exchange, oxidative damage and antioxidant activity of four Greek olive (*Olea europaea* L.) cultivars. *Plant Physiol. Biochem.* **2012**, *60*, 1–11. [CrossRef]
33. Petridis, A.; Therios, I.; Samouris, G.; Tananaki, C. Salinity-induced changes in phenolic compounds in leaves and roots of four olive cultivars (*Olea europaea* L.) and their relationship to antioxidant activity. *Environ. Exp. Bot.* **2012**, *79*, 37–43. [CrossRef]
34. Dias, M.C.; Pinto, D.C.G.A.; Figueiredo, C.; Santos, C.; Silva, A.M.S. Phenolic and lipophilic metabolite adjustments in *Olea europaea* (olive) trees during drought stress and recovery. *Phytochemistry* **2021**, *185*, 112695. [CrossRef]
35. Araújo, M.; Prada, J.; Mariz-Ponte, N.; Santos, C.; Pereira, J.A.; Pinto, D.C.G.A.; Silva, A.M.S.; Dias, M.C. Antioxidant Adjustments of Olive Trees (*Olea europaea*) under Field Stress Conditions. *Plants* **2021**, *10*, 684. [CrossRef]
36. Valente, S.; Machado, B.; Pinto, D.C.G.A.; Santos, C.; Silva, A.M.S.; Dias, M.C. Modulation of phenolic and lipophilic compounds of olive fruits in response to combined drought and heat. *Food Chem.* **2020**, *329*, 127191. [CrossRef]
37. Neugart, S.; Fiol, M.; Schreiner, M.; Rohn, S.; Zrenner, R.; Kroh, L.W.; Krumbein, A. Interaction of Moderate UV-B Exposure and Temperature on the Formation of Structurally Different Flavonol Glycosides and Hydroxycinnamic Acid Derivatives in Kale (*Brassica oleracea* var. sabellica). *J. Agric. Food Chem.* **2014**, *62*, 4054–4062. [CrossRef] [PubMed]
38. Michel, T.; Khlif, I.; Kanakis, P.; Termentzi, A.; Allouche, N.; Halabalaki, M.; Skaltsounis, A.-L. UHPLC-DAD-FLD and UHPLC-HRMS/MS based metabolic profiling and characterization of different *Olea europaea* organs of Koroneiki and Chetoui varieties. *Phytochem. Lett.* **2015**, *11*, 424–439. [CrossRef]
39. Tumlinson, J.H.; Engelberth, J. Fatty acid-derived signals that induce or regulate plant defenses against herbivory. In *Induced Plant Resistance to Herbivory*; Springer: Berlin/Heidelberg, Germany, 2008; pp. 389–407.
40. Upchurch, R.G. Fatty acid unsaturation, mobilization, and regulation in the response of plants to stress. *Biotechnol. Lett.* **2008**, *30*, 967–977. [CrossRef]
41. Dowhan, W.; Bogdanov, M.; Mileykovskaya, E. Functional Roles of Lipids in Membranes. In *Biochemistry of Lipids, Lipoproteins and Membranes*; Elsevier: Amsterdam, The Netherlands, 2016; Volume 36, pp. 1–40, ISBN 9780444634382.
42. Conde, A.; Silva, P.; Agasse, A.; Conde, C.; Geros, H. Mannitol Transport and Mannitol Dehydrogenase Activities are Coordinated in Olea europaea Under Salt and Osmotic Stresses. *Plant Cell Physiol.* **2011**, *52*, 1766–1775. [CrossRef]
43. Araújo, M.; Ferreira de Oliveira, J.M.P.; Santos, C.; Moutinho-Pereira, J.; Correia, C.; Dias, M.C. Responses of olive plants exposed to different irrigation treatments in combination with heat shock: Physiological and molecular mechanisms during exposure and recovery. *Planta* **2019**, *249*, 1583–1598. [CrossRef]
44. Bianchi, G.; Murelli, C.; Vlahov, G. Surface waxes from olive fruits. *Phytochemistry* **1992**, *31*, 3503–3506. [CrossRef]
45. Lv, Y.; Tahir, I.I.; Olsson, M.E. Factors affecting the content of the ursolic and oleanolic acid in apple peel: Influence of cultivars, sun exposure, storage conditions, bruising and Penicillium expansum infection. *J. Sci. Food Agric.* **2016**, *96*, 2161–2169. [CrossRef] [PubMed]
46. Choudhary, K.K.; Agrawal, S.B. Assessment of Fatty Acid Profile and Seed Mineral Nutrients of Two Soybean (*Glycine max* L.) Cultivars Under Elevated Ultraviolet-B: Role of ROS, Pigments and Antioxidants. *Photochem. Photobiol.* **2016**, *92*, 134–143. [CrossRef] [PubMed]
47. Le Provost, G.; Domergue, F.; Lalanne, C.; Campos, P.R.; Grosbois, A.; Bert, D.; Meredieu, C.; Danjon, F.; Plomion, C.; Gion, J.-M. Soil water stress affects both cuticular wax content and cuticle-related gene expression in young saplings of maritime pine (*Pinus pinaster* Ait). *BMC Plant Biol.* **2013**, *13*, 95. [CrossRef]
48. Liakoura, V.; Stavrianakou, S.; Liakopoulos, G.; Karabourniotis, G.; Manetas, Y. Effects of UV-B radiation on *Olea europaea*: Comparisons between a greenhouse and a field experiment. *Tree Physiol.* **1999**, *19*, 905–908. [CrossRef]
49. Allen, D.J.; Mckee, I.F.; Farage, P.K.; Baker, N.R. Analysis of limitations to CO_2 assimilation on exposure of leaves of two Brassica napus cultivars to UV-B. *Plant Cell Environ.* **1997**, *20*, 633–640. [CrossRef]
50. Correia, C.M.; Coutinho, J.F.; Bacelar, E.A.; Gonçalves, B.M.; Björn, L.O.; Moutinho Pereira, J. Ultraviolet-B radiation and nitrogen affect nutrient concentrations and the amount of nutrients acquired by above-ground organs of maize. *Sci. World J.* **2012**, *2012*, 608954. [CrossRef]
51. Forster, P.M.; Thompson, D.W.J.; Baldwin, M.P.; Chipperfield, M.P.; Dameris, M.; Haigh, J.D.; Karoly, D.J.; Kushner, P.J.; Randel, W.J.; Rosenlof, K.H.; et al. *Stratospheric Changes and Climate. Scientific Assessment of Ozone Depletion, Global Ozone Research and Monitoring Project-Report No 52*; WMO: Geneva, Switzerland; United Nations Environment Programme: Nairobi, Kenya, 2011.

plants

MDPI

Review

Impact of Nanomaterials on the Regulation of Gene Expression and Metabolomics of Plants under Salt Stress

Zainul Abideen [1], Maria Hanif [2], Neelma Munir [2,*] and Brent L. Nielsen [3,*]

[1] Dr. Muhammad Ajmal Khan Institute of Sustainable Halophyte Utilization, University of Karachi, Karachi 75270, Pakistan; zuabideen@uok.edu.pk
[2] Department of Biotechnology, Lahore College for Women University, Lahore 54000, Pakistan; mariahanif81@yahoo.com
[3] Department of Microbiology and Molecular Biology, Brigham Young University, Provo, UT 84602, USA
* Correspondence: neelma.munir@yahoo.com (N.M.); brentnielsen@byu.edu (B.L.N.)

Abstract: Plant salinity resistance results from a combination of responses at the physiological, molecular, cellular, and metabolic levels. This article focuses on plant stress tolerance mechanisms for controlling ion homeostasis, stress signaling, hormone metabolism, anti-oxidative enzymes, and osmotic balance after nanoparticle applications. Nanoparticles are used as an emerging tool to stimulate specific biochemical reactions related to plant ecophysiological output because of their small size, increased surface area and absorption rate, efficient catalysis of reactions, and adequate reactive sites. Regulated ecophysiological control in saline environments could play a crucial role in plant growth promotion and survival of plants under suboptimal conditions. Plant biologists are seeking to develop a broad profile of genes and proteins that contribute to plant salt resistance. These plant metabolic profiles can be developed due to advancements in genomic, proteomic, metabolomic, and transcriptomic techniques. In order to quantify plant stress responses, transmembrane ion transport, sensors and receptors in signaling transduction, and metabolites involved in the energy supply require thorough study. In addition, more research is needed on the plant salinity stress response based on molecular interactions in response to nanoparticle treatment. The application of nanoparticles as an aspect of genetic engineering for the generation of salt-tolerant plants is a promising area of research. This review article addresses the use of nanoparticles in plant breeding and genetic engineering techniques to develop salt-tolerant crops.

Keywords: salinity; ecophysiology; environment; salt tolerance; photosynthesis

Citation: Abideen, Z.; Hanif, M.; Munir, N.; Nielsen, B.L. Impact of Nanomaterials on the Regulation of Gene Expression and Metabolomics of Plants under Salt Stress. *Plants* **2022**, *11*, 691. https://doi.org/10.3390/plants11050691

Academic Editors: Milan S. Stankovic, Paula Baptista and Petronia Carillo

Received: 27 January 2022
Accepted: 28 February 2022
Published: 3 March 2022

1. Introduction

Soil salinization of land poses a serious threat and harms the environment, agriculture, and the economy. Salinity stress in plants may cause changes at the molecular as well as the physiological level [1]. Some plants contain salt tolerance genes while many have a salt-sensitive genetic makeup. Various complex mechanisms may alter the genetic responses in plants under abiotic conditions. Modifications in the expression of salt-responsive genes make the plants more resistant to salinity stress. Ecophysiological traits of plants and their importance for biomass production in response to variable climate change are critical for sustainable agricultural productivity [2–4]. Plants can change their ecophysiological mechanism in five known constraints including growth, water dynamics, mineral nutrition, photosynthesis rate, and oxidative stability [5,6].

The adaptation of a plant to a stressful environment is a complex and sensitive phenomenon [7,8]. This acclimation is governed by multiple genes and regulatory pathways [9]. Once the plant detects a stress, it first senses and then transduces a stress signal. Plants utilize various components for signal transduction including transcription factors, ion transporters, kinases, calcium, and hormones [10]. During abiotic stress, many physical modifications occur such as alteration in protein and other metabolites along with changes

in the cellular matrix and segregation of nucleic acid strands [11]. All these alterations may result in altered regulation of abiotic stress-responsive genes. It was observed by Tang [12] that superoxide dismutase is responsible for oxidative stress tolerance. Enhanced salt resistance in plants is due in part to the overexpression of chloroplast protein-increasing stress tolerance (CEST) [13]. The assimilation of methylglyoxal in a saline stressed potato plant was inhibited by glyoxalase activity [14]. Hasanuzzaman et al. [15] reported that selenium protects plants from damaging free radicals, improves the antioxidant defense system, and methylglyoxal detoxification. It was observed that the use of selenium nanoparticles with bitter melon induced alterations in the methylation of cytosine in DNA resulting in epigenetic modifications. The up-regulation of the *WRKY1* transcription factor was induced by a high dose of selenium nanoparticles. The transcription of phenylalanine ammonia-lyase (*PAL*) and 4-CoA-ligase (4CL) genes have also been affected by selenium nanoparticles [10].

The application of nanoparticles to plants helps to mitigate salinity stress. Nanoparticles can be used to alter plant genetic makeup to become resistant to salt stress. Nanoparticles are identified as particles that have a size of less than 100 nm in diameter [16]. They are found naturally in various resources such as minerals or as a product of bacteria and clays. Nanoparticles have been used historically for coloring metals and other purposes, with new applications over the past several years [17]. Nanoparticles that are engineered have some significant specific properties. These nanoparticles have different sizes and shapes and their composition also varies, and they differ widely from naturally occurring nanoparticles [18]. Metal and metal oxide nanoparticles reveal various physiochemical properties such as high density and possess microscopic edges on their surface. The sizes of nanoparticles vary due to differences in composition, such as $Cu^{+2}O$, $Zn^{+2}O^{-2}$, $Sn^{+4}O^{-2}{}_2$, $Al^{+3}{}_2O^{-2}{}_3$, $Mg^{+2}O^{-2}$, $Ti^{+4}O^{-2}{}_2$, and $Ce^{+4}O^{-2}{}_2$. Due to the changes in nanoparticles size, many properties including magnetic, electronic, and chemical properties are altered. Magnetic nanoparticles have achieved significant importance due to their variations in size and shape [19]. Surface, optical, thermal, and electrical properties can also be incorporated into these nanoparticles. The process of metal/metal oxide nanoparticle synthesis includes the reduction as well as oxidation of respective metal salts [20]. There are many different factors that contribute to nanoparticle reactivity with desired biomaterials. These factors are the size, dimension, and stability of the nanoparticles [21]. In the past few decades, synthesized nanoparticles have been used for various industrial and household purposes. There is continuing effort to synthesize new nanomaterials to enhance quality products. However, the environment can be contaminated due to the excess use of nanoparticles due to improper disposal of industrial wastes and other by-products [22].

Nanoparticles can be adapted for environmental conditions and their aggregation and oxidation state can be engineered [23]. The stability and behavior of nanoparticles can be affected by chemicals in the environment and by physical parameters. The properties of nanoparticles depend on their composition. The composition of nanoparticles also affects their rate of reaction, penetration ability, and translocation inside the plant. Hence, the same nanoparticles may show different responses in plants under different conditions. For instance, it was observed by Barrios et al. [24] that plant responses were influenced by citric acid-coated nanoparticles compared to bare nanoparticles. Plants constantly interact with the surrounding medium, such as water, air, and soil. The engineered nanoparticles can cause different effects caused by quantum dots, carbon-based and metal-based effects on plant growth variations, physiological and biochemical traits, food production, and quality of food. Thorough interaction studies between engineered nanoparticles and plants are needed to analyze the toxicity levels and the remediation scheme to build a sustainable environment for agriculture [25]. Plants play a significant part in the ecosystem and in the food chain. However, the effects of nanoparticles on plants are not well known. The study of nanoparticles is difficult due to a lack of detection methods in plants [26]. The most suitable technique for the identification of nanoparticles in plants is inductively coupled plasma mass spectroscopy (ICP-MS). Due to the size, shape, composition, and stability

of nanoparticles, the plant may show positive or negative impacts due to nanoparticle application. Several reported studies showed that some nanoparticles have a negative impact on plants such as declines in plant growth, production rate, and pigments [27]. Conversely, some nanoparticles may be beneficial for plants. In order to maintain their stability in agricultural crop production, synthetic nanoparticles are mostly used. These nanoparticles are used as biofertilizers, growth stimulators, soil-improving agents, and are also used as sensors [28].

2. Engineered Nanoparticles and their Effect on Plant Salt Tolerance Genes: Enzymatic Expression

Engineered nanoparticles can interact chemically and mechanically with plants. These interactions are based on their properties such as size, surface area, and catalytic interactions. Few studies have been reported regarding the effect of nanoparticles at the molecular level [29–31]. Various plant species are highly affected by ZnO nanoparticles. Nanoparticles penetrate the plant leaf and accumulate in the edible parts while some assimilate into the soil in the surrounding area of the plant. Some metal and metal oxide nanoparticles are toxic to the environment, such as Ag^{+1}, Fe^{+3}, Zn^{+2}, $Al^{+3,}$ and Ti^{+4} [32]. It was observed that when *Brassica juncea* was treated with silver nanoparticles it resulted in increased levels of antioxidant enzymes, for instance, guaiacol peroxidase, catalase, and ascorbate peroxidase, which resulted in decreased levels of reactive oxygen species (ROS) activity [33]. The activity of enzymes such as super oxide dismutase, catalase, guaiacol peroxidase, ascorbate peroxidase, and glutathione reductase increased after the treatment of *Brassica juncea* with gold nanoparticles [34]. It was found that H_2O_2 and proline content increases in gold nanoparticle-treated plants. The activity of ascorbate peroxidase, glutathione reductase, and guaiacol peroxidase is stimulated in the presence of up to 400 ppm of gold nanoparticles, while on the other hand, the activity of guaiacol peroxidase increases with 200 ppm gold nanoparticles. Plant molecular responses to silver nanoparticle treatment were analyzed in *Aradidopsis* by reverse transcription-polymerase chain reaction [35]. A whole-genome cDNA expression microarray was also used for the transcriptional response analysis of *Arabidopsis* plants subjected to silver nanoparticles. This resulted in the identification of 286 upregulated genes, including those involved with metal and oxidative stress responses such as the vacuolar proton exchanger, SOD, cytochrome P450-dependent oxidase, and peroxidase. It also identified about 81 downregulated genes along with genes that help in the plant defense system. These included auxin-regulated genes, ethylene signaling pathway, and SAR against pathogens.

A proteomic analysis of rice treated with silver nanoparticles was carried out. It was found that silver nanoparticle-responsive proteins were associated with various metabolic functions such as transcription and protein degradation, the oxidative stress response pathway, and the calcium signaling pathway [36]. Treatment with zinc oxide nanoparticles in *Arabidopsis thaliana* identified 660 up- and 826 down-regulated genes. Seedling growth and seed germination of tomato was enhanced by the up-regulation of stress-related gene expression employing multi-walled carbon nanotube-based treatment [37]. The effect of engineered nanoparticles on plant traits is shown in Figure 1.

Iron (Fe) is considered to be essential for plant growth and development as it plays a significant role in enzymatic reactions, helps in photosynthesis, and aids to improve the performance of photosystems. In plants, Fe is present in the insoluble form, i.e., Fe^{3+}. The increase in pH and aerobic conditions leads to a decreased concentration of Fe in the soil. The use of iron nanoparticles helps to improve plant resistance to different environmental abiotic stresses. The application of iron nanoparticles reacts at the molecular level of plants, which helps to enhance the nutrient uptake ability [38]. Toxicity in plants may be caused by an excess concentration of iron nanoparticles. A higher amount of free Fe ions such as Fe^{2+} and Fe^{3+} leads to the production of ROS in plants. It was reported by Rodríguez et al. [39] that in some plants, down-regulation of detoxifying proteins such as CAT2 (CATALASE 2; AT4G35090) protein and AP2 (PEROXIDASE 2; AT5G06720) protein has been observed.

A deficiency of Fe in the roots of *M. truncatula*, *P. dulcis*, and *P. persica* was correlated with superoxide dismutase expression, i.e., ATMSD1 (ARABIDOPSIS-SIS-MANGANESE SUPEROXIDE DISMUTASE 1; AT3G10920) [39]. Fe deficiency may cause the production of non-enzymatic ROS. Under Fe deficiency in *A. thaliana*, two enzymes have been reported to be expressed: GST1 (ARABIDOPSIS GLUTATHIONE S-TRANSFERASE 1; AT1G02930) and MDAR1 (MONODEHYDROASCORBATE REDUCTASE 1; AT3G52880) [40]. The ROS-eliminating enzyme aids in the stimulation of the ascorbate-glutathione cycle from GPX3 (GLUTATHIONE PEROXIDASE 3; AT2G43350) [40]. Due to the magnetic properties of superparamagnetic iron oxides, Fe_2O_3 (maghemite) and Fe_3O_4 (magnetite) nanoparticles are widely used in various applications including the mitigation of salinity effects of plants. High Fe_3O_4 nanoparticle concentration has a high impact on seed germination and root elongation of cucumber [41]. In cucurbits, the Fe_3O_4 nanoparticle aggregation occurred in the stem and roots [42]. The toxicity of superparamagnetic iron oxide nanoparticles has been tested in *Lemna gibba* [43]. It has been observed that plant chlorophyll content decreased while the photosynthetic activity and growth were also highly affected. The size and stability of nanoparticles are responsible for their toxicity level. The effect of Fe_3O_4 nanoparticles has been investigated in *Cucumis sativus*, and it was observed that seed germination and root elongation were highly affected [41]. It has been shown that Fe_3O_4 nanoparticles are translocated towards the foliage, stem, and below-ground root. Aggregation of Fe_3O_4 nanoparticles in plants may decrease the root hydraulic movement and water transport. The growth parameters of *S. lycopersicum* were studied by the application of Fe_2O_3 nanoparticles. It has been observed that these nanoparticles were clogged in root hairs, root tips, and the nodal portion of plants. Increases in Fe_2O_3 nanoparticle concentration improved iron content in plants [44]. In *Arachis hypogaea*, root length and plant height increased due to the use of Fe_2O_3 nanoparticles in saline conditions [45].

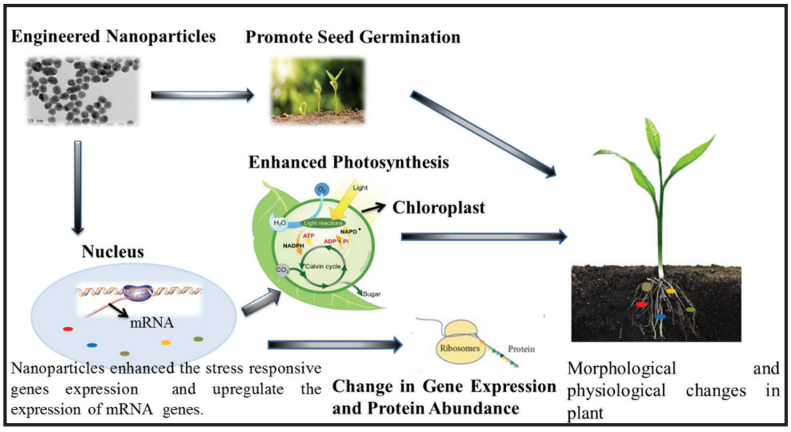

Figure 1. Effects of engineered nanoparticles on plant ecophysiological mechanisms in response to salinity.

While a number of genes with the potential for the engineering of salt tolerance have been identified and tested, additional genes and regulatory pathways need to be identified. Work in many labs is ongoing to develop genomic, transcriptomic, proteomic, and metabolomic resources.

3. Plant Metabolomics and the Linkage of Molecular Functions to Nanomaterial Application

The by-products of cellular regulatory mechanisms are metabolites. These metabolites are secreted in response to the external stimuli faced by the organism. More than 200,000 metabolites are secreted by plants and these metabolites are divided into two

classes; these are primary and secondary metabolites for plant growth and development [46]. Primary metabolites are essential and include carbohydrates, fatty acids, vitamins, amino acids, and organic acids [47]. Polyketides, alkaloids, terpenoids, glucosinolates, and phenylpropanoids are secondary metabolites synthesized from primary metabolites and are required by plants for adaptation and defense responses [48]. Throughout the plant kingdom, primary metabolites are common in all plants and conserved in their structure, while on the other hand, plant secondary compounds may vary in their chemical composition and are species-specific. Figure 2 shows the metabolomics analysis of plants exposed to engineered nanomaterials. In xenobiotic plants, the modifications in plant physiology induced by engineered nanoparticles are monitored by molecular events. These molecular events also reflect the metabolites that participate in biological pathways, for instance, the citric acid cycle, glycolysis, gluconeogenesis, and amino acid and secondary metabolite biosynthesis, nitrogen, and fatty acid metabolism. In order to defend against or adapt to various abiotic stresses, plant roots excrete metabolites as signaling molecules. Plants also alter soil chemistry and biochemical pathways to enhance nutrient bioavailability [49]. A list of halophytic species and their secondary metabolites is shown in Table 1.

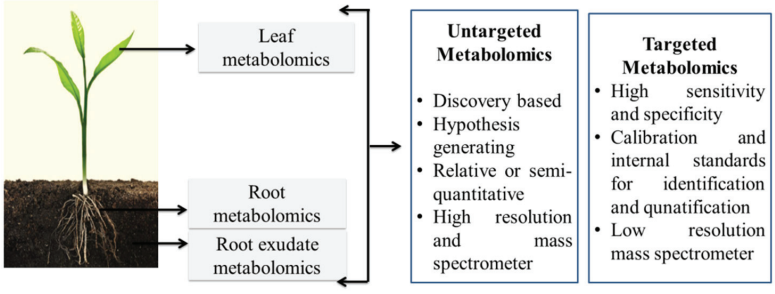

Figure 2. Metabolomics analysis in plants exposed to engineered nanomaterials.

Table 1. List of plant species and their secondary metabolites [50].

Fodder Crops	Secondary Metabolites
Atriplex nummularia	Saponin, Alkaloids, Tannins, Nitrate
Atriplex leucoclada	Saponin, Alkaloids, Tannins
Atriplex halimus	Saponin, Flavonoids, Alkaloids, Tannins, Nitrate
Diplache fusca	Flavonoids, Alkaloids
Halocnemum strobilecum	Saponin, Flavonoids, Alkaloids, Tannins, Nitrate
Haloxylon salicornicum	Saponin, Flavonoids, Alkaloids, Tannins
Kochia eriophora	Alkaloids, Tannins
Juncus acutus	Flavonoids, Alkaloids, Tannins, Nitrate
Juncus arabicus	Alkaloids, Tannins
Juncus subulatus	Alkaloids, Tannins, Flavonoids
Limonium pruinosum	Saponin, Alkaloids, Tannins
Nitraria retusa	Saponin, Tannins
Salsola glauca	Saponin, Flavonoids, Alkaloids
Suaeda fruticosa	Alkaloids, Tannins, Nitrate
Tamarix aphylla	Saponin, Tannins
Salsola tetrandra	Nitrate
Tamarix mannifera	Saponin, Tannins
Zygophyllum album	Saponin, Flavonoids, Alkaloids, Tannins, Nitrate
Sesbania sesban	Saponin, Alkaloids

4. Plant Genetic Responses to Salinity Stress

Under salt stress, genetic responses in plants occur by a complex mechanism. The synthesis of specific gene products (RNA or protein) is up-regulated while others are down-regulated. It was observed that these mechanisms may occur at different phases of the cen-

tral dogma process, such as transcription initiation, RNA processing, post-transcriptional processing, translation, and modification [51]. In order to identify the genes responsible for the stress response, transcriptional profiling is most often used, leading to the creation of extensive databases. To date, considerable information is available on the transcription factors that are included in the up- and down-regulation of plant genes and salt-responsive genes [52]. These genomic methodologies play a vital function in the encoding, cloning, and characterization of salt-responsive genes. These factors are considered important for the up-regulation and down-regulation of gene expression. *bZIP, MYB, WRKY, AP2, C2H2* zinc finger gene, *NAC,* and *DREB* family proteins are stress-responsive gene family members. The cis-acting binding of a transcription factor at a promoter region can alter the expression of individual genes [53].

Under salinity stress, up-regulation in *bZIP* gene expression was observed in a salt-sensitive variety of wheat while in the salt-tolerant cultivar, down-regulation of the gene occurred [54]. Rice contains transcriptional regulators that play a vital function under stress responses. These regulators are *DREB1/CBF, DREB2,* and *AREB/ABF* [55]. Under salt stress, up-regulation of transcription factors (*OsNAC5* and *ZFP179*) occurs. The up-regulation of these factors may affect the synthesis of proline, LEA proteins, and sugar, which in turn plays a significant role in abiotic stress tolerance [56]. Zhang et al. [57] determined that one member of one gene family, i.e., the *MYB* gene, responds to abiotic stress. Sixty full-length cDNA sequences were isolated that encode wheat *MYB* proteins. The phylogenetic tree that includes wheat, rice, and Arabidopsis *MYB* proteins was used to analyze their function and evolutionary relationship. Up-regulation of *AtWRKY8* gene expression occurs in *Arabidopsis* plants under salinity stress [58]. In diverse species of plants, many genes and transcription factors are up-regulated under salinity stress as presented in Table 2 [59], which shows associated genes, molecular chaperones, and dehydration-related transcription factors. For ion homeostasis, the *SOS* gene family plays a vital function in salt tolerance [60]. It was observed by Schmidt et al. [61] that more than 10 genes involved in the osmotic regulation process are up-regulated in *Spartia alterniflora* under salinity stress.

The salt-responsive transcription factor *ERF1* (*SERF1)* gene was characterized by Schmidt et al. [61] in *Oryza sativa*. It was observed that salt treatment and H_2O_2 may induce the expression of this gene in roots. Plants lacking the transcription factor *SERF1* are less resistant to salinity stress than wild-type plants. However, the overexpression of *SERF1* may improve salt resistance in plants. Kinases play a vital role in the adaptation of plants to salinity stress and they also regulate the activity of transcription factors. In rice, *OsRMC* acts as a negative regulator during salinity stress and it also encodes a receptor-like kinase [62]. Negative gene expression was also shown by two transcription factors, *OsEREBP1* and *OsEREB*, which belong to the *AP2/ERF* family. As with the *OsRMC* promoter, the above-mentioned transcription factors bind to the same GCC-like DNA motif. One of the major transcription factors, the basic region/leucine zipper (*bZIP*), contains a specific region that binds to the DNA and a leucine zipper dimerization motif. One of the major *ABRE*-binding transcription factors, *OSBZ8,* was also recognized in rice and is identified as the most expressed gene in salt-tolerant cultivars [63]. To respond to environmental stresses such as abiotic stress, the alternative splicing of RNA/mRNA plays a significant role by switching on/off transcriptional activities. The spliceosomal proteins play a significant function in plant development, response to harsh environmental factors, the plant immune system, and tolerance efficiency [64]. Figure 3 summarizes the signaling pathway in rice under salt stress.

Table 2. Salt responsive genes in various plant species along with their respective gene functions.

Gene Name	Plants	Gene Functions	References
SOS1,SOS2, AtNHX1	*Brassica campestris Brassica juncea*	Na^+/K^+ plasma membrane antiporter, calcium-binding protein, and protein kinase	[65]
AtSKIP	*Arabidopsis thaliana*	Transcription factor, splicing, and polyadenylation	[66]
OsHsp17.0 OsHsp23.7	*Oryza sativa* L.	Transporting proteins and heat-shock proteins	[67]
DcHsp17.7	*Daucus carota*	Cell viability and membrane stability under heat stress	[68]
JcDREB	*Arabidopsis thaliana*	Transcription factor	[69]
AtNHX1	*Arabidopsis thaliana*	Calcium-binding protein, vacuolar Na^+/K^+ antiporter	[70]
OsRab7	*Oryza sativa* L.	Vesicle trafficking gene enhanced growth and proline	[71]
PeXTH	*Populus euphratica*	Higher cell viability, water holding capacity, and membrane integrity	[72]
CYP94	*Oryza sativa*	Enhanced *CYP94C2b* expression	[73]
SOS1	*Nicotina tabacum*	Plasma membrane, Na^+/K^+ and vacuolar Na^+/K^+ antiporter	[74]
mtlD	*Escherichia coli*	Higher mannitol 1 phosphate dehydrogenase levels	[75]
TaSTRG	*Triticum aestivum*	Increase salinity and water deficit resistance	[76]
AtSTO1	*Arabidopsis thaliana*	Higher root, pith size, and photosynthesis	[77]

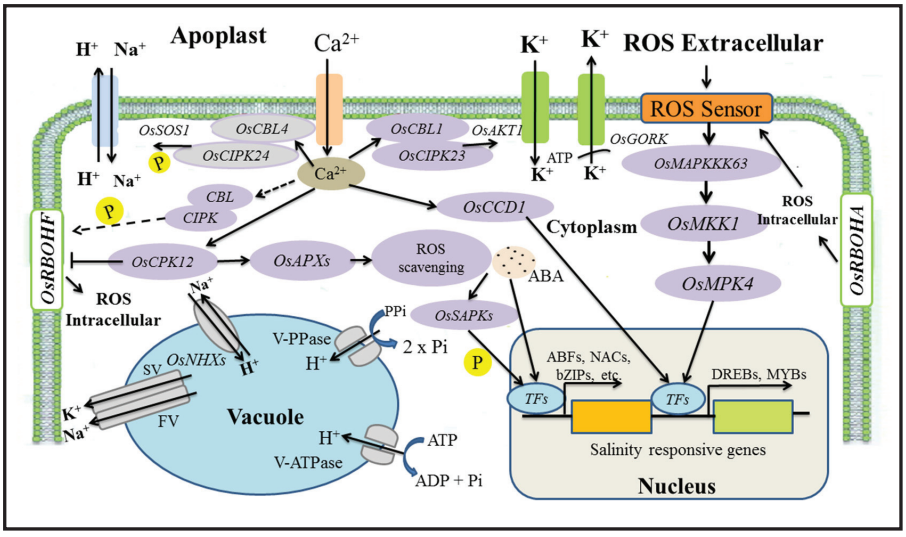

Figure 3. Signaling pathways in rice under salt stress.

MicroRNAs and small interfering RNA (siRNAs) could play a significant role in the abiotic stress responses of plants. However, post-transcriptional gene regulation has a significant impact on plant salinity resistance [78]. It has been observed that miRNAs are sensitive to biotic as well as abiotic stress. Plants face various environmental abiotic stresses such as drought, salinity, and cold. The overexpression of miR402 is induced by these environmental stresses. Figure 4 shows the post-transcriptional regulation of plant salt stress-responsive genes mediated by miRNA as studied in *Arabidopsis thaliana* and *Oryza sativa* to determine the significant role of miRNA in salt stress [79].

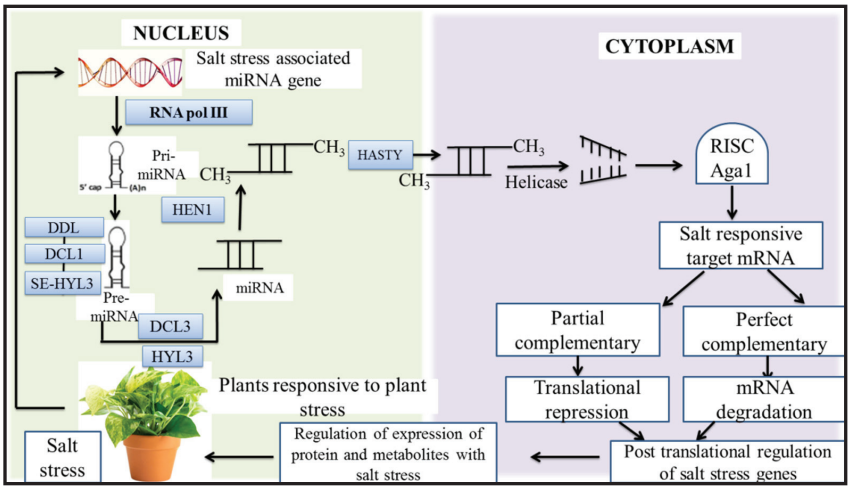

Figure 4. Pathway showing post-transcriptional regulation of salt stress-responsive plant genes mediated by miRNA.

5. Mechanisms for the Regulation of Salt Tolerance Genes

Plant transcription factors act to link salt-sensitive pathways to several tolerance responses. Certain transcription factor family genes are expressed specifically in response to external salinity stress. These transcription factor gene families include *bZIP*, *WRKY*, *APETALA2*/Ethylene Response Factor (*AP2/ERF*), *MYB*, basic helix-loop-helix (*bHLH*), and NAC. These transcription factors play a vital function in regulating the expression level of genes that may enhance the plant salt tolerance level [80]. Salt stress-induced *bZIP* transcription factor *bZIP24* is a primary example involved in adaptation to salt resistance in plants. In *Arabidopsis,* this transcription factor induces the expression of many stress-responsive genes [81]. Salt tolerance is increased in *Arabidopsis* due to the expression of *bZIP24*. It was observed that *bZIP24* down-regulated *AtHKT1;1* directly or indirectly [82]. *bZIP24* was identified by comparison of transcript regulation patterns in *Arabidopsis* and in the halotolerant *Lobularia maritima.* This halophilic model species can be utilized for the identification of novel salt tolerance mechanisms [83].

5.1. Salinity Tolerance Mechanisms

AtHKT1;1 regulates the sodium level in leaves and salt tolerance in plants. In order to modify a Na^+-resistant crop, the molecular mechanism regulating *AtHKT1;1* expression should be determined [84]. The plant salinity tolerance mechanism was analyzed by the study of the model plant *Arabidopsis* [85]. *Rice transcription factor SALT-RESPONSE ERF1 (SERF1)* functions as an enhancer of ROS-activated MAP kinase under salinity stress. The high salinity rate may induce the expression of *SERF1.* It was observed that rice plants deficient in *SERF1* exhibit a drop in salt stress tolerance genes. *serf1* mutants grown hydroponically for 3–4 weeks were observed to be salt-sensitive while *SERF1*-overexpression lines showed increased salt tolerance. The Na^+ over K^+ ratio in the foliage of the *serf1* mutant was higher than the wild-type [86].

5.2. Traditional Plant Breeding

Many approaches including conventional plant breeding have been used to enhance the salinity resistance of plants that are economically important. These traditional breeding programs have been successful in improving salt stress tolerance [87]. However, multiple salt-responsive genes are involved in tolerance to salinity in plants. These genes also function with other parts of stress signal transduction pathways. The results obtained by

traditional plant breeding may not identify genomic regions such as in perennial quantitative trait loci (QTL) that control salt resistance. By the improvement of high-throughput genotyping methods, molecular marker technology was developed to identify QTL, which is considered to be accountable for salt tolerance. In breeding programs, the selection efficiency is based on the identification of QTL regions [88]. The results of gene expression analysis and the correlation of QTLs may be easily detected at the seedling stage as compared to the developmental stages, while at the reproductive stages they are fully recognizable [89]. In recent studies, the antioxidant response in tomato plants under salinity stress was identified. The QTLs related to antioxidant content were also analyzed. The development of tomato cultivars having higher antioxidant levels may be accomplished using QTLs [90].

By using traditional breeding methods, multiple traits have been introduced into crop plants to manipulate salt tolerance. In addition, the overexpression of single genes can be used for improving plant salt tolerance. High salt tolerance has also been observed in genetically modified plants by the overexpression of genes that code for the synthesis and assimilation of osmoprotectants (proline and glycine betaine are used for osmotic adjustment). In addition, some enzymes such as glutathione S-transferase, peroxidase, ascorbate peroxidase, superoxide dismutase, and glutathione reductase are also used to modify plant salt resistance and oxidative protection [91]. Plant genetic engineering holds great promise for producing salt-tolerant crops. Salinity tolerance is multi-genic in nature, but most genetically engineered plants possess a single transgene. Various genetic tools are developed that can be utilized in gene function analysis. In order to develop salt-tolerant cultivars, the use of nanoparticle carriers to facilitate genetic engineering will be helpful to understand the mechanisms and regulation of gene expression, candidate gene usage, and tissue-specific and inducible promoters.

6. Salt Responsive Genes Present in Halophytes

Limited literature is available on the molecular defense mechanism of halophytes against salinity stress. In various studies, the ecological, physiological, anatomical, and biochemical responses of halophytes towards salinity were studied [92,93]. For the investigation of salinity stress defense molecular mechanisms, *Arabidopsis thaliana* was used as a model plant. This species was also utilized for the analysis of salt stress-responsive genes to enhance salinity tolerance in genetically modified plants [94]. It is generally understood that halophytes are salt-tolerant and glycophytes are salt sensitive. However, there are some halophyte species that are sensitive to abiotic stresses and some glycophytes are tolerant to salt. Halophytes are considered to be suitable model plants for the analysis of salt tolerance mechanisms [95]. It was observed that almost all plants likely possess similar salt tolerance regulatory mechanisms [96].

Many genomic methods have been used for the isolation and identification of salinity-responsive genes from halophytes. The overexpression of these halophytic genes under the control of the constitutive, non-specific 35SCaMV promoter in glycophytic recipients may increase abiotic stress tolerance. Many of these genes code for Na^+/H^+ antiporters, vacuolar pyrophosphatase, potassium transporters, ion channels, antioxidants, and ROS scavengers. These genes also code for proteins that are included in signal transduction and various protective functions. Many other salt-responsive genes have been identified from halophytes such as *Salicornia brachiata* [97]. Many model plants including *Arabidopsis thaliana* and salt-tolerant *Thellungiella salsuginea* were used for the study of abiotic stress tolerance. *Thellungiella* exhibits high tolerance to salt and drought stress [98]. The genetic basis of the abiotic stress defense mechanism was obtained from the analysis of the genomic sequence of *Thellungiella salsuginea.* This species was identified as the gene resource for cation transporters, abscisic acid signaling genes, and many other genes that respond to abiotic stresses [99]. The results obtained from microarray analysis revealed that only a few genes were affected under salt stress in *Thellungiella salsuginea* compared to *Arabidopsis* [100]. In another study, it was observed that in *Thellungiella salsuginea*, about 154 genes were

identified as compared to *Arabidopsis* under various stresses [101]. A diagram illustrating salt stress tolerance mechanisms in halophytes is shown in Figure 5.

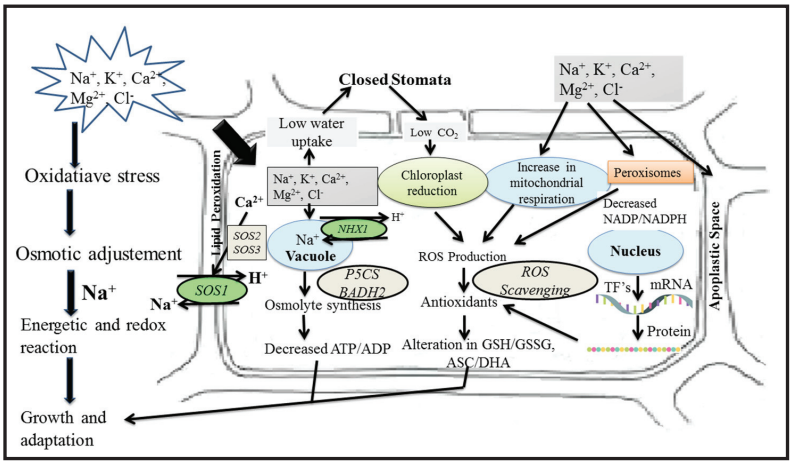

Figure 5. Salt stress tolerance mechanisms of halophytes in a saline environment.

Arabidopsis and *Lepidium crassifolium* have been studied as model plants to contrast a glycophyte with a halophyte, respectively, and to identify genes involved in oxidative and osmotic stress tolerance. Independent transgenic lines expressing random genes from *L. crassifolium* in *Arabidopsis thaliana* enhanced plant salinity tolerance [102]. Other studies were conducted with *Salicornia brachiata*, which grows in saline marshes under extreme abiotic stresses. This plant is considered to be an efficient source of stress response genes and promoters as it has the potential to grow under adverse environmental conditions [97]. Salinity-resistant transgenic plants including *Jatropha*, Cumin, and Castor were developed using salt-responsive genes isolated from *Salicornia brachiata* [103]. *Salicornia* species are considered functional foods as they contain metabolites and sulfur-rich seed storage proteins [104]. *Porteresia coarctata* is a wild halophyte that has the ability to grow in extreme saline soils. Around 152,367 unique transcript sequences were identified; 15,158 of these genes are related to salinity and submerged tolerance and the analysis of these genes will help unravel the key metabolic pathways involved in tolerance. These genes can also be utilized to introduce salinity and submerged tolerance traits in rice [105]. Table 3 shows the salt-responsive genes present in halophytes and recipient plants that express the genes.

Table 3. Salt-responsive genes present in halophytes and recipient plants.

Halophytes	Genes	Description	Recipient Plants	References
Aeluropus littoralis	*AlNHX1*	Vacuolar Na^+/H^+ antiporter	*Nicotiana tabacum*	[106]
Atriplex hortensis	*AhBADH*	Glycine betaine synthesis	*Solanum lycopersicum*	[107]
Avicennia marina	*AmMDHAR*	ROS scavenging	*Nicotiana tabacum*	[108]
Salicornia brachiata	*SbASR1*	Ascorbate regeneration and ROS scavenging	*Nicotiana tabacum*	[108]
Salicornia brachiata	*SbpAPX*	Peroxisomal ascorbate peroxidase	*Nicotiana tabacum*	[109]
Salicornia brachiata	*SbpAPX*	Peroxisomal ascorbate peroxidase	*Arachis hypogea*	[110]
Salsola soda	*SsNHX1*	Vacuolar Na^+/H^+ antiporter	*Alfalfa*	[111]
Suaeda liaotungensis	*SlBADH*	Glycine betaine synthesis	*Zea mays*	[112]
Suaeda salsa	*SsCAX1*	Vacuolar H^+/Ca^{2+} transporter	*Arabidopsis*	[113]

Table 3. *Cont.*

Halophytes	Genes	Description	Recipient Plants	References
Suaeda salsa	*SsGST*	Glutathione S-transferase	*Oryza sativa*	[114]
Suaeda salsa	*SsVP*	Vacuolar-H^+-pyrophosphatase	*Arabidopsis*	[115]
Thellungiella halophila	*ThSOS1*	Salt overly sensitive gene	*Arabidopsis*	[116]
Thellungiella salsuginea	*TsTIP1*	Tonoplast *AQP* gene	*Arabidopsis*	[117]
Tamarix androssowii	*TaMnSOD*	Manganese superoxide dismutase	*Populus*	[118]
Spartina alterniflora	*SaVHAc1*	Vacuolar H^+-ATPase subunit Cl	*Oryza sativa*	[119]
Salicornia europaea	*SeCMO*	Enhanced glycine betaine synthesis	*Nicotiana tabacum*	[120]
Kalidium foliatum	*V-ATPase*	Vacuolar-H^+-pyrophosphatase	*Arabidopsis*	[121]
Atriplex gmelini	*AgNHX1*	Vacuolar Na^+/H^+ antiporter	*Oryza sativa*	[122]

7. Promoters for Salt-Responsive Halophytic Genes

A strong promoter is needed for the genetic engineering of plant crops to attain the desired level of transgene expression. In *T. halophila*, stress-related genes are expressed constitutively as compared to *A. thaliana* where they are not [123]. This study revealed that in halophytes, a transcriptional regulatory network for stress-responsive genes is fully functional. Another study was carried out in halophytes that led to the identification of *cis*-regulatory elements of stress-responsive genes and stress-inducible motifs [124]. The promoter of the *AcBADH* gene from *Atriplex centralasiatica* contains two salt-responsive enhancer regions and one silencer region. The enhancer regions are located from −1115 to −890 and −462 to −230, while the silencer region is from −890 to −462. The *AcBADH* promoter is strongly induced by salinity stress [125].

Another strong and salt-inducible promoter is *SIBADH;* the promoter fragment (−300 bp) was identified in *Suaeda liaotungensis.* This promoter supported a 6.3-fold higher expression under salinity in contrast to non-stressed conditions [106]. To measure expression levels, GUS is widely used as a reporter gene in transformation in microorganisms and animals. It is found in various bacterial species such as *Shigella, Bacteroides* and *Clostridium, S. liaotungensis,* and *Salicornia europaea* that contain CMO genes [120]. GUS showed increased expression in transgenic *Arabidopsis*, while a halophyte *T. halophila* contains a *TsVP1* gene promoter having a 130 bp specific *cis*-acting element responsive to salt stress. The *SIPEAMT* gene of *S. liaotungensis* with an 897 bp promoter region also showed an 18.6-fold increase in the beta-glucuronidase (GUS) activity under 200 mM NaCl stress [126]. They determined that even a small portion of the promoter contains a *cis*-acting element that allows regulation of gene expression under salinity stress. A choline monooxygenase (CMO) gene was found in Chenopodiaceae and Amaranthaceae. In plants, usually, the activity of CMO is low and unstable but it can be a critical rate-limiting step in the biosynthesis of glycine betaine [127]. Promoters of these genes are inducible under salinity stress. Crassulacean acid metabolism (CAM) genes were studied in *M. crystallinum,* and the transcriptional activation of salt-responsive genes occurs due to the enhancer and silencer regions of the gene promoter [128]. CAM genes were found in various plant species. In model plant species such as *Arabidopsis* and rice, it was revealed that CAM proteins are encoded by gene families. These genes play a significant role in the regulation of growth, development, and abiotic stress resistance in plants [129].

A tissue-specific promoter *AISAP* was examined in *Aeluropus littoralis* [130]. It was found that the expression level of a *gusA* fusion with this promoter was the same in transgenic rice under the control of the *AISAP* gene as in *A. littoralis* [131]. *AISAP* and *OsSAP9* are two orthologs of the regulatory region of the promoter and provide the basis for variation in regulation specificity and stress induction in rice. The *TsVP1* gene from the halophyte *T. halophile* contains a 130 bp *cis*-acting element in the promoter region of vacuolar H^+-pyrophosphatase. It helps to enhance GUS fusion expression under

salinity stress in transgenic *Arabidopsis* [132]. Under the conditions of biotic and abiotic stresses, the expression of the reporter gene can be controlled by the *CBL1* gene promoter obtained from *Ammopiptanthus mongolicust* [133]. The enhancer and repressor binding sites in the *cis*-regulatory region were also found in the *SbpAPX* gene. This gene was found in *S. brachiata* [134]. The salt stress-responsive *cis*-regulatory motifs were present in the *SbGSTU* promoter. In *S. brachiata,* these motifs regulate the expression of the *GSTU* gene [124]. Thus, halophytes can be utilized as a source of genes for engineering abiotic stress tolerance in crops. Table 4 shows the details of promoters used to stimulate salinity resistance traits in plants.

Table 4. Promoters used to improve salt tolerance traits in crop plants [58].

Transgene	Gene Isolated	Promoters	Transgenic Crop
Ion exclusion Na^+/H^+ antiporter (*SOS1)*	*Arabidopsis*	Constitutive	*Nicotiana tabacum*
Na^+/H^+ antiporter (*SOD2)*	*Salicornia brachiata*	Stress inducible	*Oryza sativa*
Tissue tolerance Na^+/H^+ antiporter (*NHX*)	*Arabidopsis*	Constitutive	*Fagopyrum esculentum*
Tissue tolerance Trehalose-6-phosphate synthase (*TPS*)	Yeast	Constitutive	*Medicago sativa*
Tissue tolerance Trehalose-6-phosphate phosphatase (*TPP*)	Rice	Stress inducible	*Solanum lycopersicum*
Mannitol-1-phosphate dehydrogenase (*mt1D*)	*E.coli*	Shoot expression	*Oryza sativa*
Myoinositol O-methyltransferase	*M. crystallinum*	Constitutive	*Triticum aestivum*
Tissue tolerance Ascorbate (*APX*)	*Arabidopsis*	Constitutive	*Nicotiana tabacum*
Glutathione S-transferase (*GST*)	Tomato	Protein targeted to chloroplast/cytosol	*Oryza sativa*
Mitogen activated protein kinase (*MAPK*)	Chickpea	Constitutive	*Nicotiana tabacum*
Sucrose protein kinase	Rice	Inducible	*Oryza sativa*
Transcription factors *DREB*	*Pennisetum glaucum*	Constitutive & inducible	*Nicotiana tabacum*

8. Transgenic Approach for Engineered Plants Having Enhanced Salt Tolerance

It was reported by Rao et al. [53] that for salt tolerance in plants, the breeding strategy is not particularly recommended due to reproductive restrictions and there is a high probability for the transfer of undesirable traits. Genetic engineering is considered to be suitable for single gene transfer [58]. Plants have been developed from a single plant cell by the direct transfer of the gene of interest into the genome to create transgenic plants. The use of genetic engineering techniques involves traits such as resistance to pesticides, pests, better nutritional value, and improved product shelf life, which can contribute to improvements in sustainable agriculture [135]. Figure 6 shows the factors involved in enhanced salt tolerance in plants. The transgenic approach is also utilized to enhance the resistance to abiotic stress in plants [136]. Table 5 summarizes reports on gene transfer into target plants for enhanced salt tolerance.

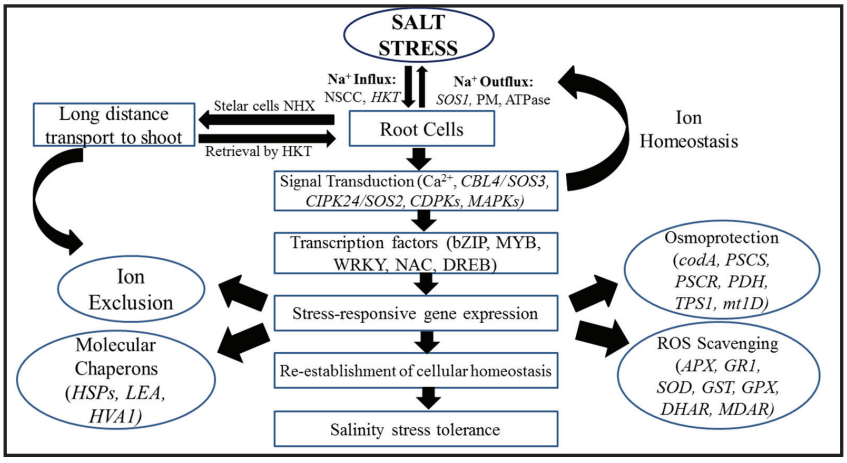

Figure 6. Factors involved in enhanced plant salt tolerance.

Table 5. Gene transfer into target plants for enhanced salt tolerance.

Desired Gene	Donor Plant	Target Plant	References
codA	*Arthrobacter globiformis*	*Solanum lycopersicum*	[137]
Cox	*Arthrobacter pascens*	*Oryza sativa*	[138]
TPS1	Yeast	*Solanum lycopersicum*	[139]
AtTPS1	*Arabidopsis*	*Nicotiana tabacum*	[140]
mtID	*Triticum aestivum*	*Escherichia coli*	[141]
S6PDH	*Malus domestica*	*Japanese Persimmon*	[142]
P5CS	*Vigna acontifolia*	*Nicotiana tabacum*	[143]
nhaA	*E.coli*	*Arabidopsis*	[141]
AtNHX1	*Arabidopsis*	*Solanum lycopersicum*	[144]
BnNHX1	Brassica	*Nicotiana tabacum*	[145]
GlyII	*Oryza sativa*	*Nicotiana tabacum*	[146]
GmbZIP1	Soybean	*Arabidopsis, Nicotiana tabacum*	[147]
BrERF4	Brassica	*Arabidopsis*	[148]
T30hsp70	*Trichoderma harzianum*	*Arabidopsis*	[149]
GhMPK2	Cotton	*Nicotiana tabacum*	[150]

9. Development of Salt Tolerant Glycophytes using Halophytic Salt Tolerance Genes

Plants are classified into two groups: salt-tolerant halophytes and salt-sensitive glycophytes depending on their growth ability in saline environments. Halophytes have the ability to grow in a saline environment including coastal marshes and inland deserts. Monocot halophytes have the potential to achieve optimum growth at less than 50 mM NaCl while in the case of dicot halophytes they can grow at approximately 100–200 mM salt [151]. Glycophytes are highly affected by saline habitats and do not grow well at 100-200 mM NaCl [92]. Various studies were conducted to identify salt tolerance genes in halophytes [96]. Over the last several years, genetic engineering has been commonly used to introduce salt tolerance in glycophytes by the transfer of salt tolerance responsive genes from halophytes [152]. For this purpose, different plants are used as model plants for the introduction of salinity tolerance genes. *Arabidopsis*, tobacco, and many other crop plants have been used to enhance ion homeostasis and salt tolerance [73].

The most commonly monitored phenomena related to salinity are the dispersion of sodium ions in vacuoles, sodium ion efflux, and the prevention of sodium ion influx by the antiporter [153]. Many antiporters have been characterized functionally after their isolation from glycophytes and halophytes. It was observed that some of the glycophytic transporters that are encoded by the *NHX*, *ATPase*, *SOS*, and *HKT* genes led to salt tolerance

in the range of 150–250 mM NaCl when expressed under the control of the constitutive CaMV35S promoter in transgenic plants [154]. For evolving salt tolerance in various crops such as tomato, maize, brassica, and wheat, constitutive expression of the glycophytic *NHX* gene obtained from *Arabidopsis thaliana* was used [155]. However, other genes such as *BnNHX1 (Brassica napus), HbNHX1(Hordeum brevisubulatum),* and *GhNHX1(Gossypium hirsutum)* were used to develop salt tolerance in tobacco. It was reported that salt tolerance was conferred by the *NHX1* gene obtained from both halophyte and glycophytes, although they differ in the level of salt tolerance. A 75% amino acid sequence similarity was observed for the antiporter *Ag*NHX1 from *Atriplex 15melina* and *At*NHX1 from *Arabidopsis thaliana.* As compared to glycophytes, transgenic plants overexpressing *AgNHX1*, *SaNHX1*, or the *SsNHX1* gene showed up to 300–400 mM NaCl tolerance [156]. In genetically modified tobacco plants, upregulation of the *SbNHX1* gene showed salt tolerance up to 200 mM NaCl while in transgenic jatropha and castor plants, salt tolerance was observed up to only 100 mM NaCl [157]. However, in transgenic plants, the upregulation of other halophytic genes such as *SbpAPX*, *SbUSP,* and *SbGSTU* also showed salt tolerance up to 200–300 mM NaCl [158]. The *TIP1* gene obtained from the halophyte *T. salsuginea* revealed enhanced salt tolerance in transgenic *Arabidopsis* plants as compared to the glycophyte *Panax ginseng* [159]. Genes from rice such as APX and GST showed tolerance of up to 150–200 mM NaCl when compared to similar genes obtained from the halophyte *S. brachiata* in transgenic plants [160]. Different levels of abiotic stress tolerance in rice, tobacco, and wheat were observed by up-regulation of the stress-associated protein *AISAP* from *Allocasuarina littoralis* [131]. It was reported that many abiotic stresses induced *AISAP* transcripts but the rice gene *OsSAP9* is also influenced by cold and heat treatments. The negative regulators of *AtHKT1; 1* expression are shown in Figure 7.

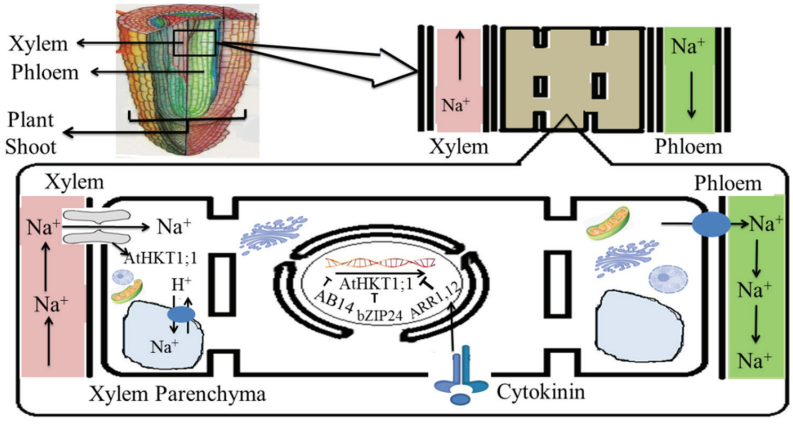

Figure 7. Model showing *AtHKT1;1* and the negative regulators of *AtHKT1;1* expression.

The antiporter SOS1 gene and its over-expression were studied in *Thellungiella* and contrasted to expression in *Arabidopsis* [161]. In *Thellungiella*, *SOS2, NHX1,* and *HKT1*, which are involved in sodium exclusion and compartmentation, have been expressed at higher levels [123]. Halophytes can serve as model plants to discover different stress-responsive genes for enhancing the salt resistance of glycophytes to allow cultivation in saline and arid areas for sustainable agriculture.

10. MicroRNAs (miRNA), a New Target for Improving Plant Tolerance to Salt Stress

Microarray and high throughput deep sequencing methods are used to identify plant miRNAs induced under salinity, as presented in Table 6. It was observed that plant miRNAs are present in all of the main plant parts such as the leaf, root, stem, and flower (Table 5). It was reported by Fu et al. [162] that among all the crops, the highest numbers of miRNAs have been identified in *Zea mays* (1077 miRNAs). *Mesembryanthemum crystallinum*, *Medicago*

truncatula, *Vicia faba*, and *Ipomoea batatas* contain 882, 876, 693, and 650 miRNAs, respectively, under saline conditions [163]. The numbers of miRNAs in plants may vary and depend on plant species, tissue specificity, development stages, and intensity of salinity stress. The degree of salt stress may up- and down-regulate the expression level of miRNAs in plants. Jodder [164] observed that the expression of miR167 in oat panicles is negatively associated with an increase in the degree of salt stress. With a 0.25% increase in NaCl, miR156, miR157, and miR172 are up-regulated in cotton, and the expression decreases with a further increase in salt concentration. Nanoparticles have the ability to affect the expression level of plant miRNAs [165].

Table 6. Numbers of salt-responsive miRNAs identified under salt stress at varying concentrations of NaCl.

Plants	NaCl Concentration	miRNA Number	References
Arabidopsis thaliana	150 mM	118	[166]
Glycine max	125 mM	238	[167]
Leymus chinensis	100 mM	148	[168]
Medicago truncatula	20 mM	876	[169]
Musa nana	300 mM	181	[170]
Oryza sativa	200 mM	498	[171]
Panicum virgatum	0.5 %	273	[172]
Suaeda maritima	255 mM	147	[173]
Zea mays	250 mM	1077	[174]
Vicia faba	150 mM	693	[175]
Thellungiella salsugniea	200 mM	246	[176]
Raphanus sativus	200 mM	204	[177]

The expression levels of miRNAs highly depend on plant developmental stages, as it was reported that few miRNAs are expressed in early growth under saline conditions while others appear in the late stages. It was observed by Luan et al. [178] that zma-miR169 shows initial up-regulation and then down-regulation under salinity stress. In cotton, miRNAs and their targets such as miR156-SPL2, miR159-TCP3, miR162-DCL1, miR395-APS1, and miR396-GRF1 show a negative correlation of expression levels [165]. Some of the miRNAs are induced under salt stress such as miR156, miR319, and miR528 while miR164 and miR397 are repressed [179]. The degree of salinity stress may increase or decrease the expression level of some miRNAs in plants. For instance, in *Arabidopsis thaliana, Triticum aestivum*, and *Agrostis stolonifera,* the expression level of miR393 increases under salt stress. However, in contrast, the expression level of miR393 decreases in *Oryza sativa*, *Gossypium* sp., and *Spartina alterniflora* under similar conditions [180]. The expression level of some miRNAs such as miR167, miR390, miR402, and miR414 have been observed only in a few plant species under salinity stress.

Glycophytes cannot tolerate high salinity levels while halophytes can tolerate and survive at up to 1000 mM NaCl. Glycophyte plants may have the potential to adapt a salt tolerance mechanism by following various strategies of gene regulation used by halophytes. The role of halophyte miRNAs may follow various strategies of salinity resistance improvements in crops by incorporating them in genetic engineering and plant selection programs. For instance, Gharat [173] observed that the expression of *Suaeda maritima* sma-miR2 and sma-miR5 increases in seawater, suggesting that their metabolic regulatory roles are restricted to saline environments. About 246 miRNAs have been identified in *E. salsugineum*. A significant response to salt stress in *E. salsugineum* was observed by the expression of 26 conserved miRNAs and four novel miRNAs [181]. Seedlings of *M. crystallinum* were treated with 200mM NaCl and it was observed that 135 conserved miRNAs and the hairpin precursor of 12 novel mcr-miRNAs were expressed [182]. In another example, *Halostachys capsica*, a salt tolerant shrub, was treated with salt and it was observed that 31 conserved miRNAs and 12 novel miRNAs were up-regulated while 48 conserved miRNAs and 13 novel miRNAs were down-regulated by salinity stress in *H. caspica* [183].

11. Conclusions and Future Perspectives

Plants integrate cellular, physiological, and molecular responses for salt stress tolerance. Various studies have been carried out on the plant salt resistance mechanisms that control ion homeostasis, osmoregulation, ROS detoxification, hormone metabolism, and stress signaling, but there is still a lack of information from genomic, transcriptomic, and proteomic studies. Genetic engineering of salt tolerance in plants has great potential. However, the continuous release of nanoparticles into the surrounding soil may affect plant growth and development. Nanoparticles may alter seed germination as well as various stages of crop production. Various kinds of nanoparticles have been found in the environment such as ZnO, CuO, TiO2, and Fe3O4. All of these nanoparticles showed some positive and negative results against seed germination, root and shoot growth, biomass production, and physiological as well as biochemical activities. These nanoparticles become adsorbed onto the plant surface and are transported to different plant tissues. However, the low concentration of nanoparticles does not show any negative effect on plants and appears to be beneficial for their growth and developmental process. Higher concentrations of nanoparticles cause toxicity by ROS which leads to the disruption of the cellular membrane. It has been considered that some nanoparticles could replace the use of toxic chemicals and fertilizers in the near future. Still, further research needs to be carried out to analyze the effect of nanoparticles on plants and the surrounding environment.

Progress has been made in developing salt-tolerant cultivars, but there are still many questions related to salt stress tolerance in plants that need to be addressed with the help of molecular marker development for gene mapping, EST library development, and integration of complete genome sequences for Arabidopsis, rice, and maize. High throughput sequencing is the most powerful technology for the identification of salt stress-responsive miRNAs. After the identification of miRNAs in plants, there is still an empty space that needs to be filled for the analysis of function carried out for salt tolerance improvement through miRNA manipulation in crops. Applications of nanoparticles will play a significant role in the modification of salt-tolerance genes in plants. Many advanced strategies have been used to date to modulate genes in plants under salinity stress, including nanoparticle transport across the plant cell and chloroplast membranes to target their genetic makeup. In addition, miRNAs can be introduced to develop salt resistance in crops. The overexpression and knocking down of miRNAs may promote the development of salinity resistance in transgenic plants.

The various modifications in small RNA sequencing technologies and analysis of miRNAs will be important for the development and growth of salt-tolerant cultivars. Many advances in genomics and metabolomics analyses of crop plants may improve the resolution of complex networks and unravel the mechanism(s) of abiotic stress tolerance. It will be essential to identify candidate gene(s) that have the ability to confer stress tolerance in plants without affecting growth and yield. It has been observed that conventional breeding methods did not significantly improve salt stress tolerance in plants and in addition, the crossing method reduced crop yield. In order to develop salt-tolerant plants, some points need to be addressed such as (i) how under the unstable natural environment genetically modified plants respond to soil salinity conditions, (ii) how soil salinity affects the transgenic plants at different growth stages including seed germination and reproductive stage, (iii) the effects of transgene expression on plant growth and development as well as nitrogen use efficiency (NUE) under saline conditions, (iv) yield of transgenic plants, and (v) disease resistance. Additional research still needs to be performed to understand stress perception, signaling, transcription factors, and genes associated with the salinity stress response.

Author Contributions: Conceptualization Z.A. and M.H.; formal analysis, Z.A. and M.H.; investigation, Z.A. and M.H.; writing—original draft preparation, Z.A. and M.H.; writing—review and editing, N.M. and B.L.N.; visualization, N.M. and B.L.N.; supervision, N.M. and B.L.N. All authors have read and agreed to the published version of the manuscript.

Funding: This research received no external funding.

Institutional Review Board Statement: Not applicable.

Informed Consent Statement: Not applicable.

Data Availability Statement: Not applicable.

Conflicts of Interest: The authors declare no conflict of interest.

References

1. Abideen, Z.; Qasim, M.; Hussain, T.; Rasheed, A.; Gul, B.; Koyro, H.W.; Ansari, R.; Khan, M.A. Salinity improves growth, photosynthesis and bioenergy characteristics of *Phragmites karka*. *Crop Pasture Sci.* **2018**, *69*, 944–953. [CrossRef]
2. Ehsen, S.; Abideen, Z.; Rizvi, R.F.; Gulzar, S.; Aziz, I.; Gul, B.; Khan, M.A.; Ansari, R. Ecophysiological adaptations and anti-nutritive status of sustainable cattle feed *Haloxylon stocksii* under saline conditions. *Flora* **2019**, *257*, 151425. [CrossRef]
3. Shoukat, E.; Ahmed, M.Z.; Abideen, Z.; Azeem, M.; Ibrahim, M.; Gul, B.; Khan, M.A. Short and long term salinity induced differences in growth and tissue specific ion regulation of *Phragmites karka*. *Flora* **2020**, *263*, 151550. [CrossRef]
4. Hussain, M.I.; Abideen, Z.; Qureshi, A.S. Soil degradation, resilience, restoration and sustainable use. In *Sustainable Agriculture Reviews*; Springer: Cham, Switzerland, 2021; Volume 52, pp. 335–365. [CrossRef]
5. Abideen, Z.; Koyro, H.W.; Huchzermeyer, B.; Ahmed, M.Z.; Gul, B.; Khan, M.A. Moderate salinity stimulates growth and photosynthesis of *Phragmites karka* by water relations and tissue specific ion regulation. *Environ. Exp. Bot.* **2014**, *105*, 70–76. [CrossRef]
6. Shoukat, E.; Abideen, Z.; Ahmed, M.Z.; Gulzar, S.; Nielsen, B.L. Changes in growth and photosynthesis linked with intensity and duration of salinity in *Phragmites karka*. *Environ. Exp. Bot.* **2019**, *162*, 504–514. [CrossRef]
7. Munir, N.; Hasnain, M.; Roessner, U.; Abideen, Z. Strategies in improving plant salinity resistance and use of salinity resistant plants for economic sustainability. *Crit. Rev. Environ. Sci. Technol.* **2021**, 1–47. [CrossRef]
8. Abideen, Z.; Koyro, H.W.; Huchzermeyer, B.; Ahmed, M.; Zulfiqar, F.; Egan, T.; Khan, M.A. *Phragmites karka* plants adopt different strategies to regulate photosynthesis and ion flux in saline and water deficit conditions. *Plant Biosyst.-An Int. J. Deal. All Asp. Plant Biol.* **2021**, *155*, 524–534. [CrossRef]
9. Lohani, N.; Jain, D.; Singh, M.B.; Bhalla, P.L. Engineering multiple abiotic stress tolerance in Canola, *Brassica napus*. *Front. Plant Sci.* **2020**, *11*, 3–11. [CrossRef]
10. Rajaee, B.S.; Iranbakhsh, A.; Ebadi, M.; Majd, A.; Ardebili, Z.O. Red elemental selenium nanoparticles mediated substantial variations in growth, tissue differentiation, metabolism, gene transcription, epigenetic cytosine DNA methylation, and callogenesis in Bittermelon (*Momordica charantia*); an In vitro experiment. *PLoS ONE* **2020**, *15*, e0235556.
11. Derbali, W.; Manaa, A.; Spengler, B.; Goussi, R.; Abideen, Z.; Ghezellou, P.; Abdelly, C.; Forreiter, C.; Koyro, H.W. Comparative proteomic approach to study the salinity effect on the growth of two contrasting quinoa genotypes. *Plant Physiol. Biochem.* **2021**, *163*, 215–229. [CrossRef]
12. Tang, W. Heterologous expression of transcription factor *ATWRKY57* alleviates salt stress-induced oxidative damage. *Open Biotechnol. J.* **2018**, *12*, 204–218. [CrossRef]
13. Yokotani, N.; Higuchi, M.; Kondou, Y.; Ichikawa, T.; Iwabuchi, M.; Hirochika, H.; Matsui, M.; Oda, K. A novel chloroplast protein, CEST induces tolerance to multiple environmental stresses and reduces photooxidative damage in transgenic *Arabidopsis*. *J. Exp. Bot.* **2011**, *62*, 557–569. [CrossRef] [PubMed]
14. Upadhyaya, C.P.; Venkatesh, J.; Gururani, M.A.; Asnin, L.; Sharma, K.; Ajappala, H.; Park, S.W. Transgenic potato overproducing l-ascorbic acid resisted an increase in methylglyoxal under salinity stress via maintaining higher reduced glutathione level and glyoxalase enzyme activity. *Biotechnol. Lett.* **2011**, *33*, 2297–2307. [CrossRef] [PubMed]
15. Hasanuzzaman, M.; Hossain, M.A.; Fujita, M. Selenium-induced up-regulation of the antioxidant defense and methylglyoxal detoxification system reduces salinity-induced damage in Rapeseed seedlings. *Biol. Trace Elem. Res.* **2011**, *143*, 1704–1721. [CrossRef]
16. Auffan, M.; Rose, J.; Bottero, J.Y.; Lowry, G.V.; Jolivet, J.P.; Wiesner, M.R. Towards a definition of inorganic nanoparticles from an environmental, health and safety perspective. *Nat. Nanotechnol.* **2009**, *4*, 634–641. [CrossRef]
17. Maurer-Jones, M.A.; Gunsolus, I.L.; Murphy, C.J.; Haynes, C.L. Toxicity of engineered nanoparticles in the environment. *Anal. Chem.* **2013**, *85*, 3036–3049. [CrossRef]
18. Radad, K.; Al-Shraim, M.; Moldzio, R.; Rausch, W.D. Recent advances in benefits and hazards of engineered nanoparticles. *Environ. Toxicol. Pharmacol.* **2012**, *34*, 661–672. [CrossRef]
19. Chavali, M.S.; Nikolova, M.P. Metal oxide nanoparticles and their applications in nanotechnology. *SN Appl. Sci.* **2019**, *1*, 3199. [CrossRef]
20. Sanchez-Dominguez, M.; Boutonnet, M.; Solans, C. A novel approach to metal and metal oxide nanoparticle synthesis: The oil-in-water microemulsion reaction method. *J. Nanopart. Res.* **2009**, *11*, 1823–1829. [CrossRef]
21. Rana, A.; Yadav, K.; Jagadevan, S. A comprehensive review on green synthesis of nature-inspired metal nanoparticles: Mechanism, application and toxicity. *J. Clean. Prod.* **2020**, *272*, 122880. [CrossRef]
22. Dumont, E.; Johnson, A.C.; Keller, V.D.; Williams, R.J. Nano silver and nano zinc-oxide in surface waters–exposure estimation for europe at high spatial and temporal resolution. *Environ. Pollut.* **2015**, *196*, 341–349. [CrossRef]

23. Levard, C.; Hotze, E.M.; Lowry, G.V.; Brown, G.E., Jr. Environmental transformations of silver nanoparticles: Impact on stability and toxicity. *Environ. Sci. Technol.* **2012**, *46*, 6900–6914. [CrossRef]
24. Barrios, A.C.; Rico, C.M.; Trujillo-Reyes, J.; Medina-Velo, I.A.; Peralta-Videa, J.R.; Gardea-Torresdey, J.L. Effects of uncoated and citric acid coated cerium oxide nanoparticles, bulk cerium oxide, cerium acetate, and citric acid on Tomato plants. *Sci. Total Environ.* **2016**, *563*, 956–964. [CrossRef] [PubMed]
25. Gardea-Torresdey, J.L.; Rico, C.M.; White, J.C. Trophic transfer, transformation, and impact of engineered nanomaterials in terrestrial environments. *Environ. Sci. Technol.* **2014**, *48*, 2526–2540. [CrossRef] [PubMed]
26. Mahdi, K.N.; Peters, R.J.; Klumpp, E.; Bohme, S.; Van der Ploeg, M.; Ritsema, C.; Geissen, V. Silver nanoparticles in soil: Aqueous extraction combined with single-particle ICP-MS for detection and characterization. *Environ. Nanotechnol. Monit. Manag.* **2017**, *7*, 24–33. [CrossRef]
27. Tripathi, D.K.; Singh, S.; Singh, S.; Srivastava, P.K.; Singh, V.P.; Singh, S.; Prasad, S.M.; Singh, P.K.; Dubey, N.K.; Pandey, A.C. Nitric oxide alleviates silver nanoparticles (Ag-NPs)-induced phytotoxicity in *Pisum sativum* seedlings. *Plant Physiol. Biochem.* **2017**, *110*, 167–177. [CrossRef] [PubMed]
28. Wang, P.; Lombi, E.; Zhao, F.J.; Kopittke, P.M. Nanotechnology: A new opportunity in plant sciences. *Trends Plant Sci.* **2016**, *21*, 699–712. [CrossRef] [PubMed]
29. Rao, S.; Shekhawat, G.S. Phytotoxicity and oxidative stress perspective of two selected nanoparticles in *Brassica juncea*. *3 Biotech* **2016**, *6*, 244. [CrossRef]
30. Taran, N.; Batsmanova, L.; Kovalenko, M.; Okanenko, A. Impact of metal nanoform colloidal solution on the adaptive potential of plants. *Nanoscale Res. Lett.* **2016**, *1*, 11–89. [CrossRef]
31. Zohra, E.; Ikram, M.; Omar, A.A.; Hussain, M.; Satti, S.H.; Raja, N.I.; Ehsan, M. Potential applications of biogenic selenium nanoparticles in alleviating biotic and abiotic stresses in plants: A comprehensive insight on the mechanistic approach and future perspectives. *Green Process. Synth.* **2021**, *10*, 456–475. [CrossRef]
32. Munir, N.; Hanif, M.; Dias, D.A.; Abideen, A. The role of halophytic nanoparticles towards the remediation of degraded and saline agricultural lands. *Environ. Sci. Pollut. Res.* **2021**, *28*, 60383–60405. [CrossRef]
33. Sharma, P.; Bhatt, D.; Zaidi, M.; Saradhi, P.P.; Khanna, P.; Arora, S. Silver nanoparticle-mediated enhancement in growth and antioxidant status of *Brassica juncea*. *Appl. Biochem. Biotechnol.* **2012**, *167*, 2225–2233. [CrossRef]
34. Gunjan, B.; Zaidi, M. Impact of gold nanoparticles on physiological and biochemical characteristics of *Brassica juncea*. *J. Plant Biochem. Physiol.* **2014**, *2*, 67–73. [CrossRef]
35. Mazumdar, H.; Ahmed, G. Phytotoxicity effect of silver nanoparticles on *Oryza sativa*. *Int. J. ChemTech Res.* **2011**, *3*, 1494–1500.
36. Mirzajani, F.; Askari, H.; Hamzelou, S.; Schober, Y.; Römpp, A.; Ghassempour, A.; Spengler, B. Proteomics study of silver nanoparticles toxicity on *Oryza sativa* L. *Ecotoxicol. Environ. Saf.* **2014**, *108*, 335–339. [CrossRef]
37. Khodakovskaya, M.; Dervishi, E.; Mahmood, M.; Xu, Y.; Li, Z.; Watanabe, F.; Biris, A.S. Carbon nanotubes are able to penetrate plant seed coat and dramatically affect seed germination and plant growth. *ACS Nano* **2009**, *3*, 3221–3227. [CrossRef]
38. Tawfik, M.; Mohamed, M.H.; Sadak, M.S.; Thalooth, A.T. Iron oxide nanoparticles effect on growth, physiological traits and nutritional contents of *Moringa oleifera* grown in saline environment. *Bull. Natl. Res. Cent.* **2021**, *45*, 177. [CrossRef]
39. Rodríguez-Celma, J.; Lattanzio, G.; Grusak, M.A.; Abadía, A.; Abadía, J.; López-Millán, A.F. Root responses of *Medicago truncatula* plants grown in two different iron deficiency conditions: Changes in root protein profile and riboflavin biosynthesis. *J. Proteome Res.* **2011**, *10*, 2590–2601. [CrossRef] [PubMed]
40. Mai, H.J.; Lindermayr, C.; Toerne, C.; Fink-Straube, C.; Durner, J.; Bauer, P. Iron and fer-like iron deficiency-induced transcription factor-dependent regulation of proteins and genes in *Arabidopsis thaliana* roots. *Proteomics* **2015**, *15*, 3030–3047. [CrossRef] [PubMed]
41. Mushtaq, Y.K. Effect of nanoscale Fe_3O_4, TiO_2 and carbon particles on cucumber seed germination. *J. Environ. Sci. Health* **2011**, *46*, 1732–1735. [CrossRef]
42. Zhu, H.; Han, J.; Xiao, J.Q.; Jin, Y. Uptake, translocation, and accumulation of manufactured iron oxide nanoparticles by Pumpkin plants. *J. Environ. Monit.* **2008**, *10*, 713–717. [CrossRef] [PubMed]
43. Barhoumi, L.; Oukarroum, A.; Taher, L.B.; Smiri, L.S.; Abdelmelek, H.; Dewez, D. Effects of superparamagnetic iron oxide nanoparticles on photosynthesis and growth of the aquatic plant *Lemna gibba*. *Arch. Environ. Contam. Toxicol.* **2015**, *68*, 510–520. [CrossRef] [PubMed]
44. Shankramma, K.; Yallappa, S.; Shivanna, M.B.; Manjanna, J. Fe_2O_3 magnetic nanoparticles to enhance *S. lycopersicum* (tomato) plant growth and their biomineralization. *Appl. Nanosci.* **2016**, *6*, 983–990. [CrossRef]
45. Rui, M.; Ma, C.; Hao, Y.; Guo, J.; Rui, Y.; Tang, X.; Zhao, Q.; Fan, X.; Zhang, Z.; Hou, T.; et al. Iron oxide nanoparticles as a potential iron fertilizer for peanut (*Arachis hypogaea*). *Fron. Plant Sci.* **2016**, *7*, 815. [CrossRef]
46. Dixon, R.A. Natural products and plant disease resistance. *Nature* **2001**, *411*, 843–847. [CrossRef]
47. Fiehn, O. Metabolomics—The link between genotypes and phenotypes. *Funct. Gen.* **2002**, *48*, 155–171. [CrossRef]
48. Hounsome, N.; Hounsome, B.; Tomos, D.; Edwards, J.G. Plant metabolites and nutritional quality of vegetables. *J. Food Sci.* **2008**, *73*, R48–R65. [CrossRef]
49. Mhlongo, M.I.; Piater, L.A.; Madala, N.E.; Labuschagne, N.; Dubery, I.A. The chemistry of plant–microbe interactions in the rhizosphere and the potential for metabolomics to reveal signaling related to defense priming and induced systemic resistance. *Front. Plant Sci.* **2018**, *9*, 112–121. [CrossRef]

50. Attia-Ismail, S.A. Plant secondary metabolites of halophytes and salt tolerant plants. In *Halophytic and Salt-Tolerant Feedstuffs*; CRC Press: Boca Raton, FL, USA, 2015; Volume 1, pp. 127–142. [CrossRef]
51. Guo, J.; Li, Y.; Han, G.; Song, J.; Wang, B. NaCl markedly improved the reproductive capacity of the euhalophyte *Suaeda salsa*. *Funct. Plant Biol.* **2018**, *45*, 350–361. [CrossRef]
52. Yao, W.; Zhao, K.; Cheng, Z.; Li, X.; Zhou, B.; Jiang, T. Transcriptome analysis of Poplar under salt stress and over-expression of transcription factor *NAC57* gene confers salt tolerance in transgenic *Arabidopsis*. *Front. Plant Sci.* **2018**, *9*, 11–21. [CrossRef]
53. Rao, A.Q.; Ud Din, S.; Akhtar, S.; Sarwar, M.B.; Ahmed, M.; Rashid, B.; Khan, M.A.U.; Qaisar, U.; Shahid, A.A.; Nasir, I.A. Genomics of salinity tolerance in plants. In *Plant Genomic*; InTechOpen: London, UK, 2016; pp. 273–299.
54. Johnson, R.R.; Wagner, R.L.; Verhey, S.D.; Walker-Simmons, M.K. The abscisic acid-responsive kinase *PKABA1* interacts with a seed-specific abscisic acid response element-binding factor, TaABF, and phosphorylates TaABF peptide sequences. *Plant Physiol.* **2002**, *130*, 837–846. [CrossRef] [PubMed]
55. Fujita, Y.; Yoshida, T.; Yamaguchi-Shinozaki, K. Pivotal role of the *AREB/ABF-SnRK2* pathway in *ABRE*-mediated transcription in response to osmotic stress in plants. *Physiol. Plant* **2013**, *147*, 15–27. [CrossRef] [PubMed]
56. Su, H.; Zhang, S.; Yuan, X.; Chen, C.; Wang, X.F.; Hao, Y.J. Genome-wide analysis and identification of stress-responsive genes of the *NAM–ATAF1, 2–CUC2* transcription factor family in Apple. *Plant Physiol. Biochem.* **2013**, *71*, 11–21. [CrossRef] [PubMed]
57. Zhang, L.; Zhao, G.; Jia, J.; Liu, X.; Kong, X. Molecular characterization of 60 isolated wheat *MYB* genes and analysis of their expression during abiotic stress. *J. Exp. Bot.* **2012**, *63*, 203–214. [CrossRef]
58. Roy, S.; Negra, S.; Tester, M. Salt resistant crop plants. *Curr. Opin. Biotechnol.* **2014**, *26*, 115–124. [CrossRef]
59. Hu, Y.; Chen, L.; Wang, H.; Zhang, L.; Wang, F.; Yu, D. Arabidopsis transcription factor *WRKY8* functions antagonistically with its interacting partner *VQ9* to modulate salinity stress tolerance. *Plant J.* **2013**, *74*, 730–745. [CrossRef]
60. Ji, H.; Pardo, J.M.; Batelli, G.; Van Oosten, M.J.; Bressan, R.A.; Li, X. The salt overly sensitive (SOS) pathway: Established and emerging roles. *Mol. Plant* **2013**, *6*, 275–286. [CrossRef]
61. Schmidt, R.; Mieulet, D.; Hubberten, H.M.; Obata, T.; Hoefgen, R.; Fernie, A.R.; Fisahn, J.; San Segundo, B.; Guiderdoni, E.; Schippers, J.H. Salt-responsive *ERF1* regulates reactive oxygen species–dependent signaling during the initial response to salt stress in Rice. *Plant Cell* **2013**, *25*, 2115–2131. [CrossRef]
62. Steinfeld, B.; Scott, J.; Vilander, G.; Marx, L.; Quirk, M.; Lindberg, J.; Koerner, K. The role of lean process improvement in implementation of evidence-based practices in behavioral health care. *J. Behav. Health Serv. Res.* **2015**, *42*, 504–518. [CrossRef]
63. Kakali, M.; Roy, C.; Bhaskar, G.; Sudhiranjan, G.; Sengupta, D. An *ABRE*-binding factor, *OSBZ8*, is highly expressed in salt tolerant cultivars than in salt sensitive cultivars of *Indica Rice*. *BMC Plant Biol.* **2006**, *6*, 18. [CrossRef]
64. Staiger, D.; Brown, J.W. Alternative splicing at the intersection of biological timing, development, and stress responses. *Plant Cell* **2013**, *25*, 3640–3656. [CrossRef] [PubMed]
65. Chakraborty, K.; Sairam, R.K.; Bhattacharya, R. Differential expression of salt overly sensitive pathway genes determines salinity stress tolerance in *Brassica* genotypes. *Plant Physiol. Biochem.* **2012**, *51*, 90–101. [CrossRef] [PubMed]
66. Lim, G.H.; Zhang, X.; Chung, M.S.; Lee, D.J.; Woo, Y.M.; Cheong, H.S.; Kim, C.S. A putative novel transcription factor, *AtSKIP*, is involved in abscisic acid signalling and confers salt and osmotic tolerance in *Arabidopsis*. *New Phytol.* **2010**, *185*, 103–113. [CrossRef] [PubMed]
67. Zou, J.; Liu, C.; Liu, A.; Zou, D.; Chen, X. Overexpression of *OsHsp17.0* and *OSHSP23.7* enhances drought and salt tolerance in Rice. *J. Plant Physiol.* **2012**, *169*, 628–635. [CrossRef] [PubMed]
68. Song, N.H.; Ahn, Y.J. *DcHsp17.7*, a small heat shock protein in Carrot, is tissue-specifically expressed under salt stress and confers tolerance to salinity. *New Biotechnol.* **2011**, *28*, 698–704. [CrossRef] [PubMed]
69. Tang, M.; Liu, X.; Deng, H.; Shen, S. Over-expression of *JcDREB*, a putative AP2/EREBP domain-containing transcription factor gene in woody biodiesel plant *Jatropha curcas*, enhances salt and freezing tolerance in transgenic *Arabidopsis thaliana*. *Plant Sci.* **2011**, *181*, 623–631. [CrossRef] [PubMed]
70. Sottosanto, J.B.; Saranga, Y.; Blumwald, E. Impact of *AtNHX1*, a vacuolar Na^+/H^+ antiporter, upon gene expression during short-and long-term salt stress in *Arabidopsis thaliana*. *BMC Plant Biol.* **2007**, *7*, 18. [CrossRef] [PubMed]
71. Peng, X.; Ding, X.; Chang, T.; Wang, Z.; Liu, R.; Zeng, X.; Cai, Y.; Zhu, Y. Overexpression of a vesicle trafficking gene, *OsRab7*, enhances salt tolerance in Rice. *Sci. World J.* **2014**, *2014*, 483526 . [CrossRef]
72. Han, Y.; Wang, W.; Sun, J.; Ding, M.; Zhao, R.; Deng, S.; Wang, F.; Hu, Y.; Wang, Y.; Lu, Y. *Populus euphratica* XTH overexpression enhances salinity tolerance by the development of leaf succulence in transgenic Tobacco plants. *J. Exp. Bot.* **2013**, *64*, 4225–4238. [CrossRef]
73. Kurotani, K.I.; Hayashi, K.; Hatanaka, S.; Toda, Y.; Ogawa, D.; Ichikawa, H.; Ishimaru, Y.; Tashita, R.; Suzuki, T.; Ueda, M. Elevated levels of *CYP94* family gene expression alleviate the Jasmonate response and enhance salt tolerance in Rice. *Plant Cell Physiol.* **2015**, *56*, 779–789. [CrossRef]
74. Yue, Y.; Zhang, M.; Zhang, J.; Duan, L.; Li, Z. SOS1 gene overexpression increased salt tolerance in transgenic Tobacco by maintaining a higher K^+/Na^+ ratio. *J. Plant Physiol.* **2012**, *169*, 255–261. [CrossRef] [PubMed]
75. Bhauso, T.D.; Thankappan, R.; Kumar, A.; Mishra, G.P.; Dobaria, J.R.; Rajam, M.V. Over-expression of bacterial *MTLD* gene confers enhanced tolerance to salt-stress and water-deficit stress in transgenic Peanut (*Arachis hypogaea*) through accumulation of mannitol. *Aust. J. Crop Sci.* **2014**, *8*, 413–424.

76. Zhou, W.; Li, Y.; Zhao, B.C.; Ge, R.C.; Shen, Y.Z.; Wang, G.; Huang, Z.J. Overexpression of *TaSTRG* gene improves salt and drought tolerance in Rice. *J. Plant Physiol.* **2009**, *166*, 1660–1671. [CrossRef] [PubMed]
77. Lawson, S.S.; Michler, C.H. Overexpression of *AtSTO1* leads to improved salt tolerance in *Populus tremula* × *P. alba*. *Transgenic Res.* **2014**, *23*, 817–826. [CrossRef] [PubMed]
78. Mangrauthia, S.K.; Agarwal, S.; Sailaja, B.; Madhav, M.S.; Voleti, S. MicroRNAs and their role in salt stress response in plants. In *Salt Stress in Plants*, 3rd ed.; Springer: Cham, Switzerland, 2013; pp. 15–46.
79. Lu, S.; Sun, Y.H.; Chiang, V.L. Stress-responsive microRNAs in *Populus*. *Plant J.* **2008**, *55*, 131–151. [CrossRef]
80. Deinlein, U.; Stephan, A.B.; Horie, T.; Luo, W.; Xu, G.; Schroeder, J.I. Plant salt-tolerance mechanisms. *Trends Plant Sci.* **2014**, *19*, 371–379. [CrossRef] [PubMed]
81. Golldack, D.; Lüking, I.; Yang, O. Plant tolerance to drought and salinity: Stress regulating transcription factors and their functional significance in the cellular transcriptional network. *Plant Cell Rep.* **2011**, *30*, 1383–1391. [CrossRef]
82. Yang, O.; Popova, O.V.; Süthoff, U.; Lüking, I.; Dietz, K.J.; Golldack, D. The *Arabidopsis* basic leucine zipper transcription factor AtbZIP24 regulates complex transcriptional networks involved in abiotic stress resistance. *Gene* **2009**, *436*, 45–55. [CrossRef]
83. Popova, O.V.; Yang, O.; Dietz, K.J.; Golldack, D. Differential transcript regulation in *Arabidopsis thaliana* and the halotolerant lobularia maritima indicates genes with potential function in plant salt adaptation. *Gene* **2008**, *423*, 142–148. [CrossRef]
84. Munns, R.; James, R.A.; Xu, B.; Athman, A.; Conn, S.J.; Jordans, C.; Byrt, C.S.; Hare, R.A.; Tyerman, S.D.; Tester, M. Wheat grain yield on saline soils is improved by an ancestral Na^+ transporter gene. *Nat. Biotechnol.* **2012**, *30*, 360–364. [CrossRef]
85. Yamaguchi, T.; Blumwald, E. Developing salt-tolerant crop plants: Challenges and opportunities. *Trends Plant Sci.* **2005**, *10*, 615–620. [CrossRef]
86. Reddy, I.N.B.L.; Kim, B.K.; Yoon, I.S.; Kim, K.H.; Kwon, T.R. Salt tolerance in rice: Focus on mechanisms and approaches. *Rice Sci.* **2017**, *24*, 123–144. [CrossRef]
87. Silva, P.; Gerós, H. Regulation by salt of vacuolar H^+-ATPase and H^+-pyrophosphatase activities and Na^+/H^+ exchange. *Plant Signal. Behav.* **2009**, *4*, 718–726. [CrossRef] [PubMed]
88. Flowers, T.; Koyama, M.; Flowers, S.; Sudhakar, C.; Singh, K.; Yeo, A. QTL: Their place in engineering tolerance of Rice to salinity. *J. Exp. Bot.* **2000**, *51*, 99–106. [CrossRef] [PubMed]
89. Alam, R.; Sazzad-ur-Rahman, M.; Seraj, Z.I.; Thomson, M.J.; Ismail, A.M.; Tumimbang-Raiz, E.; Gregorio, G.B. Investigation of seedling-stage salinity tolerance QTLS using backcross lines derived from *Oryza sativa* l. Pokkali. *Plant Breed.* **2011**, *130*, 430–437. [CrossRef]
90. Frary, A.; Göl, D.; Keleş, D.; Ökmen, B.; Pınar, H.; Şığva, H.Ö.; Yemenicioğlu, A.; Doğanlar, S. Salt tolerance in *Solanum pennellii*: Antioxidant response and related QTL. *BMC Plant Biol.* **2010**, *10*, 58. [CrossRef] [PubMed]
91. Yang, Q.; Chen, Z.Z.; Zhou, X.F.; Yin, H.B.; Li, X.; Xin, X.F.; Hong, X.H.; Zhu, J.K.; Gong, Z. Overexpression of SOS (salt overly sensitive) genes increases salt tolerance in transgenic *Arabidopsis*. *Mol. Plant* **2009**, *2*, 22–31. [CrossRef] [PubMed]
92. Shabala, S. Learning from halophytes: Physiological basis and strategies to improve abiotic stress tolerance in crops. *Ann. Bot.* **2013**, *112*, 1209–1221. [CrossRef]
93. Ventura, Y.; Eshel, A.; Pasternak, D.; Sagi, M. The development of halophyte-based agriculture: Past and present. *Ann. Bot.* **2015**, *115*, 529–540. [CrossRef]
94. Zhu, J.K. Plant salt tolerance. *Trends Plant Sci.* **2001**, *6*, 66–71. [CrossRef]
95. Himabindu, Y.; Chakradhar, T.; Reddy, M.C.; Kanygin, A.; Redding, K.E.; Chandrasekhar, T. Salt-tolerant genes from halophytes are potential key players of salt tolerance in glycophytes. *Environ. Exp. Bot.* **2016**, *124*, 39–63. [CrossRef]
96. Muchate, N.S.; Nikalje, G.C.; Rajurkar, N.S.; Suprasanna, P.; Nikam, T.D. Plant salt stress: Adaptive responses, tolerance mechanism and bioengineering for salt tolerance. *Bot. Rev.* **2016**, *82*, 371–406. [CrossRef]
97. Udawat, P.; Mishra, A.; Jha, B. Heterologous expression of an uncharacterized universal stress protein gene (SbUSP) from the extreme halophyte, *Salicornia brachiata*, which confers salt and osmotic tolerance to *E. coli*. *Gene* **2014**, *536*, 163–170. [CrossRef] [PubMed]
98. Bartels, D.; Dinakar, C. Balancing salinity stress responses in halophytes and non-halophytes: A comparison between *Thellungiella* and *Arabidopsis thaliana*. *Funct. Plant Biol.* **2013**, *40*, 819–831. [CrossRef]
99. Wu, H.J.; Zhang, Z.; Wang, J.Y.; Oh, D.H.; Dassanayake, M.; Liu, B.; Huang, Q.; Sun, H.X.; Xia, R.; Wu, Y. Insights into salt tolerance from the genome of *Thellungiella salsuginea*. *Proc. Natl. Acad. Sci. USA* **2012**, *109*, 12219–12224. [CrossRef]
100. Taji, T.; Seki, M.; Satou, M.; Sakurai, T.; Kobayashi, M.; Ishiyama, K.; Narusaka, Y.; Narusaka, M.; Zhu, J.K.; Shinozaki, K. Comparative genomics in salt tolerance between *Arabidopsis* and arabidopsis-related halophyte salt stress using *Arabidopsis* microarray. *Plant Physiol.* **2004**, *135*, 1697–1709. [CrossRef]
101. Wong, C.E.; Li, Y.; Labbe, A.; Guevara, D.; Nuin, P.; Whitty, B.; Diaz, C.; Golding, G.B.; Gray, G.R.; Weretilnyk, E.A. Transcriptional profiling implicates novel interactions between abiotic stress and hormonal responses in *Thellungiella*, a close relative of *Arabidopsis*. *Plant Physiol.* **2006**, *140*, 1437–1450. [CrossRef]
102. Rigó, G.; Valkai, I.; Faragó, D.; Kiss, E.; Van Houdt, S.; Van de Steene, N.; Hannah, M.A.; Szabados, L. Gene mining in halophytes: Functional identification of stress tolerance genes in *Lepidium crassifolium*. *Plant, Cell Environ.* **2016**, *39*, 167–181. [CrossRef]
103. Pandey, S.; Patel, M.K.; Mishra, A.; Jha, B. In planta transformed Cumin (*Cuminum cyminum* l.) plants, overexpressing the SbNHX1 gene showed enhanced salt endurance. *PLoS ONE* **2016**, *11*, e0159349.

104. Jha, B.; Singh, N.P.; Mishra, A. Proteome profiling of seed storage proteins reveals the nutritional potential of *Salicornia brachiata* Roxb., an extreme halophyte. *J. Agric. Food Chem.* **2012**, *60*, 4320–4326. [CrossRef]
105. Garg, R.; Verma, M.; Agrawal, S.; Shankar, R.; Majee, M.; Jain, M. Deep transcriptome sequencing of wild halophyte Rice, *Porteresia coarctata*, provides novel insights into the salinity and submergence tolerance factors. *DNA Res.* **2014**, *21*, 69–84. [CrossRef] [PubMed]
106. Zhang, G.H.; Su, Q.; An, L.J.; Wu, S. Characterization and expression of a vacuolar Na^+/H^+ antiporter gene from the monocot halophyte *Aeluropus littoralis*. *Plant Physiol. Biochem.* **2008**, *46*, 117–126. [CrossRef] [PubMed]
107. Jia, G.X.; Zhu, Z.Q.; Chang, F.Q.; Li, Y.X. Transformation of Tomato with the *BADH* gene from Atriplex improves salt tolerance. *Plant Cell Rep.* **2002**, *21*, 141–146. [CrossRef]
108. Harris, P.A.; Taylor, R.; Minor, B.L.; Elliott, V.; Fernandez, M.; O'Neal, L.; McLeod, L.; Delacqua, G.; Delacqua, F.; Kirby, J. The REDCap consortium: Building an international community of software platform partners. *J. Biomed. Inform.* **2019**, *95*, 15–32. [CrossRef]
109. Singh, N.; Mishra, A.; Jha, B. Over-expression of the peroxisomal ascorbate peroxidase (SbpAPX) gene cloned from halophyte *Salicornia brachiata* confers salt and drought stress tolerance in transgenic tobacco. *Mar. Biotechnol.* **2014**, *16*, 321–332. [CrossRef]
110. Singh, N.; Mishra, A.; Jha, B. Ectopic over-expression of peroxisomal ascorbate peroxidase (SbpAPX) gene confers salt stress tolerance in transgenic Peanut (*Arachis hypogaea*). *Gene* **2014**, *547*, 119–125. [CrossRef]
111. Li, W.; Wang, D.; Jin, T.; Chang, Q.; Yin, D.; Xu, S.; Liu, B.; Liu, L. The vacuolar Na^+/H^+ antiporter gene SSNHX1 from the halophyte *Salsola soda* confers salt tolerance in transgenic Alfalfa (*Medicago sativa* L.). *Plant Mol. Biol. Rep.* **2011**, *29*, 278–290. [CrossRef]
112. Wu, W.; Su, Q.; Xia, X.; Wang, Y.; Luan, Y.; An, L. The *Suaeda liaotungensis* KITAG betaine aldehyde dehydrogenase gene improves salt tolerance of transgenic maize mediated with minimum linear length of DNA fragment. *Euphytica* **2008**, *159*, 17–25. [CrossRef]
113. Qiu, W.; Liu, M.; Qiao, G.; Jiang, J.; Xie, L.; Zhuo, R. An isopentyl transferase gene driven by the stress-inducible RD29A promoter improves salinity stress tolerance in transgenic Tobacco. *Plant Mol. Biol. Rep.* **2012**, *30*, 519–528. [CrossRef]
114. Zhao, F.; Zhang, H. Salt and paraquat stress tolerance results from co-expression of the *Suaeda salsa* glutathione s-transferase and catalase in transgenic Rice. *Plant Cell Tissue Organ Cult.* **2006**, *86*, 349–358. [CrossRef]
115. Guo, S.; Yin, H.; Zhang, X.; Zhao, F.; Li, P.; Chen, S.; Zhao, Y.; Zhang, H. Molecular cloning and characterization of a vacuolar H^+-pyrophos-phatase gene, *SsVP*, from the halophyte *Suaeda salsa* and its overexpression increases salt and drought tolerance of *Arabidopsis*. *Plant Mol. Biol.* **2006**, *60*, 41–50. [CrossRef] [PubMed]
116. Oh, D.H.; Leidi, E.; Zhang, Q.; Hwang, S.M.; Li, Y.; Quintero, F.J.; Jiang, X.; D'Urzo, M.P.; Lee, S.Y.; Zhao, Y. Loss of halophytism by interference with SOS1 expression. *Plant Physiol.* **2009**, *151*, 210–222. [CrossRef] [PubMed]
117. Wang, L.L.; Chen, A.P.; Zhong, N.Q.; Liu, N.; Wu, X.M.; Wang, F.; Yang, C.L.; Romero, M.F.; Xia, G.X. The *Thellungiella salsuginea* tonoplast aquaporin TsTIP1; 2 functions in protection against multiple abiotic stresses. *Plant Cell Physiol.* **2014**, *55*, 148–161. [CrossRef] [PubMed]
118. Lin, F.; Xu, J.; Shi, J.; Li, H.; Li, B. Molecular cloning and characterization of a novel glyoxalase I gene TaGly I in Wheat (*Triticum aestivum* L.). *Mol. Biol. Rep.* **2010**, *37*, 729–737. [CrossRef]
119. Baisakh, N.; RamanaRao, M.V.; Rajasekaran, K.; Subudhi, P.; Janda, J.; Galbraith, D.; Vanier, C.; Pereira, A. Enhanced salt stress tolerance of Rice plants expressing a vacuolar H^+-ATPase subunit c1 (*SaVHAc1*) gene from the halophyte grass *Spartina alterniflora* löisel. *Plant Biotechnol. J.* **2012**, *10*, 453–464. [CrossRef]
120. Wu, S.; Su, Q.; An, L. Isolation of choline monooxygenase (CMO) gene from *Salicornia europaea* and enhanced salt tolerance of transgenic Tobacco with CMO genes. *Ind. J. Biochem. Biophys.* **2010**, *47*, 298–305.
121. Yin, X.Y.; Yang, A.F.; Zhang, K.W.; Zhang, J.R. Production and analysis of transgenic maize with improved salt tolerance by the introduction of AtNHX1 gene. *Acta Bot. Sin.-Engl. Ed.* **2004**, *46*, 854–861.
122. Ohta, M.; Hayashi, Y.; Nakashima, A.; Tsunetomi, N.; Hamada, A.; Tanaka, A.; Nakamura, T.; Hayakawa, T. Salt tolerance of Rice is conffered by introduction of a Na^+/H^+ antiporter gene from atriplex gmelini. *Plant Cell Physiol.* **2002**, *532*, 279–282. [CrossRef]
123. Taji, T.; Komatsu, K.; Katori, T.; Kawasaki, Y.; Sakata, Y.; Tanaka, S.; Kobayashi, M.; Toyoda, A.; Seki, M.; Shinozaki, K. Comparative genomic analysis of 1047 completely sequenced cDNA's from an arabidopsis-related model halophyte, *Thellungiella halophila*. *BMC Plant Biol.* **2010**, *10*, 261. [CrossRef]
124. Tiwari, V.; Patel, M.K.; Chaturvedi, A.K.; Mishra, A.; Jha, B. Functional characterization of the Tau class glutathione-s-transferases gene (*SbGSTU*) promoter of *Salicornia brachiata* under salinity and osmotic stress. *PLoS ONE* **2016**, *11*, e0148494. [CrossRef]
125. Yin, X.; Zhao, Y.; Luo, D.; Zhang, H. Isolating the promoter of a stress-induced gene encoding betaine aldehyde dehydrogenase from the halophyte *Atriplex centralasiatica* Iljin. *Biochim. Biophys. Acta-Gene Struct. Express* **2002**, *1577*, 452–456. [CrossRef]
126. Li, Q.L.; Xie, J.H.; Ma, X.Q.; Li, D. Molecular cloning of phosphoethanolamine n-methyltransferase (PEAMT) gene and its promoter from the halophyte *Suaeda liaotungensis* and their response to salt stress. *Acta Physiol. Plant* **2016**, *38*, 39–45. [CrossRef]
127. Yang, X.; Lu, M.; Wang, Y.; Wang, Y.; Liu, Z.; Chen, S. Response mechanism of plants to drought stress. *Horticulturae* **2021**, *7*, 50. [CrossRef]
128. Schaeffer, H.J.; Forsthoefel, N.R.; Cushman, J.C. Identification of enhancer and silencer regions involved in salt-responsive expression of crassulacean acid metabolism (CAM) genes in the facultative halophyte *Mesembryanthemum crystallinum*. *Plant Mol. Biol.* **1995**, *28*, 205–218. [CrossRef]

129. Zhao, Y.; Liu, W.; Xu, Y.P.; Cao, J.Y.; Braam, J.; Ca, X.Z. Genome-wide identification and functional analyses of Calmodulin genes in *Solanaceous* species. *BMC Plant Biol.* **2013**, *13*, 70. [CrossRef] [PubMed]
130. Saad, R.B.; Romdhan, W.B.; Zouari, N.; Azaza, J.; Mieulet, D.; Verdeil, J.L.; Guiderdoni, E.; Hassairi, A. Promoter of the *AlSAP* gene from the halophyte grass *Aeluropus littoralis* directs developmental-regulated, stress-inducible, and organ-specific gene expression in transgenic Tobacco. *Transgenic Res.* **2011**, *20*, 1003–1018. [CrossRef]
131. Ben-Saad, R.; Meynard, D.; Ben-Romdhane, W.; Mieulet, D.; Verdeil, J.L.; Al-Doss, A.; Guiderdoni, E.; Hassairi, A. The promoter of the ALSAP gene from the halophyte grass *Aeluropus littoralis* directs a stress-inducible expression pattern in transgenic Rice plants. *Plant Cell Rep.* **2015**, *34*, 1791–1806. [CrossRef]
132. Sun, Q.; Gao, F.; Zhao, L.; Li, K.; Zhang, J. Identification of a new 130 bp cis-acting element in the TSVP1 promoter involved in the salt stress response from *Thellungiella halophila*. *BMC Plant Biol.* **2010**, *10*, 90. [CrossRef]
133. Guo, L.; Yu, Y.; Xia, X.; Yin, W. Identification and functional characterisation of the promoter of the calcium sensor gene CBL1 from the xerophyte *Ammopiptanthus mongolicus*. *BMC Plant Biol.* **2010**, *10*, 18. [CrossRef]
134. Tiwari, V.; Chaturvedi, A.K.; Mishra, A.; Jha, B. The transcriptional regulatory mechanism of the peroxisomal ascorbate peroxidase (*pAPX*) gene cloned from an extreme halophyte, *Salicornia brachiata*. *Plant Cell Physiol.* **2014**, *55*, 201–217. [CrossRef]
135. James, C. *Global Status of Commercialized Biotech/GM Crops, 2nd ed*; International Service for the Acquisition of Agri-Biotech Applications (ISAAA): Ithaca, NY, USA, 2007; pp. 22–45.
136. Ashraf, M.; Athar, H.; Harris, P.; Kwon, T. Some prospective strategies for improving crop salt tolerance. *Adv. Agron.* **2008**, *97*, 45–110. [CrossRef]
137. Goel, D.; Singh, A.K.; Yadav, V.; Babbar, S.B.; Murata, N.; Bansal, K.C. Transformation of Tomato with a bacterial *CODA* gene enhances tolerance to salt and water stresses. *J. Plant Physiol.* **2011**, *168*, 1286–1294. [CrossRef] [PubMed]
138. Su, J.; Hirji, R.; Zhang, L.; He, C.; Selvaraj, G.; Wu, R. Evaluation of the stress-inducible production of choline oxidase in transgenic Rice as a strategy for producing the stress-protectant glycine betaine. *J. Exp. Bot.* **2006**, *57*, 1129–1135. [CrossRef] [PubMed]
139. Cortina, C.; Culiáñez-Macià, F.A. Tomato abiotic stress enhanced tolerance by trehalose biosynthesis. *Plant Sci.* **2005**, *169*, 75–82. [CrossRef]
140. Almeida, A.M.; Villalobos, E.; Araújo, S.S.; Leyman, B.; Van Dijck, P.; Alfaro-Cardoso, L.; Fevereiro, P.S.; Torné, J.M.; Santos, D.M. Transformation of tobacco with an *Arabidopsis thaliana* gene involved in trehalose biosynthesis increases tolerance to several abiotic stresses. *Euphytica* **2005**, *146*, 165–176. [CrossRef]
141. Abebe, T.; Guenzi, A.C.; Martin, B.; Cushman, J.C. Tolerance of mannitol-accumulating transgenic Wheat to water stress and salinity. *Plant Physiol.* **2003**, *131*, 1748–1755. [CrossRef]
142. Gao, M.; Tao, R.; Miura, K.; Dandekar, A.M.; Sugiura, A. Transformation of Japanese Persimmon (*Diospyros kaki thunb.*) with Apple cDNA encoding NADP-dependent sorbitol-6-phosphate dehydrogenase. *Plant Sci.* **2001**, *160*, 837–845. [CrossRef]
143. Hmida-Sayari, A.; Gargouri-Bouzid, R.; Bidani, A.; Jaoua, L.; Savouré, A.; Jaoua, S. Overexpression of δ1-pyrroline-5-carboxylate synthetase increases proline production and confers salt tolerance in transgenic potato plants. *Plant Sci.* **2005**, *169*, 746–752. [CrossRef]
144. Zhang, H.X.; Hodson, J.N.; Williams, J.P.; Blumwald, E. Engineering salt-tolerant Brassica plants: Characterization of yield and seed oil quality in transgenic plants with increased vacuolar sodium accumulation. *Proc. Natl. Acad. Sci. USA* **2001**, *98*, 12832–12836. [CrossRef]
145. Wang, J.; Zuo, K.; Wu, W.; Song, J.; Sun, X.; Lin, J.; Li, X.; Tang, K. Expression of a novel antiporter gene from *Brassica napus* resulted in enhanced salt tolerance in transgenic Tobacco plants. *Biol. Plant* **2004**, *48*, 509–515. [CrossRef]
146. Singla-Pareek, S.; Reddy, M.; Sopory, S. Genetic engineering of the glyoxalase pathway in Tobacco leads to enhanced salinity tolerance. *Proc. Natl. Acad. Sci. USA* **2003**, *100*, 14672–14677. [CrossRef] [PubMed]
147. Gao, S.Q.; Chen, M.; Xu, Z.S.; Zhao, C.P.; Li, L.; Xu, H.J.; Tang, Y.M.; Zhao, X.; Ma, Y.Z. The Soybean *GmbZIP1* transcription factor enhances multiple abiotic stress tolerances in transgenic plants. *Plant Mol. Biol.* **2011**, *75*, 537–553. [CrossRef] [PubMed]
148. Seo, Y.J.; Park, J.B.; Cho, Y.J.; Jung, C.; Seo, H.S.; Park, S.K.; Nahm, B.H.; Song, J.T. Overexpression of the ethylene-responsive factor gene *BrERF4* from *Brassica rapa* increases tolerance to salt and drought in *Arabidopsis* plants. *Mol. Cells* **2010**, *30*, 271–277. [CrossRef] [PubMed]
149. Montero-Barrientos, M.; Hermosa, R.; Cardoza, R.E.; Gutierrez, S.; Nicolas, C.; Monte, E. Transgenic expression of the *Trichoderma harzianum HSP70* gene increases *Arabidopsis* resistance to heat and other abiotic stresses. *J. Plant Physiol.* **2010**, *167*, 659–665. [CrossRef] [PubMed]
150. Zhang, L.; Xi, D.; Li, S.; Gao, Z.; Zhao, S.; Shi, J.; Wu, C.; Guo, X. A Cotton group c map kinase gene, *GhMPK2*, positively regulates salt and drought tolerance in Tobacco. *Plant Mol. Biol.* **2011**, *77*, 17–31. [CrossRef]
151. Flowers, T.J.; Colmer, T.D. Salinity tolerance in halophytes. *New Phytol.* **2008**, *179*, 945–963. [CrossRef]
152. Bose, J.; Rodrigo-Moreno, A.; Shabala, S. Ros homeostasis in halophytes in the context of salinity stress tolerance. *J. Exp. Bot.* **2014**, *65*, 1241–1257. [CrossRef]
153. Kronzucker, H.J.; Britto, D.T. Sodium transport in plants: A critical review. *New Phytol.* **2011**, *189*, 54–81. [CrossRef]
154. Volkov, V. Salinity tolerance in plants. Quantitative approach to ion transport starting from halophytes and stepping to genetic and protein engineering for manipulating ion fluxes. *Front. Plant Sci.* **2015**, *6*, 873–884. [CrossRef]
155. Mishra, A.; Tanna, B. Halophytes: Potential resources for salt stress tolerance genes and promoters. *Front. Plant Sci.* **2017**, *8*, 829. [CrossRef]

156. Lan, T.; Duan, Y.; Wang, B.; Zhou, Y.; Wu, W. Molecular cloning and functional characterization of a Na^+/H^+ antiporter gene from halophyte *Spartina anglica*. *Turk. J. Agric. For.* **2011**, *35*, 535–543.
157. Patel, M.K.; Joshi, M.; Mishra, A.; Jha, B. Ectopic expression of *SbNHX1* gene in transgenic Castor (*Ricinus communis* l.) enhances salt stress by modulating physiological process. *Plant Cell Tissue Organ Cult.* **2015**, *122*, 477–490. [CrossRef]
158. Udawat, P.; Jha, R.K.; Sinha, D.; Mishra, A.; Jha, B. Overexpression of a cytosolic abiotic stress responsive universal stress protein (*SbUSP*) mitigates salt and osmotic stress in transgenic Tobacco plants. *Front. Plant Sci.* **2016**, *7*, 518–529. [CrossRef] [PubMed]
159. Peng, Y.; Lin, W.; Cai, W.; Arora, R. Overexpression of a *Panax ginseng* tonoplast aquaporin alters salt tolerance, drought tolerance and cold acclimation ability in transgenic Arabidopsis plants. *Planta* **2007**, *226*, 729–740. [CrossRef] [PubMed]
160. Sharma, R.; Sahoo, A.; Devendran, R.; Jain, M. Over-expression of a Rice Tau class glutathione s-transferase gene improves tolerance to salinity and oxidative stresses in Arabidopsis. *PLoS ONE* **2014**, *9*, e92900.
161. Oh, D.H.; Dassanayake, M.; Haas, J.S.; Kropornika, A.; Wright, C.; d'Urzo, M.P.; Hong, H.; Ali, S.; Hernandez, A.; Lambert, G.M. Genome structures and halophyte-specific gene expression of the extremophile *Thellungiella parvula* in comparison with *Thellungiella salsuginea* (*Thellungiella halophila*) and Arabidopsis. *Plant Physiol.* **2010**, *154*, 1040–1052. [CrossRef]
162. Fu, R.; Zhang, M.; Zhao, Y.; He, X.; Ding, C.; Wang, S. Identification of salt tolerance-related microRNAs and their targets in maize (*Zea mays* L.) using high-throughput sequencing and degradome analysis. *Front. Plant Sci.* **2017**, *8*, 864. [CrossRef]
163. Yang, Z.; Zhu, P.; Kang, H.; Liu, L.; Cao, Q.; Sun, J. High-throughput deep sequencing reveals the important role that microRNAs play in the salt response in sweet potato (*Ipomoea batatas* L.). *BMC Genom.* **2020**, *21*, 164. [CrossRef]
164. Jodder, J.; Das, R.; Sarkar, D.; Bhattacharjee, P.; Kundu, P. Distinct transcriptional and processing regulations control miR167a level in tomato during stress. *RNA Biol.* **2018**, *15*, 130–143. [CrossRef]
165. Wang, M.; Wang, Q.; Zhang, B. Response of miRNAs and their targets to salt and drought stresses in cotton (*Gossypium hirsutum* L.). *Gene* **2013**, *530*, 26–32. [CrossRef]
166. Pegler, J.L.; Oultram, J.M.J.; Grof, C.P.L.; Eamens, A.L. Profiling the abiotic stress responsive microRNA landscape of *Arabidopsis thaliana*. *Plants* **2019**, *8*, 58. [CrossRef] [PubMed]
167. Dong, Z.; Shi, L.; Wang, Y.; Chen, L.; Cai, Z.; Wang, Y. Identification and dynamic regulation of microRNAs involved in salt stress responses in functional soybean nodules by high-throughput sequencing. *Int. J. Mol. Sci.* **2013**, *14*, 2717–2738. [CrossRef] [PubMed]
168. Zhou, M.; Luo, H. Role of microRNA319 in creeping bentgrass salinity and drought stress response. *Plant Signal Behav.* **2014**, *9*, e28700. [CrossRef] [PubMed]
169. Cao, C.; Long, R.; Zhang, T.; Kang, J.; Wang, Z.; Wang, P. Genome-wide identification of microRNAs in response to salt/alkali stress in *Medicago truncatula* through high-throughput sequencing. *Int. J. Mol. Sci.* **2018**, *19*, 4076. [CrossRef] [PubMed]
170. Lee, W.S.; Gudimella, R.; Wong, G.R.; Tammi, M.T.; Khalid, N.; Harikrishna, J.A. Transcripts and microRNAs responding to salt stress in *Musa acuminata colla* (AAA Group) cv. berangan roots. *PLoS ONE* **2015**, *10*, e0127526. [CrossRef]
171. Tripathi, A.; Chacon, O.; Singla-Pareek, S.L.; Sopory, S.K.; Sanan-Mishra, N. Mapping the microRNA expression profiles in glyoxalase over-expressing salinity tolerant rice. *Curr. Genom.* **2018**, *19*, 21–35. [CrossRef]
172. Xie, F.; Stewart, C.N., Jr.; Taki, F.A.; He, Q.; Liu, H.; Zhang, B. High-throughput deep sequencing shows that microRNAs play important roles in switchgrass responses to drought and salinity stress. *Plant Biotechnol. J.* **2014**, *12*, 354–366. [CrossRef]
173. Gharat, S.A.; Shaw, B.P. Novel and conserved miRNAs in the halophyte *Suaeda maritima* identified by deep sequencing and computational predictions using the ESTs of two mangrove plants. *BMC Plant Biol.* **2015**, *15*, 301. [CrossRef]
174. Xu, T.; Zhang, L.; Yang, Z.; Wei, Y.; Dong, T. Identification and functional characterization of Plant miRNA under salt stress shed light on salinity resistance improvement through miRNA manipulation in crops. *Front. Plant Sci.* **2021**, *12*, 665439. [CrossRef]
175. Alzahrani, S.M.; Alaraidh, I.A.; Khan, M.A.; Migdadi, H.M.; Alghamdi, S.S.; Alsahli, A.A. Identification and characterization of salt-responsive microRNAs in *Vicia faba* by high-throughput sequencing. *Genes* **2019**, *10*, 303. [CrossRef]
176. Zhang, Q.; Zhao, C.; Li, M.; Sun, W.; Liu, Y.; Xia, H. Genome-wide identification of *Thellungiella salsuginea* microRNAs with putative roles in the salt stress response. *BMC Plant Biol.* **2013**, *13*, 180. [CrossRef] [PubMed]
177. Sun, X.; Xu, L.; Wang, Y.; Yu, R.; Zhu, X.; Luo, X. Identification of novel and salt-responsive miRNAs to explore miRNA-mediated regulatory network of salt stress response in radish (*Raphanus sativus* L.). *BMC Genom.* **2015**, *16*, 197. [CrossRef] [PubMed]
178. Luan, M.; Xu, M.; Lu, Y.; Zhang, L.; Fan, Y.; Wang, L. Expression of zma-miR169 miRNAs and their target ZmNF-YA genes in response to abiotic stress in maize leaves. *Gene* **2015**, *55*, 178–185. [CrossRef]
179. Yuan, S.; Li, Z.; Li, D.; Yuan, N.; Hu, Q.; Luo, H. Constitutive expression of rice microRNA528 alters plant development and enhances tolerance to salinity stress and nitrogen starvation in creeping bentgrass. *Plant Physiol.* **2015**, *169*, 576–593. [CrossRef]
180. Yuan, S.; Zhao, J.; Li, Z.; Hu, Q.; Yuan, N.; Zhou, M. MicroRNA396-mediated alteration in plant development and salinity stress response in creeping bentgrass. *Hortic. Res.* **2019**, *6*, 48. [CrossRef] [PubMed]
181. Wu, Y.; Guo, J.; Cai, Y.; Gong, X.; Xiong, X.; Qi, W. Genome-wide identification and characterization of *Eutrema salsugineum* microRNAs for salt tolerance. *Physiol. Plant* **2016**, *157*, 453–468. [CrossRef]
182. Chiang, C.P.; Yim, W.C.; Sun, Y.H.; Ohnishi, M.; Mimura, T.; Cushman, J.C. Identification of ice plant (*Mesembryanthemum crystallinum* L.) microRNAs using RNA-seq and their putative roles in high salinity responses in seedlings. *Front. Plant Sci.* **2016**, *7*, 1143. [CrossRef]
183. Yang, R.; Zeng, Y.; Yi, X.; Zhao, L.; Zhang, Y. Small RNA deep sequencing reveals the important role of microRNAs in the halophyte *Halostachys caspica*. *Plant Biotechnol. J.* **2015**, *13*, 395–408. [CrossRef]

plants

MDPI

Article

Conserved and Diverse Transcriptional Reprogramming Triggered by the Establishment of Symbioses in Tomato Roots Forming *Arum*-Type and *Paris*-Type Arbuscular Mycorrhizae

Takaya Tominaga [1], Luxi Yao [2], Hikaru Saito [2] and Hironori Kaminaka [2,*]

[1] The United Graduate School of Agricultural Science, Tottori University, Tottori 680-8553, Japan; d20a1007c@edu.tottori-u.ac.jp
[2] Faculty of Agriculture, Tottori University, Tottori 680-8553, Japan; jpsmartlucy168@gmail.com (L.Y.); b18a5077y@edu.tottori-u.ac.jp (H.S.)
* Correspondence: kaminaka@tottori-u.ac.jp; Tel.: +81-857-31-5378

Abstract: Arbuscular mycorrhizal (AM) fungi allocate mineral nutrients to their host plants, and the hosts supply carbohydrates and lipids to the fungal symbionts in return. The morphotypes of intraradical hyphae are primarily determined on the plant side into *Arum*- and *Paris*-type AMs. As an exception, *Solanum lycopersicum* (tomato) forms both types of AMs depending on the fungal species. Previously, we have shown the existence of diverse regulatory mechanisms in *Arum*- and *Paris*-type AM symbioses in response to gibberellin (GA) among different host species. However, due to the design of the study, it remained possible that the use of different plant species influenced the results. Here, we used tomato plants to compare the transcriptional responses during *Arum*- and *Paris*-type AM symbioses in a single plant species. The tomato plants inoculated with *Rhizophagus irregularis* or *Gigaspora margarita* exhibited *Arum*- and *Paris*-type AMs, respectively, and demonstrated similar colonization rates and shoot biomass. Comparative transcriptomics showed shared expression patterns of AM-related genes in tomato roots upon each fungal infection. On the contrary, the defense response and GA biosynthetic process was transcriptionally upregulated during *Paris*-type AM symbiosis. Thus, both shared and different transcriptional reprogramming function in establishing *Arum*- and *Paris*-type AM symbioses in tomato plants.

Keywords: arbuscular mycorrhizal symbiosis; comparative transcriptomics; *Arum*-type; *Paris*-type; *Solanum lycopersicum*; *Rhizophagus irregularis*; *Gigaspora margarita*

Citation: Tominaga, T.; Yao, L.; Saito, H.; Kaminaka, H. Conserved and Diverse Transcriptional Reprogramming Triggered by the Establishment of Symbioses in Tomato Roots Forming *Arum*-Type and *Paris*-Type Arbuscular Mycorrhizae. *Plants* **2022**, *11*, 747. https://doi.org/10.3390/plants11060747

Academic Editors: Milan S. Stankovic, Paula Baptista and Petronia Carillo

Received: 2 February 2022
Accepted: 9 March 2022
Published: 11 March 2022

Publisher's Note: MDPI stays neutral with regard to jurisdictional claims in published maps and institutional affiliations.

1. Introduction

Approximately 80% of terrestrial plants establish a symbiotic relationship with Glomeromycotina fungi; this relationship is referred to as arbuscular mycorrhizal (AM) symbiosis [1]. Recently, how host plants and AM fungi communicate in the rhizosphere has been elucidated. AM fungal-derived short-chain chitooligosaccharides (COs) and lipo-chitooligosaccharides (LCOs) activate symbiotic signaling in host plants together with some receptor-like kinases (RLKs) [2–5]. Although AM fungal colonization triggers transient and weak defense responses in the host plants, AM fungi are known to exude some signal components to suppress plant immunity [6–9]. On the contrary, host plant roots exude strigolactones (SLs) to inform AM fungi of their presence and promote fungal growth [10,11]. SLs are classified as phytohormones and enzymatically biosynthesized from all-trans-β-carotene by DWARF 27 (D27), CAROTENOID CLEAVAGE DIOXYGENASE 7 (CCD7), CCD8, and MORE AXILLARY GROWTH 1 (MAX1) [12,13]. After AM fungi reach the host roots, some AM-specific reprogramming begins in the host root cells. For instance, several studies have demonstrated AM-promoted expression of some symbiotic genes, namely, *PHOSPHATE TRANSPORTER 4* (*PT4*) and *AMMONIUM TRANSPORTER 2;3* (*AMT2;3*) for symbiotic phosphate and ammonium transport, *REDUCED ARBUSCULAR*

MYCORRHIZA 2 (*RAM2*) and G-type ABC transporters (*STR/STR2*) for lipid production and transport, and *VAPYRIN* (*VPY*) for arbuscule development [14–19]. These AM-related genes are transcriptionally activated by several transcription factors, such as RAM1 and REQUIRED FOR ARBUSCULE DEVELOPMENT 1 (RAD1), which belong to the GRAS, GIBBERELLIC-ACID INSENSITIVE (GAI), REPRESSOR of GAI (RGA), and SCARECROW (SCR) transcription factor families [20–24]. These are known to localize on the host-derived peri-arbuscular membrane surrounding arbuscules in highly branched hyphal structures formed in root cortical cells [25].

Depending mainly on the host plant species, the mutualism established results in either *Arum*- or *Paris*-type hyphal structures of intraradical AM fungi [26–30]. In *Arum*-type AM, AM fungal hyphae elongate in the apoplastic space of plant cells and form arbuscules in the cortical cells. *Paris*-type AM is characterized by intracellular hyphal elongation and hyphal coils in the host cortical cells. Despite the distinct AM morphologies, the reasons why AM morphotypes vary among host plants has been unclear. In addition, how host plants differentially regulate AM symbioses for each AM morphotype is not fully understood.

To elucidate these enigmas, we have recently compared the regulatory mechanisms underlying *Arum*- and *Paris*-type AM symbioses using several phylogenetically distant host species [31,32]. Interestingly, the phytohormone gibberellin (GA) promotes the establishment of *Paris*-type AM symbiosis in *Eustoma grandiflorum* and *Primula malacoides* [31], whereas GA suppresses *Arum*-type AM symbiosis in legume plants and rice [33–36]. Notably, one of our previous studies demonstrated that AM fungal colonization transcriptionally promotes conserved symbiotic genes such as *STR* and *RAM1* among three host plants forming distinct AM morphotypes [32]. This previous study also showed that GA treatment alters the transcriptional responses of the symbiotic genes among the examined host plants. These studies lead us to predict that host plants have evolved to change the upstream mechanisms that regulate AM symbioses according to AM morphotype. However, previous comparative analysis on *Arum*- and *Paris*-type AM symbioses cannot thoroughly investigate our hypothesis due to the possibility that the use of different plant species influenced the results. For a more precise comparison of *Arum*- and *Paris*-type AM symbiosis regulation, a single host plant that forms both types of AMs is needed to overcome these issues.

Interestingly, *Solanum lycopersicum* (tomato) mainly has *Arum*-type AM in response to Glomeraceae fungi, such as *Rhizophagus irregularis* (formerly *Glomus intraradices*) and *Paris*-type AM, in response to Gigasporaceae fungi, such as *Gigaspora margarita* [6,37]. Here, we conducted comparative analyses on *Arum*- and *Paris*-type AM symbioses in tomato roots colonized by *R. irregularis* and *G. margarita*. *R. irregularis* and *G. margarita* infection showed *Arum*- and *Paris*-type AMs in tomato roots, respectively, and significantly promoted tomato shoot growth. In addition, transcriptome profiling of the tomato roots showed that colonization by either AM fungus triggered some shared transcriptional reprogramming in AM-related genes and the SL biosynthetic pathway in tomato roots. On the contrary, the immune response and the GA biosynthetic process were transcriptionally upregulated in *Paris*-type AM symbiosis in tomato roots. Therefore, our comparative transcriptomics identified both shared and different reprogramming in a single host species during *Arum*- and *Paris*-type AM symbioses.

2. Results

2.1. Comparison of Symbiotic Phenotypes in Tomato Plants Forming Distinct AM Morphotypes

Tomato mycorrhizal roots were sectioned and then subjected to microscopical observation of the AM fungal morphotypes of *R. irregularis* and *G. margarita* in tomato roots. Tomato roots colonized by *R. irregularis* had fungal hyphae in the intercellular space and arbuscules emerged from the intercellular hypha in the cortical cells (Figure 1a) in a manner typical of *Arum*-type AM. On the contrary, *G. margarita* infection exhibited classic *Paris*-type AM with a thick and clear hyphal coil to which the arbuscule adhered and intracellular

hyphal elongation in the tomato root cortex (Figure 1b). As several reports have demonstrated [37–39], we confirmed that AM fungal traits determine the AM morphotypes of tomato plants under the same growth conditions.

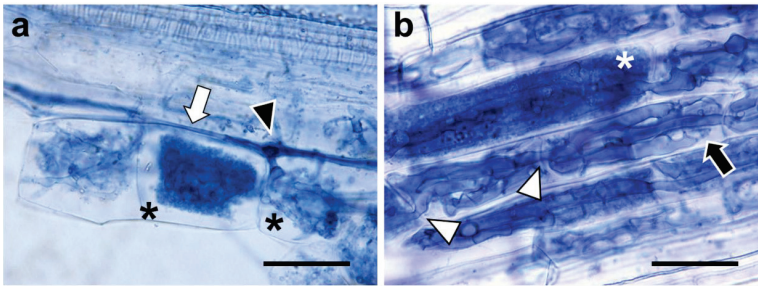

Figure 1. Arbuscular mycorrhizal (AM) morphotypes formed in tomato roots colonized by *Rhizophagus irregularis* or *Gigaspora margarita*. Tomato roots inoculated with *R. irregularis* (**a**) or *G. margarita* (**b**) were collected five weeks post-inoculation (wpi). The collected root samples were stained with 0.05% trypan blue. Scales: 20 μm. White arrow, intercellular hypha; black arrowhead, intercellular hypha penetrating the tomato cortical cell; asterisks, arbuscules; black arrow, hyphal coil; white arrowheads, intracellular hypha penetrating the adjacent tomato cortical cells.

Next, we compared the root colonization levels of the two AM fungi (Figure 2a). The quantification of AM fungal colonization revealed that the colonization rates of *G. margarita* were slightly lower than those of *R. irregularis*, although there was no statistical significance in Welch's *t*-test. In addition, the fresh weight of the tomato shoots was significantly increased by the colonization of both *R. irregularis* and *G. margarita* at five weeks post-inoculation (wpi) (Figure 2b). Taken together, the symbiotic phenotypes were comparable to each other, except for the AM morphotype.

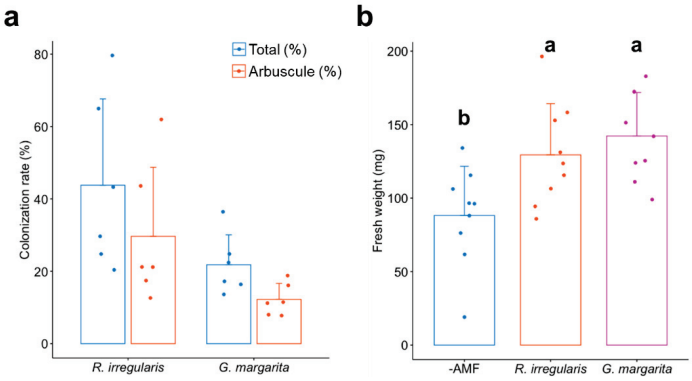

Figure 2. Quantification of AM fungal colonization rates and AM-promoted shoot growth of tomato plants. (**a**) The fungal colonization rates of *Rhizophagus irregularis* or *Gigaspora margarita* in tomato roots at five weeks post-inoculation (wpi). Total (%), the percentage of all hyphal structures observed in the tomato roots; arbuscule (%), the rate of arbuscules formed in the cortical cells. There is no statistically significant difference in the colonization rates between *R. irregularis* and *G. margarita* in Welch's *t*-test. The error bars show the standard errors (n = 6). (**b**) The shoot fresh weight of tomato colonized by *R. irregularis* and *G. margarita* at five wpi. AMF, non-colonized tomato roots; *R. irregularis*, *R. irregularis*-colonized roots; *G. margarita*, *G. margarita*-colonized roots. The bars and dots indicate the average and individual values, respectively. The error bars indicate the standard errors (n = 9). The different letters indicate statistical significance ($p < 0.05$) in analysis of variance (ANOVA) with a post hoc Tukey-Kramer test.

2.2. Comparative Transcriptomics of Tomato Mycorrhizal Roots Accommodating Different AM Fungi

Next, we conducted comparative transcriptomics between tomato roots separately colonized by *R. irregularis* and *G. margarita* to elucidate the regulatory mechanisms underlying *Arum*- and *Paris*-type AM symbioses. Our RNA-sequencing resulted in a minimum of 13 million and a maximum of 20 million raw sequence reads after trimming (Table S1). More than 80% of the filtered reads were uniquely mapped against the reference genome sequence of tomato [40]. The numbers of upregulated and downregulated differentially expressed genes (DEGs) in tomato mycorrhizae relative to non-colonized roots were 440 and 343, respectively (Figure 3a,b, Table S2). A comparison of DEGs between *R. irregularis*- and *G. margarita*-infected root samples revealed that the expression levels of 40.2% of genes were commonly promoted in both AM fungal colonizations compared with non-colonized roots (Figure 3a,c). In addition, 9.8% and 50.0% of the AM-upregulated DEGs were specific to *R. irregularis* and *G. margarita*, respectively (Figure 3a,c). On the contrary, AM-suppressed DEGs were primarily different between *R. irregularis*- and *G. margarita*-infected tomato roots (Figure 3b,c).

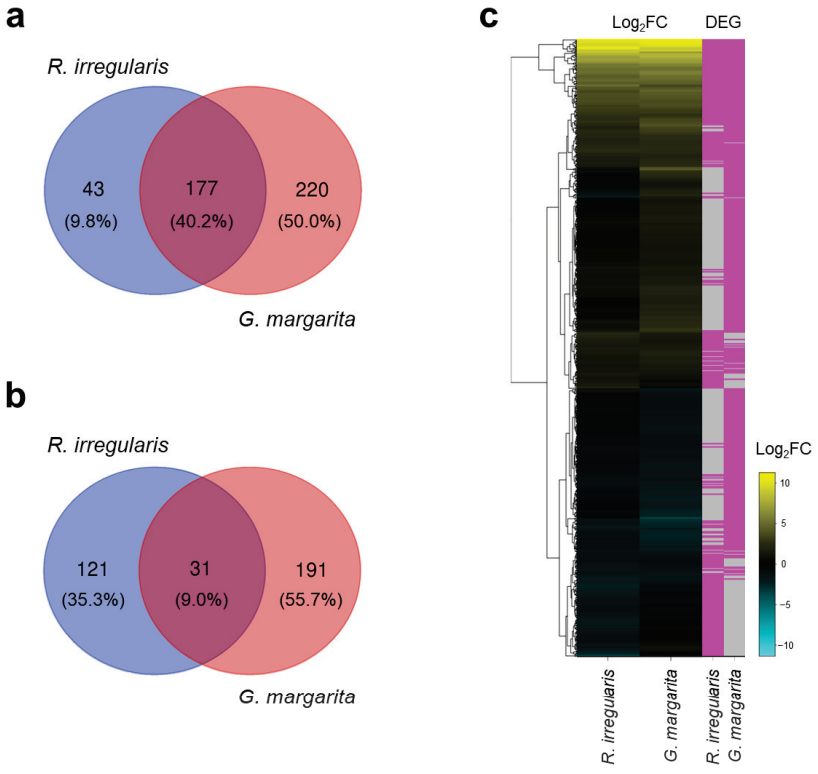

Figure 3. Differential expression analysis of tomato roots colonized by *Rhizophagus irregularis* or *Gigaspora margarita*. (**a**,**b**) Venn diagram of 440 AM-upregulated (**a**) and 343 AM-suppressed (**b**) genes compared with non-colonized roots at five weeks post-inoculation (wpi). Genes with $|\text{Log}_2\text{Fold Change (FC)}| > 1$ and a false discovery rate (FDR) < 0.05 were considered differentially expressed genes (DEGs). (**c**) Hierarchical clustering of the total AM-responsive DEGs. The left-hand heatmap shows the Log_2FC of genes expressed in colonized tomato roots relative to non-colonized roots. Blue indicates negative values; yellow, positive values; and black, zero change. The right-hand heatmap illustrates FDR values less than 0.05, with significant DEGs presented in pink. Detailed information about the DEGs can be found in Table S2.

Gene ontology (GO) enrichment analysis was conducted to gain insight into how tomato plants respond to the associating AM fungi (Figure 4, Table S3). Since half of AM-upregulated DEGs was shared between *R. irregularis*- and *G. margarita*-colonized roots, we first examined the enriched GO terms in the common DEGs. We found that some GO terms related to the lipid biosynthesis and transport, and SL production was significantly enriched during association with both AM fungi (Figure 4a). On the contrary, AM-upregulated DEGs specific to *G. margarita* had enriched GO terms related to immune response, such as the response to biotic stimuli, systemic acquired resistance, and cellular response to reactive oxygen (Figure 4b). Interestingly, GA biosynthesis in tomato roots was also transcriptionally upregulated upon *G. margarita* infection. Since the number of DEGs unique to *R. irregularis* was not sufficient for enrichment analysis, the GO terms were not analyzed.

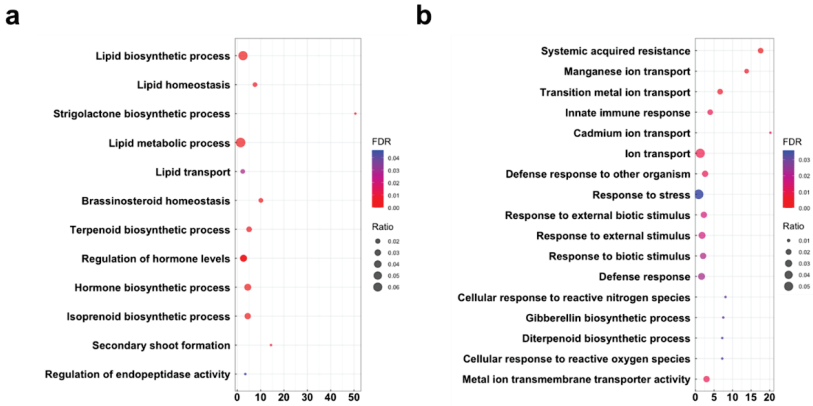

Figure 4. Gene ontology (GO) enrichment analysis on AM-upregulated genes. (**a**) GO terms enriched in the upregulated DEGs shared between tomato roots colonized by *Rhizophagus irregularis* or *Gigaspora margarita*. (**b**) GO terms enriched in DEGs upregulated only in roots infected by *G. margarita.* The representative GO terms obtained from the tested DEGs are listed. Bigger circles in the hierarchical clustering trees represent more genes annotated to the respective GO terms. The right-hand color bars indicate *p* values (< 0.05). Detailed information is presented in Table S3.

We also conducted GO enrichment analysis for AM-suppressed DEGs (Figure 3b, Table S3). Among the shared DEGs downregulated in tomato roots colonized by *R. irregularis* or *G. margarita*, some GO terms corresponding to defense-related functions were again observed with statistical significance (Table S3). In addition, the GO terms associated with response to chitin and the salicylic acid biosynthetic process were significantly and uniquely detected in *R. irregularis*- and *G. margarita*-specific downregulated DEGs, respectively (Table S3).

2.3. Expression Patterns of AM-, SL-, and Defense-Related Genes in Tomato Roots against Different AM Fungal Colonizations

Several GO terms corresponding to membrane transport, lipid biosynthesis, and SL production were significantly enriched in the shared AM-upregulated DEGs. Therefore, we studied the expression pattern of AM- and SL-related genes upon different AM fungal colonizations. For this analysis, we selected *S. lycopersicum PT4* (*SlPT4*), *SlAMT2;3*, *SlRAM1*, *SlRAD1*, *SlRAM2*, *SlSTR*/*SlSTR2*, and *SlVpy* (Table S4). AM fungal colonization significantly upregulated the transcription of all the selected genes irrespective of the associating fungal species (Figure 5a, Table S4). These results were in line with our GO enrichment analysis.

Next, we analyzed the expression patterns of SL-related genes upon AM fungal colonization. For the analysis, we selected *SlD27*, *SlCCD7*, *SlCCD8*, and *SlMAX1* for the

SL biosynthetic process and *SlD14*, *SlKAI2*, and *SlDLK2* for SL perception and signaling (Table S4) [41,42]. The expression levels of *SlD14* and *SlKAI2* were comparable to levels in non-colonized tomato roots (Figure 5b, Table S4). On the contrary, all of the selected SL biosynthetic genes and *SlDLK2* were transcriptionally upregulated by *R. irregularis* or *G. margarita* infection relative to the non-colonized roots (Figure 5b, Table S4). Together, these expression patterns of selected genes were consistent with the results of the GO enrichment analysis on the common AM-upregulated DEGs (Figure 4).

Since our GO enrichment analysis also revealed transcriptional changes in defense-related pathways (Figure 4b, Table S4), the expression patterns of the corresponding genes were investigated. We determined that genes functioning in "systemic acquired resistance" and "cellular response to reactive oxygen species (ROS)" were specifically expressed upon *G. margarita* infection (Figure 5c). In addition, the gene expression patterns associated with "response to chitin" and "salicylic acid biosynthetic process" were consistent with the GO enrichment analysis (Figure 5c, Table S4). On the contrary, the expression levels of some genes involved in "defense response to other organism" and "antibiotic metabolic process" were commonly decreased by each AM fungal colonization (Figure 5c, Table S4). These results indicate that *R. irregularis* suppressed defense responses in tomato roots, whereas *G. margarita* also stimulated some parts of the immune pathways.

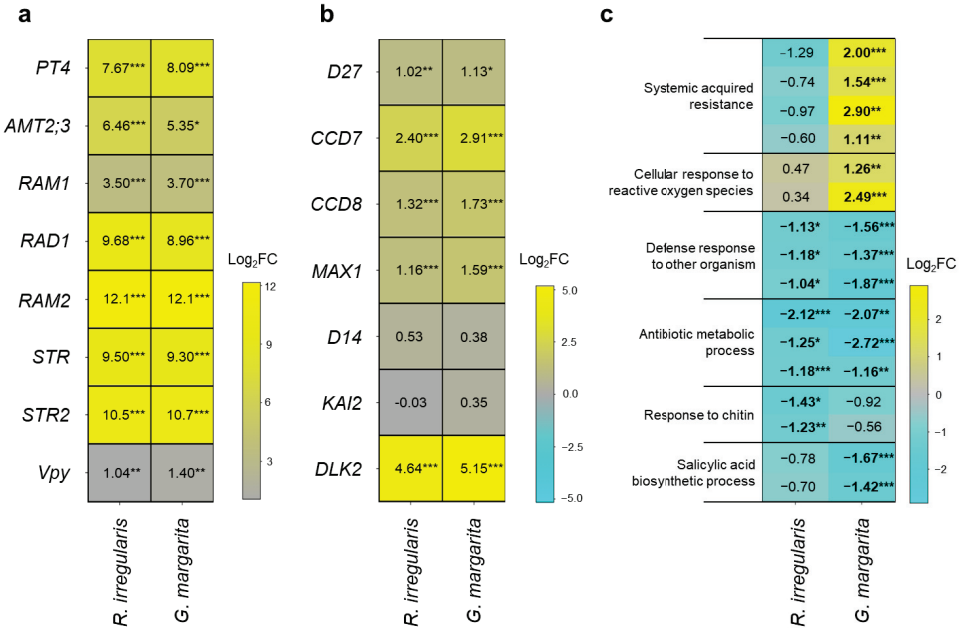

Figure 5. Expression patterns of AM-, strigolactone (SL)-, and defense-related genes during AM symbioses established by different AM fungi in tomato roots. At five weeks post-inoculation (wpi), the transcriptional response of the selected tomato genes against *Rhizophagus irregularis* or *Gigaspora margarita* colonization was analyzed. Log_2-transformed fold changes (FC) of AM-related (**a**) and SL-related (**b**) genes versus the non-colonized roots are presented in each left-hand heatmap. (**c**) The expression patterns of DEGs involved in the defense-related pathways (Figure 4b, Table S3). The calculated values are written on the heatmaps. The Log_2FC values of DEGs are shown in bold. Asterisks indicate the significance in the Log_2FC (*: false discovery rate (FDR) < 0.05, **: FDR < 0.01, and ***: FDR < 0.001). The Log_2FC and FDR values are listed in Table S4.

3. Discussion

AM morphotypes are known to change depending mainly on host traits. In previous studies, we used several host species and one AM fungal species to compare the molecular mechanisms underlying AM symbioses forming different morphotypes [31,32]. In this study, we focused on the transcriptional responses occurring in a single host species, tomato, associating with two AM fungi, namely, *R. irregularis* and *G. margarita*. Our findings revealed some shared and different transcriptional responses in tomato roots when the associating fungi and resulting AM morphotypes are distinct.

3.1. Shared Transcriptional Reprogramming upon Different AM Fungal Colonizations

This study found some shared transcriptional programs during AM symbioses in tomato roots colonized with *R. irregularis* or *G. margarita*. Membrane transport and lipid biosynthesis were transcriptionally activated in mycorrhizae accommodating *R. irregularis* or *G. margarita* (Figure 4a, Table S3). These results indicate that the nutrient exchange between the host plants and fungal symbionts is activated, which contributes to symbiotic growth promotion in tomato plants (Figure 2b). In line with these findings, the expression levels of several symbiosis-related genes required for phosphate transport (*SlPT4*), ammonium transport (*SlAMT2;3*), lipid production and transport (*SlRAM2*, *SlSTR*, *SlSTR2*), and *GRAS* transcription factors regulating these symbiotic genes (*SlRAM1*, *SlRAD1*) were commonly and significantly increased by both AM fungal colonizations (Figure 5a, Table S4). These findings indicate that the symbiotic exchange of nutrients between tomatoes and AM fungi is irrespective of AM morphotype. As for *SlVpy*, both *R. irregularis* and *G. margarita* infections enhanced the expression levels of *SlVpy*. This result indicates that *SlVpy* is necessary for the development of arbuscule in both *Arum*- and *Paris*-type AMs.

Our transcriptome analysis also revealed another shared transcriptional reprogramming upon AM fungal colonization, the SL biosynthetic process. *R. irregularis* and *G. margarita* colonization transcriptionally upregulated all selected genes for SL production at five wpi (Figure 5b, Table S4). These results were consistent with our GO enrichment analysis (Figure 4a). Moreover, the expression of *SlDLK2* was also upregulated by the two AM fungi (Figure 5b, Table S4). Recent work has elucidated the involvement of *SlDLK2* in the negative regulation of arbuscule branching [43]. In addition to AM-upregulated *SlVpy* expression, the mechanisms underlying arbuscule formation would be shared in *Arum*- and *Paris*-type AMs.

3.2. Specific Responses to Paris-Type AM Symbiosis

With respect to the different responses of tomato to AM fungal species, some genes involved in biotic stimuli such as the defense response to a pathogen and ROS were transcriptionally upregulated during *Paris*-type AM symbiosis established by *G. margarita* (Figure 4b, Table S3). In general, the perception of pathogen-associated molecular patterns, such as chitin, by pattern recognition receptors (PRRs) and penetration of the plant cell wall, triggers ROS production and transcriptional activation of some defense-responsive genes [44,45]. In addition, the disruption of the plant cell wall by pathogen penetration releases oligomeric fragments of plant cell wall polysaccharides, referred to as damage-associated molecular patterns (DAMPs), and can cause PRR-mediated local defense responses [46]. Taken together, the continuous invasion of *G. margarita* hyphae into tomato cortical cells in *Paris*-type AM roots might promote ROS production by increasing DAMPs.

Interestingly, a previous study has demonstrated that colonization by Gigasporaceae fungi in tomato (*S. lycopersicum* cv. 76R) roots results in high but transient expression levels of some defense-related genes, such as *PATHOGENESIS-RELATED PROTEIN 1* (*PR-1*) and extracellular acidic chitinase (*CHI3*) [6]. On the contrary, Gao et al. (2004) showed that relatively weak accumulations of defense-related genes are observed in tomato roots forming *Arum*-type AM with the Glomeraceae family, such as *R. irregularis* and *Glomus mosseae*. Therefore, the continuous invasion of intracellular hyphae of *G. margarita* forming *Paris*-type AM roots possibly activates biotic responses in tomato roots. In fact, we found

that *G. margarita* colonization significantly upregulated some defense pathways in tomato roots (Figures 4b and 5c, Tables S3 and S4).

Nevertheless, our study demonstrated that *G. margarita* could colonize tomato roots comparably to *R. irregularis* (Figure 2a). Recent studies have shown that LCOs, CO4, and several small, secreted proteins derived from AM fungi alleviate the immune responses in host plants [3,5,9,47], which are consistent with the AM-suppressed chitin response and salicylic acid biosynthesis (Figure 5c, Table S3). These findings lead us to predict that AM fungal chitin oligomers and/or effectors might enable the two fungi to effectively colonize tomato plants by compromising defense responses, which might show comparable fungal colonization in tomato roots (Figure 2a). In addition, the function of SAR- and ROS-related genes whose expression levels were increased by *G. margarita* infection might be irrelevant or insufficient to inhibit fungal colonization. These ideas need further investigation.

Some GO terms associated with manganese or divalent metal transport were enriched within DEGs in *G. margarita*-colonized roots (Figure 4b, Table S3). One of the annotated genes, Solyc02g092800.3, is known as *Natural Resistance-Associated Macrophage Protein 1* (*NAMP*) metal transporter [48]. The *NRAMP* genes in legume plants have been reported to be transcriptionally upregulated in root nodules and localized on the peribacteroid membrane, where host plants and rhizobia exchange nutrients [49,50]. Therefore, tomato plants could take up divalent metals, such as iron and manganese, from intraradical *G. margarita* hyphae and utilize them for their growth.

3.3. Transcriptional Activation of the GA Biosynthetic Process

Our previous work demonstrated that bioactive GA production is upregulated in *E. grandiflorum Paris*-type AMs [31]. AM-promoted bioactive GA accumulation has also been reported in *Lotus japonicus* forming *Arum*-type AM roots [34]. However, our GO enrichment analysis revealed transcriptional upregulation of the GA biosynthetic process only in tomato roots forming *Paris*-type AM with *G. margarita* (Figure 4b, Table S3). In addition, we found that *Paris*-type AM symbiosis in *E. grandiflorum* and *Primula malacoides* is promoted by exogenous GA treatment [31]. Taken together, bioactive GAs might contribute to the establishment of *Paris*-type AM symbiosis in tomatoes colonized by *G. margarita*; however, this hypothesis needs to be investigated further.

4. Materials and Methods

4.1. Biological Materials and Growth Conditions

Seeds of *Solanum lycopersicum* L. cv. Micro-Tom were obtained from the University of Tsukuba, Tsukuba Plant Innovation Research Center, through the National Bio-Resource Project. The seeds were cleaned with 70% ethanol and then rinsed twice with sterilized distilled water. The pre-washed seeds were immersed and agitated in 1.5% (*v*/*v*) NaClO solution for 15 min. After the solution was removed, the seeds were set on two pieces of filter paper in a light chamber at 24 °C and a 14-h light/10-h dark/light cycle and incubated for six days. Spores of *Gigaspora margarita* MAFF520052 were obtained from the Genebank Project (National Agriculture and Food Research Organization, Japan) and sterilized in 0.1% (*v*/*v*) NaClO and 0.04% (*v*/*v*) Tween-20 for 15 min, followed by replacement of the solution with sterilized distilled water. *Rhizophagus irregularis* DAOM197198 spores were purchased from Premier Tech (Quebec, Canada).

For the inoculation of six-day-old tomato seedlings with *R. irregularis*, 50 mL of 1/5 strength Hoagland solution (20-μM inorganic phosphate) containing 3000 spores was poured into a washed and autoclaved (121 °C for 20 min) 300-mL soil mixture of river sand and shibanome soil (2:1, *v*:*v*). Three tomato seedlings were then transplanted to the soil mixture. Each six-day-old tomato seedling was directly inoculated with 20 *G. margarita* spores. The inoculated seedlings were grown under the same conditions for five weeks. Subsequently, the lateral roots were harvested, and the fresh weight of shoots was measured.

4.2. Observation and Quantification of Mycorrhizal Roots

AM fungal colonization was quantified by staining the root samples with trypan blue and microscopically observing them as previously reported [31]. Briefly, mycorrhizal roots were fixed in a FAA solution (5% formaldehyde, 5% acetic acid, and 45% ethanol [v/v]), rinsed twice with distilled water. The fixed root samples were heated at 90 °C for 15 min and neutralized in 2% HCl solution. Subsequently, the root samples were immersed in trypan blue diluted by lactic acid at 0.05% and heated at 90 °C for 15 min. The stained samples were sliced with a scalpel under a SZX16 stereomicroscope (Olympus, Tokyo, Japan), and images were taken using a BX53 light microscope (Olympus) equipped with a digital camera (DP27; Olympus).

4.3. Extraction of RNA from Tomato Roots

To conduct transcriptome analysis by RNA-sequencing (RNA-seq), we prepared RNA samples from fresh tomato roots. The lateral roots from three seedlings in a nuclease-free tube (INA-OPTIKA, Osaka, Japan) containing two 5-mm beads were frozen in liquid nitrogen and then homogenized in a ShakeMan6 (Bio-Medical Science, Tokyo, Japan); afterward, 450 µL of Fruit-mate for RNA Purification (Takara Bio, Shiga, Japan) was added to each tube. After thoroughly mixing the tubes, the slurry was transferred to another tube and centrifuged at 12,000× g at 4 °C for 5 min. The supernatant was mixed with 450-µL ethanol and RNAiso Plus (Takara) in a new tube. The genomic DNA-free total RNA was prepared using a Zymo-spin IIICG Column (Zymo Research, Orange, CA, USA). The column membrane was treated with DNaseI (Takara) before extracting the RNA according to the manufacturer's protocols. The purity and quantity of total RNA were measured at 260 and 280 nm ($A260$: $A280$) using DeNovix DS-11 + (Scrum, Tokyo, Japan). The prepared samples were stored at −80 °C until use.

4.4. RNA-seq, Data Analysis, and Gene Identification

The library preparation and RNA-seq were performed by Genewiz (Tokyo, Japan) using DNBSEQ-G400 and resulted in more than 14 million strand-specific paired-end (2 × 150 bp) reads per sample (Table S1). The obtained raw reads were filtered (<QV30), and the adapter sequence was trimmed using Fastp [51]. The purified single-end reads were mapped to tomato genome sequence version SL4.0 and annotation ITAG4.0 built by the International Tomato Genome Sequencing Project (https://solgenomics.net/organism/Solanum_lycopersicum/genome, accessed on 2 December 2021) using the STAR program [52]. The resulting data were processed with featureCounts v1.6.4 [53] to quantify gene expression. Then, we extracted the DEGs using the EdgeR package [54] in the R software v4.0.2. In this study, genes with FDR < 0.05 were considered DEGs. In addition, the GO terms significantly enriched within the DEG datasets were identified using Shiny GO v0.61 [55]. Tomato genes with zero count in at least one of the root samples were removed before expression pattern and GO enrichment analyses. To investigate the effects of *R. irregularis* and *G. margarita* infections on the expression of AM symbiosis- or SL-related genes, we selected several tomato genes required for the mutualism. To this end, known genes in *M. truncatula* and *Arabidopsis thaliana* were used as queries for tBLASTx searches in the Sol Genomics Network using the default setting (Table S4). Raw nucleotide sequence data from this study are available from the DDBJ Sequence Read Archive under accession number DRA013369.

4.5. Biological Replicates, Statistical Analysis, and Heatmap Production

To quantify the root colonization rate (%), we considered ten pieces of root fragment from one tomato sample on a microscope slide as one biological replicate. When preparing a sample for RNA-seq, one pool of total RNA extracted from three seedlings was one biological replicate. Finally, we used three RNA samples for the RNA-seq. Statistical analysis was conducted in the R software v4.0.2. Welch's t-test and analysis of variance (ANOVA) followed by a post hoc Tukey-Kramer test were applied for the colonization

rates and shoot fresh weight, respectively. The R package heatmaply was used to draw the heatmaps [56].

5. Conclusions

We found some common AM-specific transcriptional programs for the membrane transport, arbuscule development, and SL biosynthetic pathway in *Arum*- and *Paris*-type AM symbioses in tomato roots. These similarities indicate that the primary and downstream mechanisms for accommodating AM fungi would be common, irrespective of the AM morphotype. In addition, our study demonstrated that the colonization of phylogenetically distant AM fungi differentially affected the defense-related pathways and GA biosynthetic process in tomato roots. These different transcriptional responses would enable tomatoes to fine-tune the mutualism between tomato roots and diverse AM fungi to optimize the host growth. In addition, the upstream regulation underlying *Arum*- and *Paris*-type AM symbioses in tomato plants might be differentially modulated by GA. Further investigation of how GA regulates *Paris*-type AM symbiosis established by tomato roots and *G. margarita* would improve our understanding of the regulatory mechanisms underpinning AM symbioses.

Supplementary Materials: The following supporting information can be downloaded at: https://www.mdpi.com/article/10.3390/plants11060747/s1, Table S1: Results of RNA-sequencing, read mapping, and read count; Table S2: Information of symbiosis-responsive DEGs; Table S3: Gene ontology enrichment analysis on tomato mycorrhizae; Table S4: Blastp results and expression patterns of genes listed in Figure 5.

Author Contributions: Conceptualization, T.T. and H.K.; methodology, T.T., L.Y. and H.S.; investigation, T.T., L.Y. and H.S.; writing—original draft preparation, T.T.; writing—review and editing, T.T. and H.K.; visualization, T.T. and L.Y.; supervision, T.T. and H.K.; funding acquisition, T.T and H.K. All authors have read and agreed to the published version of the manuscript.

Funding: This work was partially supported by the NIBB Cooperative Research Programs (Next-generation DNA Sequencing Initiative: 20-407, 21-301) and JSPS KAKENHI Grant-in-Aid for JSPS Fellows (Grant No. 20J21994) to T.T.

Institutional Review Board Statement: Not applicable.

Informed Consent Statement: Not applicable.

Data Availability Statement: The nucleotide sequence data obtained from our RNA sequencing has been deposited into the DDBJ Sequence Read Archive under the accession number DRA013369.

Acknowledgments: Tomato seeds (TOMJPX00001) were provided by the University of Tsukuba, Tsukuba Plant Innovation Research Center, through the National Bio-Resource Project (NBRP) of the Japan Agency for Research and Development (AMED), Japan.

Conflicts of Interest: The authors declare no conflict of interest.

References

1. Brundrett, M.C.; Tedersoo, L. Evolutionary history of mycorrhizal symbioses and global host plant diversity. *New Phytol.* **2018**, *220*, 1108–1115. [CrossRef] [PubMed]
2. Genre, A.; Chabaud, M.; Balzergue, C.; Puech-Pages, V.; Novero, M.; Rey, T.; Fournier, J.; Rochange, S.; Becard, G.; Bonfante, P.; et al. Short-chain chitin oligomers from arbuscular mycorrhizal fungi trigger nuclear Ca2+ spiking in Medicago truncatula roots and their production is enhanced by strigolactone. *New Phytol.* **2013**, *198*, 190–202. [CrossRef] [PubMed]
3. Feng, F.; Sun, J.; Radhakrishnan, G.V.; Lee, T.; Bozsoki, Z.; Fort, S.; Gavrin, A.; Gysel, K.; Thygesen, M.B.; Andersen, K.R.; et al. A combination of chitooligosaccharide and lipochitooligosaccharide recognition promotes arbuscular mycorrhizal associations in Medicago truncatula. *Nat. Commun.* **2019**, *10*, 5047. [CrossRef] [PubMed]
4. He, J.; Zhang, C.; Dai, H.; Liu, H.; Zhang, X.; Yang, J.; Chen, X.; Zhu, Y.; Wang, D.; Qi, X.; et al. A LysM receptor heteromer mediates perception of arbuscular mycorrhizal symbiotic signal in rice. *Mol. Plant* **2019**, *12*, 1561–1576. [CrossRef] [PubMed]
5. Zhang, C.; He, J.; Dai, H.; Wang, G.; Zhang, X.; Wang, C.; Shi, J.; Chen, X.; Wang, D.; Wang, E. Discriminating symbiosis and immunity signals by receptor competition in rice. *Proc. Natl. Acad. Sci. USA.* **2021**, *118*, e2023738118. [CrossRef] [PubMed]

6. Gao, L.L.; Knogge, W.; Delp, G.; Smith, F.A.; Smith, S.E. Expression patterns of defense-related genes in different types of arbuscular mycorrhizal development in wild-type and mycorrhiza-defective mutant tomato. *Mol. Plant Microbe Interact.* **2004**, *17*, 1103–1113. [CrossRef] [PubMed]
7. Liu, J.; Maldonado-Mendoza, I.; Lopez-Meyer, M.; Cheung, F.; Town, C.D.; Harrison, M.J. Arbuscular mycorrhizal symbiosis is accompanied by local and systemic alterations in gene expression and an increase in disease resistance in the shoots. *Plant J.* **2007**, *50*, 529–544. [CrossRef] [PubMed]
8. Campos-Soriano, L.; García-Martínez, J.; San Segundo, B. The arbuscular mycorrhizal symbiosis promotes the systemic induction of regulatory defence-related genes in rice leaves and confers resistance to pathogen infection. *Mol. Plant Pathol.* **2012**, *13*, 579–592. [CrossRef] [PubMed]
9. Zeng, T.; Rodriguez-Moreno, L.; Mansurkhodzaev, A.; Wang, P.; van den Berg, W.; Gasciolli, V.; Cottaz, S.; Fort, S.; Thomma, B.; Bono, J.J.; et al. A lysin motif effector subverts chitin-triggered immunity to facilitate arbuscular mycorrhizal symbiosis. *New Phytol.* **2020**, *225*, 448–460. [CrossRef]
10. Akiyama, K.; Matsuzaki, K.; Hayashi, H. Plant sesquiterpenes induce hyphal branching in arbuscular mycorrhizal fungi. *Nature* **2005**, *435*, 824–827. [CrossRef]
11. Besserer, A.; Becard, G.; Jauneau, A.; Roux, C.; Sejalon-Delmas, N. GR24, a synthetic analog of strigolactones, stimulates the mitosis and growth of the arbuscular mycorrhizal fungus *Gigaspora rosea* by boosting its energy metabolism. *Plant Physiol.* **2008**, *148*, 402–413. [CrossRef] [PubMed]
12. Umehara, M.; Hanada, A.; Yoshida, S.; Akiyama, K.; Arite, T.; Takeda-Kamiya, N.; Magome, H.; Kamiya, Y.; Shirasu, K.; Yoneyama, K.; et al. Inhibition of shoot branching by new terpenoid plant hormones. *Nature* **2008**, *455*, 195–200. [CrossRef] [PubMed]
13. Waters, M.T.; Brewer, P.B.; Bussell, J.D.; Smith, S.M.; Beveridge, C.A. The Arabidopsis ortholog of rice DWARF27 acts upstream of MAX1 in the control of plant development by strigolactones. *Plant Physiol.* **2012**, *159*, 1073–1085. [CrossRef] [PubMed]
14. Javot, H.; Penmetsa, R.V.; Terzaghi, N.; Cook, D.R.; Harrison, M.J. A *Medicago truncatula* phosphate transporter indispensable for the arbuscular mycorrhizal symbiosis. *Proc. Natl. Acad. Sci. USA* **2007**, *104*, 1720–1725. [CrossRef]
15. Pumplin, N.; Mondo, S.J.; Topp, S.; Starker, C.G.; Gantt, J.S.; Harrison, M.J. *Medicago truncatula* Vapyrin is a novel protein required for arbuscular mycorrhizal symbiosis. *Plant J.* **2010**, *61*, 482–494. [CrossRef] [PubMed]
16. Zhang, Q.; Blaylock, L.A.; Harrison, M.J. Two *Medicago truncatula* half-ABC transporters are essential for arbuscule development in arbuscular mycorrhizal symbiosis. *Plant Cell* **2010**, *22*, 1483–1497. [CrossRef]
17. Wang, E.; Schornack, S.; Marsh, J.F.; Gobbato, E.; Schwessinger, B.; Eastmond, P.; Schultze, M.; Kamoun, S.; Oldroyd, G.E. A common signaling process that promotes mycorrhizal and oomycete colonization of plants. *Curr. Biol.* **2012**, *22*, 2242–2246. [CrossRef]
18. Breuillin-Sessoms, F.; Floss, D.S.; Gomez, S.K.; Pumplin, N.; Ding, Y.; Levesque-Tremblay, V.; Noar, R.D.; Daniels, D.A.; Bravo, A.; Eaglesham, J.B.; et al. Suppression of arbuscule degeneration in *Medicago truncatula phosphate transporter4* mutants is dependent on the ammonium transporter 2 family protein AMT2;3. *Plant Cell* **2015**, *27*, 1352–1366. [CrossRef]
19. Bravo, A.; Brands, M.; Wewer, V.; Dormann, P.; Harrison, M.J. Arbuscular mycorrhiza-specific enzymes FatM and RAM2 fine-tune lipid biosynthesis to promote development of arbuscular mycorrhiza. *New Phytol.* **2017**, *214*, 1631–1645. [CrossRef]
20. Gobbato, E.; Marsh, J.F.; Vernie, T.; Wang, E.; Maillet, F.; Kim, J.; Miller, J.B.; Sun, J.; Bano, S.A.; Ratet, P.; et al. A GRAS-type transcription factor with a specific function in mycorrhizal signaling. *Curr. Biol.* **2012**, *22*, 2236–2241. [CrossRef]
21. Gobbato, E.; Wang, E.; Higgins, G.; Bano, S.A.; Henry, C.; Schultze, M.; Oldroyd, G.E. *RAM1* and *RAM2* function and expression during arbuscular mycorrhizal symbiosis and *Aphanomyces euteiches* colonization. *Plant Signal. Behav.* **2013**, *8*, e26049. [CrossRef] [PubMed]
22. Park, H.J.; Floss, D.S.; Levesque-Tremblay, V.; Bravo, A.; Harrison, M.J. Hyphal branching during arbuscule development requires *Reduced arbuscular mycorrhiza1*. *Plant Physiol.* **2015**, *169*, 2774–2788. [CrossRef] [PubMed]
23. Rich, M.K.; Schorderet, M.; Bapaume, L.; Falquet, L.; Morel, P.; Vandenbussche, M.; Reinhardt, D. The Petunia GRAS transcription factor ATA/RAM1 regulates symbiotic gene expression and fungal morphogenesis in arbuscular mycorrhiza. *Plant Physiol.* **2015**, *168*, 788–797. [CrossRef] [PubMed]
24. Xue, L.; Cui, H.; Buer, B.; Vijayakumar, V.; Delaux, P.M.; Junkermann, S.; Bucher, M. Network of GRAS transcription factors involved in the control of arbuscule development in *Lotus japonicus*. *Plant Physiol.* **2015**, *167*, 854–871. [CrossRef] [PubMed]
25. Pumplin, N.; Harrison, M.J. Live-cell imaging reveals periarbuscular membrane domains and organelle location in *Medicago truncatula* roots during arbuscular mycorrhizal symbiosis. *Plant Physiol.* **2009**, *151*, 809–819. [CrossRef] [PubMed]
26. Smith, F.A.; Smith, S.E. Tansley Review No. 96. Structural diversity in (vesicular)-arbuscular mycorrhizal symbioses. *New Phytol.* **1997**, *137*, 373–388. [CrossRef]
27. Yamato, M.; Iwasaki, M. Morphological types of arbuscular mycorrhizal fungi in roots of understory plants in Japanese deciduous broadleaved forests. *Mycorrhiza* **2002**, *12*, 291–296. [CrossRef]
28. Dickson, S. The *Arum-Paris* continuum of mycorrhizal symbioses. *New Phytol.* **2004**, *163*, 187–200. [CrossRef] [PubMed]
29. Yamato, M. Morphological types of arbuscular mycorrhizal fungi in roots of weeds on vacant land. *Mycorrhiza* **2004**, *14*, 127–131. [CrossRef] [PubMed]
30. Dickson, S.; Smith, F.A.; Smith, S.E. Structural differences in arbuscular mycorrhizal symbioses: More than 100 years after Gallaud, where next? *Mycorrhiza* **2007**, *17*, 375–393. [CrossRef]

31. Tominaga, T.; Miura, C.; Takeda, N.; Kanno, Y.; Takemura, Y.; Seo, M.; Yamato, M.; Kaminaka, H. Gibberellin promotes fungal entry and colonization during *Paris*-type arbuscular mycorrhizal symbiosis in *Eustoma grandiflorum*. *Plant Cell Physiol.* **2020**, *61*, 565–575. [CrossRef] [PubMed]
32. Tominaga, T.; Miura, C.; Sumigawa, Y.; Hirose, Y.; Yamaguchi, K.; Shigenobu, S.; Mine, A.; Kaminaka, H. Conservation and diversity in gibberellin-mediated transcriptional responses among host plants forming distinct arbuscular mycorrhizal morphotypes. *Front. Plant Sci.* **2021**, *12*, 795695. [CrossRef] [PubMed]
33. Yu, N.; Luo, D.; Zhang, X.; Liu, J.; Wang, W.; Jin, Y.; Dong, W.; Liu, J.; Liu, H.; Yang, W.; et al. A DELLA protein complex controls the arbuscular mycorrhizal symbiosis in plants. *Cell Res.* **2014**, *24*, 130–133. [CrossRef] [PubMed]
34. Takeda, N.; Handa, Y.; Tsuzuki, S.; Kojima, M.; Sakakibara, H.; Kawaguchi, M. Gibberellins interfere with symbiosis signaling and gene expression and alter colonization by arbuscular mycorrhizal fungi in *Lotus japonicus*. *Plant Physiol.* **2015**, *167*, 545–557. [CrossRef] [PubMed]
35. Pimprikar, P.; Carbonnel, S.; Paries, M.; Katzer, K.; Klingl, V.; Bohmer, M.J.; Karl, L.; Floss, D.S.; Harrison, M.J.; Parniske, M.; et al. A CCaMK-CYCLOPS-DELLA complex activates transcription of *RAM1* to regulate arbuscule branching. *Curr. Biol.* **2016**, *26*, 987–998. [CrossRef] [PubMed]
36. Nouri, E.; Surve, R.; Bapaume, L.; Stumpe, M.; Chen, M.; Zhang, Y.; Ruyter-Spira, C.; Bouwmeester, H.; Glauser, G.; Bruisson, S.; et al. Phosphate suppression of arbuscular mycorrhizal symbiosis involves gibberellic acid signalling. *Plant Cell Physiol.* **2021**, *62*, 959–970. [CrossRef] [PubMed]
37. Cavagnaro, T.R.; Gao, L.L.; Smith, F.A.; Smith, S.E. Morphology of arbuscular mycorrhizas is influenced by fungal identity. *New Phytol.* **2001**, *151*, 469–475. [CrossRef]
38. Kubota, M.; McGonigle, T.P.; Hyakumachi, M. Co-occurrence of *Arum*- and *Paris*-type morphologies of arbuscular mycorrhizae in cucumber and tomato. *Mycorrhiza* **2005**, *15*, 73–77. [CrossRef]
39. Hong, J.J.; Park, Y.S.; Bravo, A.; Bhattarai, K.K.; Daniels, D.A.; Harrison, M.J. Diversity of morphology and function in arbuscular mycorrhizal symbioses in *Brachypodium distachyon*. *Planta* **2012**, *236*, 851–865. [CrossRef]
40. Hosmani, P.S.; Flores-Gonzalez, M.; van de Geest, H.; Maumus, F.; Bakker, L.V.; Schijlen, E.; van Haarst, J.; Cordewener, J.; Sanchez-Perez, G.; Peters, S.; et al. An improved de novo assembly and annotation of the tomato reference genome using single-molecule sequencing, Hi-C proximity ligation and optical maps. *bioRxiv* **2019**, 767764. [CrossRef]
41. Waters, M.T.; Nelson, D.C.; Scaffidi, A.; Flematti, G.R.; Sun, Y.K.; Dixon, K.W.; Smith, S.M. Specialisation within the DWARF14 protein family confers distinct responses to karrikins and strigolactones in *Arabidopsis*. *Development* **2012**, *139*, 1285–1295. [CrossRef] [PubMed]
42. Vegh, A.; Incze, N.; Fabian, A.; Huo, H.; Bradford, K.J.; Balazs, E.; Soos, V. Comprehensive analysis of DWARF14-LIKE2 (DLK2) reveals its functional divergence from strigolactone-related paralogs. *Front. Plant Sci.* **2017**, *8*, 1641. [CrossRef] [PubMed]
43. Ho-Plagaro, T.; Morcillo, R.J.L.; Tamayo-Navarrete, M.I.; Huertas, R.; Molinero-Rosales, N.; Lopez-Raez, J.A.; Macho, A.P.; Garcia-Garrido, J.M. DLK2 regulates arbuscule hyphal branching during arbuscular mycorrhizal symbiosis. *New Phytol.* **2021**, *229*, 548–562. [CrossRef] [PubMed]
44. Bittel, P.; Robatzek, S. Microbe-associated molecular patterns (MAMPs) probe plant immunity. *Curr. Opin. Plant Biol.* **2007**, *10*, 335–341. [CrossRef] [PubMed]
45. Zipfel, C. Pattern-recognition receptors in plant innate immunity. *Curr. Opin. Immunol.* **2008**, *20*, 10–16. [CrossRef]
46. Hou, S.; Liu, Z.; Shen, H.; Wu, D. Damage-associated molecular pattern-triggered immunity in plants. *Front. Plant Sci.* **2019**, *10*, 646. [CrossRef]
47. Kloppholz, S.; Kuhn, H.; Requena, N. A secreted fungal effector of *Glomus intraradices* promotes symbiotic biotrophy. *Curr. Biol.* **2011**, *21*, 1204–1209. [CrossRef]
48. Tian, W.; He, G.; Qin, L.; Li, D.; Meng, L.; Huang, Y.; He, T. Genome-wide analysis of the NRAMP gene family in potato (*Solanum tuberosum*): Identification, expression analysis and response to five heavy metals stress. *Ecotoxicol. Environ. Saf.* **2021**, *208*, 111661. [CrossRef]
49. Kaiser, B.N.; Moreau, S.; Castelli, J.; Thomson, R.; Lambert, A.; Bogliolo, S.; Puppo, A.; Day, D.A. The soybean NRAMP homologue, GmDMT1, is a symbiotic divalent metal transporter capable of ferrous iron transport. *Plant J.* **2003**, *35*, 295–304. [CrossRef]
50. Tejada-Jiménez, M.; Castro-Rodríguez, R.; Kryvoruchko, I.; Lucas, M.M.; Udvardi, M.; Imperial, J.; González-Guerrero, M. *Medicago truncatula* natural resistance-associated macrophage Protein1 is required for iron uptake by rhizobia-infected nodule cells. *Plant Physiol.* **2015**, *168*, 258–272. [CrossRef]
51. Chen, S.; Zhou, Y.; Chen, Y.; Gu, J. fastp: An ultra-fast all-in-one FASTQ preprocessor. *Bioinformatics* **2018**, *34*, i884–i890. [CrossRef] [PubMed]
52. Dobin, A.; Davis, C.A.; Schlesinger, F.; Drenkow, J.; Zaleski, C.; Jha, S.; Batut, P.; Chaisson, M.; Gingeras, T.R. STAR: Ultrafast universal RNA-seq aligner. *Bioinformatics* **2013**, *29*, 15–21. [CrossRef] [PubMed]
53. Liao, Y.; Smyth, G.K.; Shi, W. featureCounts: An efficient general purpose program for assigning sequence reads to genomic features. *Bioinformatics* **2014**, *30*, 923–930. [CrossRef] [PubMed]
54. Robinson, M.D.; McCarthy, D.J.; Smyth, G.K. edgeR: A Bioconductor package for differential expression analysis of digital gene expression data. *Bioinformatics* **2010**, *26*, 139–140. [CrossRef] [PubMed]

55. Ge, S.X.; Jung, D.; Yao, R. ShinyGO: A graphical gene-set enrichment tool for animals and plants. *Bioinformatics* **2020**, *36*, 2628–2629. [CrossRef]
56. Galili, T.; O'Callaghan, A.; Sidi, J.; Sievert, C. heatmaply: An R package for creating interactive cluster heatmaps for online publishing. *Bioinformatics* **2018**, *34*, 1600–1602. [CrossRef]

plants

MDPI

Review

Realizing the Potential of *Camelina sativa* as a Bioenergy Crop for a Changing Global Climate

Dhurba Neupane [1], Richard H. Lohaus [1], Juan K. Q. Solomon [2] and John C. Cushman [1,*]

[1] MS330/Department of Biochemistry & Molecular Biology, University of Nevada, Reno, NV 89557, USA; dneupane@unr.edu (D.N.); rhlohaus25@gmail.com (R.H.L.)
[2] Department of Agriculture, Veterinary & Rangeland Sciences, University of Nevada, Reno, NV 89557, USA; juansolomon@unr.edu
* Correspondence: jcushman@unr.edu; Tel.: +1-775-784-1918

Abstract: *Camelina sativa* (L.) Crantz. is an annual oilseed crop within the Brassicaceae family. *C. sativa* has been grown since as early as 4000 BCE. In recent years, *C. sativa* received increased attention as a climate-resilient oilseed, seed meal, and biofuel (biodiesel and renewable or green diesel) crop. This renewed interest is reflected in the rapid rise in the number of peer-reviewed publications (>2300) containing "camelina" from 1997 to 2021. An overview of the origins of this ancient crop and its genetic diversity and its yield potential under hot and dry growing conditions is provided. The major biotic barriers that limit *C. sativa* production are summarized, including weed control, insect pests, and fungal, bacterial, and viral pathogens. Ecosystem services provided by *C. sativa* are also discussed. The profiles of seed oil and fatty acid composition and the many uses of seed meal and oil are discussed, including food, fodder, fuel, industrial, and medical benefits. Lastly, we outline strategies for improving this important and versatile crop to enhance its production globally in the face of a rapidly changing climate using molecular breeding, rhizosphere microbiota, genetic engineering, and genome editing approaches.

Keywords: *Camelina sativa*; semi-arid lands; biofuel feedstock; biodiesel; renewable diesel; crop breeding; transgenesis; genome editing

Citation: Neupane, D.; Lohaus, R.H.; Solomon, J.K.Q.; Cushman, J.C. Realizing the Potential of *Camelina sativa* as a Bioenergy Crop for a Changing Global Climate. *Plants* **2022**, *11*, 772. https://doi.org/10.3390/plants11060772

Academic Editor: Yin Li

Received: 11 February 2022
Accepted: 4 March 2022
Published: 14 March 2022

Publisher's Note: MDPI stays neutral with regard to jurisdictional claims in published maps and institutional affiliations.

1. Introduction

Camelina sativa (L.) Crantz., also known as false or wild flax, German sesame, gold-of-pleasure, or linseed dodder, is an allohexaploid (2n = 40) oilseed crop within the Brassicaceae [1–6]. Interest in *C. sativa* increased in recent years due to its adaptability to diverse environmental conditions, low requirements for water and nutrients, relatively strong resistance to insect pests and microbial diseases, and unique oil composition and characteristics suitable for the production of food and fodder, biofuels, and bio-based products [1,2,7,8]. These positive agronomic traits and environmental attributes, along with the recent development of methods for transgenesis [9–13] and CRISPR/Cas genome editing [14–16], triggered great interest in *C. sativa* as an industrial oilseed crop. The ongoing interest in *C. sativa* is documented by the large number of peer-reviewed publications from various databases retrieved when "camelina" was used as a search term, for example, in a query of the ScienceDirect (2309 publications from 1997–2021), Web of Science (1525 publications from 2000–2021) and Agricola (677 publications from 2000–2021) databases (reported on December 30, 2021). The large number of publications and data reported on *C. sativa* highlight the immense potential of this crop and the interest in genetic improvement to allow it to gain more widespread acceptance and economic viability. Most publications focus on the uses of *C. sativa* oil and meal, the composition of oil and fatty acids, its genetics and breeding, its physiology, and its production and agronomic management. Agronomic management refers to the practice of minimizing input factors such as fertilizer, irrigation, tillage, herbicides, fungicides, and insecticides to maximize crop yield outputs such as

seed yield, oil content, and biodiesel production. Many reviews report on various aspects of its general use as an oilseed crop [2,4,17–24], and as a platform for the production of biofuels [25–28] and industrial lipids [1,6,8]. After providing some essential background, we summarize the present status of *C. sativa* research and identify areas for its future improvement with a particular emphasis on enhancing the climate resilience of this highly versatile crop.

2. Origin and Distribution

Camelina sativa is an ancient crop, known as early as 4000 BCE in Auvervier, Switzerland [29] with evidence of widespread cultivation throughout northern Europe from Southern Scandinavia [6,30] to central Asia (eastern Turkey), from 700–900 BCE [31] to the Iron Age (100 CE–250 BCE) [24]. Archaeological sites revealed evidence that *C. sativa* was cultivated for food and oil production in Scandinavia, Romania, and eastern Turkey during the late Stone Age and middle Bronze Age (1800 BCE) [32], with widespread availability during the late Bronze age (1200 BCE) [30]. *C. sativa* cultivation declined during the Medieval Age, but grew during the last century throughout northern, central and eastern Europe, the Balkans, and Russia and to some extent in North America [33]. However, much of its former cultivation all but disappeared, being replaced almost entirely by rapeseed (*Brassica napus* L.) [24].

C. sativa was likely introduced to the Americas as a weed in flax, thus giving rise to the name false flax [4]. Today, *C. sativa* is cultivated throughout the northern USA and southern Canada [34]. Within the USA, *C. sativa* is grown effectively in the Pacific Northwest, across the North and Central Plains into the Corn Belt region [35], and in the arid Southwest with irrigation [36,37]. Within Canada, *C. sativa* is grown widely from the western Prairie Provinces [38,39] to the eastern Maritime Provinces [40].

3. Genetic Diversity and Morphological Variation

C. sativa belongs to the tribe Camelineae within the Brassicaceae. The similarity between *C. sativa* and *Arabidopsis thaliana* [41,42] makes *A. thaliana* a useful reference for the development of genetic and genomic tools in *C. sativa* [34]. The genus *Camelina* has up to 11 species, revealing taxonomic dissimilarity with its center of diversity in Eurasia (Russia or Ukraine) [43–45]. Among 11 species, five species, namely *C. sativa*, *C. microcarpa*, *C. rumelica*, *C. alyssum*, and *C. hispida,* are found in Europe and three species, namely *C. sativa*, *C. microcarpa*, and *C. alyssum,* are found in the USA and Canada [11]. Among these species, only *C. sativa* and *C. microcarpa* are cultivated [11]. *C. sativa* is an allohexaploid species with 2n = 6x = 40 [34,46]. Other *Camelina* species such as *C. hispida* (Boiss.) Hedge (2n = 2x = 14), *C. neglecta* (2n = 2x = 12) [44], and *C. laxa* C.A. Mey. (2n = 2x= 12) [47] are diploid. Other species are polyploid, including *C. rumelica* Velen., tetraploid (2n = 4x = 26); *C. microcarpa* Andrz. ex DC with three cytotypes: diploid (2n = 2x = 12), tetraploid (2n = 4x = 26), and hexaploid (2n = 6x = 40) [48]; and *C. sativa*, hexaploid (2n = 2x= 40) [49,50]. Morphologically, *C. sativa* and *C. microcarpa* are very similar except for the smaller seed size of *C. microcarpa* [51]. This phenotypic similarity suggests that *C. sativa* could potentially be the domesticated form of *C. microcarpa* [43]. Greater variations in chromosome counts within species might arise from intraspecific ploidy variations or inaccurate records suggesting past taxonomic misidentification [52]. Investigations into the genome structure of 193 *Camelina* accessions revealed three subpopulations, with two represented by domesticated *C. sativa* accessions and one composed of *C. microcarpa* species that included a newly designated *C. neglecta* diploid (née *C. microcarpa*) species [53]. Recent molecular phylogenies derived from chloroplast genome sequencing of 84 individuals revealed low intragenic variation across the *Camelina* genus [54]. However, cytotypes and chromosome counts across 82 individuals confirmed that the tetraploid *C. microcarpa* (or *C. neglecta*-like) is the proposed maternal parent and the diploid *C. hispida* is the proposed paternal parent of *C. sativa* [53,54].

Resembling other genera within the *Brassicaceae*, *Camelina* species are dicotyledonous with high morphological plasticity. Biologically, *Camelina* species can be annual spring or biennial winter types [2], with some species requiring vernalization to induce flowering [55]. Most domesticated *C. sativa* are spring types, whereas most wild relatives are winter types. Winter types are well adapted as cover crops in double- or relay-cropping systems, with soybean (*Glycine max* L. Merr.) and other short-seasoned summer crops due to their early maturity in the Great Plains and the Upper Midwestern USA [3,35,56–58]. *C. sativa* typically has a short growing cycle of 85–120 days [4,5,22,50,59]. Growing degree day (GDD) requirements for *C. sativa* during its complete life cycle (with up to 75% ripe silicles) generally range from 1200 to 1300 °C with a base temperature of 5 °C [60]. Plant height ranges from 30 to 120 cm depending upon cultivars, growing season, and amount of nitrogen fertilizer used [4,36,59,61,62]. Stems are either hairy or smooth, are branched, and become lignified when mature. Leaves are arrow-shaped and pointed, approximately 5–8 cm long with smooth to undulated edges. Flowers are 5–7 mm in diameter and are mostly autogamous [49]. Flowers are pale yellow in color and arranged within inflorescences, called raceme. The silicles are 5–14 mm long, slightly flattened, and pear-shaped, containing 8–15 golden to brown colored seeds at maturity. *C. sativa* seeds are very small, with 1000 seed weight varying between 0.8 to 1.8 g, depending upon the cultivar and growing environments during seed growth and development [4,22,24,63,64]. *C. sativa* has a deep taproot system, varying with soil type and growing conditions, which is thought to improve nutrient scavenging. The use of *C. sativa* as a cover crop can reduce nutrient run-off, particularly for winter annual cultivars [2]. *C. sativa* can also reduce soil compaction and improve infiltration capacity, similar to other species within the *Brassicaceae* [2].

4. *C. sativa* Yield Potential under Hot and Dry Conditions

Global climate change is related to increasing surface aridification and the increasing duration and frequency of droughts in many regions of the world [65,66]. Interest in *C. sativa* as a low-input crop for use on marginal lands has grown in recent years [50,67–71]. Thus, recent studies investigated *C. sativa* grown under semi-arid conditions with limited water inputs, with the goal of assessing its performance under reduced water and fertilizer inputs [36,37,59,62,72].

Many studies were conducted across semi-arid or arid regions of the globe with distinct mean annual precipitation levels to compare seed yield (kg ha^{-1}), oil content (%), protein content (%), and biodiesel production (L ha^{-1}) (Figure 1, Table 1). Differences in cultivars (genotypes), water availability, environment, physical and chemical characteristics of soils, and management practices such as irrigation, nitrogen application, sowing date, seeding methods and rates, clearly impact overall *C. sativa* productivity. Among these studies, the overall mean seed yield of *C. sativa* was 1410 kg ha^{-1} (Figure 1, Table 1). The highest reported seed yield ranges were attained in Austria (2419–3625 kg ha^{-1}) [73] and in southern Ethiopia (2795–3200 kg ha^{-1}) [74]. The lowest *C. sativa* seed yield ranges were reported by studies performed in Kansas [75] and Nevada, USA [36,37,59,62]. Low seed yield of *C. sativa* may occur due to drought and high temperatures during the flowering and pod filling stage [61,76], as well as poor soil quality [77]. Consistent with these findings, environmental factors (e.g., temperature and rainfall) were responsible for approximately 73% of the variation in seed yield in north-eastern Poland [72]. In contrast, only ~6% of the variation in seed yield was due to genetic factors [72]. Mild weather conditions, along with moderate in-season precipitation, favor higher seed yields [35,39]. Additionally, high *C. sativa* seed yields were associated with adequate moisture and mild temperatures during seed filling, which is critical for the production and transport of sugars from source to sink tissues [3,77,78]. In contrast, low seed yields were observed under conditions of hot temperature and low precipitation [79,80]. Studies showed an increase in seed yields ranging from 425 to 2867 kg ha^{-1} as a result of increasing amounts of applied irrigation ranging from 187 to 536 mm [36,69,70,81]. Seasonal water requirements range from 332–490 mm for *C. sativa* based upon cumulative evapotranspiration (ET) estimates [82–84]. Notably,

C. sativa might serve as a reliable alternative to Canola in locations where seasonal water supply is less than 250 mm [85]. In addition to increased water inputs, increasing nitrogen fertilizer application can increase seed yield. Seed yields of 1800 kg ha^{-1} can be attained with 150 kg N ha^{-1} and water inputs in the range of 320–376 mm [86]. Similar estimates for optimal N input were reported for rainfed field settings [87,88]. The use of organic fertilizers during the production of *C. sativa* for animal feed reduces its environmental impact [89].

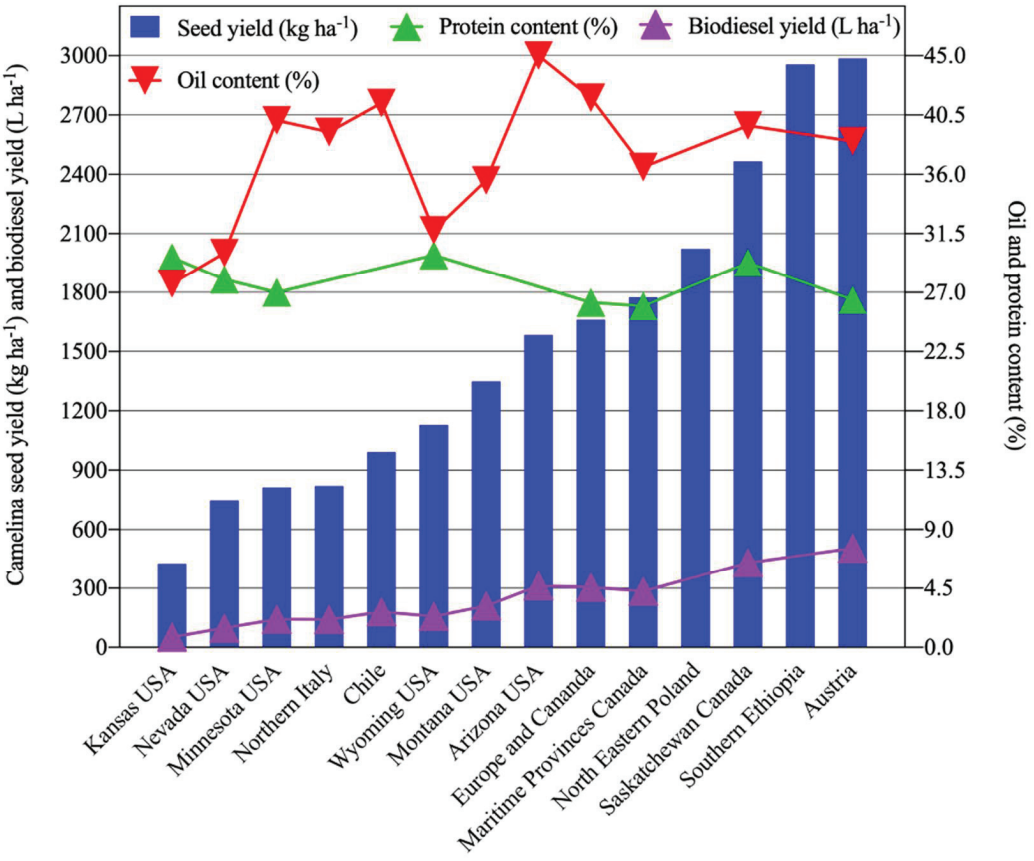

Figure 1. Average seed yield (kg ha^{-1}), oil (%), and protein content (%) of *C. sativa* grown at various locations across the world.

Another important measure of productivity for any oilseed crop is oil and protein production of the seed meal. For *C. sativa*, oil and protein content varied widely across various parts of the world, with overall mean seed oil and protein contents of ~36% and ~28%, respectively (Figure 1, Table 1). Highest seed oil contents were reported in the range of 39.8–45.7% in Chile [61], followed by 45% in Arizona, USA [84], and 38–43% in western Canada [39]. The lowest seed oil content, ranging from 25.7 to 31.8%, was observed in Nevada, USA [37]. Similarly to seed yield, oil yield is strongly influenced by environmental factors [64,90]. For example, oil content variation was chiefly associated with mean air temperature and water availability during seed development [61].

Table 1. *C. sativa* seed yield, oil, and protein content reported across various regions of the world.

Locations	Seed Yield (kg ha^{-1})		Seed Oil Content (%) [1]	Seed Meal Protein Content (%) [2]	Biodiesel Yield (L ha^{-1}) [3]	Major Sources of Variation	Reference
	Mean	Range	Range	Range	Mean		
Austria	2986	2419–3625	37.0–40.0	25.0–27.9	505	Nitrogen and sulfur rates	[73]
Southern Ethiopia	2956	2795–3200	-	-	-	Seeding rates and nitrogen fertilizer	[74]
Saskatchewan, Canada	2466	2184–2747	38 to 43 (39.7)	27 to 32 (29.3)	430	Genotypes and environment	[39]
North–Eastern Poland	2023	1700–2210	-	-	-	Genotypes	[72]
Maritime Provinces of Eastern Canada	1775	1638–1911	33.8–39.0 (36.6)	25.0–26.8 (26.0)	285	Breeding lines, nitrogen and sulfur rates	[87]
Europe and Canada	1660	1100–2700	(41.8)	(26.2)	305	Genotypes and environment	[77]
Arizona, USA	1583	1527–1638	(45)	-	313	Nitrogen rates, water use and irrigation scheduling	[84]
Montana USA	1349	546–2942	33.5–37.6 (36.0)	-	211	Cultivars and locations	[78]
Wyoming, USA	1129	832–1643	31.1–32.4	29.3–30.4	157	Nitrogen and sulfur rates	[91]
Chile	991	387–2314	39.8–45.7 (41.41)	-	180	Cultivars, planting dates, and locations	[61]
Northern Italy	820	600–940	(39.2)		141	Low input and growing seasons	[71]
Nevada, USA	899	770–1013	31.8–33.3 (32.4)	27.1–28.1 (27.5)	128	Cultivars and irrigation rates	[36]
	784	534–1010	31.8–32.6 (32.2)	26.2–30.4 (28.4)	111	Cultivars, nitrogen sources and rates	[59]
	735	34–1921	26.6–30.8	-	69.7	Cultivars and year	[37]
	570	130–921	28.4–29.5	-	72	cultivars, sowing date, and methods	[62]
Minnesota, USA	812	650–944	39.4–40.7 (40.1)	26.2–27.9 (27.0)	143	Genotypes and seeding rate	[3]
Kansas, USA	427	317–503	27–29 (27.7)	29–30 (29.7)	52	Cultivar and planting date	[75]
Overall mean	**1410**		**36.0**	**27.8**	**208.4**		

[1] Oil and [2] protein content inside brackets indicate the average oil and protein content (%). [3] Biodiesel yield was estimated by multiplying seed yield (kg ha^{-1}) and oil content (%) using the volumetric conversion factor of 1 kg ha^{-1} to 0.439 L ha^{-1} [92].

Compared with seed oil values, protein content generally varied less widely relative to the location of production across the globe, with the lowest and highest ranges of 25.0–26.8% and 27–32%, respectively, reported in Canada, with an overall mean of 27.8% (Figure 1, Table 1). However, more wide-ranging protein contents (23–47%) of *C. sativa* seeds were reported depending upon local field conditions [60,77]. High air temperatures during flowering and seed filling are generally associated with low oil contents but high protein contents within *C. sativa* seed [62]. Furthermore, increased N application rates can increase protein contents, with an associated decrease in oil contents [73,87,93,94]. Such increased nitrogen applications are known to increase protein at the expense of fatty acid synthesis due to the competition for carbon skeleton during carbohydrate metabolism [95].

A major use of *C. sativa* seed oil is biodiesel production. Biodiesel production, which is closely linked with overall oil production, varied widely with a mean of 208 L ha^{-1} across the globe (Figure 1, Table 1). The highest biodiesel yield (505 L ha^{-1}) was reported in Austria [73], followed by western Canada (430 L ha^{-1}) [39]. A multi-location study performed in Europe and Canada reported a mean biodiesel yield of 305 L ha^{-1} [77]. The lowest biodiesel yield (52 L ha^{-1}) was reported in Kansas, USA [75]. The wide variation in biodiesel production is likely accounted for by differences in temperature and water

availability, including ambient precipitation, length of growing season, and managerial factors such as fertilizer application rates and irrigation practices.

5. Biotic Production Constraints of *C. sativa*

Weeds are a major constraint to *C. sativa* production (Berti et al., 2016). *C. sativa* is considered to be very competitive against weeds with good stand establishment [22,96], due to its ability to produce and release secondary metabolites that prevent the growth of seedlings of neighboring plants [97–99]. However, the competitiveness of *C. sativa* for sunlight, nutrients, and water can be challenged by some weed species such as cheatgrass (*Bromus tectorum*), green foxtail (*Setaria viridis* L.), and Russian thistle (*Salsola kali* L.), among others [2,5,100,101]. Similarly, perennial broadleaf weeds such as field bindweed (*Convolvulus arvensis* L.), Canada thistle (*Cirsium arvense* L. Scop.), and skeleton weed (*Chondrilla juncea* L.) can also present challenges for *C. sativa*. Notably, *C. sativa* can exhibit susceptibility to dodder (*Cuscuta* spp.), a parasitic weed of many crops (D. Neupane, personal observation). *C. sativa* does not hybridize efficiently with cultivated *Brassica* species or wild *Brassica* species within the tribe *Camelineae* [102]. However, *C. sativa* does exhibit the ability to outcross with common *Brassica* weed species, such as North American weeds *C. alyssum* and *C. microcarpa* [103]. Fortunately, *C. sativa* is less competitive and shows lower invasive potential than Canola [104].

5.1. Weed Control

Both chemical and non-chemical approaches for weed control are available for *C. sativa* production systems. For chemical control, Sethoxydim (Poast®) (2-[(E)-N-ethoxy-C-propylcarbonimidoyl]-5-(2-ethylsulfanylpropyl)-3-hydroxycyclohex-2-en-1-one), a post-emergent and selective grass herbicide, which belongs to the cyclohexanone group, is currently the only registered herbicide for *C. sativa* in the USA [59,62,105,106]. Tepraloxydim (2-[(E)-N-[(E)-3-chloroprop-2-enoxy]-C-ethylcarbonimidoyl]-3-hydroxy-5-(oxan-4-yl)cyclohex-2-en-1-one) was also used to control post-emergent grass weeds [61]. Similarly, Clethodim (2-[(E)-N-[(E)-3-chloroprop-2-enoxy]-C-ethylcarbonimidoyl]-5-(2-ethylsulfanylpropyl)-3-hydroxycyclohex-2-en-1-one), which is a related post-emergent cyclohexanone herbicide, was successfully used for grassy weed control for *C. sativa* [36]. Quizalofop (2-[4-(6-chloroquinoxalin-2-yl)oxyphenoxy]propanoic acid), which is a selective, postemergence phenoxy herbicide registered in Canada and other parts of the world, was also used to control annual and perennial grass weeds of *C. sativa* [2,5,107].

In contrast to selective grass herbicides, *C. sativa* withstands very few broadleaf herbicides, and few have been approved for use on *C. sativa* in the USA [2,5,22,107,108]. Dinitroaniline pre-emergent herbicides, such as Trifluralin (2,6-dinitro-N,N-dipropyl-4-(trifluoromethyl)aniline), are widely used in the USA for early season weed control. Pre-emergent herbicides, including dimethenamid-P (2-chloro-N-(2,4-dimethylthiophen-3-yl)-N-[(2S)-1-methoxypropan-2-yl]acetamide), pendimethalin (3,4-dimethyl-2,6-dinitro-N-pentan-3-ylaniline), pyroxasulfone (3-[[5-(difluoromethoxy)-1-methyl-3-(trifluoromethyl) pyrazol-4-yl]methylsulfonyl]-5,5-dimethyl-4H-1,2-oxazole), quinclorac (3,7-dichloroquinoline-8-carboxylic acid), and S-metolachlor (2-chloro-N-(2-ethyl-6-methylphenyl)-N-[(2S)-1-methoxypropan-2-yl]acetamide), were tested at three different concentrations with *C. sativa* to examine weed control and injury to the crop [109]. Pendimethalin and S-metolachlor caused some injury, but did not lower *C. sativa* seed yields. Dimethenamid-P, used at a low rate, did not affect plant populations and seed yield; however, when applied at a high rate, it caused 60% injury with a 31% reduction in seed yield [109,110]. Quinclorac did not significantly injure the crop and was considered the safest of all the herbicides tested [109]. *C. sativa* mutants with resistance to acetolactate synthase (ALS) inhibitors were developed, displaying increased resistance to imazethapyr (5-ethyl-2-(4-methyl-5-oxo-4-propan-2-yl-1H-imidazol-2-yl)pyridine-3-carboxylic acid), sulfosulfuron (1-(4,6-dimethoxypyrimidin-2-yl)-3-(2-ethylsulfonylimidazo[1,2-a]pyridin-3-yl)sulfonylurea), and

flucarbazone (3-methoxy-4-methyl-5-oxo-N-[2-(trifluoromethoxy)phenyl]sulfonyl-1,2,4-triazole-1-carboxamide) [110].

Several non-chemical strategies for weed control were shown to be effective for *C. sativa* [96]. Mechanical weeding is a well-established and useful approach for small scale production systems (e.g., research plots). For large-scale production, early season planting that promotes stand establishment is one of the most effective strategies for overcoming weed competition in *C. sativa* fields [111]. Furthermore, increasing sowing rates can effectively suppress weeds in *C. sativa* plots, likely through increased utilization of resources by the crop at the expense of weeds [96]. Mixed cropping of *C. sativa* grain with peas (*Pisum sativum*) (or barley (*Hordeum vulgare*)) afforded significant weed suppression and acted as a smother crop and weed antagonist, leading to enhanced *C. sativa* seed yields [96,112].

Use of *C. sativa* as a winter cover crop suppressed weed abundance while increasing cash crop yields [113]. Including *C. sativa* in crop rotations for winter cereals can suppress winter weed populations and increase grain yields in semi-arid Mediterranean climates [114]. *C. sativa* was also used in innovative double- and relay-cropping systems with forage sorghum (*Sorghum bicolor*), maize (*Zea mays*), and soybean (*Glycine max*) with an increased potential for biofuel and energy feedstock production [115]. When *C. sativa* was intersown as a cover crop with maize or soybean, establishment and winter survival rates increased, with the greatest success being achieved with soybean [116]. *C. sativa* was also used as an intercrop with *Jatropha integerrima* in semi-arid regions of India with seed production improvements observed when grown alternatively with leguminous fodder crops [117]. Further exploration of the potential allelopathic effects of *C. sativa* in intercropping systems for weed suppression is needed [99].

5.2. Insect Pests

Insects can limit *C. sativa* production, but these generally present lower production barriers than weeds. *C. sativa* is known to be relatively resistant to insect predation and infestation. *C. sativa* shows resistance to several common insect pests of Canola [118,119]. For example, *C. sativa* shows high resistance to flea beetles (*Phyllotreta* spp.), a common insect pest of *B. rapa*, *B. napus*, and *B. juncea* [39,49,120,121]. This resistance is thought to be due to the presence of repellents or the absence of stimulatory volatile phytochemicals [122]. More recent studies confirmed that the presence of quercetin glycosides in *C. sativa* leaves is likely responsible for flea beetle resistance [123]. In addition to flea beetles, *C. sativa* was shown to be a poor host for the diamondback moth (*Plutella xylostella* L.) and root maggots (*Delia* spp.) [124]. Feeding damage by the Bertha armyworm (*Mamestra configurata* Walker) on *C. sativa* was consistent with Canola, but larvae and pupae weighed less when reared on *C. sativa* leaves [124]. Leafhopper (*Macrosteles quadrilineatus* Forbes) did not cause damage to *C. sativa*; however, this insect can transmit aster yellows phytoplasma, which can result in chronic, systemic disease resulting in chlorosis, phyllody, and virescence, malformed seeds, and reduced seed set [124]. *C. sativa* also appeared to show resistance against the cabbage seedpod weevil (Ceutorhyncus obstrictus (Marsh.) [125]. However, stem feeding below the soil by several weevil species (e.g., *Ceutorhynchus cyanipennis* and *C. americanus*) was associated with stand failures for fall-planted *C. sativa* [126]. Although aphids can colonize *C. sativa* under field conditions, they are not known to cause significant economic damage; however, such colonization can create a reservoir for different aphid species that can negatively impact other crops in the rotation [127].

5.3. Fungal, Bacterial, and Viral Pathogens

Similar to its apparent resistance to many insect pests, *C. sativa* shows good resistance to a variety of microbial pathogens that typically target crops within the *Brassicaceae* [18,128]. For example, *C. sativa* showed strong resistance to blackspot fungal disease caused by *Alternaria brassicae* (Berk.) Sacc. [129–131]. Such resistance is associated with the relative expression of defense-related genes [132]. Resistance to blackspot disease caused by *Alternaria brassicicola*

[(Schw.) Wiltsh] varies among *C. sativa* genebank accessions [133]. However, such resistance can be transferred to hybrids of *C. sativa* and rapid-cycling *Brassica oleracea* in an effort to confer resistance of this disease to *Brassica* vegetable crops [134,135]. Resistance to the blackspot pathogen was associated with the production of phytoalexins, specifically to camalexin, an antimicrobial phytoalexin [129,131,134,136]. Resistance was also correlated with the higher expression of chitinase gene family members in *C. sativa* relative to *B. juncea* [137]. *C. sativa* showed strong resistance to blackleg fungal disease [39] assessed using 80 different isolates of *Leptosphaeria maculans* (Desmaz.) [138]. However, for those *C. sativa* genotypes that are susceptible to blackleg disease, the fungicides metoconazole and a mixture of tebuconazole and triadimenol provided very effective control against the fungus [61].

C. sativa genotypes show various, but low, degrees of susceptibility to common *Brassicaceae* diseases, such as stem rot (*Sclerotinia sclerotiorum* (Lib.) de Bary), brown girdling root rot (*Fusarium* spp. and *R. solani*), downy mildew (*Peronospora sparsa*, *P. parasitica*), powdery mildew (*Erysiphe* sp.), grey mold (*Botrytis cinerea*), sore shin and damping-off disease (*Rhizoctonia solani*), Verticillium wilt (*Verticillium dahliae*), and white rust (*Albugo candida*) [18,128,139,140]. Some *C. sativa* genotypes are susceptible to downy mildew (*Hyaloperonospora camelinae*) [141]. Thirty diverse *C. sativa* genotypes showed varying degrees of resistance to *S. sclerotiorum* [142]. Resistance to *S. sclerotiorum* was associated with cell wall strengthening due to monolignol biosynthesis in *C. sativa* [143]. However, while camalexin production was induced by S. *sclerotiorum* inoculation, the relative degree of disease resistance was not correlated with levels of camalexin production, suggesting that other antimicrobial activities might be responsible for the observed disease resistance [142]. *C. sativa* also shows resistance to the soil-born fungus Fusarium *virguliforme* [144]. However, *C. sativa* is susceptible to other fungal diseases common to the *Brassicaceae*, such as damping-off (caused by *Rhizoctonia solani*), clubroot (*Plasmodiophora brassicae* Woronin.), and white rust (*Albugo candida* Pers. Kuntze) [128]. While susceptible, *C. sativa* showed greater resistance to *Rhizoctonia solani* than *B. napus* did, due to the presence of the phytoalexins camalexin and methoxycamelexin and two additional antimicrobial compounds in its roots [145].

C. sativa is susceptible to some bacterial diseases, such as bacterial blight (*Pseudomonas syringae* pv. spec.), phytoplasma disease, which was reported for *C. sativa* grown in Germany and Canada [139,140,146], and aster yellows diseases [124]. *C. sativa* also shows susceptibility to the bacterial pathogen *Xanthomonas campestris* Dowson pv. campestris, which causes black rot of *Brassica* crops globally [133].

Lastly, although relatively less well studied for viral diseases, *C. sativa* is susceptible to the Turnip crinkle virus and Turnip rosette virus [147], which are viral diseases transmitted by flea beetles via infested seed [2,148]. The beet western yellows mosaic virus reportedly caused up to 34% yield reductions in *C. sativa* [149]. Aphid (*Myzus persicae*) vector behavior and host palatability are key factors in the transmission of the Turnip yellows virus in *C. sativa* [150].

6. Ecosystem Services Provided by *C. sativa*

In addition to its role in crop rotations, *C. sativa* may be used to provide a range of ecosystem services, including prevention of soil loss and erosion, habitat for pollinators, and phytoremediation. Regrowth of hardy winter *C. sativa* can help to limit soil erosion and nutrient run off in the early spring [35]. In general, the use of *C. sativa* as a cover crop, with its deep tap root, is expected to benefit soil structure, promote nutrient recycling, and enhance nutrient scavenging [2]. Although *C. sativa* produces relatively small amounts of biomass compared with larger crops, these crop residues can promote soil water absorption capacity, which is particularly important in areas with dry soils [37]. Nonetheless, no-till and low-till cultivation methods are recommended for *C. sativa* to avoid or reduce soil erosion [111]. Both winter and spring *C. sativa* can provide pollinators with early season nectar and pollen for honey bees and other pollinators, as its flowers open long before most other crops grown in many regions [151,152]. Furthermore, *C. sativa* nectar sugar produced throughout anthesis can exceed that of pennycress (*Thlaspi arvense*) or Canola

(*Brassica napus*) [151]. Cocultivation of winter *C. sativa* with Persian clover was found to decrease the heavy metal (i.e., copper, lead, nickel, and zinc) content of soils [153]. Lastly, *C. sativa* can be used similarly to other cover crops, including those within the *Brassicaceae*, to promote atmospheric carbon sequestration, suppress weeds, provide erosion control, protect ground water quality, promote organic matter carbon and nitrogen accumulation in soils, and suppress the accumulation of fungal pathogens, particularly saprophytic fungal species, and nematodes [154,155].

7. Fatty Acid Synthesis and Seed Oil Profiling in *C. sativa*

C. sativa seed oil content varies from approximately 27 to 46% and has a high omega-3 fatty acid content [26,39,49,64]. *C. sativa* seed oil contains 90% unsaturated fatty acids (~60% polyunsaturated fatty acids (PUFAs), 30% monounsaturated fatty acids (MUFAs)), and 10% saturated fatty acids (SFAs). In *C. sativa* oil, palmitic (C16:0), oleic (C18:1), linoleic (C18:2), and α-linolenic (C18:3) acids are the predominant fatty acids [156]. *C. sativa* seed oil is unique in its oil composition and chemical characteristics because polyunsaturated α-linolenic acid (C18:3) is the major fatty acid, and the concentration of erucic acid (C22:1) is present in a comparatively low amount for a *Brassicaceae* species, whereas eicosenoic acid (C20:1) is produced instead as the major long-chain fatty acid [6].

The mean fatty acid composition of *C. sativa* oil includes α-linolenic acid (34.4%), linoleic acid (18.3%), oleic acid (14.7%), gadoleic acid (C20:1, 14.0%), and palmitic acid (5.8%) in descending order of relative abundance (Table 2). The mean erucic acid content was 2.9%, which is below the maximum threshold value allowed for biodiesel (5%) [157], and just above the 2% threshold required for food-grade oil in the USA [3]. Other fatty acids such as stearic acid (C18:0, 2.6%), docosaenoic acid (C22:0), nervonic acid (C24:1), ecosadienoic acid (C20:2), dihomo-gamma linolenic acid (C20:3), and docosadienoic acid (C22:3) are also present in trace amounts. The relative content of the major fatty acids varied widely depending on the study. For example, α-linolenic acid ranged from 22.8–38.4% [158] to 41% [157]. Linoleic acid ranged from 12.8–20.6% [159–161]. Oleic acid ranged from 6.9–22.1% [158]. The ranges of other fatty acids, such as gadoleic acid, palmitic acid, and erucic acid, are summarized (Table 2). The wide variations in fatty acid profiles of *C. sativa* likely arise from differences in genotypes, agronomic practices, growing environment (e.g., soil quality), weather and climatic conditions [2,90,162,163].

Table 2. Fatty acid profiles of *C. sativa* seed oil reported by various researchers. Bold font (bottom row) indicates mean values of fatty acid profile in *C. sativa* from the different reports. Dashes indicate missing data.

Concentration of Major Fatty Acids (%)										Reference
C16:0	**C18:0**	**C18:1**	**C18:2**	**C18:3**	**C20:1**	**C22:1**	**SFA**	**MUFA**	**PUFA**	
-	-	-	21–23	27–29	-	-	11–12	35–36	51–52	[75]
-	-	14–16	15–23	31–40	12–15	-	-	-	-	[2]
5.3–5.6	2.2–2.7	14.7–16.5	12.9–16.3	35	15	3	12	34	54	[159,160]
-	-	-	-	30–43	11–19	<3	-	-	-	[6]
5.4	2.4	14.3	20.6	36.9	13	2.2	-	-	-	[3]
6.29	2.73	16.5	17.7	32.5	15.6	3.1	-	-	-	[64]
5.16	2.68	15.2	17.9	34.6	15.1	2.6	8.6	33.0	54.1	[26]
5.68	-	13.9	16.6	35.1	14.3	3.0	10.1	33.5	55.9	[164]
-	-	9.1–22.1	15.2–27.1	22.8–38.4	11.6–18.2	-	-	-	-	[158]
5.5	2.4	14.4	19.1	33.5	15	3.1	-	-	-	[165]
7	2.5	6.9	14.5	41	10.9	3.5	-	-	-	[157]
6.8	2.7	18.6	19.6	32.6	12.4	2.3	-	-	-	[166]
5.1	2.4	17.6	18.7	28.6	11.9	4.2	-	-	-	[167]
5.4	2.6	14.3	14.3	38.4	16.8	2.9	-	-	-	[25]
5.7	3.4	15.0	18.5	34.7	12.7	3.2	-	-	-	[168]
4.6–5.2	2.2–2.5	12.8–14.7	16.3–17.2	36.2–39.4	14.0–15.5	2.5–3.1	8.7–8.8	-	-	[39]
5.5–9.5	-	9.1–17.1	16.1–28.6	23.5–36.2	10.5–16.4	<2	-	-	-	[161]
6.2	2.6	16.2	17.5	37.3	13.1	2.3	9.7	31.7	57.7	[71]
5.8	**2.6**	**14.7**	**18.3**	**34.4**	**14.0**	**2.9**	**10.1**	**33.5**	**54.6**	

The biosynthesis of triacylglyceride (TAG) in *C. sativa* occurs in the plastid via a Type II fatty acid synthase complex [169]. In most oilseed crops, the fatty acid chain elongates to 16 or 18 carbons in length [162]. Oleic acid (C18:1) (MUFA) is synthesized in the plastid from stearic acid (SFA) through steroyl-acyl carrier protein desaturase (SAD). Further desaturation of oleic acid to linoleic acid (C18:2) is catalyzed by fatty acid desaturase-2 (FAD2), a key enzyme responsible for the biosynthesis of PUFA in non-photosynthetic tissues, for example, the roots and developing seeds of oilseed plants in the ER and FAD 6 (plastidial enzyme) in the plastid [170,171]. α-linolenic acid (C18:3) synthesis from linoleic acid is catalyzed by FAD3 (microsomal enzyme) in the ER and FAD7/FAD8 (plastidial enzymes) in the plastid [172]. Fatty acid composition can change during seed development and varies with *C. sativa* accession. Fatty acid production can be affected by location due to climactic differences [157,173]. In oilseed crops, α-linolenic acid content differs depending on the temperature conditions during seed development. For example, at temperatures greater than 25 °C, the synthesis of α-linolenic acid declines because the activity of FAD3 decreases [2], whereas the synthesis of oleic and α-linoleic acid increases [174,175]. Similarly, biosynthesis of α-linolenic acid declined in non-irrigated compared with irrigated *C. sativa*, likely due to the higher temperatures of the non-irrigated plants [81]. Additionally, increasing temperatures from 15 °C to 35 °C reduced the expression of the FAD2 gene, suggesting a reduction in the synthesis of linoleic acid from oleic acid. A shorter duration of grain filling and a greater number of days above 25 °C resulted in a decline in linoleic acid content [176]. More recently, water-deficit stress was shown to increase oleic and linoleic acid content in *C. sativa* seeds, whereas linolenic acid content decreases, being dependent upon genotype, as one accession showed an increase in a-linolenic content following drought treatment [177]. Importantly, various environmental stress factors including heat, drought, salinity, high light, low oxygen, and high nitrogen can lead to decreases in overall seed oil content and changes in fatty acid composition [162]. Thus, an important consideration for improving overall seed oil yield is the need to improve the abiotic stress tolerance of *C. sativa*, particularly in the face of increasingly hot and dry conditions brought about by global warming.

8. Uses of *C. sativa*

C. sativa is used in a wide array of products and applications ranging from industrial, biomedical and nutraceutical products to animal feed, erosion control as ground cover, phytoremediation and carbon sequestration. *C. sativa* is also used in processed foods for human consumption. *C. sativa* is widely used as a biofuel, including biodiesel, green diesel, and renewable jet fuel. Derived products include glycerin, soaps and lotions (Figure 2).

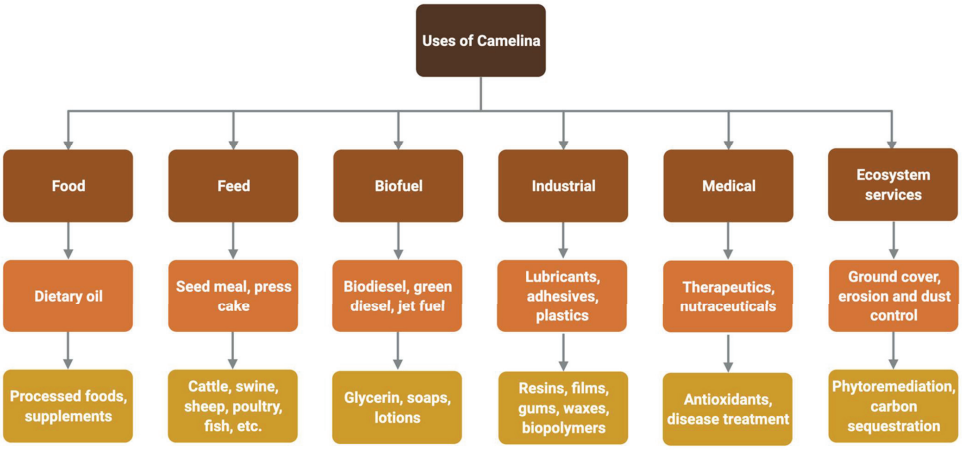

Figure 2. Diverse uses of *C. sativa* adapted from Chaturvedi et al., 2017 [17]. Created with BioRender.com.

8.1. Food and Food Products for Humans

C. sativa cooking or salad oil has potential human health benefits due to its high levels of PUFAs, omega-3-fatty acids, and antioxidants [156,178]. The consumption of *C. sativa* oil can reduce blood serum cholesterol levels [179] and improve serum lipid profiles [180,181]. Furthermore, *C. sativa* oil consumption can attenuate inflammation in peripheral blood mononuclear cells [182]. Such metabolic changes are thought to not only protect against cardiovascular risk factors, but also improve mental health in patients suffering from non-alcoholic fatty liver disease [183]. *C. sativa* oil was also used in folk medicine to treat burns and wounds to the skin and eyes [184,185]. The high levels of tocopherols, phytosterols, and carotenoids in *C. sativa* oil protect it from oxidation, imparting extended shelf life [185,186]. *C. sativa* oil displays antioxidant activities similar to those found in sunflower oil, which can effectively limit oxidation in food products, such as salad dressings and mayonnaise [156,187]. For example, *C. sativa* oil and rapeseed meal prevented the oxidation of lipids and proteins in cooked pork patties [188].

8.2. Feed for Animal Nutrition

Following oil extraction, *C. sativa* seed meal is toasted, dried, and cooled ready to use as animal feed for cattle, dairy cows, sheep, swine, and poultry, as well as for aquaculture of various fish stocks [2,189]. *C. sativa* seed and seed meal are generally considered useful and beneficial as animal feed in limited quantities. *C. sativa* seed displays a balanced profile of essential and non-essential amino acids [159,190].

8.2.1. Beef Cattle

The exceptionally high level of omega-3 fatty acids, particularly α-linolenic acid (~32–40% of total oil content), protein (40%), oil (10–15%), fiber (0–15%), and phytate (1–6%), combined with relatively low glucosinolate levels (20–44 mmoles kg^{-1} dry weight), in *C. sativa* seed meal make it a suitable feed for animals [2,21,159,160,191,192]. *C. sativa* seed meal is generally comparable to Canola meal in terms of its amino acid profile, crude protein content, and digestibility, and was demonstrated to be a valuable feedstuff for ruminants [193–195]. However, some researchers report lower degradability and palatability of *C. sativa* seed meal compared with soybean or Canola meal [196,197]. Supplementation of the diet of beef cattle with *C. sativa* seed meal resulted in reduced forage and dry matter intake, but gave rise to greater serum PUFA concentrations [198]. In a related study, addition of 10% *C. sativa* seed meal on a dry weight basis did not affect dry matter intake and improved digestion of rumen organic matter, but did reduce body weights of dairy heifers [199]. Other studies report no negative effects on animal performance when *C. sativa* seed meal comprised up to 10% of the total diet [193]. *C. sativa* seed meal is highly degradable and shows comparable total digestibility and protein absorption to other cattle feed supplements [200]. Reduced intake or weight loss might be the result of the reduced palatability of *C. sativa* seed meal, as it contains anti-nutritive compounds, such as erucic acid, sinapine, and glucosinolates [196,201]. Due to these reasons, the U.S. Food and Drug Administration (FDA) permits only a maximum of 10% *C. sativa* seed meal in rations for livestock [202]. However, the sinapine content of *C. sativa* seed meal is lower than other *Brassica* species, and thus, only the glucosinolate content is relevant when assessing palatability [192]. Glucosinate content varies widely among accessions, and thus could be reduced through conventional breeding [192,203,204]. A high erucic acid content in seed meal can lead to fat deposition and reduced contractibility of the heart muscle and is thus limited to a maximum of <2% [205]. The erucic content in *C. sativa* seed meal ranges from 1.8–4.8% in the USDA National Genetic Resources Program collection [161]. Thus, similar to low glucosinolate accessions, accessions with low erucic acid content, such as *C. sativa* accession PI 650141, could be used for conventional breeding efforts or genome-editing approaches [161].

8.2.2. Dairy Cows

C. sativa meal has a reasonably high level of histidine content, which is a good supplement for silage and grain-fed lactating cows [196]. Inclusion of seed or seed meal in the diet of dairy cows decreased dry matter intake, but did not have a significant effect on milk production [206]. However, overall milk protein and fat yield declined and resulted in a modified fatty acid profile with increased MUFAs and PUFAs, with resultant increases in butter spreadability [206]. Addition of *C. sativa* seed meal or oil to dairy cow diets did not alter dry matter intake, digestibility, or milk yield, but resulted in decreased saturated fatty acids and increased milk MUFA and PUFA content [207]. In a related study, supplementation of up to 6% *C. sativa* oil decreased milk yields and saturated fatty acid content while increasing unsaturated fatty acid content. This study concluded that 2% *C. sativa* oil could be used for commercial production without major adverse effects on animal performance [208].

8.2.3. Sheep and Goat

Inclusion of 10–20% *C. sativa* seed meal in the diet of sheep increased the content of linoleic, oleic, and α-linolenic acid content in lamb muscle [209] and reduced blood triglycerides and glucose content, while increasing insulin levels [210]. Inclusion of *C. sativa* seed meal in sheep diets improved the total omega-3 fatty acid and the ratio of omega-6/omega-3 fatty acids in lamb and yearling meat, but resulted in reduced vitamin E content, which negatively impacted color and oxidative stability upon storage [211].

Supplementation of an ewe's diet with 3–6% of *C. sativa* seed meal (or seed) in dietary dry matter increased the mono- and polyunsaturated fatty acid content of milk, resulting in milk with lower atherogenic and thrombogenic indices [212,213]. Similarly, inclusion of *C. sativa* seed meal in the diet of dairy goats increased total polyunsaturated fatty acids and decreased total saturated fatty acids in milk and kefir produced from the milk [214]. Inclusion of 10–20% *C. sativa* seed meal in the diet of dairy sheep altered the content and aroma of volatile compounds, primarily fatty acids, in raw and pasteurized ewe's milk with an overall loss of dairy or freshness aroma [215]. Sheep or goat milk with increased fatty acid content resulted in increased fermentation time and alterations in the resulting kefir, and altered its aroma [216]. Additional studies validated these effects and showed that supplementation of sheep diets with varying amounts of *C. sativa* seed meal increased the mono- and/or poly-unsaturated fatty acids content and oxidative stability of the milk, resulting in a healthier milk for human consumption [217–220].

8.2.4. Swine

After cold or expeller pressing, a comparatively high amount of oil (100–150 g kg^{-1}) remains in the meal of *C. sativa*, which provides a potential energy source for swine diets [2]. Inclusion of 5–10% *C. sativa* seed meal in swine diets resulted in increased plasma omega-3 fatty acids and reduced plasma omega-6 fatty acids in blood plasma, while reducing serum triglyceride levels [221]. During the finishing–fattening process, supplementation of the swine diet with *C. sativa* oil increased α-linolenic acid content and reduced cholesterol content in the meat, thereby improving meat quality [222], and increased n-3 polyunsaturated fatty acid and reduced cholesterol and triglyceride of the plasma, implicating improved animal health [223]. Compared with sunflower seed meal, the inclusion of 12% *C. sativa* seed meal in the swine diet did not affect growth performance, but elevated the expression of some antioxidant defense system components in the spleen [224]. Digestibility of *C. sativa* seed meal in swine was comparable to that of Canola meal [225]. However, the addition of 20% *C. sativa* seed meal lowered digestibility coefficients for amino acids and crude protein, which limits its utilization in the swine diet [226]. Inclusion of 12% *C. sativa* seed meal increased α-linolenic acid content in the heart and brain with little alteration in performance [227]. Inclusion of *C. sativa* seed meal in the diets of weaned piglets at up to 18% increased n-3 fatty acids in carcass fat depots, but did not elicit clinical signs of toxicity,

although it did result in lower average daily feed intake and weight gain than controls, probably due to an aversion to the taste of the *C. sativa* seed meal [228].

Supplementation of *C. sativa* seed meal improved feed efficiency and liver weight in 28-day-old weaned piglets, but also increased the expression of selected liver enzymes [229]. Comparison of the effects of the addition of 5%, 10%, or 15% *C. sativa* seed meal to the diet of growing–finishing pigs showed that the two higher percentages reduced average daily weight gain and marketing weight, but no negative growth performance or carcass traits were observed at 5% addition to a corn–soybean meal-based diet [230]. Incorporation of up to 30% *C. sativa* seed meal in a mixed corn/soybean meal diet for growing swine did not alter the digestible, metabolizable, or net energy, suggesting that dietary glucosinolates from *C. sativa* seed meal did not affect these dietary parameters [231].

8.2.5. Poultry

Incorporation of *C. sativa* seed meal into poultry diets benefits from the provisioning of energy and protein, increased health-promoting PUFAs and tocopherol content of meat and liver, improved antioxidant activity and lipid stability, and increased market value of the meat and eggs [189,232]. Unlike other livestock animals, chickens appear somewhat less susceptible to the taste of *C. sativa* seed meal and generally do not show reduced feeding efficiency or weight gain when provided in moderation. For example, the addition of 2.5%, 5%, and 10% *C. sativa* seed meal to a basal corn–soybean diet had little effect on weight gain and feed efficiency [233]. However, *C. sativa* seed meal resulted in significant increases in a-linolenic acid and n-3 PUFAs in white and dark meat and tissues [233]. Inclusion of 10% *C. sativa* seed meal increased egg production and increased α-linolenic acid and total n-3 PUFAs in egg yolks, compared with a corn–soybean-based diet, but reduced crude protein digestibility [234]. Addition of 8%, 16%, and 24% *C. sativa* seed meal resulted in linear increases in α-linolenic acid content in various tissues including liver, breast, and thigh, and in the proportion of n-3 PUFAs in liver and brain [235]. The supplementation of cold-pressed *C. sativa* seed cake of broiler chicken diets with or without multienzyme supplementation to improve digestibility was found to improve the energy and amino acid content of the diets [236].

Related studies tested the effects of oil supplements on poultry diets. For example, the addition of 6% of *C. sativa* oil to feed rations for broiler chickens reduced the cholesterol content in the blood plasma and increased omega-3 PUFA content in the breast, without producing an unpleasant flavor [237,238]. The addition of *C. sativa* oil to broiler chicken diets resulted in increased α-linolenic acid content in muscle and abdominal fat to a greater extent than diets supplemented with either soybean or rapeseed oil [237]. Other studies showed that *C. sativa* oil and seed meal in broiler chicken diets improved the percentage of PUFAs, particularly omega-3, and lowered the percentage of MUFAs, such as oleic acid, in the lipids of the breast muscles [239].

In addition to chicken, a variety of other poultry species were evaluated for *C. sativa* seed meal use. As with chicken diets, the inclusion of 15% to 20% *C. sativa* seed meal in duck diets resulted in significant increases in α-linolenic acid and total omega-3 PUFA in breast and leg muscles [240]. The addition of up to 5% *C. sativa* seed meal to the diets of young turkeys showed similar weight gain and feed conversion as vegetable oil and showed no negative effects [241]. However, the addition of 5% and 10% *C. sativa* cake to turkey diets caused growth depression and reduction of feed intake [242,243]. In contrast, no negative effects of weight gain or feed intake were observed when 5%, 10%, or 15% *C. sativa* seed meal was added to quail diets [244].

8.2.6. Fish

C. sativa oil and seed meal can serve as good replacements for fish oil and fish meal in fish feed. Diets of 5% *C. sativa* seed meal are acceptable substitutes to reduce reliance on fish meal [245]. Substitution of *C. sativa* oil in fish feed improved the total lipid content in salmon (*Salmo salar* L.) and Atlantic cod (*Gadus morhua* L.) without negatively affecting the sensory

quality of fish fillets [246]. *C. sativa* seed oil can be used as up to 100% replacement for fish oil without negative growth effects for Atlantic salmon raised in freshwater [245]. However, while replacing fish oil with *C. sativa* oil at ~80% had no effect on growth performance, PUFA content in the liver and muscle was reduced in Atlantic cod [247]. In another study with Atlantic cod, feeding *C. sativa* seed meal up to 24% of the diet did not affect growth in one experiment, while in a separate experiment, *C. sativa* seed diet greater than 30% resulted in depressed feed intake and growth due to reduced palatability [248]. Replacement of fish oil with oil from *C. sativa* genetically modified to express eicosapentaenoate (EPA; 20:5 n-3) and docosahexaenoate (DHA; 22:6 n-3) [249], in a feeding trial of European sea bass (*Dicentrarchus labrax*), showed no change in feed intake or growth [250]. However, the resulting fillets showed enhanced omega-3 PUFA content, indicating that *C. sativa* seed oil can effectively replace fish oil for the production of European sea bass without negative impacts on feed efficiency or growth rates [250]. *C. sativa* seed or seed meal of at least 10% can be used for feeding rainbow trout (*Oncorhynchus mykiss*) without reductions in feed conversion or weight gain [251].

8.3. Biodiesel/Renewable Diesel Fuel

One of the most important uses for *C. sativa* oil is the production of various biofuels. As with other oilseeds, the fatty acid profile of *C. sativa* oil varies depending upon the environmental conditions under which it is grown, thus resulting in variations in physical and chemical properties of the biodiesel produced. The major properties used to evaluate the quality and performance of biodiesel include cloud point (CP), cold-flow characteristics or viscosity, cetane number (CN), and oxidative stability [2,26]. Unformulated *C. sativa* B100 fails to meet the American Society for Testing and Materials (ASTM) standards for CP and oxidative stability due to exceptionally high (48–50%) polyunsaturated fatty acid content, but does meets the standard criteria for CN. However, with the addition of antioxidants, unformulated B100 can meet current ASTM standards while maintaining production costs at a level comparable with other biodiesel feedstocks [165,252]. Biodiesel produced from *C. sativa* oil generally resembles biodiesel from Canola oil (*B. napus*) [25]. The kinematic viscosity of methyl esters obtained from *C. sativa* varies from 2.9–6.4 $mm^2\ s^{-1}$ at 40 °C, which lies within the acceptable 1.9–6.0 $mm^2\ s^{-1}$ ASTM D651, and 3.5–5.0 $mm^2\ s^{-1}$ EN14214 standard values [25,26,165,166,253–255]. The CN for *C. sativa* methyl ester ranged from 49.26 to 51.17, a value higher than ASTM biodiesel standards, resulting in good ignition quality of fuel. Furthermore, the pour point of *C. sativa* methyl ester was typically between −11 °C and −8 °C, suggesting a good quality fuel under cold season temperatures. Fuel consumption and vehicle operation from *C. sativa* and Canola methyl esters are similar [25]. In addition to traditional biodiesel, *C. sativa* can be used to produce hydrogenation-derived renewable diesel (HDRD) or green diesel, which generally has chemical properties more similar to that of petroleum diesel and improved cold-flow characteristics [256], yet is more sustainable than fossil diesel based upon emission parameters [257]. Life cycle analysis of *C. sativa* for biodiesel production showed that it produces lower greenhouse gas emissions than soybean- or Canola-derived biodiesel through reduced impacts on land-use changes [258].

8.4. Hydro-Processed Renewable Jet (HRJ) Fuel

Renewable jet fuel production from *C. sativa* oil follows a two-step standard process: (1) initial hydrodeoxygenation or hydrotreatment and (2) selective cracking or hydrocracking and isomerization, followed by product separation and formulation. The linear alkanes produced during step one can be used in renewable diesel mixtures [2,166]. Compared with JP-8 (typical jet fuel), *C. sativa* HRJ fuel had superior thermal-oxidative stability [259]. Engine tests with *C. sativa* fuel showed no obvious anomalies with engine operation, with the added advantage of lower carbon monoxide emissions than JP-8. However, *C. sativa* HRJ fuel contains elastomer seal swelling capability, which might cause fuel leaks in aircrafts, but this was lower than that of JP-8 [259]. *C. sativa* HRJ fuels have similar properties

to conventional fuels used in turbine engines [259–261]. In 2009, the U.S. Air Force (USAF) tested the potential of *C. sativa* HRJ fuels as a replacement for jet fuels, with successful tests performed in fighter jets, private jets, and commercial airlines using a blend of JP-8 and *C. sativa*-based jet fuels [2,262]. *C. sativa*-based jet fuel with blending had a 75–80% lower carbon footprint compared with conventional fuel [263]. Overall, these results confirm the ability of renewable fuels derived from *C. sativa* to burn cleaner than conventional fossil fuel resources, while also removing carbon from the atmosphere during their production, resulting in overall lower carbon emissions. However, techno-economic analysis reveals that considerable investments in land area would be needed to grow *C. sativa* at large scale for economic viability [264].

8.5. Fast Pyrolysis Bio-Oil

In addition to the use of *C. sativa* for biodiesel and renewable diesel, the energetic value of the seed meal and lignocellulosic biomass was also considered. Thermochemical fast pyrolysis of the seed meal after oil extraction contains significant energetic value (29 MJ kg^{-1}) when compared with whole seeds (34.7 MJ kg^{-1}) and can provide additional volumes of high-energy, high-carbon liquid fuel intermediates for the production of renewable biofuels and jet fuel [265]. *C. sativa* residual biomass is comprised of 36.3–41.6% cellulose, 23.2–24.9% hemicellulose, and 25.0–26.3% lignin, and can be converted to bio-oil using thermal or catalytic fast pyrolysis [266]. However, the energetic value of *C. sativa* straw (15.1–15.5 MJ kg^{-1}) or straw pellets (16.6–17.1 MJ kg^{-1}) is lower than that of seeds or seed meal, but can produce gas, solid, and liquid fuel components with reduced nitrogen and sulfur contents relative to other woody or herbaceous feedstocks tested [267]. *C. sativa* straw was also used for ethanol production with an estimated total energy yield of 54.3 MJ L^{-1} ethanol [268]. Agronomic management can improve the overall energy potential of *C. sativa* biomass. For example, high rates of nitrogen and sulfur fertilization can increase the energy output of *C. sativa* seed and residual biomass by up to 186% and 155%, respectively [269]. The net energy efficiency and economic value of total *C. sativa* biomass (straw and seed) was higher than that of crambe (*Crambe abyssinica*) [270]. Thus, *C. sativa* biomass utilization, as part of an integrated biorefinery strategy where renewable diesel or jet fuel and thermal or catalytic fast pyrolysis bio-oil production are co-localized, can improve the overall energetic value of this bioenergy resource.

8.6. Industrial Applications

C. sativa oil has great potential for bio-based industrial applications. The high quantity of unsaturated fatty acids (~90%) present in *C. sativa* oil [6], enables rapid drying, and is useful for making dermatological products, cosmetics (lotions and soaps), polymers, paints, and varnishes [22,27,271]. A key limitation of using *C. sativa* oil for industrial application is its high content of PUFA, which promotes the oxidation of oils upon exposure to high temperatures [272,273]. *C. sativa* oil can be epoxidized and used for making adhesives, coatings, lubricants, and alkyd resins [274,275]. *C. sativa* meal has great potential for use in the paper industry [276]. The addition of *C. sativa* meal to recycled newspaper produced sustainable and bio-degradable green composite sheets and fibers [276]. Other applications include bio-herbicides [277], soil fungicides [278], and bio-oils [265]. *C. sativa* oil contains glucosinolates, which can be used to produce ionic thiocyanates that can serve as effective bio-herbicides against redroot pigweed (*Amaranthus retroflexus* L.) and wild oat (*Avena fatua* L.) [277]. *C. sativa* glucosinolate content ranged 9–31.4 μmol g^{-1} in seed [279,280], 14.5–23.4 μmol g^{-1} in seed meal [280], and 8.6–30.5 μmol g^{-1} in oil [281] depending upon the genotype and environmental growth conditions.

8.7. Biomedical Uses

In addition to the beneficial use of *C. sativa* seed meal for improving the quality of other foods such as meat and dairy products, the consumption of dietary oils, such as the oil from *C. sativa*, which is rich in essential omega-3 fatty acids (e.g., α-linolenic acid), was

associated with reduced risks of coronary heart disease and inflammatory diseases [282,283]. Supplementation of the human diet with *C. sativa* oil can also reduce serum cholesterol in hypercholesterolemic subjects [179]. In addition, the oil contains high nutritional value due to the presence of tocopherols, phytosterols, and carotenoids [284,285].

Leaves of *C. sativa* contain flavonols such as quercetin [286]. Methanolic and ethanolic extracts of *C. sativa* seeds show significant antibacterial and antifungal activities and potential as natural preservatives [287]. Additional therapeutic properties are associated with phenolic compounds in C. sativa seeds and oil, such as chlorogenic, caffeic, sinapinic, and phytic acids [288]. However, as mentioned earlier, *C. sativa* seeds contain glucosinolates, which have antinutritive properties [201].

The ethanolic and methanolic extracts of defatted *C. sativa* seeds were shown to reverse short-term memory impairment and reduce anxiety and depression-like behaviors in a Swiss mouse model for irritable bowel syndrome exposed to various stress tests [289]. Furthermore, these extracts decreased superoxide dismutase, but increased glutathione peroxidase activity in brain and bowel tissues as well as potentially increasing lipid peroxidation in the bowel. The authors concluded that seed extracts could improve performance and mood while exhibiting antioxidant capacity in both brain and bowel tissues [289]. In a related study, the administration of cold-pressed *C. sativa* oil was shown to ameliorate impairment of short-term memory, anxiety, and depression in a Swiss mouse zymosan-induced model for irritable bowel syndrome exposed to various stress tests [290]. Furthermore, *C. sativa* oil treatment resulted in increases in superoxide dismutase and glutathione peroxidase activity in brain and bowel tissues, resulting in decreased malondialdehyde levels, a lipid peroxidation marker, in these tissues [290].

9. Strategic Innovations for Climate-Resilient *C. sativa*

The hotter and drier conditions brought about by climate change will require novel strategies for improving the heat and drought durability of *C. sativa* in the future. Recent research suggests that *C. sativa* is able to maintain a higher shoot/root ratio under water-deficit stress and is more drought tolerant than Canola (*B. napus*) [291]. Comparisons of *C. sativa* and Canola under deficit irrigation regimes suggest that *C. sativa* performed better and gave higher seed yields than Canola under field conditions [292]. To assess the relative tolerance to water-deficit and salinity stress, screening assays of different genotypes at germination were developed. Such germination screens suggested that seedlings of *C. sativa* cv. Calena exhibited germination up to 150 mM NaCl and thus might be suitable for cultivation in saline soils [293], but additional research is required to confirm this suggestion. Comparison of two different genotypes of *C. sativa* showed that increased water-deficit stress tolerance was associated with differences in stomatal conductance and increased accumulation of osmoprotectants such as proline, sugars, amino acids, and soluble proteins [294]. Screening of winter and spring genotypes revealed differences in germination under artificial osmotic stress imposed by different concentrations of polyethylene glycol (PEG) [295]. Application of sodium selenite (Na_2SeO_3) via seed priming or foliar application was shown to increase drought tolerance in *C. sativa* (and Canola) via the accumulation of osmoprotectants and antioxidants, and to improve crop yields [296,297]. Fertilization of *C. sativa* with thiourea at the seed filling stage improved heat tolerance [298]. While such selection or treatment efforts carry a certain degree of practical utility, more direct advanced breeding and biotechnological innovations will be needed to dramatically improve the yield potential and climate resiliency of *C. sativa*.

9.1. Molecular Breeding Approaches

Characterizing the genetic diversity and population structure of available genotypes is often the first step towards developing breeding programs for improving key traits such as yield potential, oil content, resistance to biotic and abiotic stresses, and adaptability to diverse environments. Sequencing complete allohexaploid *C. sativa* transcriptomes and genomes was a key first step for advanced molecular breeding efforts [34,53,299,300].

Such information is critically important for future gene identification using genomic selection, marker-assisted selection, and genome-wide associations studies (GWAS) to guide future *C. sativa* breeding programs. For example, a recombinant inbred population from two *C. sativa* accessions (Suneson and Pryzeth) with contrasting traits, especially seed size and oil content, was developed and used to assess phenotypic differences under two environmental conditions (dryland and irrigated) [301]. Using 189 lines from this population, a genetic map was created containing 2376 single nucleotide polymorphisms (SNPs) to identify quantitative trait loci (QTLs) associated with oil content, seed size, pod size, and seed number per pod as a first step towards isolating genes that control for seed development and oil accumulation [301]. In another example, a total of 213 spring *C. sativa* accessions were collected and genotyped to assess the genetic diversity available for future breeding efforts [302]. A total of 6192 SNPs were identified using genotyping-by-sequencing technology and used to reveal two distinct populations of *C. sativa* arising from Germany and eastern Europe [302].

Various screening efforts for wildtype and mutagenized *C. sativa* were used to identify lines with desirable traits of interest. For example, analysis of *C. sativa* seedlings from 10 different cultivars using germination screens under a gradient of NaCl conditions found that 100 mM NaCl was optimal for differentiating the phenotypic performances of seedlings [303]. Screening of a spring panel of 211 *C. sativa* accessions followed by GWAS revealed a total of 17 significant trait-associated SNPs for germination rates and dry weight with potential roles in root development through mediation of phosphate metabolism, signaling, and cell membrane activities [303]. In addition, mutational breeding using gamma-ray irradiation was successfully used to alter the fatty acid profile in *C. sativa*, resulting in the identification of M_2 mutants with increased α linolenic acid content or decreased erucic acid content [304]. Screening of ethyl methanesulfonate (EMS) mutant populations resulted in the isolation of a *C. sativa* mutant with reduced seed coat mucilage, which could potentially improve the flow characteristics of the oil and reduce the washing requirements of the resultant biodiesel [305].

9.2. Improving Productivity Using Rhizosphere Microbes

In order to reduce reliance on fossil fuel-based fertilizers, interest into the use of plant growth-promoting rhizobacteria has increased in recent years. Early research indicated that the presence of nitrogen-fixing bacteria was necessary to stimulate root growth in flax (*Linum usitatissimum* L.) through aqueous washing of *C. sativa* leaves [306]. More recently, inoculation of *C. sativa* with a consortium of rhizosphere soil bacteria containing *Bacillus* species resulted in approximately a threefold increase in seed yield [307]. Similar enhancement in *C. sativa* winter hardiness and seed productivity were observed when *C. sativa* seeds were inoculated with nodule bacteria from crimson clover (*Trifolium incarnatum* L.) roots before sowing [308].

9.3. Improving Quality Traits

To complement molecular breeding and rhizosphere manipulation approaches, advances in the genetic transformation of *C. sativa* were developed [9,10,12,13]. The stable introduction of genes into *C. sativa* was used to modify or improve a wide range of agronomic traits with a focus on the manipulation of seed oil yield potential and characteristics [11]. For example, *C. sativa* was genetically modified using a set of heterologous genes to express eicosapentaenoate (EPA; 20:5 n-3) and docosahexaenoate (DHA; 22:6 n-3) as a replacement for fish oil [249]. Improving the oil content and seed yield in *C. sativa* by co-expressing *A. thaliana* diacylglycerol acyltransferase 1 (DGAT1) and yeast cytosolic glycerol-3 phosphate dehydrogenase (GPD1) genes under the control of seed-specific promoters resulted in up to 13% higher seed oil content and up to 52% higher seed mass compared with wild-type plants [309].

9.4. Improving Stress Tolerance Traits

Soil amendments containing PGPR (*Pseudomonas migulae* 8R6) that produce 1-amino cyclopropane-1-carboxylate deaminase (ACC deaminase) increased seed production in *C. sativa* by 30–50% under salinity stress by reducing stress ethylene [310]. Furthermore, plants expressing the bacterial version of the ACC deaminase (acdS) gene showed higher seed production, better seed quality, and higher levels of seed oil production under salinity stress than control lines [310]. The observed improvements in salinity tolerance were attributed to changes in the gene expression of multiple plant signaling pathway components and the modulation of genes involved in the production of reactive oxygen species (ROS) scavenging and signaling [311].

Many engineering strategies targeting improvement of abiotic stress tolerance begin with the characterization of stress-responsive genes. For *C. sativa*, stress-responsive gene discovery was performed by subjecting 15-day-old plants to 3 or 17 days of water-deficit stress and rehydration recovery for 3 days to identify hundreds of differentially expressed genes in diverse metabolic and signaling pathways based upon their relative, steady-state transcript abundance patterns [312]. Gene expression changes in *C. sativa* roots and vegetative tissues in response to salinity stress revealed hundreds of changes in relative, steady-state transcript abundance, the relative proportion of which could be assigned to each of the three *C. sativa* subgenomes [313]. Ectopic overexpression of a MYB96 transcription factor from *A. thaliana* in *C. sativa* resulted in improved water-deficit stress tolerance, due to the activation of genes involved in epicuticular wax biosynthesis [314]. Similarly, the ectopic overexpression of the CsMYB96A gene resulted in increased water-deficit stress tolerance due to the increased expression of epicuticular wax biosynthetic genes [315]. Such an approach might be useful for growing *C. sativa* on semi-arid and arid lands; however, field trials would be necessary to assess the efficacy of these modifications.

9.5. Genome-Editing Approaches

To complement molecular breeding approaches, advances in genetic transformation and genome editing using clustered regularly interspaced short palindromic repeats (CRISPR)/CRISPR-associated protein (CRISPR/Cas) are used to improve the oil contents and fatty acid profiles in oilseed crops, including *C. sativa* [316–318]. An early demonstration of this technology in *C. sativa* was the simultaneous mutation of the diacylglycerol acyltransferase (DGAT1) and phospholipid:diacylglycerol acyltransferase (PDAT1) genes, which resulted in decreased oil content and altered fatty acid composition [319]. CRISPR/Cas9 disruption of all three homoeologous fatty acid desaturase 2 (FAD2) genes in *C. sativa* resulted in a substantial increase in oleic acid content (15% to >50%) with associated decreases in linoleic (~16% to <4%) and α-linolenic acid (~35% to <10%) content in *C. sativa* seeds [16]. In a related study, disruption of all three pairs of FAD2 homeologs in *C. sativa* resulted in an 80% enhancement in MUFA content in seeds, but this resulted in severely stunted plants [319]. However, if only two homeologous gene pairs were knocked out, up to a 60% increase in seed MUFAs was obtained and the plants showed normal phenotypes [319]. This alteration in the fatty acid profile resulted in a healthier oil profile while also improving the oxidative stability of the oil, which improves its utility for biodiesel production [16]. A related study used CRISPR/Cas9 to knock out all three FAD2 homeologs in the allohexaploid *C. sativa*, resulting in increased accumulation of oleic acid in the seed oil [15]. CRISPR/Cas9-mediated knockout mutagenesis of all three fatty acid elongase 1 (FAE1) genes reduced the total content of C20-C24 very long-chain fatty acids (VLCFAs), which normally constitute 22% of fatty acids in wild-type plants, to less than 2% of total fatty acids, with a corresponding increase in desirable C18 unsaturated fatty acids for dietary or fuel uses [14]. CRISPR/Cas9 gene editing was also used to disrupt the three homeologous genes encoding CRUCIFERIN C, which resulted in an alteration in the relative abundance of other cruciferin isoforms, but did not alter total seed protein content [320]. However, the overall amino acid composition of the seed was altered along with an increase in the relative abundance of all saturated fatty acids. Other attractive

targets of genome editing to improve production traits include strategies to reduce silicle shattering and to prevent uneven seed maturation.

10. Conclusions and Future Directions

C. sativa is a highly attractive oilseed due to its low input requirements and costs and adaptability to diverse environments and soil conditions, including abandoned, marginalized, and semi-arid and arid regions. While genetic engineering and genome-editing approaches have yielded great improvements in its oil content and fatty acid profiles, *C. sativa* can also be outcrossed with related species [103], raising the possibility of targeted breeding programs to improve its yield and trait diversity. Improvements in agronomic management and commercial investments are also needed to reduce production costs and inputs and improve its overall seed yield and seed oil content relative to competing oilseeds [1,258]. In addition, improved valorization of the *C. sativa* value chain, from seed processing, oil extraction and refinement methods [321] to its co-products and lignocellulosic crop residues, is needed to better understand its integrated economic value [322] within the framework of the biorefinery concept and the bio-based economy for *C. sativa* [270,323]. More detailed examination of phenotypes is also necessary to discover natural variation in quality traits, such as the low erucic acid content of its oil [161], and production traits, such as improved heat and drought tolerance [324]. Lastly, increasing market demands for bio-based products for the renewable fuels market and improvements in value-chain cost efficiencies will likely increase future demands for this versatile crop, with great potential for agricultural production systems of the future that will increasingly rely on more climate-resilient crops such as *C. sativa*.

Author Contributions: Conceptualization, D.N. and J.C.C.; methodology, D.N. and R.H.L.; validation, D.N. and R.H.L.; formal analysis, D.N. and R.H.L.; investigation, D.N. and R.H.L.; resources, J.K.Q.S. and J.C.C.; data curation, D.N. and R.H.L.; writing—original draft preparation, D.N.; writing—review and editing, D.N. and J.C.C.; visualization, D.N. and J.C.C.; supervision, J.K.Q.S. and J.C.C. project administration, J.K.Q.S. and J.C.C.; funding acquisition, J.K.Q.S. and J.C.C. All authors have read and agreed to the published version of the manuscript.

Funding: This research was funded by Hatch grant funding from the Nevada Agricultural Experiment Station under projects NEV-00372 and NEV-00384.

Data Availability Statement: Not applicable.

Acknowledgments: The authors would like to thank Lisa Petrusa for critical reading of the manuscript.

Conflicts of Interest: The authors declare no conflict of interest. The funders had no role in the design of the study; in the collection, analyses, or interpretation of data; in the writing of the manuscript, or in the decision to publish the results.

References

1. Bansal, S.; Durrett, T.P. *Camelina sativa*: An ideal platform for the metabolic engineering and field production of industrial lipids. *Biochimie* **2016**, *120*, 9–16. [CrossRef] [PubMed]
2. Berti, M.; Gesch, R.; Eynck, C.; Anderson, J.; Cermak, S. Camelina uses, genetics, genomics, production, and management. *Ind. Crops Prod.* **2016**, *94*, 690–710. [CrossRef]
3. Gesch, R.W.; Matthees, H.L.; Alvarez, A.L.; Gardner, R.D. Winter Camelina: Crop growth, seed yield, and quality response to cultivar and seeding rate. *Crop Sci.* **2018**, *58*, 2089–2098. [CrossRef]
4. Putnam, D.H.; Budin, J.T.; Field, L.A.; Breene, W.M. Camelina: A promising low-input oilseed. In *New Crops*; Janick, J., Simon, J.E., Eds.; Wiley: New York, NY, USA, 1993; pp. 314–322.
5. Schillinger, W.F. Camelina: Long-term cropping systems research in a dry Mediterranean climate. *Field Crops Res.* **2019**, *235*, 87–94. [CrossRef]
6. Vollmann, J.; Eynck, C. Camelina as a sustainable oilseed crop: Contributions of plant breeding and genetic engineering. *Biotechnol. J.* **2015**, *10*, 525–535. [CrossRef] [PubMed]
7. Masella, P.; Martinelli, T.; Galasso, I. Agronomic evaluation and phenotypic plasticity of *Camelina sativa* growing in Lombardia, Italy. *Crop Pasture Sci.* **2014**, *65*, 453–460. [CrossRef]

8. Iskandarov, U.; Kim, H.J.; Cahoon, E.B. Camelina: An emerging oilseed platform for advanced biofuels and bio-based materials. In *Plants and Bioenergy*; Advances in Plant Biology; McCann, M., Buckeridge, M., Carpita, N., Eds.; Springer: New York, NY, USA, 2014; Volume 4, pp. 131–140.
9. Liu, X.; Brost, J.; Hutcheon, C.; Guilfoil, R.; Wilson, A.K.; Leung, S.; Shewmaker, C.K.; Rooke, S.; Nguyen, T.; Kiser, J. Transformation of the oilseed crop *Camelina sativa* by *Agrobacterium*-mediated floral dip and simple large-scale screening of transformants. *Vitr. Cell. Dev. Biol.-Plant* **2012**, *48*, 462–468. [CrossRef]
10. Lu, C.; Kang, J. Generation of transgenic plants of a potential oilseed crop *Camelina sativa* by *Agrobacterium*-mediated transformation. *Plant Cell Rep.* **2008**, *27*, 273–278. [CrossRef] [PubMed]
11. Sainger, M.; Jaiwal, A.; Sainger, P.A.; Chaudhary, D.; Jaiwal, R.; Jaiwal, P.K. Advances in genetic improvement of *Camelina sativa* for biofuel and industrial bio-products. *Renew. Sustain. Energy Rev.* **2017**, *68*, 623–637. [CrossRef]
12. Sitther, V.; Tabatabai, B.; Enitan, O.; Dhekney, S. *Agrobacterium*-mediated transformation of *Camelina sativa* for production of transgenic plants. *J. Biol. Methods* **2018**, e83. [CrossRef]
13. Yemets, A.I.; Boychuk, Y.N.; Shysha, E.N.; Rakhmetov, D.B.; Blume, Y.B. Establishment of in vitro culture, plant regeneration, and genetic transformation of *Camelina sativa*. *Cytol. Genet.* **2013**, *47*, 138–144. [CrossRef]
14. Ozseyhan, M.E.; Kang, J.; Mu, X.; Lu, C. Mutagenesis of the FAE1 genes significantly changes fatty acid composition in seeds of *Camelina sativa*. *Plant Physiol. Biochem.* **2018**, *123*, 1–7. [CrossRef]
15. Morineau, C.; Bellec, Y.; Tellier, F.; Gissot, L.; Kelemen, Z.; Nogué, F.; Faure, J.D. Selective gene dosage by CRISPR-Cas9 genome editing in hexaploid *Camelina sativa*. *Plant Biotechnol. J.* **2017**, *15*, 729–739. [CrossRef]
16. Jiang, W.Z.; Henry, I.M.; Lynagh, P.G.; Comai, L.; Cahoon, E.B.; Weeks, D.P. Significant enhancement of fatty acid composition in seeds of the allohexaploid, *Camelina sativa*, using CRISPR/Cas9 gene editing. *Plant Biotechnol. J.* **2017**, *15*, 648–657. [CrossRef]
17. Chaturvedi, S.; Bhattacharya, A.; Khare, S.K.; Kaushik, G. *Camelina sativa: An Emerging Biofuel Crop*; Springer: Berlin/Heidelberg, Germany, 2017; pp. 1–38.
18. Dharavath, R.N.; Singh, S.; Chaturvedi, S.; Luqman, S. *Camelina sativa* (L.) Crantz A mercantile crop with speckled pharmacological activities. *Ann. Phytomed.* **2016**, *5*, 6–26. [CrossRef]
19. Malik, M.R.; Tang, J.; Sharma, N.; Burkitt, C.; Ji, Y.; Mykytyshyn, M.; Bohmert-Tatarev, K.; Peoples, O.; Snell, K.D. *Camelina sativa*, an oilseed at the nexus between model system and commercial crop. *Plant Cell Rep.* **2018**, *37*, 1367–1381. [CrossRef]
20. Moser, B.R. Camelina (*Camelina sativa* L.) oil as a biofuels feedstock: Golden opportunity or false hope? *Lipid Technol.* **2010**, *22*, 270–273. [CrossRef]
21. Murphy, E.J. Camelina (*Camelina sativa*). In *Industrial Oil Crops*; McKeon, T., Hayes, D., Hildebrand, D., Weselake, R., Eds.; Elevier: London, UK, 2016; pp. 207–230.
22. Obour, K.A.; Sintim, H.Y.; O'bend, E.; Jeliazkov, V.D. Oilseed Camelina (*Camelina sativa* L. Crantz): Production systems, prospects and challenges in the USA Great Plains. *Adv. Plants Agric. Res.* **2015**, *2*, 00043. [CrossRef]
23. Waraich, E.A.; Ahmed, Z.; Ahmad, R.; Ashraf, M.Y.; Naeem, M.S.; Rengel, Z. '*Camelina sativa*', a climate proof crop, has high nutritive value and multiple-uses: A review. *Aust. J. Crop Sci.* **2013**, *7*, 1551–1559.
24. Zubr, J. Oil-seed crop: *Camelina sativa*. *Ind. Crops Prod.* **1997**, *6*, 113–119. [CrossRef]
25. Fröhlich, A.; Rice, B. Evaluation of *Camelina sativa* oil as a feedstock for biodiesel production. *Ind. Crops Prod.* **2005**, *21*, 25–31. [CrossRef]
26. Ciubota-Rosie, C.; Ruiz, J.R.; Ramos, M.J.; Pérez, Á. Biodiesel from *Camelina sativa*: A comprehensive characterisation. *Fuel* **2013**, *105*, 572–577. [CrossRef]
27. Zaleckas, E.; Makarevičienė, V.; Sendžikienė, E. Possibilities of using *Camelina sativa* oil for producing biodiesel fuel. *Transport* **2012**, *27*, 60–66. [CrossRef]
28. Agarwal, A.; Prakash, O.; Bala, M. *Camelina sativa*, a short gestation oilseed crop with biofuel potential: Opportunities for Indian scenario. *Oil Crop Sci.* **2021**, *6*, 114–121. [CrossRef]
29. *Domestication of Plants in the Old World*, 4th ed.; Oxford University Press: Oxford, UK, 2012.
30. Larsson, M. Cultivation and processing of *Linum usitatissimum* and *Camelina sativa* in southern Scandinavia during the Roman Iron Age. *Veg. Hist. Archaeobotany* **2013**, *22*, 509–520. [CrossRef]
31. Dönmez, E.O.; Belli, O. Urartian plant cultivation at Yoncatepe (Van), eastern Turkey. *Econ. Bot.* **2007**, *61*, 290–298. [CrossRef]
32. Carciumaru, M. Cultivarea plantelor in Dacia (Plants cultivation in Dacia). *Thraco-Dacica* **2007**, *8*, 1–6.
33. Knorzer, K.H. Evolution and spread of Gold of Pleasure (*Camelina sativa* S.L.). *Ber. Dtsch. Bot. Ges.* **1978**, *91*, 187–195.
34. Hutcheon, C.; Ditt, R.F.; Beilstein, M.; Comai, L.; Schroeder, J.; Goldstein, E.; Shewmaker, C.K.; Nguyen, T.; De Rocher, J.; Kiser, J. Polyploid genome of *Camelina sativa* revealed by isolation of fatty acid synthesis genes. *BMC Plant Biol.* **2010**, *10*, 233. [CrossRef]
35. Gesch, R.W. Influence of genotype and sowing date on camelina growth and yield in the north central U.S. *Ind. Crops Prod.* **2014**, *54*, 209–215. [CrossRef]
36. Neupane, D.; Solomon, J.K.Q.; McLennon, E.; Davison, J.; Lawry, T. Camelina production parameters response to different irrigation regimes. *Ind. Crops Prod.* **2020**, *148*, 112286. [CrossRef]
37. Lohaus, R.H.; Neupane, D.; Mengistu, M.A.; Solomon, J.K.Q.; Cushman, J.C. Five-year field trial of eight *Camelina sativa* cultivars for biomass to be used in biofuel under irrigated conditions in a semi-arid climate. *Agronomy* **2020**, *10*, 562. [CrossRef]
38. Blackshaw, R.; Johnson, E.; Gan, Y.; May, W.; McAndrew, D.; Barthet, V.; McDonald, T.; Wispinski, D. Alternative oilseed crops for biodiesel feedstock on the Canadian prairies. *Can. J. Plant Sci.* **2011**, *91*, 889–896. [CrossRef]

39. Gugel, R.K.; Falk, K.C. Agronomic and seed quality evaluation of *Camelina sativa* in western Canada. *Can. J. Plant Sci.* **2006**, *86*, 1047–1058. [CrossRef]
40. Urbaniak, S.D.; Caldwell, C.D.; Zheljazkov, V.D.; Lada, R.; Luan, L. The effect of seeding rate, seeding date and seeder type on the performance of *Camelina sativa* L. in the Maritime Provinces of Canada. *Can. J. Plant Sci.* **2008**, *88*, 501–508. [CrossRef]
41. Beilstein, M.A.; Al-Shehbaz, I.A.; Kellogg, E.A. Brassicaceae phylogeny and trichome evolution. *Am. J. Bot.* **2006**, *93*, 607–619. [CrossRef] [PubMed]
42. Beilstein, M.A.; Al-Shehbaz, I.A.; Mathews, S.; Kellogg, E.A. Brassicaceae phylogeny inferred from phytochrome A and ndhF sequence data: Tribes and trichomes revisited. *Am. J. Bot.* **2008**, *95*, 1307–1327. [CrossRef]
43. Brock, J.R.; Donmez, A.A.; Beilstein, M.A.; Olsen, K.M. Phylogenetics of Camelina Crantz. (Brassicaceae) and insights on the origin of gold-of-pleasure (*Camelina sativa*). *Mol. Phylogenetics Evol.* **2018**, *127*, 834–842. [CrossRef] [PubMed]
44. Brock, J.R.; Mandakova, T.; Lysak, M.A.; Al-Shehbaz, I.A. *Camelina neglecta* (Brassicaceae, Camelineae), a new diploid species from Europe. *PhytoKeys* **2019**, *115*, 51–57. [CrossRef]
45. Ghamkhar, K.; Croser, J.; Aryamanesh, N.; Campbell, M.; Konkova, N.; Francis, C. Camelina (*Camelina sativa* (L). Crantz) as an alternative oilseed: Molecular and ecogeographic analyses. *Genome* **2010**, *53*, 558–567. [CrossRef]
46. Kagale, S.; Koh, C.; Nixon, J.; Bollina, V.; Clarke, W.E.; Tuteja, R.; Spillane, C.; Robinson, S.J.; Links, M.G.; Clarke, C.; et al. The emerging biofuel crop *Camelina sativa* retains a highly undifferentiated hexaploid genome structure. *Nat. Commun.* **2014**, *5*, 3706. [CrossRef] [PubMed]
47. Galasso, I.A.; Braglia, M.L.; Ponzoni, E.; Breviario, D. Genomic fingerprinting of Camelina species using cTBP as molecular marker. *Am. J. Plant Sci.* **2015**, *6*, 1184–1200. [CrossRef]
48. Martin, S.L.; Lujan-Toro, B.E.; Sauder, C.A.; James, T.; Ohadi, S.; Hall, L.M. An update to the Canadian range, abundance, and ploidy of *Camelina* spp. (Brassicaceae) east of the Rocky Mountains. *Botany* **2017**, *95*, 405–417. [CrossRef]
49. Francis, A.; Warwick, S.I. The biology of Canadian weeds. 142. Camelina alyssum (Mill.) thell. *C. microcarpa* andrz. ex DC.; *C. sativa* (L.) crantz. *Can. J. Plant Sci.* **2009**, *89*, 791–810. [CrossRef]
50. Gehringer, A.; Friedt, W.; Luhs, W.; Snowdon, R.J. Genetic mapping of agronomic traits in false flax (*Camelina sativa* subsp. sativa). *Genome* **2006**, *49*, 1555–1563. [CrossRef] [PubMed]
51. Al-Shehbaz, I.A.; Beilstein, M.A. Flora of North America North of Mexico. *N. Y. Oxf.* **2010**, *7*, 451–453.
52. Koch, M.A.; Kiefer, M.; German, D.A.; Al-Shehbaz, I.A.; Franzke, A.; Mummenhoff, K.; Schmickl, R. BrassiBase: Tools and biological resources to study characters and traits in the Brassicaceae version 1.1. *Taxon* **2012**, *61*, 1001–1009. [CrossRef]
53. Chaudhary, R.; Koh, C.S.; Kagale, S.; Tang, L.; Wu, S.W.; Lv, Z.; Mason, A.S.; Sharpe, A.G.; Diederichsen, A.; Parkin, I.A.P. Assessing diversity in the *Camelina* genus provides insights into the genome structure of *Camelina sativa*. *G3 Genes Genomes Genet.* **2020**, *10*, 1297–1308. [CrossRef]
54. Brock, J.R.; Mandáková, T.; McKain, M.; Lysak, M.A.; Olsen, K.M. Chloroplast phylogenomics in *Camelina* (Brassicaceae) reveals multiple origins of polyploid species and the maternal lineage of *C. sativa*. *Hortic. Res.* **2022**, *9*, uhab050. [CrossRef] [PubMed]
55. Mirek, Z. Genus Camelina in Poland—Taxonomy, Distribution and Habitats. *Fragm. Florist. Geobot.* **1981**, *27*, 445–503.
56. Gesch, R.W.; Archer, D.W. Double-cropping with winter camelina in the northern corn belt to produce fuel and food. *Ind. Crops Prod.* **2013**, *44*, 718–725. [CrossRef]
57. Gesch, R.W.; Cermak, S. Sowing date and tillage effects on fall-seeded camelina in the northern Corn Belt. *Agron. J.* **2011**, *103*, 980–987. [CrossRef]
58. Johnson, G.A.; Wells, M.S.; Anderson, K.; Gesch, R.W.; Forcella, F.; Wyse, D.L. Yield tradeoffs and nitrogen between pennycress, camelina, and soybean in relay- and double-crop systems. *Agron. J.* **2017**, *109*, 2128–2135. [CrossRef]
59. Neupane, D.; Solomon, J.K.Q.; Davison, J.; Lawry, T. Nitrogen source and rate effects on grain and potential biodiesel production of camelina in the semiarid environment of northern Nevada. *Glob. Change Biol. Bioenergy* **2018**, *10*, 861–876. [CrossRef]
60. Walia, M.K.; Wells, M.S.; Cubins, J.; Wyse, D.; Gardner, R.D.; Forcella, F.; Gesch, R. Winter camelina seed yield and quality responses to harvest time. *Ind. Crops Prod.* **2018**, *124*, 765–775. [CrossRef]
61. Berti, M.; Wilckens, R.; Fischer, S.; Solis, A.; Johnson, B. Seeding date influence on camelina seed yield, yield components, and oil content in Chile. *Ind. Crops Prod.* **2011**, *34*, 1358–1365. [CrossRef]
62. Neupane, D.; Solomon, J.K.Q.; McLennon, E.; Davison, J.; Lawry, T. Sowing date and sowing method influence on camelina cultivars grain yield, oil concentration, and biodiesel production. *Food Energy Secur.* **2019**, *8*, e00166. [CrossRef]
63. Angelini, L.G.; Moscheni, E.; Colonna, G.; Belloni, P.; Bonari, E. Variation in agronomic characteristics and seed oil composition of new oilseed crops in central Italy. *Ind. Crops Prod.* **1997**, *6*, 313–323. [CrossRef]
64. Vollmann, J.; Moritz, T.; Kargl, C.; Baumgartner, S.; Wagentristl, H. Agronomic evaluation of camelina genotypes selected for seed quality characteristics. *Ind. Crops Prod.* **2007**, *26*, 270–277. [CrossRef]
65. Dai, A.; Zhao, T.; Chen, J. Climate Change and Drought: A Precipitation and Evaporation Perspective. *Curr. Clim. Change Rep.* **2018**, *4*, 301–312. [CrossRef]
66. Naumann, G.; Alfieri, L.; Wyser, K.; Mentaschi, L.; Betts, R.A.; Carrao, H.; Spinoni, J.; Vogt, J.; Feyen, L. Global changes in drought conditions under different levels of warming. *Geophys. Res. Lett.* **2018**, *45*, 3285–3296. [CrossRef]
67. McKenzie, B.A.; Smallfield, B.M.; Fasi, V.; Martin, R.J. Possible species for the production of biodiesel on marginal land. *Agron. N. Z.* **2011**, *41*, 97–108.

68. Pavlista, A.D.; Isbell, T.A.; Baltensperger, D.D.; Hergert, G.W. Planting date and development of spring-seeded irrigated canola, brown mustard and camelina. *Ind. Crops Prod.* **2011**, *33*, 451–456. [CrossRef]
69. Hergert, G.W.; Margheim, J.F.; Pavlista, A.D.; Martin, D.L.; Isbell, T.A.; Supalla, R.J. Irrigation response and water productivity of deficit to fully irrigated spring camelina. *Agric. Water Manag.* **2016**, *177*, 46–53. [CrossRef]
70. Hergert, G.W.; Margheim, J.F.; Pavlista, A.D.; Martin, D.L.; Supalla, R.J.; Isbell, T.A. Yield, irrigation response, and water productivity of deficit to fully irrigated spring canola. *Agric. Water Manag.* **2016**, *168*, 96–103. [CrossRef]
71. Matteo, R.; D'Avino, L.; Ramirez-Cando, L.J.; Pagnotta, E.; Angelini, L.G.; Spugnoli, P.; Tavarini, S.; Ugolini, L.; Foschi, L.; Lazzeri, L. Camelina (*Camelina sativa* L. Crantz) under low-input management systems in northern Italy: Yields, chemical characterization and environmental sustainability. *Ital. J. Agron.* **2020**, *15*, 132–143. [CrossRef]
72. Załuski, D.; Tworkowski, J.; Krzyżaniak, M.; Stolarski, M.J.; Kwiatkowski, J. The characterization of 10 spring Camelina genotypes grown in environmental conditions in North-eastern Poland. *Agronomy* **2020**, *10*, 64. [CrossRef]
73. Lošák, T.; Hlusek, J.; Martinec, J.; Vollmann, J.; Peterka, J.; Filipcik, R.; Varga, L.; Ducsay, L.; Martensson, A. Effect of combined nitrogen and sulphur fertilization on yield and qualitative parameters of *Camelina sativa* [L.] Crtz. (false flax). *Acta Agric. Scand. Sect. B-Soil Plant Sci.* **2011**, *61*, 313–321. [CrossRef]
74. Manore, D.; Yohanns, A. Evaluating growth, seed yield and yield attributes of Camelina (*Camelina sativa* L) in response to seeding rate and nitrogen fertilizer levels under irrigation condition, southern Ethiopia. *Agric. For. Fish.* **2019**, *8*, 31–35. [CrossRef]
75. Obeng, E.; Obour, A.K.; Nelson, N.O.; Moreno, J.A.; Ciampitti, I.A.; Wang, D.; Durrett, T.P. Seed yield and oil quality as affected by Camelina cultivar and planting date. *J. Crop Improv.* **2019**, *33*, 202–222. [CrossRef]
76. Amiri-Darban, N.; Nourmohammadi, G.; Rad, A.H.S.; Mirhadi, S.M.J.; Heravan, I.M. Potassium sulfate and ammonium sulfate affect quality and quantity of camelina oil grown with different irrigation regimes. *Ind. Crops Prod.* **2020**, *148*, 112308. [CrossRef]
77. Zanetti, F.; Eynck, C.; Christou, M.; Krzyżaniak, M.; Righini, D.; Alexopoulou, E.; Stolarski, M.J.; Van Loo, E.N.; Puttick, D.; Monti, A. Agronomic performance and seed quality attributes of Camelina (*Camelina sativa* L. crantz) in multi-environment trials across Europe and Canada. *Ind. Crops Prod.* **2017**, *107*, 602–608. [CrossRef]
78. Mohammed, Y.A.; Chen, C.; Lamb, P.; Afshar, R.K. Agronomic Evaluation of Camelina (*Camelina sativa* L. Crantz) Cultivars for Biodiesel Feedstock. *BioEnergy Res.* **2017**, *10*, 792–799. [CrossRef]
79. Obour, A.K.; Obeng, E.; Mohammed, Y.A.; Ciampitti, I.A.; Durrett, T.P.; Aznar-Moreno, J.A.; Chen, C.C. Camelina seed yield and fatty acids as influenced by genotype and wnvironment. *Agron. J.* **2017**, *109*, 947–956. [CrossRef]
80. Obour, A.K.; Chen, C.C.; Sintim, H.Y.; McVay, K.; Lamb, P.; Obeng, E.; Mohammed, Y.A.; Khan, Q.; Afshar, R.K.; Zheljazkov, V.D. Camelina sativa as a fallow replacement crop in wheat-based crop production systems in the US Great Plains. *Ind. Crops Prod.* **2018**, *111*, 22–29. [CrossRef]
81. Pavlista, A.D.; Hergert, G.W.; Margheim, J.M.; Isbell, T.A. Growth of spring camelina (*Camelina sativa*) under deficit irrigation in western Nebraska. *Ind. Crops Prod.* **2016**, *83*, 118–123. [CrossRef]
82. French, A.N.; Hunsaker, D.; Thorp, K.; Clarke, T. Evapotranspiration over a camelina crop at Maricopa, Arizona. *Ind. Crops Prod.* **2009**, *29*, 289–300. [CrossRef]
83. Hunsaker, D.J.; French, A.N.; Clarke, T.R.; El-Shikha, D.M. Water use, crop coefficients, and irrigation management criteria for camelina production in arid regions. *Irrig. Sci.* **2011**, *29*, 27–43. [CrossRef]
84. Hunsaker, D.J.; French, A.N.; Thorp, K.R. Camelina water use and seed yield response to irrigation scheduling in an arid environment. *Irrig. Sci.* **2012**, *31*, 911–929. [CrossRef]
85. George, N.; Thompson, S.E.; Hollingsworth, J.; Orloff, S.; Kaffka, S. Measurement and simulation of water-use by canola and camelina under cool-season conditions in California. *Agric. Water Manag.* **2018**, *196*, 15–23. [CrossRef]
86. Bronson, K.F.; Hunsaker, D.J.; Thorp, K.R. Nitrogen fertilizer and irrigation effects on seed yield and oil in Camelina. *Agron. J.* **2019**, *111*, 1712–1719. [CrossRef]
87. Jiang, Y.; Caldwell, C.D.; Falk, K.C.; Lada, R.R.; MacDonald, D. Camelina yield and quality response to combined nitrogen and sulfur. *Agron. J.* **2013**, *105*, 1847–1852. [CrossRef]
88. Malhi, S.S.; Johnson, E.N.; Hall, L.M.; May, W.E.; Phelps, S.; Nybo, B. Effect of nitrogen fertilizer application on seed yield, N uptake, and seed quality of *Camelina sativa*. *Can. J. Soil Sci.* **2014**, *94*, 35–47. [CrossRef]
89. Martinez, S.; Alvarez, S.; Capuano, A.; del Mar Delgado, M. Environmental performance of animal feed production from *Camelina sativa* (L.) Crantz: Influence of crop management practices under Mediterranean conditions. *Agric. Syst.* **2020**, *177*, 102717. [CrossRef]
90. Krzyżaniak, M.; Stolarski, M.J. Life cycle assessment of camelina and crambe production for biorefinery and energy purposes. *J. Clean. Prod.* **2019**, *237*, 117755. [CrossRef]
91. Sintim, H.Y.; Zheljazkov, V.D.; Obour, A.K.; Garcia y Garcia, A.; Foulke, T.K. Influence of nitrogen and sulfur application on camelina performance under dryland conditions. *Ind. Crops Prod.* **2015**, *70*, 253–259. [CrossRef]
92. Kemp, W.H. *Biodiesel: Basics and Beyond, a Comprehensive Guide to Production and Use for the Home and Farm*; Aztext Press: Tamworth, ON, Canada, 2006.
93. Bobrecka-Jamro, M.C. The effects of varied plant density and nitrogen fertilization on quantity and quality yield of *Camelina sativa* L. *Emir. J. Food Agric.* **2018**, *29*, 988–993. [CrossRef]
94. Keshavarz-Afshar, R.; Mohammed, Y.A.; Chen, C. Energy balance and greenhouse gas emissions of dryland camelina as influenced by tillage and nitrogen. *Energy* **2015**, *91*, 1057–1063. [CrossRef]

95. Rathke, G.-W.; Christen, O.; Diepenbrock, W. Effects of N source and rate on productivity and quality of winter oilseed rape (*Brassica napus* L.) grown in different crop rotations. *Field Crops Res.* **2005**, *94*, 103–113. [CrossRef]
96. Leclère, M.; Jeuffroy, M.-H.; Butier, A.; Chatain, C.; Loyce, C. Controlling weeds in camelina with innovative herbicide-free crop management routes across various environments. *Ind. Crops Prod.* **2019**, *140*, 111605. [CrossRef]
97. Lovett, J.V.; Jackson, H.F. Allelopathic activity of *Camelina sativa* (L.) Crantz inrelation to its phyllosphere bacteria. *New Phytol.* **1980**, *86*, 273–277. [CrossRef]
98. Walsh, K.D.; Sanderson, D.; Hall, L.M.; Mugo, S.; Hills, M.J. Allelopathic effects of camelina (*Camelina sativa*) and canola (*Brassica napus*) on wild oat, flax and radish. *Allelopath. J.* **2014**, *33*, 83–96.
99. Abbas, A.; Huang, P.; Hussain, S.; Saqib, M.; He, L.; Shen, F.; Du, D. Application of allelopathic phenomemna to enhance growth and production of camelina (*Camelina sativa* (L.). *Appl. Ecol. Environ. Res.* **2021**, *19*, 453–469. [CrossRef]
100. Davis, P.B.; Maxwell, B.; Menalled, F.D. Impact of growing conditions on the competitive ability of *Camelina sativa* (L.) Crantz (Camelina). *Can. J. Plant Sci.* **2013**, *93*, 243–247. [CrossRef]
101. Lenssen, A.W.; Iversen, W.M.; Sainju, U.M.; Caesar-TonThat, T.C.; Blodgett, S.L.; Allen, B.L.; Evans, R.G. Yield, pests, and water use of durum and selected crucifer oilseeds in two-year rotations. *Agron. J.* **2012**, *104*, 1295–1304. [CrossRef]
102. Julié-Galau, S.; Bellec, Y.; Faure, J.-D.; Tepfer, M. Evaluation of the potential for interspecific hybridization between *Camelina sativa* and related wild Brassicaceae in anticipation of field trials of GM camelina. *Transgenic Res.* **2014**, *23*, 67–74. [CrossRef] [PubMed]
103. Zhang, C.-J.; Auer, C. Hybridization between *Camelina sativa* (L.) Crantz and common Brassica weeds. *Ind. Crops Prod.* **2020**, *147*, 112240. [CrossRef]
104. Davis, P.B. *The Invasion Potential and Competitive Ability of Camelina sativa (L.) Crantz (Camelina) in Rangeland Ecosystems*; Montana State University-Bozeman, College of Agriculture: Bozeman, MT, USA, 2010.
105. Enjalbert, J.; Johnson, J. *Guide for Producing Dryland Camelina in Eastern Colorado*; Colorado State University Extension: Fort Collins, CO, USA, 2011.
106. WAPMC. *Biomass Crop Assistance Program: Camelina Agronomy Sheet*; NRCS: Washington, DC, USA, 2012.
107. Sobiech, Ł.; Grzanka, M.; Kurasiak-Popowska, D.; Radzikowska, D. Phytotoxic effect of herbicides on various camelina [*Camelina sativa* (L.) Crantz] genotypes and plant chlorophyll fluorescence. *Agriculture* **2020**, *10*, 185. [CrossRef]
108. Scheliga, M.; Petersen, J. Selectivity of herbicides in camelina (*Camelina sativa* (L.) Crtz.). *Jul.-Kühn-Arch.* **2016**, *452*, 154–162. [CrossRef]
109. Jha, P.; Stougaard, R.N. Camelina (*Camelina sativa*) tolerance to selected preemergence herbicides. *Weed Technol.* **2013**, *27*, 712–717. [CrossRef]
110. Walsh, D.T.; Babiker, E.M.; Burke, I.C.; Hulbert, S.H. Camelina mutants resistant to acetolactate synthase inhibitor herbicides. *Mol. Breed.* **2012**, *30*, 1053–1063. [CrossRef]
111. Schillinger, W.F.; Wysocki, D.J.; Chastain, T.G.; Guy, S.O.; Karow, R.S. Camelina: Planting date and method effects on stand establishment and seed yield. *Field Crops Res.* **2012**, *130*, 138–144. [CrossRef]
112. Saucke, H.; Ackermann, K. Weed suppression in mixed cropped grain peas and false flax (*Camelina sativa*). *Weed Res.* **2006**, *46*, 453–461. [CrossRef]
113. Almoussawi, A.; Lenoir, J.; Spicher, F.; Dupont, F.; Chabrerie, O.; Closset-Kopp, D.; Brasseur, B.; Kobaissi, A.; Dubois, F.; Decocq, G. Direct seeding associated with a mixture of winter cover crops decreases weed abundance while increasing cash-crop yields. *Soil Tillage Res.* **2020**, *200*, 104622. [CrossRef]
114. Royo-Esnal, A.; Valencia-Gredilla, F. Camelina as a rotation crop for weed control in organic farming in a semiarid Mediterranean climate. *Agriculture* **2018**, *8*, 156. [CrossRef]
115. Berti, M.; Gesch, R.; Johnson, B.; Ji, Y.; Seames, W.; Aponte, A. Double-and relay-cropping of energy crops in the northern Great Plains, USA. *Ind. Crops Prod.* **2015**, *75*, 26–34. [CrossRef]
116. Berti, M.; Samarappuli, D.; Johnson, B.L.; Gesch, R.W. Integrating winter camelina into maize and soybean cropping systems. *Ind. Crops Prod.* **2017**, *107*, 595–601. [CrossRef]
117. Chandra, K.; Sharma, D.K.; Meher, L.C.; Kulkarni, A.V.; Nasim, M. Studies of feasibility of intercropping of *Camelina sativa* in jatropha plantation in semi–arid climate in Andhra Pradesh, India. *Res. J. Agric. For. Sci.* **2014**, *2*, 23–26.
118. Robinson, R.G. Camelina: A Useful Research Crop and a Potential Oilseed Crop. **1987**, *579*. Available online: https://conservancy.umn.edu/bitstream/handle/11299/141546/SB579.pdf?sequence=1 (accessed on 10 February 2022).
119. Soroka, J.J.; Olivier, C.; Wist, T.J.; Grenkow, L. Present and potential impacts of insects on Camelina and Crambe. In *Integrated Management of Insect Pests on Canola and Other Brassica Oilseed Crops*; CABI: Boston, MA, USA, 2017; pp. 316–340.
120. Nielsen, J.K.; Hansen, M.L.; Agerbirk, N.; Petersen, B.L.; Halkier, B.A. Responses of the flea beetles *Phyllotreta nemorum* and *P. cruciferae* to metabolically engineered *Arabidopsis thaliana* with an altered glucosinolate profile. *Chemoecology* **2001**, *11*, 75–83. [CrossRef]
121. Pachagounder, P.; Lamb, R.J.; Bodnaryk, R.P. Resistance to the flea beetle *Phyllotreta cruciferae* (Coleoptera: Chrysomelidae) in false flax, *Camelina sativa* (Brassicaceae). *Can. Entomol.* **1998**, *130*, 235–240. [CrossRef]
122. Henderson, A.E.; Hallett, R.H.; Soroka, J.J. Prefeeding behavior of the crucifer flea beetle, *Phyllotreta cruciferae*, on host and nonhost crucifers. *J. Insect Behav.* **2004**, *17*, 17–39. [CrossRef]
123. Onyilagha, J.C.; Gruber, M.Y.; Hallett, R.H.; Holowachuk, J.; Buckner, A.; Soroka, J.J. Constitutive flavonoids deter flea beetle insect feeding in *Camelina sativa* L. *Biochem. Syst. Ecol.* **2012**, *42*, 128–133. [CrossRef]

124. Soroka, J.; Olivier, C.; Grenkow, L.; Séguin-Swartz, G. Interactions between *Camelina sativa* (Brassicaceae) and insect pests of canola. *Can. Entomol.* **2015**, *147*, 193–214. [CrossRef]
125. Cárcamo, H.; Olfert, O.; Dosdall, L.; Herle, C.; Beres, B.; Soroka, J. Resistance to cabbage seedpod weevil among selected Brassicaceae germplasm. *Can. Entomol.* **2007**, *139*, 658–669. [CrossRef]
126. Jewett, F.G. *Camelina sativa*: For biofuels and bioproducts. *Ind. Crops* **2015**, *9*, 157–170. [CrossRef]
127. Chesnais, Q.; Verzeaux, J.; Couty, A.; Le Roux, V.; Ameline, A. Is the oilseedcrop *Camelina sativa* a potential host for aphid pests? *BioEnergy Res.* **2015**, *8*, 91–99. [CrossRef]
128. Séguin-Swartz, G.; Eynck, C.; Gugel, R.K.; Strelkov, S.E.; Olivier, C.Y.; Li, J.L.; Klein-Gebbinck, H.; Borhan, H.; Caldwell, C.D.; Falk, K.C. Diseases of *Camelina sativa* (false flax). *Can. J. Plant Pathol.* **2009**, *31*, 375–386. [CrossRef]
129. Conn, K.L.; Tewari, J.P.; Dahiya, J.S. Resistance to *Alternaria brassicae* and phytoalexin-elicitation in rapeseed and other crucifers. *Plant Sci.* **1988**, *56*, 21–25. [CrossRef]
130. Sharma, G.; Kumar, V.D.; Haque, A.; Bhat, S.R.; Prakash, S.; Chopra, V.L. *Brassica* coenospecies: A rich reservoir for genetic resistance to leaf spot caused by *Alternaria brassicae*. *Euphytica* **2002**, *125*, 411–417. [CrossRef]
131. Jejelowo, O.A.; Conn, K.L.; Tewari, J.P. Relationship between conidial concentration, germling growth, and phytoalexin production by *Camelina sativa* leaves inoculated with *Alternaria brassicae*. *Mycol. Res.* **1991**, *95*, 928–934. [CrossRef]
132. Dixit, S.; Jangid, V.K.; Grover. Evaluation of physiological and molecular effect of variable virulence of *Alternaria brassicae* isolates in *Brassica juncea*, *Sinapis alba* and *Camelina sativa*. *Plant Physiol. Biochem.* **2020**, *155*, 626–636. [CrossRef] [PubMed]
133. Westman, A.L.; Kresovich, S.; Dickson, M.H. Regional variation in *Brassica nigra* and other weedy crucifers for disease reaction to *Alternaria brassicicola* and *Xanthomonas campestris* pv. campestris. *Euphytica* **1999**, *106*, 253–259. [CrossRef]
134. Sigareva, M.A.; Earle, E.D. Camalexin induction in intertribal somatic hybrids between *Camelina sativa* and rapid-cycling *Brassica oleracea*. *Theor. Appl. Genet.* **1999**, *98*, 164–170. [CrossRef]
135. Hansen, L.N. Intertribal somatic hybridization between rapid cycling *Brassica oleracea* L. and *Camelina sativa* (L.) Crantz. *Euphytica* **1998**, *104*, 173–179. [CrossRef]
136. Browne, L.M.; Conn, K.L.; Ayer, W.A.; Tewari, J.P. The camalexins: New phytoalexins produced in the leaves of *Camelina sativa* (Cruciferae). *Tetrahedron* **1991**, *47*, 3909–3914. [CrossRef]
137. Mir, Z.A.; Ali, S.; Shivaraj, S.M.; Bhat, J.A.; Singh, A.; Yadav, P.; Rawat, S.; Paplao, P.K.; Grover, A. Genome-wide identification and characterization of chitinase gene family in *Brassica juncea* and *Camelina sativa* in response to *Alternaria brassicae*. *Genomics* **2020**, *112*, 749–763. [CrossRef]
138. Li, H.; Barbetti, M.J.; Sivasithamparam, K. Hazard from reliance on cruciferous hosts as sources of major gene-based resistance for managing blackleg (*Leptosphaeria maculans*) disease. *Field Crops Res.* **2005**, *91*, 185–198. [CrossRef]
139. Paul, V.H.; Tewari, J.P.; Tewari, I.; Foller, I.; Henneken, M. Joint field experiment on cultivation, yield, and diseases of false flax (*Camelina sativa*) in Germany and Canada. *IOBC WPRS BULLETIN* **2000**, *23*, 205–208.
140. Föller, I.; Henneken, M.; Paul, V.H. Occurrence of false flax diseases (*Camelina sativa* (L.) CRTZ.) in field trials in Germany in 1995 and 1996. *Bull. OILB/SROP* **1998**, *21*, 65–76.
141. Putnam, M.L.; Serdani, M.; Ehrensing, D.; Curtis, M. Camelina infected by downy mildew (*Hyaloperonospora camelinae*) in the western United States: A first report. *Plant Health Prog.* **2009**, *10*, 40. [CrossRef]
142. Purnamasari, M.; Cawthray, G.R.; Barbetti, M.J.; Erskine, W.; Croser, J.S. Camalexin production in *Camelina sativa* is independent of cotyledon resistance to *Sclerotinia sclerotiorum*. *Plant Dis.* **2015**, *99*, 1544–1549. [CrossRef]
143. Eynck, C.; Séguin-Swartz, G.; Clarke, W.E.; Parkin, I.A.P. Monolignol biosynthesis is associated with resistance to *Sclerotinia sclerotiorum* in *Camelina sativa*. *Mol. Plant Pathol.* **2012**, *13*, 887–899. [CrossRef] [PubMed]
144. Kobayashi-Leonel, R.; Mueller, D.; Harbach, C.; Tylka, G.; Leandro, L. Susceptibility of cover crop plants to *Fusarium virguliforme*, causal agent of soybean sudden death syndrome, and *Heterodera glycines*, the soybean cyst nematode. *J. Soil Water Conserv.* **2017**, *72*, 575–583. [CrossRef]
145. Conn, K.L.; Browne, L.M.; Tewari, J.P.; Ayer, W.A. Resistance to *Rhizoctonia solani* and presence of antimicrobial compounds in *Camelina sativa* roots. *J. Plant Biochem. Biotechnol.* **1994**, *3*, 125–130. [CrossRef]
146. Paul, V.H.; Badent, S.; Henneken, M.; Foller, I. Results on the occurrence and seed-borne nature of the new disease bacterial blight (*Pseudomonas syringae* pv. spec) on false flax (*Camelina sativa*). *IOBC WPRS BULLETIN* **2000**, *23*, 43–50.
147. Broadbent, L.; Heathcote, G.D. Properties and host range of turnip crinkle, rosette and yellow mosaic viruses. *Ann. Appl. Biol.* **1958**, *46*, 585–592. [CrossRef]
148. Hein, A. Transmission of turnip yellow mosaic virus through seed of *Camelina sativa* (gold of pleasure). *Z. Pflanzenkrankh. Pflanzenschutz/J. Plant Dis. Prot.* **1984**, *91*, 549–551.
149. Graichen, K. Zur Bedeutung von Virusbefall fuer denAnbau von Winterraps und Leindotter. *Mitt. Biol. Bundesanst. Land-Forstwirtsch* **1995**, *310*, 102–108.
150. Chesnais, Q.; Mauck, K.E.; Bogaert, F.; Bamière, A.; Catterou, M.; Spicher, F.; Brault, V.; Tepfer, M.; Ameline, A. Virus effects on plant quality and vector behavior are species specific and do not depend on host physiological phenotype. *J. Pest Sci.* **2019**, *92*, 791–804. [CrossRef]
151. Eberle, C.A.; Thom, M.D.; Nemec, K.T.; Forcella, F.; Lundgren, J.G.; Gesch, R.W.; Riedell, W.E.; Papiernik, S.K.; Wagner, A.; Peterson, D.H. Using pennycress, camelina, and canola cash cover crops to provision pollinators. *Ind. Crops Prod.* **2015**, *75*, 20–25. [CrossRef]

152. Thom, M.D.; Eberle, C.A.; Forcella, F.; Gesch, R.; Weyers, S.; Lundgren, J.G. Nectar production in oilseeds: Food for pollinators in an agricultural landscape. *Crop Sci.* **2016**, *56*, 727–739. [CrossRef]
153. Bekuzarova, S.A.; Basiev, S.S.; Buyankin, V.I.; Kozirev, A.K.; Dulaev, T.A. Ecological significance of winter camelina in biological agriculture. *J. Pharm. Sci. Res.* **2018**, *10*, 893–895.
154. Wagg, C.; van Erk, A.; Fava, E.; Comeau, L.-P.; Mitterboeck, T.F.; Goyer, C.; Li, S.; McKenzie-Gopsil, A.; Mills, A. Full-season cover crops and their traits that promote agroecosystem services. *Agriculture* **2021**, *11*, 830. [CrossRef]
155. Ugrenović, V.; Filipović, V.; Jevremović, S.; Marjanović-Jeromela, A.; Popović, V.; Buntić, A.; Delić, D.I. Effect of Brassicaceae as cover crops. *Sel. I Semen.* **2019**, *25*, 1–8. [CrossRef]
156. Abramovič, H.; Abram, V. Physico-chemical properties, composition and oxidative stability of *Camelina sativa* oil. *Food Technol. Biotechnol.* **2005**, *43*, 63–70.
157. Rodríguez-Rodríguez, M.F.; Sánchez-García, A.; Salas, J.J.; Garcés, R.; Martínez-Force, E. Characterization of the morphological changes and fatty acid profile of developing *Camelina sativa* seeds. *Ind. Crops Prod.* **2013**, *50*, 673–679. [CrossRef]
158. Anderson, J.V.; Wittenberg, A.; Li, H.; Berti, M.T. High throughput phenotyping of *Camelina sativa* seeds for crude protein, total oil, and fatty acids profile by near infrared spectroscopy. *Ind. Crops Prod.* **2019**, *137*, 501–507. [CrossRef]
159. Zubr, J. Dietary fatty acids and amino acids of *Camelina sativa* seed. *J. Food Qual.* **2003**, *26*, 451–462. [CrossRef]
160. Zubr, J. Qualitative variation of *Camelina sativa* seed from different locations. *Ind. Crops Prod.* **2003**, *17*, 161–169. [CrossRef]
161. Hotton, S.K.; Kammerzell, M.; Chan, R.; Hernandez, B.T.; Young, H.A.; Tobias, C.; McKeon, T.; Brichta, J.; Thomson, N.J.; Thomson, J.G. Phenotypic examination of *Camelina sativa* (L.) Crantz accessions from the USDA-ARS National Genetics Resource Program. *Plants* **2020**, *9*, 642. [CrossRef]
162. Singer, S.D.; Zou, J.; Weselake, R.J. Abiotic factors influence plant storage lipid accumulation and composition. *Plant Sci.* **2016**, *243*, 1–9. [CrossRef] [PubMed]
163. Zubr, J.; Matthaus, B. Effects of growth conditions on fatty acids and tocopherols in *Camelina sativa* oil. *Ind. Crops Prod.* **2002**, *15*, 155–162. [CrossRef]
164. Krzyżaniak, M.; Stolarski, M.J.; Tworkowski, J.; Puttick, D.; Eynck, C.; Załuski, D.; Kwiatkowski, J. Yield and seed composition of 10 spring camelina genotypes cultivated in the temperate climate of Central Europe. *Ind. Crops Prod.* **2019**, *138*, 111443. [CrossRef]
165. Yang, J.; Caldwell, C.; Corscadden, K.; He, Q.S.; Li, J. An evaluation of biodiesel production from *Camelina sativa* grown in Nova Scotia. *Ind. Crops Prod.* **2016**, *81*, 162–168. [CrossRef]
166. Moser, B.R.; Vaughn, S.F. Evaluation of alkyl esters from *Camelina sativa* oil as biodiesel and as blend components in ultra low-sulfur diesel fuel. *Bioresour. Technol.* **2010**, *101*, 646–653. [CrossRef] [PubMed]
167. Wu, X.; Leung, D.Y.C. Optimization of biodiesel production from camelina oil using orthogonal experiment. *Appl. Energy* **2011**, *88*, 3615–3624. [CrossRef]
168. Hrastar, R.; Petrišič, M.G.; Ogrinc, N.; Košir, I.J. Fatty acid and stable carbon isotope characterization of *Camelina sativa* oil: Implications for authentication. *J. Agric. Food Chem.* **2009**, *57*, 579–585. [CrossRef] [PubMed]
169. Voelker, T.; Kinney, A.J. Variations in the biosynthesis of seed-storage lipids. *Annu. Rev. Plant Physiol. Plant Mol. Biol.* **2001**, *52*, 335–361. [CrossRef] [PubMed]
170. Zhang, J.; Liu, H.; Sun, J.; Li, B.; Zhu, Q.; Chen, S.; Zhang, H. Arabidopsis fatty acid desaturase FAD2 is required for salt tolerance during seed germination and early seedling growth. *PLoS ONE* **2012**, *7*, e30355. [CrossRef] [PubMed]
171. Dar, A.A.; Choudhury, A.R.; Kancharla, P.K.; Arumugam, N. The FAD2 Gene in Plants: Occurrence, Regulation, and Role. *Front Plant Sci.* **2017**, *8*, 1789. [CrossRef]
172. Bhunia, R.K.; Kaur, R.; Maiti, M.K. Metabolic engineering of fatty acid biosynthetic pathway in sesame (*Sesamum indicum* L.): Assembling tools to develop nutritionally desirable sesame seed oil. *Phytochem. Rev.* **2015**, *15*, 799–811. [CrossRef]
173. Raziei, Z.; Kahrizi, D.; Rostami-Ahmadvandi, H. Effects of climate on fatty acid profile in *Camelina sativa*. *Cell. Mol. Biol.* **2018**, *64*, 91–96. [CrossRef] [PubMed]
174. Berti, M.T.; Wilckens, R.; Fischer, S.; Araos, R. Borage: A new crop for southern Chile. In *Trends in New Crops and New Uses: Strengthin Diversity*; Janick, J., Whipkey, A., Eds.; ASHS Press: Alexandria, VA, USA, 2002; pp. 501–505.
175. Gilbertson, P.K.; Berti, M.T.; Johnson, B.L. Borage cardinal germination temperatures and seed development. *Ind. Crops Prod.* **2014**, *59*, 202–209. [CrossRef]
176. Leclère, M.; Lorent, A.-R.; Jeuffroy, M.-H.; Butier, A.; Chatain, C.; Loyce, C. Diagnosis of camelina seed yield and quality across an on-farm experimental network. *Eur. J. Agron.* **2021**, *122*, 126190. [CrossRef]
177. Borzoo, S.; Mohsenzadeh, S.; Moradshahi, A.; Kahrizi, D.; Zamani, H.; Zarei, M. Characterization of physiological responses and fatty acid compositions of *Camelina sativa* genotypes under water deficit stress and symbiosis with *Micrococcus yunnanensis*. *Symbiosis* **2021**, *83*, 79–90. [CrossRef]
178. Singh, S.K.; Rajpurohit, B.; Singha, P. Camelina (*Camelina sativa*) seed. In *Oilseeds: Health Attributes and Food Applications*; Tanwar, B., Goyal, A., Eds.; Springer: Singapore, 2021; pp. 455–471.
179. Karvonen, H.M.; Aro, A.; Tapola, N.S.; Salminen, I.; Uusitupa, M.I.; Sarkkinen, E.S. Effect of alpha-linolenic acid-rich Camelina sativa oil on serum fatty acid composition and serum lipids in hypercholesterolemic subjects. *Metabolism* **2002**, *51*, 1253–1260. [CrossRef] [PubMed]

180. Schwab, U.S.; Lankinen, M.A.; de Mello, V.D.; Manninen, S.M.; Kurl, S.; Pulkki, K.J.; Laaksonen, D.E.; Erkkilä, A.T. *Camelina sativa* oil, but not fatty fish or lean fish, improves serum lipid profile in subjects with impaired glucose metabolism—a randomized controlled trial. *Mol. Nutr. Food Res.* **2018**, *62*, 1700503. [CrossRef]
181. Manninen, S.; Lankinen, M.; Erkkilä, A.; Nguyen, S.D.; Ruuth, M.; de Mello, V.; Öörni, K.; Schwab, U. The effect of intakes of fish and *Camelina sativa* oil on atherogenic and anti-atherogenic functions of LDL and HDL particles: A randomized controlled trial. *Atherosclerosis* **2019**, *281*, 56–61. [CrossRef] [PubMed]
182. de Mello, V.D.; Dahlman, I.; Lankinen, M.; Kurl, S.; Pitkänen, L.; Laaksonen, D.E.; Schwab, U.; Erkkilä, A.T. The effect of different sources of fish and camelina sativa oil on immune cell and adipose tissue mRNA expression in subjects with abnormal fasting glucose metabolism: A randomized controlled trial. *Nutr. Diabetes* **2019**, *9*, 1. [CrossRef]
183. Saleh-Ghadimi, S.; Dehghan, P.; Farhangi, M.A.; Khoshbaten, M. Co-Supplementation of Camelina Oil and Prebiotic is more Effective in Improvement of Cardiometabolic Risk Factors and Mental Health in Patients with NAFLD: A Randomized Clinical Trial. *Food Funct.* **2021**, *in press*. [CrossRef]
184. Ergönül, P.G.; Özbek, Z.A. Cold pressed camelina (*Camelina sativa* L.) seed oil. In *Cold Pressed Oils*; Elsevier: Amsterdam, The Netherlands, 2020; pp. 255–266.
185. Ibrahim, F.M.; El Habbasha, S. Chemical composition, medicinal impacts andcultivation of camelina (*Camelina sativa*): Review. *Int. J. PharmTech Res.* **2015**, *8*, 114–122.
186. Ratusz, K.; Symoniuk, E.; Wroniak, M.; Rudzińska, M. Bioactive compounds, nutritional quality and oxidative stability of cold-pressed camelina (*Camelina sativa* L.) oils. *Appl. Sci.* **2018**, *8*, 2606. [CrossRef]
187. Eidhin, D.N.; O'Beirne, D. Oxidative stability of camelina oil in salad dressings, mayonnaises and during frying. *Int. J. Food Sci. + Technol.* **2010**, *45*, 444–452. [CrossRef]
188. Salminen, H.; Estévez, M.; Kivikari, R.; Heinonen, M. Inhibition of protein and lipid oxidation by rapeseed, camelina and soy meal in cooked pork meat patties. *Eur. Food Res. Technol. Vol.* **2006**, *223*, 461–468. [CrossRef]
189. Cherian, G. *Camelina sativa* in poultry diets: Opportunities and challenges. In *Biofuel Co-Products as Livestock Feed: Opportunities and Challenges*; Harinder, P.S., Ed.; Food and Agriculture Organization of the United Nations: Rome, Italy, 2012; pp. 303–310.
190. Bătrîna, Ş.L.; Jurcoane, Ş.; Popescu, I.; Marin, F.; Imbrea, I.M.; Crista, F.; Pop, G.; Imbrea, F. *Camelina sativa*: A study on amino acid content. *Rom. Biotechnol Lett.* **2020**, *25*, 1136–1142. [CrossRef]
191. Singh, B.K.; Bala, M.; Rai, P.K. Fatty acid composition and seed meal characteristics of *Brassica* and allied genera. *Natl. Acad. Sci. Lett.* **2014**, *37*, 219–226. [CrossRef]
192. Russo, R.; Reggiani, R. Glucosinolates and sinapine in camelina meal. *Food Nutr. Sci.* **2017**, *8*, 1063–1073. [CrossRef]
193. Paula, E.M.; da Silva, L.G.; Brandao, V.L.N.; Dai, X.; Faciola, A.P. Feeding canola, camelina, and carinata meals to ruminants. *Animals* **2019**, *9*, 704. [CrossRef] [PubMed]
194. Salas, H.; Castillejos, L.; López-Suárez, M.; Ferret, A. In vitro digestibility, in situ degradability, rumen fermentation and N metabolism of camelina co-products for beef cattle studied with a dual flow continuous culture system. *Animals* **2019**, *9*, 1079. [CrossRef] [PubMed]
195. Moriel, P.; Nayigihugu, V.; Cappellozza, B.I.; Gonçalves, E.P.; Krall, J.M.; Foulke, T.; Cammack, K.M.; Hess, B.W. Camelina meal and crude glycerin as feed supplements for developing replacement beef heifers. *J. Anim. Sci.* **2011**, *89*, 4314–4324. [CrossRef] [PubMed]
196. Colombini, S.; Broderick, G.A.; Galasso, I.; Martinelli, T.; Rapetti, L.; Russo, R.; Reggiani, R. Evaluation of *Camelina sativa* (L.) Crantz meal as an alternative protein source in ruminant rations. *J. Sci. Food Agric.* **2014**, *94*, 736–743. [CrossRef] [PubMed]
197. Llewellyn, D.A.; Rohwer, G.; Norberg, O.S.; Kimura, E.; Neibergs, J.S.; Fransen, S.C. Case study: Evaluating farm processed canola and *Camelina* meals as protein supplements for beef cattle. *J. NACAA* **2015**, *8*. Available online: https://www.nacaa.com/journal (accessed on 10 February 2022).
198. Cappellozza, B.I.; Cooke, R.F.; Bohnert, D.W.; Cherian, G.; Carroll, J.A. Effects of camelina meal supplementation on ruminal forage degradability, performance, and physiological responses of beef cattle. *J. Anim. Sci.* **2012**, *90*, 4042–4054. [CrossRef] [PubMed]
199. Lawrence, R.D.; Anderson, J.L.; Clapper, J.A. Evaluation of camelina meal as a feedstuff for growing dairy heifers. *J. Dairy Sci.* **2016**, *99*, 6215–6228. [CrossRef] [PubMed]
200. Lawrence, R.D.; Anderson, J.L. Ruminal degradation and intestinal digestibility of camelina meal and carinata meal compared with other protein sources. *Prof. Anim. Sci.* **2018**, *34*, 10–18. [CrossRef]
201. Russo, R.; Reggiani, R. Antinutritive compounds in twelve *Camelina sativa* genotypes. *Am. J. Plant Sci.* **2012**, *3*, 1408–1412. [CrossRef]
202. Schill, S.R. *Camelina* meal approved for feedlot cattle. *Biodiesel Mag.* **2009**. Available online: http://www.biodieselmagazine.com/articles/3837/camelinameal-approved-for-feedlot-cattle (accessed on 10 February 2022).
203. Berhow, M.A.; Polat, U.; Glinski, J.A.; Glensk, M.; Vaughn, S.F.; Isbell, T.; Ayala-Diaz, I.; Marek, L.; Gardner, C. Optimized analysis and quantification of glucosinolates from *Camelina sativa* seeds by reverse-phase liquid chromatography. *Ind. Crops Prod.* **2013**, *43*, 119–125. [CrossRef]
204. Russo, R.; Galasso, I.; Reggiani, R. Variability in glucosinolate content among *Camelina* species. *Am. J. Plant Sci.* **2014**, *5*, 294–298. [CrossRef]

205. Vetter, W.; Darwisch, V.; Lehnert, K. Erucic acid in Brassicaceae and salmon–An evaluation of the new proposed limits of erucic acid in food. *NFS J.* **2020**, *19*, 9–15. [CrossRef]
206. Hurtaud, C.; Peyraud, J.L. Effects of feeding camelina (seeds or meal) on milk fatty acid composition and butter spreadability. *J. Dairy Sci.* **2007**, *90*, 5134–5145. [CrossRef]
207. Halmemies-Beauchet-Filleau, A.; Kokkonen, T.; Lampi, A.M.; Toivonen, V.; Shingfield, K.J.; Vanhatalo, A. Effect of plant oils and camelina expeller on milk fatty acid composition in lactating cows fed diets based on red clover silage. *J. Dairy Sci.* **2011**, *94*, 4413–4430. [CrossRef] [PubMed]
208. Halmemies-Beauchet-Filleau, A.; Shingfield, K.J.; Simpura, I.; Kokkonen, T.; Jaakkola, S.; Toivonen, V.; Vanhatalo, A. Effect of incremental amounts of camelina oil on milk fatty acid composition in lactating cows fed diets based on a mixture of grass and red clover silage and concentrates containing camelina expeller. *J. Dairy Sci.* **2017**, *100*, 305–324. [CrossRef] [PubMed]
209. Cieslak, A.; Stanisz, M.; Wojtowski, J.; Pers-Kamczyc, E.; Szczechowiak, J.; El-Sherbiny, M.; Szumacher-Strabel, M. *Camelina sativa* affects the fattyacid contents in *M. longissimus* muscle of lambs. *Eur. J. Lipid Sci. Technol.* **2013**, *115*, 1258–1265. [CrossRef]
210. Steppa, R.; Cieślak, A.; Szumacher-Strabel, M.; Bielińska-Nowak, S.; Bryszak, M.; Stanisz, M.; Szkudelska, K. Blood serum metabolic profile and fatty acid composition in sheep fed concentrates with *Camelina sativa* cake and distillers dried grains with solubles. *Small Rumin. Res.* **2017**, *156*, 20–26. [CrossRef]
211. Ponnampalam, E.N.; Butler, K.L.; Muir, S.K.; Plozza, T.E.; Kerr, M.G.; Brown, W.G.; Jacobs, J.L.; Knight, M.I. Lipid oxidation and colour stability of lamb and yearling meat (muscle longissimus lumborum) from sheep supplemented with *Camelina*-based diets after short-, medium-, and long-term storage. *Antioxidants* **2021**, *10*, 166. [CrossRef] [PubMed]
212. Szumacher-Strabel, M.; Cieślak, A.; Zmora, P.; Pers-Kamczyc, E.; Bielińska, S.; Stanisz, M.; Wójtowski, J. *Camelina sativa* cake improved unsaturated fatty acids in ewe's milk. *J. Sci. Food Agric.* **2011**, *91*, 2031–2037. [CrossRef]
213. Mierlita, D.; Daraban, S.; Lup, F.; Chereji, A. The effect of grazing management and camelina seed supplementation in the diet on milk performance and milk fatty acid composition of dairy ewes. *J. Food Agric. Environ.* **2011**, *9*, 368–373.
214. Pikul, J.; Wójtowski, J.; Danków, R.; Teichert, J.; Czyżak-Runowska, G.; Cais-Sokolińska, D.; Cieślak, A.; Szumacher-Strabel, M.; Bagnicka, E. The effect of false flax (*Camelina sativa*) cake dietary supplementation in dairy goats on fatty acid profile of kefir. *Small Rumin. Res.* **2014**, *122*, 44–49. [CrossRef]
215. Cais-Sokolińska, D.; Majcher, M.; Pikul, J.; Bielińska, S.; Czauderna, M.; Wójtowski, J. The effect of *Camelina sativa* cake diet supplementation on sensory and volatile profiles of ewe's milk. *Afr. J. Biotechnol.* **2011**, *10*, 7245–7252. [CrossRef]
216. Cais-Sokolińska, D.; Wójtowski, J.; Pikul, J.; Danków, R.; Majcher, M.; Teichert, J.; Bagnicka, E. Formation of volatile compounds in kefir made of goat and sheep milk with high polyunsaturated fatty acid content. *J. Dairy Sci.* **2015**, *98*, 6692–6705. [CrossRef] [PubMed]
217. Mierlita, D.; Vicas, S. Dietary effect of silage type and combination with camelina seed on milk fatty acid profile and antioxidant capacity of sheep milk. *S. Afr. J. Anim. Sci.* **2015**, *45*, 1–11. [CrossRef]
218. Christodoulou, C.; Mavrommatis, A.; Mitsiopoulou, C.; Symeon, G.; Dotas, V.; Sotirakoglou, K.; Kotsampasi, B.; Tsiplakou, E. Assessing the optimum level of supplementation with Camelina seeds in ewes' diets to improve milk quality. *Foods* **2021**, *10*, 2076. [CrossRef] [PubMed]
219. Danków, R.; Pikul, J.; Wójtowski, J.; Cais-Sokolińska, D.; Teichert, J.; Bagnicka, E.; Cieślak, A.; Szumacher-Strabel, M. The effect of supplementation with gold of pleasure (*Camelina sativa*) cake on the fatty acid profile of ewe milk and yoghurt produced from it. *J. Anim. Feed Sci.* **2015**, *24*, 193–202. [CrossRef]
220. Mierlita, D. Conjugated linoleic acid and ω-3 fatty acid in sheep milk was increased by part-time grazing and camelina seed diet. *J. Food Agric. Environ.* **2015**, *13*, 76–81.
221. Eidhin, D.N.; Burke, J.; Lynch, B.; O'Beirne, D. Effects of dietary supplementation with camelina oil on porcine blood lipids. *J. Food Sci.* **2003**, *68*, 671–679. [CrossRef]
222. Hăbeanu, M.; Hebean, V.; Țăranu, I.; Marin, D.; Ropotă, M.; Tamaș, V. Effects of the dietary Camelina oil on large white pigs' meat quality. *Arch. Zootech.* **2009**, *12*, 31–45.
223. Hăbeanu, M.; Hebean, V.; Taranu, I.; Ropota, M.; Lefter, N.; Marin, D. Dietary ecologic Camelina oil: A beneficial aource of n-3 PUFA in muscle tissue and health status in finishing pigs. *Rom. Biotechnol. Lett.* **2011**, *16*, 5564–5571.
224. Taranu, I.; Gras, M.; Pistol, G.C.; Motiu, M.; Marin, D.E.; Lefter, N.; Ropota, M.; Habeanu, M. ω-3 PUFA rich Camelina oil by-products improve the systemic metabolism and spleen cell functions in fattening pigs. *PLoS ONE* **2014**, *9*, e110186. [CrossRef] [PubMed]
225. Almeida, F.N.; Htoo, J.K.; Thomson, J.; Stein, H.-H. Amino acid digestibility in camelina products fed to growing pigs. *Can. J. Anim. Sci.* **2013**, *93*, 335–343. [CrossRef]
226. Kahindi, R.K.; Woyengo, T.A.; Thacker, P.A.; Nyachoti, C.M. Energy and amino acid digestibility of camelina cake fed to growing pigs. *Anim. Feed Sci. Technol.* **2014**, *193*, 93–101. [CrossRef]
227. Hăbeanu, M.; Lefter, A.N.; Ropotă, M. Effects of the camelina cake on fatty acids composition in different organs of the pigs. *Arch. Zootech.* **2016**, *19*, 5–16.
228. Smit, M.N.; Beltranena, E. Effects of feeding camelina cake to weaned pigs on safety, growth performance, and fatty acid composition of pork. *J. Anim. Sci.* **2017**, *95*, 2496–2508. [CrossRef] [PubMed]
229. Meadus, W.J.; Duff, P.; McDonald, T.; Caine, W.R. Pigs fed camelina meal increase hepatic gene expression of cytochrome 8b1, aldehyde dehydrogenase, and thiosulfate transferase. *J. Anim. Sci. Biotechnol.* **2014**, *5*, 1–8. [CrossRef] [PubMed]

230. Hilbrands, A.M.; Johnston, L.J.; Cox, R.B.; Forcella, F.; Gesch, R.; Li, Y.Z. Effects of increasing dietary inclusion of camelina cake on growth performance of growing-finishing pigs. *Transl. Anim. Sci.* **2021**, *5*, 1–10. [CrossRef]
231. Kim, J.W.; Koo, B.; Nyachoti, C.M. Digestible, metabolizable, and net energy of camelina cake fed to growing pigs and additivity of energy in mixed diets. *J. Anim. Sci.* **2017**, *95*, 4037–4044. [CrossRef]
232. Juodka, R.; Nainienė, R.; Juškienė, V.; Juška, R.; Leikus, R.; Kadžienė, G.; Stankevičienė, D. Camelina (*Camelina sativa* (L.) Crantz) as feedstuffs in meat type poultry diet: A source of protein and n-3 fatty acids. *Animals* **2022**, *12*, 295. [CrossRef]
233. Aziza, A.E.; Quezada, N.; Cherian, G. Feeding *Camelina sativa* meal to meat-type chickens: Effect on production performance and tissue fatty acid composition. *J. Appl. Poult. Res.* **2010**, *19*, 157–168. [CrossRef]
234. Aziza, A.; Panda, A.; Quezada, N.; Cherian, G. Nutrient digestibility, egg quality, and fatty acid composition of brown laying hens fed camelina or flaxseed meal. *J. Appl. Poult. Res.* **2013**, *22*, 832–841. [CrossRef]
235. Nain, S.; Oryschak, M.A.; Betti, M.; Beltranena, E. *Camelina sativa* cake for broilers: Effects of increasing dietary inclusion from 0 to 24% on tissue fatty acid proportions at 14, 28, and 42 d of age. *Poult. Sci.* **2015**, *94*, 1247–1258. [CrossRef] [PubMed]
236. Woyengo, T.A.; Patterson, R.; Slominski, B.A.; Beltranena, E.; Zijlstra, R.T. Nutritive value of cold-pressed camelina cake with or without supplementation of multi-enzyme in broiler chickens. *Poult. Sci.* **2016**, *95*, 2314–2321. [CrossRef] [PubMed]
237. Jáskiewicz, T.; Sagan, A.; Puzio, I. Effect of the *Camelina sativa* oil on theperformance, essential fatty acid level in tissues and fat-soluble vitamins content in the livers of broiler chickens. *Livest. Sci.* **2014**, *165*, 74–79. [CrossRef]
238. Pietras, M.P.; Orczewska-Dudek, S. The effect of dietary *Camelina sativa* oil on quality of broiler chicken meat. *Ann. Anim. Sci.* **2013**, *13*, 869–882. [CrossRef]
239. Orczewska-Dudek, S.; Pietras, M. The effect of dietary *Camelina sativa* oil or cake in the diets of broiler chickens on growth performance, fatty acid profile, and sensory quality of meat. *Animals* **2019**, *9*, 734. [CrossRef] [PubMed]
240. Juodka, R.; Juska, R.; Juskiene, V.; Leikus, R.; Stankeviciene, D.; Nainiene, R. The effect of feeding with hemp and Camelina cakes on the fatty acid profile of duck muscles. *Arch. Anim. Breed.* **2018**, *61*, 293–303. [CrossRef]
241. Frame, D.D.; Palmer, M.; Peterson, B. Use of *Camelina sativa* in the diets of young turkeys. *J. Appl. Poult. Res.* **2007**, *16*, 381–386. [CrossRef]
242. Pekel, A.Y.; Kim, J.I.; Chapple, C.; Adeola, O. Nutritional characteristics of camelina meal for 3-week-old broiler chickens. *Poult Sci* **2015**, *94*, 371–378. [CrossRef] [PubMed]
243. Ryhänen, E.L.; Perttilä, S.; Tupasela, T.; Valaja, J.; Eriksson, C.; Larkka, K.E. Effect of *Camelina sativa* expeller cake on performance and meat quality of broilers. *J. Sci. Food Agric.* **2007**, *87*, 1489–1494. [CrossRef]
244. Bulbul, T.; Rahman, A.; Ozdemir, V. Effect of false flax meal on certain growth, serum and meat parameters of japanese quails. *J. Anim. Plant Sci.* **2015**, *25*, 1245–1250.
245. Ye, C.L.; Anderson, D.M.; Lall, S.P. The effects of camelina oil and solvent extracted camelina meal on the growth: Carcass composition and hindguthistology of Atlantic salmon (*Salmo salar*) parr in freshwater. *Aquaculture* **2016**, *450*, 397–404. [CrossRef]
246. Hixson, S.M.; Parrish, C.C.; Anderson, D.M. Full substitution of fish oil with camelina (*Camelina sativa*) oil, with partial substitution of fish meal with camelina meal, in diets for farmed Atlantic salmon (*Salmo salar*) and its effect on tissue lipids and sensory quality. *Food Chem.* **2014**, *157*, 51–61. [CrossRef]
247. Hixson, S.M.; Parrish, C.C.; Anderson, D.M. Effect of replacement of fish oil with camelina (*Camelina sativa*) oil on growth, lipid class and fatty acid composition of farmed juvenile Atlantic cod (*Gadus morhua*). *Fish Physiol. Biochem.* **2013**, *39*, 1441–1456. [CrossRef] [PubMed]
248. Hixson, S.M.; Parrish, C.C.; Wells, J.S.; Marie Winkowski, E.; Anderson, D.M. Inclusion of camelina meal as a protein source in diets for farmed Atlantic cod *Gadus morhua*. *Aquac. Res.* **2016**, *47*, 2607–2622. [CrossRef]
249. Ruiz-Lopez, N.; Haslam, R.P.; Napier, J.A.; Sayanova, O. Successful high-level accumulation of fish oil omega-3 long-chain polyunsaturated fatty acids in a transgenic oilseed crop. *Plant J.* **2014**, *77*, 198–208. [CrossRef] [PubMed]
250. Betancor, M.B.; MacEwan, A.; Sprague, M.; Gong, X.; Montero, D.; Han, L.; Napier, J.A.; Norambuena, F.; Izquierdo, M.; Tocher, D.R. Oil from transgenic *Camelina sativa* as a source of EPA and DHA in feed for European sea bass (*Dicentrarchus labrax* L.). *Aquaculture* **2021**, *530*, 735759. [CrossRef] [PubMed]
251. Bullerwell, C.N.; Collins, S.A.; Lall, S.P.; Anderson, D.M. Growth performance, proximate and histological analysis of rainbow trout fed diets containing *Camelina sativa* seeds, meal (high-oil and solvent-extracted) and oil. *Aquaculture* **2016**, *452*, 342–350. [CrossRef]
252. Liang, Y.; May, C.; Foon, C.; Ngan, M.; Hock, C.; Basiron, Y. The effect of natural and synthetic antioxidants on the oxidative stability of palm diesel. *Fuel* **2006**, *85*, 867–870. [CrossRef]
253. ASTM. ASTM (D6751–15ce1) Standard Specification for Biodiesel Fuel BlendStock (B100) for Middle Distillate Fuels. Am. *Soc. Test. Mater.* **2015**. Available online: https://dieselnet.com/tech/fuel_biodiesel_std.php (accessed on 10 February 2022).
254. European Standard EN 14214. EN (14214) European Specifications for Biodiesel Fuels. *Eur. Comm. Stand.* 2012. Available online: https://en.wikipedia.org/wiki/EN_14214 (accessed on 10 February 2022).
255. Soriano, N.U.; Narani, A. Evaluation of biodiesel rerived from *Camelina sativa* oil. *J. Am. Oil Chem. Soc.* **2011**, *89*, 917–923. [CrossRef]
256. Miller, P.; Kumar, A. Techno-economic assessment of hydrogenation-derived renewable diesel production from canola and camelina. *Sustain. Energy Technol. Assess.* **2014**, *6*, 105–115. [CrossRef]

257. Miller, P.; Kumar, A. Development of emission parameters and net energy ratio for renewable diesel from Canola and Camelina. *Energy* **2013**, *58*, 426–437. [CrossRef]
258. Krohn, B.J.; Fripp, M. A life cycle assessment of biodiesel derived from the "niche filling" energy crop camelina in the USA. *Appl. Energy* **2012**, *92*, 92–98. [CrossRef]
259. Corporan, E.; Edwards, T.; Shafer, L.; DeWitt, M.J.; Klingshirn, C.; Zabarnick, S.; West, Z.; Striebich, R.; Graham, J.; Klein, J. Chemical, thermal stability, sealswell, and emissions studies of alternative jet fuels. *Energy Fuels* **2011**, *25*, 955–966. [CrossRef]
260. Sivakumar, D.; Vankeswaram, S.; Sakthikumar, R.; Raghunandan, B. Analysis on the atomization characteristics of aviation biofuel discharging from simplex swirl atomizer. *Int. J. Multiph. Flow* **2015**, *72*, 88–96. [CrossRef]
261. Sivakumar, G.; Vail, D.R.; Xu, J.; Burner, D.M.; Lay, J.O.; Ge, X.; Weathers, P.J. Bioethanol and biodiesel: Alternative liquid fuels for future generations. *Eng. Life Sci.* **2010**, *10*, 8–18. [CrossRef]
262. Agusdinata, D.B.; Zhao, F.; Ileleji, K.; DeLaurentis, D. Life cycle assessment of potential biojet fuel production in the United States. *Environ. Sci. Technol.* **2011**, *45*, 9133–9143. [CrossRef] [PubMed]
263. Shonnard, D.R.; Williams, L.; Kalnes, T.N. Camelina-derived jet fuel and diesel: Sustainable advanced biofuels. *Env. Prog Sustain Energy* **2010**, *29*, 382–392. [CrossRef]
264. Shila, J.; Johnson, M.E. Techno-economic analysis of Camelina-derived hydroprocessed renewable jet fuel within the US context. *Appl. Energy* **2021**, *287*, 116525. [CrossRef]
265. Boateng, A.A.; Mullen, C.A.; Goldberg, N.M. Producing stable pyrolysis liquids from the oil-seed presscakes of mustard family plants: Pennycress (*Thlaspi arvense* L.) and Camelina (*Camelina sativa*). *Energy Fuels* **2010**, *24*, 6624–6632. [CrossRef]
266. Hernando, H.; Fermoso, J.; Moreno, I.; Coronado, J.M.; Serrano, D.P.; Pizarro, P. Thermochemical valorization of camelina straw waste via fast pyrolysis. *Biomass Convers. Biorefinery* **2017**, *7*, 277–287. [CrossRef]
267. Gómez-Monedero, B.; Bimbela, F.; Arauzo, J.; Faria, J.; Ruiz, M.P. Pyrolysis of red eucalyptus, camelina straw, and wheat straw in an ablative reactor. *Energy Fuels* **2015**, *29*, 1766–1775. [CrossRef]
268. Mohammad, B.T.; Al-Shannag, M.; Alnaief, M.; Singh, L.; Singsaas, E.; Alkasrawi, M. Production of multiple biofuels from whole Camelina material: A renewable energy crop. *BioResources* **2018**, *13*, 4870–4883.
269. Jankowski, K.J.; Sokólski, M. Spring camelina: Effect of mineral fertilization on the energy efficiency of biomass production. *Energy* **2021**, *220*, 119731. [CrossRef]
270. Stolarski, M.J.; Krzyżaniak, M.; Kwiatkowski, J.; Tworkowski, J.; Szczukowski, S. Energy and economic efficiency of camelina and crambe biomass production on a large-scale farm in north-eastern Poland. *Energy* **2018**, *150*, 770–780. [CrossRef]
271. Kasetaite, S.; Ostrauskaite, J.; Grazuleviciene, V.; Svediene, J.; Bridziuviene, D. Camelina oil- and linseed oil-based polymers with bisphosphonate crosslinks. *Appl. Polym.* **2014**, *131*, 8536–8543. [CrossRef]
272. Fox, N.J.; Stachowiak, G.W. Vegetable oil-based lubricants- a review of oxidation. *Tribol. Int.* **2007**, *40*, 1035–1046. [CrossRef]
273. Knothe, G. Dependence of biodiesel fuel properties on the structure of fatty acid alkyl esters. *Fuel Processing Technol.* **2005**, *86*, 1059–1070. [CrossRef]
274. Kim, N.; Li, Y.; Sun, X.S. Epoxidation of *Camelina sativa* oil and peel adhesion properties. *Ind. Crops Prod.* **2015**, *64*, 1–8. [CrossRef]
275. Nosal, H.; Nowicki, J.; Warzała, M.; Nowakowska-Bogdan, E.; Zarębska, M. Synthesis and characterization of alkyd resins based on *Camelina sativa* oil and polyglycerol. *Prog. Org. Coat.* **2015**, *86*, 59–70. [CrossRef]
276. Kim, J.T.; Netravali, A.N. Non-food application of camelina meal: Development of sustainable and green biodegradable paper-camelina composite sheets and fibers. *Polym. Compos.* **2012**, *33*, 1969–1976. [CrossRef]
277. Cao, Y.; Gu, Z.; Muthukumarappan, K.; Gibbons, W. Separation of glucosinolates from Camelina seed meal via membrane and acidic aluminum oxide column. *J. Liq. Chromatogr. Relat. Technol.* **2015**, *38*, 1273–1278. [CrossRef]
278. Ma, Y.; Gentry, T.; Hu, P.; Pierson, E.; Gu, M.; Yin, S. Impact of brassicaceous seed meals on the composition of the soil fungal community and the incidence of Fusarium wilt on chili pepper. *Appl. Soil Ecol.* **2015**, *90*, 41–48. [CrossRef]
279. Schuster, A.; Friedt, W. Glucosinolate content and composition as parameters of quality of *Camelina* seed. *Ind. Crops Prod.* **1998**, *7*, 297–302. [CrossRef]
280. Matthäus, B.; Zubr, J. Variability of specific components in *Camelina sativa* oilseed cakes. *Ind. Crops Prod.* **2000**, *12*, 9–18. [CrossRef]
281. Maršalkienė, N.; Žilėnaitė, L.; Karpavičienė, B. Oil content and composition in seeds of *Camelina sativa* and *Crambe abyssinica* cultivars. *J. Ementol.* **2020**, *25*, 1399–1412. [CrossRef]
282. Zubr, J. Unique dietary oil from *Camelina sativa* seed. *Agrafood Ind. Hi-Tech* **2009**, *20*, 42–46.
283. De Lorgeril, M.; Renaud, S.; Salen, P.; Monjaud, I.; Mamelle, N.; Martin, J.; Guidollet, J.; Touboul, P.; Delaye, J. Mediterranean alpha-linolenic acid-rich diet in secondary prevention of coronary heart disease. *Lancet* **1994**, *343*, 1454–1459. [CrossRef]
284. Budin, J.T.; Breene, W.M.; Putnam, D.H. Some compositional properties of camelina (*Camelina sativa* L. Crantz) seeds and oils. *J. Am. Oil Chem. Soc.* **1995**, *72*, 309–315. [CrossRef]
285. Onyilagha, J.; Bala, A.; Hallett, R.; Gruber, M.; Soroka, J.; Westcott, N. Leaf flavonoids of the cruciferous species, *Camelina sativa*, *Crambe* spp., *Thlaspi arvense* and several other genera of the family Brassicaceae. *Biochem. Syst. Ecol.* **2003**, *31*, 1309–1322. [CrossRef]
286. Kumar, K.; Gupta, S.M.; Arya, M.C.; Nasim, M. In vitro antimicrobial and antioxidant activity of camelina seed extracts as potential source of bioactive compounds. *Proc. Natl. Acad. Sci. India Sect. B Biol. Sci.* **2017**, *87*, 521–526. [CrossRef]
287. Kurasiak-Popowska, D.; Ryńska, B.; Stuper-Szablewska, K. Analysis of distribution of selected bioactive compounds in *Camelina sativa* from seeds to pomace and oil. *Agronomy* **2019**, *9*, 168. [CrossRef]

288. Cojocariu, R.O.; Balmus, I.-M.; Lefter, R.; Hritcu, L.; Ababei, D.C.; Ciobica, A.; Copaci, S.; Mot, S.E.L.; Copolovici, L.; Copolovici, D.M.; et al. *Camelina sativa* methanolic and ethanolic extract potential in alleviating oxidative stress, memory deficits, and affective impairments in stress exposure-based irritable bowel syndrome mouse models. *Oxidative Med. Cell. Longev.* **2020**, *2020*, 9510305. [CrossRef] [PubMed]
289. Cojocariu, R.; Balmus, I.; Lefter, R.; Hritcu, L.; Ababei, D.; Ciobica, A.; Copaci, S.; Copolovici, L.; Copolovici, D.; Jurcoane, S. Beneficial effects of *Camelina sativa* oil on behavioural (memory, anxiety, depression and social-related) manifestations and oxidative stress parameters in a mice model of irritable bowel syndrome. *Rom. Biotechnol. Lett.* **2020**, *25*, 1532–1540. [CrossRef]
290. Gao, L.; Caldwell, C.D.; Jiang, Y. Photosynthesis and growth of camelina and canola in response to water deficit and applied nitrogen. *Crop Sci.* **2018**, *58*, 393–401. [CrossRef]
291. Waraich, E.A.; Ahmad, R.; Ahmad, R.; Ahmed, Z.; Ahmad, Z.; Barutcular, C.; Erman, M.; Cig, F.; Saneoka, H.; Öztürk, F. Comparative study of growth, physiology and yield attributes of camelina (*Camelina sativa* L.) and canola (*Brassica napus* L.) under different irrigation regimes. *Pak. J. Bot.* **2020**, *52*, 1537–1544. [CrossRef]
292. Yadav, P.V.; Khatri, D.; Nasim, M. Salt and PEG induced osmotic stress tolerance at germination and seedling stage in *Camelina sativa*: A potential biofuel crop. *J. Seed Sci.* **2017**, *10*, 27–32. [CrossRef]
293. Ahmed, Z.; Waraich, E.A.; Rashid, A.; Shahbaz, M. Morpho-physiological and biochemical responses of camelina (*Camelina sativa* Crantz) genotypes under drought stress. *Int. J. Agric. Biol.* **2017**, *19*, 1–7. [CrossRef]
294. Čanak, P.; Jeromela, A.M.; Vujošević, B.; Kiprovski, B.; Mitrović, B.; Alberghini, B.; Facciolla, E.; Monti, A.; Zanetti, F. Is drought stress tolerance affected by biotypes and seed size in the emerging oilseed crop Camelina? *Agronomy* **2020**, *10*, 1856. [CrossRef]
295. Ahmad, Z.; Anjum, S.; Skalicky, M.; Waraich, E.A.; Tariq, R.M.S.; Ayub, M.A.; Hossain, A.; Hassan, M.M.; Brestic, M.; Islam, M.S.; et al. Selenium alleviates the adverse effect of drought in oilseed crops Camelina (*Camelina sativa* L.) and Canola (*Brassica napus* L.). *Molecules* **2021**, *26*, 1699. [CrossRef] [PubMed]
296. Ahmad, Z.; Waraich, E.A.; Barutcular, C.; Alharby, H.; Bamagoos, A.; Kizilgeci, F.; Öztürk, F.; Hossain, A.; Bayoumi, Y.; El Sabagh, A. Enhancing drought tolerance in *Camelina sativa* L. and canola (*Brassica napus* L.) through application of selenium. *Pak. J. Bot.* **2020**, *52*, 1927–1939. [CrossRef]
297. Ahmad, M.; Waraich, E.A.; Zulfiqar, U.; Ullah, A.; Farooq, M. Thiourea application improves heat tolerance in camelina (*Camelina sativa* L. Crantz) by modulating gas exchange, antioxidant defense and osmoprotection. *Ind. Crops Prod.* **2021**, *170*, 113826. [CrossRef]
298. Liang, C.; Liu, X.; Yiu, S.-M.; Lim, B.L. De novo assembly and characterization of *Camelina sativa* transcriptome by paired-end sequencing. *BMC Genom.* **2013**, *14*, 146. [CrossRef]
299. Nguyen, H.T.; Silva, J.E.; Podicheti, R.; Macrander, J.; Yang, W.; Nazarenus, T.J.; Nam, J.W.; Jaworski, J.G.; Lu, C.; Scheffler, B.E.; et al. Camelina seed transcriptome: A tool for meal and oil improvement and translational research. *Plant Biotechnol. J.* **2013**, *11*, 759–769. [CrossRef] [PubMed]
300. King, K.; Li, H.; Kang, J.; Lu, C. Mapping quantitative trait loci for seed traits in *Camelina sativa*. *Theor. Appl. Genet.* **2019**, *132*, 2567–2577. [CrossRef]
301. Luo, Z.; Brock, J.; Dyer, J.M.; Kutchan, T.; Schachtman, D.; Augustin, M.; Ge, Y.; Fahlgren, N.; Abdel-Haleem, H. Genetic diversity and population structure of a *Camelina sativa* spring panel. *Front. Plant Sci.* **2019**, *10*, 184. [CrossRef] [PubMed]
302. Luo, Z.; Szczepanek, A.; Abdel-Haleem, H. Genome-wide association study (GWAS) analysis of Camelina seedling germination under salt stress sondition. *Agronomy* **2020**, *10*, 1444. [CrossRef]
303. Vollmann, J.; A, D.; Baumgartner, S.; Ruckenbauer, P. Selection of induced mutants with improved linolenic acid content in camelina. *Fett/Lipid* **1997**, *99*, 357–361. [CrossRef]
304. Lohaus, R.H.; Zager, J.J.; Kosma, D.K.; Cushman, J.C. Characterization of seed, oil, and fatty acid methyl esters of an ethyl methanesulfonate mutant of *Camelina sativa* with reduced seed-coat mucilage. *J. Am. Oil Chem. Soc.* **2020**, *97*, 157–174. [CrossRef]
305. Lovett, J.V.; Sagar, G.R. Influence of bacteria in the phyllosphere of *Camelina sativa* (L.) Crantz on germination of *Linum usitatissimum* L. *New Phytol.* **1978**, *81*, 617–625. [CrossRef]
306. Miyashita, H.; Fujita, K. Improvement of *Camelina sativa* yield using a plant growth-promoting rhizobacterium. *Soil Sci. Plant Nutr.* **2019**, *65*, 566–569. [CrossRef]
307. Bekuzarova, S.A.; Weisfeld, L.I.; Dulaev, T.A. Biological methods increasing the productivity of the winter false flax *Camelina silvestris* L. In *Antioxidants in Systems of Varying Complexity*; Apple Academic Press: Palm Bay, FL, USA, 2019; pp. 293–304.
308. Chhikara, S.; Abdullah, H.M.; Akbari, P.; Schnell, D.; Dhankher, O.P. Engineering *Camelina sativa* (L.) Crantz for enhanced oil and seed yields by combining diacylglycerol acyltransferase1 and glycerol-3-phosphate dehydrogenase expression. *Plant Biotechnol J.* **2018**, *16*, 1034–1045. [CrossRef] [PubMed]
309. Heydarian, Z.; Yu, M.; Gruber, M.; Glick, B.R.; Zhou, R.; Hegedus, D.D. Inoculation of soil with plant growth promoting bacteria producing 1-aminocyclopropane-1-carboxylate deaminase or expression of the corresponding acdS gene in transgenic plants increases salinity tolerance in *Camelina sativa*. *Front. Microbiol.* **2016**, *7*, 1966. [CrossRef]
310. Heydarian, Z.; Gruber, M.; Glick, B.R.; Hegedus, D.D. Gene expression patterns in roots of *Camelina sativa* with enhanced salinity tolerance arising from inoculation of soil with plant growth promoting bacteria producing 1-aminocyclopropane-1-carboxylate deaminase or expression the corresponding acds gene. *Front. Microbiol.* **2018**, *9*, 1297. [CrossRef] [PubMed]
311. Kanth, B.K.; Kumari, S.; Choi, S.H.; Ha, H.-J.; Lee, G.-J. Generation and analysis of expressed sequence tags (ESTs) of *Camelina sativa* to mine drought stress-responsive genes. *Biochem. Biophys. Res. Commun.* **2015**, *467*, 83–93. [CrossRef]

312. Heydarian, Z.; Yu, M.; Gruber, M.; Coutu, C.; Robinson, S.J.; Hegedus, D.D. Changes in gene expression in *Camelina sativa* roots and vegetative tissues in response to salinity stress. *Sci. Rep.* **2018**, *8*, 9804. [CrossRef] [PubMed]
313. Lee, S.B.; Kim, H.; Kim, R.J.; Suh, M.C. Overexpression of Arabidopsis MYB96 confers drought resistance in *Camelina sativa* via cuticular wax accumulation. *Plant Cell Rep.* **2014**, *33*, 1535–1546. [CrossRef]
314. Kim, R.J.; Kim, H.U.; Suh, M.C. Development of camelina enhanced with drought stress resistance and seed oil production by co-overexpression of MYB96A and DGAT1C. *Ind. Crops Prod.* **2019**, *138*, 111475. [CrossRef]
315. Subedi, U.; Jayawardhane, K.N.; Pan, X.; Ozga, J.; Chen, G.; Foroud, N.A.; Singer, S.D. The potential of genome editing for improving seed oil content and fatty acid composition in oilseed crops. *Lipids* **2020**, *55*, 495–512. [CrossRef] [PubMed]
316. Kawall, K. Genome-edited *Camelina sativa* with a unique fatty acid content and its potential impact on ecosystems. *Environ. Sci. Eur.* **2021**, *33*, 38. [CrossRef]
317. Yuan, L.; Li, R. Metabolic engineering a model oilseed *Camelina sativa* for the sustainable production of high-value designed oils. *Front. Plant Sci.* **2020**, *11*, 11. [CrossRef]
318. Aznar-Moreno, J.A.; Durrett, T.P. Simultaneous targeting of multiple gene homeologs to alter seed oil production in *Camelina sativa*. *Plant Cell Physiol.* **2017**, *58*, 1260–1267. [CrossRef] [PubMed]
319. Lee, K.-R.; Jeon, I.; Yu, H.; Kim, S.-G.; Kim, H.-S.; Ahn, S.-J.; Lee, J.; Lee, S.-K.; Kim, H.U. Increasing monounsaturated fatty acid contents in hexaploid *Camelina sativa* seed oil by FAD2 gene knockout using CRISPR-Cas9. *Front. Plant Sci.* **2021**, 12. [CrossRef] [PubMed]
320. Lyzenga, W.J.; Harrington, M.; Bekkaoui, D.; Wigness, M.; Hegedus, D.D.; Rozwadowski, K.L. CRISPR/Cas9 editing of three CRUCIFERIN C homoeologues alters the seed protein profile in *Camelina sativa*. *BMC Plant Biol.* **2019**, *19*, 292. [CrossRef] [PubMed]
321. Veljković, V.B.; Kostić, M.D.; Stamenković, O.S. Camelina seed harvesting, storing, pretreating, and processing to recover oil: A review. *Ind. Crops Prod.* **2022**, *178*, 114539. [CrossRef]
322. Pagnotta, E.; Ugolini, L.; Matteo, R.; Lazzeri, L.; Foschi, L.; Angelini, L.; Tavarini, S. Exploring the *Camelina sativa* value chain: A new opportunity for bio-based products and overall crop sustainability. *La Riv. Italliana Delle Sostanze Grasse* **2019**, *96*, 259–268.
323. Righini, D.; Zanetti, F.; Monti, A. The bio-based economy can serve as the springboard for camelina and crambe to quit the limbo. *Oilseeds Fats Crops Lipids (OCL)* **2016**, *23*, D504. [CrossRef]
324. Ahmad, M.; Waraich, E.A.; Zulfiqar, U.; Ullah, A.; Farooq, M. Thiourea application increases seed and oil yields in Camelina under heat stress by modulating the plant water relations and antioxidant defense system. *J. Soil Sci. Plant Nutr.* **2022**, 1–18. [CrossRef]

plants

MDPI

Article

Identification of Genes in *Xanthomonas euvesicatoria* pv. *rosa* That Are Host Limiting in Tomato

Qiurong Fan [1,†], Shaheen Bibi [1,†], Gary E. Vallad [1,2], Erica M. Goss [1,3], Jason C. Hurlbert [4], Matthews L. Paret [1,5], Jeffrey B. Jones [1,*] and Sujan Timilsina [1,*]

1 Department of Plant Pathology, University of Florida, Gainesville, FL 32611, USA; chiaki@ufl.edu (Q.F.); shaheen110@ufl.edu (S.B.); gvallad@ufl.edu (G.E.V.); emgoss@ufl.edu (E.M.G.); paret@ufl.edu (M.L.P.)
2 Gulf Coast Research and Education Center, University of Florida, Balm, FL 33598, USA
3 Emerging Pathogens Institute, University of Florida, Gainesville, FL 32610, USA
4 Department of Chemistry, Physics and Geology, Winthrop University, Rock Hill, SC 29733, USA; hurlbertj@winthrop.edu
5 North Florida Research and Education Center, University of Florida, Quincy, FL 32351, USA
* Correspondence: jbjones@ufl.edu (J.B.J.); sujan.timilsina@ufl.edu (S.T.)
† These authors contributed equally to this work.

Abstract: *Xanthomonas euvesicatoria* pv. *rosa* strain *Xer07* causes a leaf spot on a *Rosa* sp. and is closely related to *X. euvesicatoria* pv. *euvesicatoria* (*Xee*) and *X. perforans* (*Xp*), causal agents of bacterial spot of tomato. However, *Xer07* is not pathogenic on tomato and elicits a hypersensitive reaction (HR). We compared the genomes of the three bacterial species to identify the factors that limit *Xer07* on tomato. Comparison of pathogenicity associated factors including the type III secretion systems identified two genes, *xopA* and *xer3856*, in *Xer*07 that have lower sequence homology in tomato pathogens. *xer3856* is a homolog of genes in *X. citri* (*xac3856*) and *X. fuscans* pv. *aurantifolii*, both of which have been reported to elicit HRs in tomato. When *xer3856* was expressed in *X. perforans* and infiltrated in tomato leaflets, the transconjugant elicited an HR and significantly reduced bacterial populations compared to the wildtype *X. perforans* strain. When *xer*3856 was mutated in *Xer07*, the mutant strain still triggered an HR in tomato leaflets. The second gene identified codes for type III secreted effector XopA, which contains a harpin domain that is distinct from the *xopA* homologs in *Xee* and *Xp*. The *Xer07-xopA*, when expressed in *X. perforans*, did not elicit an HR in tomato leaflets, but significantly reduced bacterial populations. This indicates that *xopA* and *xer3856* genes in combination with an additional factor(s) limit *Xer07* in tomato.

Keywords: *Xanthomonas euvesicatoria*; host associate factor; comparative genomics

Citation: Fan, Q.; Bibi, S.; Vallad, G.E.; Goss, E.M.; Hurlbert, J.C.; Paret, M.L.; Jones, J.B.; Timilsina, S. Identification of Genes in *Xanthomonas euvesicatoria* pv. *rosa* That Are Host Limiting in Tomato. *Plants* **2022**, *11*, 796. https://doi.org/10.3390/plants11060796

Academic Editors: Milan S. Stankovic, Paula Baptista and Petronia Carillo

Received: 25 January 2022
Accepted: 2 March 2022
Published: 17 March 2022

1. Introduction

Florida is the leading producer of shrub roses in the U.S. [1]. A bacterial spot disease on rose (*Rosa* sp.) was reported in southern states including Florida and Texas in which *Xanthomonas* strains were isolated and shown to be pathogenic [2]. Multilocus sequence analysis and 16S rRNA sequences along with fatty acid profiles suggested that these rose pathogenic strains were highly similar to *X. alfalfae* subsp. *citrumelonis*. In a later study, Barak et al. [3] compared the whole genome sequence of GEV-Rose-07, one of the rose pathogenic strains, with other closely related *Xanthomonas* strains. Based on whole genome sequence analysis, GEV-Rose-07 was closely related to the taxonomic group Rademaker 9.2, which includes *X. euvesicatoria* (*Xe*) 85-10, *X. perforans* (*Xp*) 91-118, *X. euvesicatoria* pv. *allii* (*Xea*) CFBP 6369, *X. alfalfae* subsp. *citrumelonis* (*Xac*) F1, and *X. dieffenbachiae* (*Xd*) LMG 12,749 [4]. With pairwise average nucleotide identity values >97% with *X. euvesicatoria*, GEV-Rose-07 was designated as a pathovar of *X. euvesicatoria*; *X. euvesicatoria* pv. *rosa* (*Xer*) [3].

Host range can tremendously vary among strains within a species due to variation in pathogenicity associated genes. Although taxonomically classified as *X. euvesicatoria* pv. *rosa* and closely related to *X. perforans* and *X. euvesicatoria* that cause bacterial spot disease on tomato and pepper, strain GEV-Rose-07, henceforth referred to as *Xer07*, is not pathogenic on either pepper or tomato, showing only minor chlorosis or HR-like symptoms at the inoculation site [2]. Due to its close relationship to strains infecting other hosts, identifying pathogenicity associated factors of strain *Xer07* may improve understanding of the key factors influencing the host-pathogen interactions in this group of *Xanthomonas* and risk of host range expansion.

Host specificity, to a large extent, is dictated by delivery of type III secreted effectors (T3SEs) via the type III secretion system (T3SS) into host cells. T3SEs influence host-pathogen interactions by manipulating cellular activities [5]. In some cases, host plants carry resistance genes that recognize corresponding T3SEs (avirulence genes) and this interaction results in hypersensitive response (HR), characterized by rapid cell death to prevent bacterial spread [6,7]. For example, *X. perforans* and *X. euvesicatoria* contain effectors which limit their host range to tomato and/or pepper [8–10]. *X. perforans*, which does not infect *Nicotiana benthamiana,* contains two effectors, AvrBsT and XopQ, that when mutated allowed for host range expansion to *Nicotiana benthamiana* [10]. Barak et al. [3] computationally analyzed *Xer07* for the presence, absence, or variation in effectors compared to *Xp* and *Xe* to identify potential host-limiting factor(s) in *Xer07* and observed a stepwise erosion of T3SE genes in *X. euvesicatoria,* relative to the common ancestor of the group. However, they did not identify any obvious factors that would limit *Xer07* pathogenicity in tomato and pepper.

In addition to T3SEs, other pathogenicity-associated factors in xanthomonads include genes encoding cell wall degrading enzymes such as endoxylanases, endoglucanases and pectate lyases [5,11]. Members of the glycosyl hydrolase (GH) family, XynA and XynB, were implicated in the reduction of virulence [12,13], and XynC also has been reported to contribute to bacterial virulence [14]. Likewise, Steffens et al. [15], determined that the lipopolysaccharide (LPS) synthesis clusters found in a *Xanthomonas translucens* pv. *translucens* elicted a stress response and were involved in pathogen signaling.

In the study by Barak et al. [3], analysis of T3SEs in several strains including the *Xer07* strain that were placed in *X. euvesicatoria* did not identify any obvious factors that would limit *Xer07* in tomato and pepper. Therefore, further comparative genomics are necessary to identify potential factor(s) in *Xer07* that limit it from being pathogenic in tomato and pepper. The aim of this study was to identify host limiting factors in *Xer07* that prevent disease on tomato, despite *Xer07* being closely related to tomato pathogens *X. perforans* and *X. euvesicatoria*. We identified two genes in *Xer07* that, when expressed in *Xp*, successfully limited the ability of the bacterium to grow in tomato. Our results support a model in which host-specificity in *Xanthomonas* involves a complex interplay of multiple factors.

2. Results

2.1. Whole-Genome Sequence Similarity

The *Xer07* genome was compared with 6 *Xanthomonas* species or pathovars available from the NCBI sequence database: *X. perforans* (36 straiens), *X. euvesicatoria* (37 strains), *X. gardneri* (13 strains), *X. alfalfae* (1 strain), *X. axonopodis* (1 strain) and *X. vesicatoria* (7 strains) (Supplementary Table S1). Whole-genome sequence information of *Xer07* along with some of the reference strains are listed in Table 1. Pairwise ANI comparisons based on Nucmer (Supplementary Table S1) showed *Xer07* shared overall higher sequence similarities with strains of *X. perforans* (>99% sequence identity) and *X. euvesicatoria* (ANI between 98.7–99%). Following the study by Barak et al. [3], we further compared the pairwise ANI and in-silico DDH values within members of the Rademaker group 9.2 [2]. Both ANI and isDDH yielded consistent results in which *Xer07* had slightly higher similarity values with *X. perforans* compared to *X. euvesicatoria* strains (Supplementary Table S1).

Table 1. Whole-genome sequence information of *Xer* 07 along with reference strains.

Strain	Host Name	GenBank Accession No.	Total Sequence Length (bp)	GC Content (%)	Gene Count
X. euvesicatoria pv. *rosa* GEV-Rose-07	*Rosa* sp.	GCA_001855615.1	4,970,862	64.87	4510
X. euvesicatoria pv. *allii* CFBP 6369	*Allium cepa* (onion)	GCA_000730305.1	5,427,242	64.35	4696
X. alfalfae subsp. *citrumelonis* F1	*Rutaceae citrus* (citrus)	GCA_000225915.1	4,967,469	64.92	4188
X. euvesicatoria LMG 12749	Philodendron	GCA_001401675.2	4,886,158	64.91	4388
X. perforans 91-118	*S. lycopersicum* (tomato)	GCA_000192045.3	4,898,349	65.04	4186
X. euvesicatoria 85-10	*C. annuum* (pepper)	GCA_000009165.1	5,420,152	64.56	4707
X. gardneri ATCC 19865	Tomato	GCA_000192065.2	5,528,124	63.68	5424
X. vesicatoria ATCC 35937	Tomato	GCA_000192025.2	5,531,089	64.07	5117

2.2. Type III Secreted Effectors Repertoires

We identified 26 putative type III secreted effectors in the genome of *Xer07* based on sequence homology with effectors found in other closely related xanthomonads (Table 2). *Xer07* effector sequences were compared with representative strains of the closely related species *Xanthomonas euvesicatoria* pv. *allii* (*Xea*) CFBP 6369, *X. alfalfae* subsp. *citrumelonis* (*Xac*) F1, *X. perforans* (*Xp*) 91-118, and *X. euvesicatoria* (*Xe*) 85-10 (Table 2). Among the 26 effectors identified in *Xer07*, 22 of these effectors were present in all of the reference strains. Effector XopAE present in Xer07 was absent in Xe 85-10; XopAF was absent in Xe 85-10 and Xac F1; XopE2 was found in *Xer07* and *Xe* 85-10; and XopAJ was found in *Xer07*, Xe85-10, and Xac F1. Effectors found in multiple strains had high sequence homology, with overall amino acid identity above 95% except for XopA.

We further examined XopA due to its $^{+}$divergence from homologs in related strains. XopA in *Xer07* is significantly different from *Xp* 91-118 (51%) and *Xe* 85-10 (50%) but identical to the XopA effector from *Xac* F1 and *Xea* CFBP6369. We aligned the amino acid sequence of XopA from additional representative genomes including pathogenic pepper strains *Xe* 85-10 and *Xp* 2010, pathogenic tomato strains *Xp* 91-118, *Xp* 17-12, *Xp* GEV904, and *Xp* GEV839, and other strains including *Xe* LMG12749, *Xea* CFBP6369, *Xac* F1, and *Xooc* RS105. The *xopA* gene in *Xer07* contains a distinct glutamine and glycine repeat region unlike *Xe* 85-10 and *Xp* 91-118 (Figure 1A) similar to the motif found in the harpin, HpaG [16,17]. Previous sequence comparisons of the HpaG and Hpa1 amino acid sequences from *X. oryzae* pv. *oryzicola* and *X. oryzae* pv. o*ryzae,* respectively [18], identified two distinct domains that are conserved in many harpin-like proteins within *Xanthomonas*. The first region was required to prevent aggregation of the expressed proteins into inclusion bodies when the genes are expressed in *E. coli,* as deletion of the twelve amino acids (QGISEKQLDQLL) resulted in expression of insoluble proteins as inclusion bodies. The second region had no effect on inclusion body formation or elicitation of a hypersensitive response in tobacco leaves. Multiple sequence alignment of the amino acid sequences of XopA from *Xp* 91-118 and *Xe*07 with the amino acid sequences of HpaG and Hpa1 from *X. oryzae* pv. *oryzicola* and *X. oryzae* pv. o*ryzae* (Figure 1B) show that all four proteins have the two domains, with 100% amino acid identity shared between all four proteins in region 1 and an 88.5% amino acid identity shared between all four species in the second domain. The presence of these canonical *Xanthomonas* harpin domains suggests that some other factor may be responsible for the difference in hypersensitive response in tomato observed between *Xp* 91-118 and *Xer*07.

Table 2. Putative type III secreted effectors in the genome of *Xer07* and other xanthomonads including *X. euvesicatoria* 85-10, *X. perforans* 91-118, *X. alfalfa* subsp. *citrumelonis* F1 and *X. euvesicatoria* pv. *allii CFBP6369* based on sequence homology.

Effectors	Synonyms	*Xer07*	*Xe* 85-10	*Xp* 91-118	*Xac* F1	*Xea* CFBP6369
AvrBs2		+ [1]	704/714 (99%) [2]	708/714 (99%)	708/714 (99%)	710/714 (99%)
XopE1	*avrXacE1*	+	397/400 (99%)	394/400 (99%)	393/400 (98%)	396/400 (99%)
HpaA		+	273/275 (99%)	272/275 (99%)	272/275 (99%)	271/275 (99%)
XopA	Hpa1	+	69/133 (52%)	68/133 (51%)	132/132 (100%)	132/132 (100%)
XopAD		+	510/530 (96%)	530/530 (100%)	463/531 (87%)	461/530 (87%)
XopAE	HpaF/G	+	– [3]	644/650 (99%)	632/650 (97%)	643/650 (99%)
XopAP		+	417/423 (99%)	417/423 (99%)	424/427 (99%)	419/423 (99%)
XopAU		+	515/517 (99%)	513/517 (99%)	511/517 (99%)	513/517 (99%)
XopAW		+	216/221 (98%)	221/221 (100%)	220/221 (99%)	221/221 (100%)
XopC2		+	206/206 (100%) &196/200 (98%) [4]	432/437 (99%)	432/437 (99%)	434/437 (99%)
XopF1	Hpa4	+	664/670 (99%)	661/672 (98%)	668/670 (99%)	666/670 (99%)
XopF2		+	653/667 (98%)	662/667 (99%)	660/667 (99%)	639/647 (99%)
XopK		+	630/634 (99%)	634/634 (100%)	614/634 (97%)	614/635 (97%)
XopL		+	634/661 (96%)	641/661 (97%)	633/661 (96%)	639/661 (97%)
XopN		+	718/733 (98%)	731/733 (99%)	724/733 (99%)	728/733 (99%)
XopQ		+	460/464 (99%)	460/464 (99%)	459/464 (99%)	456/464 (98%)
XopR		+	399/404 (99%)	400/404 (99%)	401/404 (99%)	399/404 (99%)
XopS		+	298/308 (97%)	301/308 (98%)	295/307 (96%)	302/307 (98%)
XopV		+	338/346 (98%)	339/346 (98%)	341/346 (98%)	342/346 (99%)
XopX		+	688/721 (95%)	683/714 (96%)	680/714 (95%)	683/721 (95%)
XopZ		+	1376/1388 (99%)	1369/1388 (99%)	1372/1388 (99%)	1377/1388 (99%)
XopP		+	567/577 (98%) +50/51 (98%)	622/627 (99%)	617/627 (98%)	629/641 (98%)
XopAF	avrXv3	+	–	217/218 (99%)	–	217/218 (99%)
XopI		+	443/450 (98%)	443/450 (98%)	444/450 (99%)	443/450 (98%)
XopE2	avrXacE3 /avrXccE1	+	352/358 (98%)	–	–	–
XopAJ	avrRxo1	+	412/421 (98%)	–	320/324 (99%)	–

[1] Symbol "+" indicates presence of type III effector in *Xer07*; [2] Type III effector nucleotide sequence identity of each isolate when compared to *Xer07*; [3] Symbol "–" indicates the absence of type III effector in respective isolates; [4] Symbol "&" indicates the type III effector distributed in two different contigs.

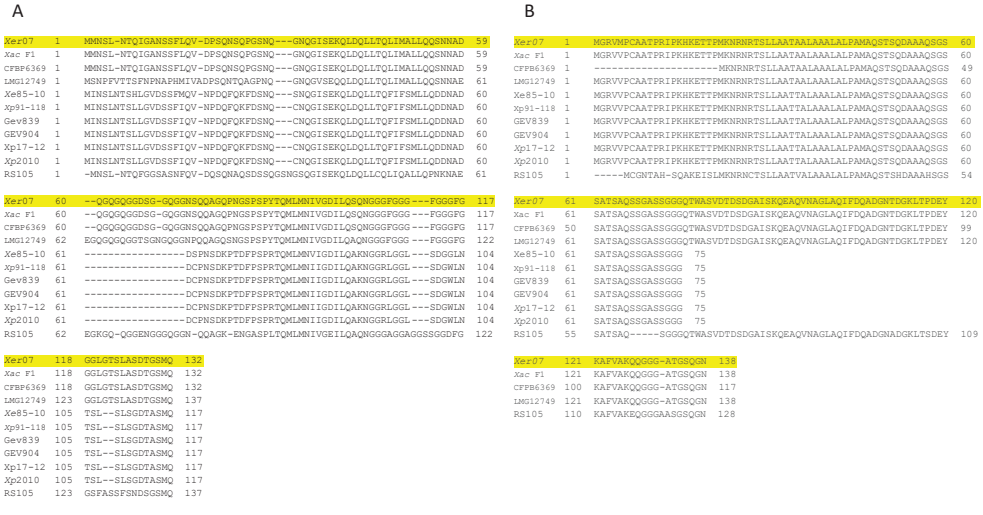

Figure 1. Comparison of XopA and Xer3856 amino acid sequences in *Xer*07 with sequences in other xanthomonads including *X. alfalfae* subsp. *citrumelonis* F1, *X. euvesicatoria* pv. *allii* CFBP6369, *X. euvesicatoria* 85-10, *X. perforans* 91-118 and *X. perforans* GEV904, *X. perforans Xp*17-12, *X. perforans* GEV839, *X. perforans* Xp2010, *X. euvesicatoria* LMG12749, *X. oryzae* pv. *oryzicola* RS105. (**A**) *xopA* gene missing distinct harpin motif (depicted by dashes) in *X. euvesicatoria* (85-10) and *X. perforans* (91-118) but present in *X. euvesicatoria* (*Xer*07). (**B**) *xer3856* gene found in *Xer* 07.

We determined that 16 effectors were absent in *Xer07* but present in either *Xe* or *Xp* (Table 2). AvrBs1, AvrRxv, XopAA, HolPsyAE, XopAV, XopAX, XopB, XopC, XopG, XopH, and XopO were found in *Xe* 85-10, while XopAK, XopJ4 and an ortholog of XopX were present in strain *Xp* 91-118. Sequence length of XopAK varied within all of the strains that were compared to *Xer07*, missing a significant coding region with only 142 amino acids out of 485, suggesting that the gene may be non-functional in *Xer07*. Interestingly, the same copy of this gene in addition to the XopAK effector was found in strain *Xp* 91-118. XopD, a SUMO protease effector [19], that is present in both *Xp* 91-118 and *Xe* 85-10 is also absent in *Xer07* (Table 2).

2.3. xer3856 as Host-Limiting Candidate

A homolog of Xac3856 in *X. citri* and a homolog in *X. fuscans* pv. *aurantifolii* (Xfa) designated Xfa3856 were identified in *Xer07* and designated as *Xer*3856 (Figure 1B, Supplementary Figure S1). This was considered a potential host-limiting factor, since the Xfa3856 was shown to induce a hypersensitive response in tomato independent of type III secretion system, whereas homologs present in tomato strains do not elicit an HR [20]. Homologs of *xac3856* and *xfa3856* were found to be present in all strains used in this study. However, the sequences varied significantly in length (Figure 1B). Strains infecting pepper (*Xe* 85-10, *Xp* 2010) and tomato (*Xp* 91-118, *Xp* GEV904, *Xp* 17-12, *Xp* GEV839) were missing 63 amino acids compared to *Xer07-xer*3856. Rather interestingly, the *Xer07-xer3856* was over 99% identical to genes found in both *Xac* F1 from citrus and *Xe* LMG12749 from *Philodendron*.

2.4. XopA and Xer3856 Are Host-Limiting Factors in Tomato

Given that comparative genomics indicated XopA and Xer3856 were potential candidates for limiting the ability of *Xer07* to infect tomato, the two genes were cloned from *Xer07* and expressed in tomato strain *Xp* 91-118 to evaluate their role in limiting growth in tomato. *xopA* and *xer3856* clones were conjugated into tomato pathogenic strain *Xp* 91-118 via triparental mating to generate *Xp* 91-118::*Xer07-xopA* and *Xp* 91-118::*Xer07-xer3856*. Bacterial suspensions of transconjugants adjusted to 10^8 CFU/mL were infiltrated into the mesophyll of susceptible cultivar Bonny Best along with the wildtype *Xp* 91-118. *Xp* 91-118::*Xer07-xer3856* induced a strong HR within 36 h post inoculation (Figure 2A) but *Xp* 91-118::*Xer07-xopA* didn't induce a visible HR (Figure 2B). Simultaneously, the strains were also infiltrated at concentrations of 10^5 CFU/mL in tomato to determine bacterial population over time. The results showed that the *Xp* 91-118::*Xer07-xopA* and the *Xp* 91-118::*xer3856* populations were significantly lower than those in the wildtype *Xp* 91-118 strain (Figure 2C,D).

In order to determine if inactivation of *xer3856* eliminates an HR when *Xer07* is infiltrated in tomato, the gene was mutated using pCR2.1TOPO-vector from *Xer07* to generate the insertion mutant *Xer07* Ω*xer3856* (Table 3). Both *Xer07* and *Xer07* Ω*xer*3856 induced an HR in tomato (Figure 3A). Furthermore, the *Xer07* Ω*xer*3856, *Xer07* and *Xp* 91-118::pUFR strains were infiltrated into leaflets of Bonny Best tomato cultivar to quantify bacterial populations. *Xp* 91-118 populations were ~2 log CFU/mL higher than *Xer07* Ω*xer*3856 and wildtype *Xer07* over the sampling period following infiltration (Figure 3B).

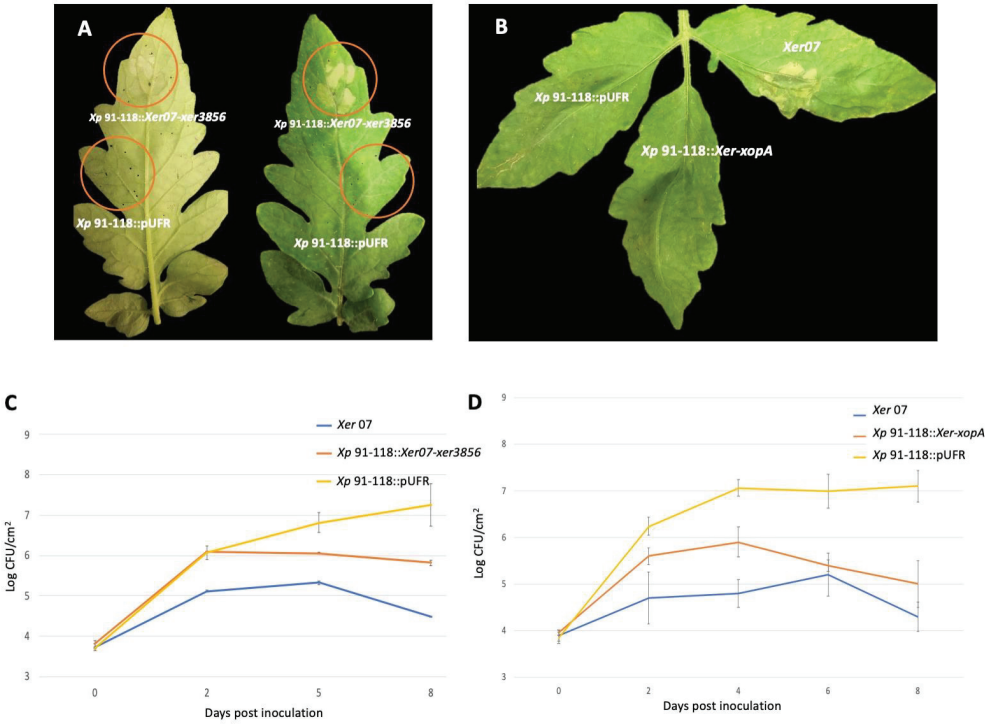

Figure 2. Hypersensitive reaction and population dynamics following infiltration of Bonny Best tomato leaflets. Infiltration of suspensions of (**A**) *Xp* 91-118::*Xer07-xer3856* and (**B**) *Xp* 91-118::*Xer-xopA* in tomato at ~5 × 10^8 CFU/mL concentration. Note HR in leaflet infiltrated with *Xp* 91-118::*xer3856* but not *Xp* 91-118::*Xer-xopA* (**C**) Bacterial populations of *Xp* 91-118::pUFR, wildtype *Xer07*, and *Xp* 91-118::*xer-3856*, and (**D**) Population of *Xp* 91-118::pUFR, wildtype *Xer07*, and Xp91-118::*Xer-xopA* following infiltration with suspensions adjusted to ~10^5 CFU/mL at ~10^5 CFU/mL in tomato.

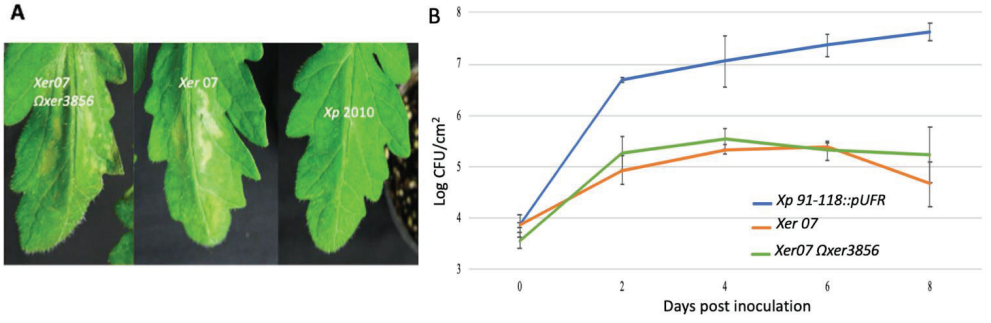

Figure 3. Hypersensitive reaction and population dynamics following infiltration of Bonny Best tomato leaflets. (**A**) Hypersensitive reactions on tomato following infiltration with *Xer07* Ω*xer3856*, *Xer*07, and *Xp* 2010 (a pepper isolate susceptible on tomato) at concentration of ~5 × 10^8 CFU/mL. HR was observed 24 h post inoculation with *Xer07* Ω*xer*3856 and *Xer*07 no no significant damage was observed in leaflet infiltrated with *Xp* 2010. (**B**) Population dynamics of *Xer07* Ω*xer*3856, *Xer*07 and *Xp* 91-118::pUFR in tomato leaflets at various times after infiltration of bacterial suspension at concentration of 10^5 CFU/mL. Populations were significantly lower for Xer07 Ωxer3856 and *Xer*07 in comparison with *Xp* 91-118::pUFR. Vertical lines indicate standard error.

Table 3. List of strains used in the study.

Strain	Characteristics	Source
Xer07	*Xanthomonas* strain isolated from Rose	This study
Xp 91-118	*X. perforans* isolated from tomato	This study
Xe 85-10	*X. euvesicatoria* isolated from pepper	This study
E. coli DH5α	Competent cell for hosting the plasmid	Bethesda Research Laboratories
Xer07Ω*xer3856* (TOPO-*xer3856*)	*Xer07*, *xer3856* mutated using TOPO, KanR	This study
Xp 91-118::*xer3856* (pUFR034::*xer3856*)	Xp 91-118 complemented with *xer3856*, KanR	This study
Xp 91-118::*xopA* (pUFR034::*xopA*)	Xp 91-118, complemented with *xopA* from Xer 07, KanR	This study
	Plasmids	
pCR2.1-TOPO	TOPO plasmid, KanR	Thermofisher
pCR2.1-TOPO-*xer3856*	PCR product of *xer3856*-int-F and *xer3856*-int-R into pCR2.1-TOPO, KanR	This study
pUFR034	Cloning vector, KanR	
pUFR034-*xer3856*	PCR product of *xer3856*-out-F and *xer3856*-out-R into pUFR034, KanR	This study
pUFR034-*xopA*	PCR product of *xopA*-F and *xopA*-R from *Xer07* into pUFR034, KanR	This study
pGEM-T Easy	Cloning vector, AmpR	Promega
pGEM-T Easy-*xer3856*	*xer3856* in pGEM-T for cloning, AmpR	This study
pGEM-T Easy-*xopA*	*xopA* from *Xer07* in pGEM-T for cloning to pUFR034-*xopA*, AmpR	This study

2.5. Structure of XopA

XopA found in *Xer*07 carried an additional Glutamine and Glycine repeat region different from the *X. perforans* and *X. euvesicatoria* strains that are pathogenic on tomato. Four different protein structure prediction models from Phyre2, RaptorX, iTasser, and trRosetta were used to evaluate the possible structural differences between the XopA proteins found in *Xer*07 and *X. perforans* 91-118. The Phyre2 server could only model 6% (8 amino acids) of the submitted sequence for the *Xer07* XopA protein with 28% confidence and 14% (16 amino acids) with 22% confidence of the *Xp* 91-118 XopA protein. The two other homology modeling algorithms used, RaptorX and iTasser, varied widely in the models returned for each protein, with each model of each protein having a completely different predicted tertiary structure than the other model created for the same input sequence. This is not surprising as harpin proteins vary widely in their amino acid sequence and localization, either extracellularly or as an effector protein injected into the host cell via the T3SS [18,21]. Superpositions of the models generated by RaptorX (Figure 4A) show two alpha helices that are superposable, the first spanning amino acids 36-54 in *Xp* 91-118 (37-52 in *Xer*07), and the second spanning amino acids 37-52 in *Xp* 91-118 (88-103 in *Xer*07). None of the remaining amino acids are superposable, in large part due to the fifteen amino acid deletion in the *Xp* 91-118 XopA protein. In XopA from *Xer07* and *Xoo*, an amino acid sequence of QGQGGDSGGQGGNSQ is present (Figure 5), resulting in an extended loop being formed between amino acids 59 and 86 (Figure 4B). Since the proteins from all four organisms contain the two regions demonstrated to be necessary for function [18], we hypothesize that this additional loop in the *Xer*07 XopA protein adopts an alpha-helical secondary structure when in the presence of its cognate binding partner, much the same as is seen in the *X. oryzae* pv. *oryzae* and *X. oryzae* pv. o*ryzicola* homologs. The formation of a complex between the *Xer*07 XopA protein and a plant protein may be the reason why *Xer07* XopA homolog is capable of eliciting a defense response in tomato, but *Xp* 91-118 XopA is not.

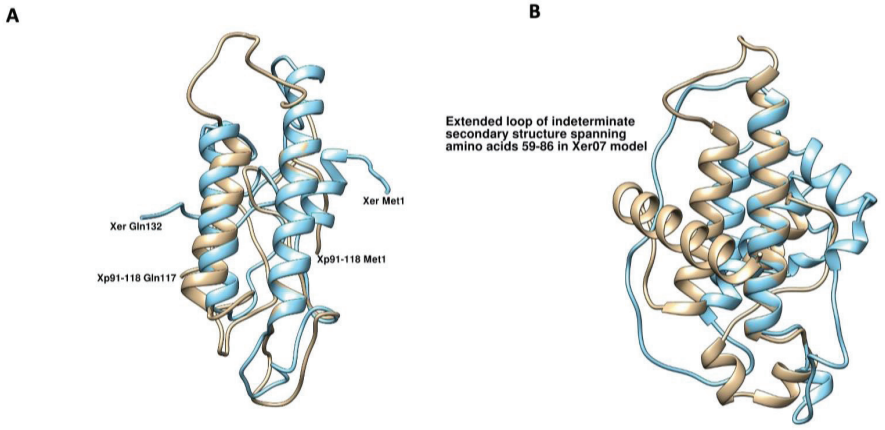

Figure 4. (**A**) Superposition of the lowest energy homology models of XopA from *X. perforans* (91-118) (Tan) and *Xer*07 (blue). The amino and carboxy-terminal residues of each protein are labelled. (**B**) Superposition of the lowest energy *de novo* models of *X. perforans* (91-118) (Tan) and *Xer*07 (blue) created by trRosetta.

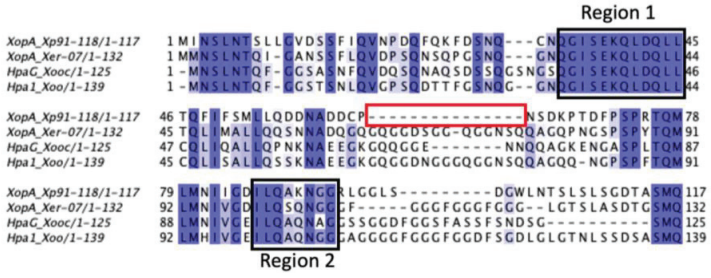

Figure 5. Sequence alignment of the XopA genes from *X. perforans* 91-118, Xer 07, the HpaG gene from *X. oryzae* pv. oryzicola and the Hpa1 gene from *X. oryzae* pv. oryzae. The two regions previously shown to be conserved between the *X. oryzae* pathovars and that are found in *X. perforans* 91-118 and Xer 07 are shown as is the deleted region (red box) in the *X. perforans* 91-118 sequence.

2.6. Comparative Genomics of Other Pathogenicity Associated Factors

We compared the genes for proteins secreted by the type II secretion system that are conserved in *Xanthomonas* genus (Supplementary Tables S2 and S3). The arrangement and content of genes encoding three xylanase genes (*xyn10A*, *xyn10B* and *xyn10C*) were similar among *Xer07*, *Xp* 91-118, *Xe* 85-10, *Xac* F1, *Xea* CFBP 6369, and *Xe* LMG12749 (Supplementary Figure S2 and Supplementary Table S2). When comparing the genetic organization of the two type II secretion systems, *xcs* and *xps* gene clusters (Supplementary Figure S3) of *Xer07*, Xcs- D, E, F, G and H shared homology to Xps proteins, whereas no homology to XpsI, XpsJ, XpsK, XpsL, XpsM, and XpsN was identified. Meanwhile, gene clusters encoding for diffusible signal factors (DSF) present in *Xer07* were highly similar to those in other strains except for *Xg* and *Xv* strains and ranged from 98.25 to 100% (Supplementary Table S3); *rpfH* in *Xer07* was 100% identical to *Xea* CFBP 6369 and *Xac* F1; and *rpfG* in *Xer07* also shared 100% similarity to *Xea* CFBP 6369.

Similarly, *Xer07* contains two glycosyl transferase genes (*wbdA1*, *wbdA2*) in region 1 that were present in *Xe* 85-10 strains but were different from *Xg* and *Xv* (Supplementary Figure S4). *Xer07* has a similar LPS gene cluster as *Xe* 85-10, *Xg*, and *Xv* strains but different from *Xp* 91-118 and *Xe* LMG 12749 strains (Supplementary Figure S4).

3. Discussion

We compared genes involved in pathogenicity and host range in related xanthomonads from pepper, tomato, and other host species to those in strain *Xer07* from rose. *Xer07* is closely related to *X. perforans* based on ANI and *in silico* DDH, but causes an HR in tomato, the primary host of *X. perforans*. We identified two host associated factors in *X. euvesicatoria* pv. *rosa* that limited its ability to cause disease on tomato. Our results further confirmed that *Xanthomonas* taxonomy is not driven by host range and showed that differences in multiple specific pathogenicity factors among phylogenetically similar strains can alter host specificity.

We identified two genes in *Xer07* that contributed to limiting infection in tomato. The first gene, *xer*3856, a homolog of genes in *X. citri* and *X. fuscans* pv. *aurantifollii* was identified in *Xer07*. In two studies, *xfa*3856, when expressed in the tomato pathogen *Xp* 91-118 and infiltrated in tomato leaves resulted in elicitation of an HR [20,22]. *Xfa*3856 homologs are also present in *X. euvesicatora* and *X. perforans* with high sequence similarity, although the latter two homologs encode for a truncated protein. *Xfa*3856 is predicted to have a putative transmembrane helix and two EF-hand calcium binding motifs at the C-terminus [20]. When *xer3856* was cloned and expressed in *Xp* 91-118, the transconjugant induced an HR in tomato plants. However, the mutated version, *Xer07* Ω*xer*3856, performed similarly as wild-type *Xer07*, and still triggered HR in tomato. These results indicated that *xer*3856 from *Xer07* elicits a resistant reaction in tomato and is one of multiple host limiting factors for *Xer07* in tomatoes.

The type III secretion system is crucial for pathogenic *Xanthomonas* to colonize plants and to translocate type III effectors to interfere with cellular functions. We identified 26 potential type III effectors/*Xanthomonas* outer proteins (Xops) present in *Xer07*. XopA is the name designated for the Hpa1 protein that contains harpin-like protein and is secreted through T3SS transfer [23]. Interestingly, XopA homologs were present in all *Xanthomonas* strains in this study. XopA was found to be necessary for strain *Xe* 85-10 to grow in planta and maintain full virulence [24]. Deletion of XopA delayed an HR and water-soaking symptom and reduced bacterial growth in pepper leaves compared to wild-type *Xe* 85-10. In this study, we observed that the x*opA* gene from strains pathogenic to different hosts varied in sequence. Tomato and pepper pathogenic strains, including *Xp* 91-118, *Xe* 85-10, *Xp* 17-12, *Xp* GEV904, *Xp* GEV839, and *Xp* 2010, shared only ~50% amino acid identity in XopA with *Xer07*, *Xac* F1 and CFBP 6369. Similarity among species may be ancestral (trans-specific variation) or the result of recombination event within or including the gene. A study by [25], showed that HpaG (also referred as Hpa1) with the feature of harpins, was able to elicit an HR in pepper but not in tomato plants, and Hpa1 from *X. oryzae* pv. *oryzae* induced HR in tobacco plants. A recent study also confirmed that the expression of XopA from *X. oryzae* pv. *oryzicola* RS105 in *N. benthamiana* was able to trigger HR symptoms [26]. We expressed XopA from *Xer07* in *Xp* 91-118 to evaluate if it can independently act as a host limiting factor. Interestingly, the bacterial populations of *Xp* 91-118::*Xer07-xopA* were reduced by more than 2 log-folds compared to the *Xp* 91-118::pUFR (Empty vector).

In addition to their individual role as an effector, several possibilities have been studied to gain insights into the function of harpin-type bacterial proteins. The XopA/Hpa1-like effectors have been found to play a significant role in translocation of associated effectors [27]. Wang et al. [18], demonstrated that Hpa1 is a type III translocator which is critical for translocation of two transcription activation like (TAL) effectors PthXo1 and AvrXa10 that affect the phenotype in susceptible and resistant genotypes. Although the XopA harpin in *Xer07* when expressed in *X. perforans* resulted in a reduction in bacterial populations in tomato, the reason remains to be determined. In other studies, XopA homologs in transconjugants expressing an extra copy of HrpG were shown to elicit an HR in tobacco or citrus [25,28]. Kim et al. [25], determined that *X. axonopodis* pv. *glycines* expressing extra copies of HrpG also overexpressed *hpa1* which was associated with elicitation of an HR in tobacco leaves. In this study there may have been a slight increase in expression of *xopA*, although not to the level observed in transconjugants expressing multiple copies of HrpG.

The results confirm multiple factors can limit pathogenicity towards a host and can either induce a phenotypic reaction as Xer3856 or limit the population growth as XopA.

The Glutamine and Glycine repeat region found in the XopA of *Xer07* was similar to a motif, motif 2 found in the HpaG harpin protein from *X. axonopodis* pv. *glycines*. The motif 2 region of HpaG is homologous to the prion-forming domain of the yeast prion protein Rnq1p [16] and HpaG secretion was shown to induce HR in plants by formation of amyloid-like fibrils [17]. Among the three motifs described in HpaG from *X. axonopodis* pv. *glycines*, homologs to motifs 1 and 3 were found in other genomes compared in this study.

We identified differences in the effector repertoires of *Xer07*, *X. euvesicatoria*, *X. perforans*, and other closely related species that could be explored in future studies. As an example, XopD is absent from *Xer07* but present in both *X. euvesicatoria* and *X. perforans* strains. Based on protein analysis of XopD, it was shown to contain a small ubiquitin-like modifier (SUMO) protease domain that belongs to the C48 protease family as reversible post-translational modifiers [29]. Mutation of *xopD* gene in *Xe* 85-10 followed by inoculation resulted in plants exhibiting severe chlorosis and tissue necrosis and increased salicylic acid levels compared to wild-type, which suggested XopD's ability to delay symptom progression and function as a tolerance-promoting factor [19,23]. It is apparent that *Xer07* strain expressing XopD should be created to determine whether XopD is linked to virulence on tomato and pepper. However, this can only be evaluated once we can successfully eliminate the HR phenotype that restricts *Xer07* in tomato. Additionally, the absence of XopD and 11 other effectors that were found in *Xe* 85-10 and *Xp* 91-118 could be other potential genes that could influence *Xer07* pathogenicity in different hosts.

Among the two type II secretion systems found in many xanthomonads, T2SS-xps is conserved in all *Xanthomonas* spp. [5]. In a study by Szczesnyet al. [14], the *xps* system was shown to be required for extracellular protease and xylanase activity, as deletion of the *xps* but not *xcs* in *Xe* 85-10 significantly reduced halo formation when incubated on NYG plates containing milk or xylan. Sequence identity of DSF cell-cell signaling system and the arrangement and content of xylanolytic enzyme clusters were found to be conserved among the Rademaker group 9.2 strains that encompasses the *Xer07*, compared to *Xv* and *Xg* strains. Meanwhile the xylanase genes *xynC/xyn5A* were not present in *Xv* ATCC 35937 and *Xg* ATCC 19,865 but in the Rademaker group 9.2 strains. A deletion of *xynC* in *Xe* 85-10 caused a reduction in bacterial growth in planta suggesting *xynC/xyn5A* is an active xylanase and can contribute to virulence [14]. Similar high sequence and cluster similarity was found in LPS gene cluster among the *Xer07* and *Xe* 85-10 that was distinct from the *X. perforans* strain 91-118. Potnis et al. [11] predicted a putative horizontal gene transfer event resulting in the acquisition of novel LPS gene cluster in *X. perforans* that may have played a major role in *X. perforans* specificity in tomato.

In this comparative study we demonstrate that *Xer07* is closely related to *Xp* and *Xe.* As we focused on identifying host limiting factors in GEV-Rose-07, we successfully demonstrated that *xer*3856 gene induced an HR in tomato and XopA from *Xer07* significantly limited bacterial growth in tomato. Recognition of these host-limiting factors in *Xer07* improves our knowledge in host pathogen interactions of *Xp* and *Xe* on tomato and pathogen host range evolution that can be used to design durable resistance mechanisms in plant hosts.

4. Material and Methods

4.1. Bacterial Strains and Growth Conditions

Bacterial strains that were used for assaying pathogenicity and quantifying internal bacterial population dynamics included *Xer* GEV-Rose-07 strain (pathogenic on *Rosa* spp.), *Xe* E3 (pathogenic to pepper), *Xe* 85-10 (pathogenic to pepper), and *Xp* 91-118 (pathogenic to tomato) (Table 3). The strains were stored at −80 °C in 30% glycerol for long term storage. Fresh cultures used in this study were obtained by streaking the bacterium on nutrient agar (NA) plates followed by incubation at 28 °C for 48 h. Individual colonies were then streaked on NA plates and incubated at 28 °C for 24 h for use during experiments. For

Escherichia coli strains used during mutant constructions, the plates were incubated at 37 °C. The list of strains and plasmid constructs are listed in Table 3.

4.2. Genome Collection and Genome Statistics

Representative complete and draft genome sequences of *Xanthomonas* spp. were obtained from GenBank database (Supplementary Table S1). The assembled genomes were compared with pairwise average nucleotide identity (ANI) analysis and in-silico DNA-DNA hybridization (isDDH) analysis based on genome-to-genome comparisons [30,31]. The pairwise ANI values were obtained from nucmer (NUCleotide MUMmer). Similarly, isDDH was estimated using the Genome-to-Genome Distance Calculator (GGDC) 2.0 Web server (http://ggdc.dsmz.de/distcalc2.php) (accessed on 15 March 2019).

4.3. Effector Repertoire and Pathogenicity Associated Genes

With the objective of identifying host specificity factors in *Xer07*, the annotated sequences from IMG/JGI were downloaded and searched by BLAST analysis for effectors using a list of 81 type III effectors compiled from different *Xanthomonas* species (Potnis and Iruegas-Bocardo, personal communication; www.xanthomonas.org (accessed on 9 May 2018)). Effector sequences were extracted based on amino acid sequence homology using local BLAST [32]. Effector with more than 70% sequence homology compared with the reference was considered as being present. The sequences for the effectors predicted for *Xer07* were further evaluated manually and compared with annotations from IMG/JGI to the confirm their presence. The *xer3856* gene and its homology to the *xfa3856* was determined based on BLAST comparisons.

4.4. Mutants, Transconjugants and Population Dynamics

The *xer3856* gene was mutated in *Xer07* using pCR2.1-TOPO vector (TOPO® TA Cloning Kit, invitrogen™ [33]) to generate *Xer07*Δ*xer3856*. In order to determine if *xer3856* is the factor responsible for eliciting an HR in tomato and pepper, we infiltrated Bonny Best tomato leaflets with suspensions adjusted to ~10^8 CFU/mL of strains *Xer07*Δ*xer3856*, and *Xer07* along with the tomato pathogen, *X. perforans, Xp* 91-118. Additionally, the bacterial populations of *Xer07*Δ*xer3856*, *Xer07* and *Xp* 91-118 were evaluated in tomato by quantifying bacterial growth as described above. In order to independently evaluate the role of Xer3856 and XopA in tomato pathogenicity, plasmids carrying these individual genes were conjugated into *Xp* 91-118. To create these plasmids, the genes *xopA* and *xer3856* were amplified using primers as specified in Supplementary Table S4. The amplicon was cloned with pGEM-T easy vector and subsequently excised from pGEM-T vector and ligated into pUFR034 and mobilized into *Xp* 91-118 through triparental mating for in planta analysis.

4.5. Comparative Genomics

In addition to the type III secreted effectors, additional pathogenicity factors were compared between *Xer07*, *Xp* 91-118, *Xe* 85-10, *Xac* F1, *Xea* CFBP6369, *X. gardneri* ATCC19865 (*Xg* ATCC19865) and *X. vesicatoria* ATCC35937 (*Xv* ATCC35937). Type III secretion system cluster, cell-wall degrading enzyme cluster, lipopolysaccharide biosynthetic clusters and diffusible signal factors that are considered important for bacterial virulence were compared among the four closely related strains. The reference genes and their homologs were identified using BLAST and homology search was carried out using the IMG/JGI online platform (www.img.jgi.doe.gov) (accessed on 1 April 2019).

4.6. Pathogenicity Assay

In order to evaluate pathogenicity/resistance in tomato, bacterial strains used in the study were inoculated at variable concentrations. Bacterial inoculum was adjusted to 10^8 CFU/mL (A_{600} = ~0.3 at) and infiltrated with a hypodermic needle syringe into Bonny Best tomato leaflets to determine HR. Plants were placed in growth chambers at 28 °C and the infiltrated area was observed for HR or susceptible reaction. HR was confirmed

by the presence of confluent necrosis in infiltrated area due to rapid cell death, 24 to 48 h post inoculation.

Bacterial populations were also determined in Bonny Best tomato. Bacterial suspensions at ~10^5 CFU/mL were infiltrated into the leaflets and plants were placed in growth chamber at 28 °C. Inoculated leaf tissue was sampled every 48 h for 10 days. A 1-cm^2 leaf disk was sampled from each leaflet and the tissue was ground in sterile tap water and the resulting suspensions were serially diluted between 10^{-1}–10^{-5} fold. Fifty-microliters from the suspensions were plated on NA and the plates were incubated at 28 °C. The assay was replicated three times for determining bacterial populations in planta.

Supplementary Materials: The following supporting information can be downloaded at: https://www.mdpi.com/article/10.3390/plants11060796/s1, Supplementary Figure S1: Open reading frame search of of *xer3856* protein homology in *Xer07* including 100 bp upstream. Other xanthomonads include *X. alfalfae* subsp. *citrumelonis* F1, *X. euvesicatoria* pv. *allii* CFBP6369, *X. euvesicatoria* 85-10, *X. perforans* 91-118 and *X. perforans* GEV904, *X. perforans Xp*17-12, *X. perforans* GEV839, *X. perforans* Xp2010, *X. euvesicatoria* LMG12749. Sequence highlighted in red indicates open reading frame according to https://web.expasy.org/translate/, accessed on 23 November 2021; Supplementary Figure S2: The arrangement and content of the xylanolytic enzyme cluster within different *Xanthomonas* genomes including *X. euvesicatoria* GEV-rose-07, *X. perforans* 91-118 *X. euvesicatoria* 85-10, *X. alfalfae* subsp. *citrumelonis* F1, *X. euvesicatoria* pv. *allii* CFBP6369, *X. euvesicatoria* LMG12749, *X. vesicatoria* ATCC35937, and *X. gardneri* ATCC19865, Symbols '[' and ']' stand for the contig break. Color code represents homologues genes; Supplementary Figure S3: The arrangement and content of the *xcs* and *xps* clusters within different *Xanthomonas* genomes including *X. euvesicatoria* GEV-rose-07, *X. perforans* 91-118 *X. euvesicatoria* 85-10, *X. alfalfae* subsp. *citrumelonis* F1, *X. euvesicatoria* pv. *allii* CFBP6369, *X. euvesicatoria* LMG12749, *X. vesicatoria* ATCC35937, and *X. gardneri* ATCC19865, Symbols '[' and ']' stand for the contig break. Color code represents for the different genes; Supplementary Figure S4: The structure of the LPS cluster within different *Xanthomonas* genomes including *X. euvesicatoria* GEV-rose-07, *X. perforans* 91-118 *X. euvesicatoria* 85-10, *X. alfalfae* subsp. *citrumelonis* F1, *X. euvesicatoria* pv. *allii* CFBP6369, *X. euvesicatoria* LMG12749, *X. vesicatoria* ATCC35937, and *X. gardneri* ATCC19865, Symbols '[' and ']' stand for the contig break. Color code represents homologous genes in different genomes. 'Hpo pro' indicates a hypothetical protein. Supplementary Table S1: ANI and in silico DDH comparisons of Xer07 with representative strains of *X. axonopodis*, *X. alfalfa*, *X. euvesicatoria*, *X. gardneri*, *X. perforans*, and *X. vesicatoria* genomes available in NCBI database; Supplementary Table S2: Locus tags of cell wall degrading enzymes in *X. euvesicatoria* GEV-ROSE-07 (Xer07) and in other xanthomonads including *X. perforans* 91-118, *X. euvesicatoria* 85-10, *X. alfalfae* subsp. *citrumelonis* F1, *X. euvesicatoria* pv. *allii* CFBP6369, *X. euvesicatoria* LMG12749, *X. gardneri* ATCC19865 and *X. vesicatoria* ATCC35937; Supplementary Table S3. Locus tags and sequence identities (%) of *X. euvesicatoria* GEV-ROSE-07 (Xer07), *X. perforans* 91-118, *X. euvesicatoria* 85-10, *X. alfalfae* subsp. *citrumelonis* F1, *X. euvesicatoria* pv. *allii* CFBP6369, *X. euvesicatoria* LMG12749, *X. gardneri* ATCC19865 and *X. vesicatoria* ATCC35937 genes associated with diffusible signal factor (DSF) involved in cell-cell signaling system; Supplementary Table S4. List of primers used in this study.

Author Contributions: Conceptualization, Q.F., S.B., G.E.V., E.M.G., M.L.P., J.B.J. and S.T.; formal analysis, Q.F., S.B. and S.T.; methodology, Q.F., S.B. and J.C.H.; validation, Q.F., S.B., J.B.J. and S.T.; writing—original draft, Q.F., S.B., J.C.H., J.B.J., and S.T.; writing—review and editing, Q.F., S.B., G.E.V., E.M.G., J.C.H., J.B.J. and S.T. All authors have read and agreed to the published version of the manuscript.

Funding: The United States Department of Agriculture (USDA) National Institute of Food and Agriculture (NIFA) Specialty Crop Research Initiative Grants Program Grant Number: 2015-51181-24312. JCH is supported in part by grant P20GM103499-20 (SC INBRE) from the National Institute of General Medical Sciences, National Institutes of Health and an award from the National Science Foundation [#OIA-1655740].

Institutional Review Board Statement: Not applicable.

Informed Consent Statement: Not applicable.

Data Availability Statement: All the data is available within the article or its Supplementary Materials.

Conflicts of Interest: The authors declare no conflict of interest.

References

1. USDA National Agricultural Statistics Service. *Floriculture Crops 2020 Summary*; USDA National Agricultural Statistics Service: Washington, DC, USA, 2021.
2. Huang, C.-H.; Vallad, G.E.; Adkison, H.; Summers, C.; Margenthaler, E.; Schneider, C.; Hong, J.; Jones, J.B.; Ong, K.; Norman, D.J. A Novel Xanthomonas sp. Causes Bacterial Spot of Rose (*Rosa* spp.). *Plant Dis.* **2013**, *97*, 1301–1307. [CrossRef] [PubMed]
3. Barak, J.D.; Vancheva, T.; Lefeuvre, P.; Jones, J.B.; Timilsina, S.; Minsavage, G.V.; Vallad, G.E.; Koebnik, R. Whole-Genome Sequences of Xanthomonas euvesicatoria Strains Clarify Taxonomy and Reveal a Stepwise Erosion of Type 3 Effectors. *Front. Plant Sci.* **2016**, *7*, 1805. [CrossRef] [PubMed]
4. Rademaker, J.L.; Louws, F.; Schultz, M.H.; Rossbach, U.; Vauterin, L.; Swings, J.; De Bruijn, F.J. A Comprehensive Species to Strain Taxonomic Framework for Xanthomonas. *Phytopathology* **2005**, *95*, 1098–1111. [CrossRef]
5. Timilsina, S.; Potnis, N.; Newberry, E.A.; Liyanapathiranage, P.; Iruegas-Bocardo, F.; White, F.F.; Goss, E.M.; Jones, J.B. Xanthomonas diversity, virulence and plant–pathogen interactions. *Nat. Rev. Genet.* **2020**, *18*, 415–427. [CrossRef]
6. He, S.Y.; Nomura, K.; Whittam, T.S. Type III protein secretion mechanism in mammalian and plant pathogens. *Biochim. Biophys. Acta Mol. Cell Res.* **2004**, *1694*, 181–206. [CrossRef] [PubMed]
7. Buüttner, D.; He, S.Y. Type III Protein Secretion in Plant Pathogenic Bacteria. *Plant Physiol.* **2009**, *150*, 1656–1664. [CrossRef]
8. Astua-Monge, G.; Minsavage, G.V.; Stall, R.E.; Davis, M.J.; Bonas, U.; Jones, J.B. Resistance of Tomato and Pepper to T3 Strains of *Xanthomonas campestris* pv. *Vesicatoria* Is Specified by a Plant-Inducible Avirulence Gene. *Mol. Plant-Microbe Interact.* **2000**, *13*, 911–921. [CrossRef]
9. Minsavage, G.; Dahlbeck, D.; Whalen, M.; Kearney, B.; Bonas, U.; Staskawicz, B.; Stall, R. Gene-for-gene relationships specifying disease resistance in *Xanthomonas campestris* pv. *vesicatoria*-pepper interactions. *Mol. Plant-Microbe Interact.* **1990**, *3*, 41–47. [CrossRef]
10. Schwartz, A.R.; Potnis, N.; Timilsina, S.; Wilson, M.; Patané, J.; Martins, J.J.; Minsavage, G.V.; Dahlbeck, D.; Akhunova, A.; Almeida, N.; et al. Phylogenomics of Xanthomonas field strains infecting pepper and tomato reveals diversity in effector repertoires and identifies determinants of host specificity. *Front. Microbiol.* **2015**, *6*, 535. [CrossRef]
11. Potnis, N.; Krasileva, K.; Chow, V.; Almeida, N.F.; Patil, P.B.; Ryan, R.P.; Sharlach, M.; Behlau, F.; Dow, J.M.; Momol, M.; et al. Comparative genomics reveals diversity among xanthomonads infecting tomato and pepper. *BMC Genom.* **2011**, *12*, 146. [CrossRef]
12. Li, J.; Wang, N. Genome-Wide Mutagenesis of *Xanthomonas axonopodis* pv. *citri* Reveals Novel Genetic Determinants and Regulation Mechanisms of Biofilm Formation. *PLoS ONE* **2011**, *6*, e21804. [CrossRef]
13. Rajeshwari, R.; Jha, G.; Sonti, R.V. Role of an In Planta-Expressed Xylanase of *Xanthomonas oryzae* pv. *oryzae* in Promoting Virulence on Rice. *Mol. Plant-Microbe Interact.* **2005**, *18*, 830–837. [CrossRef] [PubMed]
14. Szczesny, R.; Jordan, M.; Schramm, C.; Schulz, S.; Cogez, V.; Bonas, U.; Büttner, D. Functional characterization of the Xcs and Xps type II secretion systems from the plant pathogenic bacterium Xanthomonas campestris pv vesicatoria. *New Phytol.* **2010**, *187*, 983–1002. [CrossRef] [PubMed]
15. Steffens, T.; Duda, K.; Lindner, B.; Vorhölter, F.-J.; Bednarz, H.; Niehaus, K.; Holst, O. The lipopolysaccharide of the crop pathogen *Xanthomonas* translucenspv. translucens: Chemical characterization and determination of signaling events in plant cells. *Glycobiology* **2017**, *27*, 264–274. [CrossRef]
16. Dueholm, M.S. Biophysical Characterization of Naturally Occurring Bacterial Amyloids. Ph.D. Thesis, Aalborg University, Aalborg, Denmark, 2010.
17. Shanmugam, N.; Baker, M.O.D.G.; Ball, S.R.; Steain, M.; Pham, C.L.L.; Sunde, M. Microbial functional amyloids serve diverse purposes for structure, adhesion and defence. *Biophys. Rev.* **2019**, *11*, 287–302. [CrossRef]
18. Wang, X.; Zhang, L.; Ji, H.; Mo, X.; Li, P.; Wang, J.; Dong, H. Hpa1 is a type III translocator in Xanthomonas oryzae pv. *oryzae*. *BMC Microbiol.* **2018**, *18*, 105. [CrossRef]
19. Kim, J.-G.; Taylor, K.W.; Hotson, A.; Keegan, M.; Schmelz, E.A.; Mudgett, M.B. XopD SUMO Protease Affects Host Transcription, Promotes Pathogen Growth, and Delays Symptom Development in Xanthomonas-Infected Tomato Leaves. *Plant Cell* **2008**, *20*, 1915–1929. [CrossRef] [PubMed]
20. Bibi, S.; Pereira, J.; Timilsina, S.; Minsavage, G.V.; Hulbert, J.C.; Jones, J.B. 2018. Examining The Role of an EF-Hand Protein in Regulating Virulence in Xanthomonas. In Proceedings of the International Congress of Plant Pathology (ICPP 2018), Boston, MA, USA, 29 July–3 August 2018.
21. Charkowski, A.O.; Alfano, J.R.; Preston, G.; Yuan, J.; He, S.Y.; Collmer, A. The Pseudomonas syringae pv. tomato HrpW Protein Has Domains Similar to Harpins and Pectate Lyases and Can Elicit the Plant Hypersensitive Response and Bind to Pectate. *J. Bacteriol.* **1998**, *180*, 5211–5217. [CrossRef] [PubMed]
22. Figueiredo, J. Genetic and molecular analysis of pathogenicity genes in Xanthomonas citri subsp. citri. Ph.D. Thesis, University of Florida, Gainesville, FL, USA, 2009.
23. White, F.F.; Potnis, N.; Jones, J.B.; Koebnik, R. The type III effectors of Xanthomonas. *Mol. Plant Pathol.* **2009**, *10*, 749–766. [CrossRef]
24. Noël, L.; Thieme, F.; Nennstiel, D.; Bonas, U. Two Novel Type III-Secreted Proteins of *Xanthomonas campestris* pv. *vesicatoria* Are Encoded within the hrp Pathogenicity Island. *J. Bacteriol.* **2002**, *184*, 1340–1348. [CrossRef]

25. Kim, J.-G.; Park, B.K.; Yoo, C.-H.; Jeon, E.; Oh, J.; Hwang, I. Characterization of the *Xanthomonas axonopodis* pv. *glycines* Hrp Pathogenicity Island. *J. Bacteriol.* **2003**, *185*, 3155–3166. [CrossRef] [PubMed]
26. Li, S.; Wang, Y.; Wang, S.; Fang, A.; Wang, J.; Liu, L.; Zhang, K.; Mao, Y.; Sun, W. The Type III Effector AvrBs2 in *Xanthomonas oryzae* pv. *oryzicola* Suppresses Rice Immunity and Promotes Disease Development. *Mol. Plant-Microbe Interact.* **2015**, *28*, 869–880. [CrossRef] [PubMed]
27. Li, P.; Zhang, L.; Mo, X.; Ji, H.; Bian, H.; Hu, Y.; Majid, T.; Long, J.; Pang, H.; Tao, Y.; et al. Rice aqua-porin PIP1;3 and harpin Hpa1 of bacterial blight pathogen cooperate in a type III effector translocation. *J. Exp. Bot.* **2019**, *70*, 3057–3073. [CrossRef]
28. Rybak, M.; Minsavage, G.V.; Stall, R.E.; Jones, J.B. Identification of Xanthomonas citri ssp. citri host specificity genes in a heterologous expression host. *Mol. Plant Pathol.* **2009**, *10*, 249–262. [CrossRef] [PubMed]
29. Chosed, R.; Tomchick, D.; Brautigam, C.; Mukherjee, S.; Negi, V.S.; Machius, M.; Orth, K. Structural Analysis of Xanthomonas XopD Provides Insights into Substrate Specificity of Ubiquitin-like Protein Proteases. *J. Biol. Chem.* **2007**, *282*, 6773–6782. [CrossRef] [PubMed]
30. Auch, A.F.; Von Jan, M.; Klenk, H.-P.; Göker, M. Digital DNA-DNA hybridization for microbial species delineation by means of genome-to-genome sequence comparison. *Stand. Genom. Sci.* **2010**, *2*, 117–134. [CrossRef]
31. Delcher, A.; Phillippy, A.; Carlton, J.; Salzberg, S. Fast algorithms for large-scale genome alignment and comparison. *Nucleic Acids Res.* **2002**, *30*, 2478–2483. [CrossRef]
32. Altschul, S.F.; Gish, W.; Miller, W.; Myers, E.W.; Lipman, D.J. Basic local alignment search tool. *J. Mol. Biol.* **1990**, *215*, 403–410. [CrossRef]
33. Aranda, J.; Poza, M.; Pardo, B.G.; Rumbo, S.; Rumbo, C.; Parreira, J.R.; Rodríguez-Velo, P.; Bou, G. A rapid and simple method for constructing stable mutants of Acinetobacter baumannii. *BMC Microbiol.* **2010**, *10*, 279. [CrossRef]

plants

MDPI

Article

A Comprehensive Phytochemical Analysis of Terpenes, Polyphenols and Cannabinoids, and Micromorphological Characterization of 9 Commercial Varieties of *Cannabis sativa* L.

Eugenia Mazzara [1], Jacopo Torresi [1], Gelsomina Fico [2,3], Alessio Papini [4], Nicola Kulbaka [5], Stefano Dall'Acqua [6], Stefania Sut [6], Stefania Garzoli [7], Ahmed M. Mustafa [1,8], Loredana Cappellacci [1], Dennis Fiorini [9], Filippo Maggi [1,*], Claudia Giuliani [2,3] and Riccardo Petrelli [1]

1 Chemistry Interdisciplinary Project (CHIP), School of Pharmacy, University of Camerino, Via Madonna delle Carceri, 62032 Camerino, Italy; eugenia.mazzara@unicam.it (E.M.); jacopo.torresi@unicam.it (J.T.); ahmed.mustafa@unicam.it (A.M.M.); loredana.cappellacci@unicam.it (L.C.); riccardo.petrelli@unicam.it (R.P.)
2 Department of Pharmaceutical Sciences, University of Milan, Via Mangiagalli 25, 20133 Milan, Italy; gelsomina.fico@unimi.it (G.F.); claudia.giuliani@unimi.it (C.G.)
3 Ghirardi Botanic Garden, Department of Pharmaceutical Sciences, University of Milan, Via Religione 25, 25088 Toscolano Maderno, Italy
4 Department of Biology, University of Florence, Via La Pira 4, 50121 Florence, Italy; alessio.papini@unifi.it
5 Società Agricola Everweed Di G.Di Vietri & C. SS, Frazione Conti 2, 63857 Amandola, Italy; everweed.nicola@gmail.com
6 Natural Product Laboratory, Department of Pharmaceutical and Pharmacological Sciences, University of Padova, 35131 Padova, Italy; stefano.dallacqua@unipd.it (S.D.); stefania.sut@unipd.it (S.S.)
7 Department of Drug Chemistry and Technology, Sapienza University, 00185 Rome, Italy; stefania.garzoli@uniroma1.it
8 Department of Pharmacognosy, Faculty of Pharmacy, Zagazig University, Zagazig 44519, Egypt
9 Chemistry Interdisciplinary Project (CHIP), School of Science and Technology, University of Camerino, Via Madonna delle Carceri, 62032 Camerino, Italy; dennis.fiorini@unicam.it
* Correspondence: filippo.maggi@unicam.it; Tel.: +39-07-37-404-506

Citation: Mazzara, E.; Torresi, J.; Fico, G.; Papini, A.; Kulbaka, N.; Dall'Acqua, S.; Sut, S.; Garzoli, S.; Mustafa, A.M.; Cappellacci, L.; et al. A Comprehensive Phytochemical Analysis of Terpenes, Polyphenols and Cannabinoids, and Micromorphological Characterization of 9 Commercial Varieties of *Cannabis sativa* L. *Plants* **2022**, *11*, 891. https://doi.org/10.3390/plants11070891

Academic Editors: Milan S. Stankovic, Paula Baptista, Petronia Carillo and Seok-Geun Lee

Received: 9 March 2022
Accepted: 25 March 2022
Published: 27 March 2022

Publisher's Note: MDPI stays neutral with regard to jurisdictional claims in published maps and institutional affiliations.

Abstract: New hemp (*Cannabis sativa* L.) strains developed by crossbreeding selected varieties represent a novel research topic worthy of attention and investigation. This study focused on the phytochemical characterization of nine hemp commercial cultivars. Hydrodistillation was performed in order to collect the essential oils (EO), and also the residual water and deterpenated biomass. The volatile fraction was analyzed by GC-FID, GC-MS, and SPME-GC-MS, revealing three main chemotypes. The polyphenolic profile was studied in the residual water and deterpenated biomass by spectrophotometric assays, and HPLC-DAD-MS^n and ^{1}H-NMR analyses. The latter were employed for quali–quantitative determination of cannabinoids in the deterpenated material in comparison with the one not subjected to hydrodistillation. In addition, the glandular and non-glandular indumentum of the nine commercial varieties was studied by means of light microscopy and scanning electron microscopy in the attempt to find a possible correlation with the phytochemical and morphological traits. The EO and residual water were found to be rich in monoterpene and sesquiterpene hydrocarbons, and flavonol glycosides, respectively, while the deterpenated material was found to be a source of neutral cannabinoids. The micromorphological survey allowed us to partly associate the phytochemistry of these varieties with the hair morphotypes. This research sheds light on the valorization of different products from the hydrodistillation of hemp varieties, namely, essential oil, residual water, and deterpenated biomass, which proved to be worthy of exploitation in industrial and health applications.

Keywords: *Cannabis sativa* L.; chemovars; secondary metabolites; trichomes; residual by-products

1. Introduction

Hemp (*Cannabis sativa* L.) is a versatile crop, for a long time cultivated in different parts of the world, and its cultivation has recently been considered as a good opportunity for agriculture production. Legally cultivated hemp has been selected in order to keep the psychotropic δ-9-tetrahydrocannabinol (THC) at levels lower than 0.2% [1]. The main non-psychotropic cannabinoid found in hemp, namely, cannabidiol (CBD), has recently been included in the list of the ingredients that can be used in cosmetics, thus offering new opportunities for the development of hemp products. In fact, up to now, the use of CBD has been approved in the cosmeceutical industry [2]. For medicinal applications, CBD has been registered as a drug (Epidiolex®) in the EU for the treatment of some epilepsy forms [3]. CBD regulation in the food or food supplements area is not uniform in European countries; thus, CBD products can be produced in some countries as food supplements, but they cannot be in others. Many studies have been developed in the last few years on CBD's potential uses as medicine, but CBD-fortified or CBD-labeled health products and CBD-associated health claims lack a rigorous scientific foundation [4]. At present, many research groups are studying CBD and other cannabinoids for possible applications in healthcare, medicine, food supplements, and cosmetics. In this regard, improving the knowledge on different hemp varieties or cultivars to obtain extracts enriched in specific phytoconstituents may be advantageous.

Moreover, hemp inflorescences, usually regarded as waste material of the fiber industry, are instead valuable sources of volatile constituents, secreted in the form of essential oils (EO), that can be obtained by distillation procedures [5]. Specifically, hemp is endowed with secretory structures, namely trichomes, representing the main site to produce secondary metabolites. Among them, cannabinoids and terpenes are contained in a sort of resin released by capitate-stalked glandular hairs localized on flower bracts and, to a minor extent, by capitate sessile and bulbous trichomes occurring also on other vegetative organs [6]. Notably, volatile terpenes of hemp glandular trichomes are recovered as a yellowish and odorous EO [7,8]. Morphological descriptions of hemp trichomes play a significant role in forensic investigations and legal/illegal cannabis identification. Given the high variability in *C. sativa* morphological features, the study of such anatomical characteristics appears to be necessary and useful for varieties classification and characterization [9]. For these reasons, traditional optical, electron, and fluorescence microscopy, and the more common Raman spectroscopy [10], have been employed for the localization and analysis of cannabinoids in cannabis trichomes.

As a source of certified new products, hemp EO is gaining more interest from agrochemical, cosmeceutical, pharmaceutical, and nutraceutical perspectives [11]. Indeed, this EO exhibited repellent, acaricidal [12,13], and insecticidal activity [14,15], to be exploited in the development of safe botanical pesticides in organic farming and parasite-control programs, as a promising alternative to conventional synthetic agents [16]. Hemp EO can also be employed as a scent in cosmetics, such as soaps and perfumes [17]. Moreover, the displayed antifungal, anti-inflammatory [18], antiprotozoal and antioxidant [19] effects support its use in infectious diseases, in the form of dermatological preparations and as an ingredient in protective masks against COVID-19 [18]. In addition, recent studies on the use of plant EOs as natural food preservatives evidenced the capability of hemp EO to enhance the shelf-life of trout fillets, due to its antimicrobial properties, which were improved by nano-encapsulation [20]. These results support further applications of hemp EO in green active packaging to maintain food safety and quality.

Hemp inflorescence distillation of EO produces two by-products, namely, residual water and deterpenated plant material, which are currently under-studied. The aqueous residues could be rich in phenolic compounds and can be extracted with safe solvents, such as ethanol and water [21]. Hemp polyphenols are interesting biomolecules, able to reduce the progression of cardiovascular and neurodegenerative diseases, asthma, inflammatory conditions, tumors, and others [22]. Among cannabis-typical flavones, cannflavin A and B are particularly attractive compounds, with anti-inflammatory [23], antiparasitic [24], anti-

cancer, and antiviral properties [25]. Flavonoids contribute to plant protection, especially from UV light, due to their antioxidant and radical scavenger activity. In fact, cannflavin A was detected at a high level in hemp varieties under the influence of strong solar radiation and cold temperatures [26].

The inflorescences and, to a minor extent, the leaves can also be considered as good sources of cannabinoids, especially CBD. In hemp plant material, cannabinoids are mostly present in the acidic form, and the heating of biomass at temperatures near 100 °C induces the decarboxylation of these compounds. So, this material can be used after distillation for the extraction of CBD and other minor cannabinoids. Indeed, some authors recently affirmed that hemp deterpenated biomass should no longer be considered as a waste [27], since it represents a source of phytocannabinoids [28]. CBD is nowadays of great interest for several applications, and less investigated minor cannabinoids, such as cannabigerol (CBG), can be equally promising on a pharmaceutical level. Specific chemovars characterized by other cannabinoids represent a challenging research area and can be the source of new appealing products [29]. For example, the French cultivar Santhica, characterized by a significant CBG content, could be employed to develop new hemp strains as reservoirs of this cannabinoid [30]. Actually, CBD and CBG, used in combination, showed antioxidant and anti-inflammatory activity [31], as well as antidiabetic and antimicrobial potential [32,33]. In particular, CBG reduced cachexia caused by chemotherapy [34], and was found to be active against several tumoral cell lines, including glioblastoma [35]. In addition, CBG could be a candidate in therapy against inflammatory bowel disease [36].

Most of the published papers on *C. sativa* are related to certified industrial hemp varieties or legal cannabis for recreational and therapeutic purposes, while studies on commercial cultivars of cannabis with low THC content are scarce. The crossbreeding of selective varieties with interesting terpenoids and phytocannabinoids profiles could allow obtaining new hemp breeding lines with diverse medicinal and pharmacological properties, and with potential industrial applications, such as antiseptics and biopesticides [37]. On this basis, this work aims to carry out a complete phytochemical characterization of several commercial hemp strains, cultivated for research purposes and to produce craft beers. Our study explored the opportunity to obtain three high-value products from hydrodistillation of the hemp inflorescences, namely, EO, residual water, and deterpenated plant material. The EO and residual water are sources of volatile terpenes and polyphenols, respectively. Moreover, the strong heating during distillation may induce the decarboxylation of cannabinoids in the plant deterpenated material. In this study, nine different hemp commercial varieties have been used as training model plants to establish the value of this complete extraction process. This research also aimed at offering new opportunities to develop a smart extraction approach to valorize hemp by-products, supporting their further utilization in the pharmaceutical, nutraceutical, cosmeceutical, and food sectors.

Furthermore, to substantiate this approach, a comprehensive micromorphological and histochemical study of glandular and non-glandular hairs has been carried out in the attempt to correlate the phytochemistry and morphological traits of these commercial varieties with the morphotype, abundance, distribution, and secretory products of trichomes.

2. Results and Discussion

2.1. Analysis of the Volatile Fraction

2.1.1. Analysis of EOs Yields

The yields of the EOs from the nine studied commercial varieties ranged from 0.485% *w*/*w* in Pablito to 1.814% *w*/*w* in Amnesia Cookies (Table 1). It is worth noting that in the literature, the maximum yield value for hemp EO was 0.60% [38], so the values registered in this work were considerably high, with respect to those obtained for the EOs from the certified European hemp varieties [7,39]. The EO yield can be influenced by several factors, such as genetics, plant biomass status, environmental and climatic conditions, post-harvesting, drying, etc. For this work, only non-pollinated female inflorescences were processed, and this aspect could explain the significant EO yields obtained. In fact,

it is known to hemp growers, and it has also been demonstrated, that the pollination of *Cannabis* plants should be prevented to ensure EO yields twice those deriving from pollinated flowers [40]. Some stress conditions, such as the temperature changes involved in the harvesting periods of the nine varieties, could enhance the secretion of EO, with cannabinoids and terpenes produced as plant defense agents [41]. Moreover, slow air drying in a dark environment prevented humidity and degradation of the biomass by microorganisms, by protecting the inflorescences against sun light, with the consequent preservation of the aroma and organoleptic features of each variety.

Table 1. GC-FID analysis results for the 9 commercial varieties' EOs and their yield values (%).

Compound	Hemp Variety								
	White Shark	Lemon Conti Kush New	Lemon Conti Kush	Venom OG	Pablito	24 K	Fresh Mountain	Amnesia Cookies	Gorilla Glue
	(g/100 g)								
α-pinene	8.53	3.24	11.48	21.19	8.35	0.73	9.32	21.16	0.74
β-pinene	3.59	2.78	4.67	4.79	3.21	0.68	3.66	7.45	0.82
myrcene	20.28	11.14	17.13	10.57	12.56	8.12	27.46	29.23	7.16
limonene	9.17	5.97	3.38	4.28	3.30	4.18	4.10	2.20	6.79
1,8-cineole	0.07	0.13	0.04	0.07	0.03	0.02	0.04	0.04	0.02
(*E*)-β-ocimene	0.10	4.51	0.16	0.05	0.06	0.03	0.02	0.02	0.03
terpinolene	9.51	30.47	1.33	1.65	0.52	3.69	0.25	0.18	0.27
(*E*)-caryophyllene	10.79	10.40	11.91	17.19	18.15	18.12	19.70	18.91	18.94
humulene	2.96	3.04	4.46	4.64	6.82	5.35	5.51	8.57	4.86
caryophyllene oxide	3.52	3.34	3.88	5.60	7.97	8.00	1.28	3.93	6.62
CBD	5.54	2.91	4.26	5.25	3.13	4.02	3.86	2.30	3.06
Δ-9-THC	0.13	0.09	0.10	0.13	0.12	0.12	0.12	0.20	0.20
Yields (%)	0.64	1.51	1.03	0.86	0.49	1.08	1.23	1.81	1.33

2.1.2. GC-FID Quantitative Determination of Hemp EO Main Constituents

The quantitative GC-FID analysis results for the nine EOs, shown in Table 1, highlight the presence of α-pinene, myrcene, terpinolene, and (*E*)-caryophyllene as the major terpenes. The highest content of α-pinene was detected in Venom OG (21.2 g/100 g), while Amnesia Cookies proved to be the richest in myrcene (29.2 g/100 g). The best concentration value of terpinolene was found in Lemon Conti Kush New (30.5 g/100 g), while (*E*)-caryophyllene reached the greatest amount in Fresh Mountain (19.7 g/100 g). The limonene, α-humulene, and caryophyllene oxide percentages were lower than those of the above compounds (for a total of 9.2 g/100 g in White Shark, 8.6 g/100 g in Amnesia Cookies and 8.0 g/100 g in 24 K). The other quantified terpenes, namely, 1,8-cineole and (*E*)-β-ocimene, were detected at a very low level in all the investigated EOs. CBD content ranged from 2.3 g/100 g in Amnesia Cookies to 5.5 g/100 g in White Shark EOs. It is worth noting that in all the analyzed EOs, the THC content was within the limit of 0.2%, which is far below that stated by EU regulation for industrial hemp biomass (Table 1).

2.1.3. GC-MS Analysis of EOs

A comprehensive GC-MS analysis was carried out using two columns of different polarities, namely, HP-5MS and DB-WAX, to obtain an overview of the chemical profiles of the nine EOs. The results of the two analyses were comparable, confirming the presence of the same main compounds in each variety. Interestingly, the more apolar HP-5MS stationary phase allowed us to obtain, for several components, higher relative abundances, with respect to those found by employing the more polar DB-WAX column. For this reason, Table 2 reports the percentage values provided by the analysis performed with the HP-5MS column.

Table 2. GC-MS analysis results for the 9 commercial varieties EOs.

						Variety									
						Pablito	White Shark	Gorilla Glue	24 K	Fresh Mountain	Venom OG	Lemon Conti Kush	Lemon Conti Kush New	Amnesia Cookies	
N	Component [a]	RI [b] HP-5MS	RI [c] lit. apol.	RI [d] DB-WAX	RI [e] lit. polar	% HP-5MS									ID [f]
1	heptanal	901	901	1187	1184	0.9	0.3	0.2	0.2	0.2	0.3	0.6	0.1	tr [g]	RI,MS
2	α-thujene	926	924	1028	1025		0.1		0.2			tr	0.3	tr	RI,MS
3	α-pinene	932	933	1026	1027	9.0	11.3	0.7	0.2	11.0	23.3	12.5	3.5	24.6	Std
4	camphene	947	946	1071	1063	0.1	0.3	0.1	0.2	0.2	0.4	0.2	0.1	0.3	Std
5	β-pinene	975	974	1114	1112	3.0	4.2	0.7	0.2	4.0	5.0	4.8	2.7	8.2	Std
6	myrcene	990	988	1164	1165	10.7	21.5	6.6	0.2	26.0	9.7	14.9	9.5	27.1	Std
7	α-phellandrene	1004	1002	1169	1167	tr	0.5			tr	tr	tr	1.3	tr	Std
8	δ-3-carene	1009	1008	1153	1152		0.4					tr	1.0		Std
9	α-terpinene	1016	1014	1184	1193	tr	0.4		0.1	tr	tr	tr	1.3	tr	Std
10	limonene	1027	1024	1203	1193	2.7	10.2	6.8	4.6	3.9	3.9	2.8	5.4	1.8	Std
11	1,8-cineole	1030	1026	1217	1212	0.1	tr		1.5		tr		0.1	0.2	Std
12	(*Z*)-β-ocimene	1038	1032				tr				tr		tr		Std
13	(*E*)-β-ocimene	1048	1044	1253	1252	tr	tr					tr	4.0		Std
14	γ-terpinene	1058	1054	1250	1257	tr	0.3	tr	0.3		tr	0.1	1.0	tr	Std
15	terpinolene	1087	1086	1288	1282	0.3	11.8	0.3	0.4	0.2	0.1	1.0	30.2	0.1	RI,MS
16	linalool	1099	1095	1547	1549	0.2	1.0	0.9	2.9	0.1	1.0	0.4	0.4	tr	Std
17	*endo*-fenchol	1112	1114	1589	1582	0.2	0.8	1.7	1.0	0.8	0.7	0.6	0.4	tr	RI,MS
18	*trans*-pinene hydrate	1120	1119			0.1	0.5	1.1	0.6	0.5	0.4	0.4	0.3	tr	RI,MS
19	borneol	1164	1165	1711	1701	0.1	0.2	0.4	0.3	0.2	0.3	0.2	0.1	tr	Std
20	α-terpineol	1189	1186	1703	1698	0.3	1.0	1.4	1.3	0.6	0.7	0.4	1.0	0.1	Std
21	hexyl isobutanoate	1192	1191					0.1			tr	0.3			RI,MS
22	sativene	1393	1390					0.1		tr		0.1	tr		RI,MS
23	α-*cis*-bergamotene	1416	1411	1577	1577		0.1	0.1	0.2	tr	0.1	0.1			RI,MS
24	(*E*)-caryophyllene	1420	1417	1612	1612	15.5	11.4	17.6	19.9	16.0	17.1	10.7	8.2	15.3	Std
25	α-*trans*-bergamotene	1436	1432	1594	1583	0.2	1.0	1.3	1.4	0.4	0.7	0.9	0.1	0.1	RI,MS
26	α-guaiene	1439	1439					tr		2.8					RI,MS
27	α-humulene	1455	1452	1685	1667	6.5	3.0	4.7	6.3	4.7	4.9	4.1	2.4	7.6	Std
28	(*E*)-β-farnesene	1457	1454	1668	1674	0.1	1.1	1.2	1.5	0.2	0.6	0.8	0.1	tr	Std
29	*allo*-aromadendrene	1462	1458			0.1		tr	0.2	tr	tr	0.2	tr	tr	RI,MS
30	γ-muurolene	1478	1478					0.1		0.1		0.1			RI,MS
31	γ-curcumene	1480	1481					0.1	tr						RI,MS
32	β-selinene	1487	1489	1736	1734	0.8	0.2	0.2		0.6	0.1	0.5	0.6	1.3	RI,MS
33	valencene	1494	1496			0.2		0.4			0.1			0.1	RI,MS
34	α-selinene	1496	1498	1740	1737	0.7	0.2	0.5	0.1	0.8	0.1	0.8	0.7	1.1	RI,MS
35	β-dihydro-agarofuran	1501	1503			0.1	tr	0.1	0.1		0.1	tr	tr	tr	RI,MS
36	α-bulnesene	1507	1509			0.1				6.3					RI,MS
37	β-bisabolene	1509	1505	1734	1727	0.7	0.1	1.4	1.9	1.1	0.1	1.6	0.6	0.1	RI,MS
38	β-curcumene	1512	1514				0.1	0.2	0.2		tr	0.1			RI,MS
39	sesquicineole	1515	1515			tr	0.1	0.1	0.5	0.1	0.2	0.3	tr		RI,MS
40	zonarene	1522	1528			0.1	tr	0.9		0.3	tr				RI,MS
41	selina-4(15),7(11)-diene	1536	1544			0.3	0.1	7.1		3.5	0.1	5.0	3.4	0.1	RI,MS
42	selina-3,7(11)-diene	1543	1538	1796	1791		0.3	12.5		7.8	0.3	8.7	6.4	0.7	RI,MS
43	(*E*)-α-bisabolene	1543	1544	1780	1784	1.7			1.8						RI,MS
44	caryophyllene oxide	1584	1582	2008	2005	0.8	0.2	0.2	0.5	0.6	1.0	0.4	0.1	0.1	Std
45	guaiol	1598	1600	2100	2103	7.5	3.0	5.8	9.7	tr	5.9	3.3	2.1	2.1	RI,MS

Table 2. *Cont.*

						Variety									
						Pablito	White Shark	Gorilla Glue	24 K	Fresh Mountain	Venom OG	Lemon Conti Kush	Lemon Conti Kush New	Amnesia Cookies	
N	Component [a]	RI [b] HP-5MS	RI [c] lit. apol.	RI [d] DB-WAX	RI [e] lit. polar	% HP-5MS									ID [f]
46	eudesmol-5-*epi*-7-*epi*-α	1606	1607			0.4	0.1	0.2	0.4		0.2	0.1	0.1	tr	RI,MS
47	10-*epi*-γ-eudesmol	1621	1622	2124	2137	7.6	4.1	7.0	10.2	tr	6.5	4.6	3.1	3.0	RI,MS
48	γ-eudesmol	1633	1630			1.7	0.5	0.8	1.5		1.0	0.5	0.3	0.3	RI,MS
49	β-eudesmol	1651	1649			3.1	1.3	1.8	3.4	tr	2.3	1.1	0.7	0.7	RI,MS
50	α-eudesmol	1654	1652			4.3	2.0	2.8	4.7	0.2	3.2	1.7	1.1	1.1	RI,MS
51	eudesmol-7-*epi*-α	1659	1658			0.8	0.3	0.5	0.9		0.6	0.3	0.1	0.1	RI,MS
52	bulnesol	1668	1670	2201	2196	6.0	2.6	4.4	7.2		3.9	2.7	1.7	1.7	RI,MS
53	α-bisabolol	1684	1685	2215	2219	8.6	0.2	2.7	8.4	4.3	0.5	5.2	1.9	tr	Std
54	eudesm-7(11)-4-ol	1697	1700			tr	tr	0.1		tr	tr	0.3	0.1		RI,MS
55	cannabidiol	2427	2430			0.2	0.6	0.2	0.4	0.5	1.0	0.5	0.1	0.1	Std
56	cannabichromene	2434	2440			tr	tr	tr	tr	tr	tr	tr	tr	tr	RI,MS
	Total identified (%)					96.07	97.51	96.13	95.42	98.13	96.63	93.80	96.47	98.42	

[a] Order of compounds is according to their elution from the HP-5MS column. [b] Linear retention index calculated using a mixture of *n*-alkanes (C_8–C_{30}) with respect to HP-5MS column. [c] Retention index values for apolar columns taken from ADAMS library. [d] Linear retention index calculated using a mixture of *n*-alkanes (C_8–C_{30}) with respect to the DB-WAX column. [e] Retention index values for polar columns taken from NIST 17 library. [f] Peak assignment method: Std, comparison with an available analytical standard; MS, MS matching with those stored in ADAMS, WILEY 275, NIST 17 and FFNSC2 libraries; RI, comparison of the calculated RI with those reported in ADAMS, NIST 17 and FFNSC2 libraries. [g] tr, traces (% < 0.1).

Among the monoterpenes, α-pinene, myrcene, and terpinolene were again the most abundant compounds detected in the EOs from the nine commercial varieties. Only one of them, namely Venom OG, showed prevalence of α-pinene over the other terpenes, as reported in the GC-FID analysis (Section 2.1.2). Indeed, this component accounted for 23.3% of the whole chemical profile, followed by (*E*)-caryophyllene (17.1%). Myrcene was the predominant constituent of the EOs from Amnesia Cookies, Fresh Mountain, White Shark, and Lemon Conti Kush (27.1%, 26.0%, 21.5%, and 14.9% of the total composition, respectively) confirming the GC-FID outcomes (Table 1). Along with myrcene, Amnesia Cookies' EO was characterized by a significant content of α-pinene (24.6%) and (*E*)-caryophyllene (15.6%). In addition to myrcene, other abundant constituents were (*E*)-caryophyllene (16.0%) and α-pinene (11.0%) in Fresh Mountain, and terpinolene (11.8%), (*E*)-caryophyllene (11.4%), α-pinene (11.3%) and limonene (10.2%) in White Shark. Myrcene was followed by α-pinene (12.5%) and (*E*)-caryophyllene (10.7%) in Lemon Conti Kush. Differently from the latter, the Lemon Conti Kush New EO presented terpinolene as the predominant component, accounting for a remarkable 30.2% of the total composition, followed by myrcene (9.5%). This EO was also the one with the highest content of terpinolene among all the EOs, as shown by the GC-FID analysis results.

Unlike the previous ones, 24 K, Gorilla Glue, and Pablito EOs were dominated by sesquiterpenes. Among them, (*E*)-caryophyllene was the most prevalent compound, in line with GC-FID analysis, representing 19.9%, 17.6%, and 15.5% of EO, respectively. It was followed by 10-*epi*-γ-eudesmol (10.2%) and guaiol (9.7%) in 24 K, and by selina-3,7(11)-diene (12.5%) and selina-4(15),7(11)-diene (7.1%) in Gorilla Glue. With respect to the other EOs, Pablito contained a higher relative percentage of α-bisabolol (8.6%).

Regarding cannabinoids, the only compounds detected in the nine commercial varieties' EOs were CBD and cannabichromene (CBC). While CBC was found only in traces in all the EOs, CBD content ranged from 0.1% to 0.6%, except in Venom OG, where it reached 1.0% (Table 2).

The above-described GC-MS outcomes highlight a certain variability in the chemical profiles of the investigated EOs, among each other and also, in some cases, with respect to those obtained by the certified industrial hemp varieties which were the relatives of the nine commercial cultivars considered in this study. In fact, the Pablito EO was characterized by the prevalence of (*E*)-caryophyllene and other sesquiterpenes, while its original monoecious variety Santhica 70 was reported to be richer in monoterpenes, especially myrcene, although its EO was obtained by steam distillation [42]. 24 K and Gorilla Glue, deriving from Carmagnola CS, presented the sesquiterpenes class and, particularly, (*E*)-caryophyllene as predominant constituents; notably, Carmagnola EO showed a higher amount of monoterpenes (especially myrcene) in the case of steam-distilled fresh inflorescences [43], but a higher sesquiterpene content (notably (*E*)-caryophyllene) when hydrodistillation of dry inflorescences was carried out [44]. Regarding Lemon Conti Kush, Fresh Mountain, and Amnesia Cookies, originated by the Kompolti variety, a considerable abundance of myrcene and other monoterpenes was detected in their EOs. This was in accordance with some literature findings in which the Kompolti EO from dried inflorescences appeared to be richer in the same compounds, rather than in sesquiterpenes [45]. So, it could be deduced that such differences in the distribution of mono- and sesquiterpenes in hemp EOs seem to be dependent on the extraction method and plant material status.

Interestingly, in some EOs from the nine commercial varieties, the presence of several sesquiterpenes structurally different from (*E*)-caryophyllene was found at noteworthy levels (Figure 1). Among them, 10-*epi*-γ-eudesmol and guaiol in 24 K, selina-3,7(11)-diene and selina-4(15),7(11)-diene in Gorilla Glue, and α-bisabolol in Pablito could be mentioned as the most representative compounds (Table 2). These sesquiterpenes were not frequent in hemp EOs from other studies. For instance, they were missing in the Kompolti EO analyzed by Novak et al. [46], while in Bertoli et al. [5], selina-3,7(11)-diene and α-bisabolol were detected, but in very low amounts (<1%), as for all the other minor sesquiterpenes identified in Carmagnola EO.

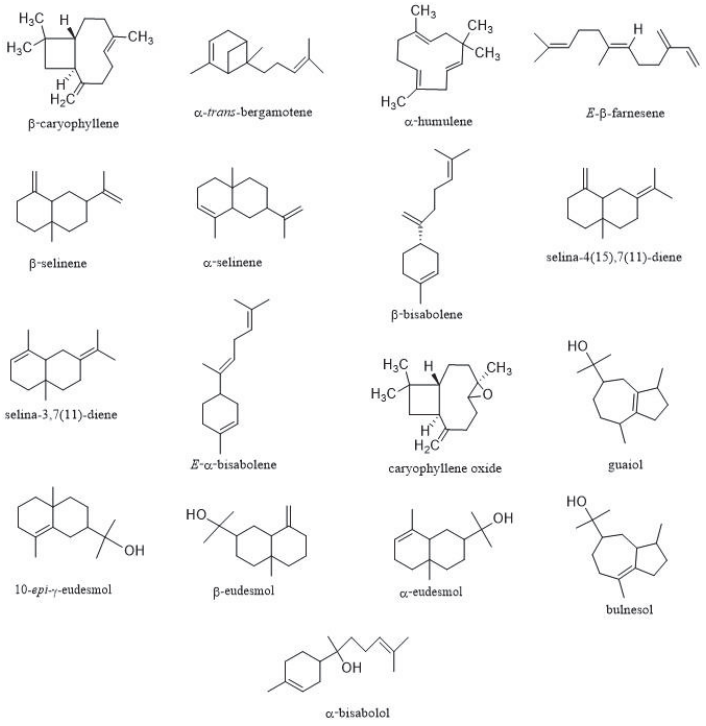

Figure 1. Chemical structures of the main sesquiterpenes found in the 9 EOs.

2.1.4. Chiral GC-MS Analysis of EOs

The EOs from the nine commercial varieties were subjected to chiral GC-MS analysis to determine the enantiomeric distribution of α-pinene, β-pinene, limonene, linalool, (*E*)-caryophyllene and caryophyllene oxide. This analysis could be helpful to detect the origin of the EO samples based on the enantiomeric ratio shown by the main constituents. In this regard, Table 3 reports the ratios within the enantiomeric pairs of these chiral terpenes. Both the enantiomers of α-pinene and limonene were detected in all the varieties. For α-pinene, the predominance of the (+)-form was observed, while the (−)-enantiomeric form was the prevalent one in the case of limonene. No significant differences in the enantiomeric ratios were obtained for these two compounds among the nine studied varieties. On the other hand, β-pinene and linalool were characterized by higher variability in the enantiomeric ratios. In fact, the (+)-enantiomer of β-pinene was generally predominant, although the presence of only the (−)-form was found in EOs from two varieties, namely, 24 K and Gorilla Glue. Moreover, the prevalence of the (+)-enantiomer of linalool was detected, and it was the only recognized form in Fresh Mountain, Gorilla Glue and Venom OG EOs. It is worth noting that the elution order of the enantiomeric forms of α-pinene and β-pinene was compliant with that found in one of our previous works, where the same column was employed [8]. Interestingly, (+)-α-pinene and (+)-β-pinene, as the main enantiomers in the nine EOs, were reported to be endowed with antibacterial and antifungal properties [47]. Concerning sesquiterpenes, (*E*)-caryophyllene and caryophyllene oxide were present exclusively in the (−)-enantiomeric form (Table 3), as confirmed by another study on hemp EOs [8]. From the findings provided, it is possible to conclude that the enantiomeric ratio of the main volatile terpenes does not allow us to differentiate most of the varieties analyzed, apart from 24 K and Gorilla Glue, which showed the predominance of the (−)-β-pinene.

Table 3. Chiral GC-MS analysis results for the 9 commercial varieties EOs.

Variety	Enant. %					
	α-Pinene (−):(+)	β-Pinene (+):(−)	Limonene (−):(+)	Linalool (−):(+)	(*E*)-Caryophyllene (+):(−)	Caryophyllene Oxide (+):(−)
White Shark	11.6:88.4	70.9:29.1	93.5:6.5	8.4:91.6	0:100	0:100
Lemon Conti Kush	4.9:95.1	78.4:21.6	92.4:7.6	6.9:93.1	0:100	0:100
Lemon Conti Kush New	3.2:96.8	66.4:33.6	91.4:8.6	34.8:65.2	0:100	0:100
Pablito	1.6:98.5	84.8:15.2	90.4:9.6	12.3:87.7	0:100	0:100
Fresh Mountain	7.8:92.2	74.6:25.4	93.0:7.0	0:100	0:100	0:100
Amnesia Cookies	2.9:97.1	88.6:11.4	74.1:25.9	28.2:71.8	0:100	0:100
24 K	7.0:93.0	0:100	97.4:2.6	2.8:97.2	0:100	0:100
Venom OG	4.6:95.4	81.0:19.0	87.9:12.1	0:100	0:100	0:100
Gorilla Glue	7.9:92.1	0:100	97.4:2.6	0:100	0:100	0:100

2.1.5. SPME-GC-MS Analysis of Untreated Material

The dry female inflorescences (untreated material, UM) of the investigated hemp commercial varieties, provided by Everweed farm (Section 3.2), were evaluated for their organoleptic and aromatic features through the solid-phase microextraction (SPME) technique coupled to GC-MS. The detected volatile compounds belonged to the monoterpene and sesquiterpene classes, and, among them, α-pinene, myrcene, terpinolene, and (*E*)-caryophyllene represented the main fractions (Table 4). Myrcene dominated the volatile fractions of Pablito (35.2%), White Shark (44.6%), Fresh Mountain (39.2%), and Amnesia Cookies (37.2%) varieties, supporting the results on EOs (Sections 2.1.2 and 2.1.3). Similarly, terpinolene was the most abundant compound in Lemon Conti Kush New (24.1%), and, to a minor extent, in White Shark (17.1%), as reported by the previous analyses on EOs. Concerning sesquiterpenes, 24 K, Gorilla Glue, Venom OG, and Lemon Conti Kush were characterized by higher levels of (*E*)-caryophyllene (50.3, 43.8, 36.5 and 25.7%, respectively). In compliance with the EOs' GC-MS results, selina-3,7(11)-diene and selina-4(15),7(11)-diene were detected especially in Gorilla Glue (10.0 and 6.3%, respectively) and, in minor amounts, in Lemon Conti Kush and Lemon Conti Kush New (Table 4).

Regarding sesquiterpenes, the literature data suggest that a mountain environment could promote the production of these compounds, in particular (*E*)-caryophyllene and α-humulene, and other minor ones, such as selina-3,7(11)-diene [48]. In the cited study, dry inflorescences obtained from Kompolti grown in a mountainous area, analyzed with DVB/CAR/PDMS fiber as in the current work, presented significant amounts of the above sesquiterpenes, with respect to those obtained by lowland plants. In contrast to our research outcomes, the almost total absence of less common components, such as selina diene-, bisabolene-, and eudesmol-type sesquiterpenes, should be pointed out in other publications regarding the SPME analysis of inflorescences from several hemp varieties, including Carmagnola and Carmagnola CS [5]. Incidentally, the employed DVB/CAR/PDMS fiber was selected as the best one for the extraction of volatiles from *C. sativa* inflorescences [49].

2.2. Spectrophotometric Analysis of Lyophilized Extract and Deterpenated Material

The two hydrodistillation by-products, namely the water and plant biomass remaining in the round flask, were recovered separately and treated to obtain the lyophilized extracts (LE) and the dried deterpenated material (DM), as reported in Sections 3.3 and 3.5.1, respectively. LE and DM, obtained from the nine commercial varieties, were analyzed for their polyphenols and flavonoids content, and also for their antioxidant activity, in order to evaluate their possible reuse in pharmaceutical, nutraceutical, and cosmeceutical applications. In this regard, Table 5 shows the results of the spectrophotometric assays performed on the LE. The lowest and highest polyphenols and flavonoids contents were recorded in Fresh Mountain and Lemon Conti Kush New, respectively (between 40.4 and 72.2 mg of gallic acid equivalents (GAE) per g of dry extract (DE) for TPC, and from 18.2 to 46.3 mg of rutin equivalents (RE)/g DE for TFC). Moreover, the DPPH radical scavenging activity of LE varied from 90.3 to 143.0 mg of trolox equivalents (TE)/g DE in Fresh Mountain and Venom OG, respectively. As regards the studies on the antioxidant capacity

of EU-approved hemp water extracts, Orlando et al. [50] found TPC, TFC, and DPPH values of 21.2 mg GAE/$g_{extract}$, 7.1 mg RE/$g_{extract}$ and 14.9 mg TE/$g_{extract}$, respectively, for Futura 75 freeze-dried aqueous extract. As another example, a TPC value of around 55.0 mg GAE/$g_{extract}$ was detected by Gunjevic et al. [51] in the lyophilized extract obtained from the residual water after Monoica hemp EO distillation. Notably, the TPC, TFC, and DPPH levels of all the nine varieties of the present study were much higher than those found by Orlando et al. [50]. The TPC values for only Fresh Mountain and Lemon Conti Kush LE were lower than those found by Gunjevic et al. [51], as well. Interestingly, the TPC and TFC levels for the LE obtained from all the investigated hemp varieties (apart from Fresh Mountain) were significantly above those ascribed to aqueous extracts of mulberry fruits (39.6 and 18.5 mg GAE/$g_{extract}$ for TPC and TFC, respectively), which are well recognized and valorized for their antioxidant capacity [52].

As expected, due to the high-water solubility of these compounds, the polyphenols and flavonoids levels and the antioxidant activity in DM (Table 6) were lower than those belonging to LE. Nevertheless, DM could still represent potential sources of phenolic constituents, responsible for preventing the damaging effects of oxidation. The TPC values were in the range of 15.5–23.9 mg GAE per g of dry hemp (DW), reaching the minimum and maximum in Lemon Conti Kush and Venom OG DM, respectively. In the case of TFC, the results were between 8.3 mg RE/g DW in Amnesia Cookies and 22.0 mg RE/g DW in 24 K, while DPPH scavenging activity varied from 24.1 to 41.7 mg TE/g DW in Fresh Mountain and Venom OG, respectively. For comparative purposes, the same spectrophotometric tests were also performed on the dry inflorescences of Carmagnola CS, Santhica 70, and Kompolti, which were extracted with an ethanol-water 1:1 solution. As a result, the nine commercial varieties showed an improved TPC, TFC, and DPPH profile compared to the values obtained for the original certified ones (Table 6). These findings were confirmed by literature data. For instance, André et al. [53] indicated a TPC between 4.7 and 16.5 mg GAE/g DW for methanol:water extracts from Santhica 70 dried inflorescences. Moreover, Drinić et al. [54] reported TPC values ranging from 9.3 to 17.1 mg GAE/g DW for Helena aerial part extracts (50% ethanol in water). This solvent:water ratio, which was also chosen in the current research to carry out the tests, guaranteed the best extraction efficiency for phenolic constituents [54]. Based on the provided outcomes, the LE and DM from the nine hemp commercial varieties could represent interesting products that could be exploited for their antioxidant properties. Interestingly, LEs, currently recognized as waste obtained during distillation, represent valuable products to be used on an industrial level.

2.3. ^{1}H-NMR Analysis of UM and DM

To assess the multiple ways to extract valuable compounds from residual biomass resulting from distillation, the ^{1}H-NMR approach was used as a first general attempt to establish what changes in composition were observable before and after the hydrodistillation of the nine hemp varieties. For this reason, UM and DM were used to perform ^{1}H-NMR measurements, and samples were prepared using extractive solvents in sequence with increasing polarity. As a result, the UM chloroform extract showed the presence of cannabinoid acidic forms, the UM methanol extract presented a limited amount of phenolics and sugars, while the UM water extract was characterized by the presence of sugars (Figure 2). On the other hand, the DM chloroform extract showed the presence of cannabinoids, but the CBDA was in large part decarboxylated, being converted into CBD (Figure 3). The DM methanol and water extracts presented a limited amount of phenolics. Thus, the preliminary investigation by ^{1}H-NMR revealed that DM, in comparison to UM, contained decarboxylated cannabinoids, with potential usefulness as a starting material for the extraction of these bioactive phytoconstituents.

Table 4. SPME-GC-MS analysis results for the 9 commercial varieties' UM.

No	Compound	Variety								
		Lemon Conti Kush	Fresh Mountain	24 K	Gorilla Glue	White Shark	Venom OG	Lemon Conti Kush New	Amnesia Cookies	Pablito
		%								
1	α-thujene					tr		0.2		
2	α-pinene	14.4	10.7	1.5	1.4	12.0	3.6	2.0	18.3	12.4
3	camphene	0.2	0.2	tr	0.1	0.2	0.4		0.2	0.2
4	β-pinene	6.1					6.8		6.4	
5	myrcene	21.3	39.2	18.3	15.0	44.6	31.8	15.9	37.2	35.2
6	α-phellandrene					0.6		0.9	tr	0.3
7	α-terpinene									0.2
8	limonene	3.8	3.8	6.2	8.3	11.0	8.2	5.4	1.8	5.9
9	*p*-cymene					0.1				
10	(Z)-β-ocimene				0.1	0.1	1.1	5.5		1.2
11	γ-terpinene					0.3		0.4		0.2
12	*p*-cymenene					0.2				
13	terpinolene	1.7	1.0	5.2	2.7	17.1	1.3	24.1	tr	9.2
14	*cis*-ocimenol									0.2
15	copaene									0.1
16	aristolene								0.1	
17	fenchol	0.1		0.2	0.4	0.1				
18	butanoic acid, hexyl ester	0.2								
19	α-terpineol	0.3	0.1	0.5	0.6	0.4	0.3	0.4		
20	ylangene	0.3						0.1		
21	α-santalene	0.2		0.3	0.4	tr	0.1			
22	*trans*-α-bergamotene			0.9	0.4					
23	β-caryophyllene	25.7	23.1	50.3	43.8	10.9	36.5	22.8	23.0	21.8
24	α-guaiene		3.6				0.4			
25	α-himachalene	2.3	1.7							
26	(*E*)-β-farnesene	0.2		0.4						
27	β-bisabolene			3.2	2.2					
28	α-humulene	7.1	5.1	10.6	7.4	1.9	8.0	5.6	9.0	6.5
29	aromadendrene	0.3		0.2						
30	β-eudesmene	0.6	0.7			0.2			1.3	0.7
31	α-farnesene	0.1	0.1		0.5			0.6		
32	δ-selinene							0.4	0.4	

Table 4. *Cont.*

No	Compound	Variety								
		Lemon Conti Kush	Fresh Mountain	24 K	Gorilla Glue	White Shark	Venom OG	Lemon Conti Kush New	Amnesia Cookies	Pablito
		%								
33	valencene				0.4					
34	δ-guaiene		5.8				0.7		1.1	
35	β-sesquiphellandrene	0.1								
36	δ-cadinene	0.1								
37	*trans*-α-bisabolene	1.9	1.6	2.1			0.3	2.4	0.6	1.1
38	selina-4(15),7-(11)-diene	5.1	0.3		6.3			5.2		1.8
39	selina-3,7(11)-diene	7.6	3.0		10.0	0.1	0.3	7.9	0.3	2.6
40	guaia-3,9-diene									0.4
	Total identified (%)	99.7	100.0	99.9	100.0	99.8	99.8	99.8	99.7	100.0

Table 5. TPC, TFC, and antioxidant activity results for the nine commercial varieties' LE.

Variety	TPC (mg GAE/g DE)	TFC (mg RE/g DE)	DPPH (mg TE/g DE)
Lemon Conti Kush New	72.18	46.30	142.33
Lemon Conti Kush	54.74	30.00	111.89
Pablito	66.28	41.63	135.33
Fresh Mountain	40.38	18.15	90.33
24 K	65.00	40.37	138.11
Venom OG	69.62	42.96	143.00
Amnesia Cookies	57.82	25.56	109.67
White Shark	62.69	30.78	115.89
Gorilla Glue	57.56	31.48	120.78

Table 6. TPC, TFC, and antioxidant activity results for the 9 commercial varieties DM.

Variety	TPC (mg GAE/g DW)	TFC (mg RE/g DW)	DPPH (mg TE/g DW)
Lemon Conti Kush	15.51	12.58	25.07
Pablito	16.31	13.58	36.84
Fresh Mountain	16.13	10.33	24.11
24 K	23.00	22.00	39.07
Venom OG	23.90	20.08	41.67
Amnesia Cookies	15.82	8.33	26.62
White Shark	18.10	13.58	34.40
Gorilla Glue	20.28	16.92	38.62
Carmagnola CS	9.54	3.25	13.04
Santhica	12.36	4.33	10.22
Kompolti	15.10	6.50	15.56

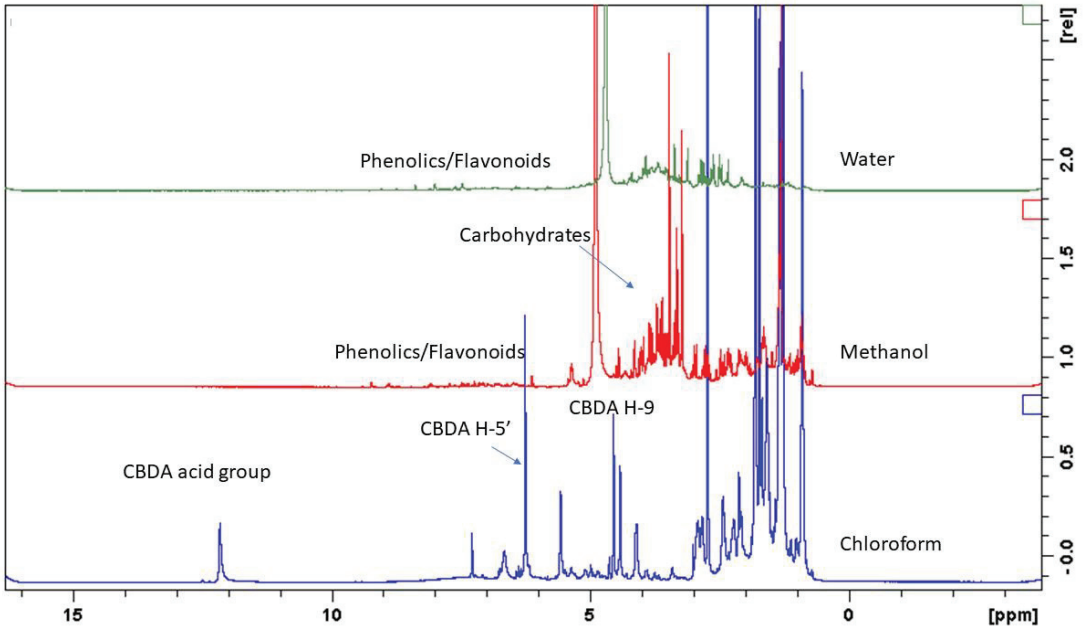

Figure 2. ^{1}H-NMR spectra showing the composition of UM chloroform, methanol and water extracts.

2.4. HPLC-DAD-MS^n Analysis of LE, DM and UM

The HPLC-DAD-MS^n analysis of flavones in the nine commercial cultivars allowed us to identify 11 compounds, such as luteolin, apigenin, quercetin glycosides, and the hemp-specific flavonoids cannflavin A and B. Furthermore, the lignanamides cannabisin A and B were also identified and quantified. These compounds have been previously identified mainly in the seeds and are considered markers for hemp [55]. UM presented large variations in the amounts of these 11 phenolic derivatives. Among them, luteolin glucuronide was observed in a larger amount (more than 7.0 mg/g in Pablito UM and 4.2 mg/g in Lemon Conti Kush UM). Considering the sum of all the phenolic and lignanamide derivatives, Pablito UM presented these compounds in larger amounts, accounting for a total of more than 12.0 mg/g. Considering DM, a general decrease in the contents of the 11 detected compounds was observed, probably due to the washing away caused by water during the hydrodistillation process. Nevertheless, DM still contained a significant amount of certain phenolics. Notably, not all the compounds were washed away during EO distillation; these include cannflavins, which present low water solubility, and were quantified in a comparable amount in UM and DM of most varieties. On the other hand, glycosidic flavonoids, such as luteolin glycosides or rutin, which are in general more soluble in water at high temperatures, were less present in DM than in UM (Table 7).

LE presented significant amounts of phenolic compounds (Table 8). Very high levels of rutin have been observed in Venom OG, White Shark, 24 K, and Lemon Conti Kush LE. Other varieties, for example Fresh Mountain, contained only a limited concentration (0.3 mg/g) of rutin. Vitexin-2″-O-glucoside was observed in significant amounts in Venom OG (5.0 mg/g), Lemon Conti Kush (3.5 mg/g), and 24 K (3.2 mg/g). As expected, cannabinoids were present in negligible amounts in LE, due to their poor water solubility.

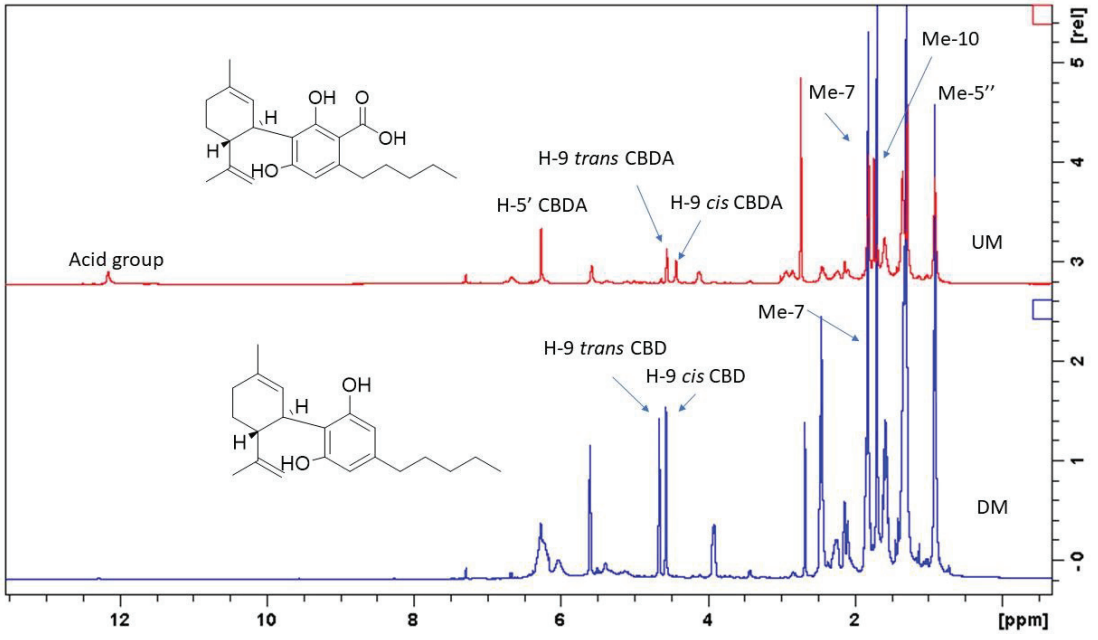

Figure 3. ^{1}H-NMR spectra showing the cannabinoids profiles of UM and DM chloroform extract.

UM and DM were also studied for their cannabinoid composition, and the results are summarized in Table 9. As previously indicated by the preliminary investigation by ^{1}H-NMR all the varieties were rich in acidic forms of cannabinoids, mostly CBDA. The cultivar Pablito presented CBGA as the most abundant cannabinoid. Very limited amounts

of δ-9-THC have been detected, and the maximum observed levels were all below 0.2 mg/g. Comparing the levels of cannabinoids in UM and DM, most of the CBDA was converted to CBD in DM. In fact, DM possessed a larger amount of CBD, compared to the corresponding UM, due to decarboxylation reaction and conversion of CBDA in CBD. The cannabinoid levels were remarkably higher with respect to some data published on Finola and Futura varieties [56] and were comparable with those of other studies reporting on the amount of CBD in several hemp varieties cultivated in Slovenia [57].

2.5. Multivariate Statistical Analysis of EOs and UM

PCA was carried out to better visualize, within the nine commercial varieties, the behaviors of the main constituents belonging to the three studied fractions, namely, terpenes, polyphenols, and cannabinoids, in the plant biomass (inflorescences).

The first PCA (Figure 4A) was performed to identify the correlation groups for terpene distribution in EOs, based on the GC-FID analysis results. The plots reported 53.56% of data variability on the first principal component (PC 1), and 29.61% on the second one (PC 2). The variance was caused mainly by terpinolene and, to a minor extent, by α-pinene and myrcene on PC 1, and by (*E*)-caryophyllene and caryophyllene oxide on PC 2. Specifically, the Lemon Conti Kush New cultivar was distinguishable for its high content of terpinolene, while Fresh Mountain and Amnesia Cookies were differentiated by the significant presence of α-pinene and myrcene. The other varieties belonged to the third correlation group, characterized by the sesquiterpenes prevalence.

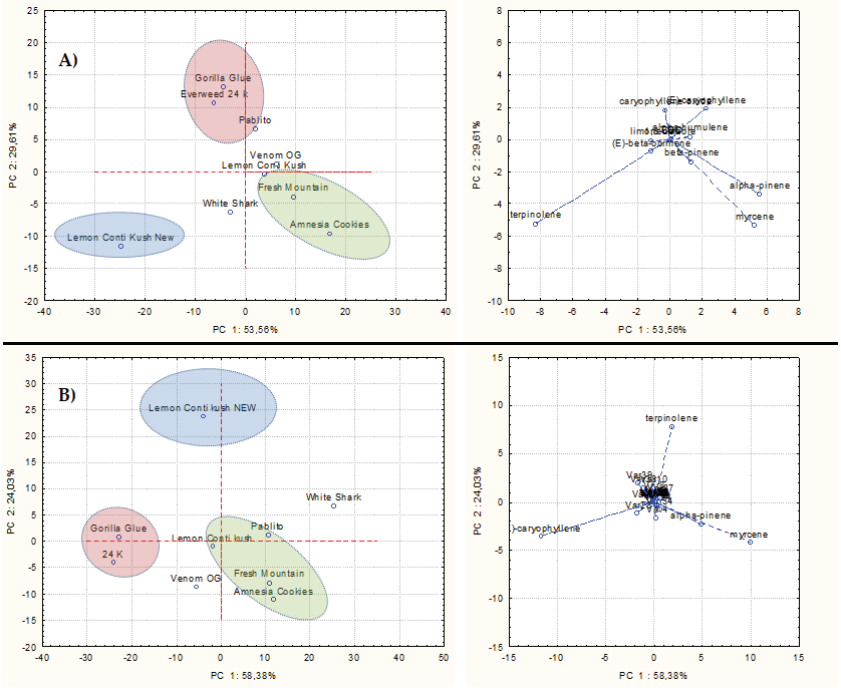

Figure 4. (**A**) Representation of PCA score and loading plots reporting hemp varieties and components found in the 9 EOs. (**B**) Representation of PCA score and loading plots depicting hemp varieties and volatiles extracted by SPME.

Table 7. HPLC-DAD-MS^n characterization of flavonoids in UM and DM.

Compound	Variety																	
	White Shark		24 K		Lemon Conti Kush		Lemon Conti Kush New		Pablito		Venom OG		Gorilla Glue		Fresh Mountain		Amnesia Cookies	
	UM	DM	UM	DM	UM	DM	UM	DM	UM	DM	UM	DM	UM	DM	UM	DM	UM	DM
	mg/g																	
cannabisin A	0.18	0.02	0.07	0.02	0.25	0.03	0.58		0.06	0.01	0.57	0.02	0.86	0.12	0.03	0.01	0.05	0.08
cannabisin B	0.38	0.12	0.05	0.05	0.12	0.14	1.35		0.23	0.02	0.82	0.08	0.81	0.13	0.02	0.004	0.54	0.12
luteolin-C-hexoside-O-rutinoside	0.72	0.05	0.05	0.05	0.16	0.03	0.63	0.03	0.50	0.03	0.66	0.12	0.51	0.02	0.18		0.38	0.06
rutin	0.53	0.04	0.30	0.02	0.33	0.03	0.33	0.06	0.07	0.11	0.51	0.03	0.27	0.04	0.03	0.03	0.21	0.03
luteolin-hexoside-hexoside	0.16	0.04	0.12	0.04	0.13	0.02	0.06	0.03	0.50	0.02	0.15	0.06	0.04	0.02	0.01		0.18	0.06
vitexin 2″-O-glucoside	0.12	0.03	0.12	0.05	0.09	0.02	0.17	0.04	0.30	0.07	0.29	0.03	0.15	0.02	0.17	0.04	0.05	0.03
apigenin-hexoside-glucuronide	0.20	0.06	0.15	0.03	0.17	0.54	0.06	0.02	0.12	0.03	0.18	0.03	0.13	0.46	0.16	0.04	0.13	0.02
luteolin 7-glucuronide	2.77	0.56	3.11	0.69	4.18	0.12	2.58	0.99	7.26	1.49	3.52	0.30	3.10	0.12	1.43	0.29	2.00	0.30
apigenin 7-glucuronide	0.94	0.27	0.46	0.13	0.67	0.07	0.23	0.20	0.21	0.37	0.02	0.15	0.37	0.07	0.48	0.13	0.63	0.14
cannflavin B	0.89	0.88	0.72	0.75	0.67	0.43	0.36	0.9	0.51	0.56	0.58	0.42	0.33	0.25	0.34	0.51	0.35	0.43
cannflavin A	1.13	1.38	2.08	2.66	0.38	1.92	1.46	2.43	2.15	2.87	0.53	0.74	1.35	1.41	0.97	1.3	0.68	0.16

Table 8. HPLC-DAD-MS^n characterization of flavonoids in LE.

Compound	Variety								
	White Shark	24 K	Lemon Conti Kush	Lemon Conti Kush New	Pablito	Venom OG	Gorilla Glue	Fresh Mountain	Amnesia Cookies
	(mg/g)								
cannabisin A	0.33	0.39	0.22	0.30	0.57	0.11	0.33	0.33	0.12
cannabisin B	0.71	2.57	2.37	0.35	3.03	3.57	0.30	0.22	0.18
luteolin-C-hexoside-O-rutinoside	0.23	1.18	0.51	0.50	1.48	1.39	2.51	0.22	0.32
rutin	7.93	7.93	8.79	0.35	5.63	12.18	0.75	0.30	0.58
luteolin-hexoside-hexoside	0.21	0.20	0.49	2.35	0.21	0.34	0.21	0.38	0.21
vitexin 2″-O-glucoside	0.29	3.19	3.48	0.63	0.55	5.01	0.40	0.57	0.37
apigenin-hexoside-glucuronide	1.12	0.79	1.43	0.32	1.84	1.21	0.79	0.46	0.32
luteolin 7-glucuronide	0.05	0.30	0.20	0.27	0.22	0.05	0.29	0.34	0.22
apigenin 7-glucuronide	0.22	0.07	0.04	0.27	0.23	0.22	0.31	0.23	0.08
cannflavin B	0.05	0.04	0.08	0.23	0.09	0.16	0.12	0.06	0.20
cannflavin A	0.24	0.19	0.15	0.27	0.12	0.20	0.62	0.20	0.24

Table 9. HPLC-DAD-MS^n characterization of cannabinoids in UM and DM.

Compound	Variety																	
	White Shark		24 K		Lemon Conti Kush		Lemon Conti Kush New		Pablito		Venom OG		Gorilla Glue		Fresh Mountain		Amnesia Cookies	
	UM	DM	UM	DM	UM	DM	UM	DM	UM	DM	UM	DM	UM	DM	UM	DM	UM	DM
	mg/g																	
CBDA	46.12	0.68	59.07	2.34	46.92	1.22	62.45	2.95	20.68	0.35	53.70	1.45	63.52	2.61	67.77	2.44	64.14	2.40
CBD	0.35	1.56	0.74	2.89	0.43	2.38	0.72	3.71	0.16	0.61	0.56	3.25	0.94	3.93	1.10	4.58	0.77	4.04
CBGA	2.11	0.46	3.07	0.43	0.99	0.41	0.54	0.32	23.50	0.50	3.25	0.41	4.91	0.45	3.26	0.42	2.24	0.43
CBG	0.13	0.16		0.28		0.12	0.11	0.82	0.26	2.57	0.14	0.58	0.17	0.93	0.05	0.48	0.14	0.85
CBN	0.44	1.13	0.35	0.11	0.38	0.13	0.04			0.14	0.08					0.33	0.07	0.08
Δ-9-THC	0.10	0.01	0.13	0.11	0.09	0.05	0.01				0.07	0.02	0.16		0.14	0.02	0.05	
CBC	0.46	0.05	0.34	0.27	0.25	0.15				0.56	0.13	0.65				0.01		
Δ-9-THCA	0.88	0.68	0.31	0.14	1.30	0.02	0.23	0.16	0.01	0.01	0.10	0.13				0.38		

Another PCA (Figure 4B) was conducted on volatiles obtained by SPME of UM and confirmed the clustering of the first PCA conducted on EOs. In fact, data variability, accounting for 58.38% along the first PC and 24.03% along the second one, was again produced by terpinolene, α-pinene, and myrcene among the monoterpenes, and by the sesquiterpene (*E*)-caryophyllene. Thus, the nine varieties so grouped reflected the trend observed in the first PCA.

The third PCA was carried out on terpenes, polyphenols, and cannabinoids fractions simultaneously (Figure 5), using data related to the dry biomass weight. In this case, PC 1 and PC 2 showed 92.89% and 4.75% variability, respectively. The data distribution was affected especially by CBDA on the first PC and CBGA on the second PC. The Pablito variety was recognized as the one with the highest content of CBGA, and, on the other hand, the CBDA-rich cluster included most of the studied cultivars, namely, Fresh Mountain, Gorilla Glue, Amnesia Cookies, 24 K, and Lemon Conti Kush New.

The last PCA focused exclusively on the polyphenolic profiles of the nine commercial varieties UM (Figure 6). The plots represented 78.49% of the variation in PC 1 and 8.95% in PC 2. On the first PC, the data variability was influenced mostly by luteolin glucuronide, which was predominant in the Pablito variety; on the second PC, cannflavin A emerged as the main phenolic compound in 24 K and Fresh Mountain.

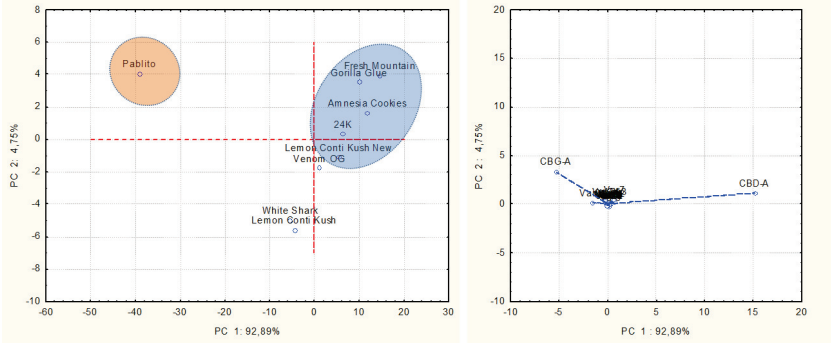

Figure 5. Representation of PCA score and loading plots reporting hemp varieties and their contents of terpenes, polyphenols, and cannabinoids.

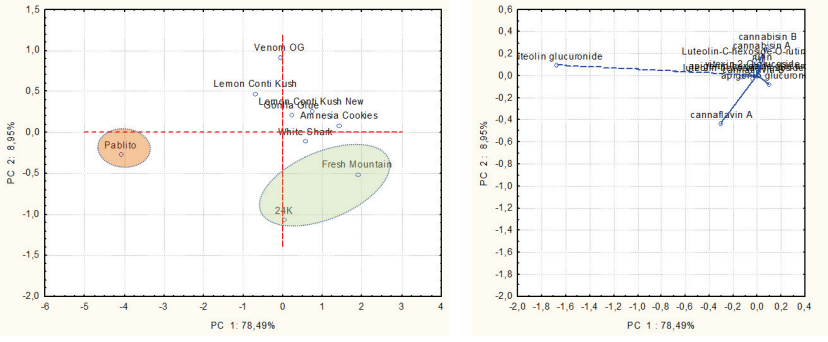

Figure 6. Representation of PCA score and loading plots reporting hemp varieties and the main polyphenols in UM.

In summary, the nine hemp commercial varieties were clustered, through PCA analyses, based on volatiles, phenols and cannabinoids content. Regarding the aromatic profile, apart from Lemon Conti Kush New, characterized by terpinolene predominance, the cultivars could be classified as α-pinene/myrcene-rich and (*E*)-caryophyllene-rich chemotypes.

Concerning polyphenols and cannabinoids, Pablito was one of the most interesting varieties, because it was marked by the highest concentration of CBGA and luteolin glucuronide. For this reason, it is differentiated from the other cultivars, in which CBDA was prevalent.

2.6. Micromorphological Analysis

The pistillate flowers of *C. sativa* are grouped into pairs in crowded, short pauciflore inflorescences at the axillae or terminals of branches. The flower, subtended by a bract, consists of one unilocular ovary and of two elongated, hairy stigmas. A hood-shaped bracteole surrounds the base of the ovary, a typical characteristic of the family Cannabaceae.

The micromorphological survey on the investigated cultivars involved bracts, bracteoles, and inflorescence axes. Within the same variety, the *indumentum* features proved consistent across the replicates, as regards trichome morphotypes, distribution pattern, and density on the examined plant parts.

In all the investigated hemp varieties, the plant epidermis was densely covered by an *indumentum* composed of diverse trichome morphotypes (Table 10; Figures 7–9).

Hooked hair-like lithocysts were observed on the bract, bracteole, and inflorescence axis surfaces. They were simple and unicellular with an acute apex; the cell diameter was progressively smaller moving from the base to the apex (Figure 7). The cuticle was smooth in Venom OG (Figure 7), and characterized by micropapillae, sometimes lacking on the basal cells, in all the other examined varieties. The overall length of this hair kind appeared variable, being lower on the interveinal regions of bracts and bracteoles and higher along the vein systems. Their distribution patterning and the compositions of the cystoliths have been used in the past in the forensic identification of marijuana [58].

In previous literature contributions, glandular trichomes of various morphotypes have been defined under diverse, controversial terms over time [6,9,59–61]. Therefore, an update of trichome terminology would be highly desirable to redefine the gland morphotypes. We decided, however, to adopt the current terminology and, consistently with the critical considerations that appeared in the paper by Casiraghi et al. [60], recognized two main trichome groups.

The first was capitate, with a head made up of 8–16 cells arranged in a single disc and a multiseriate stalk composed of four to eight cell rows. The secretory head was surrounded by a broad storing chamber, giving to the apex of each trichome a spherical shape. Cuticular rupture is often observed in SEM micrographs, in the form of a detached cap or following a horizontal line of apparent fragility in the diametrical region of the head. The stalk was variable in length due to the diverse elongation degree of the epidermal multiseriate stalk (pseudo-stalks) supporting it. Therefore, the so-called capitate-stalked glands and capitate-sessile glands were grouped together. They invariably co-occurred on the inflorescence axis, on the bracts and especially on bracteoles in all the investigated varieties. The second group was bulbous, with a uni- or bicellular head, a short, biseriate stalk and a two-foot cell lying at the level of the epidermis [59]. We recorded their distributions on the surfaces of all the examined plant parts. As a whole, neither the density rate nor the distribution pattern of the different types of trichomes represented features with diagnostic value for varietal recognition (Table 10). However, the diverse elongation degrees and the variable diameters of the pseudo-stalks of the capitate-stalked trichomes appeared as microcharacters useful in the recognition of some examined cultivars. Indeed, in Lemon Conti Kush and Lemon Conti Kush New, the pseudo-stalk appeared typically shorter and wider at the base in comparison to the other examined varieties.

Table 10. Distribution pattern of the glandular and non-glandular trichomes in the examined *C. sativa* varieties.

Plant Part	Trichome Morphotype	24 K	Gorilla Glue	Lemon Conti Kush	Fresh Mountain	Amnesia Cookies	Pablito	White Shark	Venon OG	Lemon Conti Kush New
bract	hair-like lithocysts	++	++	+	++	++	+	++	++	+
	bulbous	++	++	++	++	++	++	++	++	++
	capitate-stalked	++	++	++	++	++	++	++	++	++
	capitate sessile	+	+	+	+	+	+	+	+	+
bracteole	hair-like lithocysts	++	++	+	++	++	+	++	+	+
	bulbous	+	+	+	+	++	+	+	+	+
	capitate-stalked	++	++	++	++	++	++	++	++	++
	capitate sessile	++	+	++	+	++	++	+	++	++
inflorescence axis	hair-like lithocysts	+	+	+	++	++	++	+	+	+
	bulbous	+	+	+	++	++	++	+	++	+
	capitate-stalked	+	+	++	++	++	++	+	++	++
	capitate sessile	+	+	+	+	+	+	+	+	+

Trichome distribution: (+) present in all the replicates; (++) abundant in all the replicates.

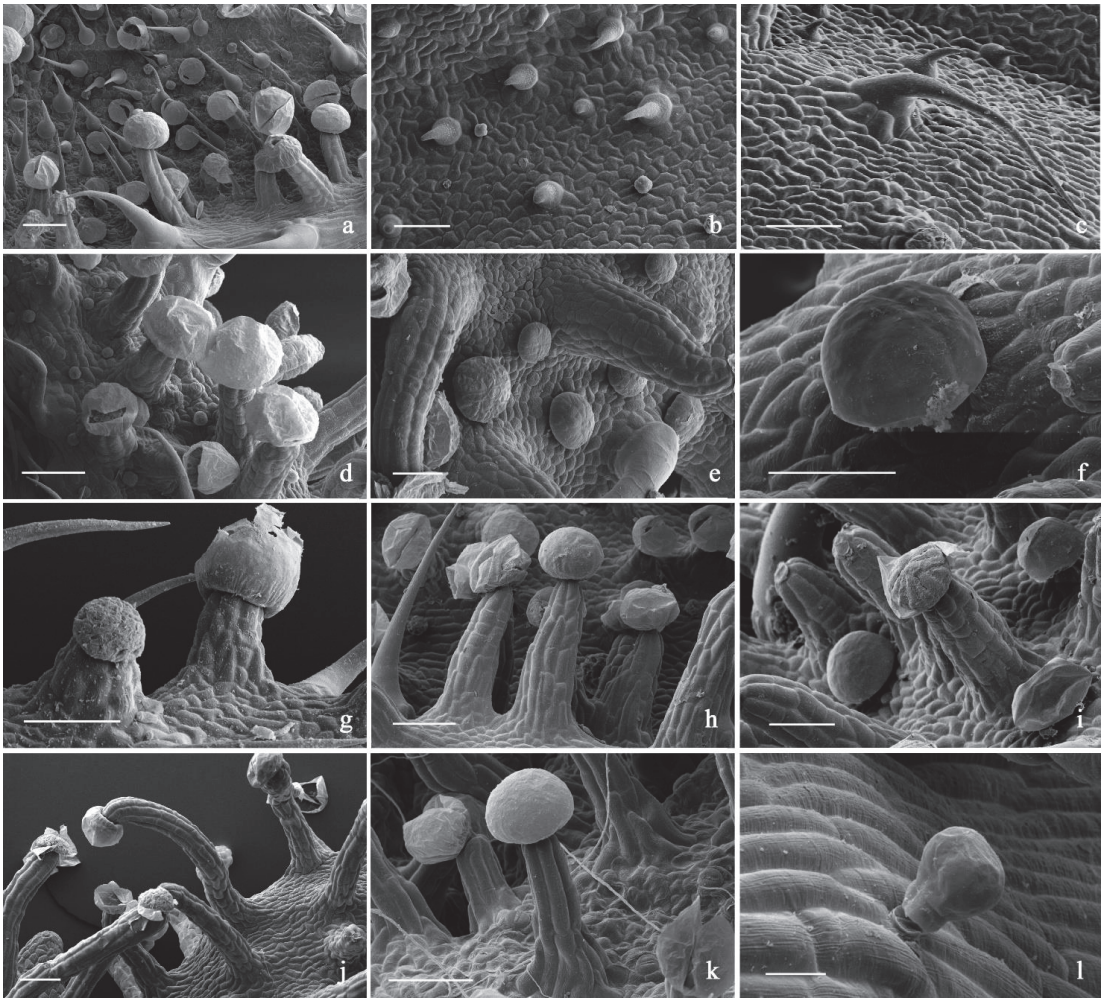

Figure 7. SEM micrographs showing the trichome morphotypes in the investigated *C. sativa* varieties. (**a**) General view of the bract abaxial surface with hair-like lithocysts, capitate-stalked, capitate-sessile and bulbous trichomes; (**b**) short hair-like lithocysts; (**c**) long hair-like lithocysts; (**d**) particular with groups of capitate-stalked and bulbous trichomes; (**e**,**f**) capitate-sessile trichomes; (**g**–**k**) capitate-stalked trichomes with diverse elongation degree of the pseudo-stalk; (**l**) bulbous trichome. *Scale bars = 100 µm (**a**–**k**); 20 µm (**l**).*

Due to the dense *indumentum* and the overall small sizes of the bulbous hairs, histochemical observation under light microscope mostly involved capitate glands. Copious secretory products fully covering the heads and the stalks of capitates were observed. They were mainly composed of terpenes, both for capitate-stalked and capitate-sessile hairs, as indicated by the intense positive responses to the NADI reagent, with a minor polyphenolic fraction, as suggested by the green-brownish colorations after the application of the Ferric Tricloride stain (Figure 10). The bulbous hairs occasionally exhibited faintly positive responses to terpenes and polyphenols. Cannabinoid production, however, takes place mainly in the capitate trichomes, especially the stalked ones, as was largely confirmed by gas–liquid chromatographic evidence, by the identification of the candidate biosynthetic genes [6], and by CARS microscopy [10].

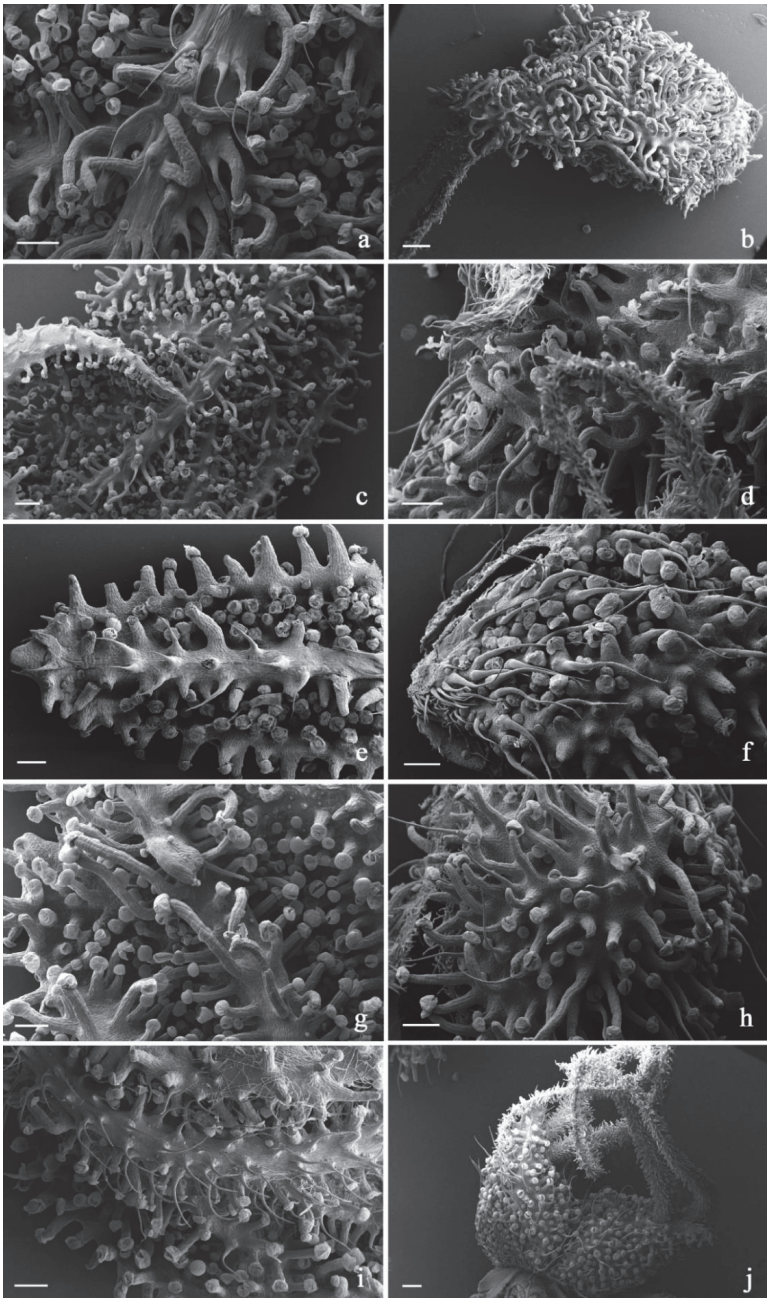

Figure 8. SEM micrographs showing the trichome distribution pattern on bracts and bracteoles of the investigated *C. sativa* varieties. (**a**,**b**) 24 K hemp variety: abaxial surfaces of bract (**a**) and bracteole (**b**); (**c**,**d**) Gorilla Glue hemp variety: abaxial surfaces of bract (**c**) and bracteole (**d**); (**e**,**f**) Lemon Conti Kush hemp variety: abaxial surfaces of bract (**e**) and bracteole (**f**); (**g**,**h**) Fresh Mountain hemp variety: abaxial surfaces of bract (**g**) and bracteole (**h**); (**i**,**j**) Amnesia Cookies hemp variety: abaxial surfaces of bract (**i**) and bracteole (**j**). *Scale bars = 200 µm (**a**,**c**–**i**); 250 µm (**b**,**j**).*

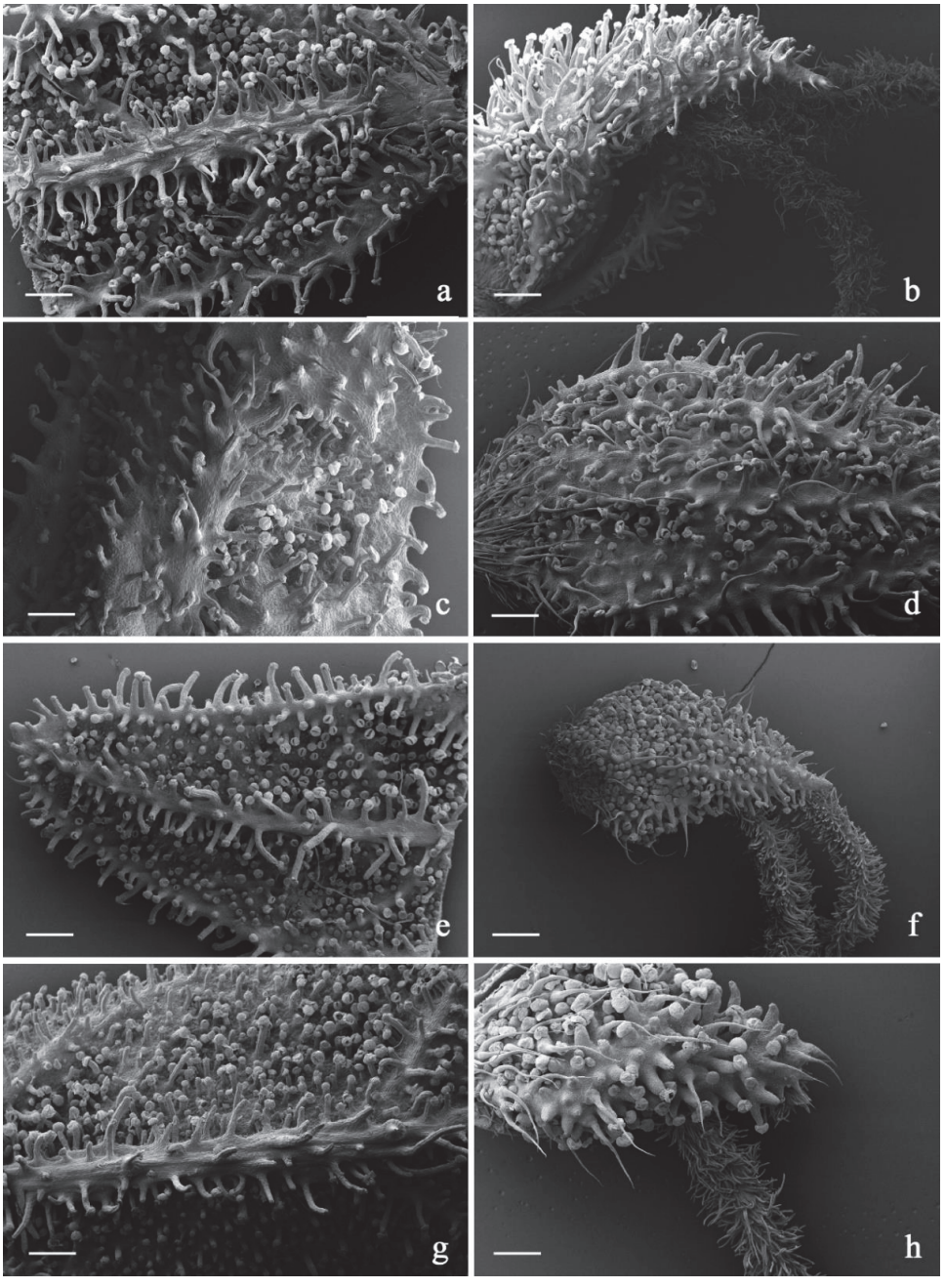

Figure 9. SEM micrographs showing the trichome distribution pattern on bracts and bracteoles of the investigated *C. sativa* varieties. (**a**,**b**) Pablito hemp variety: abaxial surfaces of bract (**a**) and bracteole (**b**); (**c**,**d**) White Shark hemp variety: abaxial surfaces of bract (**c**) and bracteole (**d**); (**e**,**f**) Venom OG hemp variety: abaxial surfaces of bract (**e**) and bracteole (**f**); (**g**,**h**) Lemon Conti Kush New hemp variety: abaxial surfaces of bract (**g**) and bracteole (**h**). *Scale bars = 500 µm (**a**–**g**); 200 µm (**h**).*

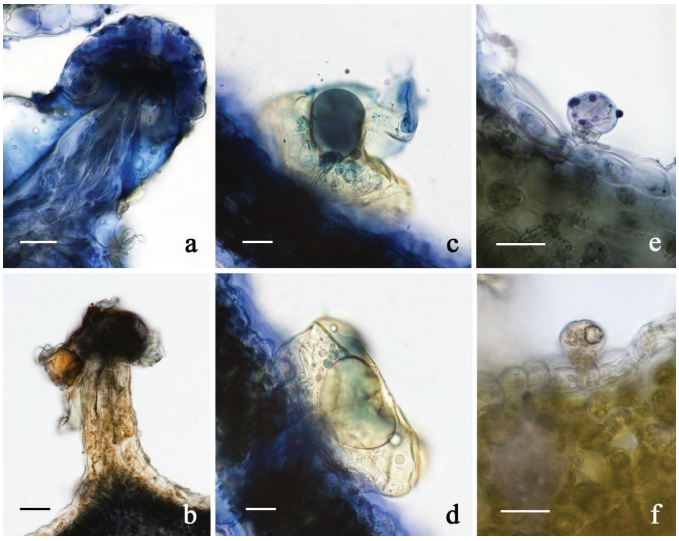

Figure 10. LM micrographs showing the results of the histochemical investigation on the glandular trichomes in the investigated *C. sativa* varieties. (**a**,**b**) Capitate-stalked trichome: Nadi reagent (**a**), Ferric Tricloride (**b**); (**c**,**d**) capitate-sessile trichome: Nadi reagent; (**e**,**f**) bulbous trichome: Nadi reagent (**e**), Ferric Tricloride (**f**). *Scale bars = 20 µm*.

3. Materials and Methods

3.1. Origin of the Commercial Varieties

The 9 investigated commercial varieties of *C. sativa*, namely, 24 K, Gorilla Glue, Lemon Conti Kush, Lemon Conti Kush New, Fresh Mountain, Amnesia Cookies, Pablito, White Shark, and Venom OG, were provided by the farm Everweed of G.Di Vietri & C. SS, sited in the national park of Monti Sibillini, in the municipality of Amandola, district of Ascoli Piceno, central Italy (GPS coordinates: 42°58′42.6″ N, 13°24′19.3″ E). They were obtained by crossbreeding between EU-approved cultivars, which has not been fully disclosed due to potential patent protection. Specifically, 24 K and Gorilla Glue derived from male inflorescences of Carmagnola CS; Lemon Conti Kush, Fresh Mountain and Amnesia Cookies originated from Kompolti male inflorescences; Pablito was generated from Santhica 70. In addition, White Shark and Venom OG were produced by replanting 24 K seeds; Lemon Conti Kush New was obtained from Lemon Conti Kush seeds. Voucher specimens of the 9 hemp varieties were stored in the *Herbarium Camerinensis* of the School of Bioscience and Veterinary Medicine, University of Camerino.

3.2. Growing and Harvesting Conditions

Hemp plants were cultivated in semi-hilly fields belonging to the farm Everweed. After 18 h of light at the vegetative stage, the agamic reproduction with cuttings was carried out. The cuttings were then positioned in a hydroponic greenhouse, where they were left to take root. The plants were transferred to the ground, and they grew to about 60 cm in height. Drip irrigation and NPK macronutrients were employed, without using pesticides, herbicides, and chemical fertilizers. The inflorescences were harvested from September to the second week of October 2020. Larger leaves were then removed, and the plants were air-dried in the dark, by means of fans and dehumidifiers. After slow drying, flowers were separated from branches, and smaller leaves were mechanically and, if necessary, manually eliminated. The product (untreated material, UM), represented by female inflorescences of the 9 varieties, was placed in plastic bags under vacuum and stored in the dark, until use.

3.3. Hydrodistillation

In order to obtain the EOs, 200 g of UM for each variety were subjected to hydrodistillation in a 10 L round flask, filled with 6 L of distilled water. UM was left to soak for 30 min before extraction. A Falc MA heating mantle (Falc Instruments, Treviglio, Italy), and a Clevenger-type apparatus were employed for the process, which was carried out for 5 h. The provided EOs were separated from the aqueous layer and collected in glass vials, to be stored at 4 °C until further analysis. The EOs yields were calculated on a dry matter basis (*w*/*w*).

Along with EOs, two other hydrodistillation products were recovered, namely, the water and plant biomass remaining in the round flask. The aqueous residues were filtered with filter paper and maintained at −20 °C, while the deterpenated material was dried for 24 h at 60 °C within a Biosec desiccator (Tauro Essiccatori, Vanzo Nuovo, Vicenza, Italy), and stored at room temperature in the dark for the following analyses.

3.4. Analysis of the Volatile Fraction

3.4.1. GC-FID Analysis of EOs

The quantified EO marker compounds were α-pinene, β-pinene, myrcene, limonene, 1,8-cineole, (*E*)-β-ocimene, terpinolene, (*E*)-caryophyllene, α-humulene, caryophyllene oxide, CBD and THC. Their analytical standards, provided by Sigma Aldrich (Milan, Italy), were injected to build the calibration curves in the range 0.005–10 mg/mL. The EOs obtained from the 9 commercial hemp varieties were diluted 1:100 in analytical-grade *n*-hexane; 0.5 µL of this solution was analyzed in split mode (1:30), by employing an HP-5 coated capillary column (HP-5, 30 m l., 0.32 mm i.d., 0.25 µm f.t., Agilent Technologies), placed in an Agilent 6850 Gas-Chromatograph (GC). A generator PGH2-250 (DBS Analytical Instruments, Vigonza, Italy) was used to produce hydrogen flowing at 3.7 mL/min. The injector temperature was set at 300 °C, while that of the GC oven was programmed as follows: 60 °C for 3 min, then 350 °C at 25 °C/min for 1 min. The FID detector temperature was 360 °C, and the hydrogen and air flow were 40 and 400 mL/min, respectively.

3.4.2. GC-MS Analysis of EOs

The qualitative chemical compositions of the EOs from the 9 varieties were evaluated through an Agilent 8890 GC, with a single quadrupole Agilent 5977B Mass Spectrometer (MSD) (Santa Clara, CA, USA), and a PAL RTC 120 autosampler (CTC Analytics AG, Zwingen, Switzerland). The non-polar HP-5MS (5% phenylmethylpolysiloxane; length: 30 m, 0.25 mm i.d., 0.25 µm f.t.) and the polar DB-WAX (polyethylene glycol; length: 60 m, 0.25 mm i.d., 0.25 µm f.t.) columns were employed as stationary phases. Helium (He) flow rate was 1 mL/min. The oven temperature programs were set as below: for the HP-5MS column, 60 °C for 5 min, then up to 220 °C at 4 °C/min, and on to 280 °C at 11 °C/min, for 15 min, and finally to 300 °C at 15 °C/min for 0.5 min; for the DB-WAX column, 60 °C for 5 min, increased to 220 °C at 4 °C/min, and later to 250 °C at 11 °C/min, for 15 min. The EOs were diluted 1:100 in *n*-hexane (LC-MS) and the injection was done in split mode (1:200). Data were acquired in SCAN mode (40–400 *m*/*z*) and analyzed through MSD ChemStation software (Agilent, Version G1701DA D.01.00), using the NIST Mass Spectral Search Program for the NIST/EPA/NIH EI and NIST Tandem Mass Spectral Library v. 2.3. A mix of *n*-alkanes (C_8-C_{30}, Supelco, Bellefonte, CA, USA) was injected to calculate linear retention indices (RI), and EO constituents were identified by checking the correspondence between their RI and mass spectra (MS) and those of commercial libraries, in particular ADAMS in the case of the analysis performed with the HP5-MS column, and NIST 17 when the DB-WAX column was used [62,63]. Relative abundance (peak area percentages) was obtained by normalization without using correction factors.

3.4.3. Chiral GC-MS Analysis of EOs

The separation of the enantiomeric pairs of α-pinene, β-pinene, limonene, linalool, (*E*)-caryophyllene and caryophyllene oxide in the 9 EOs was achieved with an Agilent HP

20β capillary column (20% β-cyclodextrin, length: 30 m, 0.25 mm i.d., 0.25 μm f.t.). The employed GC-MS system, along with the EOs dilution and injection mode, were the same as those used in the previous analyses (Section 3.4.2). The oven temperature was set at 50 °C, which was then raised to 220 °C at 2 °C/min for 1 min. The injector temperature was 250 °C, while the ionization source and quadrupole temperatures were set at 230 °C and 150 °C, respectively. The analytical standards (Sigma-Aldrich) of (+)-α-pinene, (−)-α-pinene, (−)-β-pinene, (+)-limonene, (−)-linalool, (−)-(*E*)-caryophyllene and (−)-caryophyllene oxide were injected as reference compounds.

3.4.4. SPME-GC-MS Analysis of UM

To analyze the volatile composition of UM, an SPME device from Supelco (Bellefonte, PA, USA) with 1 cm fiber coated with 50/30 μm DVB/CAR/PDMS (divinylbenzene/carboxen/polydimethylsiloxane) was used. The operative conditions for the sampling were the following: equilibration time of 30 min, and sampling time of 60 min at 35 °C. Lastly, the SPME fiber was inserted into the injector of the GC-MS system, maintained at 250 °C and operating as below. A gas chromatograph equipped with a FID and coupled with a mass spectrometer (Clarus 500 model Perkin Elmer-Waltham, MA, USA) was used. The capillary column was a Varian Factor Four VF-1, and the optimized temperature program was the following: from 70 °C to 120 °C at 6 °C/min; from 120 °C to 220 °C at 7 °C/min and held for 10 min. The components were identified by comparison between their calculated linear retention indices (LRIs) and those relating to a mix of *n*-alkanes. Furthermore, the matching of their mass spectra against commercial libraries (NIST) was performed. All analyses were conducted in triplicate and the results were expressed as average percentages calculated by peak area normalization from GC-FID chromatograms, without the use of an internal standard or correction factors.

3.5. Spectrophotometric Analysis of LE and DM

3.5.1. Samples Treatment

The frozen remaining water after EO distillation was freeze-dried at − 54 °C and 0.05 mbar, through a BUCHI Lyovapor™ L-200 freeze-dryer (Büchi Labortechnik AG, Flawil, Switzerland). The lyophilized extracts (LE) were ground in a mortar and the obtained powders were maintained at 4 °C until further analyses.

3.5.2. Total Polyphenols Content

The total polyphenols content (TPC) in LE was measured by applying the Folin–Ciocalteu method [64], with little variation. Briefly, 0.5 mL of aqueous solutions of LE (1 mg/mL), after being added to 2.5 mL of Folin–Ciocalteu reagent solution (diluted 10 times in water) and 7 mL of 7.5% Na_2CO_3 solution, were stored for 2 h at room temperature in the dark. The spectrophotometric assay was carried out with a Cary 8454 UV-Vis (Agilent Technologies, Woburn, MA, USA) at 735 nm. The calibration curve of gallic acid was employed in order to determine the TPC, which was reported as the mean of two measurements, and indicated as mg of gallic acid equivalents (GAE) per g of dry extract (DE). The TPC was evaluated also for the dried deterpenated material (DM). In this case, 1 g of DM was extracted in an ultrasound bath with 10 mL of a 50% ethanol aqueous solution, and 0.5 mL of the supernatant was subjected to the spectrophotometric test, following the same previous procedure. The results were expressed as mg GAE per g of dry hemp (DW).

3.5.3. Total Flavonoids Content

The total flavonoids content (TFC) determination was performed by following the procedure by Chen et al. [65], with few modifications. More precisely, 0.5 mL LE solutions in water at a concentration of 1.5 mg/mL were treated with 0.15 mL of $NaNO_2$ (0.5 M), with the following addition with stirring of 3.2 mL of 30% MeOH and 0.15 mL of $AlCl_3 \cdot 6H_2O$ (0.3 M). After adding 1 mL of NaOH (1 M) 5 min later, the absorbance of the mixed solution was evaluated spectrophotometrically at 506 nm. Rutin calibration curve (100–1000 ppm) was

used, and the results are given as mg of rutin equivalents (RE) per g of DE. DM was extracted with a 50% ethanol solution in water for TFC determination, operating in the same way as the TPC analysis of DM. The spectrophotometric assay was carried out as already described in this section and the obtained data were reported as mg RE per g of DW.

3.5.4. Radical Scavenging Activity

The antioxidant activity was determined in compliance with Mustafa et al. [64], by using 2,2-diphenyl-1-picrylhydrazyl (DPPH) free radical. Specifically, 4.5 mL of DPPH in EtOH (0.1 mM) were added to the aqueous solutions of LE (0.5 mL), to be then kept at room temperature for 30 min in the dark. The analysis was performed at 517 nm, with the same spectrophotometer employed for TPC and TFC evaluation. The radical scavenging activity was expressed, referring to the trolox calibration curve, as mg of trolox equivalents (TE) per g of DE. For DM, the same ethanol/water extracts were prepared, as for the two previous spectrophotometric tests, and then they were analyzed as reported in the present section. The antioxidant capacity was measured as mg TE per g of DW.

3.6. ^{1}H-NMR Analysis of UM and DM

As a preliminary characterization approach, UM and DM were subjected to ^{1}H-NMR analysis. In detail, 100 mg of ground samples were extracted with 800 µL of $CDCl_3$, sonicated for 10 min and centrifuged. The liquid was then collected in an NMR tube, while the plant material was dried under a nitrogen flow and then re-extracted with deuterated methanol and water, sonicated for 10 min and centrifuged. In these cases, the liquid fractions were collected in NMR tubes and analyzed. The spectra were acquired using a Bruker Ultrashield Plus 400 MHz spectrometer.

3.7. HPLC-DAD-MS^n Analysis of LE, DM and UM

An Agilent 1260 chromatograph with an autosampler and a diode array detector (DAD), interfaced with a Varian MS 500 ion trap mass spectrometer, was employed to quantify cannabinoids and phenolic compounds in the LE, DM, and UM of the 9 hemp commercial varieties. For the analysis of flavonoids and minor compounds, the column was an Agilent Eclipse XDB C18 (3.0 m × 150 mm × 3.5 µm), and the mobile phase was represented by a mixture of 1% formic acid in water (A) and acetonitrile (B). At the beginning, the gradient was 95% A, and in 30 min reached 100% B, with a flow rate of 0.4 mL/min. Data were collected by DAD in the λ range of 200–400 nm. The mass spectrometer was provided with an electrospray ion (ESI) source, which was employed in negative ion mode. The MS parameters were the following: spray chamber temperature, 45 °C; needle voltage, 4700 V; capillary voltage, 85 V; RF loading, 80%; nebulizing gas pressure, 25 psi (nitrogen); drying gas pressure, 15 psi; drying gas temperature, 300 °C. Spectra were acquired in the 50–1000 *m/z* range. Chromatograms were acquired from the turbo data depending on the scanning (TDDS) mode, allowing the generation of fragmentation spectra for the most intense ionic species. For the analysis of cannabinoids, an Agilent XDB (4.6 m × 250 mm × 5.0 µm) was used as the stationary phase. The gradient of elution was performed using water 1% formic acid (A) acetonitrile (B) and methanol (C). The gradient started with 30% A and 70% B, and in 20 min arrived at 70% B and 30% C; in 23 min it reached 100% C and stayed isocratic up to 33 min. Data were detected with DAD in the λ range of 200–400 nm. ESI-MS spectra were collected in positive ion mode for the neutral cannabinoids, and in negative ion mode for the acidic forms. Compounds were identified based on *m/z* values and retention times, and by comparison with authentic standards. For quantitative purposes, standard solutions in concentration from 0.1 to 100 µg/mL were set up to develop the calibration curves. For this purpose, CBD, cannabidiolic acid (CBDA), THC, and δ-9-tetrahydrocannabinolic acid (THCA) were used for cannabinoids' quantification, while rutin and quercetin-3-O-glucoside were selected for phenols content determination. For the analyses, LE, DM and UM samples were finely ground and about 200 mg were weighed and extracted with 25 mL of MeOH/H_2O 70:30.

The extracts were sonicated in an ultrasound bath for 15 min and centrifuged, and then the supernatants were taken and inserted into HPLC vials.

3.8. Multivariate Statistical Analysis of EOs and UM

Principal Component Analysis (PCA) was executed on the compositions of EOs and UM of the 9 commercial varieties, using STATISTICA software v. 7.1 (Stat Soft Italia S.r.l., Vigonza, Italy). GC-FID (Section 2.1.2) and SPME (Section 2.1.5) results for terpenes, and HPLC data (Section 2.4) for polyphenols and cannabinoids, were employed to build the score and loading plots (missing values were replaced with 0.001).

3.9. Micromorphological Analysis

For each hemp cultivar, a micromorphological survey on female inflorescences (bracts, bracteoles and inflorescence axes) was carried out by means of light microscopy (LM) and scanning electron microscopy (SEM) in order to document the features of the glandular indumentum. The samples were collected at comparable anthesis phenological stages. A minimum of ten replicates per each plant part were studied to assess the variability in the micromorphological features. Referring to the trichome distribution, we qualitatively evaluated it using the following symbols: (+) present in all the replicates; (++) abundant in all the replicates with a distribution on the whole organ surface.

3.9.1. Light Microscopy (LM)

The fresh examined plant parts were preliminarily observed by LM using hand-cut sections. The following histochemical dyes were used to characterize the chemical nature of the secretory products of the glandular trichomes: Toluidine Blue as a general dye [66], Nadi reagent for terpenes [67], Alcian Blue for mucopolysaccharides [66], and Ferric Trichloride for polyphenols [68]. Control stainings were simultaneously carried out. Observations were performed under a Leitz DM-RB Fluo optical microscope equipped with a Nikon digital camera.

3.9.2. Scanning Electron Microscopy (SEM)

Small hand-prepared segments of each plant part were FAA-fixed for 7 days, dehydrated in ascending ethanol series up to absolute, critical-point-dried, mounted on stubs and carbon gold-coated. Observations were performed under a Zeiss® EVO MA15 SEM operating at 10 kV at the Interdepartmental Center for Electron Microscopy and Microanalysis Services (M.E.M.A.) of the University of Florence (Florence, Italy).

4. Conclusions

The findings of this work highlight new opportunities for the working area on hemp. In addition to the most common applications and uses of hemp, its aerial parts, in particular the inflorescences, can be exploited to obtain essential oil by hydrodistillation, a niche and valuable product to be employed especially in the area of perfumes, and in agriculture as natural pest-control agent, though new applications remain to be identified. Concerning the residual fractions after hydrodistillation, the aqueous residue was found to be rich in phenolic compounds, thus it can be a source of antioxidant constituents used as additive in food and cosmetics. In addition, the deterpenated material has been proven to contain a significant amount of decarboxylated cannabinoids, this being a valuable starting material for the extraction of such compounds for the pharmaceutical market. From a phytochemical point of view, the nine commercial hemp varieties showed significant differences in terms of volatile profiles and, to a minor extent, the major cannabinoids. Interestingly, Lemon Conti Kush New was characterized by high levels of the monoterpene terpinolene, while Pablito was distinguishable from the others for the high levels of cannabigerol. In terms of polyphenols, the latter was the only one showing high contents of luteolin-3-glucuronide, while 24 K and Freh Mountain contained a high level of cannflavin A. The micromorphological and histochemical survey on the examined hemp commercial varieties allowed us,

for the first time, to sketch a link between the hair morphotypes and their phytochemical profiles. However, neither the trichomes' density rate, nor their distribution patterns on inflorescences, represented features with diagnostic value for varietal differentiation. Only the smooth cuticle of the hooked hair-like lithocysts and the shorter pseudo-stalks of the capitate-stalked trichomes proved valuable for the recognition of Venom OG and Lemon Conti Kush/Lemon Conti Kush New varieties, respectively.

Author Contributions: The contributions of the respective authors are as follows: F.M., R.P., S.D. and C.G., conceptualization as well as interpreting the data to prepare the manuscript; E.M., J.T., N.K., S.D., S.S., D.F. and A.M.M., collecting plant material, hydrodistillation, polyphenols, HPLC, NMR, and GC analyses; C.G., G.F., A.P. and S.G. conducted the micromorphological analysis as well as interpreting the relative data; C.G., R.P., S.D., G.F., L.C., D.F. and F.M., drafting, reviewing, and editing. All authors have read and agreed to the published version of the manuscript.

Funding: R.P. thanks the PRIN grant from the Italian Ministry of Health (PRIN 2017 CBNCYT) for the financial support.

Institutional Review Board Statement: Not applicable.

Informed Consent Statement: Not applicable.

Data Availability Statement: Not applicable.

Acknowledgments: The authors want to thank the Società Agricola Everweed of G.Di Vietri & C. SS, Amandola (Italy), for providing the nine commercial varieties of *C. sativa* and Federica Compieta for her contribution on the extraction of hemp samples.

Conflicts of Interest: The authors declare no conflict of interest.

References

1. Pacifici, R.; Pichini, S.; Pellegrini, M.; Tittarelli, R.; Pantano, F.; Mannocchi, G.; Rotolo, M.C.; Busardò, F.P. Determination of cannabinoids in oral fluid and urine of "light cannabis" consumers: A pilot study. *Clin. Chem. Lab. Med.* **2019**, *57*, 238–243. [CrossRef] [PubMed]
2. Mnekin, L.; Ripoll, L. Topical Use of *Cannabis sativa* L. Biochemicals. *Cosmetics* **2021**, *8*, 85. [CrossRef]
3. Nabbout, R.; Thiele, E.A. The role of cannabinoids in epilepsy treatment: A critical review of efficacy results from clinical trials. *Epileptic Disord.* **2020**, *22*, S23–S28. [CrossRef]
4. Nelson, K.M.; Bisson, J.; Singh, G.; Graham, J.G.; Chen, S.N.; Friesen, J.B.; Dahlin, J.L.; Niemitz, M.; Walters, M.A.; Pauli, G.F. The essential medicinal chemistry of cannabidiol (CBD). *J. Med. Chem.* **2020**, *63*, 12137–12155. [CrossRef] [PubMed]
5. Bertoli, A.; Tozzi, S.; Pistelli, L.; Angelini, L.G. Fibre hemp inflorescences: From crop-residues to essential oil production. *Ind. Crops Prod.* **2010**, *32*, 329–337. [CrossRef]
6. Happyana, N.; Agnolet, S.; Muntendam, R.; Van Dam, A.; Schneider, B.; Kayser, O. Analysis of cannabinoids in laser-microdissected trichomes of medicinal *Cannabis sativa* using LCMS and cryogenic NMR. *Phytochemistry* **2013**, *87*, 51–59. [CrossRef]
7. Fiorini, D.; Molle, A.; Nabissi, M.; Santini, G.; Benelli, G.; Maggi, F. Valorizing industrial hemp (*Cannabis sativa* L.) by-products: Cannabidiol enrichment in the inflorescence essential oil optimizing sample pre-treatment prior to distillation. *Ind. Crops Prod.* **2019**, *128*, 581–589. [CrossRef]
8. Fiorini, D.; Scortichini, S.; Bonacucina, G.; Greco, N.G.; Mazzara, E.; Petrelli, R.; Torresi, J.; Maggi, F.; Cespi, M. Cannabidiol-enriched hemp essential oil obtained by an optimized microwave-assisted extraction using a central composite design. *Ind. Crops Prod.* **2020**, *154*, 112688. [CrossRef]
9. Raman, V.; Lata, H.; Chandra, S.; Khan, I.A.; ElSohly, M.A. Morpho-anatomy of marijuana (*Cannabis sativa* L.). In *Cannabis sativa L.-Botany and Biotechnology*, 1st ed.; Chandra, S., Lata, H., ElSohly, M.A., Eds.; Springer: New York, NY, USA, 2017; pp. 123–136.
10. Ebersbach, P.; Stehle, F.; Kayser, O.; Freier, E. Chemical fingerprinting of single glandular trichomes of *Cannabis sativa* by Coherent anti-Stokes Raman scattering (CARS) microscopy. *BMC Plant Biol.* **2018**, *18*, 275. [CrossRef] [PubMed]
11. Zheljazkov, V.D.; Sikora, V.; Dincheva, I.; Kačániová, M.; Astatkie, T.; Semerdjieva, I.B.; Latkovic, D. Industrial, CBD, and wild hemp: How different are their essential oil profile and antimicrobial activity? *Molecules* **2020**, *25*, 4631. [CrossRef] [PubMed]
12. Górski, R.; Sobieralski, K.; Siwulski, M. The effect of hemp essential oil on mortality *Aulacorthum solani Kalt*. and *Tetranychus urticae* Koch. *Ecol. Chem. Eng. S* **2016**, *23*, 505–511. [CrossRef]
13. Tabari, M.A.; Khodashenas, A.; Jafari, M.; Petrelli, R.; Cappellacci, L.; Nabissi, M.; Maggi, F.; Pavela, R.; Youssefi, M.R. Acaricidal properties of hemp (*Cannabis sativa* L.) essential oil against Dermanyssus gallinae and Hyalomma dromedarii. *Ind. Crops Prod.* **2020**, *147*, 112238. [CrossRef]
14. Thomas, T.G.; Sharma, S.K.; Anand, P.; Sharma, B.R. Insecticidal properties of essential oil of *Cannabis sativa* Linn. against mosquito larvae. *Entomon* **2000**, *25*, 21–24.

15. Benelli, G.; Pavela, R.; Petrelli, R.; Cappellacci, L.; Santini, G.; Fiorini, D.; Sut, S.; Dall'Acqua, S.; Canale, A.; Maggi, F. The essential oil from industrial hemp (*Cannabis sativa* L.) by-products as an effective tool for insect pest management in organic crops. *Ind. Crops Prod.* **2018**, *122*, 308–315. [CrossRef]
16. Thakore, Y. The biopesticide market for global agricultural use. *Ind. Biotechnol.* **2006**, *2*, 194–208. [CrossRef]
17. Crini, G.; Lichtfouse, E.; Chanet, G.; Morin-Crini, N. Applications of hemp in textiles, paper industry, insulation and building materials, horticulture, animal nutrition, food and beverages, nutraceuticals, cosmetics and hygiene, medicine, agrochemistry, energy production and environment: A review. *Environ. Chem. Lett.* **2020**, *18*, 1451–1476. [CrossRef]
18. Orlando, G.; Adorisio, S.; Delfino, D.; Chiavaroli, A.; Brunetti, L.; Recinella, L.; Leone, S.; D'Antonio, M.; Zengin, G.; Acquaviva, A.; et al. Comparative investigation of composition, antifungal, and anti-inflammatory effects of the essential oil from three industrial hemp varieties from Italian cultivation. *Antibiotics* **2021**, *10*, 334. [CrossRef]
19. Menghini, L.; Ferrante, C.; Carradori, S.; D'Antonio, M.; Orlando, G.; Cairone, F.; Cesa, S.; Filippi, A.; Fraschetti, C.; Zengin, G.; et al. Chemical and bioinformatics analyses of the anti-leishmanial and anti-oxidant activities of hemp essential oil. *Biomolecules* **2021**, *11*, 272. [CrossRef]
20. Majidiyan, N.; Hadidi, M.; Azadikhah, D.; Moreno, A. Protein complex nanoparticles reinforced with industrial hemp essential oil: Characterization and application for shelf-life extension of Rainbow trout fillets. *Food Chem.* **2022**, *13*, 100202. [CrossRef]
21. Matešić, N.; Jurina, T.; Benković, M.; Panić, M.; Valinger, D.; Gajdoš Kljusurić, J.; Jurinjak Tušek, A. Microwave-assisted extraction of phenolic compounds from *Cannabis sativa* L.: Optimization and kinetics study. *Sep. Sci. Technol.* **2021**, *56*, 2047–2060. [CrossRef]
22. Andre, C.M.; Hausman, J.F.; Guerriero, G. *Cannabis sativa*: The plant of the thousand and one molecules. *Front. Plant Sci.* **2016**, *7*, 19. [CrossRef]
23. Werz, O.; Seegers, J.; Schaible, A.M.; Weinigel, C.; Barz, D.; Koeberle, A.; Allegrone, G.; Pollastro, F.; Zampieri, L.; Grassi, G.; et al. Cannflavins from hemp sprouts, a novel cannabinoid-free hemp food product, target microsomal prostaglandin E2 synthase-1 and 5-lipoxygenase. *PharmaNutrition* **2014**, *2*, 53–60. [CrossRef]
24. Pollastro, F.; Minassi, A.; Fresu, L.G. Cannabis phenolics and their bioactivities. *Curr. Med. Chem.* **2018**, *25*, 1160–1185. [CrossRef] [PubMed]
25. Bautista, J.L.; Yu, S.; Tian, L. Flavonoids in *Cannabis sativa*: Biosynthesis, bioactivities, and biotechnology. *ACS Omega* **2021**, *6*, 5119–5123. [CrossRef] [PubMed]
26. Calzolari, D.; Magagnini, G.; Lucini, L.; Grassi, G.; Appendino, G.B.; Amaducci, S. High added-value compounds from *Cannabis* threshing residues. *Ind. Crops Prod.* **2017**, *108*, 558–563. [CrossRef]
27. Vuerich, M.; Ferfuia, C.; Zuliani, F.; Piani, B.; Sepulcri, A.; Baldini, M. Yield and quality of essential oils in hemp varieties in different environments. *Agronomy* **2019**, *9*, 356. [CrossRef]
28. Zheljazkov, V.D.; Maggi, F. Valorization of CBD-hemp through distillation to provide essential oil and improved cannabinoids profile. *Sci. Rep.* **2021**, *11*, 1–11. [CrossRef]
29. Smith, C.J.; Vergara, D.; Keegan, B.; Jikomes, N. The phytochemical diversity of commercial cannabis in the United States. *BioRxiv* **2021**. [CrossRef]
30. Clarke, R.C.; Merlin, M.D. *Cannabis* domestication, breeding history, present-day genetic diversity, and future prospects. *CRC Crit. Rev. Plant Sci.* **2016**, *35*, 293–327. [CrossRef]
31. Mammana, S.; Cavalli, E.; Gugliandolo, A.; Silvestro, S.; Pollastro, F.; Bramanti, P.; Mazzon, E. Could the combination of two non-psychotropic cannabinoids counteract neuroinflammation? Effectiveness of cannabidiol associated with cannabigerol. *Medicina* **2019**, *55*, 747. [CrossRef]
32. Smeriglio, A.; Giofrè, S.V.; Galati, E.M.; Monforte, M.T.; Cicero, N.; D'Angelo, V.; Grassi, G.; Circosta, C. Inhibition of aldose reductase activity by *Cannabis sativa* chemotypes extracts with high content of cannabidiol or cannabigerol. *Fitoterapia* **2018**, *127*, 101–108. [CrossRef] [PubMed]
33. Zagožen, M.; Čerenak, A.; Kreft, S. Cannabigerol and cannabichromene in *Cannabis sativa* L. *Acta Pharm.* **2021**, *71*, 355–364. [CrossRef]
34. Brierley, D.I.; Harman, J.R.; Giallourou, N.; Leishman, E.; Roashan, A.E.; Mellows, B.A.; Bradshaw, H.B.; Swann, J.R.; Patel, K.; Whalley, B.J.; et al. Chemotherapy-induced cachexia dysregulates hypothalamic and systemic lipoamines and is attenuated by cannabigerol. *J. Cachexia Sarcopenia Muscle* **2019**, *10*, 844–859. [CrossRef]
35. Lah, T.T.; Novak, M.; Pena Almidon, M.A.; Marinelli, O.; Žvar Baškovič, B.; Majc, B.; Mlinar, M.; Bošnjak, R.; Breznik, B.; Zomer, R.; et al. Cannabigerol is a potential therapeutic agent in a novel combined therapy for glioblastoma. *Cells* **2021**, *10*, 340. [CrossRef] [PubMed]
36. Borrelli, F.; Fasolino, I.; Romano, B.; Capasso, R.; Maiello, F.; Coppola, D.; Orlando, P.; Battista, G.; Pagano, E.; Di Marzo, V.; et al. Beneficial effect of the non-psychotropic plant cannabinoid cannabigerol on experimental inflammatory bowel disease. *Biochem. Pharmacol.* **2013**, *85*, 1306–1316. [CrossRef] [PubMed]
37. Rocha, E.D.; Silva, V.E.; Pereira, F.; Jean, V.M.; Souza, F.L.C.; Baratto, L.C.; Vieira, A.; Carvalho, V.M. Qualitative terpene profiling of *Cannabis* varieties cultivated for medical purposes. *Rodriguésia* **2020**, *71*. [CrossRef]
38. Abdollahi, M.; Sefidkon, F.; Calagari, M.; Mousavi, A.; Mahomoodally, M.F. A comparative study of seed yield and oil composition of four cultivars of Hemp (*Cannabis sativa* L.) grown from three regions in northern Iran. *Ind. Crops Prod.* **2020**, *152*, 112397. [CrossRef]

39. Rossi, P.; Cappelli, A.; Marinelli, O.; Valzano, M.; Pavoni, L.; Bonacucina, G.; Petrelli, R.; Pompei, P.; Mazzara, E.; Ricci, I.; et al. Mosquitocidal and anti-inflammatory properties of the essential oils obtained from monoecious, male, and female inflorescences of hemp (*Cannabis sativa* L.) and their encapsulation in nanoemulsions. *Molecules* **2020**, *25*, 3451. [CrossRef] [PubMed]
40. Meier, C.; Mediavilla, V. Factors influencing the yield and the quality of hemp (*Cannabis sativa* L.) essential oil. *J. Int. Hemp Assoc.* **1998**, *5*, 16–20.
41. Pate, D.W. Chemical ecology of *Cannabis*. *J. Int. Hemp Assoc.* **1994**, *2*, 32–37.
42. Iseppi, R.; Brighenti, V.; Licata, M.; Lambertini, A.; Sabia, C.; Messi, P.; Pellati, F.; Benvenuti, S. Chemical Characterization and Evaluation of the Antibacterial Activity of Essential Oils from Fibre-Type *Cannabis sativa* L. (Hemp). *Molecules* **2019**, *24*, 2302. [CrossRef]
43. Nissen, L.; Zatta, A.; Stefanini, I.; Grandi, S.; Sgorbati, B.; Biavati, B.; Monti, A. Characterization and antimicrobial activity of essential oils of industrial hemp varieties (*Cannabis sativa* L.). *Fitoterapia* **2010**, *81*, 413–419. [CrossRef] [PubMed]
44. Pieracci, Y.; Ascrizzi, R.; Terreni, V.; Pistelli, L.; Flamini, G.; Bassolino, L.; Fulvio, F.; Montanari, M.; Paris, R. Essential Oil of *Cannabis sativa* L: Comparison of Yield and Chemical Composition of 11 Hemp Genotypes. *Molecules* **2021**, *26*, 4080. [CrossRef] [PubMed]
45. Palmieri, S.; Maggio, F.; Pellegrini, M.; Ricci, A.; Serio, A.; Paparella, A.; Lo Sterzo, C. Effect of the Distillation Time on the Chemical Composition, Antioxidant Potential and Antimicrobial Activity of Essential Oils from Different *Cannabis sativa* L. Cultivars. *Molecules* **2021**, *26*, 4770. [CrossRef] [PubMed]
46. Novak, J.; Zitterl-Eglseer, K.; Deans, S.G.; Franz, C.M. Essential oils of different cultivars of *Cannabis sativa* L. and their antimicrobial activity. *Flavour Fragr. J.* **2001**, *16*, 259–262. [CrossRef]
47. Silva, A.C.R.D.; Lopes, P.M.; Azevedo, M.M.B.D.; Costa, D.C.M.; Alviano, C.S.; Alviano, D.S. Biological activities of α-pinene and β-pinene enantiomers. *Molecules* **2012**, *17*, 6305–6316. [CrossRef] [PubMed]
48. Giupponi, L.; Leoni, V.; Pavlovic, R.; Giorgi, A. Influence of altitude on phytochemical composition of hemp inflorescence: A metabolomic approach. *Molecules* **2020**, *25*, 1381. [CrossRef] [PubMed]
49. Pellati, F.; Brighenti, V.; Sperlea, J.; Marchetti, L.; Bertelli, D.; Benvenuti, S. New methods for the comprehensive analysis of bioactive compounds in *Cannabis sativa* L.(hemp). *Molecules* **2018**, *23*, 2639. [CrossRef]
50. Orlando, G.; Recinella, L.; Chiavaroli, A.; Brunetti, L.; Leone, S.; Carradori, S.; Di Simone, S.; Ciferri, M.C.; Zengin, G.; Ak, G.; et al. Water extract from inflorescences of industrial hemp futura 75 variety as a source of anti-inflammatory, anti-proliferative and antimycotic agents: Results from in silico, in vitro and ex vivo studies. *Antioxidants* **2020**, *9*, 437. [CrossRef] [PubMed]
51. Gunjević, V.; Grillo, G.; Carnaroglio, D.; Binello, A.; Barge, A.; Cravotto, G. Selective recovery of terpenes, polyphenols and cannabinoids from Cannabis sativa L. inflorescences under microwaves. *Ind. Crops Prod.* **2021**, *162*, 113247. [CrossRef]
52. Mustafa, A.M.; Mazzara, E.; Abouelenein, D.; Angeloni, S.; Nunez, S.; Sagratini, G.; Lopez, V.; Cespi, M.; Vittori, S.; Caprioli, G.; et al. Optimization of Solvent-Free Microwave-Assisted Hydrodiffusion and Gravity Extraction of *Morus nigra* L. Fruits Maximizing Polyphenols, Sugar Content, and Biological Activities Using Central Composite Design. *Pharmaceuticals* **2022**, *15*, 99. [CrossRef] [PubMed]
53. André, A.; Leupin, M.; Kneubühl, M.; Pedan, V.; Chetschik, I. Evolution of the polyphenol and terpene content, antioxidant activity and plant morphology of eight different fiber-type cultivars of *Cannabis sativa* L. cultivated at three sowing densities. *Plants* **2020**, *9*, 1740. [CrossRef] [PubMed]
54. Drinić, Z.; Vidović, S.; Vladić, J.; Koren, A.; Kiprovski, B.; Sikora, V. Effect of extraction solvent on total polyphenols content and antioxidant activity of *Cannabis sativa* L. *Lek. Sirov.* **2018**, *38*, 17–21. [CrossRef]
55. Chen, T.; He, J.; Zhang, J.; Li, X.; Zhang, H.; Hao, J.; Li, L. The isolation and identification of two compounds with predominant radical scavenging activity in hempseed (seed of *Cannabis sativa* L.). *Food Chem.* **2012**, *134*, 1030–1037. [CrossRef] [PubMed]
56. Pavlovic, R.; Panseri, S.; Giupponi, L.; Leoni, V.; Citti, C.; Cattaneo, C.; Cavaletto, M.; Giorgi, A. Phytochemical and ecological analysis of two varieties of hemp (*Cannabis sativa* L.) grown in a mountain environment of Italian Alps. *Front. Plant Sci.* **2019**, *10*, 1265. [CrossRef]
57. Glivar, T.; Eržen, J.; Kreft, S.; Zagožen, M.; Čerenak, A.; Čeh, B.; Benković, E.T. Cannabinoid content in industrial hemp (*Cannabis sativa* L.) varieties grown in Slovenia. *Ind. Crops Prod.* **2020**, *145*, 112082. [CrossRef]
58. Evert, R.F. *Esau's Plant Anatomy: Meristems, Cells, and Tissues of the Plant Body: Their Structure, Function, and Development*, 3rd ed.; John Wiley & Sons: Hoboken, NJ, USA, 2006.
59. Mahlberg, P.G.; Kim, E.S. Accumulation of cannabinoids in glandular trichomes of *Cannabis* (Cannabaceae). *J. Ind. Hemp* **2004**, *9*, 15–36. [CrossRef]
60. Casiraghi, A.; Roda, G.; Casagni, E.; Cristina, C.; Musazzi, U.M.; Franzè, S.; Rocco, P.; Giuliani, C.; Fico, G.; Minghetti, P.; et al. Extraction method and analysis of cannabinoids in cannabis olive oil preparations. *Planta Med.* **2018**, *84*, 242–249. [CrossRef] [PubMed]
61. Brousseau, V.D.; Wu, B.S.; MacPherson, S.; Morello, V.; Lefsrud, M. Cannabinoids and Terpenes: How Production of Photo-Protectants Can Be Manipulated to Enhance *Cannabis sativa* L. Phytochemistry. *Front. Plant Sci.* **2021**, *12*, 620021. [CrossRef] [PubMed]
62. Adams, R.P. *Identification of Essential Oil Components by Gas Chromatography/Mass Spectrometry*, 4th ed.; Allured Publishing Corp. Carol Stream: Carol Stream, IL, USA, 2007.
63. *Mass Spectral Library (NIST/EPA/NIH)*; NIST 17; National Institute of Standards and Technology: Gaithersburg, MD, USA, 2017.

64. Mustafa, A.M.; Maggi, F.; Öztürk, N.; Öztürk, Y.; Sagratini, G.; Torregiani, E.; Vittori, S.; Caprioli, G. Chemical and biological analysis of the by-product obtained by processing *Gentiana lutea* L. and other herbs during production of bitter liqueurs. *Ind. Crops Prod.* **2016**, *80*, 131–140. [CrossRef]
65. Chen, G.L.; Chen, S.G.; Xiao, Y.; Fu, N.L. Antioxidant capacities and total phenolic contents of 30 flowers. *Ind. Crops Prod.* **2018**, *111*, 430–445. [CrossRef]
66. Beccari, N.; Mazzi, V. *Manuale Di Tecnica Microscopica*, 6th ed.; Società Editrice Libraria: Milano, Italy, 1966.
67. David, R.; Carde, J.P. Histochimie–coloration differentielle des inclusions lipidiques et terpeniques des pseudophylles du pin maritime au moyen du reactif NADI. *C. R. Biol.* **1964**, *258*, 1338–1340.
68. Gahan, P.B. *Plant Histochemistry and Cytochemistry*; Academic Press: London, UK, 1984.

MDPI
St. Alban-Anlage 66
4052 Basel
Switzerland
www.mdpi.com

Plants Editorial Office
E-mail: plants@mdpi.com
www.mdpi.com/journal/plants

Academic Open
Access Publishing

mdpi.com

ISBN 978-3-0365-8421-8